**The Effects of Blast Loading on the Interface of Concrete Masonry Units and Mortar**

by

Kelsey Rae Doan

A thesis submitted to the Graduate Faculty of
Auburn University
in partial fulfillment of the
requirements for the Degree of
Master of Science in Civil Engineering

Auburn, Alabama
May 4, 2019

Keywords: Dynamic Loading, Contact Interface, Concrete Masonry Unit, Finite Element Modeling, Strain Rate, Mortar Joint

Approved by

James S. Davidson, Committee Chair, Professor of Civil Engineering
Robert Barnes, Associate Professor of Civil Engineering
Justin D. Marshall, Associate Professor of Civil Engineering
Catherine Stephens, Research Civil Engineer, Engineer Research and Development Center

## Abstract

Masonry has always been a very efficient building material because of its low cost, availability, versatility, and construction simplicity. In terms of blast protection, masonry presents an enormous challenge: when subjected to blast loading, unreinforced masonry walls tend to break up into fragments that are propelled into the building interior at hazardous velocities. For these reasons, the response of unreinforced masonry walls subjected to impulse loads has been extensively studied through testing and advanced analyses and case studies of actual explosion events. However, as demonstrated by numerous blast load tests and investigations, the weakest part of an unreinforced masonry wall system is the interface between the masonry unit and mortar. However, as seen from observing previous relevant research, there is still a large amount of variation in approaches used to simulate that critical bond interface. This thesis therefore presents the results of an investigation intended to define the influence of masonry-mortar bond strength on the response of unreinforced masonry walls to far-field blast loads, and ultimately to provide guidance on optimum techniques for use in advanced finite element simulations. As a result of this work, it was determined that properly modeling the mortar in finite element models is important to obtain accurate results. It was also found that the shear and tensile strength of the connection between mortar and concrete masonry unit needed to be increased with dynamic loading. A testing setup for future testing was decided upon to validate such conclusions.

## Acknowledgments

I would like to thank my family and friends for supporting me during this long process and sticking with me all the way to the end. A special thanks to my parents, John and Lynn Doan, who were my biggest supporters in my time here at Auburn. Without their continuous encouragement, I would not have made it this far. I would also like to specifically thank my boyfriend, William Hyche, for coming into my life at the beginning of this process and being the calm to the storm that came with everything with grad school. A huge shout out to the many friends who have helped keep me sane throughout the years, including, but not limited to, Anna Quinn, Kendall Franklin, Vince Sellers, Ciara Morgan, and so many more people who have touched my life.

I would like to thank the faculty and staff at Auburn who made the journey as enjoyable as possible, specifically my advisor, Dr. Jim Davidson, and my committee members, Dr. Justin Marshall and Dr. Robert Barnes. There was never a time I felt like I could not approach any of them with any troubles I had and not get the assistance I needed, both in school life and anything overwhelming in my personal life. Also, this work was completed in part with resources provided by the Auburn University Hopper Cluster.

A special thanks to the Engineer Research and Development Center in Vicksburg, Mississippi for not only funding this research, but for also guiding me along the way. Especially Don Nelson, a modeling genius, for his insight into using the modeling software and his patient answers to my never-ending questions.

## Table of Contents

## List of Tables:

**List of Figures:**

# Chapter 1: Introduction and Objective

## 1.1 Overview

Blast engineering and the research behind how a structure reacts to the dynamic effects of explosions is a relatively new field within engineering. In the past, these types of loads were typically only considered for facilities where explosions would only happen from a chemical reaction or by accident. But due to events such as the Oklahoma City Bombing and the bombing of the World Trade Center, the importance behind understanding how to design a building to withstand such events outside of accidental explosions has been recognized. The main goal is not necessarily to keep the event from happening, because such events are not able to be eradicated, but to design structures to keep the damage compartmentalized to ensure life safety during the response of the structure. Today, many hospitals, schools, military buildings, and other high-risk structures are required to be designed with blast loads in consideration. There is continuous improvement within the design practices for all structures, and blast loads is a field where there is still much to be determined. There are some aspects of blast design that have still not been researched.

The main focus of blast engineering is life safety – keeping the occupants inside the structures as safe as possible during such an event. Glass and masonry are two of the worst materials in terms of life safety as they are easier to break and have a lot of debris velocity after a blast. A lot of research has been done and is still ongoing to better understand the best way to enhance such building components to decrease the likelihood of casualties due to such an event.

There are two main types of blast loads – accidental, such as from utility lines or chemical facilities, and terrorist attacks from a wide assortment of potential explosions. An example of an accidental explosion is the explosion that occurred in Bozeman, Montana in 2009. A natural gas explosion destroyed an entire downtown block in Bozeman. The damage included five historical buildings that were destroyed, as well as the businesses found inside, and, unfortunately, one life was lost. An example of a terrorist attack is the Oklahoma City bombing that occurred in 1995. This explosion occurred from explosives that were in a truck in front of the Alfred P. Murrah Federal Building. This explosion took many lives, the final count reaching 168. Due to the destruction of such events, it has become apparent as to why such a field in engineering is important. Better enhancing structures to be able to withstand the force of such awful events can help save lives as it has, unfortunately, become apparent that these events will not stop on their own.

Modeling has also been a key factor in understanding blast loads and their effects on structures. Being able to accurately model the response of a structure can open a whole new level of understanding on how the specific structure at hand responds to a load and how to appropriately transfer this knowledge to structures that have not been physically tested before. This is important as physical testing that involves explosives can be time consuming as well as quite expensive. But this leads one to wonder – how detailed does a model need to get and on how small of a level must one model a structure to produce the most accurate of results? The focus of this thesis is to target a part of blast engineering that although it may be small in size, can play a large part in understanding the overall effects of such a load. The topic of this thesis is to better understand the relationship at the interface of mortar and concrete masonry units in shear when subjected to high impulse loads from blasts. The objectives to obtain such information is twofold – first, to

determine the implications on this interface due to increased strain rate effects and, second, to decide on a testing configuration that could be performed to validate the found implications. The effects of blast load on the interface between mortar and the surface of the concrete masonry unit may be a small characteristic, but one that is important in understanding how the relationship between the two materials works under a high shear loading of high impulse from high pressure. It has been determined in previous reports, which will be discussed later in this thesis, that this interface is the primary failure mode of masonry walls, or where a larger scale of failure originates. Therefore, understanding how such a failure happens at this interface can be useful in determining a more accurate way to model such a connection.

### 1.2 Defining the Problem

There is currently very little available literature discussing the specific relationship between mortar and the concrete masonry unit surface at loading rates above quasi-static. There is information available for the relationship under quasi-static loading but not much was found for tests at a faster loading rate, such as from a blast load or a high pressure high impulse load. There is also an adequate amount of information about loading in the plane of the concrete masonry unit wall, such as seismic loading, but not necessarily for out of plane loading, such as from a blast load. It is important to understand how the faster loading rate would affect the relationship and at what amount it would do so. Knowing how this relationship works could lead to ways of enhancing the strength and performance at the interface and lead to a greater ability for the wall to resist loadings at such a high impulse from high pressure.

Throughout the process of understanding where past research has been accomplished in regards to the interface between mortar and concrete masonry unit, some questions have been brought to light. Such questions include what happens at this interface in terms of shear only? Can these

testing methods be implemented at higher strain rates? Is there a type of dynamic increase factor for this interface similar to that seen in concrete? Have modelers been improperly modeling such a connection without realizing? It has become apparent that there is a lack of information on what truly happens at the interface between mortar and concrete masonry unit at dynamic loadings and also the importance of understanding such a phenomenon, especially in terms of knowing how to properly model such a scenario, has been brought to light.

This project was funded by the Engineer Research and Development Center (ERDC) in Vicksburg, Mississippi to help tackle a finding that has recently been brought to light. It has been found that in order to accurately model blast loading on concrete masonry unit walls that the shear bond strength found in the bed joints of the wall must be increased in order to get accurate results. This location on the wall is subjected to more of a pure shear loading that the rest of the wall. It was then wondered if there is some sort of dynamic increase in shear bond strength that occurs when certain parts of concrete masonry unit walls are under more of a pure shear loading. Therefore, the idea to look more into pure shear failure at the bond between concrete masonry units and mortar came to be.

### 1.3 Proposed Solution

The proposed solution to the lack of information available is to develop a model to portray as accurately as possible the interface when subjected to high impulse loadings. This, of course, cannot be validated until physical testing is accomplished. However, it is desired that this research will pave the way to the most efficient way to acquire such physical testing data. This model will be created using finite element modeling software using typical modeling techniques as instructed by a modeler at ERDC. Data will be obtained to better understand the relationship at the joint as well as the effects from this joint being subjected to such a load. The particular values will not be

analyzed as these are irrelevant unless the appropriate material values and model parameters are used, but more so the behavior of the model and the implications it shows for what happens when the strain rate is increased.

The purpose of this research is to determine an efficient and accurate testing setup to model with a finite element approach to understand this relationship and correctly portray how this failure happens. With the use of LS-DYNA as the finite element modeling tool, a testing setup was modeled and many scenarios were tested in hopes of proving the accuracy of such a setup. It is desired that with this finite element modeling that physical testing may be accomplished to validate the model.

### 1.4 Objective

The objective of this research is twofold:

1) to determine a realistic experimental testing method that can be utilized in future work with the available equipment at ERDC, and

2) to determine what the effects of increasing strain rate on the bond at the interface of the concrete masonry unit and the mortar.

### 1.5 Scope of Work and Methodology

To reach this objective, first a literature review was performed. The aim of this research is to develop a simplistic and realistic finite element model to analyze the effects of high strain rates on the bond at the interface of the mortar and concrete masonry units. Finite element models were created within LS-PrePost and run through LS-DYNA solver to obtain results. These results were then used to determine the effects on the relationship between the mortar and concrete masonry units. A parametric study was performed using the methods within LS-DYNA by changing the

specifics of how the mortar and concrete masonry unit were connected and determining what type of relationship, if any, was found as the impulse load on the unit was increased. It is the overall goal of this thesis to produce a finite element model to aid in the overall modeling of concrete masonry unit walls subjected to blast loading to better understand what is actually happening at the interface between mortar and concrete masonry units. Based on results of these models, modelers will have a better indication of the types of parameters of this interface to produce more accurate results. It is desired to one day validate this model with the available equipment at ERDC.

### 1.6 Organization of Thesis

**Chapter 2** discusses the findings from current produced literature about the relationship at the interface between the mortar and the concrete masonry unit. There is currently scant information on this specific aspect of concrete masonry unit walls, but the articles that were discovered with similar characteristics were used to further expand on the specific topic at hand. Most articles focused on testing at lower strain rates with shear, or higher strain rates but with flexure or tension. Not many articles focused specifically on high strain rates with shear and focusing on the interface. There were various testing setups that were discovered through this process, one of which was chosen to be the setup used in the remainder of this research. The main goal of this literature review was to determine if such a topic of bond failure in shear had been observed before and if there were signs for a need of such research to be performed. The findings from this literature review are summarized in the following chapter.

**Chapter 3** focuses on the testing setup that was desired and how it was modeled in the finite element modeling program chosen, LS-DYNA. The various ways that modelers have been modeling the connection between mortar and concrete masonry units was also explored here,

introducing new models to be run to observe the behavior changes within the model for these changed parameters.

**Chapters 4** presents the results that were discovered for various loading cases as well as for the different parameters analyzed. Any relationship found for each set of runs is also observed and discussed in this chapter.

**Chapter 5** summarizes these findings with recommendations for future work.

# Chapter 2: Literature Review

## 2.1 Overview

In 2000, a test series was performed by the engineers at ERDC's Geotechnical and Structural Laboratories. These tests consisted of forty-three different quarter-scale walls with varying discharge weights and distances as well as varying wall types. All walls consisted of quarter scale concrete masonry units, mortar, and different groups of walls included grouted cells, vertical steel reinforcement, and sometimes retrofitting. Walls were split into different groups, including the following types:

- Simple Supports Unreinforced Ungrouted (SSUU)
- Simple Supports Unreinforced Fully Grouted (SSUG)
- Simple Supports Reinforced Partially Grouted (SSRP)
- Simple Supports Reinforced Fully Grouted (SSRG)
- Fixed-Simple Reinforced Partially Grouted (FSRP)
- Simple Supports Unreinforced Ungrouted FRP Wrap
- Simple Supports Reinforced Partially Grouted FRP Wrap
- Simple Supports Unreinforced Ungrouted Line-X
- Simple Supports Reinforced Partially Grouted Line-X
- Simple Supports Reinforced Partially Grouted Line-X with Steel Plates
- Simple Supports Reinforced Partially Grouted FRP Wrap with Steel Plates
- Simple Supports Reinforced Partially Grouted with Sheet Metal

A significant amount of data was obtained through these tests including high speed video, before and after pictures, as well as data from the accelerometers and pressure gages. Many various reports were written on this work over the years, some of which will be discussed below and have included finite element modeling. This particular modeling typically consisted of the walls being modeled as a single unit-wide column and loaded as such. It was not until 2016 that a modeler at ERDC started to model the walls as a full wall model. This process was started with the simplest group of walls, the simple supports ungrouted unreinforced group, and the model was arranged till results were appropriate before moving on to the next group of walls. Below in Figure 2-1 by Don Nelson at ERDC shows the effective strain fringe plot for such a model.

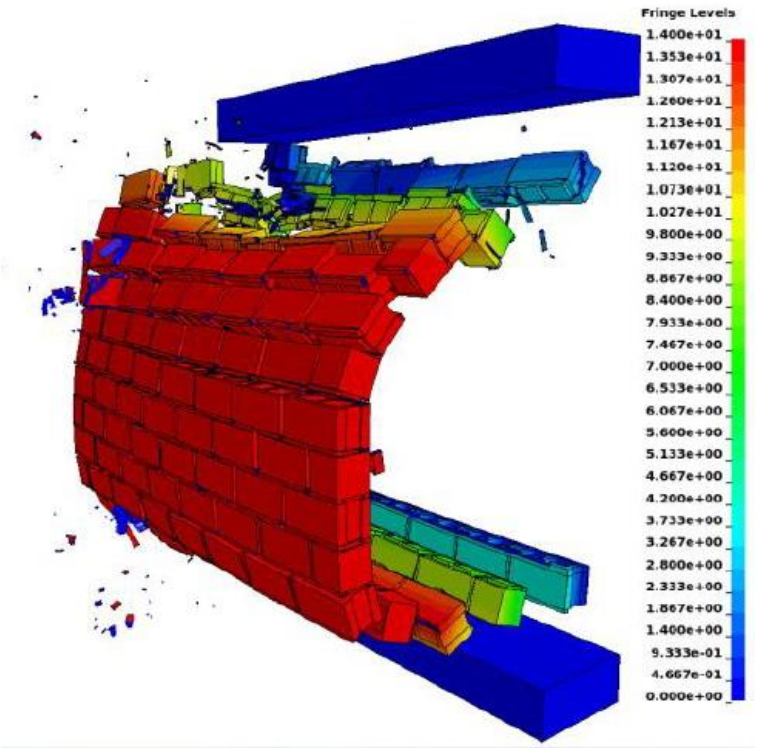


**Figure 2-1: Example of Full Wall Model from ERDC**

It was observed during this process that the values for the tensile and shear strength of the interface connection between the mortar and the concrete masonry units at the bed joint had to be artificially

increased in order to obtain accurate results. This particular location in the wall is the area where the most pure form of shear failure occurs. While the overall failure behavior of the wall is typically flexural failure, the locations of most pure shear failure happen on the uppermost and lowest locations on the wall. It was found that without an increased bond shear strength value that the wall was not failing with the correct shape, the boundary blocks were failing too soon to produce more accurate results for the rest of the model, and the velocity of the wall was not matching with the velocity obtained from the physical testing. This is where the idea was formed to take a closer look at this interface and a more pure shear failure mode, which is the overall topic of this thesis.

The literature review process began by first looking into the work performed by Eamon, Baylot, and O'Daniel in their article named "Modeling Concrete Masonry Walls Subjected to Explosive Loads" (2004). This was based off of tests done in 2000 by ERDC. Many articles were written on this specific test data, most of which will be discussed below, but the need to understand how the bond between the mortar and concrete masonry unit acted under such a high impulse load became apparent.

In order to understand more on this topic, a thorough literature review was performed. This review covered a wide array of testing setups, loading rates, material types, as well as countries that performed such work. As the literature review process came to a close, a specific testing configuration was decided upon and used for the basis of this thesis.

It was determined by the end of this process that little data or tests to better understand this connection at dynamic loads and in shear have been conducted as of this time. There was a large amount of data found for compressive and tensile strength, as these are two of the most important components of most materials. Shear was also a large topic between articles, but the problem arose

with the strain rates utilized – most of the strain rates for testing in shear were either static or quasi-static, but not past that strain rate to reach an actual dynamic loading.

It was also observed that shear is not a predominant reason for failure in the overall concrete masonry unit wall, rather flexural failure of the wall tends to be the driving factor in wall failure. However, as the wall starts to fail in flexure, the connection between the mortar and the concrete masonry units start to fail in tension or shear until these connections fail. So while shear is not a common failure mode of the overall wall, shear of the connection between the components of the wall occur due to the overall wall reaching a flexural failure mode, which is the type of shearing that is the focus of this research.

Of the articles that did discuss shear in concrete masonry unit walls, the main focus was on the in-plane direction rather than the out-of-plane direction. Examples of in-plane dynamic loading includes earthquake loading while an example of out-of-plane loading is loading from blast. There were many articles that discussed some of the parameters that were being searched for, but did not include enough of what exactly was being searched for to make use of the data and methods that were utilized. To use this data for this topic would have largely extrapolated the data that had already been obtained, but this is also in a region that extrapolation would not be appropriate for since materials act differently in different phases and under dynamic loadings than if it were to stay in the elastic region of loading and with a more static loading than that of a blast load.

It was, however, determined that a similar test setup that was used in these articles could be used to obtain the desired data. After careful consideration, a testing setup was decided upon and finite element modeling was able to be performed to obtain theoretical data for future use.

## 2.2 Results from Original Test Series from 2000

To begin this literature review process, it was desired to take a closer look at the articles published from the test data from the 2000 test series discussed above. As discussed, this test series consisted of forty-three different tests all falling into one of many wall types. These wall types also included some work on retrofitting, but these tests were not further looked into as retrofitting changes the behavior of the wall and this work focuses on such a small aspect of the wall itself. Blast pressures were induced by various charge weights at various standoff distances. Walls were also reinforced with steel dowels at every third cell. Explosives were detonated and results were obtained by five pressure gages around the frame and two accelerometers located on various locations on the wall. High-speed photography was also used for a better visual of the deformations that occurred during testing. Average pressure histories were obtained from testing and applied to the model for comparison. Walls were made from 1/4-scale concrete masonry units and placed in a rigid frame to hold the wall into place at the top and the bottom while the sides were free to move in and out of the plane.

The first of these articles was "Modeling Concrete Masonry Walls Subjected to Explosive Loads" by Eamon, Baylot, and O'Daniel (2004). For this specific article, fourteen of the above tests were used and categorized into three different ranges of blast pressures as well as three different types of failure modes. The tests were divided into three different pressure cases – high pressure cases, where failure resulted in the wall breaking into three large pieces; moderate pressure cases, where failure resulted in the wall breaking into two large pieces; and low pressure cases, where failure was not necessarily a result as the walls did not collapse, but there were large permanent deformations as a result of the testing. Examples of these failure modes are shown in Figure 2-1 below.

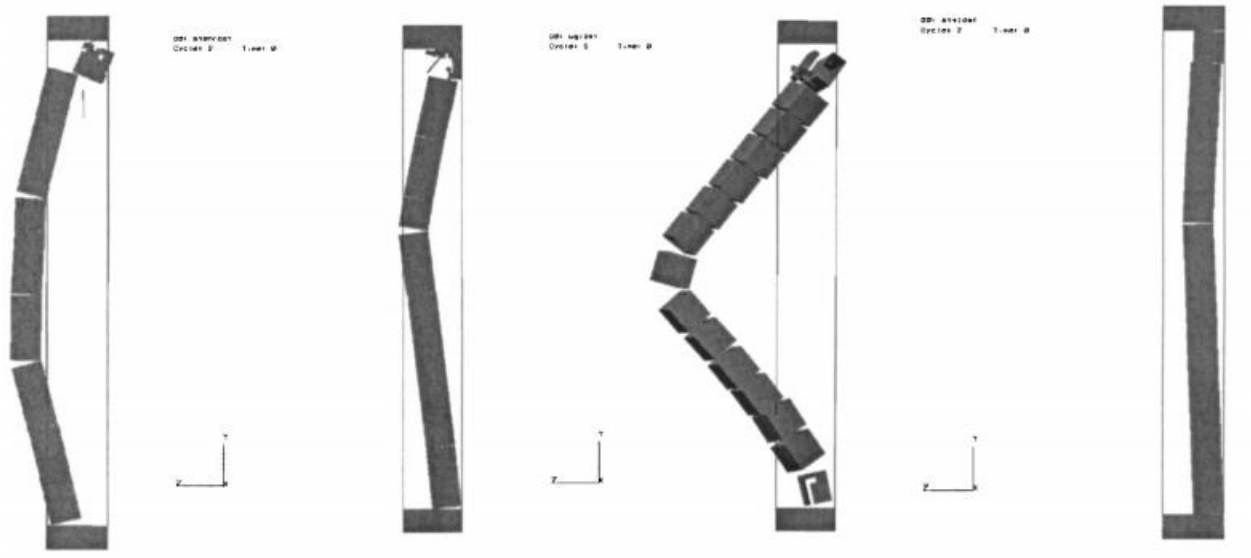

**Figure 2-2: Failure Modes Found by Eamon, Baylot, and O'Daniel (2004)**

The analytical model was obtained through work done in DYNA3D, "a large strain, large-displacement Lagrangian nonlinear finite element code with an explicit (central difference) solver" (Eamon, Baylot and O'Daniel 2004). DYNA3D is a government version of LS-DYNA, which was used for the modeling done for this research. Elements for this analysis were 8-node hexahedrals with trilinear shape functions. The walls were modeled as a single width concrete masonry unit column because the walls responded as a one-way system, signifying that width did not have a significant impact on the behavior of the wall. The mortar was "modeled as a zero-thickness contact surface" (Eamon, Baylot and O'Daniel 2004) with the actual mortar thickness included in the dimensions of the concrete masonry units. Adjustments in the mesh density did not affect the results, and it was determined that this "suggests that CMU interconnectivity and contact parameters along joint lines, rather than individual block deformations, govern global wall behavior" (Eamon, Baylot and O'Daniel 2004).

The model was validated by the results of the physical testing by correctly indicating whether or not the wall would fail and, if so, which failure mode was predominant. In the end, it was determined that because of variations in both material properties and construction that an accurate model for all cases is not likely. Further testing and analysis was suggested.

The second article from this work was "Response of 1/4-Scale Concrete Masonry Unit (CMU) Walls to Blast" by Dennis, Baylot, and Woodson (2002). This article starts with static testing that was also performed during the 2000 test series, ensuring that the model corresponded to the results of the physical testing before increasing the loading rate to a dynamic loading and determining if the model was still appropriate. In the model, the concrete masonry unit was composed of eight-node solid elements and each unit was connected by slide surfaces to represent the mortar. Similar to before, the wall in the model consisted of a single concrete masonry unit wide column. It was determined that the model was accurate to the point of maximum capacity of the wall, but not past this point. The stiffness of the wall in the model was determined to be accurate up to a pressure load of approximately 30 kPa but resulted in a wall stiffer than experimental results past this point.

This model was used to analyze the wall when subjected to a triangular pressure pulse representing the effects of blast load. Pressures were varied and the point at which failure begins was obtained for each case to determine a pressure-impulse diagram. Failure was designated as the point at which the wall does not return. It was determined that "the analysis displacement history matches the data history, initially indicating that the mass, initial loading, and initial stiffness are modeled accurately" (Dennis, Baylot and Woodson 2002). The relationship of the stiffness between experimental and analytical results for the static testing were also apparent for the dynamic testing. It was determined that the model was appropriate for both static loading and dynamic loading and provided conservative results.

The next article that was observed from the 2000 test series was "Blast Response of Lightly Attached Concrete Masonry Unit Walls" by Baylot, Bullock, Slawson, and Woodson (2005). The main objective of this study was to better improve the code used in predicting the response of elements exposed to blast loads, the Wall Analysis Code (WAC). The two main objectives of this work were to obtain more information in terms of wall damage and the degree of hazard from the debris. The tests that were used categorized the walls into degrees of damage, from little damage, or low hazard, to failure of the wall, or high hazard. It was determined that the velocity of the particles from the wall were related to the impulse of the load. However, a relationship between the velocity and the degree of hazard was determined to have no correlation. It was also observed that the "predominant failure mechanism of the walls was bond failure at the mortar joint" (Baylot, et al. 2005), but there was no additional investigations into such a failure within this article.

The last article found and used in this literature review was "Reliability of Concrete Masonry Unit Walls Subjected to Explosive Loads" by Eamon (2007). In this article, it was the attempt of the author to determine the probability of a wall being subjected to a blast load and develop models to determine the extent of damage to the structure in question as well as the probability of occupants being struck by debris from the blast. The main objective of this article was to develop a procedure to determine the reliability of masonry walls after being exposed to such a load, which is determined based on wall failure and injury to its occupants. Both fully grouted and ungrouted walls were utilized, as well as three different blast pressure categories – low pressure, moderate pressure, and high pressure. It was determined that "the most influential random variables that affect wall resistance are mortar joint strength and contact surface friction" (Eamon 2007). It was determined that in terms of wall failure, fully grouted walls were safer than ungrouted walls. In terms of debris velocity, it is less sensitive than wall failure and does not depend on the type of

wall failure. It was determined that for moderate and high pressure cases that wall failure and debris velocity were both likely to occur, whereas for low pressure cases, wall failure was more likely to occur without the presence of debris velocity.

These four articles were ones found that specifically worked off of the original data obtained from the 2000 test series. Of all of these articles, the finite element modeling consisted of a single concrete masonry unit wide column with zero-thickness mortar, where the mortar is not modeled at all and the concrete masonry units are connected with a contact parameter to indicate the mortar joint. Once the modeling was started in 2016 using a full wall model, which modeled the mortar joints as separate entities and multiple contact parameters between mortar joints and concrete masonry units, it was determined that such a model was more inclusive and accurate in terms of overall wall failure and debris velocity than what was seen in previous work. However, it was also noted that a better understanding of the mortar to concrete masonry unit connection was necessary as the strength values of the connection had to be increased to achieve the desired response of the model. Therefore, the literature review process began in an attempt to better understand if such a relationship had previously been discovered or if there was still much work to be done on such a topic.

### 2.3 Shear Bond Strength

Articles that discussed the effects of shear bond strength of masonry units and mortar were found, but most testing was done with static or quasi-static loading rather than dynamic loading or loading with a high strain rate. Some of these articles focused on the smaller scale of looking at the joint itself, where some of the research found included the effects of the overall wall. Work done on concrete specifically rather than concrete masonry units and mortar were also explored in an

attempt to correlate such work to the topic at hand. The articles discussed below include ones that were reviewed and fall into these categories.

"Tests on the Shear Bond Behaviour in the Bed-Joints of Masonry" by Stöckl and Hofman (1986) focused on the joints between the mortar and the masonry units to better understand the effects of shear stressed masonry. The test specimen consisted of five different types of bricks, all a type of clay brick or sand-lime brick, and three different types of mortar – Class II, IIa, and III. Both wet and dry specimen of each type of brick and mortar group was also prepared and tested. The test method selected "ensured a constant, uniformly distributed, freely selectable, normal stress in the mortar joint of a two-unit specimen" (Stockl and Hofmann 1986). Figure 2-1 displays the test setup utilized.

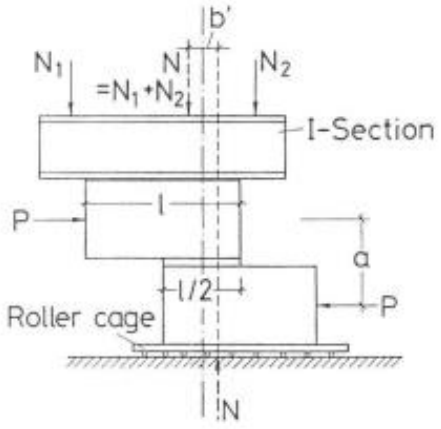


**Figure 2-3: Two Brick Test Specimen (Stockl and Hofmann 1986)**

The results were analyzed and the influence of the normal stress, type of brick, mortar strength, and state of the bricks upon being placed were all observed. It was found that an increase in normal stress resulted in a stiffer system and a corresponding deformation. However, it was also observed that an increase in the normal stress had little effect on the shear stress. When compared to the clay bricks, the sand-lime bricks resulted in stiffer behavior of the bed joints. It was noted that the

bearing surface of the sand-lime bricks should be taken into consideration because of how smooth they are, stating that the "sand-lime bricks seem to have a different type of bond, which may be better characterized with the term "gluing" in contrast to "indentation" in the case of clay bricks" (Stockl and Hofmann 1986). Increasing the mortar strength resulted in an increased stiffness of the bed joint for both types of bricks. It was observed that the increase in mortar strength had an effect on both the contact surface and the deformation. The clay bricks that were wet upon being laid resulted in a greater suction capacity which led to a higher value for the ultimate shear stress. An influence on the deformation of the bed joints was also observed but mostly for low strength bricks whereas there was little effect on high strength bricks in terms of the deformation. The placement of wet or dry bricks had little effect on the results of the sand-lime specimens.

Lourenco, Barros, and Oliveria (2004) tested stack bonded masonry in "Shear Testing of Stack Bonded Masonry". Stack bonded masonry is a type of placement utilized other the typical running bond placement, but is not as common of a placement type (Lourenco, Barros and Oliveria 2004). This type of placement allows for a continuous vertical joint which is typical when used to build masonry shells. The test specimen was a triplet which included three courses with a vertical pre-compression load, the top and bottom course held under a constant pressure, and a load applied to the middle course until it started to slide. The result of this test was the shear strength found in the joints due to in-plane loading. The cohesion and friction angle of the joints were observed at three different pre-compression stresses. The main failure mode observed throughout these tests was failure of the bond at the bottom of the units. For some of the tests, a diagonal crack through the brick or fissures occurred as well. A relationship was plotted between the normal stress and the shear stress following the trend as expected by the Coulomb friction law. A value for the cohesion

and the tangent of the friction angle were determined and deemed appropriate by falling into the range of acceptable values.

Ductility of reinforced masonry walls was observed by Mayrhofer (2002) in "Reinforced Masonry Walls under Blast Loading". It was observed that as a dynamic force is applied to a masonry wall that the wall will "change brittleness and gain ductility with reinforcement in the bed joint" (Mayrhofer 2002). Ductile behavior is desirable from walls subjected to such a load and was the focus of this article. Support conditions varied throughout the tests and the dynamic response was evaluated by using a single-degree-of-freedom (SDOF) system. Tests were performed with both a static loading and a dynamic loading. The walls were tested using the shock tube to observe the effects of reinforcement in the bed joint as well as observing the difference in using various types of bricks. The schematic of the shock tube is shown in Figure 2-2.

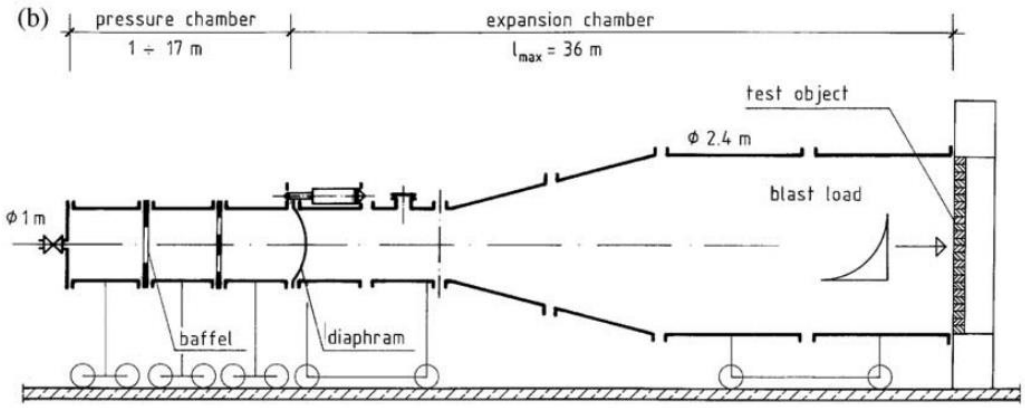


**Figure 2-4: Schematic of Shock Tube (Mayrhofer 2002)**

Results of the static loading condition showed that the type of brick used determined the amount of bond strength of the wall. Both clay bricks and sand-lime bricks produced walls with a higher bond strength. Various failure modes were observed in these tests, such as "exceeding of the brick material strength, the bond between the brick and the bed joint or by exceeding the tensile strength

of the reinforcement" (Mayrhofer 2002). It was also observed that a higher ductility of the wall itself was a result of using a lower amount of reinforcement. For the dynamic results, a dynamic load factor was used to convert the static problem to a dynamic problem. It was determined that for reinforced walls, failure by deflection was 10 to 13 times the elastic deflection while for unreinforced walls, failure by deflection was 30 times the elastic deflection. It was stressed that this increase was not necessarily because of the ductility of the wall, but because of the limited flexibility when reinforcement was present. Although the failure mode of the bond was mentioned, further information about the bond failure was not provided.

Moisture and strain rate effects on concrete were both observed by Ross, Jerome, Tedesco, and Hughes (1996) in "Moisture and Strain Rate Effects on Concrete Strength". Both wet and dry concretes were tested at various strain rates in both tension and compression to determine the effects of moisture and strain rate on the behavior of concrete. Transition regions were noticed for both tension and compression tests and increases in strengths for both wet and dry specimens were also observed. It was determined that for dry concrete, strength increase was only observed above this transition region. However, for wet concrete, strength increase was observed both above and below the transition region. Therefore, the moisture content plays an important role on how sensitive the specific specimen is to the strain rate.

Three types of specimens were tested – wet, half dry, and completely dry. Both static and dynamic tests were completed on all specimen types using a split-Hopkinson pressure bar system. A dynamic increase factor was used to compare the dynamic strength to the static strength to create a more uniform way of observing the data. It was observed that the wet and half dry specimens had a greater increase in strength at higher strain rates than those that were observed at lower strain rates. The wet specimens also had an increase in strength but not near as large of an increase as

what was seen in the dry and half dry specimens. From static testing, the wet and half dry specimens exhibited less strength than the dry tests. It was concluded that at higher strain rates, the excess water in the wet and half dry specimens actually improved the strength of the concrete.

"Response Evaluation of Reinforced Concrete Block Structural Walls Subjected to Blast Loading" by ElSayed, El-Dakhakhni, and Tait (2015) makes the point that structural walls tend to deal with larger loads under the same type of blast load than a single column because of the large increase in surface area of a wall when compared to a column. It is also noted that there is a possibility of a brittle failure when the wall is bent about its weak axis, attributing to the necessity of looking at the entire wall rather than simply a column. Wall specimens include fully grouted, 1/3-scale reinforced masonry structural walls. Physical testing on twelve specimen was performed to obtain rotation in the support, damage to the walls, and the failure mode. These were then compared to a single-degree-of-freedom model "described in UFC 3-340-02 and then correlated to code-specified damage threshold levels, and corresponding system-level performance" (ElSayed, El-Dakhakhni and Tait 2015). The scaled distance approach was used to correlate the results of three different charge weights. Boundary conditions included both simply supported and fixed-fixed. For the simply supported setup, the top and bottom of the wall was capped with steel C-channels. For the fixed-fixed setup, walls were welded to the top and bottom C-channels by their vertical reinforcement and additional steel members were used to prevent rotation. Three walls with same steel reinforcement ratios and boundary conditions were tested with a quasi-static loading rate. These reinforcement ratios are low (0.33%), moderate (0.62%), and high (1.07%). Three different charge masses were also used - moderate, heavy, and hazardous failure. The different amounts corresponded to different groups of walls, with Group I subjected to 5 kg of explosive charge, Group II with 10 kg of explosive charge, and Group III with 25 kg of explosive charge. To measure

the response of these walls, displacement transducers were used to monitor out-of-plane displacements, strain gauges were used on the vertical reinforcement, and three piezoelectric pressure transducers were used around the wall to measure reflected pressure.

Group I walls "developed tension cracks in the bed joints of the mid-height zone of the walls on the rear face" (ElSayed, El-Dakhakhni and Tait 2015). Spalling did not occur in a majority of the walls tested and tension cracks propagated "into the grout cells for more than half the wall thickness" (ElSayed, El-Dakhakhni and Tait 2015). The damage for Group I walls was classified as superficial, or damage that is unlikely to be permanent. Boundary conditions and reinforcement ratio did not impact the results of Group I walls because all walls showed this superficial, or not permanent, damage.

Group II walls resulted in cracks horizontally in the joints with minor cracks in the blocks. The cracks observed were indicative of a loss in bond between the block and the mortar. The damage for Group II walls was classified as heavy damage, or damage that is most likely irreparable but component failure is not necessarily problematic.

Group III walls resulted in much more damage, as well as the walls with a low reinforcement ratio splitting in half. Wall splitting, tensile cracks, compressive spalling, cracks propagating to blocks, and necking in reinforcement were all observed throughout the various walls in this group. The damage for Group III walls was classified as hazardous, or damage that results in an expected component failure. It was recommended that for Group III walls "that a balance between ductility and strength should be carefully considered in blast-resistant RM (reinforced masonry) walls, as increased ductility with reduced strength might result in a wall displacement demand, under a specific range of DBT (design basis threat) levels, that might exceed the displacement capacity of the wall or result in permanent deformations that might be detrimental to the wall. Conversely,

having a less ductile but a stronger wall would result in reduced permanent deformations and increased blast resistance; all the while introducing the risk of a brittle failure mode should the strength demand exceed the capacity." (ElSayed, El-Dakhakhni and Tait 2015). In other words, the higher the load from blast pressure, the more brittle the failure mode becomes. Flexural response was the most demanding response in all cases.

The response of these walls was compared to the results of a nonlinear single-degree-of-freedom model as specified in UFC 3-340-02 (U.S. Army Corps of Engineers 2008) and the results were fairly consistent across the board. It was also noted that when observing the damage on these walls, the quantitative and qualitative descriptors may not necessarily match up for all cases. It is also important to note that while structural walls are designed to be ductile from typical in-plane loads, this is not necessarily the case for out-of-plane loads, where failure can be more brittle.

### 2.4 Testing Methods

Testing methods that were found and utilized throughout the various reports in the literature review process include a vacuum chamber, split Hopkinson pressure bar, servo-controlled direct shear apparatus, and biaxial test. Testing specimen included couplet testing configurations, triplet testing configurations, and full wall testing configurations. Each of these types of tests and the results that were obtained from them are discussed below.

The static vacuum chamber was capable of testing full-scale infill wall systems as tested by Brown (2004) in "Evaluation of Wall Systems Subjected to Lateral Pressure for Blast Resistant Design", allowing there to be no concerns with scaling of the results. "The static-vacuum testing chamber is essentially a reinforced steel cube with the test wall, covered by a flexible membrane, creating the final side of the cube" (Brown 2004). Boundary conditions of the full-scale infill wall systems were simulated by concrete. This setup was designed to contain the entire specimen, allowing

those performing the tests to be present without the possibility of injury. However these results were from more of a static type of testing, which cannot necessarily be utilized for dynamic loading.

The split Hopkinson pressure bar was utilized by various reports that were reviewed. The first of these was "Split-Hopkinson Pressure-Bar Tests on Concrete and Mortar in Tension and Compression" by Ross, Thompson, and Tedesco (1989). From this report, it was determined that an increase in strain rate leads to an increase in strength in both tension and in compression. The increase was much greater for tension, which found an increase in strength from 1.5 to 3 times as much at strain rates of 10 to 100/sec than the tensile strength at quasi-static strain rates, than for compression. Figure 2-3 shows the testing setup that was utilized by Ross, Thompson, and Tedesco (1989).

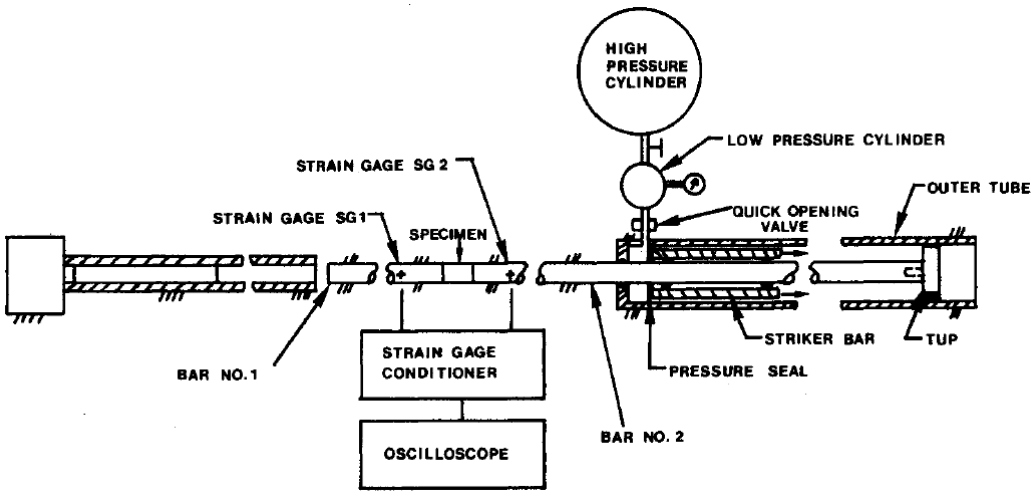


**Figure 2-5: Split-Hopkinson Pressure Bar Setup (Ross, Thompson and Tedesco 1989)**

"Experimental and Numerical Analysis of High Strain Rate Splitting Tensile Tests" by Tedesco, Ross, and Kuennen (1993) used a 50.8 mm diameter Split-Hopkinson pressure bar and was loaded at strain rates of $10^{-7}$ /sec to $10^{2}$ /sec. These tests were performed to observe the deformations and

cracking that occurred within the specimen, as well as to compare the tensile strength versus strain rate to that of a compressive strength versus strain rate. It was found that there was not a significant effect of strain rates above that of 1.0/sec, which was found to be about one hundred times less than that for compressive strength.

"Effects of Strain Rate on Concrete Strength" by Ross, Tedesco, and Kunnen (1995) was written based on results from three different types of testing – direct compression, direct tension, and splitting tensile. The specimen that were tested were 51 mm in diameter and at strain rates of 1.0/sec to 300/sec, as well as quasi-static rates from $10^{-7}$/sec to $10^{-3}$/sec. It was shown that tension and compressive strengths both showed an increase as the strain rate was increasing. A critical strain rate, or the final value of strain for which concrete showed an increase in strength, was determined to be 5/sec for tension and 60/sec for compression. Results showed that the tensile strength data was much more sensitive and that larger increases happened at lower strain rates than that for compressive strength. It was also stated that "higher strain-rate sensitivity, supposedly attributed to excess water content after the normal curing time, appears to be a function of the inherent lower wet concrete strength as well as excess water content" (Ross, Tedesco and Kuennen 1995).

The servo-controlled direct shear apparatus was used by Atkinson, Amadei, Saeb, and Sture in "Response of Masonry Bed Joints in Direct Shear" (1989) that tested a total of forty-four different tests on old clay units and nine tests on new clay units. The results concluded that the masonry bed joints showed a peak strength during the first cycle that then had a residual shear strength. The results had friction coefficients between 0.64 and 0.75 and were conclusive with the Mohr Coulumb criterion. There were various set-ups that were discussed in this report, each with their own list of advantages and disadvantages. These are briefly discussed in the following paragraphs.

The first of these setups was used by Nuss (1978) and Hamid and Drysdale (1980). The specimen would collapse in an unstable manner once a peak strength was reached, making any post-peak, load reversal, or deformation values, impossible to retrieve. Advantageous results from such a setup included factors that affect the peak shear resistance. A schematic of this setup can be seen in Figure 2-4.

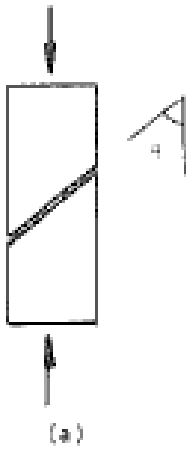


**Figure 2-6: Compressive Loading of Masonry with Bed Joint at an Angle (Atkinson, et al. 1989)**

The next setup was on used by various researchers, but the work of Yokel and Fattal (1975); Calvi, Macchi, and Zanon, (1985); and Meli (1973) were all referenced within this report. This setup was done to test the tension and shear strength of the masonry in the diagonal direction, which created a complex state of stress. One of the disadvantages of this setup and test was that the stresses along the bed joint was nonuniform, resulting in an averaged value for failures. This resulted in values that were different than the actual material property. Figure 2-5 displays such a testing setup.

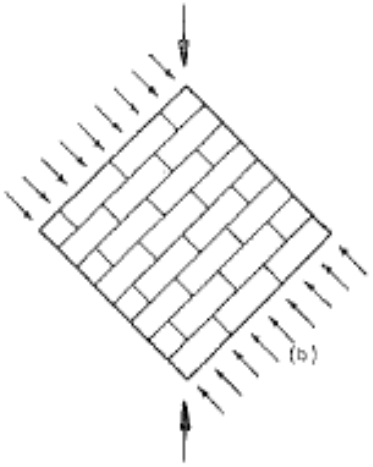


**Figure 2-7: Testing Configuration with Concentrated Diagonal Load for Complex Stress State (Atkinson, et al. 1989)**

The subsequent setup discussed was utilized by Meli (1973); Sinha and Hendry (1969); Dawe and McBride (1985); and Mayes and Clough (1975). This setup was accomplished by testing a wall with both a vertical and horizontal load at the top of the wall. This was used to look at loads applied in the plane of a shear wall. The results obtained from this setup were from the complex stresses and the gradients found in the testing. It was determined though that "this test is better suited to providing information on the response of structural subassemblages or structural components (macromodels) due to specific loading conditions than for revealing basic material properties (micromodels)" (Atkinson, et al. 1989). This setup can be seen in Figure 2-6.

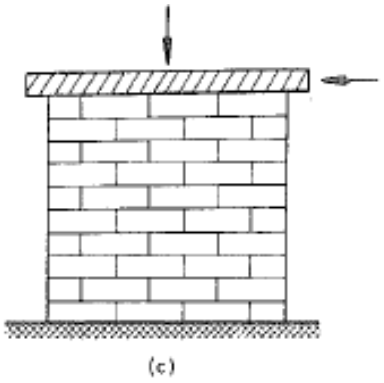


**Figure 2-8: Racking Test Setup (Atkinson, et al. 1989)**

The following setup was one tested by Meli (1973) and Hamid (1978) which targeted the bond and friction in bed joints with varying types of concrete masonry units. It was determined that bond strength varied depending on the mortar and type of concrete masonry unit used. Meli (1973) also observed that normal joint precompression was present but that the shear strength also varied linearly. He also determined that an increase in precompression stress would lead to a decreased value for the coefficient of friction. Other findings included that grouted concrete masonry had a lower initial shear stiffness than ungrouted concrete masonry and that an increase in normal stress led to an increase in shear strength and shear stiffness. Figure 2-7 shows the setup that was used to obtain such results.

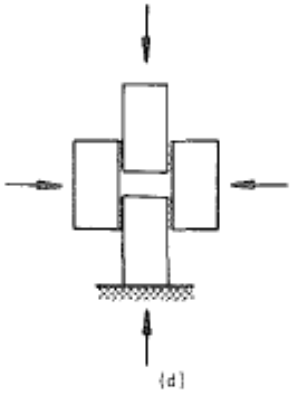


**Figure 2-9: Masonry Prism Configuration for Testing of Bond and Bed Joints (Atkinson, et al. 1989)**

The final setup discussed in this report was used by Hegemier et al. (1978). This setup utilized a triplet configuration with the specimen. His results showed that there was no dependence on the shear resistance on velocity when determining the shear displacement velocity. Furthermore, after the first cycle of stress reversal, the shear resistance found in the bed joint became a constant value which was determined by the remaining shear resistance. This triplet specimen setup can be seen in Figure 2-8.

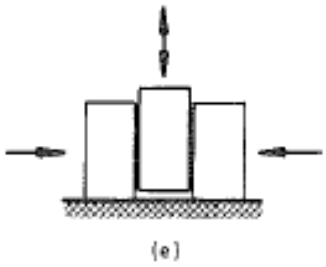


**Figure 2-10: Triplet Test Specimen (Atkinson, et al. 1989)**

The results from this report showed that "the coefficient of friction decreased with an increase in precompression stress and that grouted specimens yielded friction coefficients that were considerably higher than ungrouted specimens" (Atkinson, et al. 1989).

The biaxial test was the method used in two separate reports. The first of these was "Shear Behavior of Bed Joints" by Vad der Plujim, Rutten, and Ceelen (2000). The focus of this work was on the failure envelope, mode II fracture energy, cohesion softening, and dilatancy. The testing specimen used for this testing were wired cut clay bricks with general purpose mortar and masonry containing calcium silicate blocks with a prefabricated thin layer of mortar. Normal stresses were held constant at different levels for different sets of tests while the shear deformation was increased. The objective for the failure envelope portion of this report and test results was to be able to plot points on the failure envelope for points within the high tensile stress range.

Failure mechanisms observed were bond failure, failure in mortar and bond failure, bond failure and tensile fracture of the units near their heads, and diagonal tensile failure of the units. Such failure mechanisms are shown in Figure 2-9, and the testing setup utilized is shown in Figure 2-10.

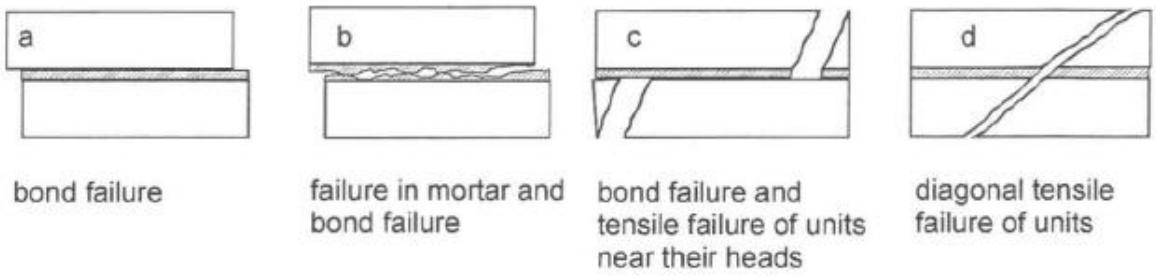


**Figure 2-11: Failure Mechanisms observed by Van der Plujim, Rutten, and Ceelen (2000)**

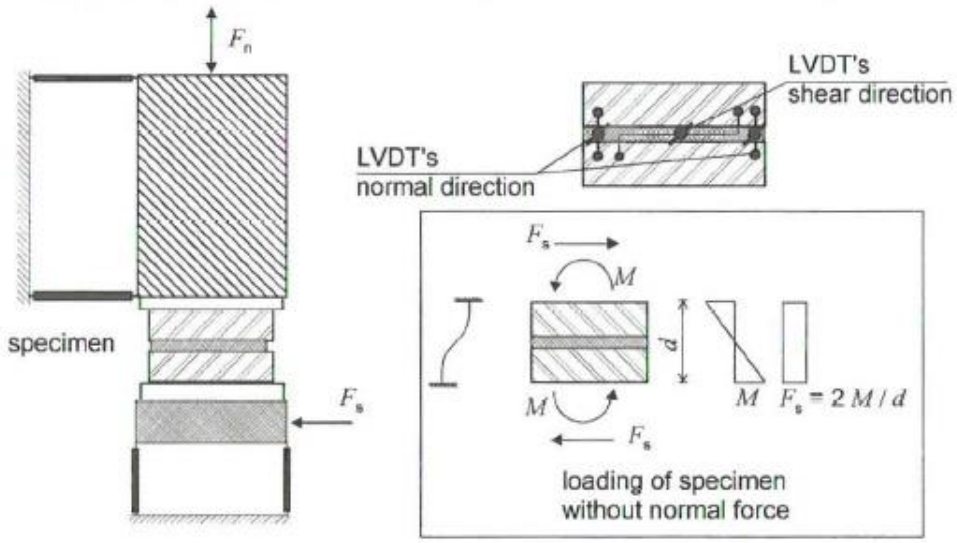


**Figure 2-12: Bi-axial Test Setup (Van der Pluijm, Rutten and Ceelen 2000)**

Another report utilizing the biaxial test was "Experimental Study of Shear Bond Strength of Traditional Masonry" by Bei and Papayianni (2004). The specimen used for this testing was compressed earth bricks with mud mortars and fired bricks with lime mortars. The configuration of these specimen for testing purposes was in the form of a triplet similar to the last test setup shown above by Atkinson et al. (1989). The configurations were placed in the testing apparatus so that the applied shear force was parallel to the mortar joints. A hydraulic jack was also used to keep the prisms steady, applying a normal force just enough to keep the configuration from shifting. Transducers were used to obtain displacements, both vertically and horizontally. Shear loads were applied at a rate of 0.4 N/mm$^2$/min while the normal force varied. Results showed that an increase in the applied normal stress results in an increase in the shear strength of the bed joint. A comparison between the two types was conducted to determine that earth brick masonries had a lower shear strength and higher values of slip. It was also determined that "failure type and detachment pattern of the joint may be related to the values of bond strength" (Bei and Papayianni 2004). Figure 2-11 shows the schematic of the testing setup used by Bei and Papayianni (2004).

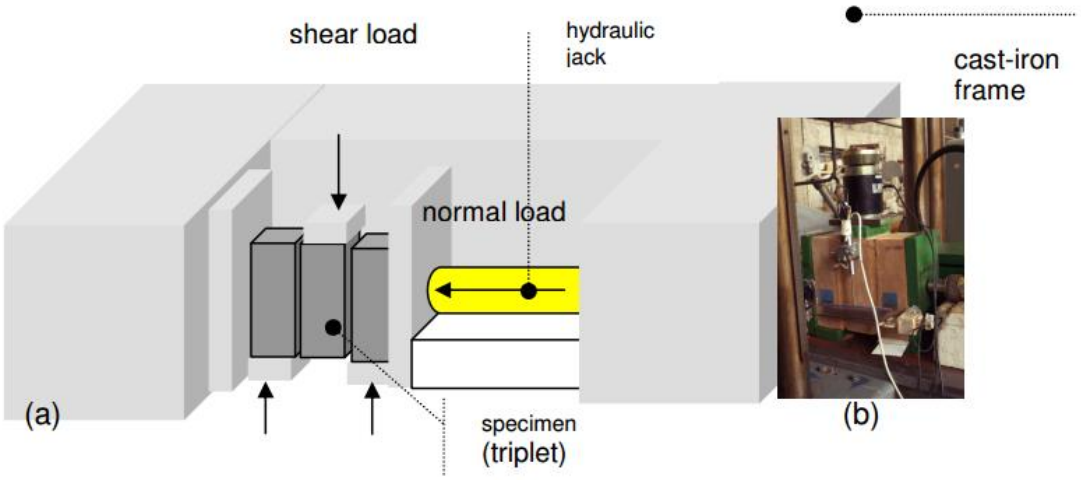


**Figure 2-13: Testing Setup Used (a) and Arrangement in Laboratory (b) (Bei and Papayianni 2004)**

## 2.5 Dynamic Testing

The triplet specimen setup was also utilized by Beattie, Molyneaux, Gilbert, and Burnett in the work titled "Masonry Shear Strength under Impact Loading" (2001). This article was written as a summary of work performed by Beattie in his thesis titled "Joint Fracture in Reinforced and Unreinforced Masonry under Quasi-Static and Dynamic Loading" (1996) at Liverpool University. This work consisted of two phases where work from Liverpool, Sheffield, and Teeside Universities all contributed to the overall goal of understanding the fundamental characteristics of masonry walls subjected to impact loads from vehicles. The objective of this work for Liverpool was the "development of small scale reinforced and unreinforced test methods in order to provide the dynamic and quasi-static material data required for the finite element modeling" (G. Beattie 1996). This led to physical testing of a triplet brick specimen in a drop hammer rig apparatus which was then accompanied with finite element modeling. The triplet test consisted of sixty-six different tests whose purpose was to "investigate shear strength, mode II fracture energy, and angle of

dilitancy with varying amounts of precompresssion applied" (G. Beattie 1996). Other tests were performed on couplets, columns, and beams resulted in adequate information for Liverpool to complete the specific tasks for the overall project.

Beattie used a drop hammer rig to test the triplet specimen as an impact loading. An electro-magnetic release mechanism was constructed by Liverpool University to conduct consistent loadings on the specimen. Reaction forces of the outer bricks were obtained using load cells and strain gages were also utilized for the drop bar itself. After the testing rig was validated, testing was then completed at higher strain rates to explore the effects on the reaction forces. These results were then plotted to create a shear stress to static shear stress ratio versus stress rate plot. Figure 2-12 shows such results from this testing.

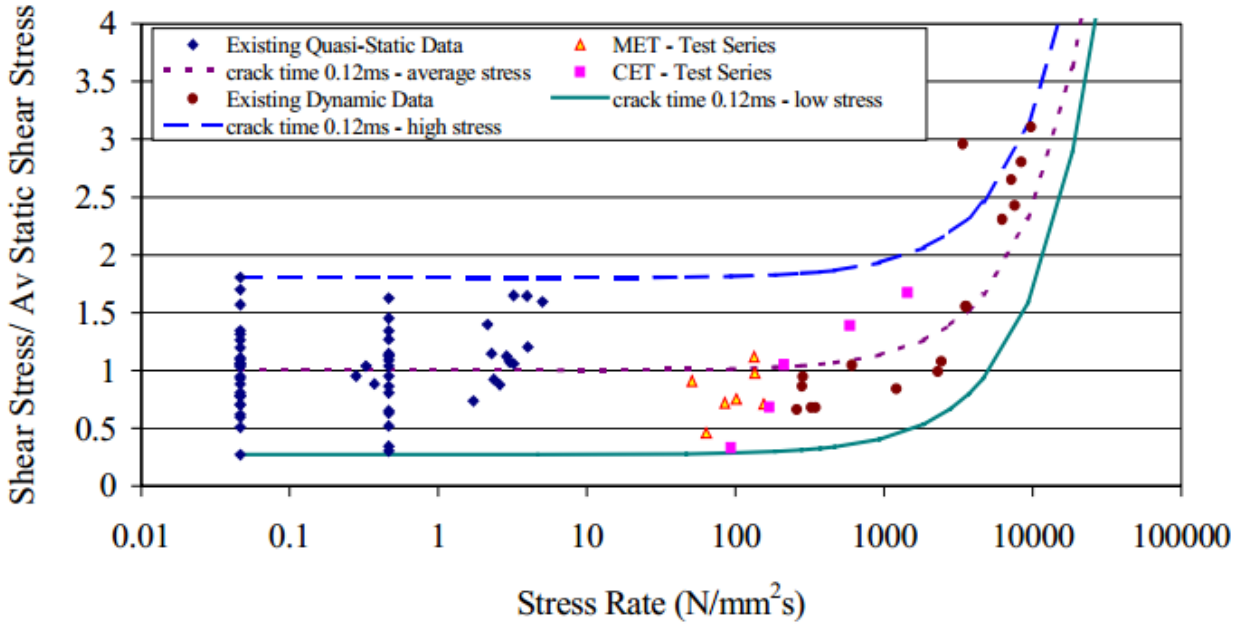


**Figure 2-14: Shear Stress to Static Shear Stress Ratio versus Stress Rate for Impact Loaded Triplets (Beattie, Molyneaux, et al. 2001)**

This plot shows a similar phenomenon that is seen in a typical dynamic increase factor plots for concrete materials. An exponential curve was also fit to the data and crack speed was also implemented to obtain the curves found on the graph. This work and this particular figure gave hope into the possibility of somehow proving the necessity for increased shear and tensile strength values in the connection.

This same phenomena was also discovered by Molyneaux in his work titled "Vehicle Impact on Masonry Parapets" (1995). The focus of this particular work was investigating the impact loading felt by masonry parapet walls after being struck by vehicles. During the material testing portion of this work, it was stated that "the most striking finding was the degree to which the shear strength of the mortar joint is sensitive to strain rate" (Molyneaux 1995). This same behavior was also noticed in the modeling portion of this work as the shear and tensile strengths of the connection had to be increased for the model to exhibit an adequate response of the panels. It was observed that the "dynamic strength of mortar joints in walls is significantly greater than the static strength". (Molyneaux 1995).

Another interesting find from the work done by Beattie was the cracking pattern found in the mortar joint. This was observed to be dependent upon the type of support conditions and loading condition utilized in the testing method. When a uniform pressure was applied to the top of the center brick and therefore resulted in a uniform reaction on the bottoms of the outer bricks, the failure was more of a tensile failure between the mortar and the brick. When the applied force was more of a point load directed exactly at the edge of the mortar and brick interface, the failure was more of a shear failure within the joint. Due to this finding, it was stated that it was not a pure shear strength increase that could be attributed to the previous strength increase findings. Figure

2-13 displays the two types of failure that were indicated above, the first being tensile failure and the second being the shear failure.

**Figure 2-15: Tensile and Shear Bond Failure in Triplet Specimens (Beattie, Molyneaux, et al. 2001)**

There were three main conclusions observed from the work by Beattie, Molyneaux, Gilbert, and Burnett. The first was that there was, in fact, an increase in the bond strength from an increased impact loading on the specimens. Second, that the support and loading conditions should be carefully considered as the results of the overall testing are very sensitive to such conditions. The last observation was that the crack propagation velocity of the mortar joint may be of importance when attempting to produce an accurate finite element model.

Many other articles were found to have used the triplet testing specimen as well. Such work was performed by Hegemier, Arya, Krisnamoorthy, Nachbar, and Furgerson (1978); Singh and Munjal (2017); Beattie, Molyneaux, Gilbert, and Burnett (2001); Sarangapani, Venkatarama Reddy, and Jagadish (2005); Thamboo, Dhanasekar, and Yan (2013); Thamboo and Dhanasekar (2015); Ghazali and Riddington (1988); Riddington and Ghazali (1990); Mendoza Puchades, Judge, and

Beattie (2016); and Beattie (1996). This work varied between static loading or dynamic loading, as well as between the ways that these loadings were applied to the specimen. Some of this work also included modeling the testing in a finite element modeling software.

The most recent and prominent, especially in terms of dynamic loading, is the work accomplished by Beattie (1996) and the work referencing the physical testing done by Beattie included loading rates above the quasi-static region. The findings from this work provided hope that this triplet specimen and loading it at higher strain rates would result in very useful results. From these results, it is desired to have a better understanding of why a higher tensile and shear strength value of the connection is needed and how to appropriately implement them.

## 2.6 Summary of Literature Review

In summary, there is little previous work that was found discussing the relationship at the interface between the mortar and the concrete masonry unit for shear loading. Most information found was for loading in tension or compression, or analyzing an entire masonry wall rather than looking at the smaller scale of the interface. It was determined that for both tension and compression that an increase in loading rate led to an increase in concrete strength. It is desired to find a similar relationship when observing the bond strength of mortar and concrete masonry units at higher strain rates.

However, many articles discussed the importance of bond strength and bond failure as a predominant failure mode, but did not discuss the bond in further detail. The work by Beattie (1996) gave hope into finding an interesting relationship between the bond strength and strain rate. After finding this work implementing impact testing on triplet specimens, it was desired to perform similar testing to obtain more information in regards to the possibility of an increased bond strength under pure shear loading. The triplet specimen similar to that shown in Figure 2-11 above was

then implemented into the finite element parametric study for this research. Such a testing setup can easily be implemented to work with the machines available at ERDC when physical testing becomes a reality. It is the hope that the findings shown above by previous research and that with the implications of the parametric study below that the most efficient course of action as possible can be implemented when physical testing is started.

## Chapter 3: Finite Element Modeling

### 3.1 Introduction to LS-DYNA

LS-DYNA is a finite element modeling software that is typically used by structural engineers to accurately model situations where blast loads may be involved. There are, however, many other applications for LS-DYNA that can be useful in the analysis world. The government version of LS-DYNA is called DYNA3D and mentioned previously in various articles discussed in the literature review. LS-DYNA was described by Hallquist as "an explicit three-dimensional finite element code for analyzing the large deformation dynamic response of inelastic solids. A contact-impact algorithm permits gaps and sliding along material interfaces. By a specialization of this algorithm, such interfaces can be rigidly ties to admit variable zoning without the need of transition regions" (Hallquist 1979). To run these analyses, intense calculations are performed on supercomputers to quickly produce results that can accurately describe what happens with a dynamic event. With the speeds of computers nowadays, these calculations can be completed in a much more efficient manner than when DYNA3D was first introduced. Intense calculations that would take days to perform can now be completed in a matter of minutes or hours. Over the years, many modifications have been implemented and new capabilities were included to continue to increase the efficiency, dependency, and accuracy of the models run on the application.

Contact parameters can be specified to link one part to another and appropriate material models can be assigned to each part. There are many various applications for using LS-DYNA or the finite element method as an object can be broken down to a desired number of elements to

mathematically simulate what happens to the overall object by looking at each individual element and how it behaves itself as well as with the elements surrounding it. A finer mesh with more elements included leads to a more accurate solution, but can also lead to issues with computation time as more elements results in a necessity for much more computing power and time. Therefore, it is important to have a good balance between having enough elements to run an accurate simulation but not too many to be inefficient.

A geometry is created in LS-PrePost with the pre-processing side of the application. Once a design is finalized, the input file, or "keyword" file, is transferred to a supercomputer system with the LS-DYNA program loaded into it and ran in this system. There are supercomputers both at ERDC as well as at Auburn University and both were used for this thesis. The modeling process started with ERDC supercomputer, called Topaz, and then moved to the supercomputer at Auburn University, called Hopper. Most of the preliminary design was completed on Topaz but a majority of the modeling done for this thesis, including all the results and images found within, was completed on Hopper. Once the job was completed on the supercomputer, the output files were then opened in LS-PrePost and analyzed using the post-processing side of the application. It is here that the behavior of the model, as well as graphs, tables, and a variety of other output platforms, were observed. This chapter will discuss the parameters, values, and methods chosen to be implemented with this design.

### 3.2 Initial Design

Once the triplet concrete masonry unit specimen was decided upon, the next step was to create the model in LS-PrePost. This was done using the student version that was available online from Livermore Software Technology Corporation. Using the pre-processing side of the application, a model was made to include a desired meshing and element size, boundary conditions, contact

interface, appropriate material models, and loading of the specimen. The below sections will go into detail about the specifics of the model.

### 3.2.1 Element Sizing and Meshing

Although the test series that this thesis was derived from used quarter scale concrete masonry units, when physical testing of this work is performed, it is desired to use full scale concrete masonry units. Therefore, the nominal size of 8 inches by 8 inches by 16 inches was used. This corresponds to an actual concrete masonry unit size of 7-5/8 inches by 7-5/8 inches by 15-5/8 inches with a 3/8 inch mortar joint between all concrete masonry units.

The three concrete masonry units were modeled first using the actual concrete masonry unit size and leaving 3/8 of an inch in between for the two mortar lines. All parts, the three concrete masonry units and the two mortar interfaces, were modeled as an 8 noded hexahedron solid box elements. The concrete masonry units were split into elements with an approximate square size of 0.381 inches on each side, leading to an object with 20 elements by 20 elements by 41 elements. The mortar line had the smallest meshing size to allow for three elements through the thickness of the mortar. From work previously accomplished with modelers at ERDC, a minimum of three elements through the thickness is typical for most modeling techniques. This is typically done to account for a coarse model undergoing flexure, allowing one element to carry tension, one to carry compression, and the other to represent a neutral axis between the two. Otherwise, the neutral axis may fall right in the center of the element and since single point integration of the elements is accomplished by looking in the center of the element, it will not accurately portray what is happening within the object as it will continue to see a value of zero while it is still at the neutral axis. The mortar elements had an approximate square size of 0.125 inches on each side, which resulted in mortar objects with 3 elements by 61 elements by 125 elements. Each element, for

both the concrete masonry units and the mortar line, were made to be as close to square as possible. The model with this meshing and geometry can be seen in Figure 3-1.

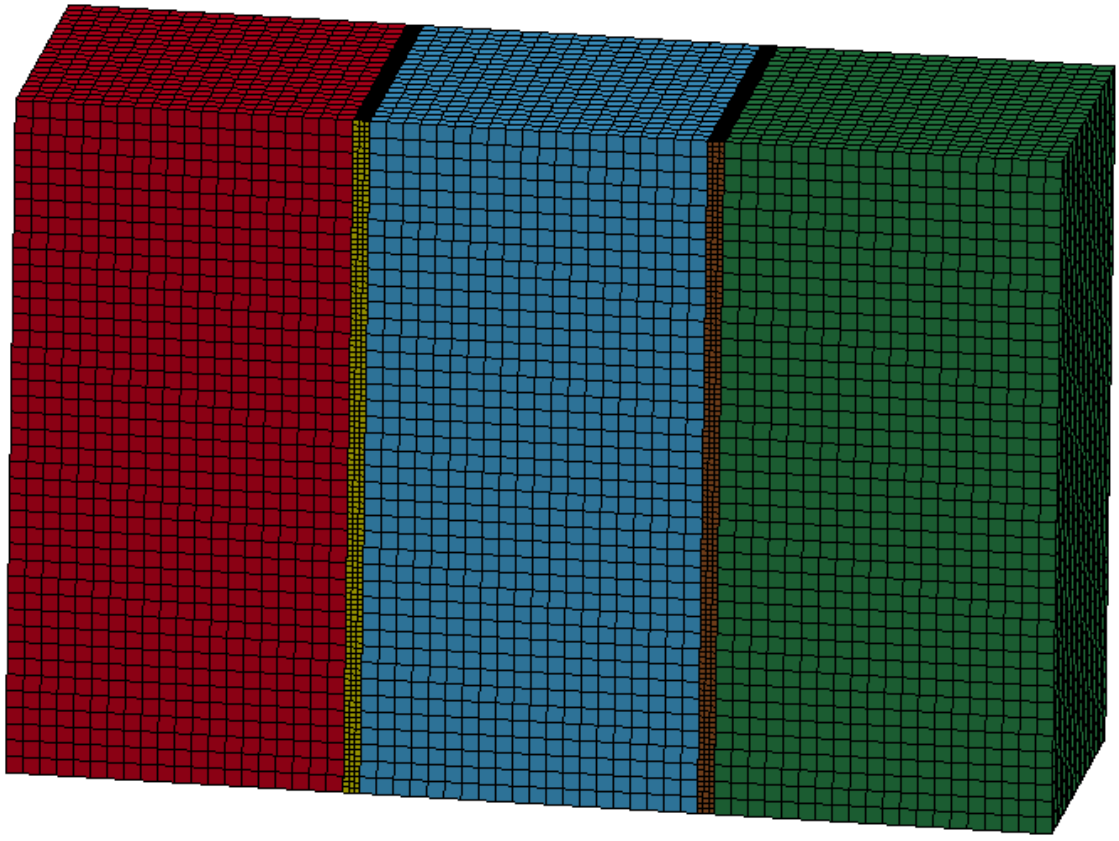

**Figure 3-1: Meshing and Geometry of Initial Model Setup**

It was decided to model the concrete masonry units as solid concrete masonry unit objects rather than the typical concrete masonry units with holes in the middle. It is also to be noted that the setup used is more of a stack bonded masonry configuration rather than the typical running bond masonry configuration that is used in most construction. For both of these observations, it was determined to be adequate as the concrete masonry units were not the main focus of the thesis, but the contact interface and the mortar itself.

### 3.2.2 Boundary Conditions

To create an appropriate model, boundary conditions must be implemented – with no boundary conditions, there would be nothing to stop the model from floating continuously in free space after the driving force is applied. The only force being applied to this specimen was downward on the center concrete masonry unit, so only a vertical restraining boundary condition would be necessary to oppose this driving force.

The way the model was preferred to be set up, only the middle concrete masonry unit would feel the force of the impact being applied and it was desired to continue pushing this concrete masonry unit while holding the outer concrete masonry units still and potentially failing in either the contact between mortar and concrete masonry unit or within the mortar itself. Therefore only the bottom nodes of the outer concrete masonry units were restrained by vertical movement only. This was done to allow the concrete masonry units to still flatten and potentially expand in the horizontal direction while also leaving room for the edges to rotate if the concrete masonry unit so desired. With this simple boundary condition, the behavior of the model would more closely resemble how the real world experiment would behave.

### 3.2.3 Contact Interfaces between Parts

Since the individual components were modeled as individual objects within the model, a contact card was used to characterize the relationship between the various parts. This was done with the tiebreak surface-to-surface option, which allowed the user to input values to describe this relationship such as friction values and both tensile and shear failure stress of the connection. It should also be noted that once the tiebreak fails, the contact "behaves as a surface-to-surface contact with no thickness offsets" (Livermore Software Technology Corporation 2015).

Therefore, once the limiting values for the shear or tensile failure stress were exceeded, the model would continue to run and "slip" along the surface according to the friction values specified.

For the tiebreak surface-to-surface contact, segment sets were created to include the surfaces of the elements that were desired to be implemented in the contact. These segment sets include not only the nodes but also the sides of the elements and is more of an area contact. Of these segment sets, one was assigned as the master segment set and the other as the slave segment set. During a simulation, LS-DYNA checks to see if penetration occurs from one side to the other in terms of slave side nodes versus master side nodes. The type of contact used will determine if only one side, the slave side, is observed or if both sides are observed. Using the tiebreak surface-to-surface contact, LS-DYNA used the nodes or segments specified in the master and slave sides for penetration into the other. It is standard practice to use the segment set with the finer mesh as the slave segment set, therefore the mortar side was assigned as the slave for each tiebreak. This is because there are fewer calculations required for the coarser side and a smaller chance that any type of penetration was missed. For this model, there were four tiebreak surface-to-surface contacts used, all with the same values for friction.

### 3.2.4 Material Model

There is a wide array of material models available within LS-DYNA that can be implemented for work to involve liquids, concrete, elastic materials, thermal materials, and even a random material with whatever assigned properties the user desires. For this model, the 072R3 Concrete Damage Release 3 concrete constitutive model was used. This is the third release of the KCC Concrete Model, a concrete model that is within LS-DYNA and commonly used as it is very user friendly, needing only the mass density ($\rho$) value, Poisson's ratio, and the compressive strength of the

concrete. The material model can then use the compressive strength provided to calculate any other material values it may need to run the analyses.

The KCC model is commonly used for structural response of concrete models within LS-DYNA. Work by Wu, Crawford, Lan, and Magallanes (2014) indicate that the parameters within this model greatly affect the results. One of these parameters is the strain rate enhancement. There is a built in strain rate enhancement function within the model that is utilized to effectively include the effects of strain rate. It was stated, however, that "the automatic generation feature does not apply to dynamic increase factor (DIF) in current LS-DYNA code. To activate the strain rate effect, the user needs to input a nonzero number under "LCRate" and define a load curve with LDIC = LCRate" (Wu, et al. 2014). There is a default strain rate enhancement that is based off of the work done by Wu, Crawford, Lan, and Magallanes which is calculated based off of the current strain rate, the reference strain rate, and unconfined compressive strength of the concrete, and the confined compressive strength of the concrete. Overall, Wu, Crawford, Lan, and Magallanes found that the KCC model worked well in accurately portraying the effects of blast load on concrete structures but heeded warning when considering the appropriate use for strain rate effects. Work accomplished by Schwer and Malvar (2005) also provided results to show that the "model provides an excellent material model for modeling the complex behavior of concrete when only the most minimal information about the concrete, i.e. its unconfined compression strength, is known."

Since the model created in LS-DYNA for this particular research is not based on any physical testing and mainly to look at the relative behavior of such a situation, these values, as well as all the values in this model, were chosen arbitrarily. The initial values were actually those taken from doing previous work with the modelers at the ERDC and Table 3-1 displays the values used for

both the concrete masonry units and the mortar. It is to be noted that for the units to be properly implemented into the model, the effects of gravity were included to convert to the necessary values and numbers.

**Table 3-1: Material Properties for Concrete Materials Used**

| Material | Concrete Masonry Units | Mortar |
|---|---|---|
| Mass Density, ρ ($lbs \cdot ms^2/in^4$) | 224 | 162 |
| Poisson's Ratio | 0.22 | 0.22 |
| Compressive Strength (psi) | 3000 | 2300 |

### 3.2.5 Loading of the Model

There were a two different loading cases that were desired to include in the model – first, the applied precompresion on the outer faces of the outer concrete masonry units and, second, the driving force for hitting the middle concrete masonry unit and creating the movement desired. It is to be noted that both pressure loadings were applied to the model through segment sets so that the pressure would be applied to the entire face of the concrete masonry unit sections as desired rather than only being applied to the nodes or the entire elements.

For the precompression loading, this was chosen to be implemented as this is more realistic with a real world situation of a structure built with concrete masonry units because of the self-weight of the wall as well as other confining factors as the wall is loading from high pressure loading. The actual value of this can vary depending on how high the wall is or where on this wall a specific concrete masonry unit is located. A value of 500 psi was arbitrarily chosen to be sufficient for the purposes of this model. The specific value of precompression was also used as a parametric value to be changed and behaviors observed later in the model. Figure 3-2 displays what the loading curve for the precompression looked like in the LS-DYNA model for the initial model:

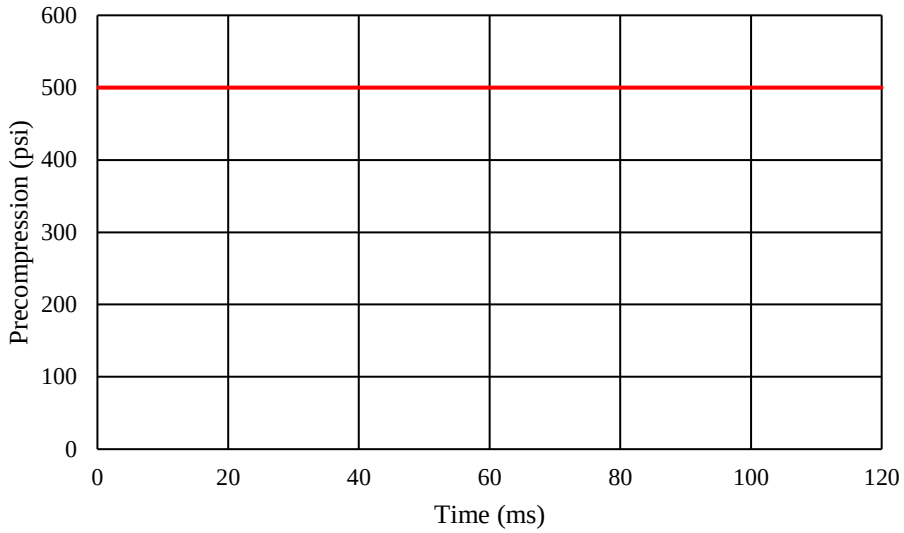


**Figure 3-2: Precompression Curve for Initial Model Setup**

The second loading curve to be used was for the applied pressure to the center block, which was the driving force behind this model. Since this work was first started by looking at walls subjected to blast loads, it was decided to use a similar type loading for this model. Therefore, a pressure time curve similar to what can be seen from a blast load was used. Figure 3-3 shows a typical pressure time curve for a blast load, including both the positive phase and the negative phase.

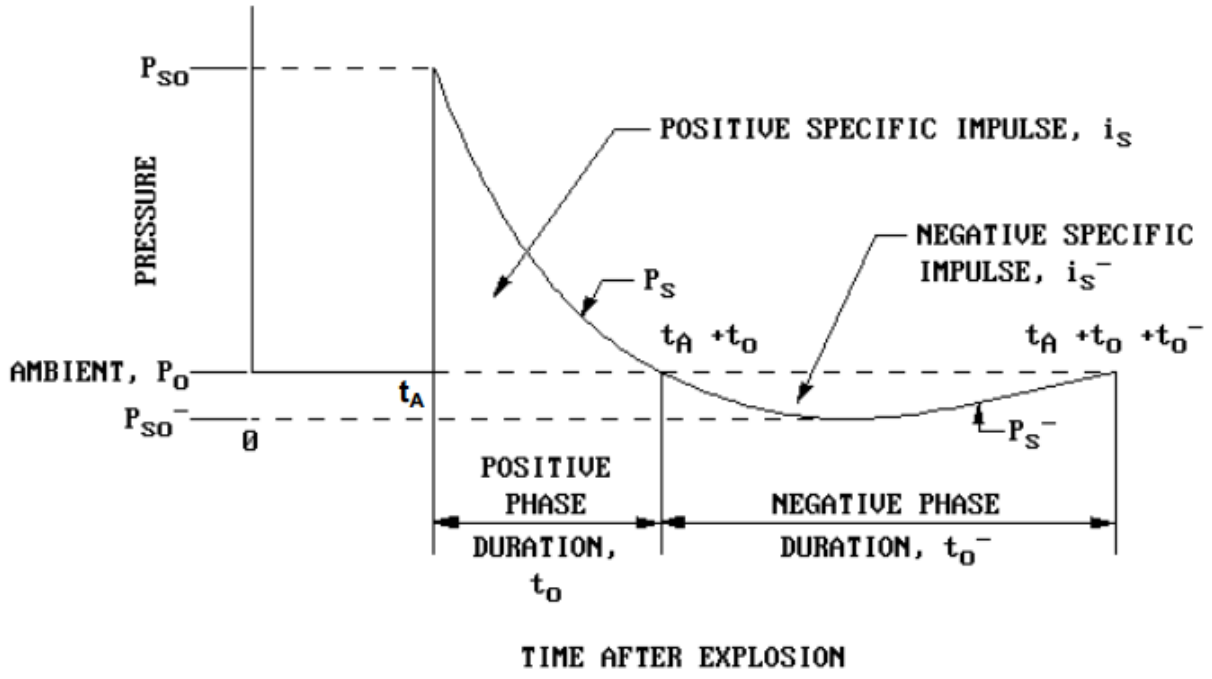


**Figure 3-3: Typical Pressure-Time Curve for Blast Load (U.S. Army Corps of Engineers 2008)**

The positive phase indicated in the figure above shows when the blast hits the structure, instantaneously increasing to the peak pressure point, then declining till it hits the negative phase, where the pressure is actually below the ambient pressure and a suction force is felt by the pressure wave. This figure is a generalization of a typical blast pressure curve as the actual pressure wave will not be as perfect of a curve because of the imperfect nature of the wave itself.

For the purposes of defining the pressure curve in the model, an even more simplified pressure-time curve was adopted. This curve was just simply a triangular pressure loading with no negative phase. There are options in LS-DYNA to include an actual blast wave by indicating the weight of the explosive as well as the location in respect to the structure desired to be analyzed. However, since this model is desired to be validated at a later time with physical testing which would not

include actual explosives, a simple pressure curve was utilized to be more realistic in what the experimental approach would be. Figure 3-4 shows the pressure curve that was used in the model in LS-DYNA.

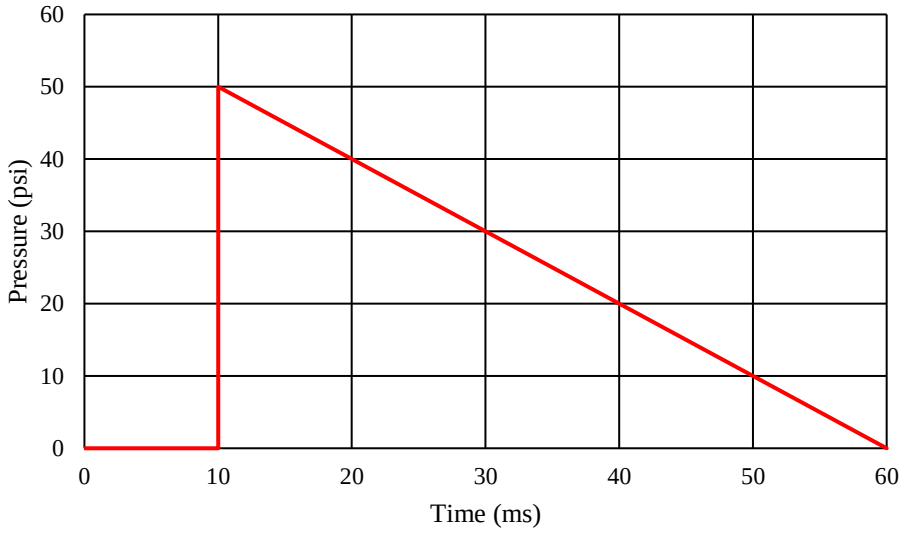


**Figure 3-4: Pressure-Time Curve for Loading of Model**

As stated, this is a very simplified form of a typical blast pressure curve. This was the main parameter that was changed with each test to see how the model changed with increased pressure. The duration, 50 milliseconds, stayed constant with each test while the pressure value was increased. The impulse of each test was able to easily be determined by calculating the area under this pressure-time curve. To start, the pressure was increased in intervals of 50 psi until either movement in the model parts or failure of the elements was noticed.

### 3.2.6 Additional Modeling Parameters Needed

After the model was created using all of the steps discussed above, the finer tunings of the model was completed by implementing other cards in the control and database sections of LS-DYNA. These cards include adjusting settings for items such as the energy through the system, the timestep

desired for output files, the output file types, and so much more. The following discusses the various cards used and how they were implemented.

Hourglass energy was included to be computed by LS-DYNA during the analysis process. Hourglassing is a common issue seen in finite element modeling where the elements tend to distort into hourglass shapes during the analysis, hence the term "hourglass" energy. This can lead to instability of the model and is a geometrical anomaly where nodal displacements can results in zero internal energy. If this happens, the program will not update the stress and strain states of the model or the internal energy. Sometimes, the distortions from hourglass effects can lead to degradation of the mesh and can even affect the overall results of the model if not handled adequately. Within LS-DYNA, there are various ways to counteract the effect of hourglassing, done through the hourglass cards with various algorithms available. For this particular model, hourglass energy was accomplished by Belytschko and Bindeman (1993) method which assumes a co-rotational stiffness. Essentially, the energy of hourglassing associated with the model to keep the elements from being improperly distorted needs to be minimized. A way to check the model is to verify that the hourglass energy is low compared to the internal energy of the model.

There were a few cards used for inputting the various timesteps used in LS-DYNA. There is a timestep within LS-DYNA that is used in the analysis process and can either be input by the user or can be determined as best seen by LS-DYNA. The default options within this card were used. There are also timesteps that can be specified for the timestep between the desired output files. The d3plot output file was desired, as this outputs the database for the entire model. The content included in these files can be adjusted with the extent binary card and was adjusted to include plastic and thermal strain within the model as well as the stress values at all integration points within the model. The timestep first chosen for these output files was first chosen as 1 millisecond

but could easily be adjusted later on if it was seen that a smaller timestep was necessary. A card was also used to include the material energies and global data of the model. These timesteps were also set at 1 millisecond for the initial model setup.

## 3.3 Final Design

After running many jobs using the initial model setup described above, adjustments were made to the model to make a more efficient and realistic model. Appendix A shows an example of the specific parameters and cards that were used, not including the node positions and numbering that was included in the input file. The following sections include specifics about what was changed in the model to get to the final desired result.

### 3.3.1 Adding Steel Bases

Once the first sets of analyses were completed for the model, it was determined that the best way to get results from this model was to obtain the reaction forces at the bottom of the outer concrete masonry units and compare these values to what was obtained as higher pressure forces were applied. To first accomplish this, steel bases were added under the outer two concrete masonry units as supports. These parts were given typical steel properties and the boundary conditions were adjusted to not allow the nodes of the blocks to move. The concrete masonry units themselves were still allowed to move and to flatten against these steel bases.

A new interface was needed for the connection between the concrete masonry units and the steel bases. For this, a general automatic surface-to-surface interface was implemented. Similar characteristics for the interface connection between the concrete masonry units and the mortar was used here but shear and tensile strengths of the connection were not defined. Figure 3-5 shows the new geometry of the model that was used for the final design.

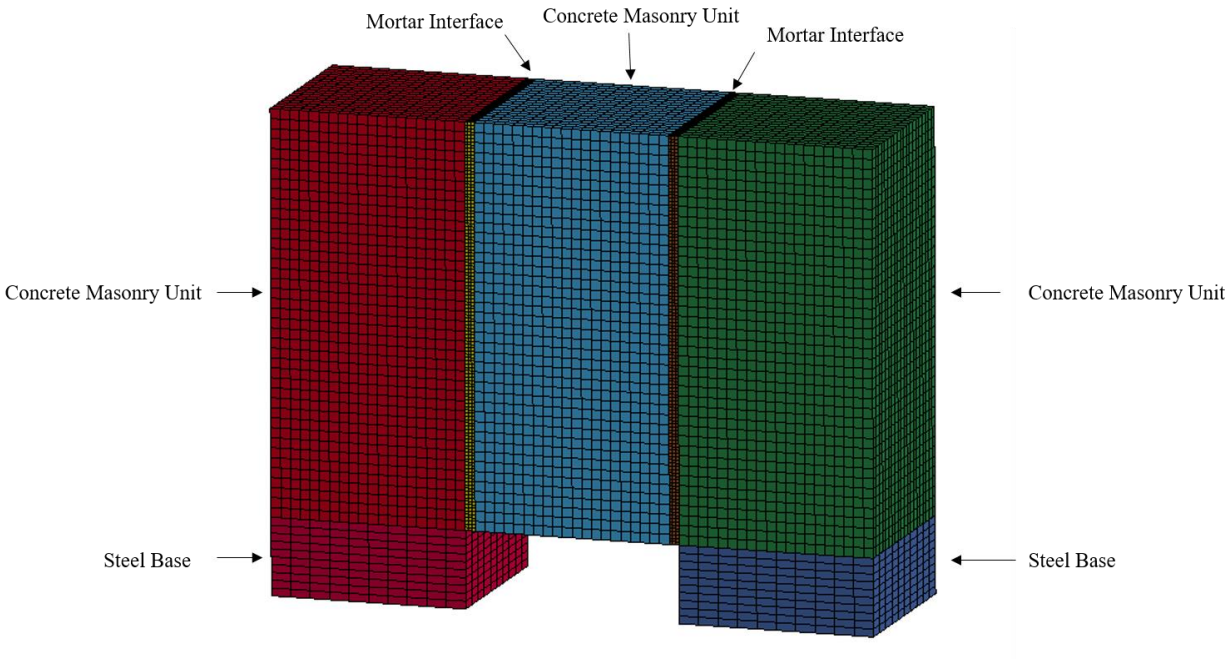


**Figure 3-5: Meshing and Geometry of Final Model Setup**

### 3.3.2 New Output Files

To obtain the reaction forces, another output file was needed to look at the interfaces and therefore obtain the information happening at these locations. The intfor file type was used and when displayed, this file type show only the interfaces that were created in the input file and post-processing can be accomplished on these interfaces. It was here that interface normal forces could be acquired which resulted in the maximum reaction forces in the model.

### 3.3.3 Erosion

Based on some of the results from previous runs, erosion was decided to be implemented. Erosion can be beneficial to include in models, as it can make the results seem more realistic, but it can also construe the results if not implemented in a proper way. Analyzing the initial runs led to some unusual behavior of the elements themselves, which seemed to be deforming too much in a manner that would not be possible of concrete masonry units. Concrete masonry units are brittle materials

and are not expected to expand or stretch as much as what was being seen in the model, and so erosion was decided to be used. Once erosion was implemented, the model seemed to behave more like what would be expected when concrete materials are tested, the elements would crumble and disconnect as would be expected of a brittle material like concrete.

### 3.3.4 Precompression Curve

It was noticed that the precompression curve was acting more dynamically than statically as desired. Some changes in the precompression curve in the initial model runs drastically changed the results that were seen. It was desired to have a more gradual increase to the desired precompression level rather than hitting it with the full pressure at one instant, hoping to take out the dynamic factor of such a load. After some adjustments in the precompression curve, Figure 3-6 shows the curve was deemed most appropriate to use without having too much of an influence on the results themselves.

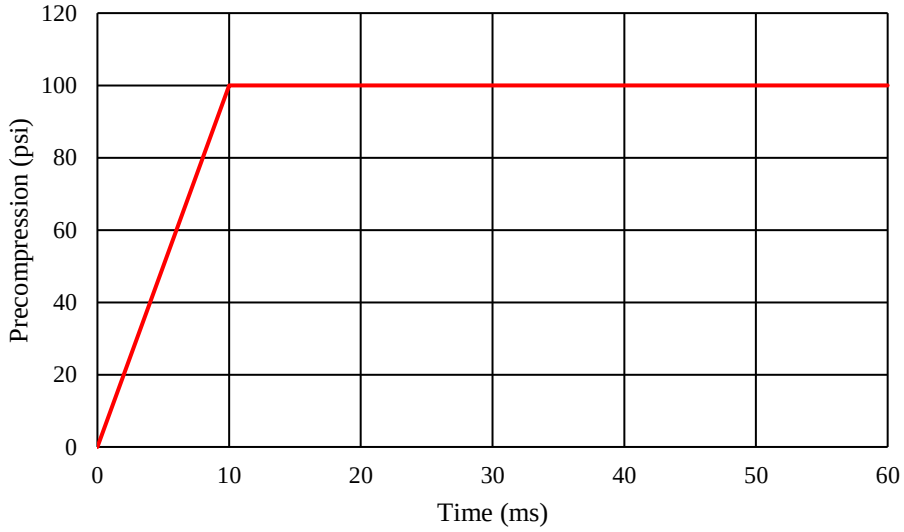


**Figure 3-6: Final Precompression Curve**

### 3.3.5 Timestep Adjustment

Each analysis resulted in a large number of very large files, which resulted in a very tedious post-processing routine. The files needed to be transferred from Hopper to a local hard drive in order to properly be analyzed in the post-processing portion of LS-DYNA. With the number of jobs that were desired to be processed though, this took a very long time and was too inefficient with the timestep for the output files that was originally chosen. When the timestep was increased to a larger interval, it was observed that the maximum values were being skipped over due to the large timestep size. But with too little of a timestep, the number of files greatly increased and, therefore, so did the transfer time.

There is a curve option in LS-DYNA to adjust the timestep value as a function of time. It was observed in all of the previous runs that the maximum value always occurred within 10 milliseconds to 15 milliseconds, right after the peak pressure of the pressure curve was applied. Therefore, a timestep curve was included to decrease to a smaller timestep size between 9 milliseconds, right before the peak pressure hit the middle concrete masonry unit, to 20 milliseconds to ensure that the peak reaction had time to be recorded. A timestep of 0.1 milliseconds was chosen during this interval with a value of 0.5 for the remainder of the analysis. This change drastically decreased the number of files needing to be transferred and greatly helped with the transfer times to make for a more efficient post-processing process. Figure 3-7 displays the timestep curve used in the model.

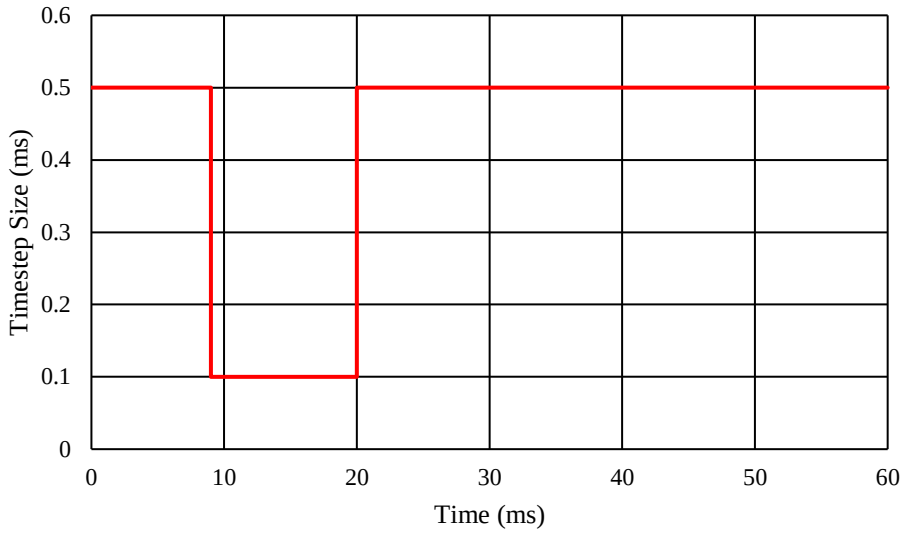


**Figure 3-7: Timestep Curve for Output Files**

## 3.4 Model Verification

Since there was no physical testing data to use to validate this model, certain aspects within the model were checked to verify that the mechanics of the model were happening appropriately. One of these checks was ensuring that the kinetic energy of the model was being dissipated appropriately. If the energy was dissipated too quickly or not at all, it indicated that the model was not handling the energy transfer through the system as one would see of actual testing. Figure 3-8 shows the plot of kinetic energy that was produced for the first test run.

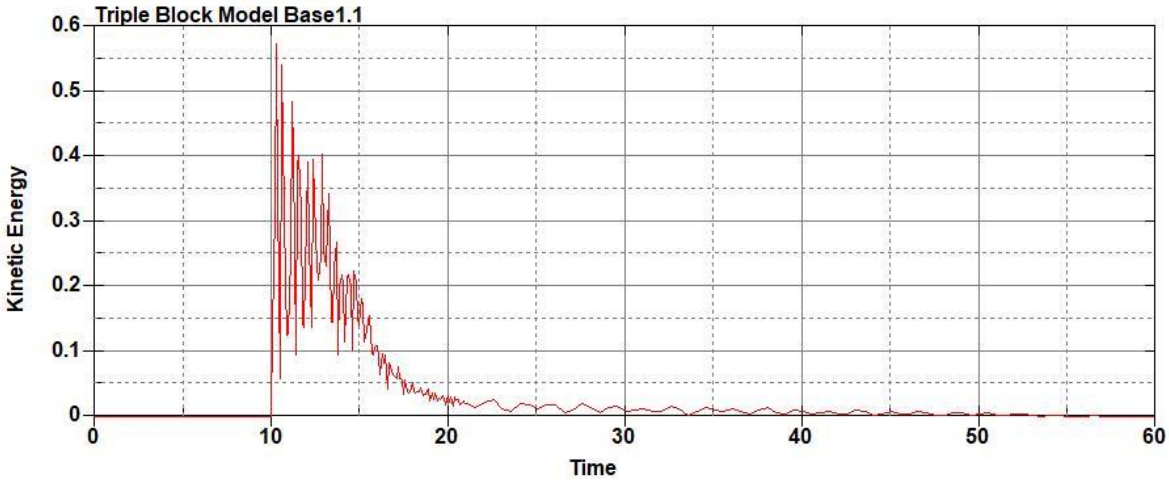


**Figure 3-8: Kinetic Energy of First Base Run 1.1 (lbf·in, ms)**

From Figure 3-8, the kinetic energy follows along with a typical pressure curve for the type of loading being applied to the model. It does not dissipate too quickly and eventually flattens out to right at the zero mark. The total energy of the system, along with the kinetic energy figure above, was also looked at in terms of checking the damping of the system. If damping was required, the input card for damping could be implemented. Damping may not be necessary though as dissipation of energy could be addressed through the hourglass energy or even the friction forces within the tiebreak cards. If damping was deemed necessary to add to the model, it could be done so with the dampening card. Figure 3-9 shows the total energy of the first run.

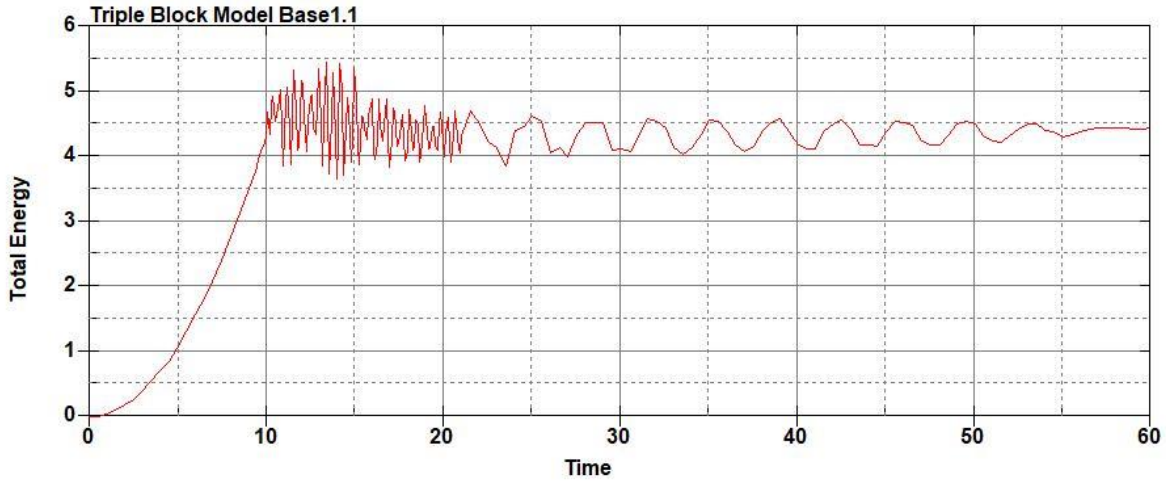


**Figure 3-9: Total Energy of First Base Run 1.1 (lbf·in, ms)**

From both the kinetic energy and the total energy, damping does not seem to be a problem and the system also does not look overdamped. Therefore, it was decided to not include additional damping effects on the model.

It was also desired to look at the hourglass energy plot associated with the run and ensure that the energy produced from hourglassing did not drive the model. It is a typical rule of thumb for the hourglass energy to be ten percent or less of the overall energy in the system. To check if the hourglass energy was appropriate for this model, Figure 3-10 was analyzed.

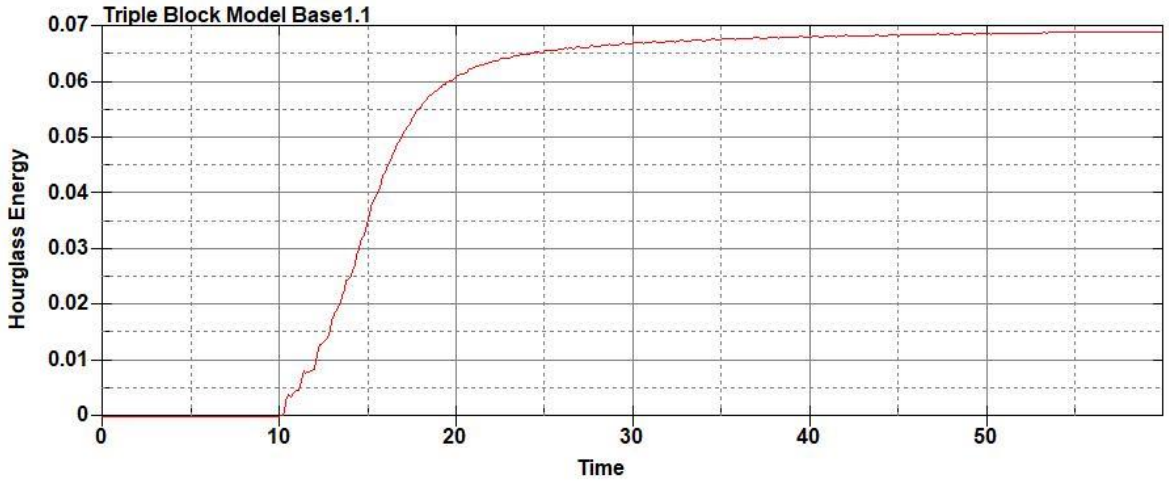


**Figure 3-10: Hourglass Energy of First Base Run 1.1 (lbf·in, ms)**

When comparing the hourglass energy plot to the total energy plot above, it can be seen that the maximum hourglass energy was less than ten percent of the total energy plots. Based on this comparison, it was determined that the hourglass energy parameters used did not drive the results of the model. Therefore, the model was deemed appropriate continue to be used for this research.

### 3.5 Parameters Desired to be Included

Once the final model was ready to be used, various tests were run to include the parametric changes desired to look at the behavioral differences. The material model itself was not chosen to be one of the changed parameters as the material model chosen is one typically used by modelers to include all concrete materials. However, there is a parameter within the model to either include or not include strain rate effects. The user can define the desired strain rate curve or a default curve, as discussed above and based on equations by Wu, Crawford, Lan, and Maganelles 2014, can be implemented. Since one of the main goals of this work is to determine the effects of strain rate on the bond between the concrete masonry unit and mortar, this was desired to be one of the parameters to be changed.

Another parameter that was decided to be adjusted throughout this research was the shear and tensile strength limits of the tiebreak surface-to-surface connection between the concrete masonry units and the mortar. The initial values for both strengths were taken from the work previously done with the modelers at the ERDC but these values were based off of material property tests that were done statically, not dynamically. So it was desired to increase these values and see how this increase would affect the overall results. It was believed that there would be an expected increase in these values once testing dynamically, following along with the typical behavior of concrete tested dynamically with a dynamic increase factor. Since physical testing has not yet been completed for such a test, this theory cannot yet be proved.

The next parameter desired to be adjusted was the number of elements though the thickness of the mortar. As discussed earlier, a minimum of three elements has been recommended to properly portray what happens within the object at hand. It was desired to see what would happen with increasing the element size and therefore decreasing the number of elements through the thickness of the object.

The precompression value and time increment to reach the maximum precompression value were also desired to be further analyzed. This came about because of the results acquired from tests in the initial phase of testing that were applying the precompression at too quick of a time increment versus ones that were lengthened.

With the desired number of parametric changes, a total of sixteen different series were desired to be run. The “LCRATE Value” column indicates either including or not including the strain rate effects in the material model, with a 0 indicating no effects included and a -1 indicating the effects are included with the default implemented in LS-DYNA. The “Shear/Tensile Strength” column shows the values used for each of these strengths included in the interface parameters. These

numbers can be input in separately and can therefore be different, and they most likely will be in physical testing, but both were changed and increased in this study. The next column represents the slope of the incline for the precompression curve. The first number indicates the change in precompression and the second indicates how long this change took before hitting the maximum value, which was then held constant for the remainder of the test. The last column is labeled "Number of Elements" and indicate which series was run to investigate the effects of element size as well as number of elements through the thickness. The various runs chosen for this study and the values used can be described in Table 3-2.

**Table 3-2: Parametric Values Used in Analysis**

| Series Name | LCRATE Value | Shear/Tensile Strength (psi) | Precompression Pressure (psi per ms) | Number of Elements |
|---|---|---|---|---|
| Base1 | 0 | 400 | 100/10 | 3 |
| Base2 | -1 | 400 | 100/10 | 3 |
| Base3 | 0 | 1000 | 100/10 | 3 |
| Base4 | -1 | 1000 | 100/10 | 3 |
| Base5 | 0 | 1500 | 100/10 | 3 |
| Base6 | -1 | 1500 | 100/10 | 3 |
| Base7 | 0 | 400 | 100/10 | 1 |
| Base8 | -1 | 400 | 100/10 | 1 |
| Base9 | 0 | 1000 | 250/10 | 3 |
| Base10 | 0 | 1000 | 500/10 | 3 |
| Base11 | 0 | 1500 | 500/10 | 3 |
| Base12 | 0 | 100000 | 500/10 | 3 |
| Base13 | -1 | 100000 | 500/10 | 3 |
| Model1 | 0 | 400 | 500/2 | 3 |
| Model7 | 0 | 400 | 500/10 | 3 |
| Model8 | 0 | 400 | 0/0 | 3 |

# Chapter 4: Results and Discussion

## 4.1 Results from Individual Tests

For each series listed above, tests were run and analyzed until failure, or breakage, was first indicated in the model itself. Failure was indicated by one of two occurrences – the first being failure of the bond, in which the model would slip along the interface connections between the mortar and the concrete masonry units, and the second being failure of the elements themselves, in which the elements would become so stressed that they would fail. In the cases where the failure was driven by the bond, the series was continued till there was obvious movement and therefore failure of the bond. The breaking pressure values varied depending on the parameters that were changed and will be seen in the below results. For each individual test, there were a number of results that were gathered to be used in the overall comparison. The first of these results was obtaining the reaction force found at the base of each of the outer concrete masonry units. This was accomplished using the intfor output files and using the analysis tools available within LS-DYNA to plot the y-interface force for the desired part. Figure 4-1 shows such a plot for the right support from the first test that was run.

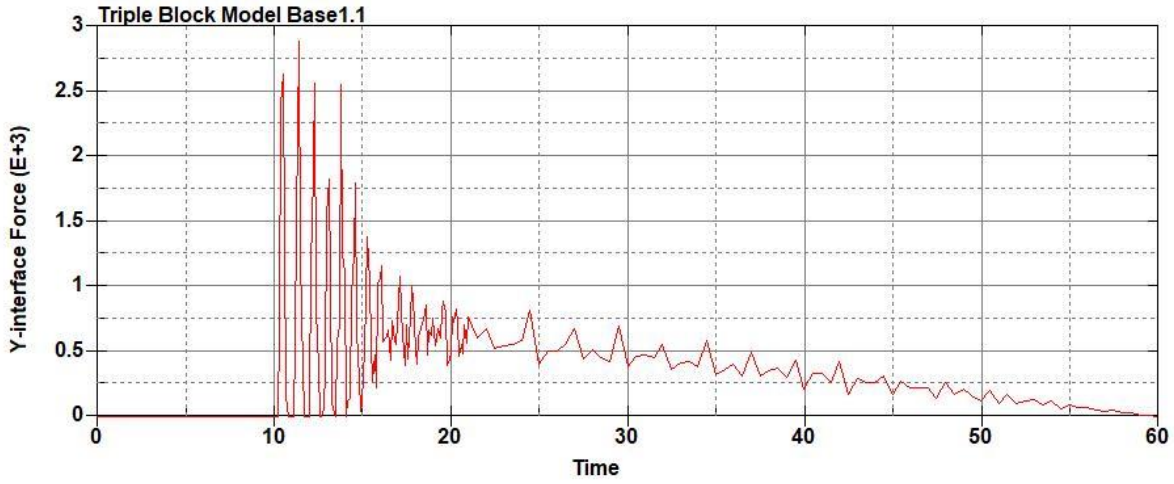


**Figure 4-1: Y-Interface Force (lbs) versus Time (ms) Plot from LS-DYNA for Right Support for First Base Run 1.1 – 50 psi**

From the above figure, the data points were able to be exported into excel and maximum force values were found for each case. These maximum values were then used in the overall comparison from one run to the other. For each run, two plots like the one shown above were obtained – one for the right support and one for the left support. The values were kept separated throughout the post-processing process to also observe whether or not the analysis was symmetrical from the applied load.

Another figure that was obtained from the results of each run was observing how the model behaved throughout the time that the load was applied. This was done using the figure from the d3plot files, which showed the overall model itself through this process and shows how the model behaved as a whole as well as at the elemental level. Figures were obtained at the end of each run time, 60 milliseconds for each run, to see if there was any physical damage or breaking. This was done with two separate figures – the first which was the model itself and the second was a fringe

plot with the effective plastic strain contours present. Figure 4-2 shows the first of these figures for the first run of the first series.

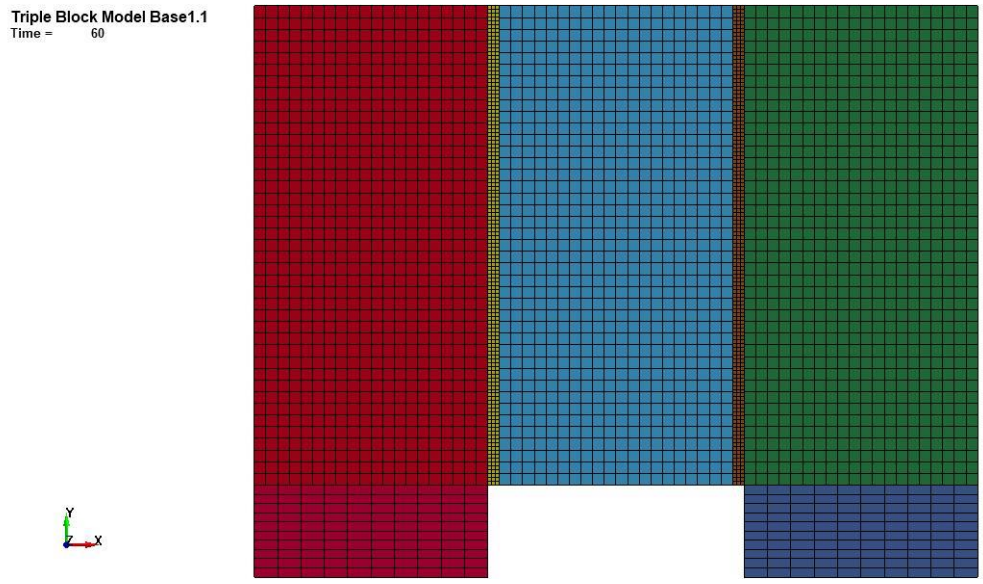


**Figure 4-2: Last State at 60 Milliseconds for First Base Run 1.1 – 50 psi**

The effective plastic strain fringe plot ranges from a blue color, where there is no damage, to a red color, which corresponds to a value of 2.0 or failure of the element. With this figure, the failure pattern of the model was able to be seen as the pressure propagated through the model itself as well as how the increase in applied pressure changed from the previous runs. Figure 4-3 shows the effective plastic strain fringe plot for a run later on in the first series which first started to show failure propagating through the model.

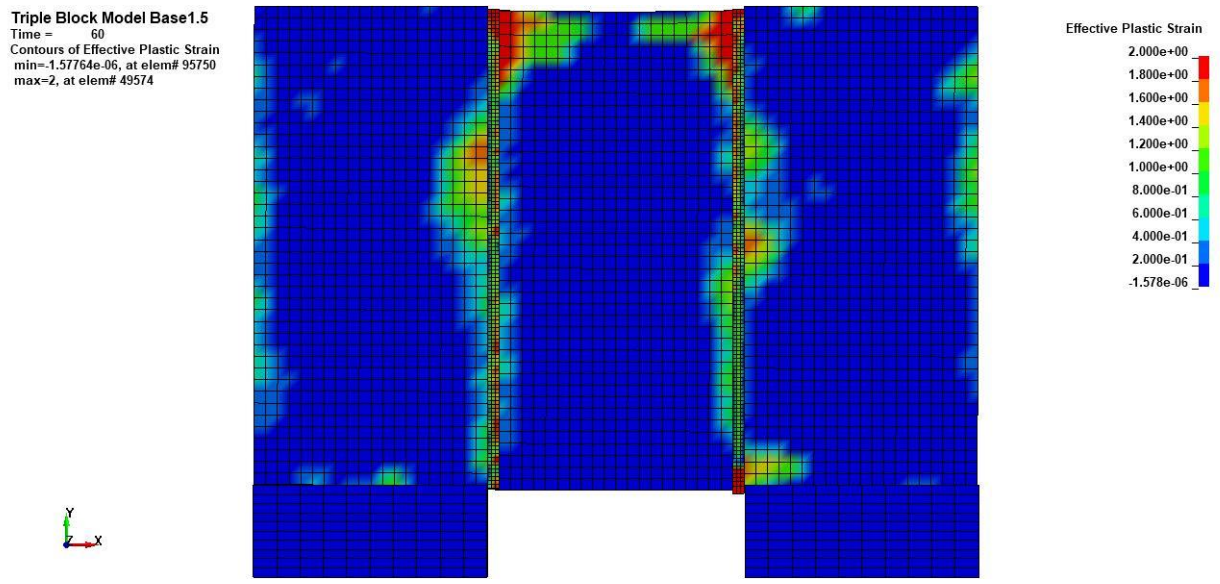


**Figure 4-3: Effective Plastic Strain Fringe Plot for Last State at 60 Milliseconds for Fifth Base Run 1.5 – 250 psi**

Using both of these figures, the behavior of the model was visualized and it was simpler to determine how high the pressure should be increased till breakage occurred within the specimen. For later cases where failure was observed, movement and distortion of the elements was observed from the first figure while the second figure showed which elements had either failed or were very close to failure, helping to indicate what the failure pattern would be for the model. While the above figures were just those from two separate runs, Appendix B shows the figures from all runs that were analyzed for this work.

For each test series, the overall behavior of the model was the same for each series. As the pressure wave propagated through the model, the effective plastic strain would first show no signs of failure anywhere within the model. As the applied pressure increased, element failure would slowly start to occur at the bottom of the mortar joints. The failure would slowly start to increase upward in the joint as the applied pressure continued to increase till failure of the tiebreak occurred. It was

when this failure happened that the test series was completed and results were able to be compared between series.

### 4.2 Comparison of Results

Once the results of each of the runs was analyzed, comparisons between the various base run series were able to be made. Using these comparisons, it would become apparent whether or not changing the various parameters within LS-DYNA would produce differing results. Plots were made using the maximum load values that were obtained in the above section and plotting these loads versus the applied pressure for each specific test. Figure 4-4 shows how such a plot looks for the first series in this work.

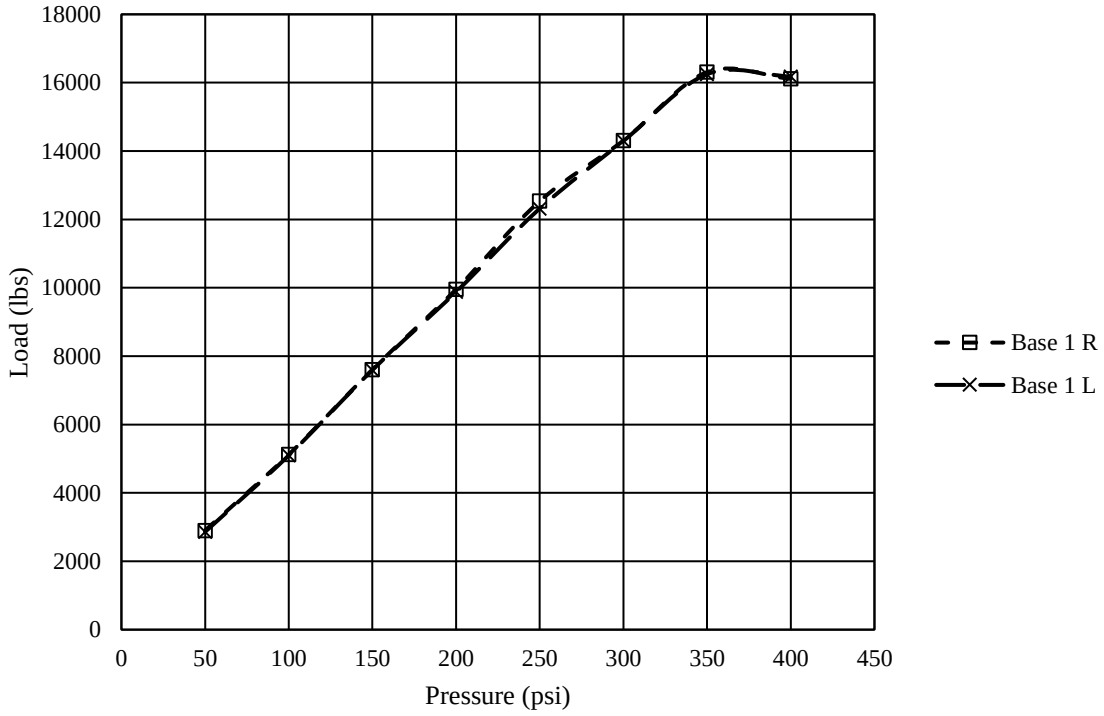


**Figure 4-4: Maximum Loads (lbs) versus Applied Pressure (psi) for the First Base Series**

Once the above plot was acquired for all test series desired, comparisons were able to be made. There were numerous comparison plots created in an attempt to not only understand what these parameter changes do within the program, but to also provide an indication to future modelers to better understand how certain parametric changes can affect the results of the model. The different types of parametric changes that were analyzed include strain rate effects, precompression values, tiebreak values, element size, and precompression timing. Each of these will be displayed in the sections below.

### 4.2.1 Parametric Change – Strain Rate Effects

For this section, all comparisons were made between test series that had the same tiebreak values, precompression values, and element sizes. The first plot below shows the comparison between Base Series 1 and Base Series 2. For this plot, the only difference between the two is that one series is run without the strain rate effects included in the material model (Base Series 1) while the other included the default strain rate effects in LS-DYNA (Base Series 2). Figure 4-5 can be seen below.

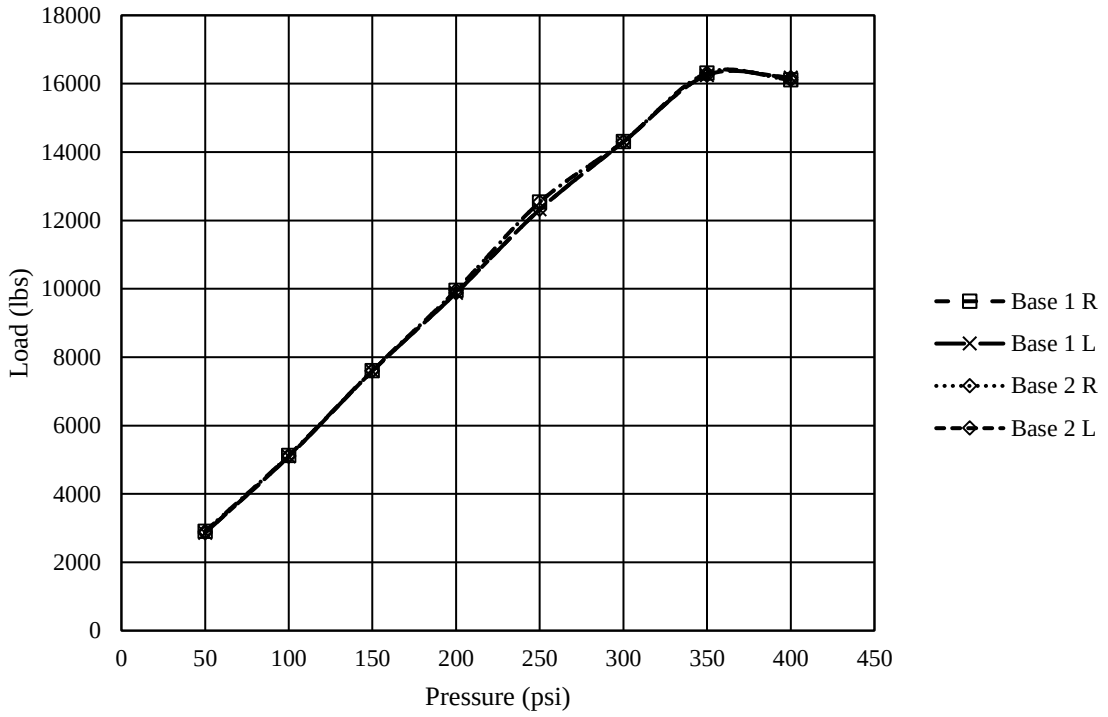


**Figure 4-5: Maximum Load (lbs) versus Pressure (psi) Comparison for Base Series 1 and Base Series 2**

From the above plot, there was no difference in the results between Base Series 1 and Base Series 2. Both test series indicated some initial slippage around the 250 psi test, but incremental increase in pressure was continued until obvious failure was noted. It was also at this point that the elements themselves were first initially very stressed from the applied pressure. Around the 350 psi test, the model showed drastic failure where a complete failure of the bond was observed as well as failure and breakage of some of the mortar elements.

Figure 4-6, Figure 4-7, Figure 4-8, and Figure 4-9 show the other comparisons that were made with the only difference between series was including the strain rate effects or not including these effects. The comparison is made between Base Series 3 and Base Series 4, Base Series 5 and Base Series 6, Base Series 7 and Base Series 8, then Base Series 12 and Base Series 13.

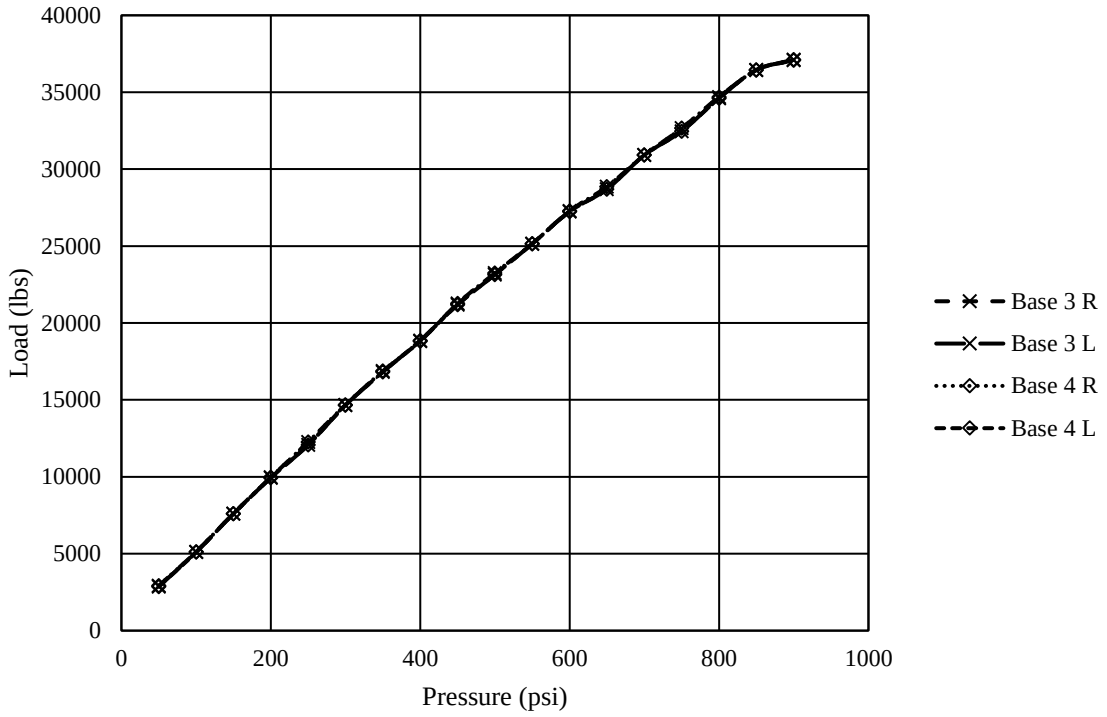


**Figure 4-6: Maximum Load (lbs) versus Pressure (psi) Comparison for Base Series 3 and Base Series 4**

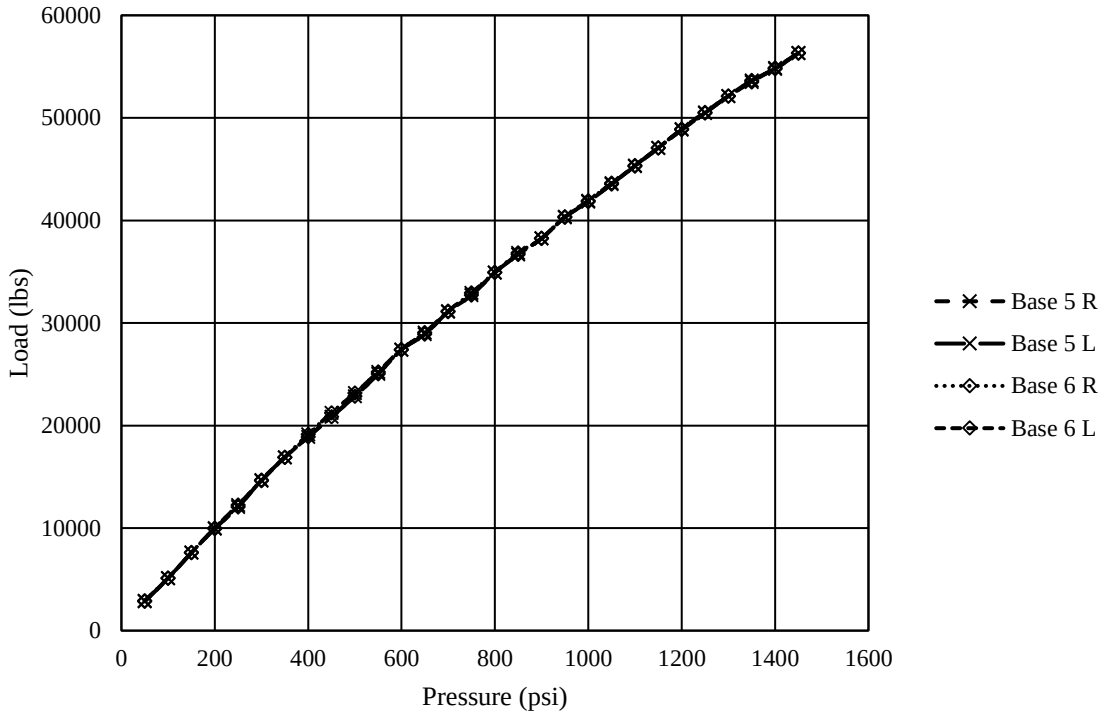


**Figure 4-7: Maximum Load (lbs) versus Pressure (psi) Comparison for Base Series 5 and Base Series 6**

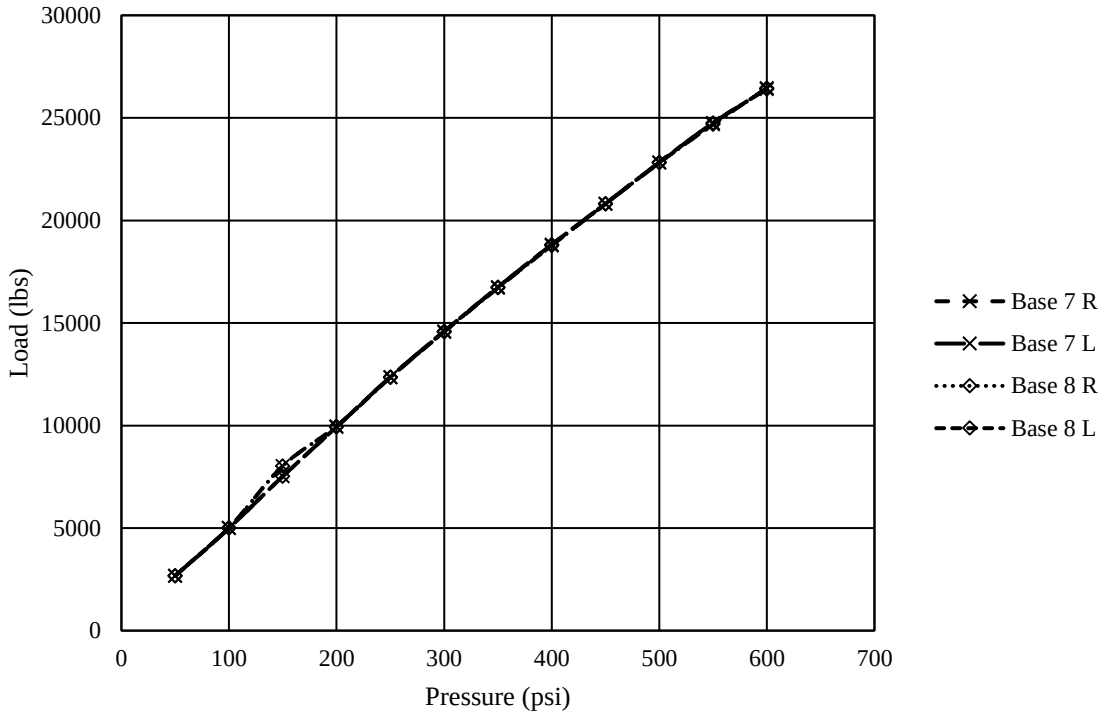


**Figure 4-8: Maximum Load (lbs) versus Pressure (psi) Comparison for Base Series7 and Base Series 8**

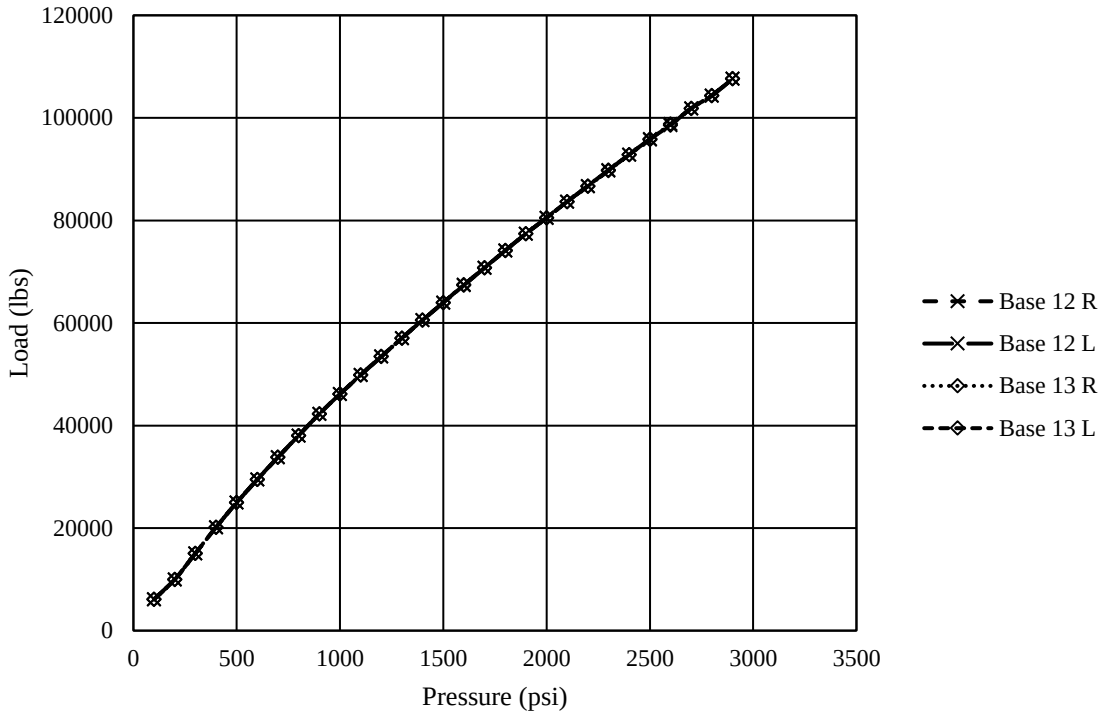


**Figure 4-9: Maximum Load (lbs) versus Pressure (psi) Comparison for Base Series 12 and Base Series 13**

Each of the above comparisons show the same behavior as the comparison between Base Series 1 and Base Series 2 in regards to the fact that there is no difference between results when strain rate effects are included and when they are not included. Also, each test series showed the same behavior of the overall model in regards to when slipping was first noticed and at what pressure value initiated failure of the model.

### 4.2.2 Parametric Change – Precompression Values

For this section, strain rate effects, element size, and tiebreak values were all held constant between comparisons. The only change was in the final and constant precompression value that was applied to the sides of the outer concrete masonry units. There were two comparisons that were made for this parametric change – one for Base Series 5 and Base Series 11 and the other for a comparison

between Base Series 3, Base Series 9, and Base Series 10. Figure 4-10 and Figure 4-11 can be seen below.

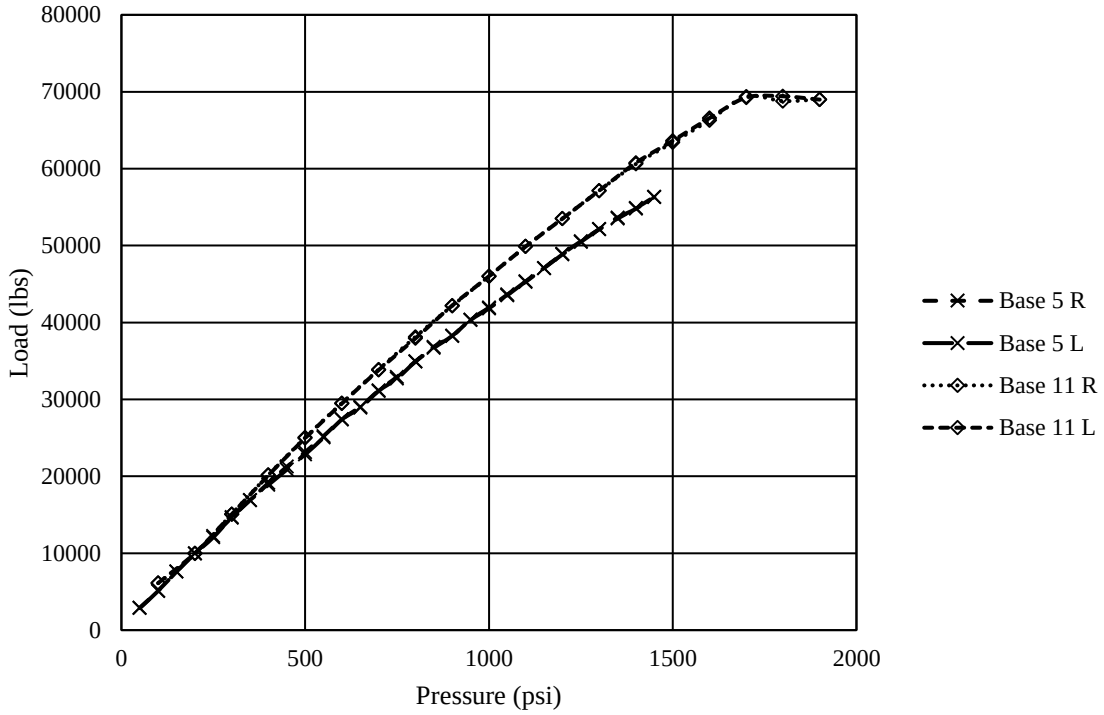


**Figure 4-10: Maximum Load (lbs) versus Pressure (psi) Comparison for Base Series 5 and Base Series 11**

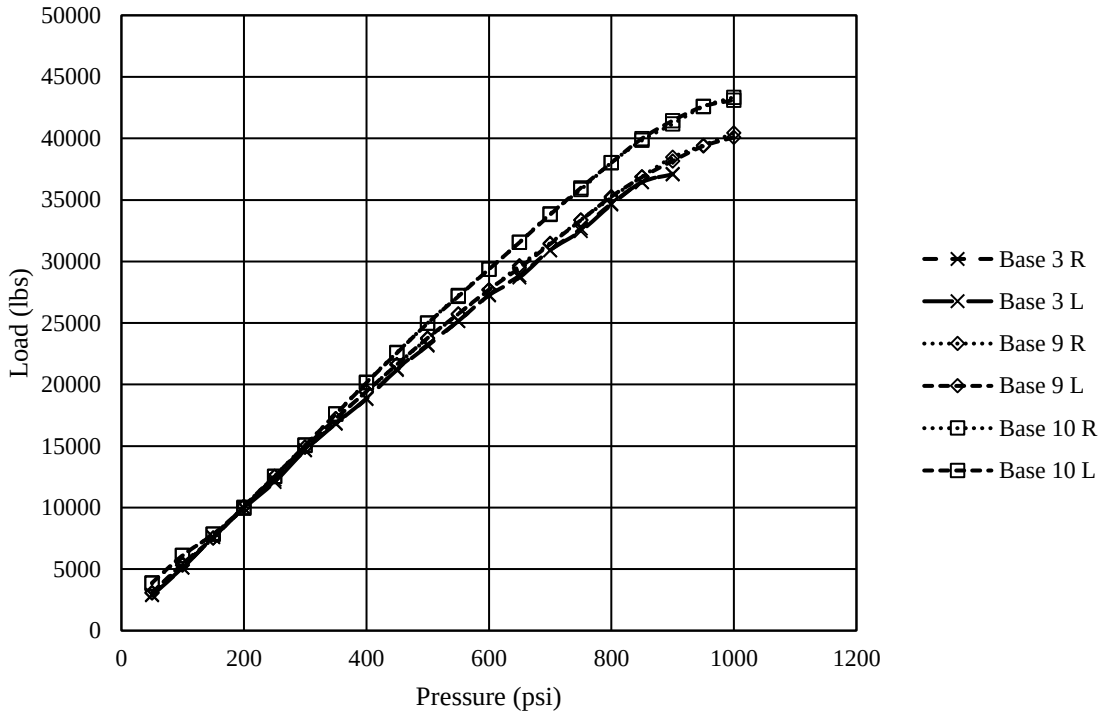


**Figure 4-11: Maximum Load (lbs) versus Pressure (psi) Comparison for Base Series 3, Base Series 9, and Base Series 13**

For both comparisons, the maximum loads were the same for all series being analyzed and started on the same initial slope. Eventually, as the elements began to become more stressed with the increased applied pressure, the test series with the larger final precompression values showed larger reaction forces than the test series with the lower precompression values.

During the initial modeling portion of this research, it was also desired to display what would happen to the results of the model if no precompression was implemented at the sides of the outer concrete masonry units. Since this was done in the earlier stages of modeling, this comparison will be shown using Model Series 7 and Model Series 8, which were intermediate test series between initial modeling and the final model. For both of these test series, the strain rate effects, tiebreak values, and element size was held constant. The only different between the two was that

Model Series 7 had precompression applied whereas Model Series 8 had no precompression. Figure 4-12 can be seen below.

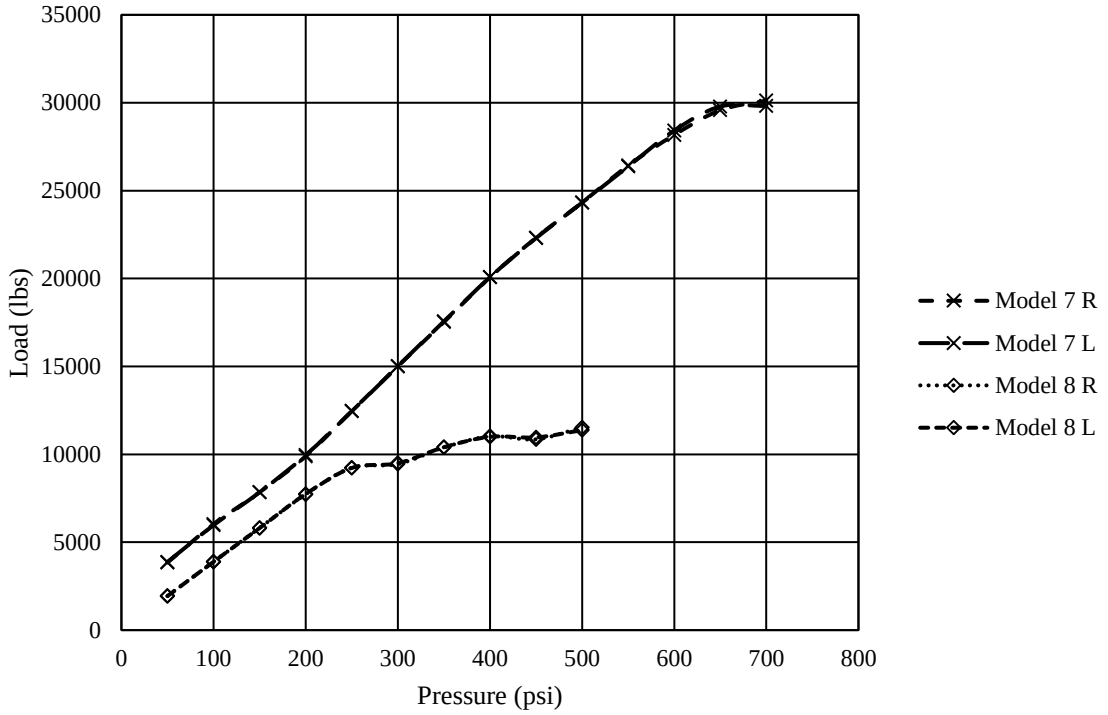


**Figure 4-12: Maximum Load (lbs) versus Pressure (psi) Comparison for Model Series 7 and Model Series 8**

Although not at the same values, both series started off at the same slope. As failure started to initiate in the elements and the overall model, the model with no precompression quickly started to show failure and trail off from the nearly linear increase in the curve. It should be noted that this case is not likely to ever occur due to the fact that there will always be some precompression on the outer edges of the concrete masonry units from self-weight of the wall or structure alone. This comparison was performed to validate that the precompression being applied was not construing and controlling the results of the models too much.

### 4.2.3 Parametric Change – Tiebreak Values

For this section, strain rate effects, element size, and precompression value were all held constant between comparisons. Two different comparisons were made between three test series each – the first between Base Series 1, Base Series 3, and Base Series 5 while the second was between Base Series 2, Base Series 4, and Base Series 6. Figure 4-13 and Figure 4-14 show these comparisons.

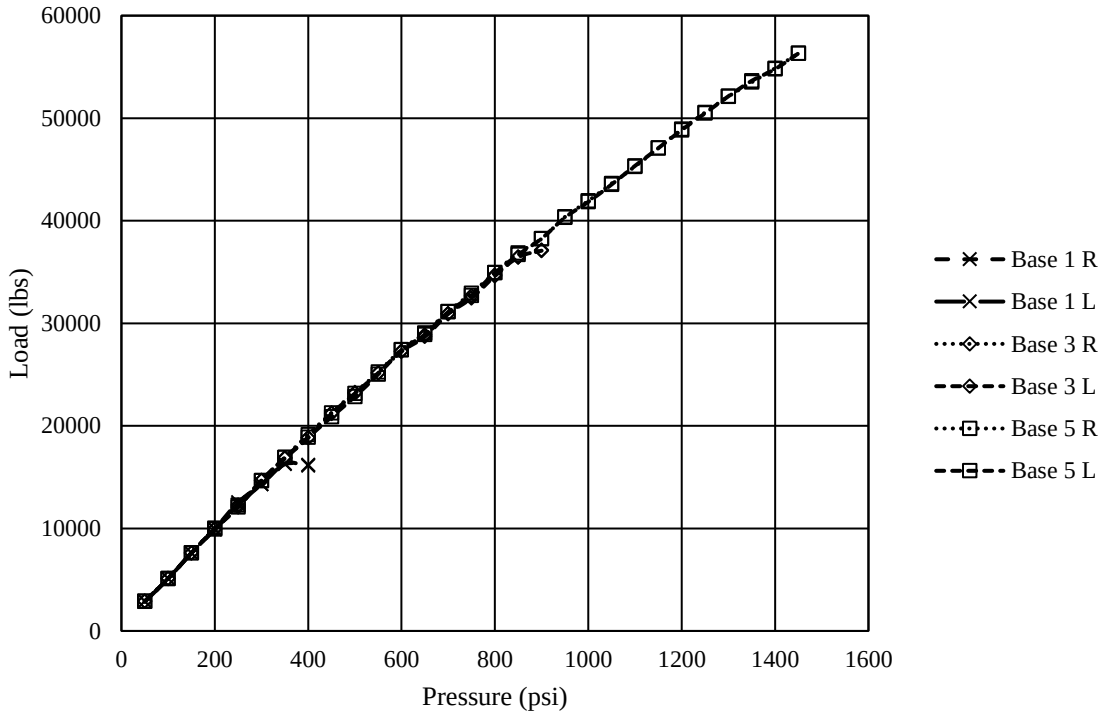


**Figure 4-13: Maximum Load (lbs) versus Pressure (psi) Comparison for Base Series 1, Base Series 3, and Base Series 5**

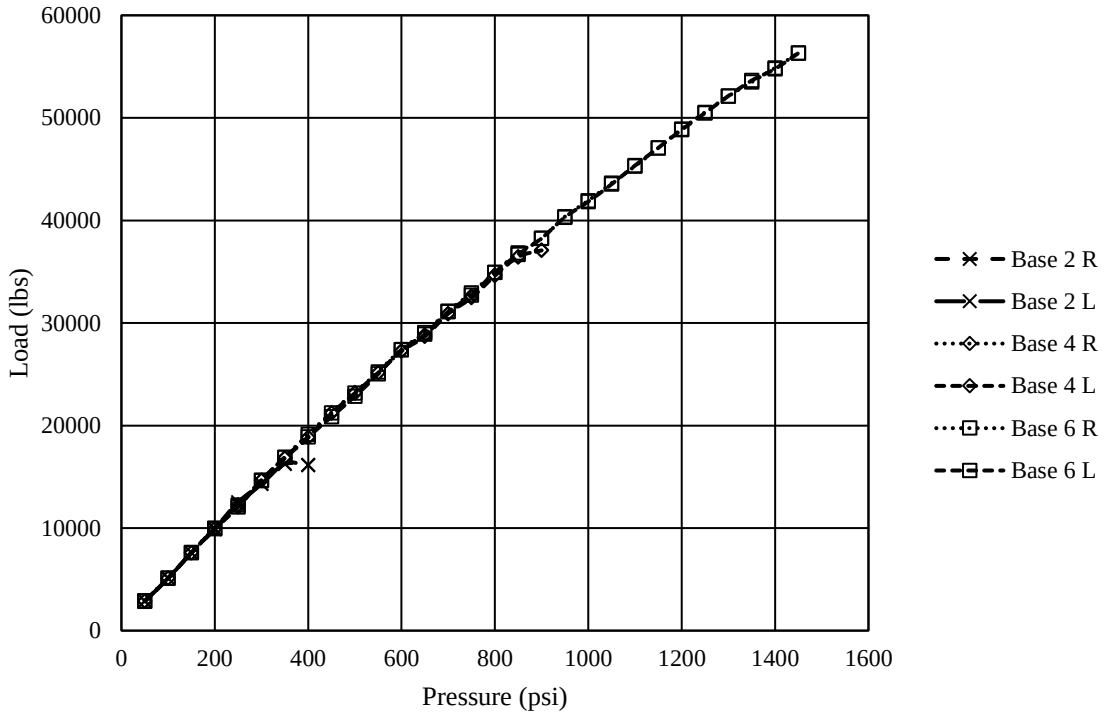


**Figure 4-14: Maximum Load (lbs) versus Pressure (psi) Comparison for Base Series 2, Base Series 4, and Base Series 6**

In both comparisons, all tests follow along the same slope and show the same behavior in each of the first few tests. It is not until the pressure is increased that changes are seen between tests with the same applied pressure. For the lower tiebreak values, failure of the model is observed at a pressure value of 350 psi. As the tiebreak values increase, failure is not seen until higher values of pressure are applied. For the highest tiebreak value, it is not until a pressure of 1400 that failure is seen in the model.

### 4.2.4 Parametric Change – Element Size

For this section, the precompression value, tiebreak value, and strain rate were all held constant. It is known from typical rule of thumb in finite element modeling that it is good practice to include at least three elements through the thickness of any object being modeled within LS-DYNA.

However, it is also known that there have been numerous ways that mortar has been modeled in the past, once of which is a single element thickness for the mortar. Therefore, it was desired to include a comparison between a single element mortar thickness and a three element mortar thickness. This is done so between Base Series 1 and Base Series 7, as well as between Base Series 2 and Base Series 8, both of which are shown in Figure 4-15 and Figure 4-16.

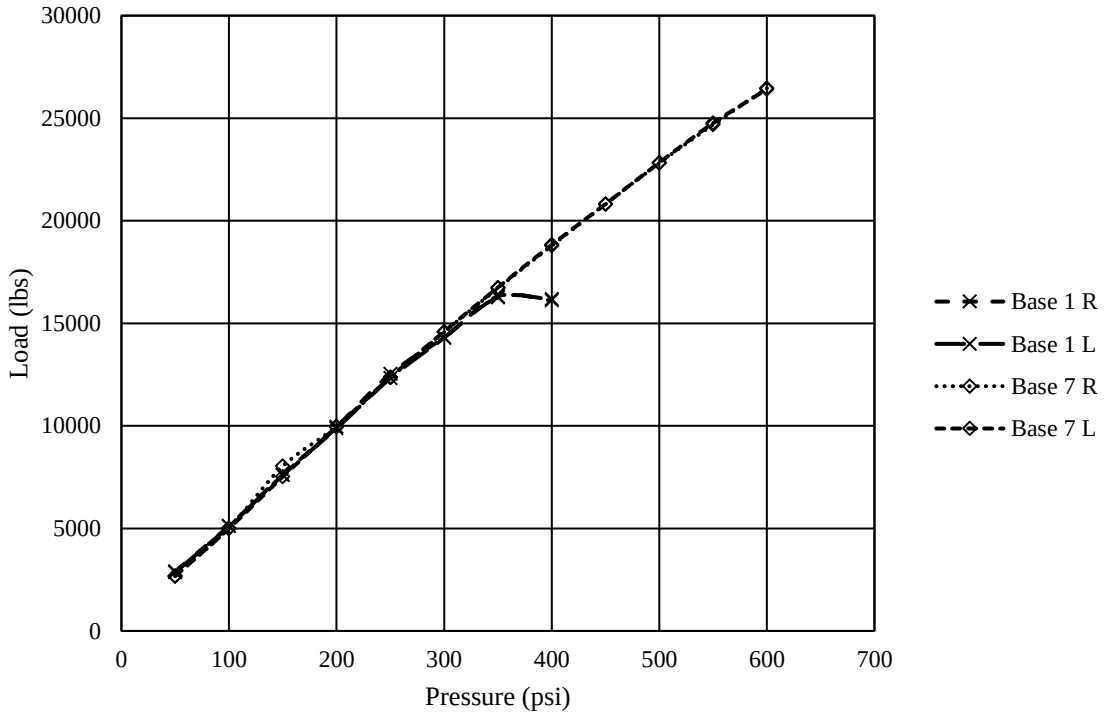


**Figure 4-15: Maximum Load (lbs) versus Pressure (psi) Comparison for Base Series 1 and Base Series 7**

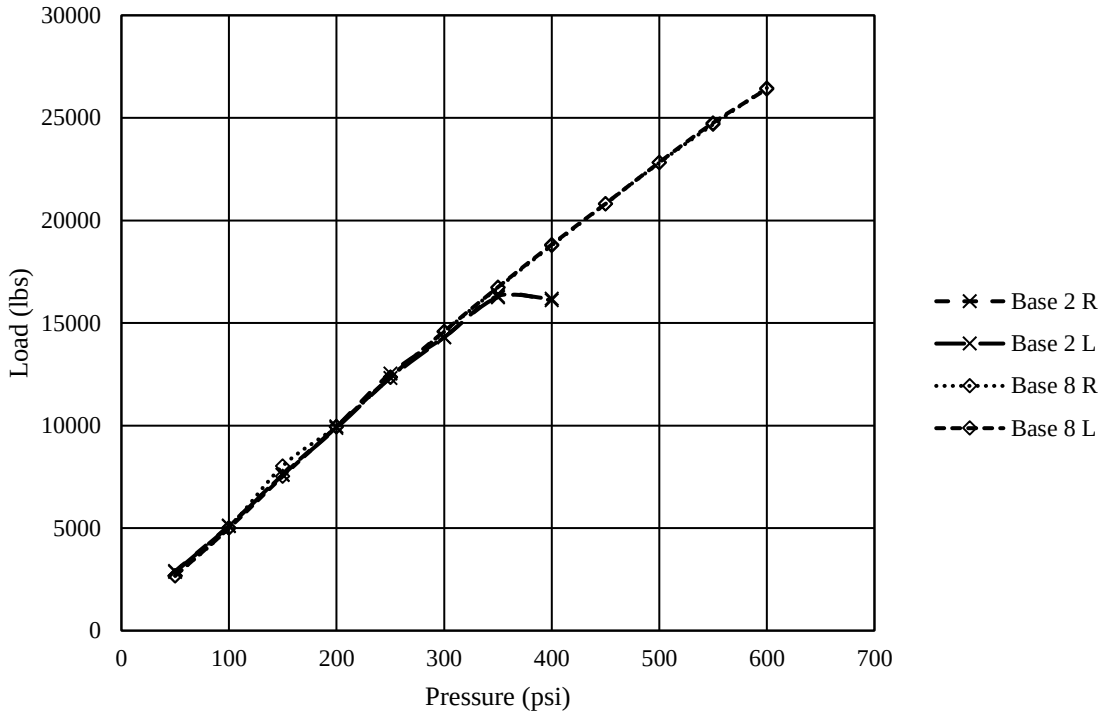


**Figure 4-16: Maximum Load (lbs) versus Pressure (psi) Comparison for Base Series 2 and Base Series 8**

For both of these comparisons, the results from the single element mortar thickness shows a greater strength of the model than the model with the three element mortar thickness. The model with the three elements shows failure and even the next increment in applied pressure shows approximately the same reaction force, whereas in the single element, after failure is first seen the reaction force recorded continues to increase.

### 4.2.5 Parametric Change – Precompression Timing

This section refers to the amount of time that the precompression curve takes to reach the final constant precompression value. This became a parameter of curiosity through the initial modeling phase of this research. It was noticed that when the precompression was ramped up at a smaller time interval, that the results of the maximum reaction forces versus pressures showed dips in the

plot. As the model was adjusted to what is now the final version, it showed that as the precompression was ramped up over a longer time interval that these dips did not appear. The figure below shows the results between Model Series 1 and Model Series 7. For both of these test series, strain rate, tiebreak values, and element size were held constant. The only difference between the two was the Model Series 1 had the precompression of 500 psi applied over 2 milliseconds while Model Series 7 had the precompression of 500 psi applied over 10 milliseconds. This comparison can be seen in Figure 4-17.

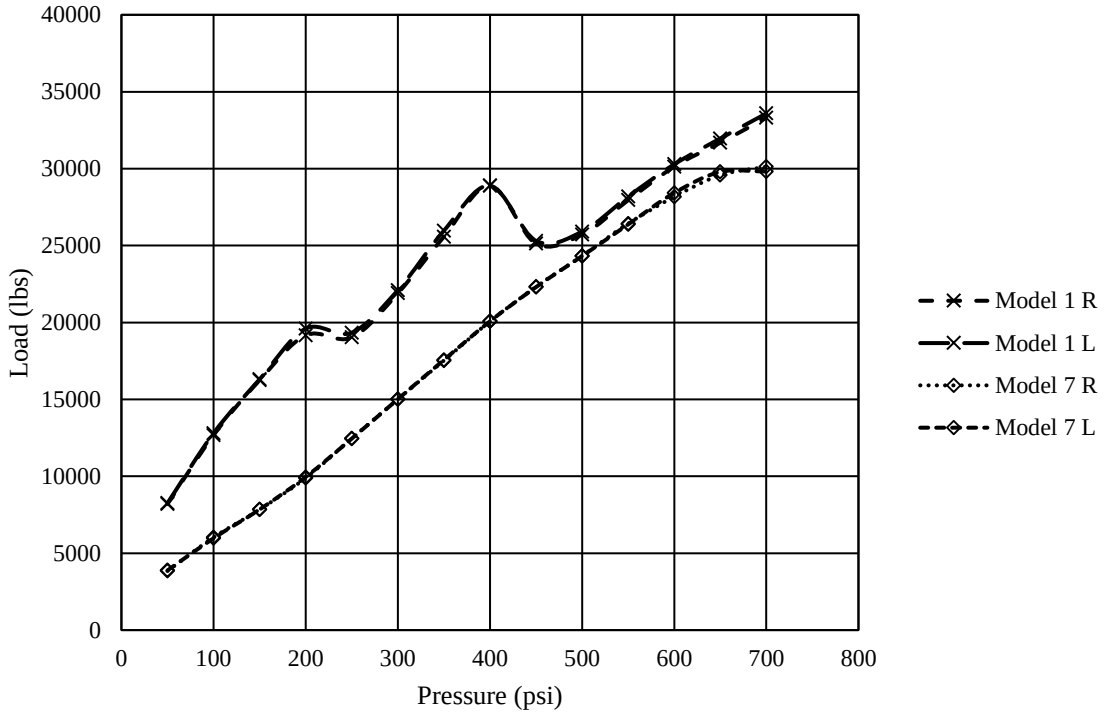


**Figure 4-17: Maximum Load (lbs) versus Pressure (psi) Comparison for Model Series 1 and Model Series 7**

As discussed above, the test series where the precompression was increased over 2 milliseconds showed inconsistensies in the curve and dips in the maximum reaction forces recorded. As the

precompression curve flattened out and was increased over a longer time increment, the curve flattened out as well and become linear, no longer having the dips in the values.

## 4.3 Discussion of Results

In the below sections, a more in-depth discussion of the results displayed above can be found. Potential reasoning for the behavior and characteristics found will be discussed, one section at a time. These sections will focus on strain rate effects, precompression values, tiebreak values, element size, and precompression timing.

### 4.3.1 Discussion of Strain Rate Effects

As can be seen in the many plots comparing the test series performed with and without the strain rate effects, there was no difference in the results between the two cases. This indicates that simply turning on the default strain rate effect for the material model will not produce more accurate results. One of the potential reasons this is the case may be that the default strain rate effect equations and analyses may not be sufficient for all cases. Another potential reason may be the element sizing. The element size of the mortar may be too small for the strain rate effects to be implemented properly. To better understand if this is simply an issue with the element size or the strain rate effect function itself, a more in-depth study on these specifics will need to be performed. It should also be noted that since these models focus on a pure shear loading condition, that the strain rate enhancement included within the material model may not occur.

Since the tiebreak was the main failure mode of these models, this is what led to Base Series 12 and Base Series 13 where the tiebreak strengths were drastically increased in an attempt to make the material fail first to see if the strain rate effects would come into play and affect the results. This was accomplished in these test series but, as indicated in the plot in the results section, the strain rate effects did not alter the results.

### 4.3.2 Discussion of Precompression Values

There were a total of three precompression value comparison plots provided in the text above. The first was a comparison between a final precompression value of 100 psi and 500 psi. The second was a comparison between a final compression value of 100 psi, 250 psi, and 500 psi. The final was a comparison between 500 psi and no precompression at all. For the first two comparisons, all test series started at approximately the same values and increased in the same slope. This indicated that for lower applied pressure values that the precompression value itself did not matter and did not drive any of the results. As the applied pressure continued to increase and failure in the elements started to initiate and spread, the lines started to diverge with the series with the highest precompression value resulting in the higher reaction forces. This is because the higher precompression that is applied enhances the bond strength at higher applied pressures. As the applied pressure continued to climb, the divergence between lines continued but the 100 psi and the 250 psi test series stayed much closer when compared to the 500 psi line. This shows that there is no direct comparison between the differences in precompression values to the amount of divergence between lines, but that simply the higher precompression value diverges more so than the smaller difference in precompression values.

For the comparison between no precompression and precompression, both lines started off with the same slope, although at different values. As failure of the elements started and as this failure propagated throughout the model, the series with no precompression trailed off and resulted in abrupt failure around 200 psi applied load. On the other hand, the model with applied precompression slowly led to failure with elements slowly failing, failure propagating more through the mortar itself, and ultimately to failure of the connection or the tiebreak. Based on this plot, when precompression is present, the bond strength is increased regardless of what the applied

pressure value is in comparison to having no precompression applied. This once again follows with the statement that precompression increases the bond strength seen in the model.

### 4.3.3 Discussion of Tiebreak Values

For the comparison between tiebreak values, all lines followed along the same line and each series slowly started to drop off depending on the tiebreak value. This shows that the tiebreak, or the connection, was the main source of failure. As the tiebreak value increased, so did the final applied pressure value till failure occurred. This goes to show that the value chosen for the shear and normal strength of the tiebreak within LS-DYNA is very important. If the value is too high, it can lead to false strength of the model itself. On the other hand, there may be a need for an increase of these values to get an overall accurate response of the model itself. It is hopeful that based on the research provided in this thesis that physical testing can be performed to prove whether or not such an increase in tiebreak strength in shear is accurate or not.

### 4.3.4 Discussion of Element Size

As seen in both of the figures comparing the results of one element mortar thickness and three element mortar thickness, both series start at the same values and follow along the same slope. Once failure is first seen in the series with three element mortar thickness, the increase in maximum reaction forces is stopped. However, the series with the single element mortar thickness continues to increase and does not show failure till 550 psi. In fact, this failure happens so abruptly that for the model with 500 psi, there is very minimal damage found within the elements themselves. This goes to show that modeling mortar as a single element thickness does not accurately represent how the stress travels between element to element throughout the entire model. This can also be related back to simple finite element methods, where elements use single integration and determine strains at the center of the elements, therefore neglecting what is happening on the edges. When the

thickness is broken up into multiple elements, the strain is determining at multiple points throughout the thickness and can therefore better represent the stresses and strains transferred from one to the other.

### 4.3.5 Discussion of Precompression Timing

As discussed and seen above, when the precompression was applied over too short of a time period, there were dips and inconsistencies within the curve. This can be attributed to a phenomenon known as "dynamic relaxation", which can be adjusted with certain cards in LS-DYNA if necessary but for this case, was not needed after lengthening the precompression timing. When the precompression was applied at a smaller time interval, it was acting too much like a dynamic load and was controlling the results of the series. However, when the precompression timing was lengthened, the dynamic effects of the precompression load seemed to level out and become less of a driving factor. Once these dips were no longer a concern, it was determined that the behavior and characteristics of the results were adequate. Utilizing the dynamic relaxation cards within LS-DYNA in future work could further prove whether or not this assumption is accurate and could lead to better values in the results when validated this model to physical results.

# Chapter 5: Conclusions

## 5.1 Conclusions

In conclusion, there is no set way that mortar can be and should be modeled within LS-DYNA. There are a variety of ways that have been implemented by various modelers, but from previous work it has been found that neglecting the mortar altogether and modeling just the concrete masonry units themselves has not been a sufficient tactic. As discussed in the previous chapter, a single thickness element size has also proven to not be an accurate solution as it leads to an abrupt failure with no element failure propagation through the model. Therefore, element sizing is important when attempting to accurately model mortar.

From the results in this research alone, the importance of accuracy in tiebreak values has been shown. If too high of a value is selected, this could lead to false strength of the model as the final pressure till failure was much higher for the series with higher tiebreak values. However, from the work done by modelers at the ERDC it seems that there should in fact be an increase in these tiebreak values when looking at dynamic loading. This therefore indicates that there could in fact be a dynamic increase factor sort of phenomenon with the connection, and is also displayed in this current work.

The precompression loading of the apparatus is not as important of a factor but needs to be accurately modeled based on how physical testing is performed. If the precompression is applied over too short of a period, the dynamic effects of the precompression can drive the results of the

overall system. It was shown above, however, that the actual value of the maximum precompression loading does not necessarily alter the overall behavior.

## 5.2 Future Recommendations

It has been shown that when concrete masonry unit walls are subjected to higher pressure loads, such as blast loads, that there seems to be an enhancement in the strength of the connection. There has not been any physical testing to prove such a statement, and it is the hopes that this research will pave the way for such physical testing to be performed.

Using the work accomplished within this research, it is hoped that one day physical testing can be performed in a similar manner to how the model was setup and executed. When this becomes a reality though, there will need to be work done beforehand to determine how to deal with the inertia effects of the concrete masonry units themselves. For the model, nothing was done to alter the mass of the objects but there is the capability to remove the mass and test the model as a massless object.

Another topic to look into with future work would be the limitations of the strain rate effects within LS-DYNA. It is a possibility that the strain rate effects in shear have not been included, but only results for tension and compression. Although there is no possible way for something to be in pure shear or pure tension as the two are related, it is possible that the strain rate effects only show themselves during tension or compression effects in the model. It may also be possible that the default strain rate curve within the material model is not sufficient for looking at masonry as the KCC Material Model is based off of concrete. It leads to a compelling question of whether or not the strain rate effects in the material model include only effects from pure tension or pure compression.

In conclusion, it is recommended that physical testing be performed similar to the test setup used in the model to obtain actual physical data. Once this is accomplished, the values in the model can be updated and therefore validated. After this is accomplished, it is desired that the behavior of the interface connection between the mortar and concrete masonry units can be better understood and that if there truly is an increase in strength based on the pressure applied, the adequate way to include this in a model can be found and implemented in future modeling work.

## References


Atkinson, R. H., B. P. Amadei, S. Saeb, and S. Sture. 1989. "Response of Masonry Bed Joints in Direct Shear." *Journal of Structural Engineering 115 (9)* 2276-2296.

Baylot, James T., Billy Bullock, Thomas R. Slawson, and Stanley C. Woodson. 2005. "Blast Response of Lightly Attached Concrete Masonry Unit Walls." *Journal of Structural Engineering 131 (8)* (Journal of Structural Engineering) 1186-1193.

Beattie, G. 1996. *Investigation into the Variation of Masonry Shear Strength under Static and Dynamic Loading.* Report No. CE/01/01, University of Liverpool.

Beattie, G., TCK Molyneaux, M. Gilbert, and S. Burnett. 2001. "Masonry Shear Strength Under Impact Loading." *9th Canadian Masonry Symposium.*

Beattie, Gregor. 2003. *Joint Fracture in Reinforced and Unreinforced Masonry under Quasi-Static and Dynamic Loading.* M. Eng (Hons) CEng MICE, The University of Liverpool.

Bei, G., and I. Papayianni. 2004. "Experimental Study of Shear Bond Strength of Traditional Masonry." *13th International Brick and Brick Masonry Conference.* Amsterdam. 1-10.

Belytschko, Ted, and Lee P. Bindeman. 1993. "Assumed Strain Stabilization of the Eight Node Hexahedral Element." *Computer Methods in Applied Mechanics and Engineering 105* 225-260.

Brown, J. A. 2004. "Evaluation of Wall Systems Subjected to Lateral Pressure for Blast Resistant Design." M.S. Thesis, Department of Civil and Environmental Engineering, University of Missouri, Columbia, MO.

Calvi, B. M., G. Macchi, and P. Zanon. 1985. "Random Cyclic Behavior of Reinforced Masonry under Shear Action." *Proceedings of 7th International Brick Masonry Conference.* Melbourne, Australia.

Dawe, J. L., and R. T. McBride. 1985. "Experimental Investigation of the Shear Resistance of Masonry Panels in Steel Frames." *Proceedings of 7th International Brick Masonry Conference.* Melbourne, Australia.

Dennis, Scott T., James T. Baylot, and Stanley C. Woodson. 2002. "Response of 1/4-Scale Concrete Masonry Unit (CMU) Walls to Blast." *Journal of Engineering Mechanics 128 (2)* (Journal of Engineering Mechanics) 134-142.

Eamon, Christopher D. 2007. "Reliability of Concrete Masonry Unit Walls Subjected to Explosive Loads." *Journal of Structural Engineering 133 (7)* 935-944.

Eamon, Christopher D., James T. Baylot, and James L. O'Daniel. 2004. "Modeling Concrete Masonry Walls Subjected to Explosive Loads." *Journal of Engineering Mechanics 130(9)* (Journal of Engineering Mechanics) 1098-1106.

ElSayed, Mostafa, Wael El-Dakhakhni, and Michael Tait. 2015. "Response Evaluation of Reinforced Concrete Structural Walls Subjected to Blast Loading." *Journal of Structural Engineering 141 (11)* (Journal of Structural Engineering).

Ghazali, M. Z. , and J. R. Riddington. 1988. "Simple Test Method for Masonry Shear Strength." *Proceedings of the Institution of Civil Engineers, Part 2, 85.* 567-574.

Hallquist, J. O. 1979. *Preliminary User's Manual for DYNA3D and DYNAP (Nonlinear Dynamic Analysis of Solids in Three Dimensions).* Report UCID-17268 Rev. 1, Livermore, California: Lawrence Livermore National Laboratory.

Hamid, A. A. 1978. "Behvior Characteristics of Concrete Masonry." PhD Thesis, McMaster University, Hamilton, Canada.

Hamid, A. A., and R. G. Drysdale. 1980. "Behavior of Brick Masonry Under Combined Shear and Compression Loading." *Proceedings of 2nd Canadian Masonry Symposium.* Otawa, Canada.

Hegemier, G. A., S. K. Arya, G. Krishnamoorthy, W. Nachbar, and R. Furgerson. 1978. "On the Behavior of Joints in Concrete Masonry." *Proceedings of North American Masonry Conference.* Boulder, Colorado.

Livermore Software Technology Corporation. 2015. *LS-DYNA Keyword User's Manual.* Livermore, California: Livermore Software Technology Corporation.

Lourenco, P. B., J. O. Barros, and J. T. Oliveria. 2004. "Shear Testing of Stack Bonded Masonry." *Construction and Building Materials 18* 125-132.

Malvar, Javier L., and Allen C. Ross. 1998. "Review of Strain Rate Effects for Concrete in Tension." *ACI Materials Journal 95-M73* 735-739.

Mayes, R. L., and R. W. Clough. 1975. *A Literature Survey - Compressive, Tensile, Bond and Shear Strength of Masonry*. Dept. No. 75-13, Berkeley, California: University of California.

Mayes, R. L., and R. W. Clough. 1975. *State-of-the-art in Seismic Shear Strength of Masonry - An Evaluation and Review*. Dept. No. EERC 75-21, Berkeley, California: University of California.

Mayrhofer, Chr. 2002. "Reinforced Masonry Walls under Blast Loading." *International Journal of Mechanical Sciences 44* (International Journal of Mechanical Sciences 44) 1067-1080.

Meli, R. 1973. "Behavior of Masonry Walls under Lateral Loads." *Proceedings of 5th World Congress on Earthquake Engineering.* 853-862.

Mendoza Puchades, M., R. Judge, and G. Beattie. 2016. "Uncertainty in the Numerical Modelling of Masonry Triplet Tests Under Dynamic Loading." *International Journal of Computational Methods and Experimental Measurements 0 (0)* 1-11.

Molyneaux, T. C. K. 1995. "Vehicle Impact on Masonry Parapets." *The Society for Earthquake and Civil Engienering Dynamics Newsletter Volume 9, No 1* (The Society for Earthquake and Civil Engineering Dynamics) 7-9.

Nuss, L. K. 1978. "The Parameters Influencing Shear Strength between Clay Masonry Units and Mortar Tested using Shear Masonry Specimens." M.S. Thesis, University of Colorado, Boulder, CO.

Oh, Byung Hwan. 1987. "Behavior of Concrete under Dynamic Tensile Loads." *ACI Materials Journal 84-M2* 8-13.

Riddington, J. R., and M. Z. Ghazali. 1990. "Hypothesis for Shear Failure in Masonry Joints." *Proceedings of the Institution of Civil Engineers, Part 2, 89.* 89-102.

Ross, Allen C., David M. Jerome, Joseph W. Tedesco, and Mary L. Hughes. 1996. "Moisture and Strain Rate Effects on Concrete Strength." *ACI Materials Journal 93-M33* 293-298.

Ross, Allen C., Joseph W. Tedesco, and Steven T. Kuennen. 1995. "Effects of Strain Rate on Concrete Strength." *ACI Materials Journal 92-M5* 37-45.

Ross, Allen C., P. Y. Thompson, and J. W. Tedesco. 1989. "Split-Hopkinson Pressure-Bar Tests on Concrete and Mortar in Tension and Compression." *ACI Materials Journal 86-M43* 475-481.

Sarangapani, G., B. V. Venkatarama Reddy, and K. S. Jagadish. 2005. "Brick-Mortar Bond and Masonry Compressive Strength." *Journal of Materials in Civil Engineering 17 (2)* 229-237.

Schwer, Leonard E, and L. Javier Malvar. 2005. "Simplified Concrete Modeling with *MAT_CONCRETE_DAMAGE_REL3." *JRI LS-DYNA Users Week* 1-14.

Singh, S.B., and Pankaj Munjal. 2017. "Bond Strength and Compressive Stress-Strain Characteristics of Brick Masonry." *Journal of Building Engineering 9* 10-16.

Sinha, B. P., and A. W. Hendry. 1969. "Racking tests on Storey-Height Shear Wall Strucutres with Openings, Subjected to Precompression." *Proceedings of International Conference on Masonry Structural Systems.* University of Texas at Austin, Texas. 192-199.

Stockl, Siegfried, and Peter Hofmann. 1986. "Tests on the Shear Bond Behaviour in the Bed-Joints of Masonry." *8th International Brick and Block Masonry Conference.* London: Elsevier Applied Science. 292-303.

Tedesco, Joseph W., Allen C. Ross, and Steven T. Kuennen. 1993. "Experimental and Numerical Analysis of High Strain Rate Splitting Tensile Tests." *ACI Materials Journal 90-M17* 162-169.

Thamboo, Julian Ajith, Manicka Dhanasekar, and Cheng Yan. 2013. "Flexural and Shear Bond Characteristics of Thin Layer Polymer Cement Mortared Concrete Masonry." *Construction and Building Materials 46* 104-113.

Thamboo, Julilan Ajith, and Manicka Dhanasekar. 2015. "Characterisation of Thin Layer Polymer Cement Mortared Concrete." *Construction and Building Materials 82* 71-80.

U.S. Army Corps of Engineers. 2008. *Unified Facilities Criteria (UFC) Structures to Resist the Effects of Accidental Explosions.* UFC 3-340-02, U.S. Army Corps of Engineers.

Van der Pluijm, Rob, Harry Rutten, and Martien Ceelen. 2000. "Shear Behaviour of Bed Joints." *12th International Brick and Block Masonry Conference.* Madrid, Spain. 1849-1862.

Wu, Youcai, John E. Crawford, Shengrui Lan, and Joseph M. Magallanes. 2014. "Validation Studies for Concrete Constitutive Models with Blast Test Data." *13th International LS-DYNA Users Conference: Constitutive Modeling.* Detroit. 1-1 - 1-12.

Yokel, F. Y., and S. G. Fattal. 1975. *A Failure Hypothesis for Masonry Shear Walls.* Report No. NBSIR 75-703, Washington D.C.: National Bureau of Standards.

## Appendix A: Input Data

```
$# LS-DYNA Keyword file created by LS-PrePost(R) V4.5.21 - 31May2018
$# Created on Feb-27-2019 (19:11:00)
*KEYWORD
*TITLE
$#                                                                         title
Triple Block Model Base1.1
*CONTROL_ENERGY
$#    hgen      rwen    slnten     rylen
         2         2         1         1
*CONTROL_MPP_DECOMPOSITION_AUTOMATIC
*CONTROL_TERMINATION
$#  endtim    endcyc     dtmin    endeng    endmas     nosol
      60.0         0       0.0       0.01.000000E8         0
*CONTROL_TIMESTEP
$#  dtinit    tssfac      isdo    tslimt     dt2ms      lctm     erode     ms1st
       0.0       0.9         0       0.0       0.0         0         0         0
$#  dt2msf   dt2mslc     imscl    unused    unused     rmscl
       0.0         0         0                             0.0
*DATABASE_GLSTAT
$#      dt    binary      lcur     ioopt
       0.1         0         0         1
*DATABASE_MATSUM
$#      dt    binary      lcur     ioopt
       0.1         0         0         1
*DATABASE_BINARY_D3PLOT
$#      dt      lcdt      beam     npltc    psetid
       0.1         3         0         0         0
$#   ioopt
         0
*DATABASE_BINARY_INTFOR
$#      dt      lcdt      beam     npltc    psetid
       0.1         3         0         0         0
$#   ioopt
         0
*DATABASE_BINARY_RUNRSF
$#    cycl        nr      beam     npltc    psetid
     100.0         0         0         0         0
*DATABASE_EXTENT_BINARY
$#   neiph     neips    maxint    strflg    sigflg    epsflg    rltflg    engflg
         0         0         3        11         1         1         1         1
$#  cmpflg    ieverp    beamip     dcomp      shge     stssz    n3thdt   ialemat
         0         0         0         1         1         1         2         1
$# nintsld   pkp_sen      sclp     hydro     msscl     therm    intout    nodout
         0         0       1.0         0         0         0STRESS    STRESS
$#    dtdt    resplt     neipb     quadr     cubic
         0         0         0         0         0
*BOUNDARY_SPC_SET_ID
$#      id                                                              heading
```

```
         1Front and Rear Slide Planes
$#    nsid       cid      dofx      dofy      dofz     dofrx     dofry     dofrz
         1         0         0         1         0         0         0         0
         2Boundary Conditions
         2         0         0         1         0         0         0         0
*LOAD_SEGMENT_SET_ID
$#      id                                                             heading
         1Left Side Confinement
$#    ssid      lcid        sf        at
         9         1       1.0       0.0
*LOAD_SEGMENT_SET_ID
$#      id                                                             heading
         2Right Side Confinement
$#    ssid      lcid        sf        at
        10         1       1.0       0.0
*LOAD_SEGMENT_SET_ID
$#      id                                                             heading
         3Pressure Curve
$#    ssid      lcid        sf        at
        11         2       1.0       0.0
*CONTACT_TIEBREAK_SURFACE_TO_SURFACE_ID
$#     cid                                                               title
         1Cont btw left brick and left mortar
$#    ssid      msid     sstyp     mstyp    sboxid    mboxid       spr       mpr
         2         1         0         0         0         0         1         1
$#      fs        fd        dc        vc       vdc    penchk        bt        dt
       0.6       0.5       0.2    1155.0       0.0         0       0.01.00000E20
$#     sfs       sfm       sst       mst      sfst      sfmt      fsf       vsf
       1.0       1.0       0.0       0.0       1.0       1.0       1.0       1.0
$#    nfls      sfls    tblcid    thkoff
     400.0     400.0         0         0
*CONTACT_TIEBREAK_SURFACE_TO_SURFACE_ID
$#     cid                                                               title
         2Cont btw left mortar and middle brick
$#    ssid      msid     sstyp     mstyp    sboxid    mboxid       spr       mpr
         3         4         0         0         0         0         1         2
$#      fs        fd        dc        vc       vdc    penchk        bt        dt
       0.6       0.5       0.2    1155.0       0.0         0       0.01.00000E20
$#     sfs       sfm       sst       mst      sfst      sfmt      fsf       vsf
       1.0       1.0       0.0       0.0       1.0       1.0       1.0       1.0
$#    nfls      sfls    tblcid    thkoff
     400.0     400.0         0         0
*CONTACT_TIEBREAK_SURFACE_TO_SURFACE_ID
$#     cid                                                               title
         3Cont btw middle brick and right mortar
$#    ssid      msid     sstyp     mstyp    sboxid    mboxid       spr       mpr
         6         5         0         0         0         0         1         1
$#      fs        fd        dc        vc       vdc    penchk        bt        dt
       0.6       0.5       0.2    1155.0       0.0         0       0.01.00000E20
$#     sfs       sfm       sst       mst      sfst      sfmt      fsf       vsf
       1.0       1.0       0.0       0.0       1.0       1.0       1.0       1.0
$#    nfls      sfls    tblcid    thkoff
     400.0     400.0         0         0
*CONTACT_TIEBREAK_SURFACE_TO_SURFACE_ID
$#     cid                                                               title
         4Cont btw right mortar and right brick
$#    ssid      msid     sstyp     mstyp    sboxid    mboxid       spr       mpr
```

```
         7         8         0         0         0         0         1         1
$#      fs        fd        dc        vc       vdc    penchk        bt        dt
       0.6       0.5       0.2    1155.0       0.0         0       0.01.00000E20
$#     sfs       sfm       sst       mst      sfst      sfmt      fsf       vsf
       1.0       1.0       0.0       0.0       1.0       1.0       1.0       1.0
$#    nfls      sfls    tblcid    thkoff
     400.0     400.0         0         0
*CONTACT_SURFACE_TO_SURFACE_ID
$#     cid                                                              title
         5Left Boundary Contact
$#    ssid      msid     sstyp     mstyp    sboxid    mboxid       spr       mpr
        12        13         0         0         0         0         1         1
$#      fs        fd        dc        vc       vdc    penchk        bt        dt
       0.6       0.5       0.2    1155.0       0.0         0       0.01.00000E20
$#     sfs       sfm       sst       mst      sfst      sfmt      fsf       vsf
       1.0       1.0       0.0       0.0       1.0       1.0       1.0       1.0
*CONTACT_SURFACE_TO_SURFACE_ID
$#     cid                                                              title
         6Right Boundary Contact
$#    ssid      msid     sstyp     mstyp    sboxid    mboxid       spr       mpr
        14        15         0         0         0         0         1         1
$#      fs        fd        dc        vc       vdc    penchk        bt        dt
       0.6       0.5       0.2    1155.0       0.0         0       0.01.00000E20
$#     sfs       sfm       sst       mst      sfst      sfmt      fsf       vsf
       1.0       1.0       0.0       0.0       1.0       1.0       1.0       1.0
*CONTACT_ERODING_SINGLE_SURFACE_ID
$#     cid                                                              title
         7Eroding Contact between all parts
$#    ssid      msid     sstyp     mstyp    sboxid    mboxid       spr       mpr
         1         0         2         0         0         0         0         0
$#      fs        fd        dc        vc       vdc    penchk        bt        dt
       0.6       0.5       0.2    1155.0       0.0         0       0.01.00000E20
$#     sfs       sfm       sst       mst      sfst      sfmt      fsf       vsf
       1.0       1.0       0.0       0.0       1.0       1.0       1.0       1.0
$#    isym    erosop      iadj
         0         0         0
*SET_PART_LIST_TITLE
Part Set for Erosion
$#     sid       da1       da2       da3       da4    solver
         1       0.0       0.0       0.0       0.0MECH
$#    pid1      pid2      pid3      pid4      pid5      pid6      pid7      pid8
         1         2         3         4         5         6         7         0
*PART
$#                                                                       title
Left Brick
$#     pid     secid       mid     eosid      hgid      grav    adpopt      tmid
         1         1         1         0         1         0         0         0
*SECTION_SOLID_TITLE
Block Left Section
$#   secid    elform       aet
         1         1         0
*MAT_CONCRETE_DAMAGE_REL3_TITLE
CMU Material
$#     mid        ro        pr
         1     224.0      0.22
$#      ft        a0        a1        a2        b1     omega       a1f
     500.0   -3000.0       0.0       0.0       0.0       0.0       0.0
```

```
$# slambda      nout     edrop     rsize       ucf    lcrate  locwidth      npts
       0.0       0.0       0.0       0.0       0.0         0       0.3       0.0
$# lambda1   lambda2   lambda3   lambda4   lambda5   lambda6   lambda7   lambda8
       0.0       0.0       0.0       0.0       0.0       0.0       0.0       0.0
$#lambda09  lambda10  lambda11  lambda12  lambda13        b3       a0y       a1y
       0.0       0.0       0.0       0.0       0.0       0.0       0.0       0.0
$#    eta1      eta2      eta3      eta4      eta5      eta6      eta7      eta8
       0.0       0.0       0.0       0.0       0.0       0.0       0.0       0.0
$#   eta09     eta10     eta11     eta12     eta13        b2       a2f       a2y
       0.0       0.0       0.0       0.0       0.0       0.0       0.0       0.0
*HOURGLASS_TITLE
Hourglass control for CMUs
$#    hgid       ihq        qm       ibq        q1        q2    qb/vdc        qw
         1         6       0.1         0       1.5      0.06       0.1       0.1
*PART
$#                                                                         title
Middle Brick
$#     pid     secid       mid     eosid      hgid      grav    adpopt      tmid
         2         2         1         0         1         0         0         0
*SECTION_SOLID_TITLE
Block Middle Section
$#   secid    elform       aet
         2         1         0
*PART
$#                                                                         title
Right Brick
$#     pid     secid       mid     eosid      hgid      grav    adpopt      tmid
         3         3         1         0         1         0         0         0
*SECTION_SOLID_TITLE
Block Right Section
$#   secid    elform       aet
         3         1         0
*PART
$#                                                                         title
Left Mortar
$#     pid     secid       mid     eosid      hgid      grav    adpopt      tmid
         4         4         2         0         2         0         0         0
*SECTION_SOLID_TITLE
Mortar Left Section
$#   secid    elform       aet
         4         1         0
*MAT_CONCRETE_DAMAGE_REL3_TITLE
Mortar Material
$#     mid        ro        pr
         2     162.0      0.22
$#      ft        a0        a1        a2        b1     omega       a1f
     500.0   -2300.0       0.0       0.0       0.0       0.0       0.0
$# slambda      nout     edrop     rsize       ucf    lcrate  locwidth      npts
       0.0       0.0       0.0       0.0       0.0         0       0.3       0.0
$# lambda1   lambda2   lambda3   lambda4   lambda5   lambda6   lambda7   lambda8
       0.0       0.0       0.0       0.0       0.0       0.0       0.0       0.0
$#lambda09  lambda10  lambda11  lambda12  lambda13        b3       a0y       a1y
       0.0       0.0       0.0       0.0       0.0       0.0       0.0       0.0
$#    eta1      eta2      eta3      eta4      eta5      eta6      eta7      eta8
       0.0       0.0       0.0       0.0       0.0       0.0       0.0       0.0
$#   eta09     eta10     eta11     eta12     eta13        b2       a2f       a2y
       0.0       0.0       0.0       0.0       0.0       0.0       0.0       0.0
```

```
*HOURGLASS_TITLE
Hourglass control for mortar
$#    hgid       ihq        qm       ibq        q1        q2    qb/vdc        qw
         2         6       0.1         0       1.5      0.06       0.1       0.1
*PART
$#                                                                         title
Right Mortar
$#     pid     secid       mid     eosid      hgid      grav    adpopt      tmid
         5         5         2         0         2         0         0         0
*SECTION_SOLID_TITLE
Mortar Right Section
$#   secid    elform       aet
         5         1         0
*PART
$#                                                                         title
Left Section
$#     pid     secid       mid     eosid      hgid      grav    adpopt      tmid
         6         1         3         0         1         0         0         0
*MAT_ELASTIC_TITLE
Steel
$#     mid        ro         e        pr        da        db  not used
         3     733.02.900000E7       0.3       0.0       0.0         0
*PART
$#                                                                         title
Right Section
$#     pid     secid       mid     eosid      hgid      grav    adpopt      tmid
         7         3         3         0         1         0         0         0
*MAT_ADD_EROSION_TITLE
Erosion for Mortar
$#     mid      excl    mxpres     mneps    effeps    voleps    numfip       ncs
         2       0.0       0.0       0.0       0.0       0.8       1.0       1.0
$#  mnpres     sigp1     sigvm     mxeps     epssh     sigth   impulse    failtm
       0.0       0.0       0.0       0.9       0.0       0.0       0.0       0.0
$#    idam    dmgtyp     lcsdg     ecrit    dmgexp     dcrit    fadexp    lcregd
         0       0.0         0       0.0       1.0       0.0       1.0         0
$#   lcfld             epsthin    engcrt    radcrt
         0         0       0.0       0.0       0.0
*MAT_ADD_EROSION_TITLE
Erosion for CMU
$#     mid      excl    mxpres     mneps    effeps    voleps    numfip       ncs
         1       0.0       0.0       0.0       0.0       0.8       1.0       1.0
$#  mnpres     sigp1     sigvm     mxeps     epssh     sigth   impulse    failtm
       0.0       0.0       0.0       0.9       0.0       0.0       0.0       0.0
$#    idam    dmgtyp     lcsdg     ecrit    dmgexp     dcrit    fadexp    lcregd
         0       0.0         0       0.0       1.0       0.0       1.0         0
$#   lcfld             epsthin    engcrt    radcrt
         0         0       0.0       0.0       0.0
*DEFINE_CURVE_TITLE
Precompression Curve
$#    lcid      sidr       sfa       sfo      offa      offo    dattyp     lcint
         1         0       1.0       1.0       0.0       0.0         0         0
$#                a1                  o1
                0.0                 0.0
               10.0                100.0
               60.0                100.0
*DEFINE_CURVE_TITLE
Pressure Curve
```

```
$#    lcid      sidr       sfa       sfo      offa      offo    dattyp     lcint
         2         0       1.0       1.0       0.0       0.0         0         0
$#                a1                  o1
                 0.0                 0.0
                10.0                 0.0
                10.0                50.0
                60.0                 0.0
*DEFINE_CURVE_TITLE
Timestep Curve
$#    lcid      sidr       sfa       sfo      offa      offo    dattyp     lcint
         3         0       1.0       1.0       0.0       0.0         0         0
$#                a1                  o1
                 0.0                 0.5
                 9.0                 0.5
                 9.0                 0.1
                21.0                 0.1
                21.0                 0.5
                60.0                 0.5
*END
```

## Appendix B: Raw Data

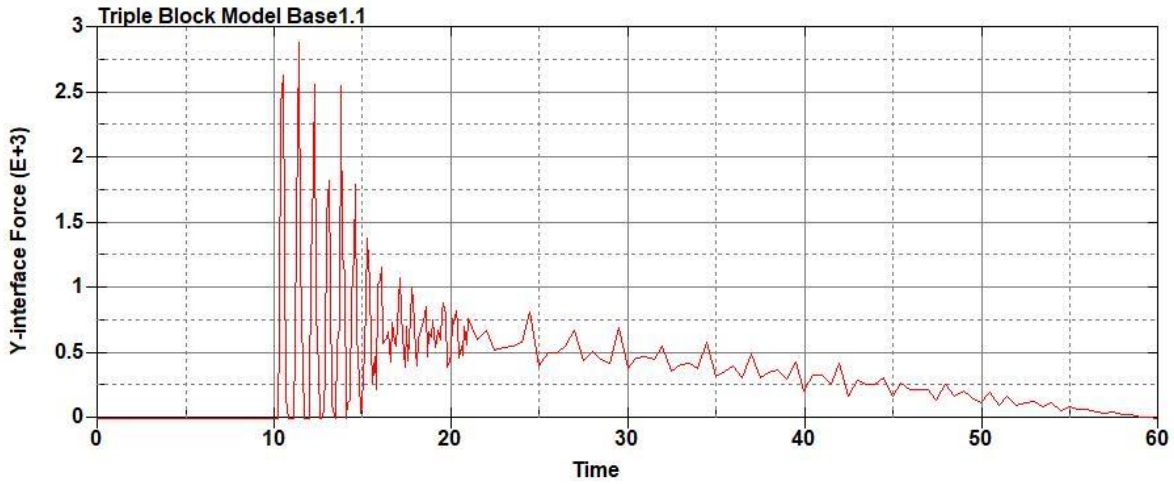


**Figure B-1: Base Run 1.1 Right Support Y-Interface Force (lbs) versus Time (ms) – 50 psi**

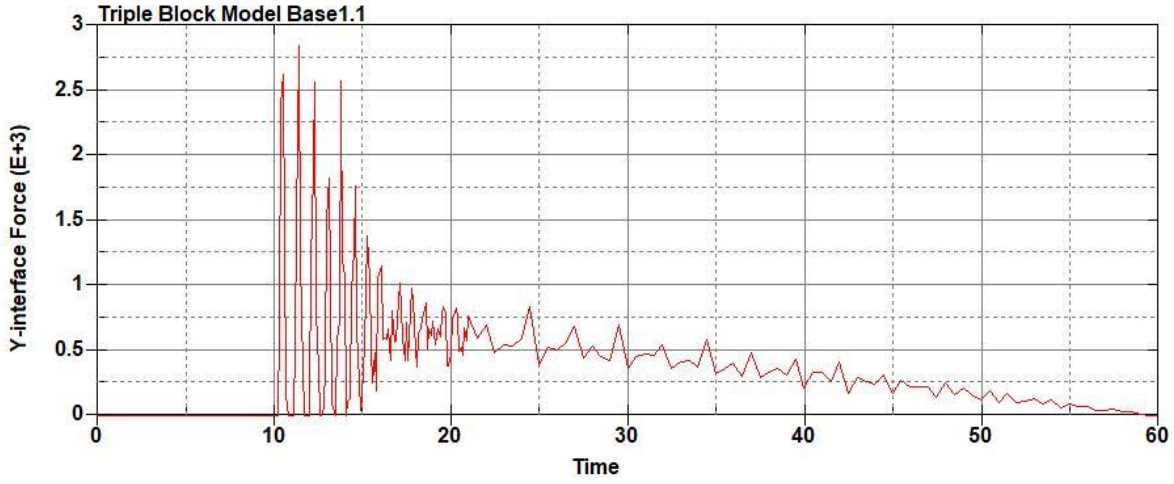


**Figure B-2: Base Run 1.1 Left Support Y-Interface Force (lbs) versus Time (ms) – 50 psi**

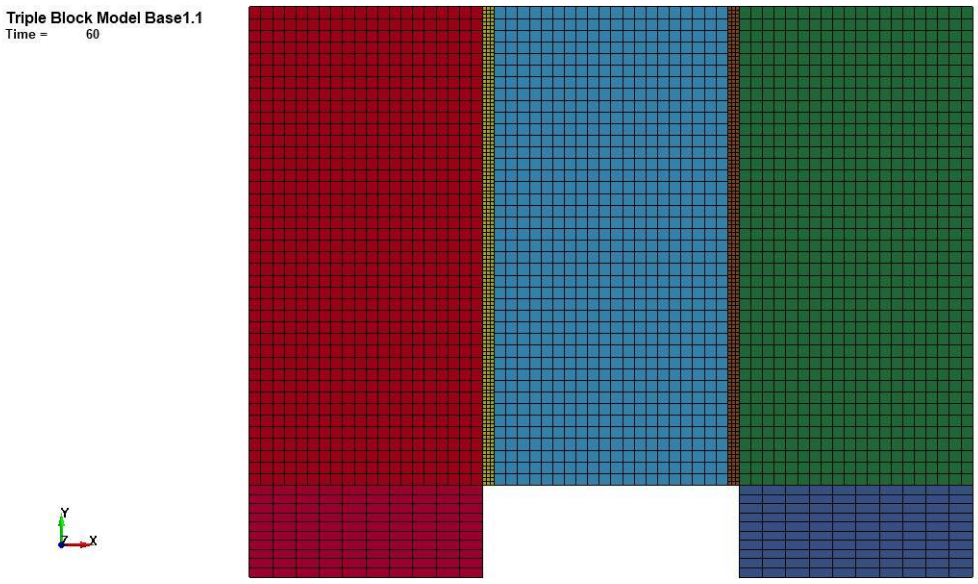


**Figure B-3: Last State at 60 Milliseconds for Base Run 1.1 – 50 psi**

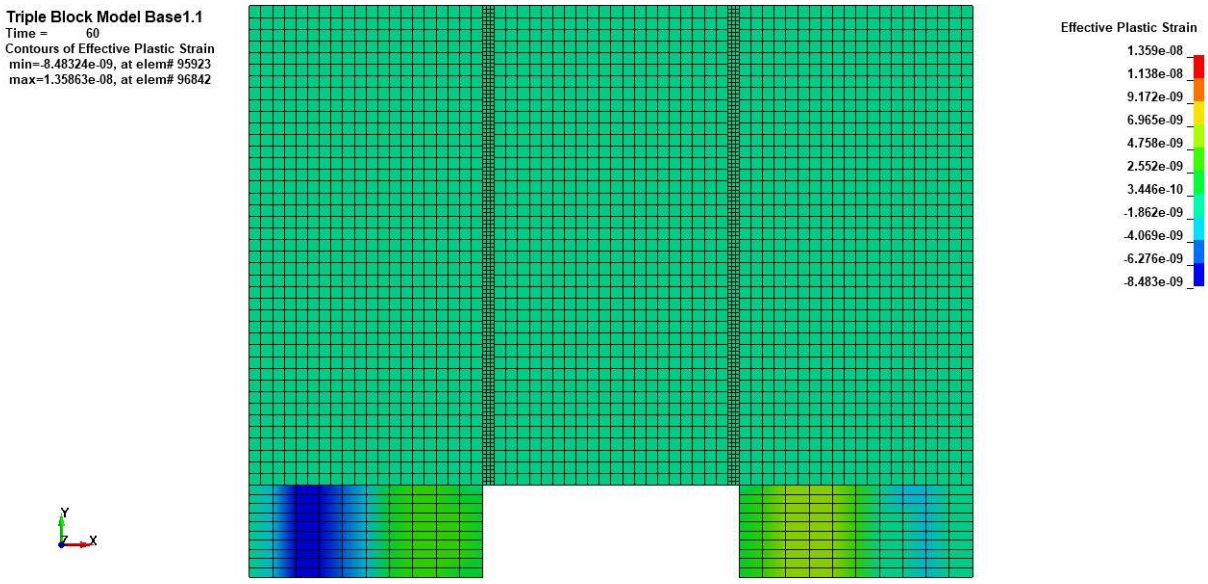


**Figure B-4: Effective Plastic Strain Fringe Plot for Last State at 60 Milliseconds for Base Run 1.1 – 50 psi**

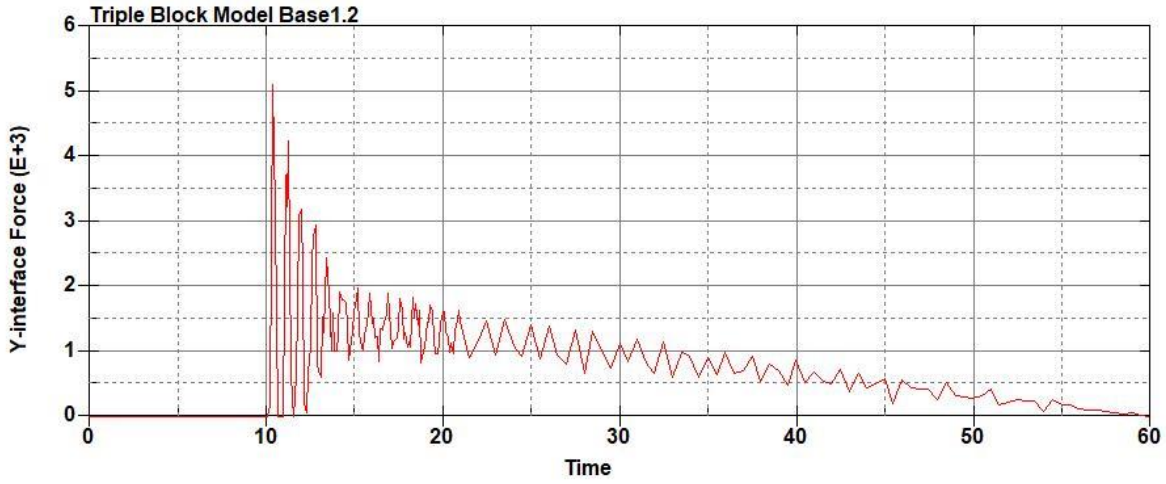


**Figure B-5: Base Run 1.2 Right Support Y-Interface Force (lbs) versus Time (ms) – 100 psi**

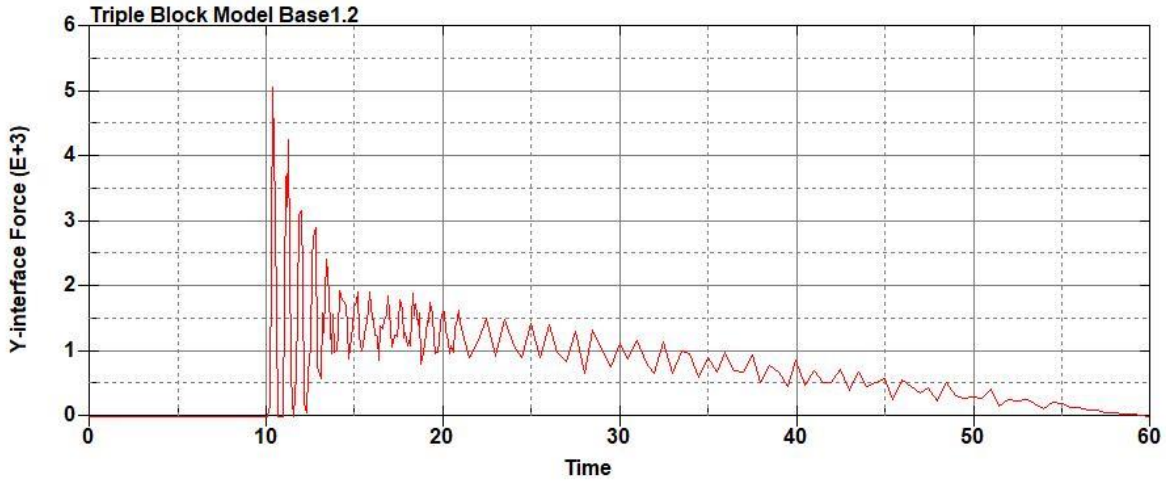


**Figure B-6: Base Run 1.2 Left Support Y-Interface Force (lbs) versus Time (ms) – 100 psi**

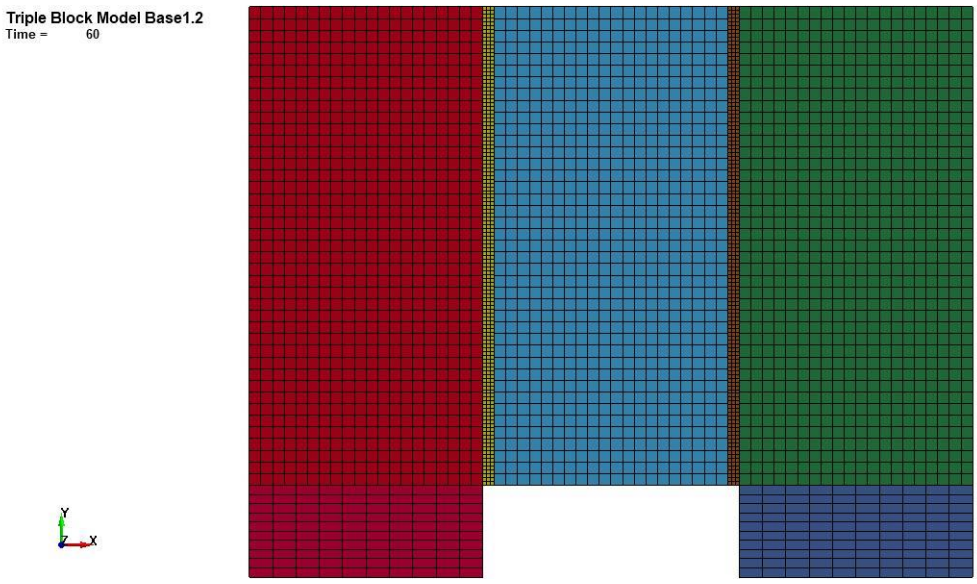


**Figure B-7: Last State at 60 Milliseconds for Base Run 1.2 – 100 psi**

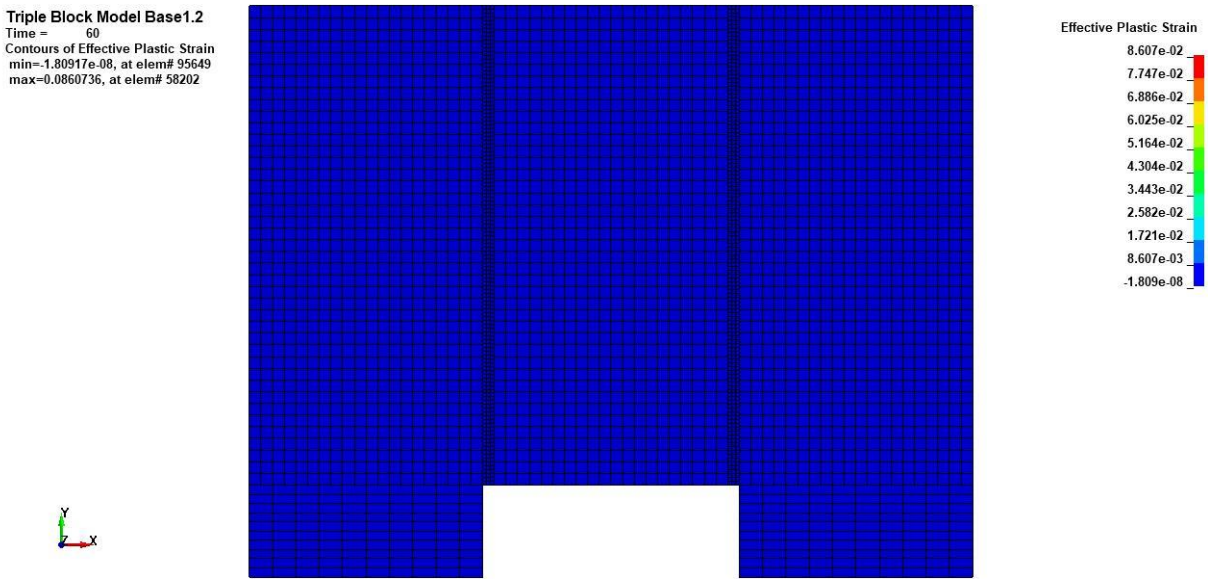


**Figure B-8: Effective Plastic Strain Fringe Plot for Last State at 60 Milliseconds for Base Run 1.2 – 100 psi**

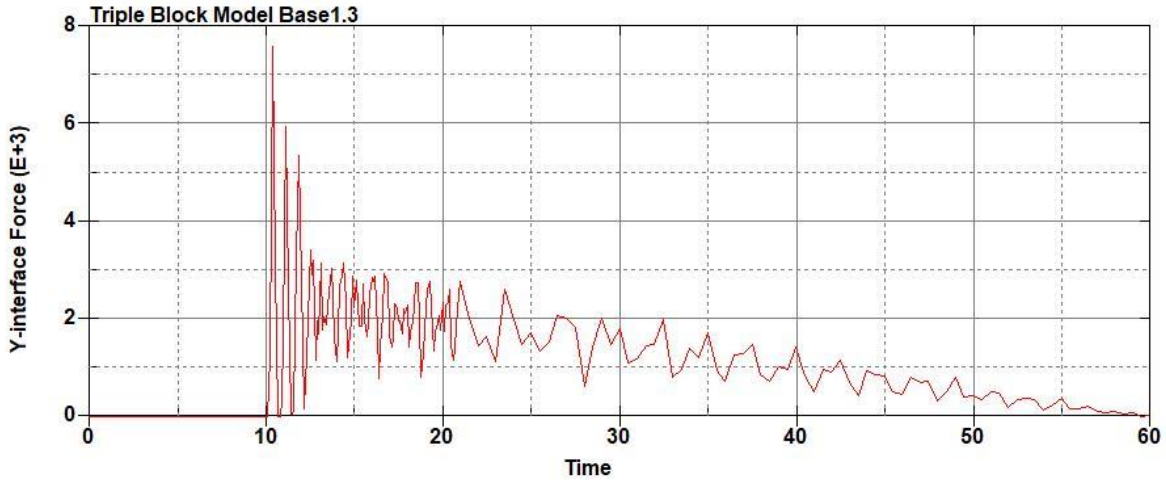


**Figure B-9: Base Run 1.3 Right Support Y-Interface Force (lbs) versus Time (ms) – 150 psi**

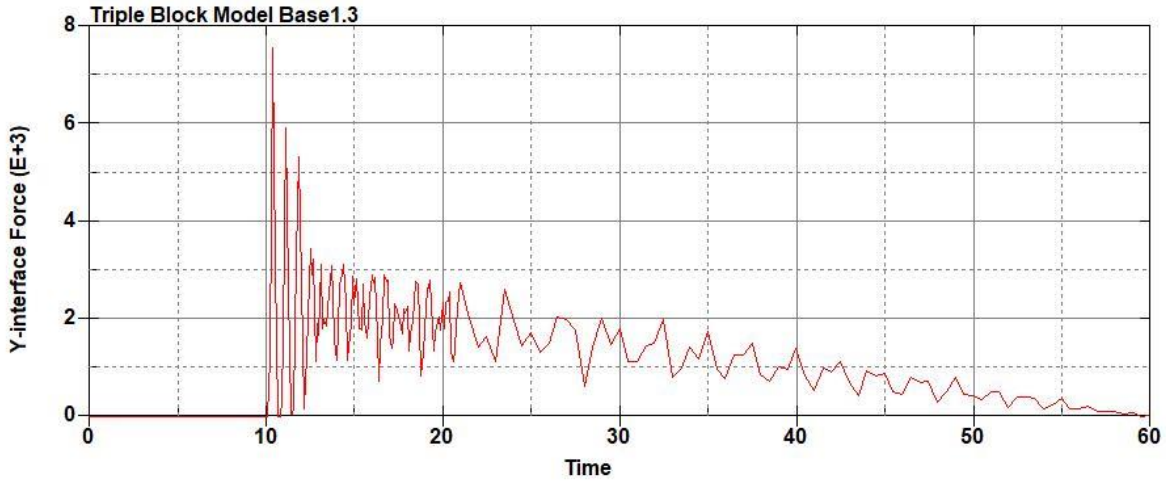


**Figure B-10: Base Run 1.3 Left Support Y-Interface Force (lbs) versus Time (ms) – 150 psi**

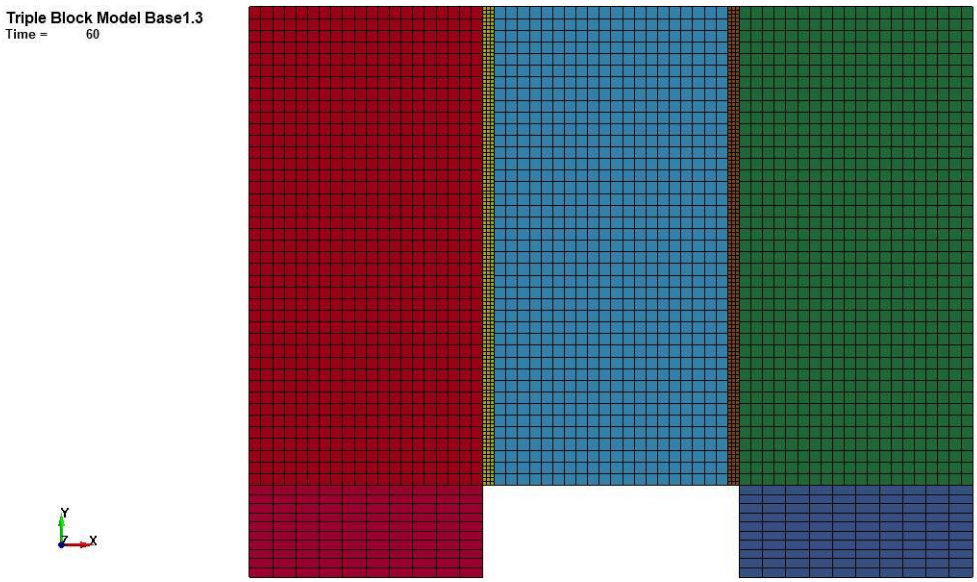


**Figure B-11: Last State at 60 Milliseconds for Base Run 1.3 – 150 psi**

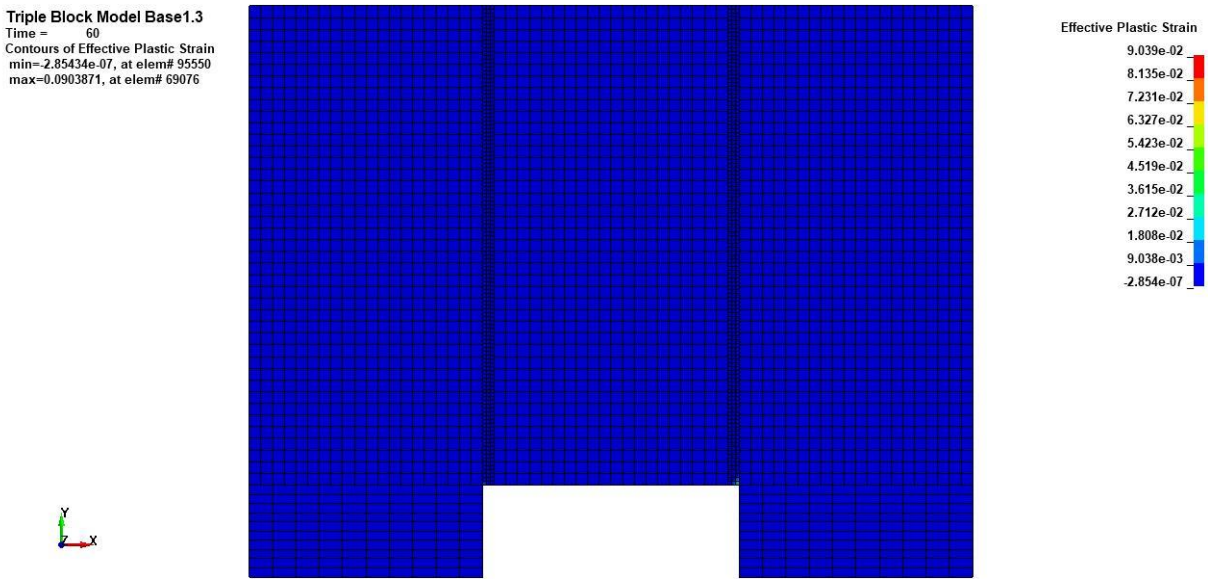


**Figure B-12: Effective Plastic Strain Fringe Plot for Last State at 60 Milliseconds for Base Run 1.3 – 150 psi**

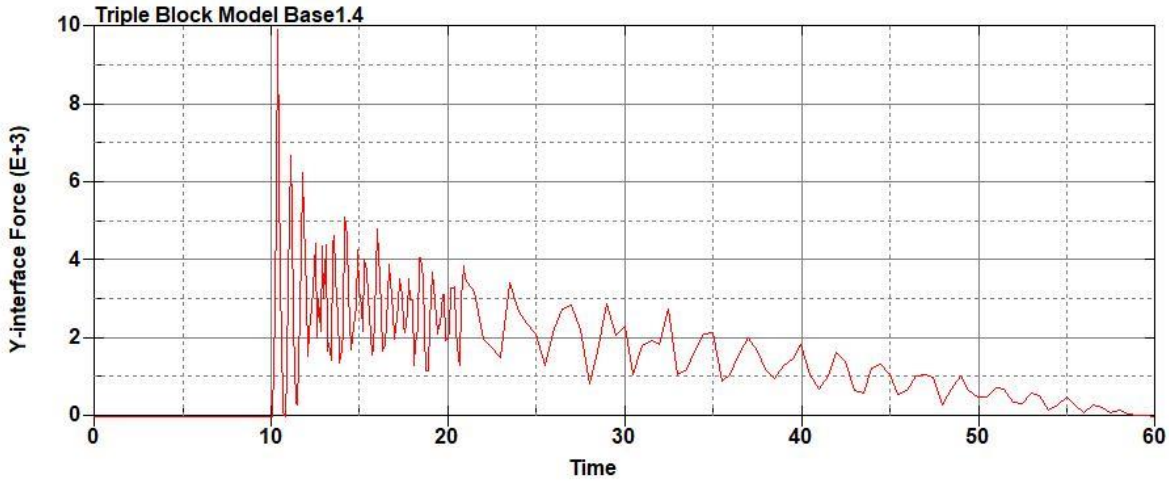


**Figure B-13: Base Run 1.4 Right Support Y-Interface Force (lbs) versus Time (ms) – 200 psi**

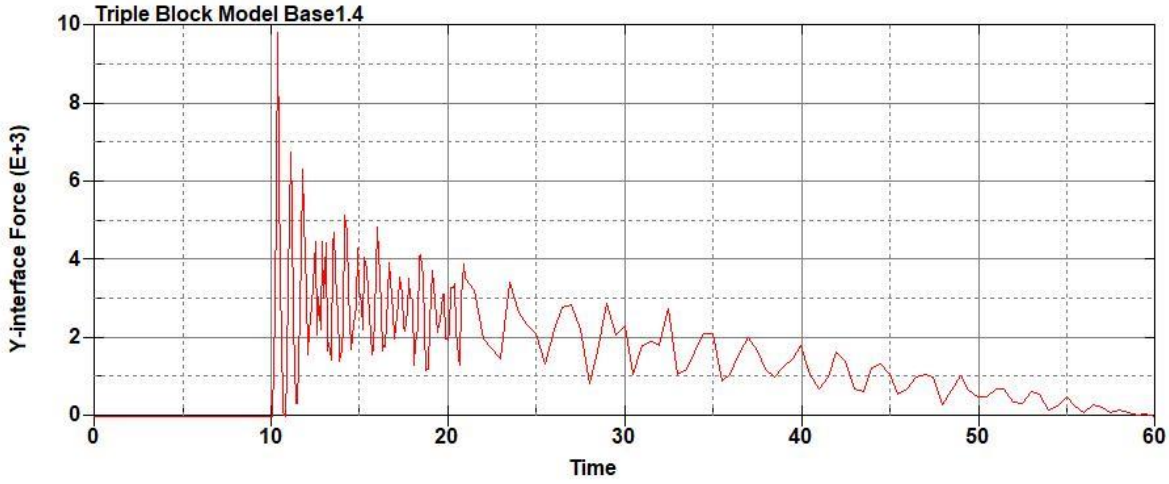


**Figure B-14: Base Run 1.4 Left Support Y-Interface Force (lbs) versus Time (ms) – 200 psi**

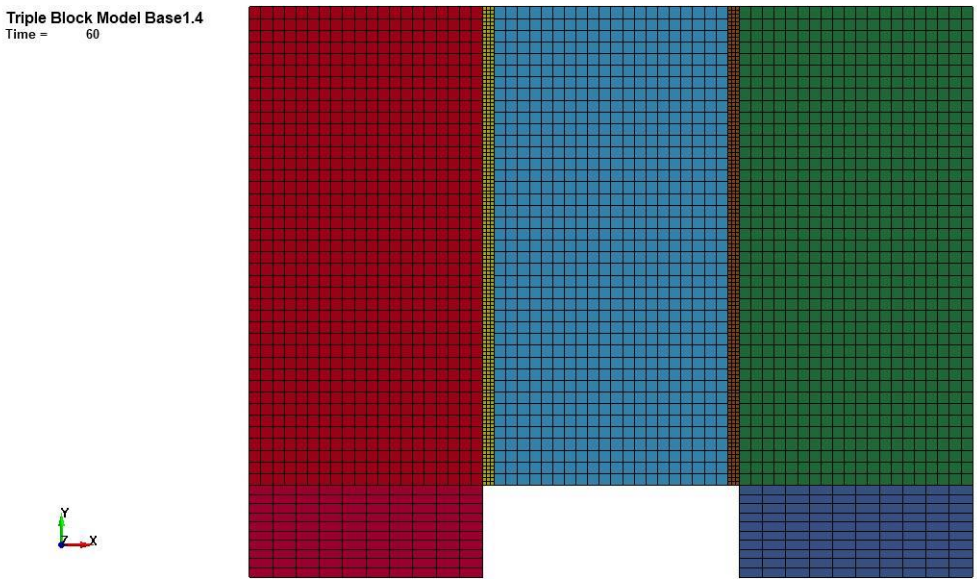


**Figure B-15: Last State at 60 Milliseconds for Base Run 1.4 – 200 psi**

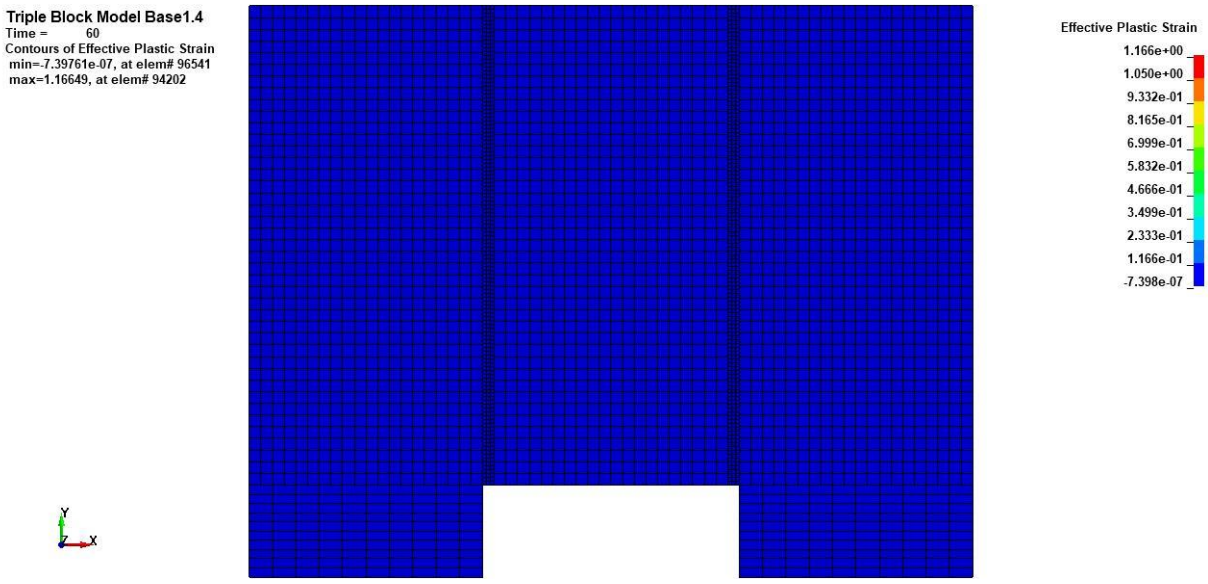


**Figure B-16: Effective Plastic Strain Fringe Plot for Last State at 60 Milliseconds for Base Run 1.4 – 200 psi**

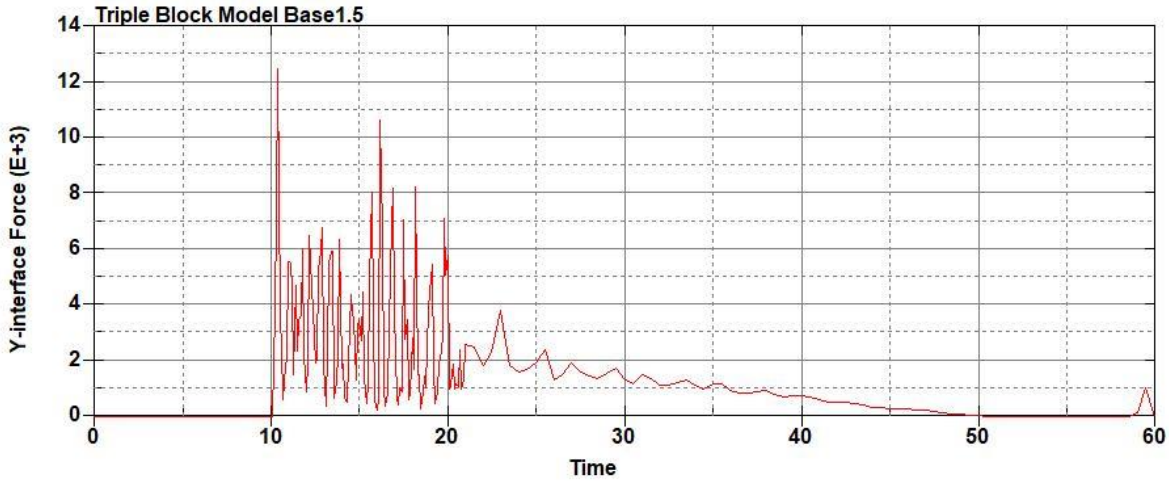


**Figure B-17: Base Run 1.5 Right Support Y-Interface Force (lbs) versus Time (ms) – 250 psi**

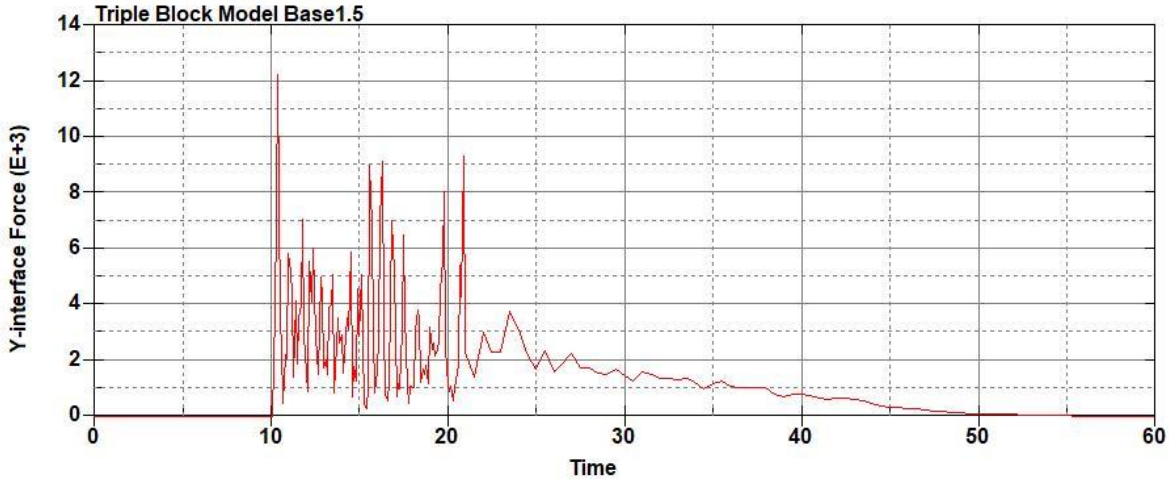


**Figure B-18: Base Run 1.5 Left Support Y-Interface Force (lbs) versus Time (ms) – 250 psi**

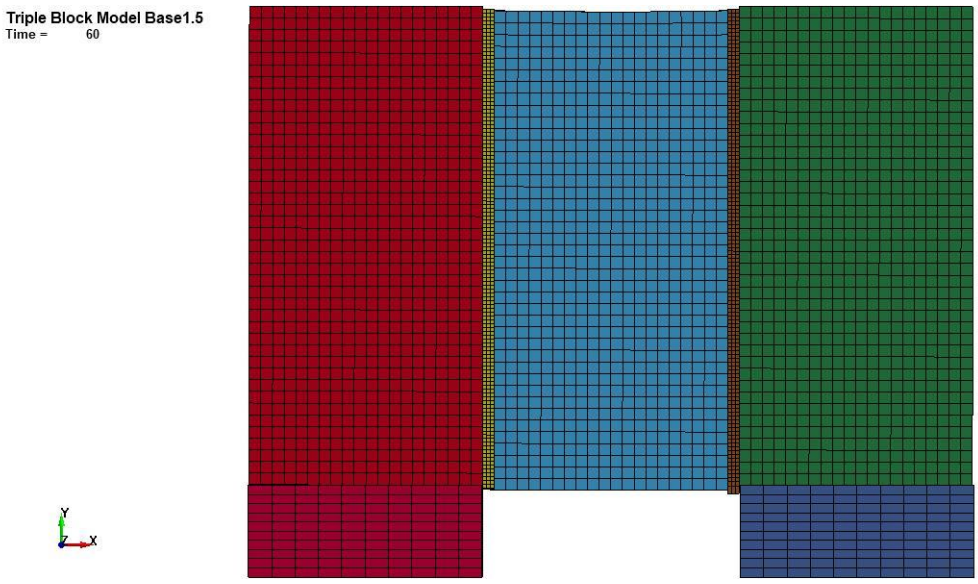


**Figure B-19: Last State at 60 Milliseconds for Base Run 1.5 – 250 psi**

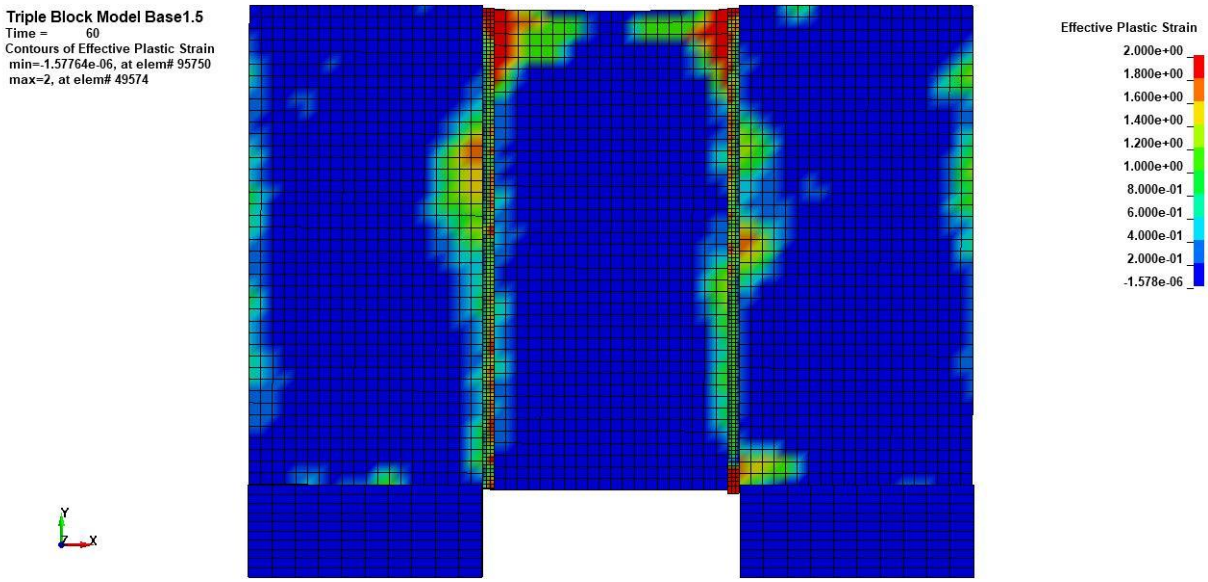


**Figure B-20: Effective Plastic Strain Fringe Plot for Last State at 60 Milliseconds for Base Run 1.5 – 250 psi**

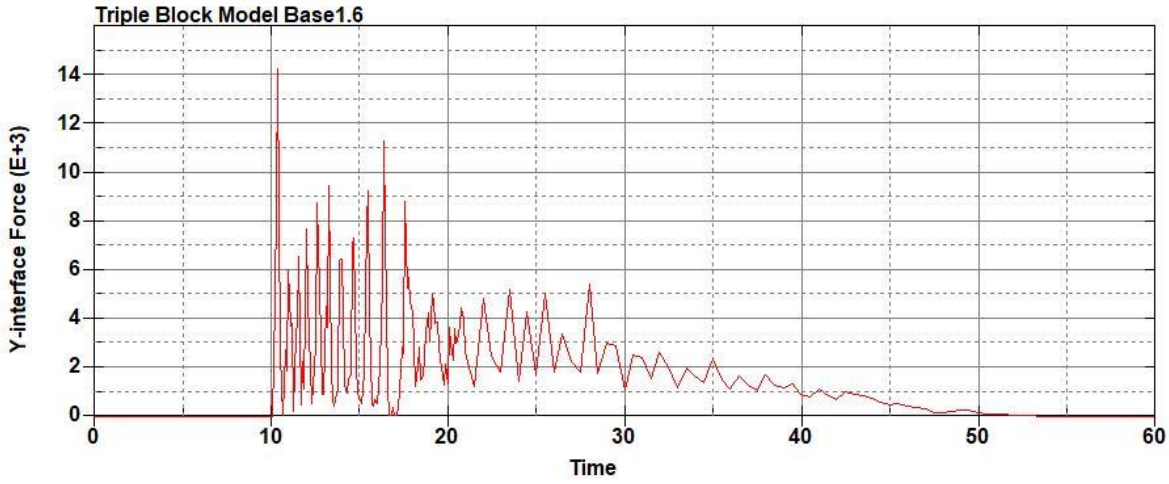


**Figure B-21: Base Run 1.6 Right Support Y-Interface Force (lbs) versus Time (ms) – 300 psi**

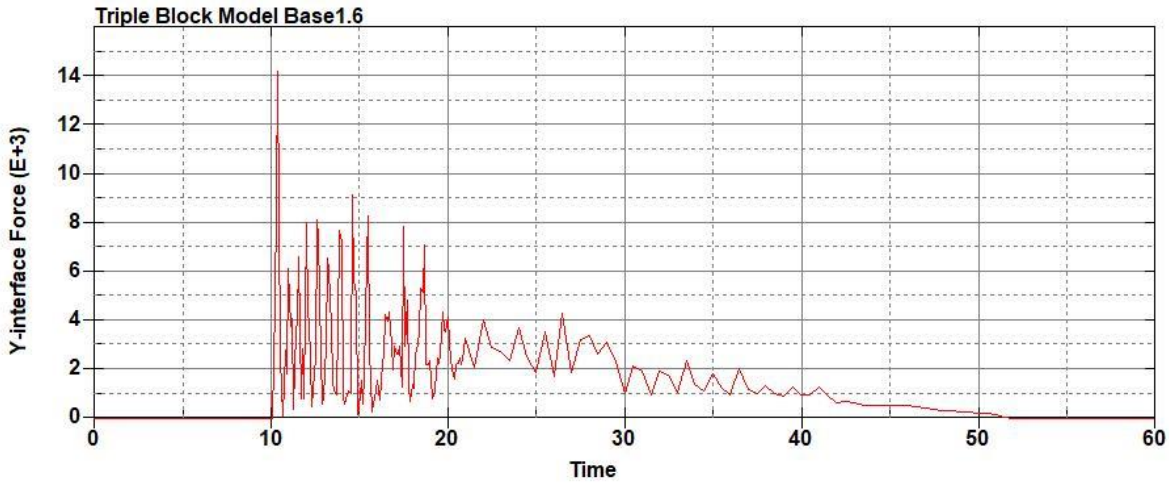


**Figure B-22: Base Run 1.6 Left Support Y-Interface Force (lbs) versus Time (ms) – 300 psi**

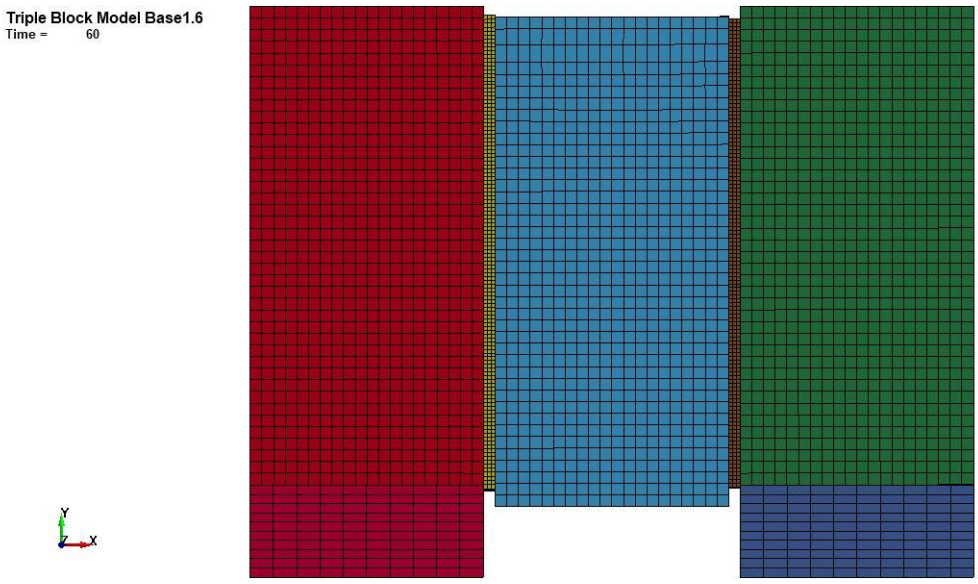


**Figure B-23: Last State at 60 Milliseconds for Base Run 1.6 – 300 psi**

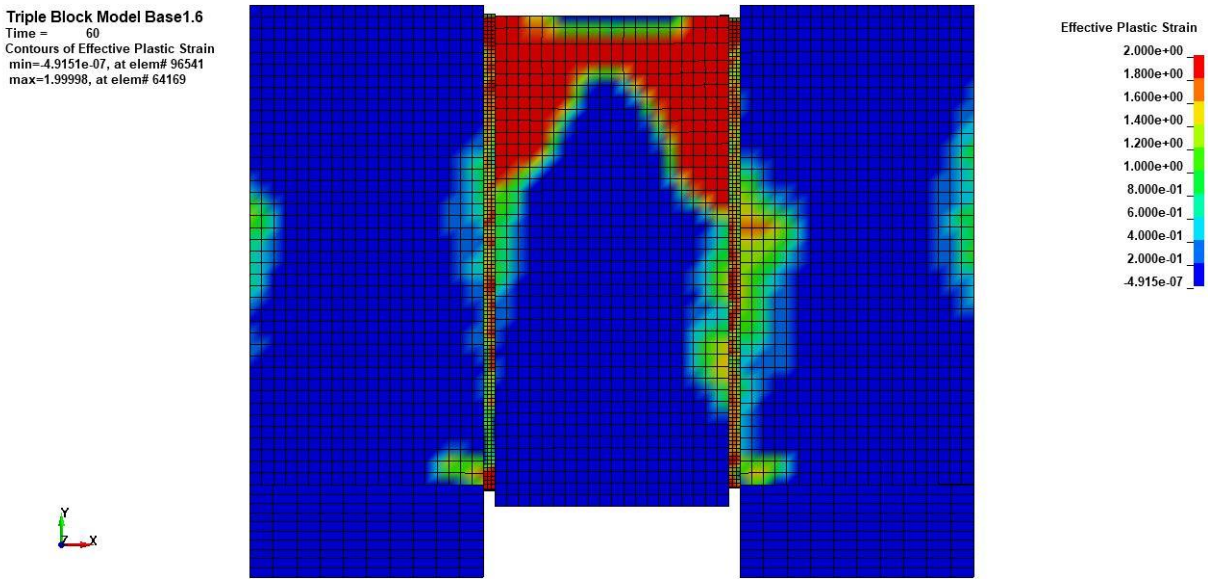


**Figure B-24: Effective Plastic Strain Fringe Plot for Last State at 60 Milliseconds for Base Run 1.6 – 300 psi**

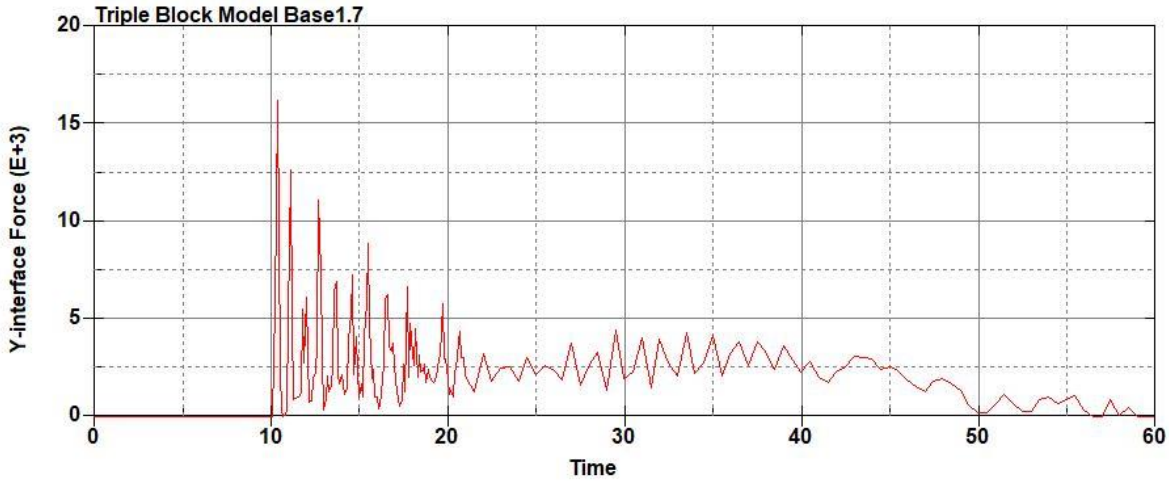


**Figure B-25: Base Run 1.7 Right Support Y-Interface Force (lbs) versus Time (ms) – 350 psi**

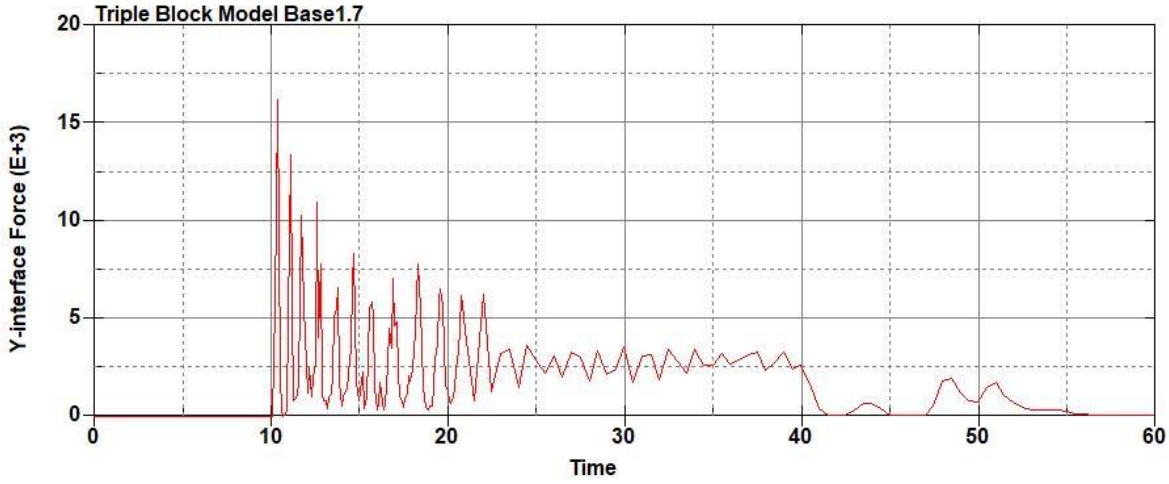


**Figure B-26: Base Run 1.7 Left Support Y-Interface Force (lbs) versus Time (ms) – 350 psi**

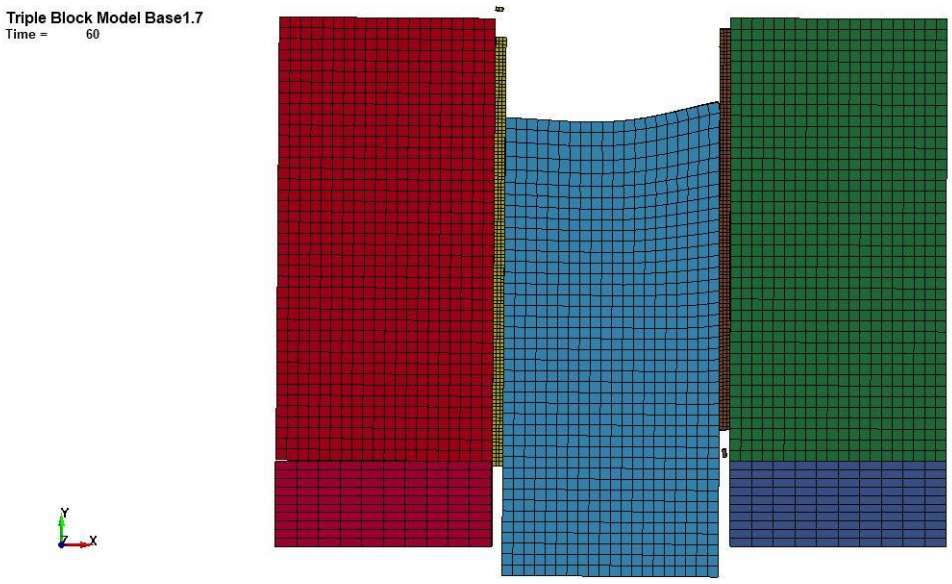


**Figure B-27: Last State at 60 Milliseconds for Base Run 1.7 – 350 psi**

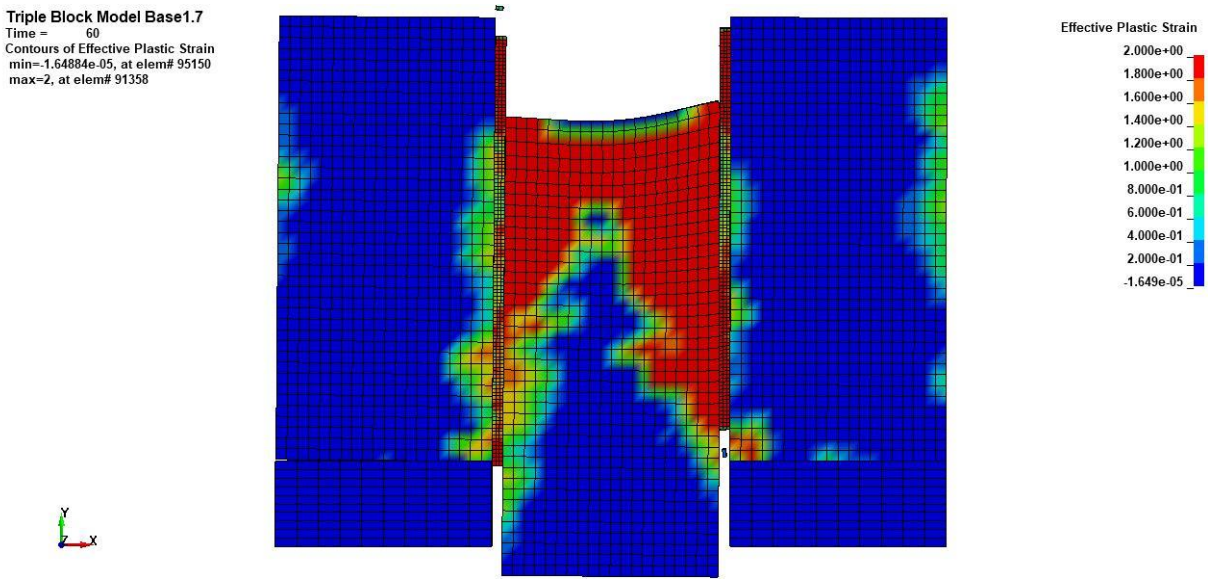


**Figure B-28: Effective Plastic Strain Fringe Plot for Last State at 60 Milliseconds for Base Run 1.7 – 350 psi**

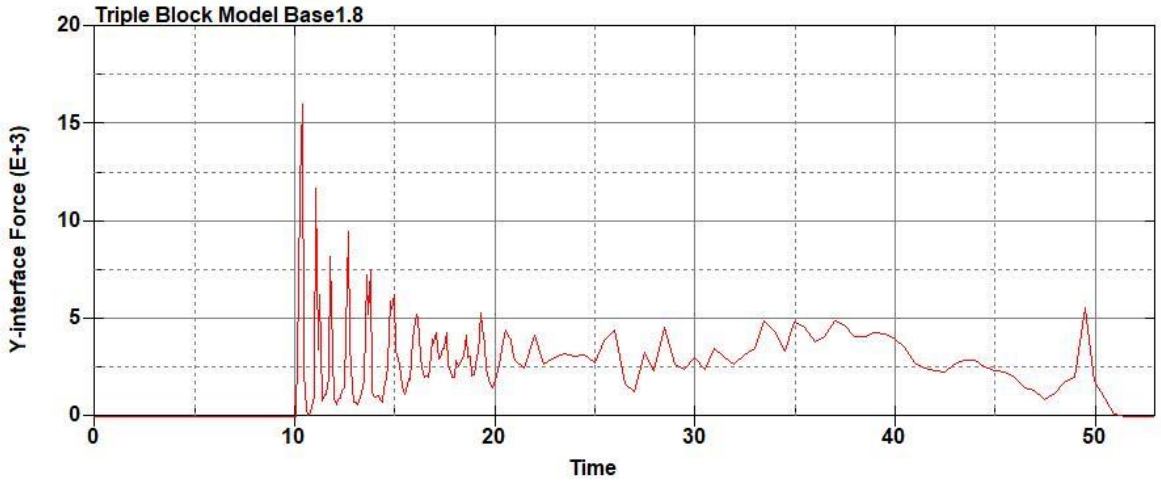


**Figure B-29: Base Run 1.8 Right Support Y-Interface Force (lbs) versus Time (ms) – 400 psi**

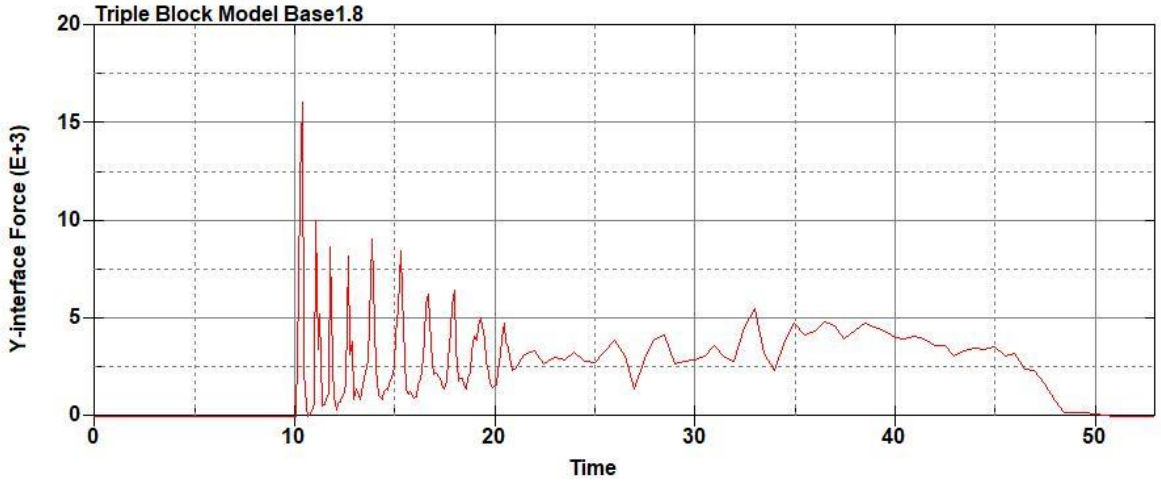


**Figure B-30: Base Run 1.8 Left Support Y-Interface Force (lbs) versus Time (ms) – 400 psi**

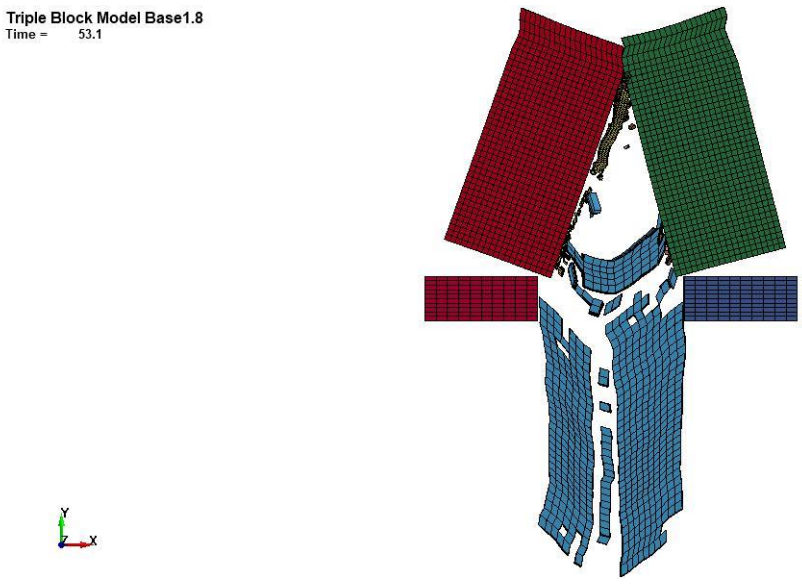


**Figure B-31: Last State at 53.1 Milliseconds for Base Run 1.8 – 400 psi**

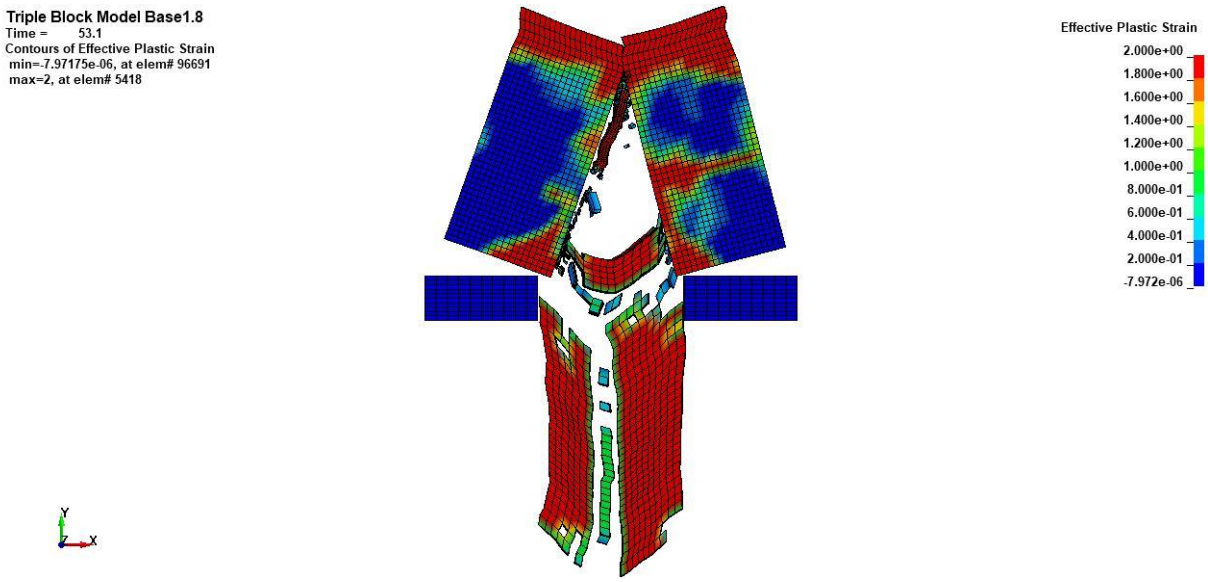


**Figure B-32: Effective Plastic Strain Fringe Plot for Last State at 53.1 Milliseconds for Base Run 1.8 – 400 psi**

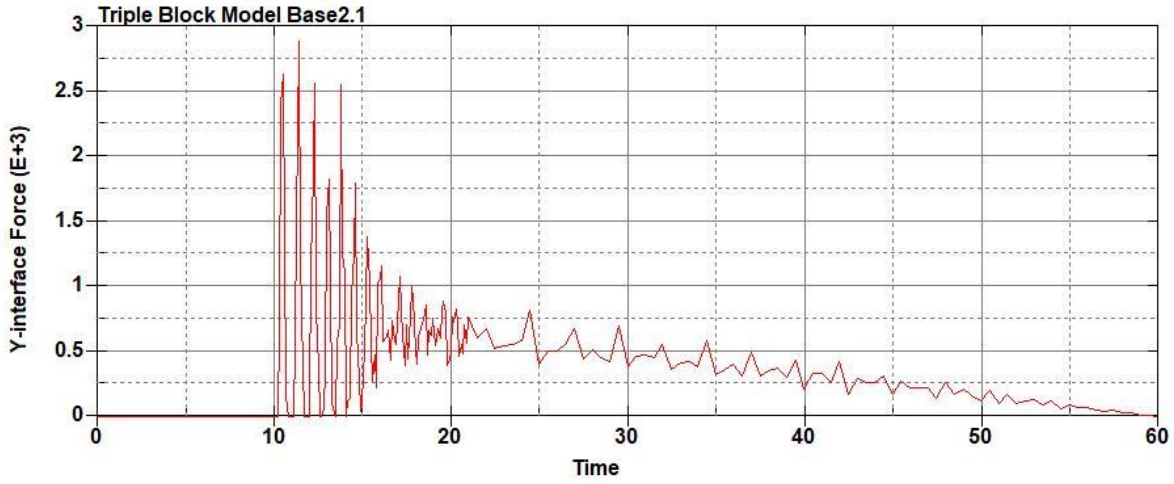


**Figure B-33: Base Run 2.1 Right Support Y-Interface Force (lbs) versus Time (ms) – 50 psi**

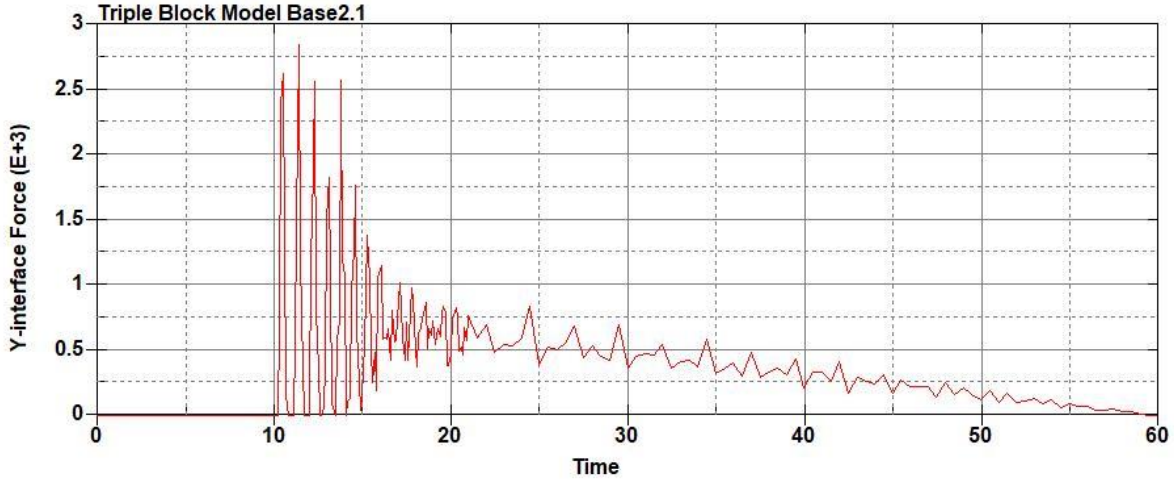


**Figure B-34: Base Run 2.1 Left Support Y-Interface Force (lbs) versus Time (ms) – 50 psi**

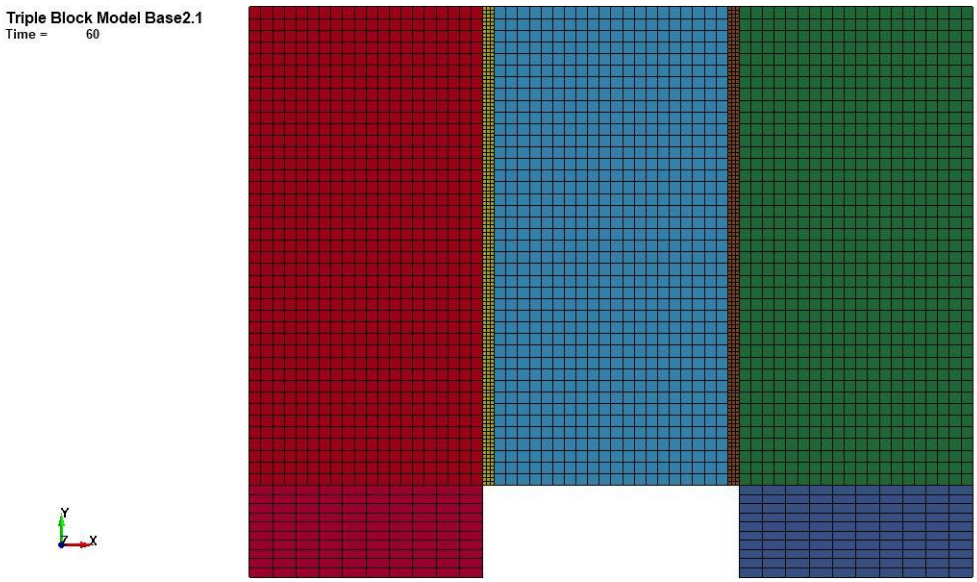


**Figure B-35: Last State at 60 Milliseconds for Base Run 2.1 – 50 psi**

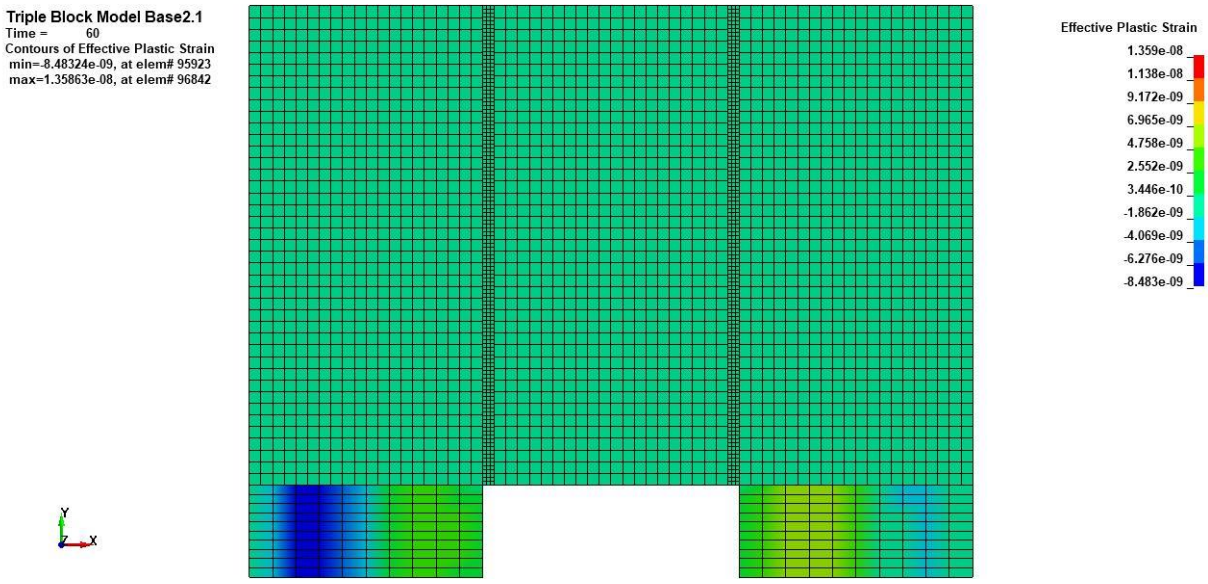


**Figure B-36: Effective Plastic Strain Fringe Plot for Last State at 60 Milliseconds for Base Run 2.1 – 50 psi**

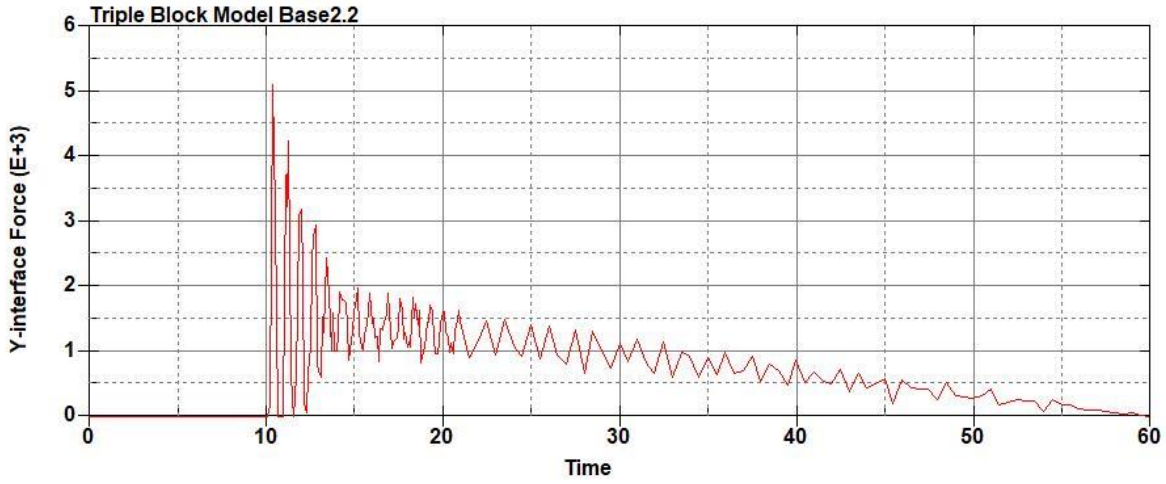


**Figure B-37: Base Run 2.2 Right Support Y-Interface Force (lbs) versus Time (ms) – 100 psi**

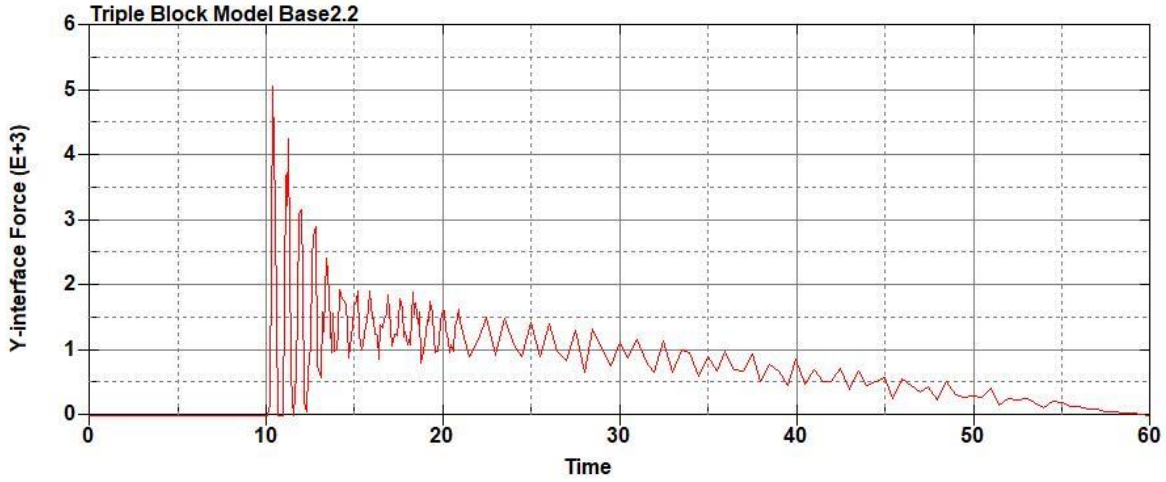


**Figure B-38: Base Run 2.2 Left Support Y-Interface Force (lbs) versus Time (ms) – 100 psi**

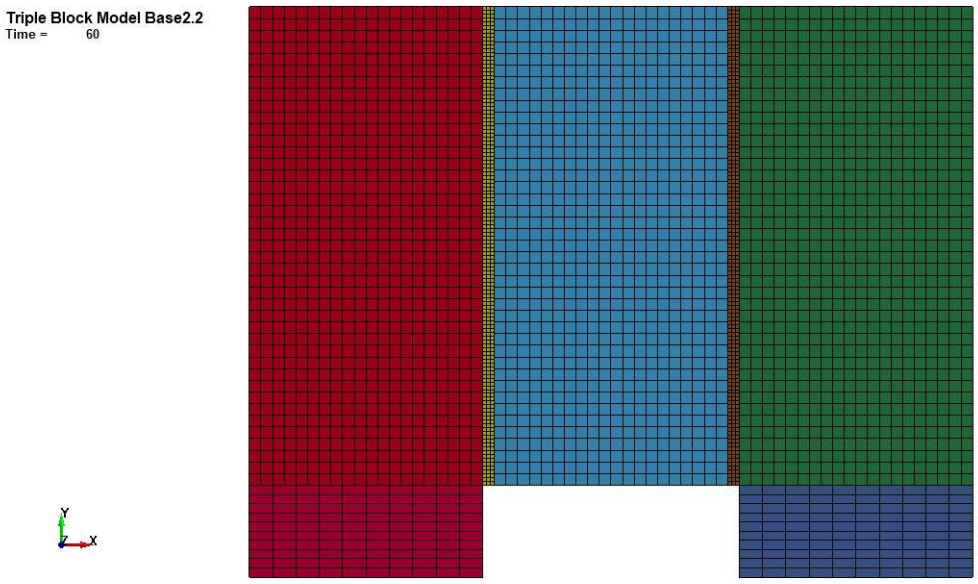


**Figure B-39: Last State at 60 Milliseconds for Base Run 2.2 – 100 psi**

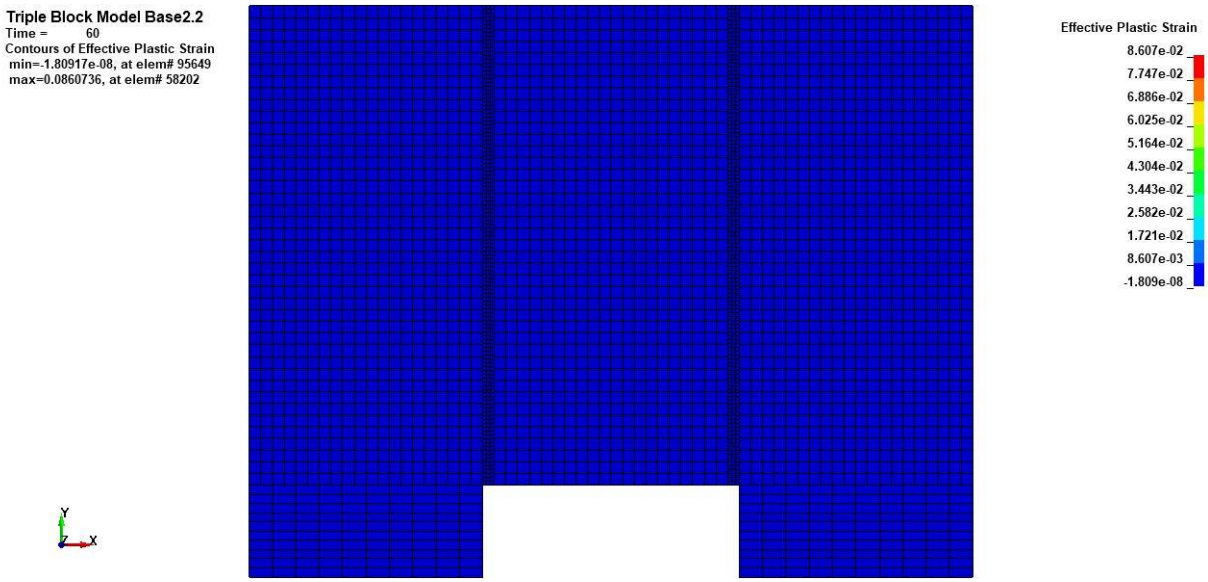


**Figure B-40: Effective Plastic Strain Fringe Plot for Last State at 60 Milliseconds for Base Run 2.2 – 100 psi**

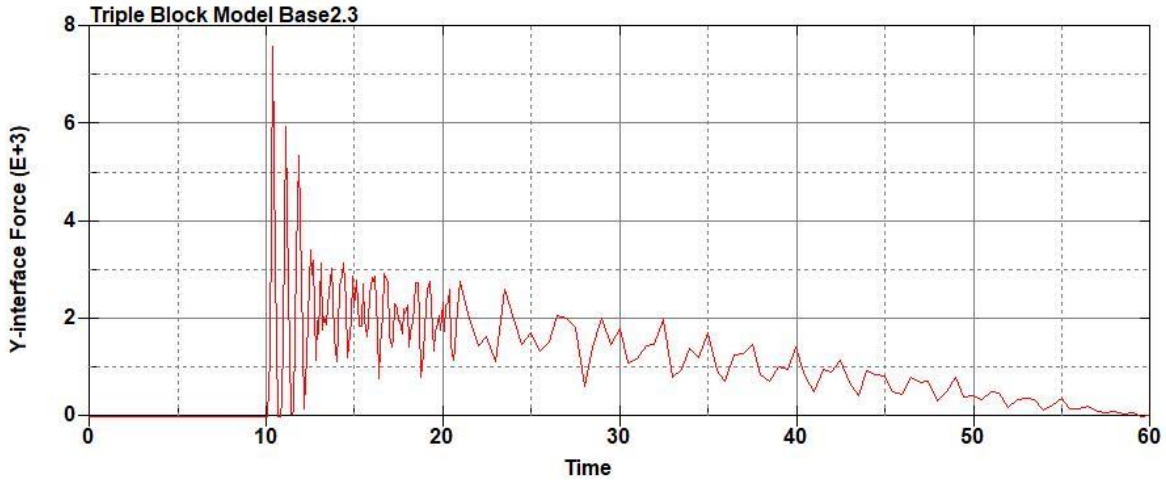


**Figure B-41: Base Run 2.3 Right Support Y-Interface Force (lbs) versus Time (ms) – 150 psi**

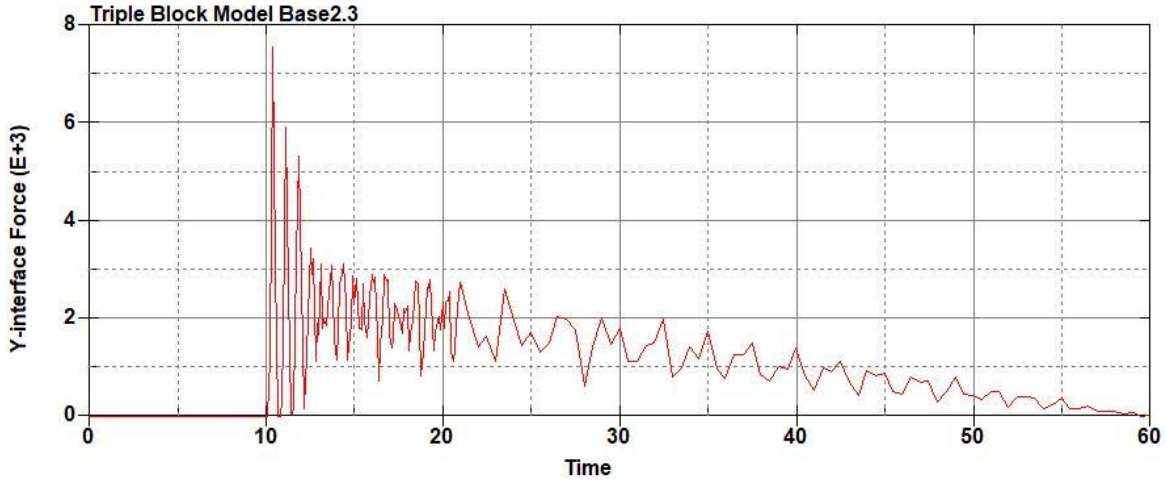


**Figure B-42: Base Run 2.3 Left Support Y-Interface Force (lbs) versus Time (ms) – 150 psi**

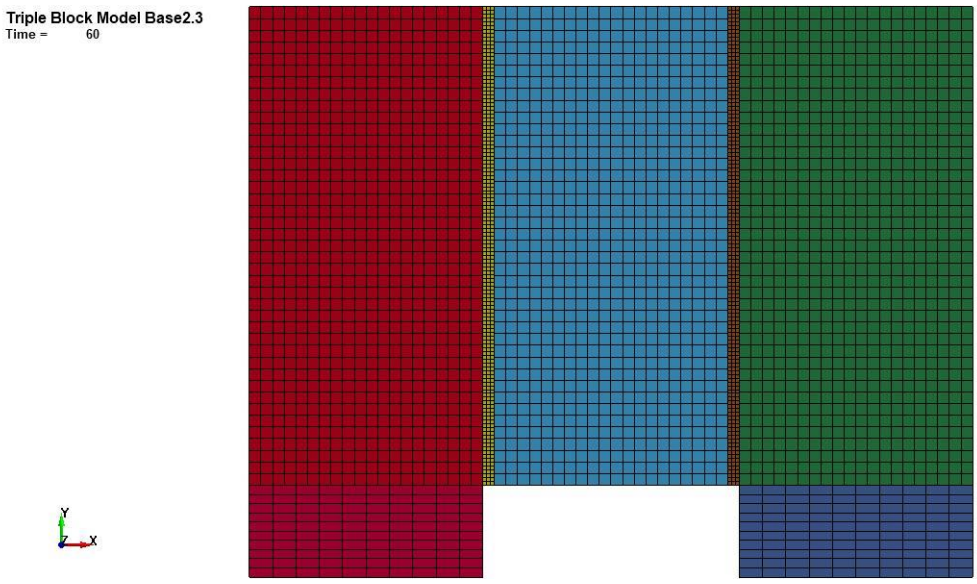


**Figure B-43: Last State at 60 Milliseconds for Base Run 2.3 – 150 psi**

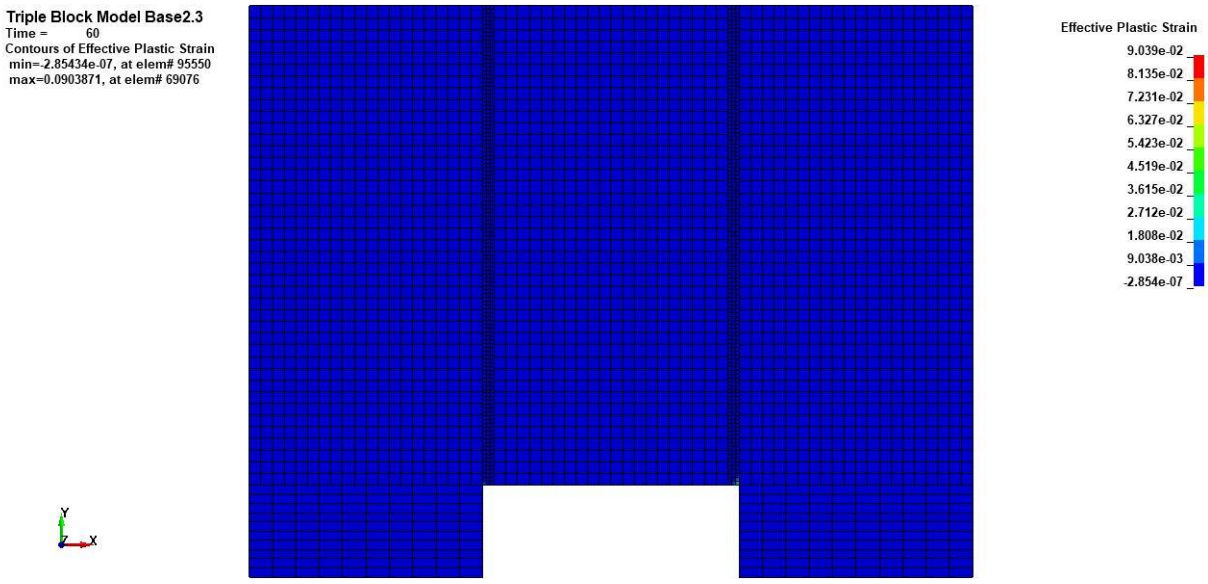


**Figure B-44: Effective Plastic Strain Fringe Plot for Last State at 60 Milliseconds for Base Run 2.3 – 150 psi**

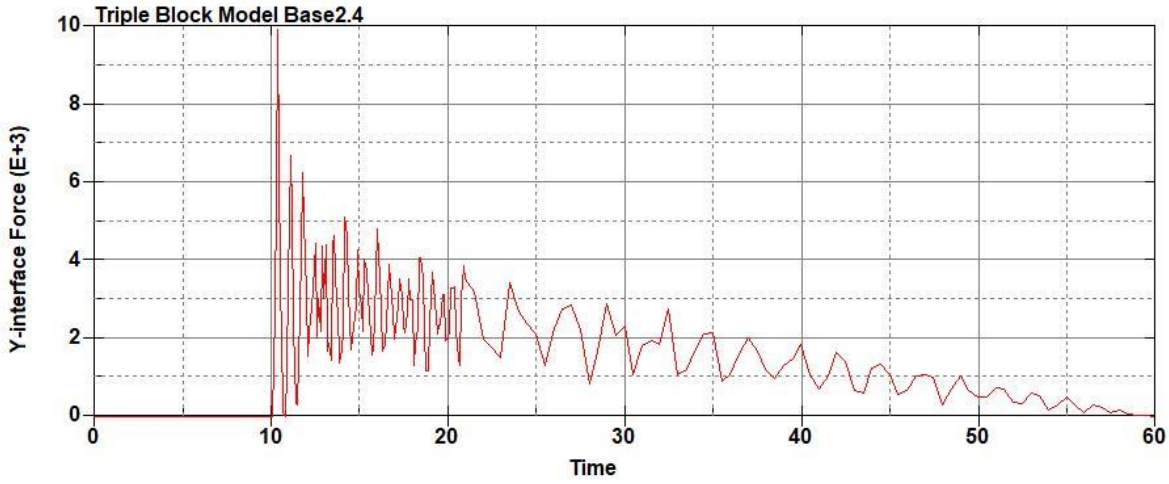


**Figure B-45: Base Run 2.4 Right Support Y-Interface Force (lbs) versus Time (ms) – 200 psi**

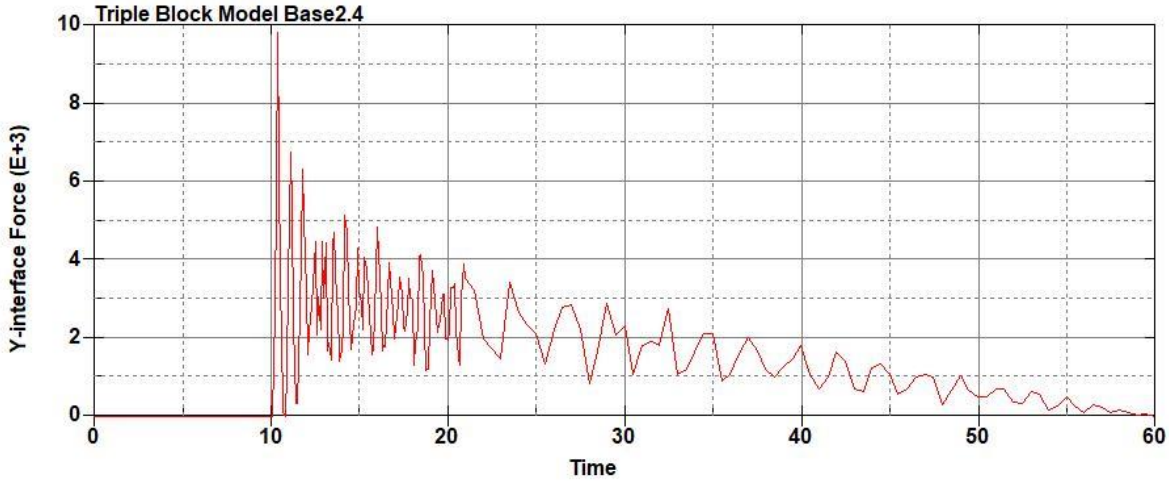


**Figure B-46: Base Run 2.4 Left Support Y-Interface Force (lbs) versus Time (ms) – 200 psi**

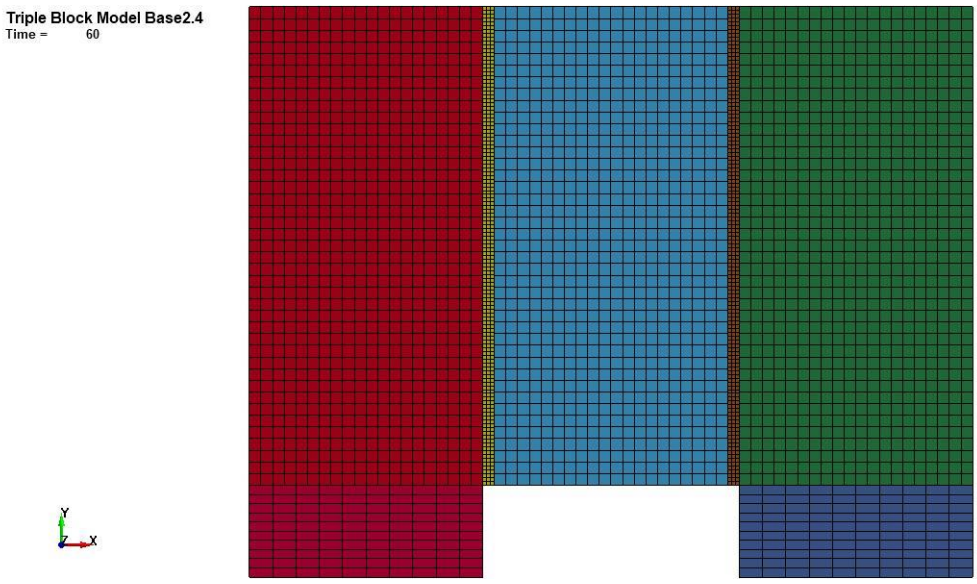


**Figure B-47: Last State at 60 Milliseconds for Base Run 2.4 – 200 psi**

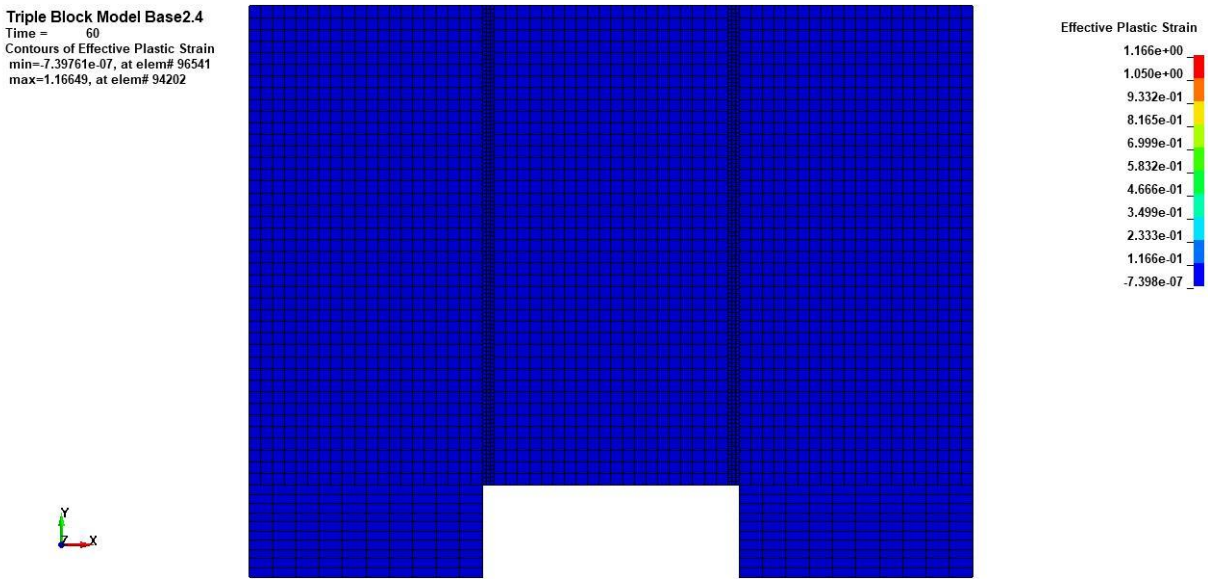


**Figure B-48: Effective Plastic Strain Fringe Plot for Last State at 60 Milliseconds for Base Run 2.4 – 200 psi**

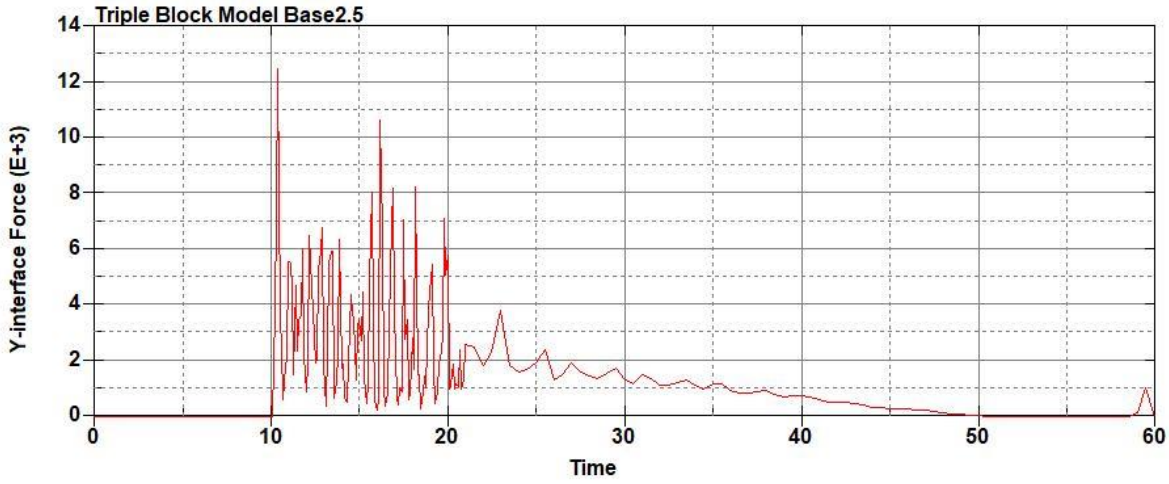


**Figure B-49: Base Run 2.5 Right Support Y-Interface Force (lbs) versus Time (ms) – 250 psi**

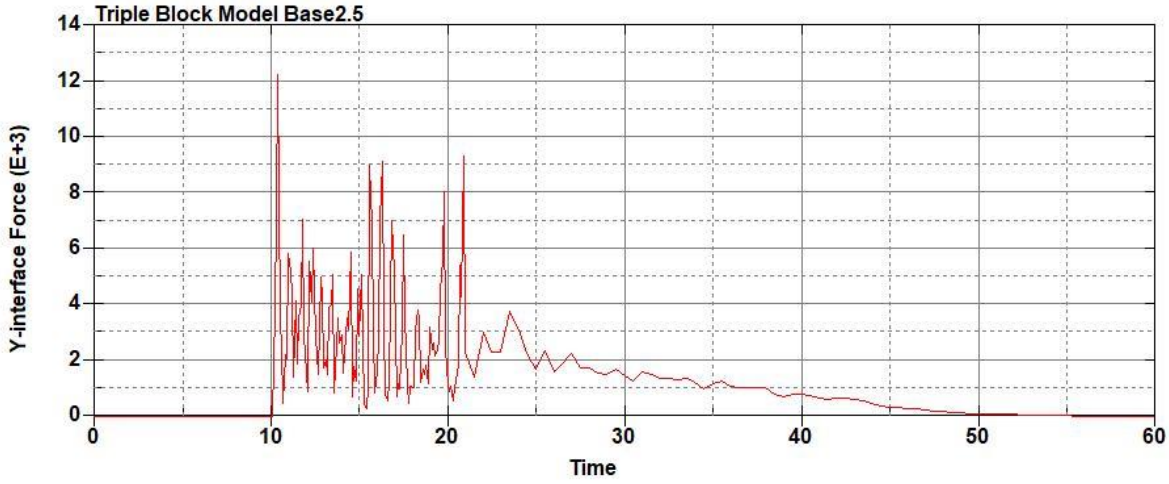


**Figure B-50: Base Run 2.5 Left Support Y-Interface Force (lbs) versus Time (ms) – 250 psi**

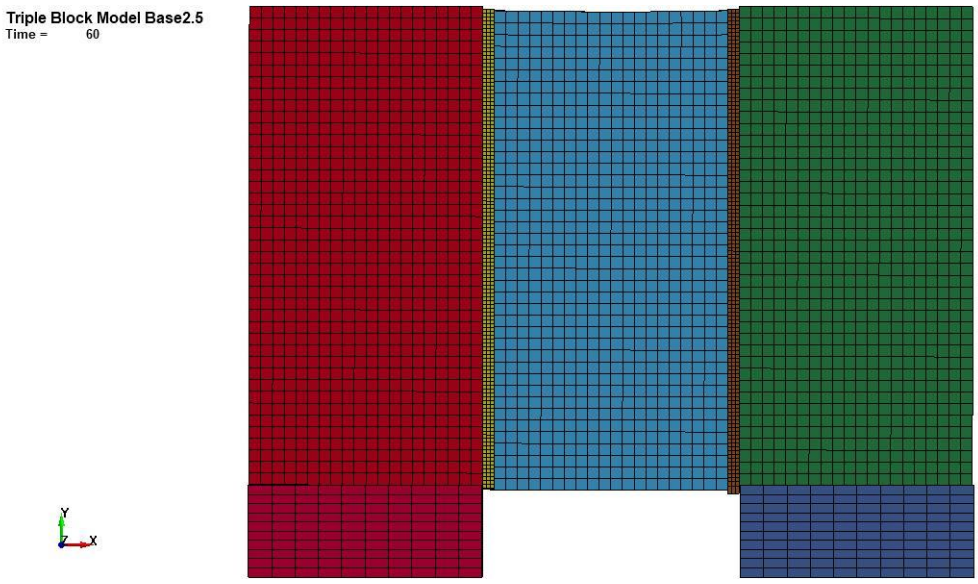


**Figure B-51: Last State at 60 Milliseconds for Base Run 2.5 – 250 psi**

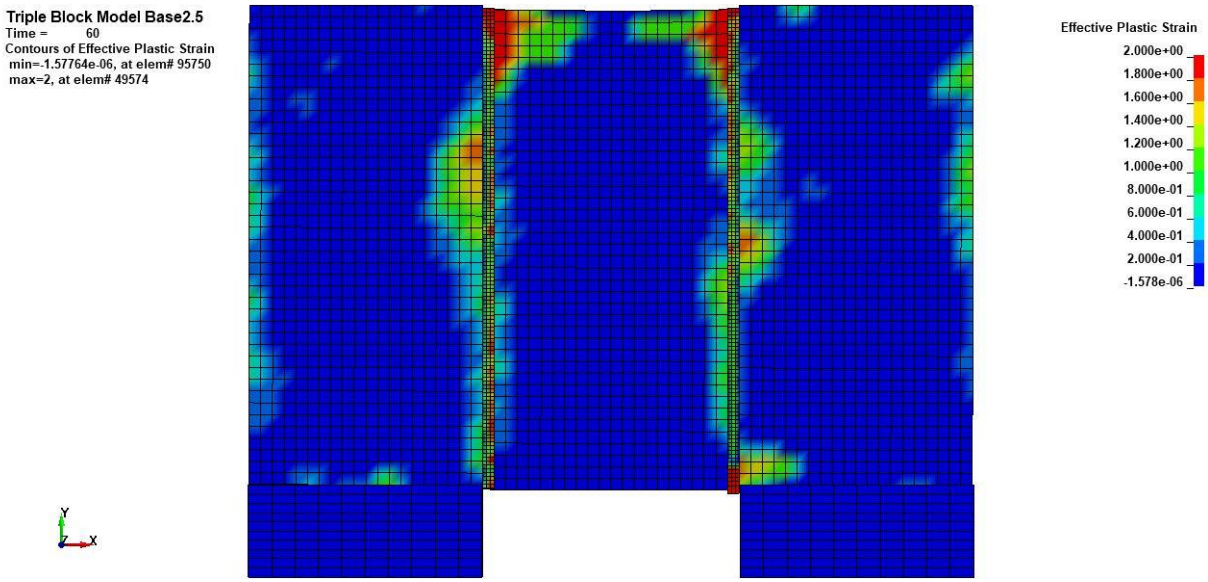


**Figure B-52: Effective Plastic Strain Fringe Plot for Last State at 60 Milliseconds for Base Run 2.5 – 250 psi**

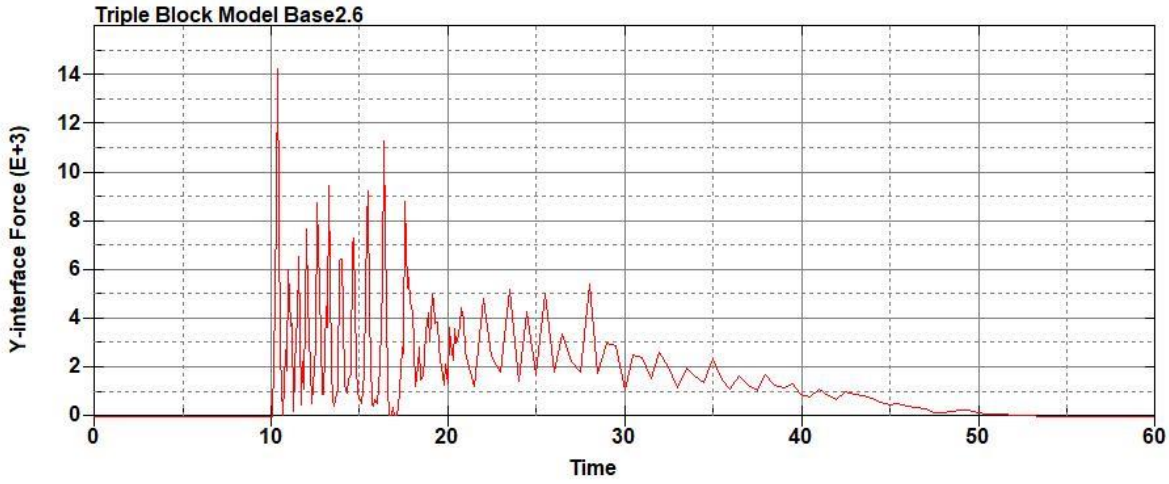


**Figure B-53: Base Run 2.6 Right Support Y-Interface Force (lbs) versus Time (ms) – 300 psi**

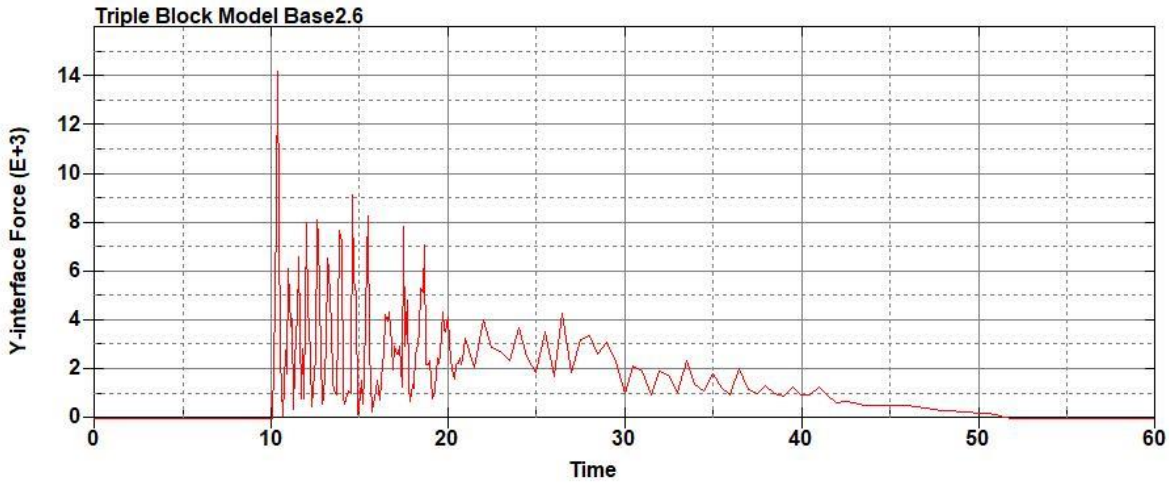


**Figure B-54: Base Run 2.6 Left Support Y-Interface Force (lbs) versus Time (ms) – 300 psi**

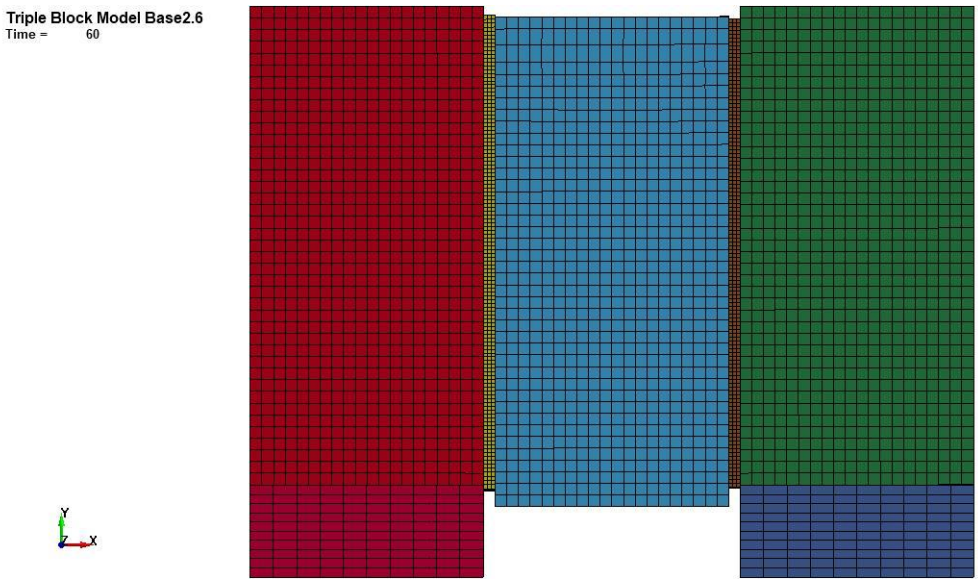


**Figure B-55: Last State at 60 Milliseconds for Base Run 2.6 – 300 psi**

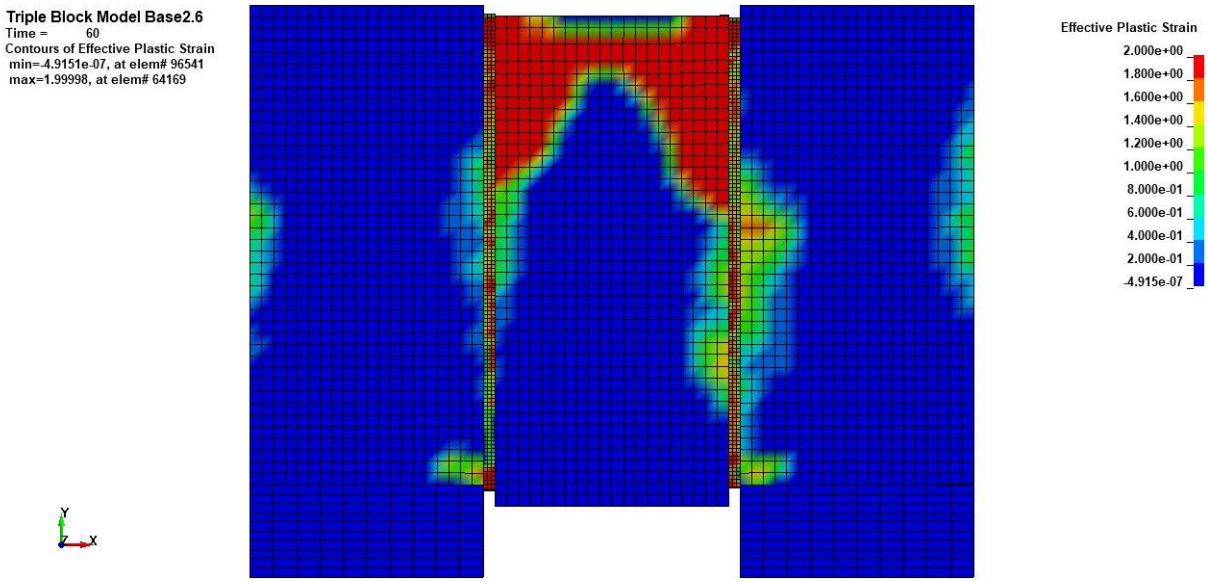


**Figure B-56: Effective Plastic Strain Fringe Plot for Last State at 60 Milliseconds for Base Run 2.6 – 300 psi**

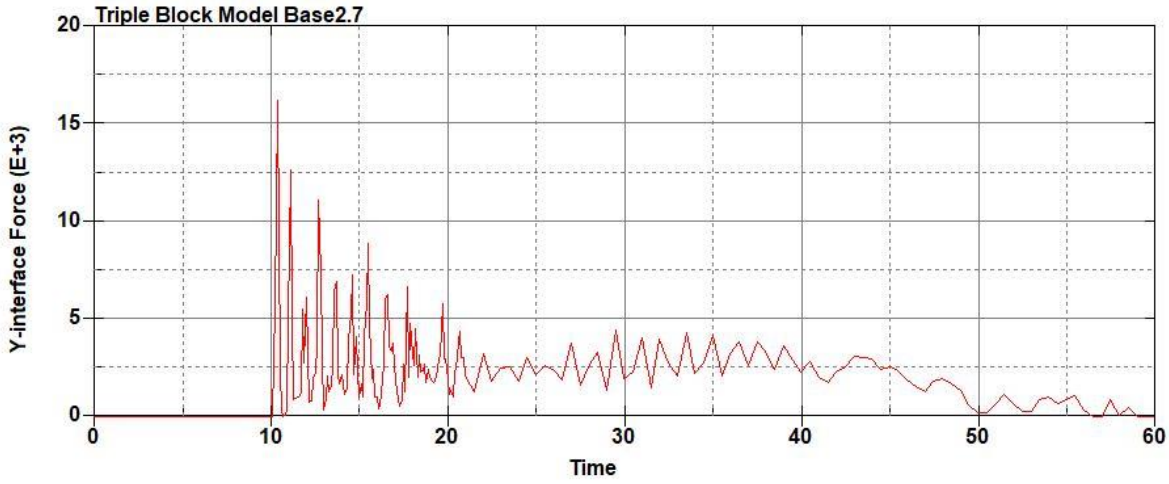


**Figure B-57: Base Run 2.7 Right Support Y-Interface Force (lbs) versus Time (ms) – 350 psi**

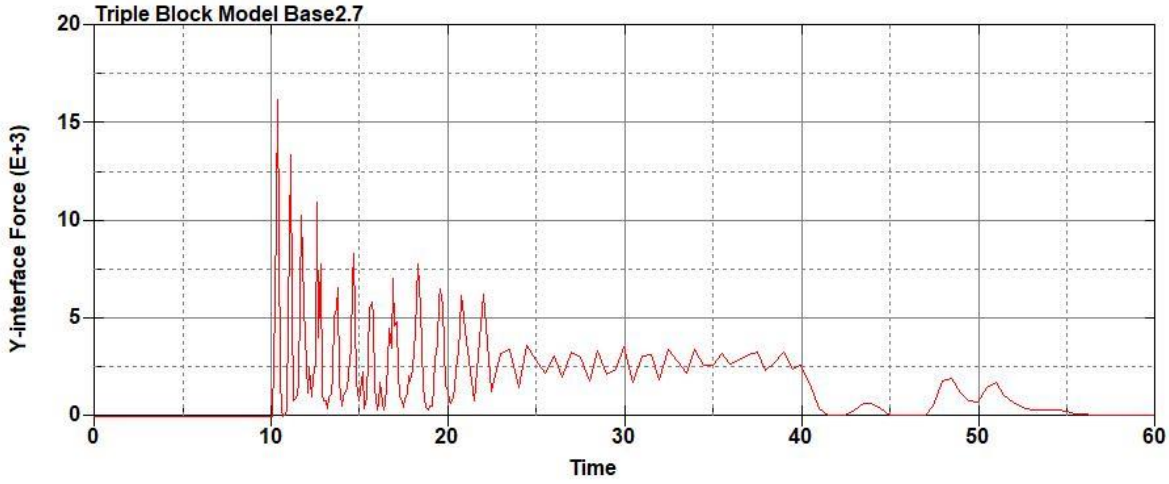


**Figure B-58: Base Run 2.7 Left Support Y-Interface Force (lbs) versus Time (ms) – 350 psi**

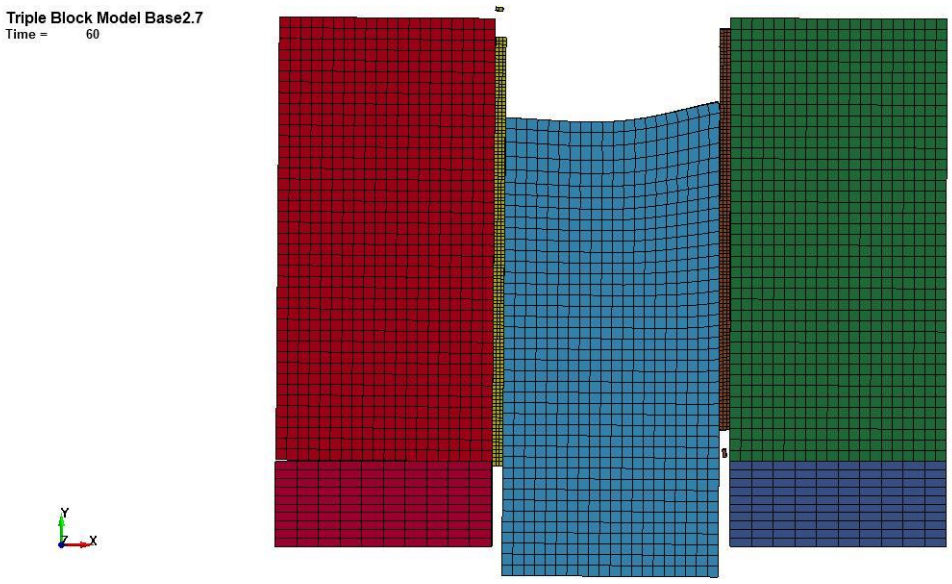


**Figure B-59: Last State at 60 Milliseconds for Base Run 2.7 – 350 psi**

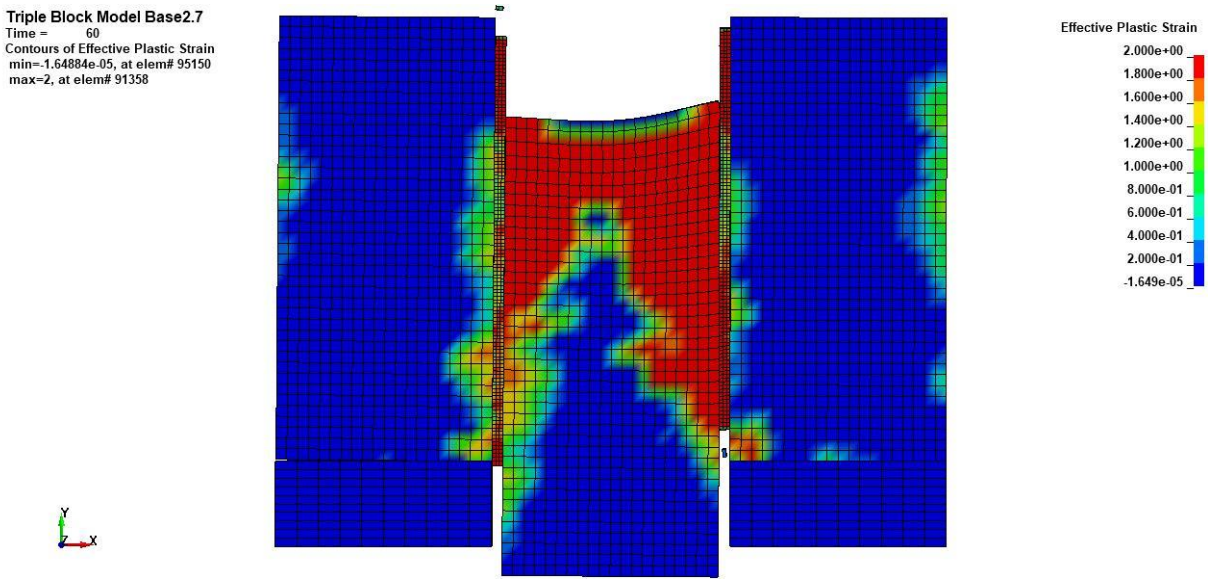


**Figure B-60: Effective Plastic Strain Fringe Plot for Last State at 60 Milliseconds for Base Run 2.7 – 350 psi**

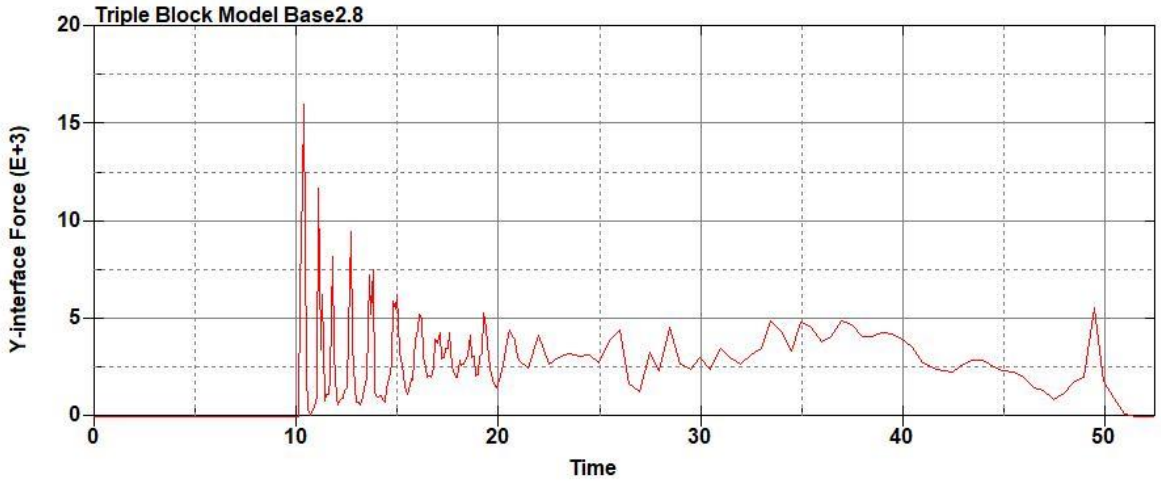


**Figure B-61: Base Run 2.8 Right Support Y-Interface Force (lbs) versus Time (ms) – 400 psi**

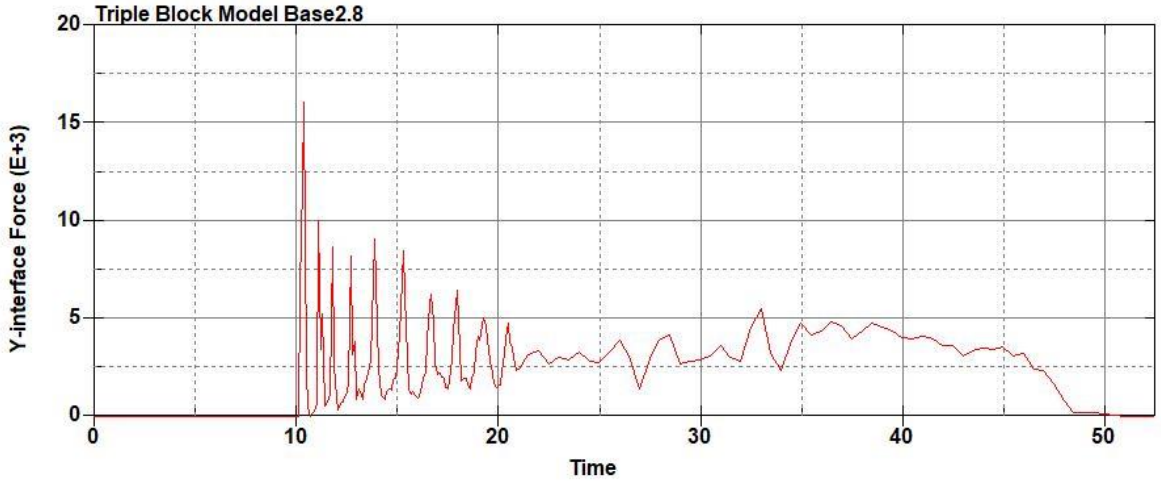


**Figure B-62: Base Run 2.8 Left Support Y-Interface Force (lbs) versus Time (ms) – 400 psi**


**Figure B-63: Last State at 52.6 Milliseconds for Base Run 2.8 – 400 psi**

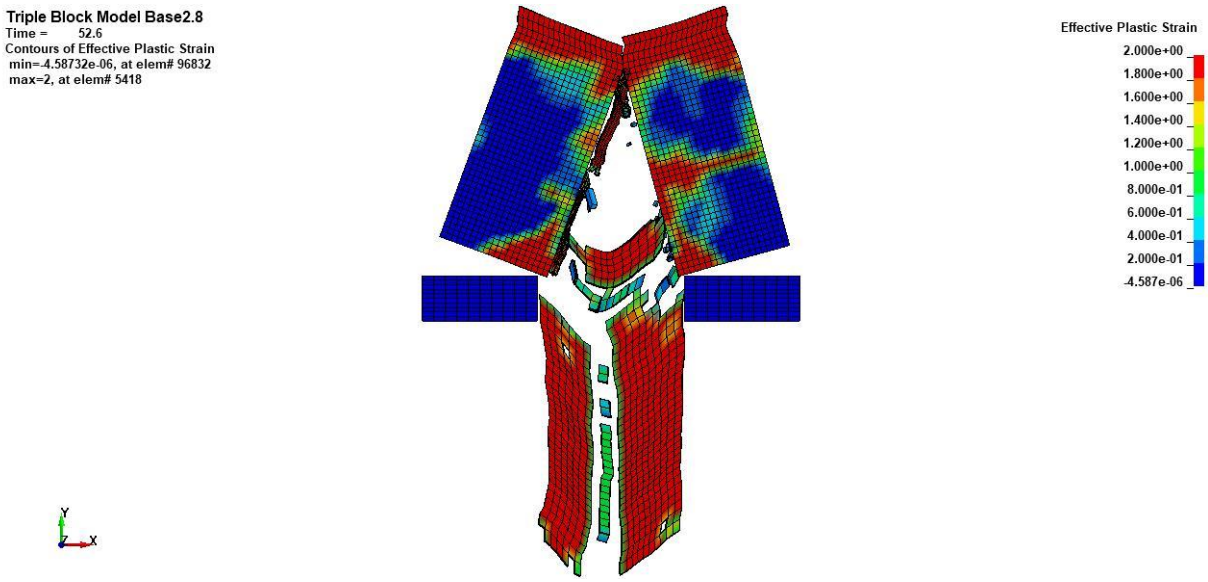


**Figure B-64: Effective Plastic Strain Fringe Plot for Last State at 52.6 Milliseconds for Base Run 2.8 – 400 psi**

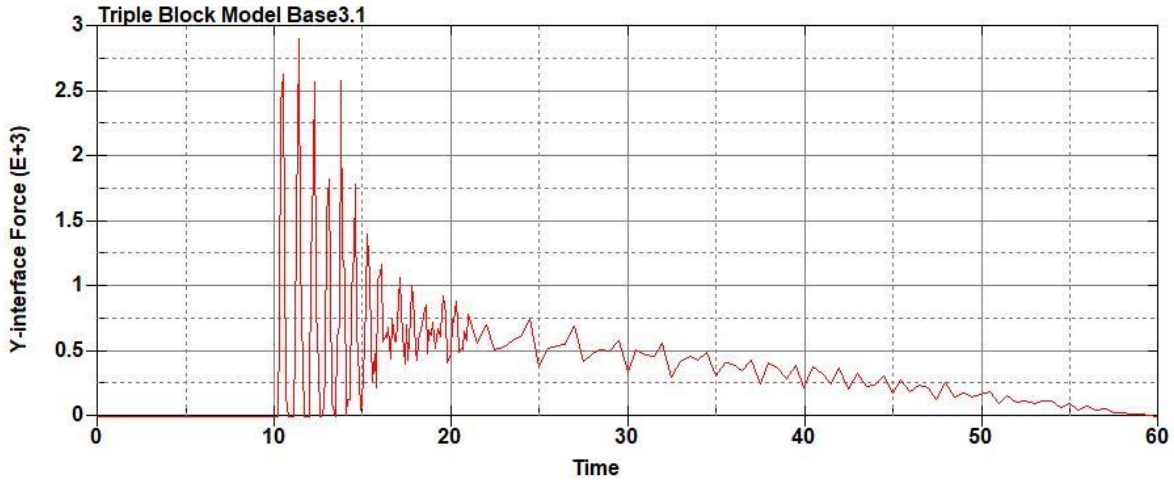


**Figure B-65: Base Run 3.1 Right Support Y-Interface Force (lbs) versus Time (ms) – 50 psi**

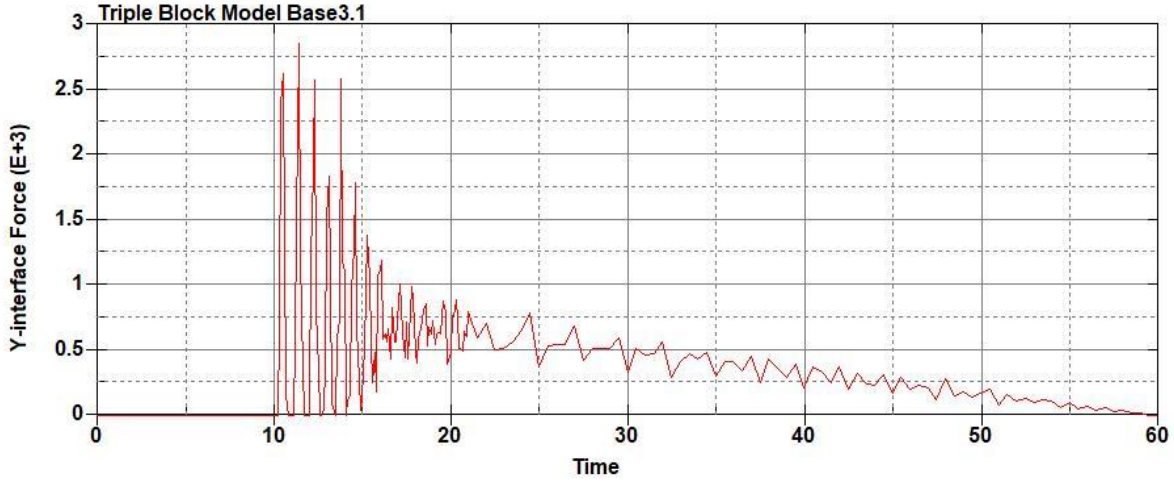


**Figure B-66: Base Run 3.1 Left Support Y-Interface Force (lbs) versus Time (ms) – 50 psi**

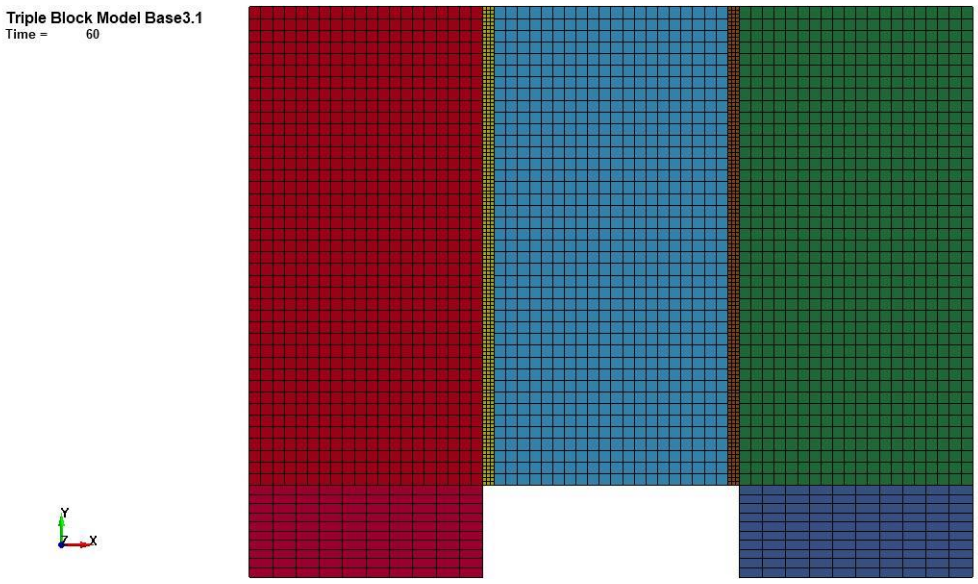


**Figure B-67: Last State at 60 Milliseconds for Base Run 3.1 – 50 psi**

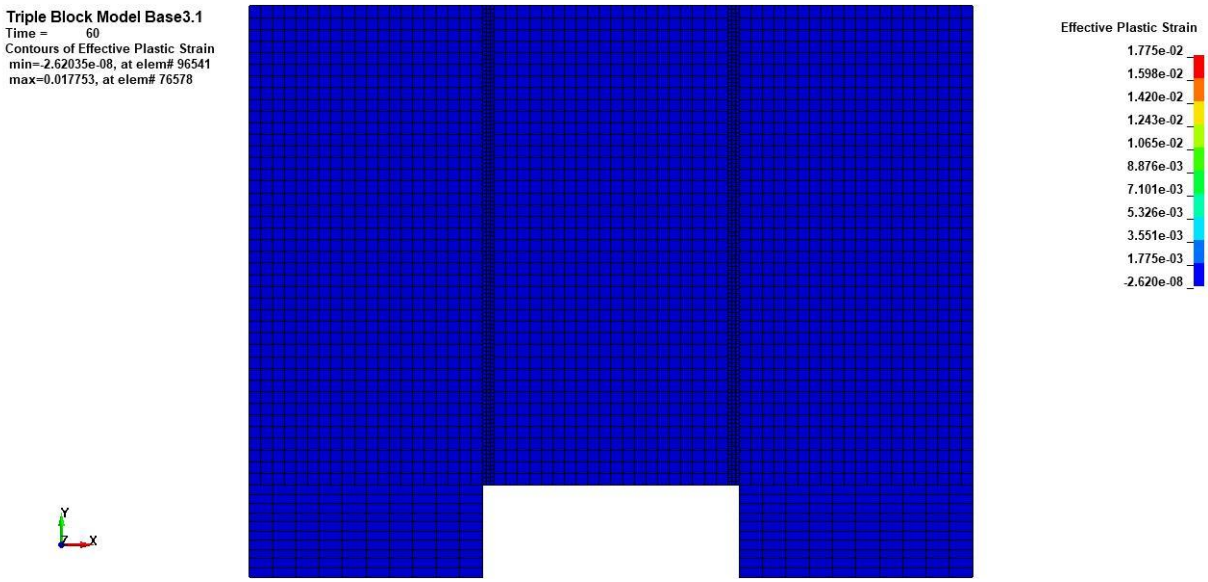


**Figure B-68: Effective Plastic Strain Fringe Plot for Last State at 60 Milliseconds for Base Run 3.1 – 50 psi**

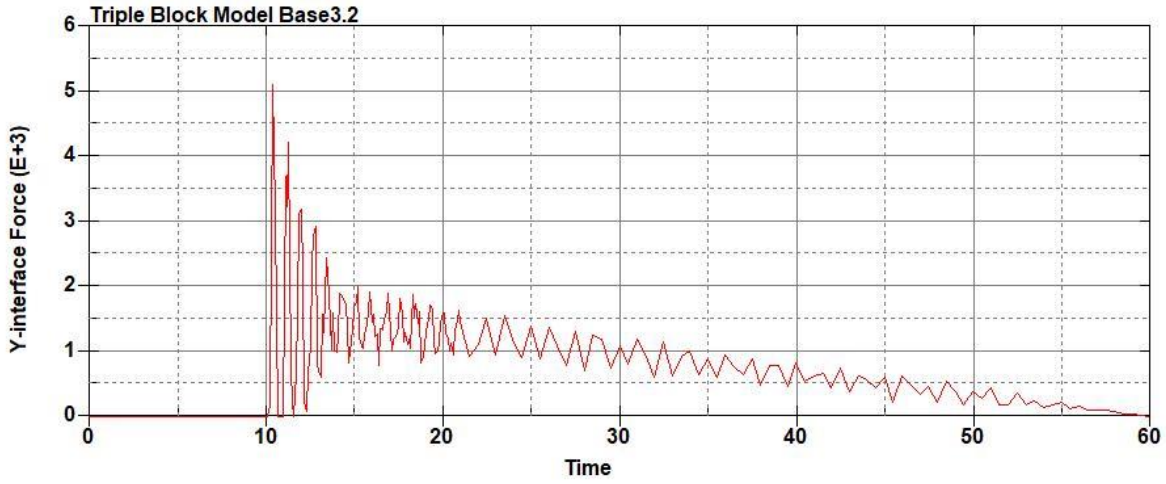


**Figure B-69: Base Run 3.2 Right Support Y-Interface Force (lbs) versus Time (ms) – 100 psi**

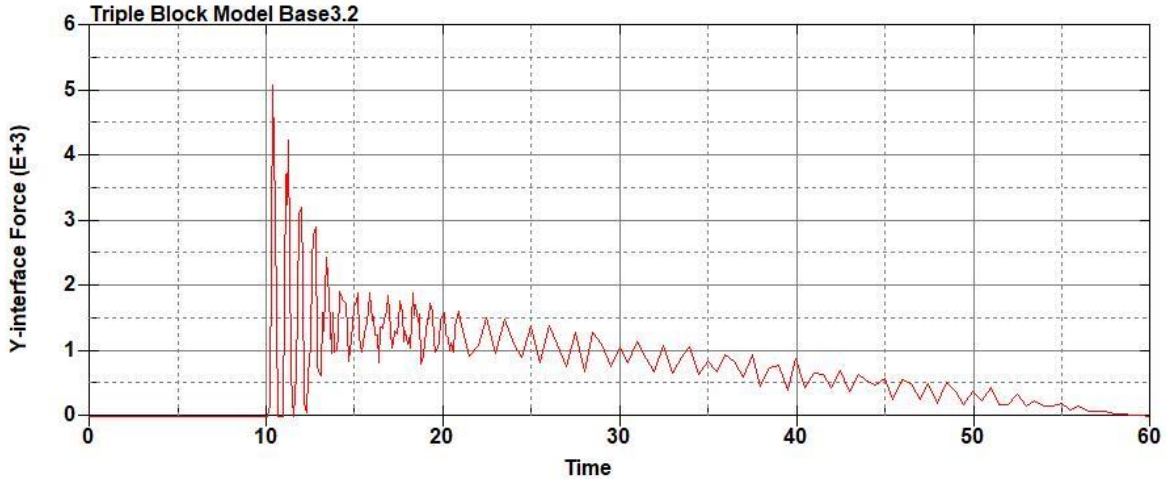


**Figure B-70: Base Run 3.2 Left Support Y-Interface Force (lbs) versus Time (ms) – 100 psi**

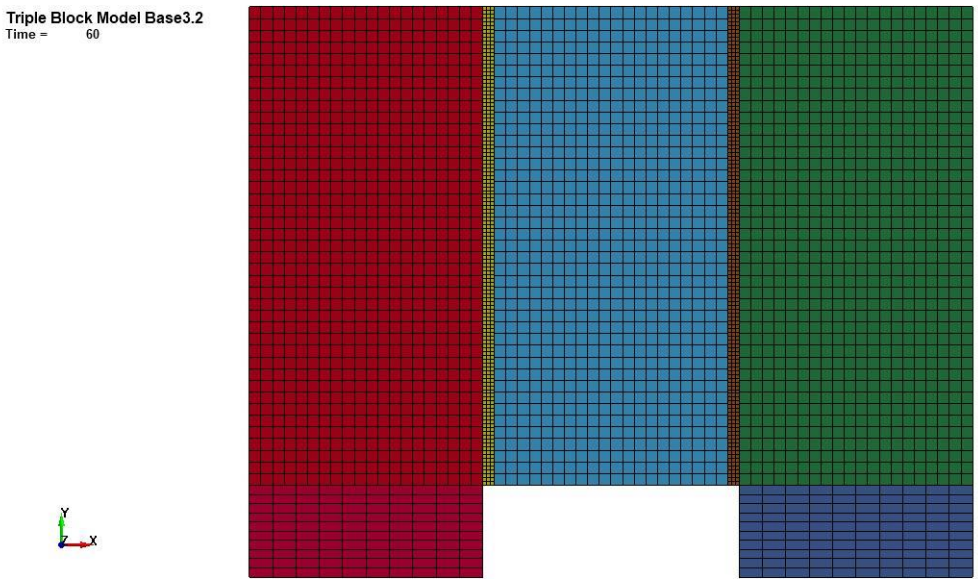


**Figure B-71: Last State at 60 Milliseconds for Base Run 3.2 – 100 psi**

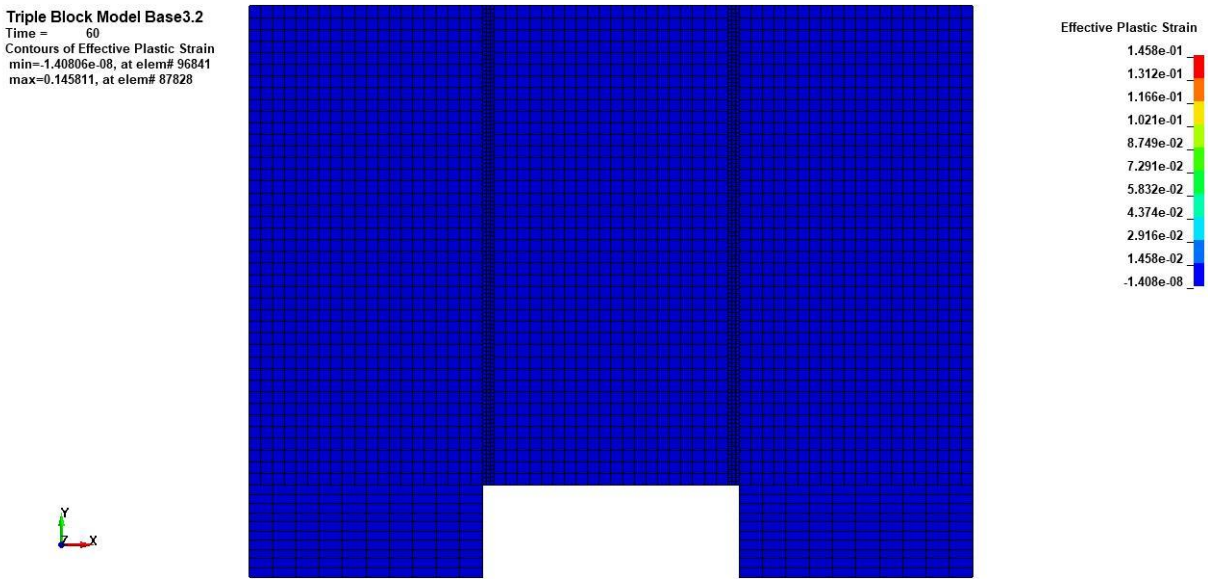


**Figure B-72: Effective Plastic Strain Fringe Plot for Last State at 60 Milliseconds for Base Run 3.2 – 100 psi**

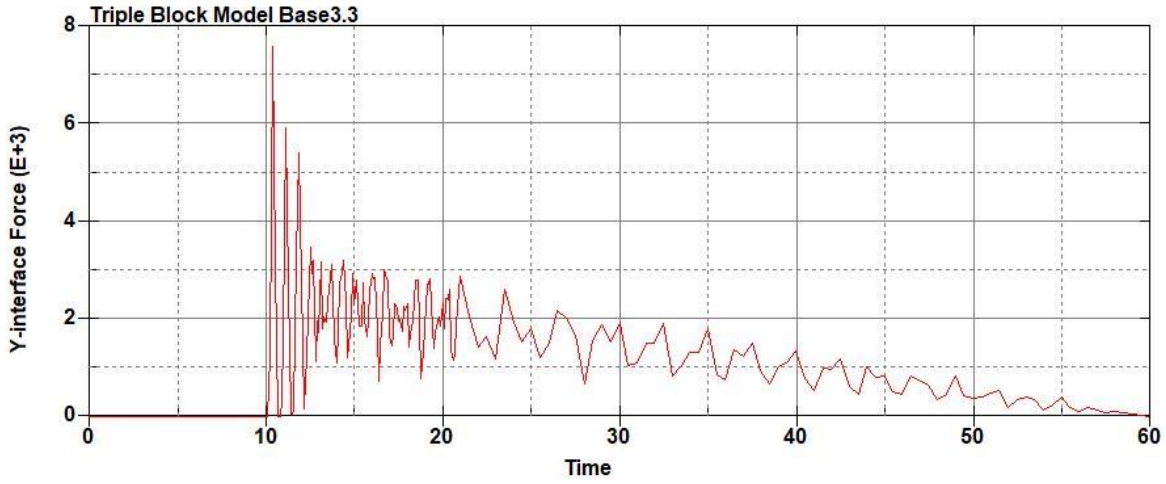


**Figure B-73: Base Run 3.3 Right Support Y-Interface Force (lbs) versus Time (ms) – 150 psi**

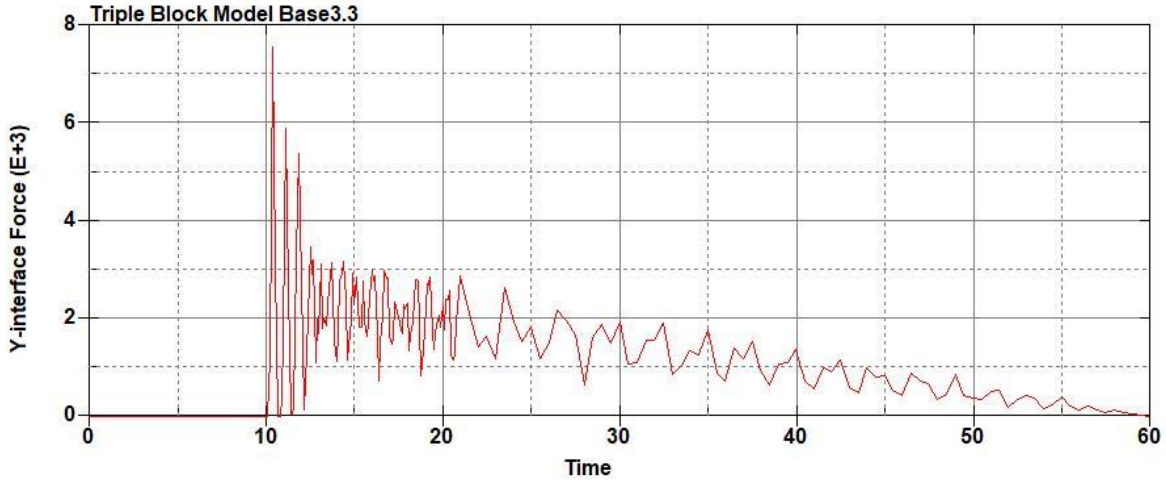


**Figure B-74: Base Run 3.5 Left Support Y-Interface Force (lbs) versus Time (ms) – 150 psi**

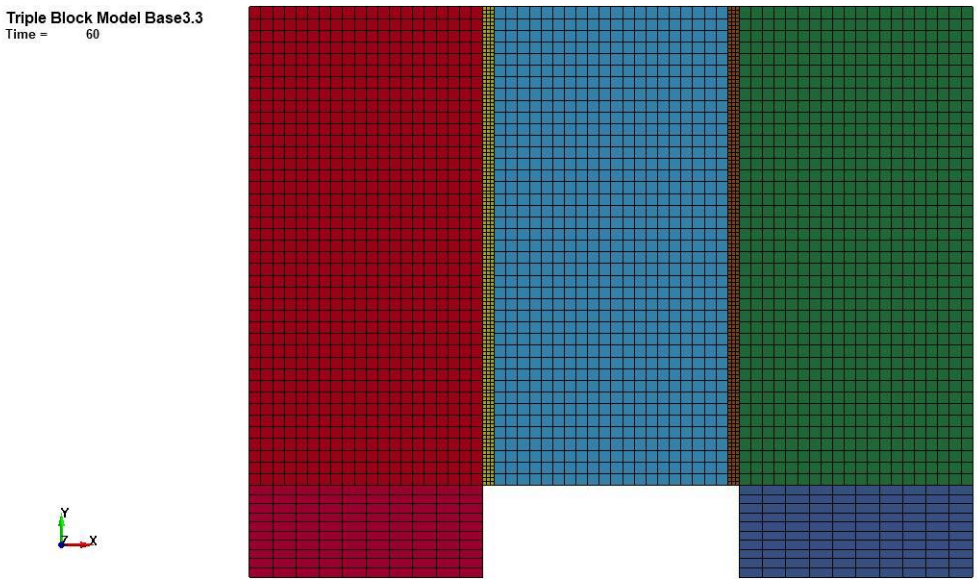


**Figure B-75: Last State at 60 Milliseconds for Base Run 3.3 – 150 psi**

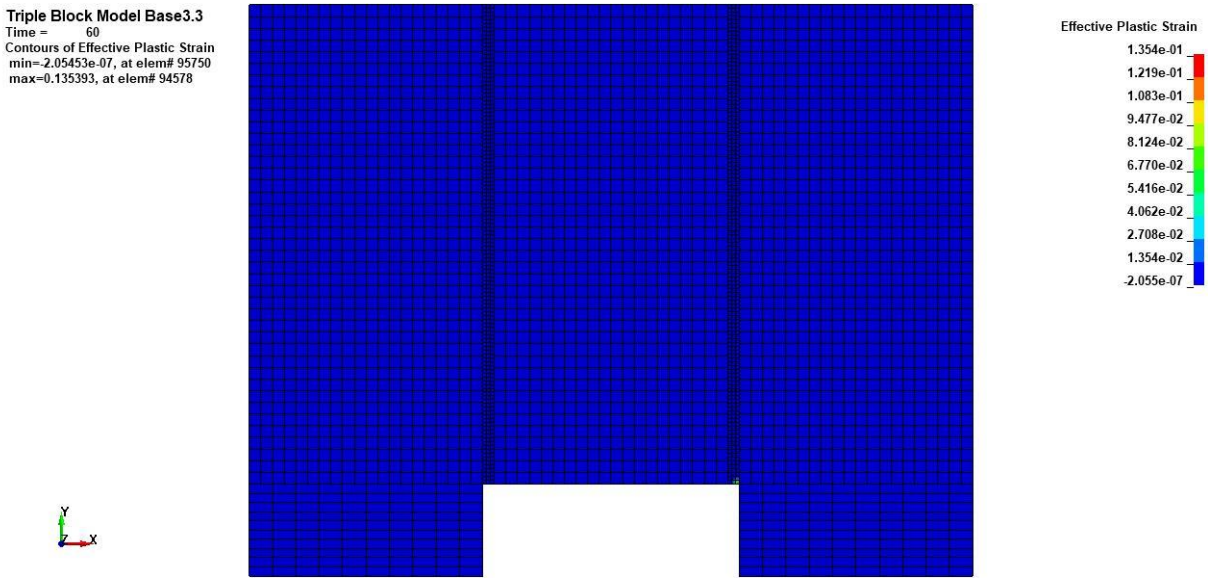


**Figure B-76: Effective Plastic Strain Fringe Plot for Last State at 60 Milliseconds for Base Run 3.3 – 150 psi**

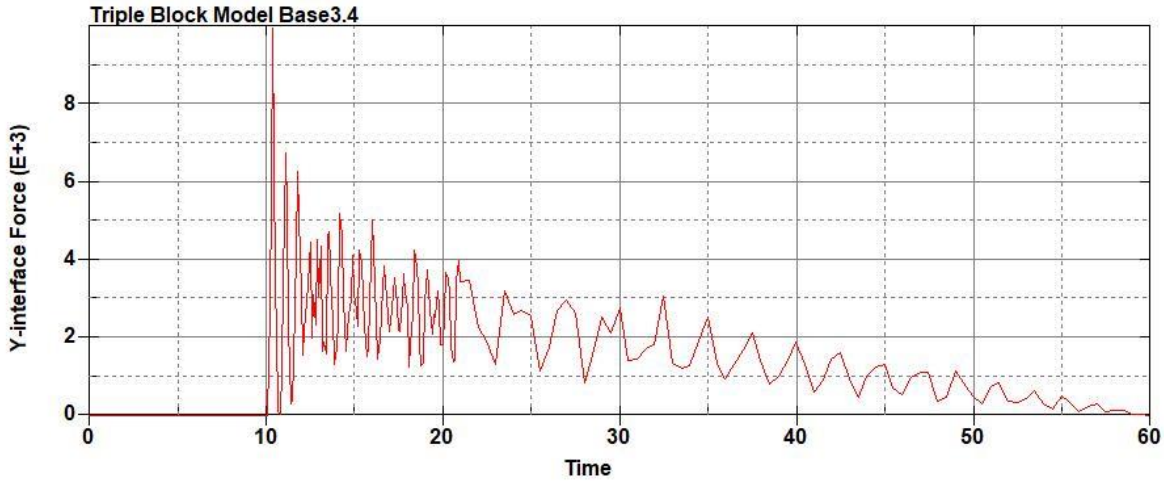


**Figure B-77: Base Run 3.4 Right Support Y-Interface Force (lbs) versus Time (ms) – 200 psi**

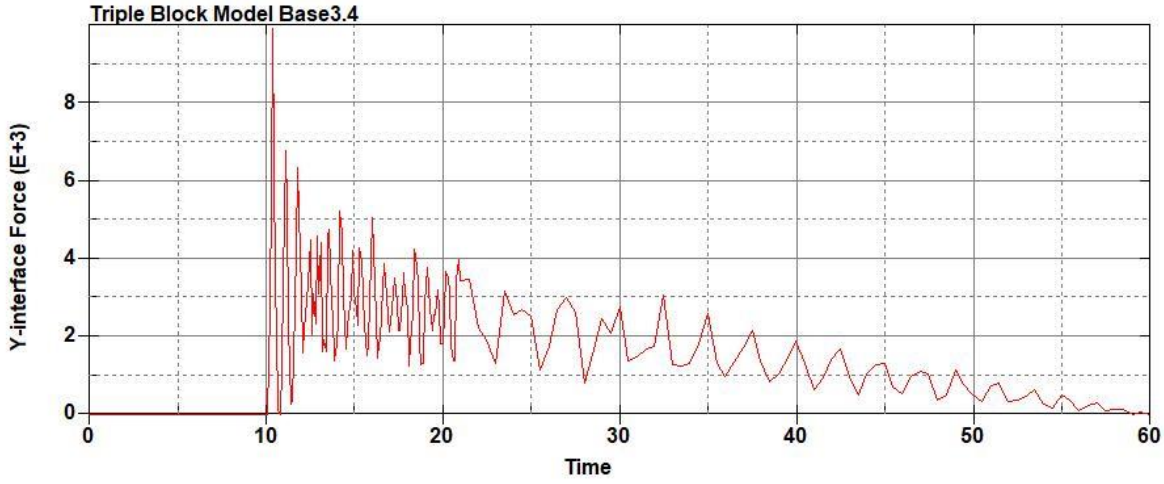


**Figure B-78: Base Run 3.4 Left Support Y-Interface Force (lbs) versus Time (ms) – 200 psi**

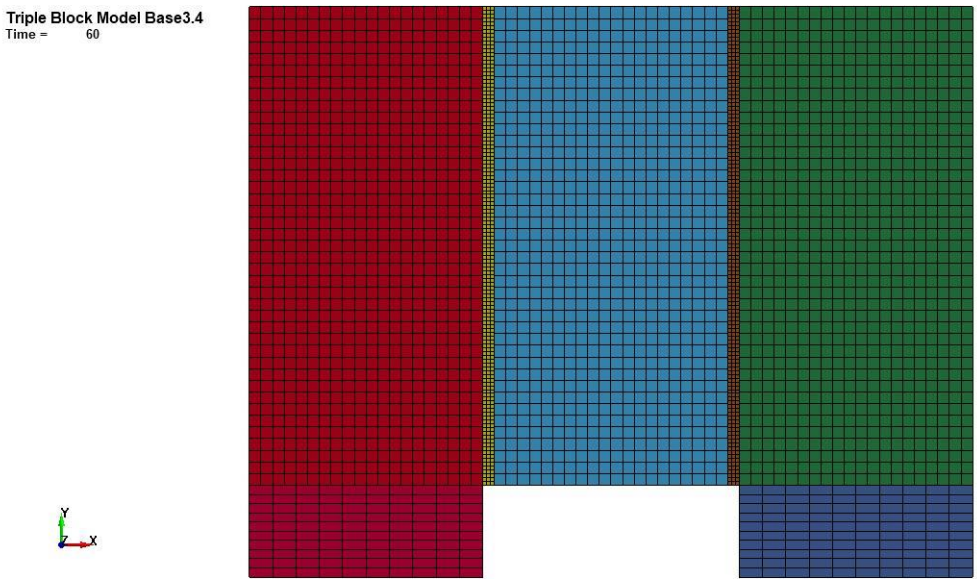


**Figure B-79: Last State at 60 Milliseconds for Base Run 3.4 – 200 psi**

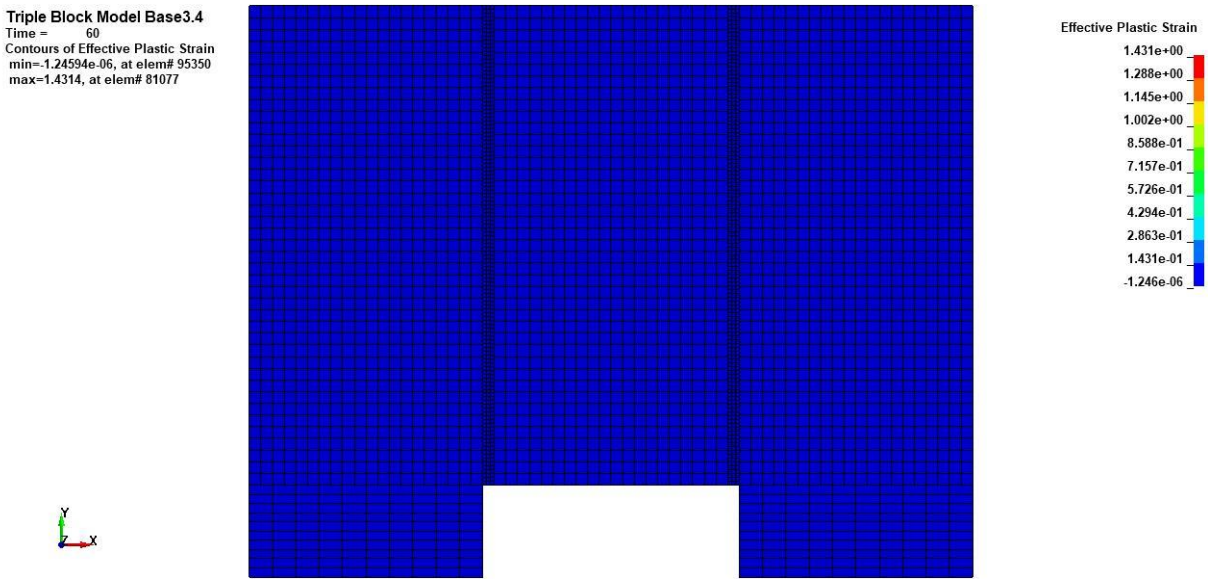


**Figure B-80: Effective Plastic Strain Fringe Plot for Last State at 60 Milliseconds for Base Run 3.4– 200 psi**

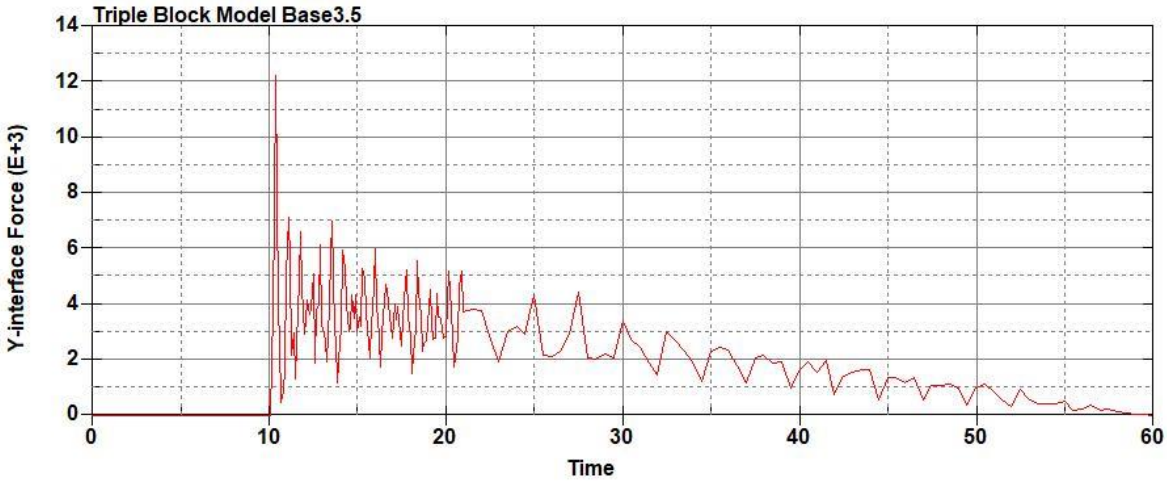


**Figure B-81: Base Run 3.5 Right Support Y-Interface Force (lbs) versus Time (ms) – 250 psi**

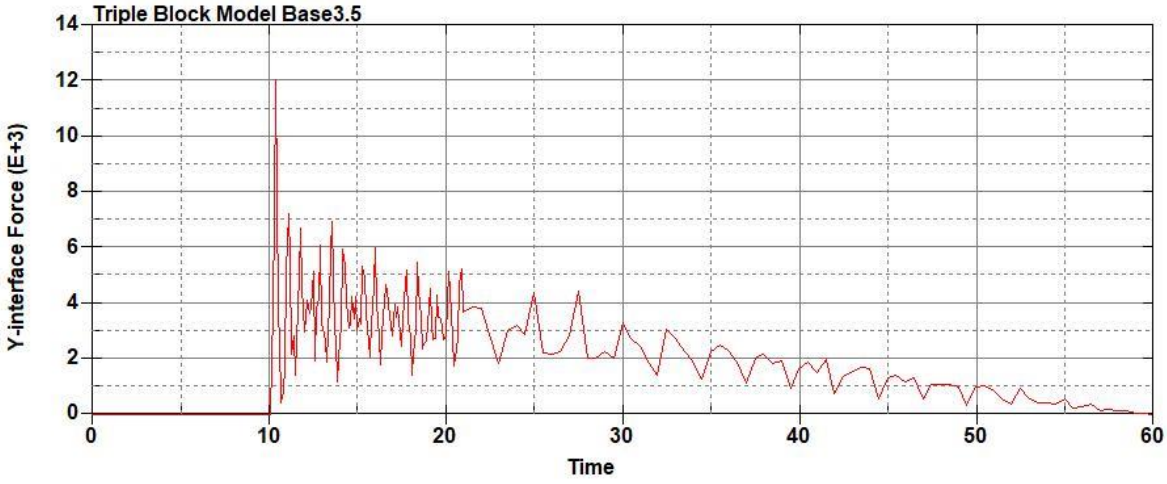


**Figure B-82: Base Run 3.5 Left Support Y-Interface Force (lbs) versus Time (ms) – 250 psi**

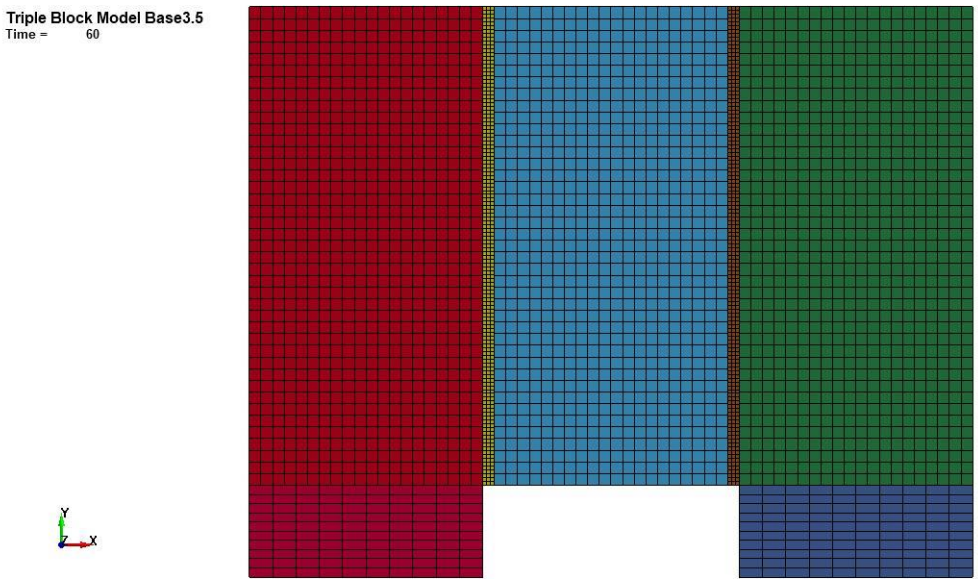


**Figure B-83: Last State at 60 Milliseconds for Base Run 3.5 – 250 psi**

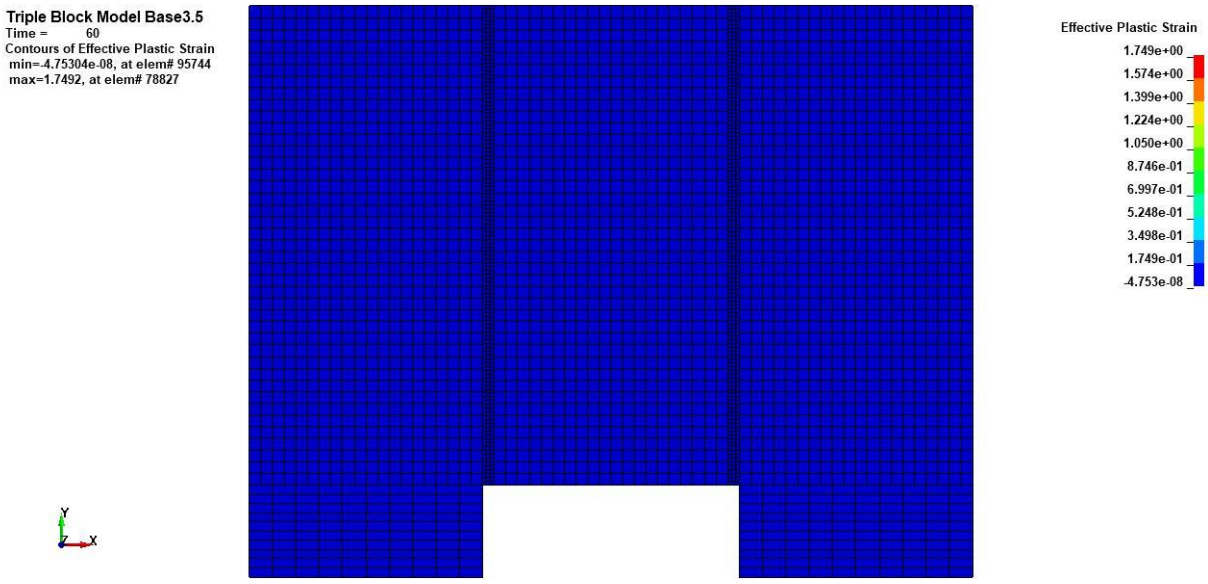


**Figure B-84: Effective Plastic Strain Fringe Plot for Last State at 60 Milliseconds for Base Run 3.5 – 250 psi**

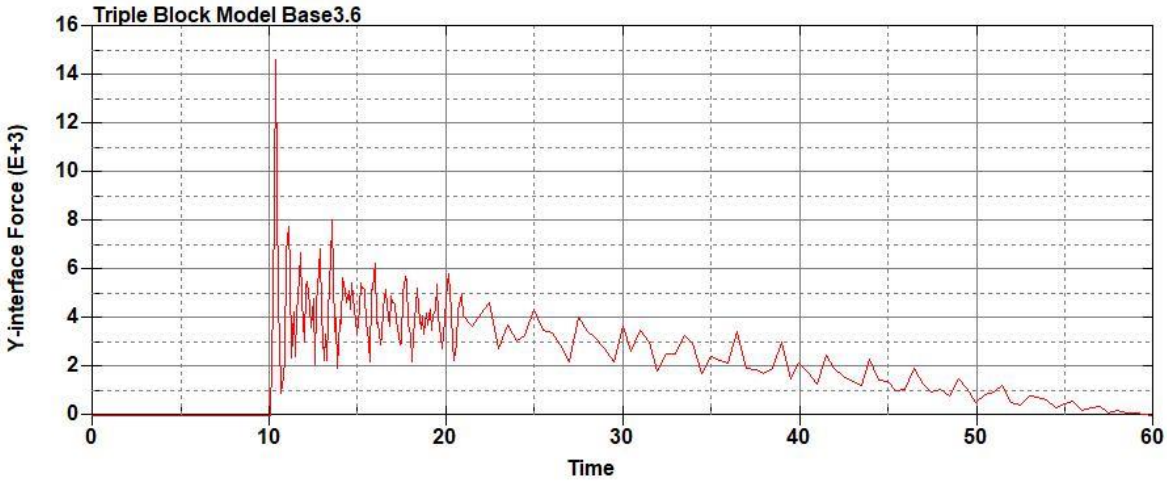


**Figure B-85: Base Run 3.6 Right Support Y-Interface Force (lbs) versus Time (ms) – 300 psi**

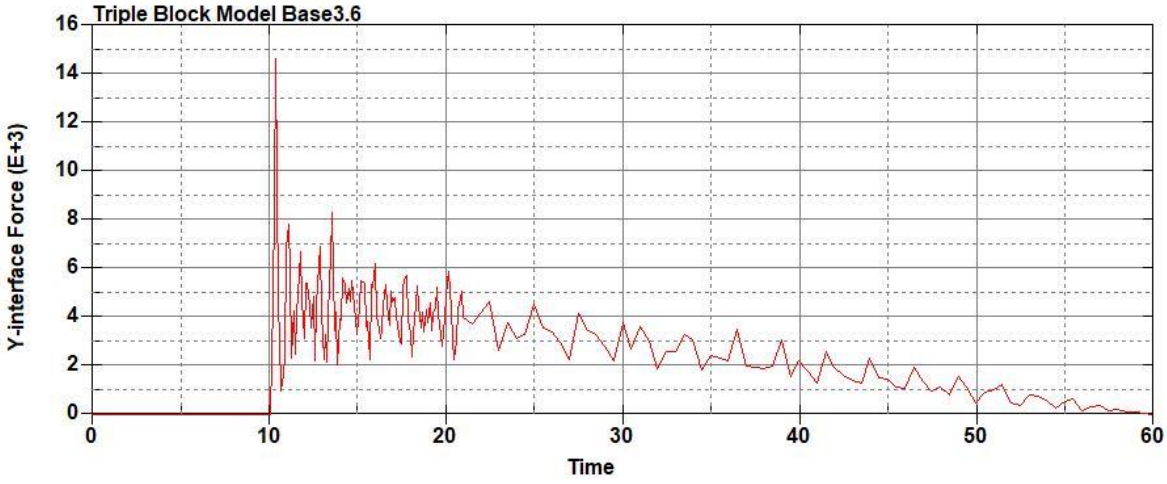


**Figure B-86: Base Run 3.6 Left Support Y-Interface Force (lbs) versus Time (ms) – 300 psi**

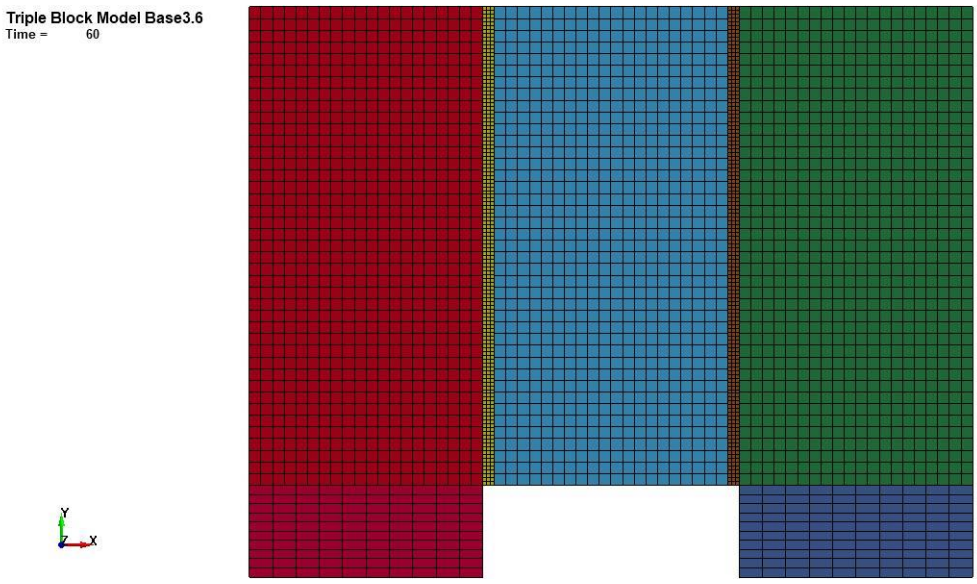


**Figure B-87: Last State at 60 Milliseconds for Base Run 3.6 – 300 psi**

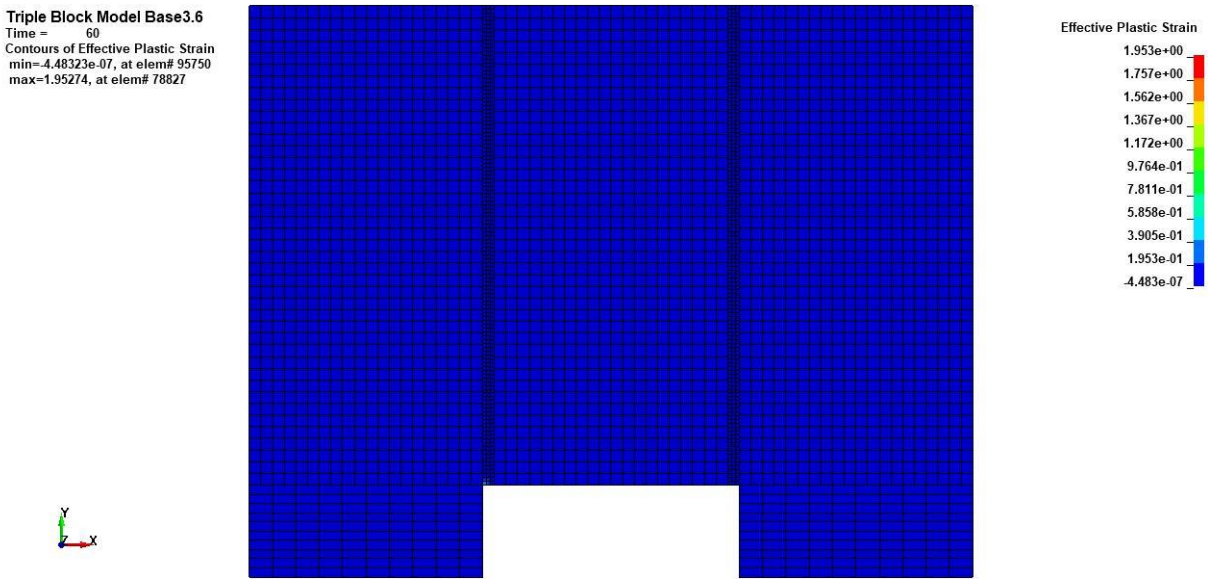


**Figure B-88: Effective Plastic Strain Fringe Plot for Last State at 60 Milliseconds for Base Run 3.6 – 300 psi**

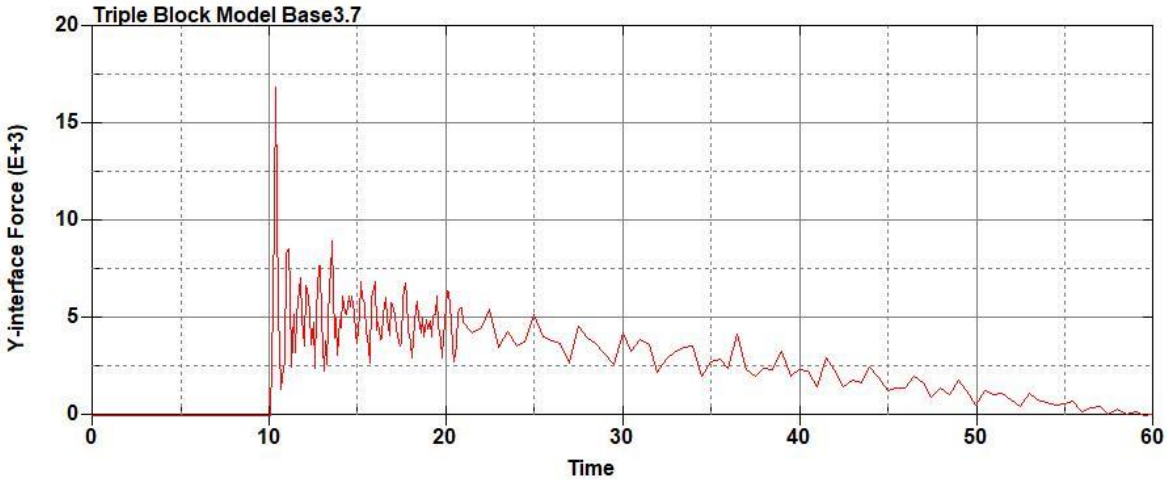


**Figure B-89: Base Run 3.7 Right Support Y-Interface Force (lbs) versus Time (ms) – 350 psi**

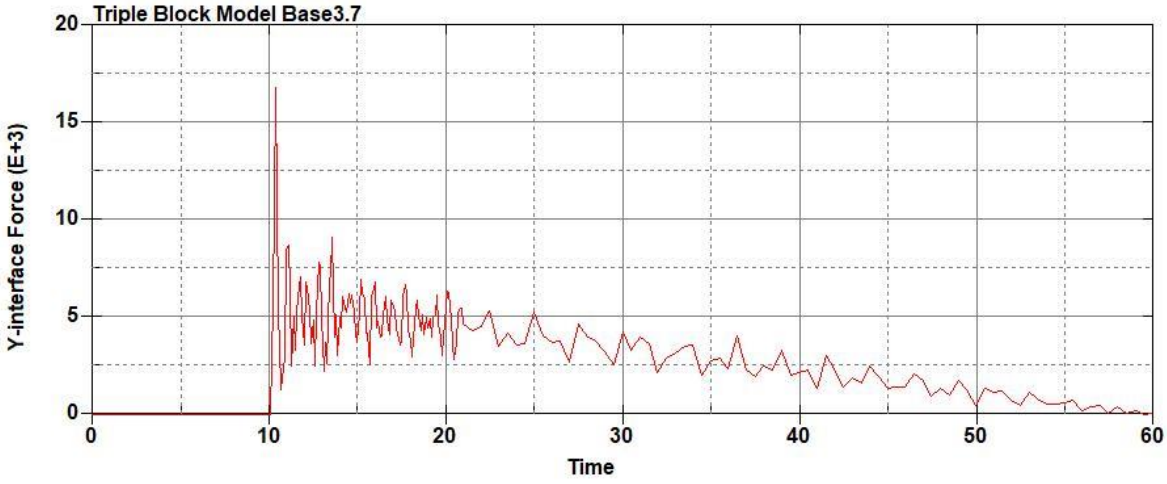


**Figure B-90: Base Run 3.7 Left Support Y-Interface Force (lbs) versus Time (ms) – 350 psi**

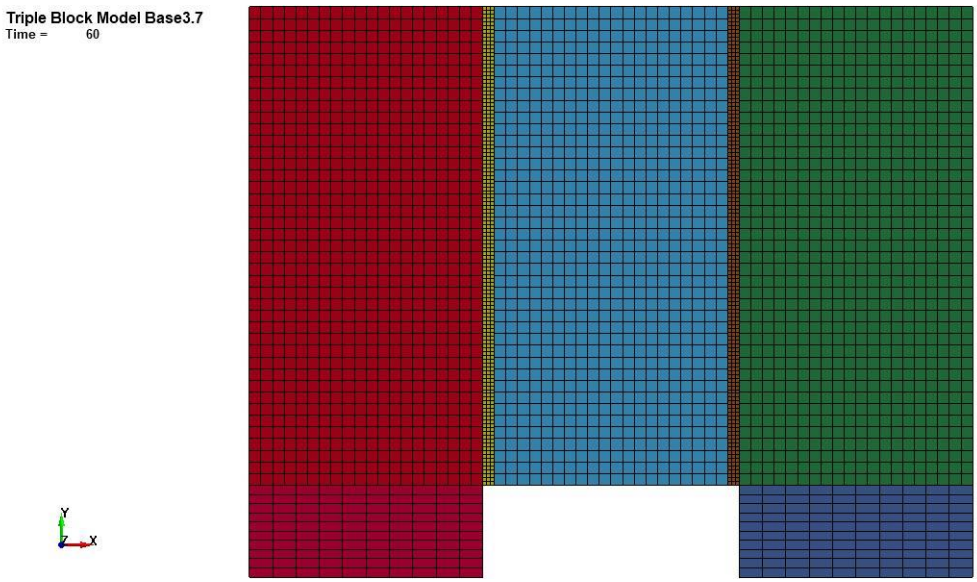


**Figure B-91: Last State at 60 Milliseconds for Base Run 3.7 – 350 psi**

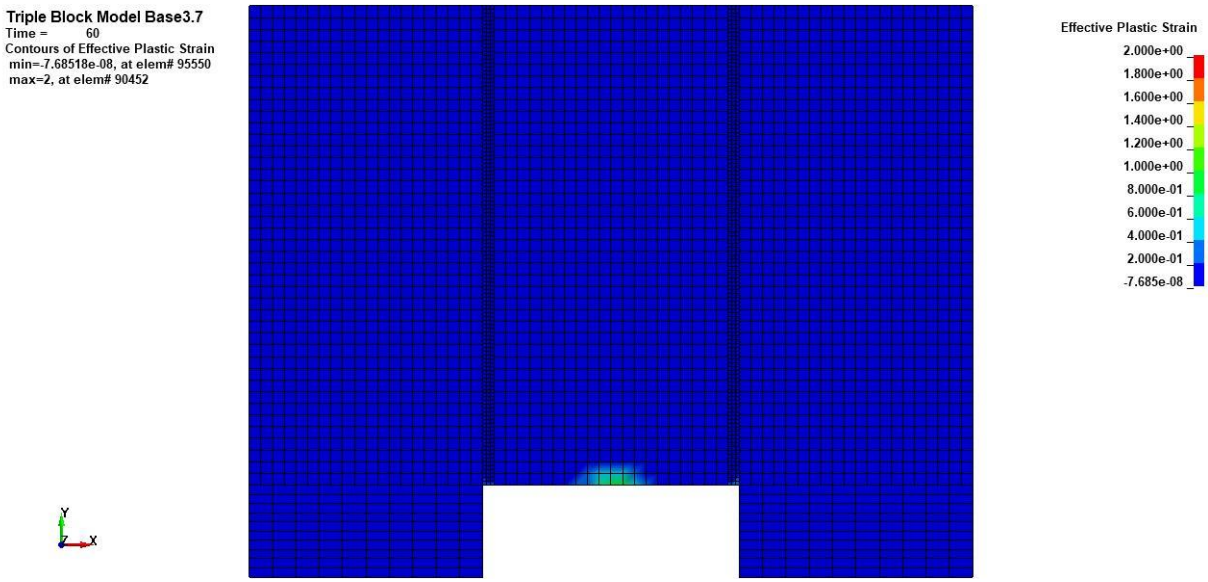


**Figure B-92: Effective Plastic Strain Fringe Plot for Last State at 60 Milliseconds for Base Run 3.7 – 350 psi**

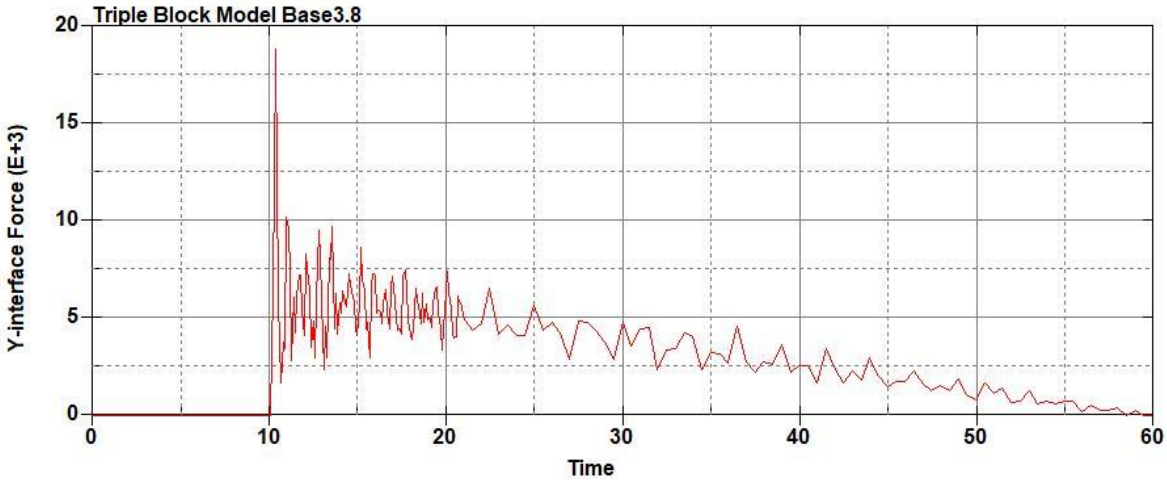


**Figure B-93: Base Run 3.8 Right Support Y-Interface Force (lbs) versus Time (ms) – 400 psi**

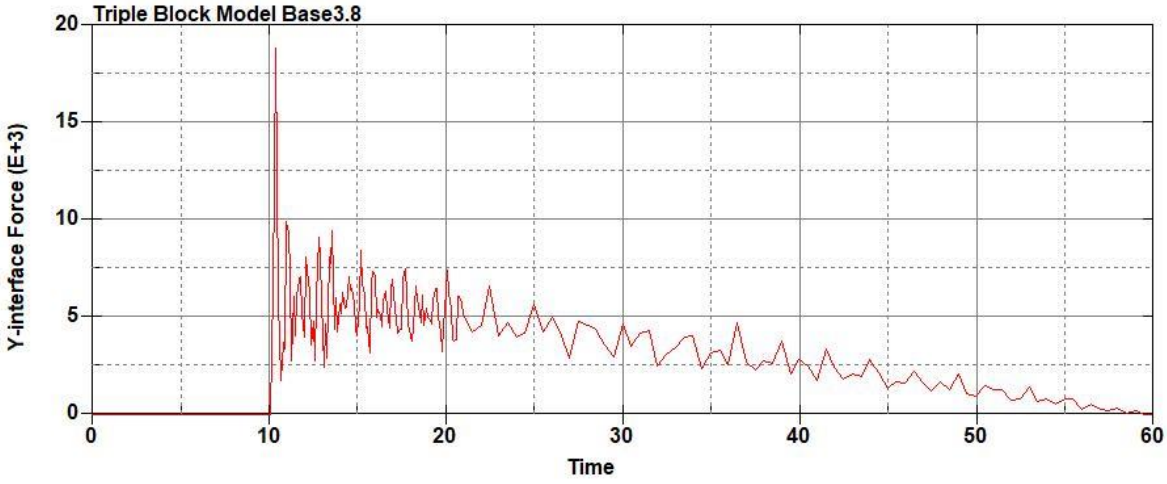


**Figure B-94: Base Run 3.8 Left Support Y-Interface Force (lbs) versus Time (ms) – 400 psi**

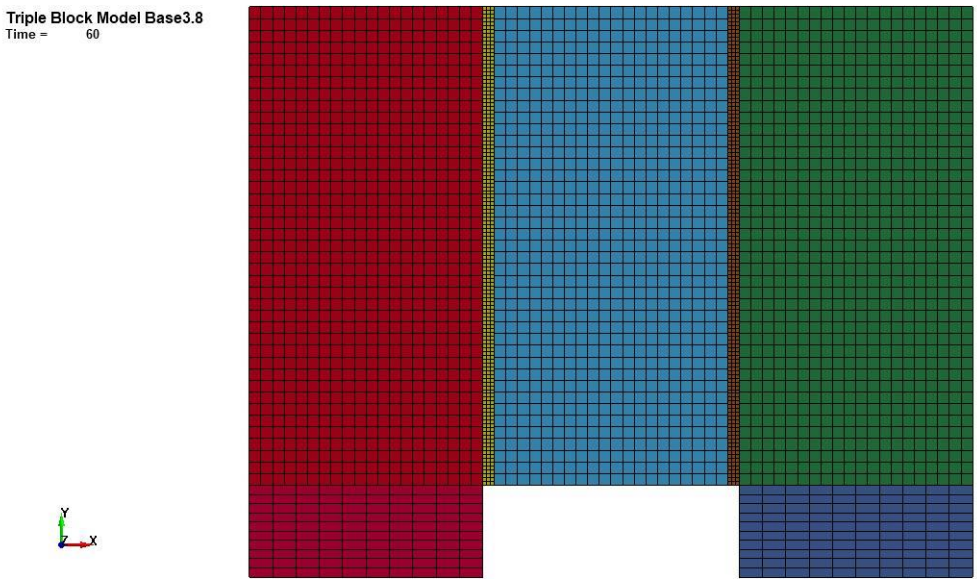


**Figure B-95: Last State at 60 Milliseconds for Base Run 3.8 – 400 psi**

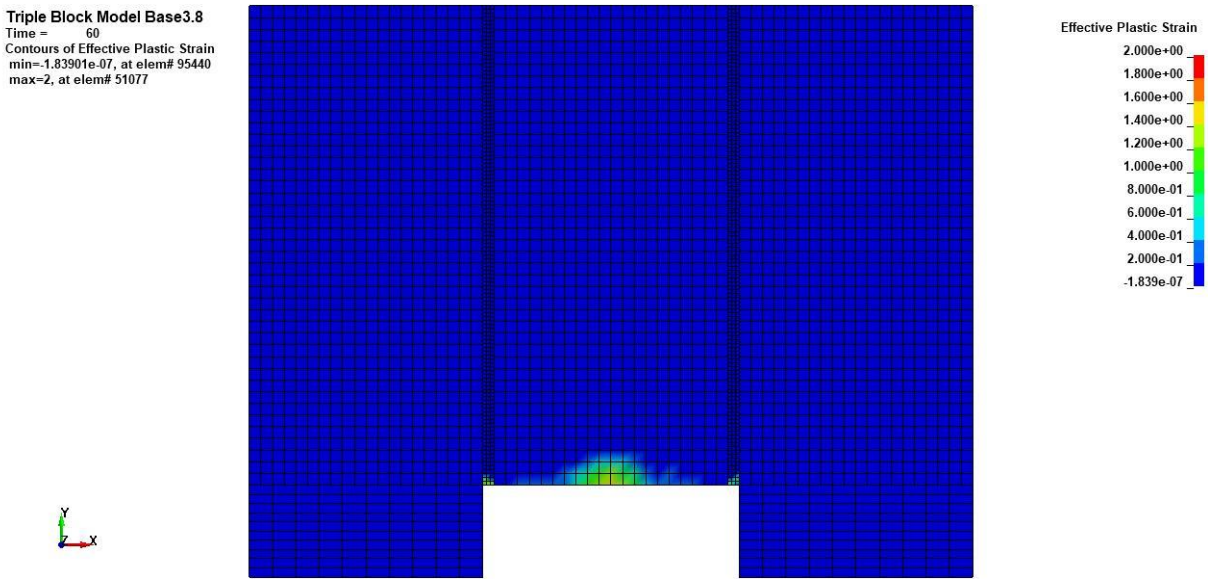


**Figure B-96: Effective Plastic Strain Fringe Plot for Last State at 60 Milliseconds for Base Run 3.8 – 400 psi**

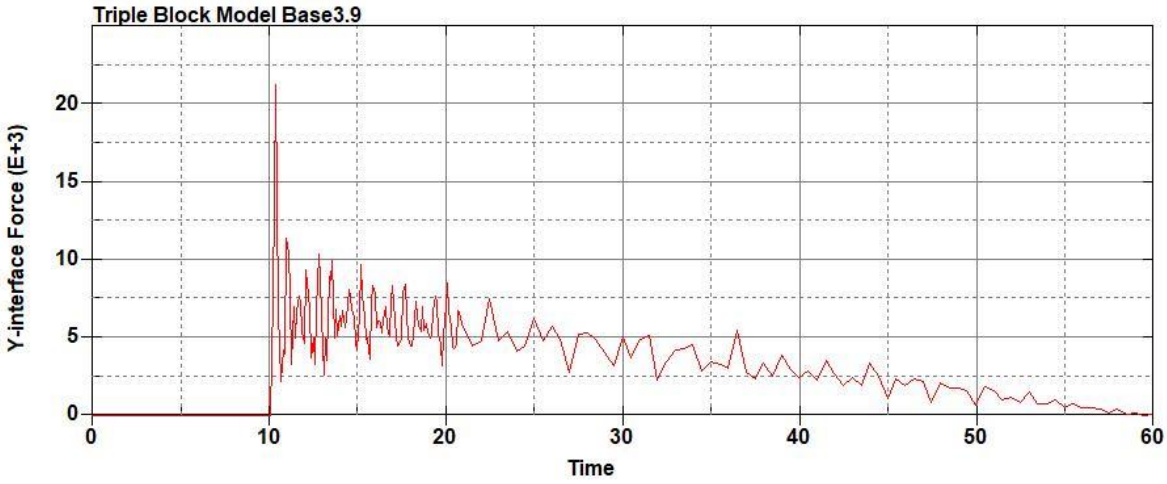


**Figure B-97: Base Run 3.9 Right Support Y-Interface Force (lbs) versus Time (ms) – 450 psi**

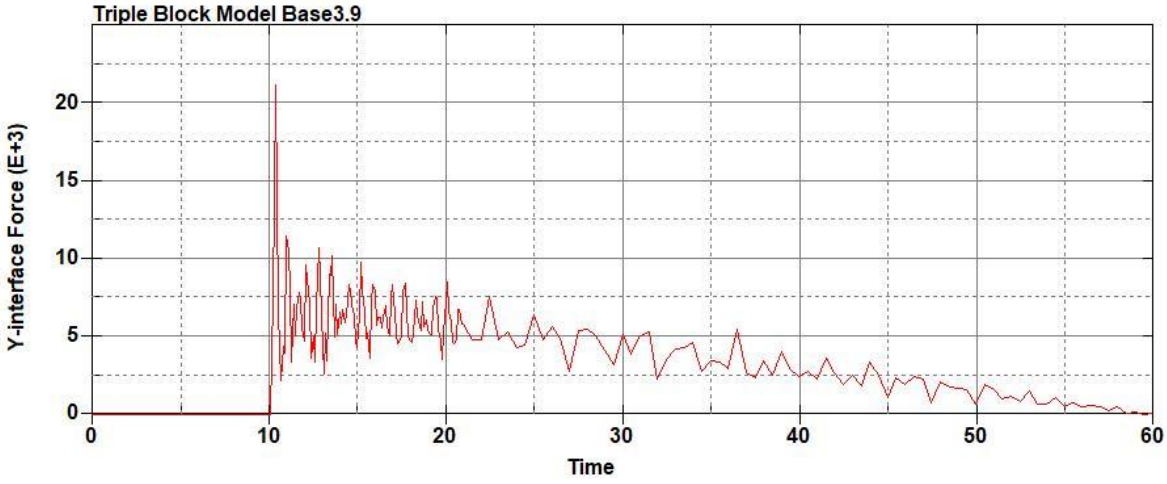


**Figure B-98: Base Run 3.9 Left Support Y-Interface Force (lbs) versus Time (ms) – 450 psi**

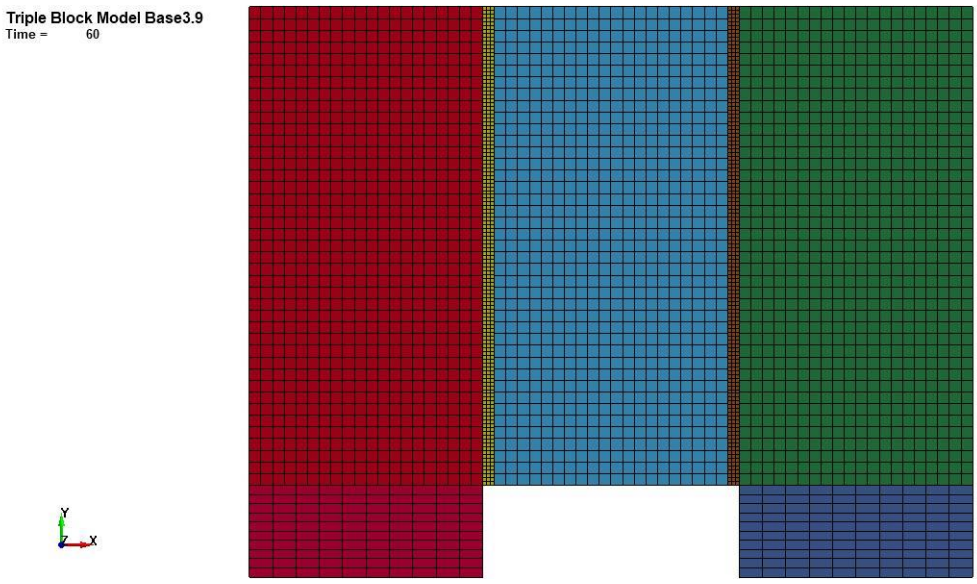


**Figure B-99: Last State at 60 Milliseconds for Base Run 3.9 – 450 psi**

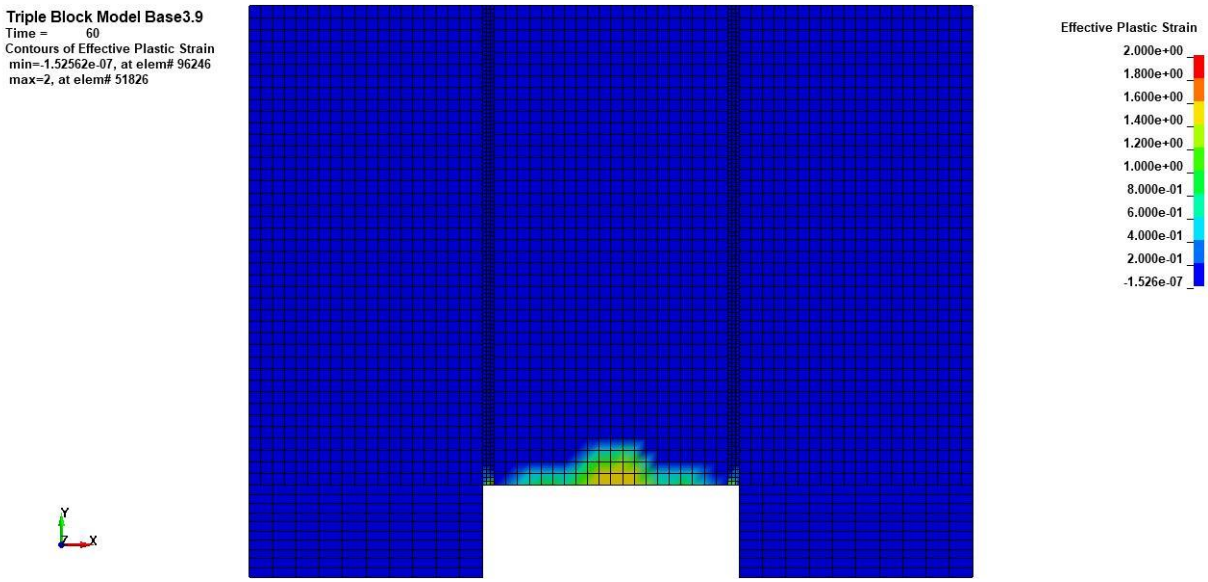


**Figure B-100: Effective Plastic Strain Fringe Plot for Last State at 60 Milliseconds for Base Run 3.9 – 450 psi**

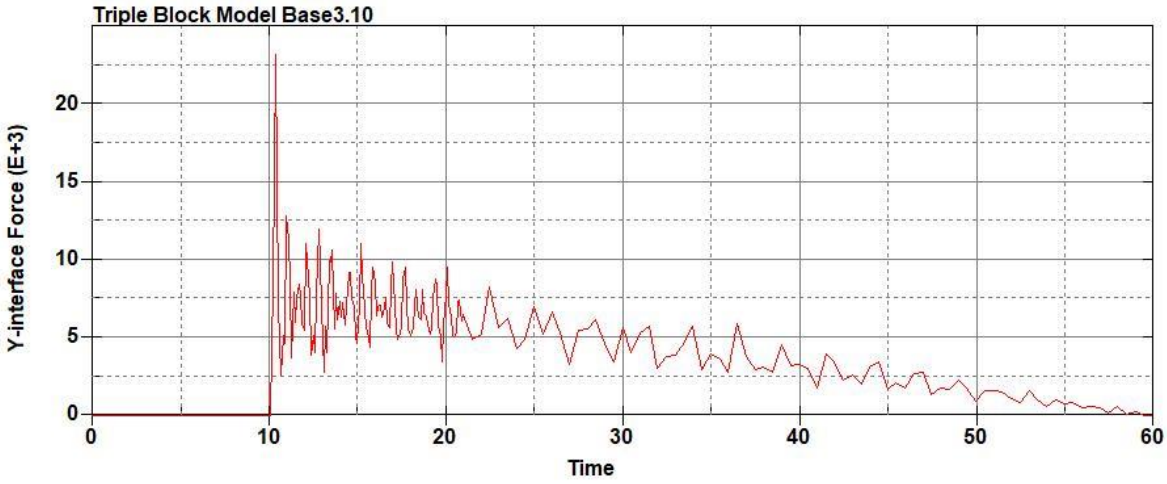


**Figure B-101: Base Run 3.10 Right Support Y-Interface Force (lbs) versus Time (ms) – 500 psi**

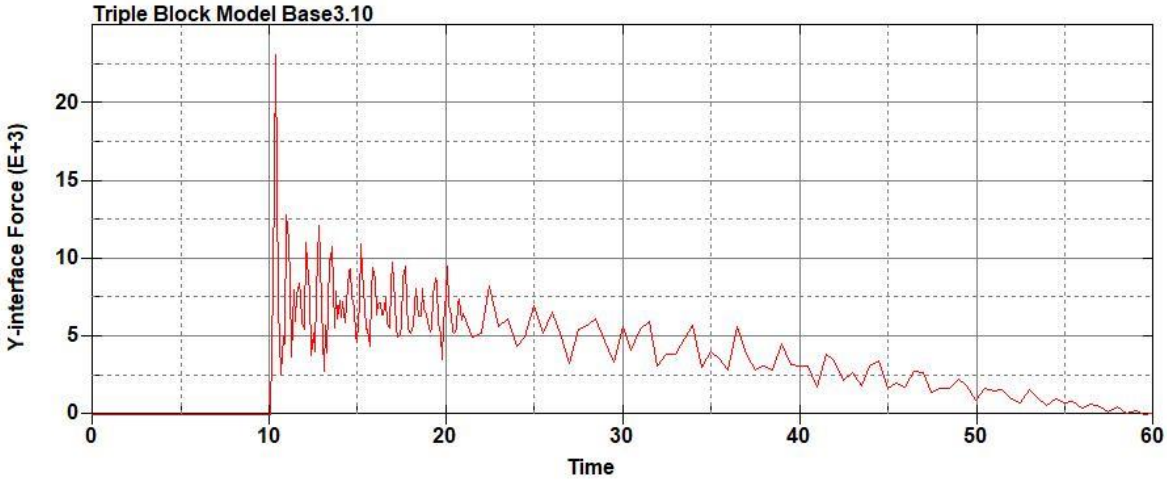


**Figure B-102: Base Run 3.10 Left Support Y-Interface Force (lbs) versus Time (ms) – 500 psi**

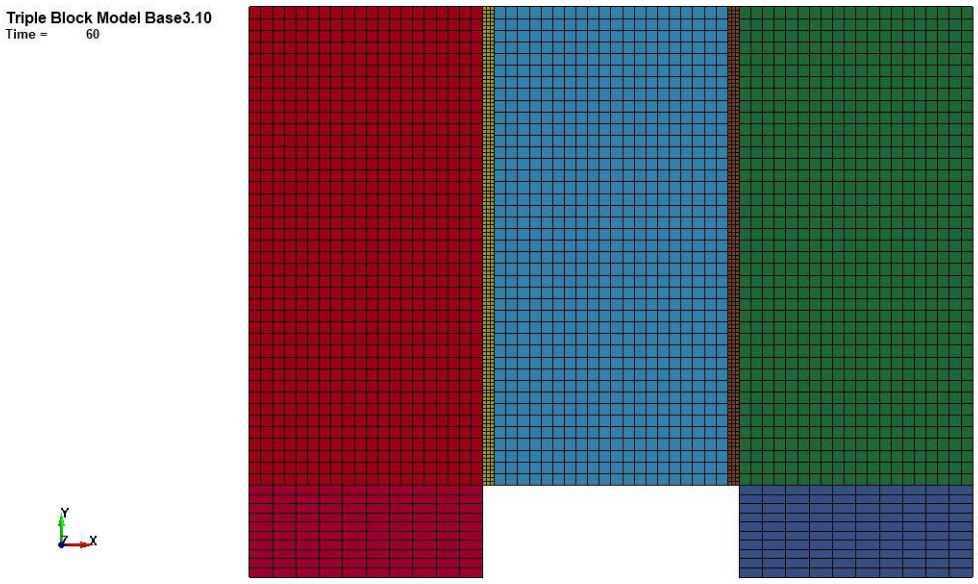


**Figure B-103: Last State at 60 Milliseconds for Base Run 3.10 – 500 psi**

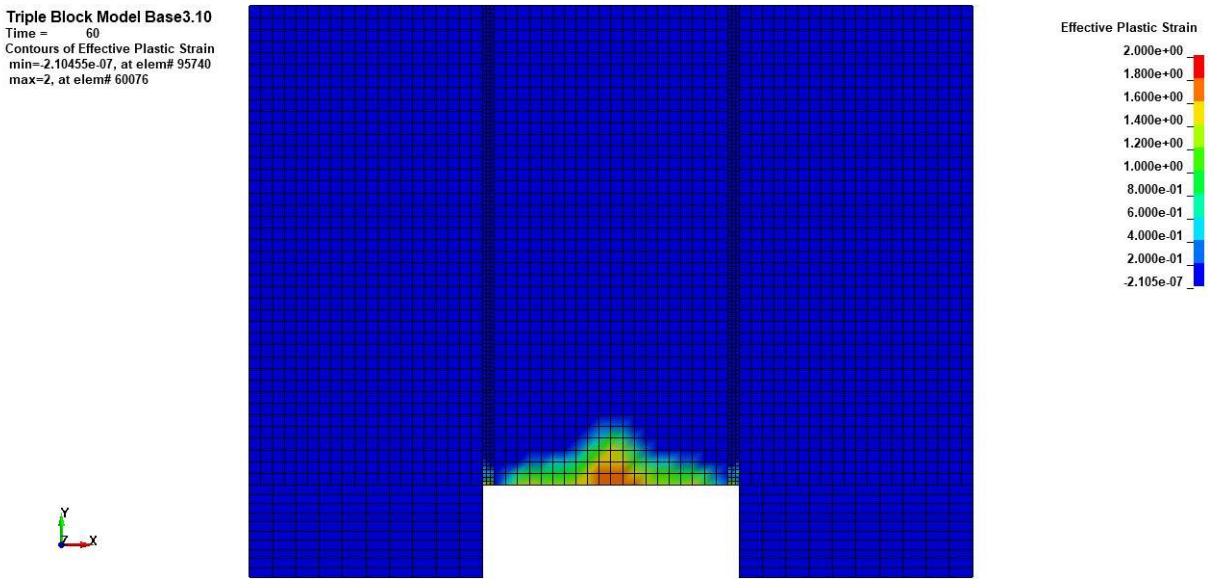


**Figure B-104: Effective Plastic Strain Fringe Plot for Last State at 60 Milliseconds for Base Run 3.10 – 500 psi**

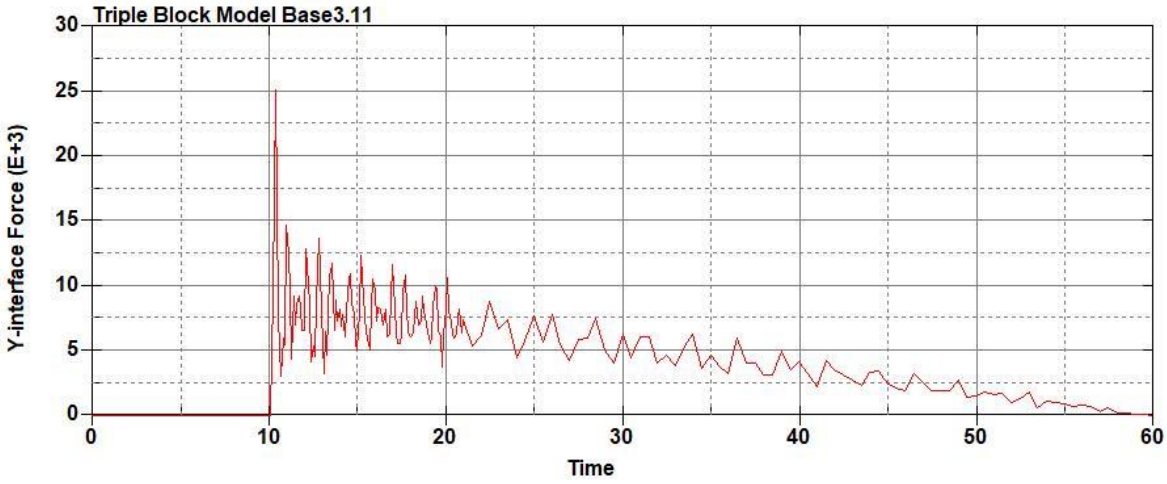


**Figure B-105: Base Run 3.11 Right Support Y-Interface Force (lbs) versus Time (ms) – 550 psi**

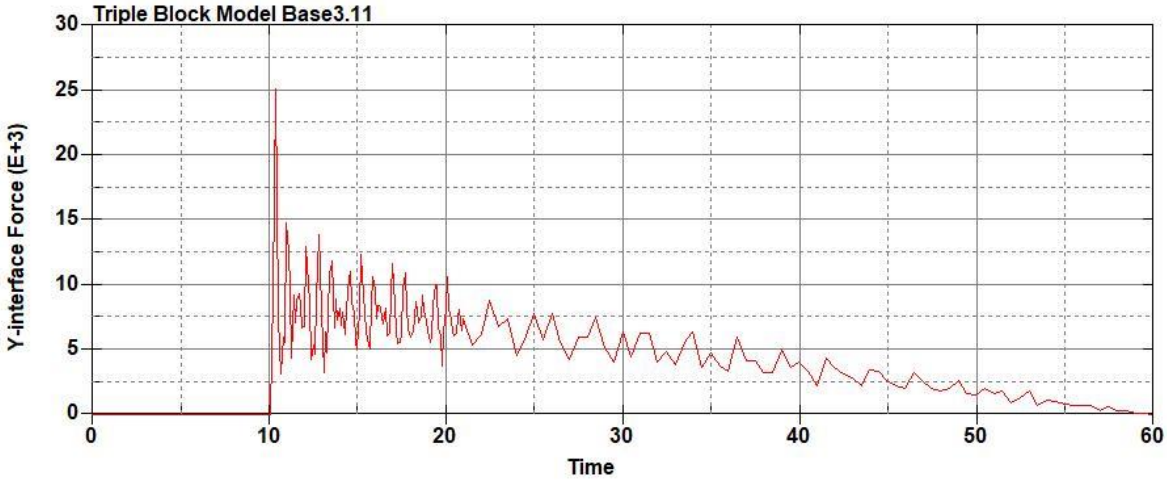


**Figure B-106: Base Run 3.11 Left Support Y-Interface Force (lbs) versus Time (ms) – 550 psi**

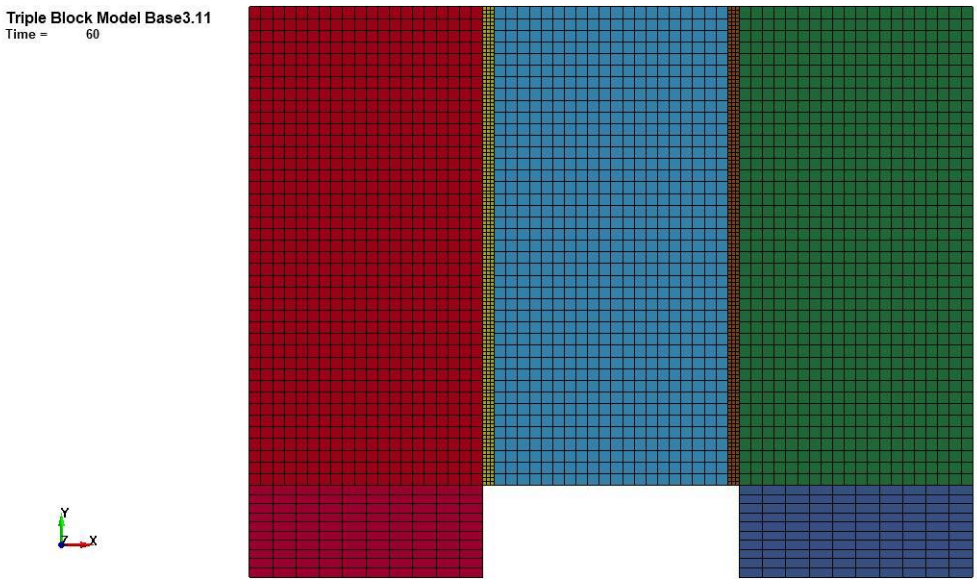


**Figure B-107: Last State at 60 Milliseconds for Base Run 3.11 – 550 psi**

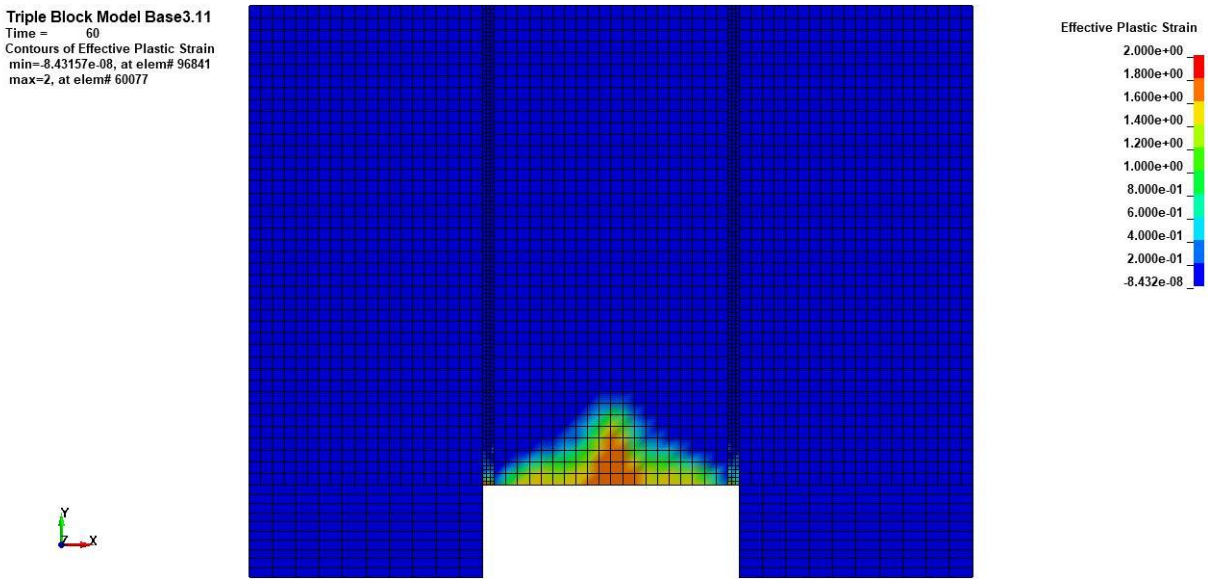


**Figure B-108: Effective Plastic Strain Fringe Plot for Last State at 60 Milliseconds for Base Run 3.11 – 550 psi**

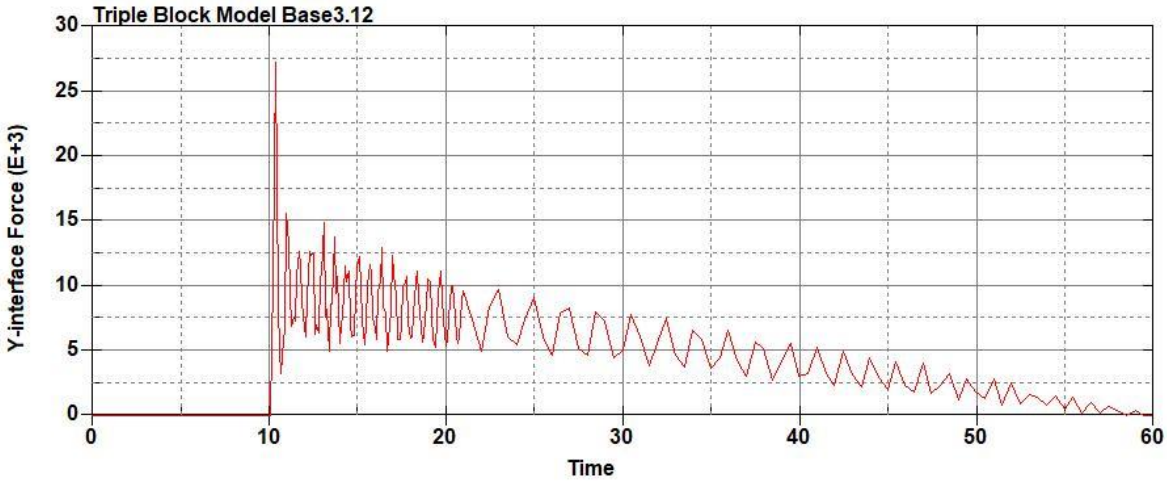


**Figure B-109: Base Run 3.12 Right Support Y-Interface Force (lbs) versus Time (ms) – 600 psi**

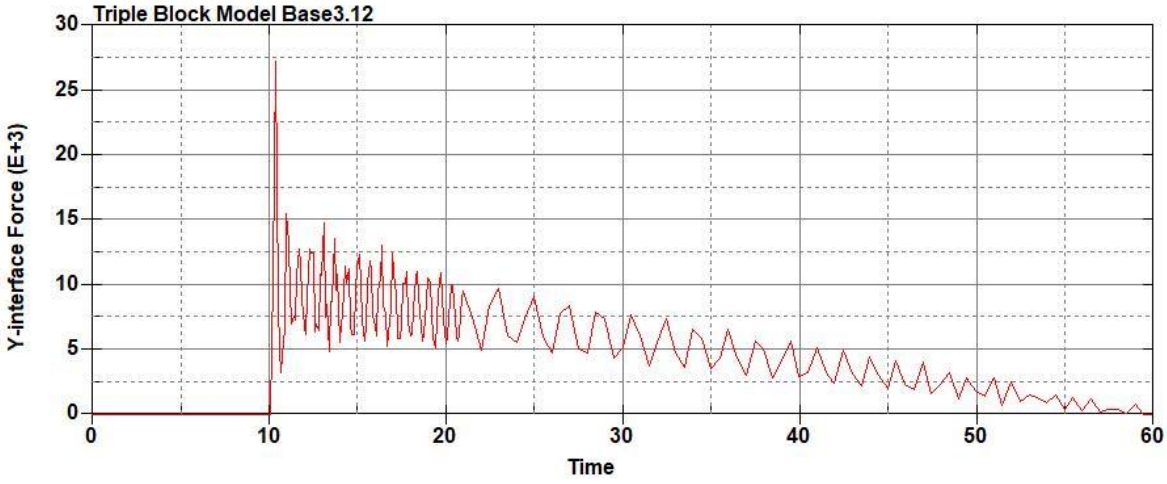


**Figure B-110: Base Run 3.12 Left Support Y-Interface Force (lbs) versus Time (ms) – 600 psi**

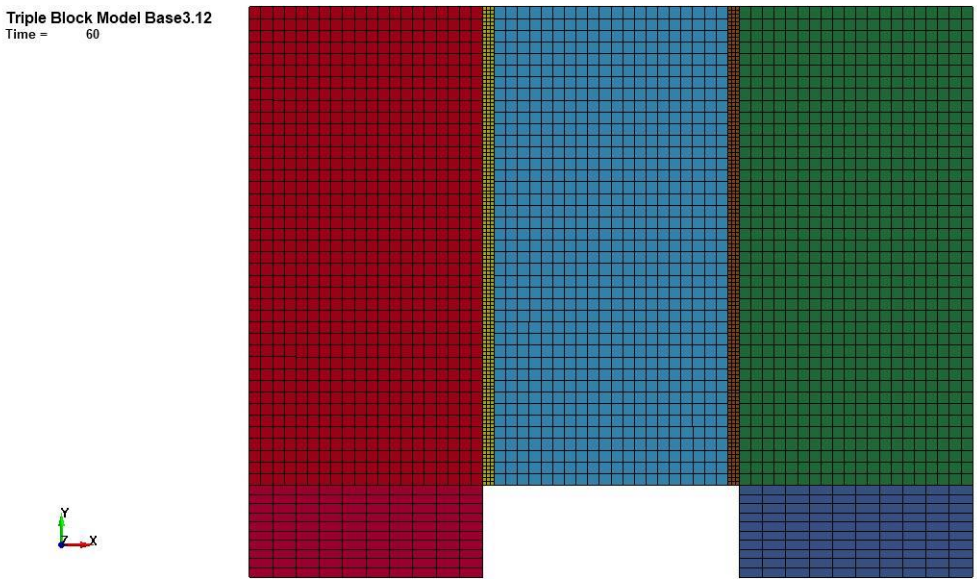


**Figure B-111: Last State at 60 Milliseconds for Base Run 3.12 – 600 psi**

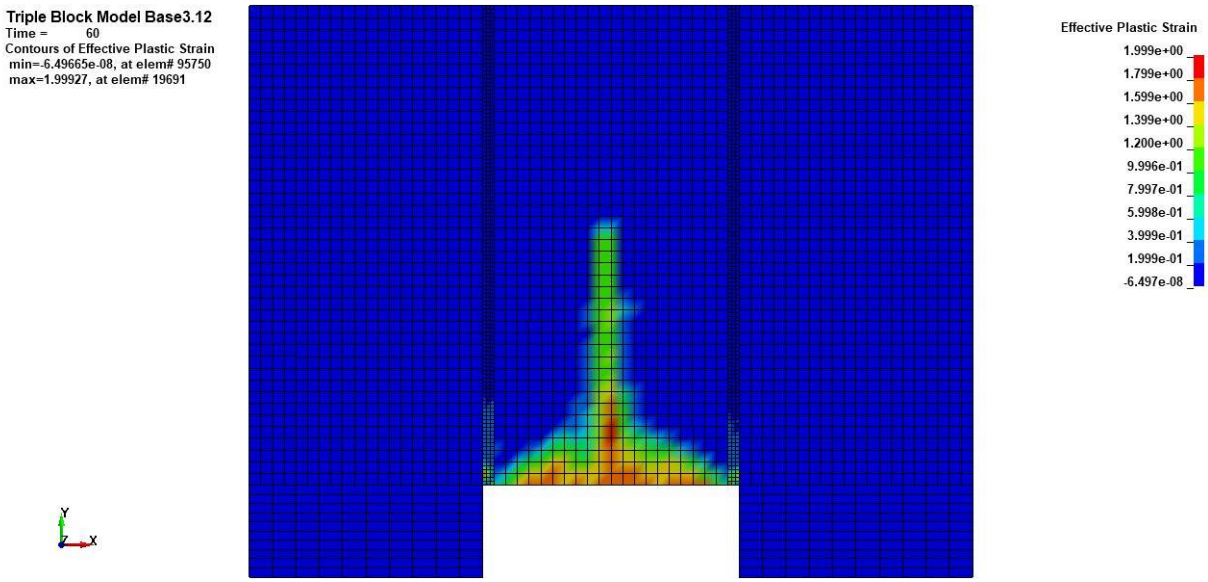


**Figure B-112: Effective Plastic Strain Fringe Plot for Last State at 60 Milliseconds for Base Run 3.12 – 600 psi**

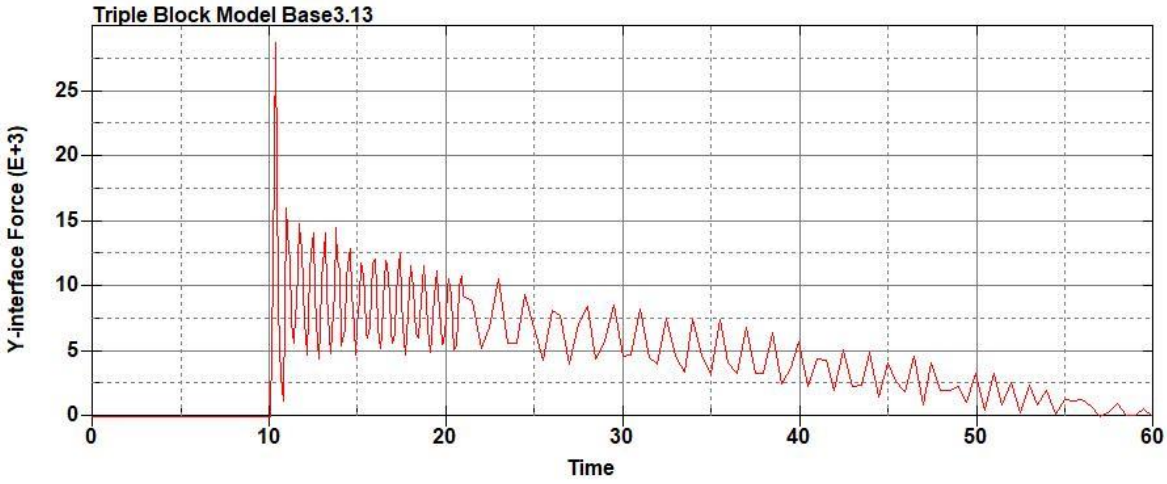


**Figure B-113: Base Run 3.13 Right Support Y-Interface Force (lbs) versus Time (ms) – 650 psi**

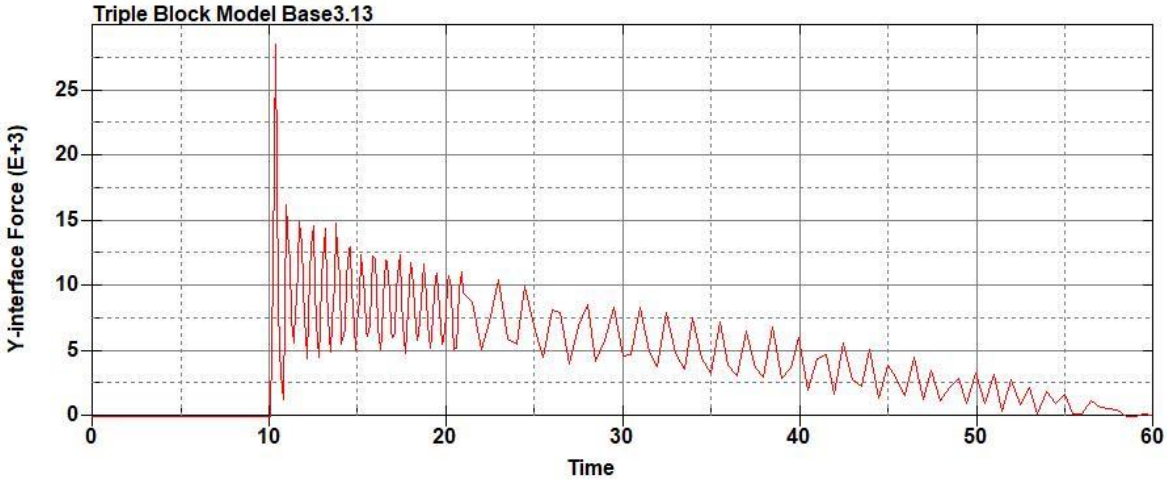


**Figure B-114: Base Run 3.13 Left Support Y-Interface Force (lbs) versus Time (ms) – 650 psi**

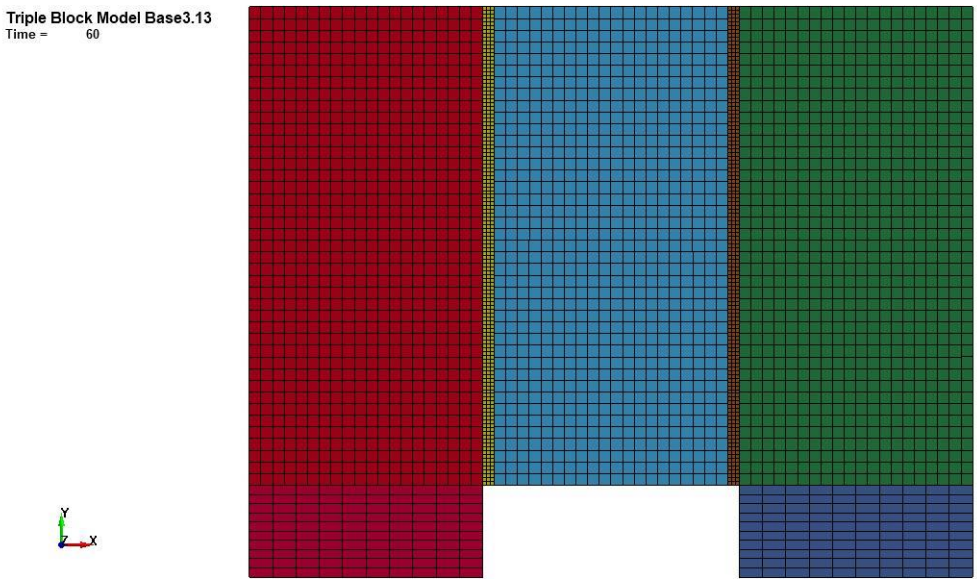


**Figure B-115: Last State at 60 Milliseconds for Base Run 3.13 – 650 psi**

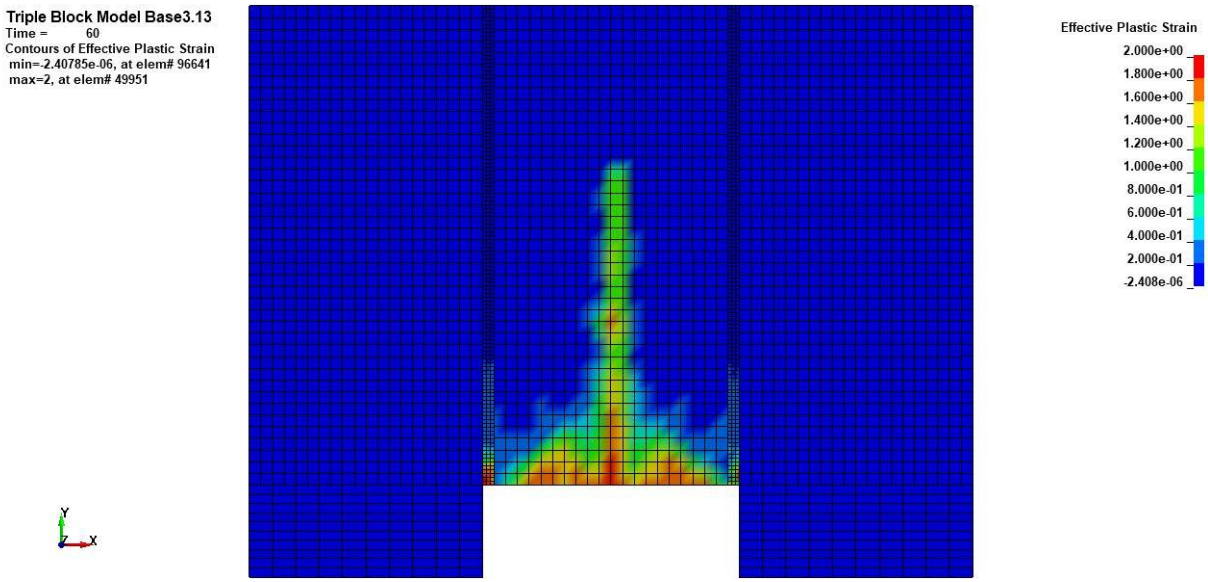


**Figure B-116: Effective Plastic Strain Fringe Plot for Last State at 60 Milliseconds for Base Run 3.13 – 650 psi**

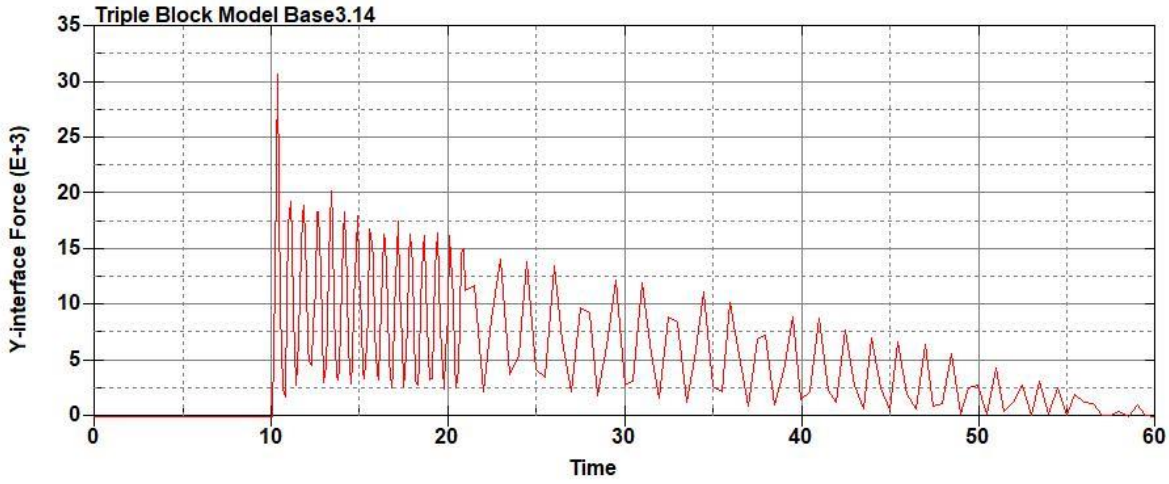


**Figure B-117: Base Run 3.14 Right Support Y-Interface Force (lbs) versus Time (ms) – 700 psi**

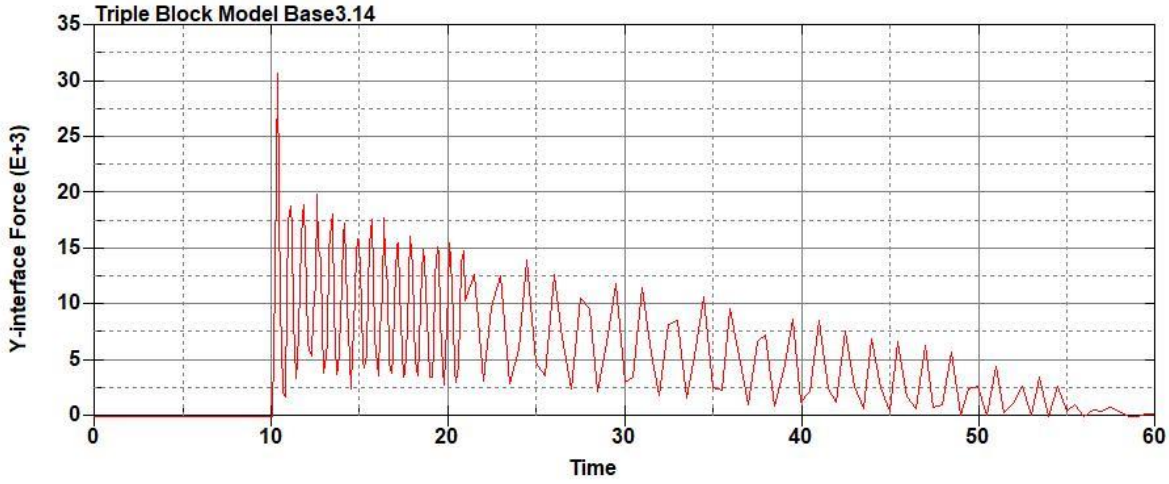


**Figure B-118: Base Run 3.14 Left Support Y-Interface Force (lbs) versus Time (ms) – 700 psi**

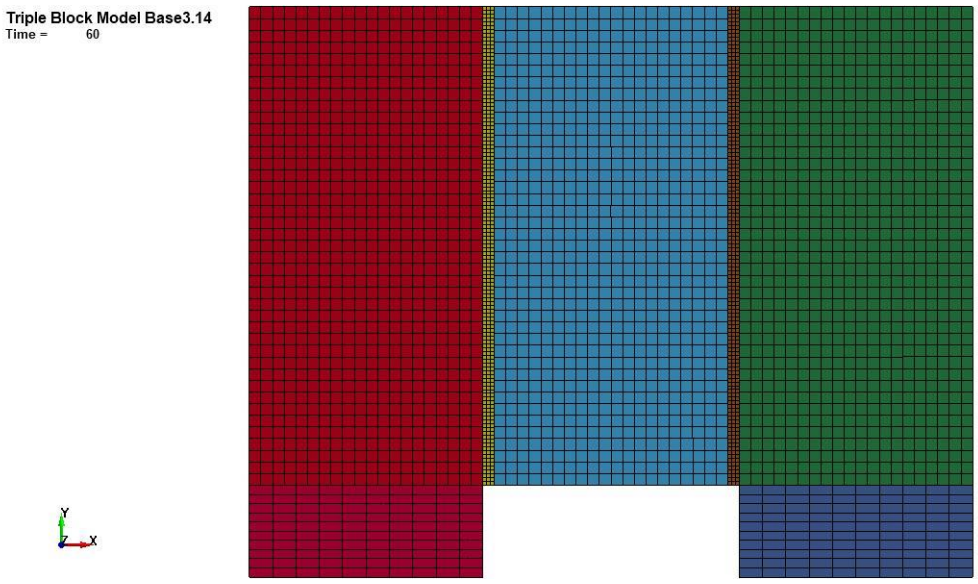


**Figure B-119: Last State at 60 Milliseconds for Base Run 3.14 – 700 psi**

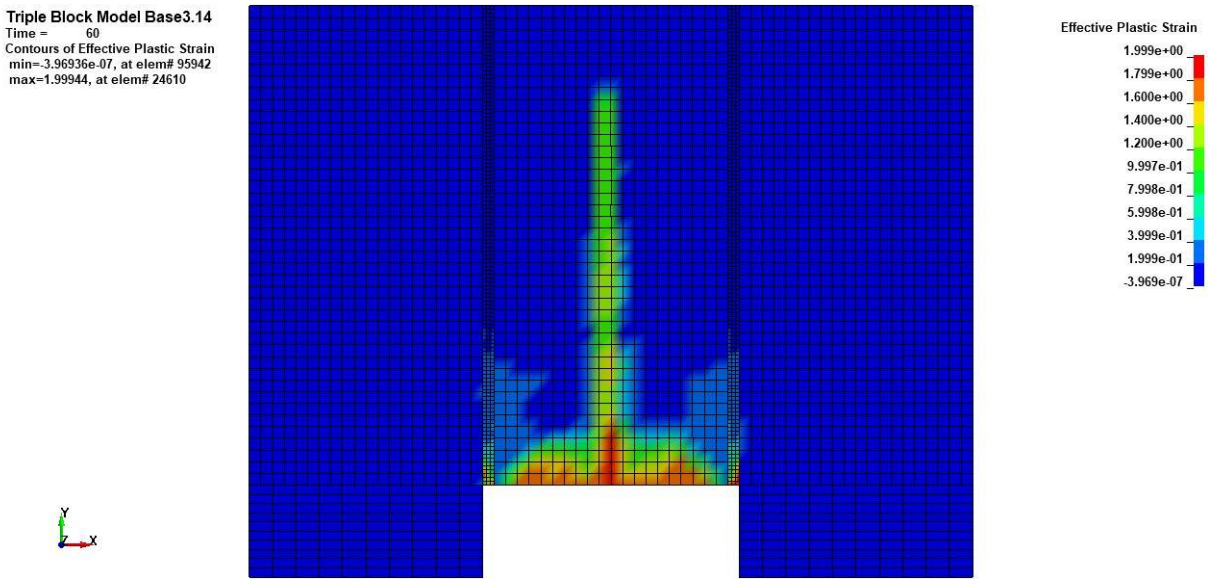


**Figure B-120: Effective Plastic Strain Fringe Plot for Last State at 60 Milliseconds for Base Run 3.14 – 700 psi**

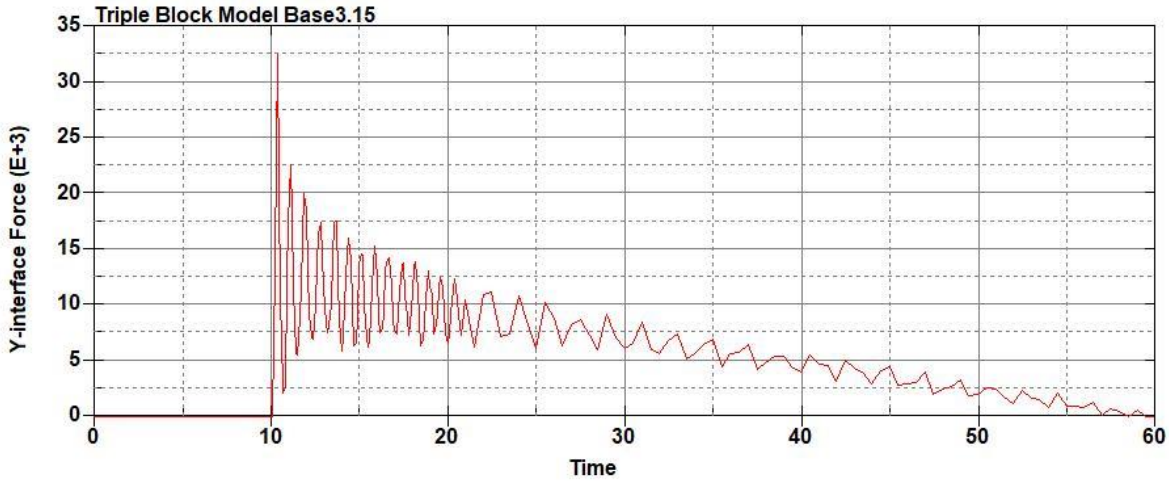


**Figure B-121: Base Run 3.15 Right Support Y-Interface Force (lbs) versus Time (ms) – 750 psi**

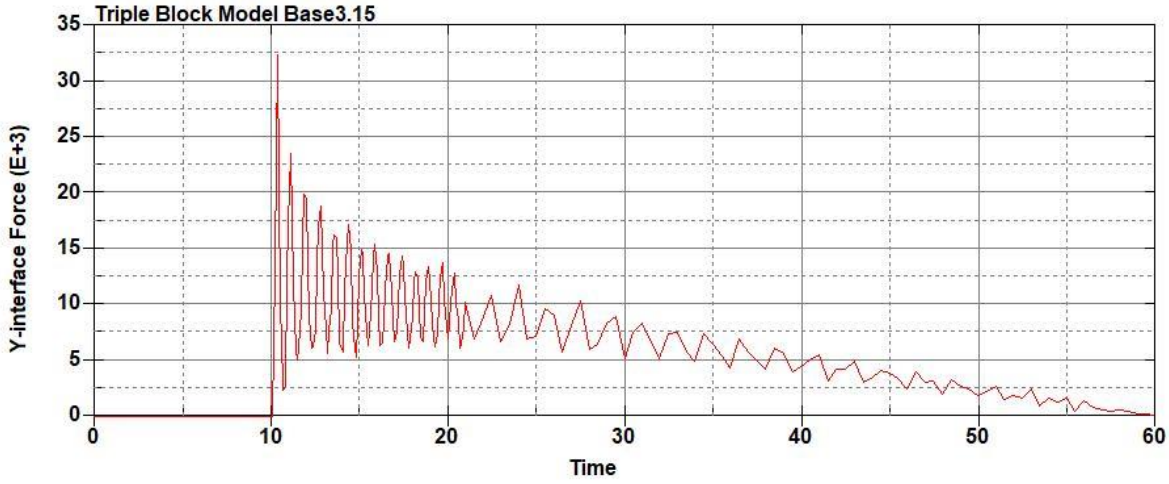


**Figure B-122: Base Run 3.15 Left Support Y-Interface Force (lbs) versus Time (ms) – 750 psi**

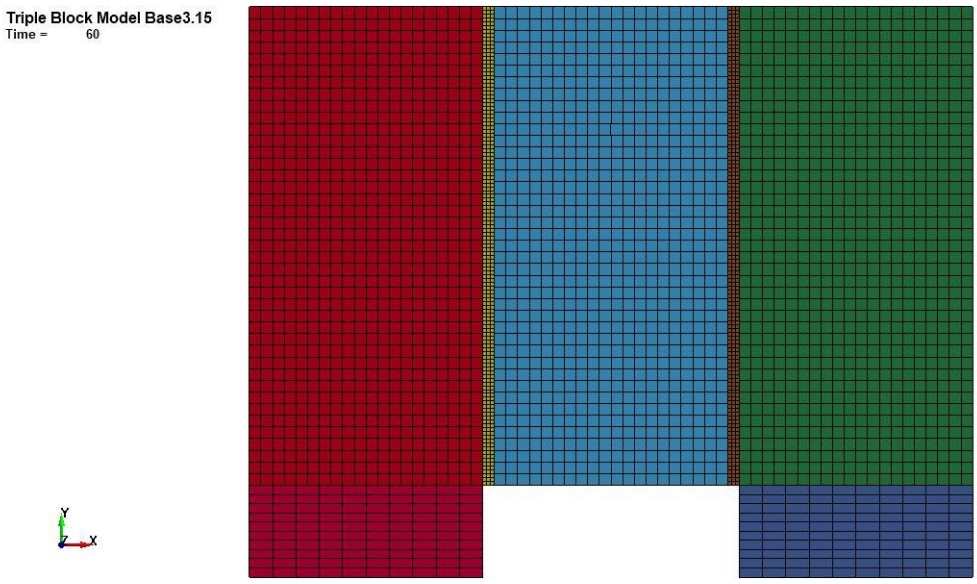


**Figure B-123: Last State at 60 Milliseconds for Base Run 3.15 – 750 psi**

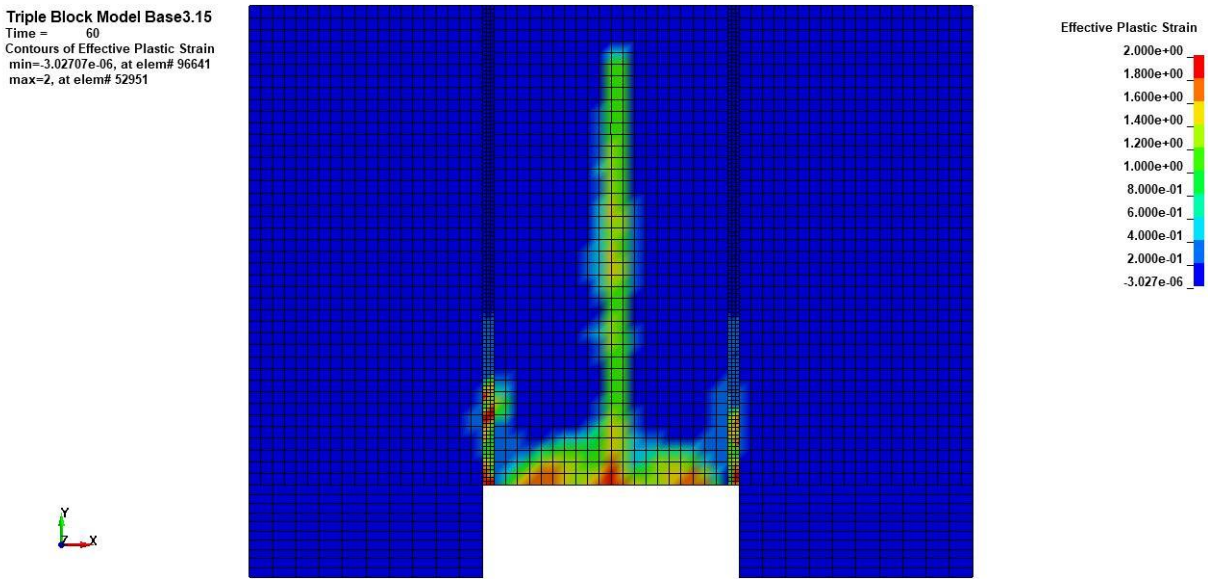


**Figure B-124: Effective Plastic Strain Fringe Plot for Last State at 60 Milliseconds for Base Run 3.15 – 750 psi**

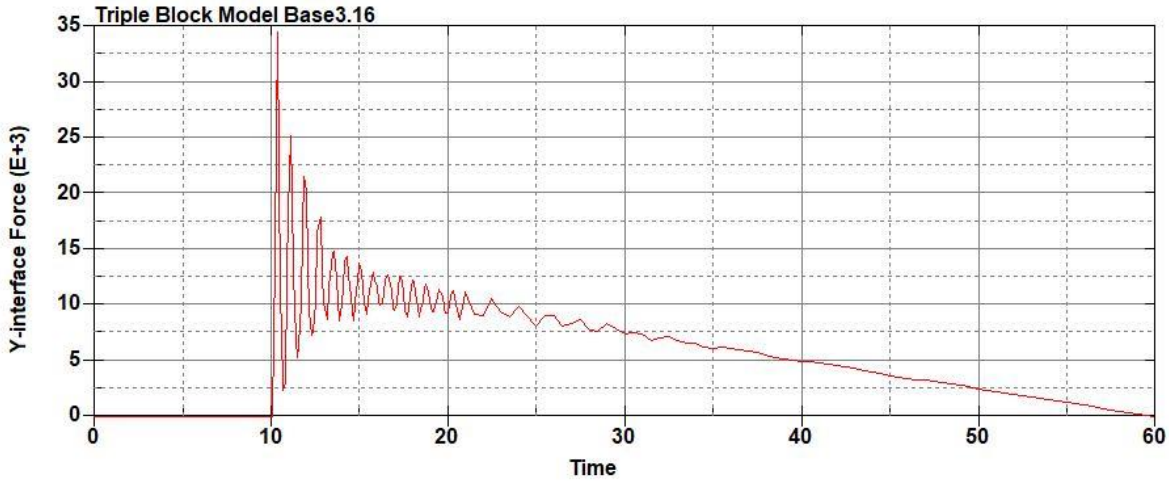


**Figure B-125: Base Run 3.16 Right Support Y-Interface Force (lbs) versus Time (ms) – 800 psi**

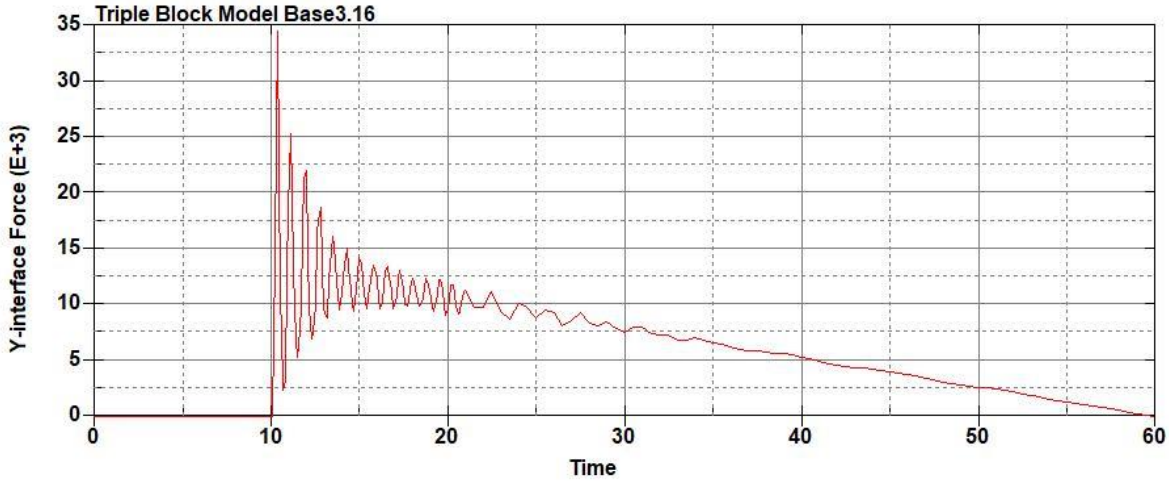


**Figure B-126: Base Run 3.16 Left Support Y-Interface Force (lbs) versus Time (ms) – 800 psi**

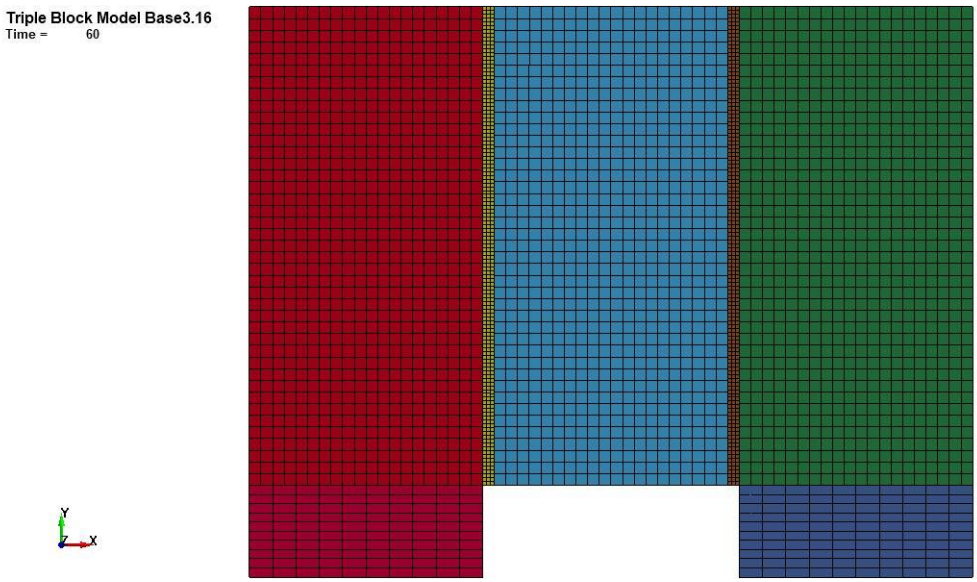


**Figure B-127: Last State at 60 Milliseconds for Base Run 3.16 – 800 psi**

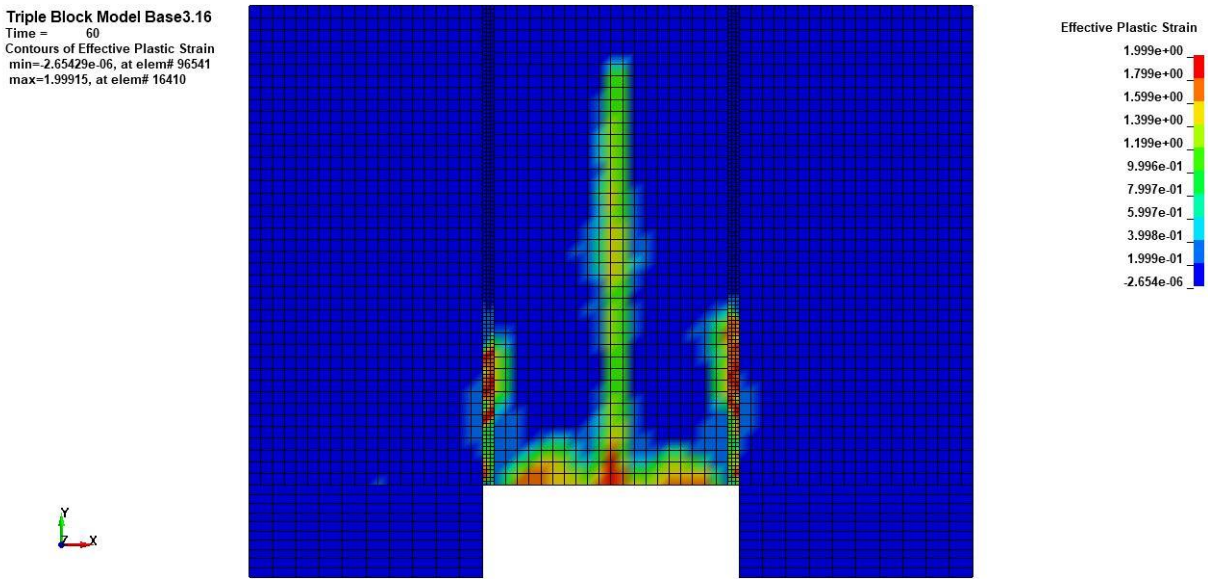


**Figure B-128: Effective Plastic Strain Fringe Plot for Last State at 60 Milliseconds for Base Run 3.16 – 800 psi**

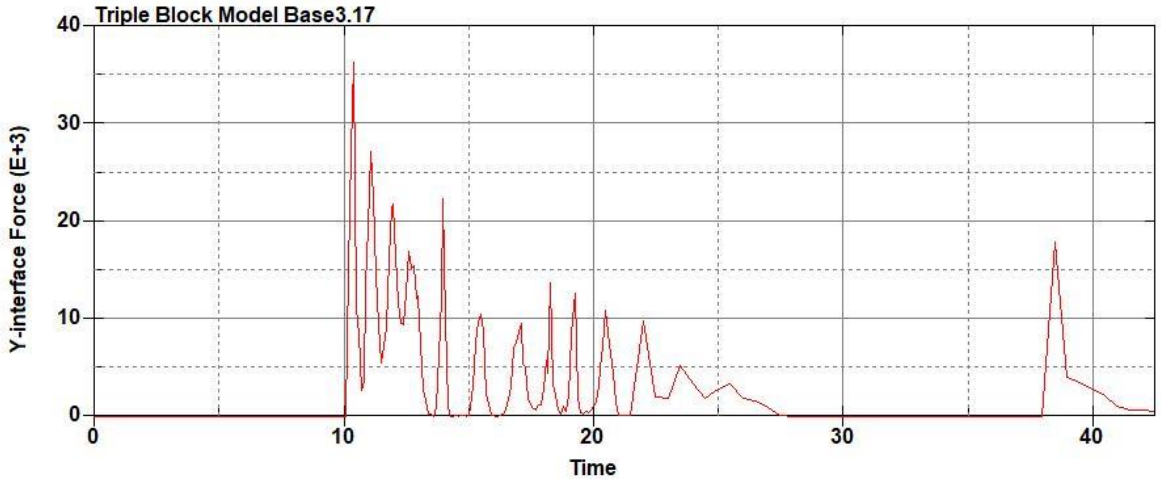


**Figure B-129: Base Run 3.17 Right Support Y-Interface Force (lbs) versus Time (ms) – 850 psi**

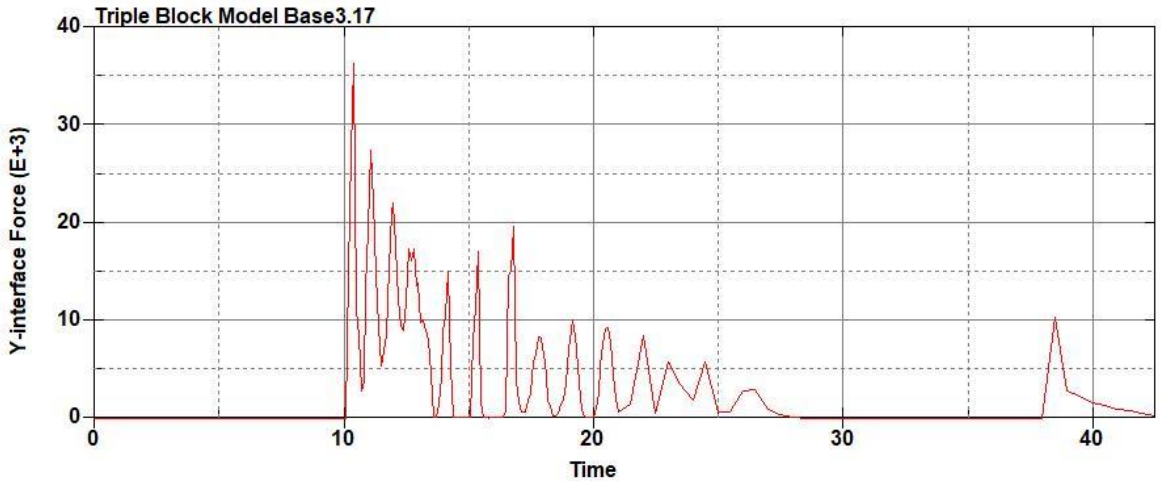


**Figure B-130: Base Run 3.17 Left Support Y-Interface Force (lbs) versus Time (ms) – 850 psi**

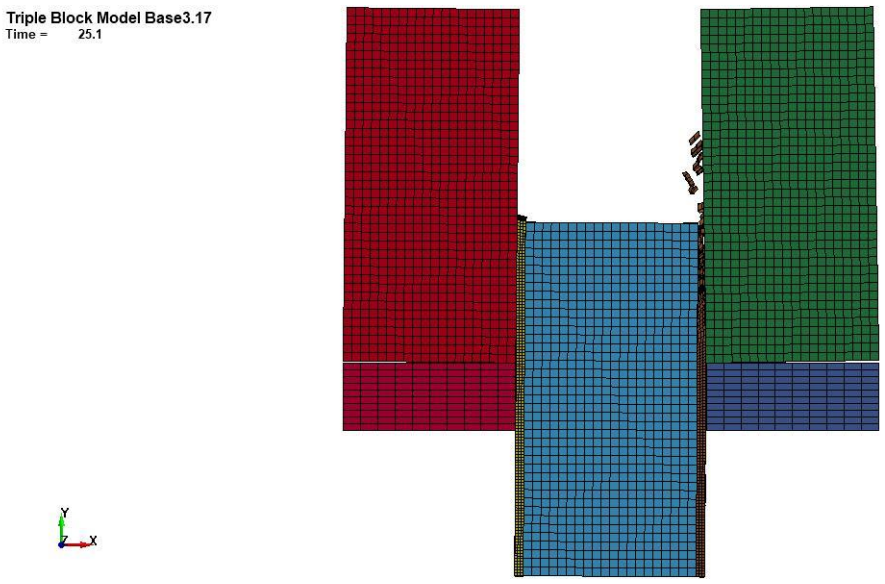


**Figure B-131: Last State at 60 Milliseconds for Base Run 3.17 – 850 psi**

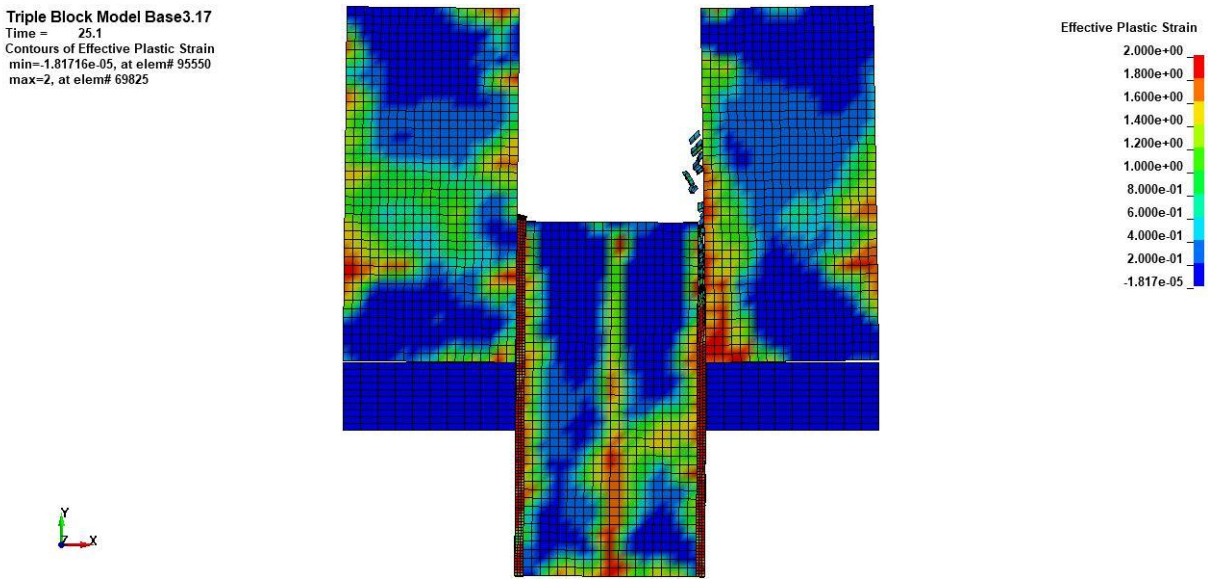


**Figure B-132: Effective Plastic Strain Fringe Plot for Last State at 60 Milliseconds for Base Run 3.17 – 850 psi**

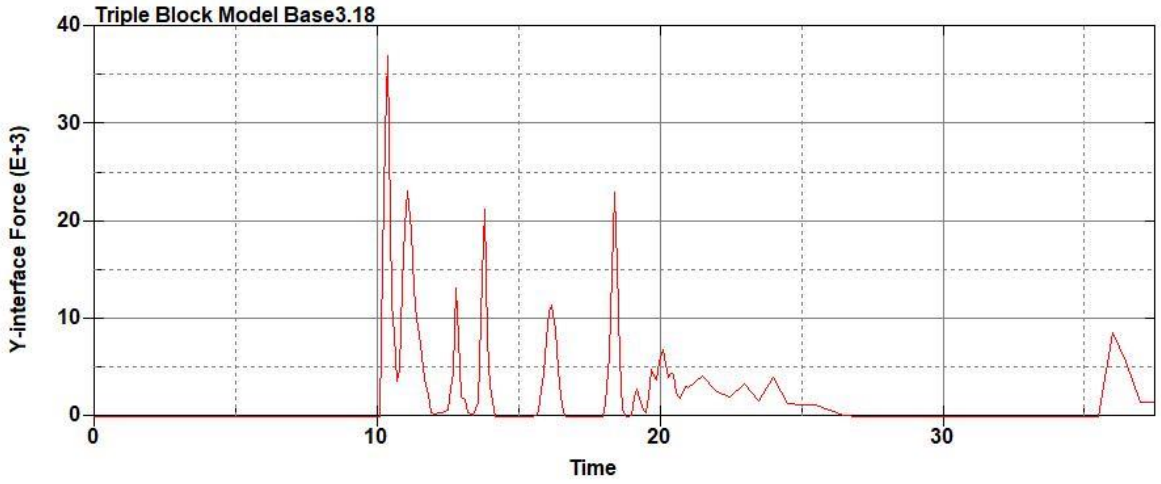


**Figure B-133: Base Run 3.18 Right Support Y-Interface Force (lbs) versus Time (ms) – 900 psi**

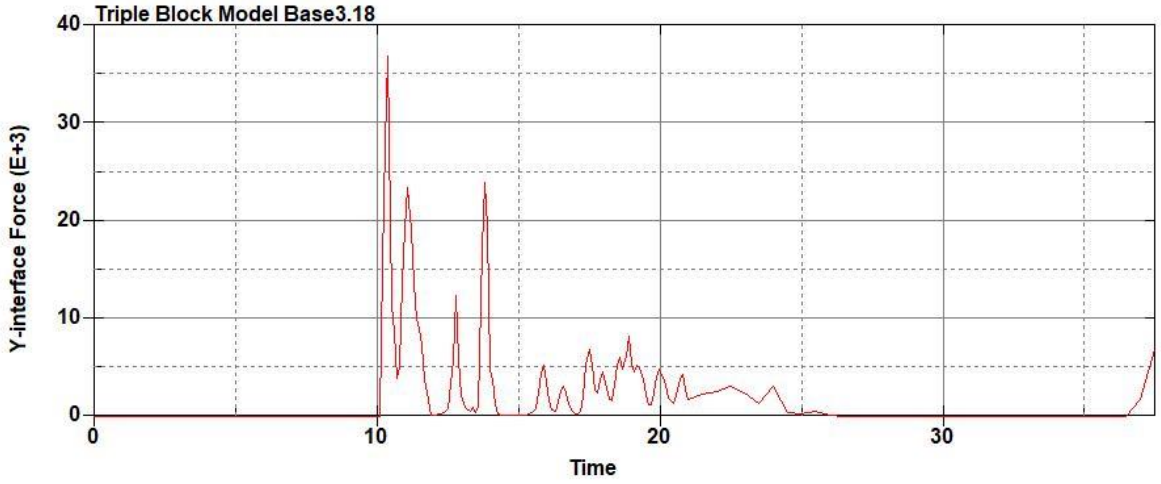


**Figure B-134: Base Run 3.18 Left Support Y-Interface Force (lbs) versus Time (ms) – 900 psi**

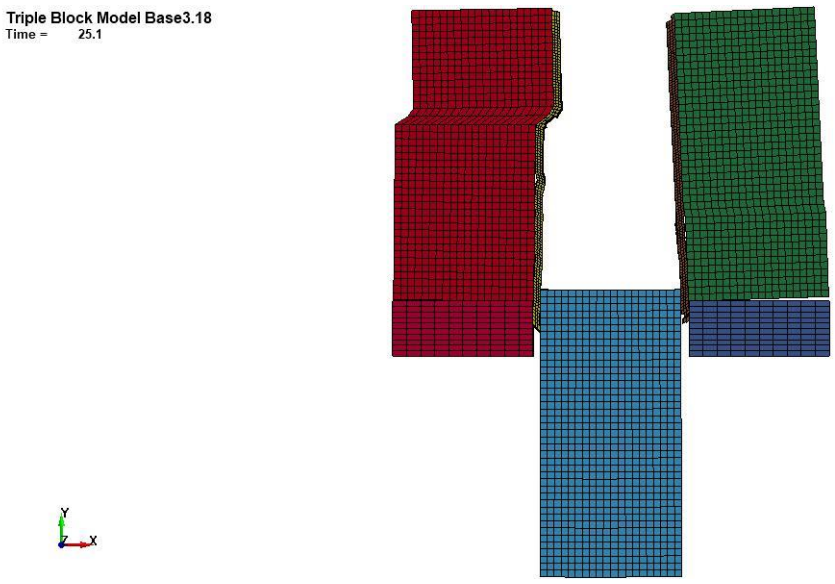


**Figure B-135: Last State at 60 Milliseconds for Base Run 3.18 – 900 psi**

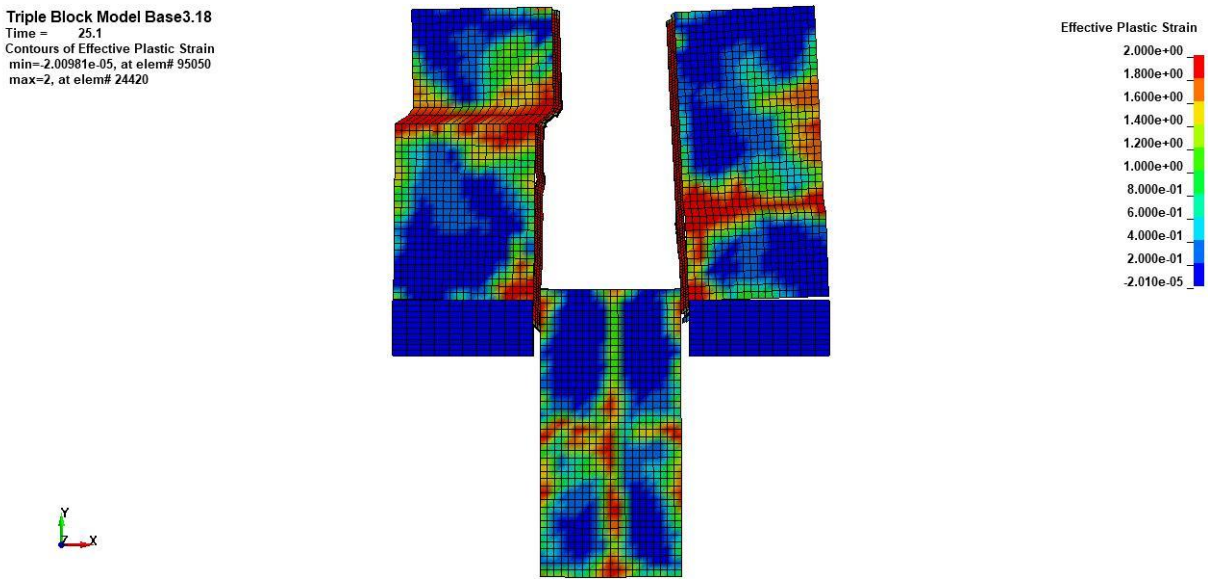


**Figure B-136: Effective Plastic Strain Fringe Plot for Last State at 60 Milliseconds for Base Run 3.18 – 900 psi**

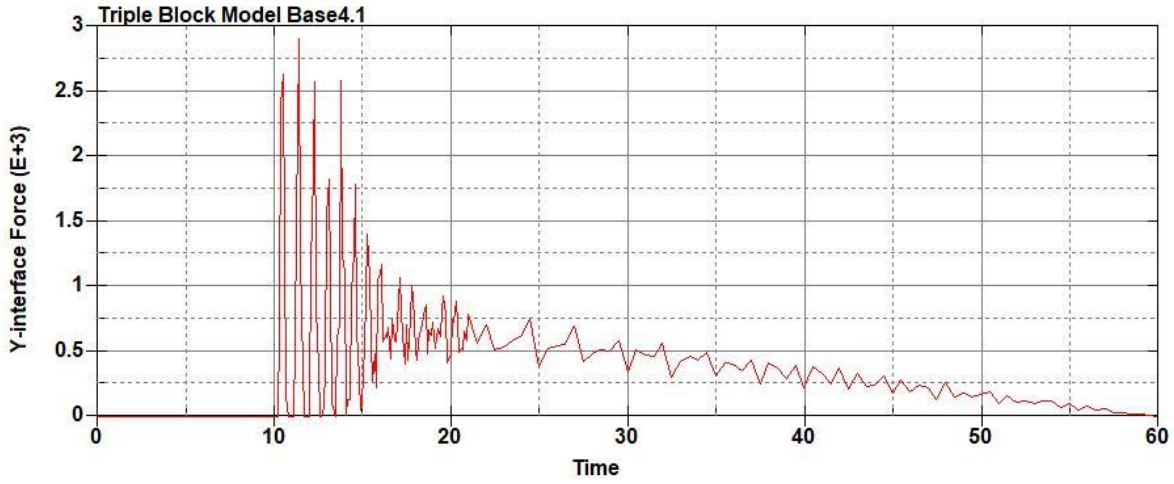


**Figure B-137: Base Run 4.1 Right Support Y-Interface Force (lbs) versus Time (ms) – 50 psi**

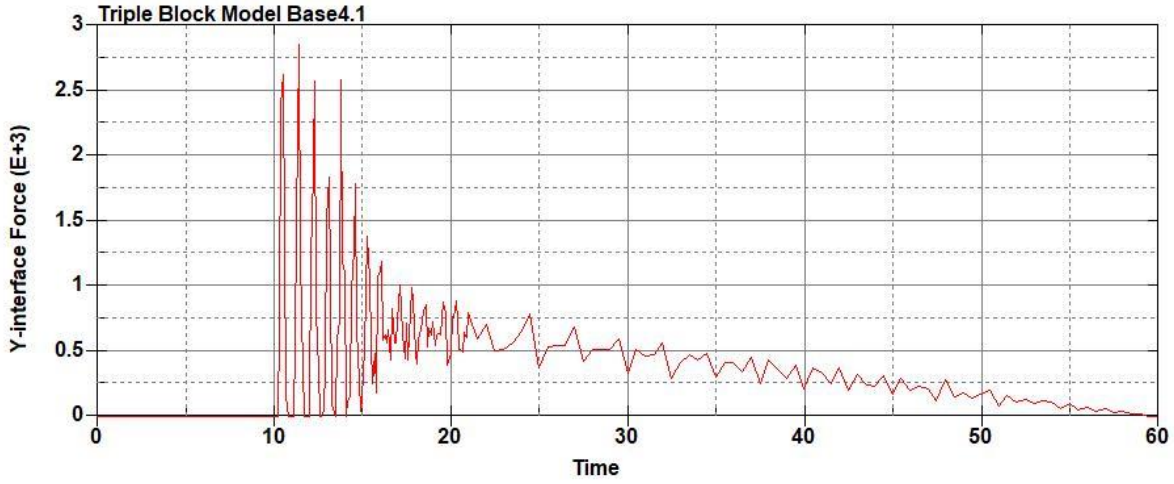


**Figure B-138: Base Run 4.1 Left Support Y-Interface Force (lbs) versus Time (ms) – 50 psi**

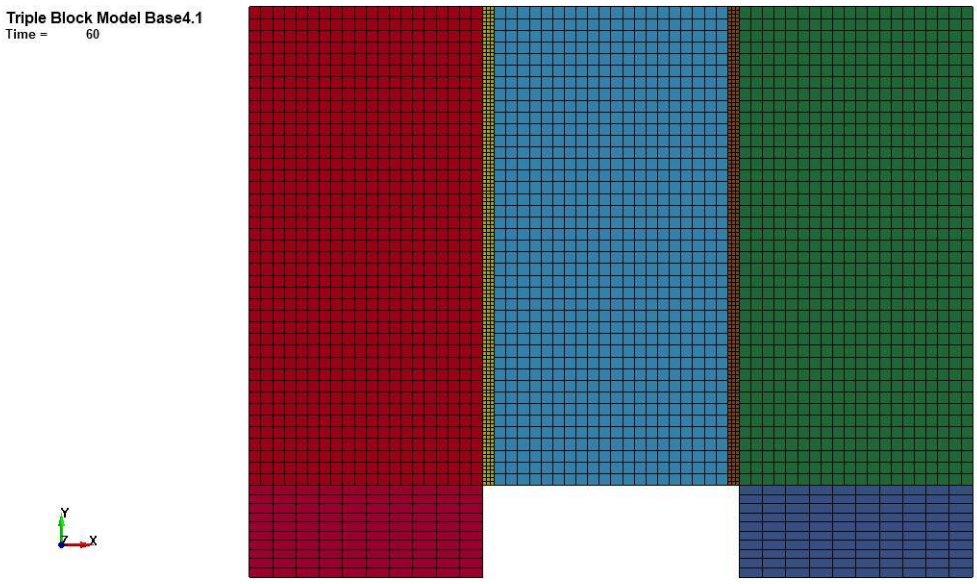


**Figure B-139: Last State at 60 Milliseconds for Base Run 4.1 – 50 psi**

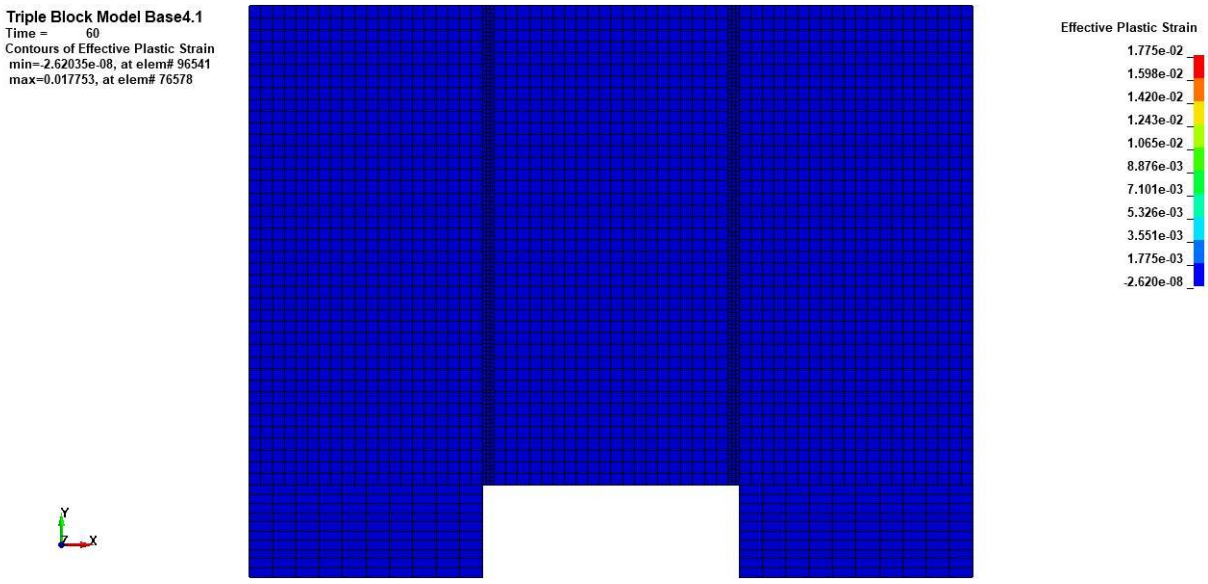


**Figure B-140: Effective Plastic Strain Fringe Plot for Last State at 60 Milliseconds for Base Run 4.1 –50 psi**

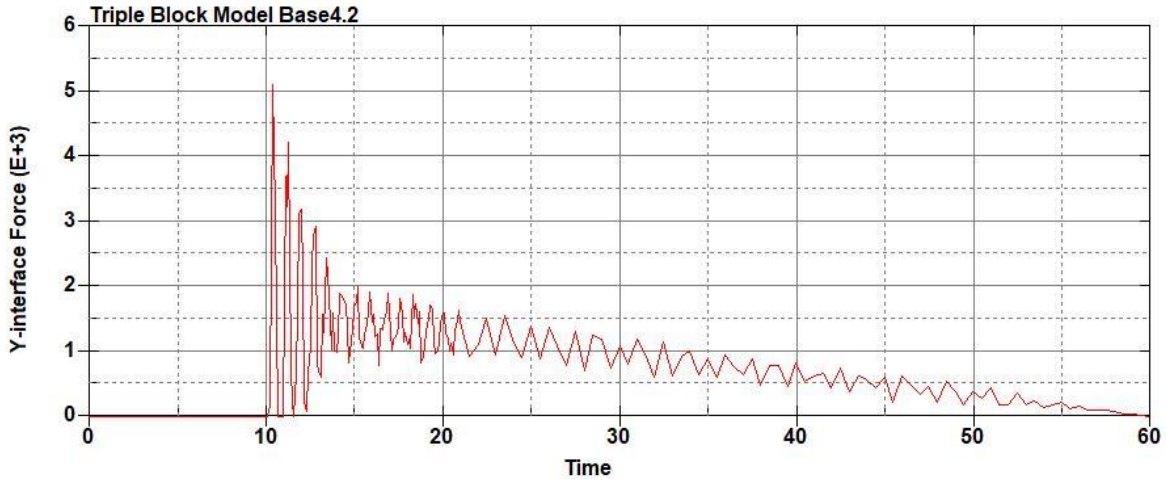


**Figure B-141: Base Run 4.2 Right Support Y-Interface Force (lbs) versus Time (ms) – 100 psi**

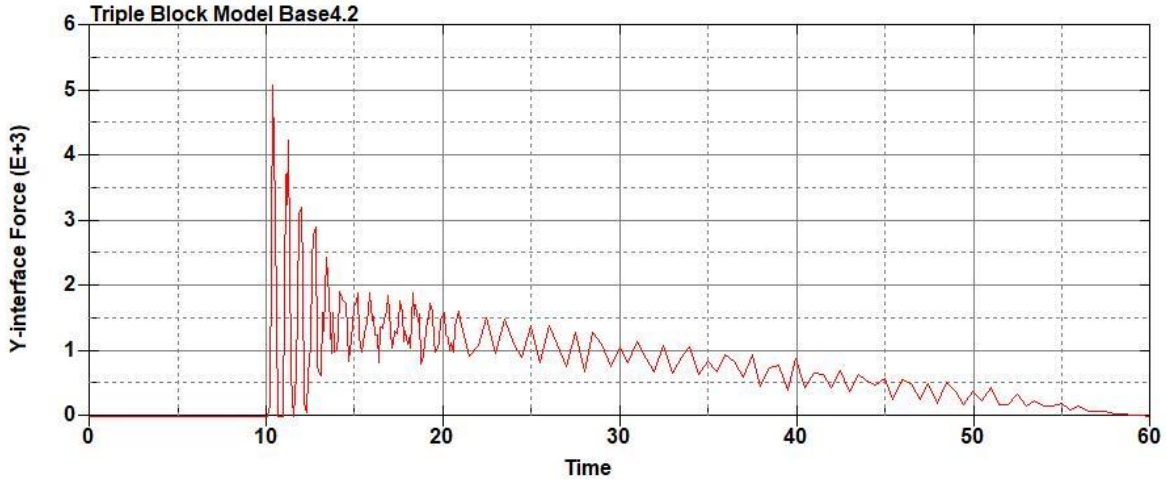


**Figure B-142: Base Run 4.2 Left Support Y-Interface Force (lbs) versus Time (ms) – 100 psi**

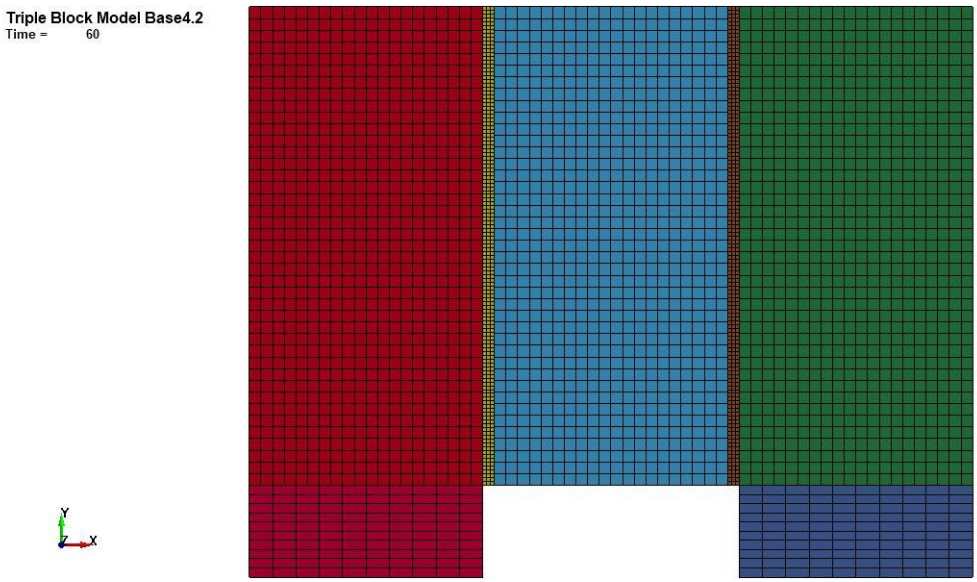


**Figure B-143: Last State at 60 Milliseconds for Base Run 4.2 – 100 psi**

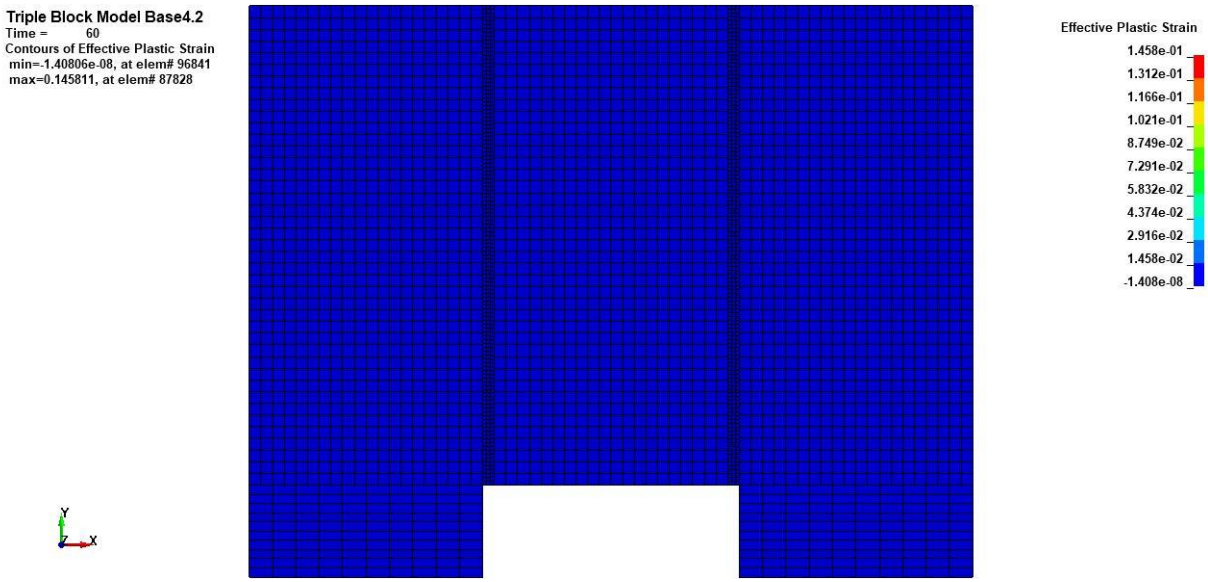


**Figure B-144: Effective Plastic Strain Fringe Plot for Last State at 60 Milliseconds for Base Run 4.2 – 100 psi**

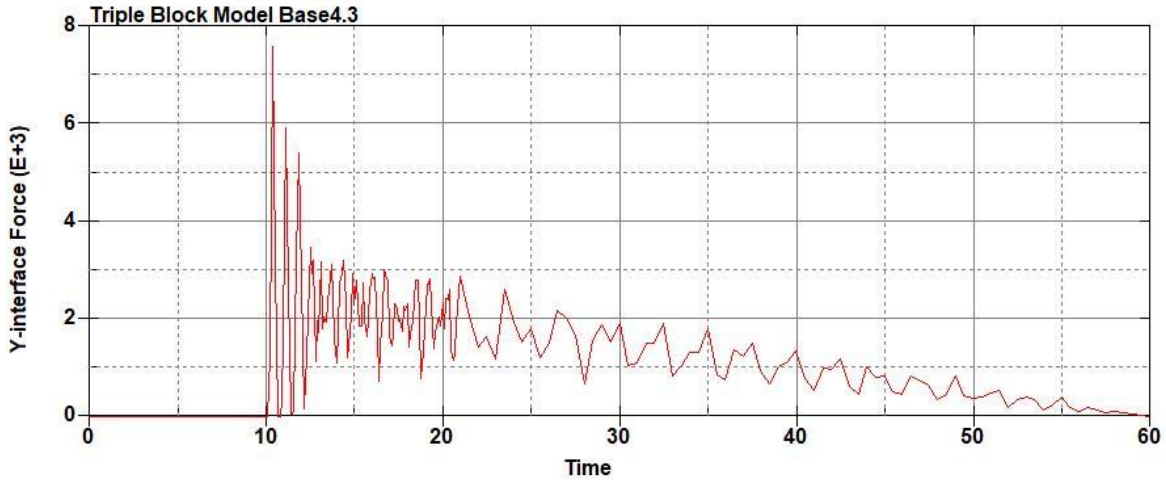


**Figure B-145: Base Run 4.3 Right Support Y-Interface Force (lbs) versus Time (ms) – 150 psi**

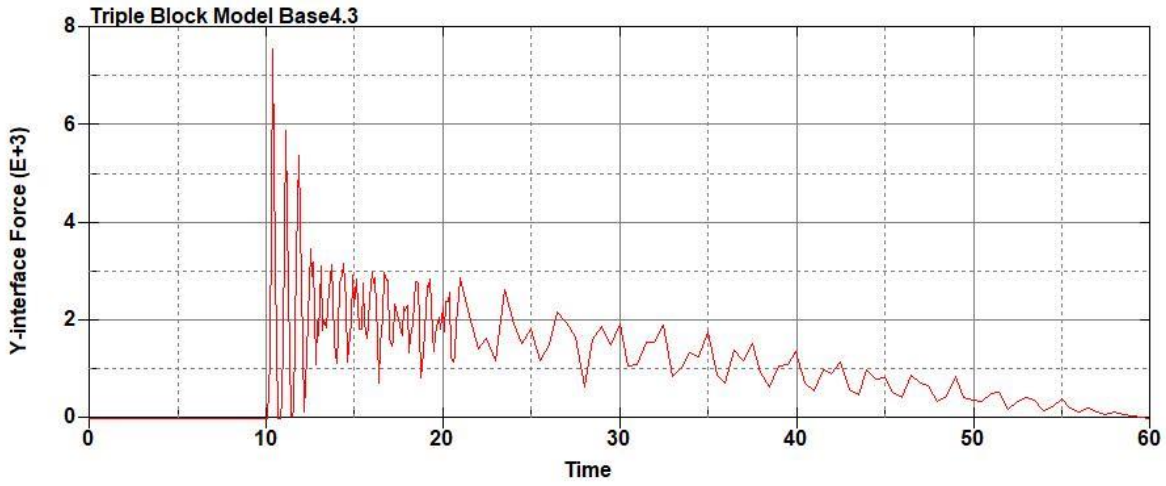


**Figure B-146: Base Run 4.3 Left Support Y-Interface Force (lbs) versus Time (ms) – 150 psi**

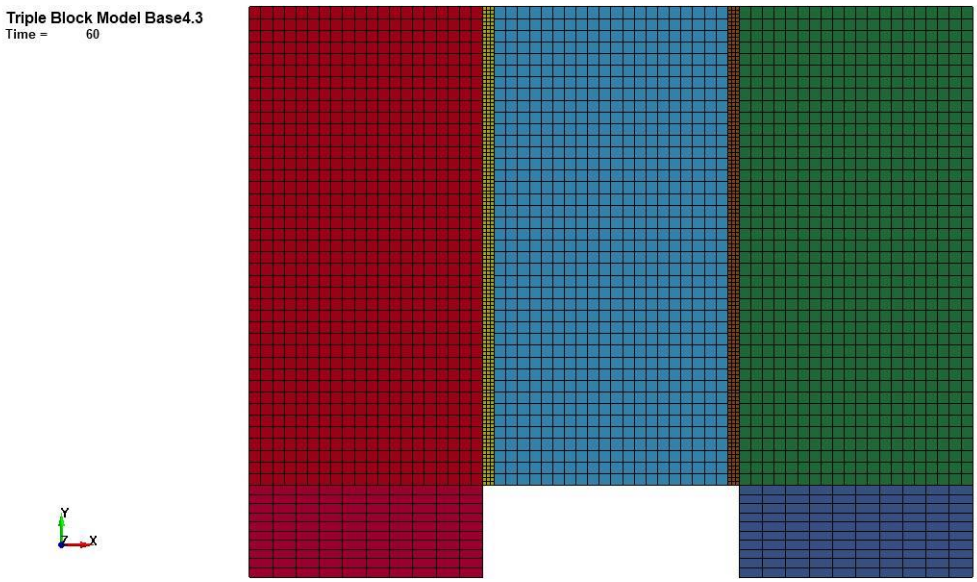


**Figure B-147: Last State at 60 Milliseconds for Base Run 4.3 – 150 psi**

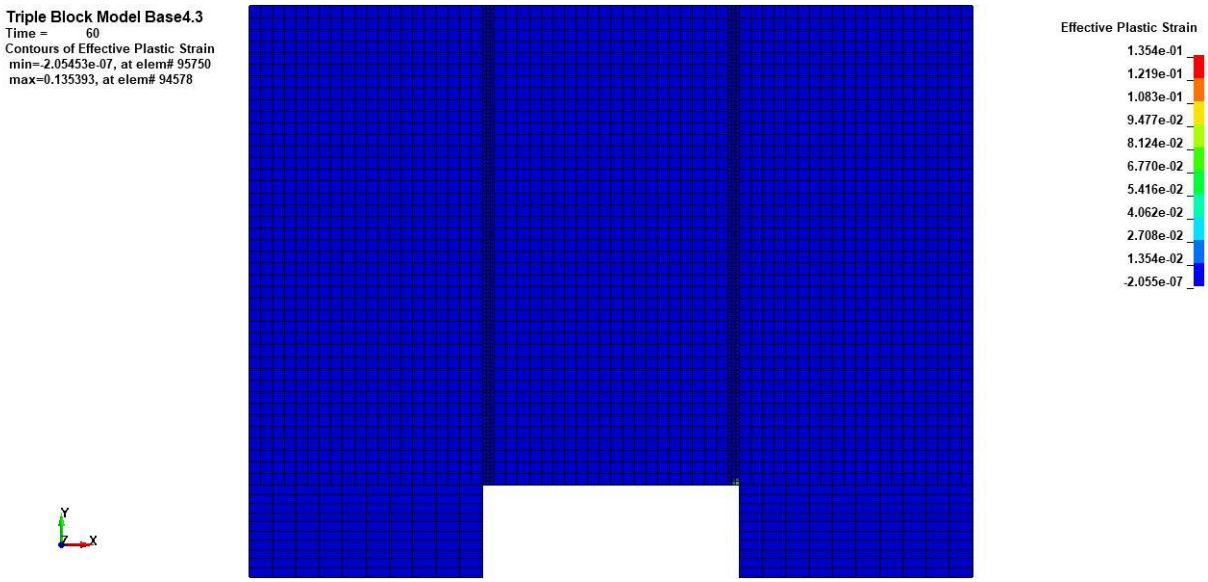


**Figure B-148: Effective Plastic Strain Fringe Plot for Last State at 60 Milliseconds for Base Run 4.3 – 150 psi**

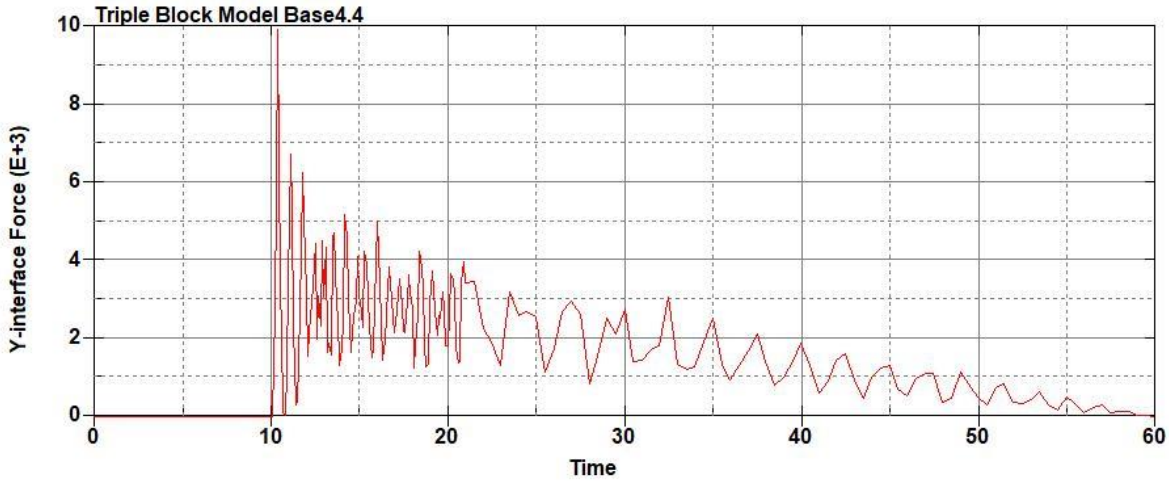


**Figure B-149: Base Run 4.4 Right Support Y-Interface Force (lbs) versus Time (ms) – 200 psi**

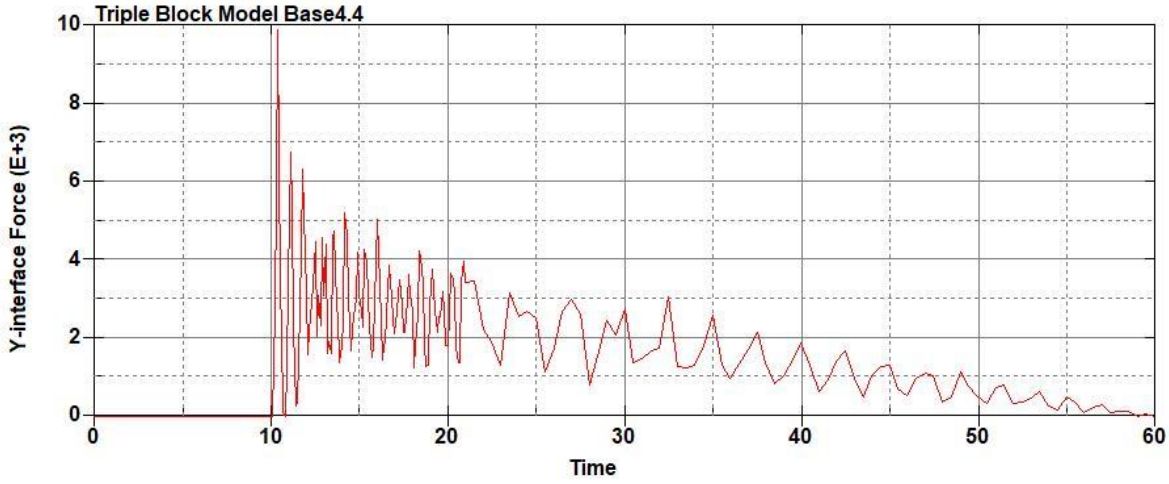


**Figure B-150: Base Run 4.4 Left Support Y-Interface Force (lbs) versus Time (ms) – 200 psi**

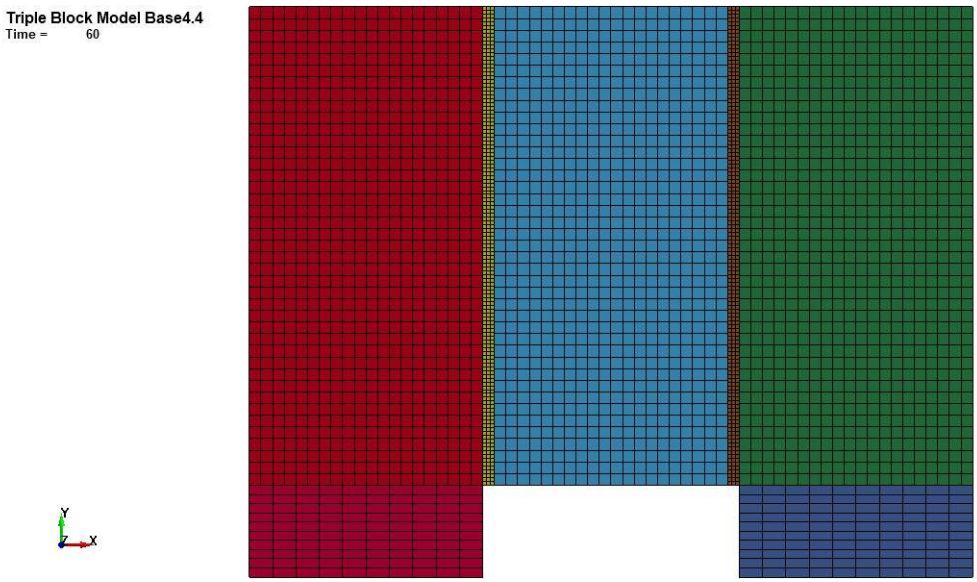


**Figure B-151: Last State at 60 Milliseconds for Base Run 4.4 – 200 psi**

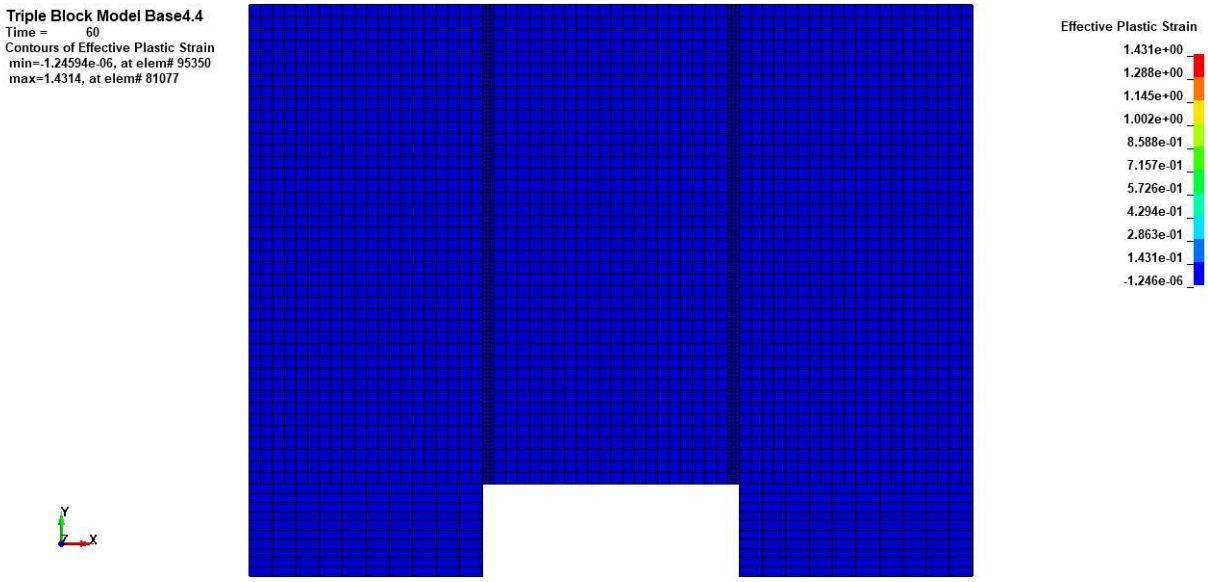


**Figure B-152: Effective Plastic Strain Fringe Plot for Last State at 60 Milliseconds for Base Run 4.4 – 200 psi**

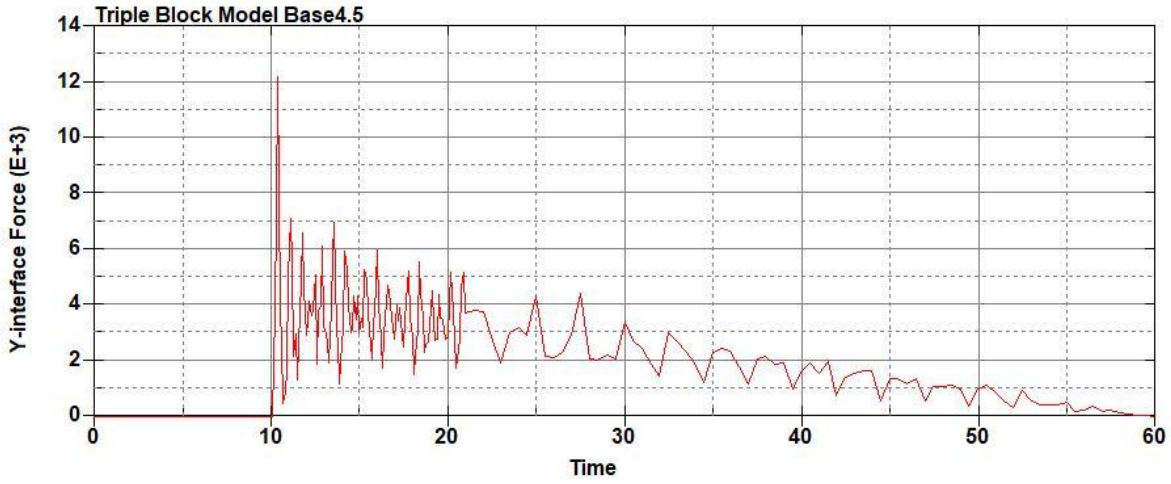


**Figure B-153: Base Run 4.5 Right Support Y-Interface Force (lbs) versus Time (ms) – 250 psi**

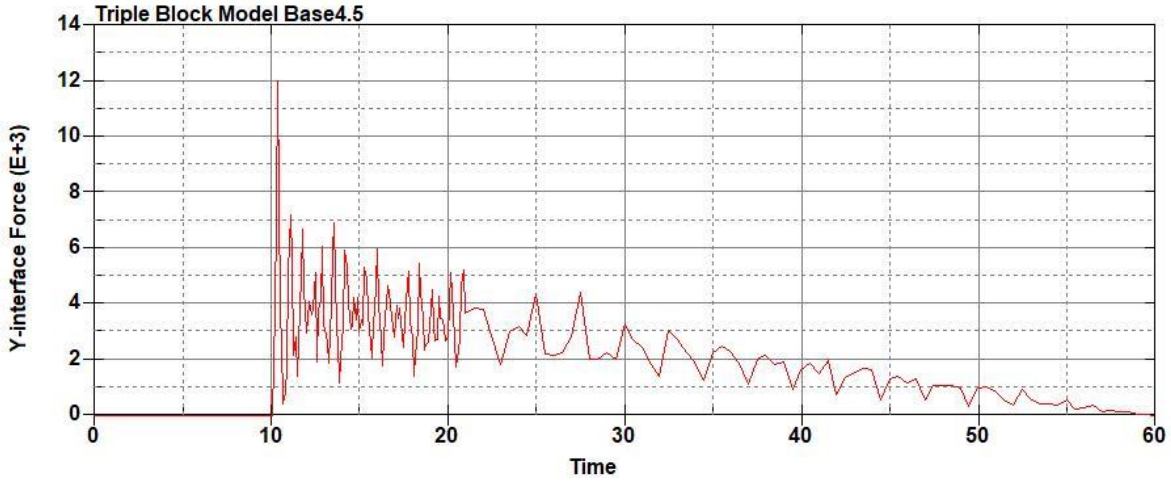


**Figure B-154: Base Run 4.5 Left Support Y-Interface Force (lbs) versus Time (ms) – 250 psi**

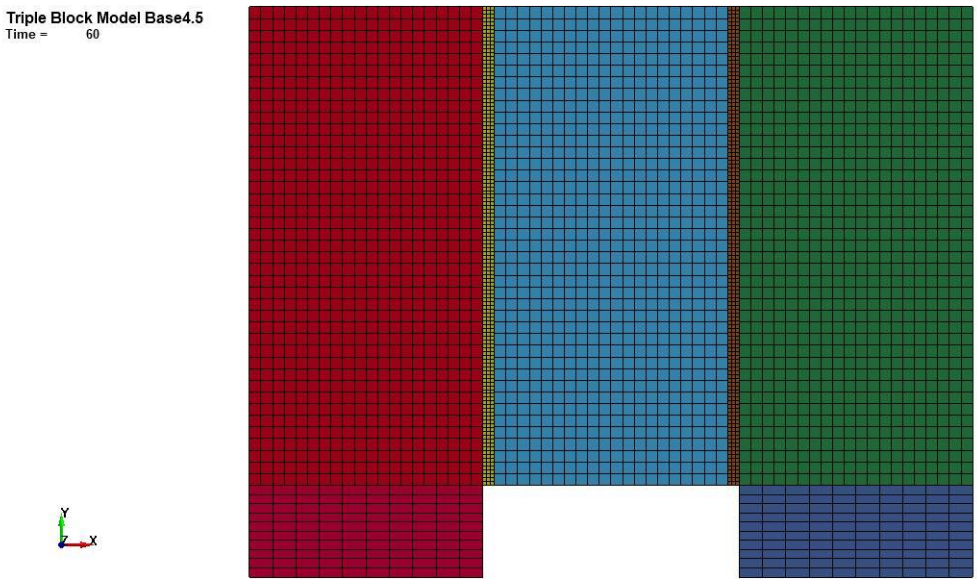


**Figure B-155: Last State at 60 Milliseconds for Base Run 4.5 – 250 psi**

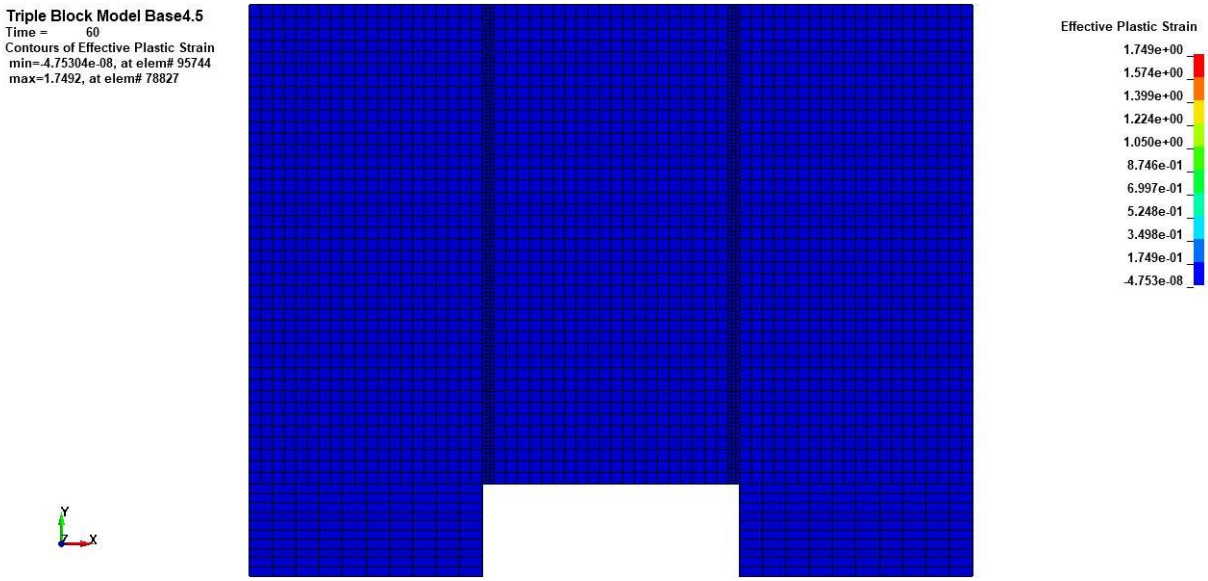


**Figure B-156: Effective Plastic Strain Fringe Plot for Last State at 60 Milliseconds for Base Run 4.5 – 250 psi**

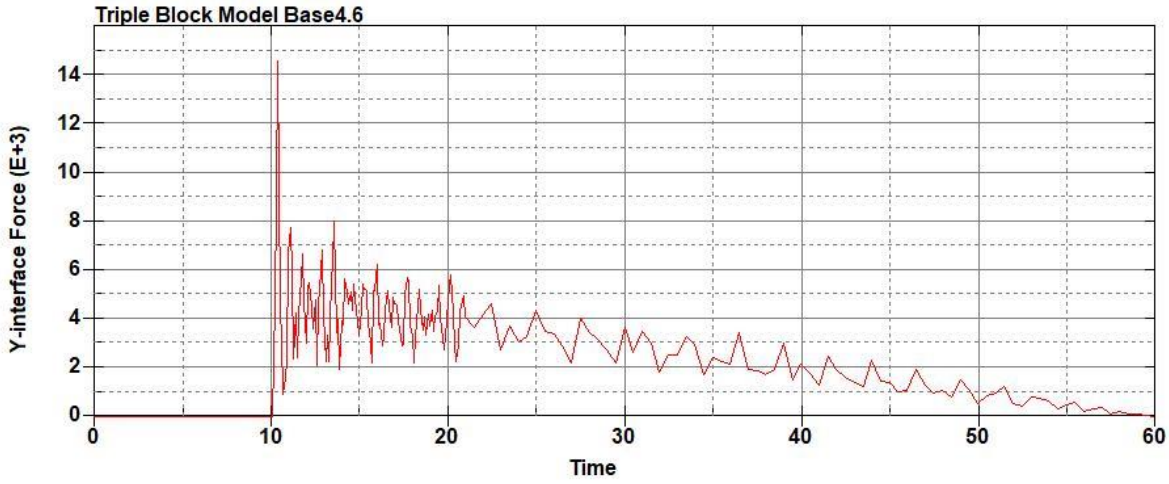


**Figure B-157: Base Run 4.6 Right Support Y-Interface Force (lbs) versus Time (ms) – 300 psi**

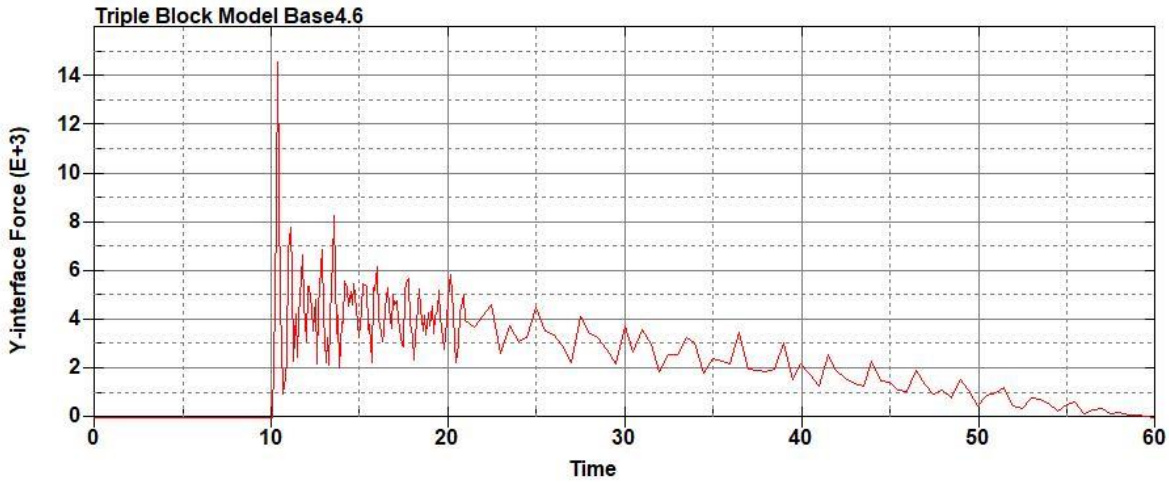


**Figure B-158: Base Run 4.6 Left Support Y-Interface Force (lbs) versus Time (ms) – 300 psi**

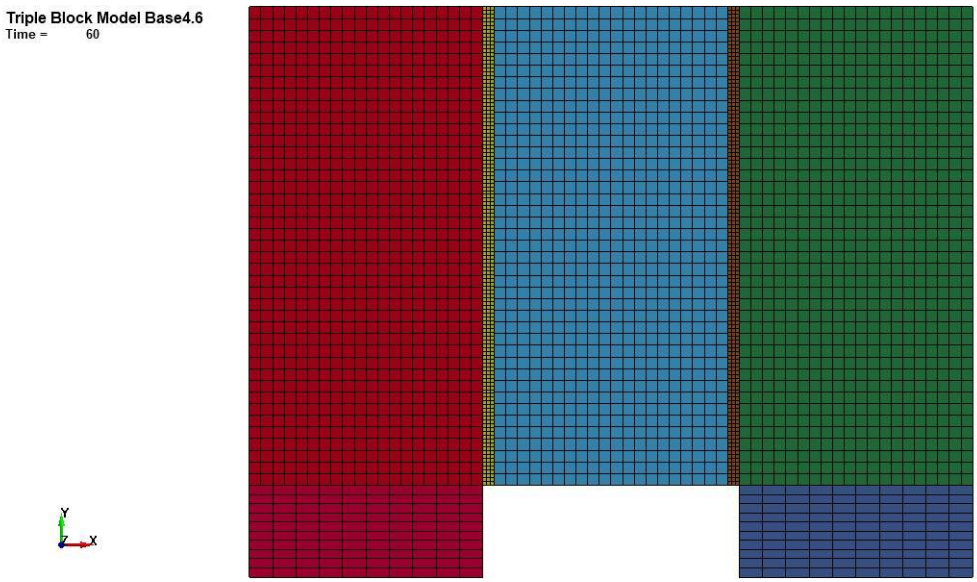


**Figure B-159: Last State at 60 Milliseconds for Base Run 4.6 – 300 psi**

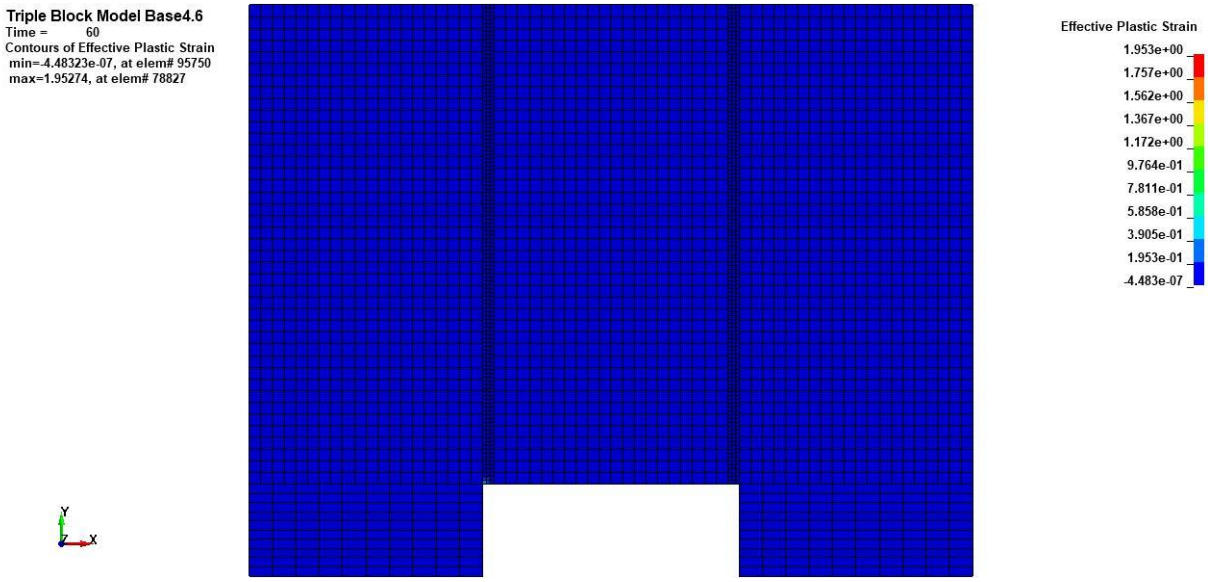


**Figure B-160: Effective Plastic Strain Fringe Plot for Last State at 60 Milliseconds for Base Run 4.6 – 300 psi**

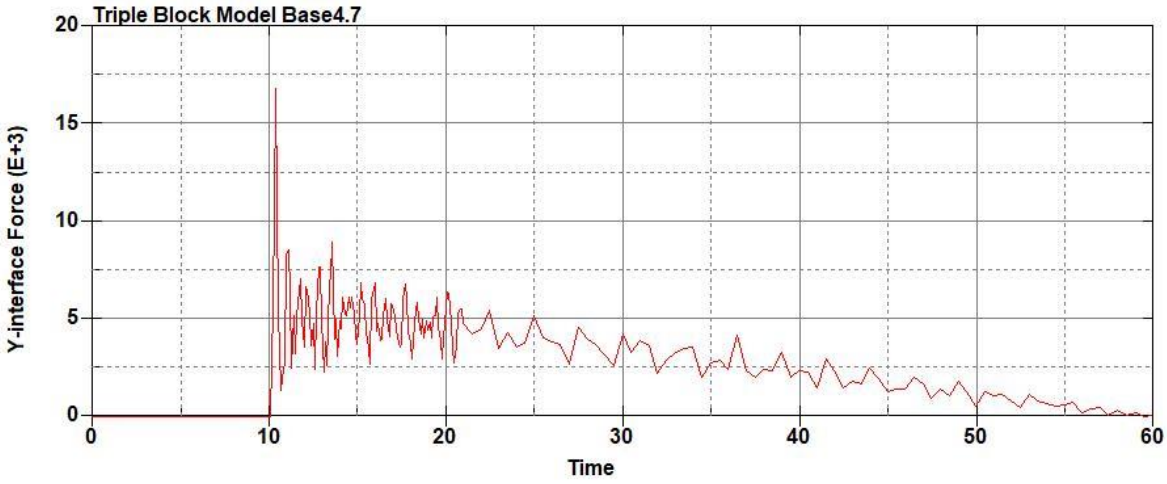


**Figure B-161: Base Run 4.7 Right Support Y-Interface Force (lbs) versus Time (ms) – 350 psi**

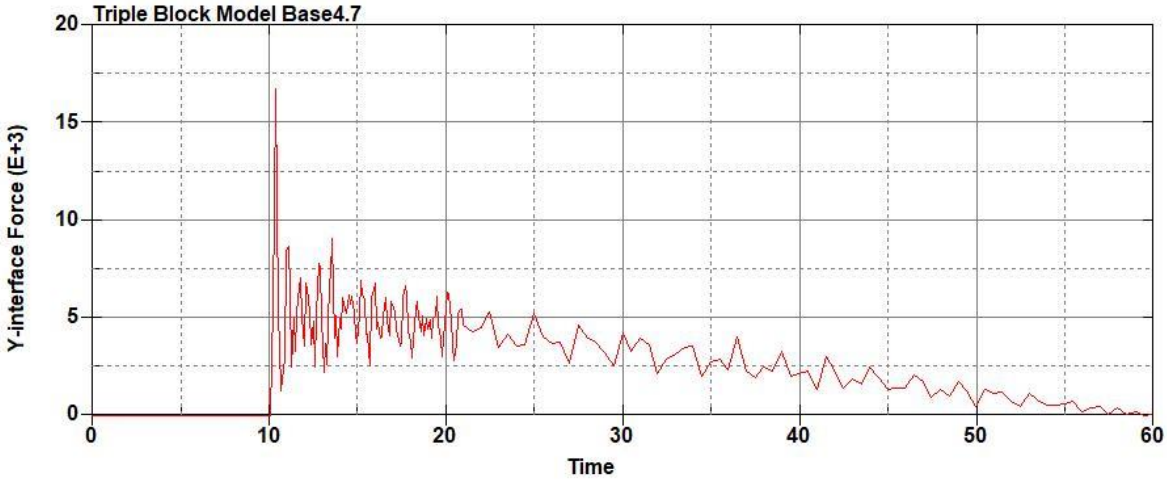


**Figure B-162: Base Run 4.7 Left Support Y-Interface Force (lbs) versus Time (ms) – 350 psi**

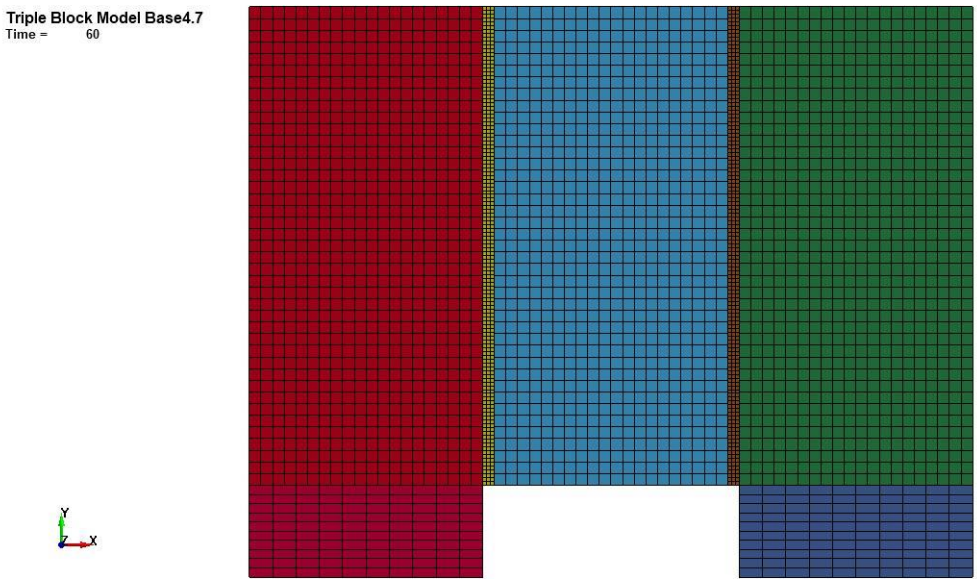


**Figure B-163: Last State at 60 Milliseconds for Base Run 4.7 – 350 psi**

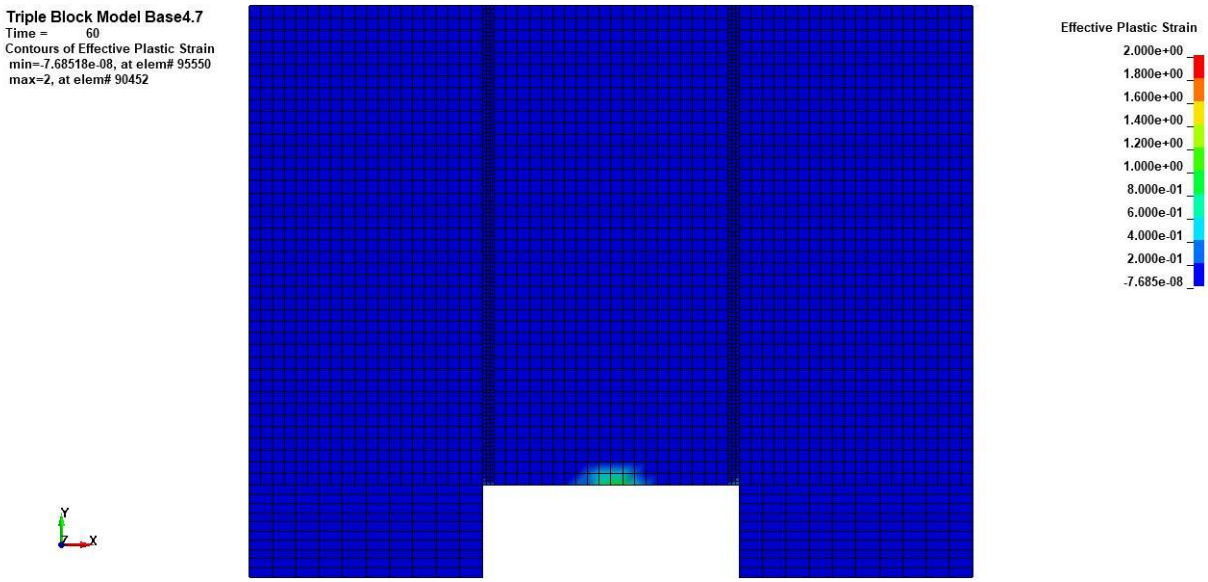


**Figure B-164: Effective Plastic Strain Fringe Plot for Last State at 60 Milliseconds for Base Run 4.7 – 350 psi**

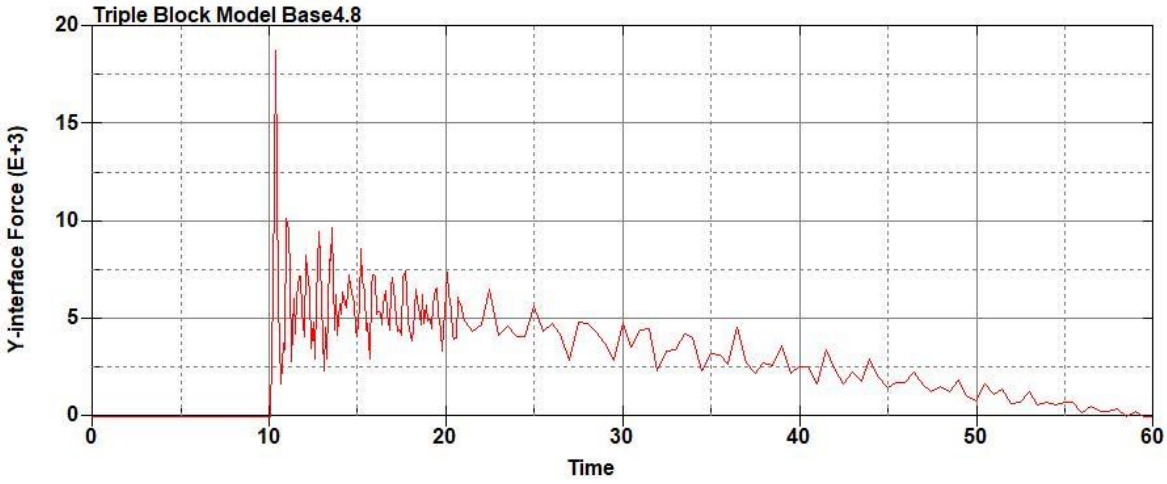


**Figure B-165: Base Run 4.8 Right Support Y-Interface Force (lbs) versus Time (ms) – 400 psi**

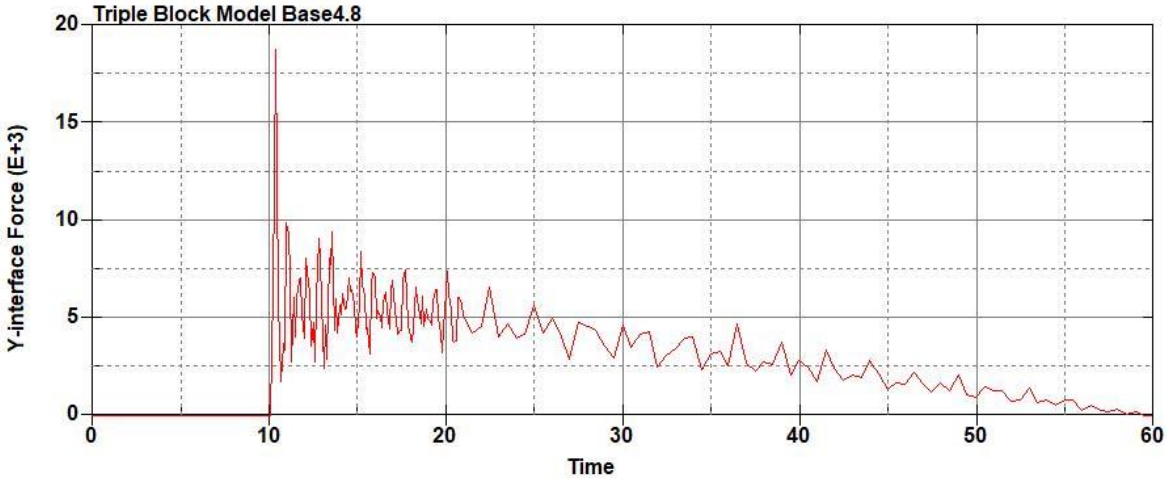


**Figure B-166: Base Run 4.8 Left Support Y-Interface Force (lbs) versus Time (ms) – 400 psi**

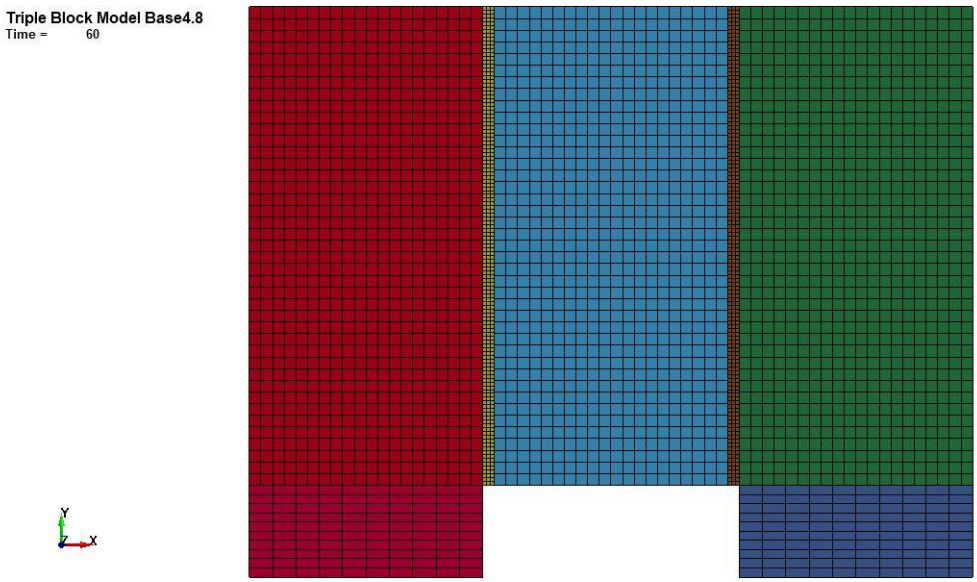


**Figure B-167: Last State at 60 Milliseconds for Base Run 4.8 – 400 psi**

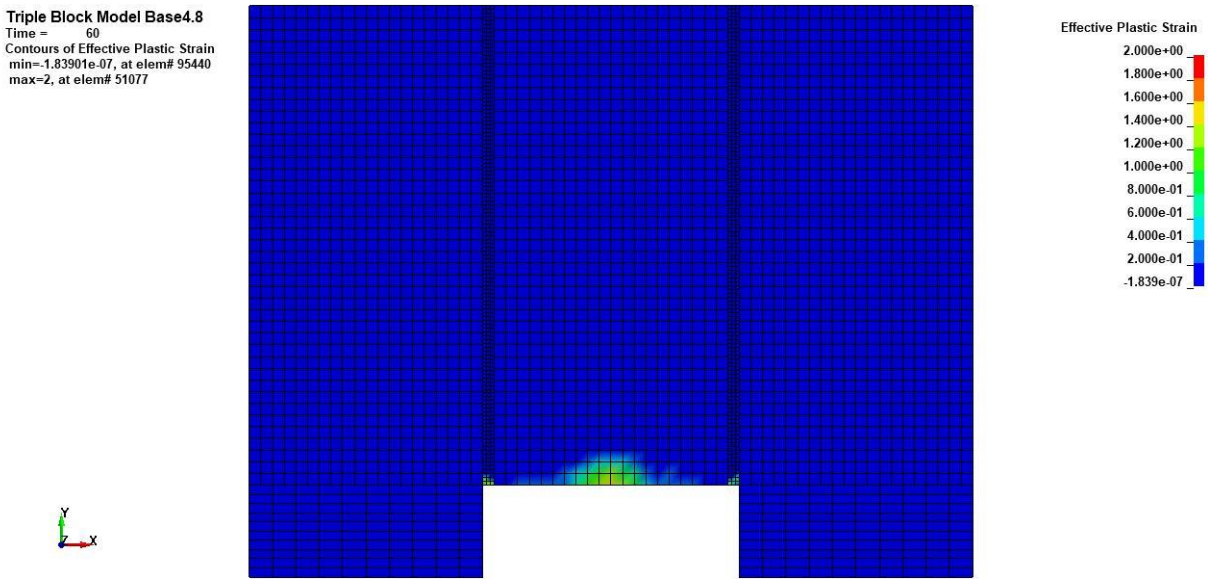


**Figure B-168: Effective Plastic Strain Fringe Plot for Last State at 60 Milliseconds for Base Run 4.8 – 400 psi**

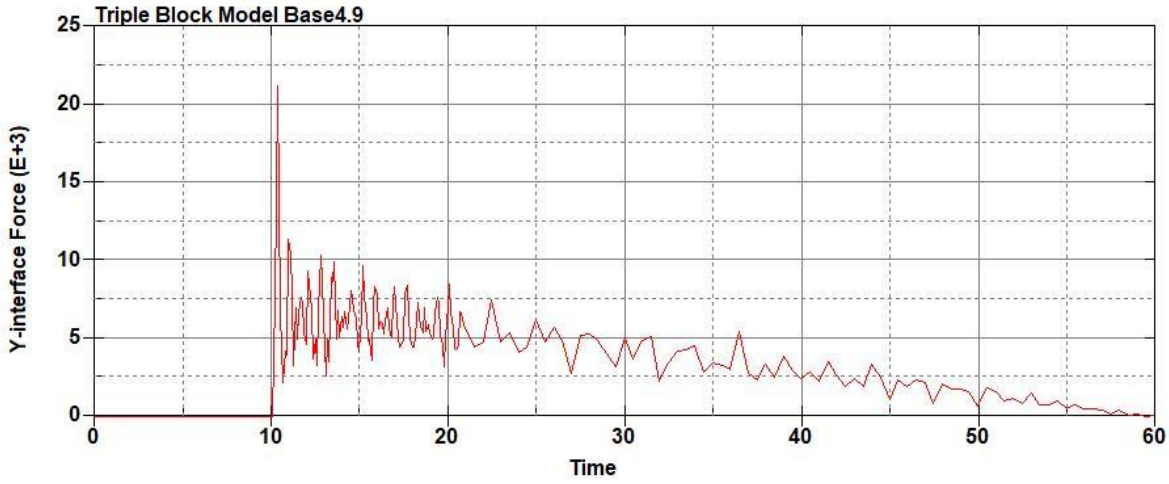


**Figure B-169: Base Run 4.9 Right Support Y-Interface Force (lbs) versus Time (ms) – 450 psi**

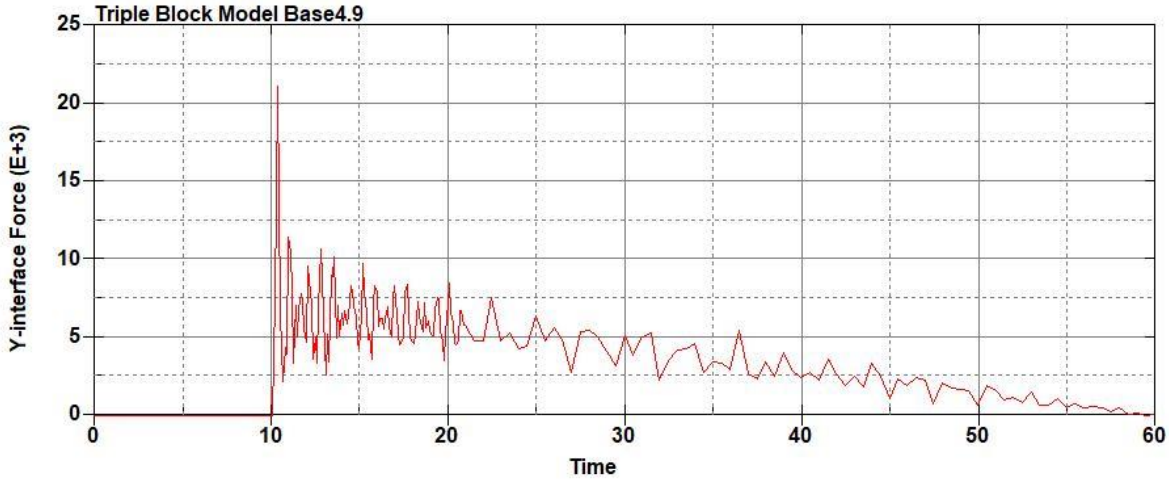


**Figure B-170: Base Run 4.9 Left Support Y-Interface Force (lbs) versus Time (ms) – 450 psi**

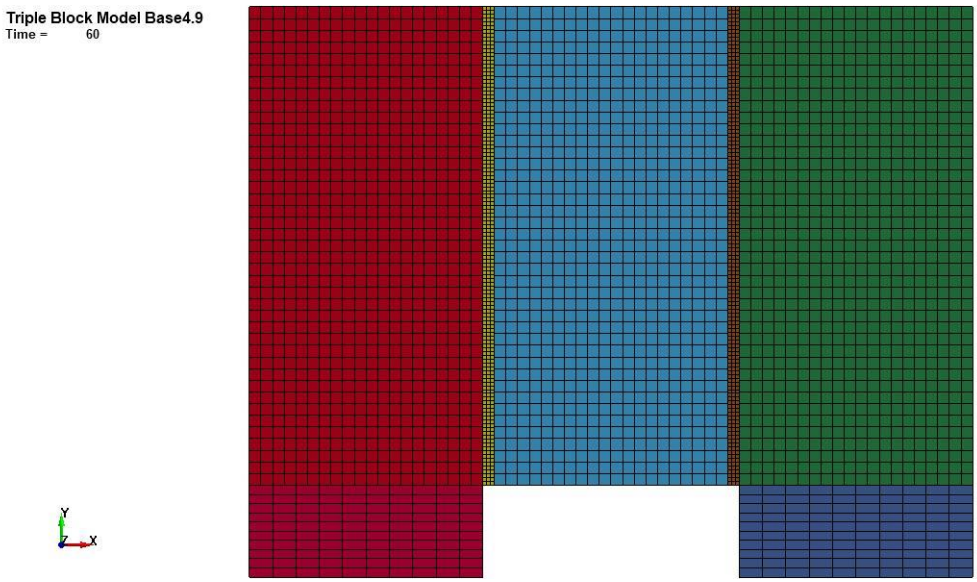


**Figure B-171: Last State at 60 Milliseconds for Base Run 4.9 – 450 psi**

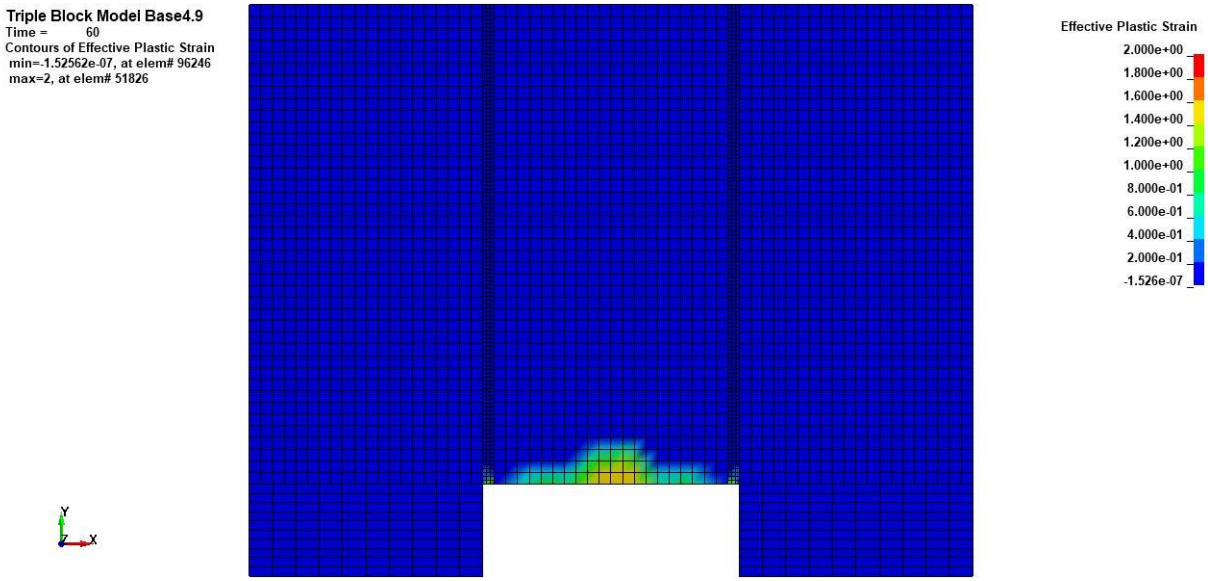


**Figure B-172: Effective Plastic Strain Fringe Plot for Last State at 60 Milliseconds for Base Run 4.9 – 450 psi**

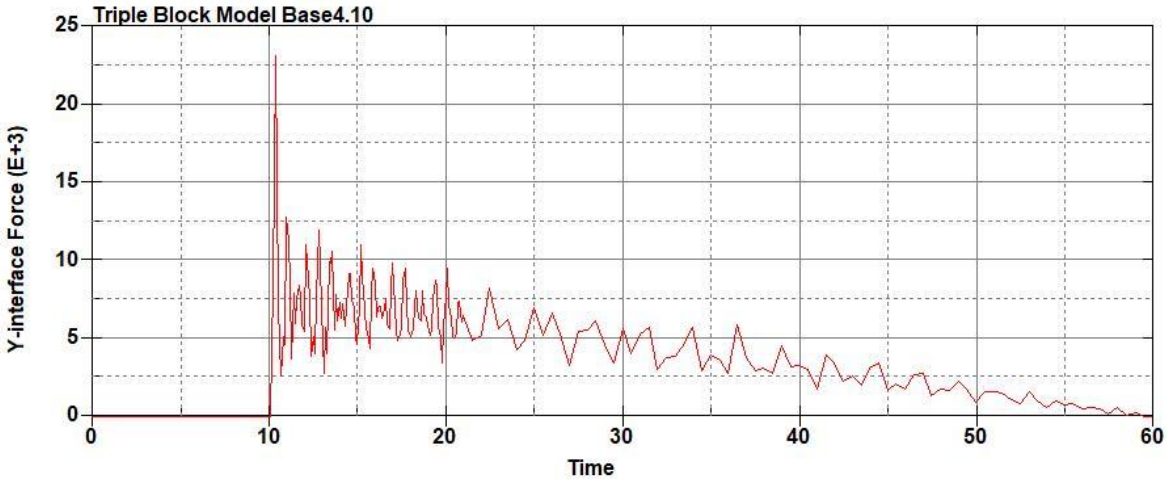


**Figure B-173: Base Run 4.10 Right Support Y-Interface Force (lbs) versus Time (ms) – 500 psi**

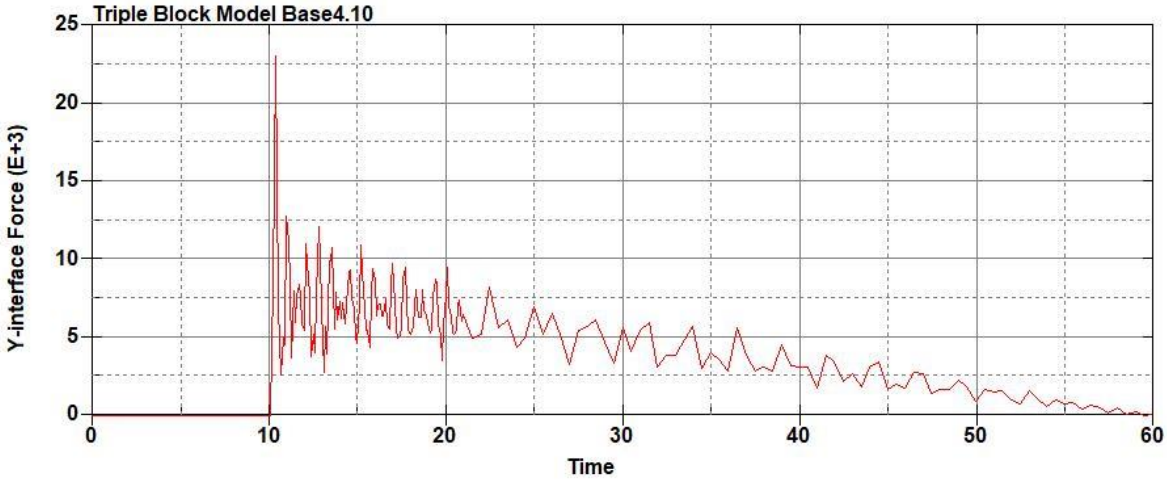


**Figure B-174: Base Run 4.10 Left Support Y-Interface Force (lbs) versus Time (ms) – 500 psi**

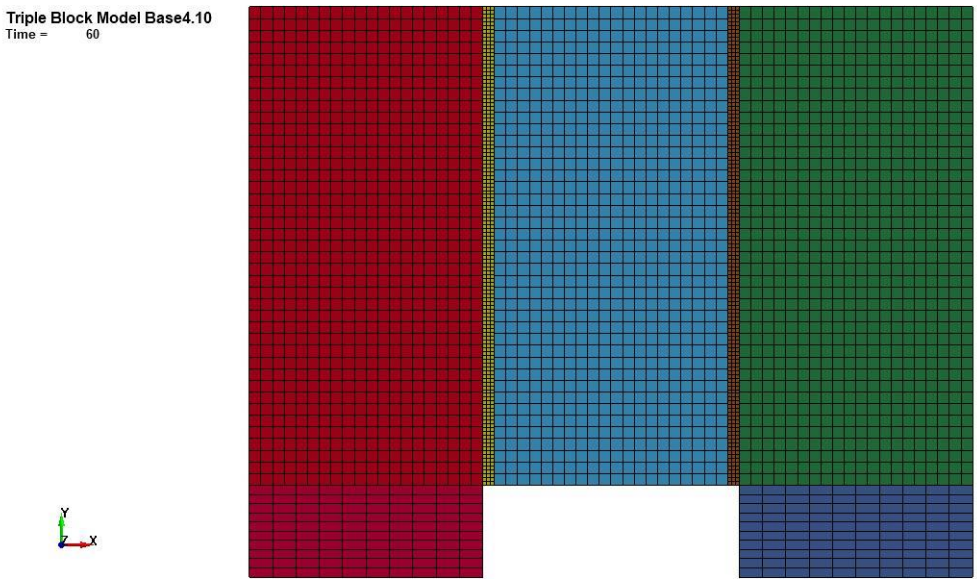


**Figure B-175: Last State at 60 Milliseconds for Base Run 4.10 – 500 psi**

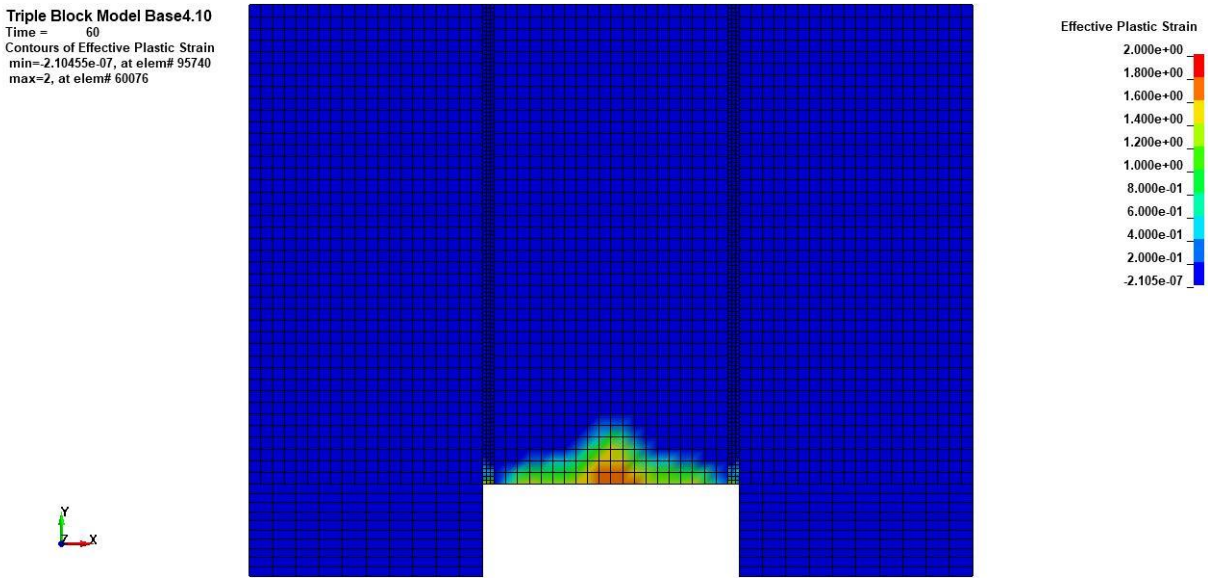


**Figure B-176: Effective Plastic Strain Fringe Plot for Last State at 60 Milliseconds for Base Run 4.10 – 500 psi**

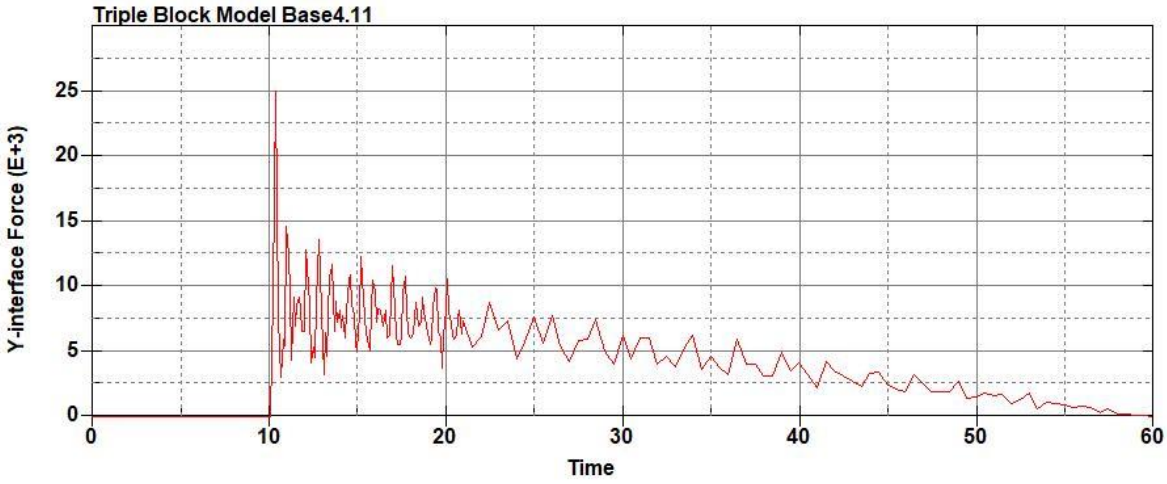


**Figure B-177: Base Run 4.11 Right Support Y-Interface Force (lbs) versus Time (ms) – 550 psi**

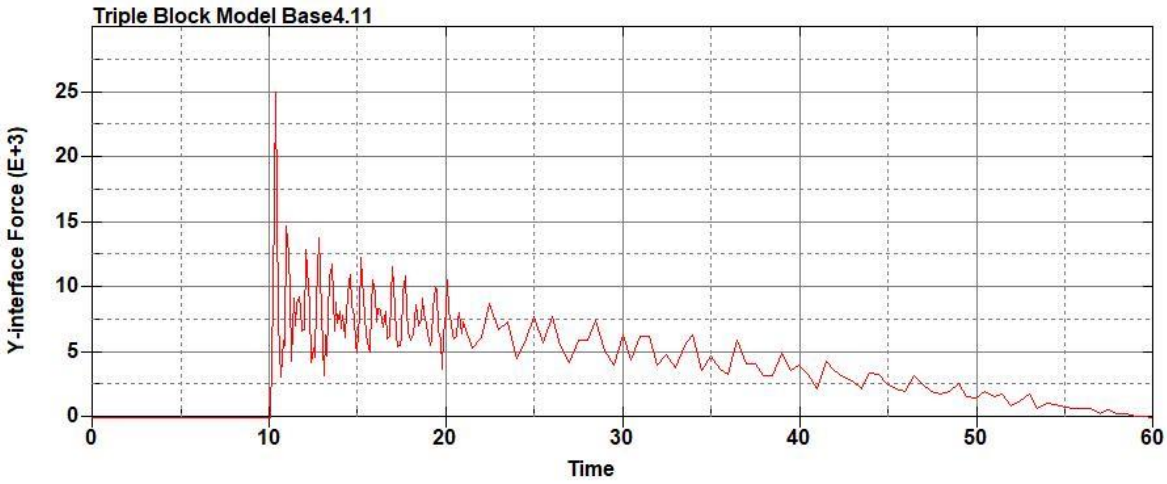


**Figure B-178: Base Run 4.11 Left Support Y-Interface Force (lbs) versus Time (ms) – 550 psi**

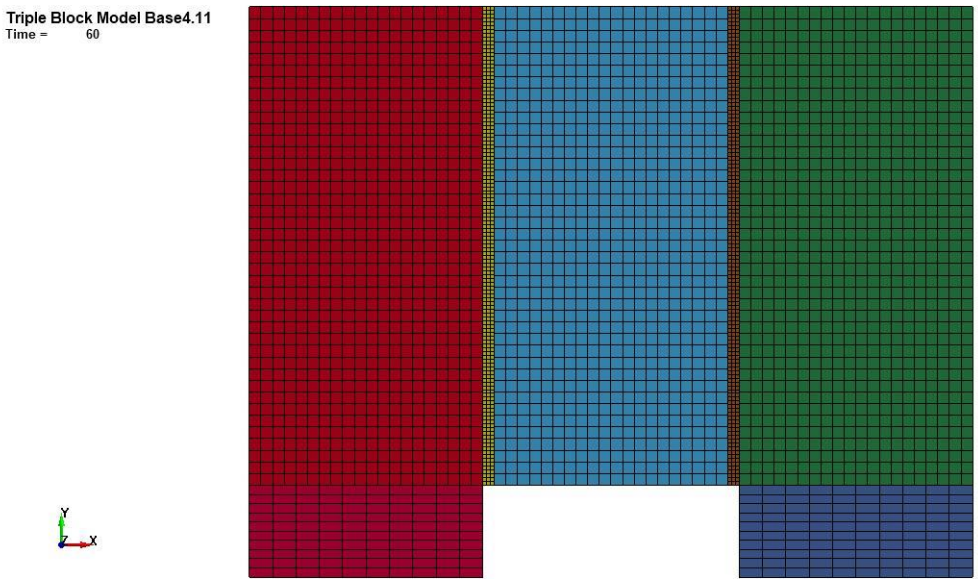


**Figure B-179: Last State at 60 Milliseconds for Base Run 4.11 – 550 psi**

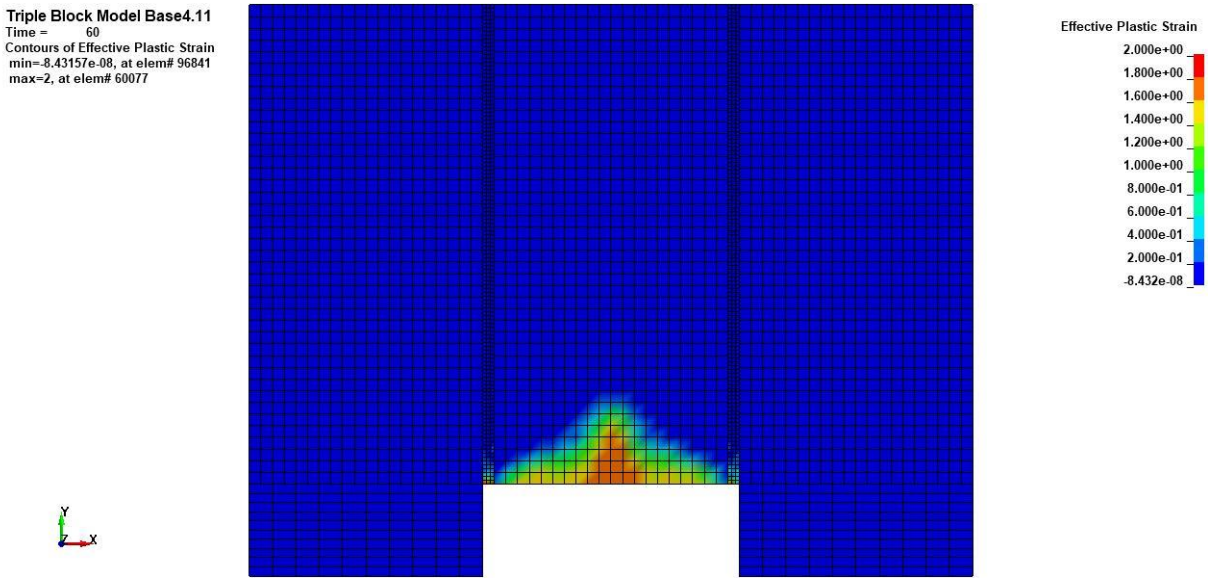


**Figure B-180: Effective Plastic Strain Fringe Plot for Last State at 60 Milliseconds for Base Run 4.11 – 550 psi**

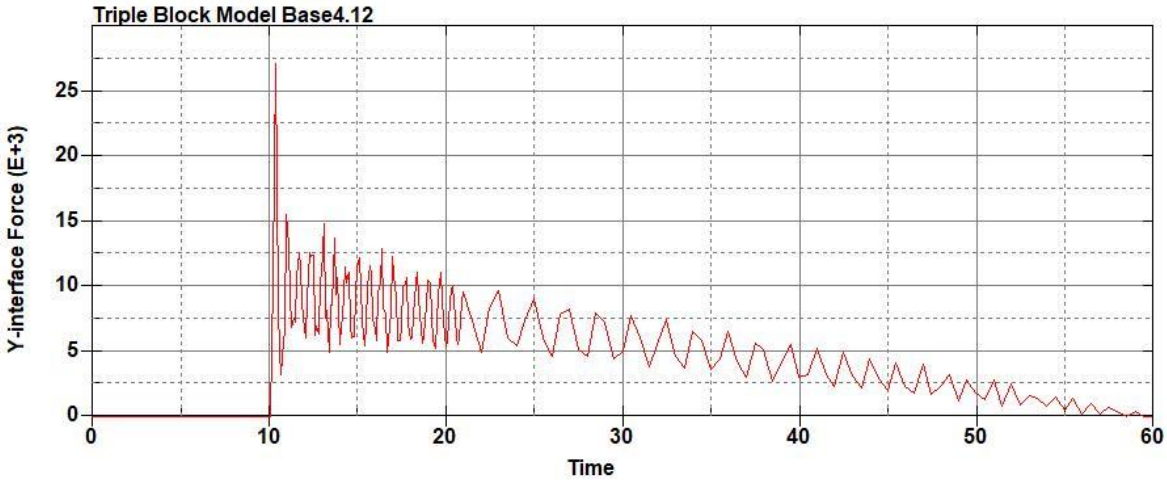


**Figure B-181: Base Run 4.12 Right Support Y-Interface Force (lbs) versus Time (ms) – 600 psi**

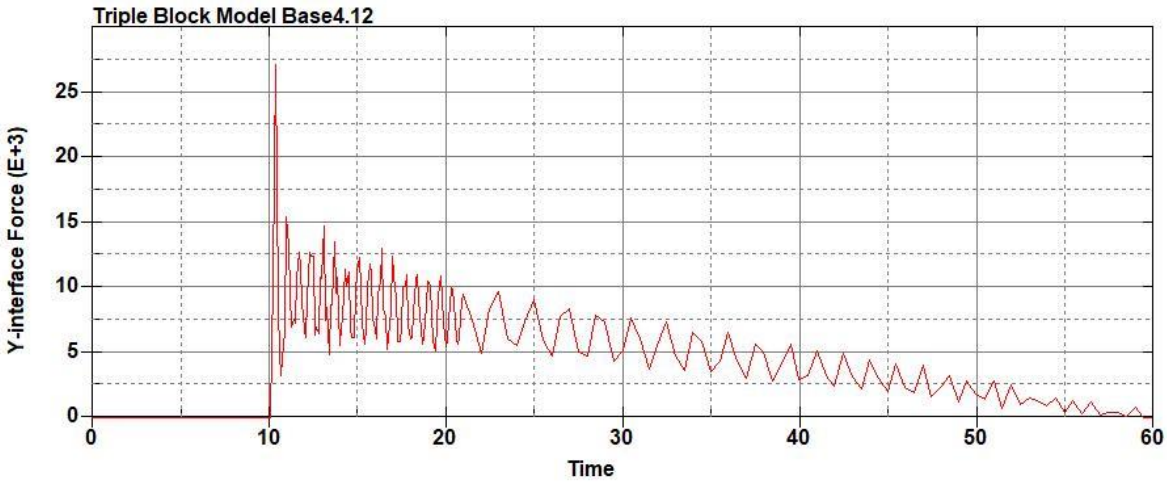


**Figure B-182: Base Run 4.12 Left Support Y-Interface Force (lbs) versus Time (ms) – 600 psi**

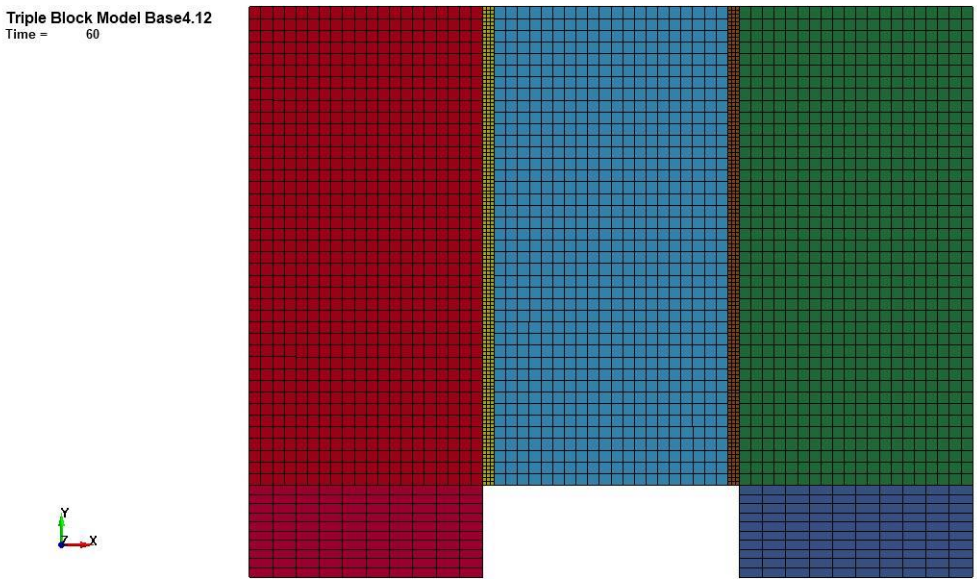


**Figure B-183: Last State at 60 Milliseconds for Base Run 4.12 – 600 psi**

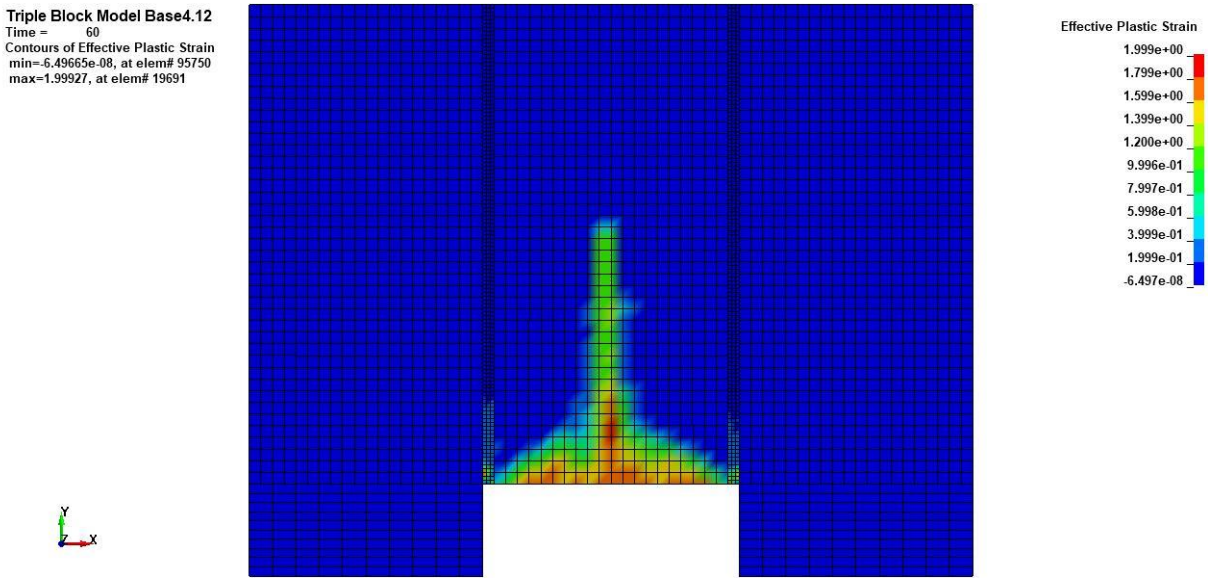


**Figure B-184: Effective Plastic Strain Fringe Plot for Last State at 60 Milliseconds for Base Run 4.12 – 600 psi**

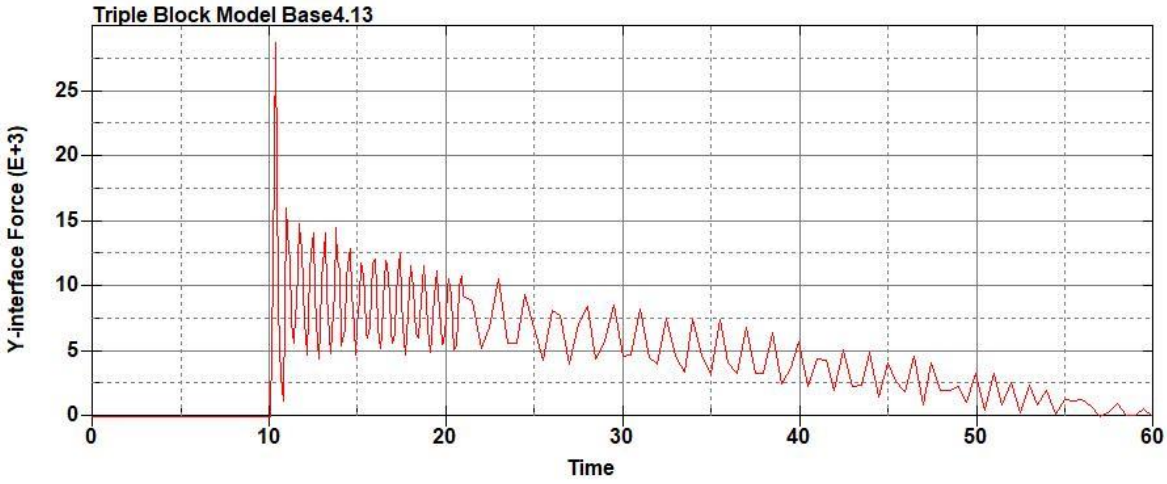


**Figure B-185: Base Run 4.13 Right Support Y-Interface Force (lbs) versus Time (ms) – 650 psi**

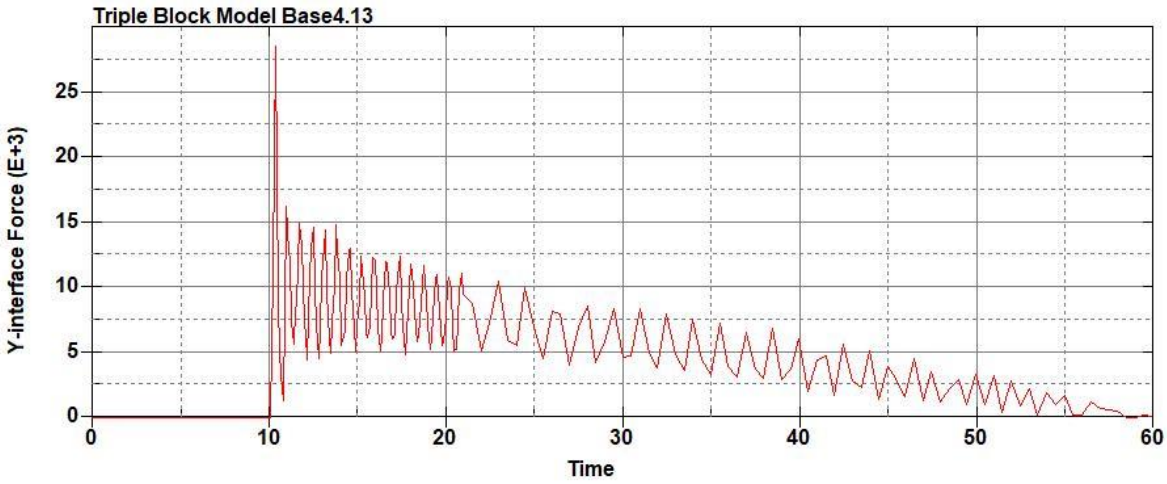


**Figure B-186: Base Run 4.13 Left Support Y-Interface Force (lbs) versus Time (ms) – 650 psi**

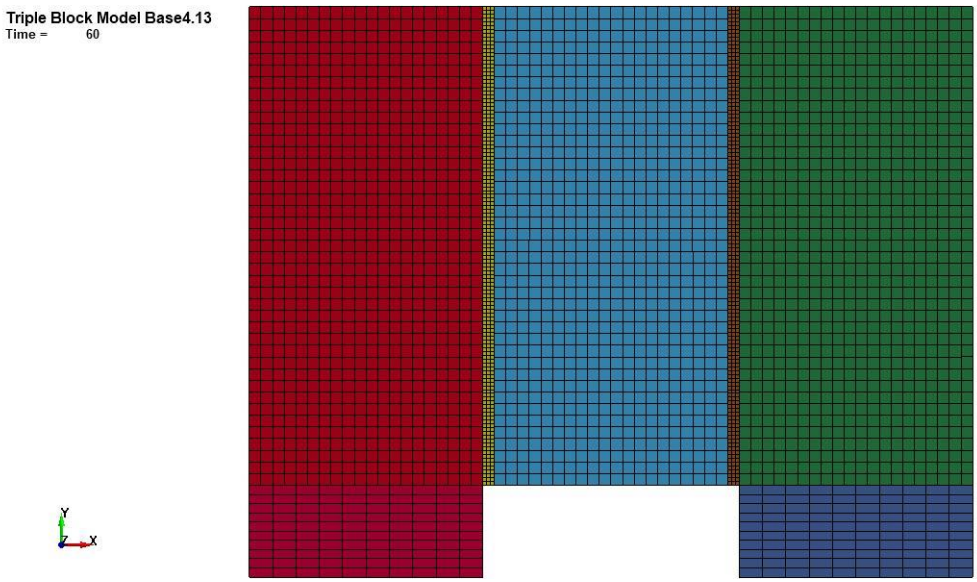


**Figure B-187: Last State at 60 Milliseconds for Base Run 4.13 – 650 psi**

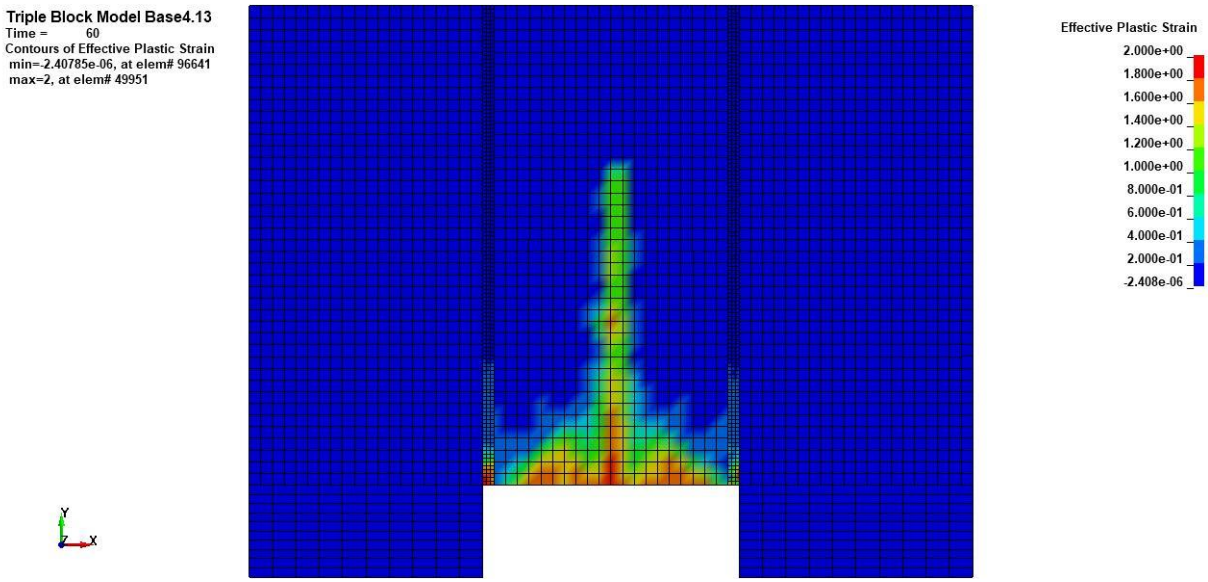


**Figure B-188: Effective Plastic Strain Fringe Plot for Last State at 60 Milliseconds for Base Run 4.13 – 650 psi**

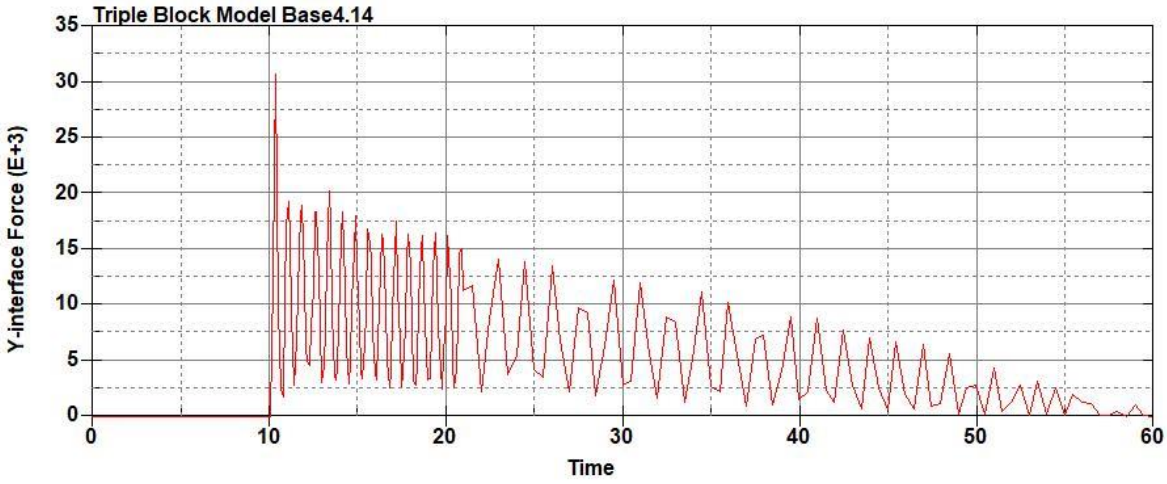


**Figure B-189: Base Run 4.14 Right Support Y-Interface Force (lbs) versus Time (ms) – 700 psi**

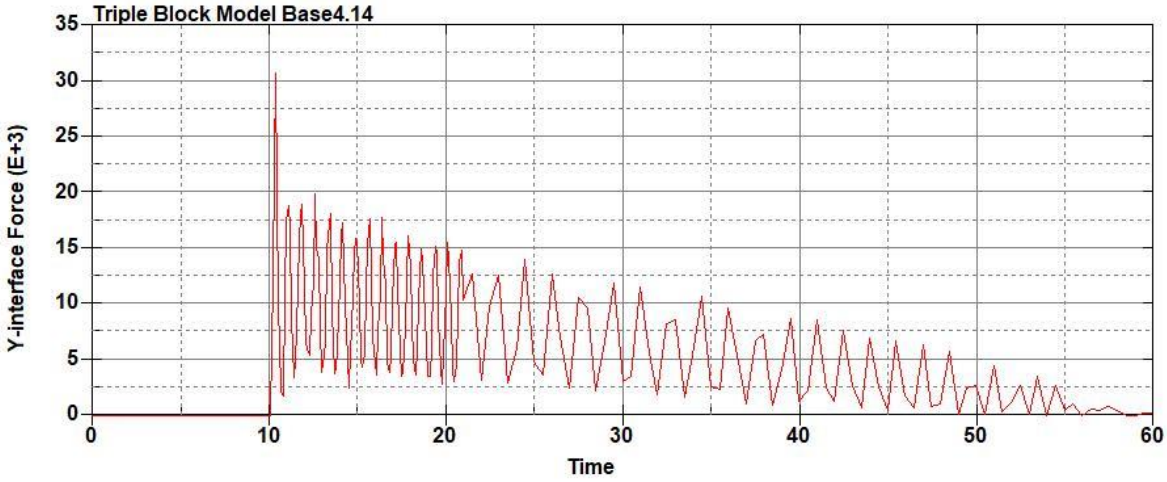


**Figure B-190: Base Run 4.14 Left Support Y-Interface Force (lbs) versus Time (ms) – 700 psi**

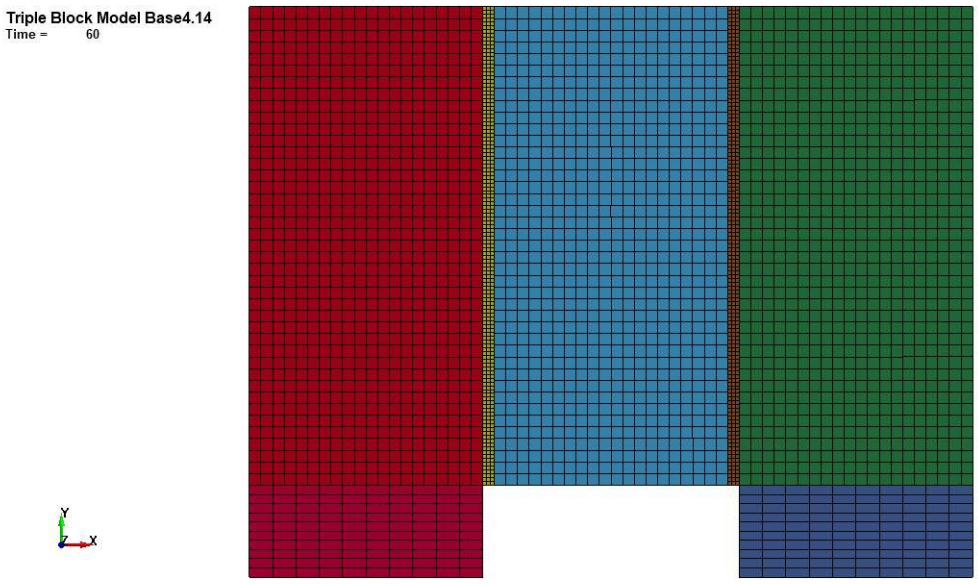


**Figure B-191: Last State at 60 Milliseconds for Base Run 4.14 – 700 psi**

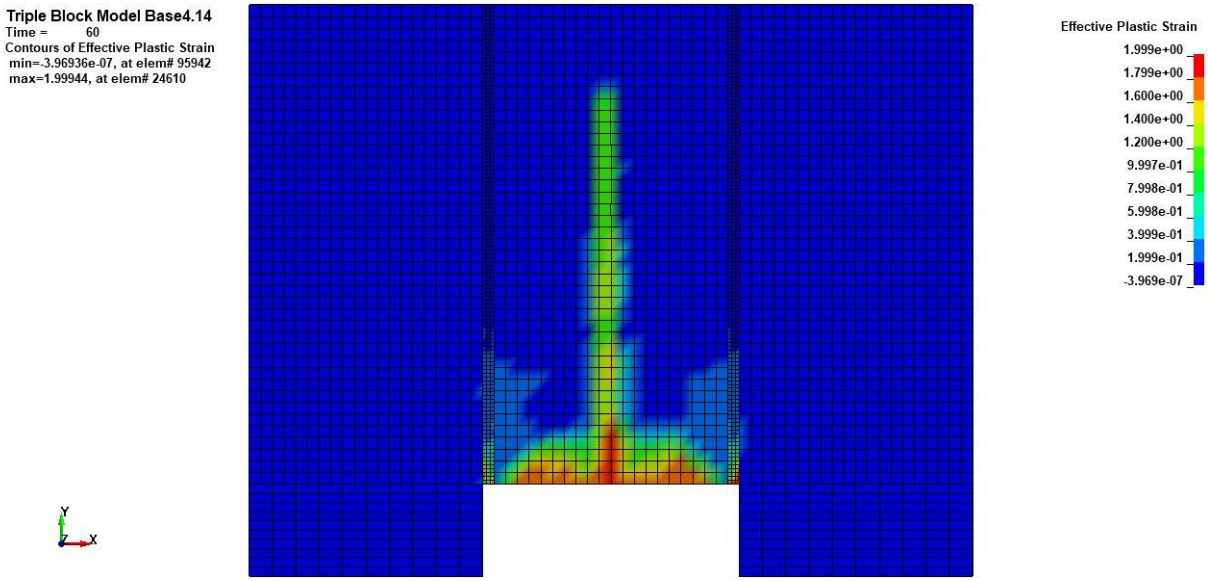


**Figure B-192: Effective Plastic Strain Fringe Plot for Last State at 60 Milliseconds for Base Run 4.14 – 700 psi**

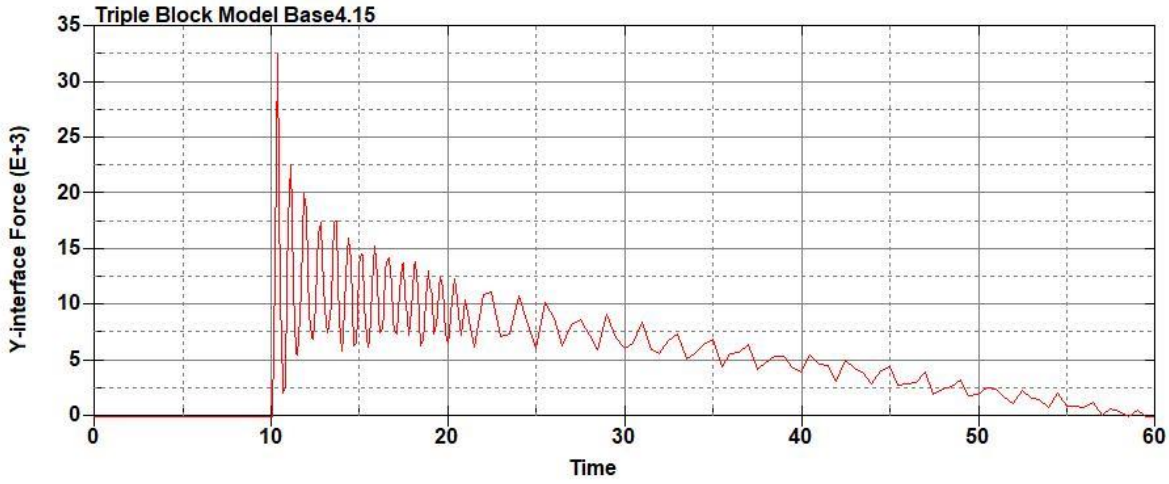


**Figure B-193: Base Run 4.15 Right Support Y-Interface Force (lbs) versus Time (ms) –750 psi**

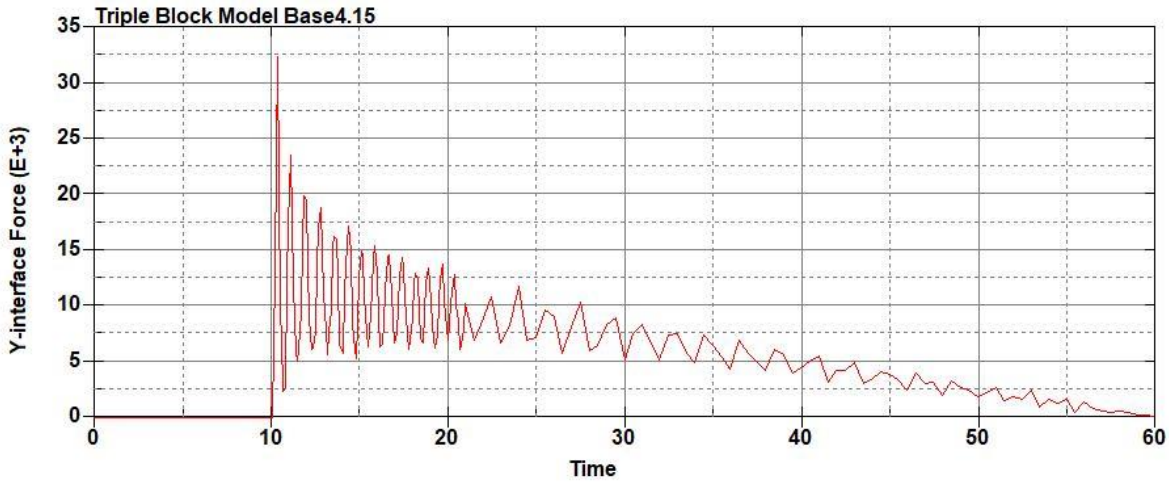


**Figure B-194: Base Run 4.15 Left Support Y-Interface Force (lbs) versus Time (ms) – 750 psi**

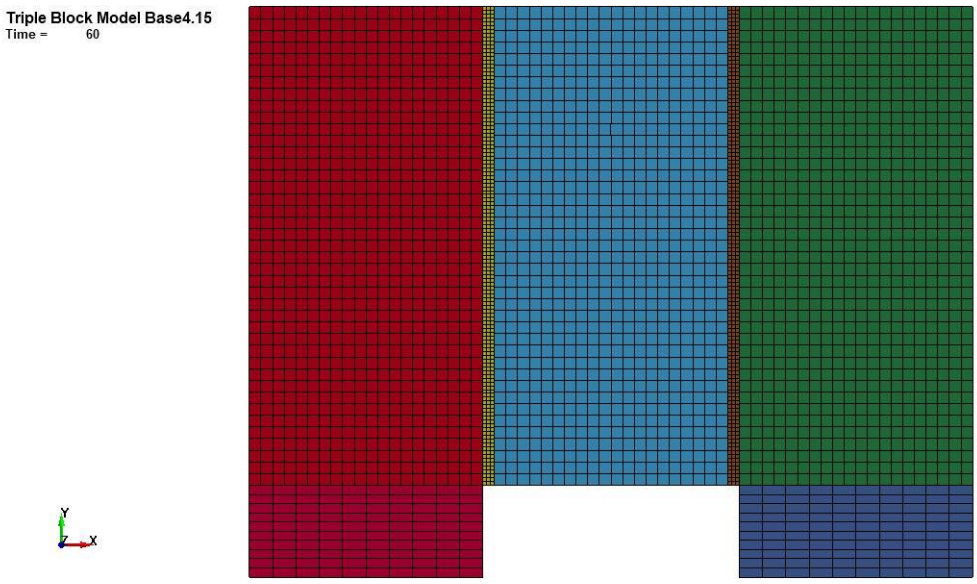


**Figure B-195: Last State at 60 Milliseconds for Base Run 4.15 – 750 psi**

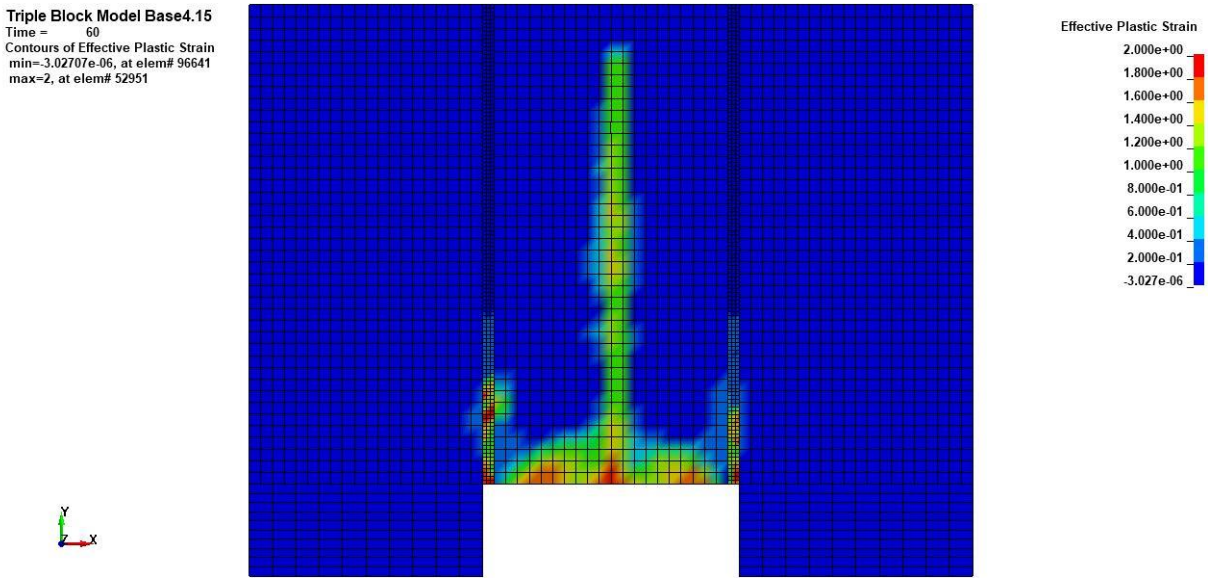


**Figure B-196: Effective Plastic Strain Fringe Plot for Last State at 60 Milliseconds for Base Run 4.15 – 750 psi**

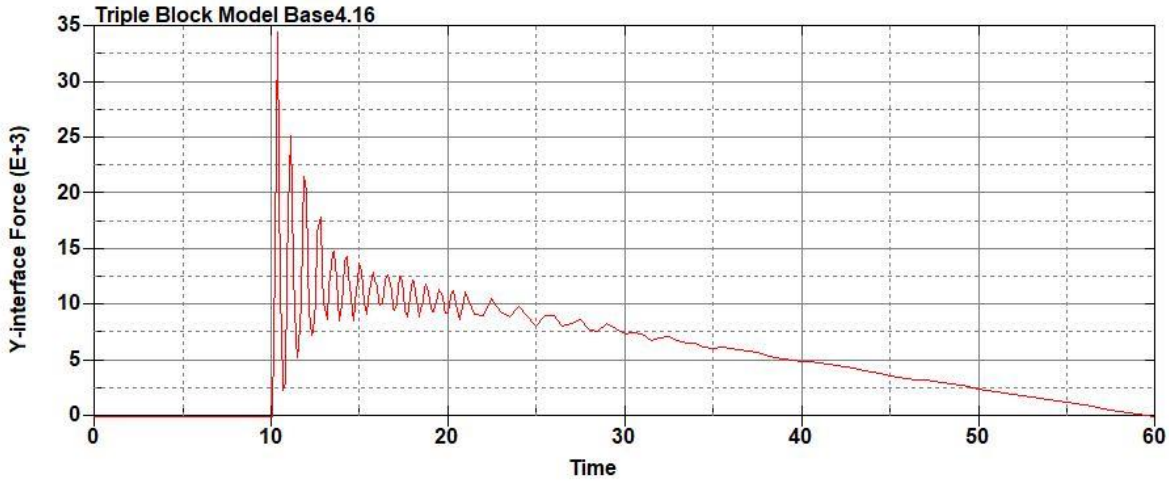


**Figure B-197: Base Run 4.16 Right Support Y-Interface Force (lbs) versus Time (ms) – 800 psi**

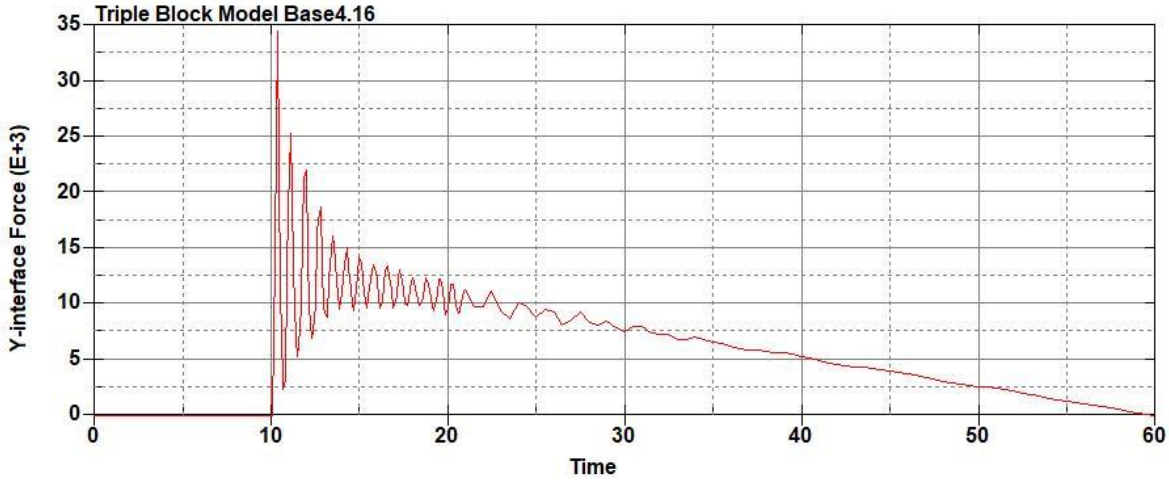


**Figure B-198: Base Run 4.16 Left Support Y-Interface Force (lbs) versus Time (ms) – 800 psi**

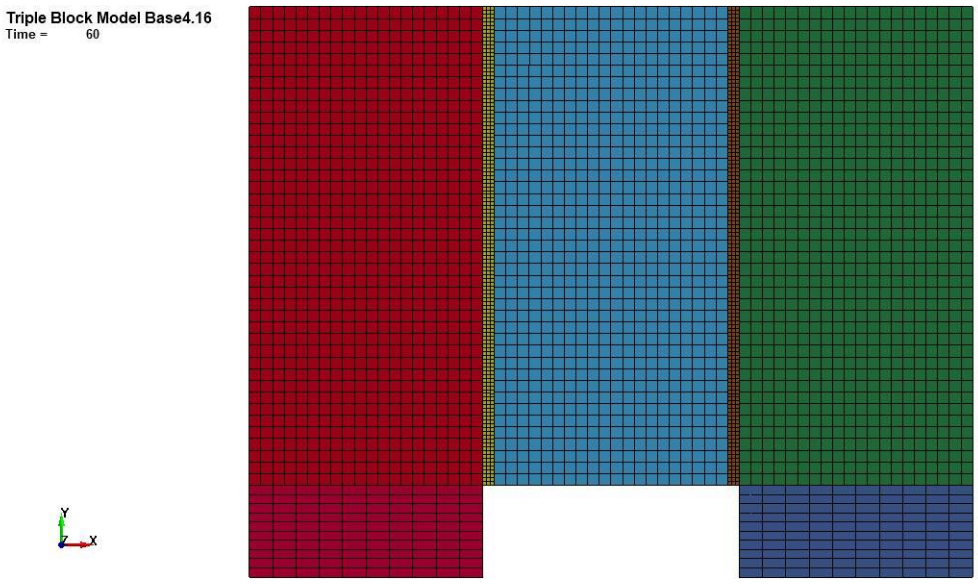


**Figure B-199: Last State at 60 Milliseconds for Base Run 4.16 – 800 psi**

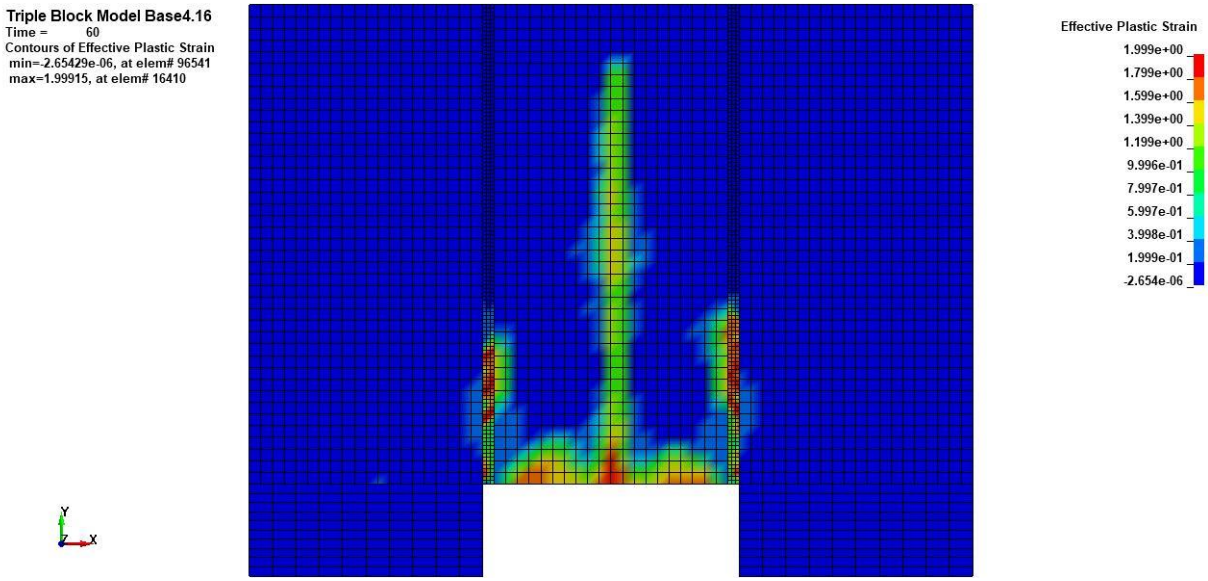


**Figure B-200: Effective Plastic Strain Fringe Plot for Last State at 60 Milliseconds for Base Run 4.16 – 800 psi**

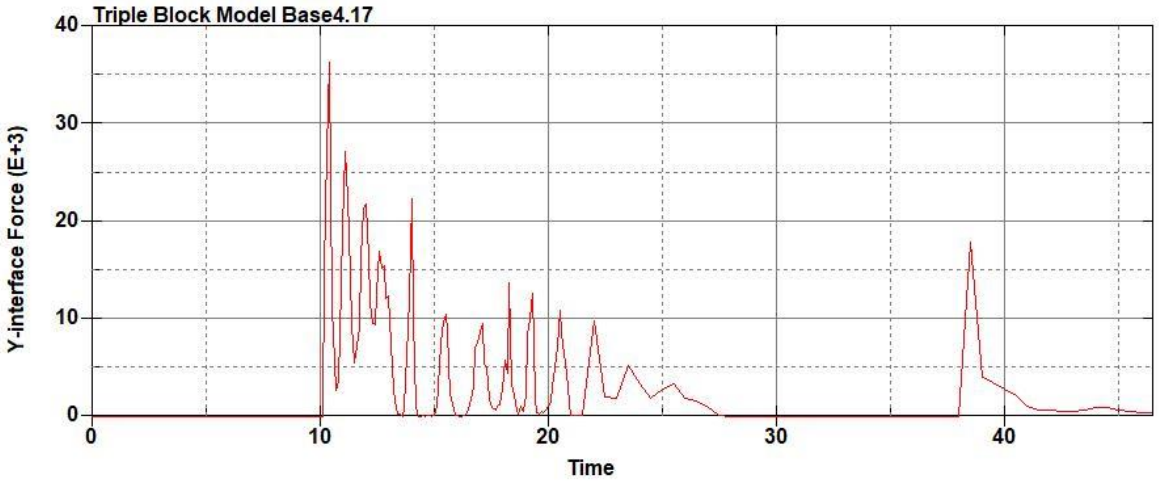


**Figure B-201: Base Run 4.17 Right Support Y-Interface Force (lbs) versus Time (ms) – 850 psi**

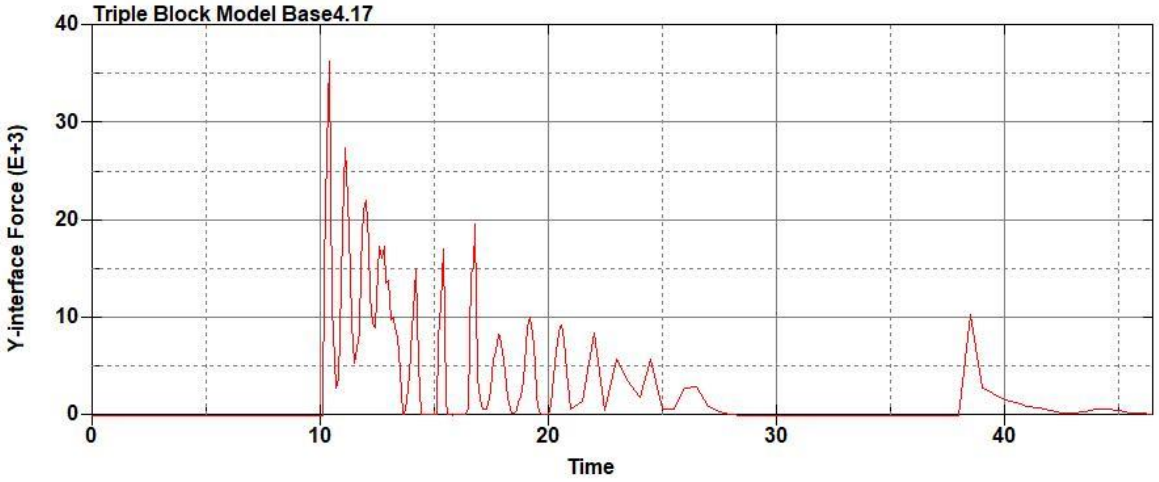


**Figure B-202: Base Run 4.17 Left Support Y-Interface Force (lbs) versus Time (ms) – 850 psi**

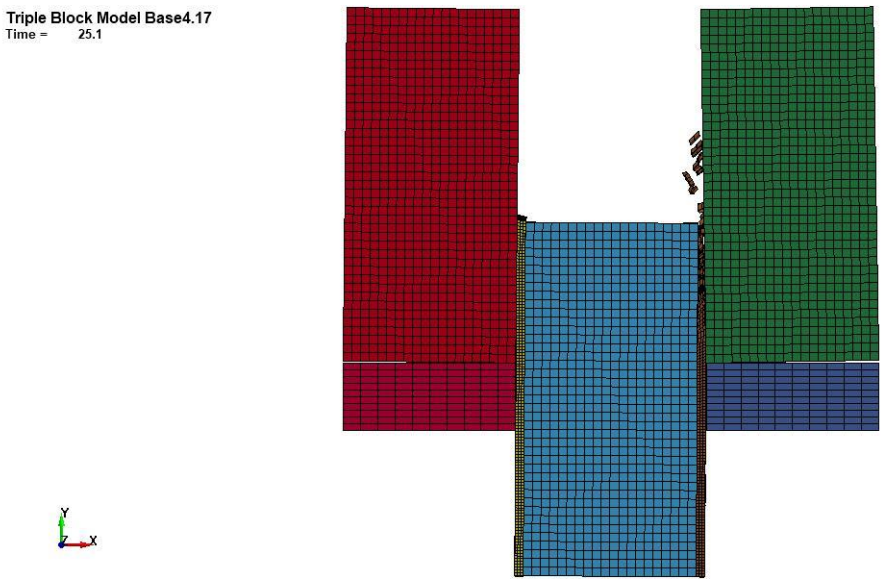


**Figure B-203: Last State at 25.1 Milliseconds for Base Run 4.17 – 850 psi**

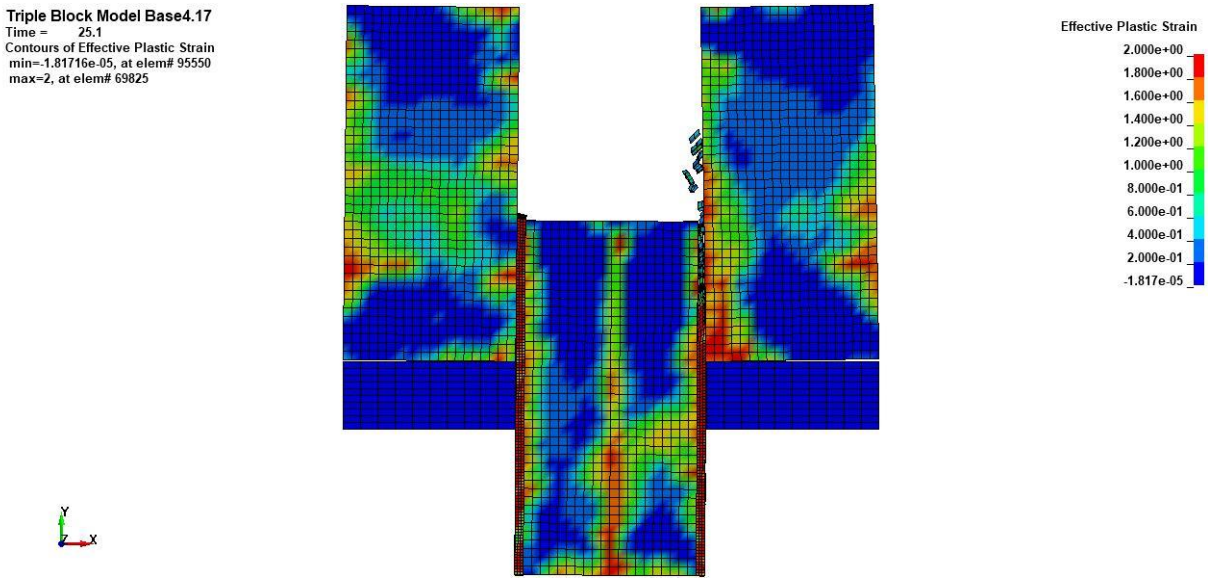


**Figure B-204: Effective Plastic Strain Fringe Plot for Last State at 25.1 Milliseconds for Base Run 4.17 – 850 psi**

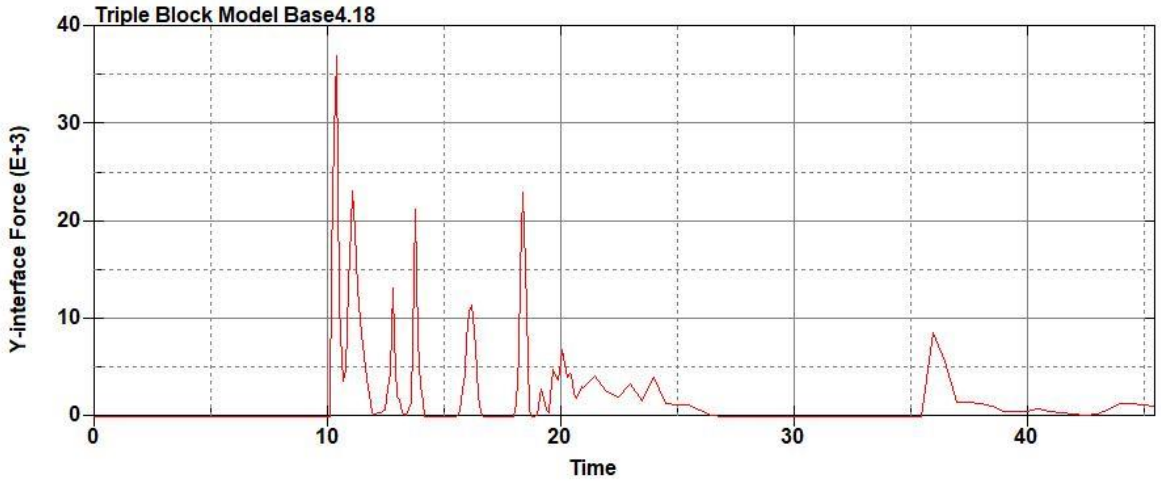


**Figure B-205: Base Run 4.18 Right Support Y-Interface Force (lbs) versus Time (ms) – 900 psi**

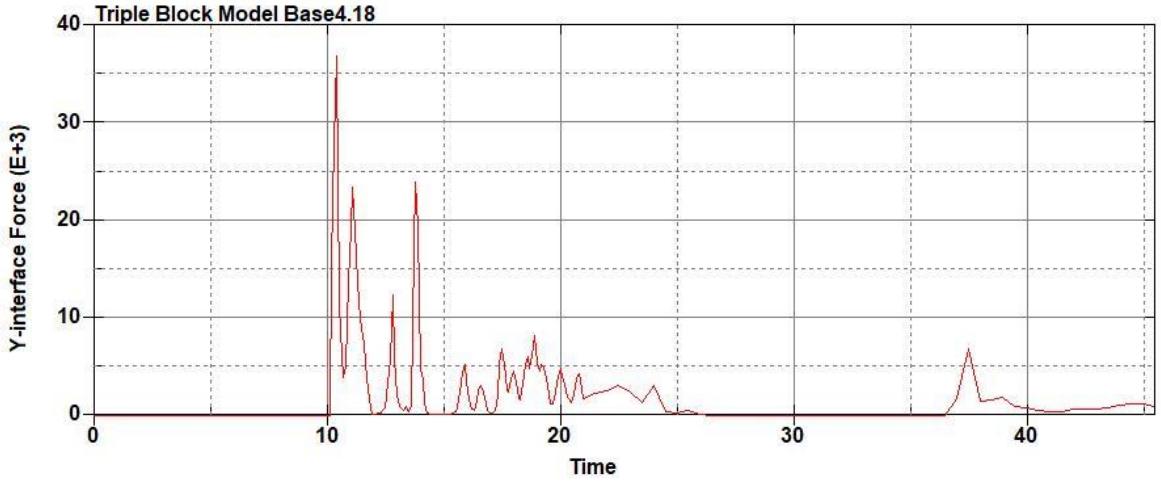


**Figure B-206: Base Run 4.18 Left Support Y-Interface Force (lbs) versus Time (ms) – 900 psi**

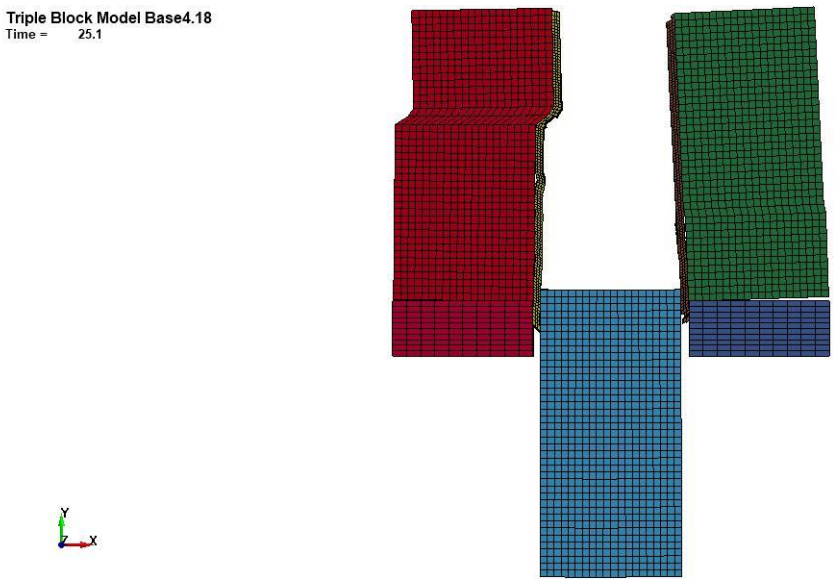


**Figure B-207: Last State at 25.1 Milliseconds for Base Run 4.18 – 900 psi**

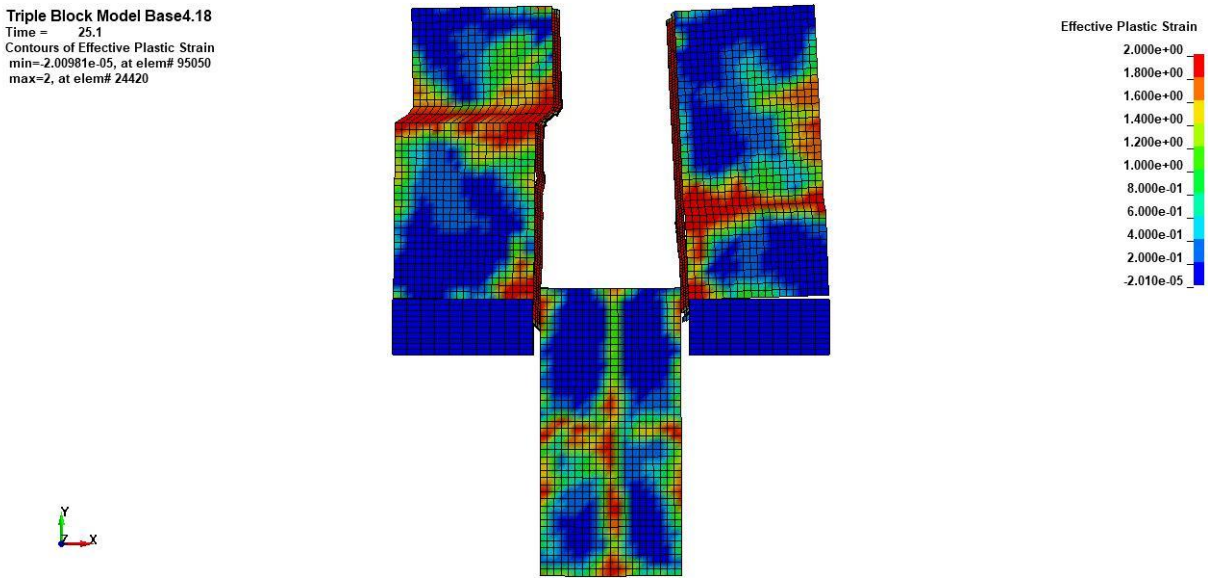


**Figure B-208: Effective Plastic Strain Fringe Plot for Last State at 25.1 Milliseconds for Base Run 4.18 – 900 psi**

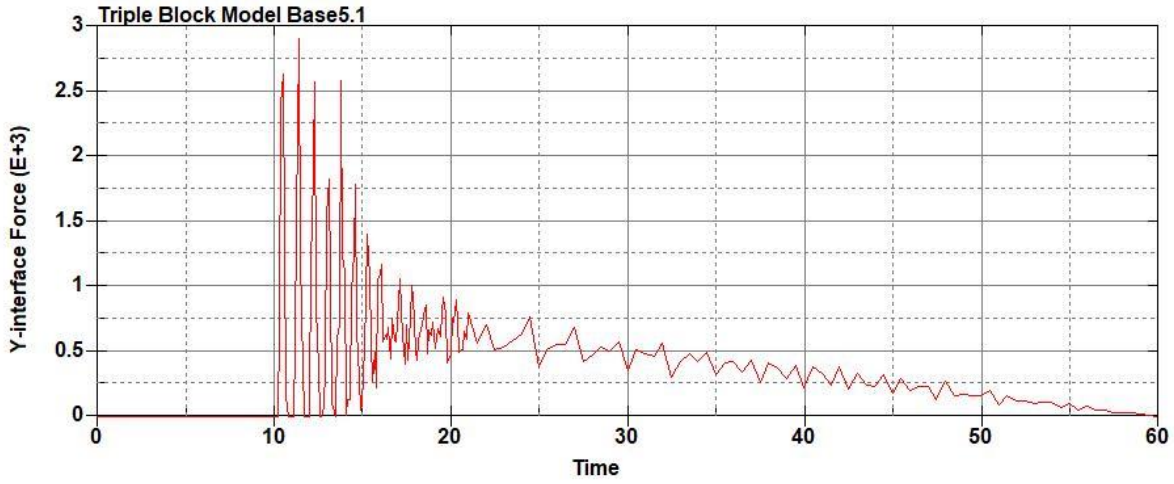


**Figure B-209: Base Run 5.1 Right Support Y-Interface Force (lbs) versus Time (ms) – 50 psi**

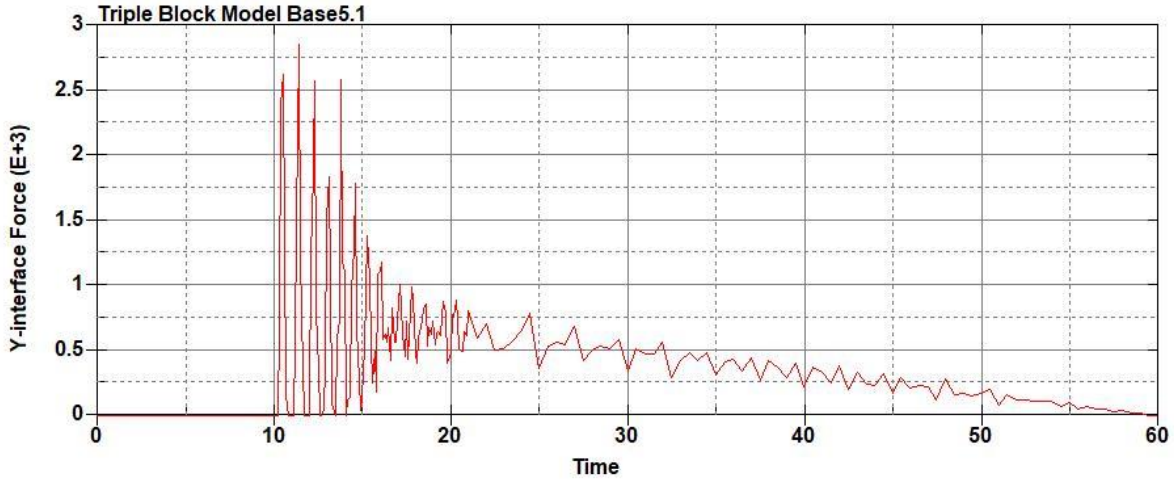


**Figure B-210: Base Run 5.1 Left Support Y-Interface Force (lbs) versus Time (ms) – 50 psi**

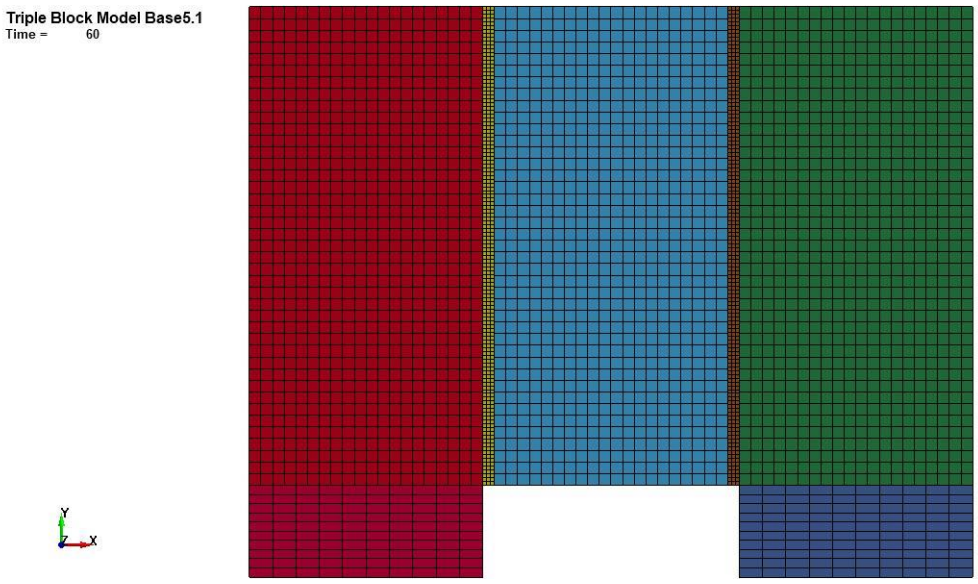


**Figure B-211: Last State at 60 Milliseconds for Base Run 5.1 – 50 psi**

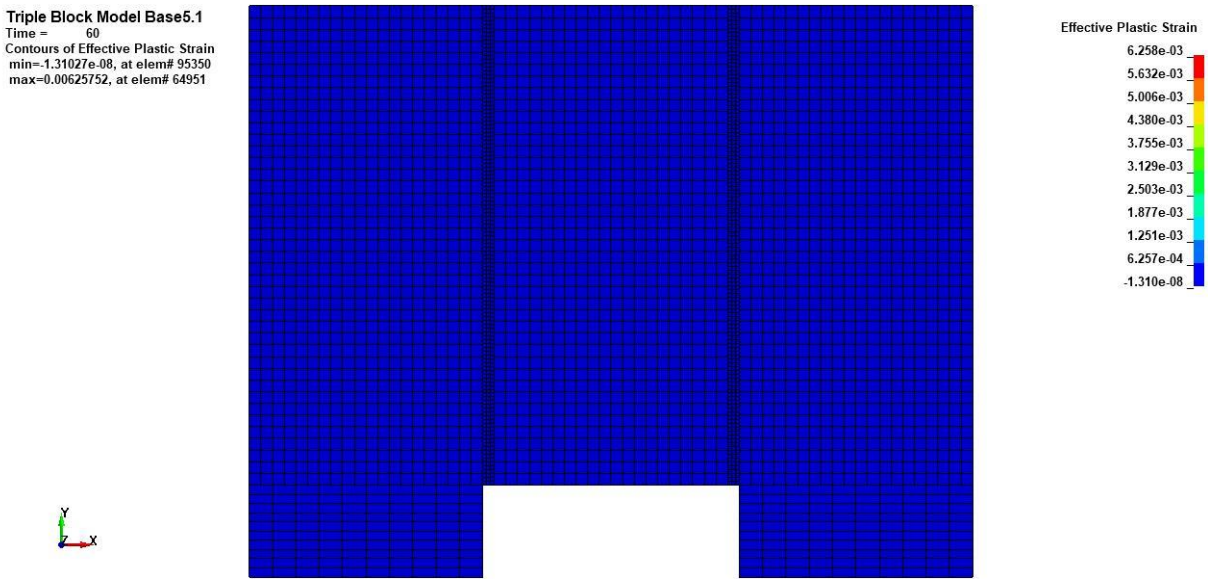


**Figure B-212: Effective Plastic Strain Fringe Plot for Last State at 60 Milliseconds for Base Run 5.1 – 50 psi**

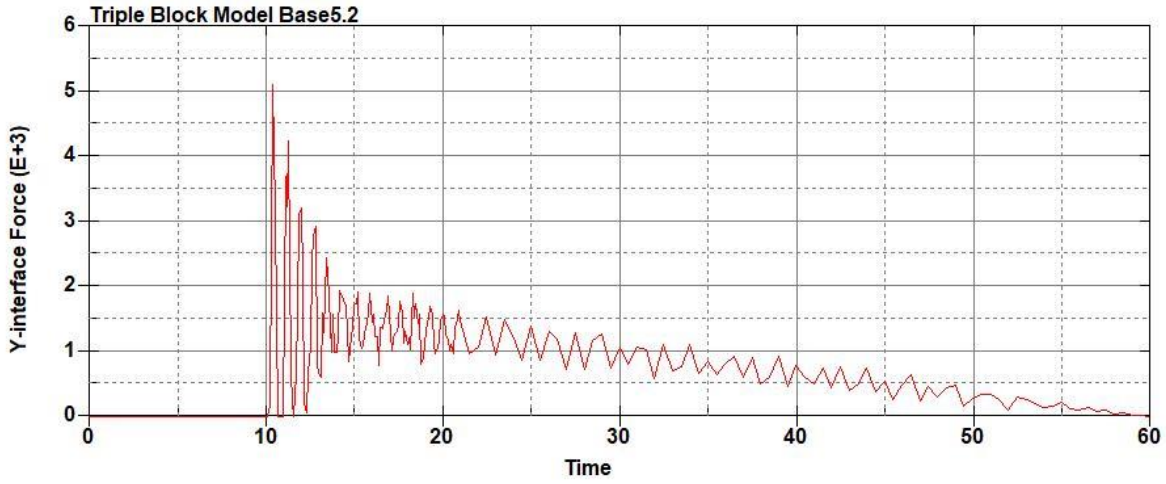


**Figure B-213: Base Run 5.2 Right Support Y-Interface Force (lbs) versus Time (ms) – 100 psi**

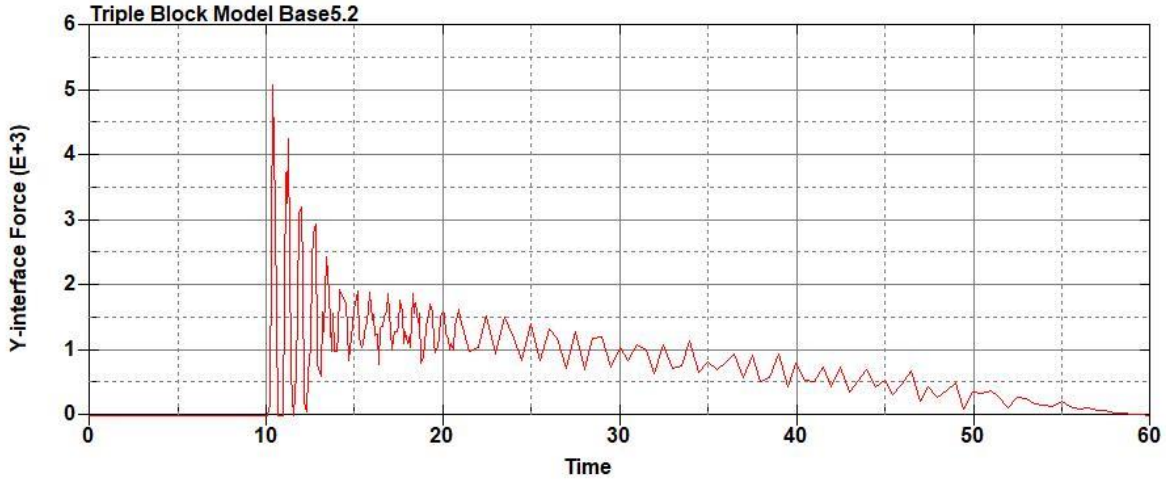


**Figure B-214: Base Run 5.2 Left Support Y-Interface Force (lbs) versus Time (ms) – 100 psi**

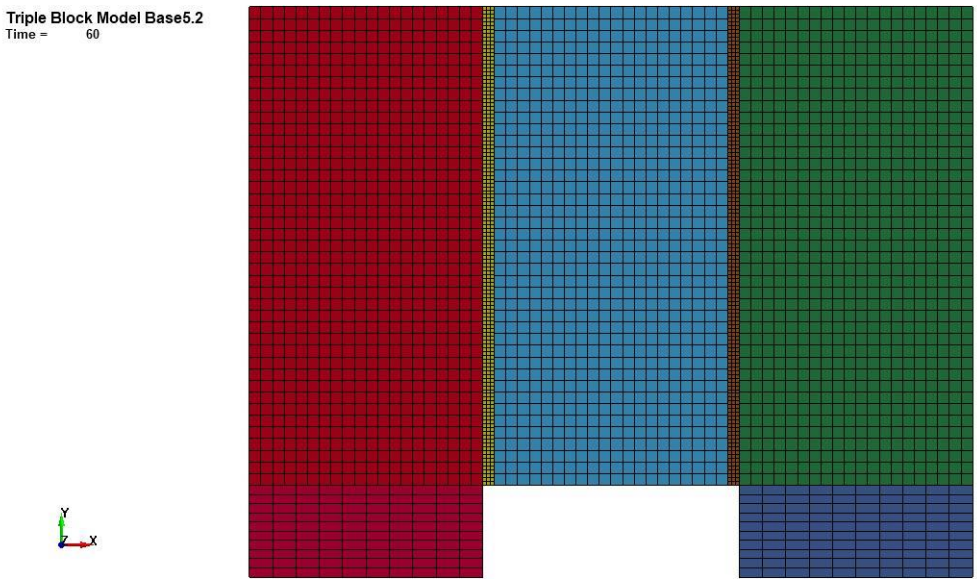


**Figure B-215: Last State at 60 Milliseconds for Base Run 5.2 – 100 psi**

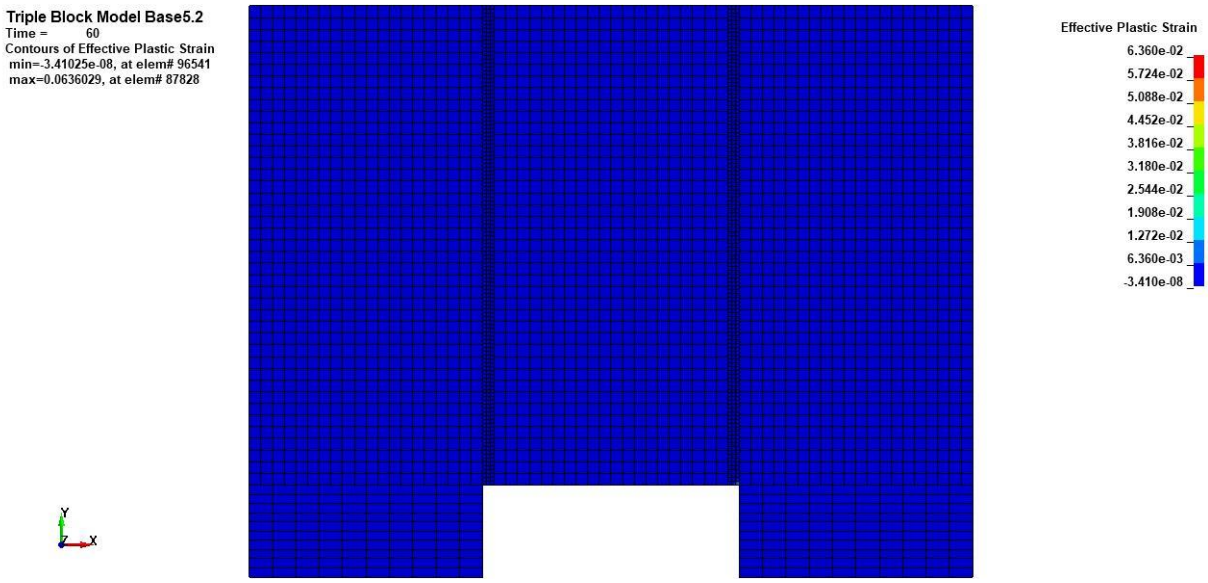


**Figure B-216: Effective Plastic Strain Fringe Plot for Last State at 60 Milliseconds for Base Run 5.2 – 100 psi**

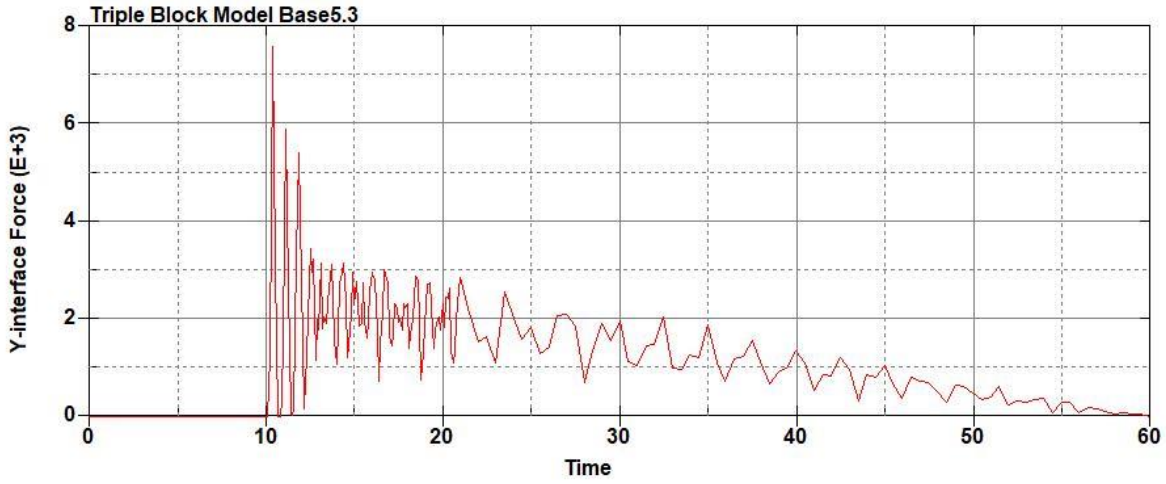


**Figure B-217: Base Run 5.3 Right Support Y-Interface Force (lbs) versus Time (ms) – 150 psi**

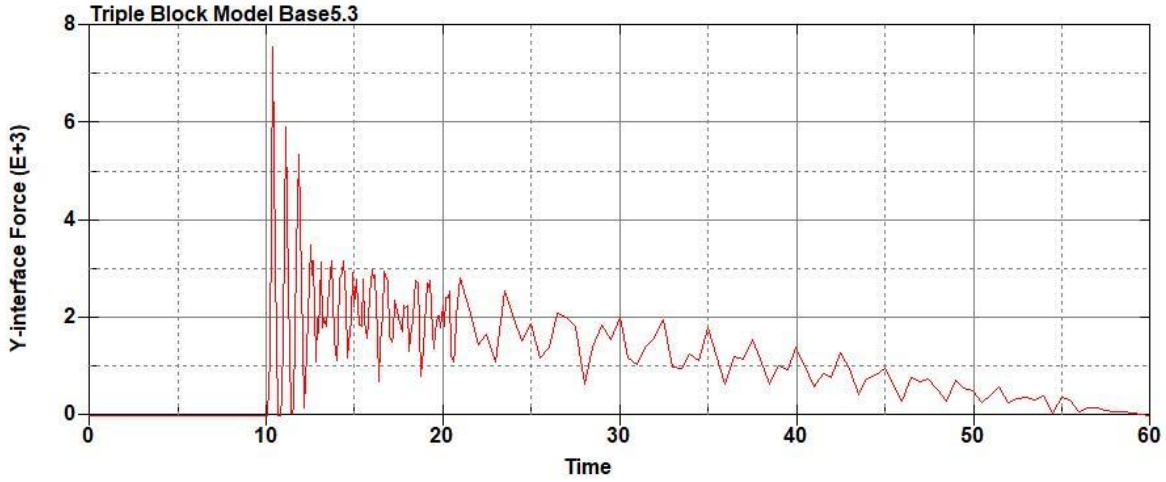


**Figure B-218: Base Run 5.3 Left Support Y-Interface Force (lbs) versus Time (ms) – 150 psi**

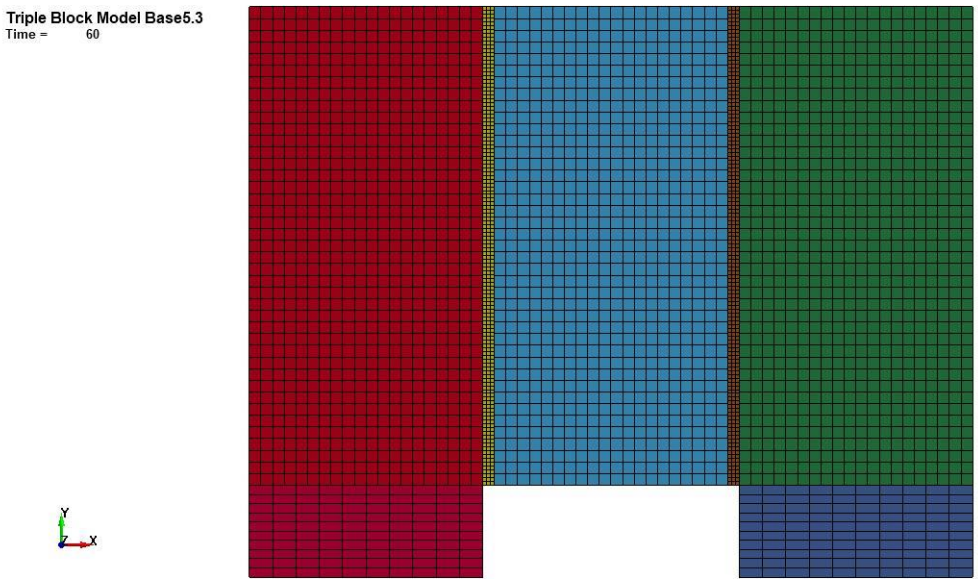


**Figure B-219: Last State at 60 Milliseconds for Base Run 5.3 – 150 psi**

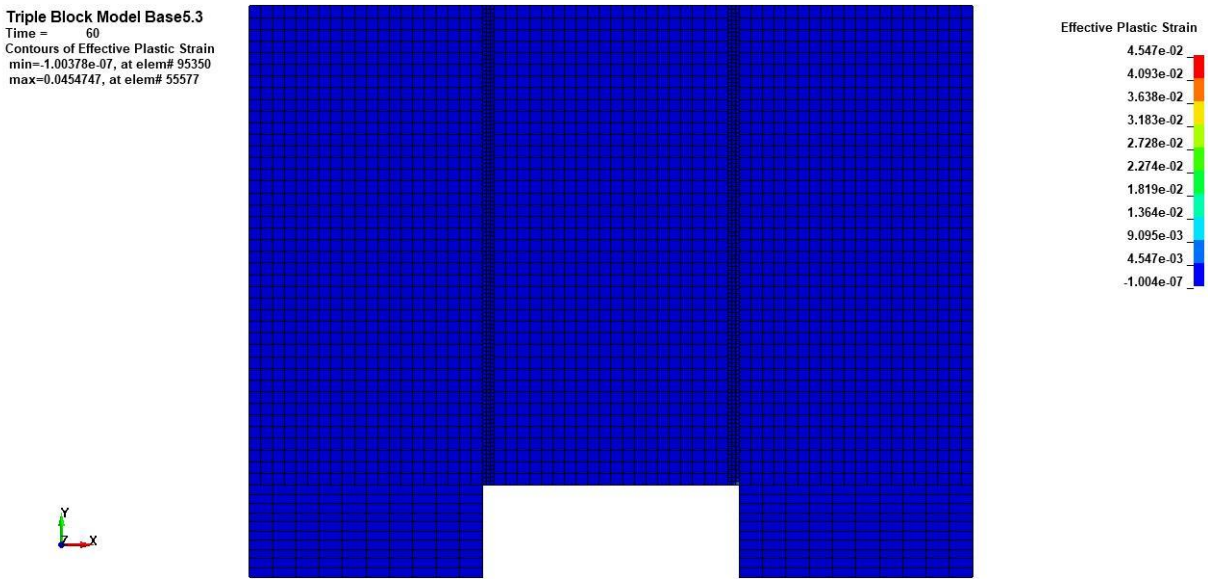


**Figure B-220: Effective Plastic Strain Fringe Plot for Last State at 60 Milliseconds for Base Run 5.3 – 150 psi**

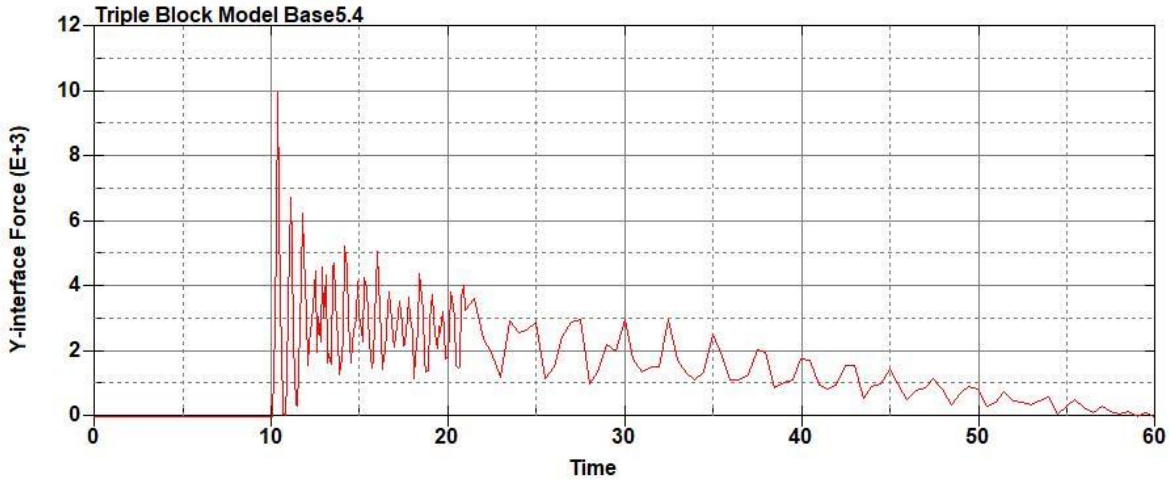


**Figure B-221: Base Run 5.4 Right Support Y-Interface Force (lbs) versus Time (ms) – 200 psi**

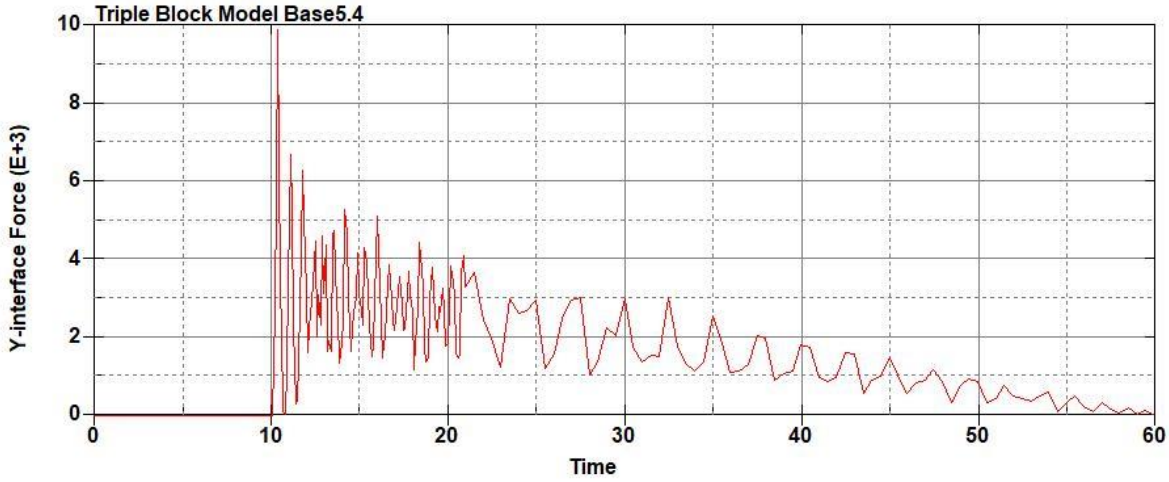


**Figure B-222: Base Run 5.4 Left Support Y-Interface Force (lbs) versus Time (ms) – 200 psi**

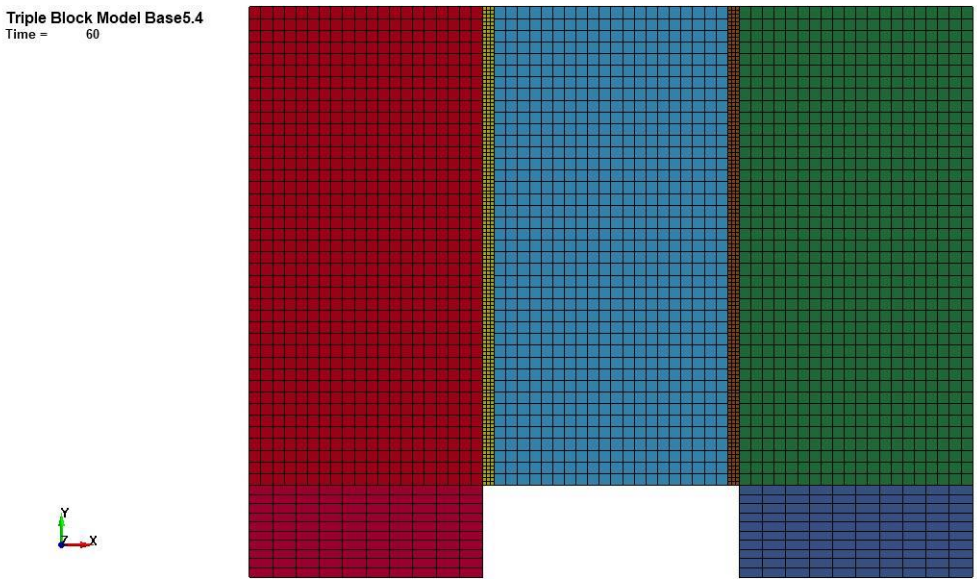


**Figure B-223: Last State at 60 Milliseconds for Base Run 5.4 – 200 psi**

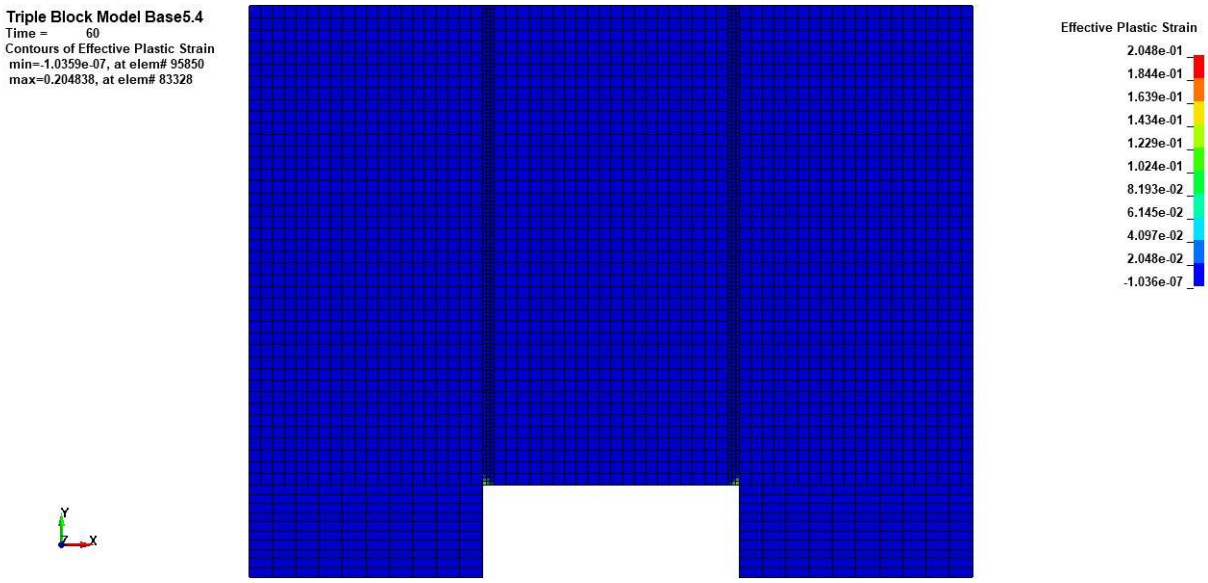


**Figure B-224: Effective Plastic Strain Fringe Plot for Last State at 60 Milliseconds for Base Run 5.4 – 200 psi**

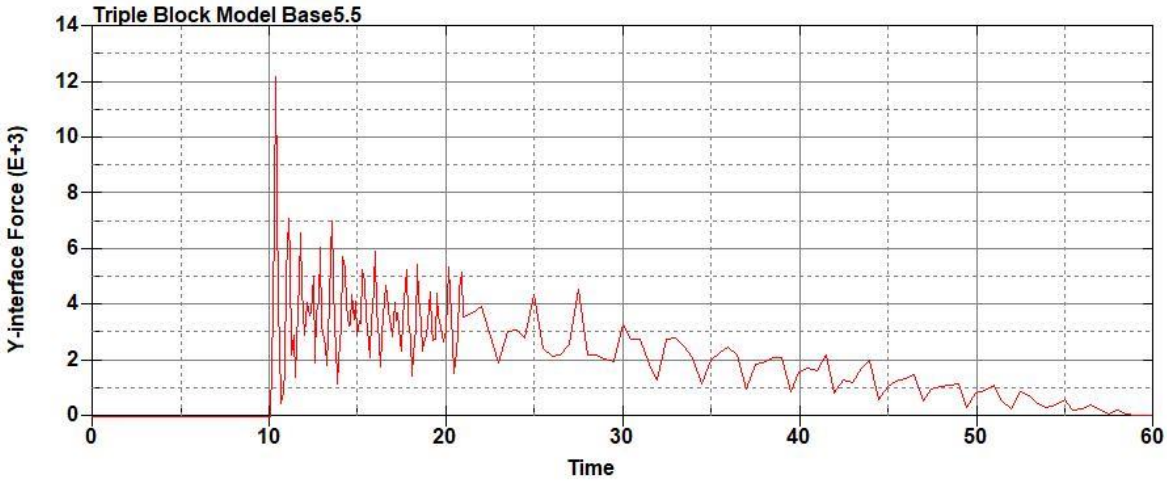


**Figure B-225: Base Run 5.5 Right Support Y-Interface Force (lbs) versus Time (ms) – 250 psi**

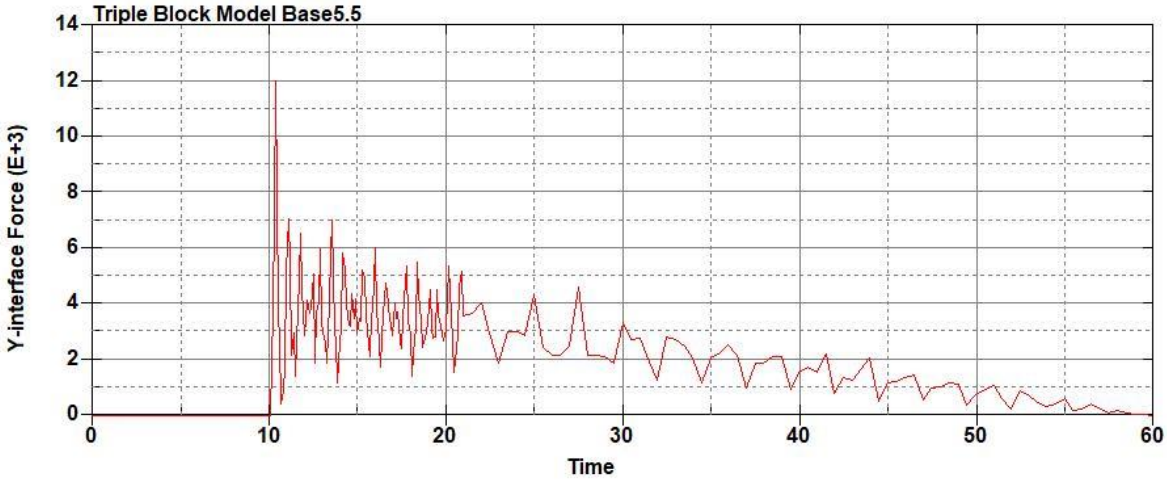


**Figure B-226: Base Run 5.5 Left Support Y-Interface Force (lbs) versus Time (ms) – 250 psi**

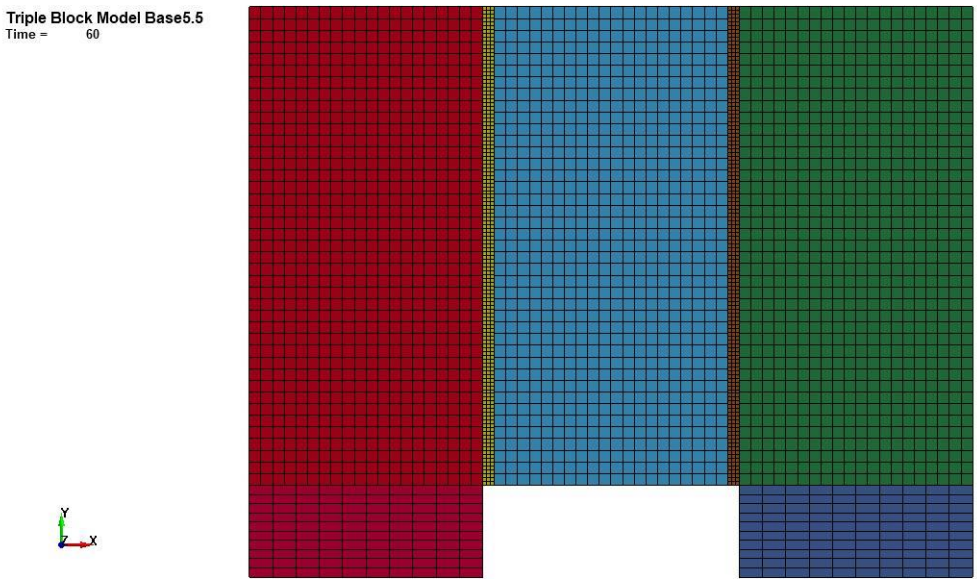


**Figure B-227: Last State at 60 Milliseconds for Base Run 5.5 – 250 psi**

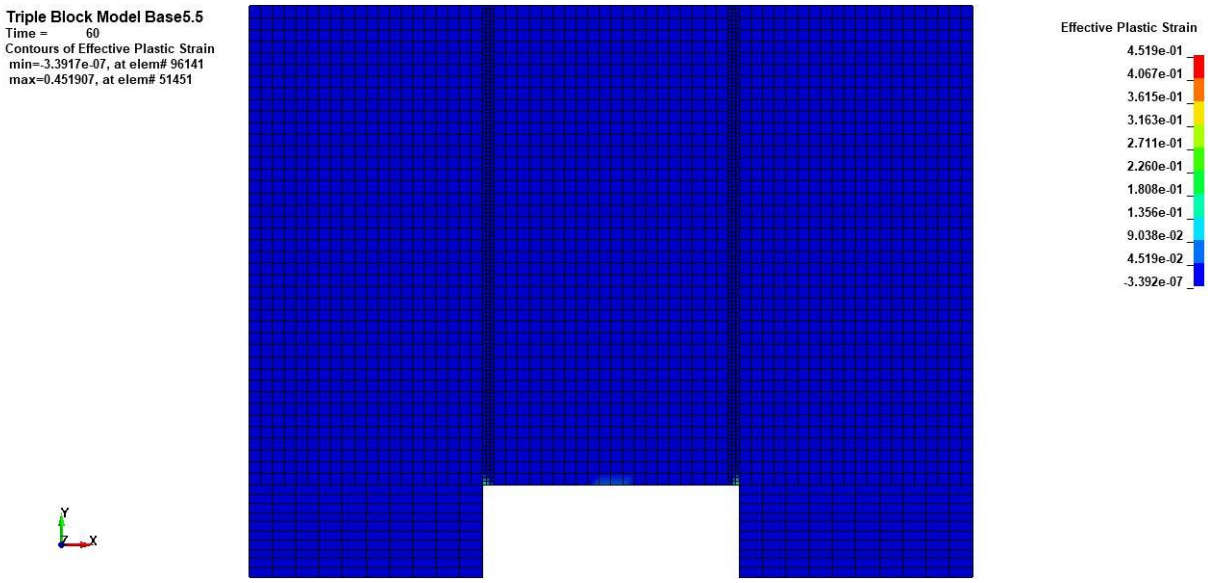


**Figure B-228: Effective Plastic Strain Fringe Plot for Last State at 60 Milliseconds for Base Run 5.5 – 250 psi**

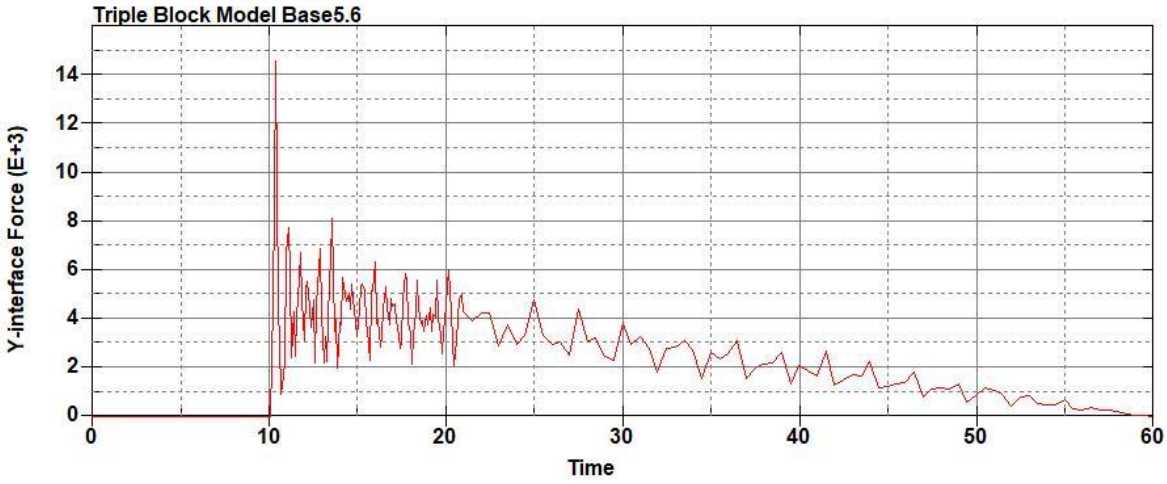


**Figure B-229: Base Run 5.6 Right Support Y-Interface Force (lbs) versus Time (ms) – 300 psi**

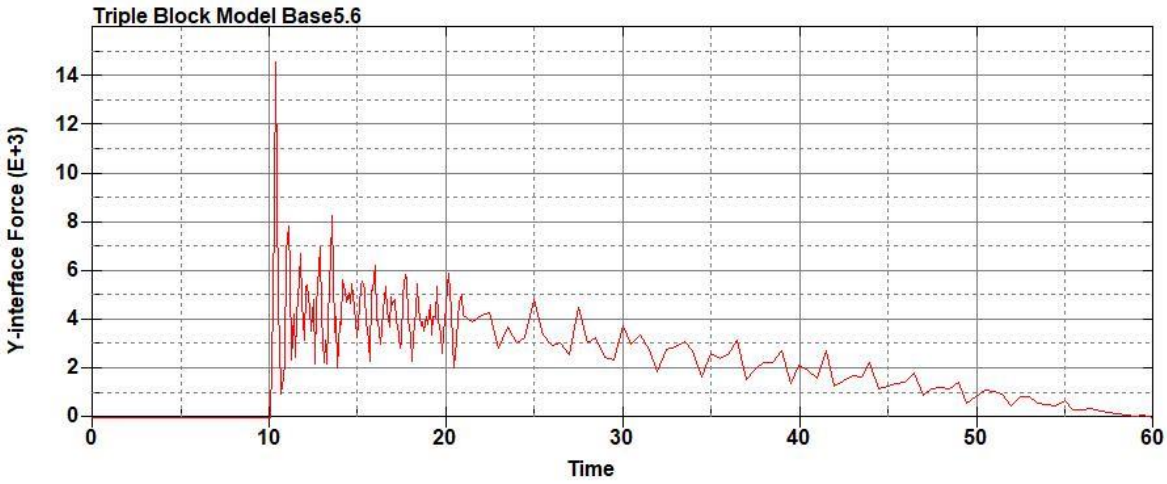


**Figure B-230: Base Run 5.6 Left Support Y-Interface Force (lbs) versus Time (ms) – 300 psi**

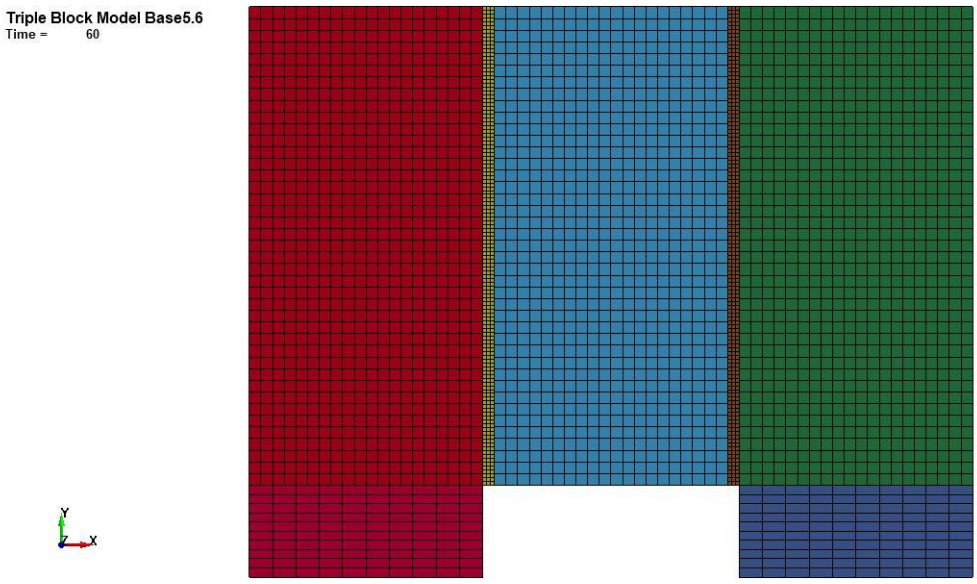


**Figure B-231: Last State at 60 Milliseconds for Base Run 5.6 – 300 psi**

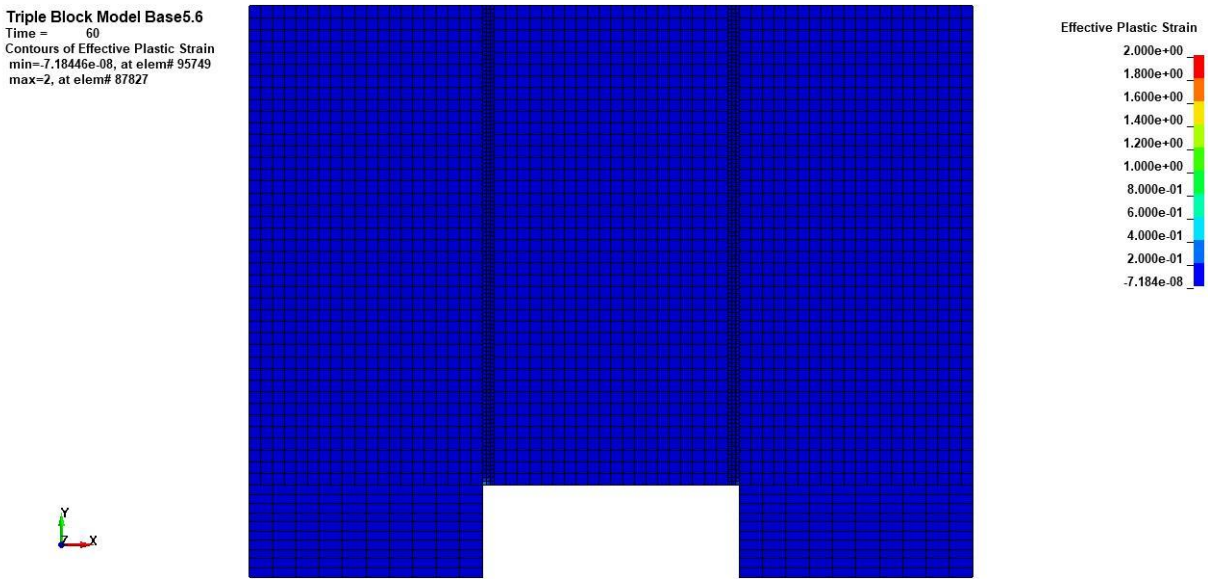


**Figure B-232: Effective Plastic Strain Fringe Plot for Last State at 60 Milliseconds for Base Run 5.6 – 300 psi**

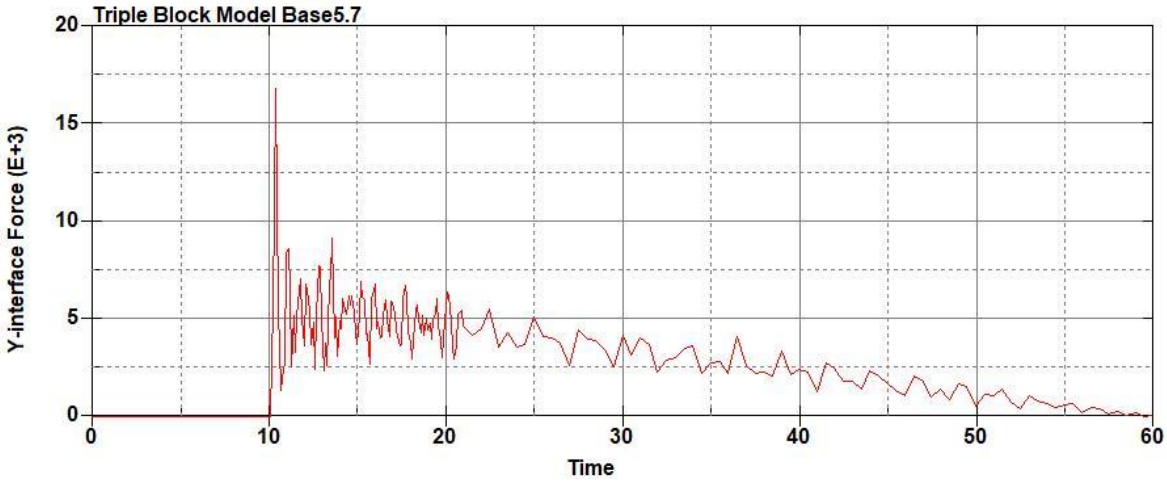


**Figure B-233: Base Run 5.7 Right Support Y-Interface Force (lbs) versus Time (ms) – 350 psi**

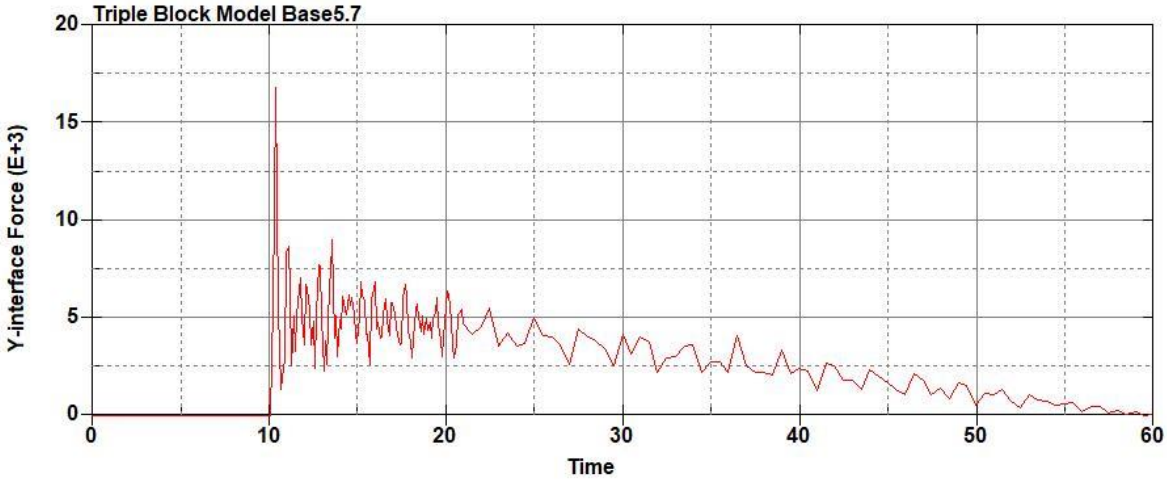


**Figure B-234: Base Run 5.7 Left Support Y-Interface Force (lbs) versus Time (ms) – 350 psi**

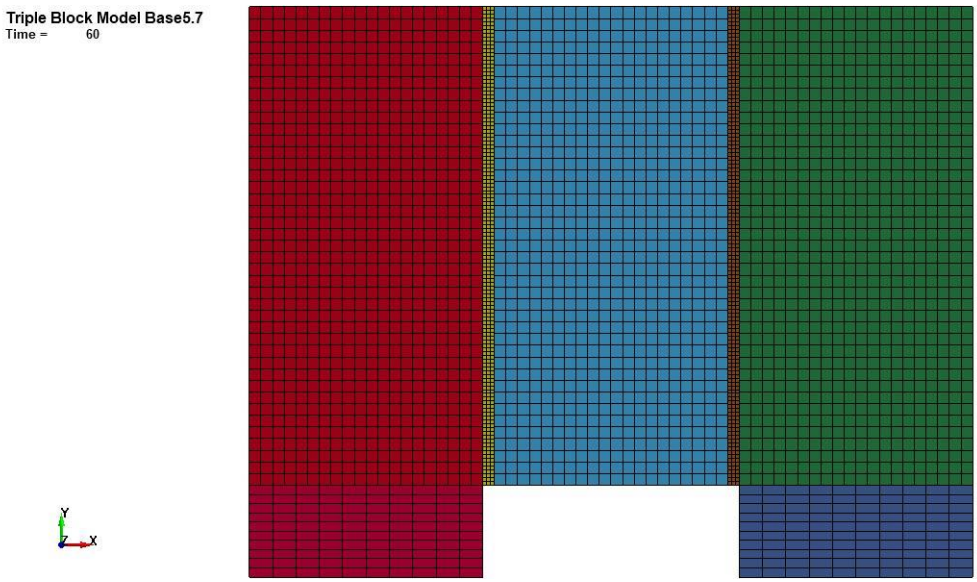


**Figure B-235: Last State at 60 Milliseconds for Base Run 5.7 – 350 psi**

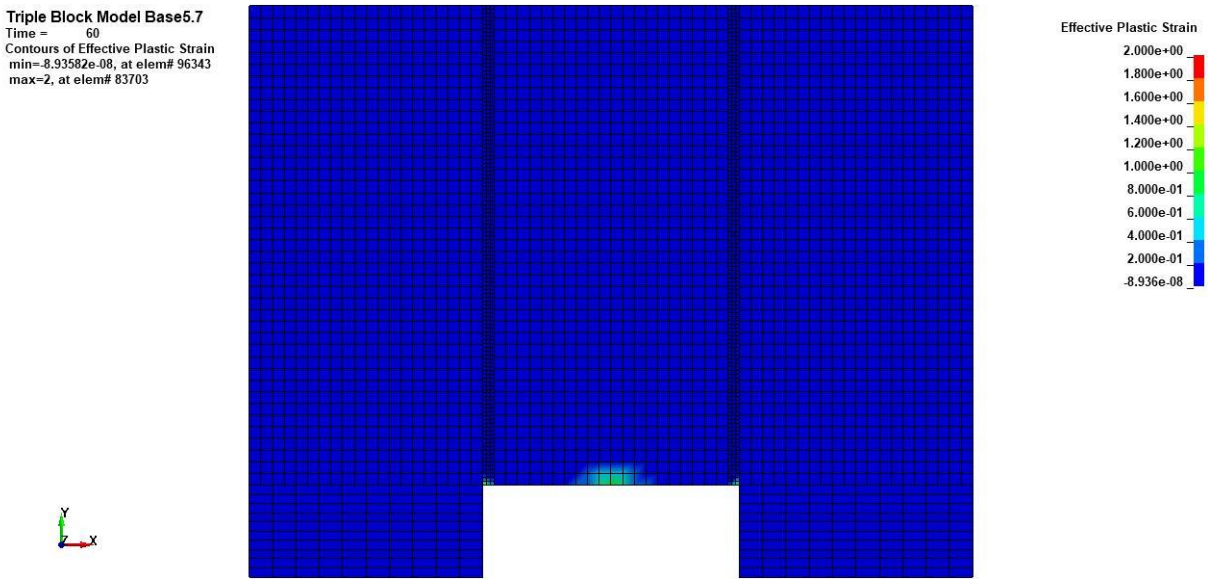


**Figure B-236: Effective Plastic Strain Fringe Plot for Last State at 60 Milliseconds for Base Run 5.7 – 350 psi**

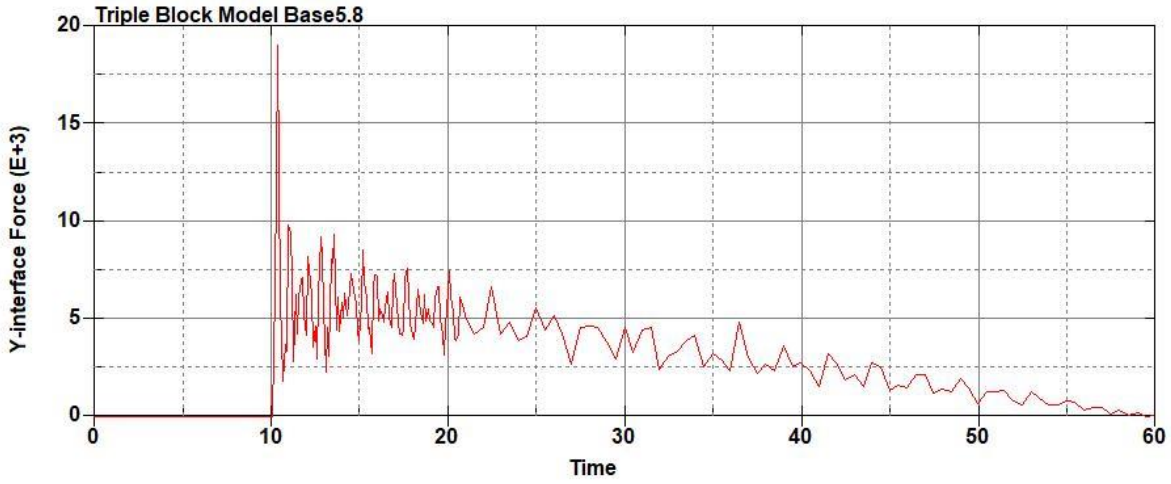


**Figure B-237: Base Run 5.8 Right Support Y-Interface Force (lbs) versus Time (ms) – 400 psi**

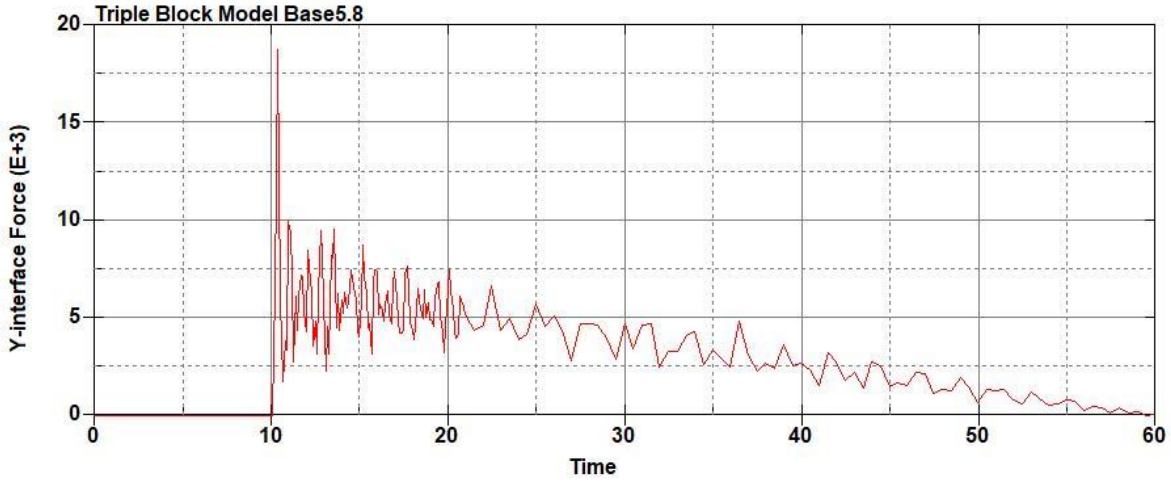


**Figure B-238: Base Run 5.8 Left Support Y-Interface Force (lbs) versus Time (ms) – 400 psi**

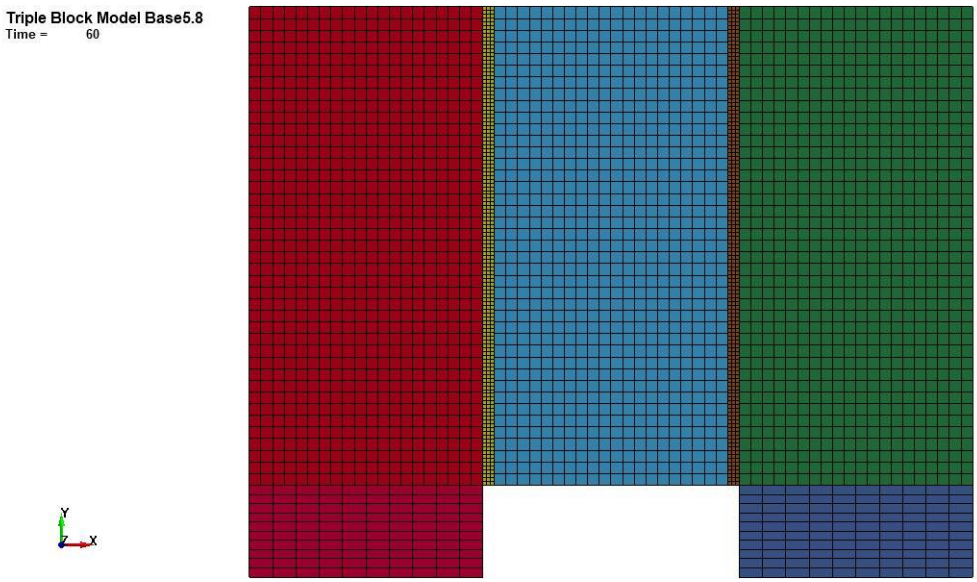


**Figure B-239: Last State at 60 Milliseconds for Base Run 5.8 – 400 psi**

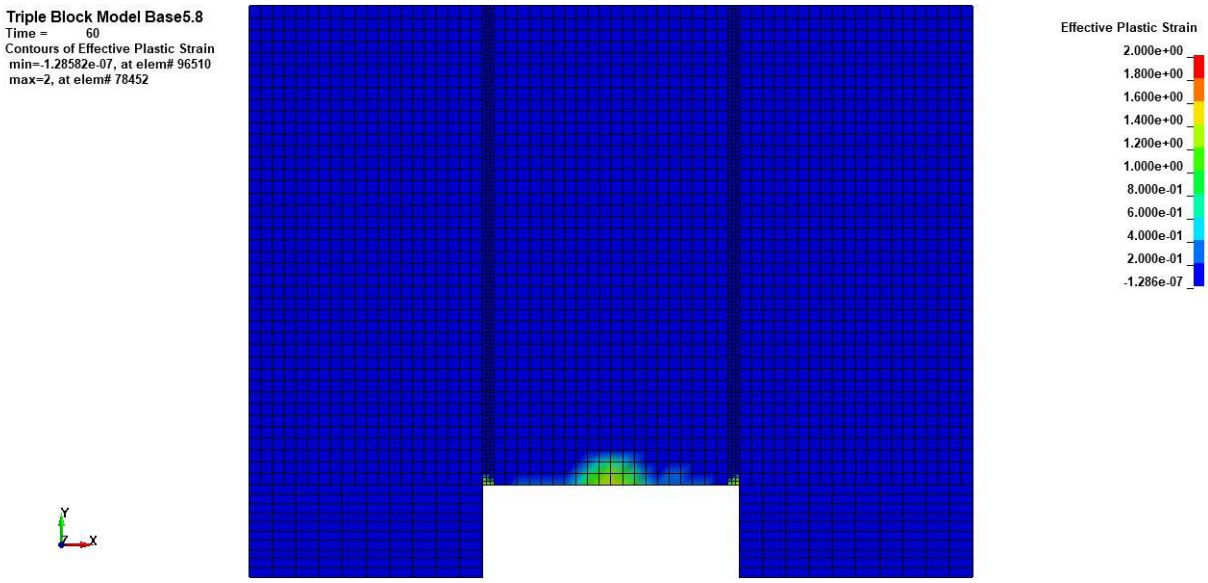


**Figure B-240: Effective Plastic Strain Fringe Plot for Last State at 60 Milliseconds for Base Run 5.8 – 400 psi**

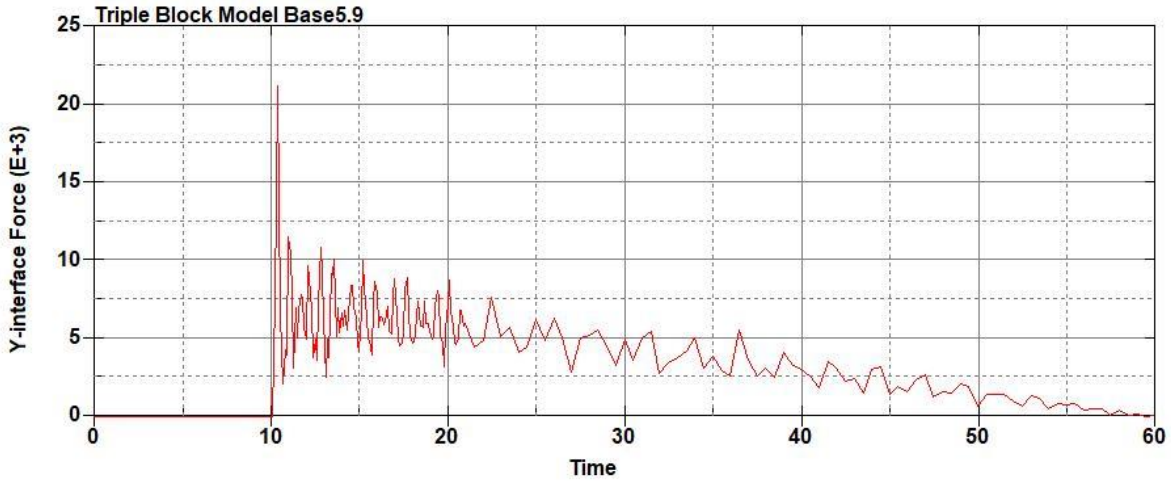


**Figure B-241: Base Run 5.9 Right Support Y-Interface Force (lbs) versus Time (ms) – 450 psi**

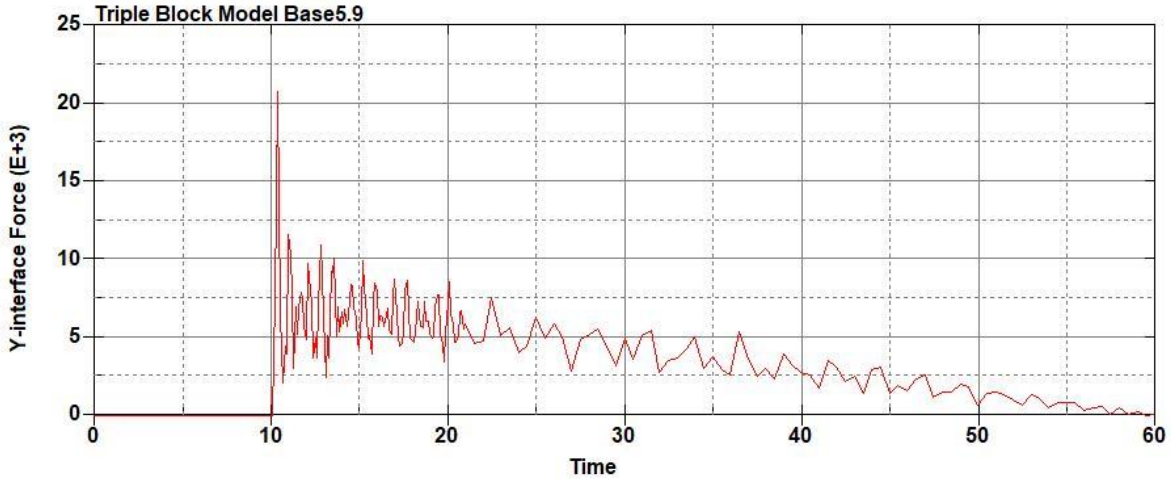


**Figure B-242: Base Run 5.9 Left Support Y-Interface Force (lbs) versus Time (ms) – 450 psi**

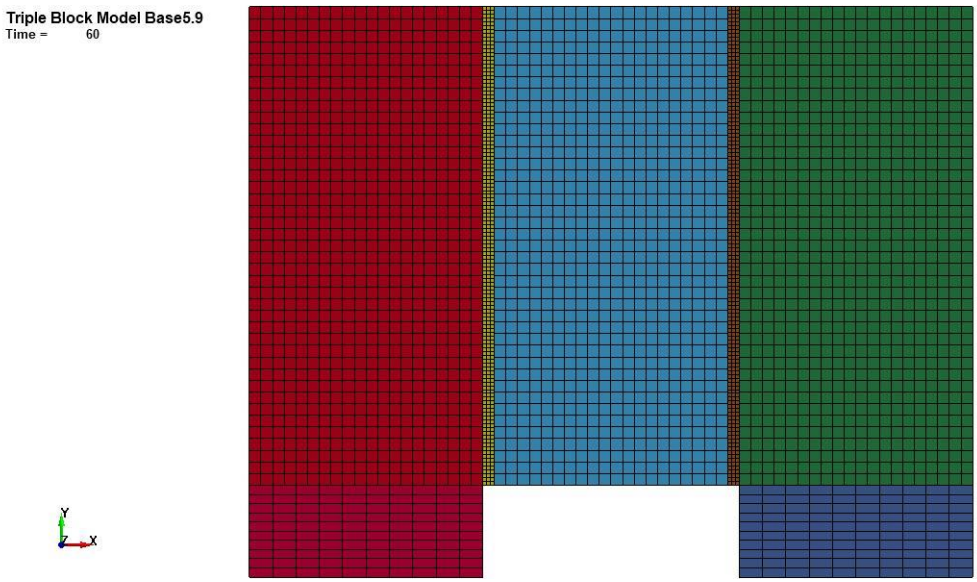


**Figure B-243: Last State at 60 Milliseconds for Base Run 5.9 – 450 psi**

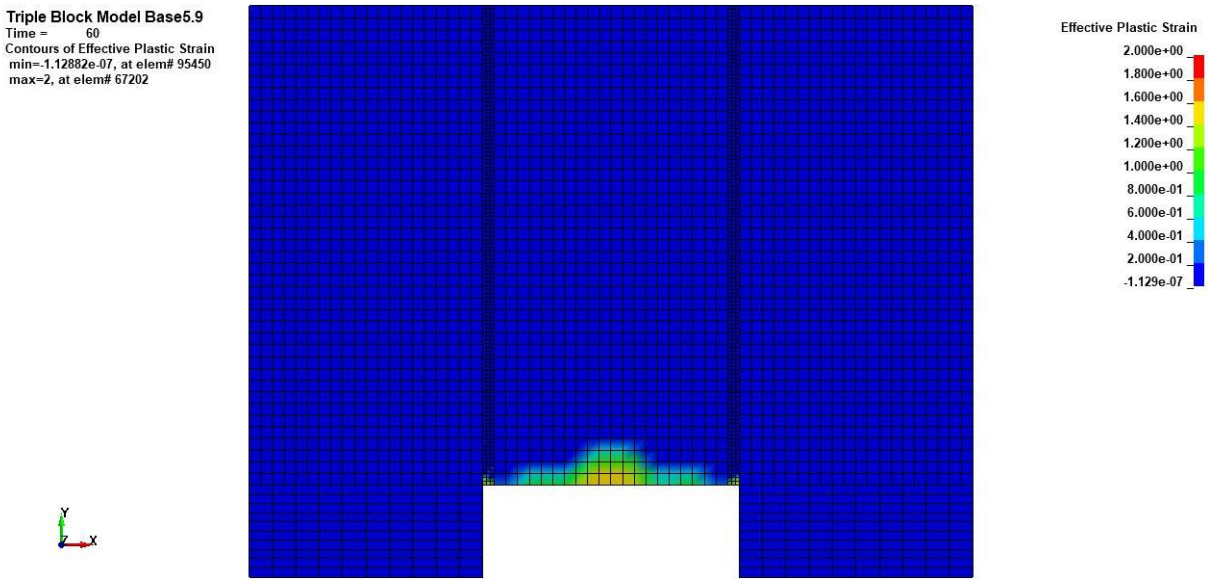


**Figure B-244: Effective Plastic Strain Fringe Plot for Last State at 60 Milliseconds for Base Run 5.9 – 450 psi**

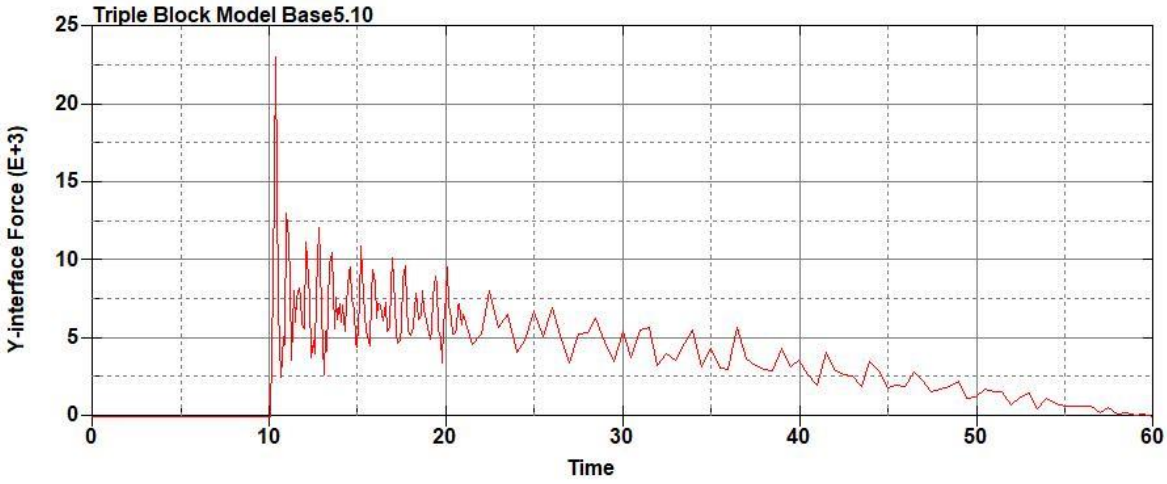


**Figure B-245: Base Run 5.10 Right Support Y-Interface Force (lbs) versus Time (ms) – 500 psi**

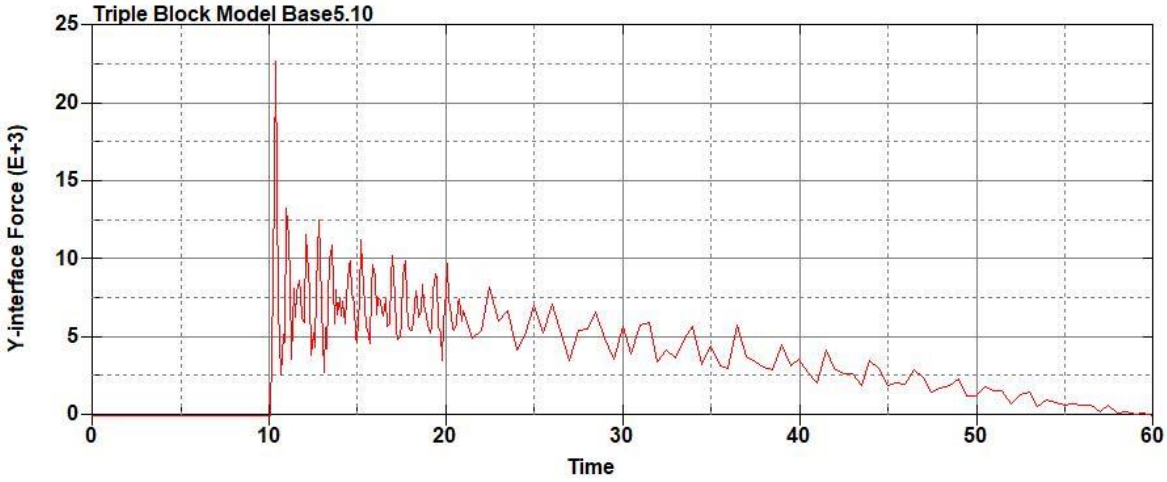


**Figure B-246: Base Run 5.10 Left Support Y-Interface Force (lbs) versus Time (ms) – 500 psi**

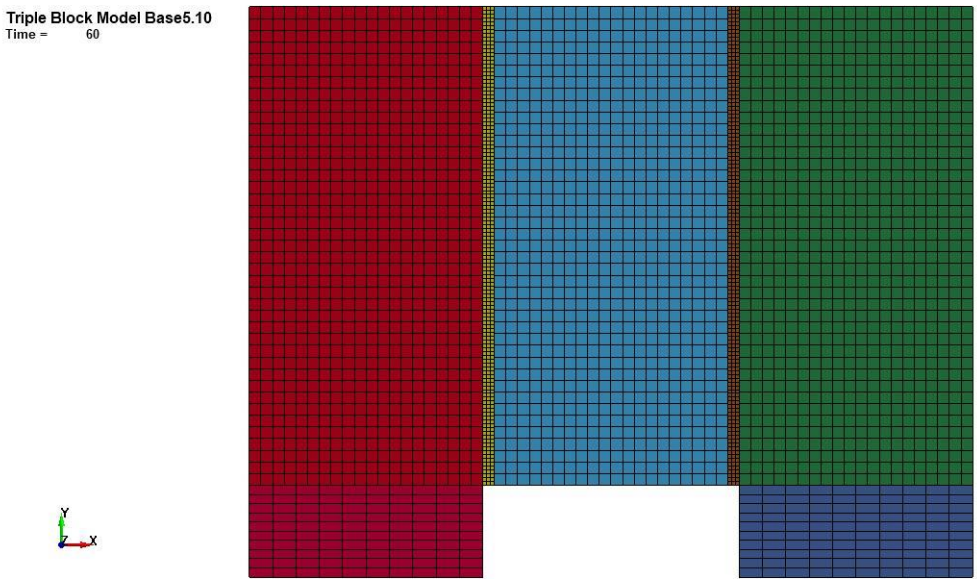


**Figure B-247: Last State at 60 Milliseconds for Base Run 5.10 – 500 psi**

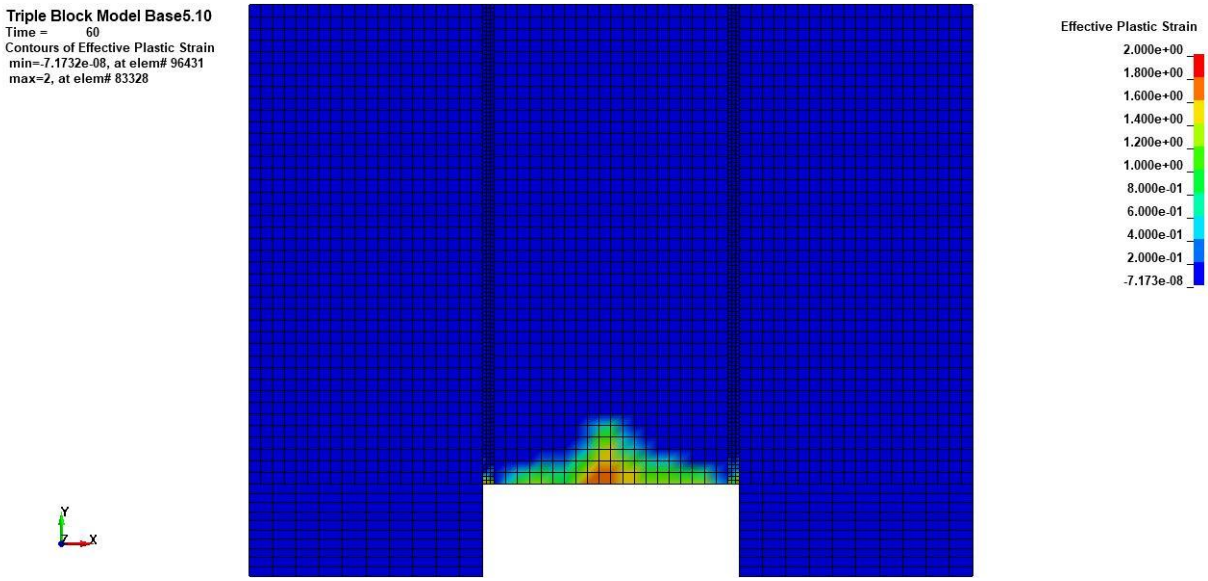


**Figure B-248: Effective Plastic Strain Fringe Plot for Last State at 60 Milliseconds for Base Run 5.10 – 500 psi**

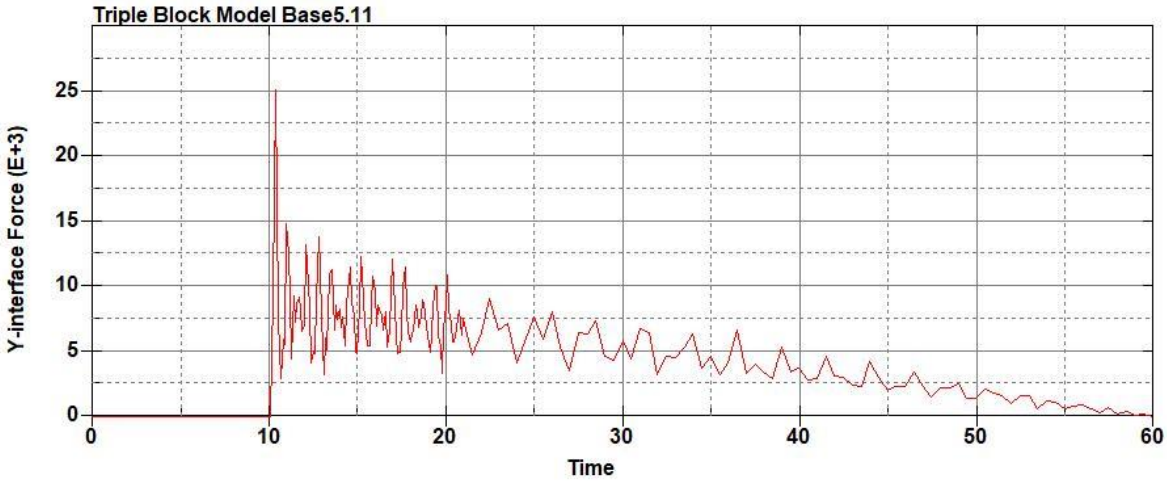


**Figure B-249: Base Run 5.11 Right Support Y-Interface Force (lbs) versus Time (ms) – 550 psi**

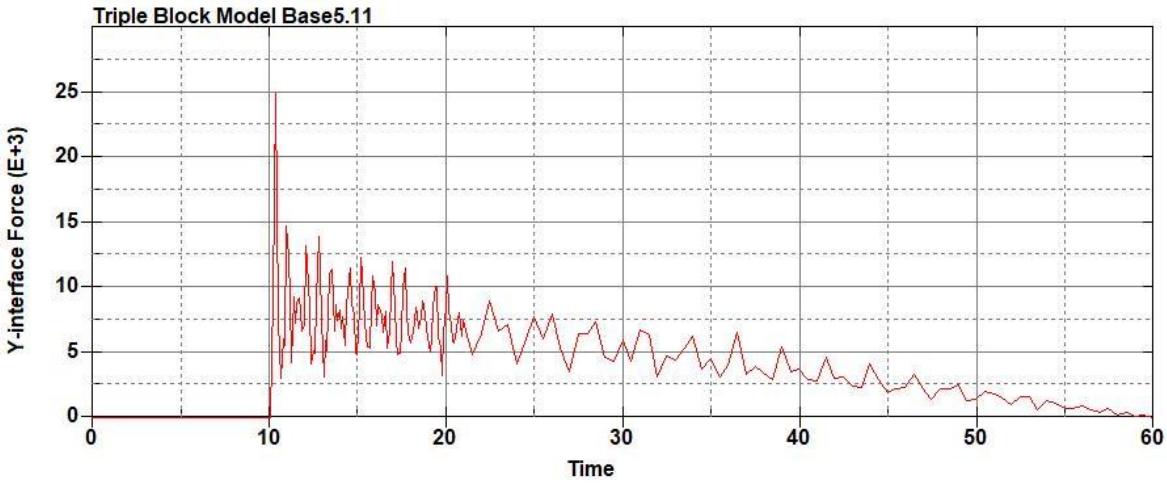


**Figure B-250: Base Run 5.11 Left Support Y-Interface Force (lbs) versus Time (ms) – 450 psi**

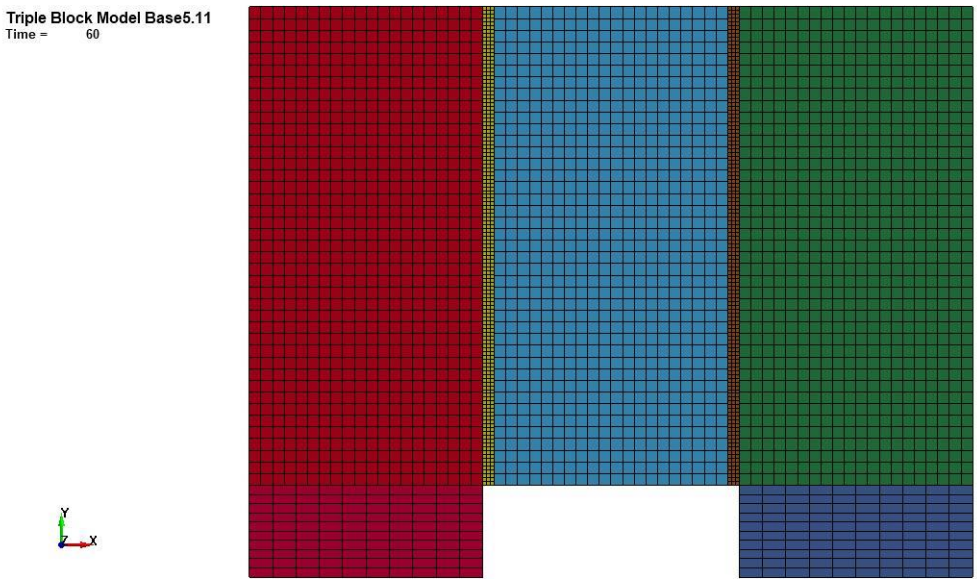


**Figure B-251: Last State at 60 Milliseconds for Base Run 5.11 – 550 psi**

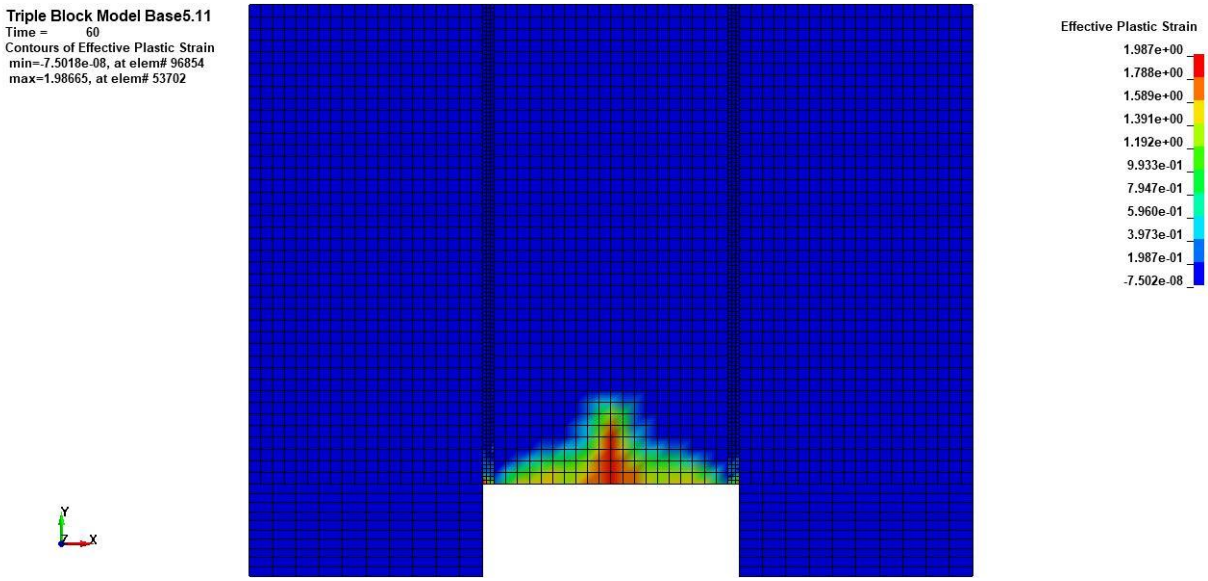


**Figure B-252: Effective Plastic Strain Fringe Plot for Last State at 60 Milliseconds for Base Run 5.11 – 550 psi**

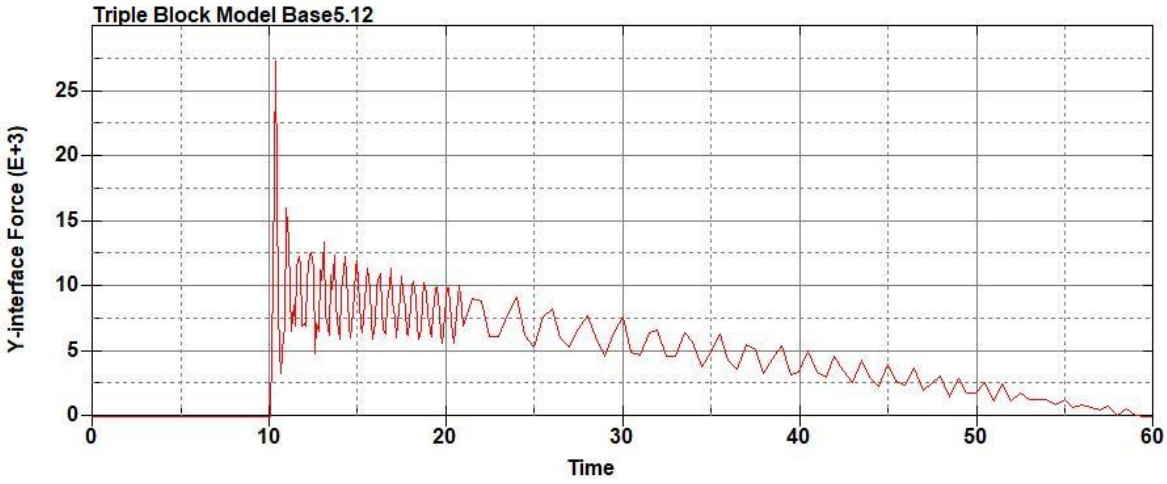


**Figure B-253: Base Run 5.12 Right Support Y-Interface Force (lbs) versus Time (ms) – 600 psi**

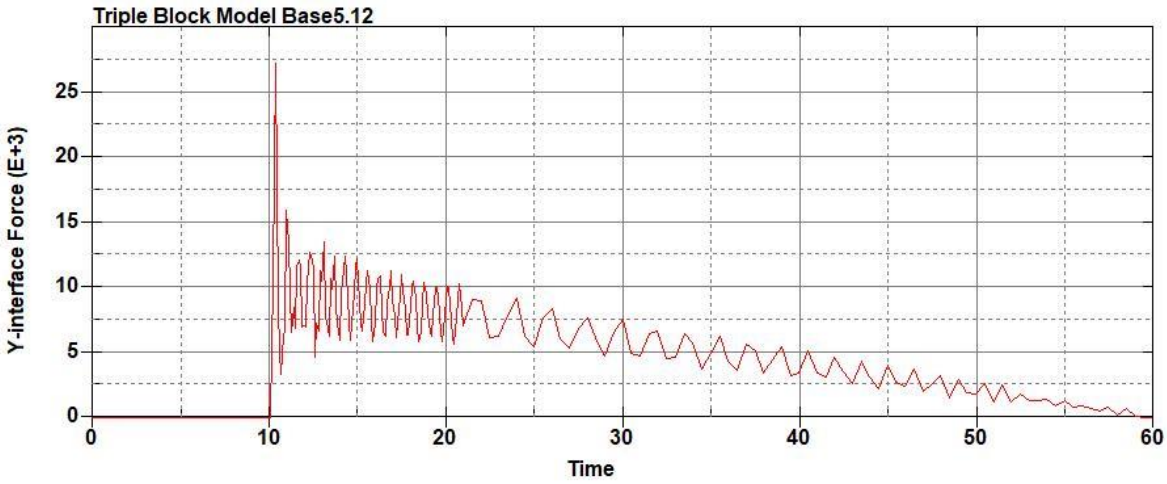


**Figure B-254: Base Run 5.12 Left Support Y-Interface Force (lbs) versus Time (ms) – 600 psi**

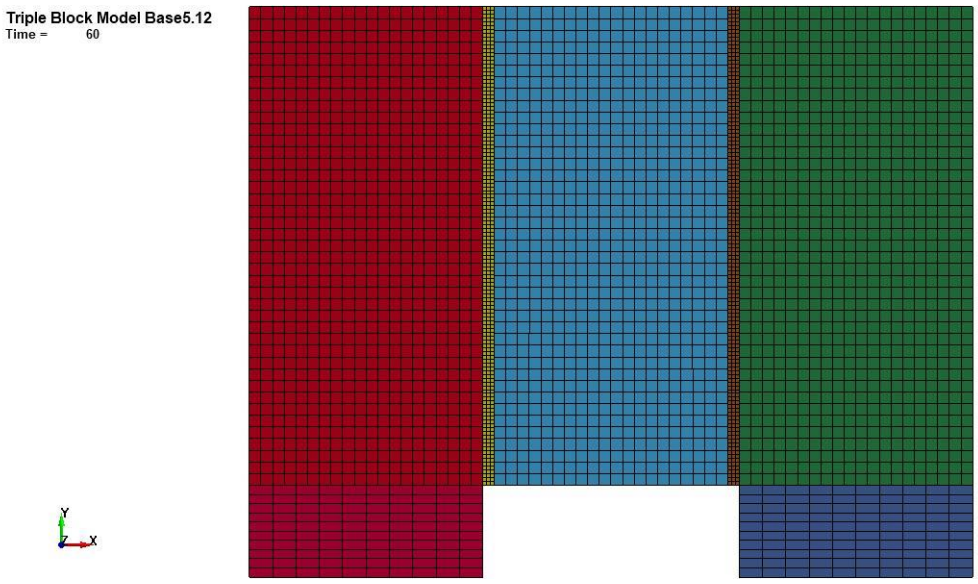


**Figure B-255: Last State at 60 Milliseconds for Base Run 5.12 – 600 psi**

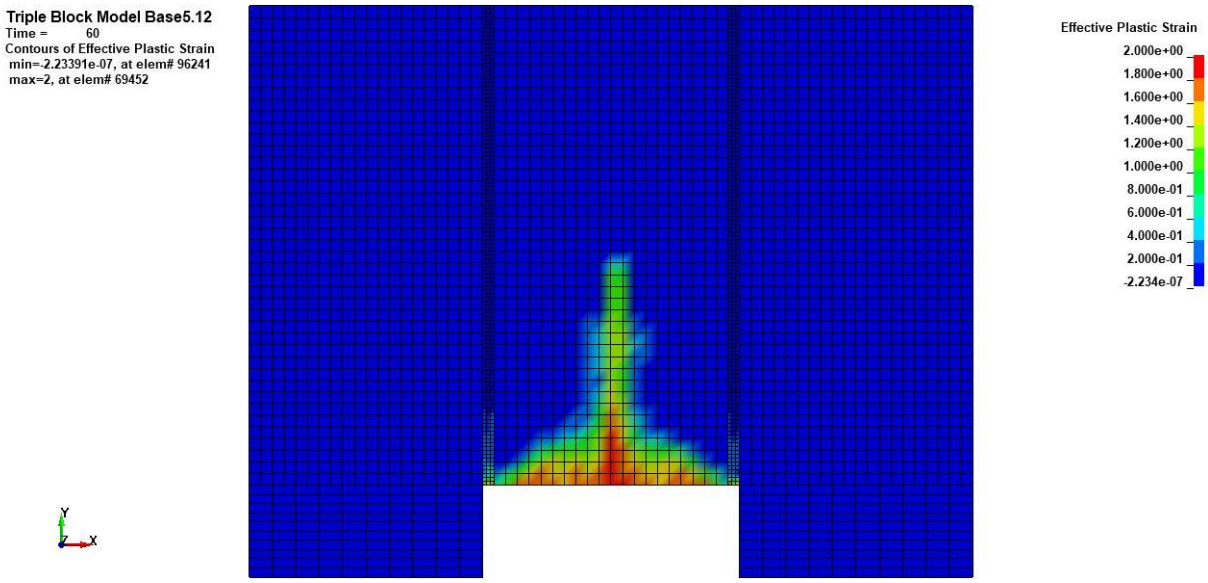


**Figure B-256: Effective Plastic Strain Fringe Plot for Last State at 60 Milliseconds for Base Run 5.12 – 600 psi**

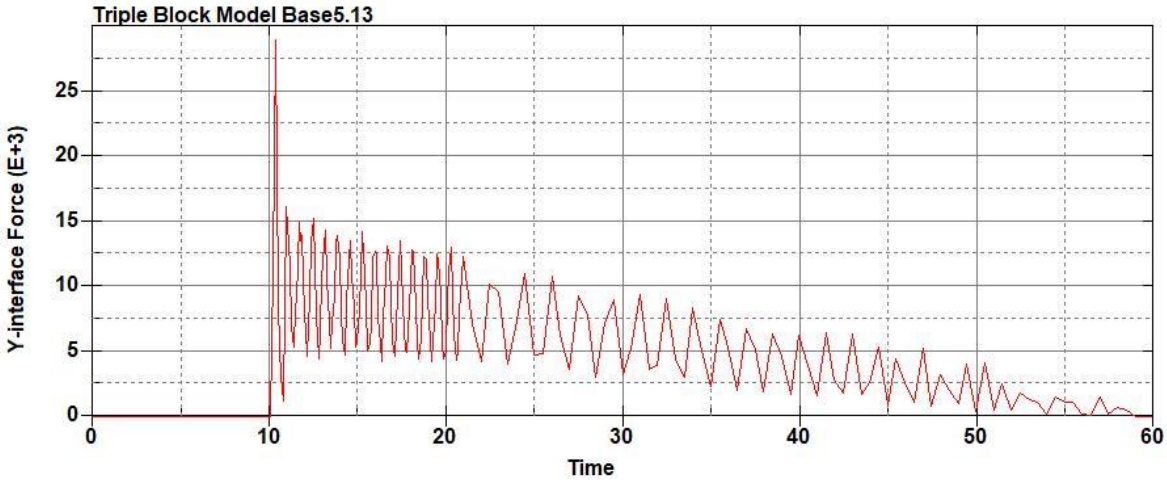


**Figure B-257: Base Run 5.13 Right Support Y-Interface Force (lbs) versus Time (ms) – 650 psi**

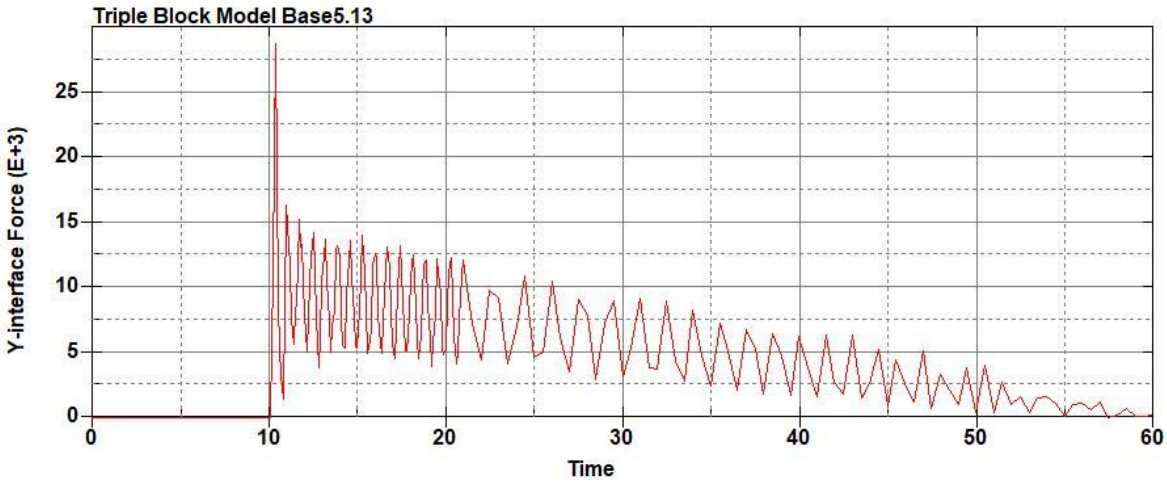


**Figure B-258: Base Run 5.13 Left Support Y-Interface Force (lbs) versus Time (ms) – 650 psi**

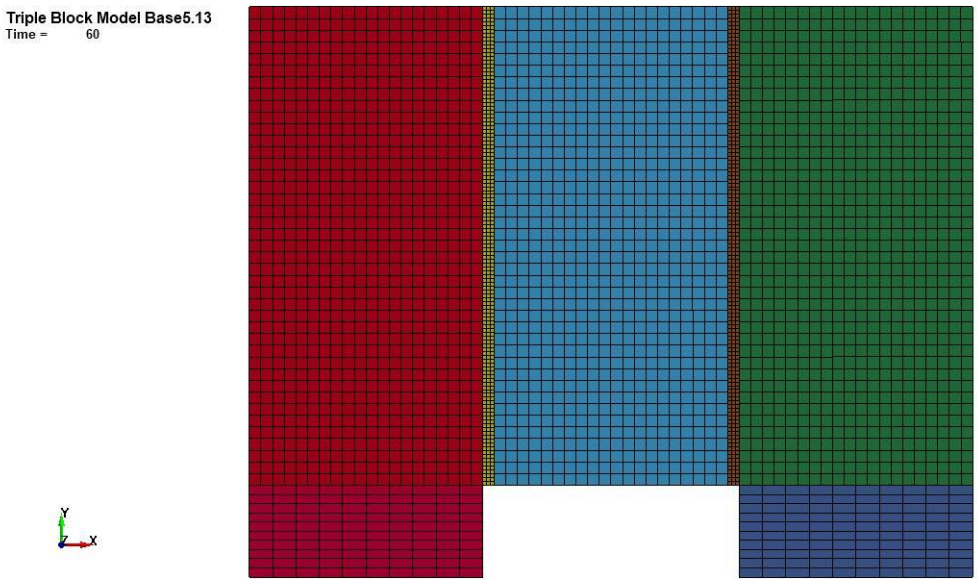


**Figure B-259: Last State at 60 Milliseconds for Base Run 5.13 – 650 psi**

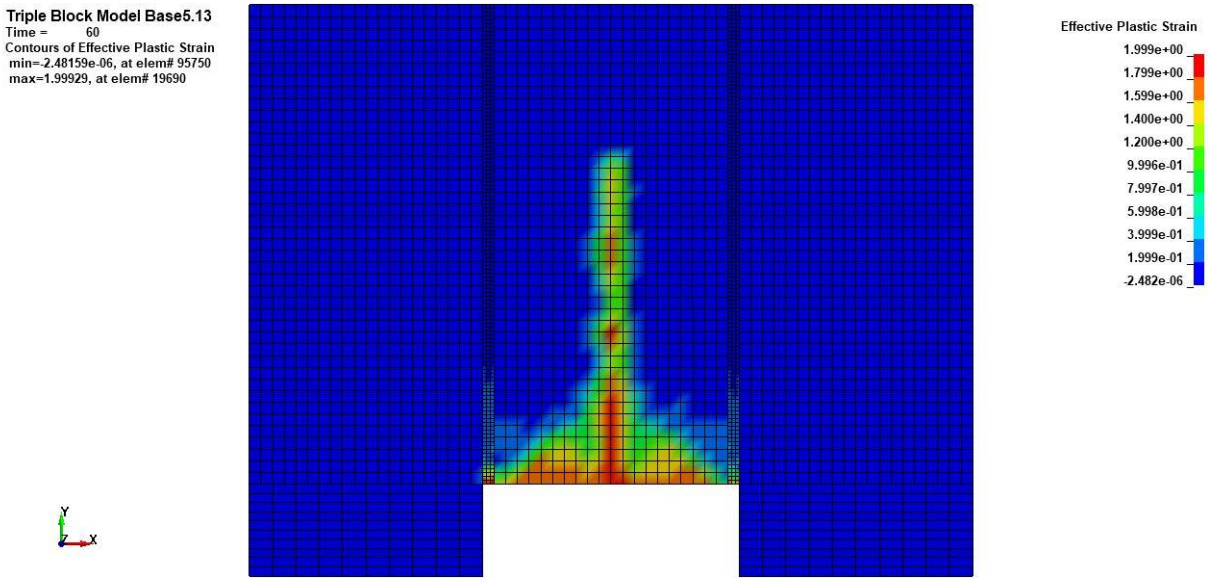


**Figure B-260: Effective Plastic Strain Fringe Plot for Last State at 60 Milliseconds for Base Run 5.13 – 650 psi**

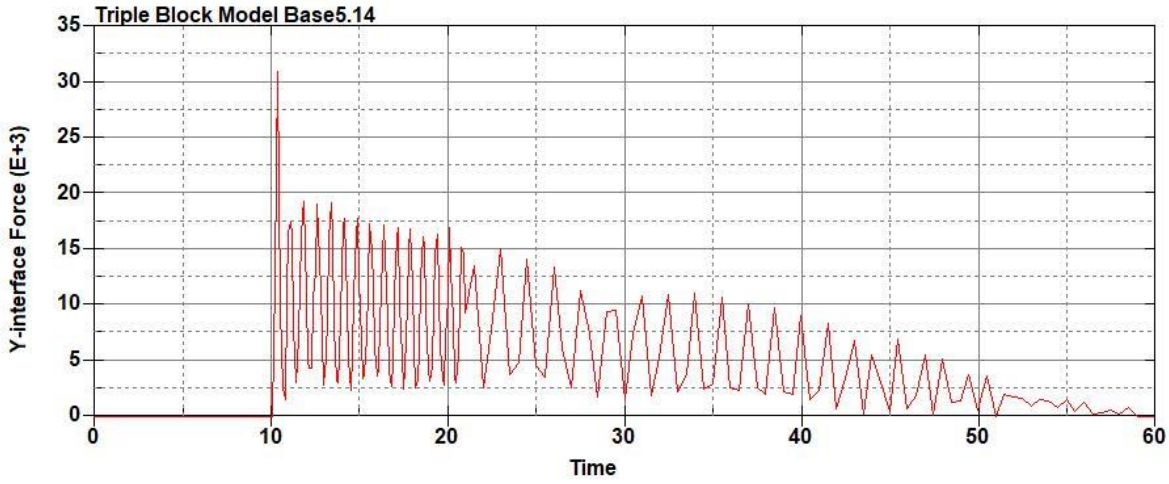


**Figure B-261: Base Run 5.14 Right Support Y-Interface Force (lbs) versus Time (ms) – 700 psi**

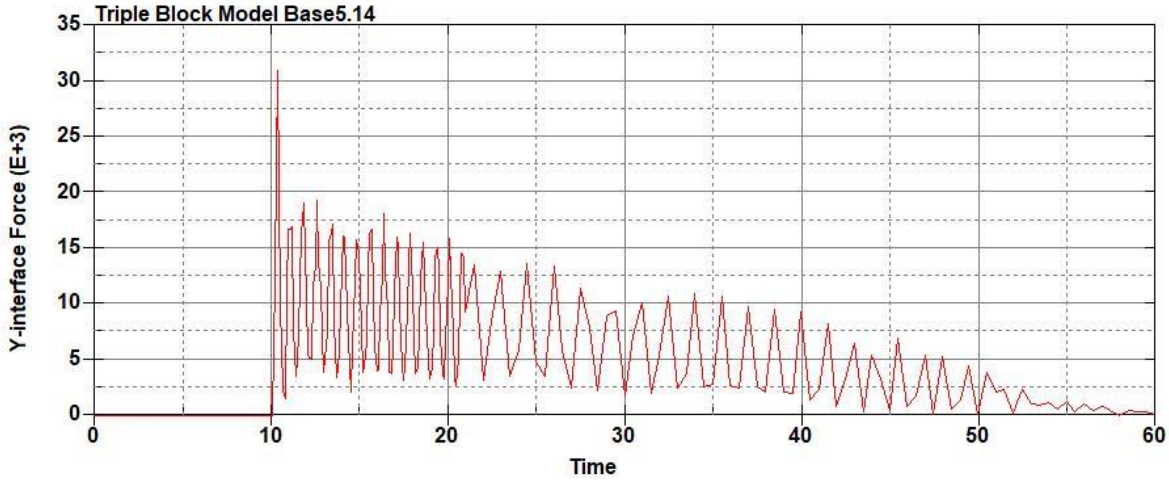


**Figure B-262: Base Run 5.14 Left Support Y-Interface Force (lbs) versus Time (ms) – 700 psi**

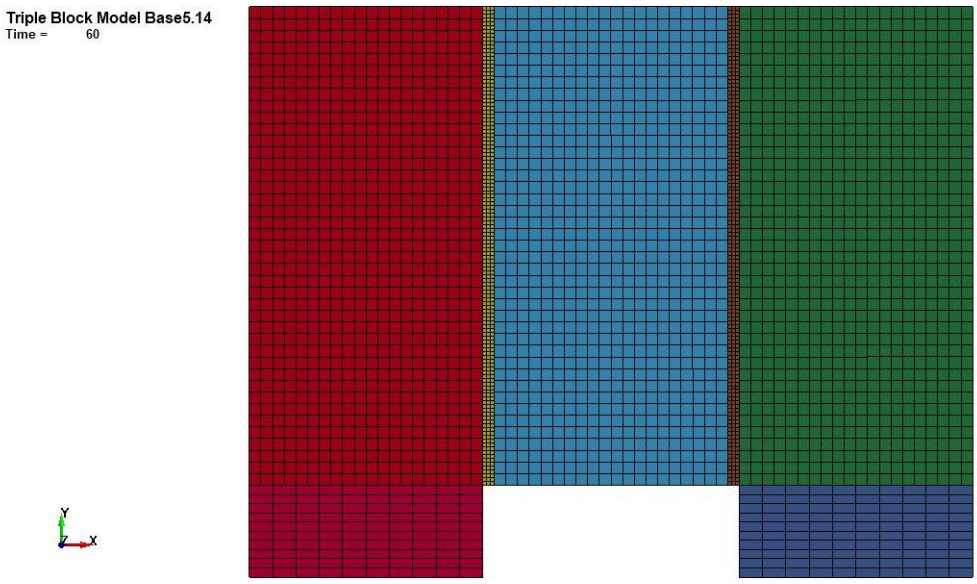


**Figure B-263: Last State at 60 Milliseconds for Base Run 5.14 – 700 psi**

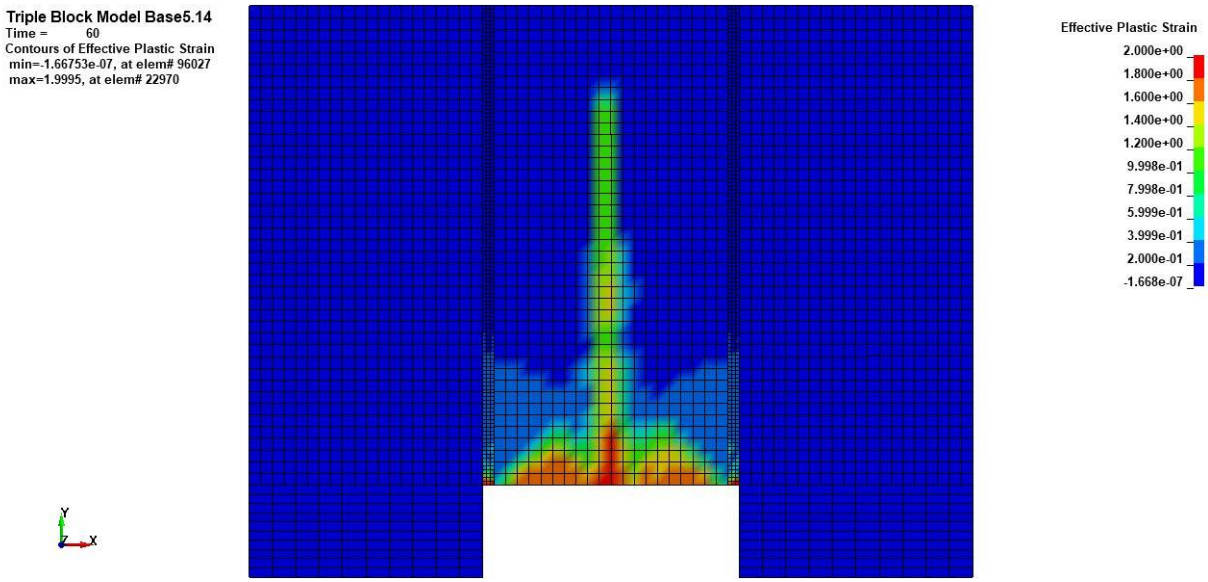


**Figure B-264: Effective Plastic Strain Fringe Plot for Last State at 60 Milliseconds for Base Run 5.14 – 700 psi**

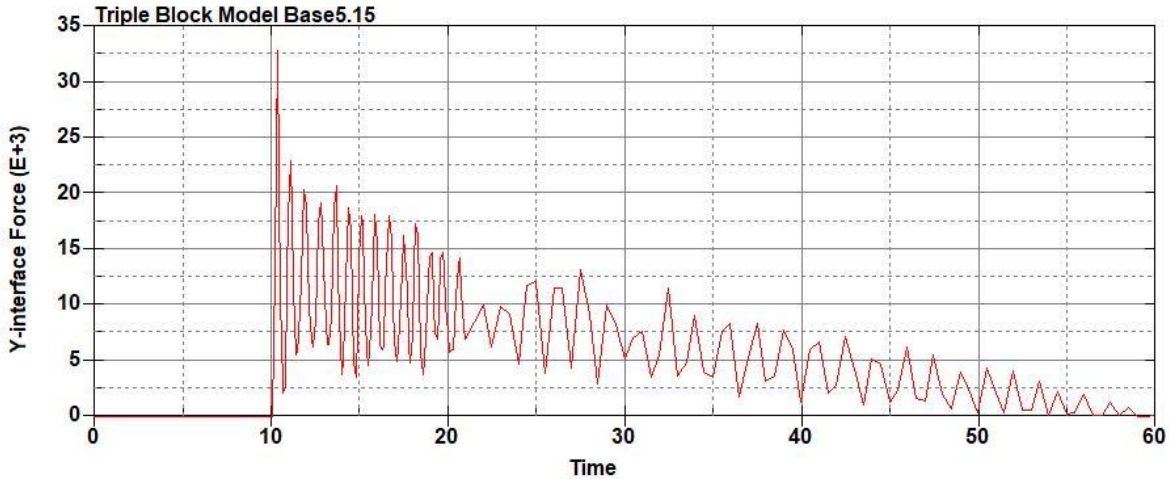


**Figure B-265: Base Run 5.15 Right Support Y-Interface Force (lbs) versus Time (ms) – 750 psi**

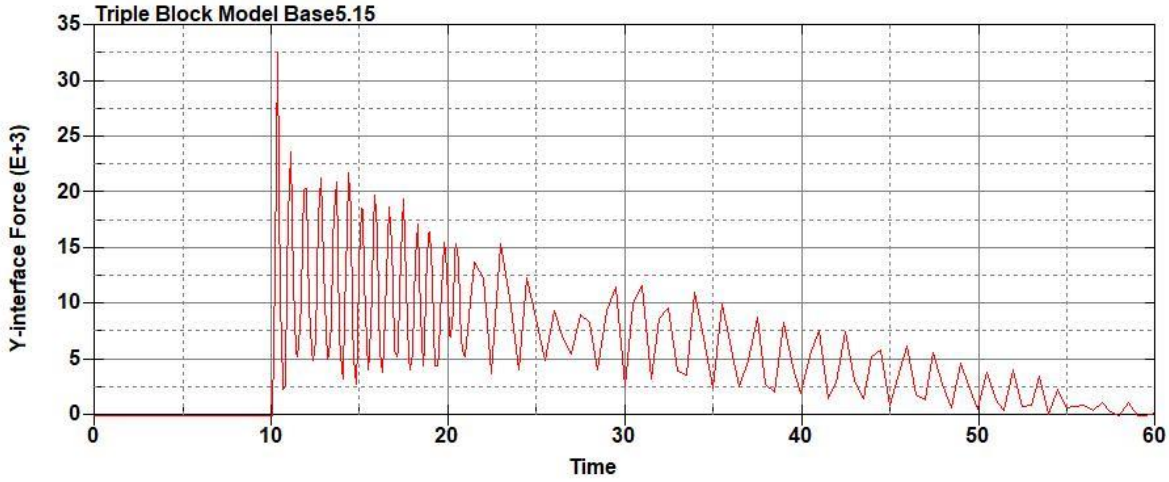


**Figure B-266: Base Run 5.15 Left Support Y-Interface Force (lbs) versus Time (ms) – 750 psi**

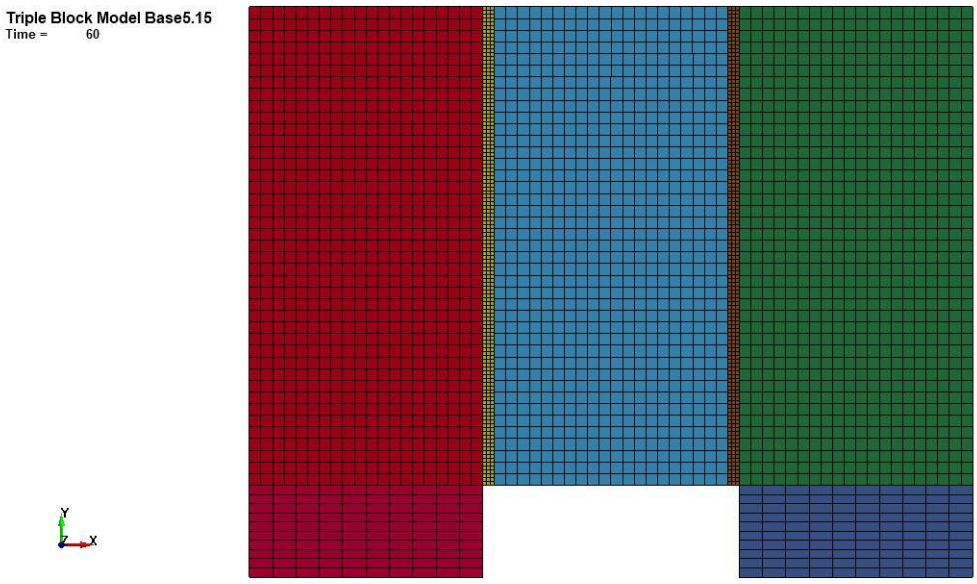


**Figure B-267: Last State at 60 Milliseconds for Base Run 5.15 – 750 psi**

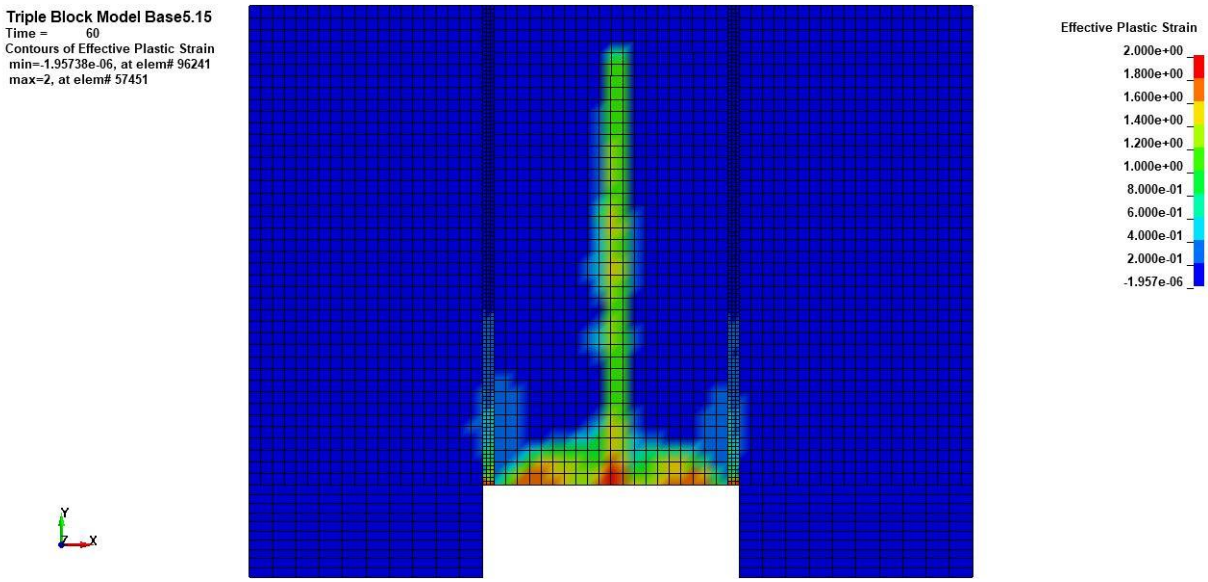


**Figure B-268: Effective Plastic Strain Fringe Plot for Last State at 60 Milliseconds for Base Run 5.15 – 750 psi**

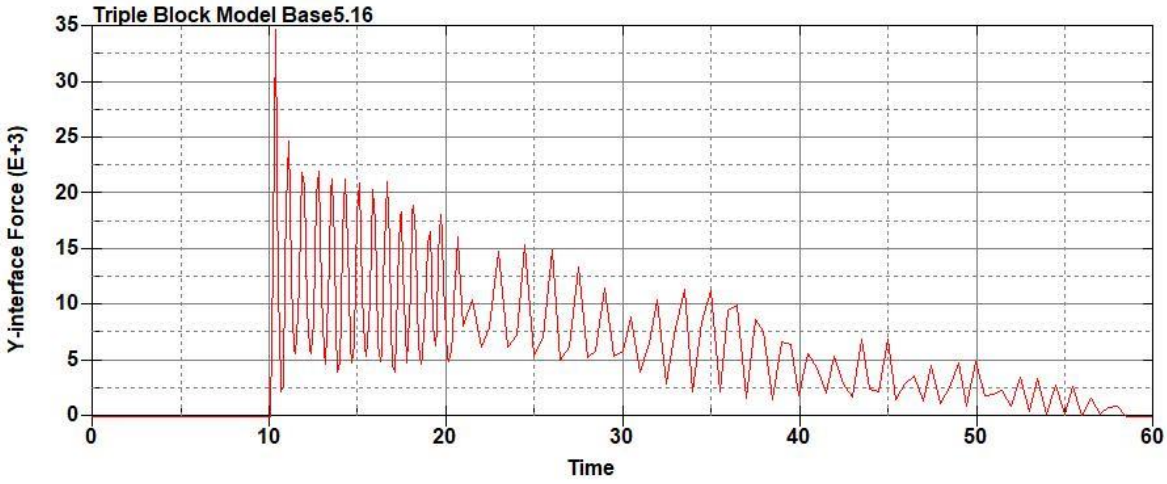


**Figure B-269: Base Run 5.16 Right Support Y-Interface Force (lbs) versus Time (ms) – 800 psi**

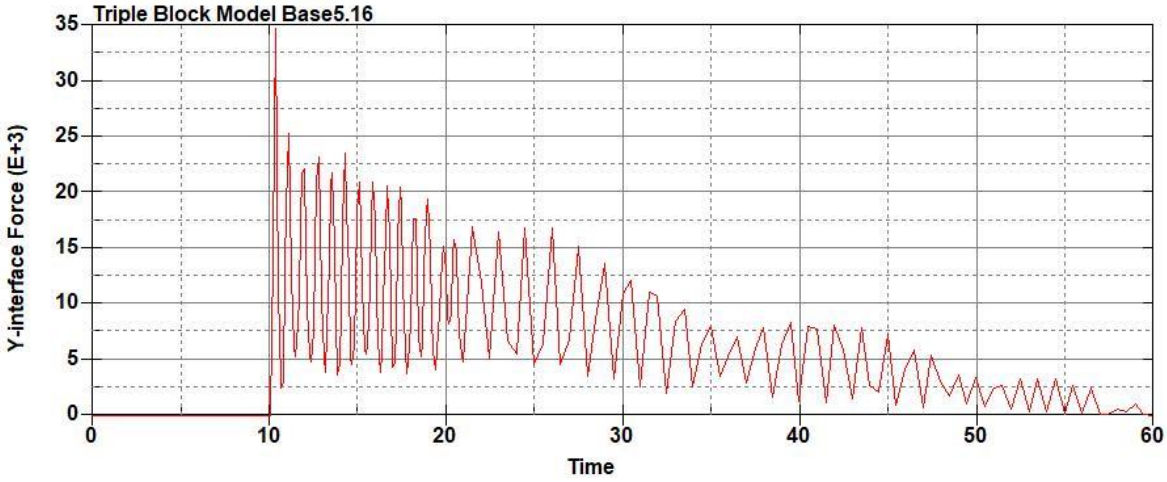


**Figure B-270: Base Run 5.16 Left Support Y-Interface Force (lbs) versus Time (ms) – 800 psi**

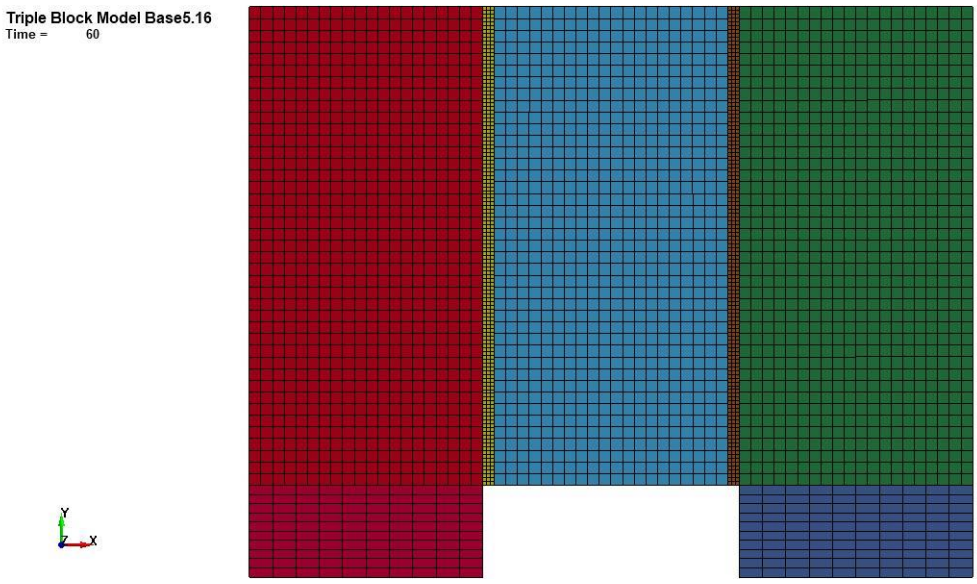


**Figure B-271: Last State at 60 Milliseconds for Base Run 5.16 – 800 psi**

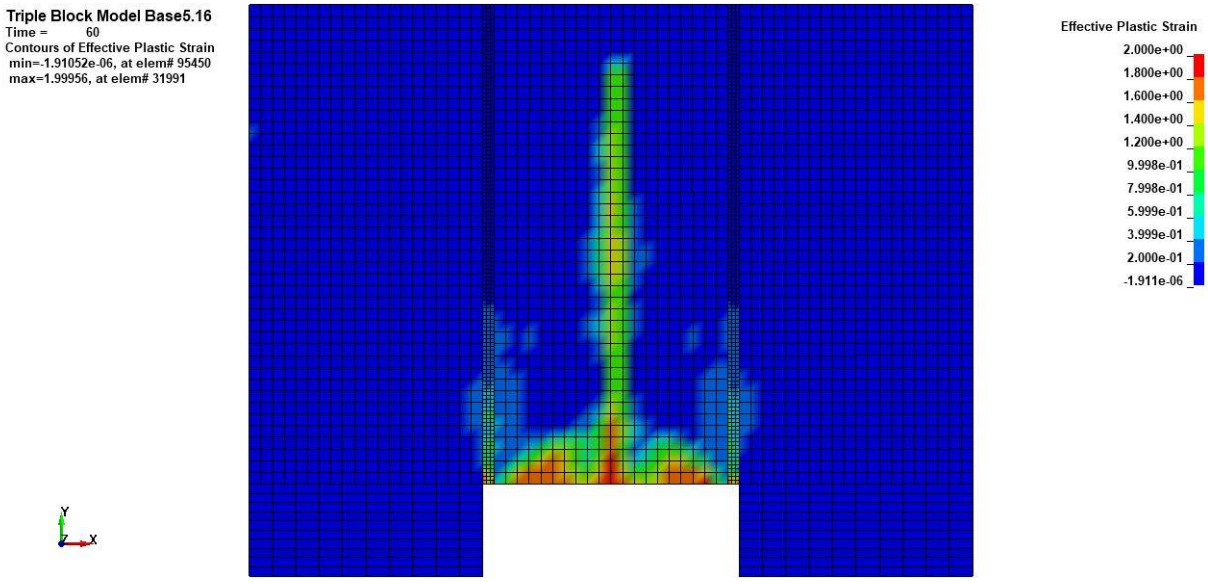


**Figure B-272: Effective Plastic Strain Fringe Plot for Last State at 60 Milliseconds for Base Run 5.16 – 800 psi**

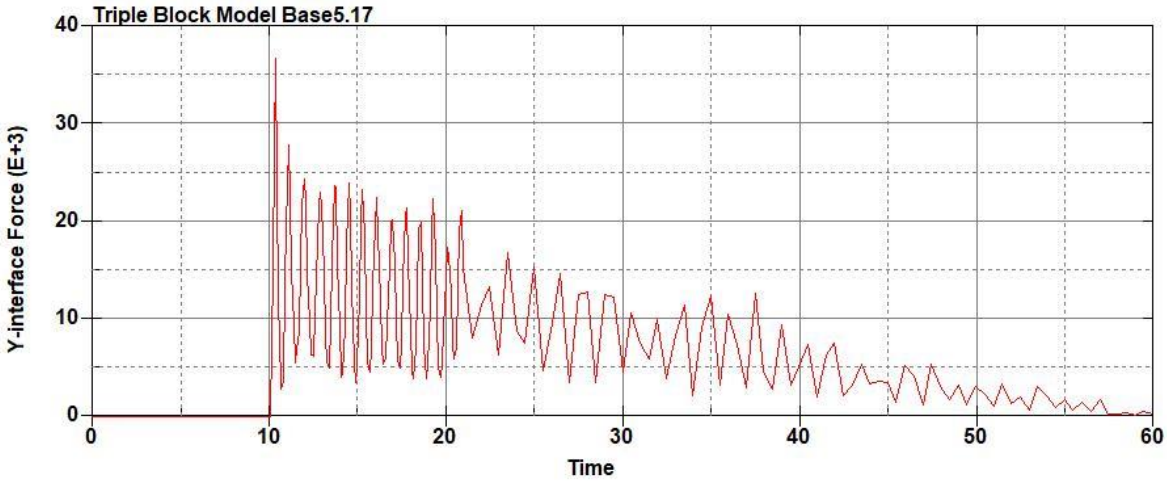


**Figure B-273: Base Run 5.17 Right Support Y-Interface Force (lbs) versus Time (ms) – 850 psi**

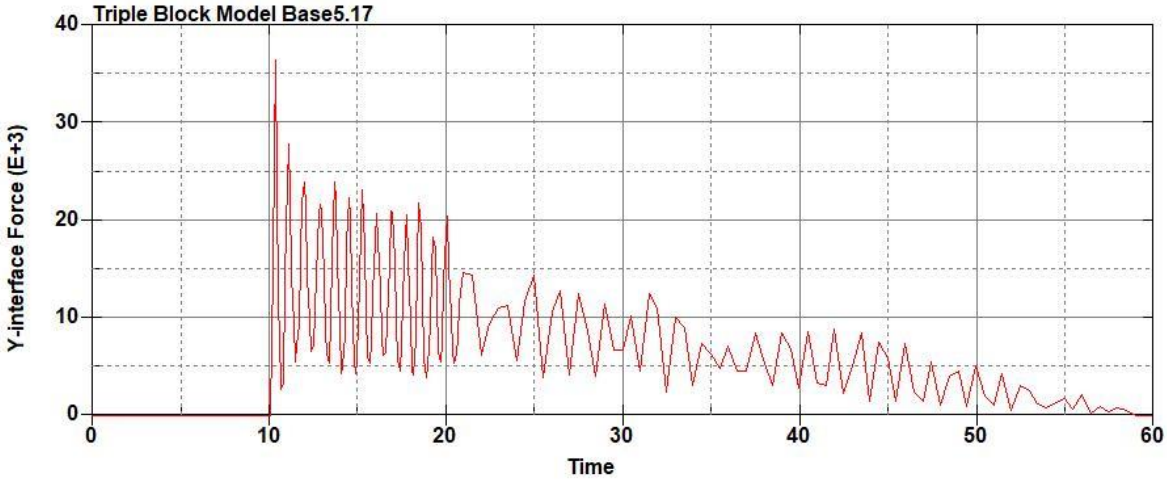


**Figure B-274: Base Run 5.17 Left Support Y-Interface Force (lbs) versus Time (ms) – 850 psi**

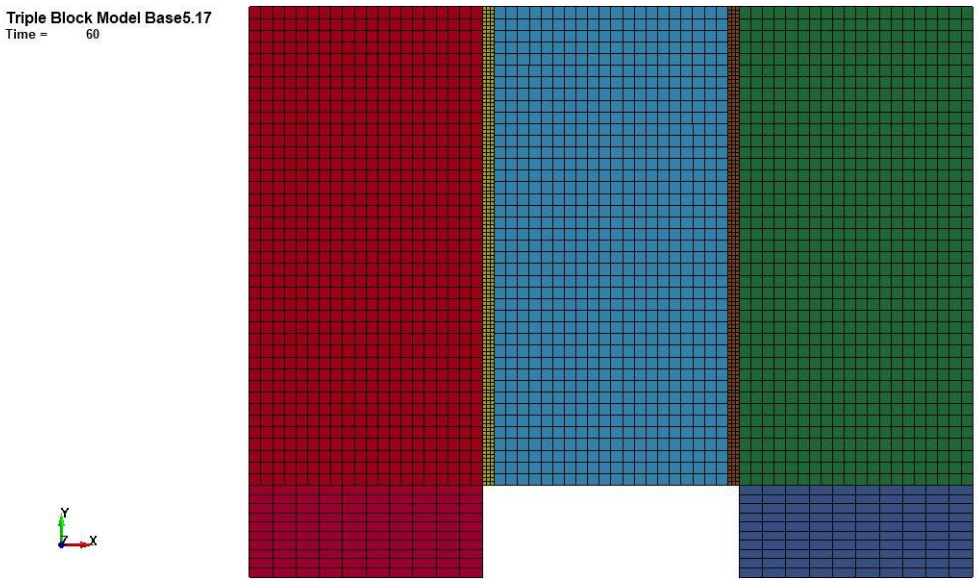


**Figure B-275: Last State at 60 Milliseconds for Base Run 5.17 – 850 psi**

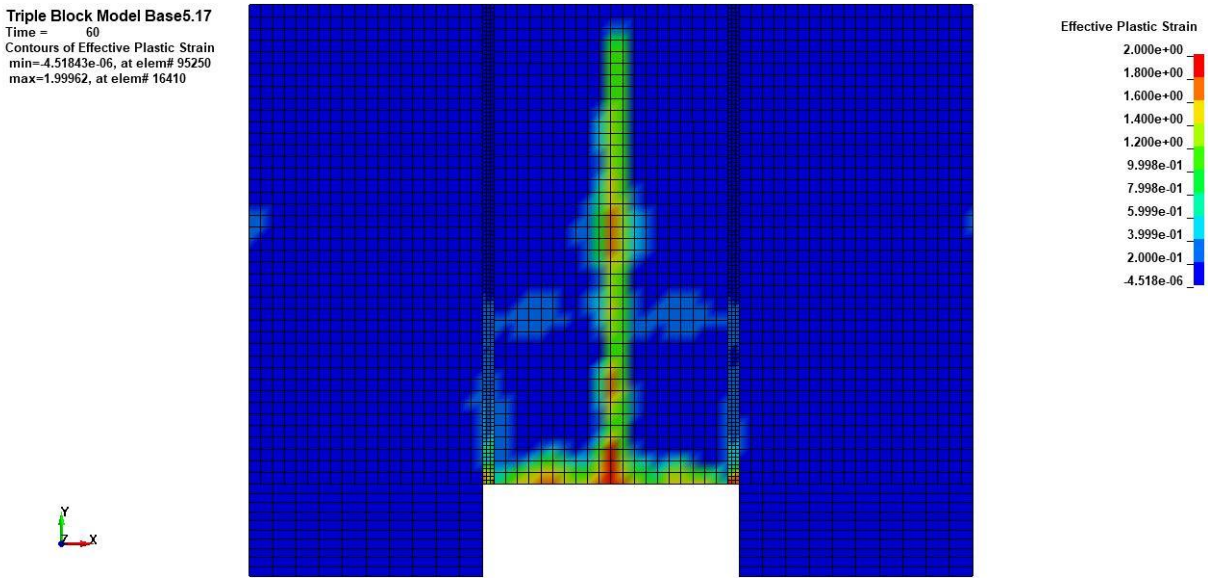


**Figure B-276: Effective Plastic Strain Fringe Plot for Last State at 60 Milliseconds for Base Run 5.17 – 850 psi**

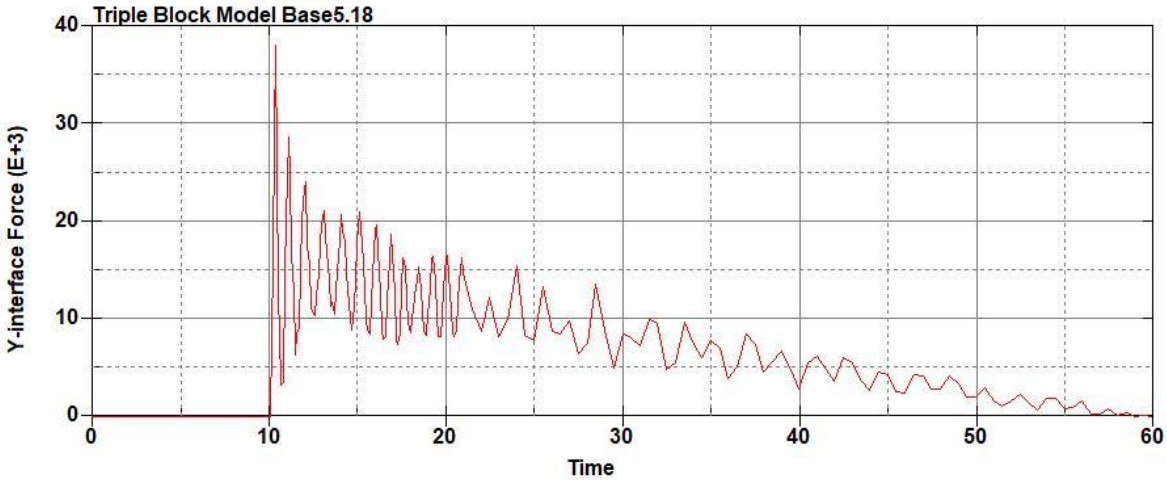


**Figure B-277: Base Run 5.18 Right Support Y-Interface Force (lbs) versus Time (ms) – 900 psi**

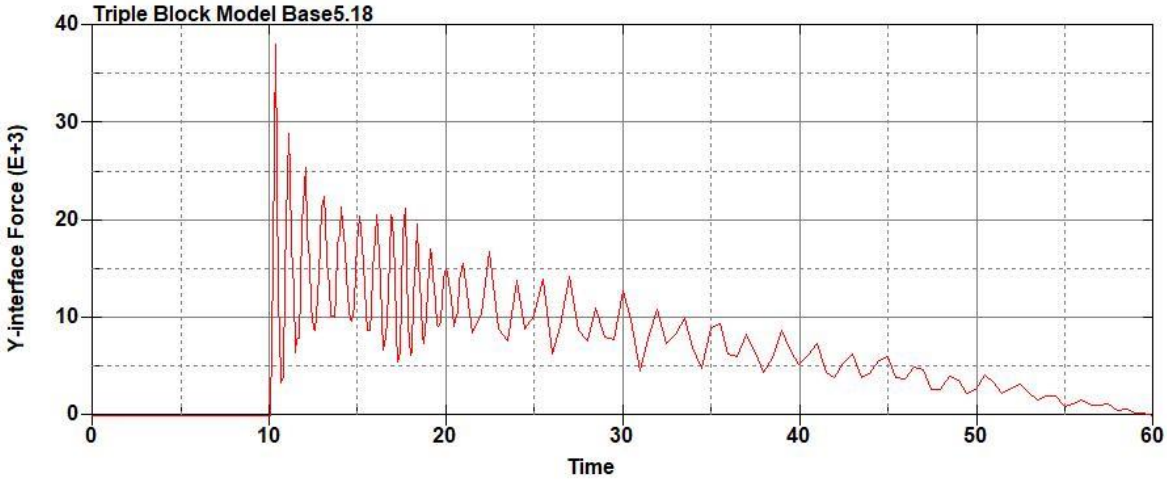


**Figure B-278: Base Run 5.18 Left Support Y-Interface Force (lbs) versus Time (ms) – 900 psi**

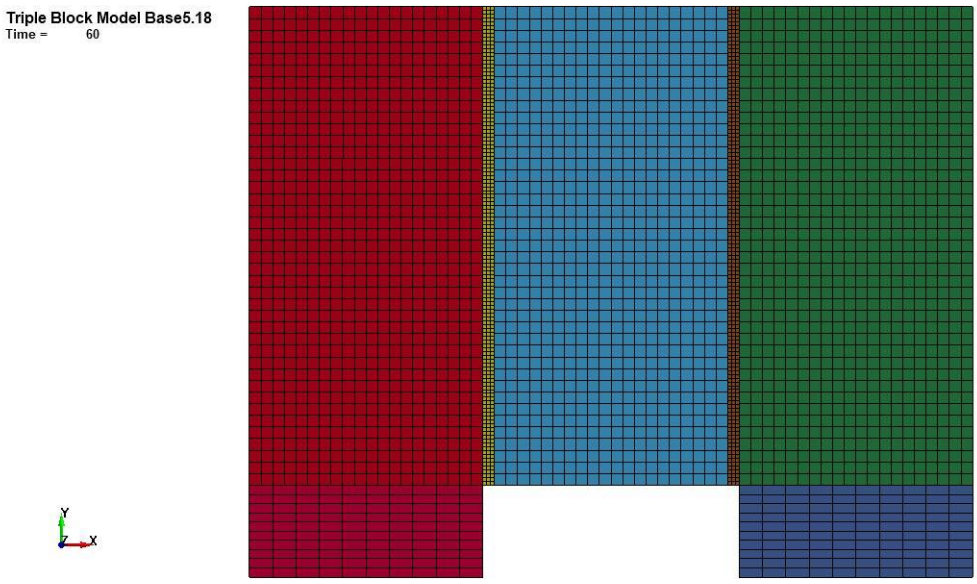


**Figure B-279: Last State at 60 Milliseconds for Base Run 5.18 – 900 psi**

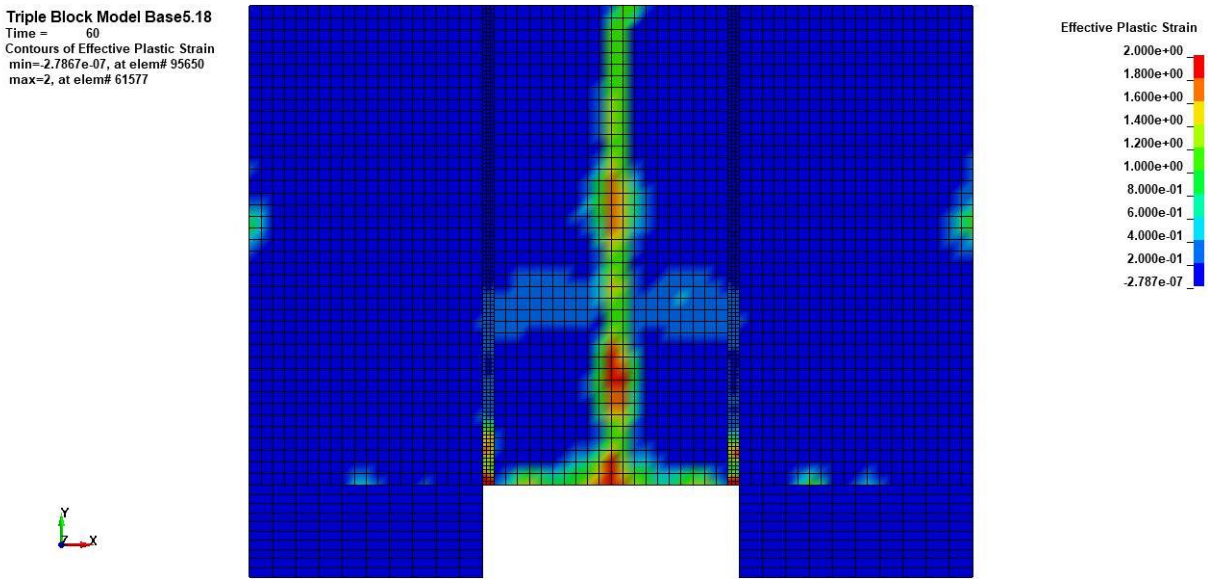


**Figure B-280: Effective Plastic Strain Fringe Plot for Last State at 60 Milliseconds for Base Run 5.18 – 900 psi**

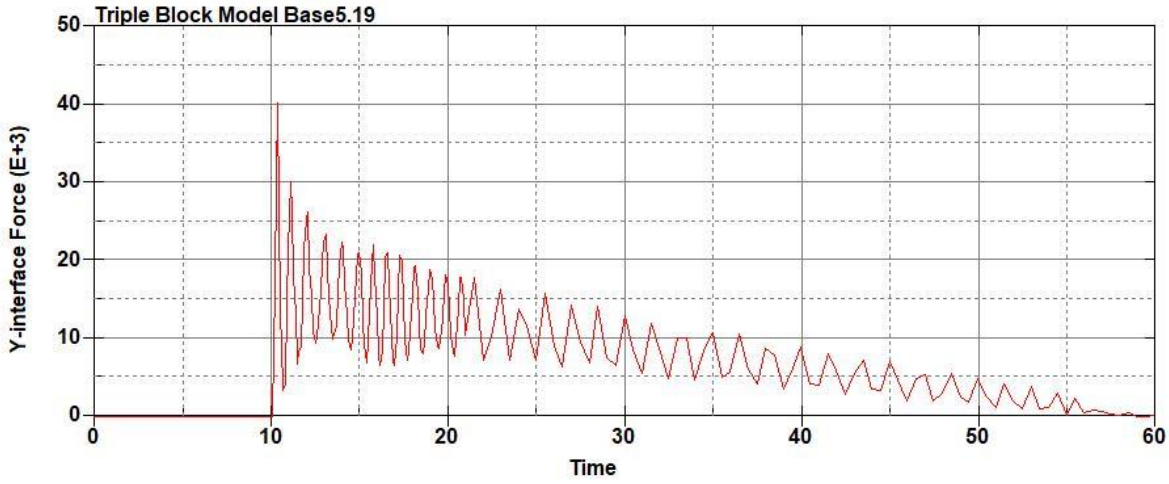


**Figure B-281: Base Run 5.19 Right Support Y-Interface Force (lbs) versus Time (ms) – 950 psi**

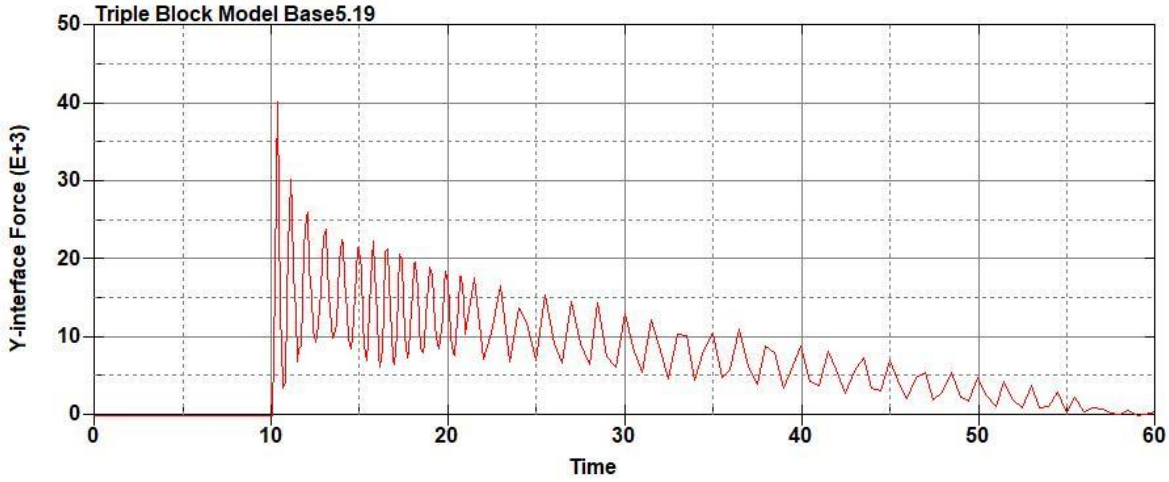


**Figure B-282: Base Run 5.19 Left Support Y-Interface Force (lbs) versus Time (ms) – 950 psi**

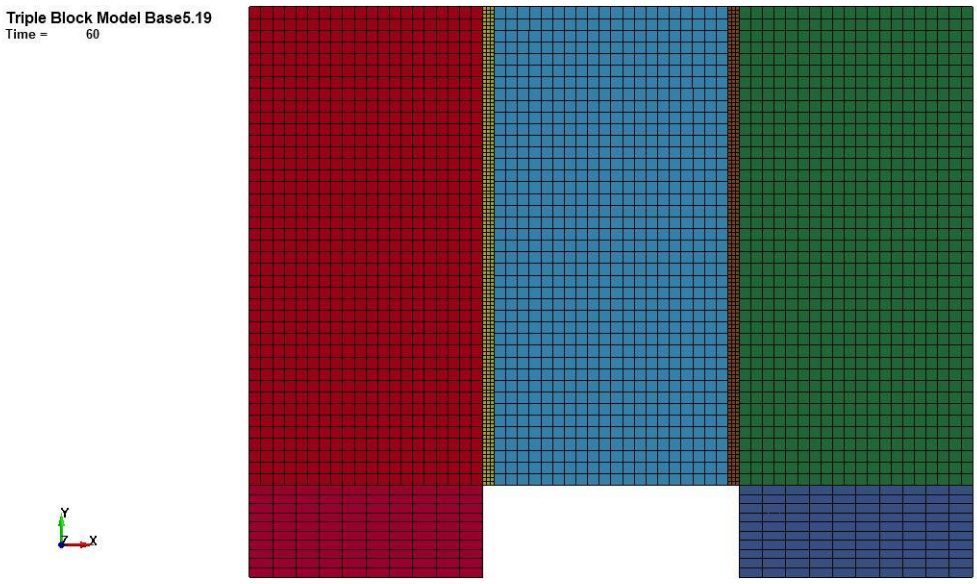


**Figure B-283: Last State at 60 Milliseconds for Base Run 5.19 – 950 psi**

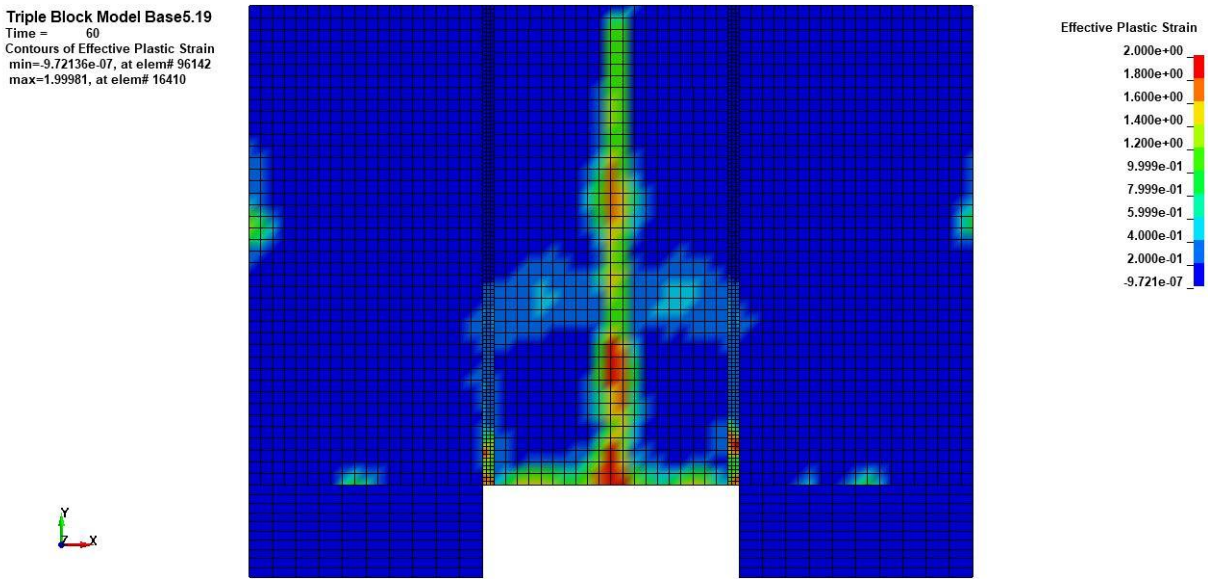


**Figure B-284: Effective Plastic Strain Fringe Plot for Last State at 60 Milliseconds for Base Run 5.19 – 950 psi**

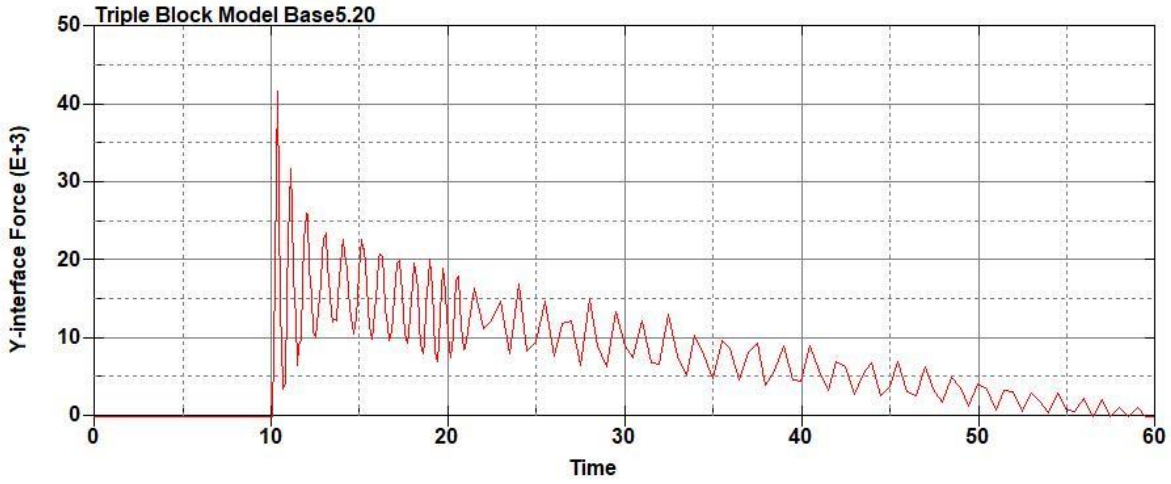


**Figure B-285: Base Run 5.20 Right Support Y-Interface Force (lbs) versus Time (ms) – 1000 psi**

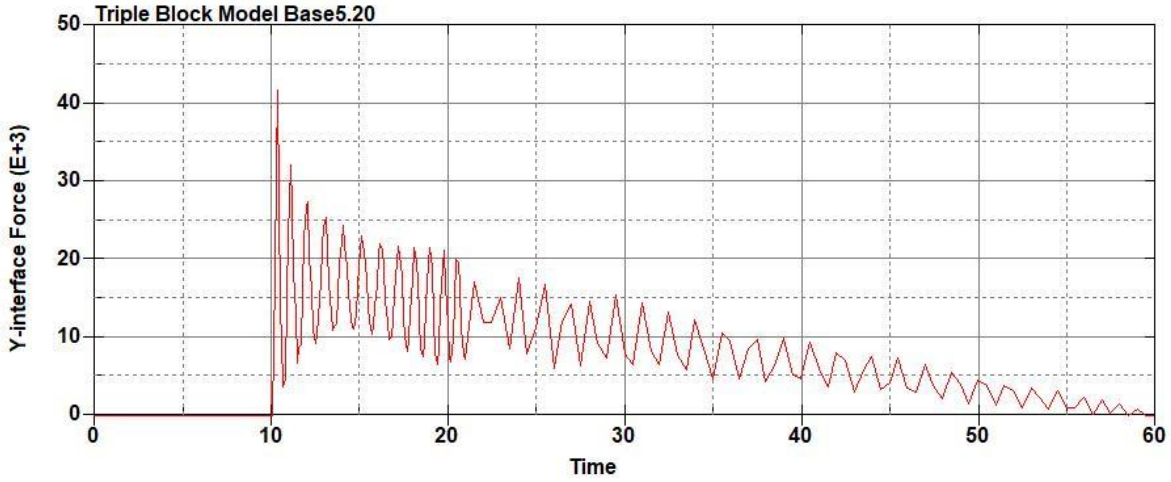


**Figure B-286: Base Run 5.20 Left Support Y-Interface Force (lbs) versus Time (ms) – 1000 psi**

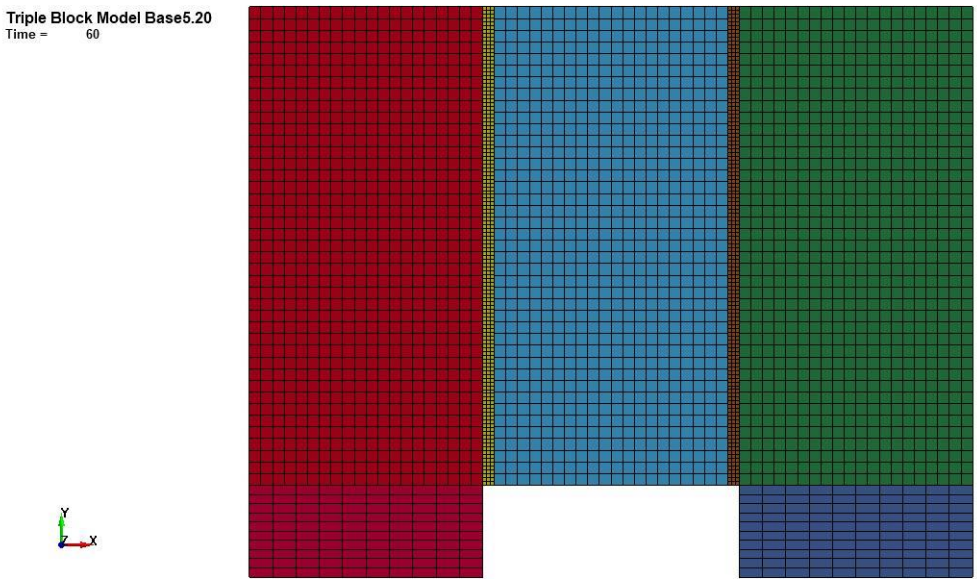


**Figure B-287: Last State at 60 Milliseconds for Base Run 5.20 – 1000 psi**

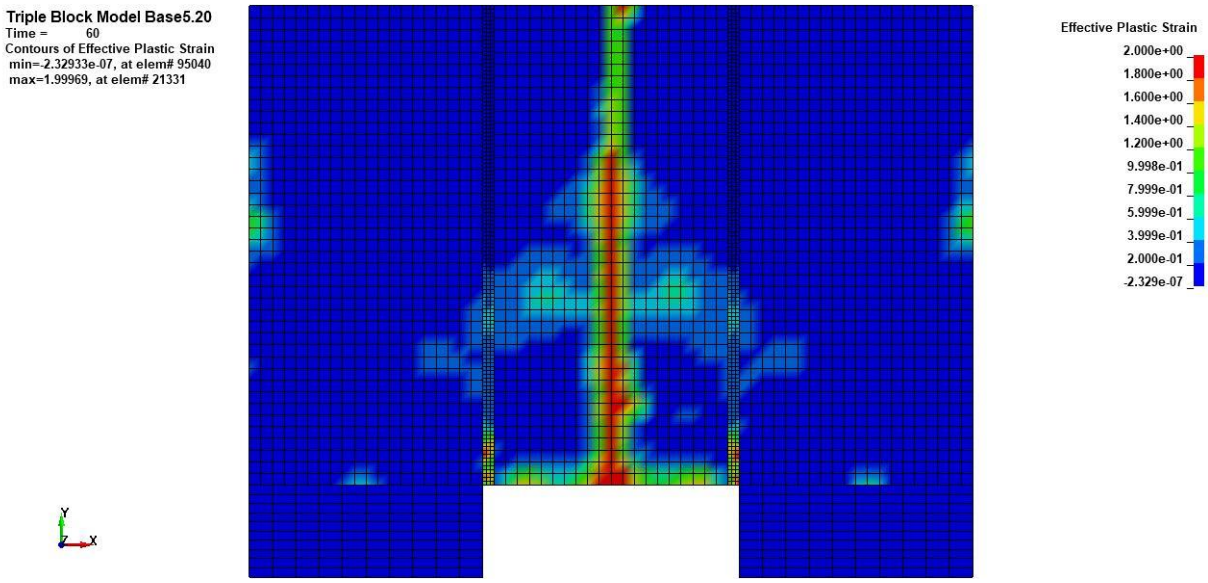


**Figure B-288: Effective Plastic Strain Fringe Plot for Last State at 60 Milliseconds for Base Run 5.20 – 1000 psi**

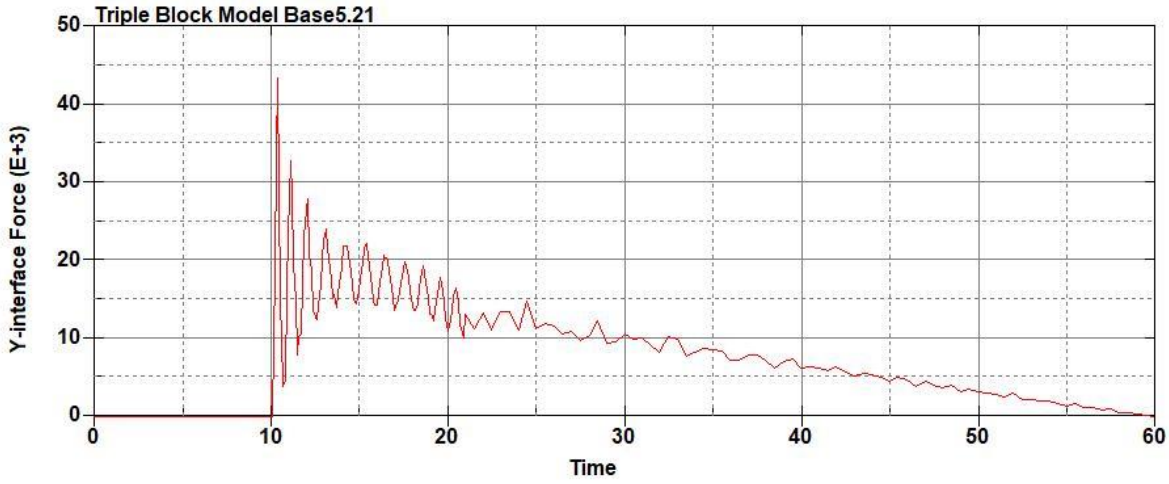


**Figure B-289: Base Run 5.21 Right Support Y-Interface Force (lbs) versus Time (ms) – 1050 psi**

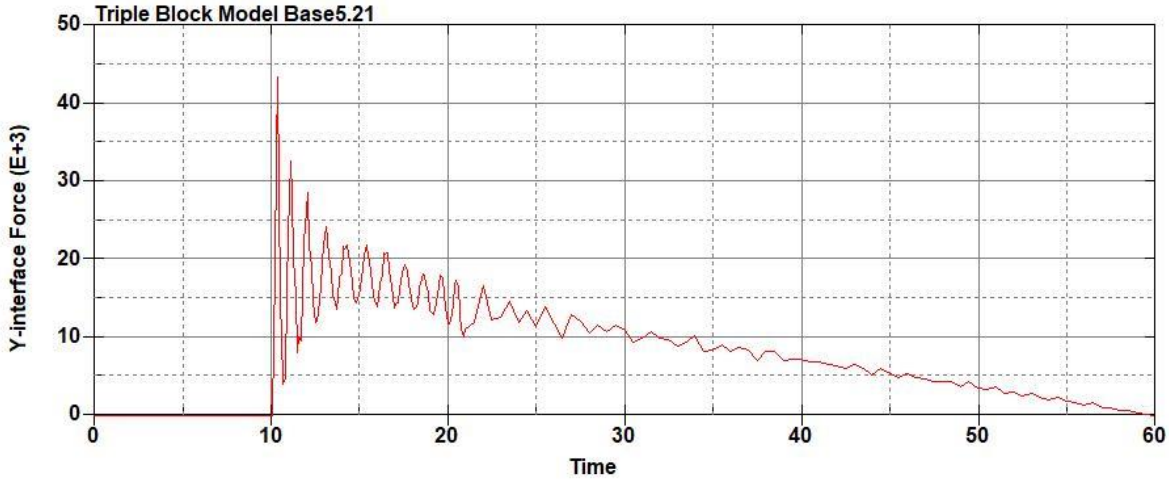


**Figure B-290: Base Run 5.21 Left Support Y-Interface Force (lbs) versus Time (ms) – 1050 psi**

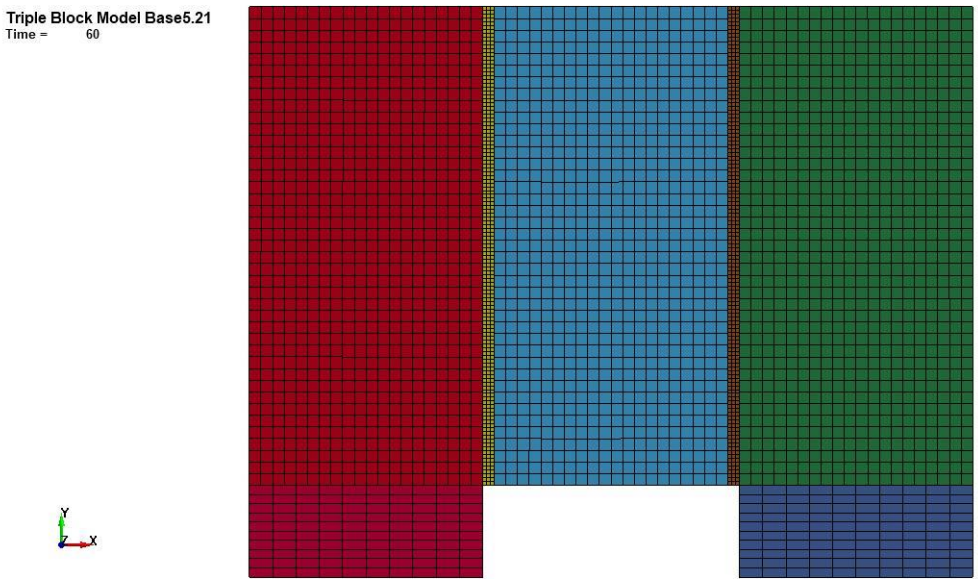


**Figure B-291: Last State at 60 Milliseconds for Base Run 5.21 – 1050 psi**

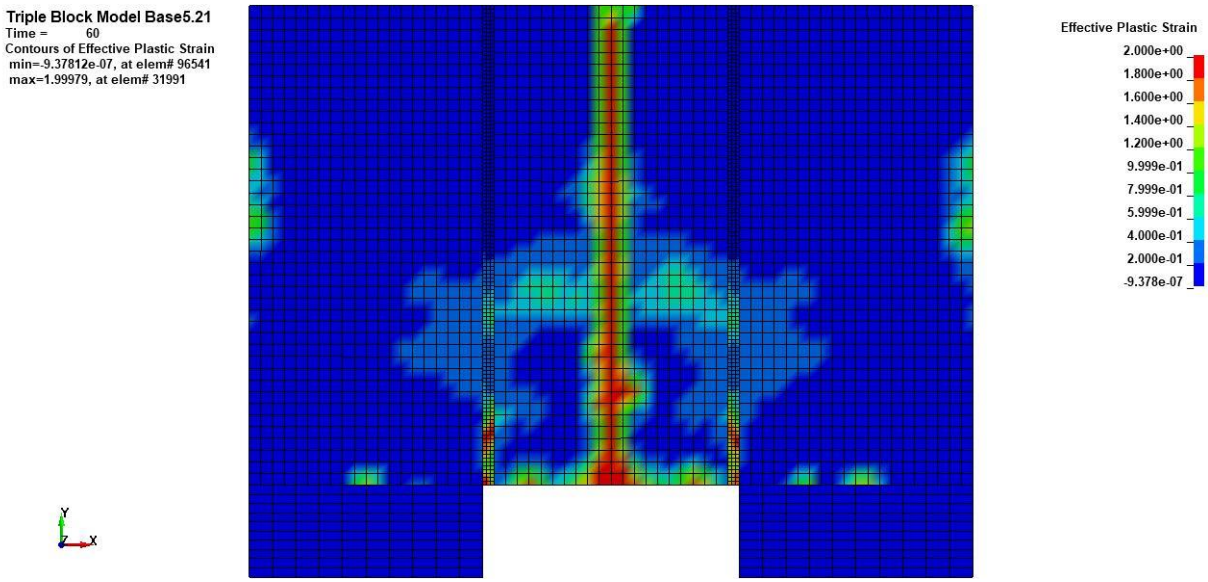


**Figure B-292: Effective Plastic Strain Fringe Plot for Last State at 60 Milliseconds for Base Run 5.21 – 1050 psi**

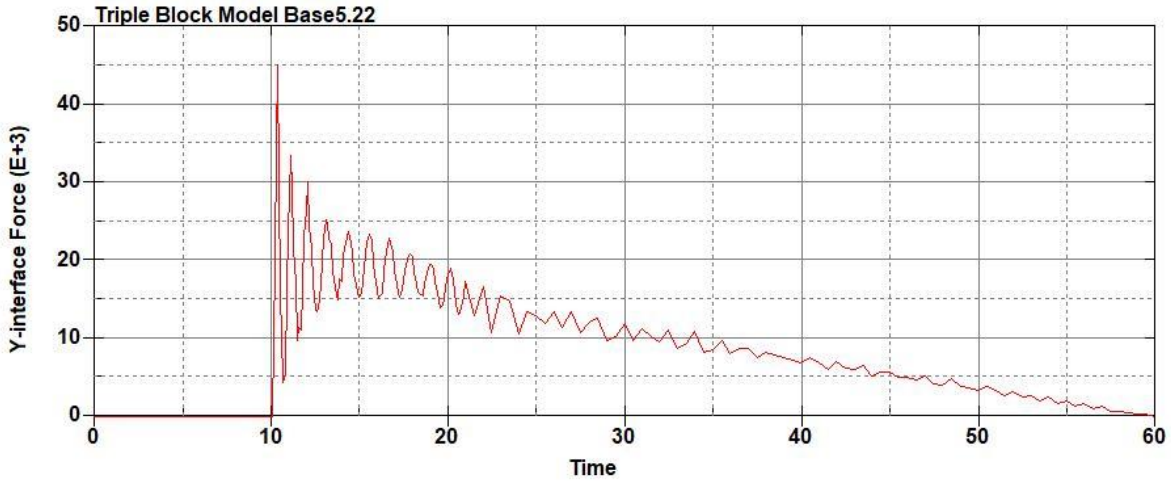


**Figure B-293: Base Run 5.22 Right Support Y-Interface Force (lbs) versus Time (ms) – 1100 psi**

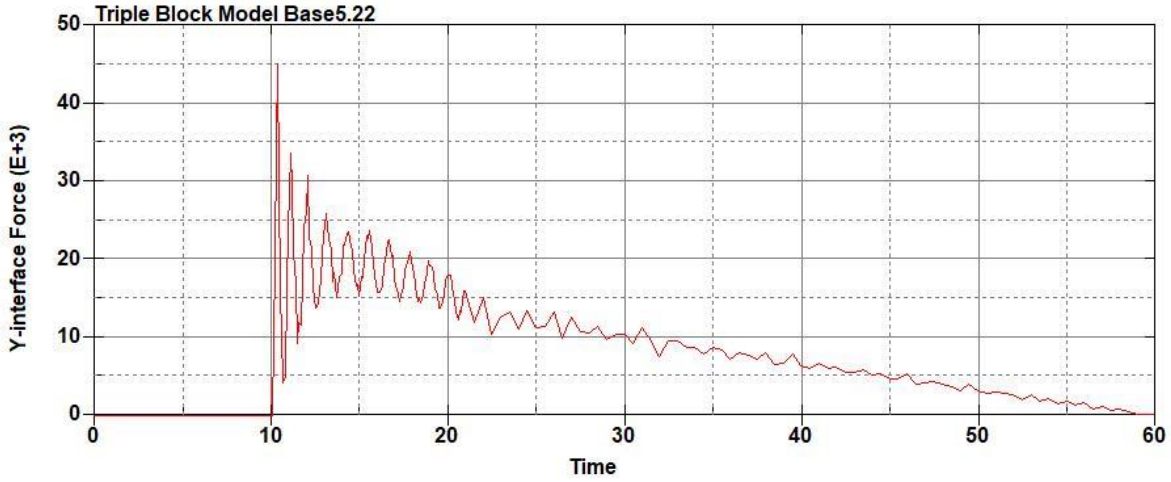


**Figure B-294: Base Run 5.22 Left Support Y-Interface Force (lbs) versus Time (ms) – 1100 psi**

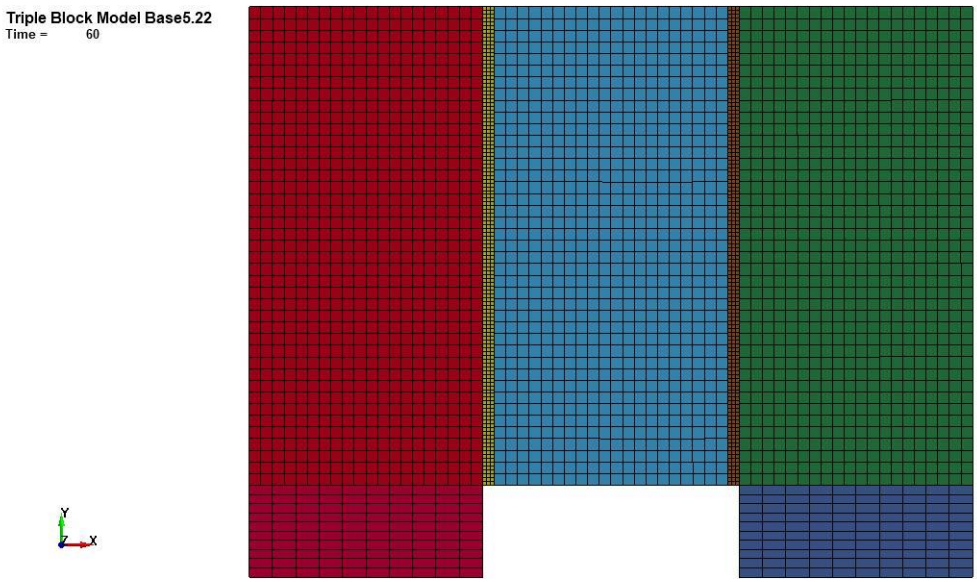


**Figure B-295: Last State at 60 Milliseconds for Base Run 5.22 – 1100 psi**

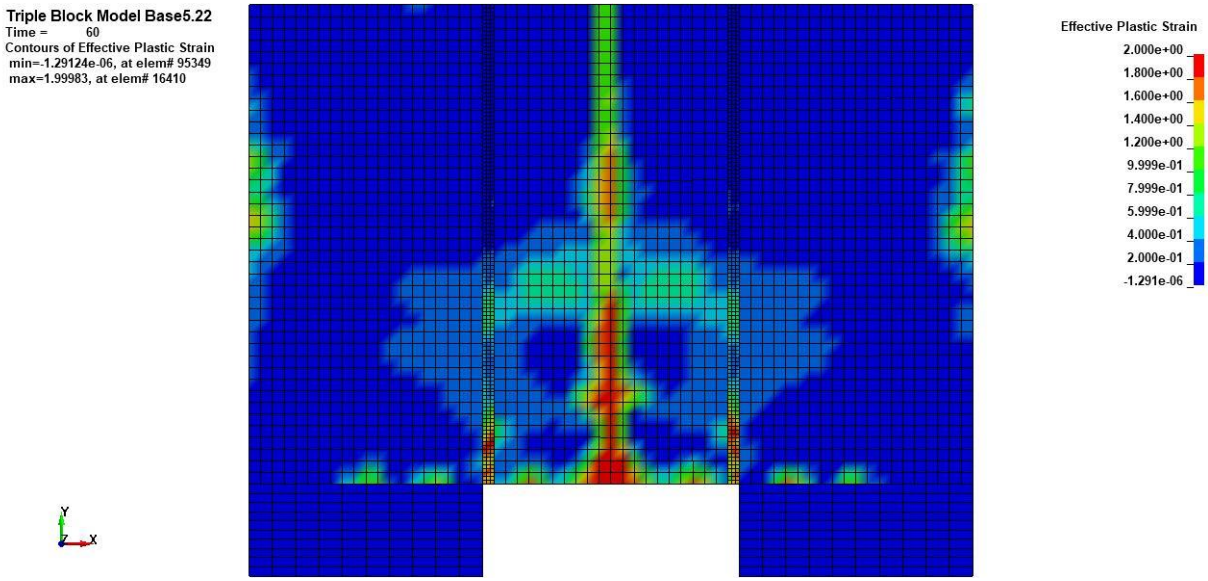


**Figure B-296: Effective Plastic Strain Fringe Plot for Last State at 60 Milliseconds for Base Run 5.22 – 1100 psi**

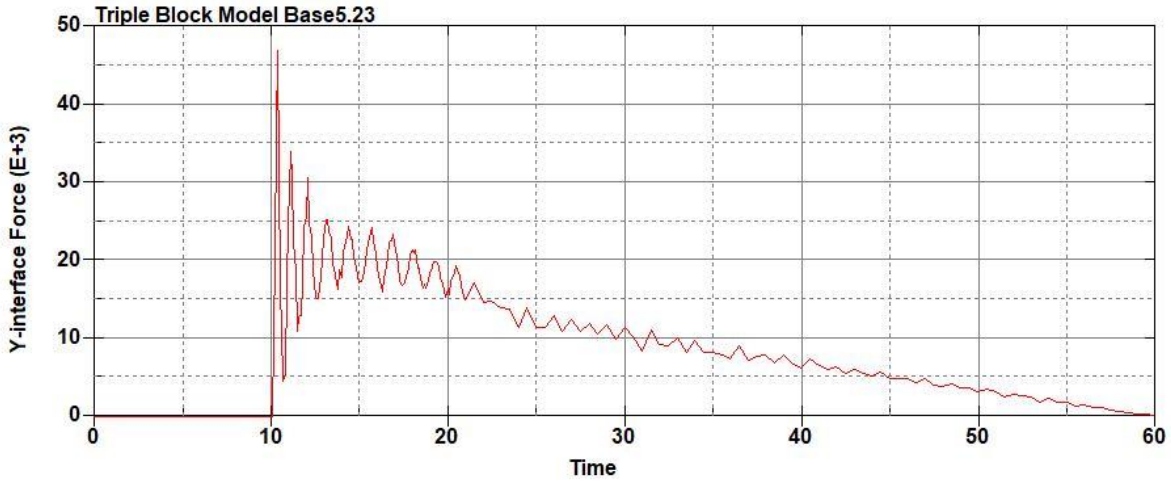


**Figure B-297: Base Run 5.23 Right Support Y-Interface Force (lbs) versus Time (ms) – 1150 psi**

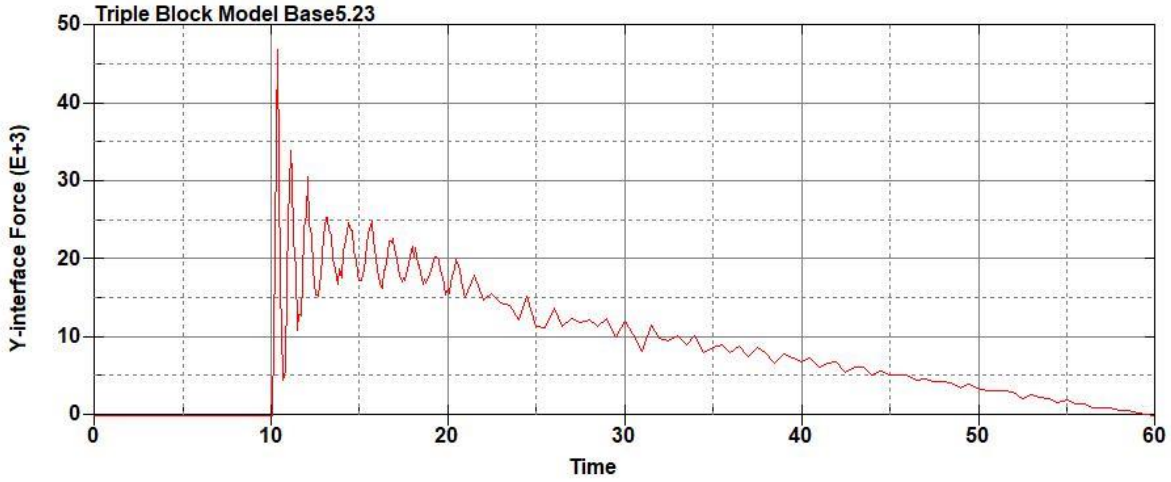


**Figure B-298: Base Run 5.23 Left Support Y-Interface Force (lbs) versus Time (ms) – 1150 psi**

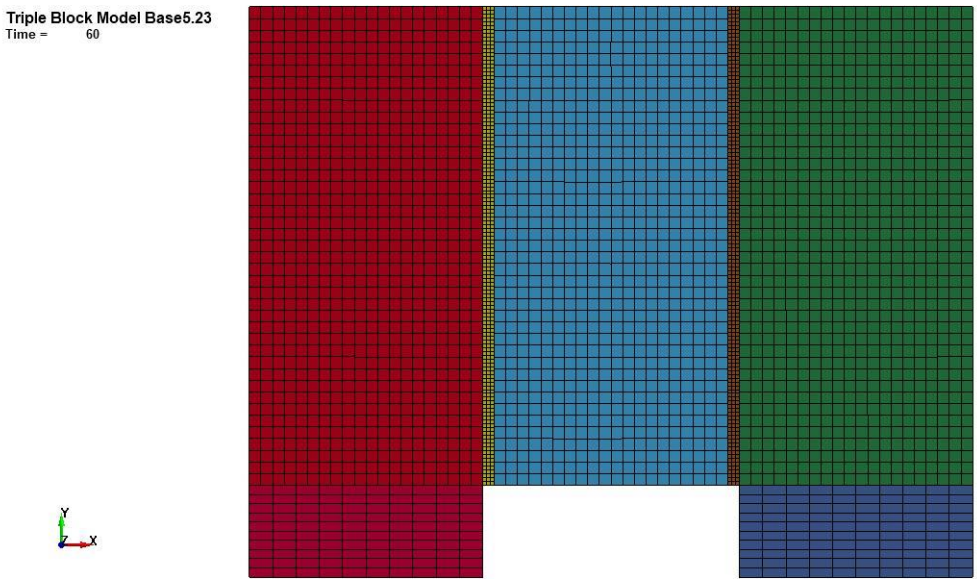


**Figure B-299: Last State at 60 Milliseconds for Base Run 5.23 – 1150 psi**

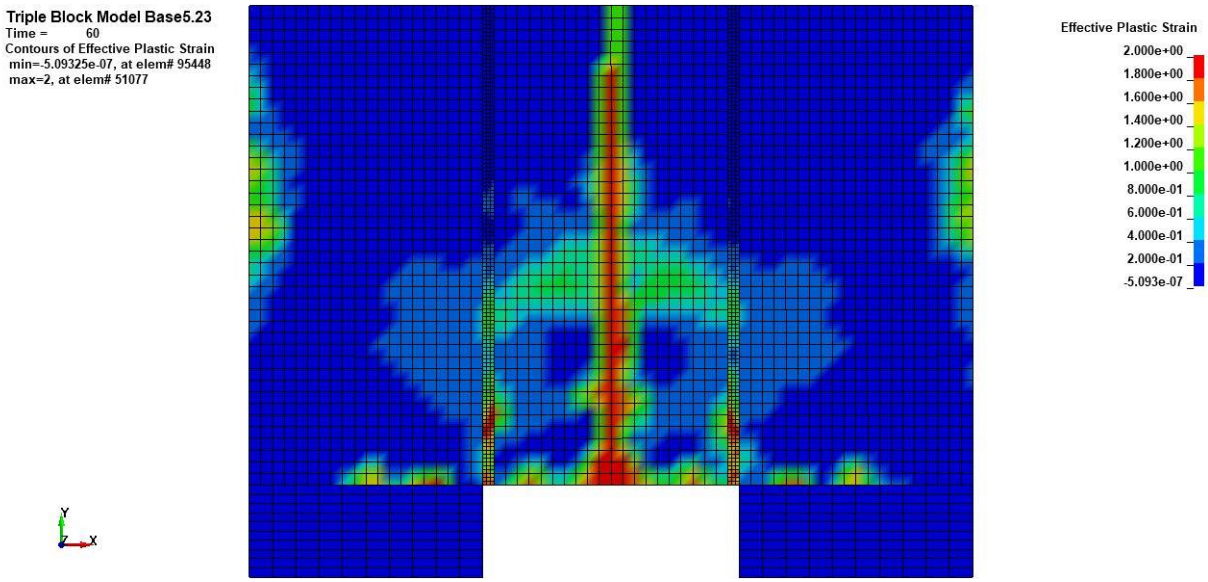


**Figure B-300: Effective Plastic Strain Fringe Plot for Last State at 60 Milliseconds for Base Run 5.23 – 1150 psi**

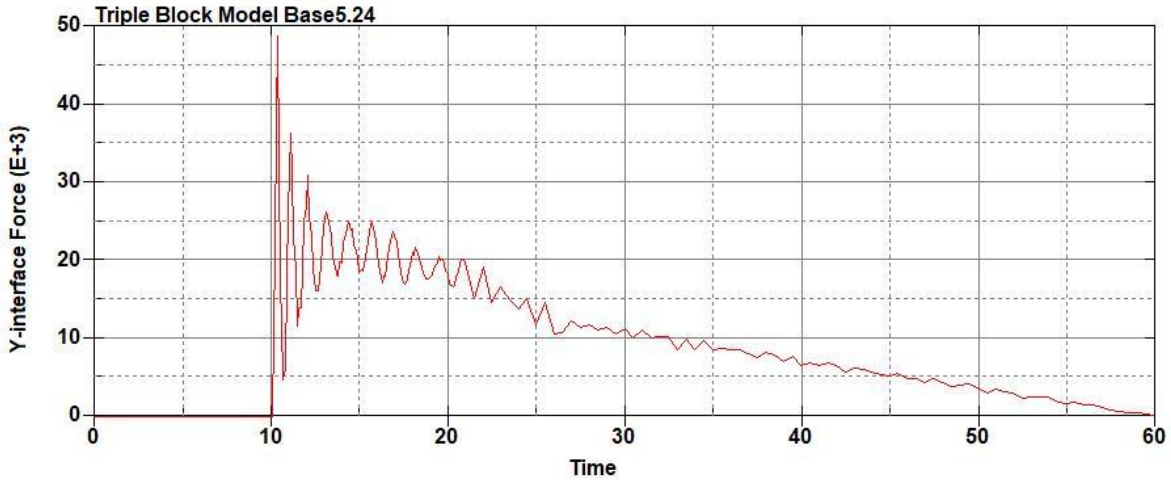


**Figure B-301: Base Run 5.24 Right Support Y-Interface Force (lbs) versus Time (ms) – 1200 psi**

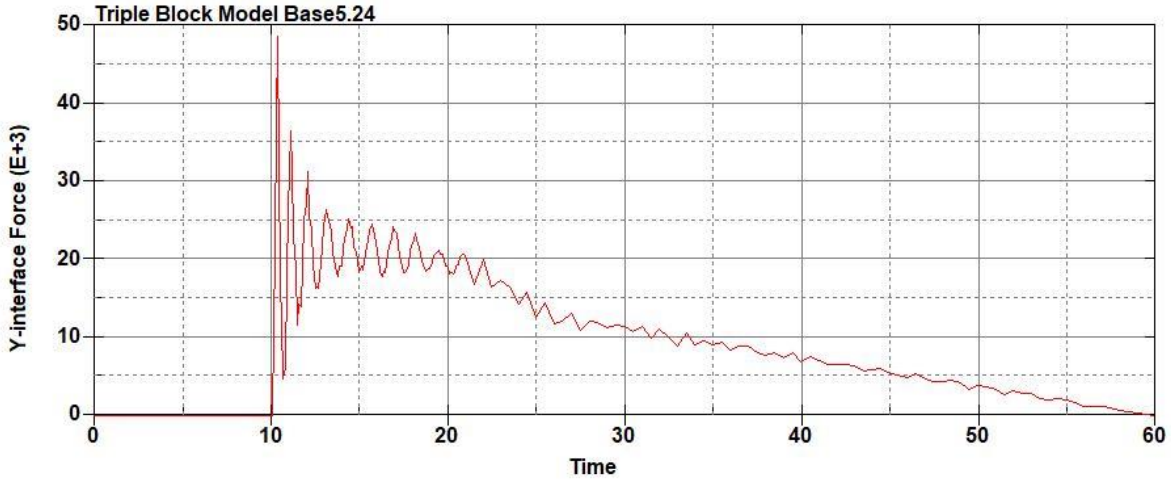


**Figure B-302: Base Run 5.24 Left Support Y-Interface Force (lbs) versus Time (ms) – 1200 psi**

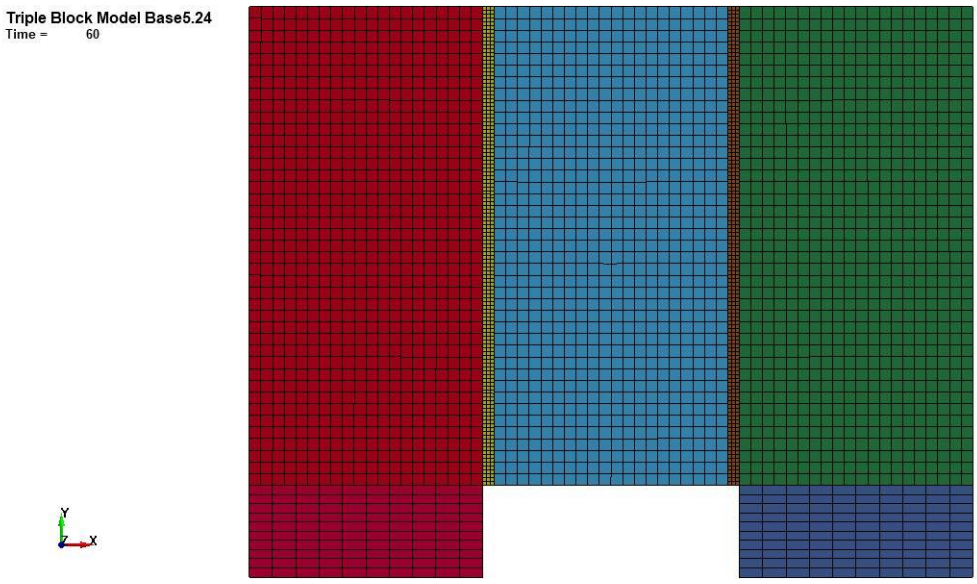


**Figure B-303: Last State at 60 Milliseconds for Base Run 5.24 – 1200 psi**

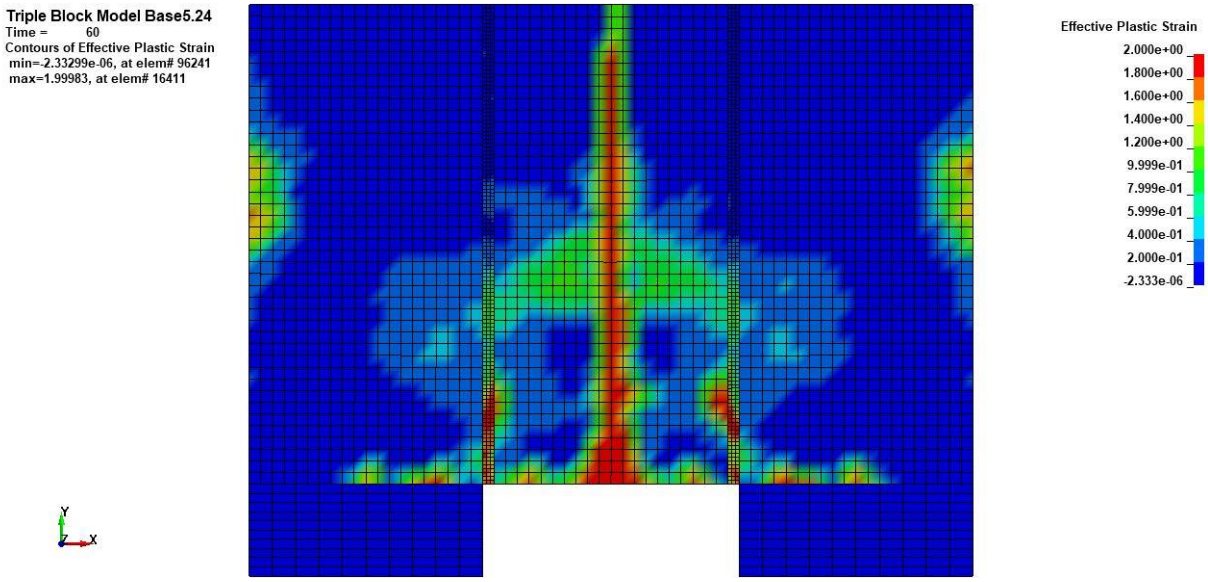


**Figure B-304: Effective Plastic Strain Fringe Plot for Last State at 60 Milliseconds for Base Run 5.24 – 1200 psi**

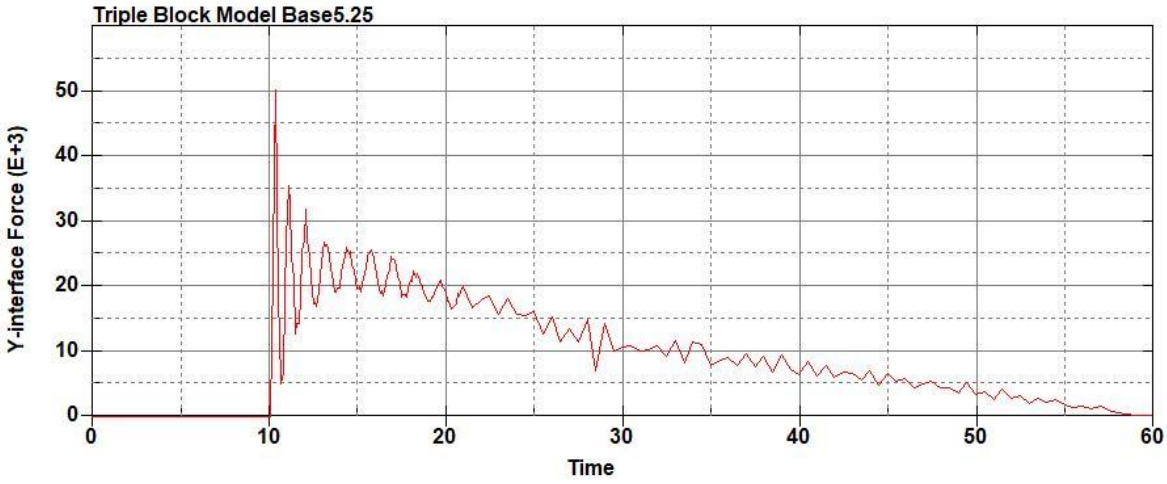


**Figure B-305: Base Run 5.25 Right Support Y-Interface Force (lbs) versus Time (ms) – 1250 psi**

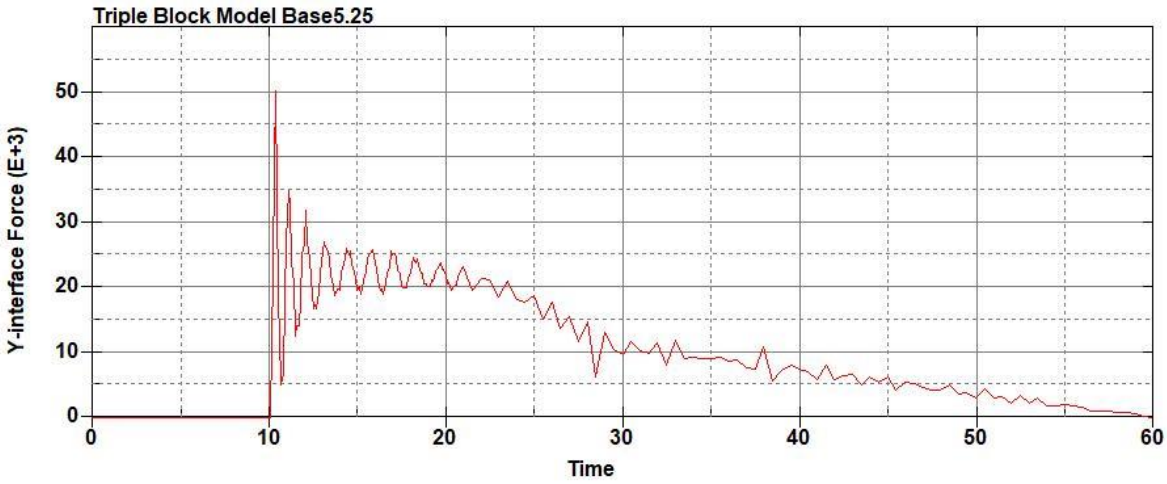


**Figure B-306: Base Run 5.25 Left Support Y-Interface Force (lbs) versus Time (ms) – 1250 psi**

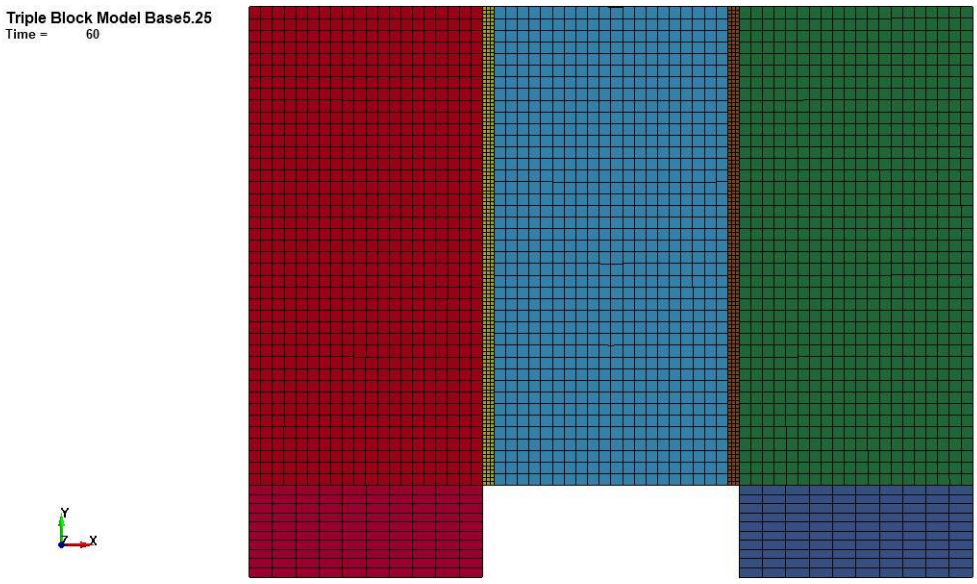


**Figure B-307: Last State at 60 Milliseconds for Base Run 5.25 – 1250 psi**

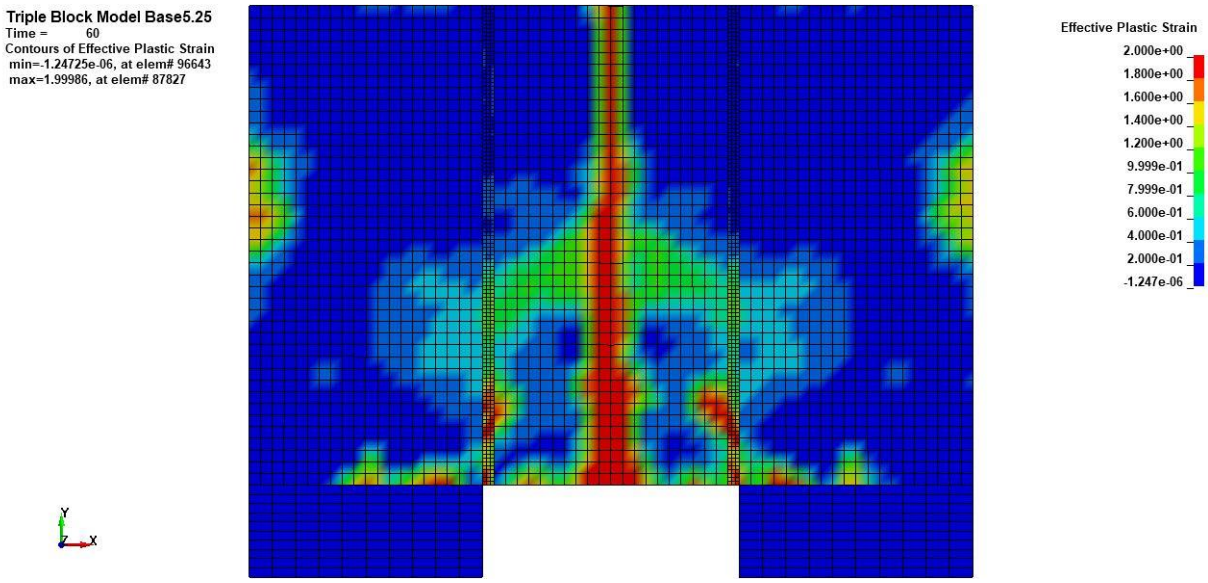


**Figure B-308: Effective Plastic Strain Fringe Plot for Last State at 60 Milliseconds for Base Run 5.25 – 1250 psi**

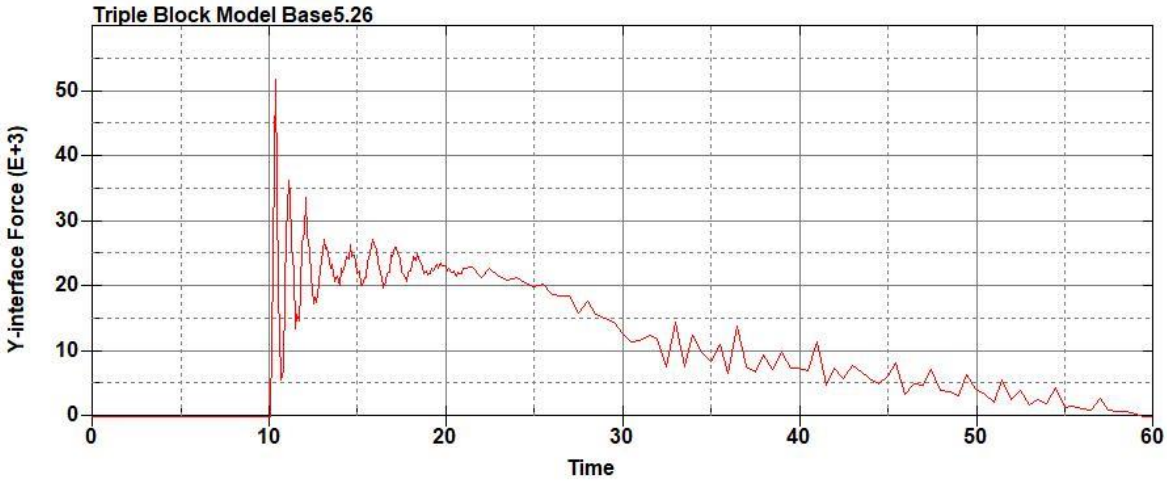


**Figure B-309: Base Run 5.26 Right Support Y-Interface Force (lbs) versus Time (ms) – 1300 psi**

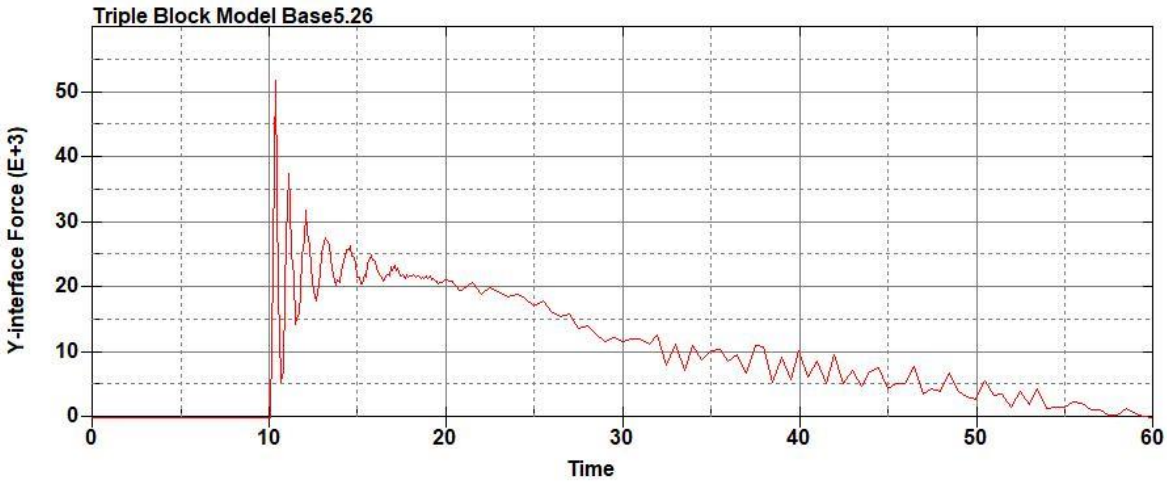


**Figure B-310: Base Run 5.26 Left Support Y-Interface Force (lbs) versus Time (ms) – 1300 psi**

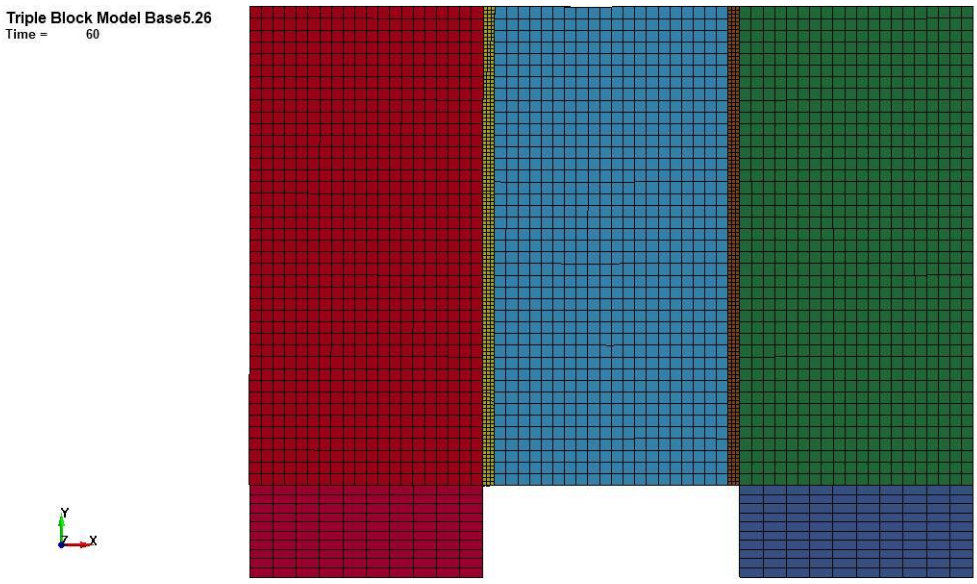


**Figure B-311: Last State at 60 Milliseconds for Base Run 5.26 – 1300 psi**

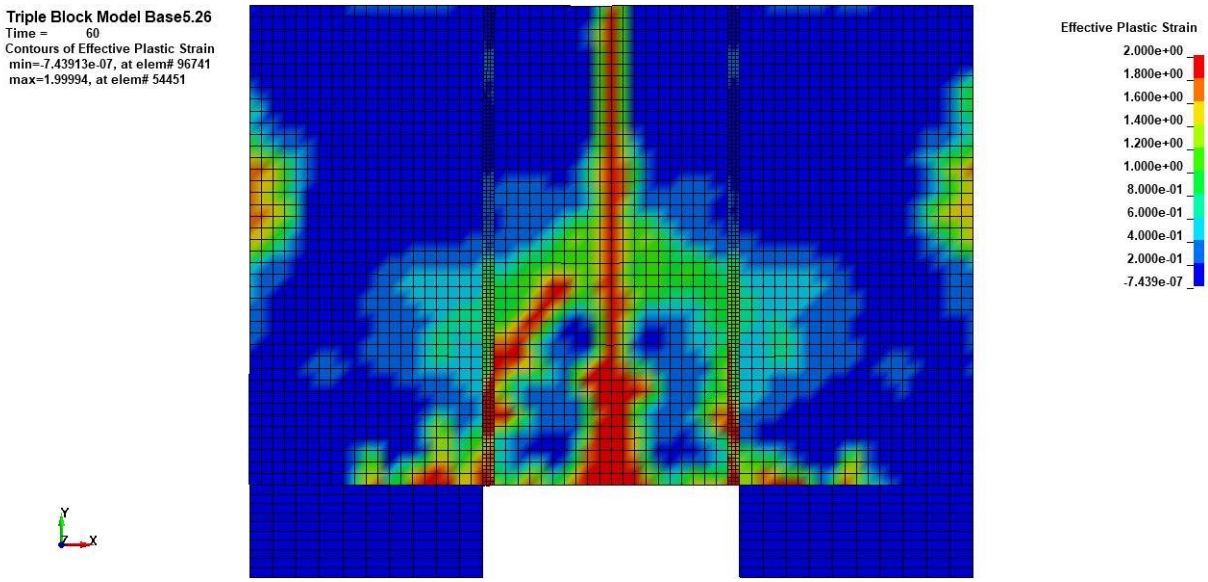


**Figure B-312: Effective Plastic Strain Fringe Plot for Last State at 60 Milliseconds for Base Run 5.26 – 1300 psi**

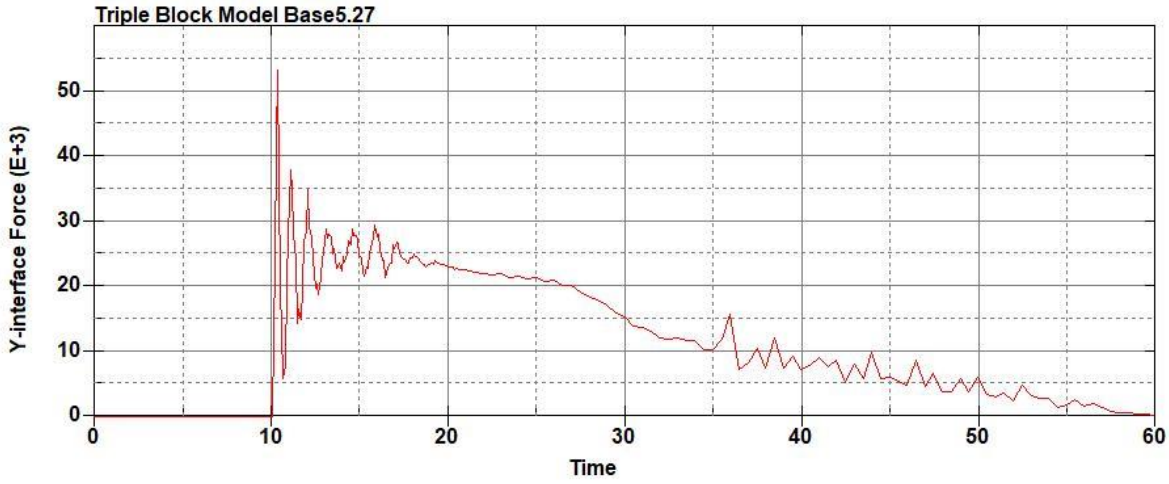


**Figure B-313: Base Run 5.27 Right Support Y-Interface Force (lbs) versus Time (ms) – 1350 psi**

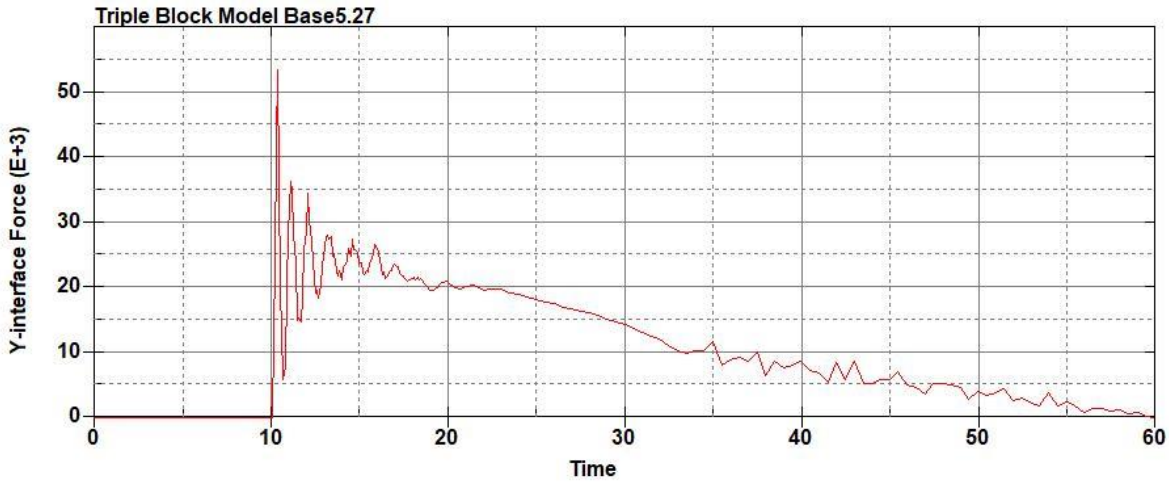


**Figure B-314: Base Run 5.27 Left Support Y-Interface Force (lbs) versus Time (ms) – 1350 psi**

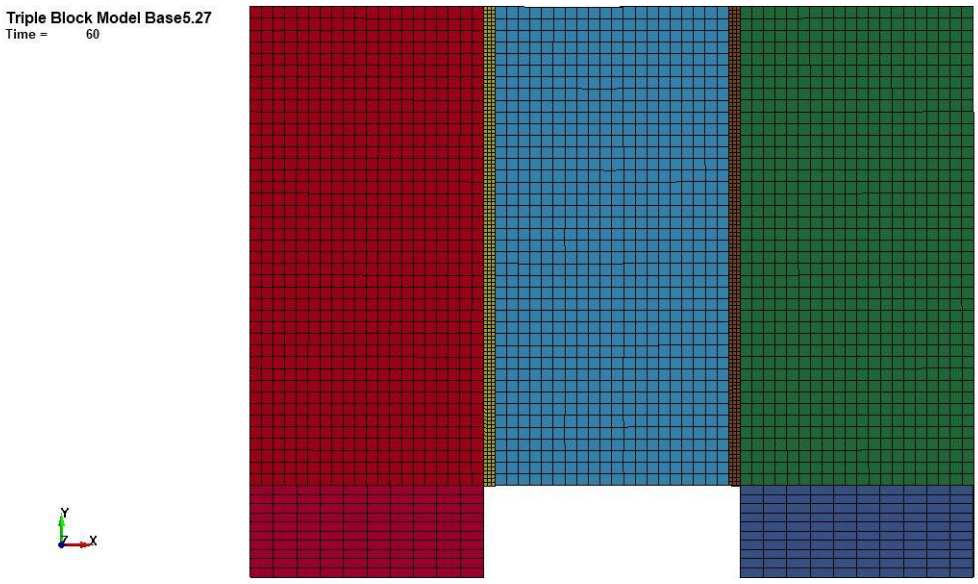


**Figure B-315: Last State at 60 Milliseconds for Base Run 5.27 – 1350 psi**

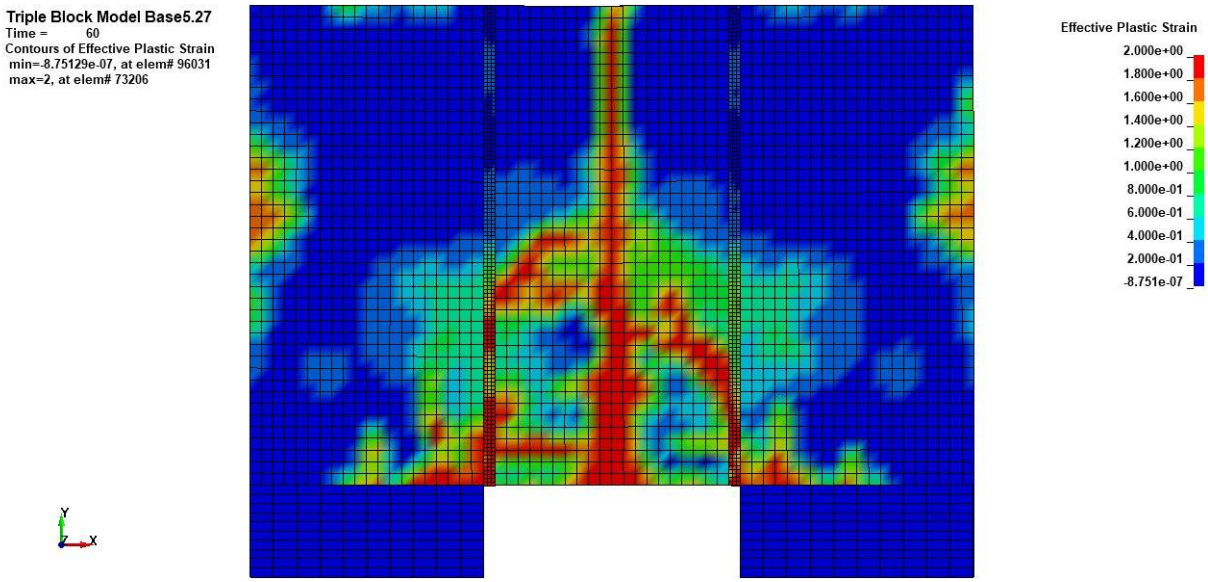


**Figure B-316: Effective Plastic Strain Fringe Plot for Last State at 60 Milliseconds for Base Run 5.27 – 1350 psi**

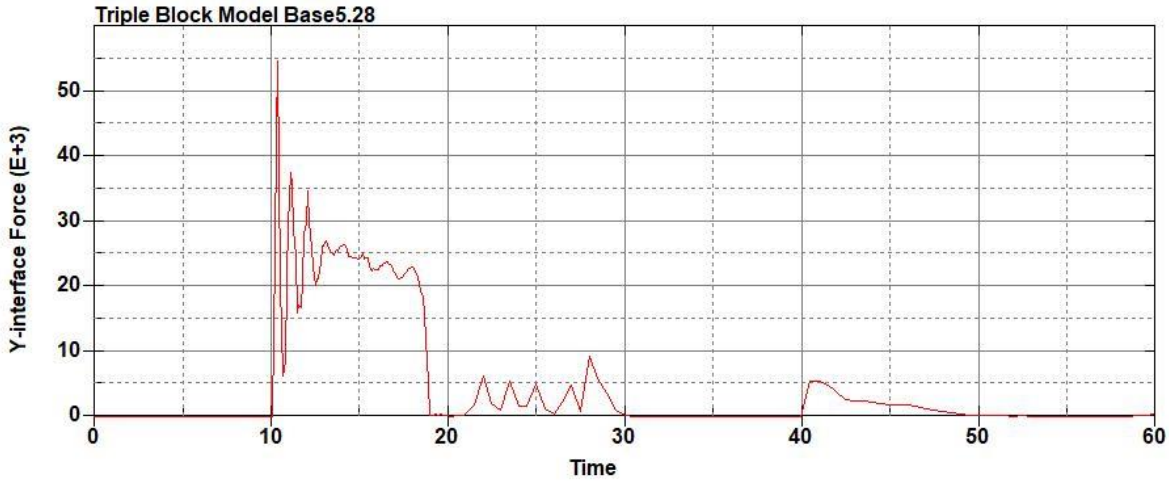


**Figure B-317: Base Run 5.28 Right Support Y-Interface Force (lbs) versus Time (ms) – 1400 psi**

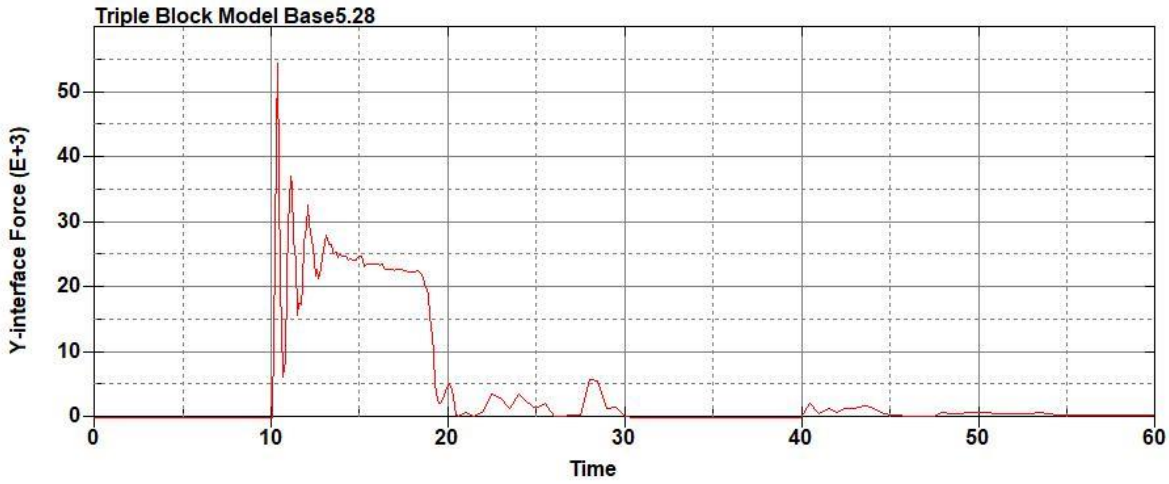


**Figure B-318: Base Run 5.28 Left Support Y-Interface Force (lbs) versus Time (ms) – 1400 psi**

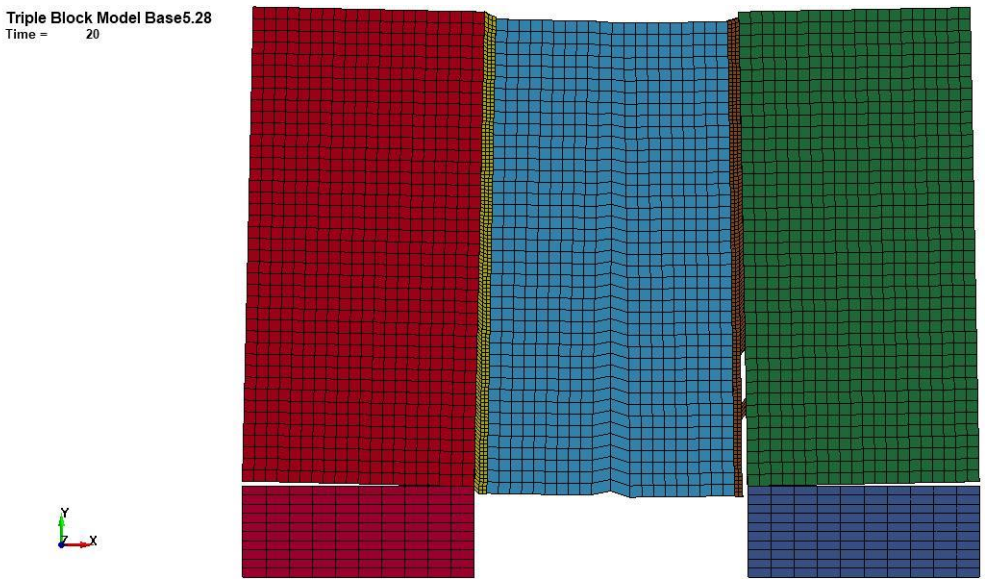


**Figure B-319: Last State at 20 Milliseconds for Base Run 5.28 – 1400 psi**

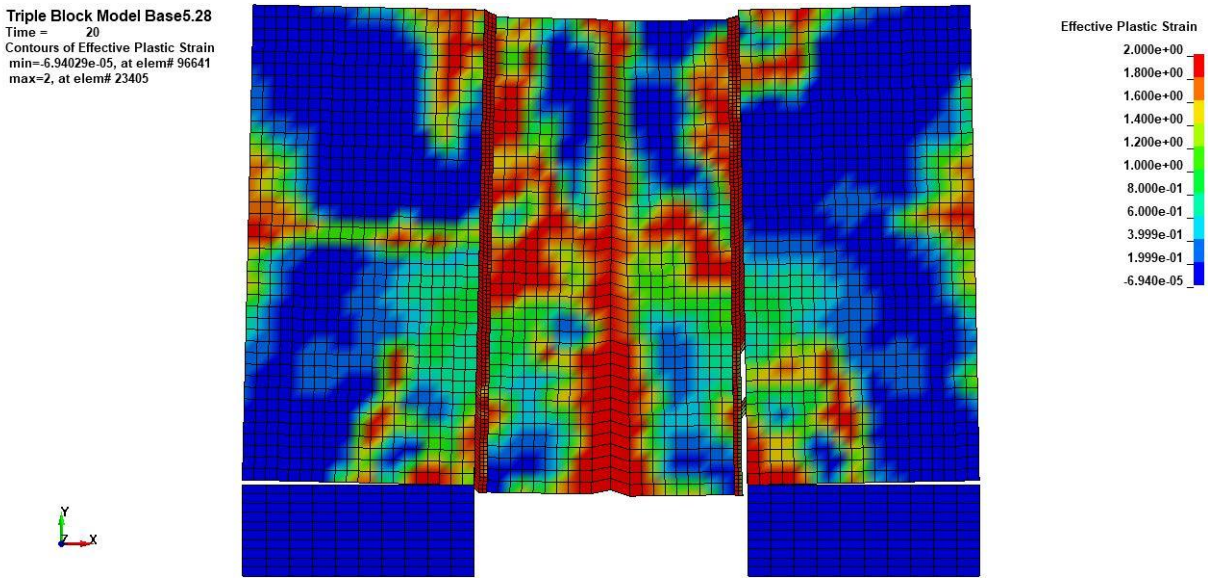


**Figure B-320: Effective Plastic Strain Fringe Plot for Last State at 20 Milliseconds for Base Run 5.28 – 1400 psi**

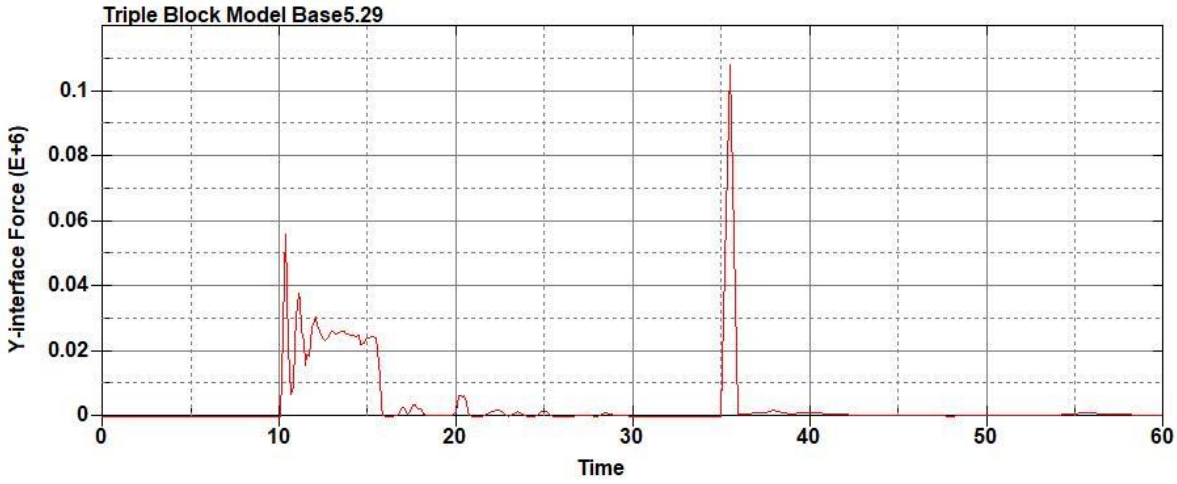


**Figure B-321: Base Run 5.29 Right Support Y-Interface Force (lbs) versus Time (ms) – 1450 psi**

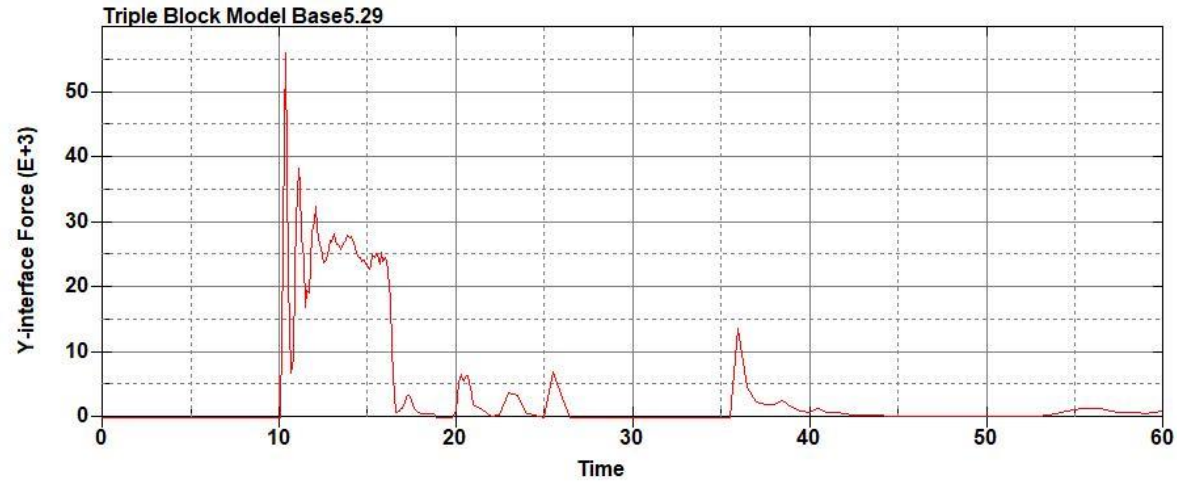


**Figure B-322: Base Run 5.29 Left Support Y-Interface Force (lbs) versus Time (ms) – 1450 psi**

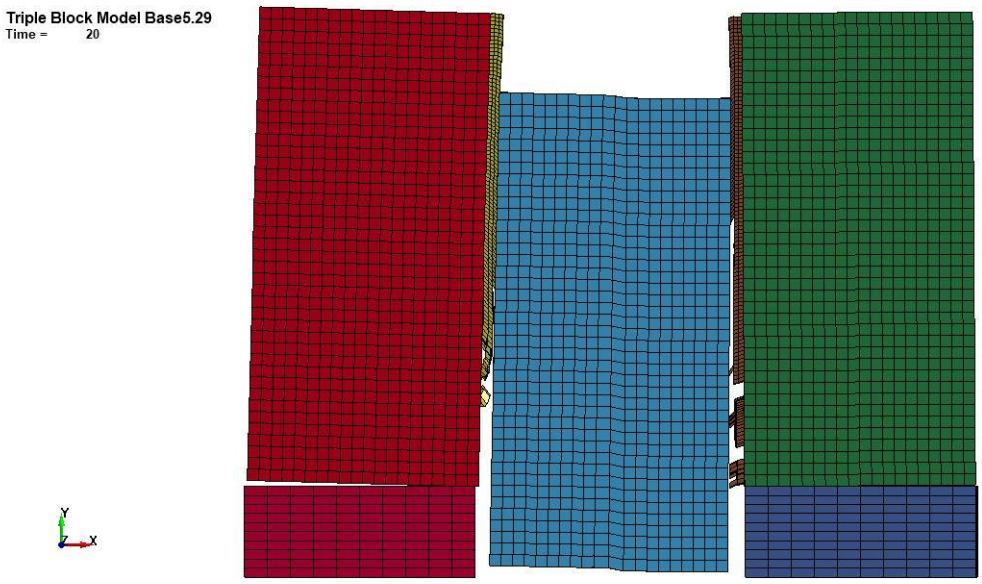


**Figure B-323: Last State at 20 Milliseconds for Base Run 5.29 – 1450 psi**

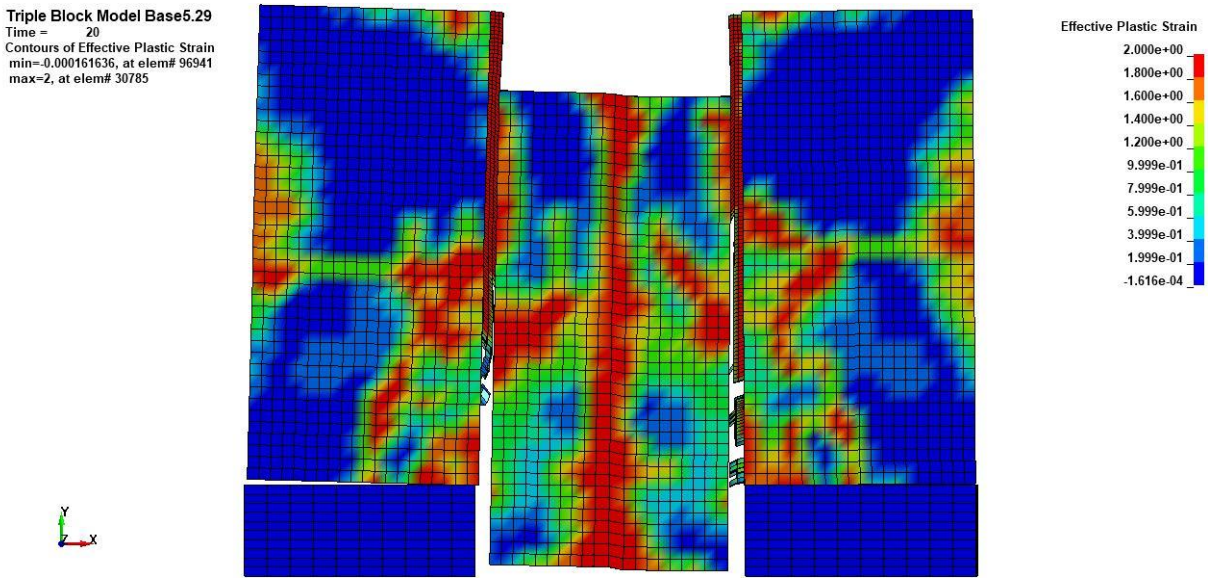


**Figure B-324: Effective Plastic Strain Fringe Plot for Last State at 20 Milliseconds for Base Run 5.29 – 1450 psi**

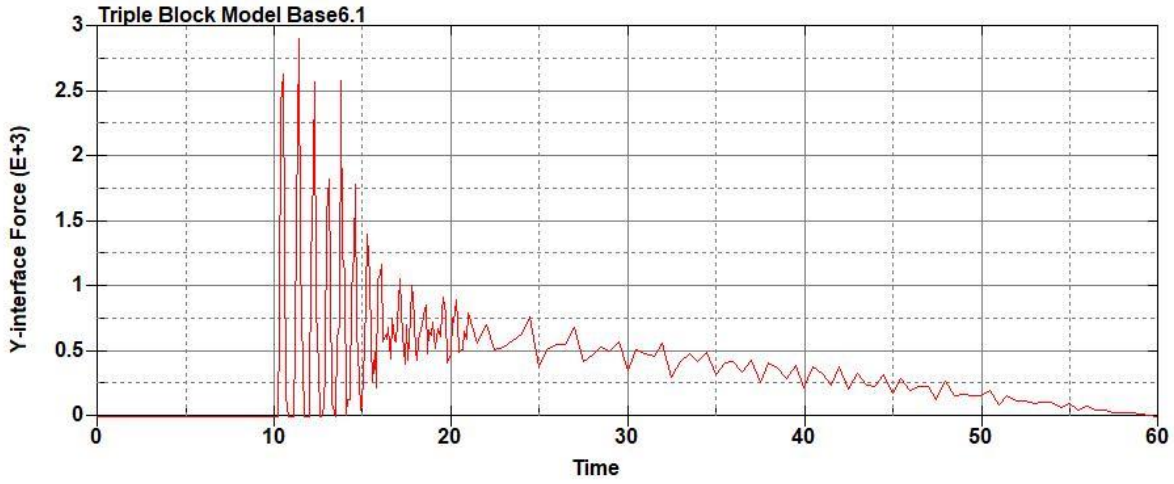


**Figure B-325: Base Run 6.1 Right Support Y-Interface Force (lbs) versus Time (ms) – 50 psi**

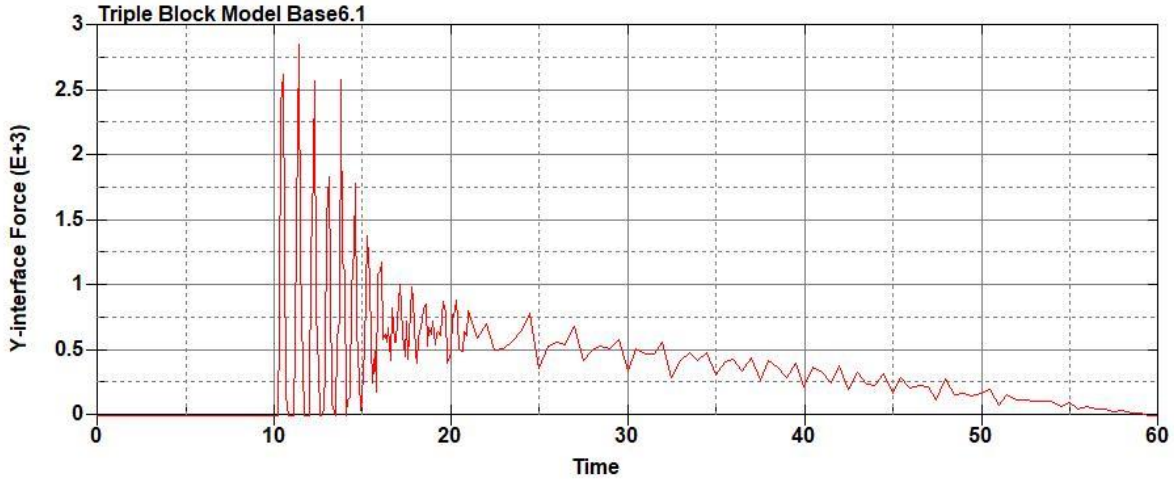


**Figure B-326: Base Run 6.1 Left Support Y-Interface Force (lbs) versus Time (ms) – 50 psi**

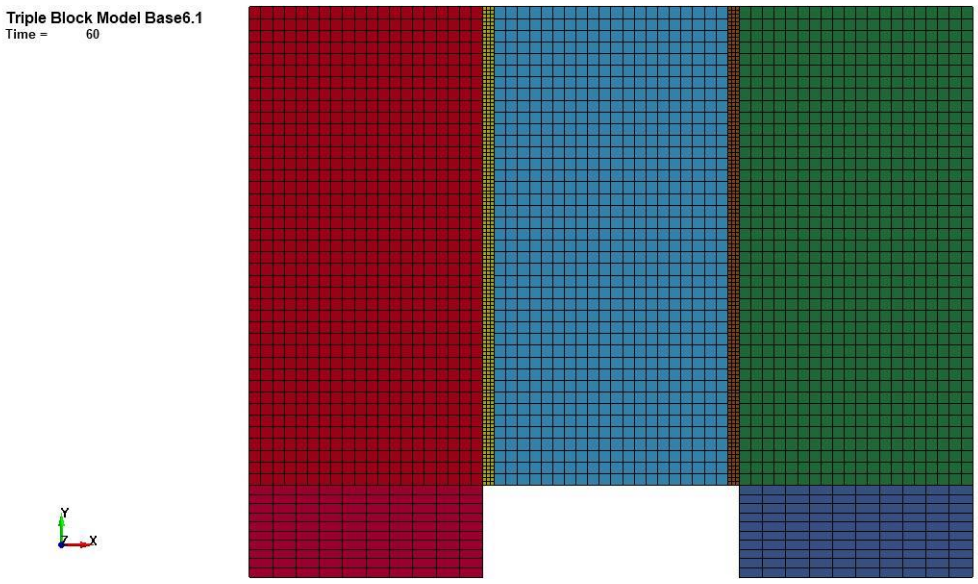


**Figure B-327: Last State at 60 Milliseconds for Base Run 6.1 – 50 psi**

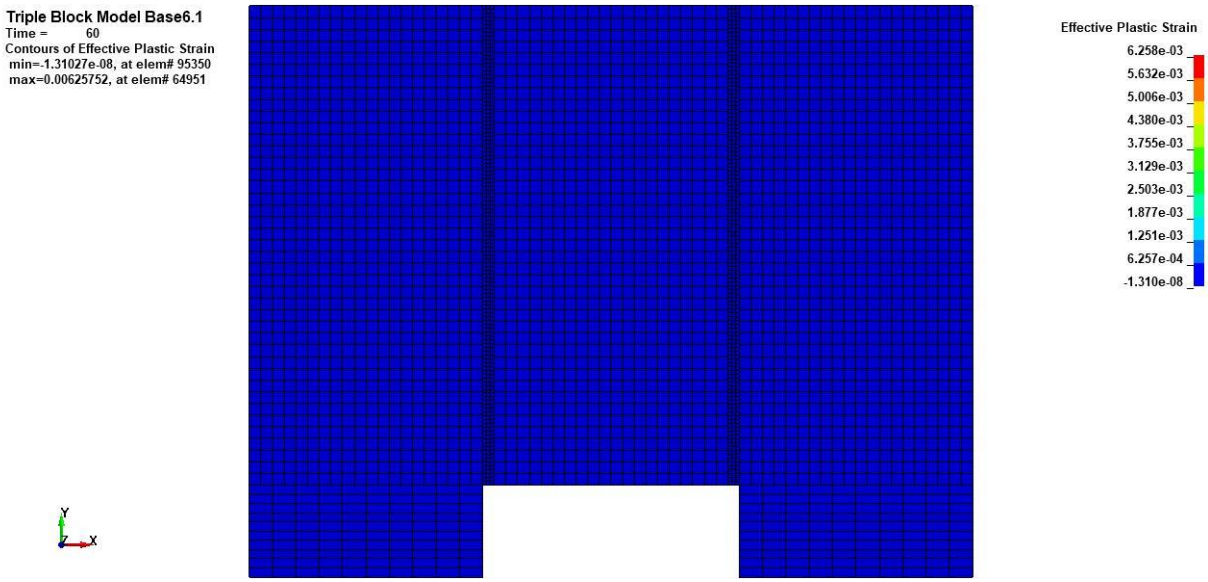


**Figure B-328: Effective Plastic Strain Fringe Plot for Last State at 60 Milliseconds for Base Run 6.1 – 50 psi**

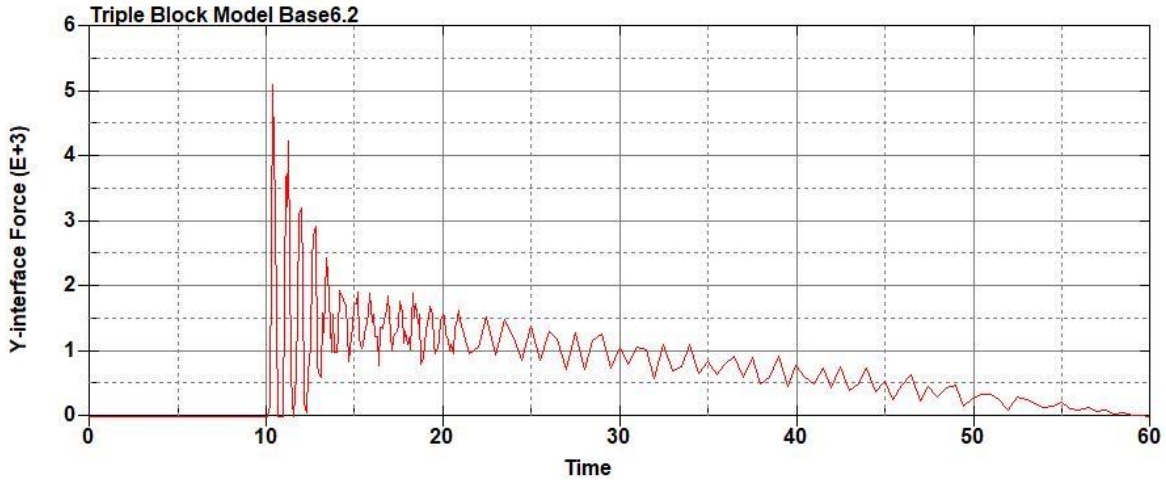


**Figure B-329: Base Run 6.2 Right Support Y-Interface Force (lbs) versus Time (ms) – 100 psi**

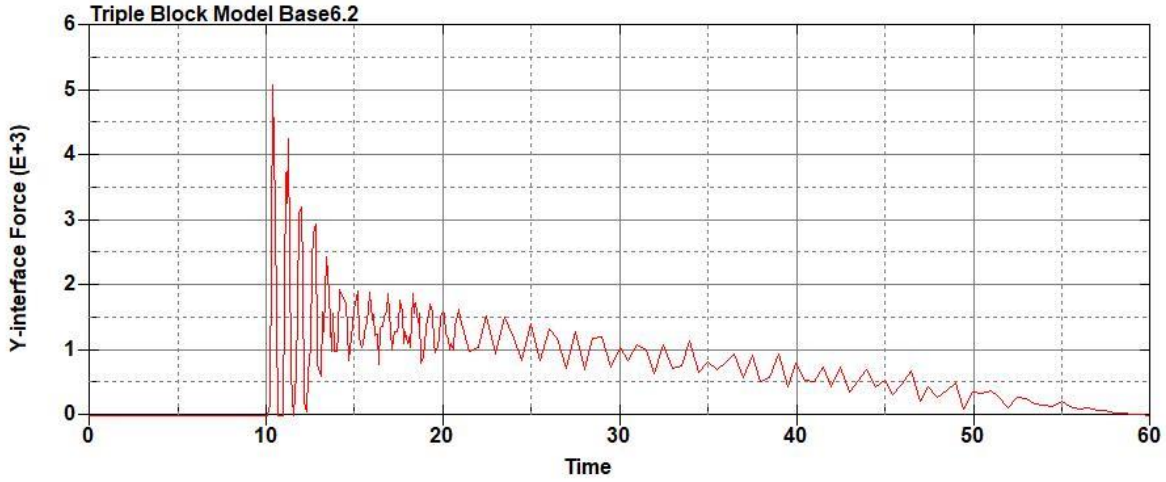


**Figure B-330: Base Run 6.2 Left Support Y-Interface Force (lbs) versus Time (ms) – 100 psi**

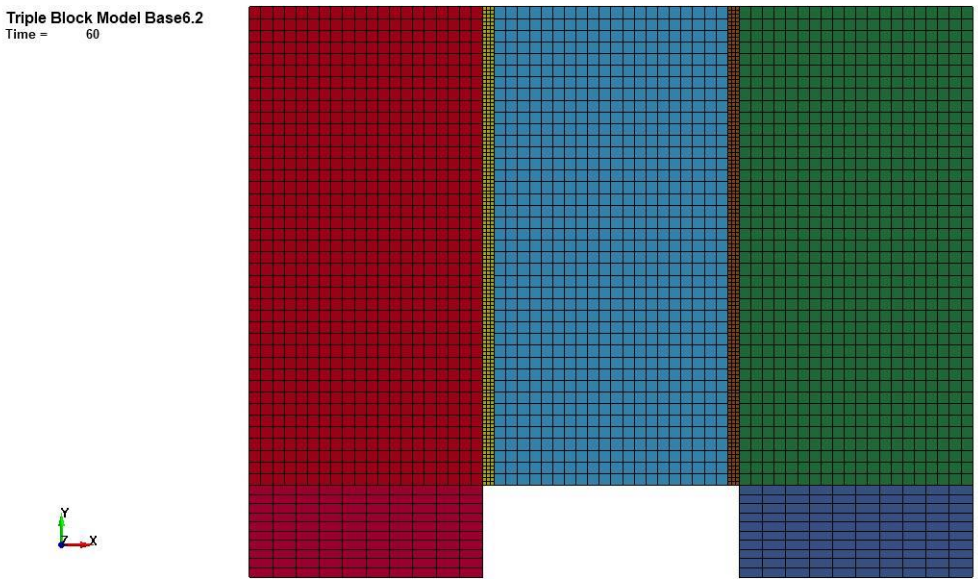


**Figure B-331: Last State at 60 Milliseconds for Base Run 6.2 – 100 psi**

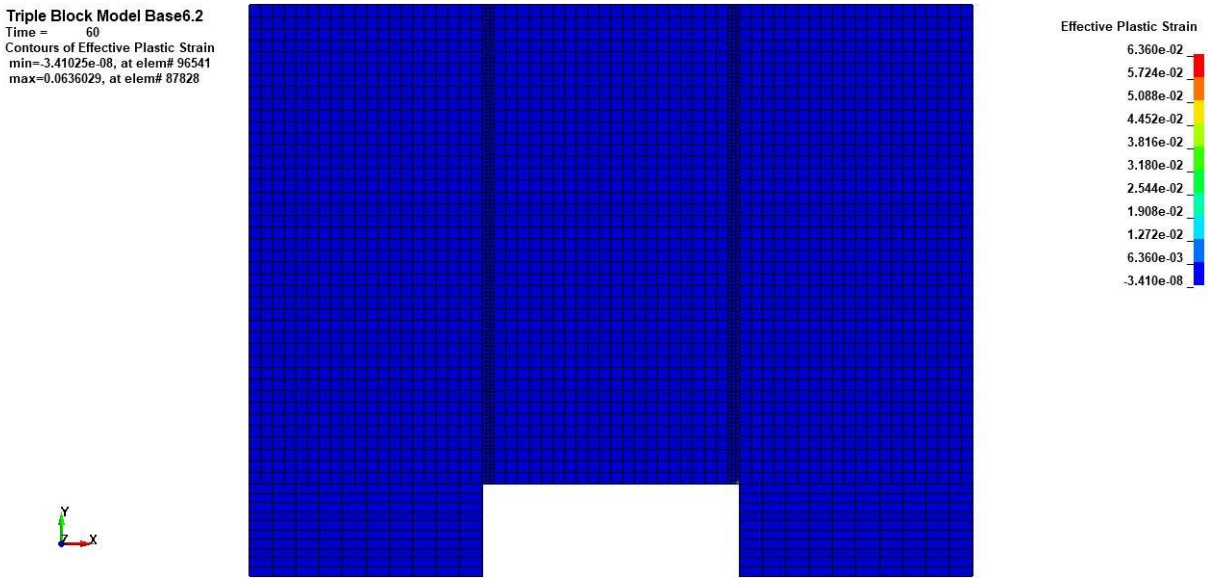


**Figure B-332: Effective Plastic Strain Fringe Plot for Last State at 60 Milliseconds for Base Run 6.2 – 100 psi**

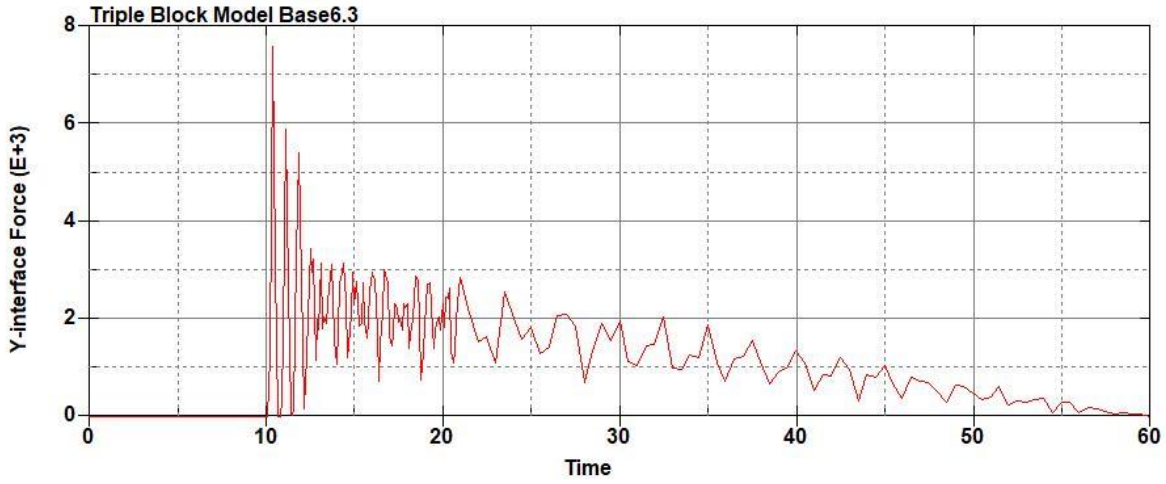


**Figure B-333: Base Run 6.3 Right Support Y-Interface Force (lbs) versus Time (ms) – 150 psi**

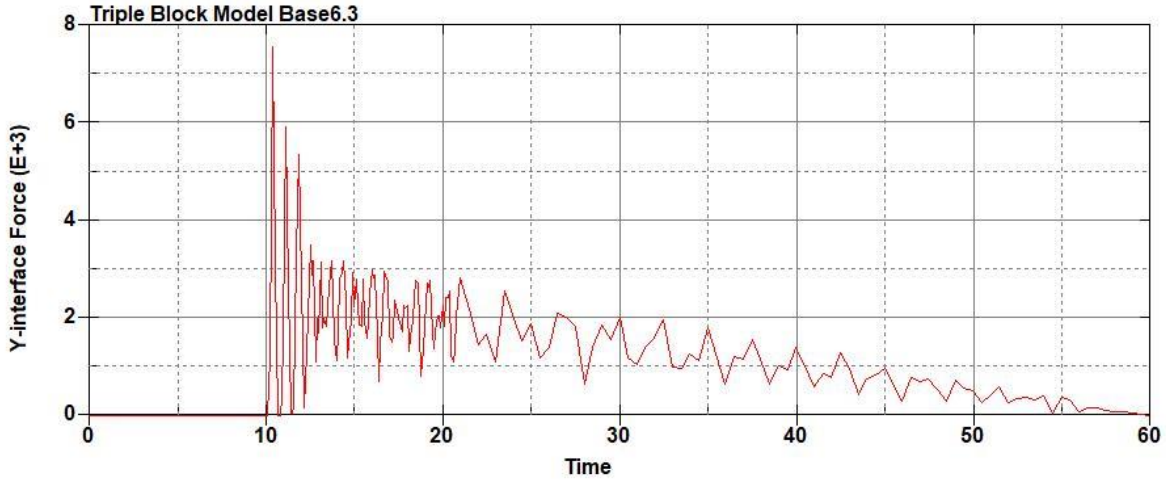


**Figure B-334: Base Run 6.3 Left Support Y-Interface Force (lbs) versus Time (ms) – 150 psi**

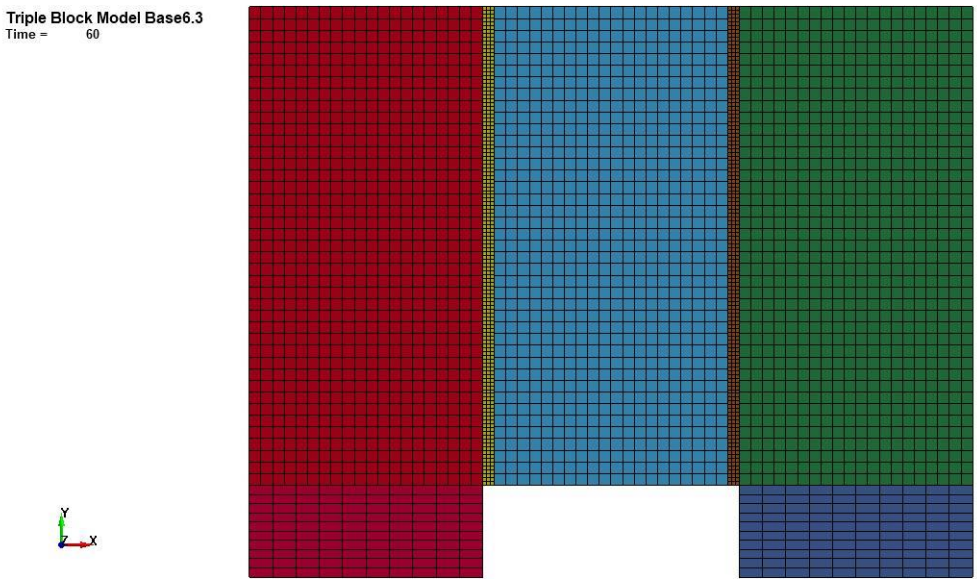


**Figure B-335: Last State at 60 Milliseconds for Base Run 6.3 – 150 psi**

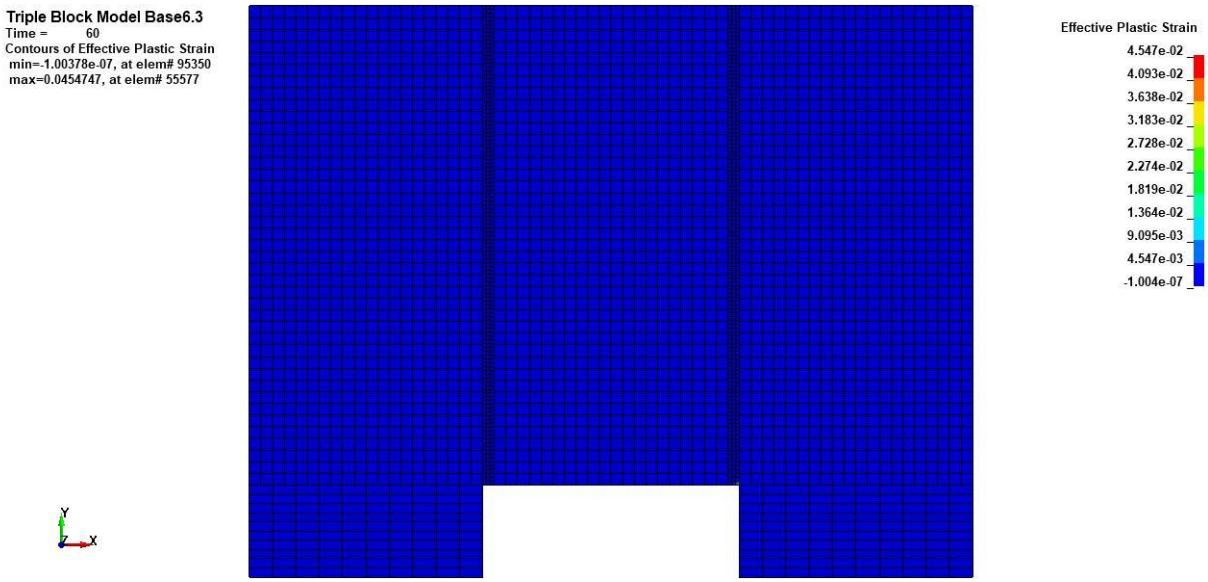


**Figure B-336: Effective Plastic Strain Fringe Plot for Last State at 60 Milliseconds for Base Run 6.3 – 150 psi**

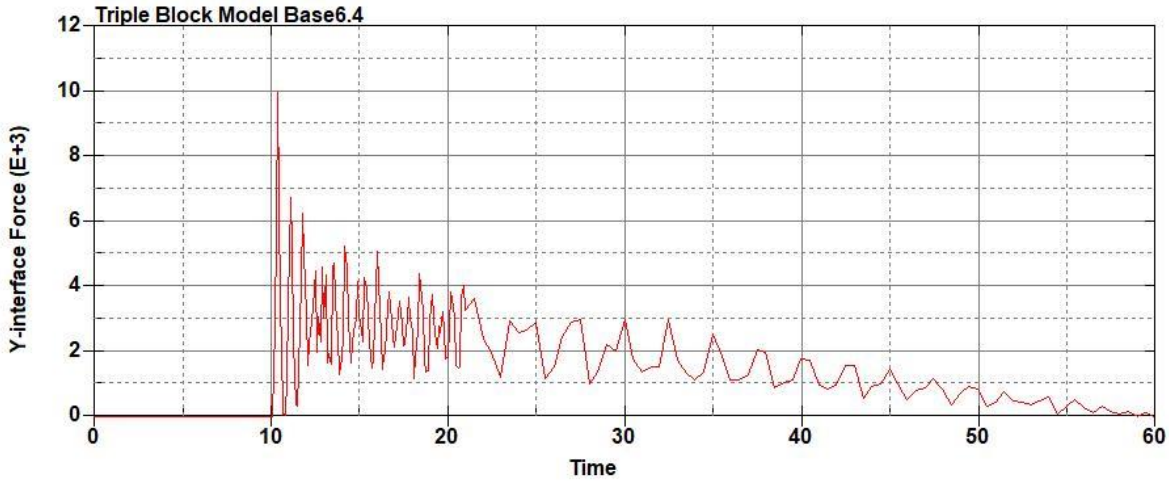


**Figure B-337: Base Run 6.4 Right Support Y-Interface Force (lbs) versus Time (ms) – 200 psi**

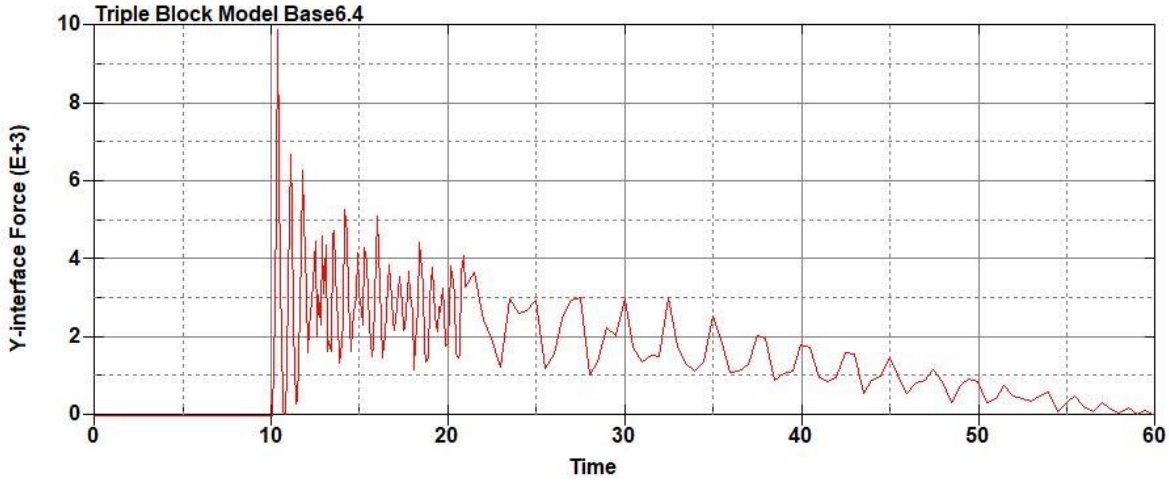


**Figure B-338: Base Run 6.4 Left Support Y-Interface Force (lbs) versus Time (ms) – 200 psi**

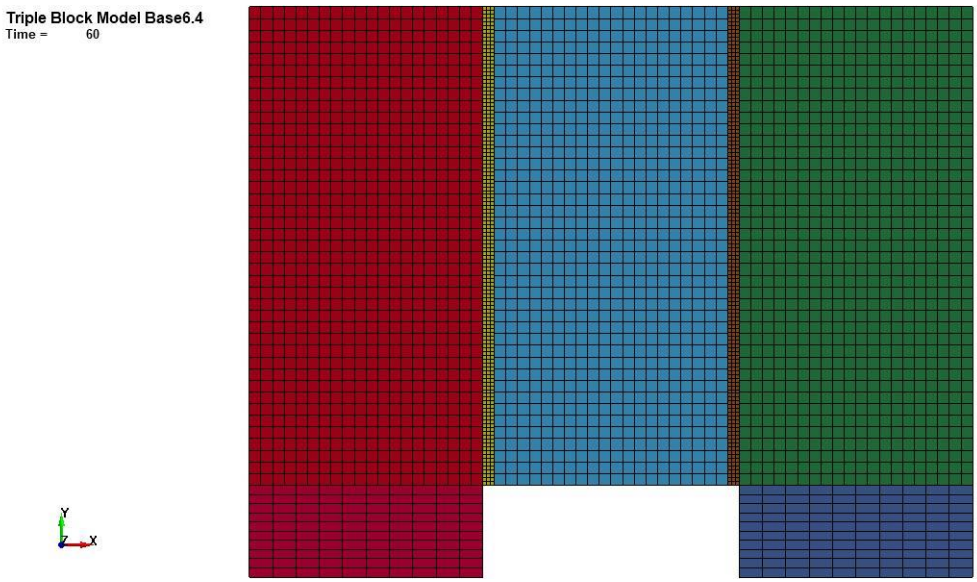


**Figure B-339: Last State at 60 Milliseconds for Base Run 6.4 – 200 psi**

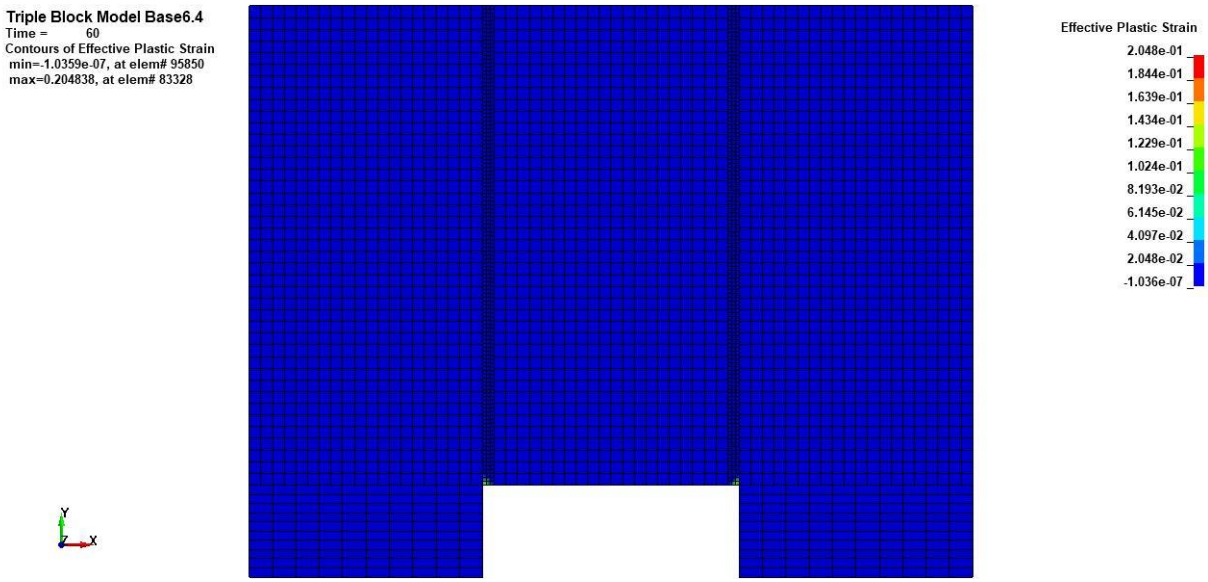


**Figure B-340: Effective Plastic Strain Fringe Plot for Last State at 60 Milliseconds for Base Run 6.4 – 200 psi**

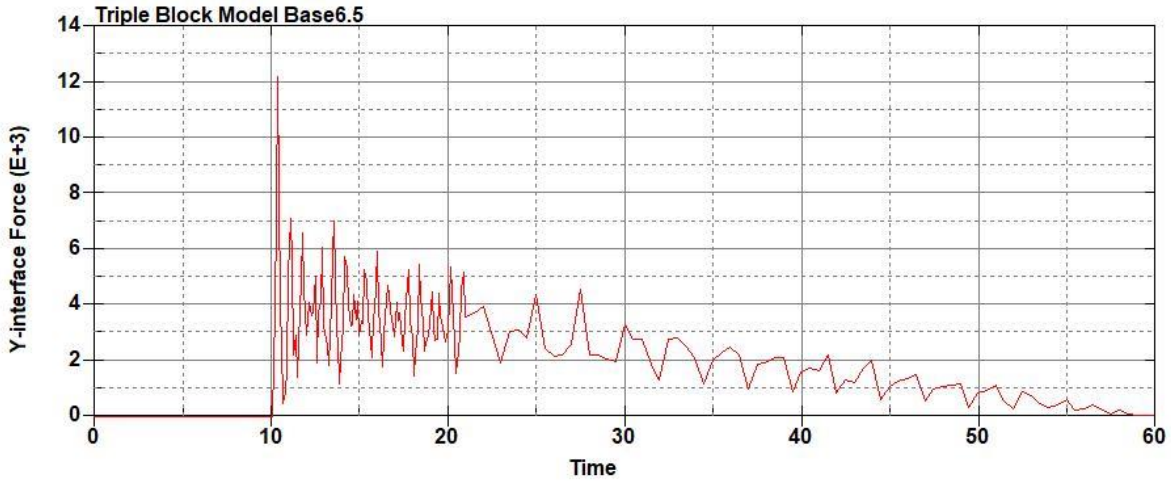


**Figure B-341: Base Run 6.5 Right Support Y-Interface Force (lbs) versus Time (ms) – 250 psi**

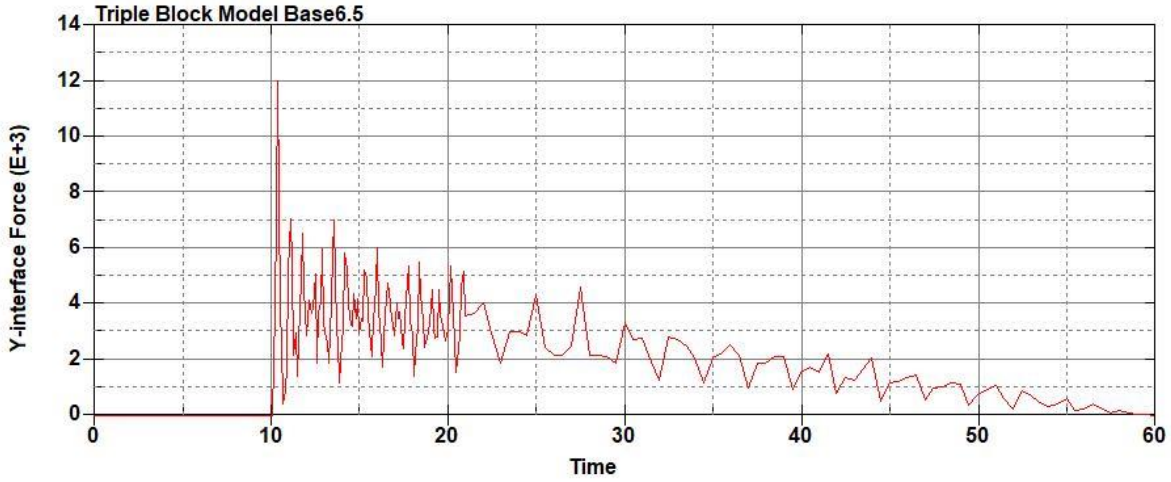


**Figure B-342: Base Run 6.5 Left Support Y-Interface Force (lbs) versus Time (ms) – 250 psi**

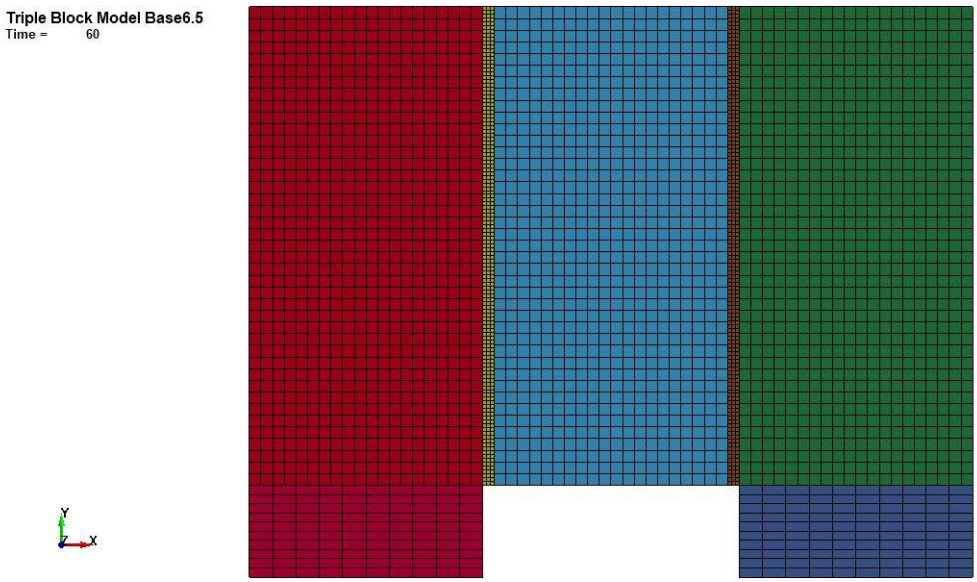


**Figure B-343: Last State at 60 Milliseconds for Base Run 6.5 – 250 psi**

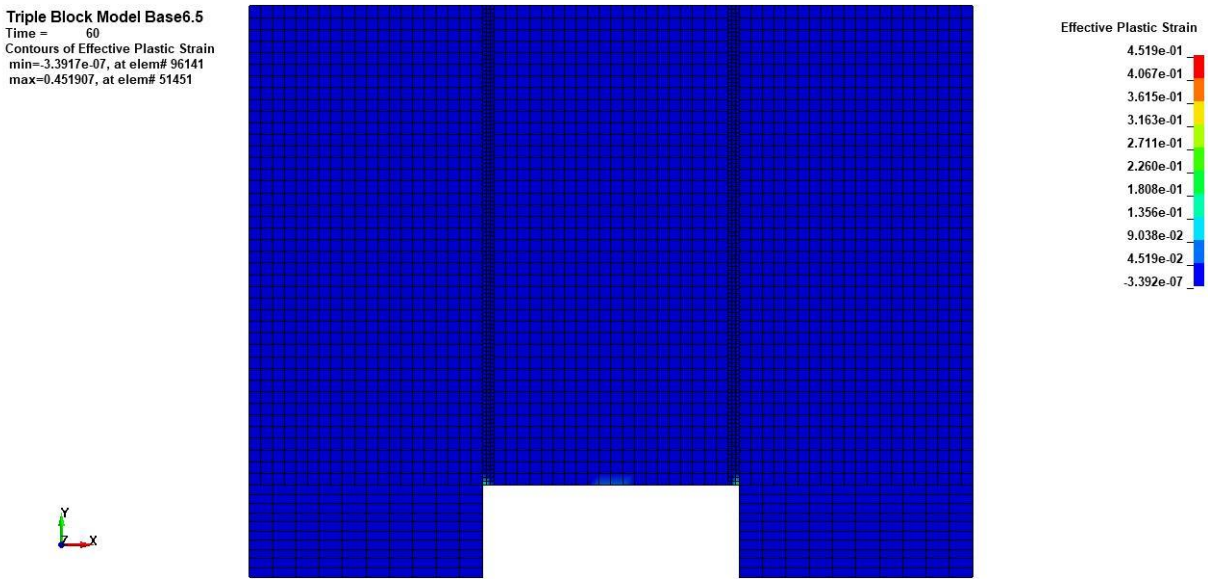


**Figure B-344: Effective Plastic Strain Fringe Plot for Last State at 60 Milliseconds for Base Run 6.5 – 250 psi**

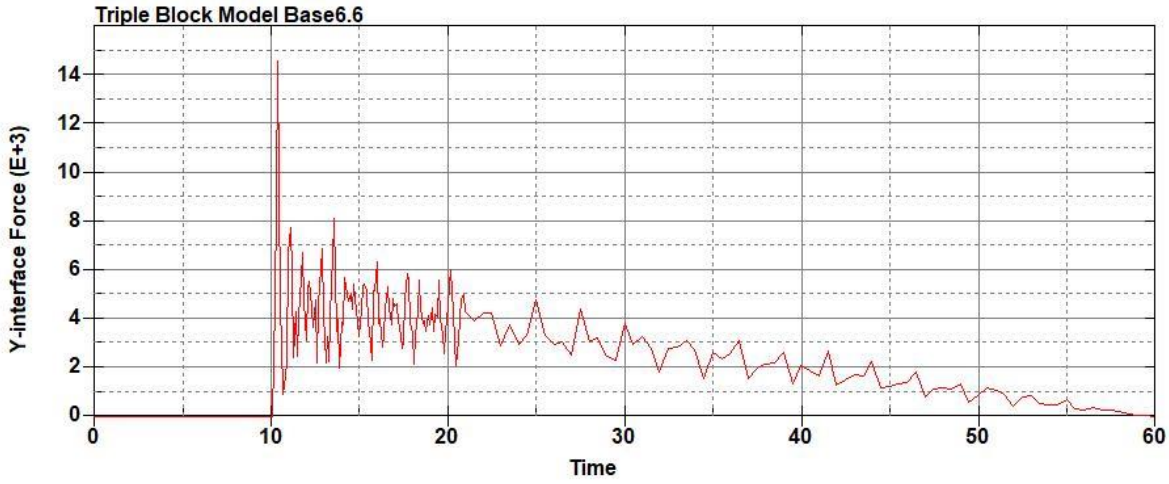


**Figure B-345: Base Run 6.6 Right Support Y-Interface Force (lbs) versus Time (ms) – 300 psi**

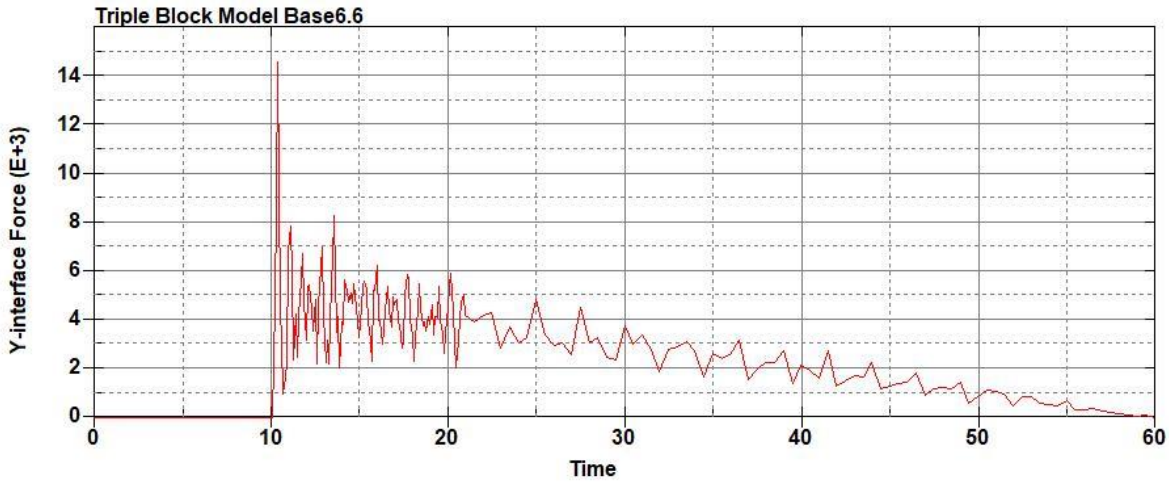


**Figure B-346: Base Run 6.6 Left Support Y-Interface Force (lbs) versus Time (ms) – 300 psi**

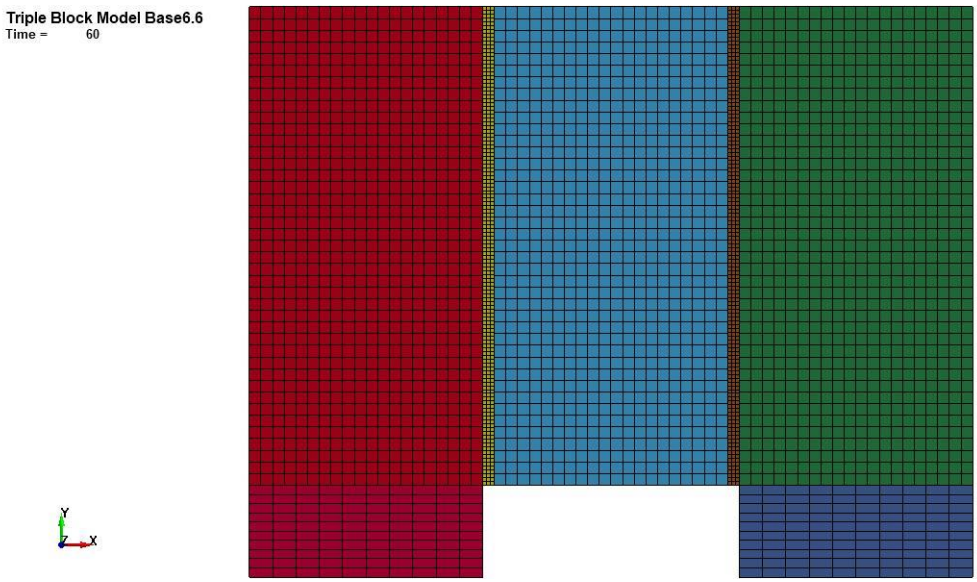


**Figure B-347: Last State at 60 Milliseconds for Base Run 6.6 – 300 psi**

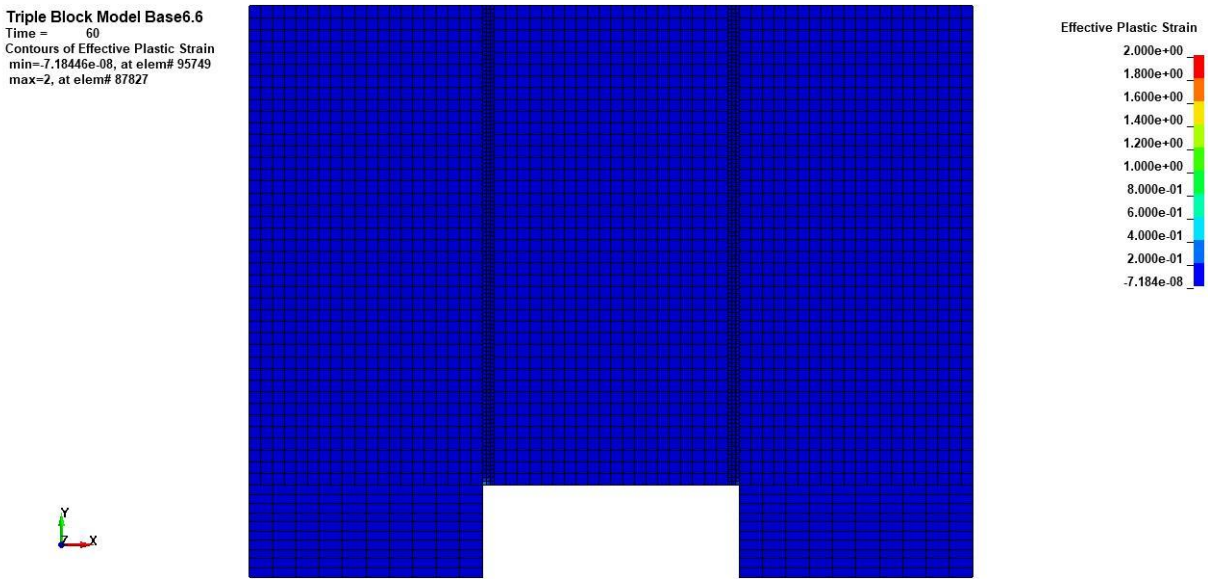


**Figure B-348: Effective Plastic Strain Fringe Plot for Last State at 60 Milliseconds for Base Run 6.6 – 300 psi**

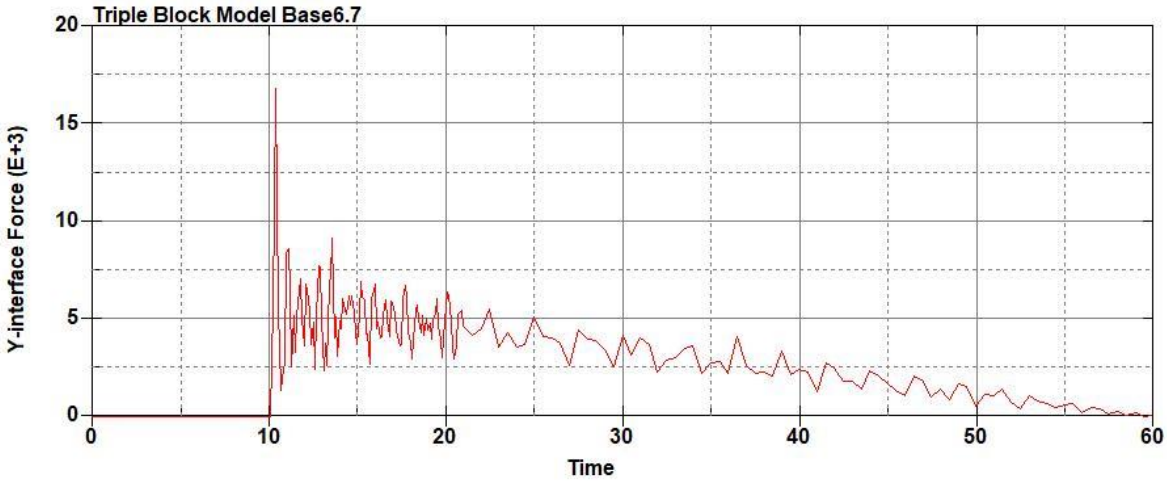


**Figure B-349: Base Run 6.7 Right Support Y-Interface Force (lbs) versus Time (ms) – 350 psi**

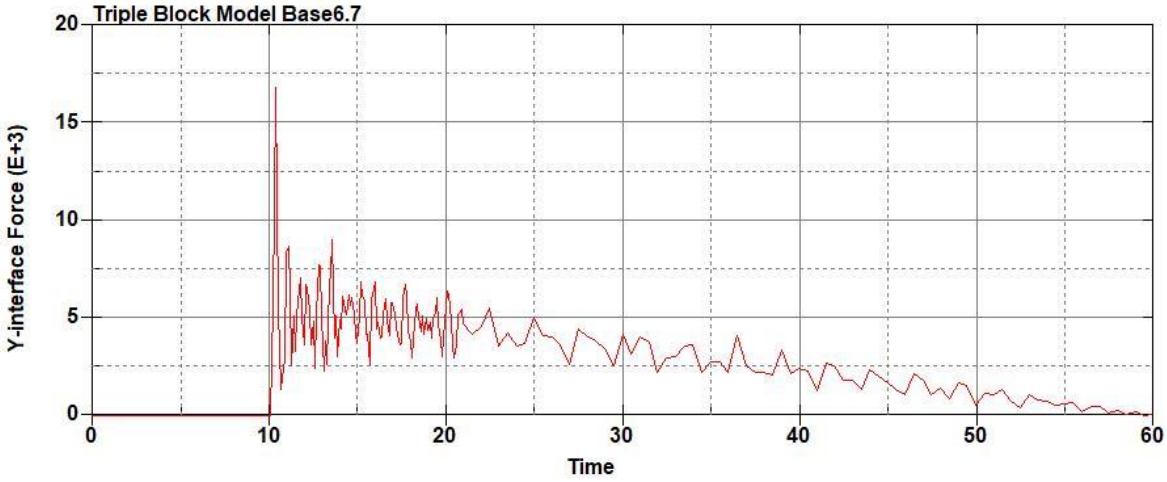


**Figure B-350: Base Run 6.7 Left Support Y-Interface Force (lbs) versus Time (ms) – 350 psi**

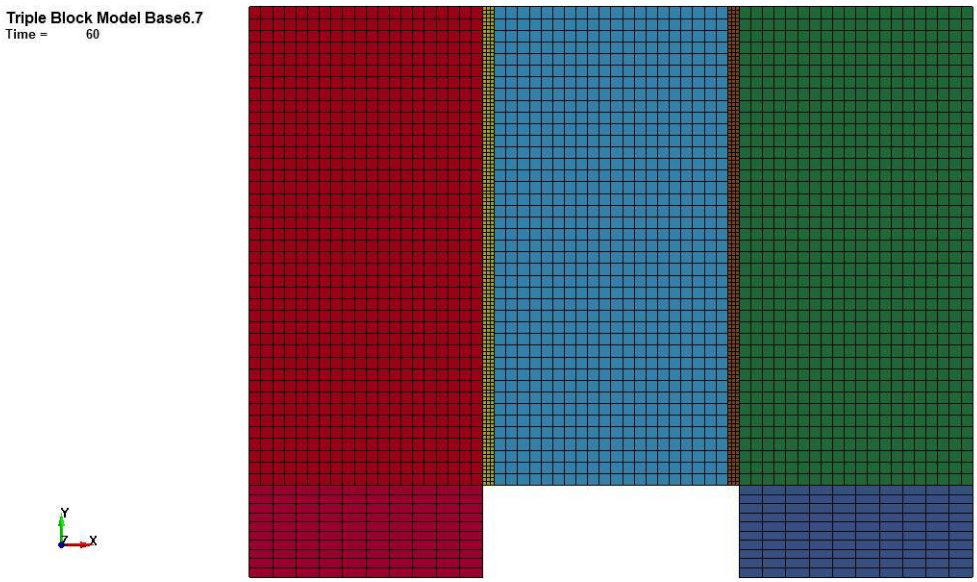


**Figure B-351: Last State at 60 Milliseconds for Base Run 6.7 – 350 psi**

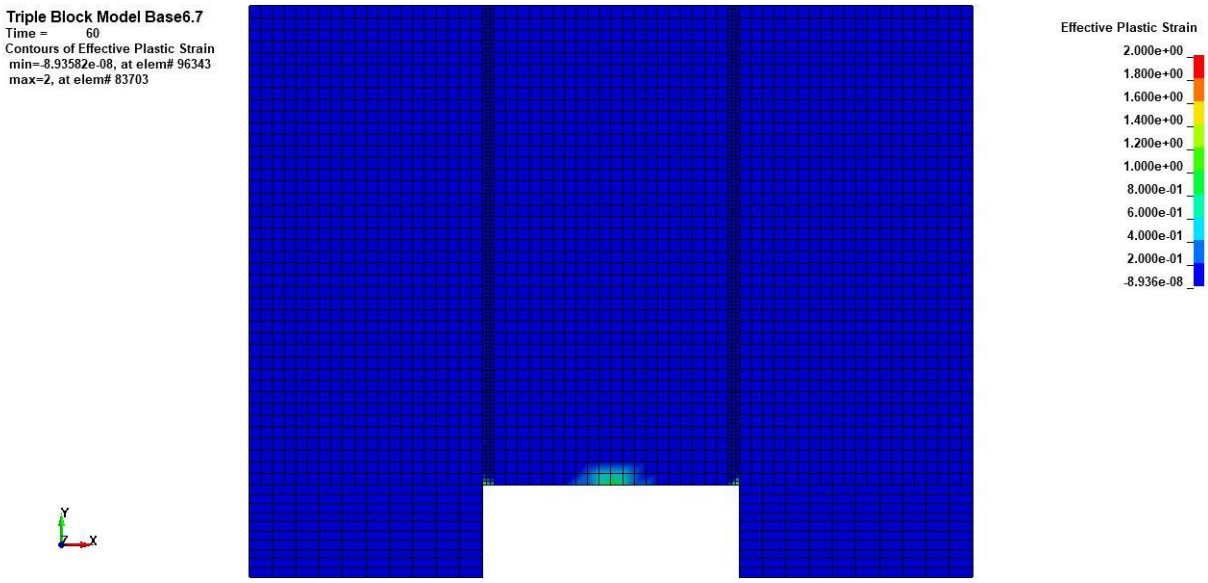


**Figure B-352: Effective Plastic Strain Fringe Plot for Last State at 60 Milliseconds for Base Run 6.7 – 350 psi**

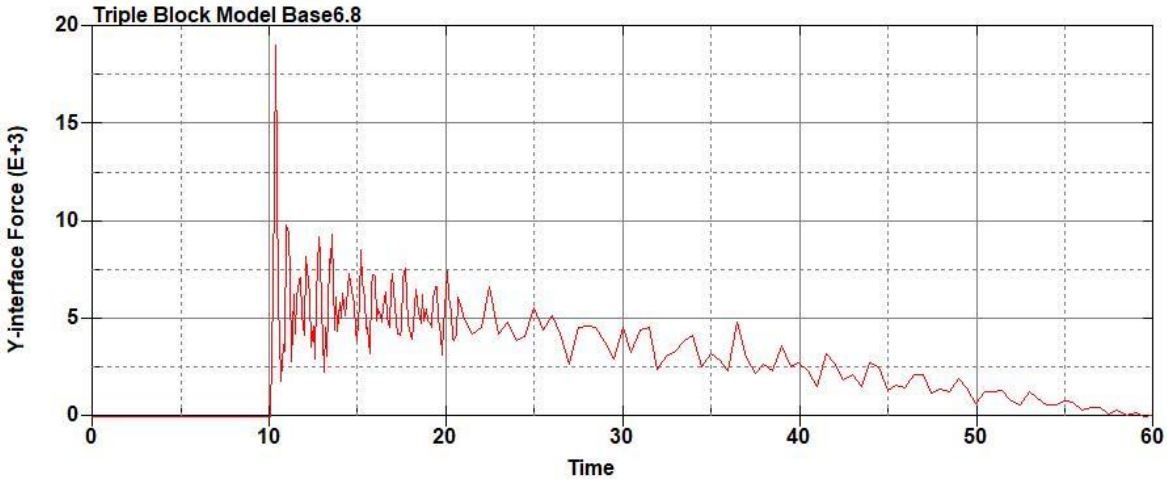


**Figure B-353: Base Run 6.8 Right Support Y-Interface Force (lbs) versus Time (ms) – 400 psi**

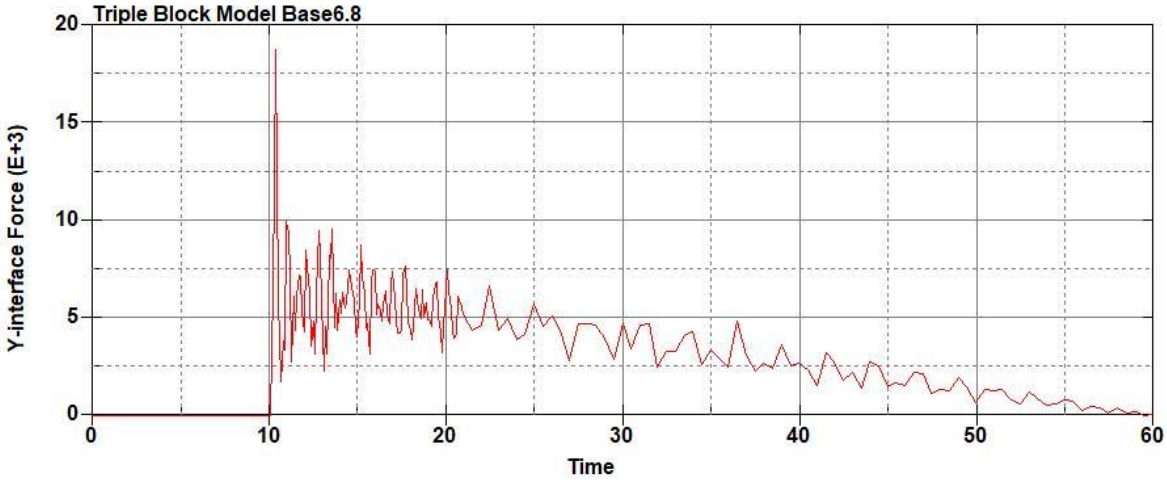


**Figure B-354: Base Run 6.8 Left Support Y-Interface Force (lbs) versus Time (ms) – 400 psi**

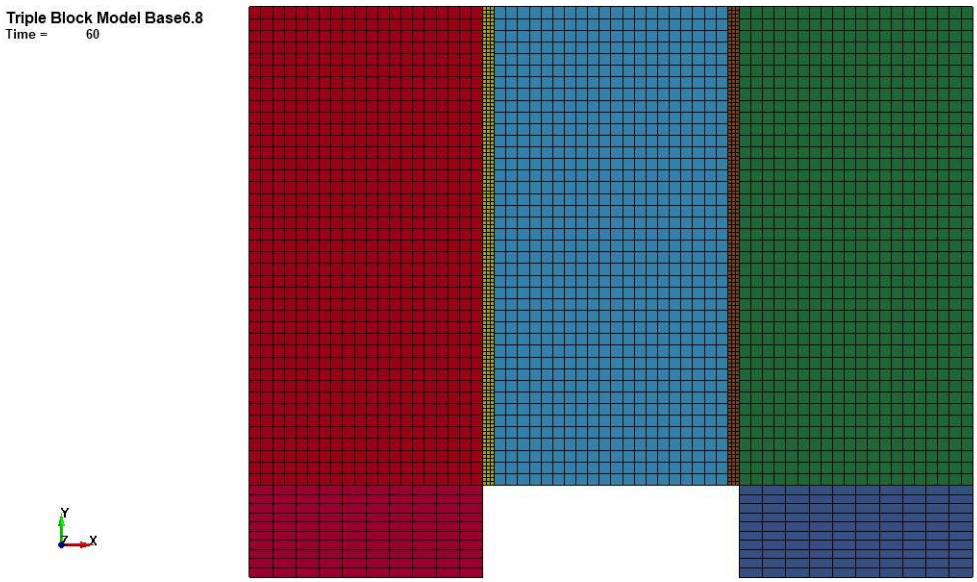


**Figure B-355: Last State at 60 Milliseconds for Base Run 6.8 – 400 psi**

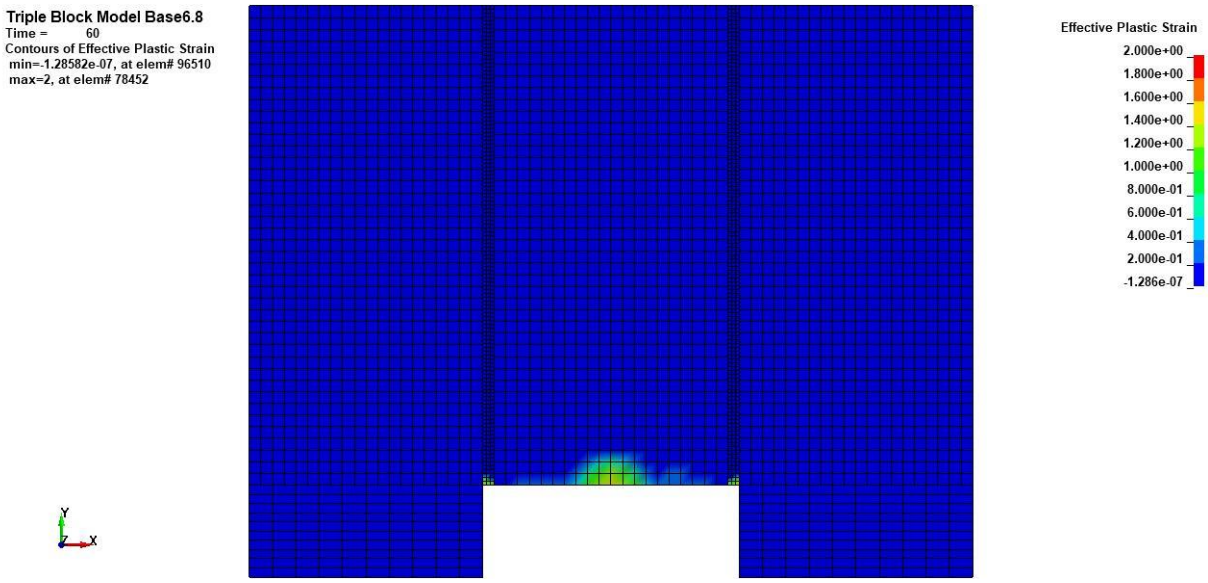


**Figure B-356: Effective Plastic Strain Fringe Plot for Last State at 60 Milliseconds for Base Run 6.8 – 400 psi**

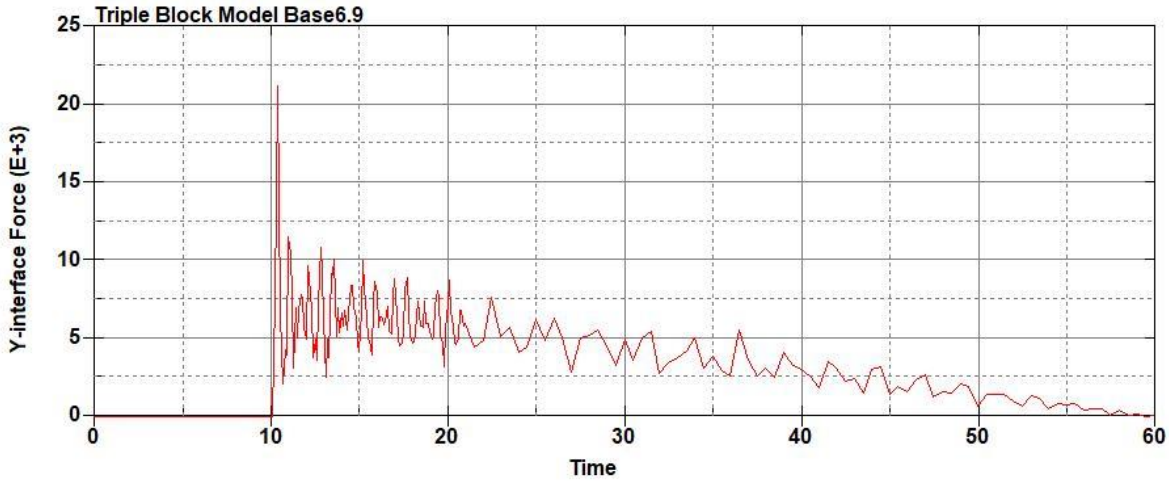


**Figure B-357: Base Run 6.9 Right Support Y-Interface Force (lbs) versus Time (ms) – 450 psi**

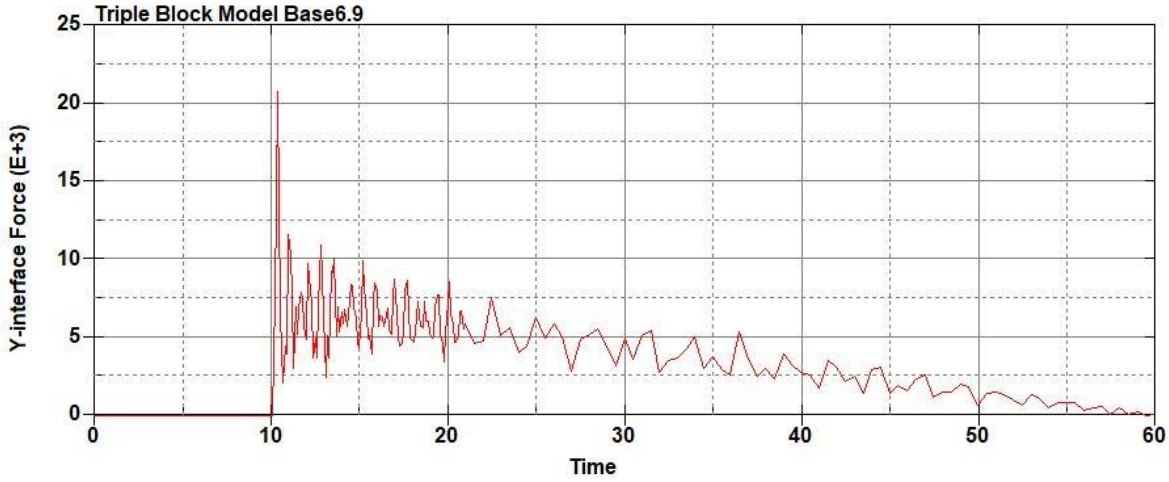


**Figure B-358: Base Run 6.9 Left Support Y-Interface Force (lbs) versus Time (ms) – 450 psi**

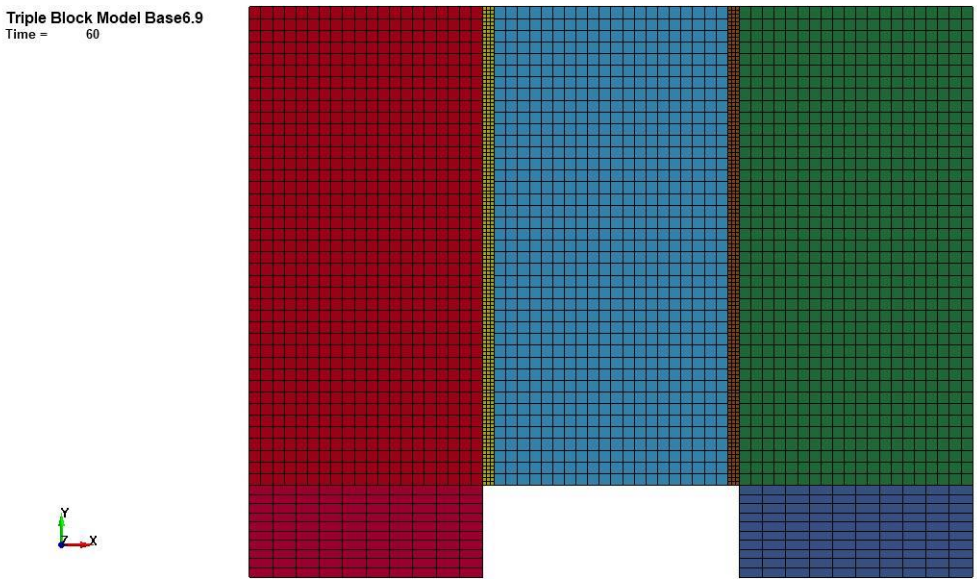


**Figure B-359: Last State at 60 Milliseconds for Base Run 6.9 – 450 psi**

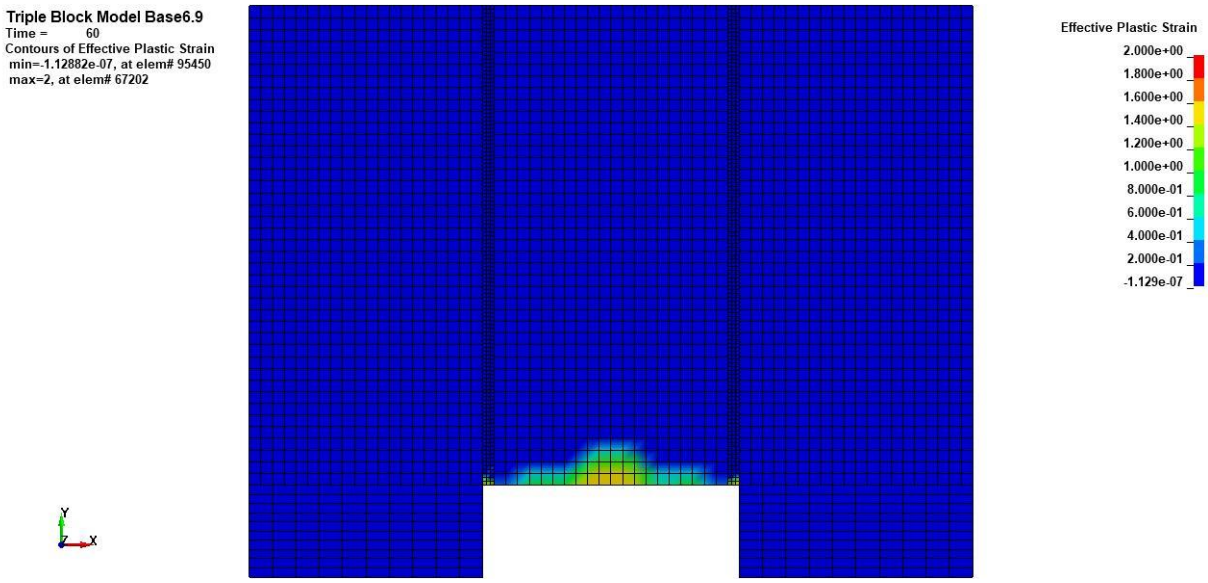


**Figure B-360: Effective Plastic Strain Fringe Plot for Last State at 60 Milliseconds for Base Run 6.9 – 450 psi**

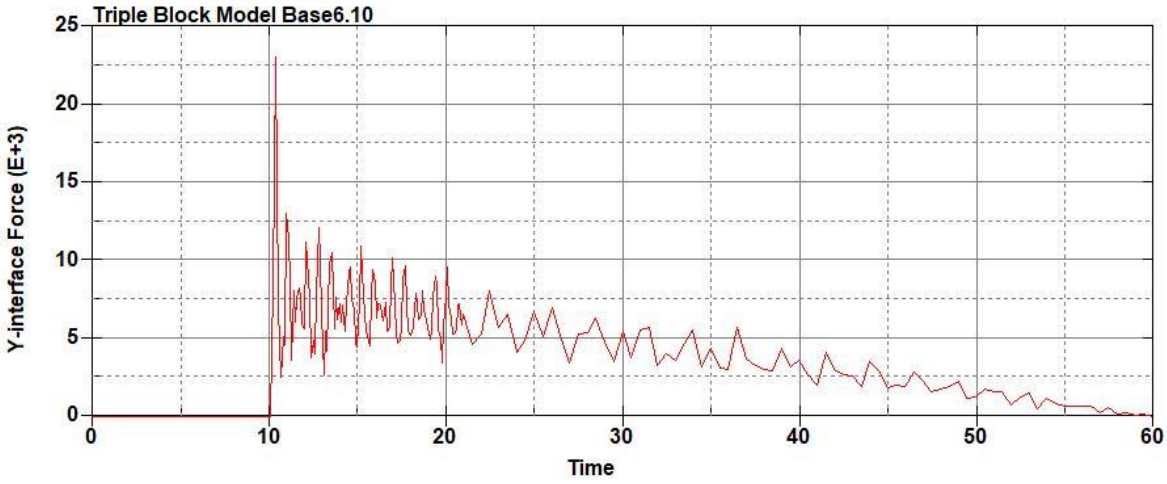


**Figure B-361: Base Run 6.10 Right Support Y-Interface Force (lbs) versus Time (ms) – 500 psi**

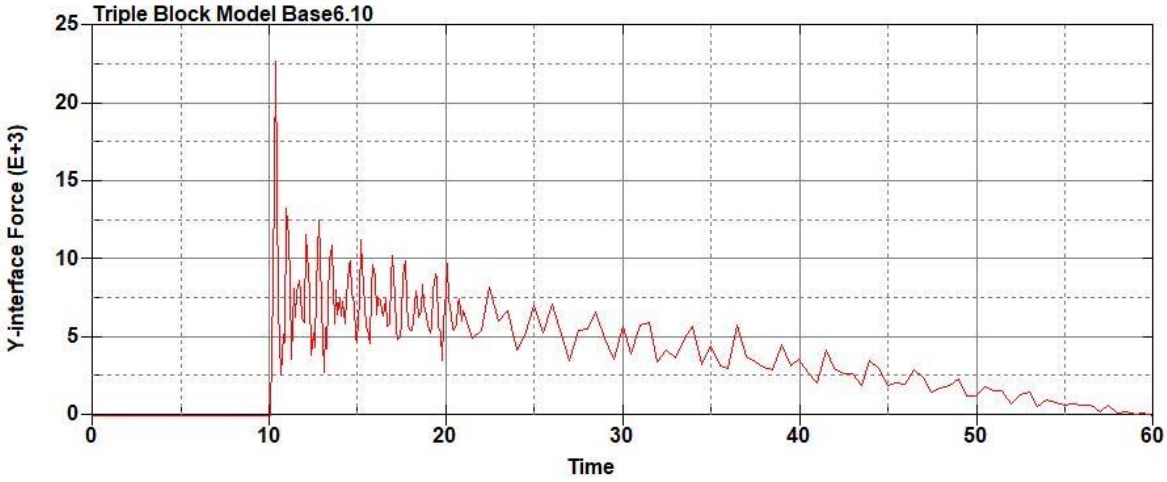


**Figure B-362: Base Run 6.10 Left Support Y-Interface Force (lbs) versus Time (ms) – 500 psi**

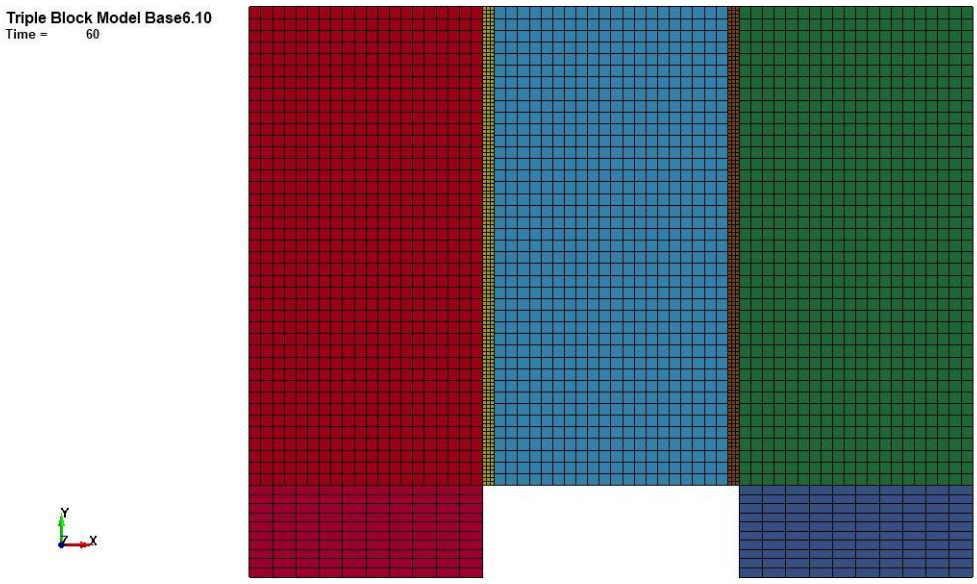


**Figure B-363: Last State at 60 Milliseconds for Base Run 6.10 – 500 psi**

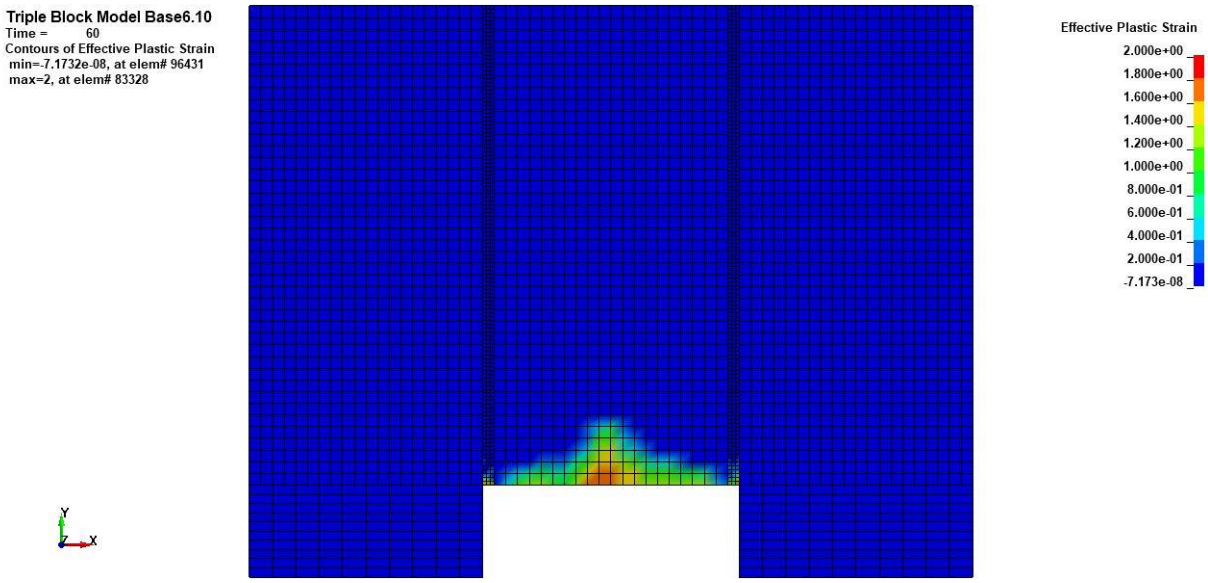


**Figure B-364: Effective Plastic Strain Fringe Plot for Last State at 60 Milliseconds for Base Run 6.10 – 500 psi**

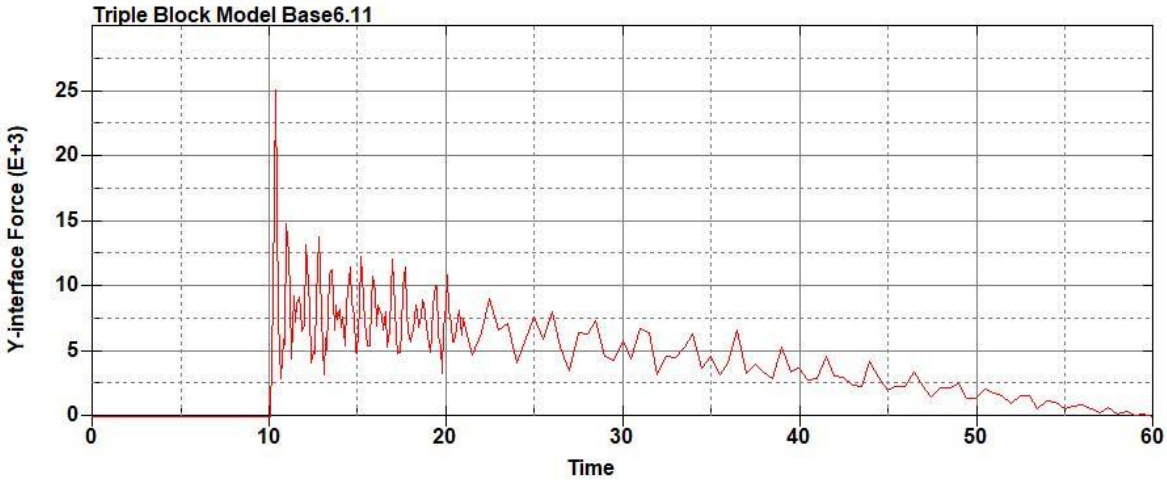


**Figure B-365: Base Run 6.11 Right Support Y-Interface Force (lbs) versus Time (ms) – 550 psi**

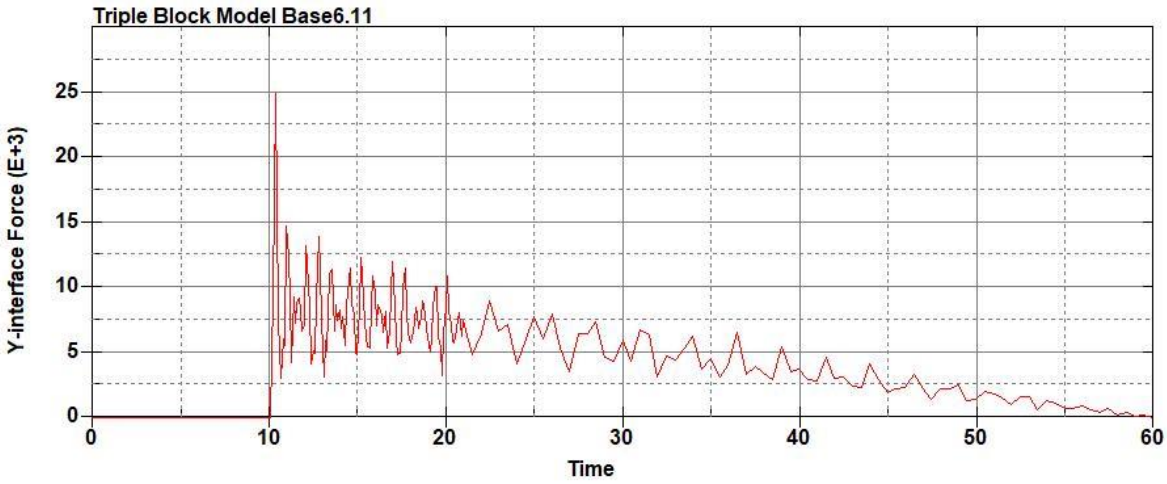


**Figure B-366: Base Run 6.11 Left Support Y-Interface Force (lbs) versus Time (ms) – 550 psi**

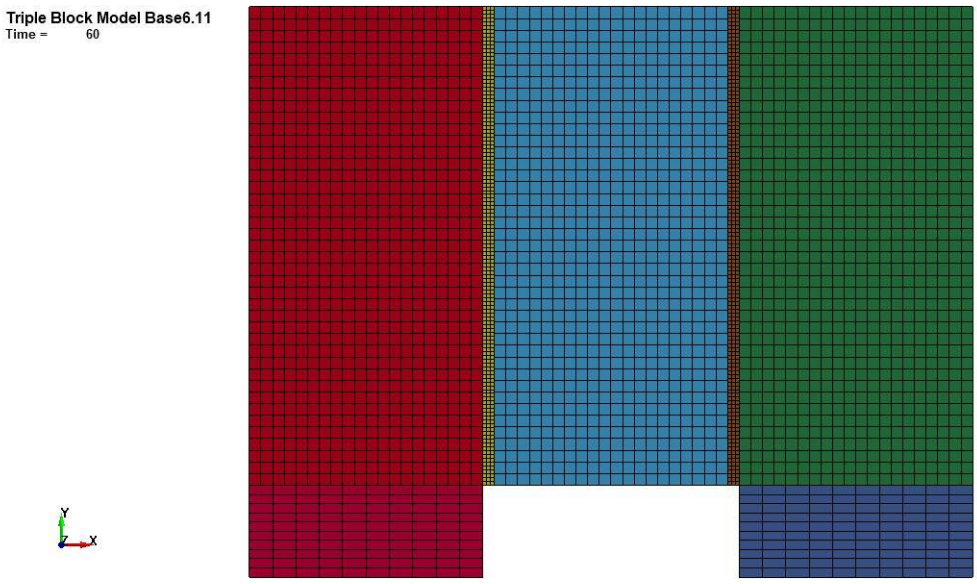


**Figure B-367: Last State at 60 Milliseconds for Base Run 6.11 – 550 psi**

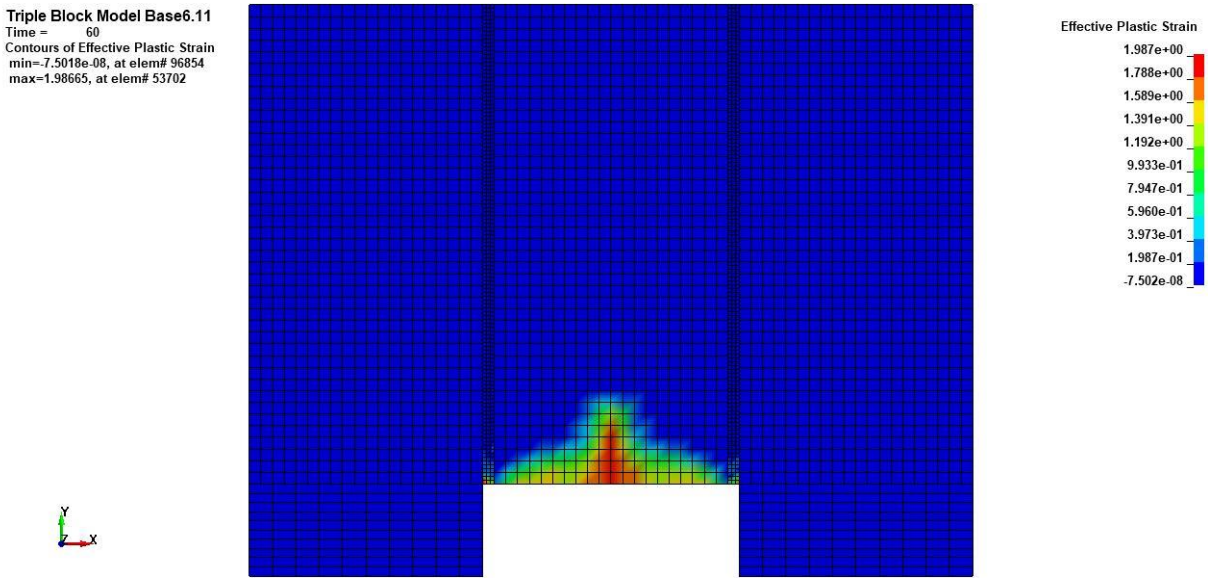


**Figure B-368: Effective Plastic Strain Fringe Plot for Last State at 60 Milliseconds for Base Run 6.11 – 550 psi**

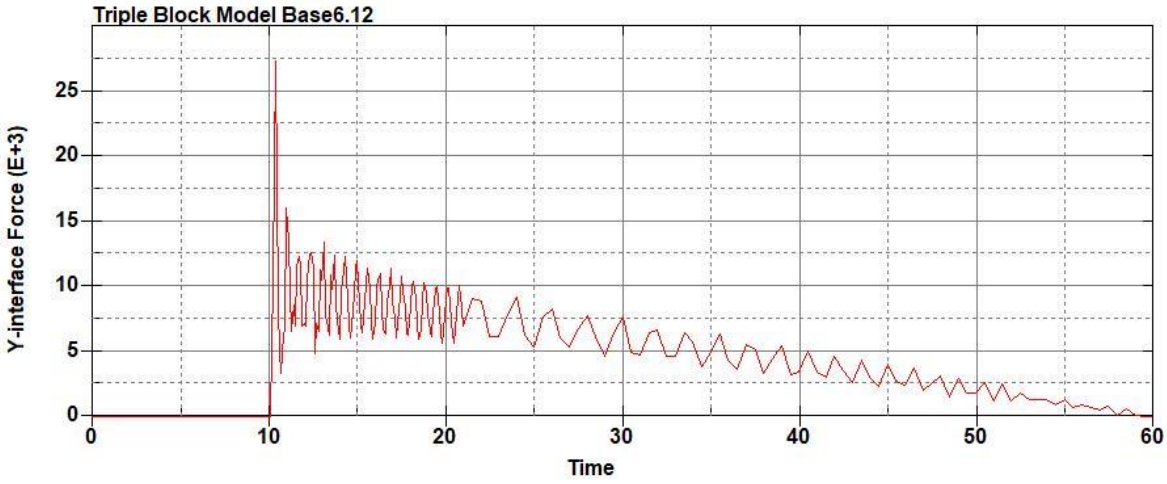


**Figure B-369: Base Run 6.12 Right Support Y-Interface Force (lbs) versus Time (ms) – 600 psi**

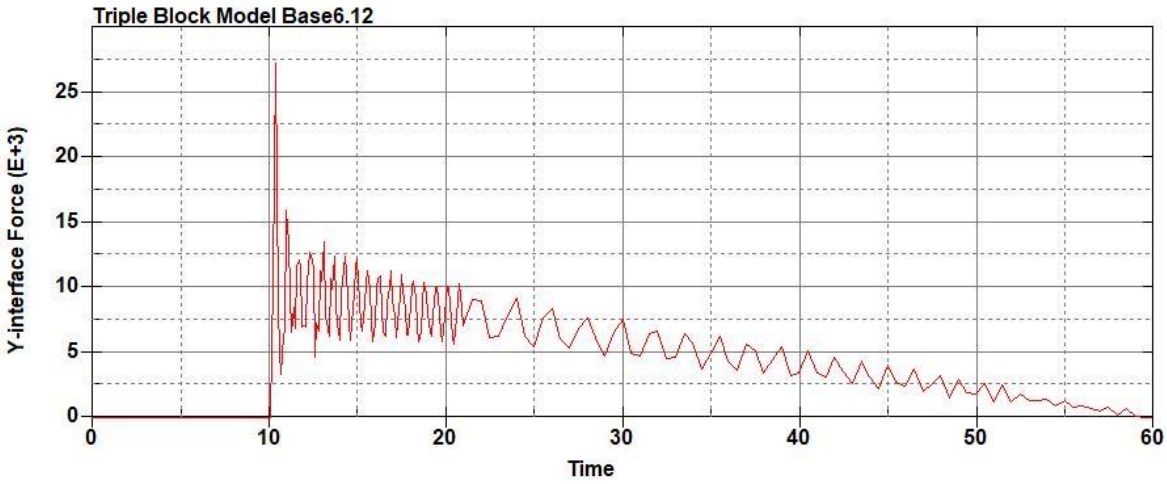


**Figure B-370: Base Run 6.12 Left Support Y-Interface Force (lbs) versus Time (ms) – 600 psi**

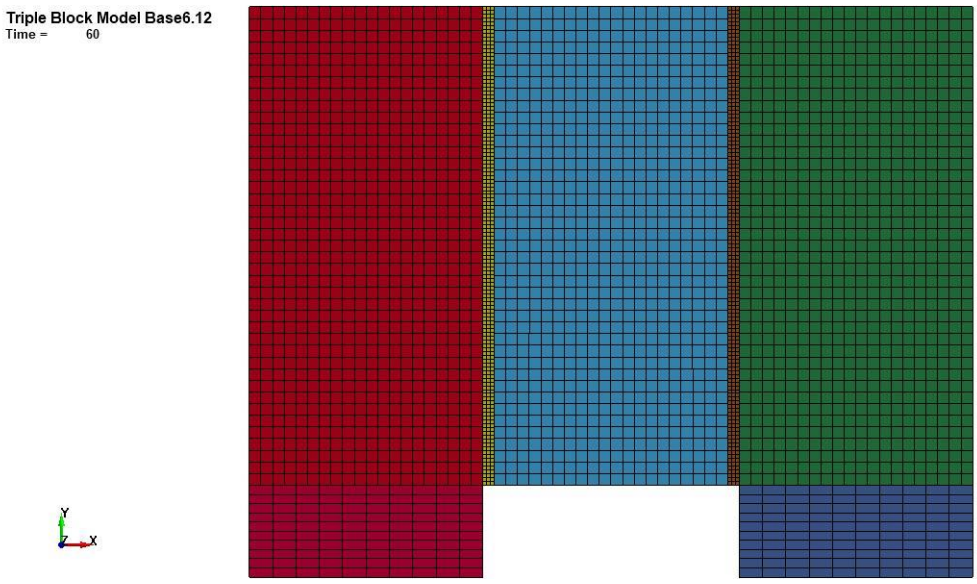


**Figure B-371: Last State at 60 Milliseconds for Base Run 6.12 – 600 psi**

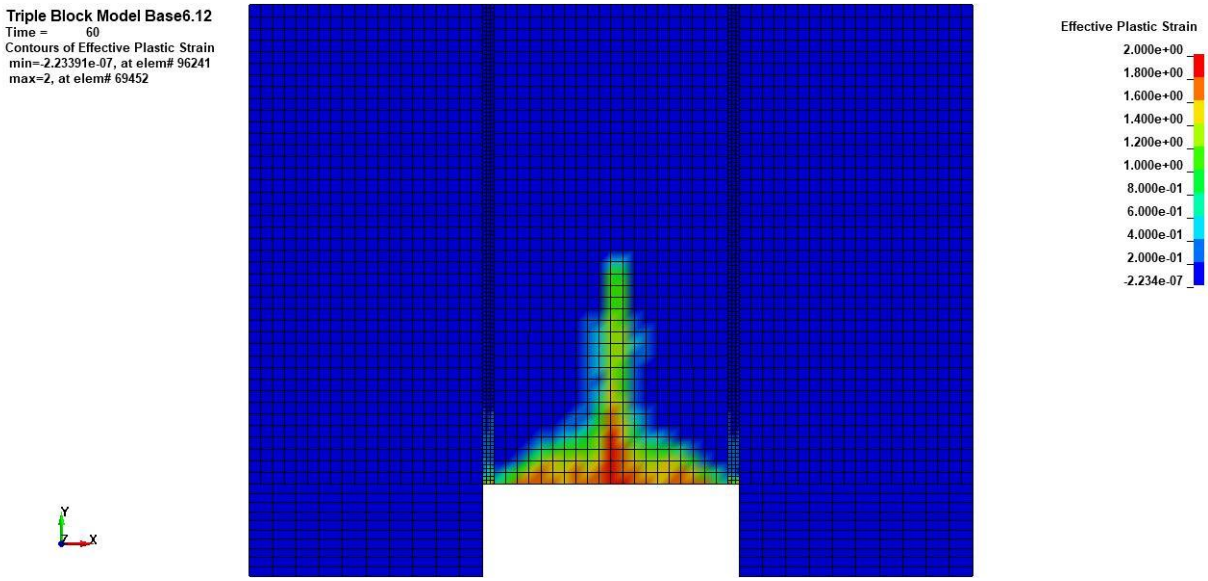


**Figure B-372: Effective Plastic Strain Fringe Plot for Last State at 60 Milliseconds for Base Run 6.12 – 600 psi**

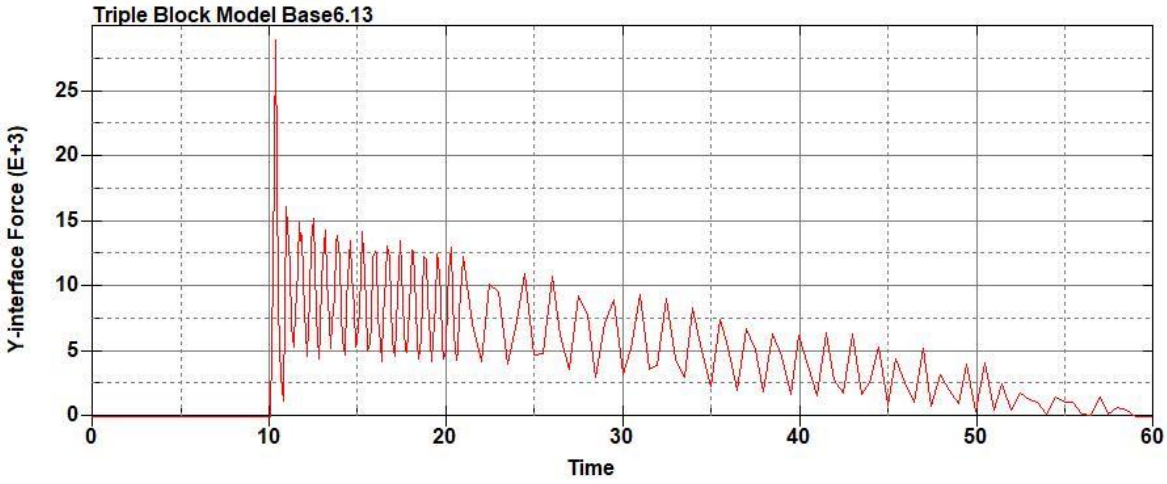


**Figure B-373: Base Run 6.13 Right Support Y-Interface Force (lbs) versus Time (ms) – 650 psi**

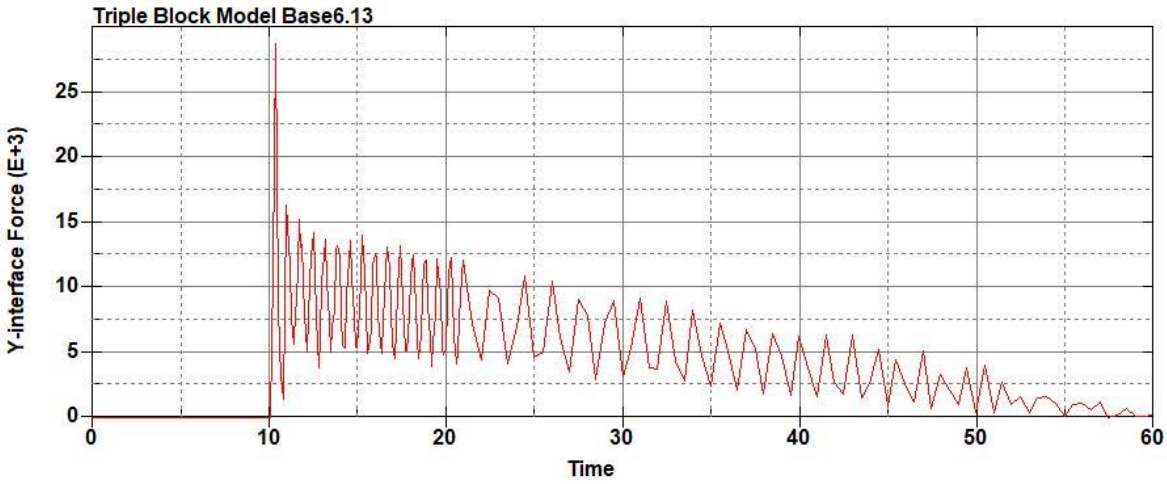


**Figure B-374: Base Run 6.13 Left Support Y-Interface Force (lbs) versus Time (ms) – 650 psi**

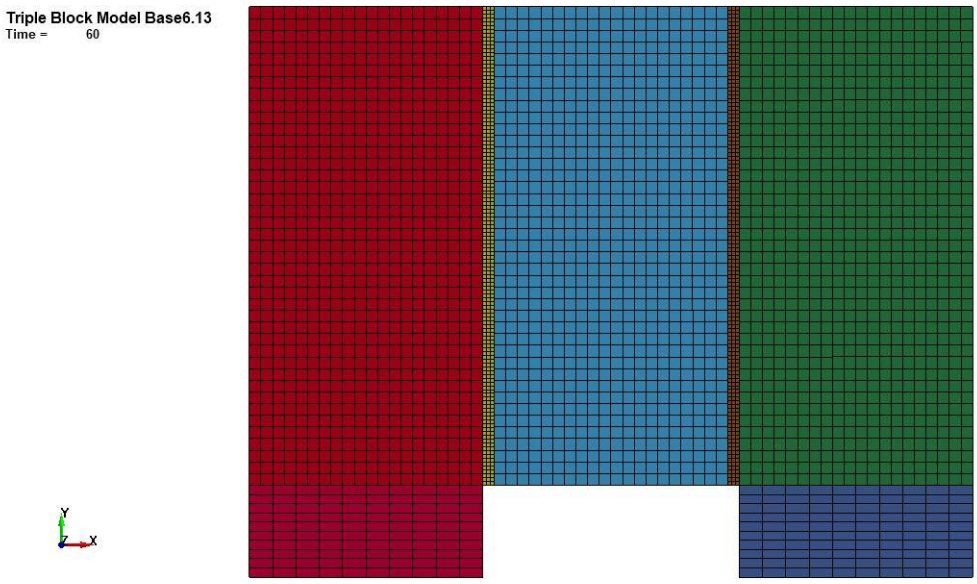


**Figure B-375: Last State at 60 Milliseconds for Base Run 6.13 – 650 psi**

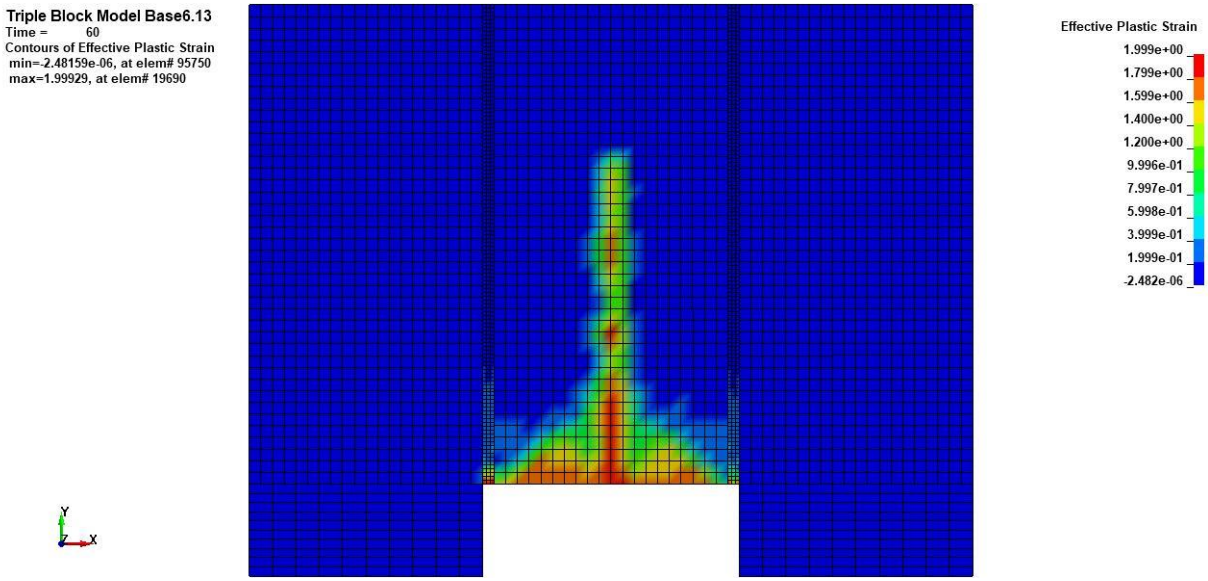


**Figure B-376: Effective Plastic Strain Fringe Plot for Last State at 60 Milliseconds for Base Run 6.13 – 650 psi**

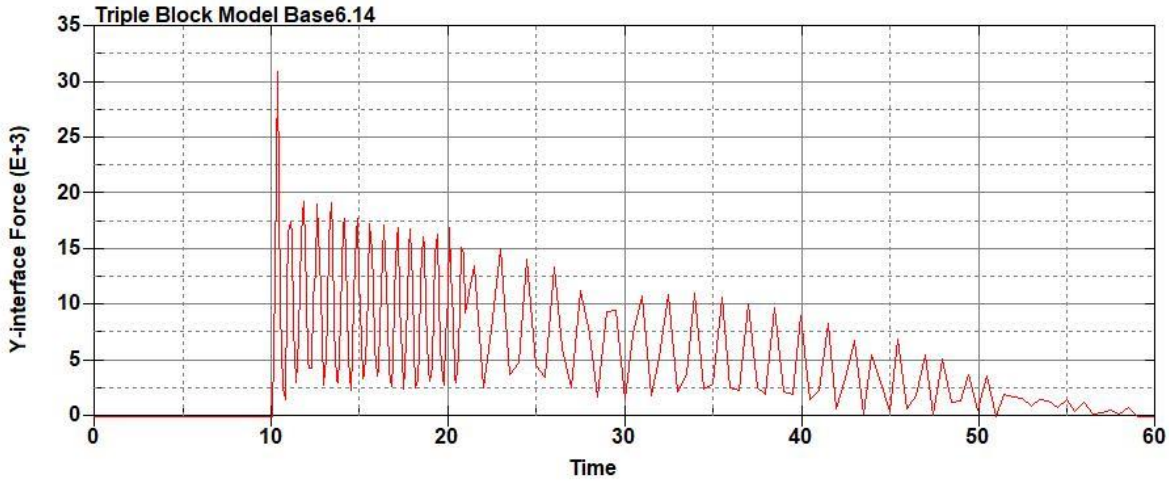


**Figure B-377: Base Run 6.14 Right Support Y-Interface Force (lbs) versus Time (ms) – 700 psi**

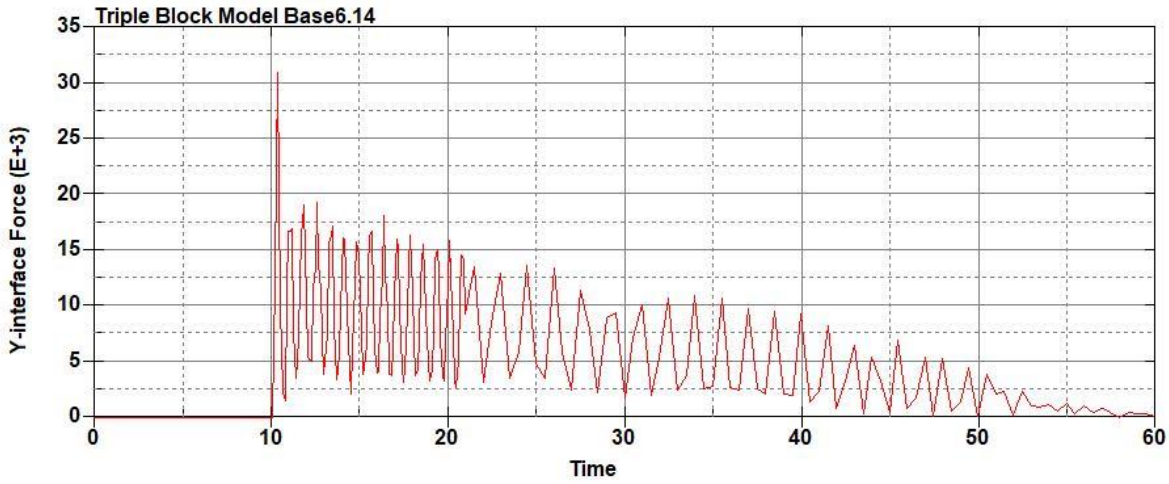


**Figure B-378: Base Run 6.14 Left Support Y-Interface Force (lbs) versus Time (ms) – 700 psi**

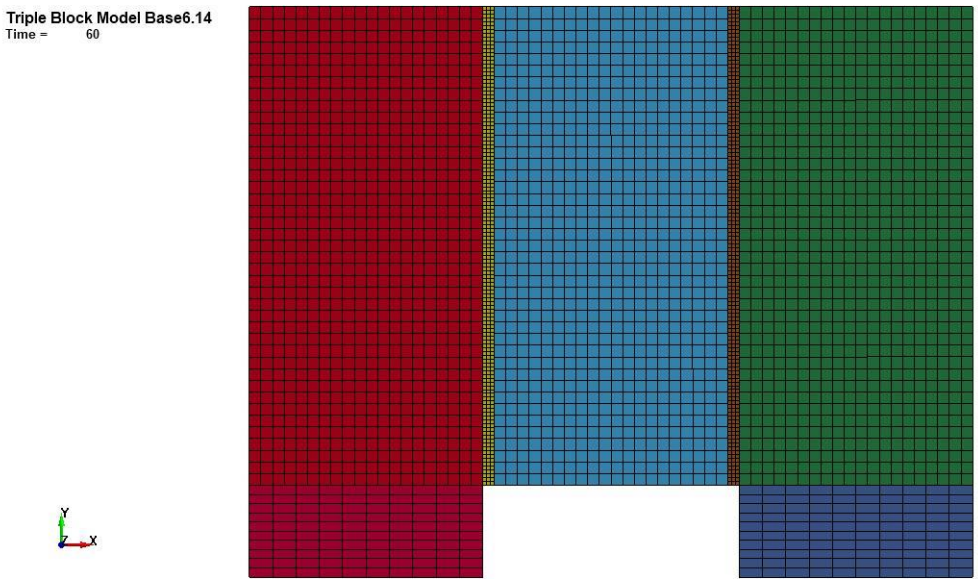


**Figure B-379: Last State at 60 Milliseconds for Base Run 6.14 – 700 psi**

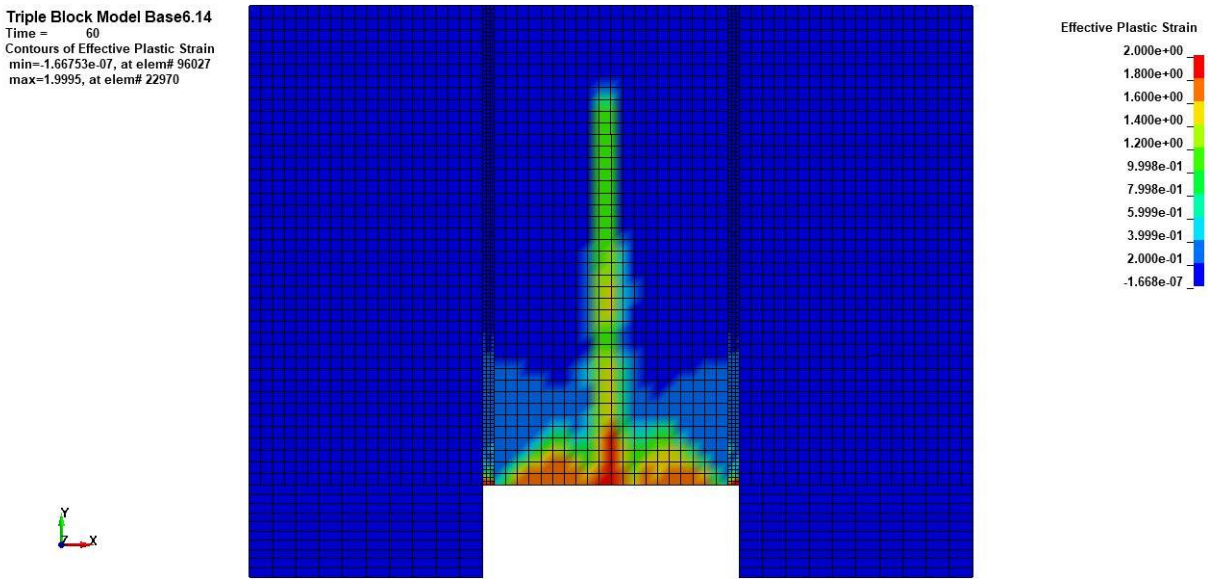


**Figure B-380: Effective Plastic Strain Fringe Plot for Last State at 60 Milliseconds for Base Run 6.14 – 700 psi**

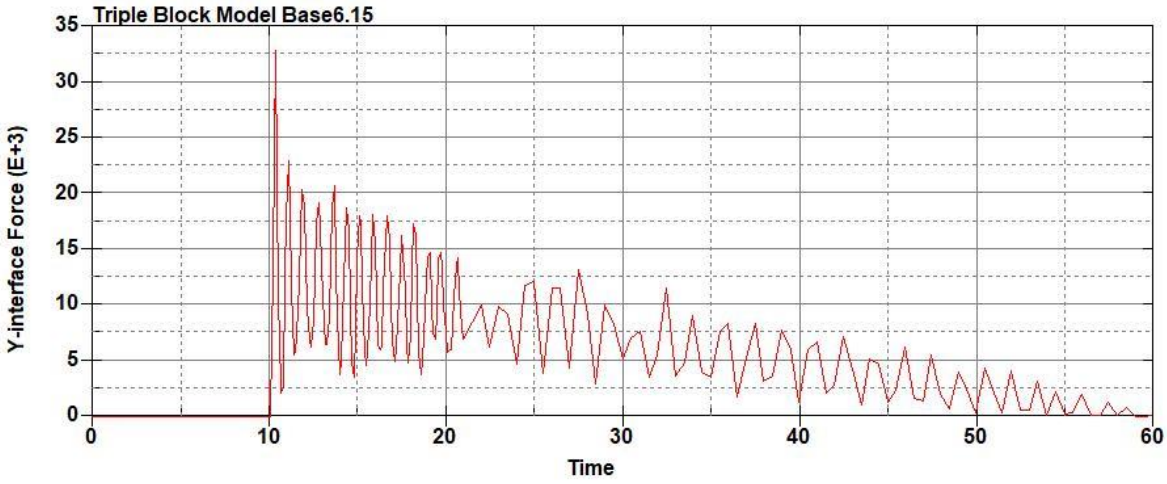


**Figure B-381: Base Run 6.15 Right Support Y-Interface Force (lbs) versus Time (ms) – 750 psi**

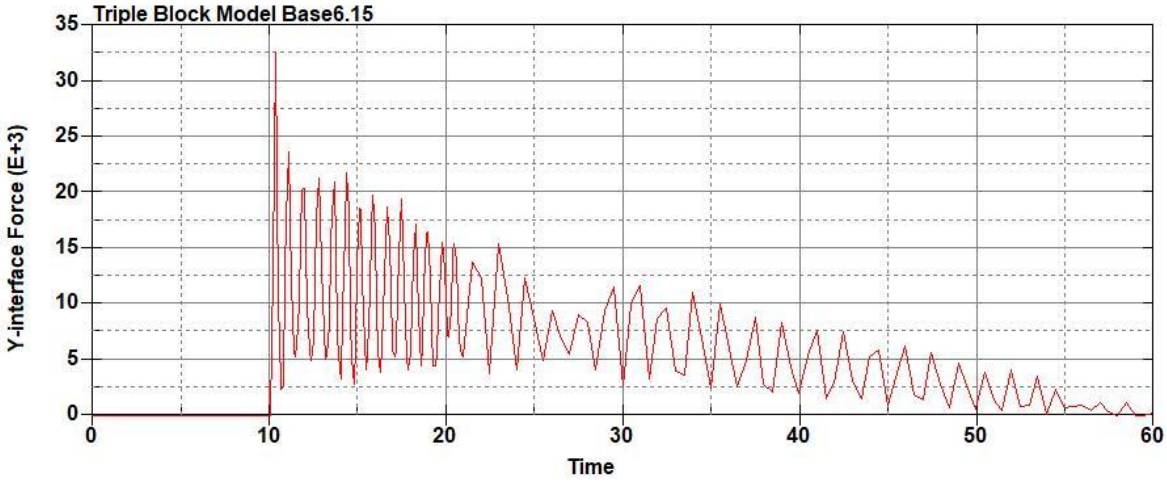


**Figure B-382: Base Run 6.15 Left Support Y-Interface Force (lbs) versus Time (ms) – 750 psi**

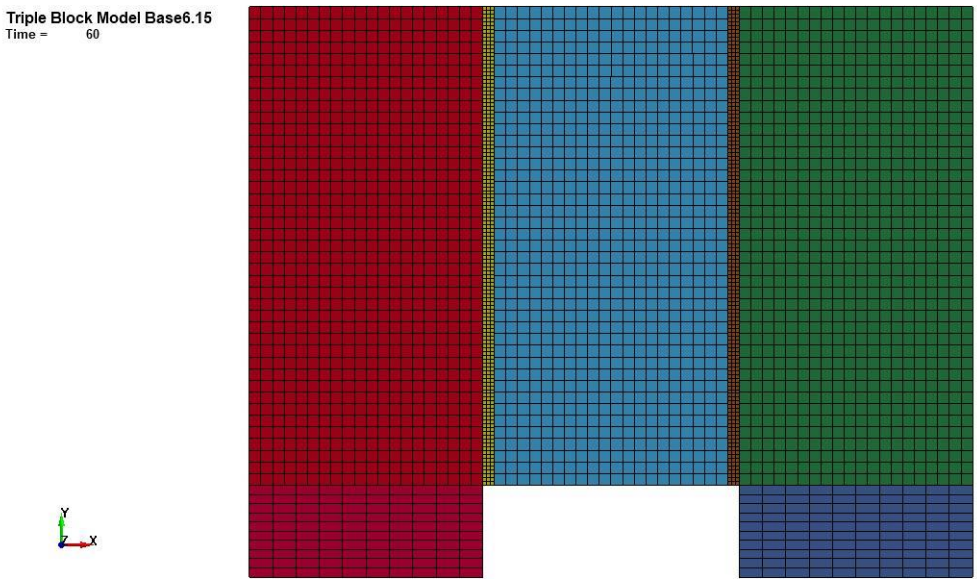


**Figure B-383: Last State at 60 Milliseconds for Base Run 6.15 – 750 psi**

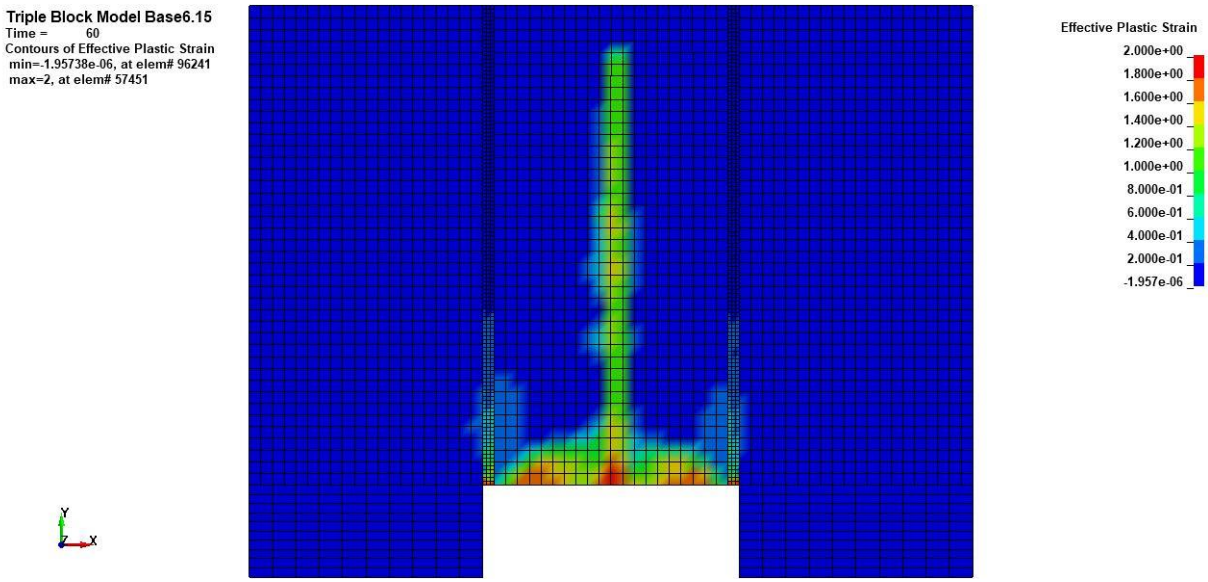


**Figure B-384: Effective Plastic Strain Fringe Plot for Last State at 60 Milliseconds for Base Run 6.15 – 750 psi**

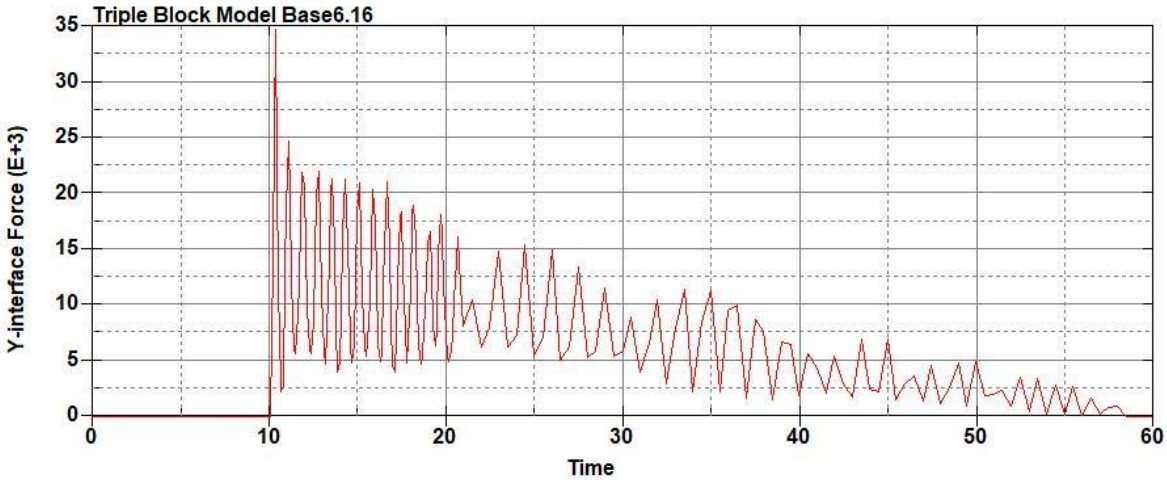


**Figure B-385: Base Run 6.16 Right Support Y-Interface Force (lbs) versus Time (ms) – 800 psi**

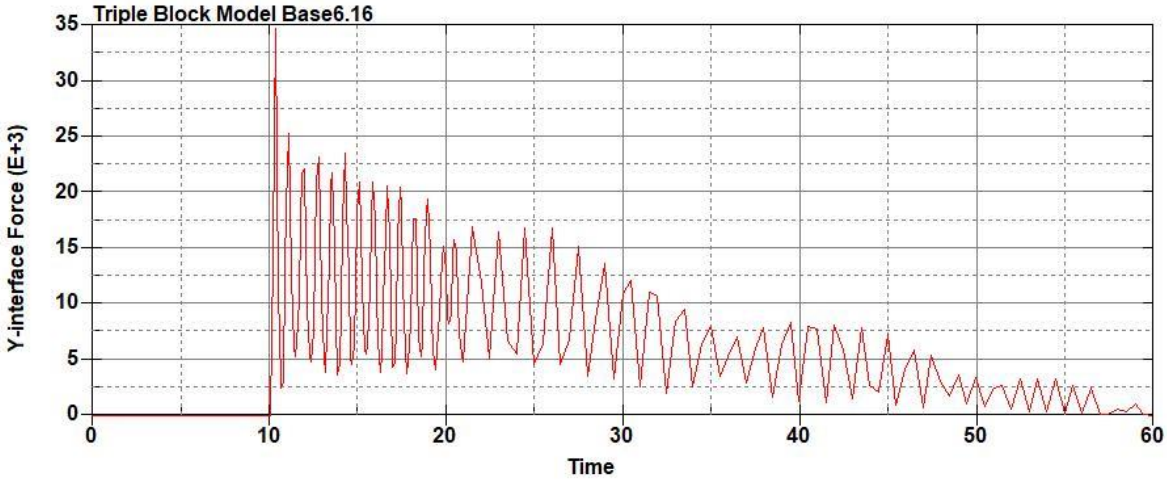


**Figure B-386: Base Run 6.16 Left Support Y-Interface Force (lbs) versus Time (ms) – 800 psi**

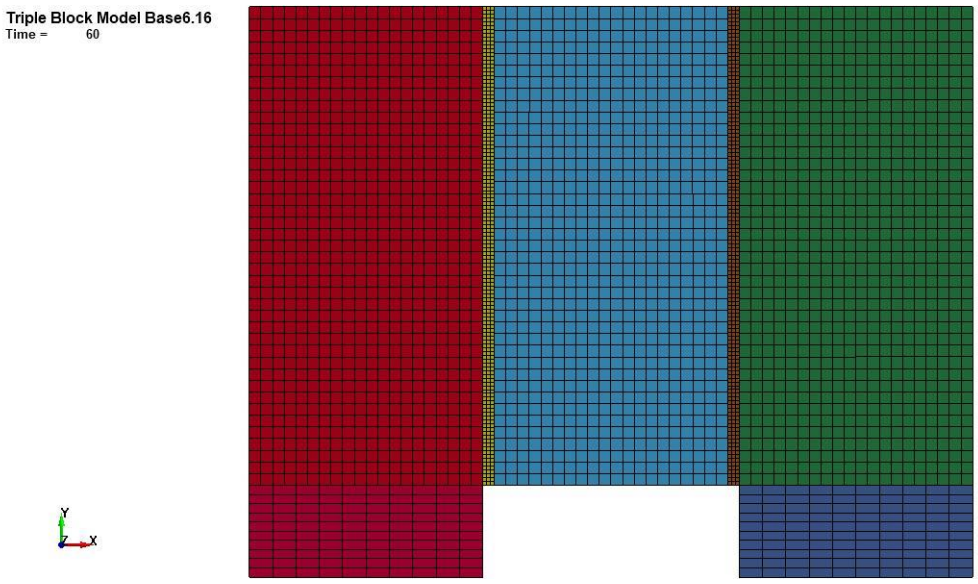


**Figure B-387: Last State at 60 Milliseconds for Base Run 6.16 – 800 psi**

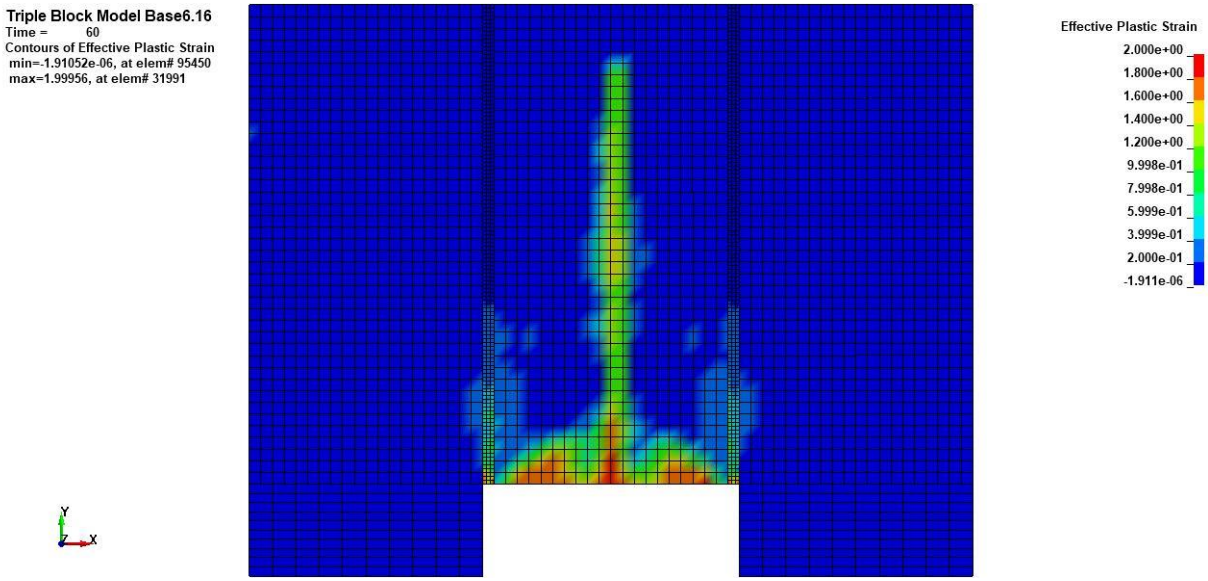


**Figure B-388: Effective Plastic Strain Fringe Plot for Last State at 60 Milliseconds for Base Run 6.16 – 800 psi**

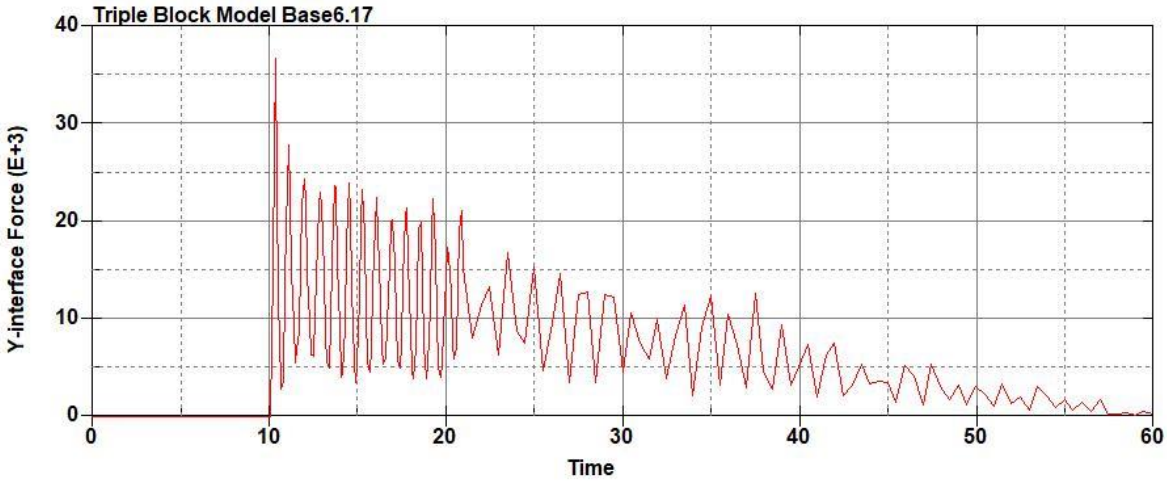


**Figure B-389: Base Run 6.17 Right Support Y-Interface Force (lbs) versus Time (ms) – 850 psi**

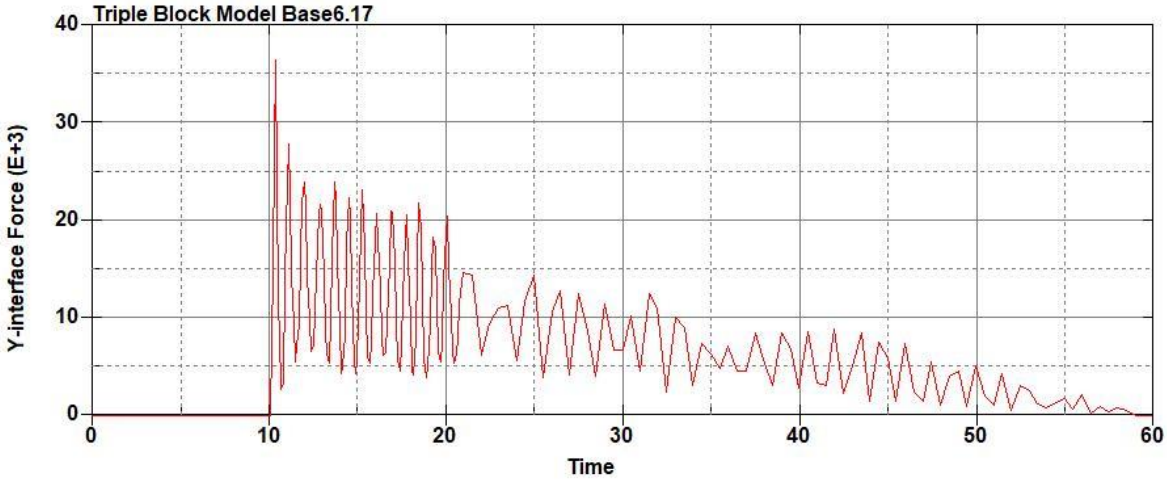


**Figure B-390: Base Run 6.17 Left Support Y-Interface Force (lbs) versus Time (ms) – 850 psi**

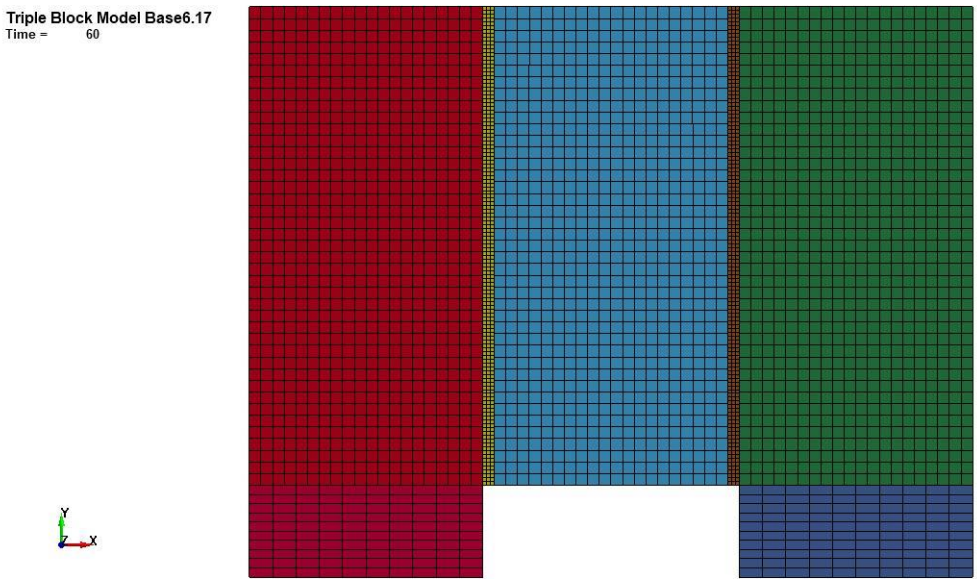


**Figure B-391: Last State at 60 Milliseconds for Base Run 6.17 – 850 psi**

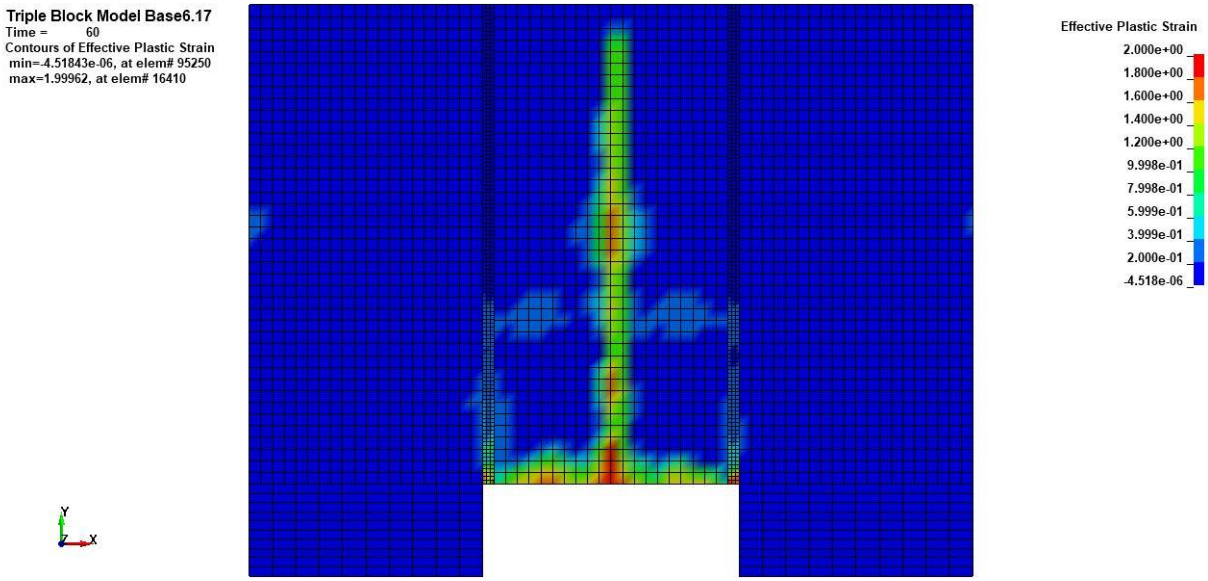


**Figure B-392: Effective Plastic Strain Fringe Plot for Last State at 60 Milliseconds for Base Run 6.17 – 850 psi**

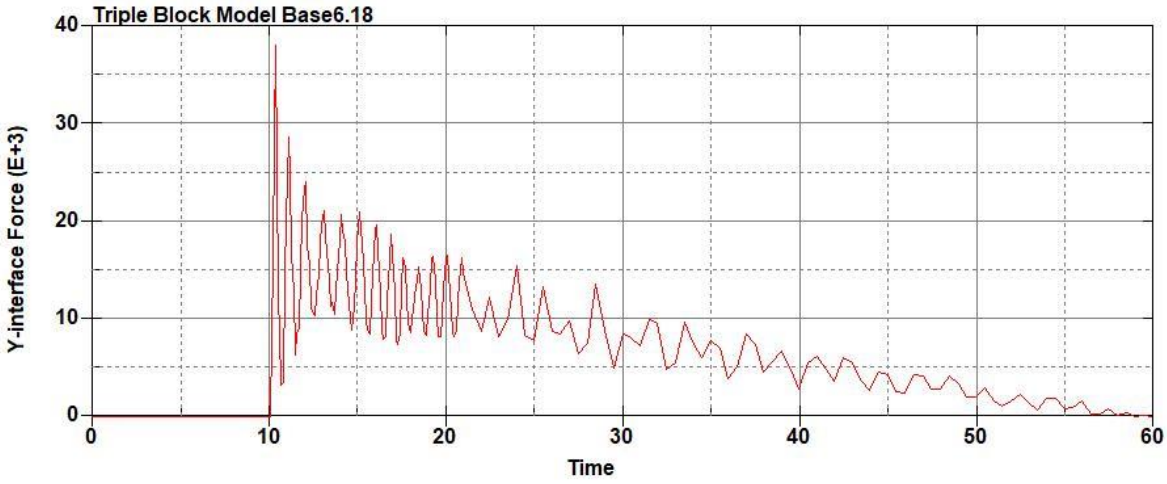


**Figure B-393: Base Run 6.18 Right Support Y-Interface Force (lbs) versus Time (ms) – 900 psi**

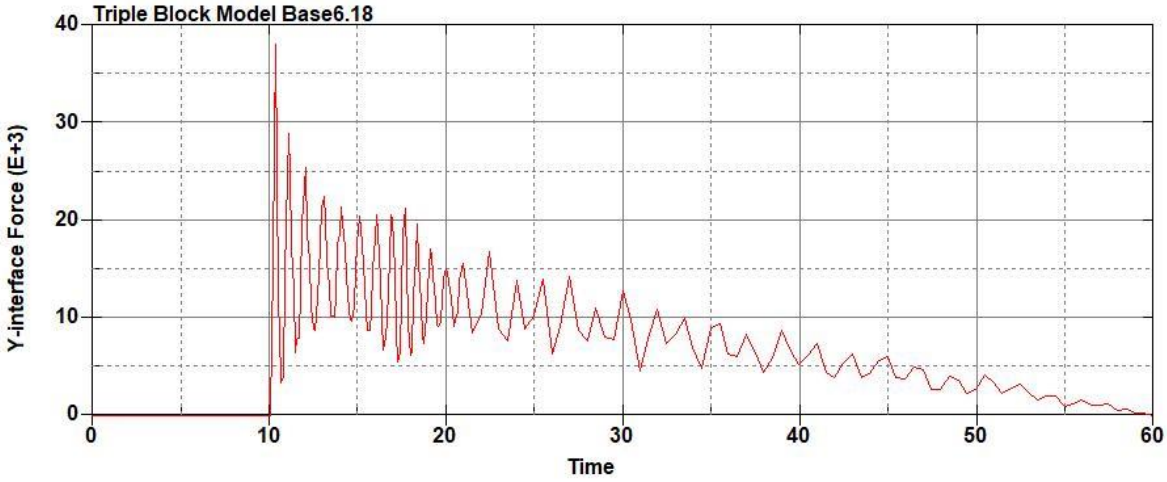


**Figure B-394: Base Run 6.18 Left Support Y-Interface Force (lbs) versus Time (ms) – 900 psi**

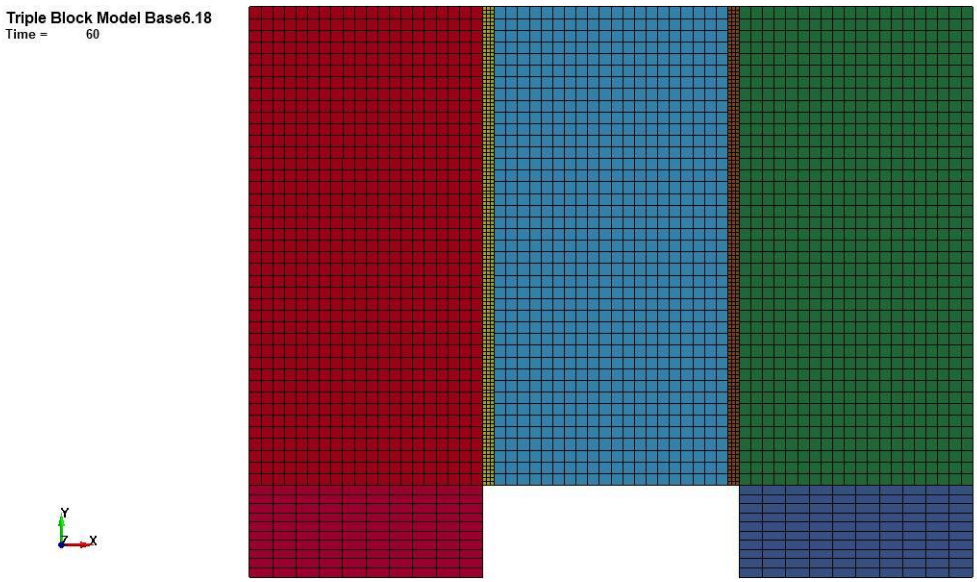


**Figure B-395: Last State at 60 Milliseconds for Base Run 6.18 – 900 psi**

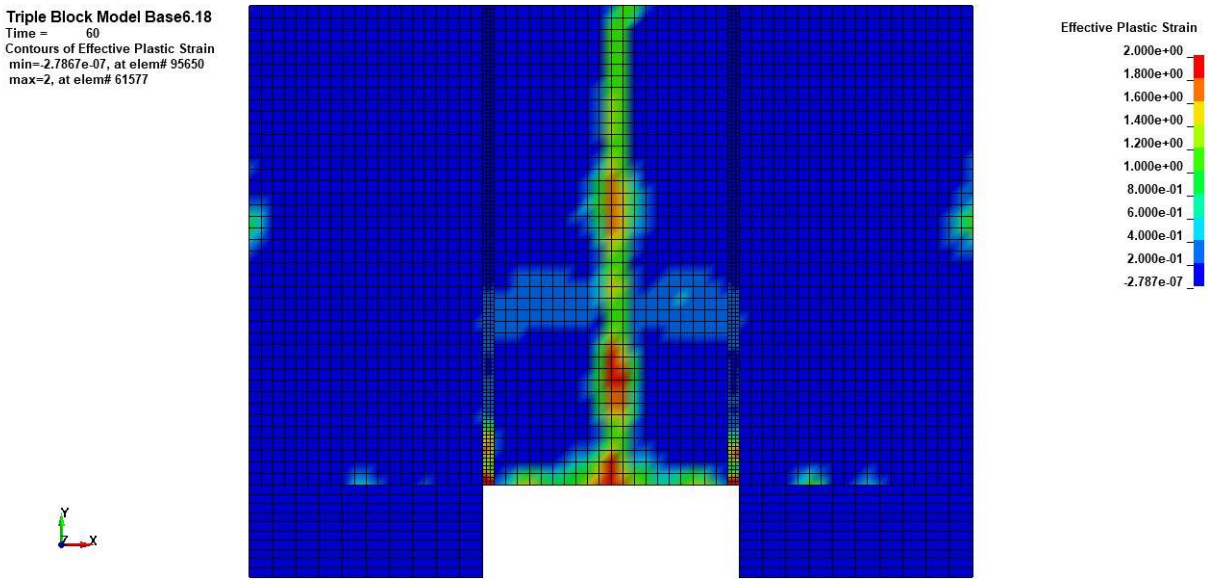


**Figure B-396: Effective Plastic Strain Fringe Plot for Last State at 60 Milliseconds for Base Run 6.18 – 900 psi**

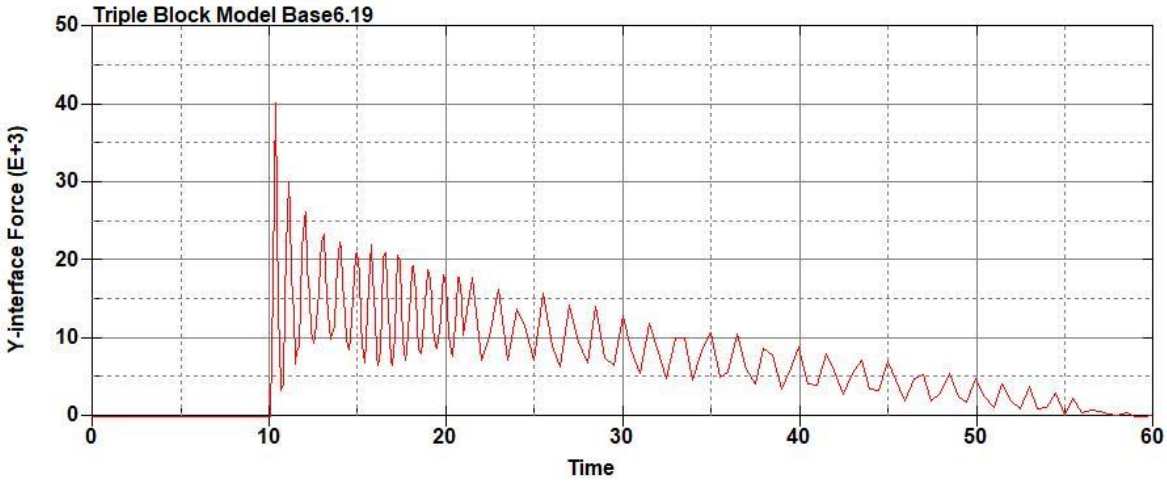


**Figure B-397: Base Run 6.19 Right Support Y-Interface Force (lbs) versus Time (ms) – 950 psi**

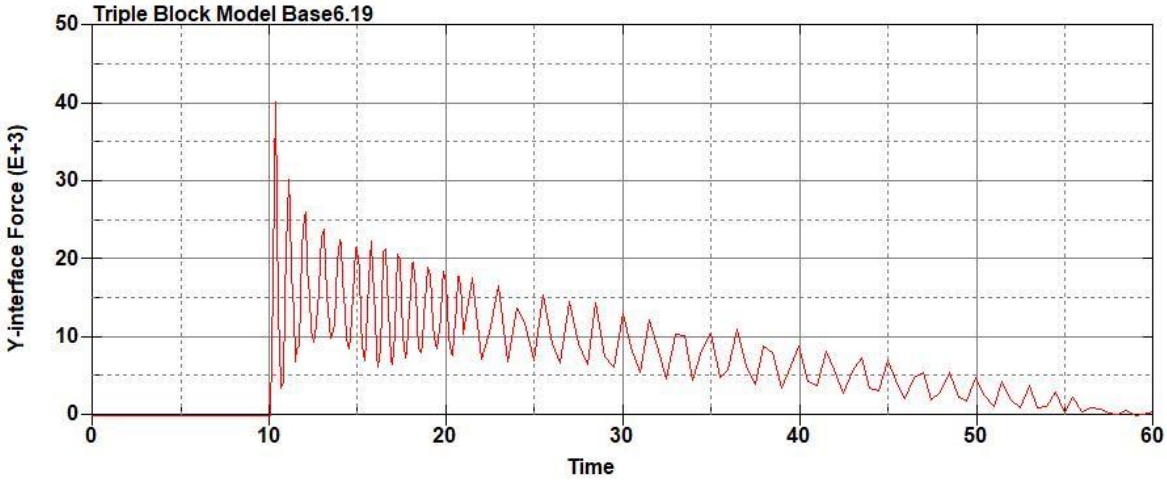


**Figure B-398: Base Run 6.19 Left Support Y-Interface Force (lbs) versus Time (ms) – 950 psi**

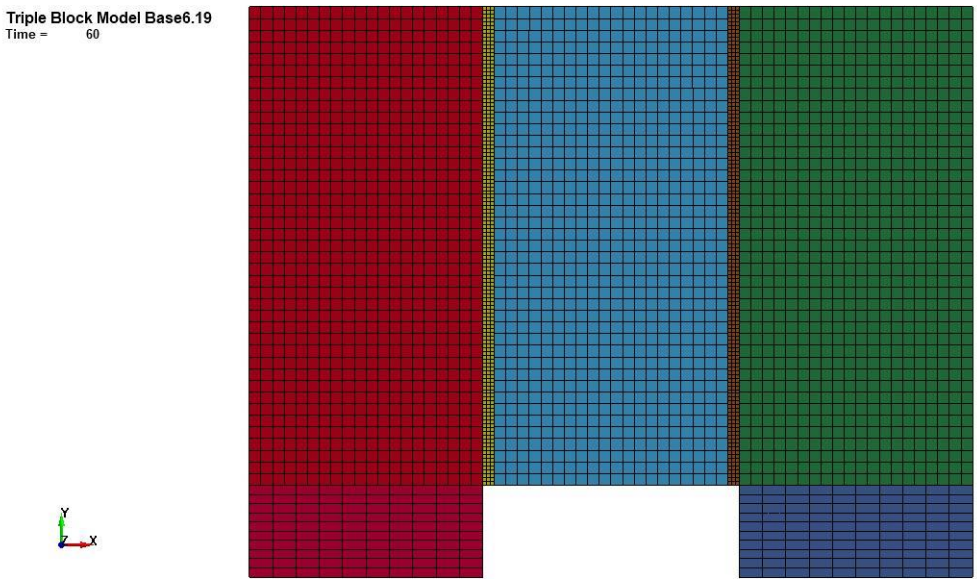


**Figure B-399: Last State at 60 Milliseconds for Base Run 6.19 – 950 psi**

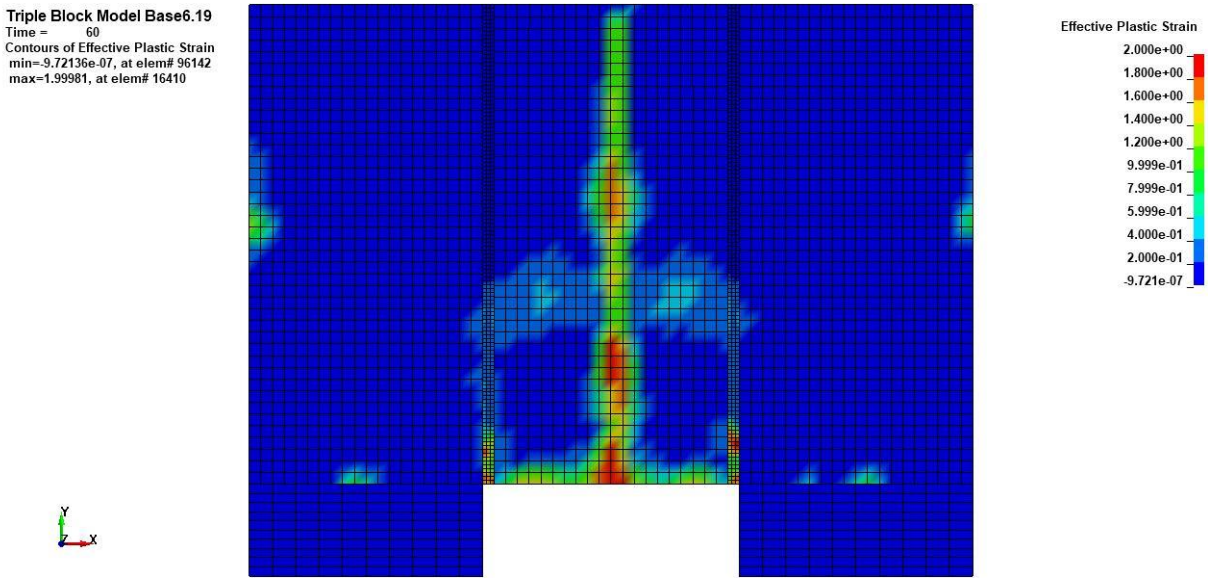


**Figure B-400: Effective Plastic Strain Fringe Plot for Last State at 60 Milliseconds for Base Run 6.19 – 950 psi**

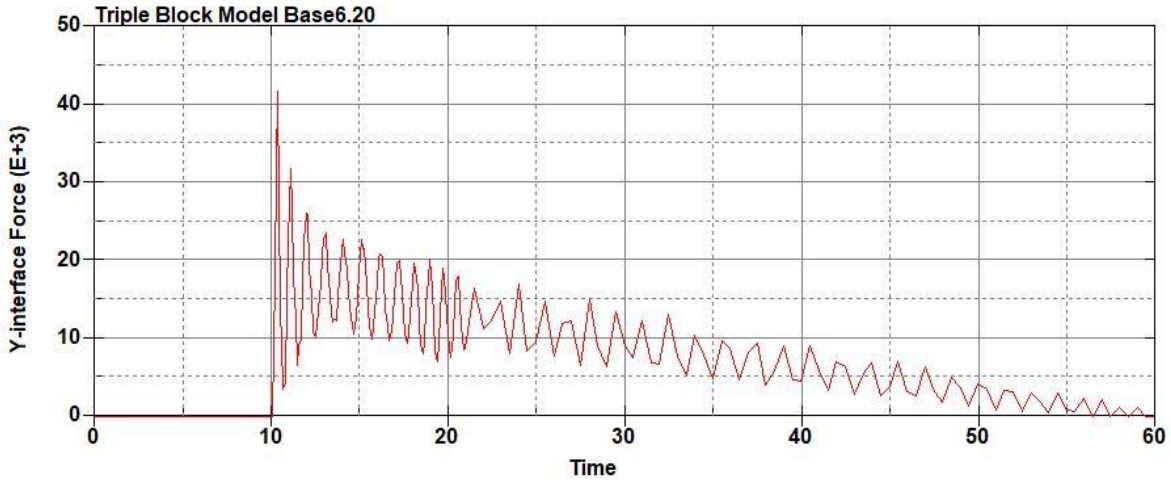


**Figure B-401: Base Run 6.20 Right Support Y-Interface Force (lbs) versus Time (ms) – 1000 psi**

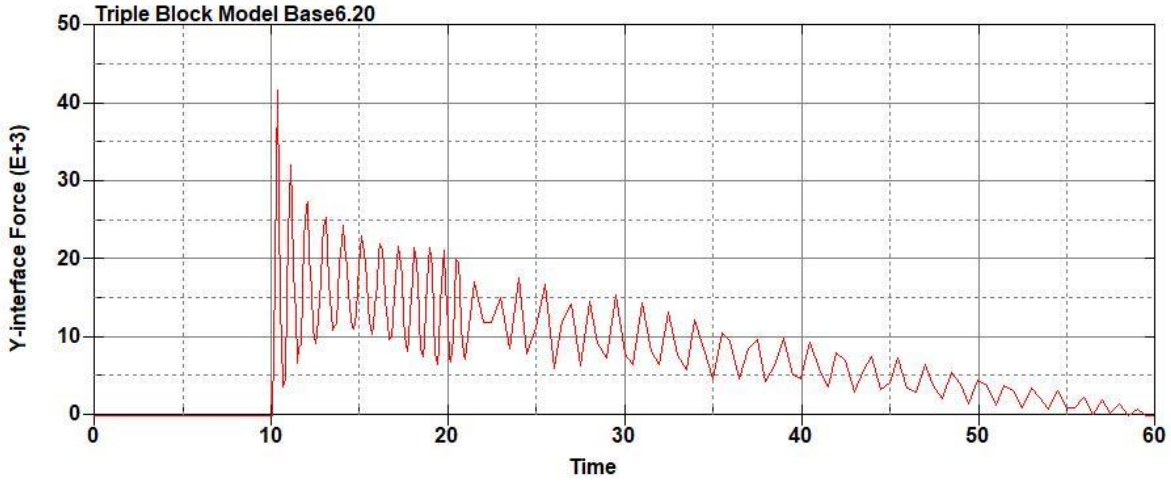


**Figure B-402: Base Run 6.20 Left Support Y-Interface Force (lbs) versus Time (ms) – 1000 psi**

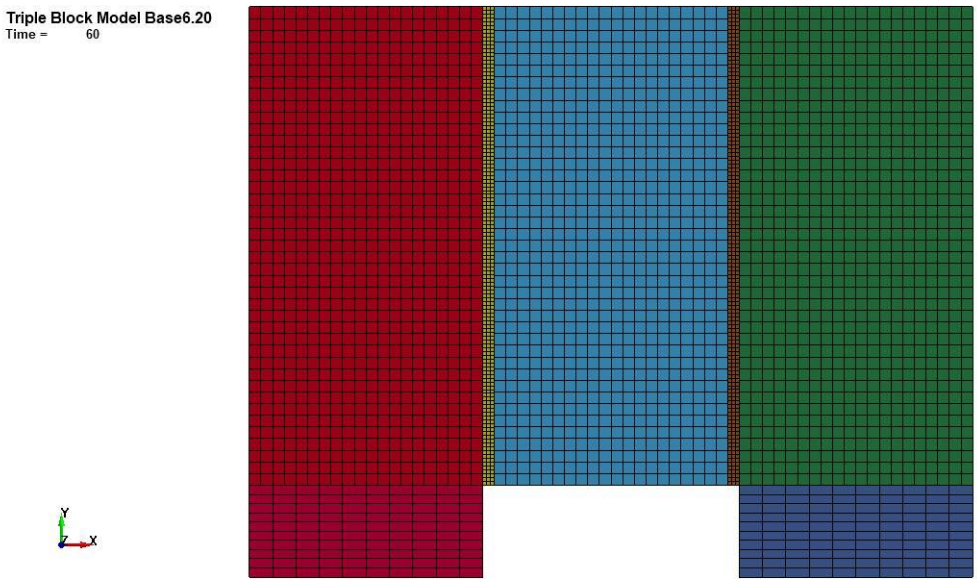


**Figure B-403: Last State at 60 Milliseconds for Base Run 6.20 – 1000 psi**

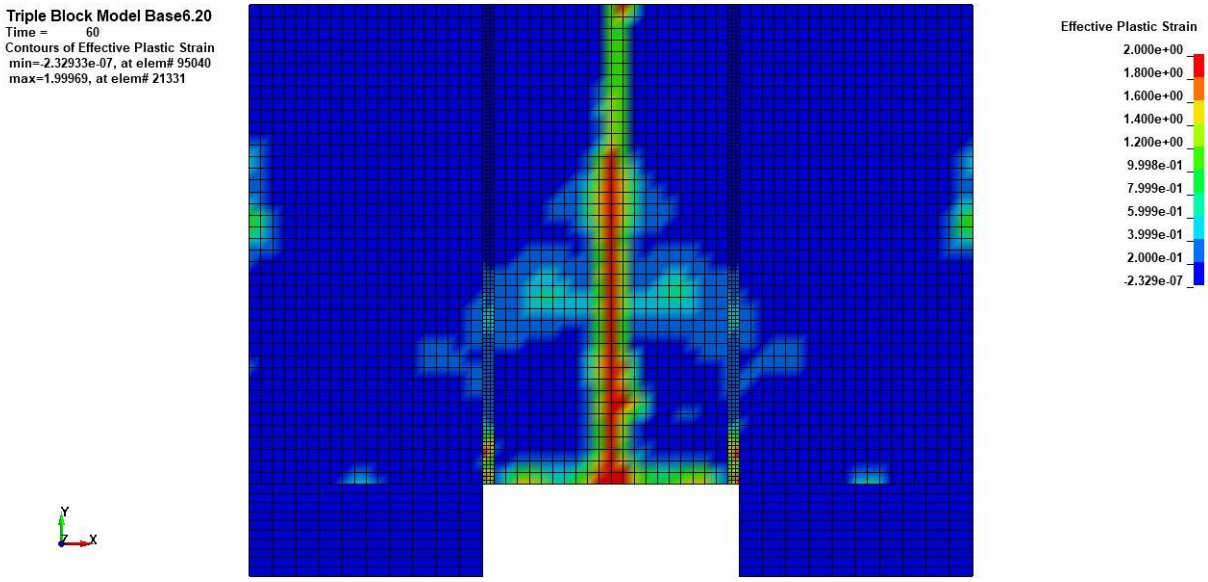


**Figure B-404: Effective Plastic Strain Fringe Plot for Last State at 60 Milliseconds for Base Run 6.20 – 1000 psi**

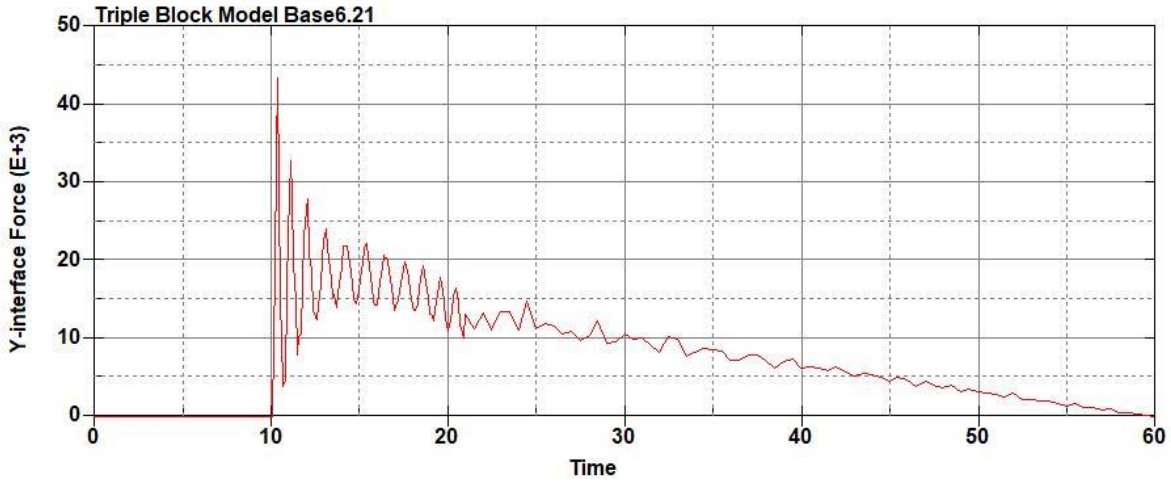


**Figure B-405: Base Run 6.21 Right Support Y-Interface Force (lbs) versus Time (ms) – 1050 psi**

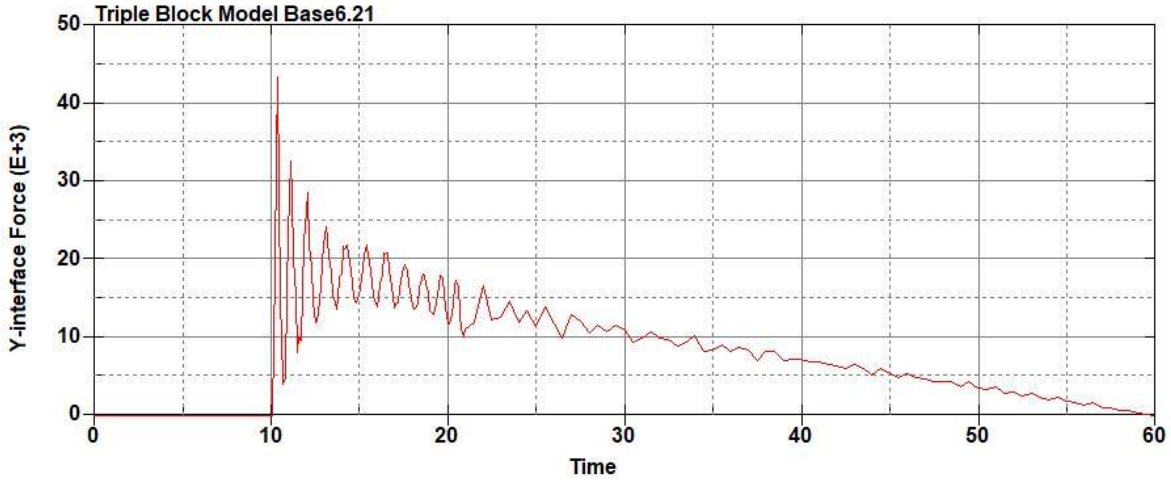


**Figure B-406: Base Run 6.21 Left Support Y-Interface Force (lbs) versus Time (ms) – 1050 psi**

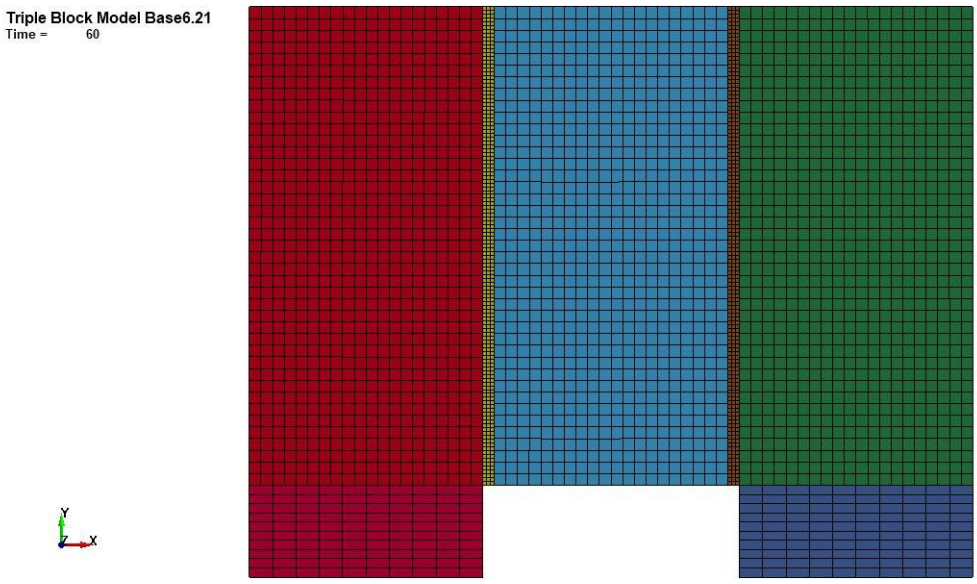


**Figure B-407: Last State at 60 Milliseconds for Base Run 6.21 – 1050 psi**

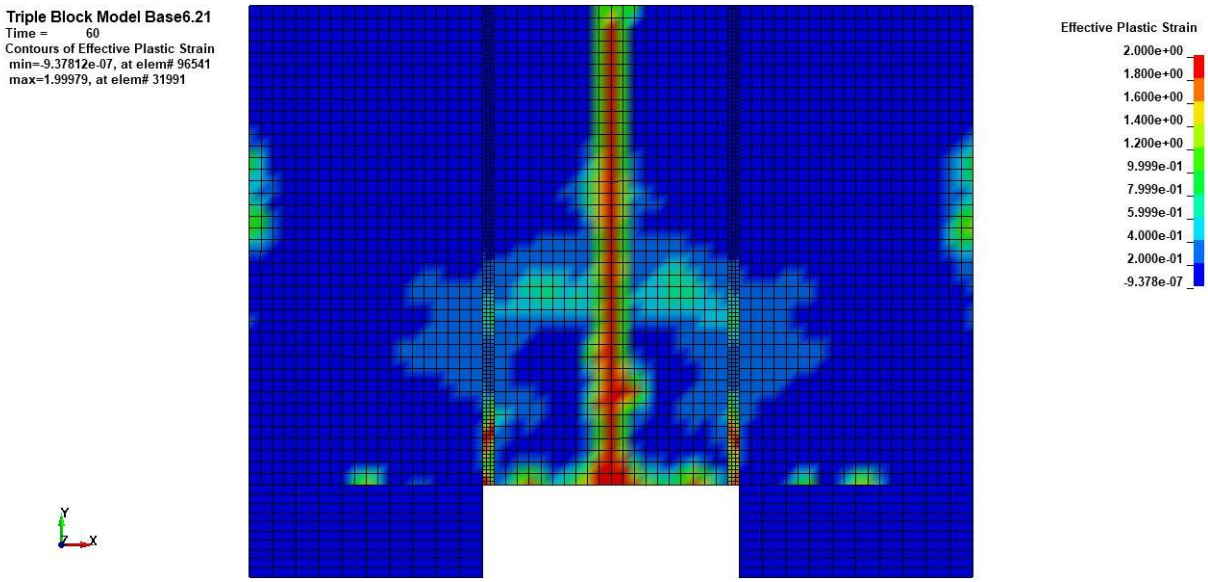


**Figure B-408: Effective Plastic Strain Fringe Plot for Last State at 60 Milliseconds for Base Run 6.21 – 1050 psi**

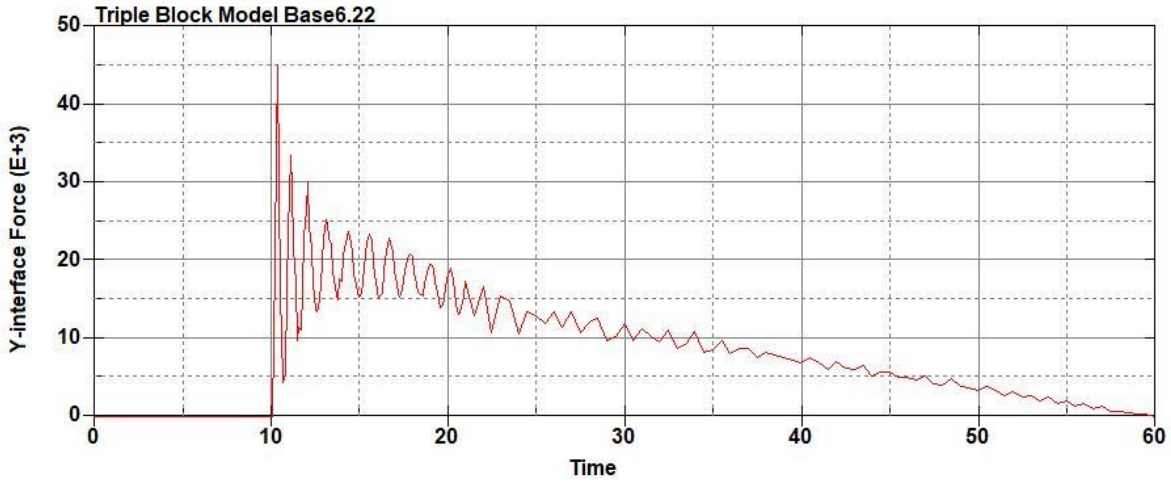


**Figure B-409: Base Run 6.22 Right Support Y-Interface Force (lbs) versus Time (ms) – 1100 psi**

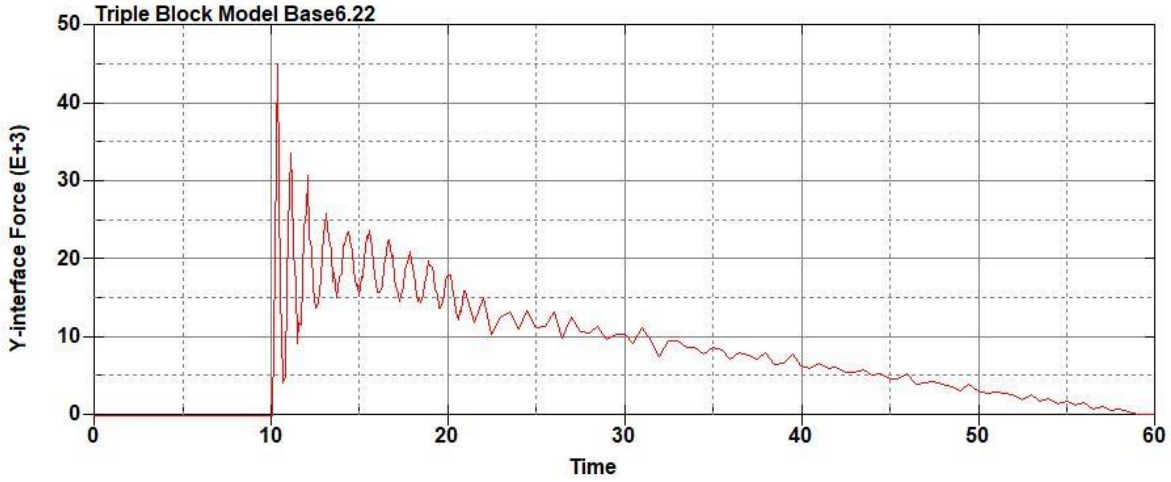


**Figure B-410: Base Run 6.22 Left Support Y-Interface Force (lbs) versus Time (ms) – 1100 psi**

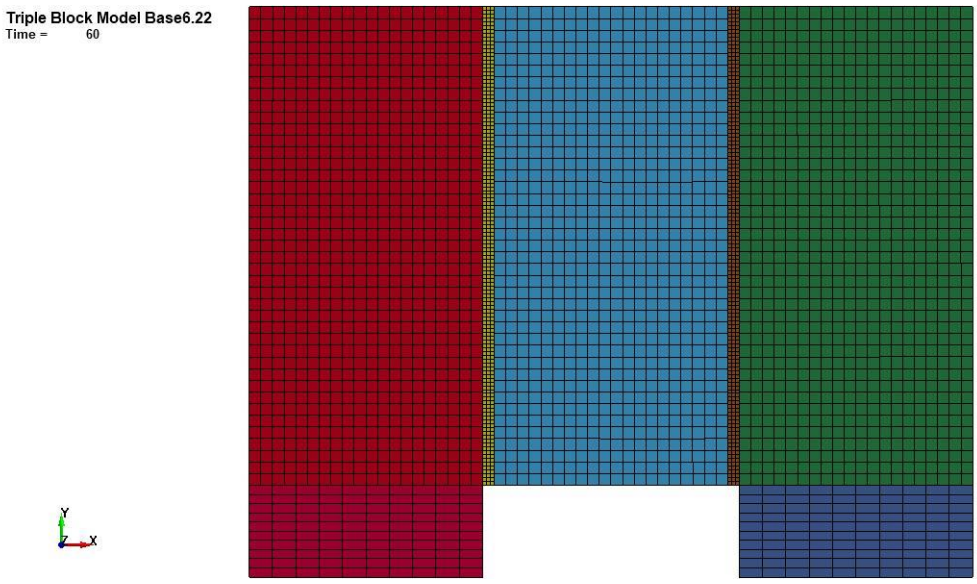


**Figure B-411: Last State at 60 Milliseconds for Base Run 6.22 – 1100 psi**

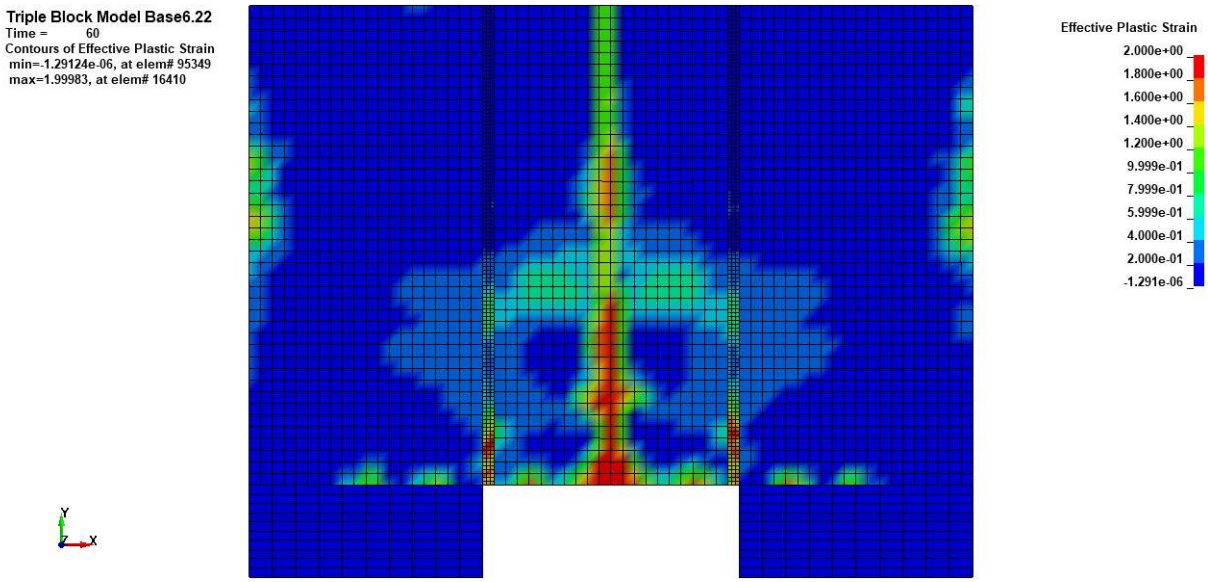


**Figure B-412: Effective Plastic Strain Fringe Plot for Last State at 60 Milliseconds for Base Run 6.22 – 1100 psi**

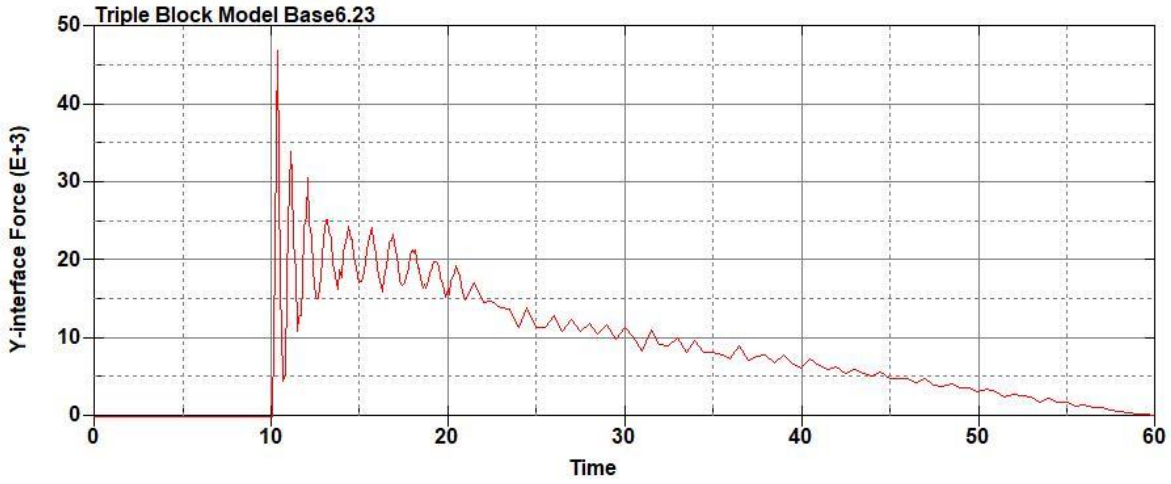


**Figure B-413: Base Run 6.23 Right Support Y-Interface Force (lbs) versus Time (ms) – 1150 psi**

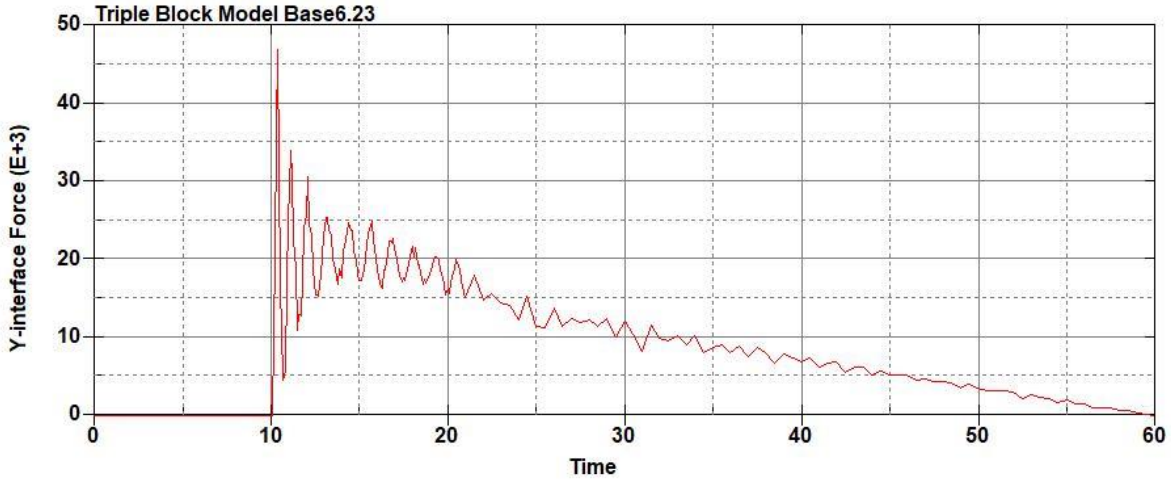


**Figure B-414: Base Run 6.23 Left Support Y-Interface Force (lbs) versus Time (ms) – 1150 psi**

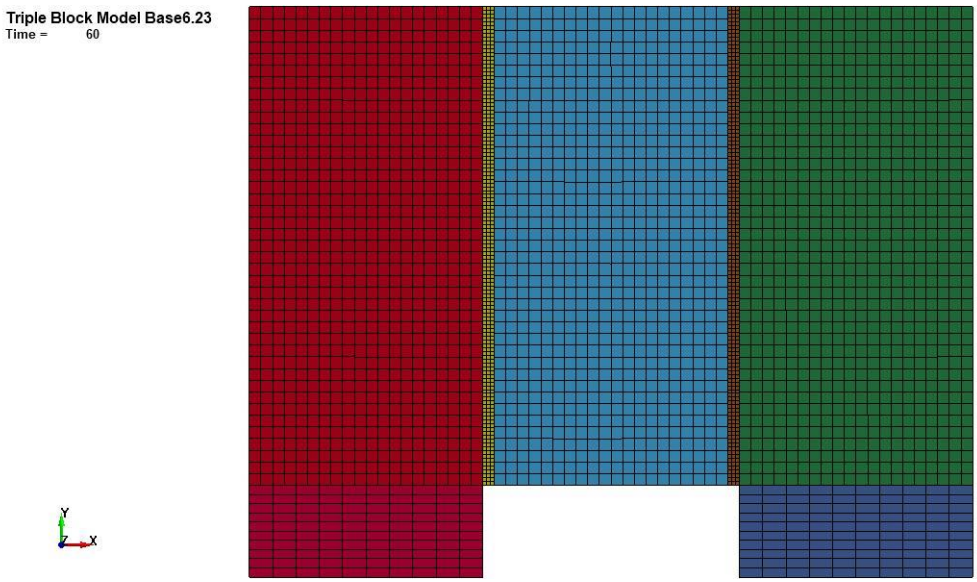


**Figure B-415: Last State at 60 Milliseconds for Base Run 6.23 – 1150 psi**

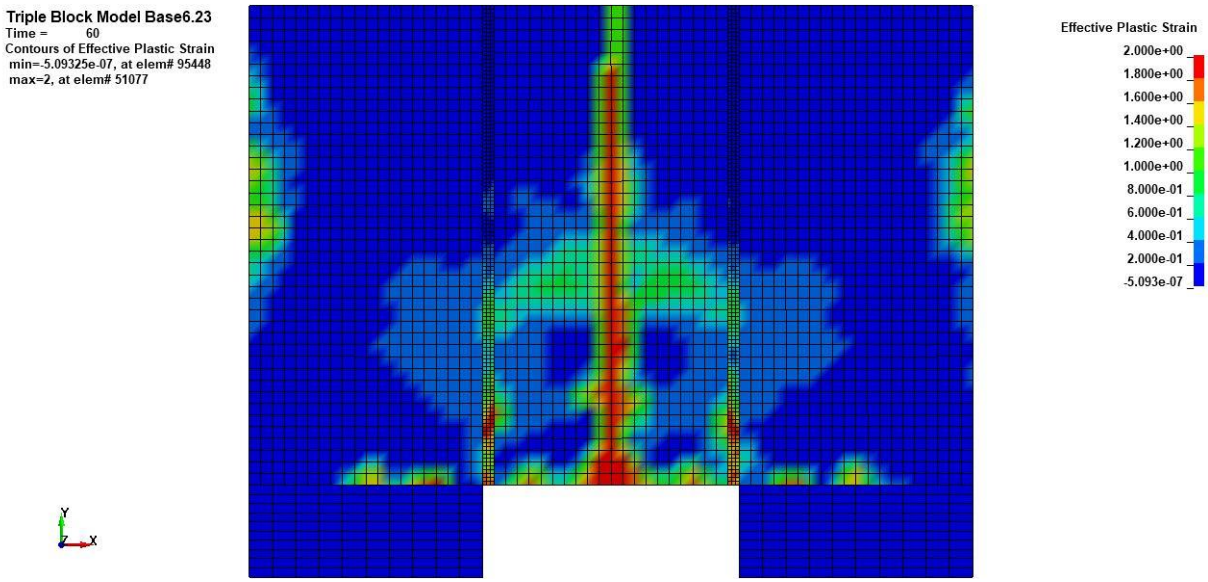


**Figure B-416: Effective Plastic Strain Fringe Plot for Last State at 60 Milliseconds for Base Run 6.23 – 1150 psi**

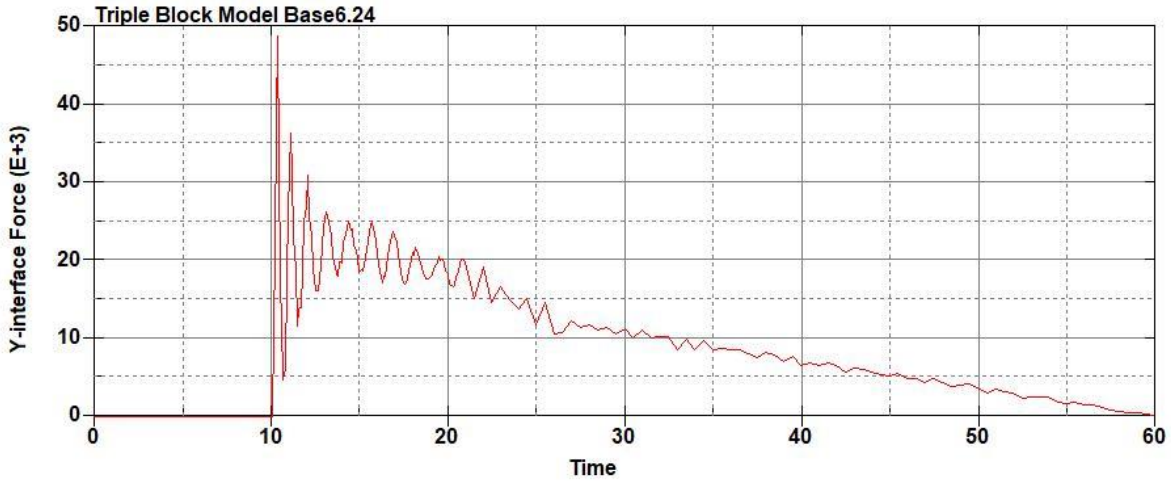


**Figure B-417: Base Run 6.24 Right Support Y-Interface Force (lbs) versus Time (ms) – 1200 psi**

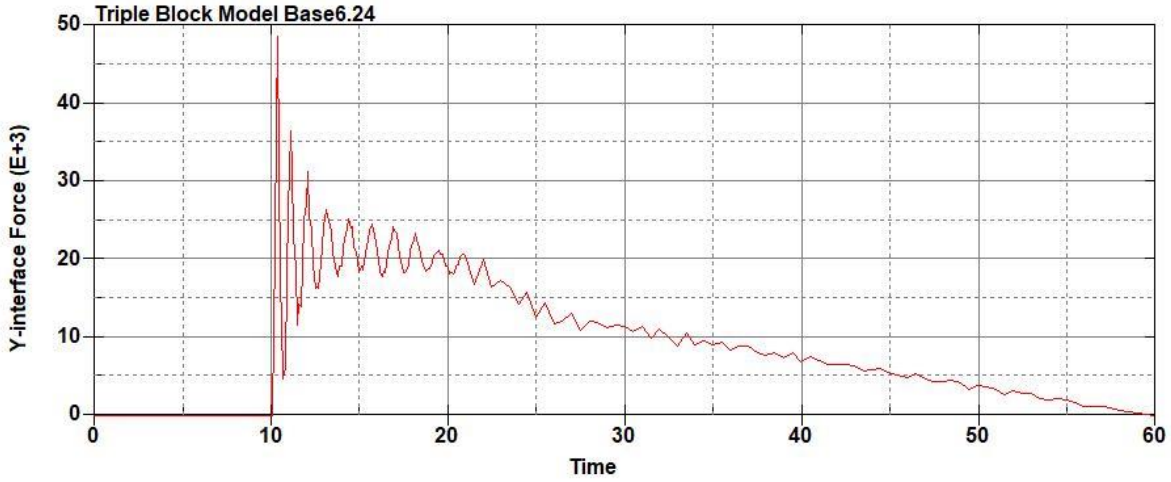


**Figure B-418: Base Run 6.24 Left Support Y-Interface Force (lbs) versus Time (ms) – 1200 psi**

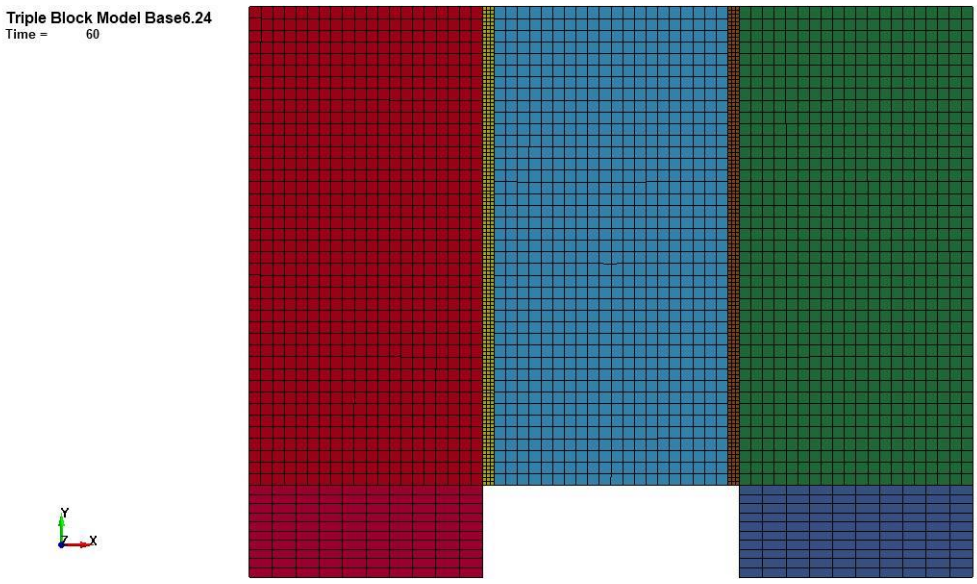


**Figure B-419: Last State at 60 Milliseconds for Base Run 6.24 – 1200 psi**

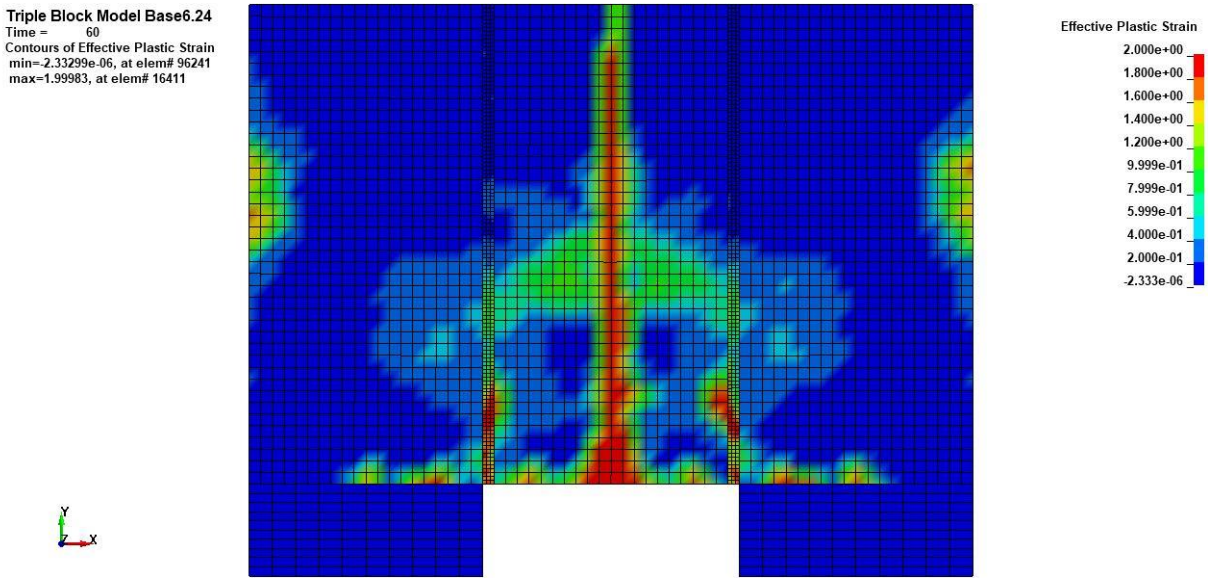


**Figure B-420: Effective Plastic Strain Fringe Plot for Last State at 60 Milliseconds for Base Run 6.24 – 1200 psi**

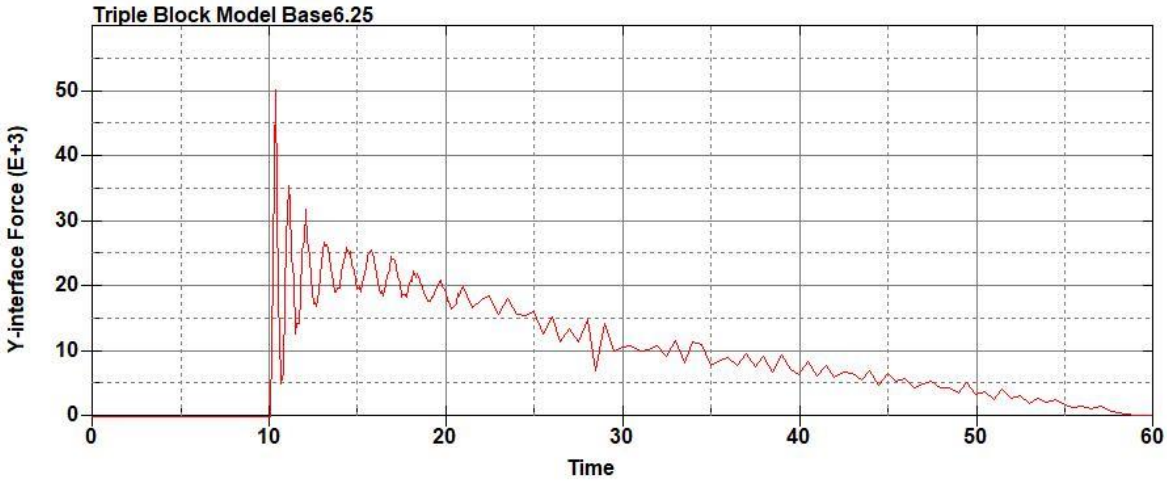


**Figure B-421: Base Run 6.25 Right Support Y-Interface Force (lbs) versus Time (ms) – 1250 psi**

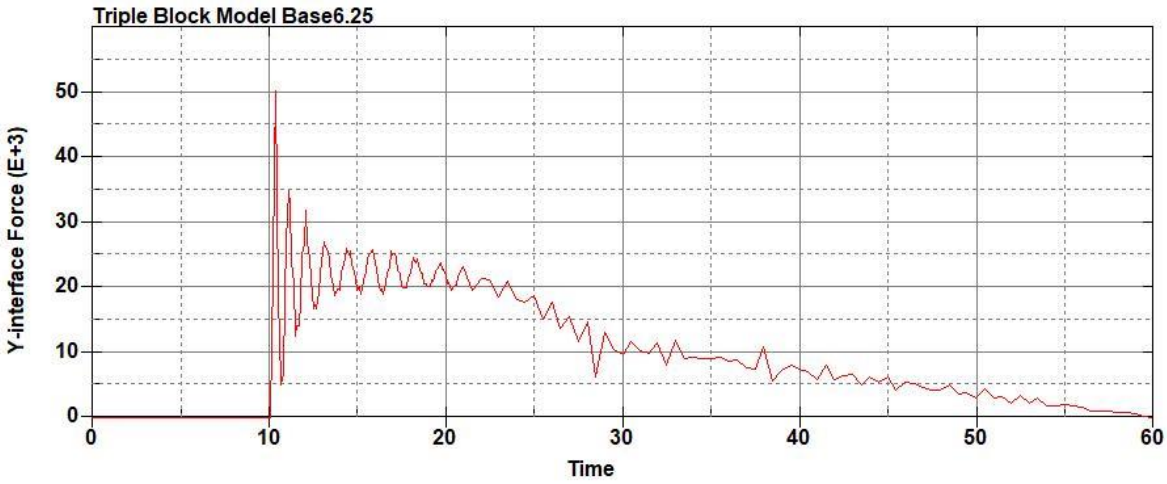


**Figure B-422: Base Run 6.25 Left Support Y-Interface Force (lbs) versus Time (ms) – 1250 psi**

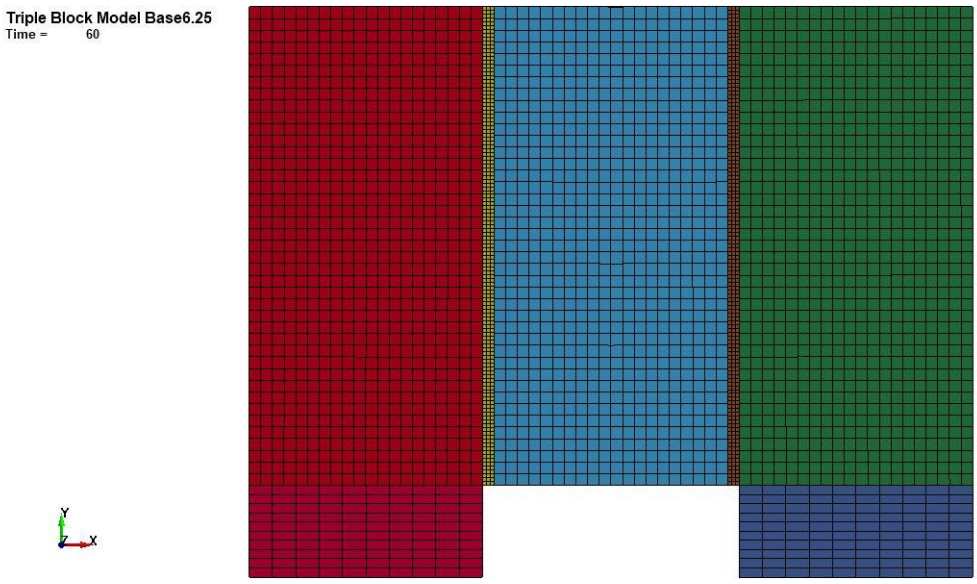


**Figure B-423: Last State at 60 Milliseconds for Base Run 6.25 – 1250 psi**

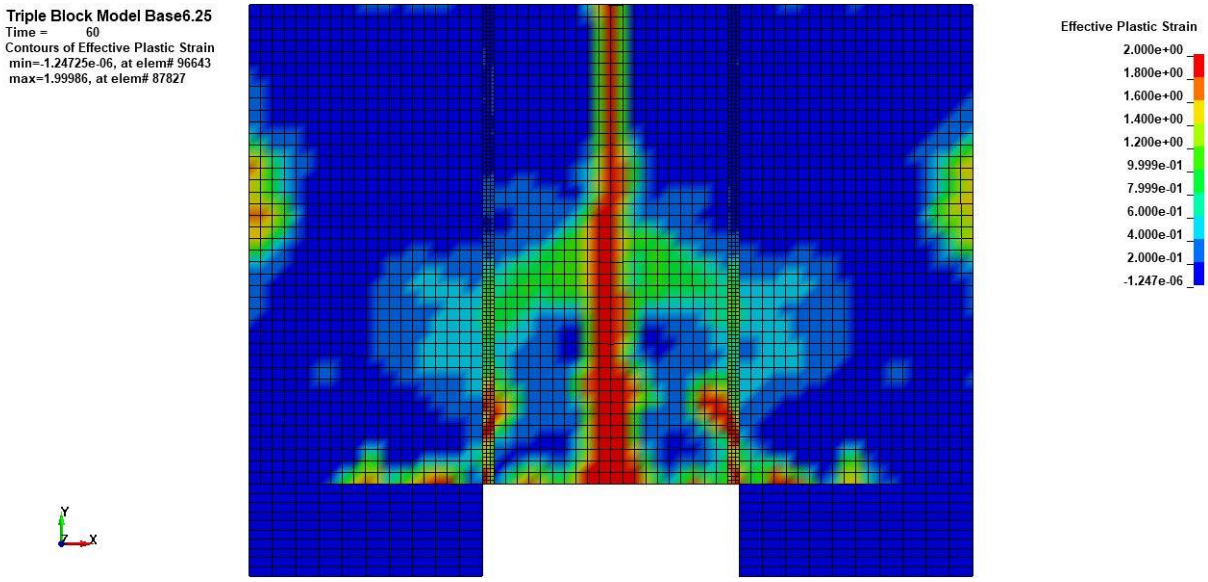


**Figure B-424: Effective Plastic Strain Fringe Plot for Last State at 60 Milliseconds for Base Run 6.25 – 1250 psi**

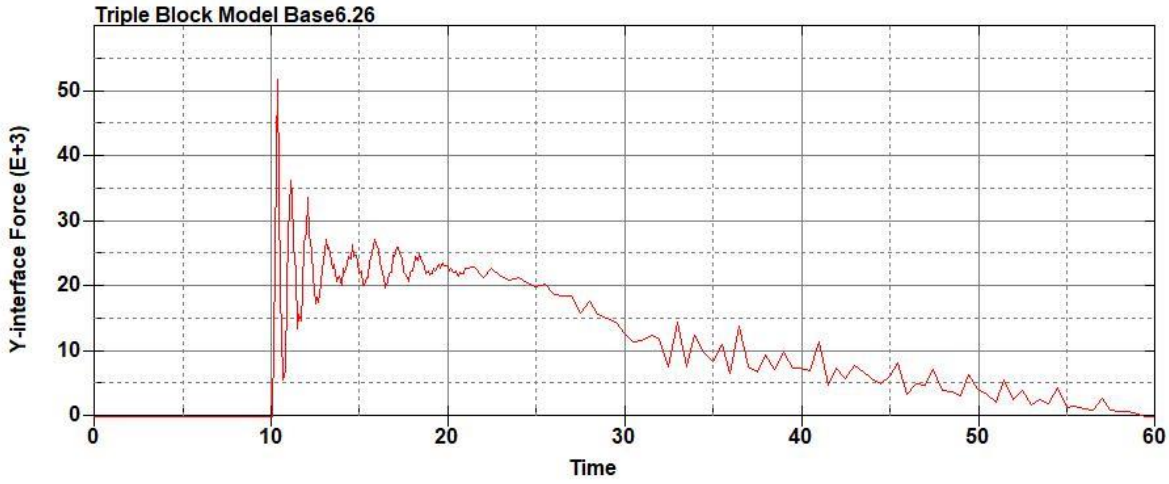


**Figure B-425: Base Run 6.26 Right Support Y-Interface Force (lbs) versus Time (ms) – 1300 psi**

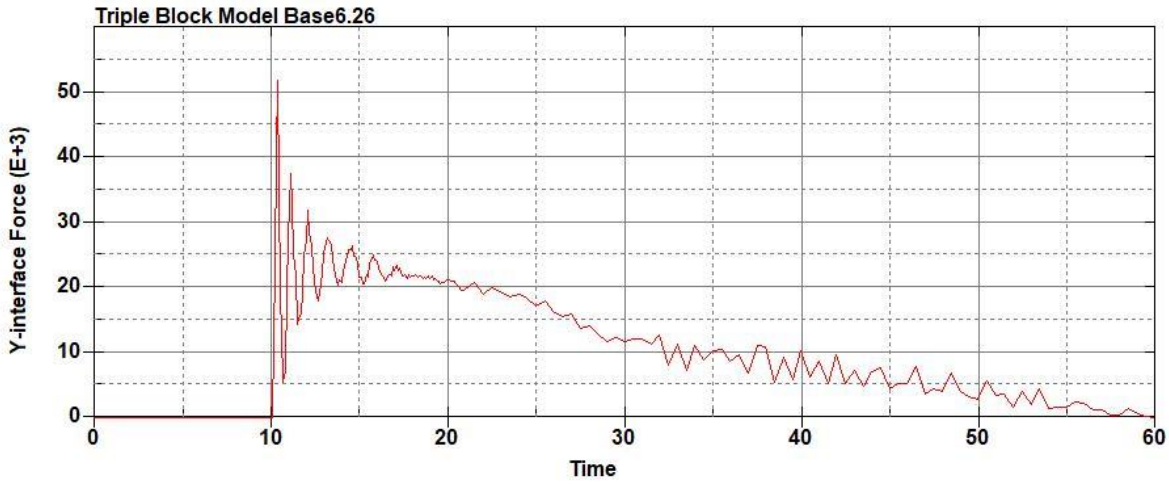


**Figure B-426: Base Run 6.26 Left Support Y-Interface Force (lbs) versus Time (ms) – 1300 psi**

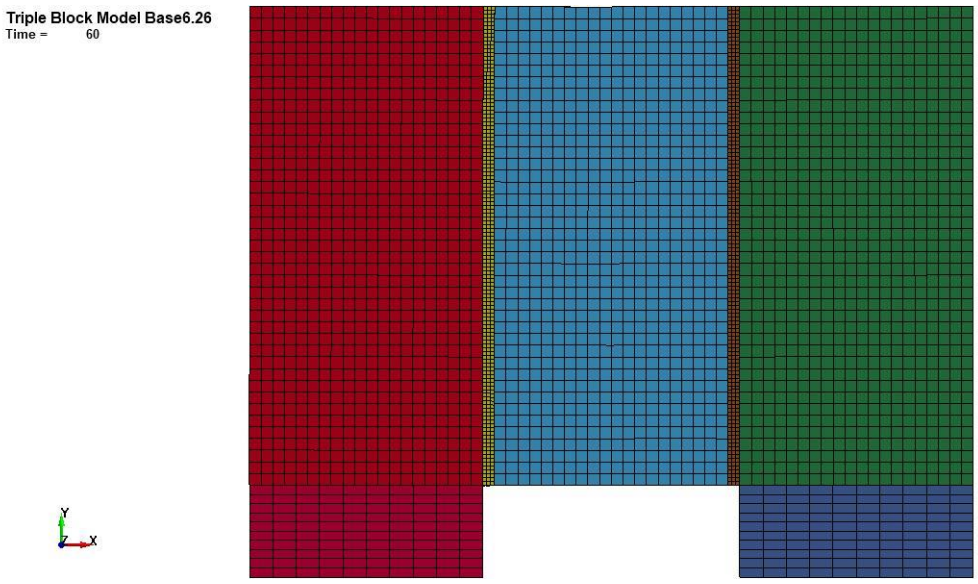


**Figure B-427: Last State at 60 Milliseconds for Base Run 6.26 – 1300 psi**

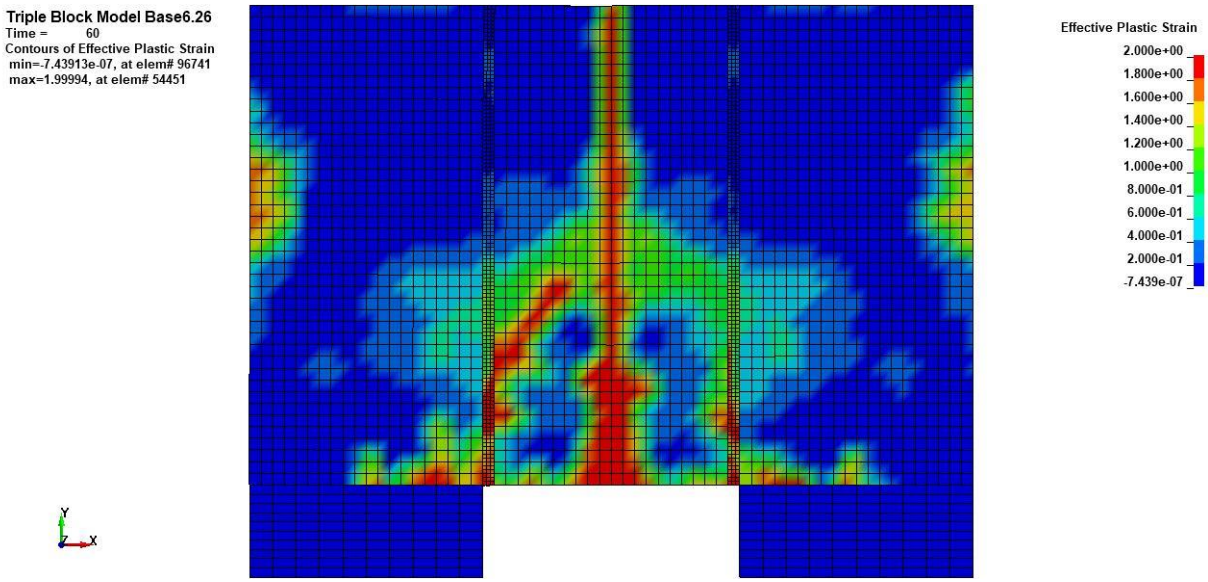


**Figure B-428: Effective Plastic Strain Fringe Plot for Last State at 60 Milliseconds for Base Run 6.26 – 1300 psi**

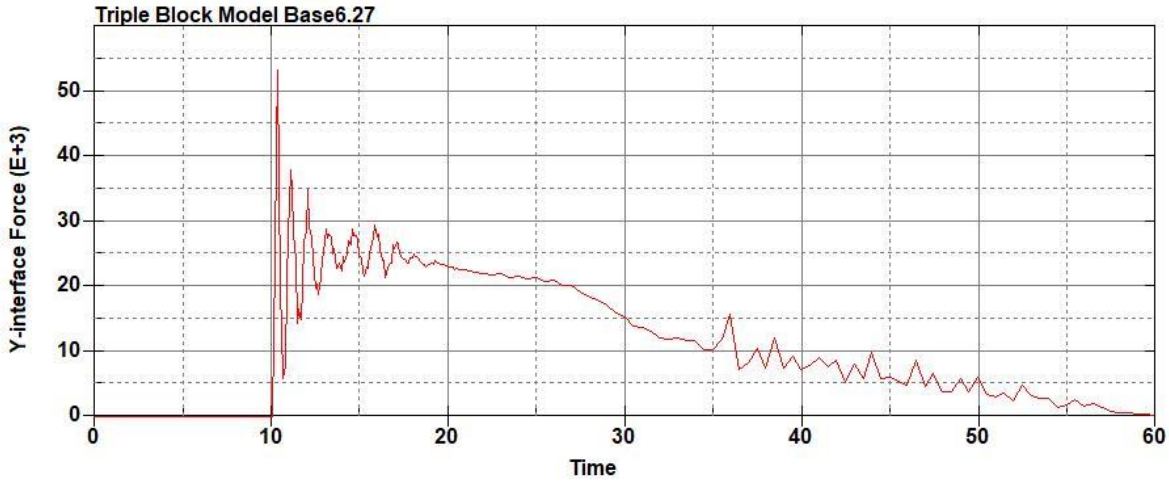


**Figure B-429: Base Run 6.27 Right Support Y-Interface Force (lbs) versus Time (ms) – 1350 psi**

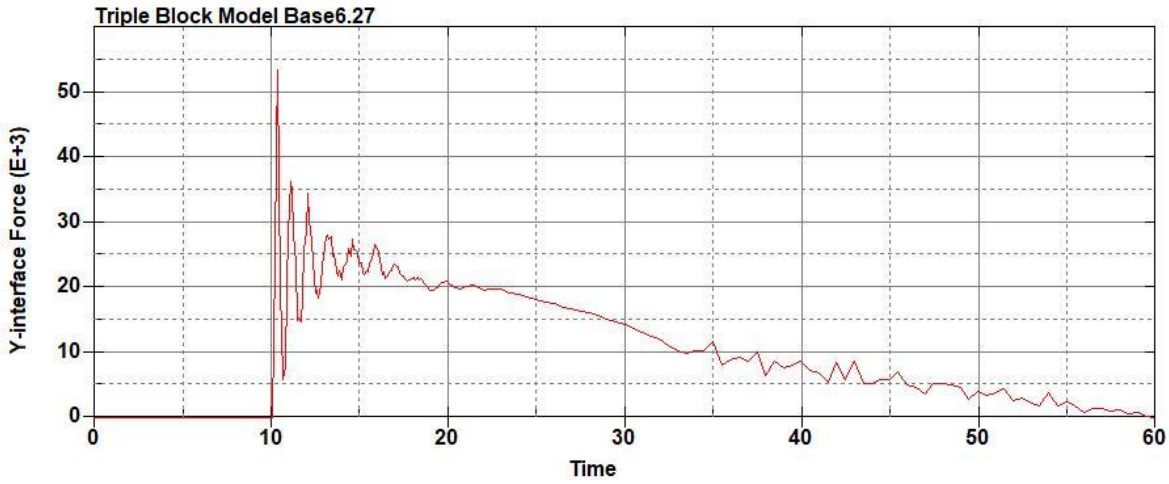


**Figure B-430: Base Run 6.27 Left Support Y-Interface Force (lbs) versus Time (ms) – 1350 psi**

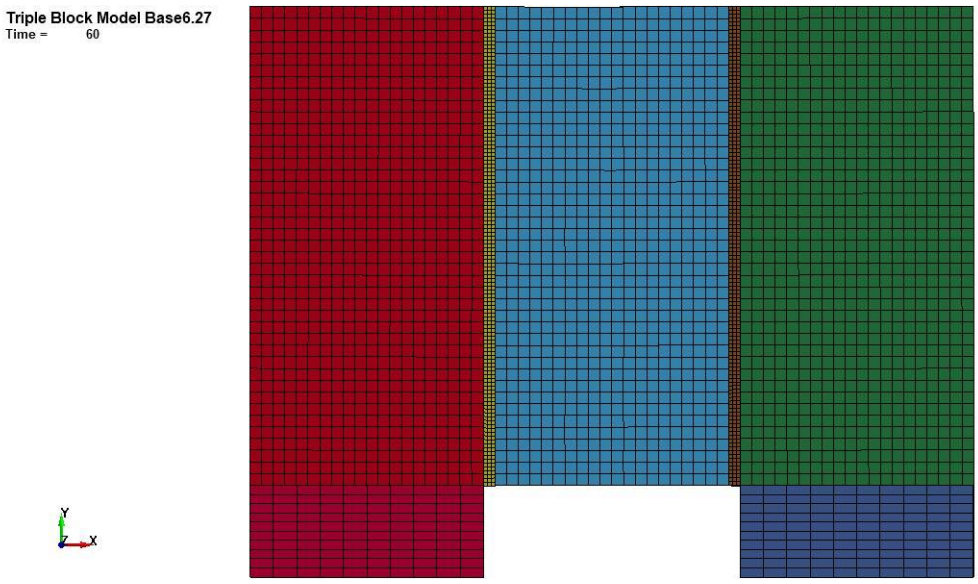


**Figure B-431: Last State at 60 Milliseconds for Base Run 6.27 – 1350 psi**

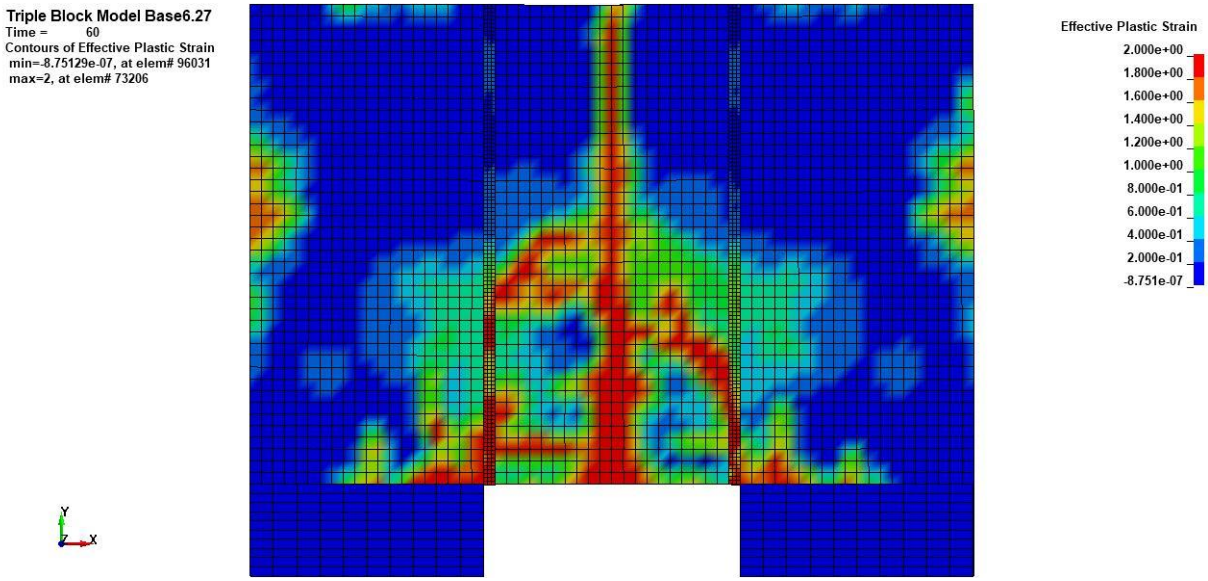


**Figure B-432: Effective Plastic Strain Fringe Plot for Last State at 60 Milliseconds for Base Run 6.27 – 1350 psi**

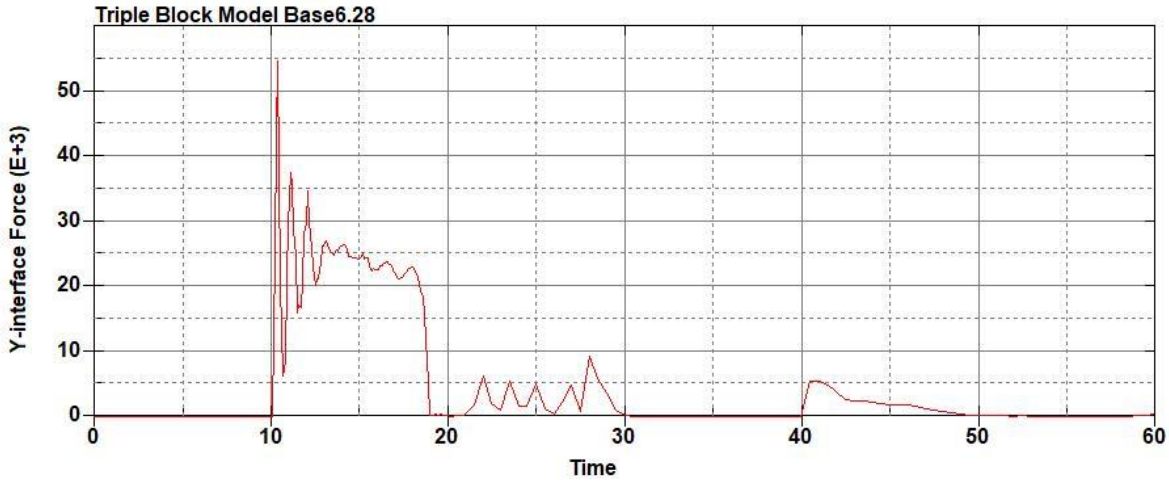


**Figure B-433: Base Run 6.28 Right Support Y-Interface Force (lbs) versus Time (ms) – 1400 psi**

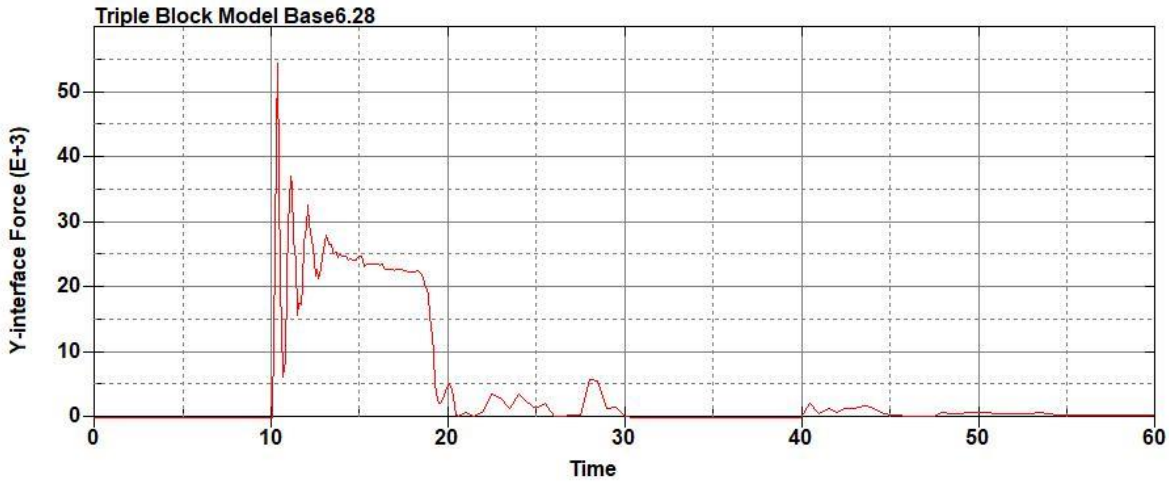


**Figure B-434: Base Run 6.28 Left Support Y-Interface Force (lbs) versus Time (ms) – 1400 psi**

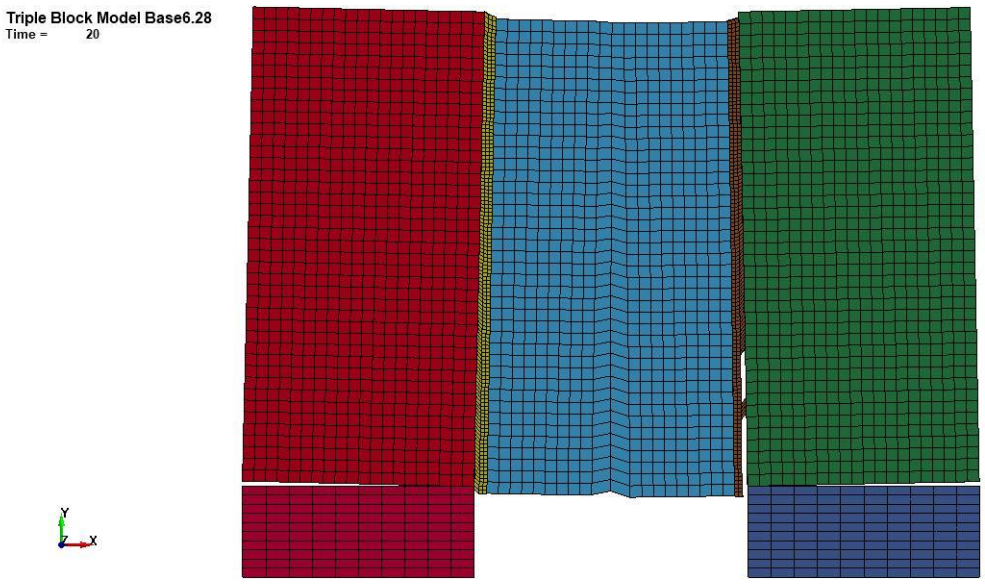


**Figure B-435: Last State at 20 Milliseconds for Base Run 6.28 – 1400 psi**

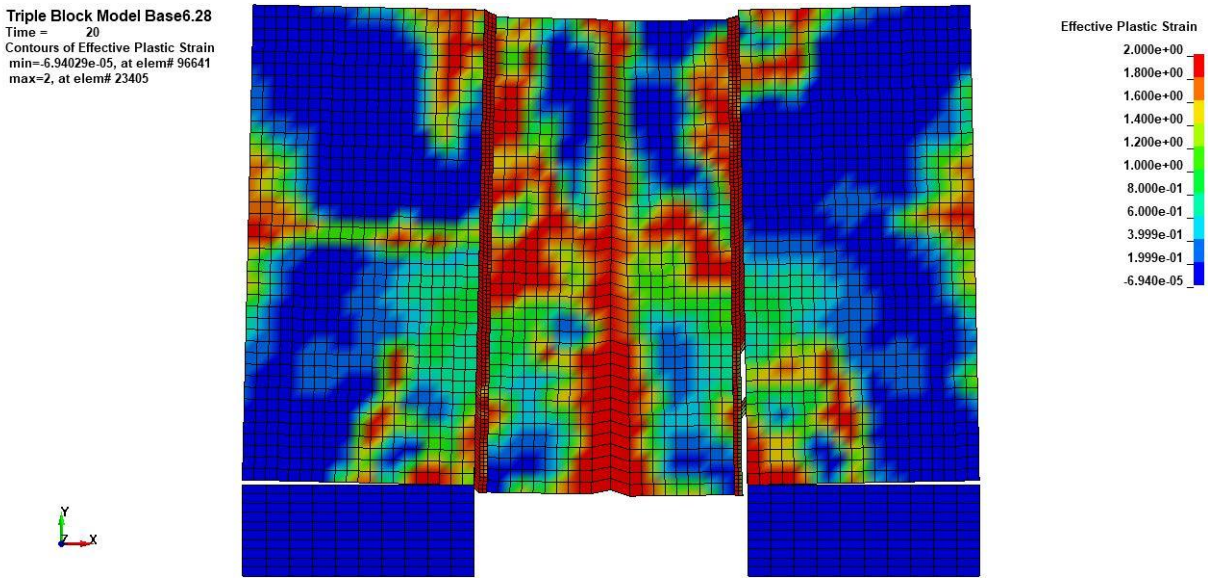


**Figure B-436: Effective Plastic Strain Fringe Plot for Last State at 20 Milliseconds for Base Run 6.28 – 1400 psi**

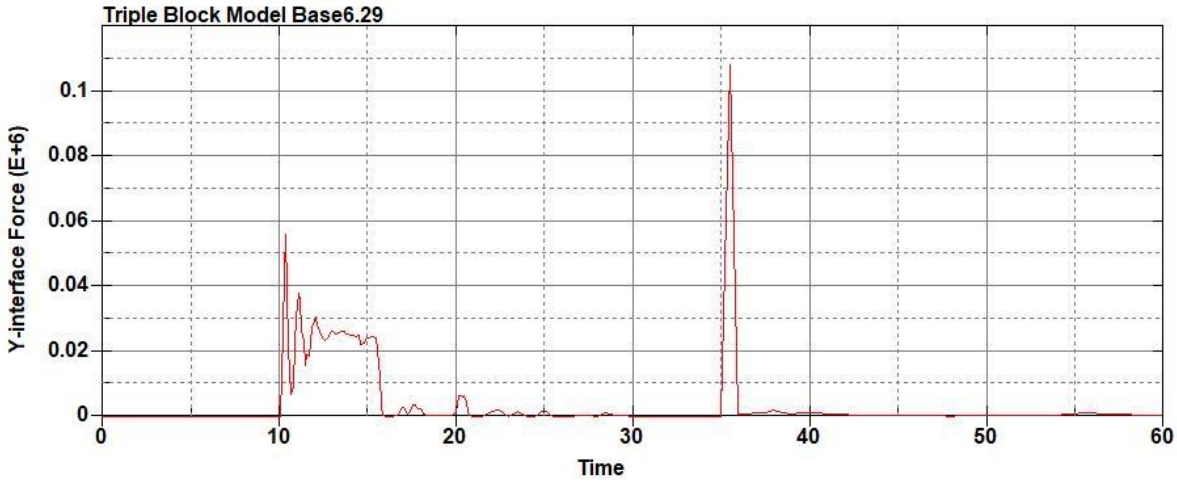


**Figure B-437: Base Run 6.29 Right Support Y-Interface Force (lbs) versus Time (ms) – 1450 psi**

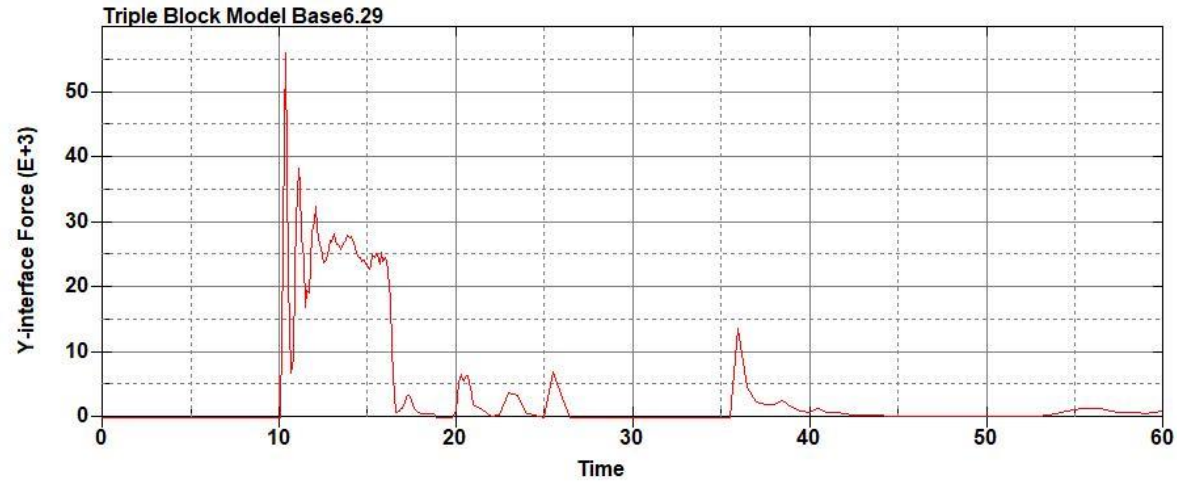


**Figure B-438: Base Run 6.29 Left Support Y-Interface Force (lbs) versus Time (ms) – 1450 psi**

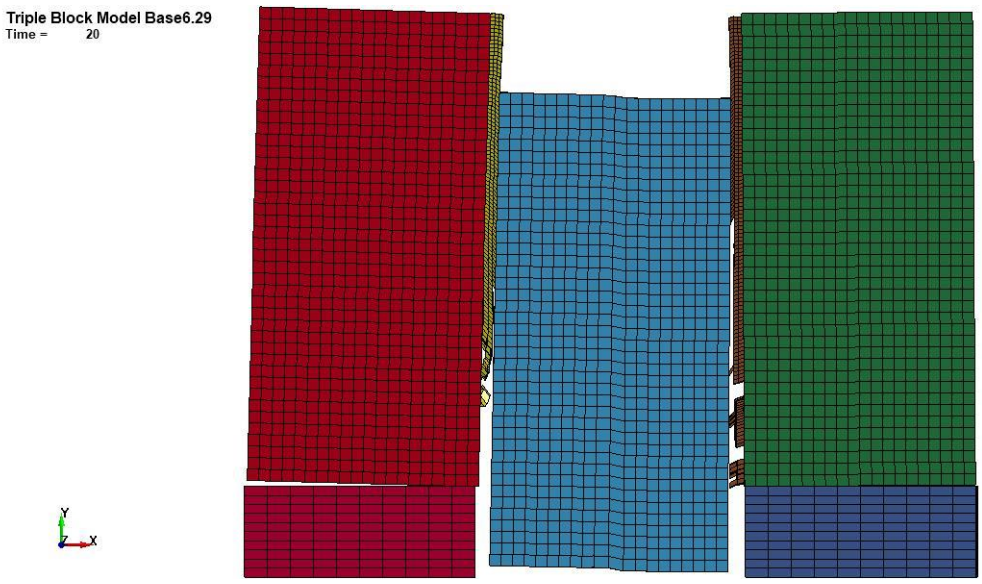


**Figure B-439: Last State at 20 Milliseconds for Base Run 6.29 – 1450 psi**

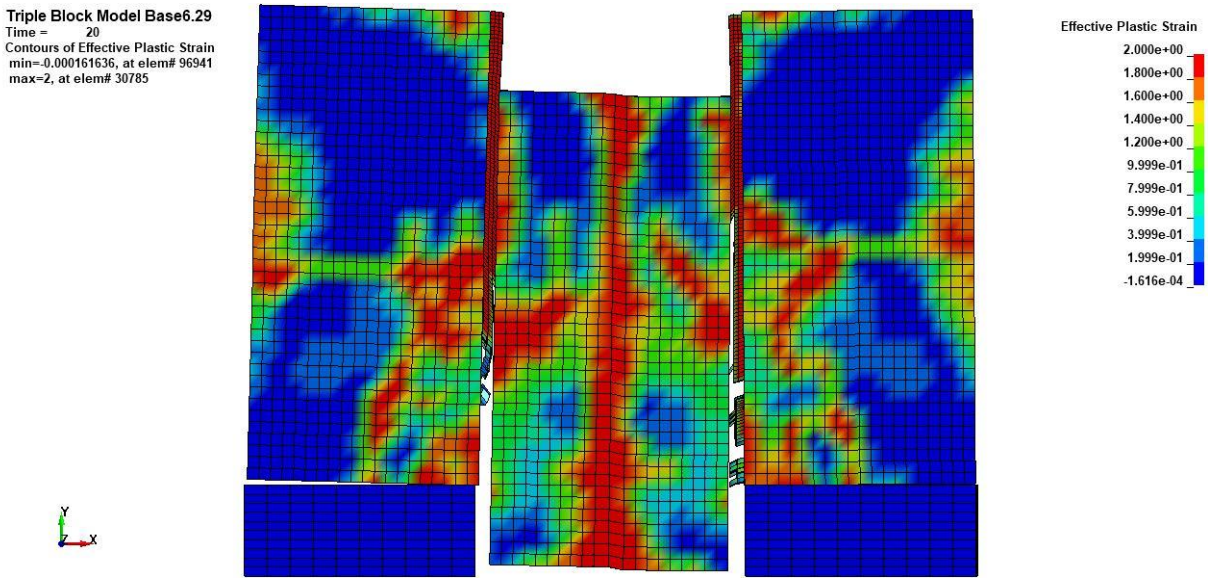


**Figure B-440: Effective Plastic Strain Fringe Plot for Last State at 20 Milliseconds for Base Run 6.29 – 1450 psi**

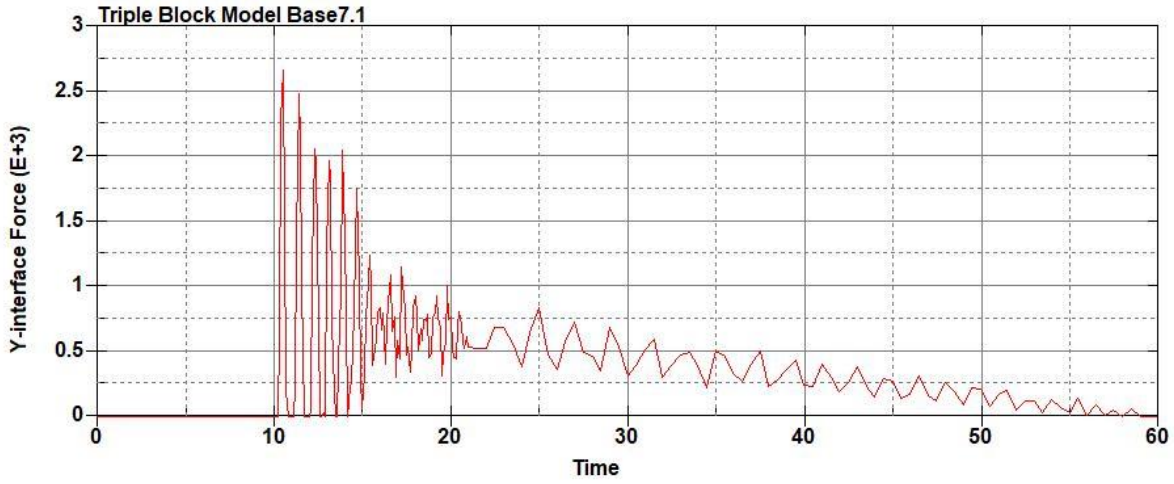


**Figure B-441: Base Run 7.1 Right Support Y-Interface Force (lbs) versus Time (ms) – 50 psi**

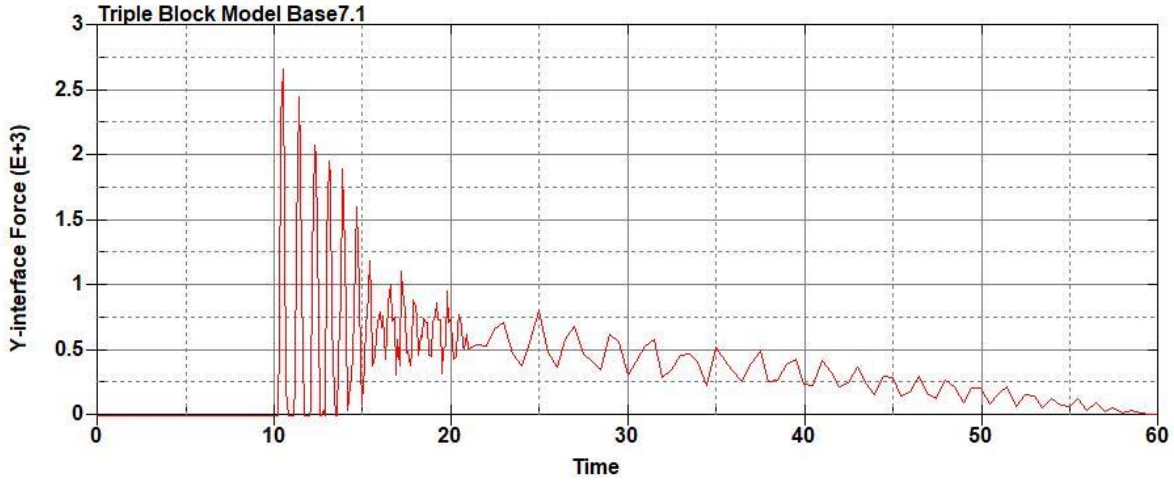


**Figure B-442: Base Run 7.1 Left Support Y-Interface Force (lbs) versus Time (ms) – 50 psi**

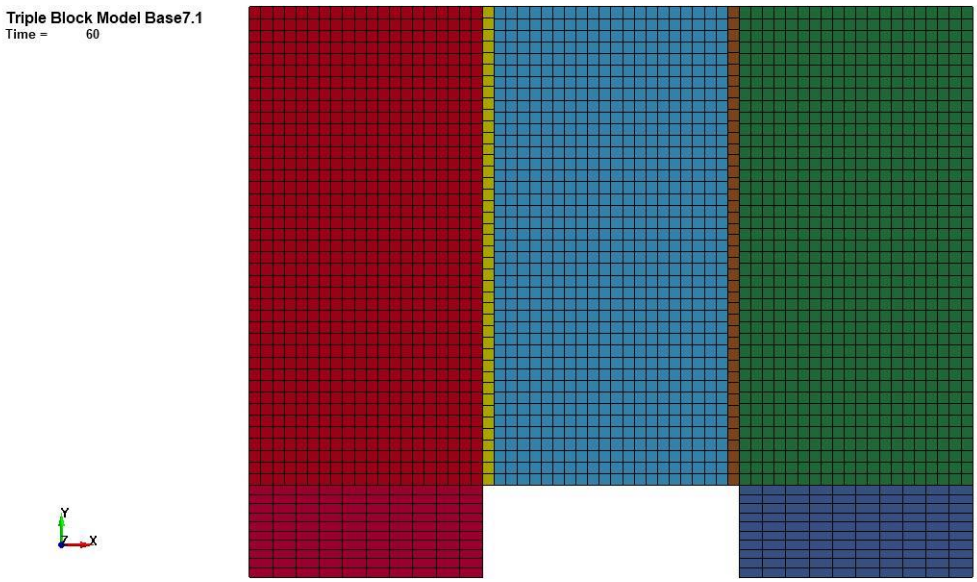


**Figure B-443: Last State at 60 Milliseconds for Base Run 7.1 – 50 psi**

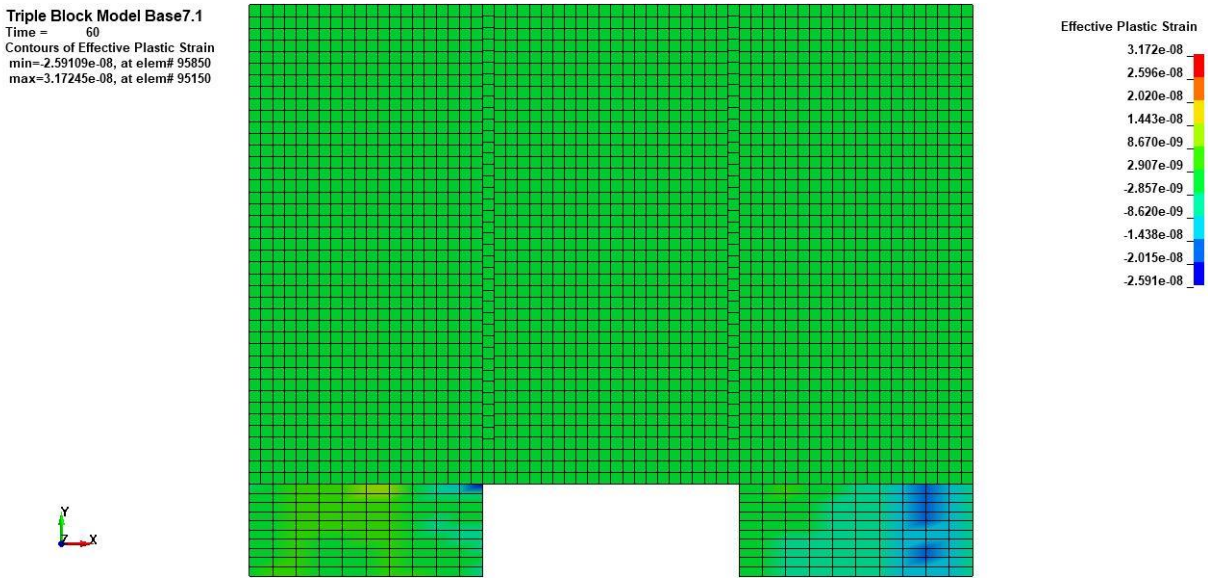


**Figure B-444: Effective Plastic Strain Fringe Plot for Last State at 60 Milliseconds for Base Run 7.1 – 50 psi**

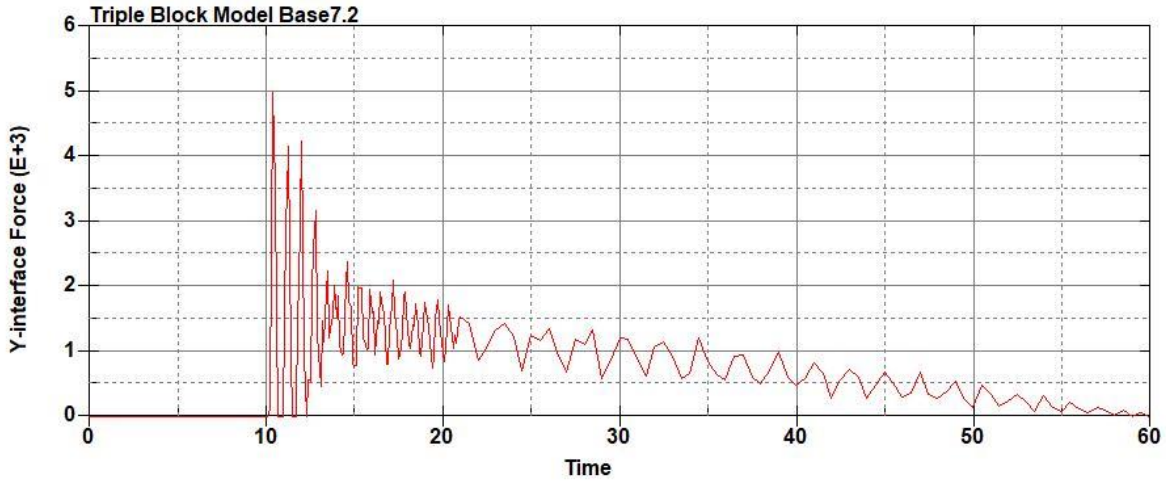


**Figure B-445: Base Run 7.2 Right Support Y-Interface Force (lbs) versus Time (ms) – 100 psi**

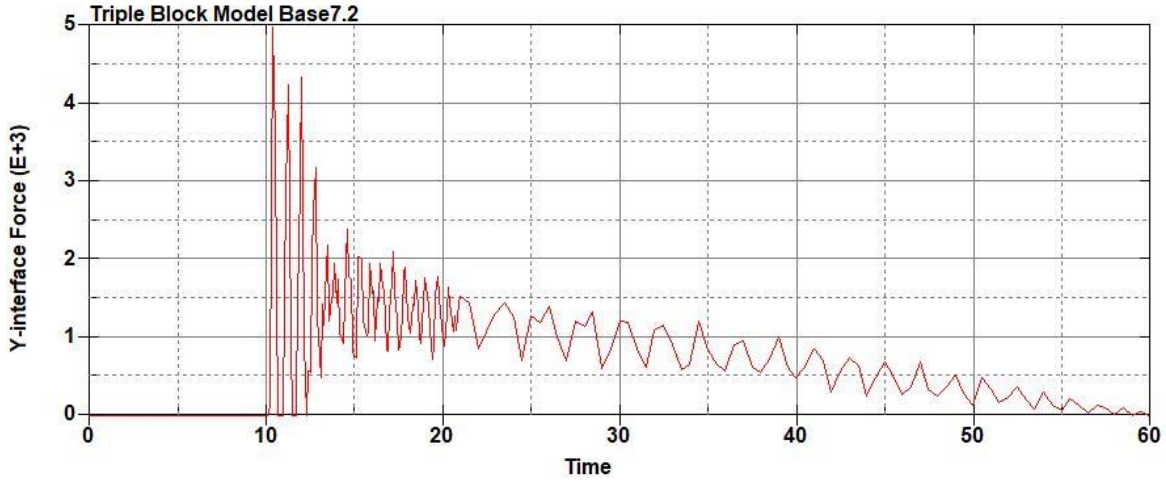


**Figure B-446: Base Run 7.2 Left Support Y-Interface Force (lbs) versus Time (ms) – 100 psi**

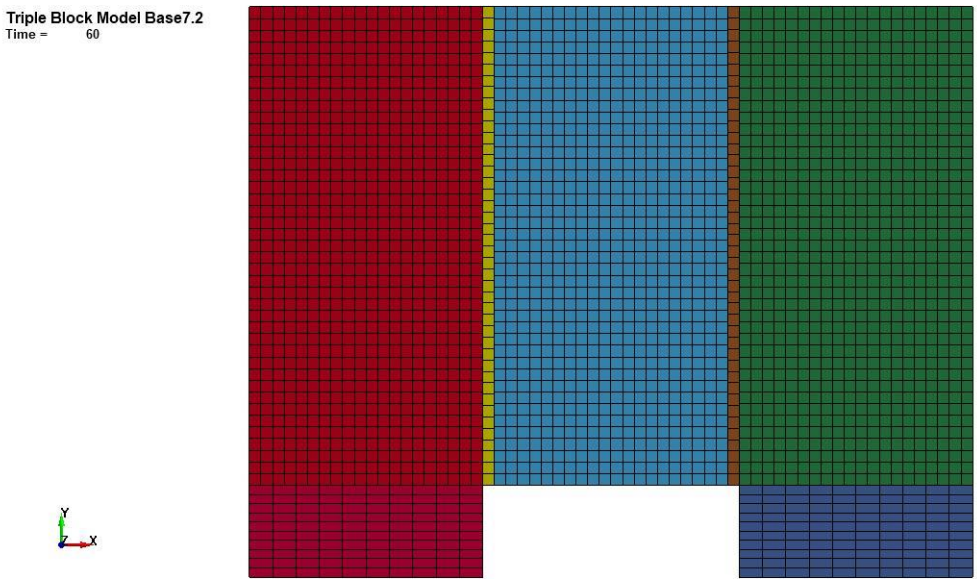


**Figure B-447: Last State at 60 Milliseconds for Base Run 7.2 – 100 psi**

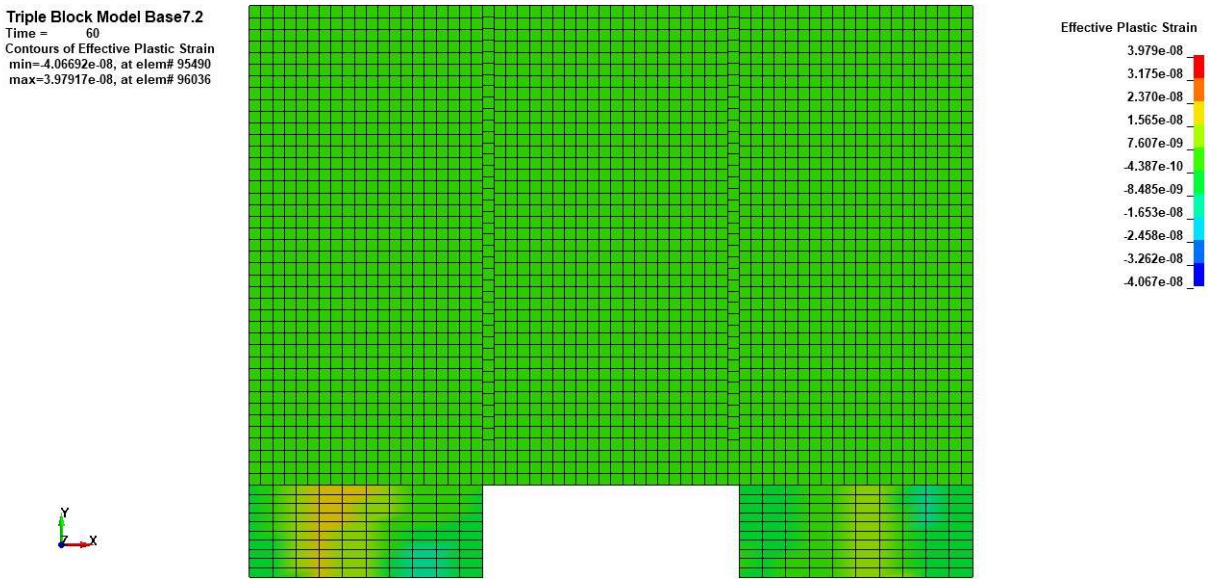


**Figure B-448: Effective Plastic Strain Fringe Plot for Last State at 60 Milliseconds for Base Run 7.2 – 100 psi**

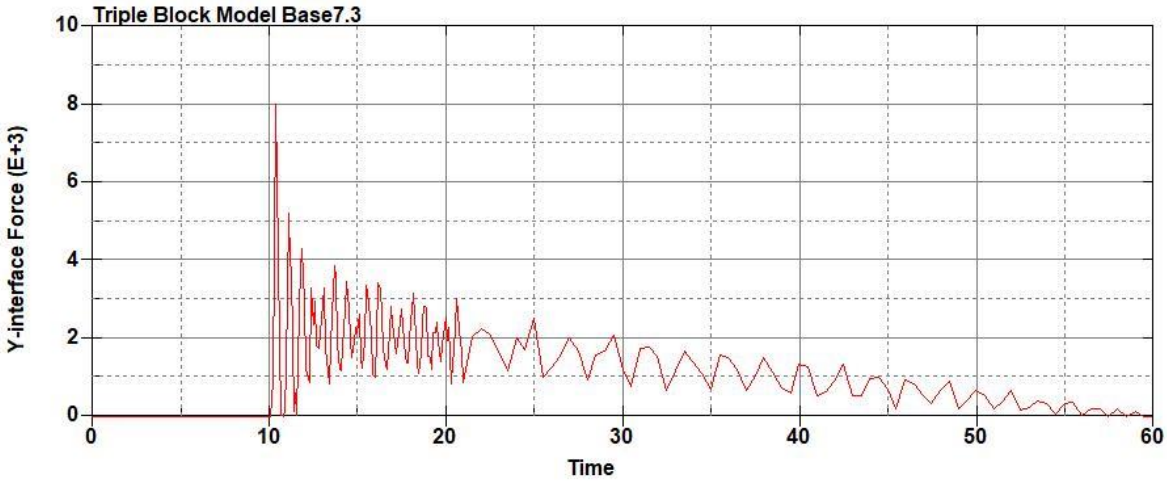


**Figure B-449: Base Run 7.3 Right Support Y-Interface Force (lbs) versus Time (ms) – 150 psi**

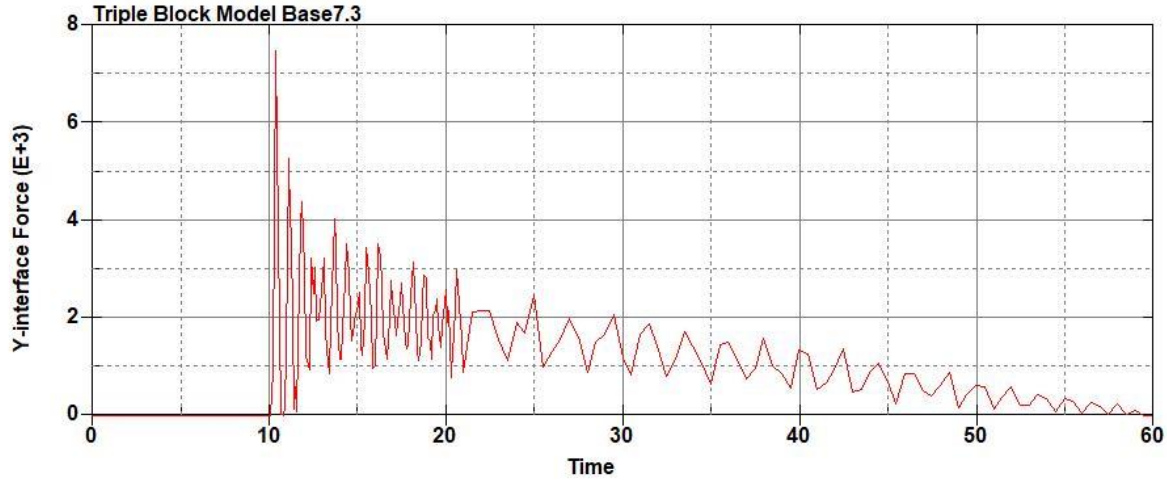


**Figure B-450: Base Run 7.3 Left Support Y-Interface Force (lbs) versus Time (ms) – 150 psi**

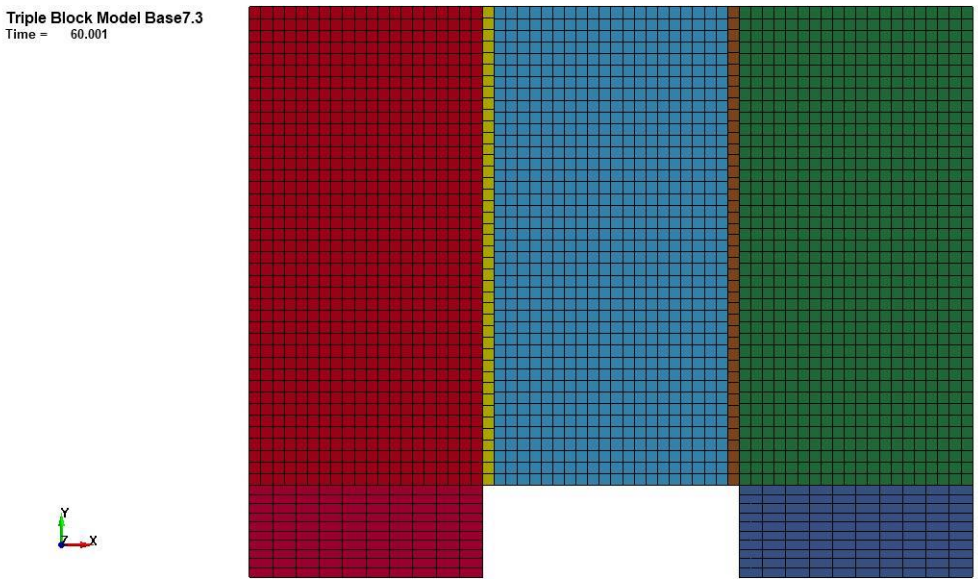


**Figure B-451: Last State at 60 Milliseconds for Base Run 7.3 – 150 psi**

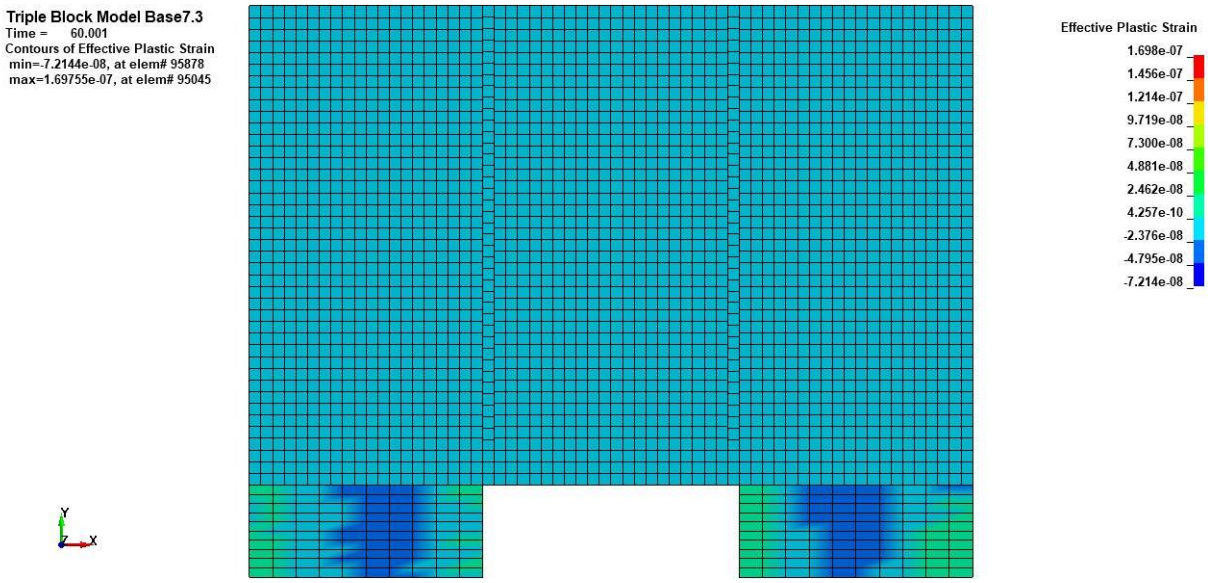


**Figure B-452: Effective Plastic Strain Fringe Plot for Last State at 60 Milliseconds for Base Run 7.3 – 150 psi**

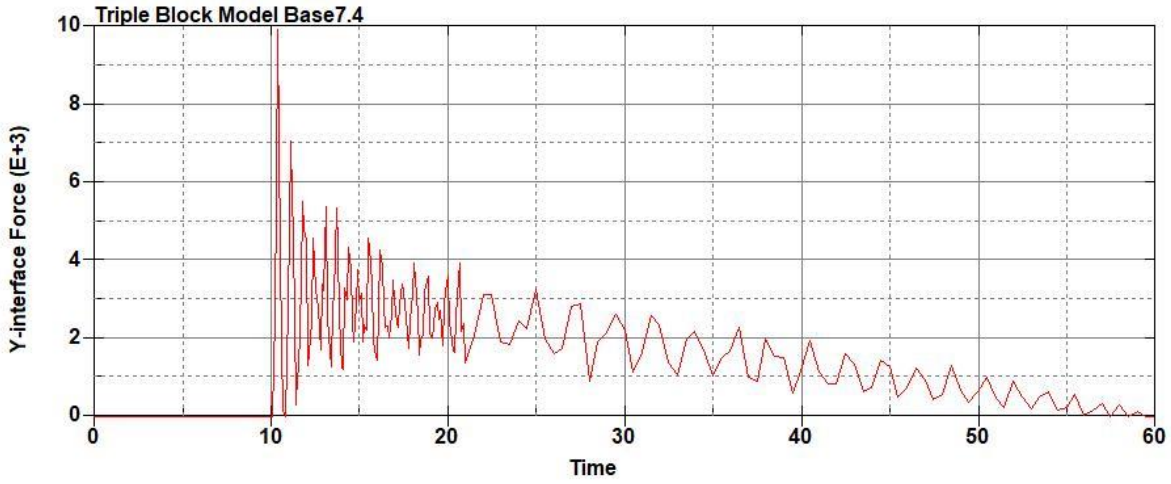


**Figure B-453: Base Run 7.4 Right Support Y-Interface Force (lbs) versus Time (ms) – 200 psi**

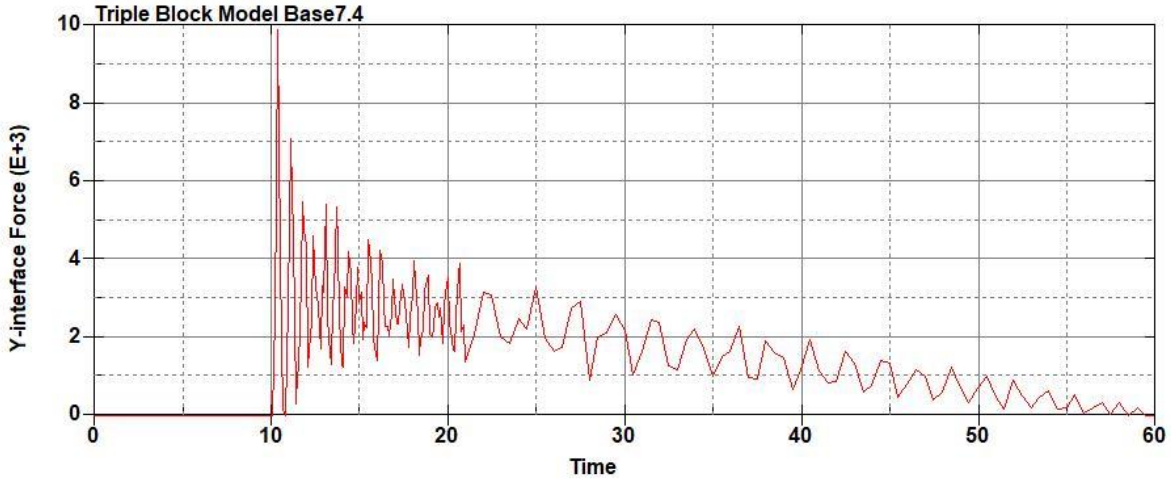


**Figure B-454: Base Run 7.4 Left Support Y-Interface Force (lbs) versus Time (ms) – 200 psi**

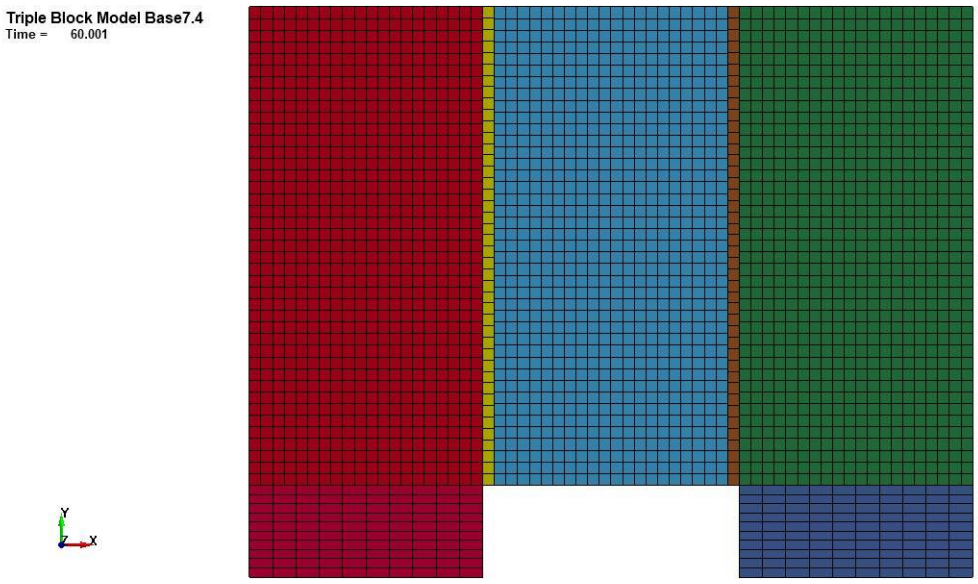


**Figure B-455: Last State at 60 Milliseconds for Base Run 7.4 – 200 psi**

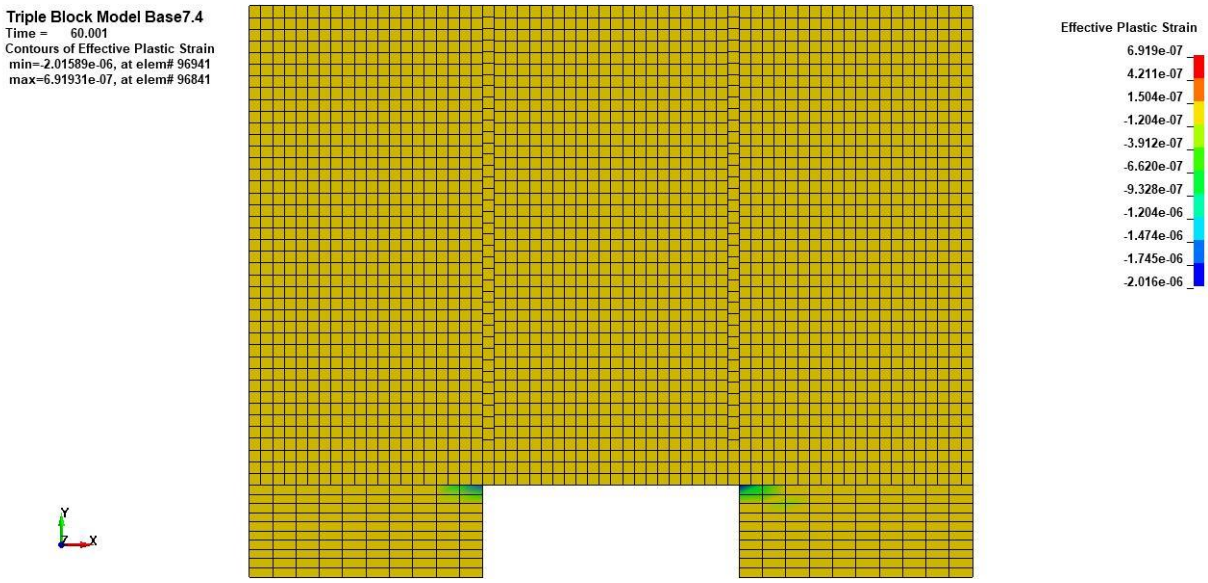


**Figure B-456: Effective Plastic Strain Fringe Plot for Last State at 60 Milliseconds for Base Run 7.4 – 200 psi**

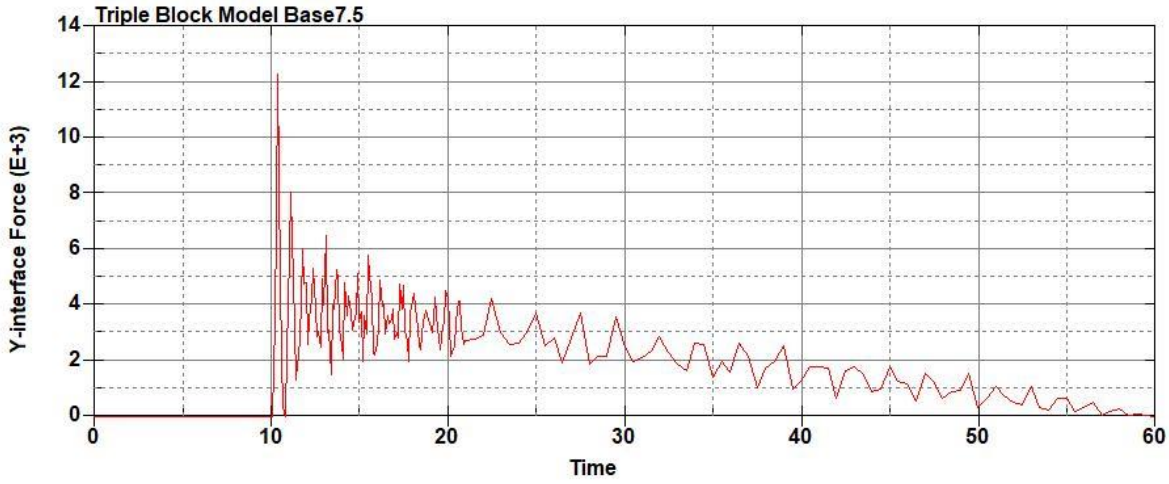


**Figure B-457: Base Run 7.5 Right Support Y-Interface Force (lbs) versus Time (ms) – 250 psi**

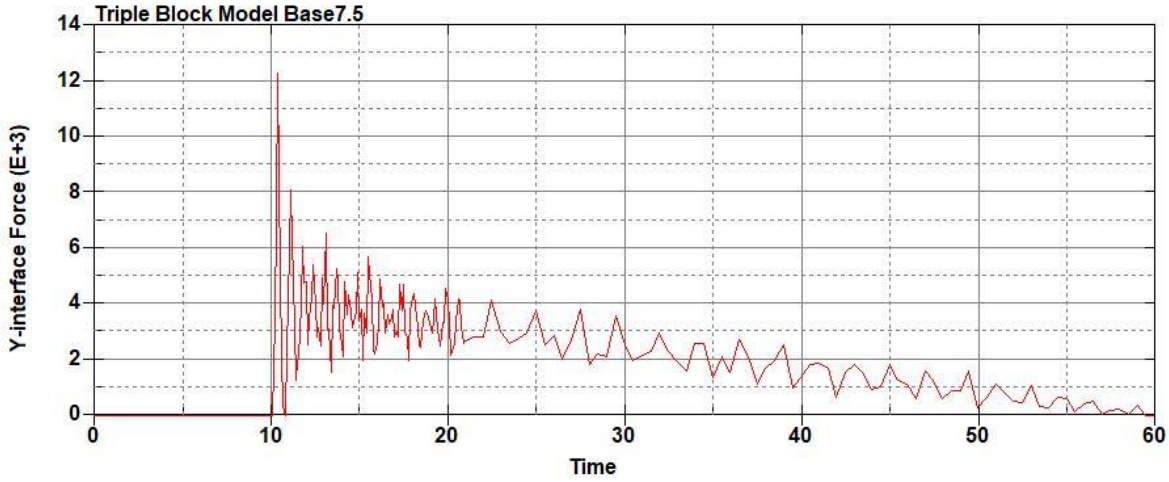


**Figure B-458: Base Run 7.5 Left Support Y-Interface Force (lbs) versus Time (ms) – 250 psi**

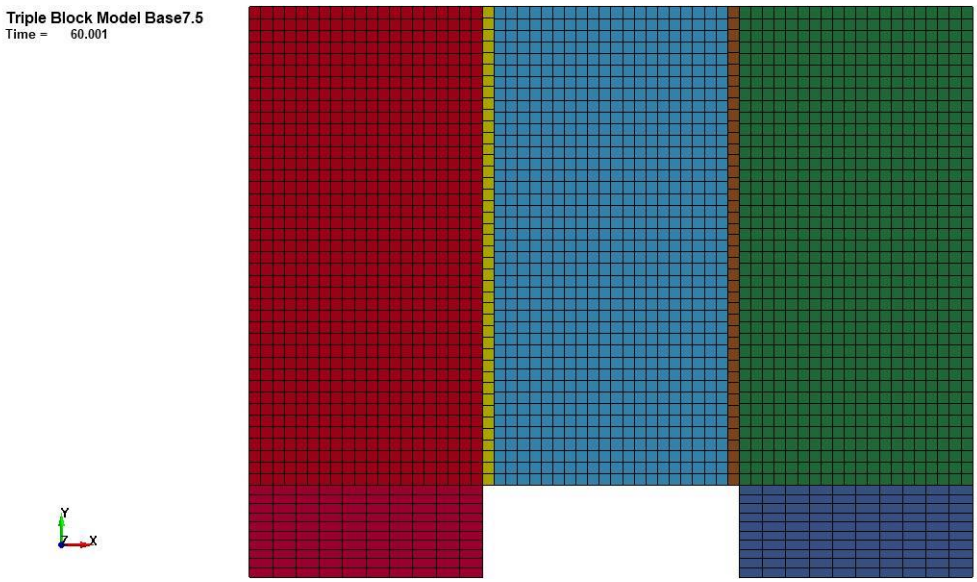


**Figure B-459: Last State at 60 Milliseconds for Base Run 7.5 – 250 psi**

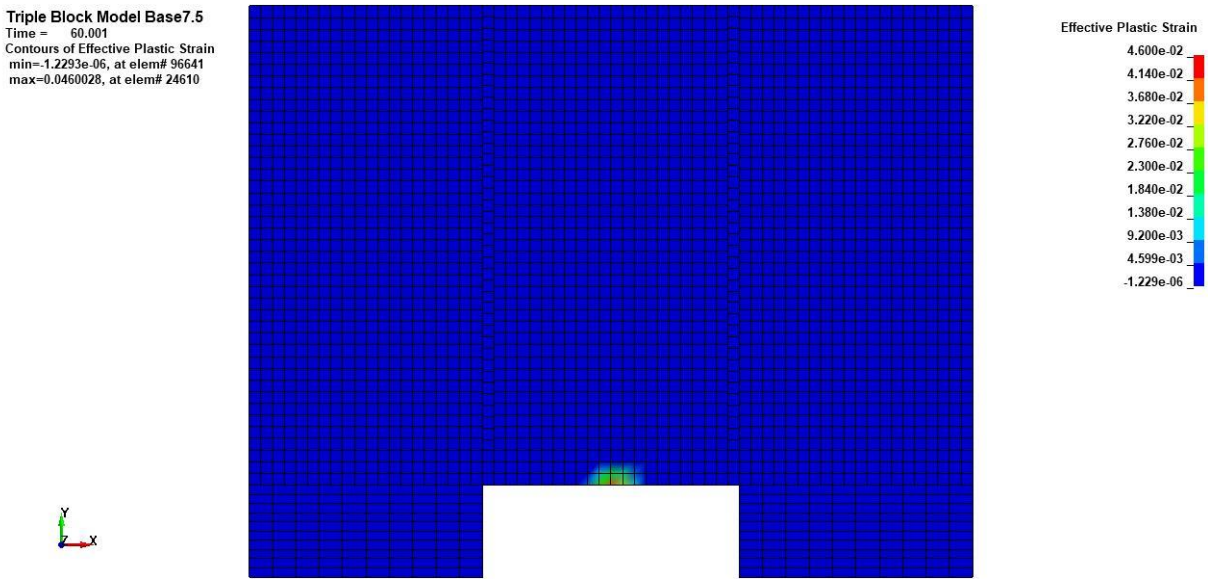


**Figure B-460: Effective Plastic Strain Fringe Plot for Last State at 60 Milliseconds for Base Run 7.5 – 250 psi**

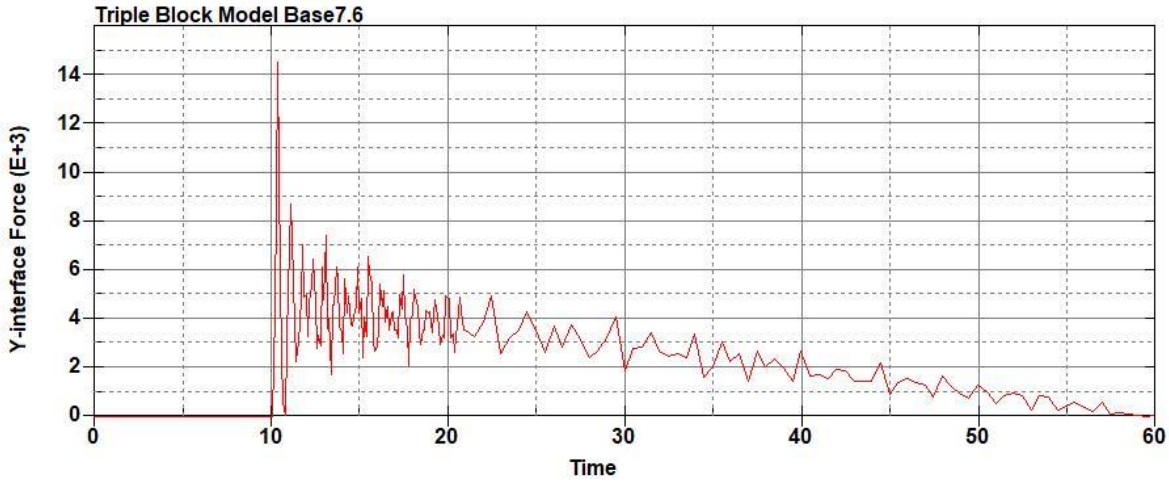


**Figure B-461: Base Run 7.6 Right Support Y-Interface Force (lbs) versus Time (ms) – 300 psi**

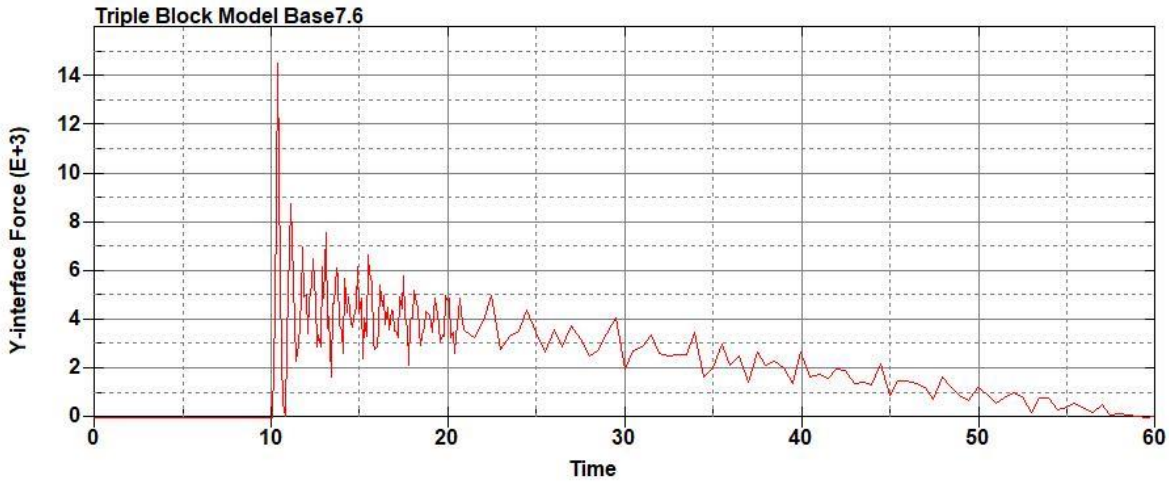


**Figure B-462: Base Run 7.6 Left Support Y-Interface Force (lbs) versus Time (ms) – 300 psi**

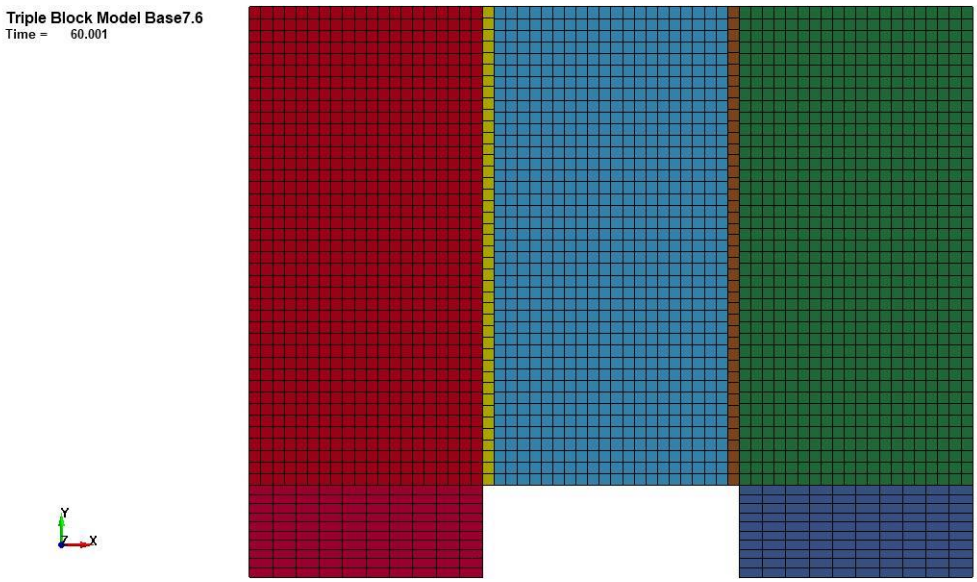


**Figure B-463: Last State at 60 Milliseconds for Base Run 7.6 – 300 psi**

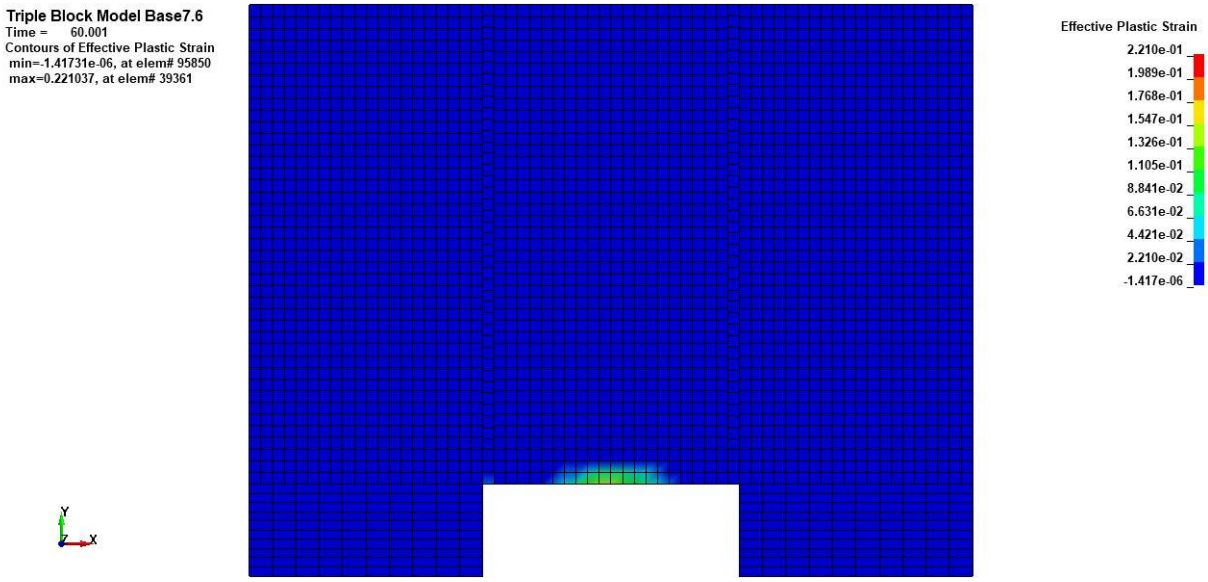


**Figure B-464: Effective Plastic Strain Fringe Plot for Last State at 60 Milliseconds for Base Run 7.6 – 300 psi**

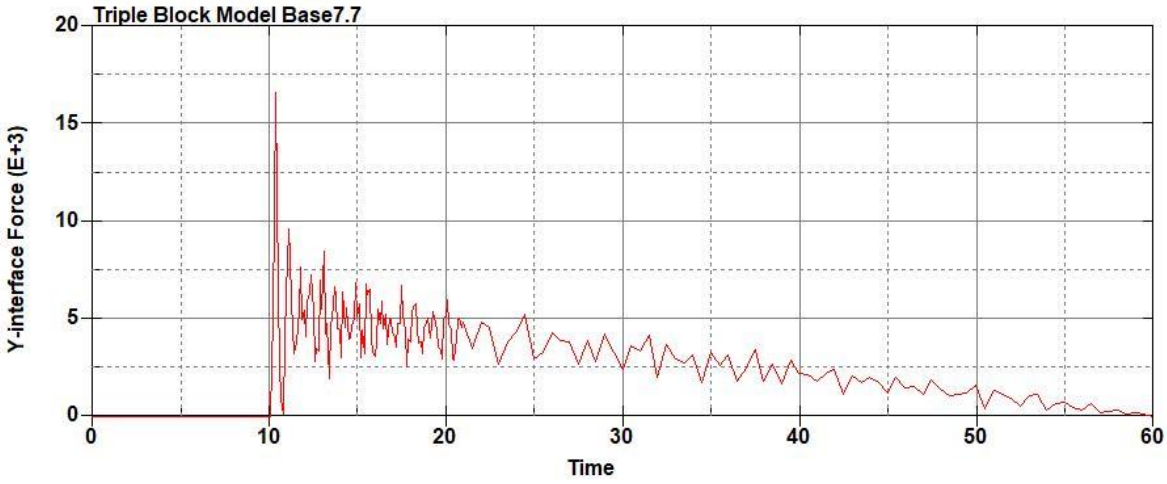


**Figure B-465: Base Run 7.7 Right Support Y-Interface Force (lbs) versus Time (ms) – 350 psi**

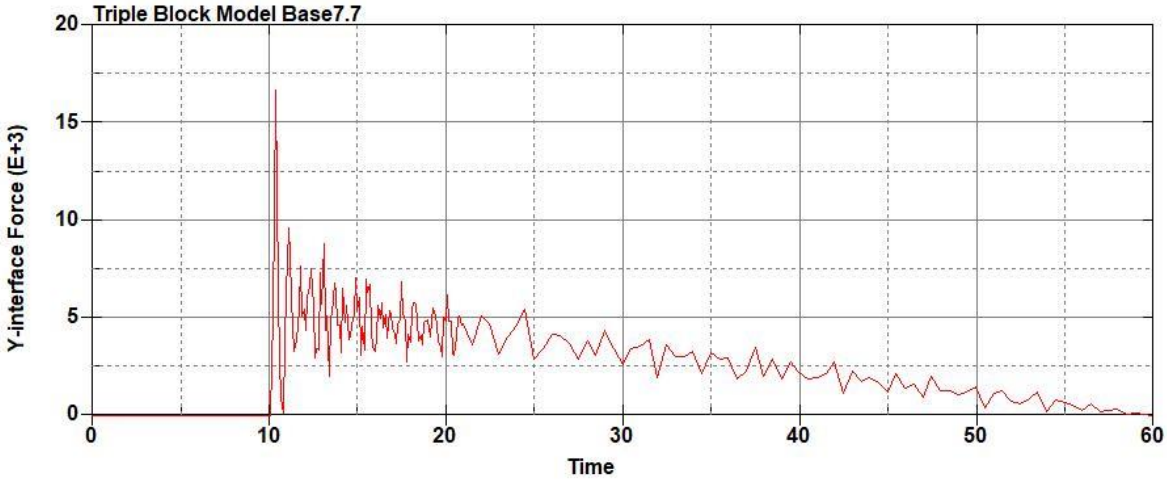


**Figure B-466: Base Run 7.7 Left Support Y-Interface Force (lbs) versus Time (ms) – 350 psi**

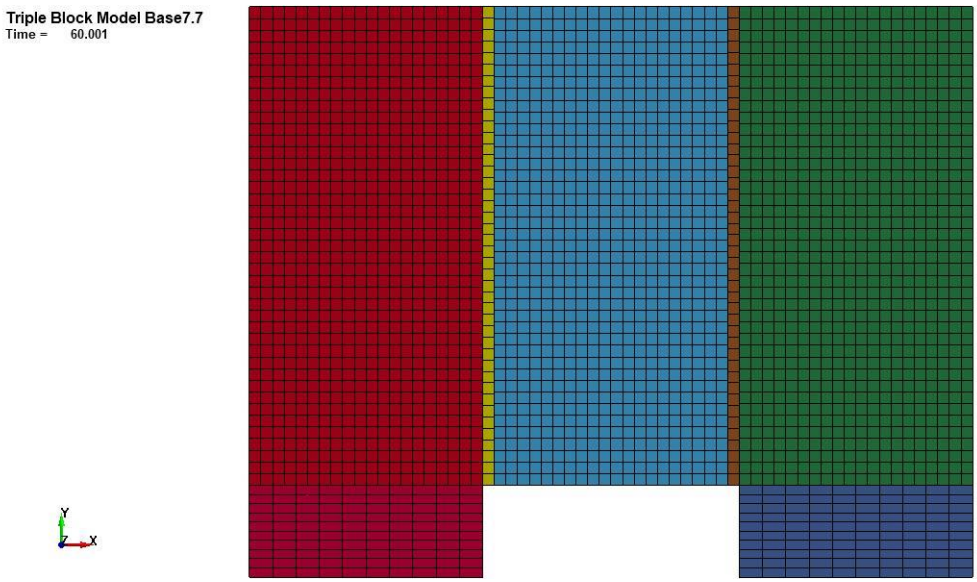


**Figure B-467: Last State at 60 Milliseconds for Base Run 7.7 – 350 psi**

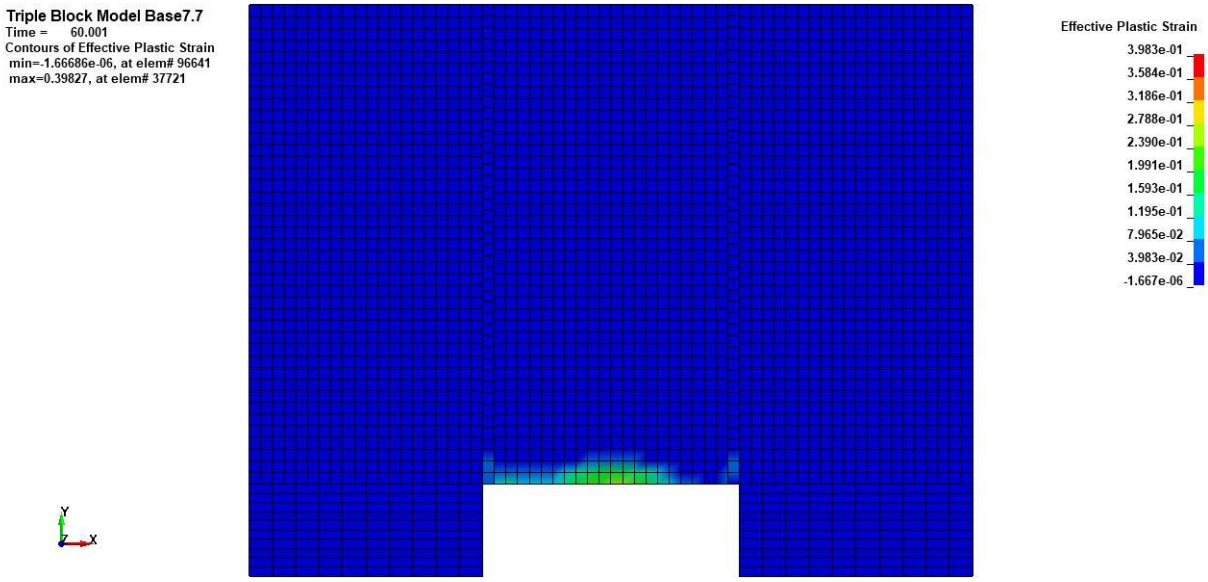


**Figure B-468: Effective Plastic Strain Fringe Plot for Last State at 60 Milliseconds for Base Run 7.7 – 350 psi**

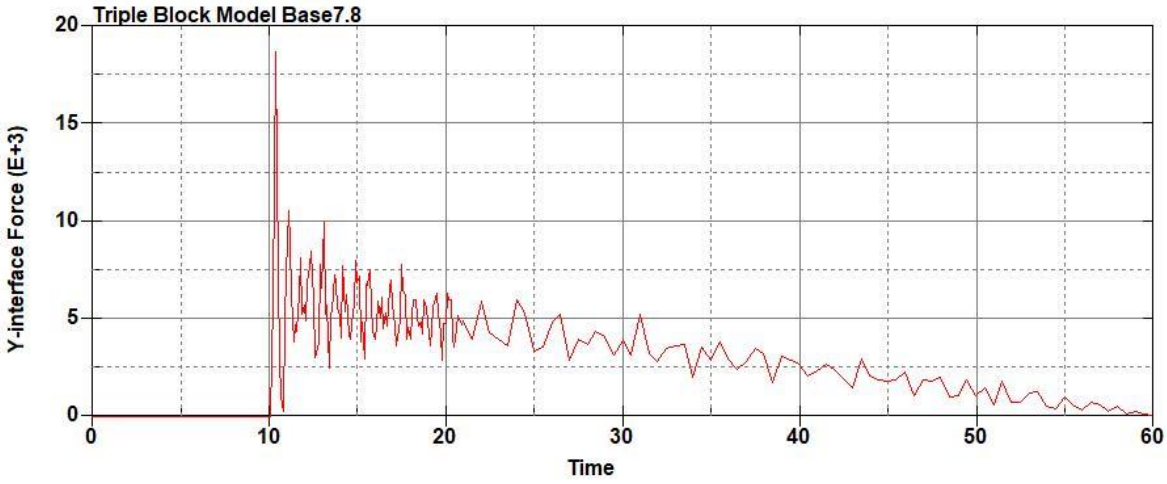


**Figure B-469: Base Run 7.8 Right Support Y-Interface Force (lbs) versus Time (ms) – 400 psi**

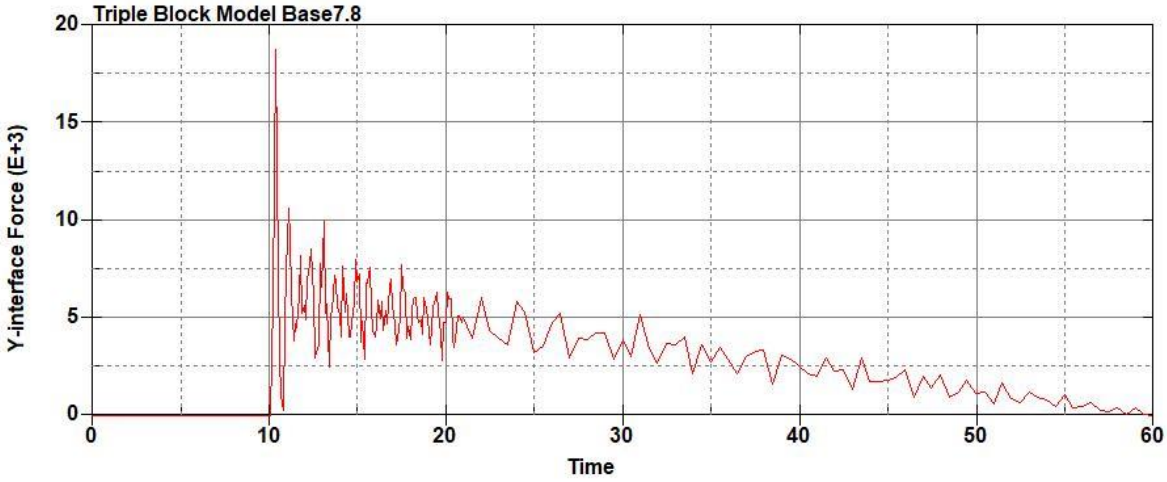


**Figure B-470: Base Run 7.8 Left Support Y-Interface Force (lbs) versus Time (ms) – 400 psi**

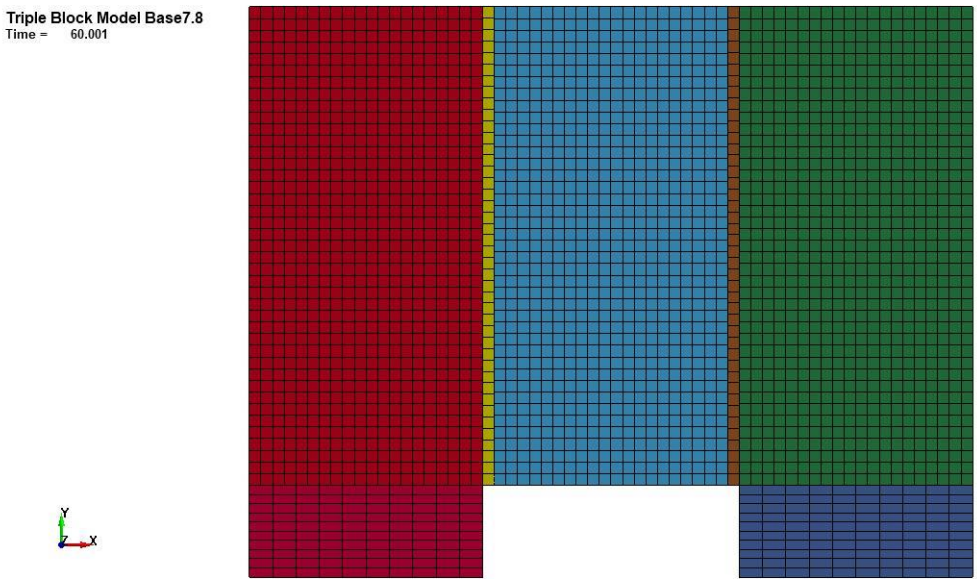


**Figure B-471: Last State at 60 Milliseconds for Base Run 7.8 – 400 psi**

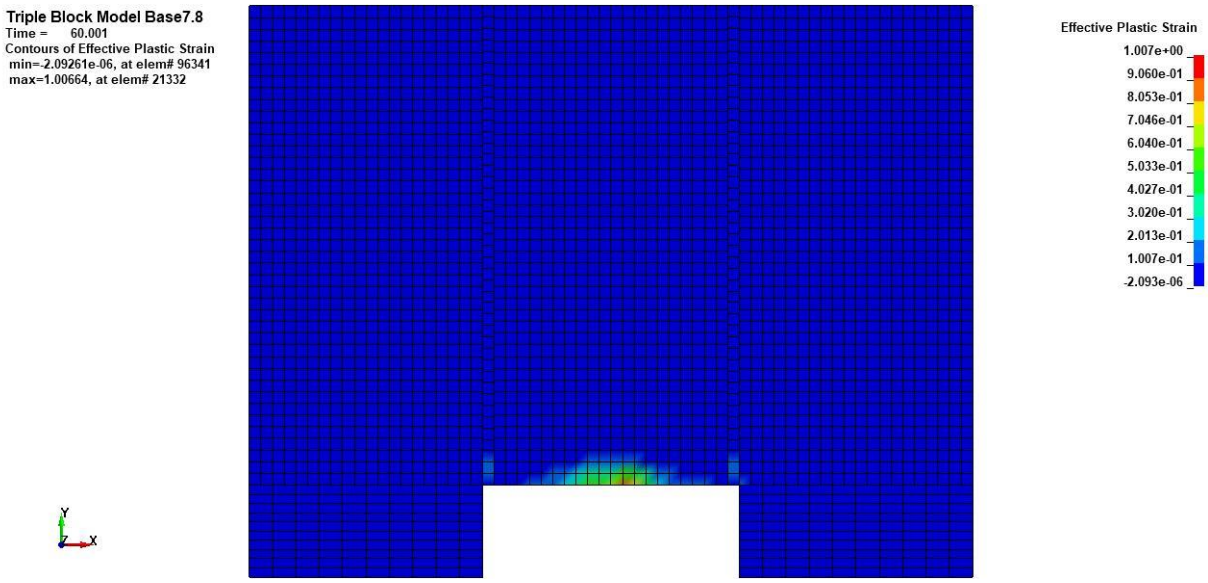


**Figure B-472: Effective Plastic Strain Fringe Plot for Last State at 60 Milliseconds for Base Run 7.8 – 400 psi**

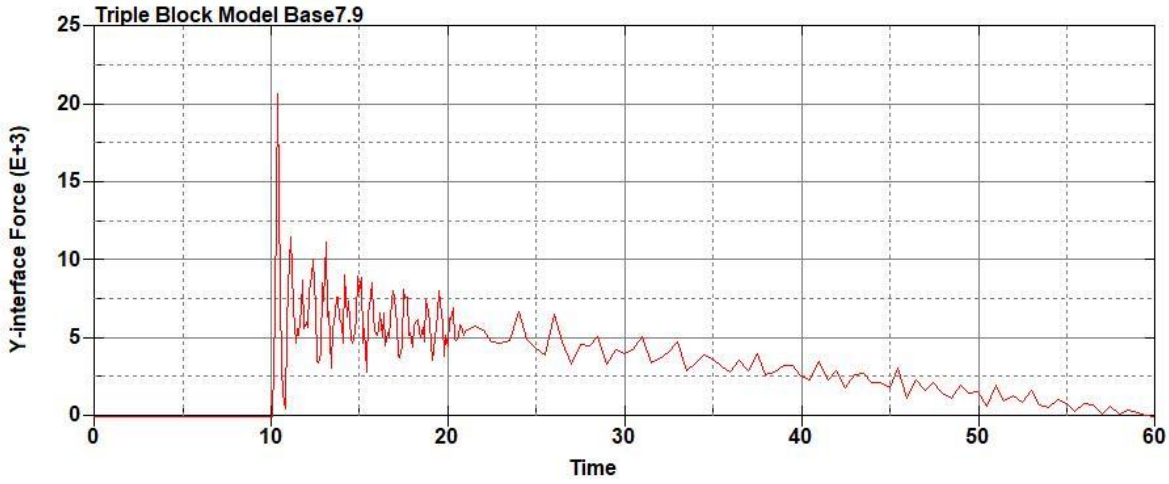


**Figure B-473: Base Run 7.9 Right Support Y-Interface Force (lbs) versus Time (ms) – 450 psi**

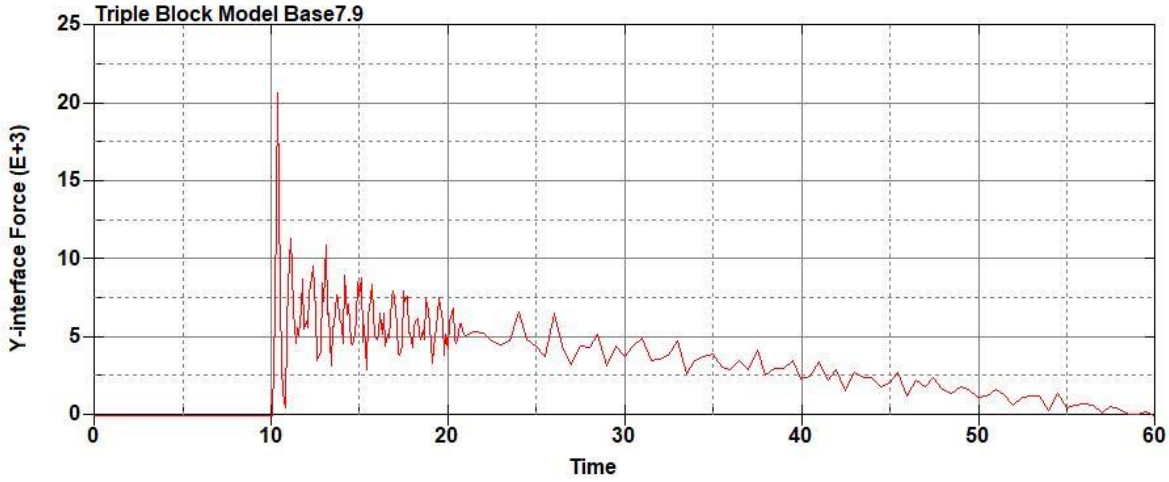


**Figure B-474: Base Run 7.9 Left Support Y-Interface Force (lbs) versus Time (ms) – 450 psi**

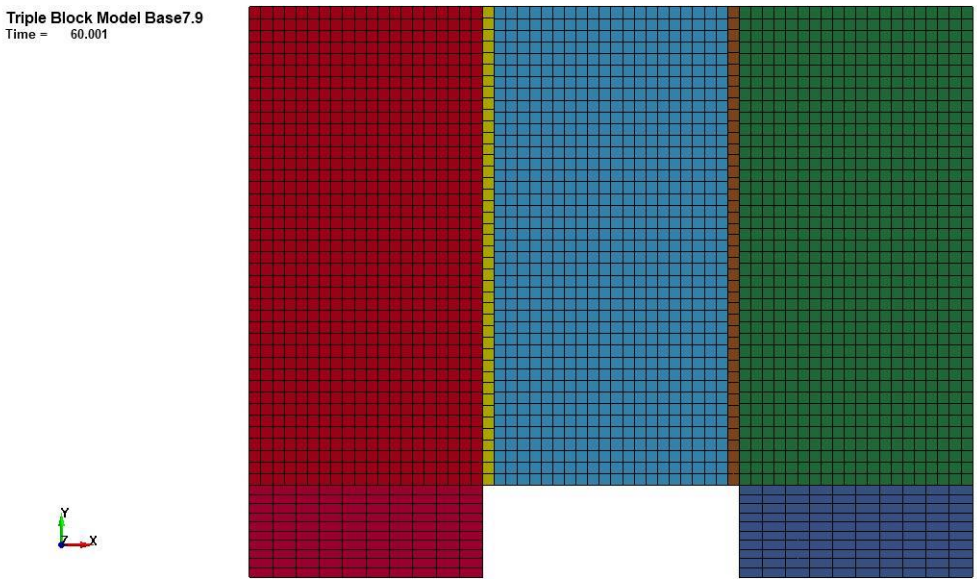


**Figure B-475: Last State at 60 Milliseconds for Base Run 7.9 – 450 psi**

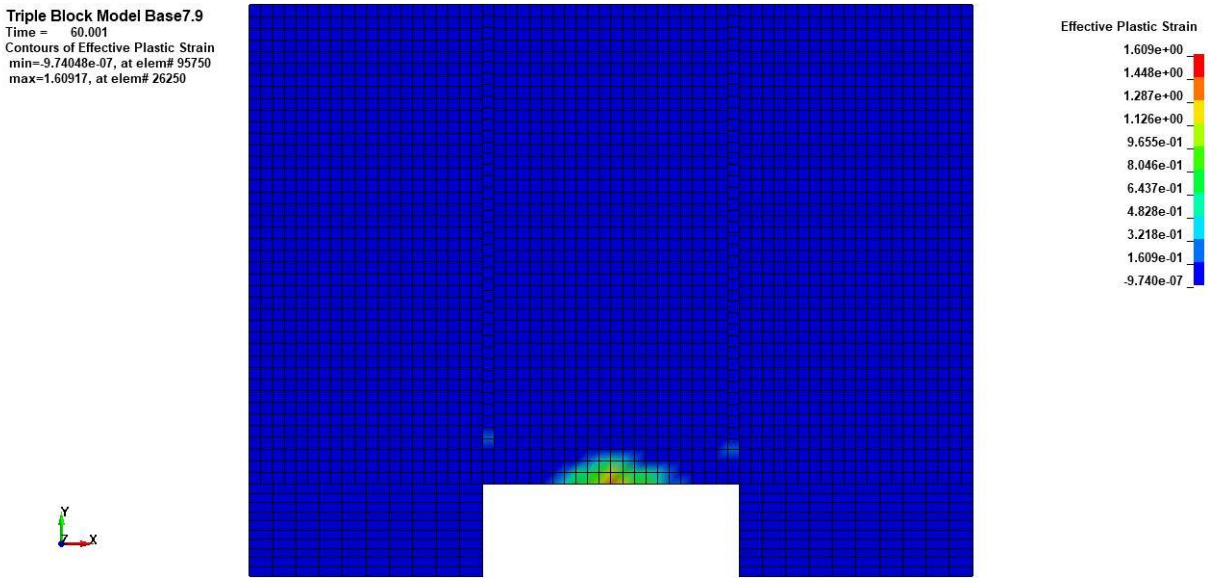


**Figure B-476: Effective Plastic Strain Fringe Plot for Last State at 60 Milliseconds for Base Run 7.9 –450 psi**

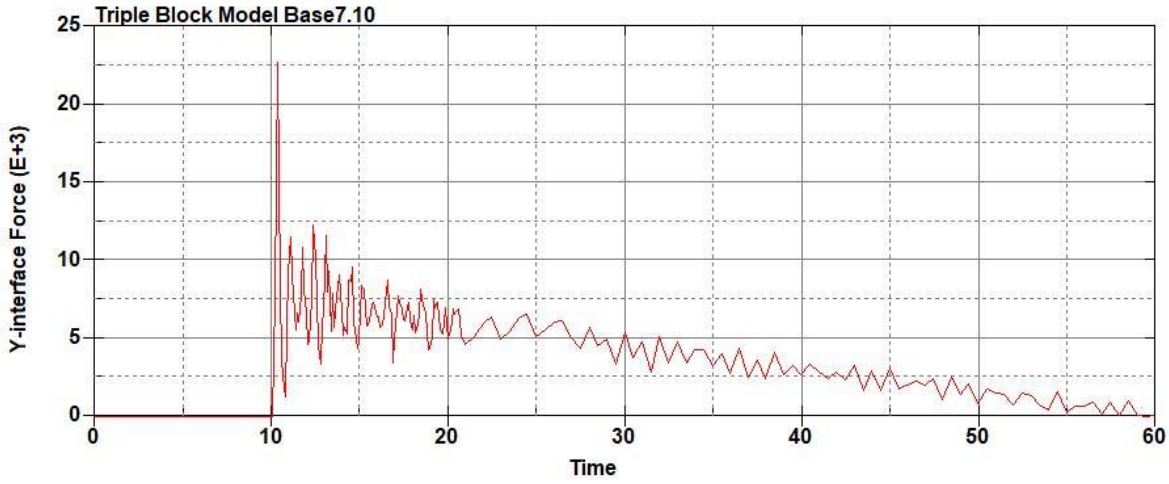


**Figure B-477: Base Run 7.10 Right Support Y-Interface Force (lbs) versus Time (ms) – 500 psi**

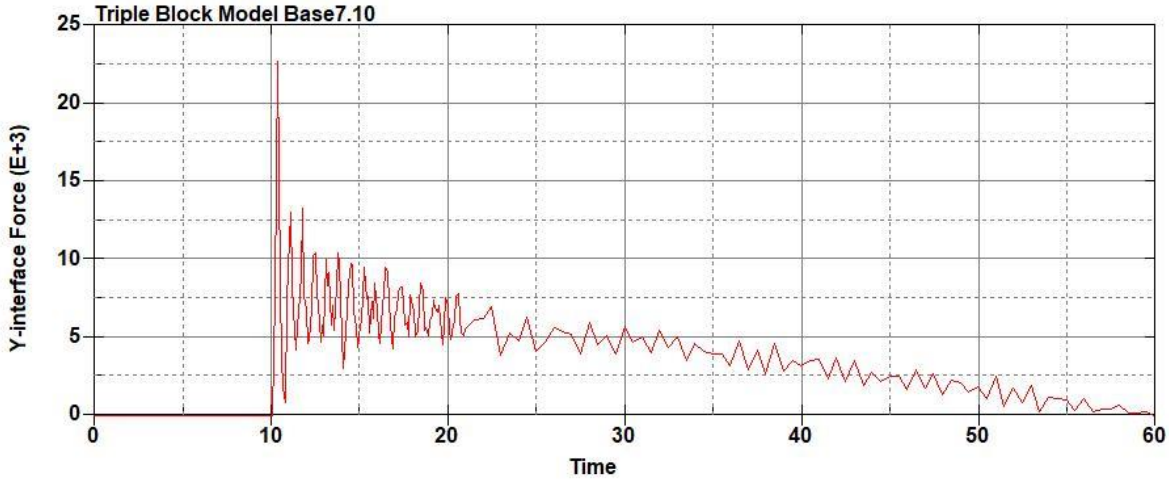


**Figure B-478: Base Run 7.10 Left Support Y-Interface Force (lbs) versus Time (ms) – 500 psi**

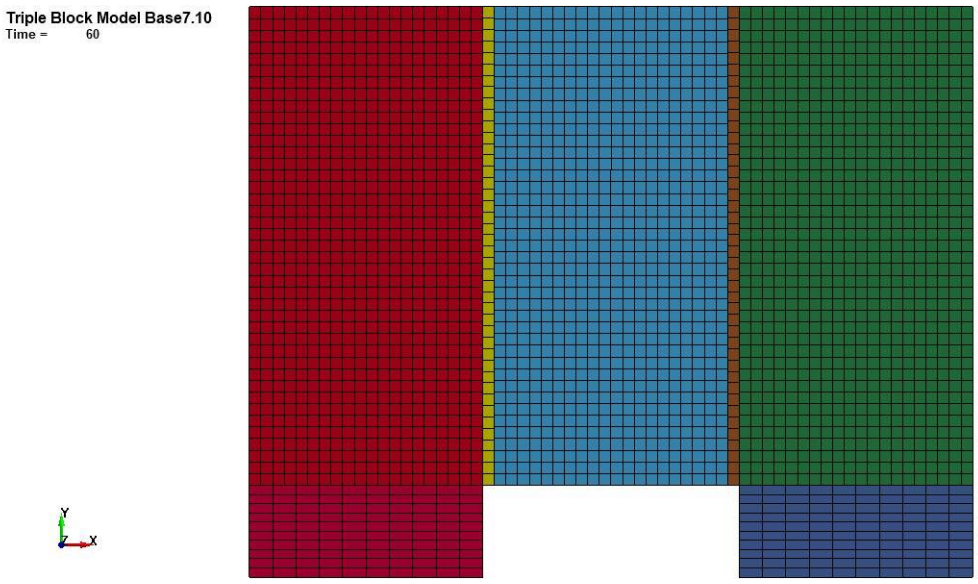


**Figure B-479: Last State at 60 Milliseconds for Base Run 7.10 – 500 psi**

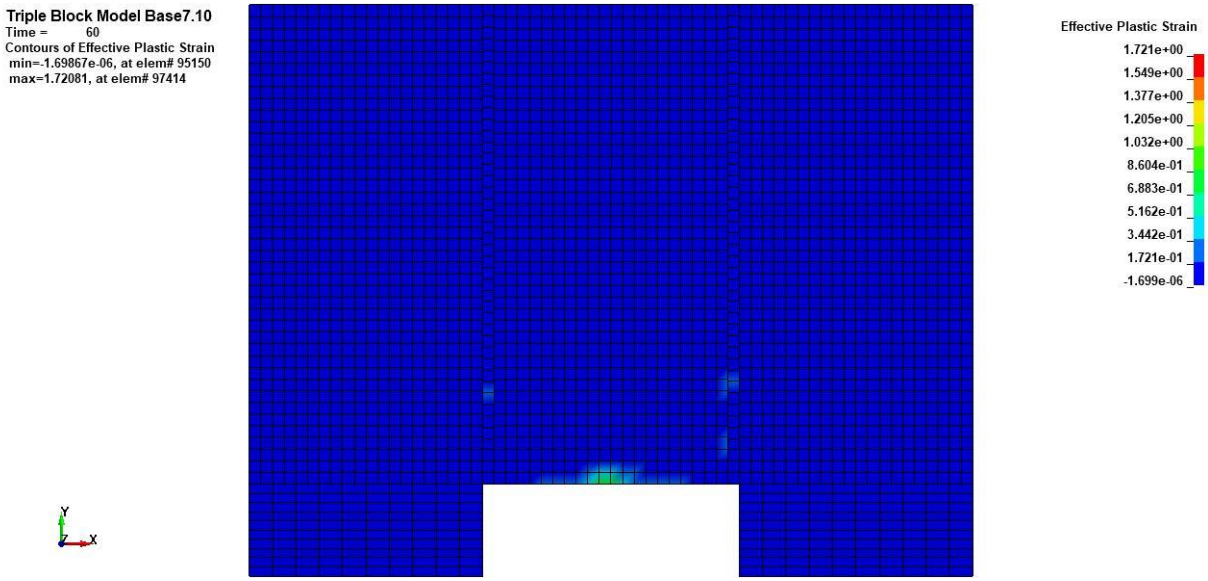


**Figure B-480: Effective Plastic Strain Fringe Plot for Last State at 60 Milliseconds for Base Run 7.10 – 500 psi**

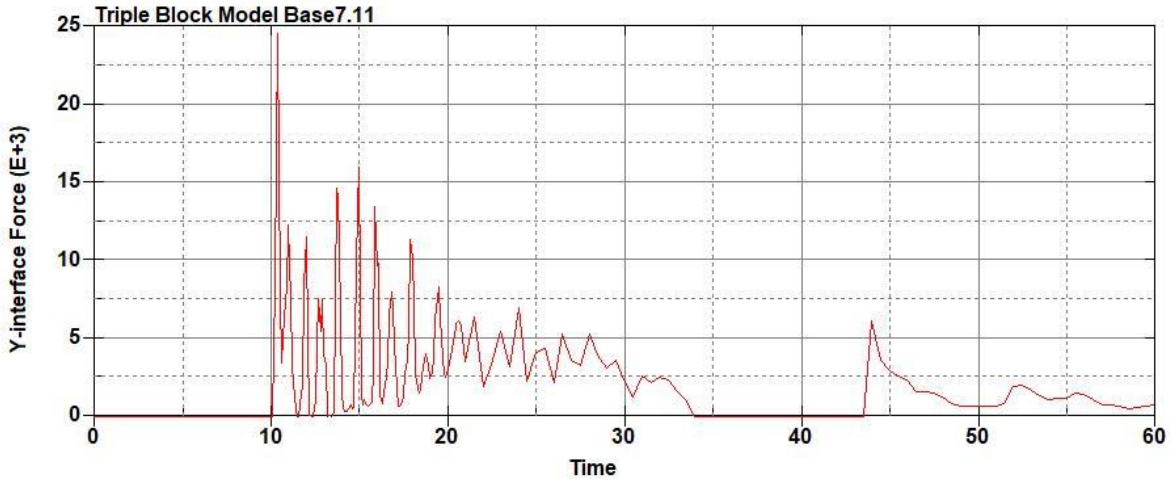


**Figure B-481: Base Run 7.11 Right Support Y-Interface Force (lbs) versus Time (ms) – 550 psi**

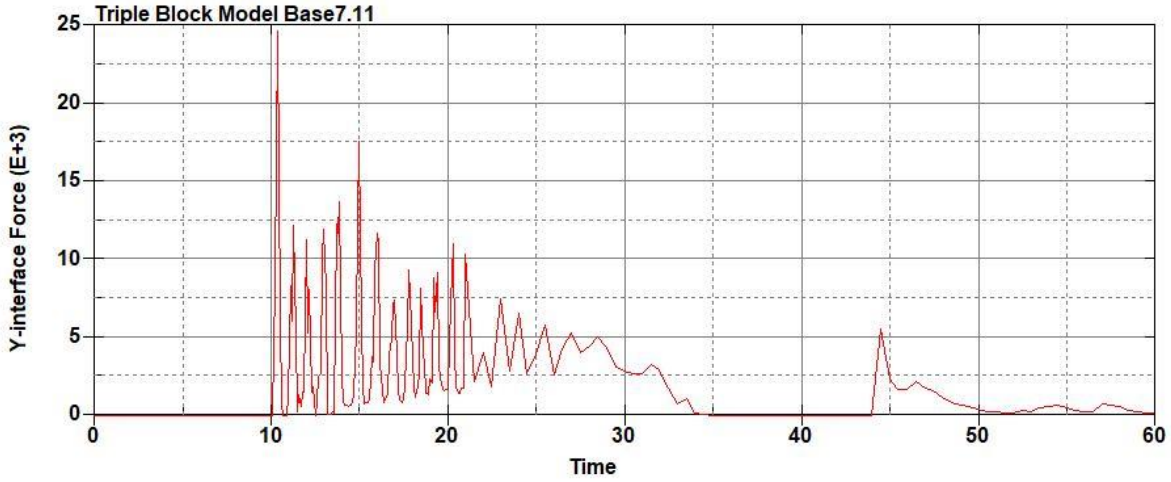


**Figure B-482: Base Run 7.11 Left Support Y-Interface Force (lbs) versus Time (ms) – 550 psi**

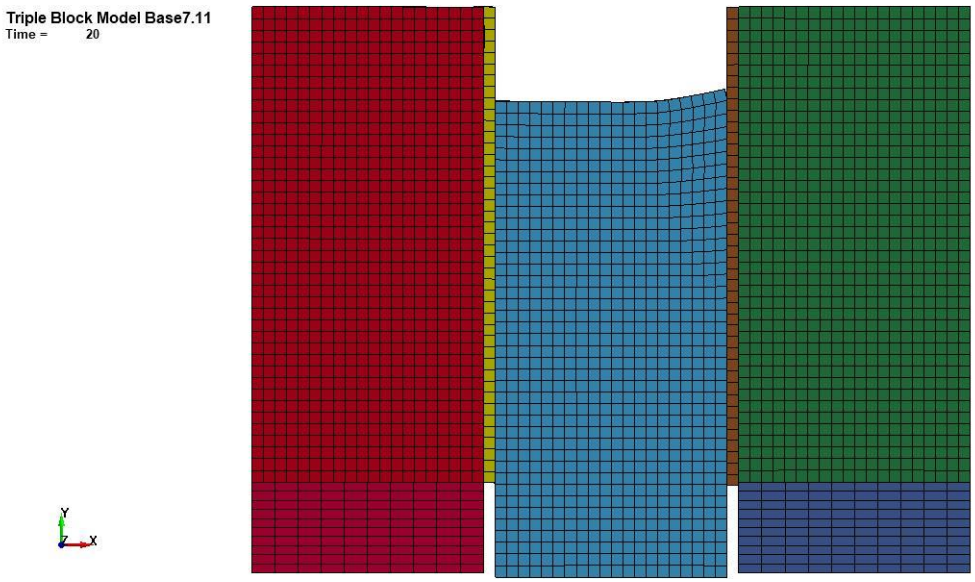


**Figure B-483: Last State at 20 Milliseconds for Base Run 7.11 – 550 psi**

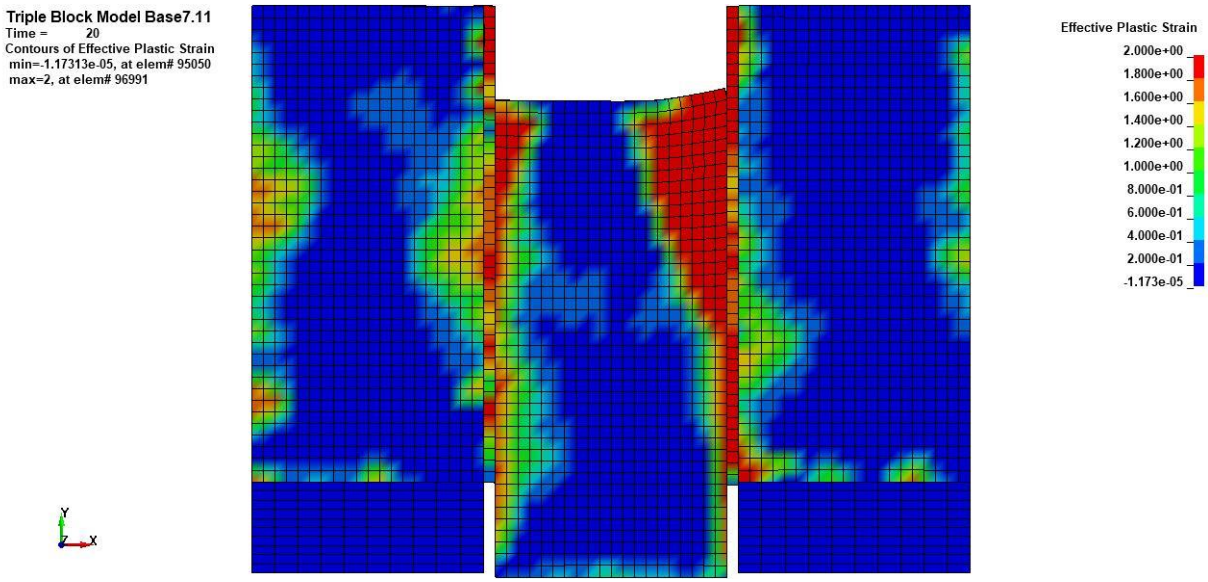


**Figure B-484: Effective Plastic Strain Fringe Plot for Last State at 20 Milliseconds for Base Run 7.11 – 550 psi**

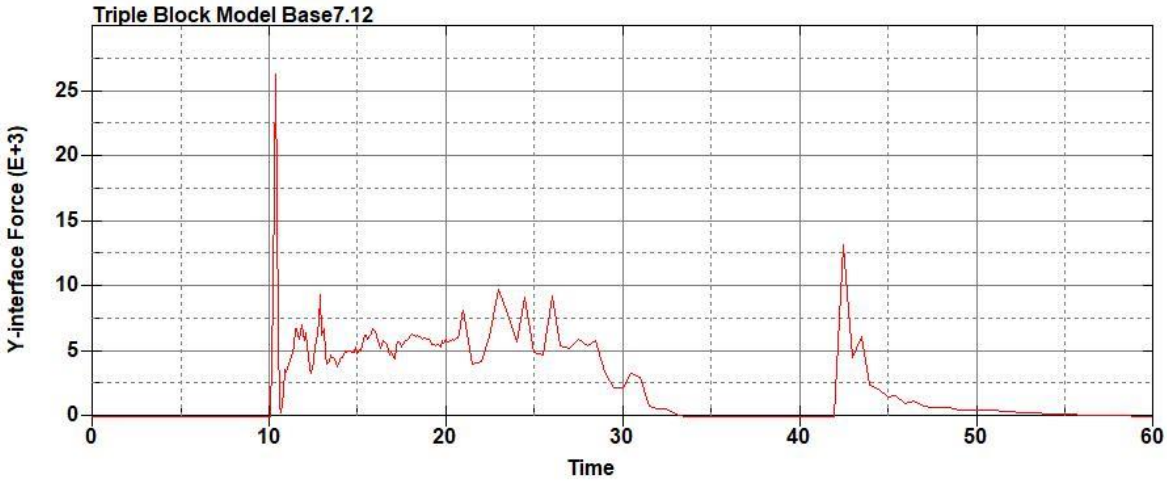


**Figure B-485: Base Run 7.12 Right Support Y-Interface Force (lbs) versus Time (ms) – 600 psi**

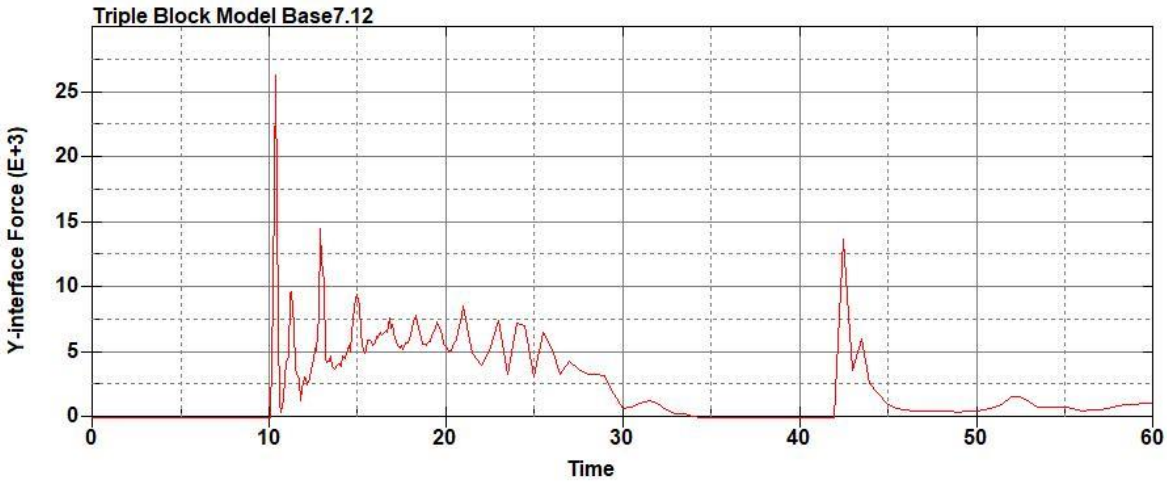


**Figure B-486: Base Run 7.12 Left Support Y-Interface Force (lbs) versus Time (ms) – 600 psi**

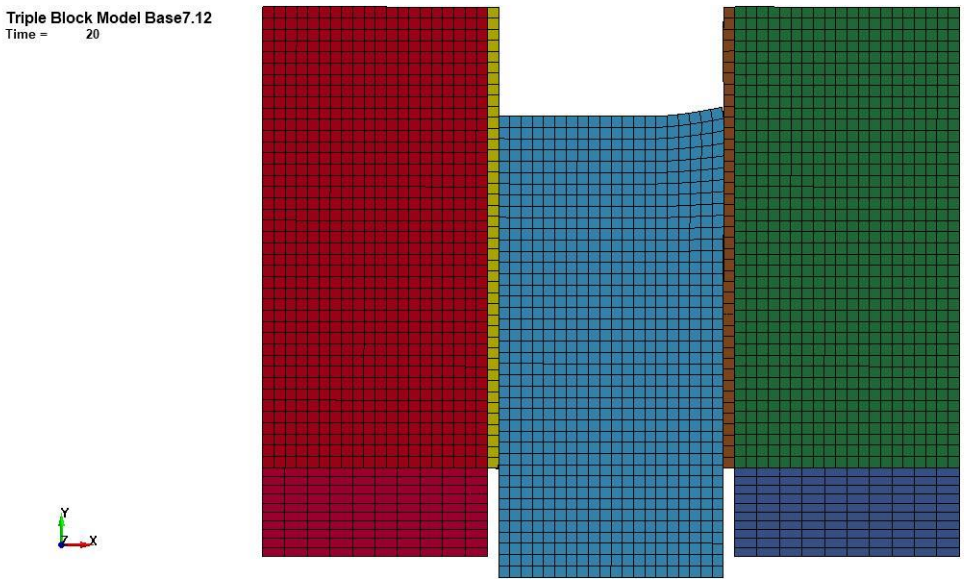


**Figure B-487: Last State at 20 Milliseconds for Base Run 7.12 – 600 psi**

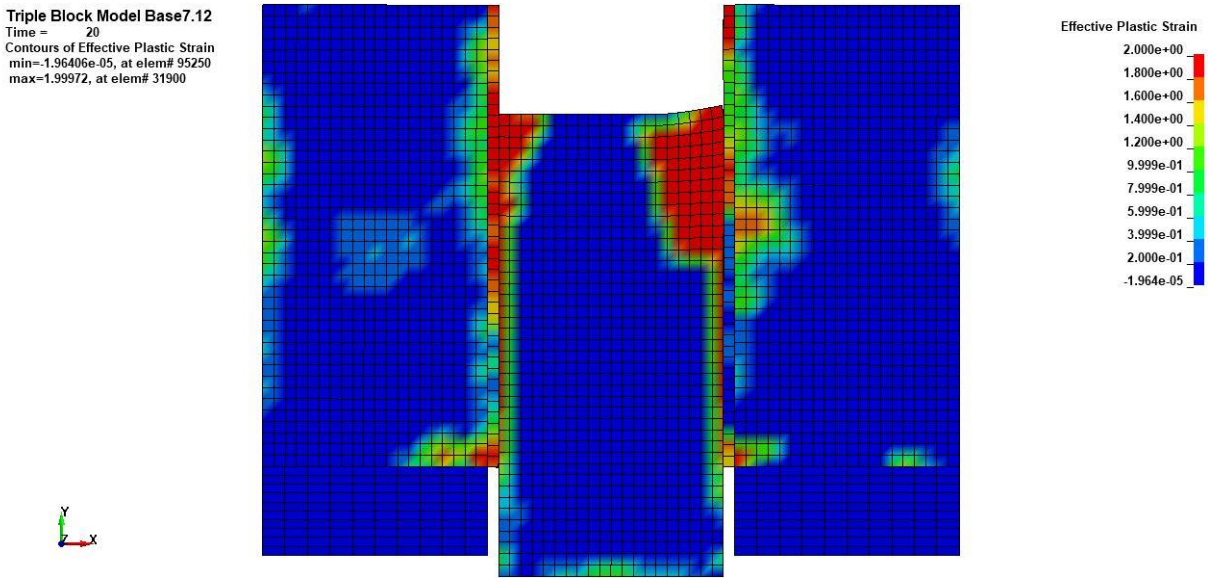


**Figure B-488: Effective Plastic Strain Fringe Plot for Last State at 20 Milliseconds for Base Run 7.12 – 600 psi**

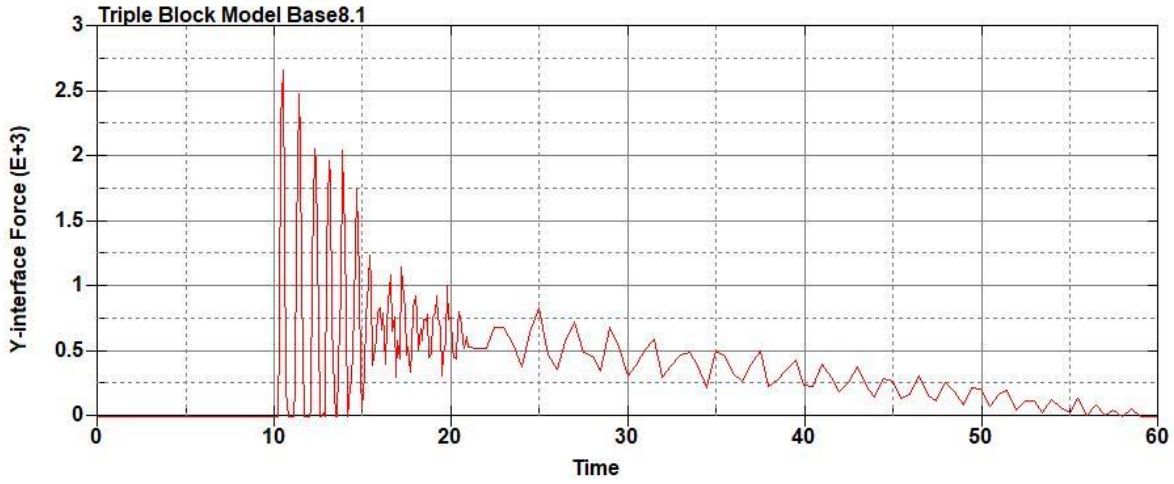


**Figure B-489: Base Run 8.1 Right Support Y-Interface Force (lbs) versus Time (ms) – 50 psi**

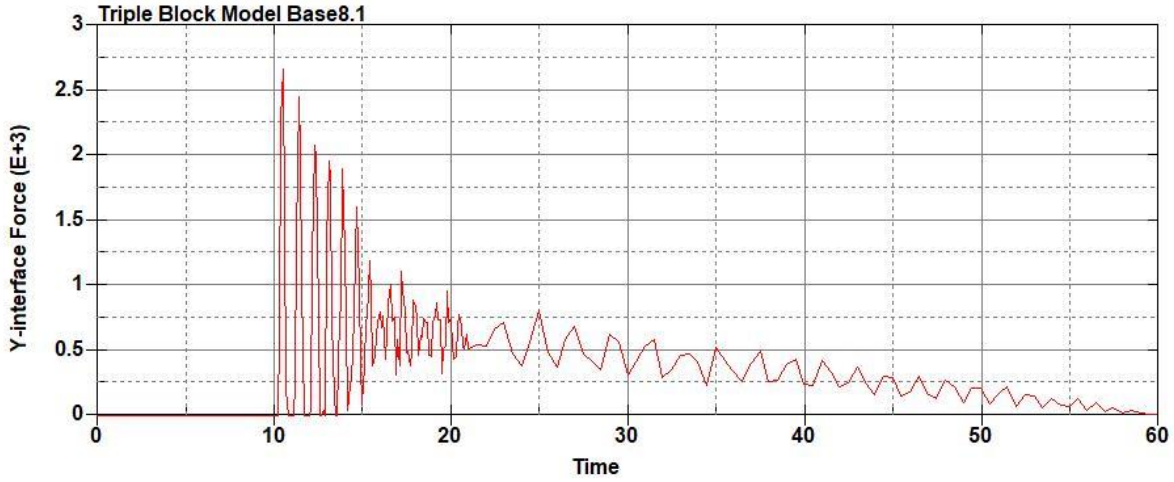


**Figure B-490: Base Run 8.1 Left Support Y-Interface Force (lbs) versus Time (ms) – 50 psi**

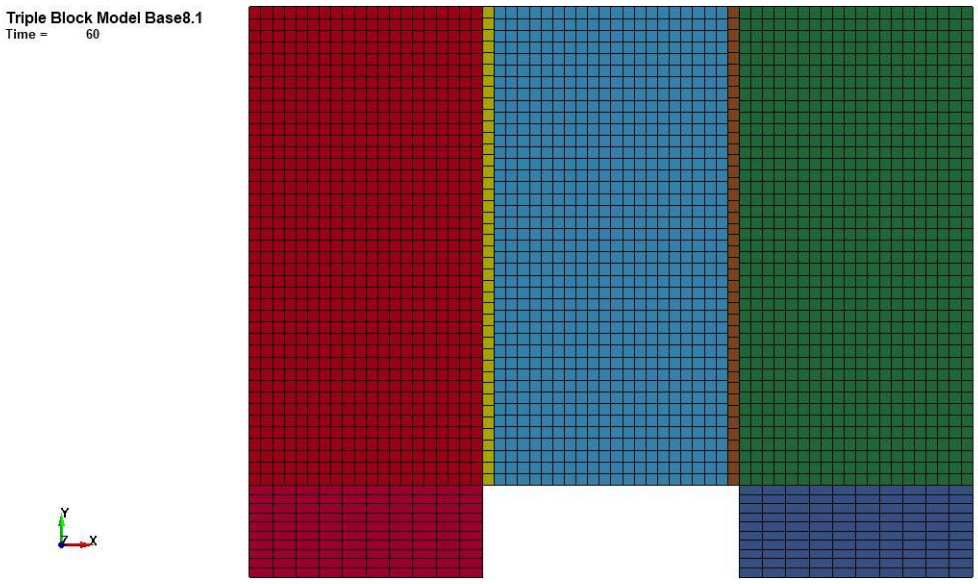


**Figure B-491: Last State at 60 Milliseconds for Base Run 8.1 – 50 psi**

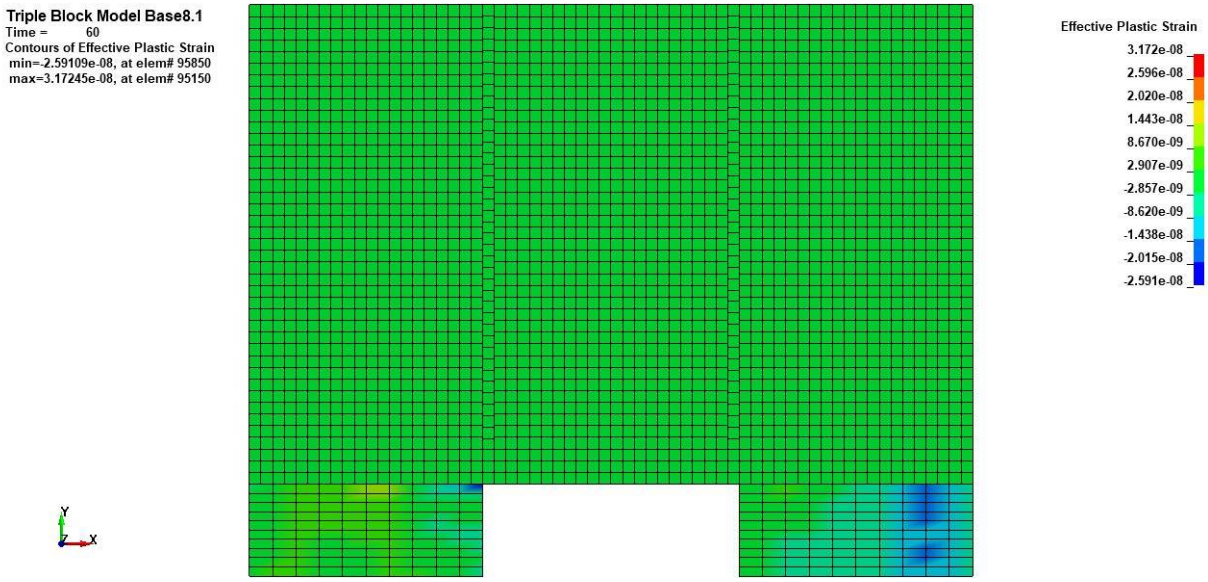


**Figure B-492: Effective Plastic Strain Fringe Plot for Last State at 60 Milliseconds for Base Run 8.1 – 50 psi**

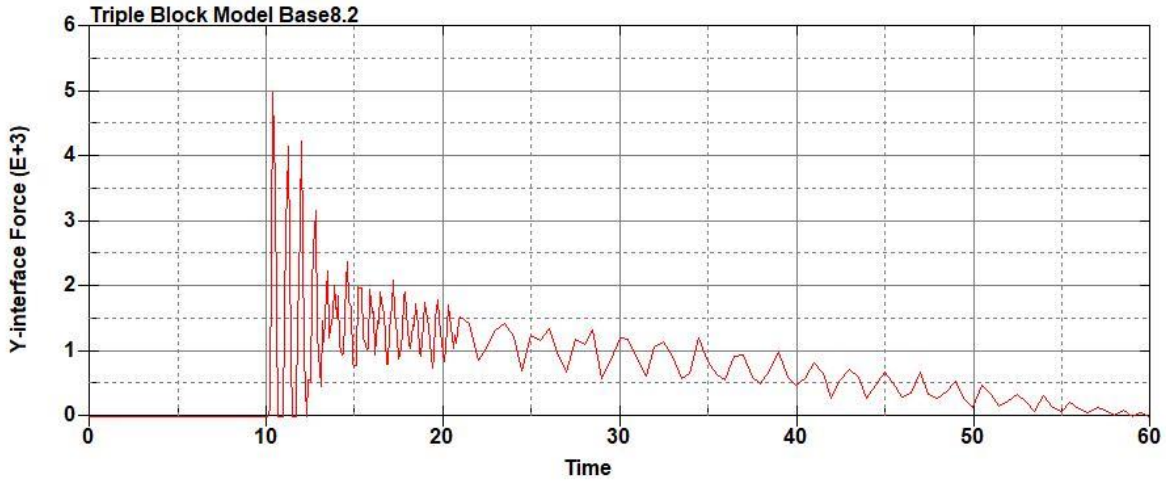


**Figure B-493: Base Run 8.2 Right Support Y-Interface Force (lbs) versus Time (ms) – 100 psi**

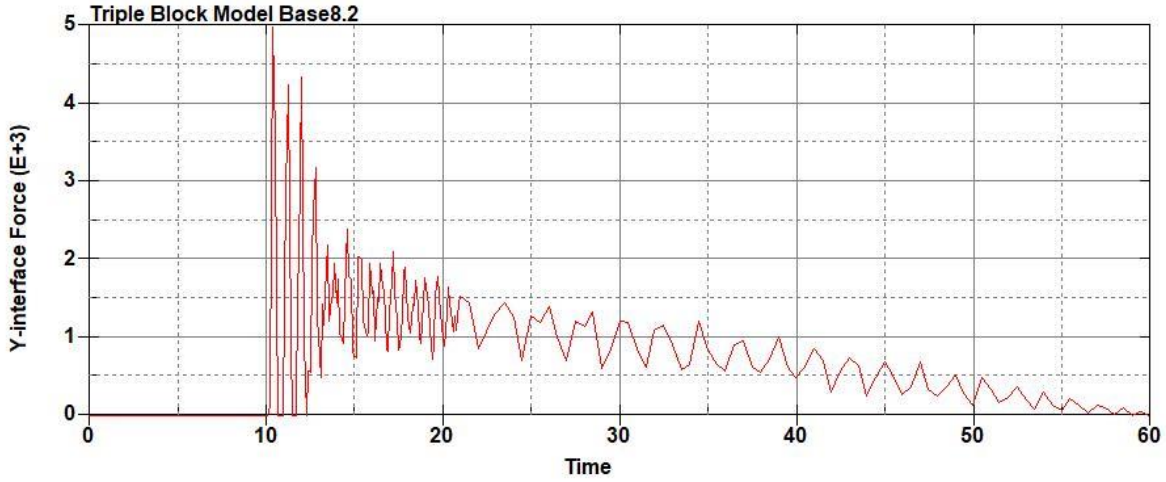


**Figure B-494: Base Run 8.2 Left Support Y-Interface Force (lbs) versus Time (ms) – 100 psi**

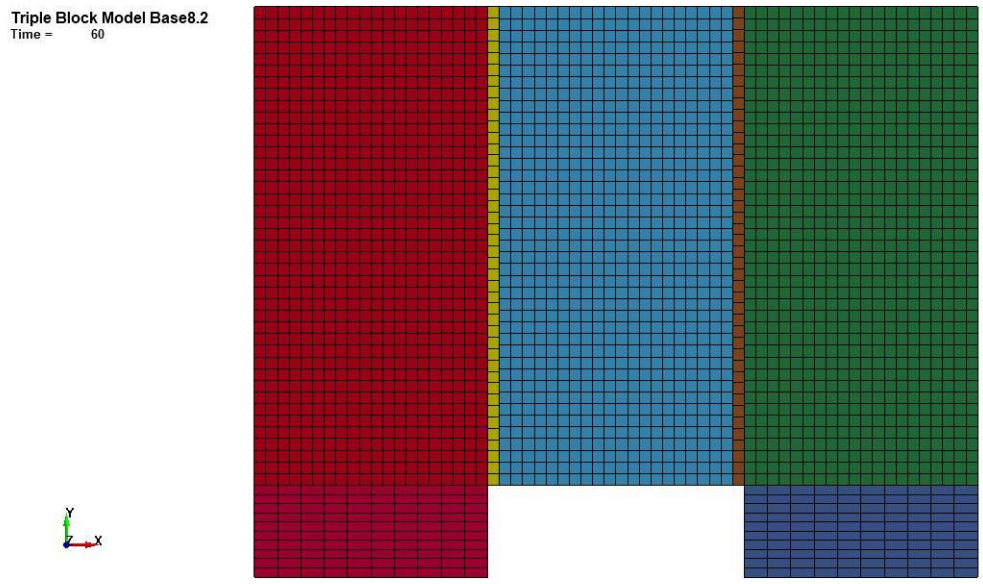


**Figure B-495: Last State at 60 Milliseconds for Base Run 8.2 – 100 psi**

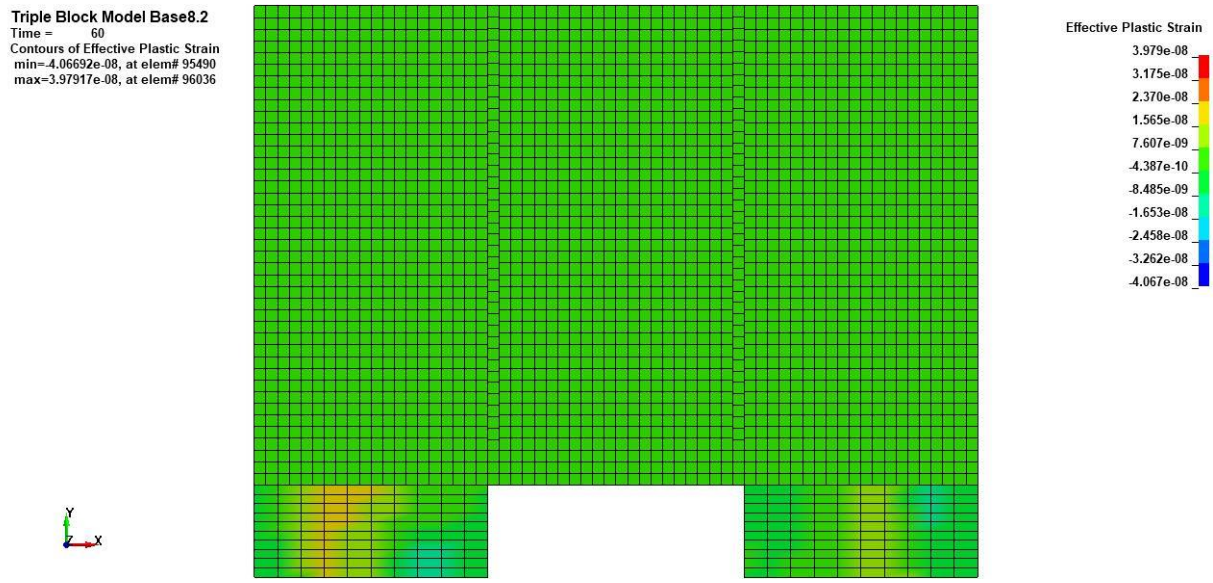


**Figure B-496: Effective Plastic Strain Fringe Plot for Last State at 60 Milliseconds for Base Run 8.2 – 100 psi**

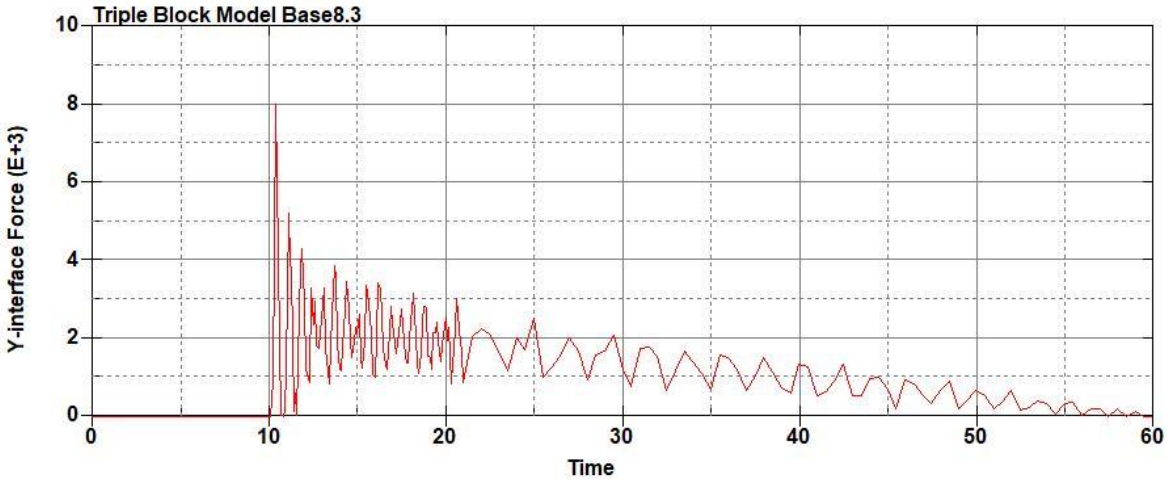


**Figure B-497: Base Run 8.3 Right Support Y-Interface Force (lbs) versus Time (ms) – 150 psi**

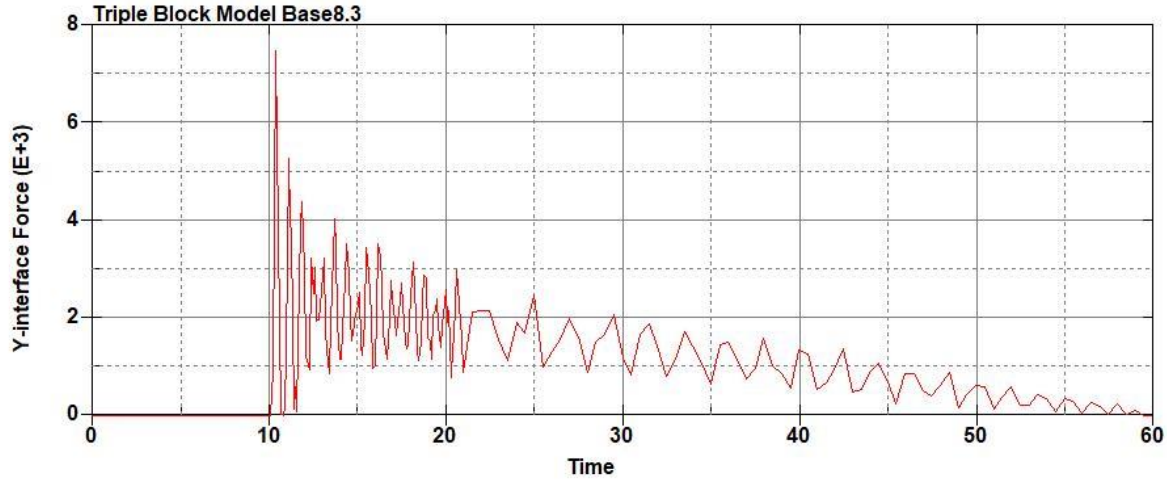


**Figure B-498: Base Run 8.3 Left Support Y-Interface Force (lbs) versus Time (ms) – 150 psi**

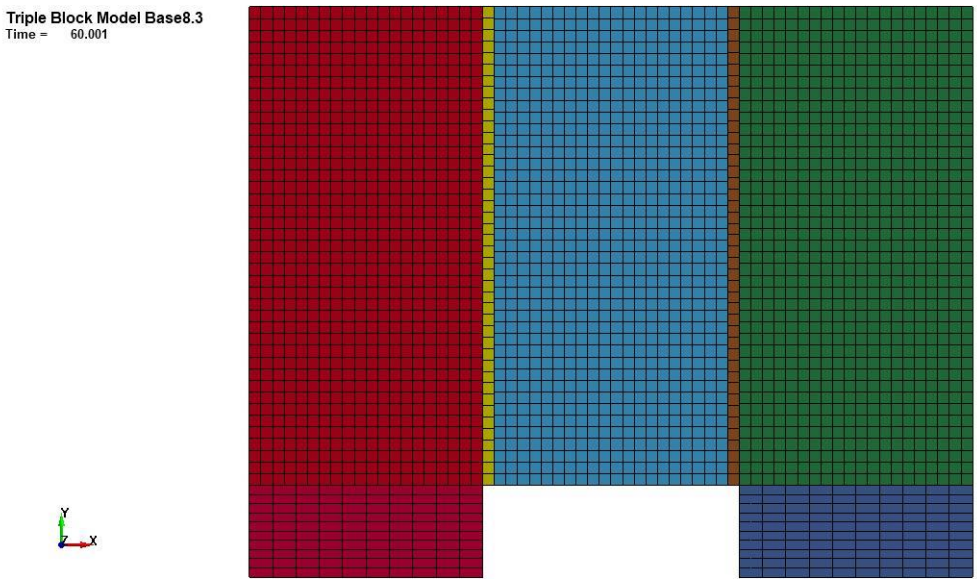


**Figure B-499: Last State at 60 Milliseconds for Base Run 8.3 – 150 psi**

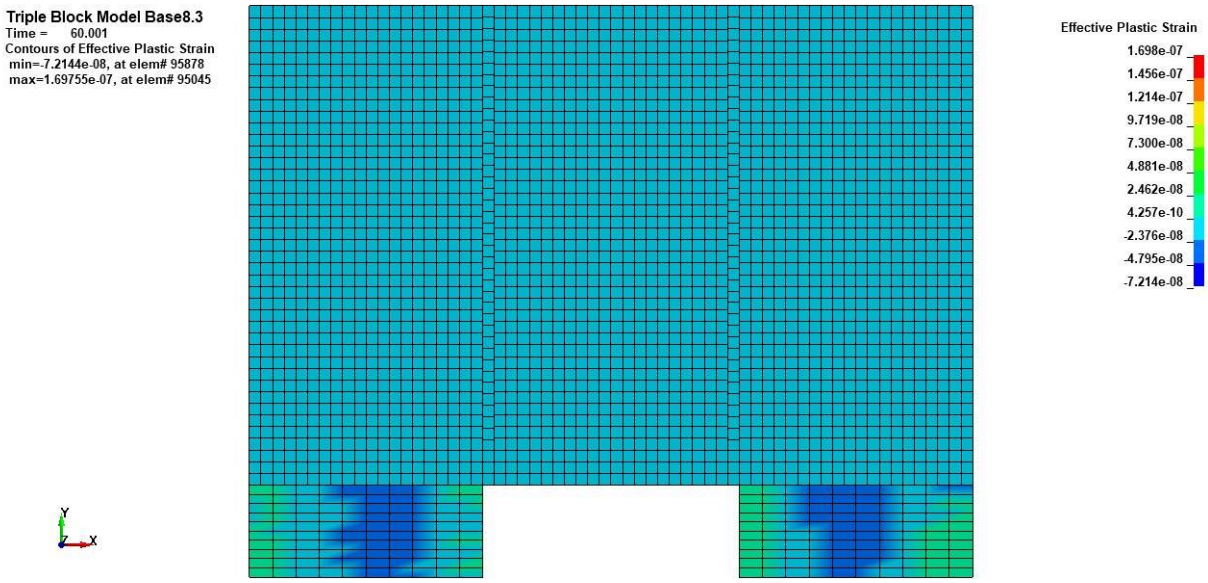


**Figure B-500: Effective Plastic Strain Fringe Plot for Last State at 60 Milliseconds for Base Run 8.3 – 150 psi**

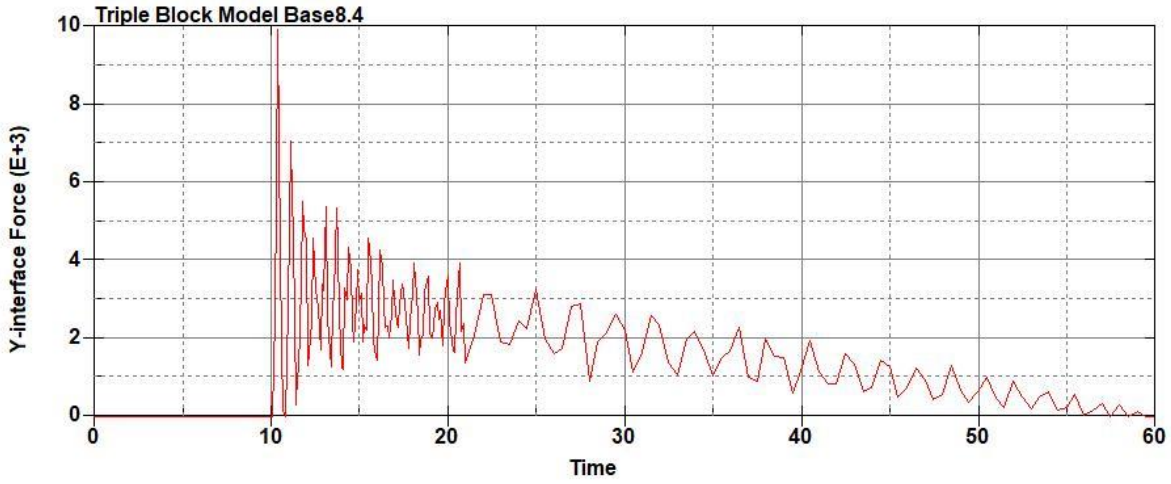


**Figure B-501: Base Run 8.4 Right Support Y-Interface Force (lbs) versus Time (ms) – 200 psi**

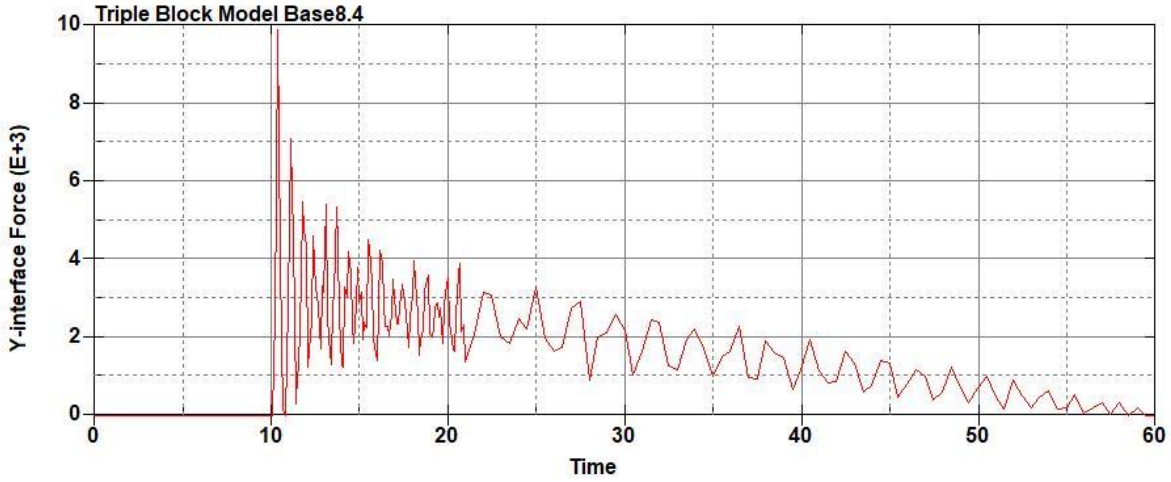


**Figure B-502: Base Run 8.4 Left Support Y-Interface Force (lbs) versus Time (ms) – 200 psi**

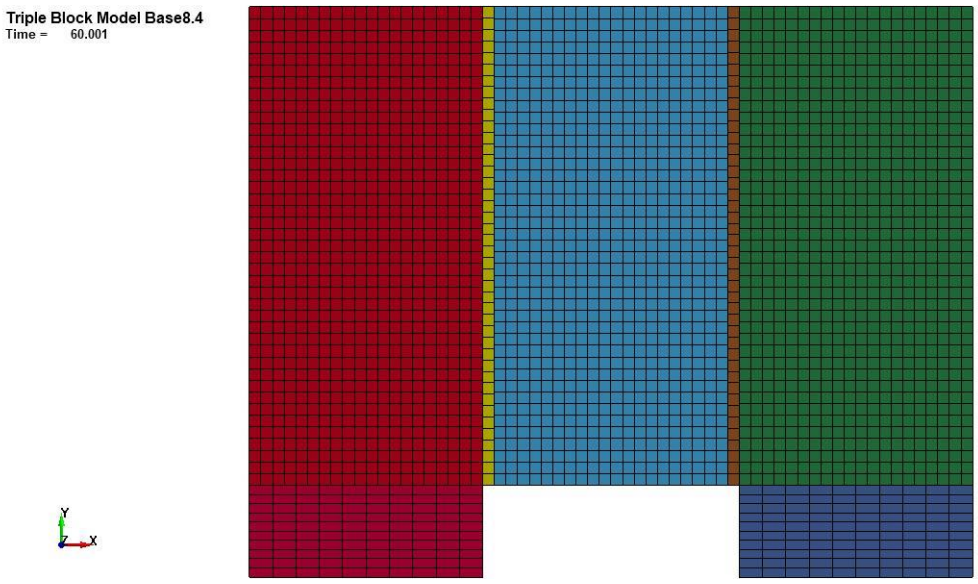


**Figure B-503: Last State at 60 Milliseconds for Base Run 8.4 – 200 psi**

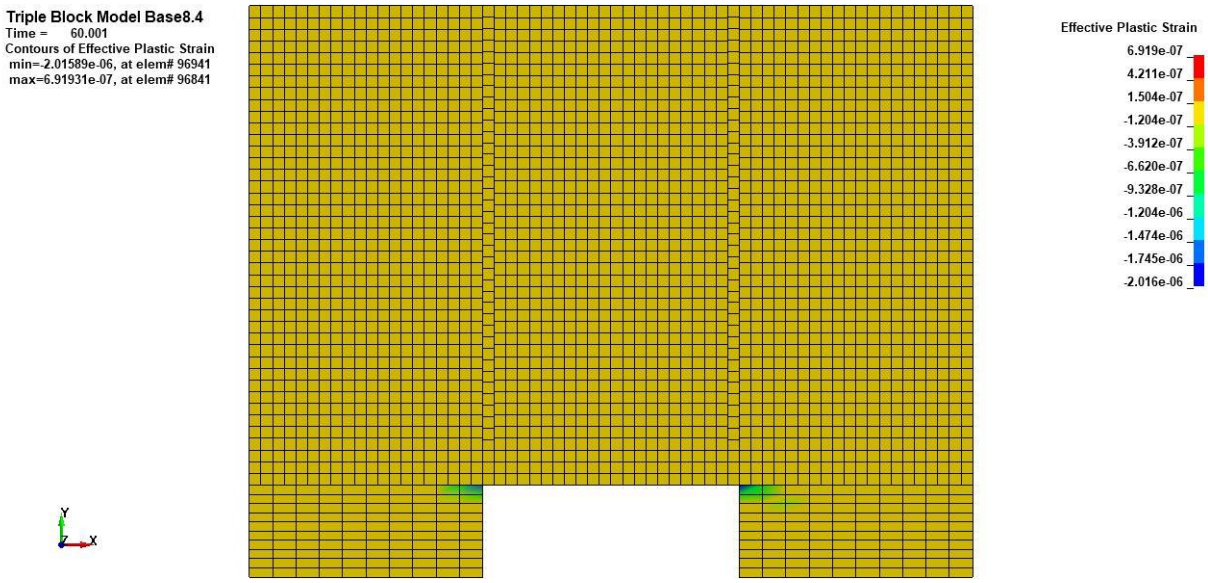


**Figure B-504: Effective Plastic Strain Fringe Plot for Last State at 60 Milliseconds for Base Run 8.4 – 200 psi**

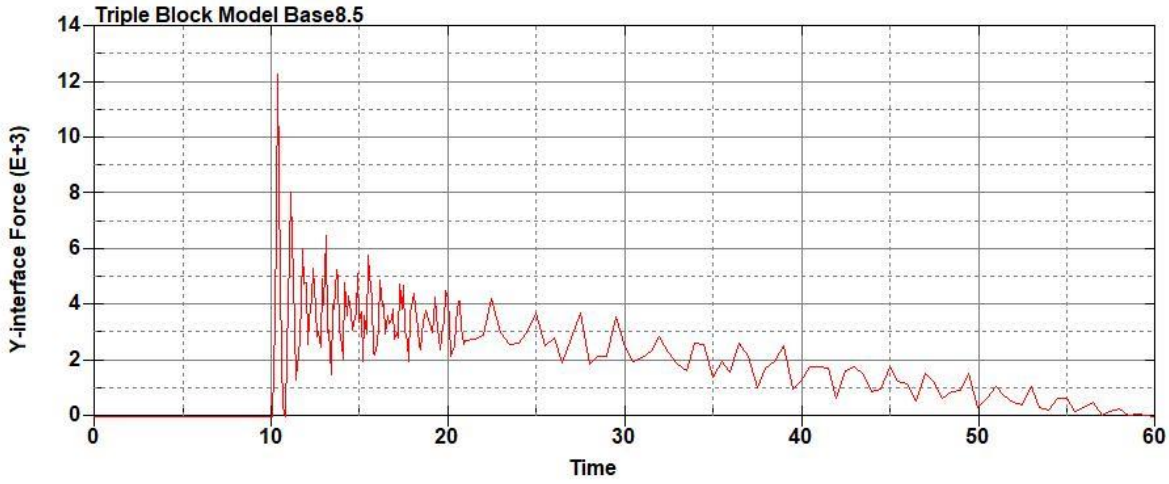


**Figure B-505: Base Run 8.5 Right Support Y-Interface Force (lbs) versus Time (ms) – 250 psi**

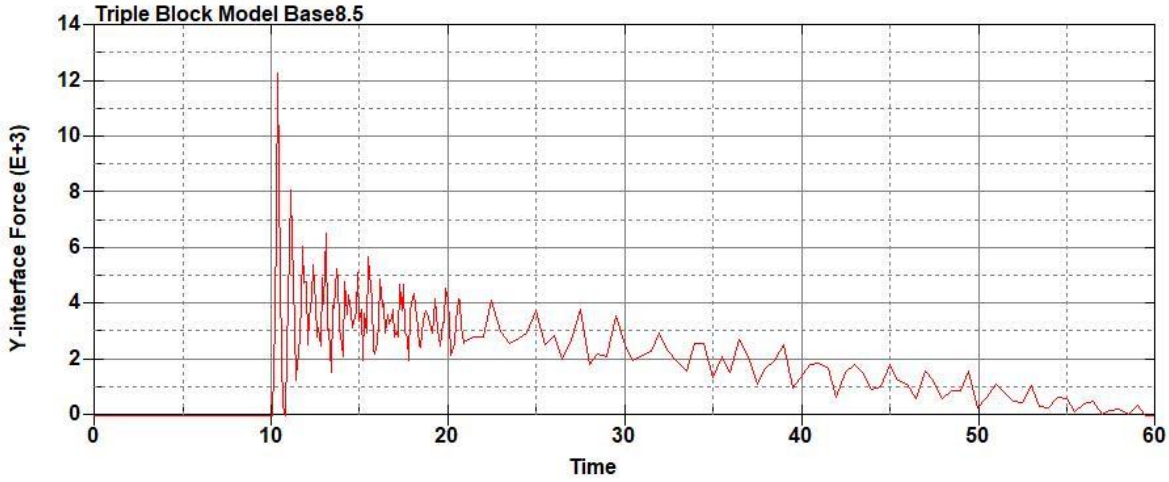


**Figure B-506: Base Run 8.5 Left Support Y-Interface Force (lbs) versus Time (ms) – 250 psi**

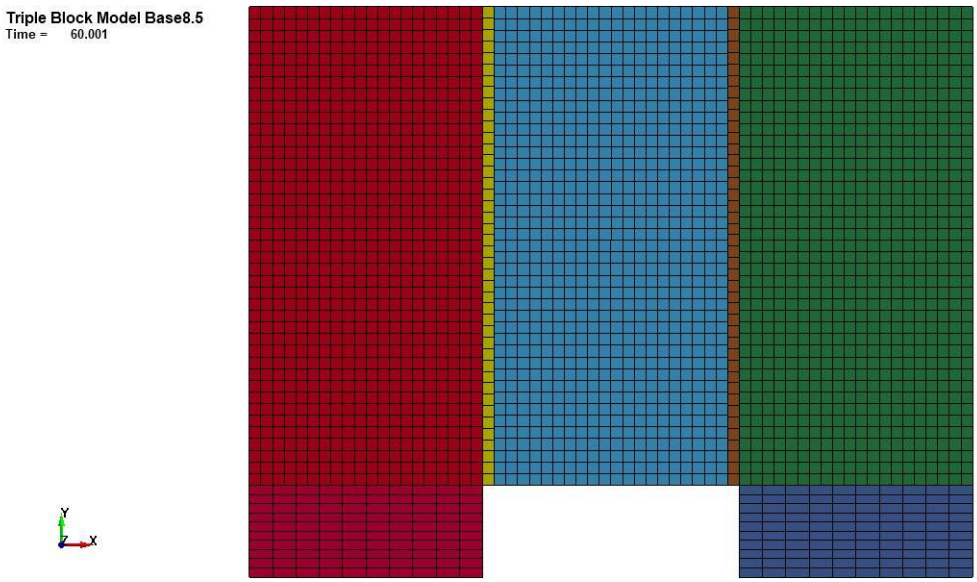


**Figure B-507: Last State at 60 Milliseconds for Base Run 8.5 – 250 psi**

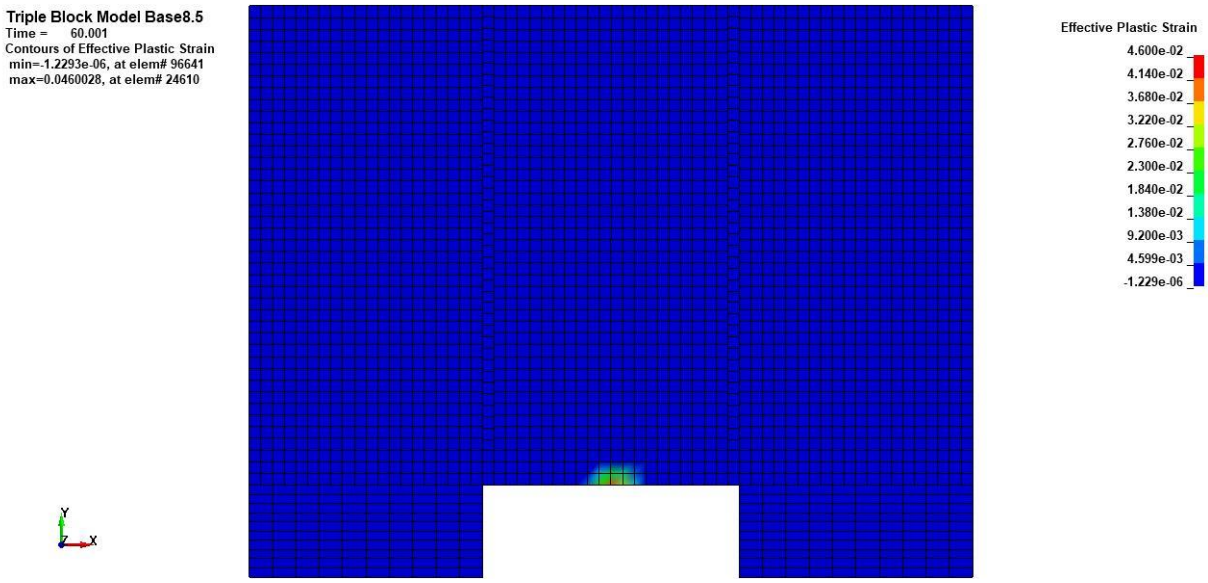


**Figure B-508: Effective Plastic Strain Fringe Plot for Last State at 60 Milliseconds for Base Run 8.5 – 250 psi**

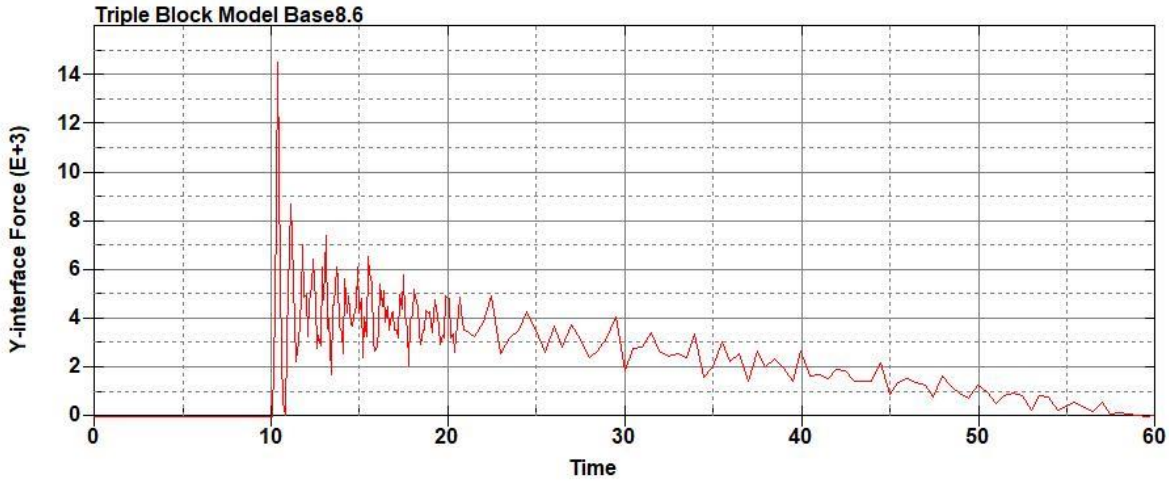


**Figure B-509: Base Run 8.6 Right Support Y-Interface Force (lbs) versus Time (ms) – 300 psi**

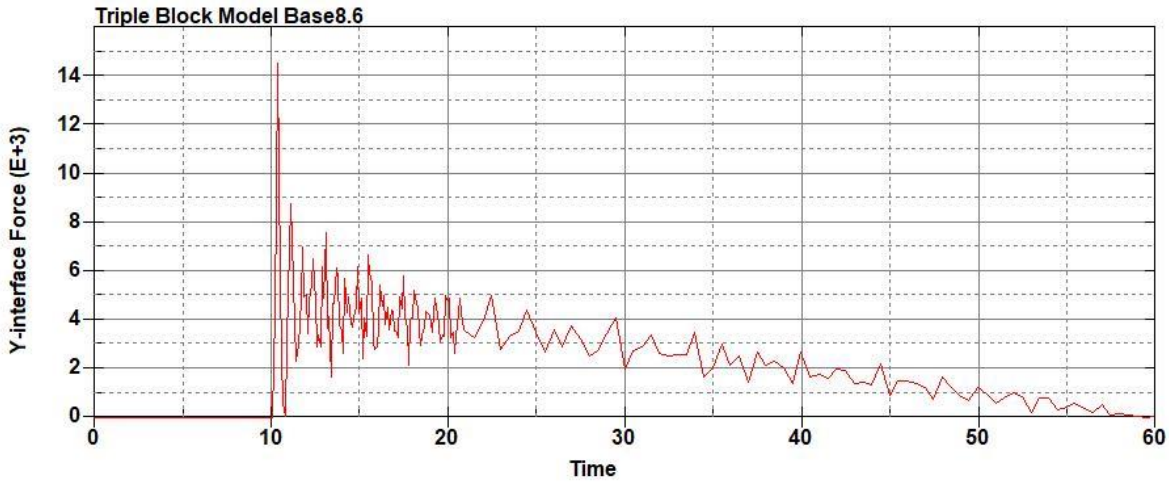


**Figure B-510: Base Run 8.6 Left Support Y-Interface Force (lbs) versus Time (ms) – 300 psi**

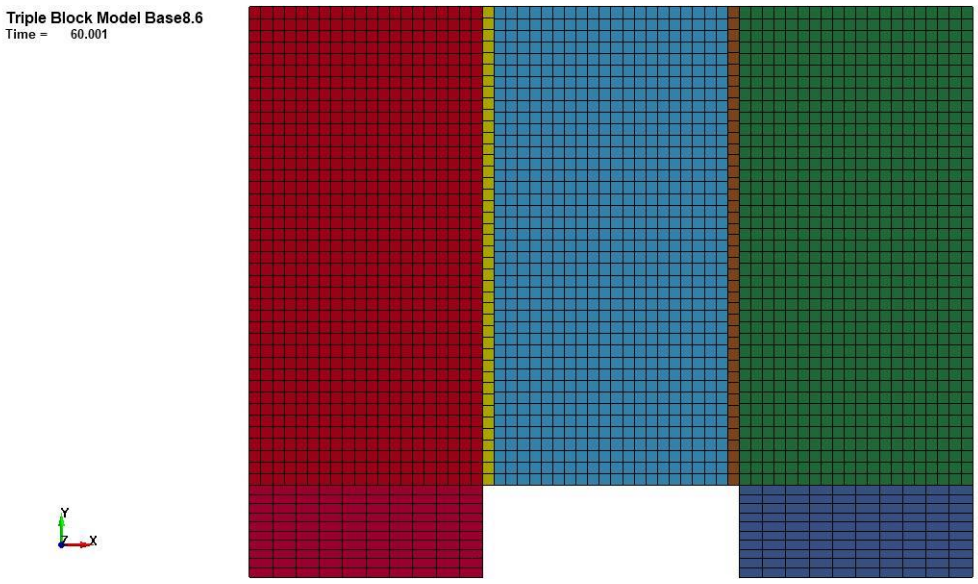


**Figure B-511: Last State at 60 Milliseconds for Base Run 8.6 – 300 psi**

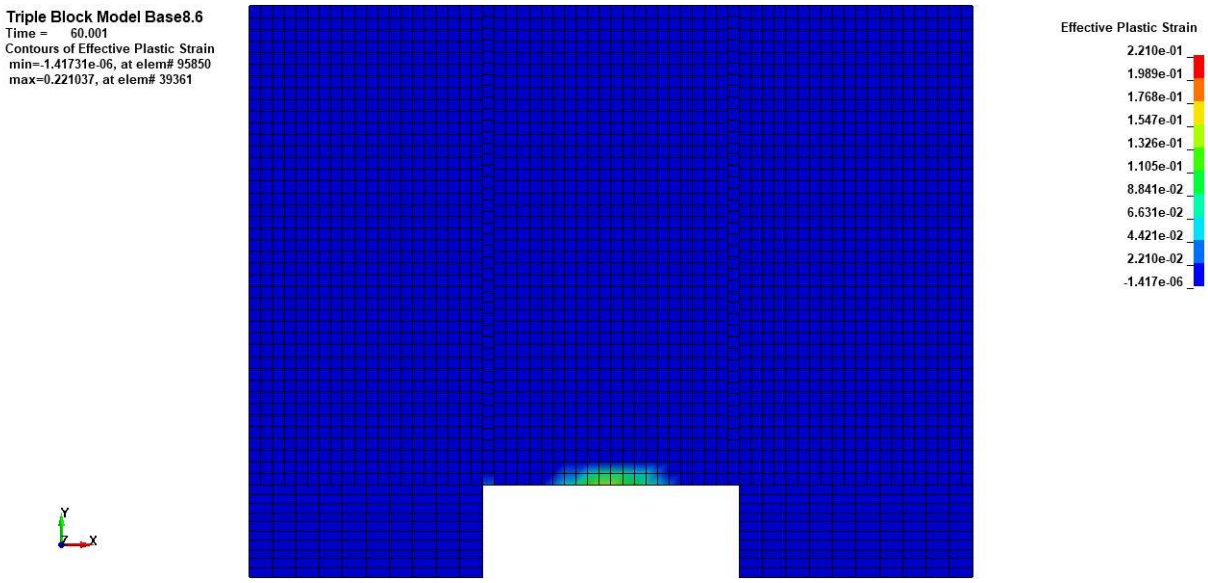


**Figure B-512: Effective Plastic Strain Fringe Plot for Last State at 60 Milliseconds for Base Run 8.6 – 300 psi**

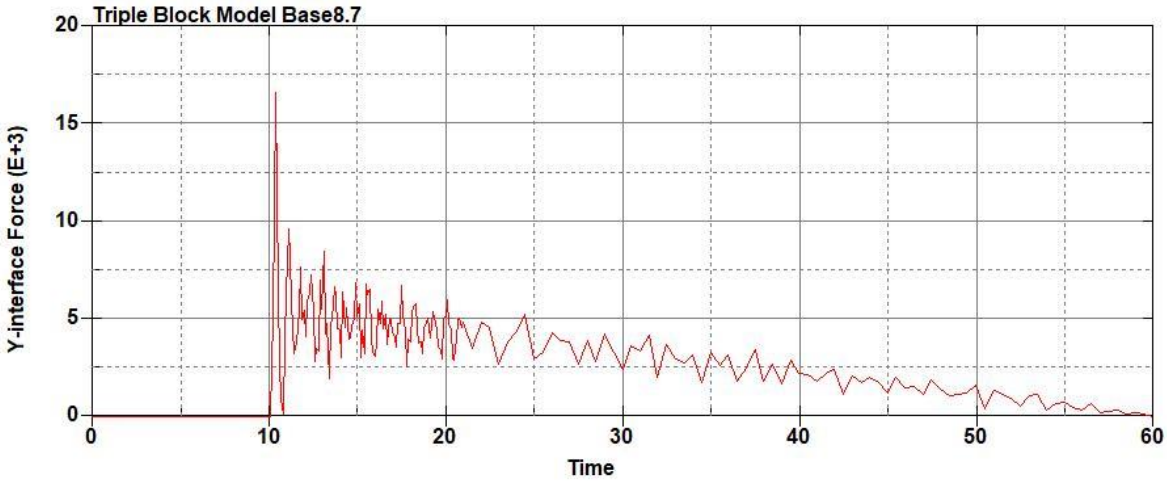


**Figure B-513: Base Run 8.7 Right Support Y-Interface Force (lbs) versus Time (ms) – 350 psi**

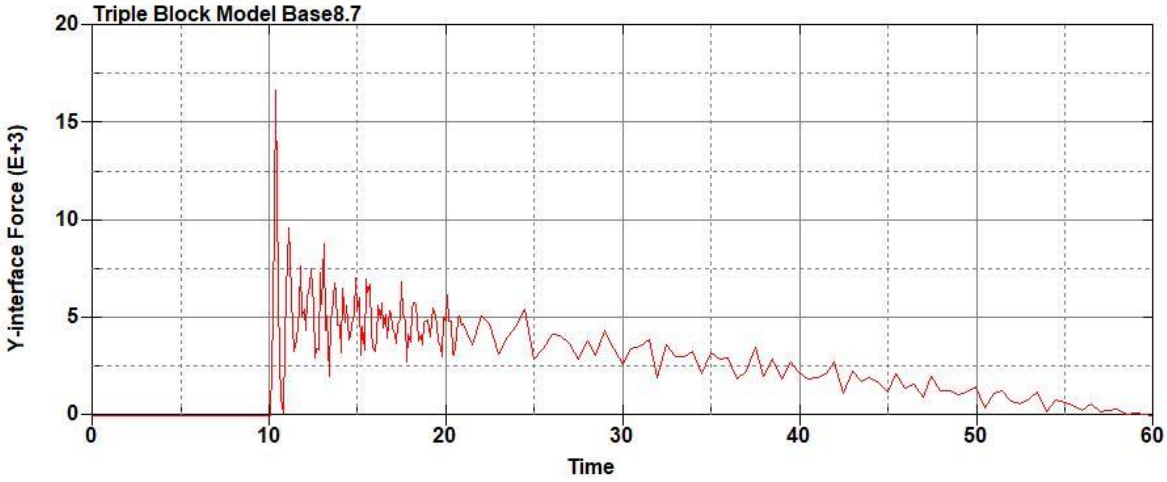


**Figure B-514: Base Run 8.7 Left Support Y-Interface Force (lbs) versus Time (ms) – 350 psi**

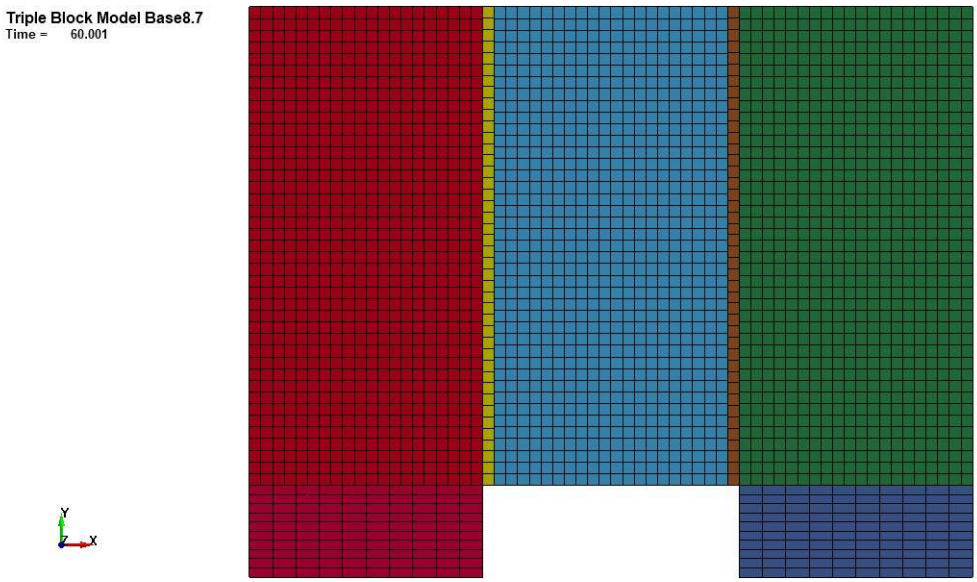


**Figure B-515: Last State at 60 Milliseconds for Base Run 8.7 – 350 psi**

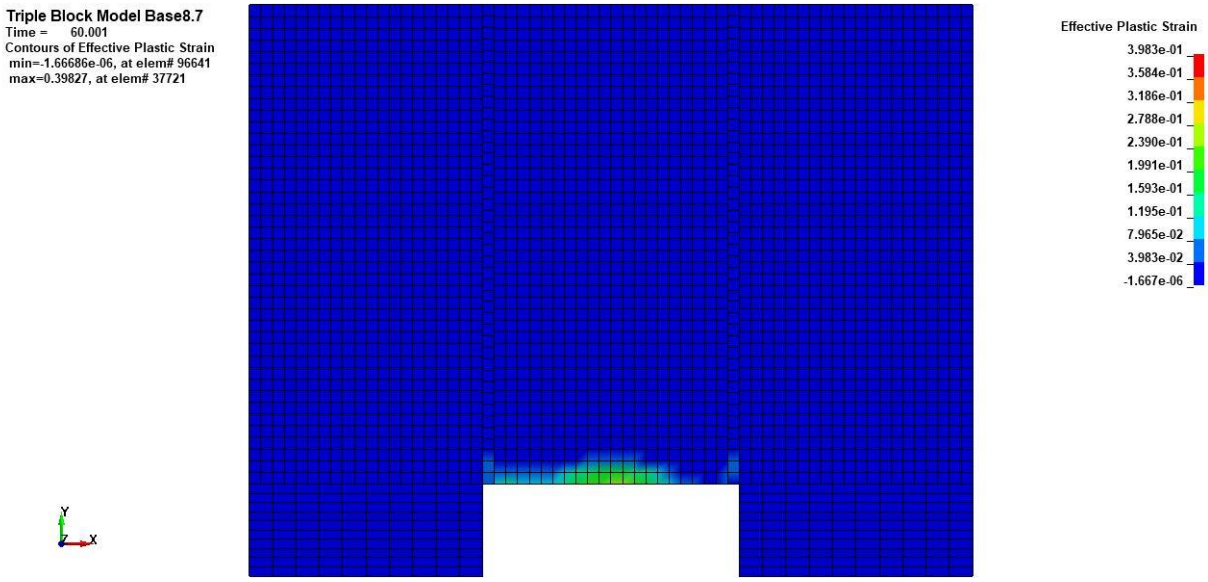


**Figure B-516: Effective Plastic Strain Fringe Plot for Last State at 60 Milliseconds for Base Run 8.7 – 350 psi**

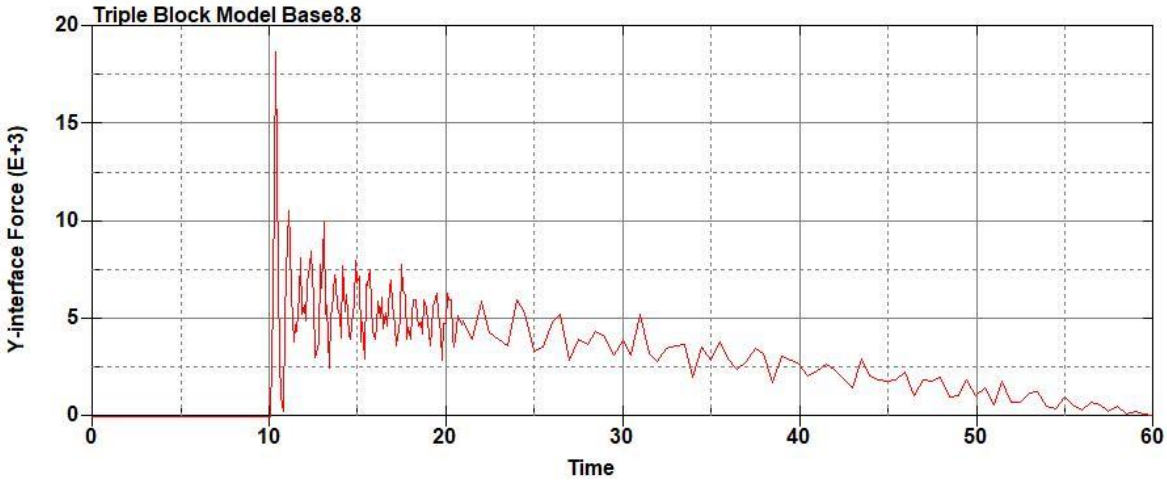


**Figure B-517: Base Run 8.8 Right Support Y-Interface Force (lbs) versus Time (ms) – 400 psi**

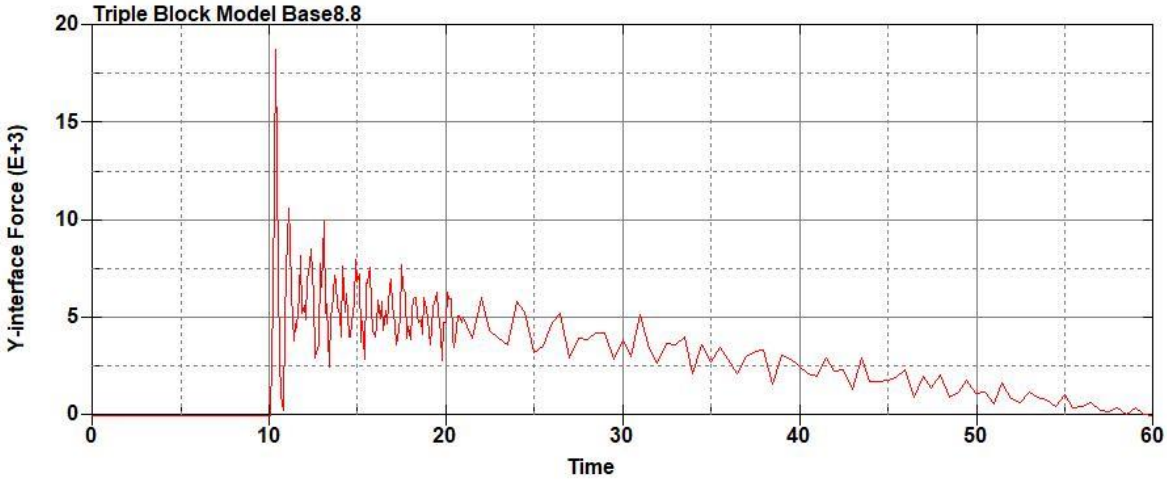


**Figure B-518: Base Run 8.8 Left Support Y-Interface Force (lbs) versus Time (ms) – 400 psi**

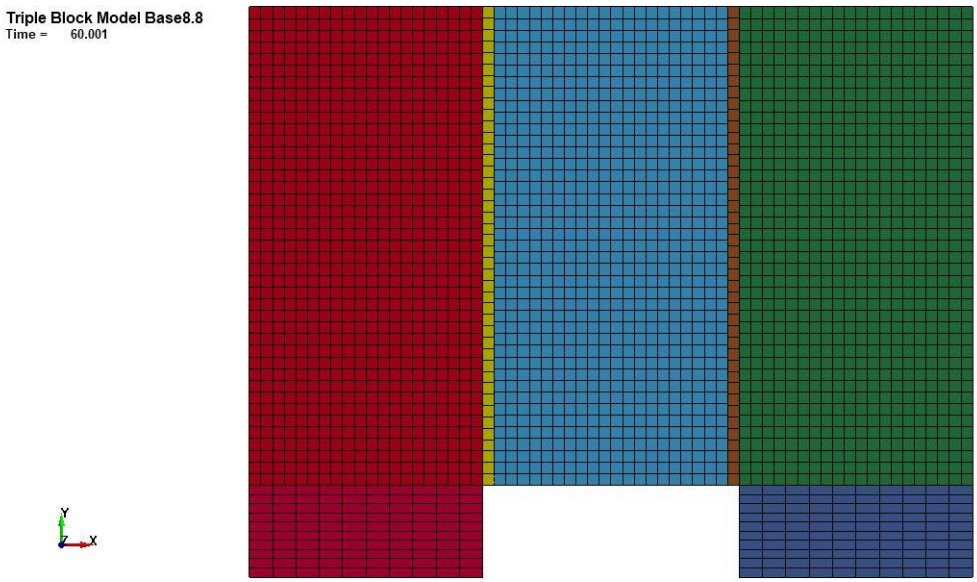


**Figure B-519: Last State at 60 Milliseconds for Base Run 8.8 – 400 psi**

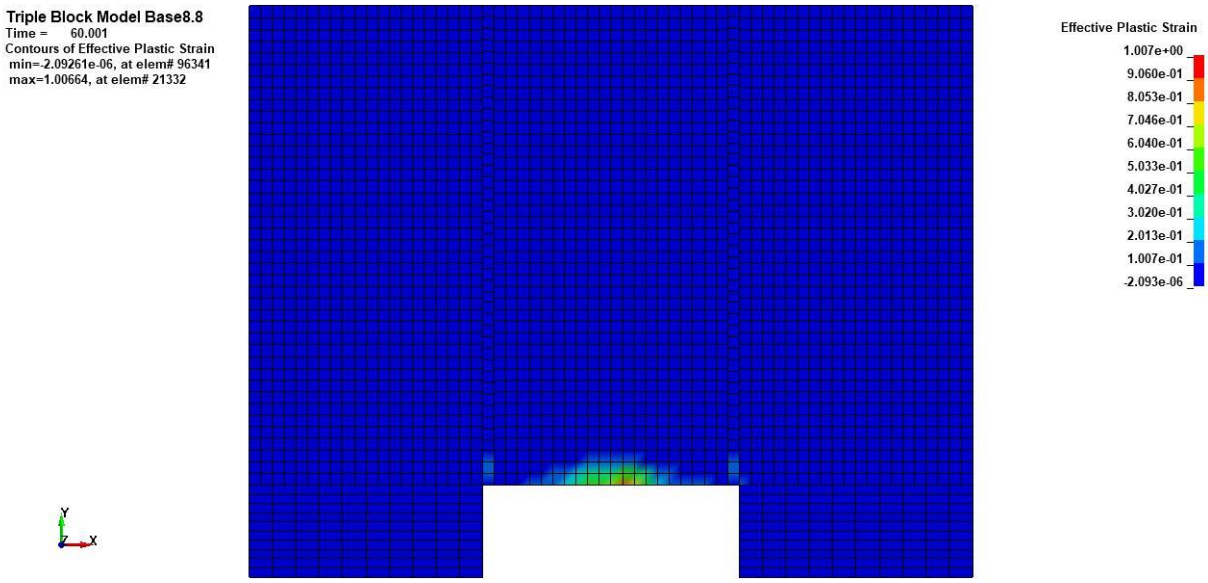


**Figure B-520: Effective Plastic Strain Fringe Plot for Last State at 60 Milliseconds for Base Run 8.8 – 400 psi**

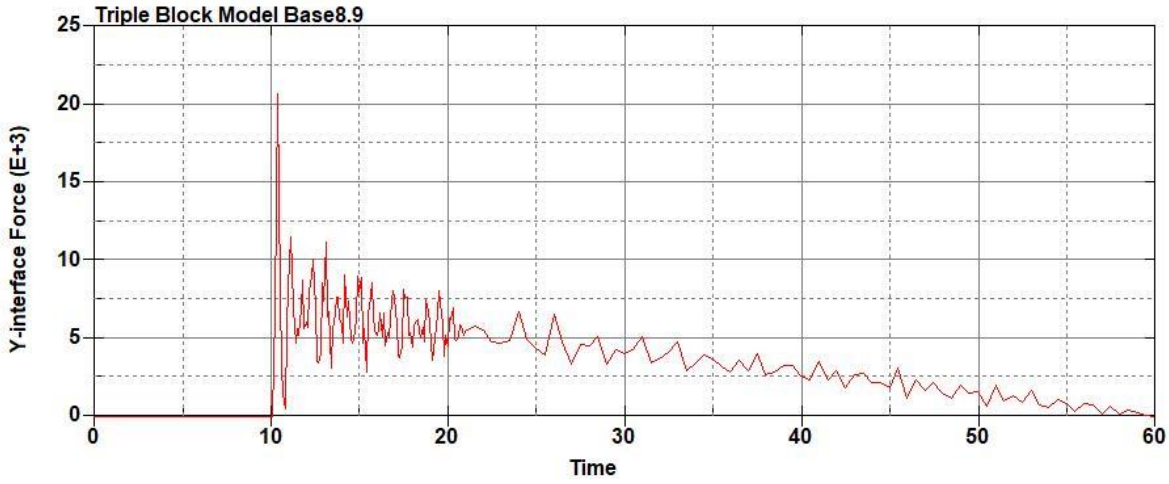


**Figure B-521: Base Run 8.9 Right Support Y-Interface Force (lbs) versus Time (ms) – 450 psi**

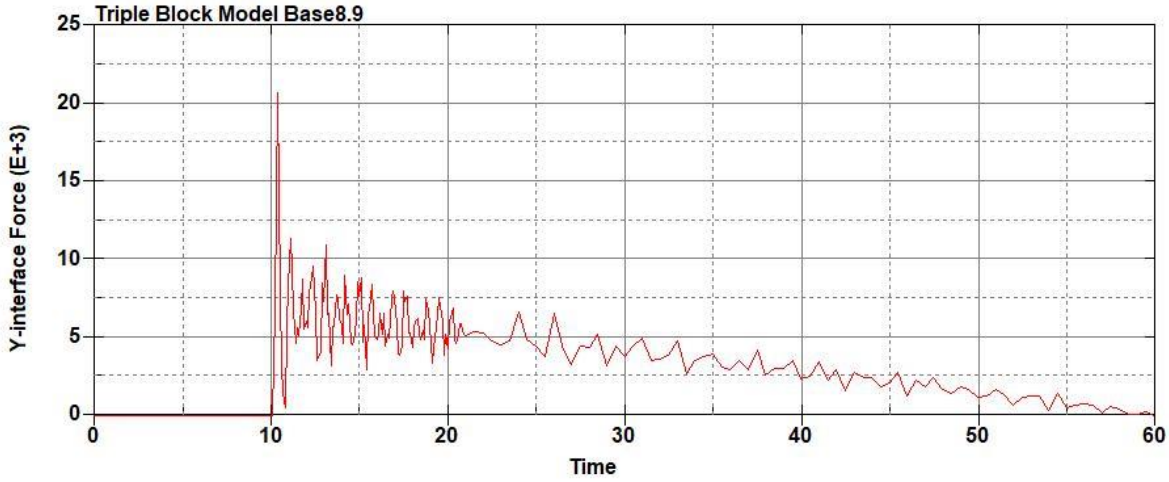


**Figure B-522: Base Run 8.9 Left Support Y-Interface Force (lbs) versus Time (ms) – 450 psi**

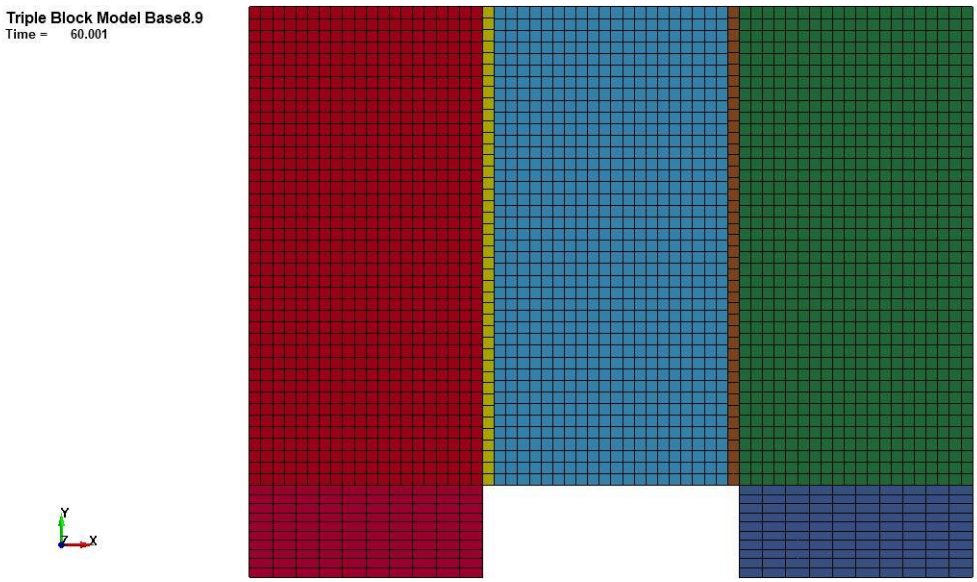


**Figure B-523: Last State at 60 Milliseconds for Base Run 8.9 – 450 psi**

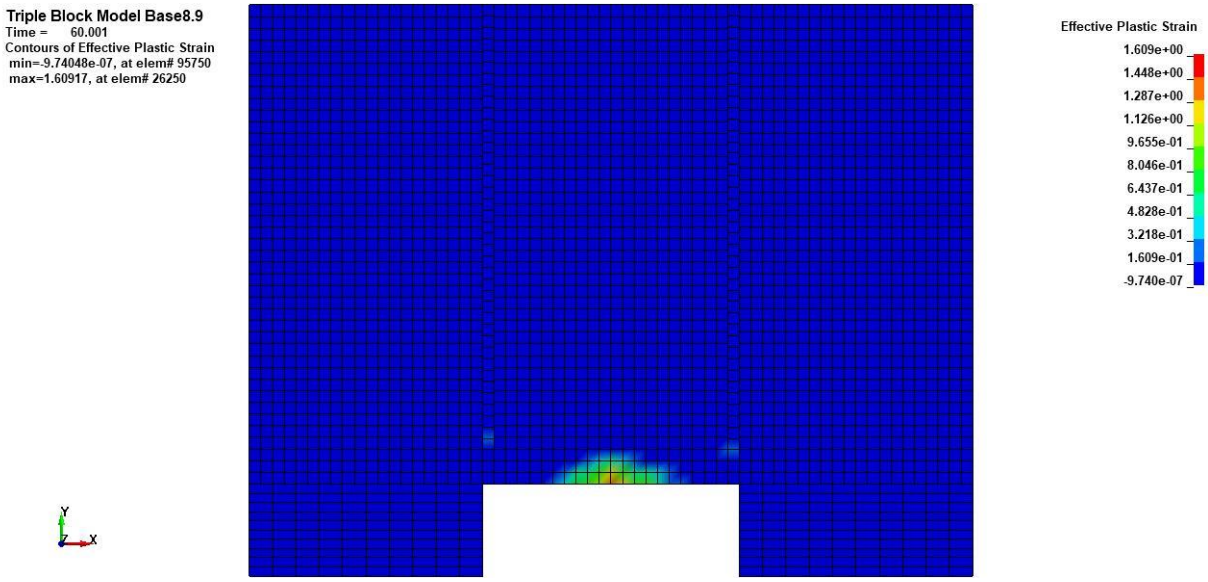


**Figure B-524: Effective Plastic Strain Fringe Plot for Last State at 60 Milliseconds for Base Run 8.9 – 450 psi**

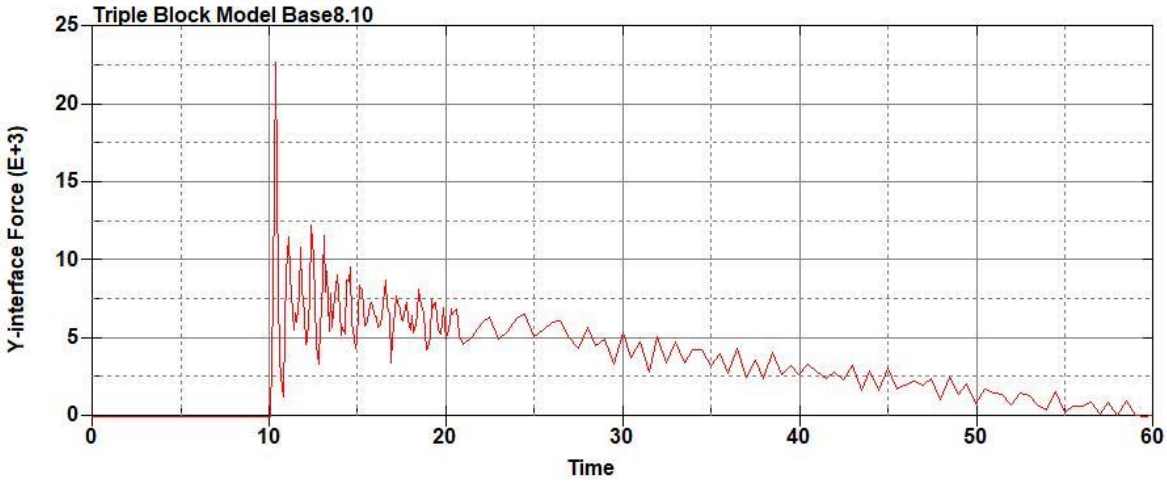


**Figure B-525: Base Run 8.10 Right Support Y-Interface Force (lbs) versus Time (ms) – 500 psi**

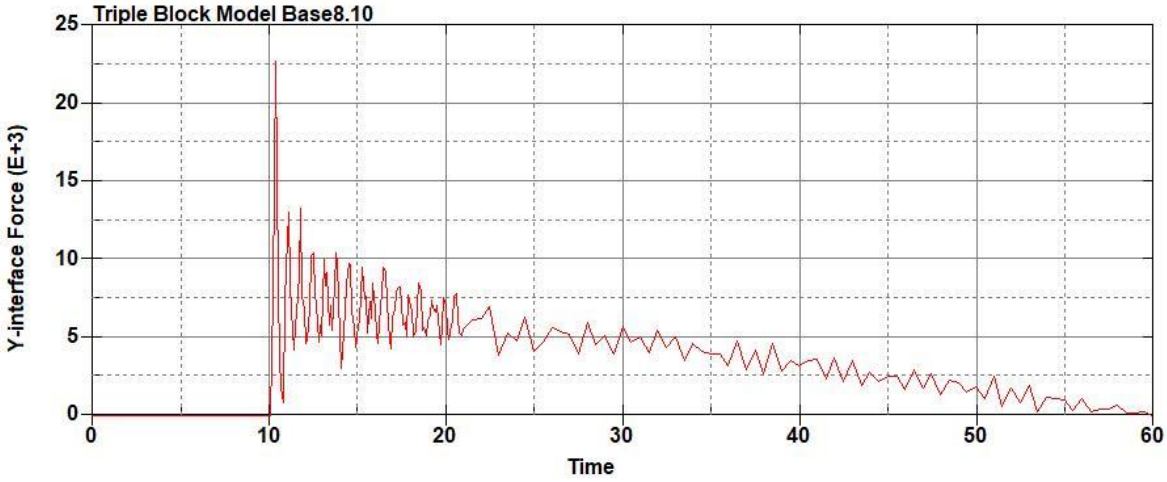


**Figure B-526: Base Run 8.10 Left Support Y-Interface Force (lbs) versus Time (ms) – 500 psi**

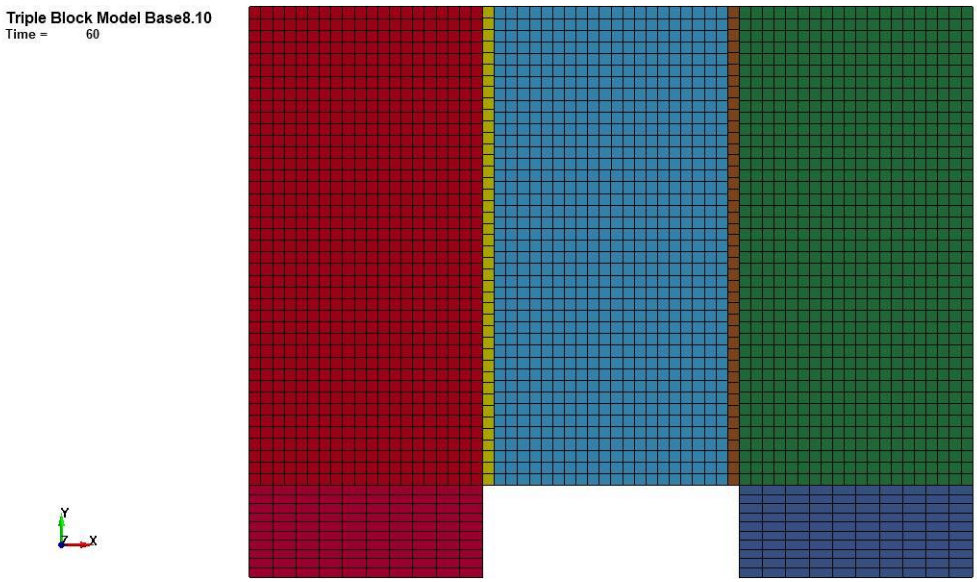


**Figure B-527: Last State at 60 Milliseconds for Base Run 8.10 – 500 psi**

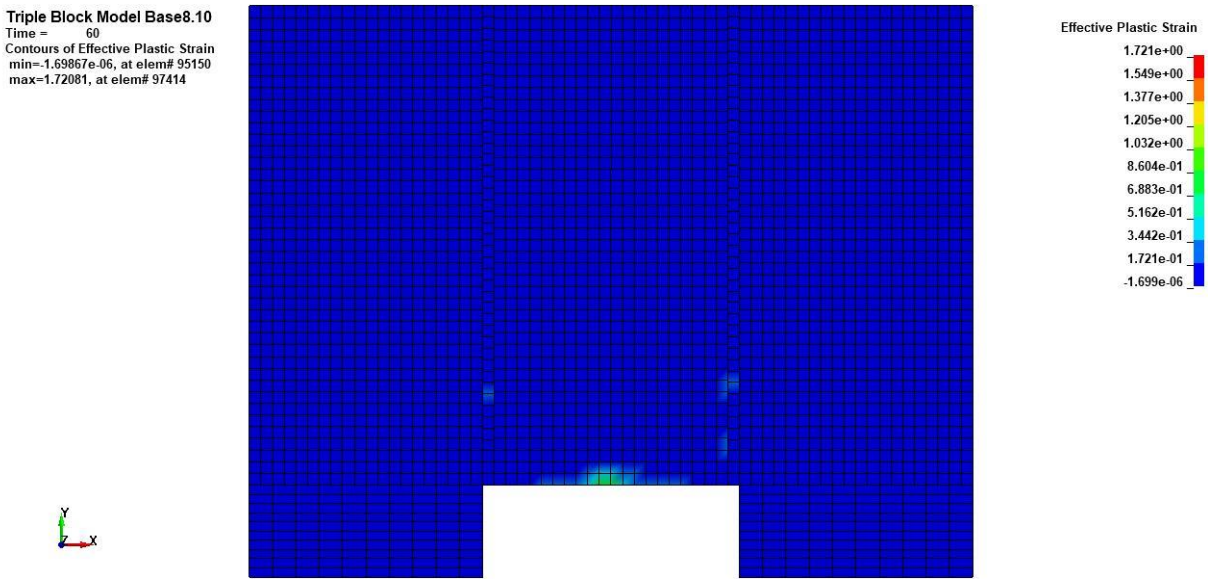


**Figure B-528: Effective Plastic Strain Fringe Plot for Last State at 60 Milliseconds for Base Run 8.10 – 500 psi**

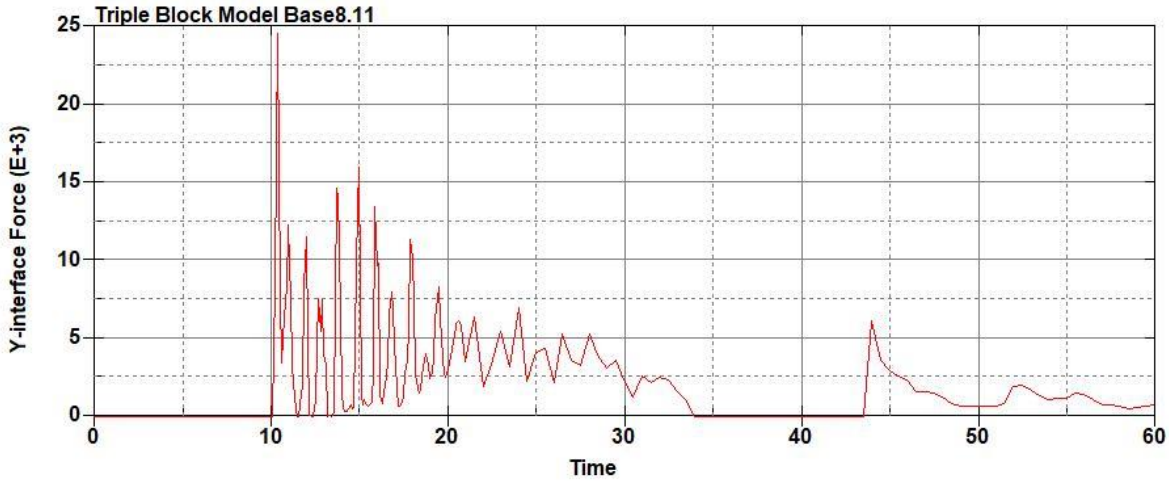


**Figure B-529: Base Run 8.11 Right Support Y-Interface Force (lbs) versus Time (ms) – 550 psi**

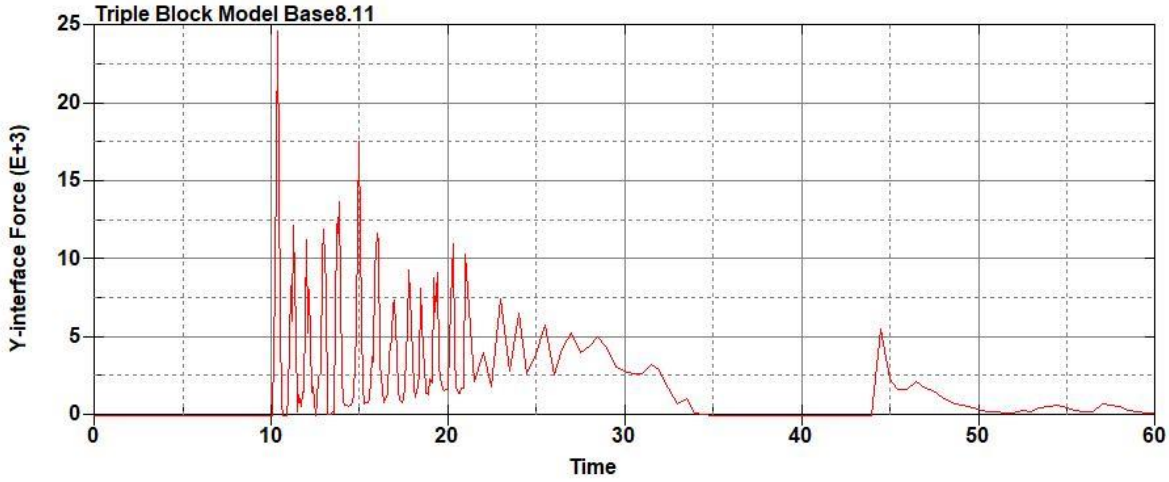


**Figure B-530: Base Run 8.11 Left Support Y-Interface Force (lbs) versus Time (ms) – 550 psi**

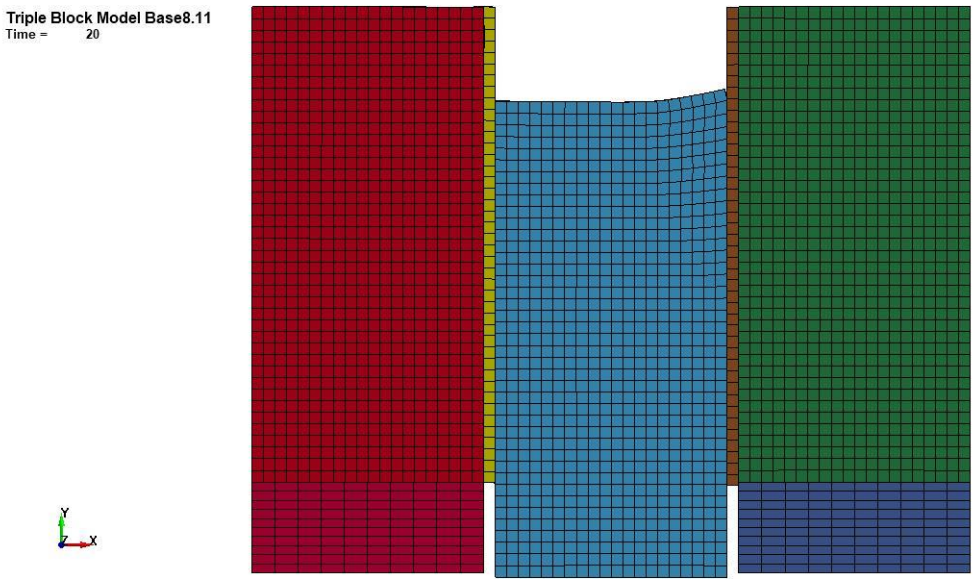


**Figure B-531: Last State at 20 Milliseconds for Base Run 8.11 – 550 psi**

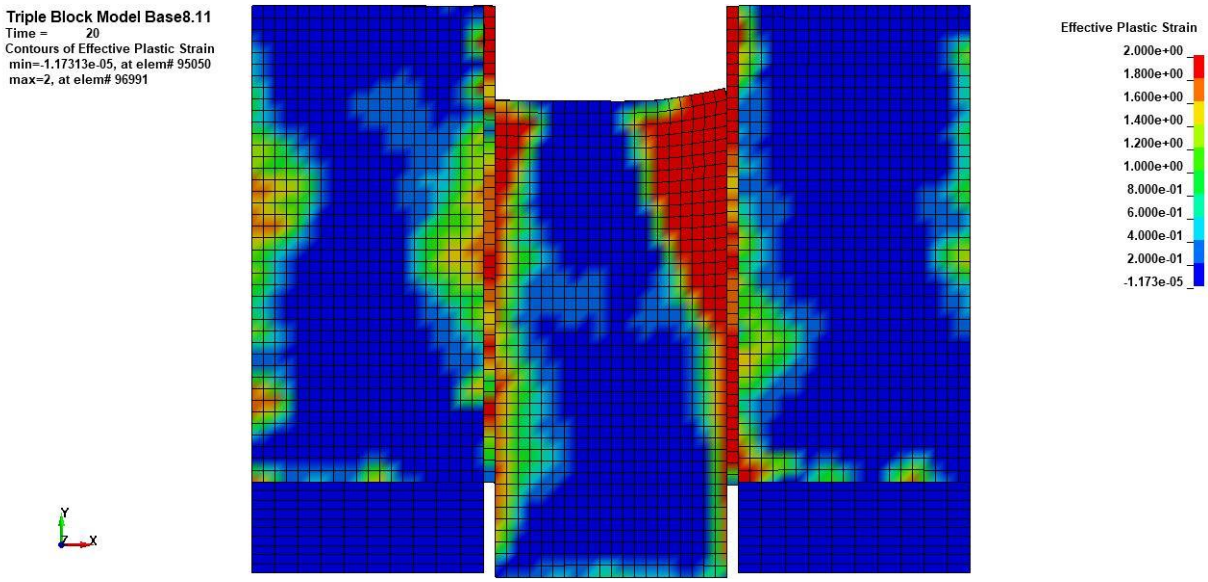


**Figure B-532: Effective Plastic Strain Fringe Plot for Last State at 20 Milliseconds for Base Run 8.11 – 550 psi**

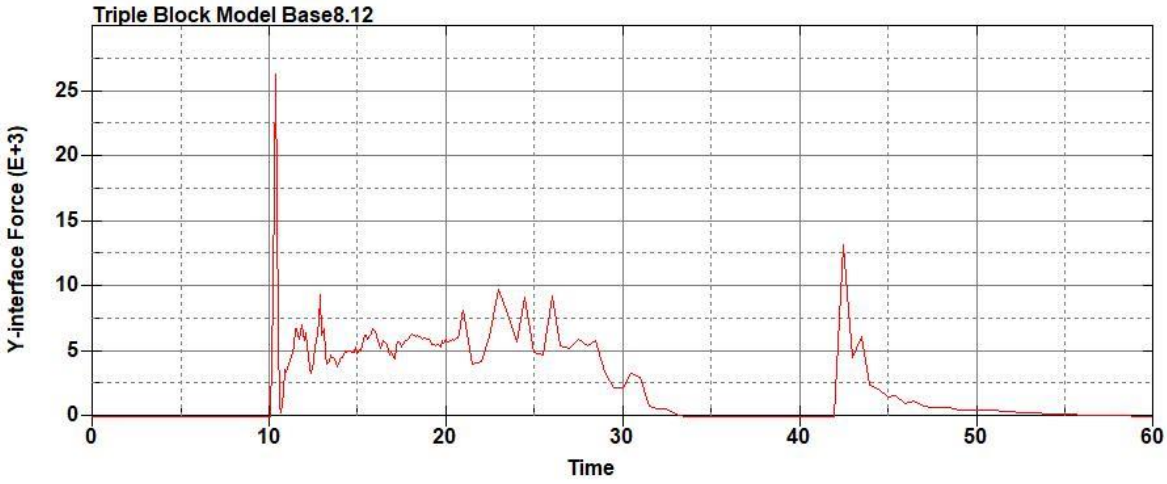


**Figure B-533: Base Run 8.12 Right Support Y-Interface Force (lbs) versus Time (ms) – 600 psi**

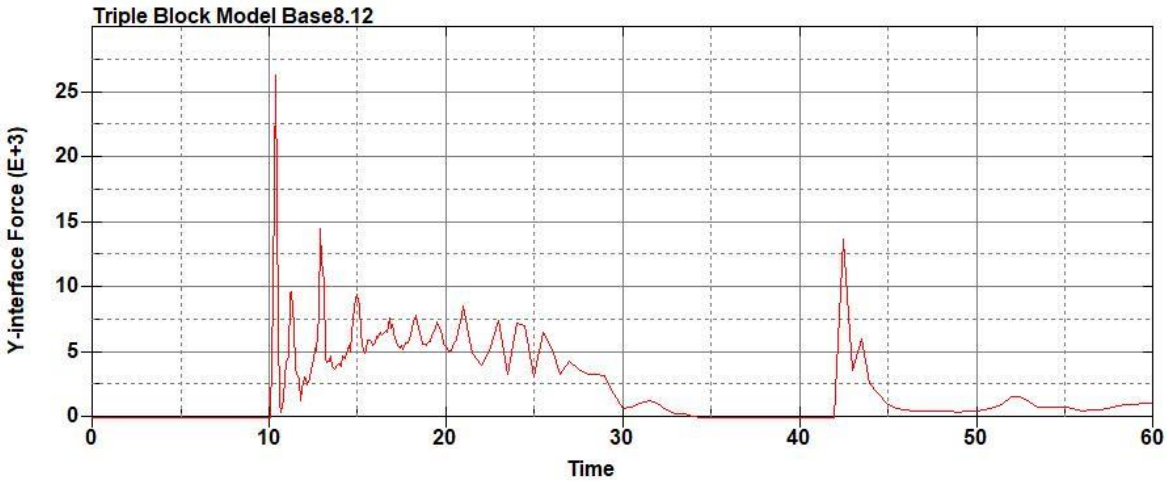


**Figure B-534: Base Run 8.12 Left Support Y-Interface Force (lbs) versus Time (ms) – 600 psi**

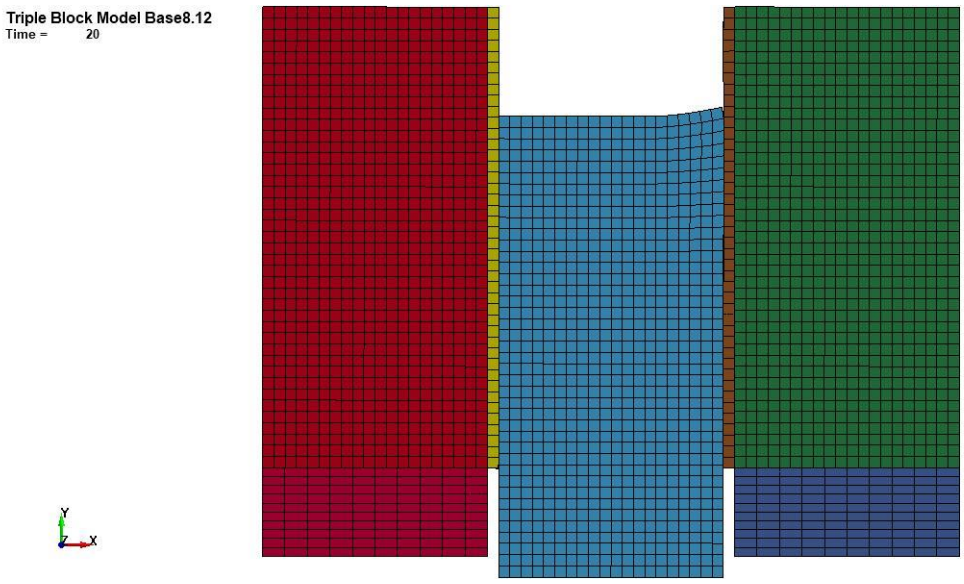


**Figure B-535: Last State at 20 Milliseconds for Base Run 8.12 – 600 psi**

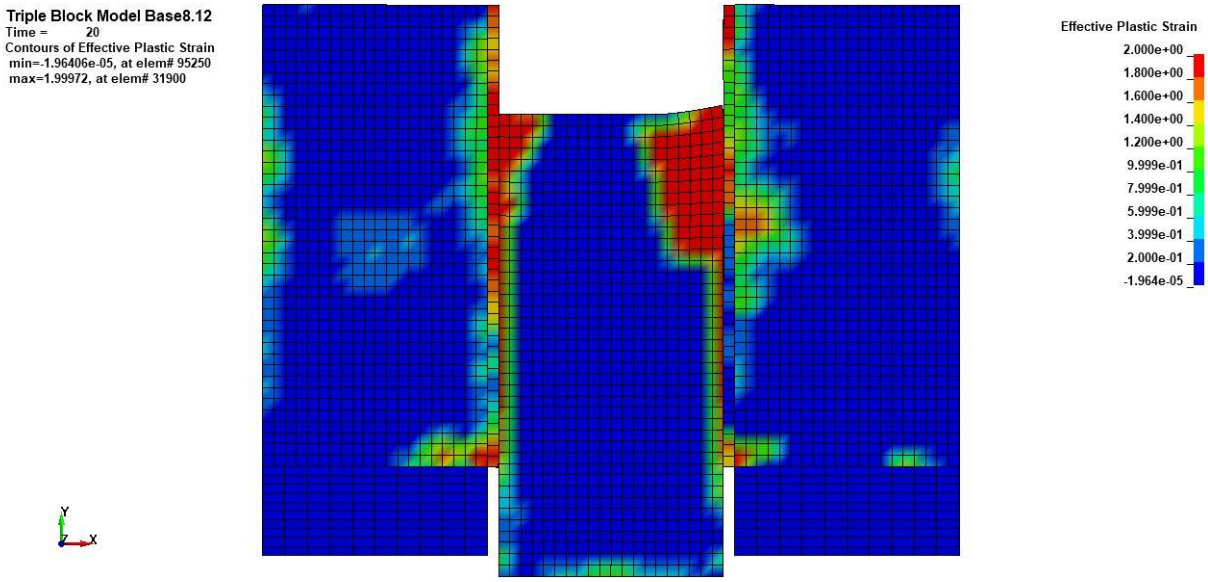


**Figure B-536: Effective Plastic Strain Fringe Plot for Last State at 20 Milliseconds for Base Run 8.12 – 600 psi**

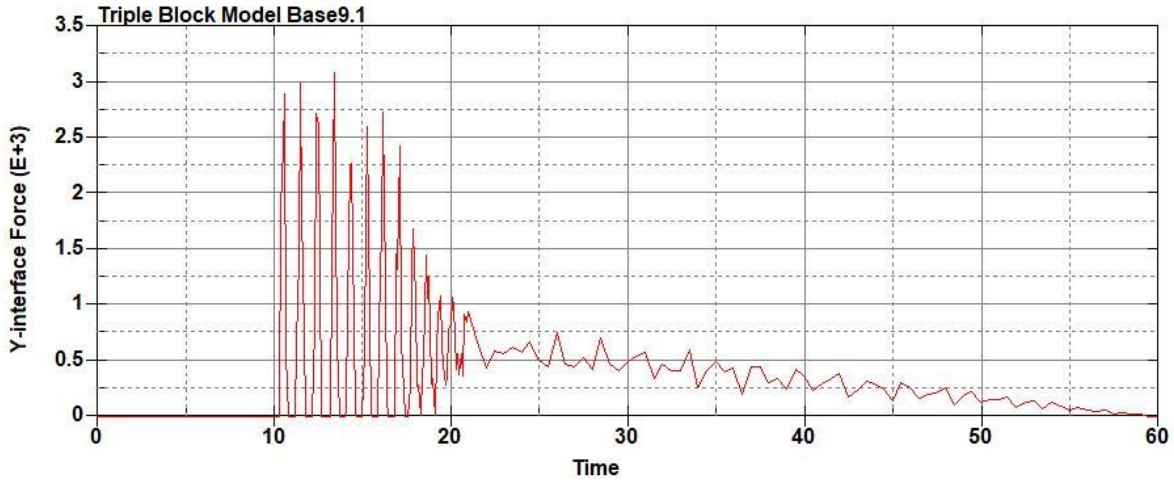


**Figure B-537: Base Run 9.1 Right Support Y-Interface Force (lbs) versus Time (ms) – 50 psi**

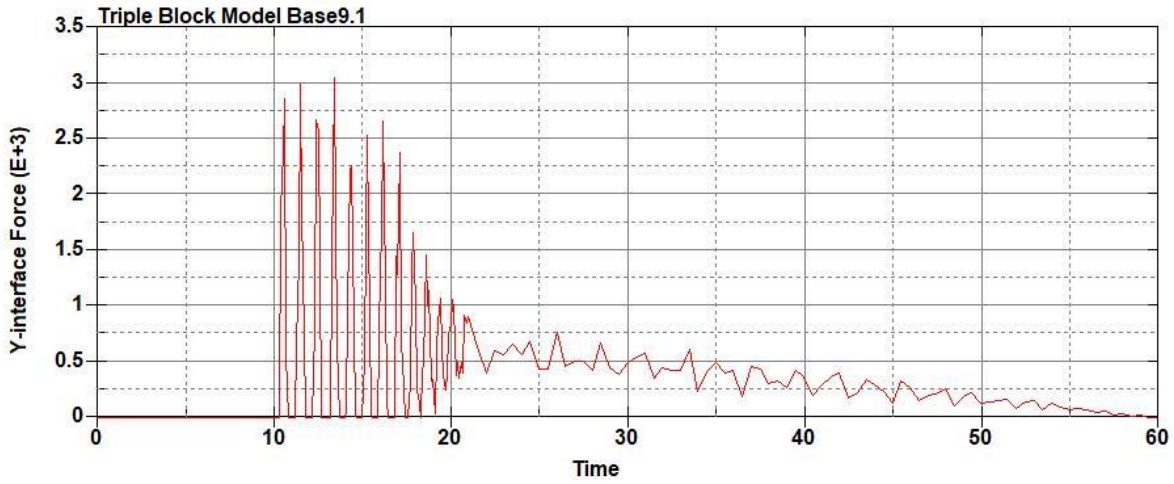


**Figure B-538: Base Run 9.1 Left Support Y-Interface Force (lbs) versus Time (ms) – 50 psi**

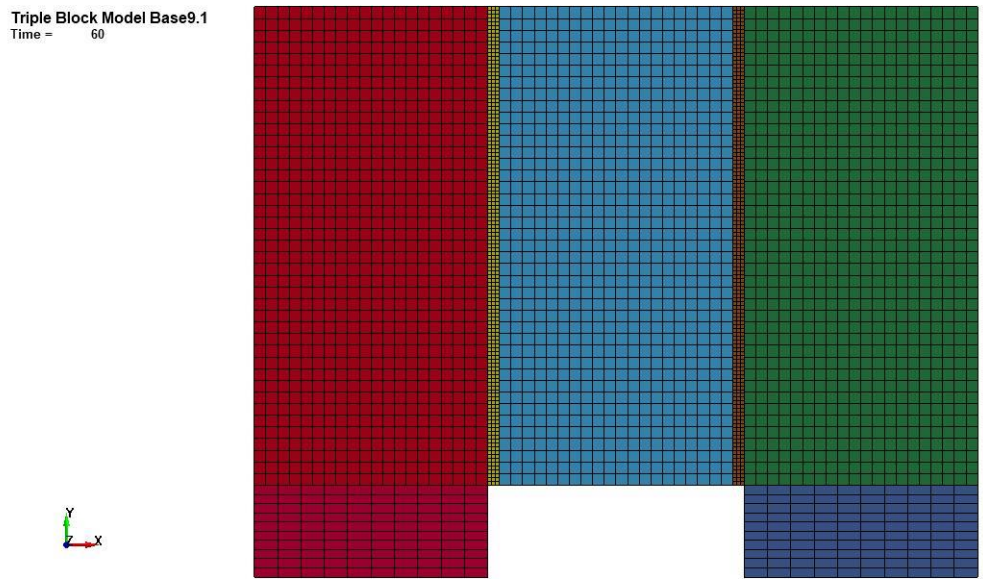


**Figure B-539: Last State at 60 Milliseconds for Base Run 9.1 – 50 psi**

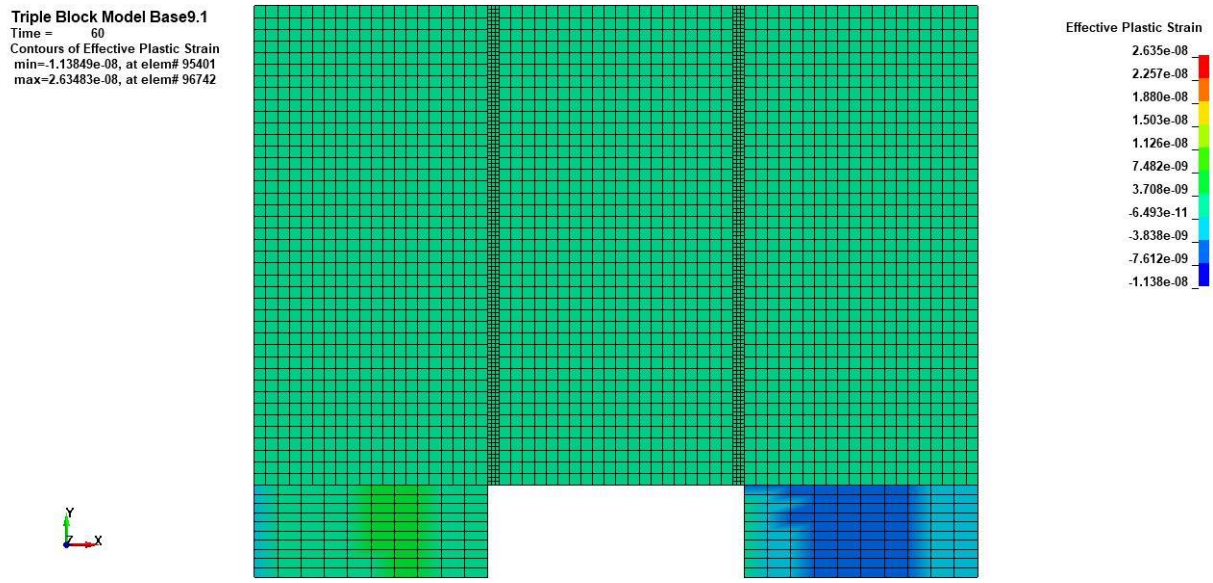


**Figure B-540: Effective Plastic Strain Fringe Plot for Last State at 60 Milliseconds for Base Run 9.1 – 50 psi**

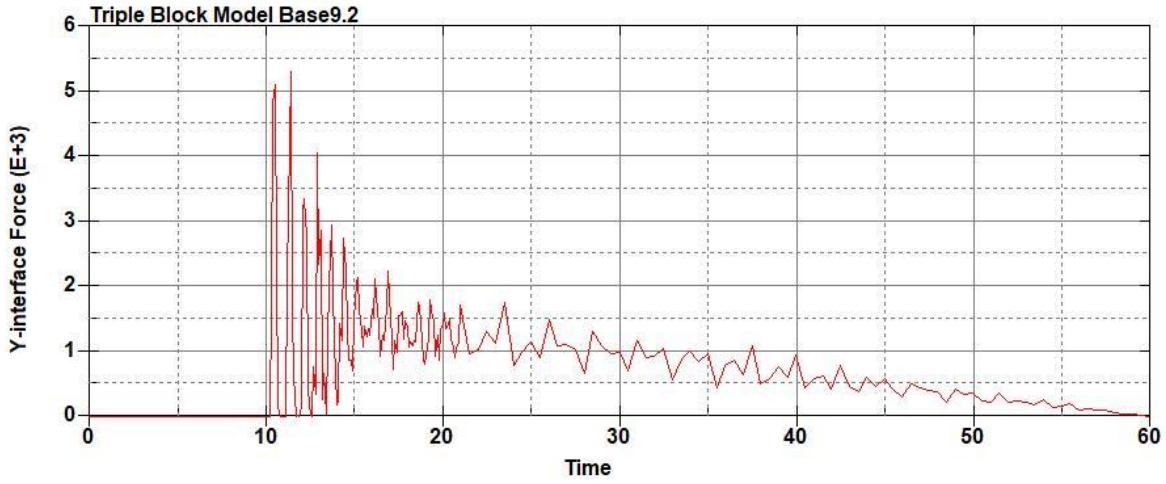


**Figure B-541: Base Run 9.2 Right Support Y-Interface Force (lbs) versus Time (ms) – 100 psi**

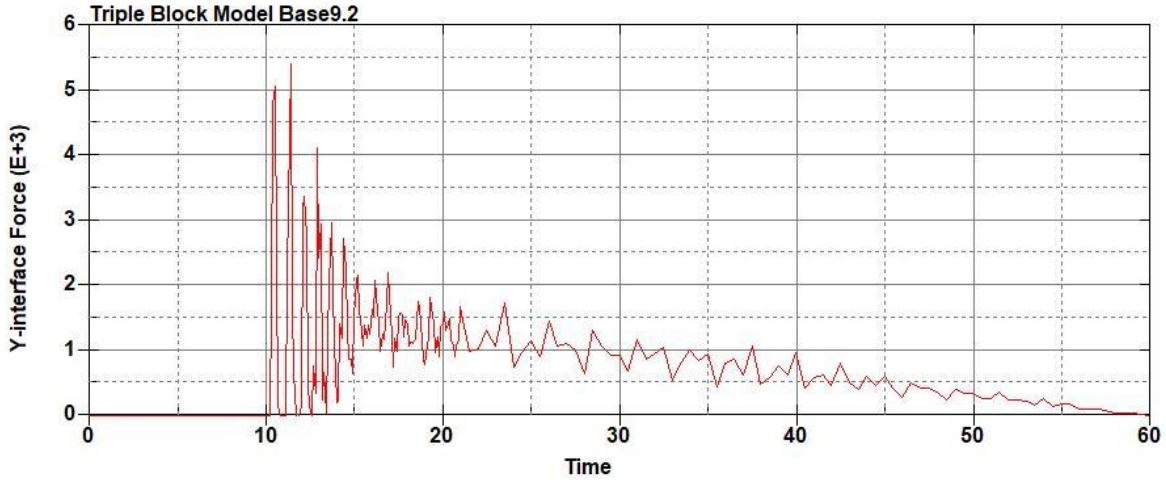


**Figure B-542: Base Run 9.2 Left Support Y-Interface Force (lbs) versus Time (ms) – 100 psi**

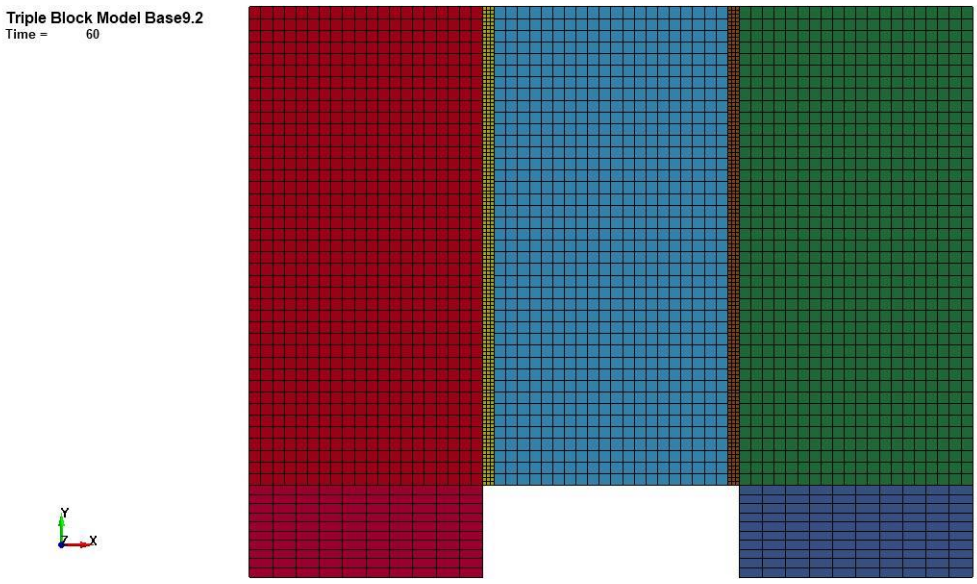


**Figure B-543: Last State at 60 Milliseconds for Base Run 9.2 – 100 psi**

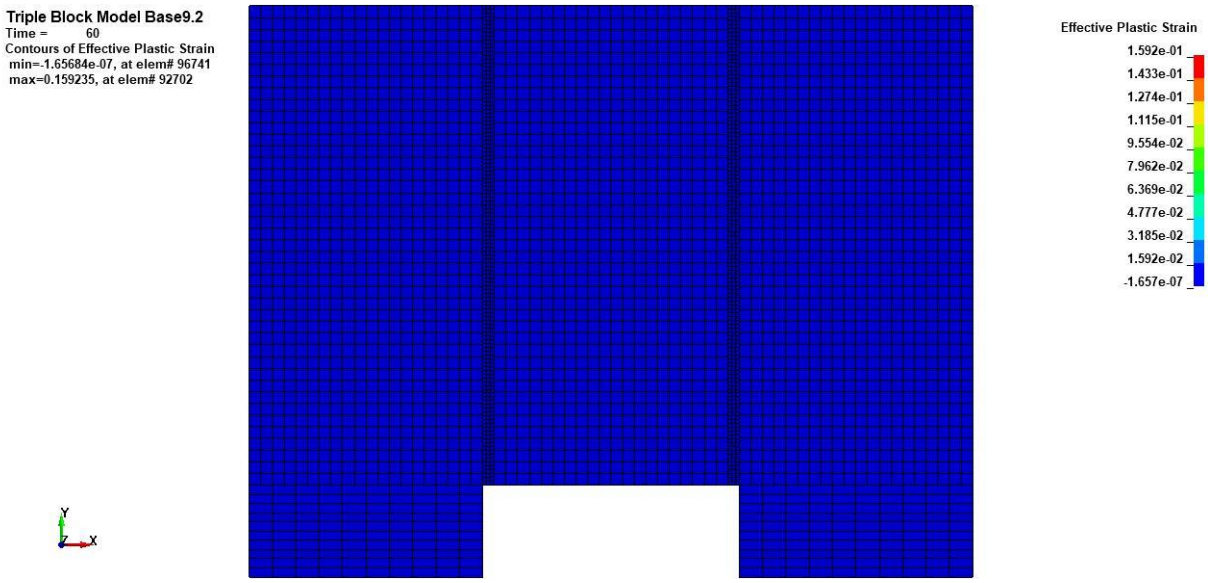


**Figure B-544: Effective Plastic Strain Fringe Plot for Last State at 60 Milliseconds for Base Run 9.2 – 100 psi**

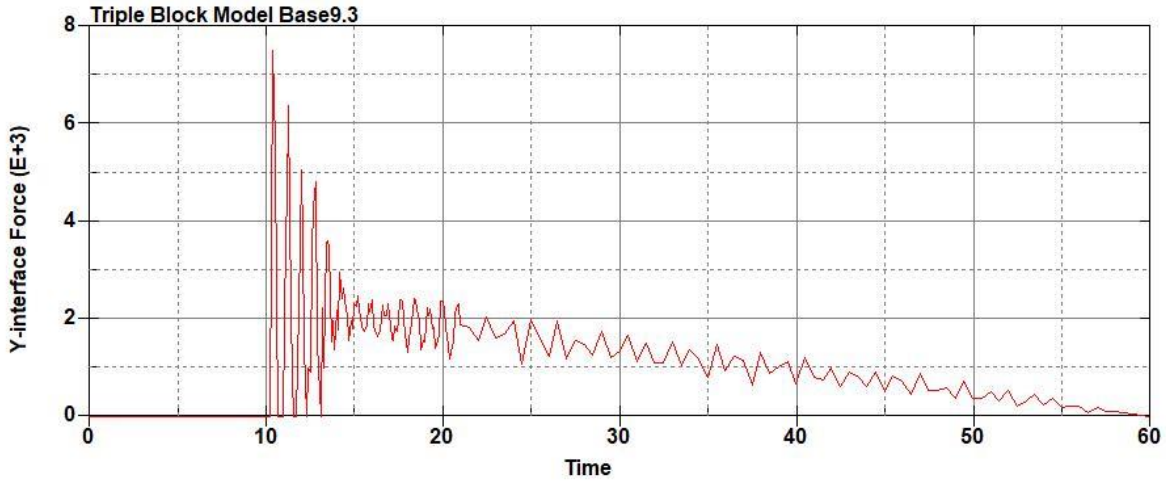


**Figure B-545: Base Run 9.3 Right Support Y-Interface Force (lbs) versus Time (ms) – 150 psi**

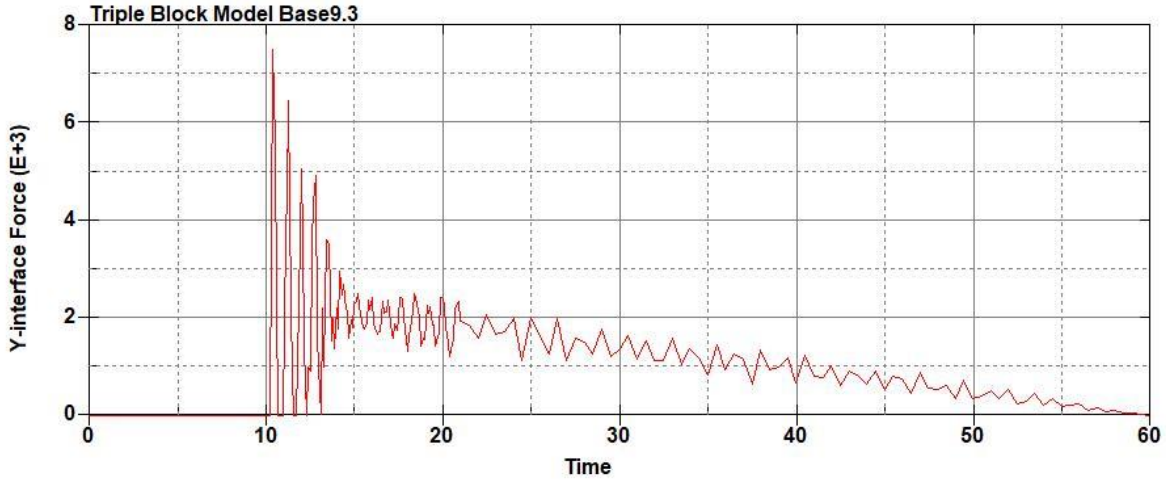


**Figure B-546: Base Run 9.3 Left Support Y-Interface Force (lbs) versus Time (ms) – 150 psi**

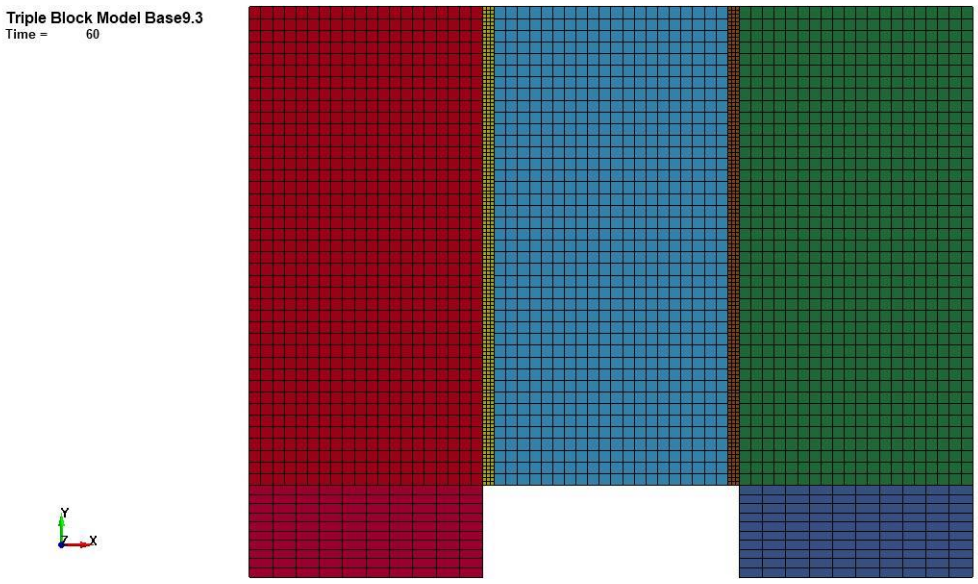


**Figure B-547: Last State at 60 Milliseconds for Base Run 9.3 – 150 psi**

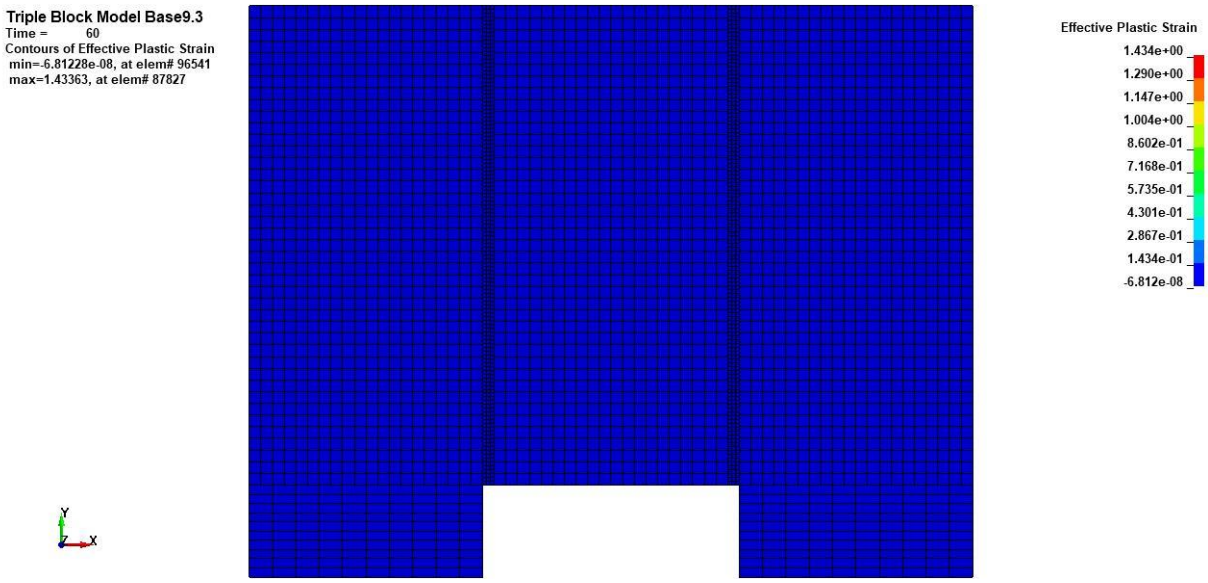


**Figure B-548: Effective Plastic Strain Fringe Plot for Last State at 60 Milliseconds for Base Run 9.3 – 150 psi**

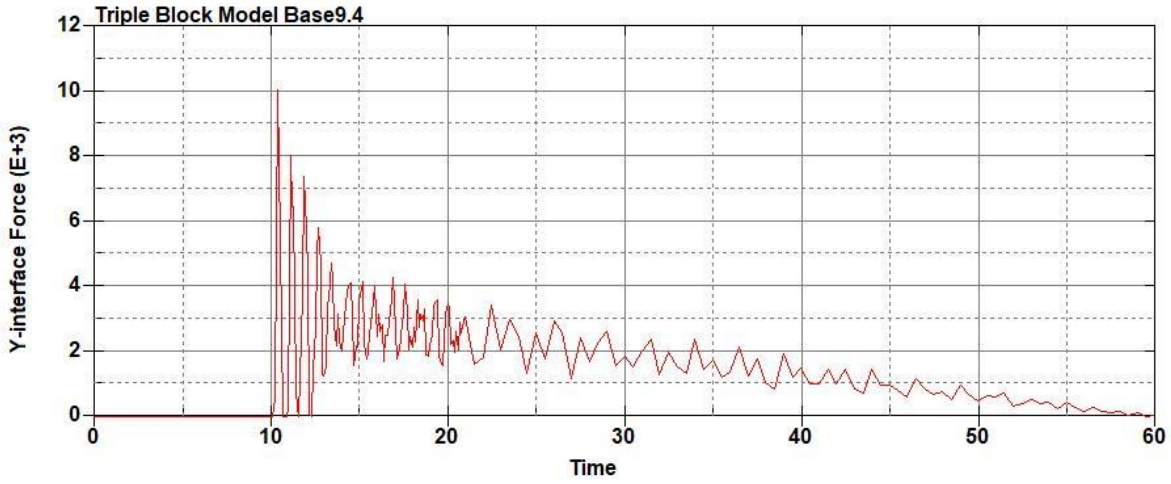


**Figure B-549: Base Run 9.4 Right Support Y-Interface Force (lbs) versus Time (ms) – 200 psi**

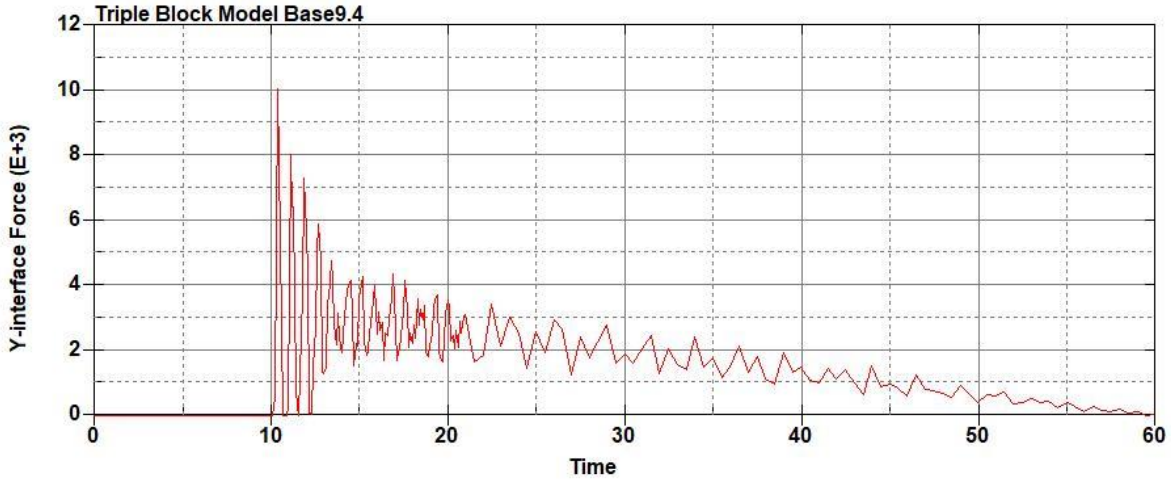


**Figure B-550: Base Run 9.4 Left Support Y-Interface Force (lbs) versus Time (ms) – 200 psi**

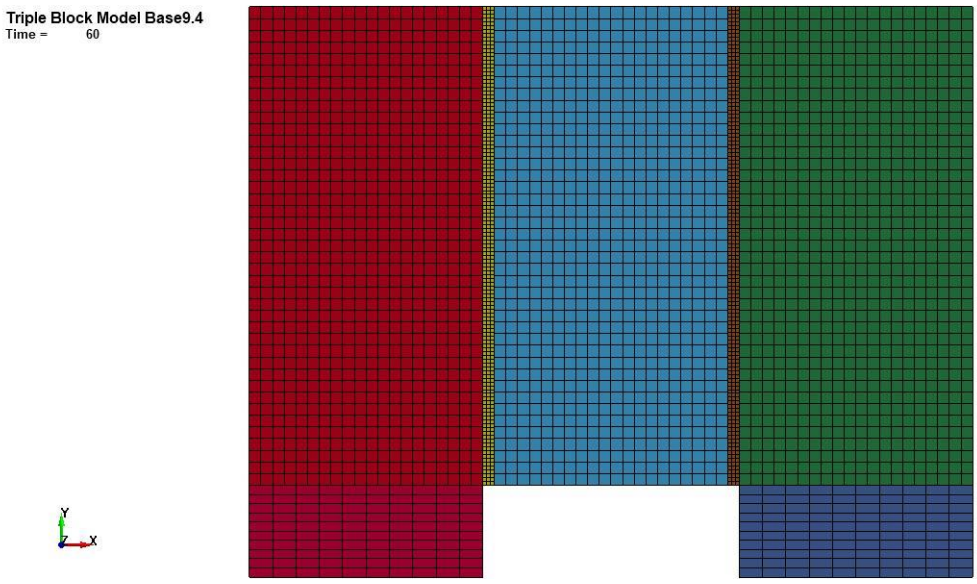


**Figure B-551: Last State at 60 Milliseconds for Base Run 9.4 – 200 psi**

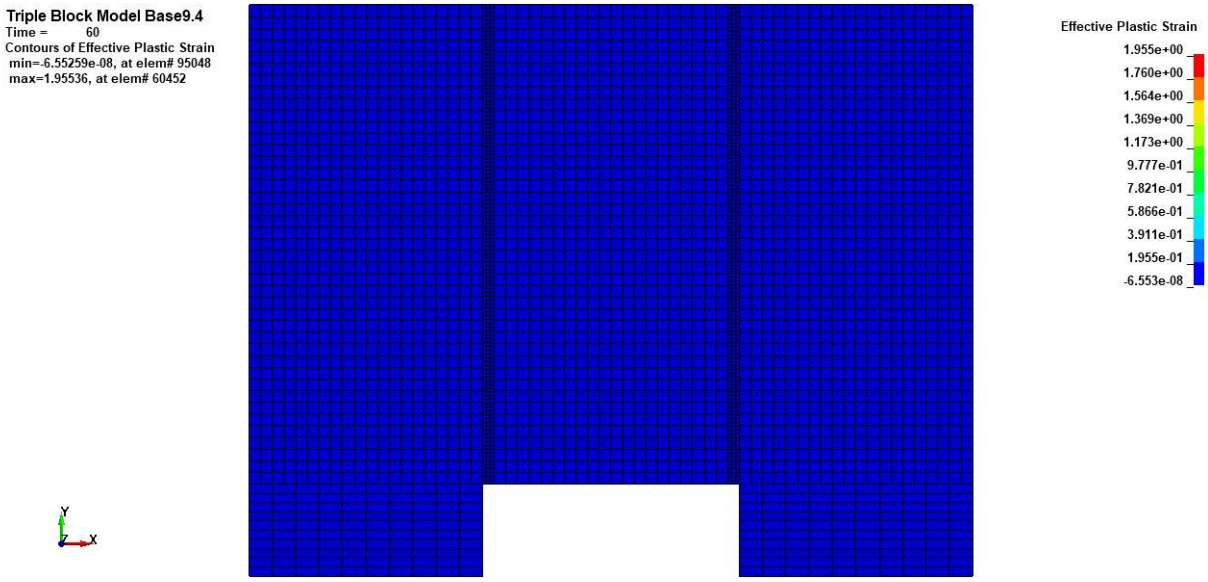


**Figure B-552: Effective Plastic Strain Fringe Plot for Last State at 60 Milliseconds for Base Run 9.4 – 200 psi**

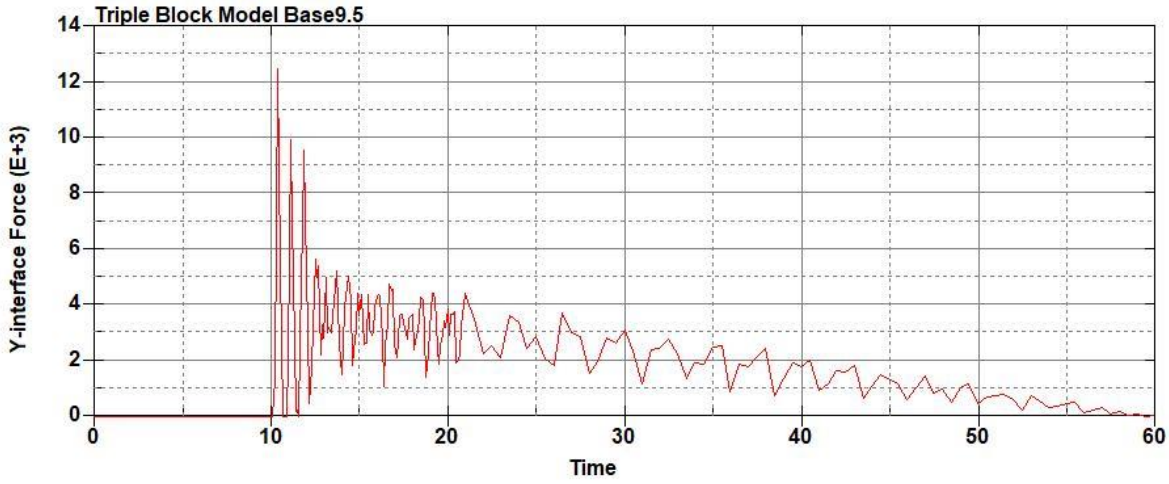


**Figure B-553: Base Run 9.5 Right Support Y-Interface Force (lbs) versus Time (ms) – 250 psi**

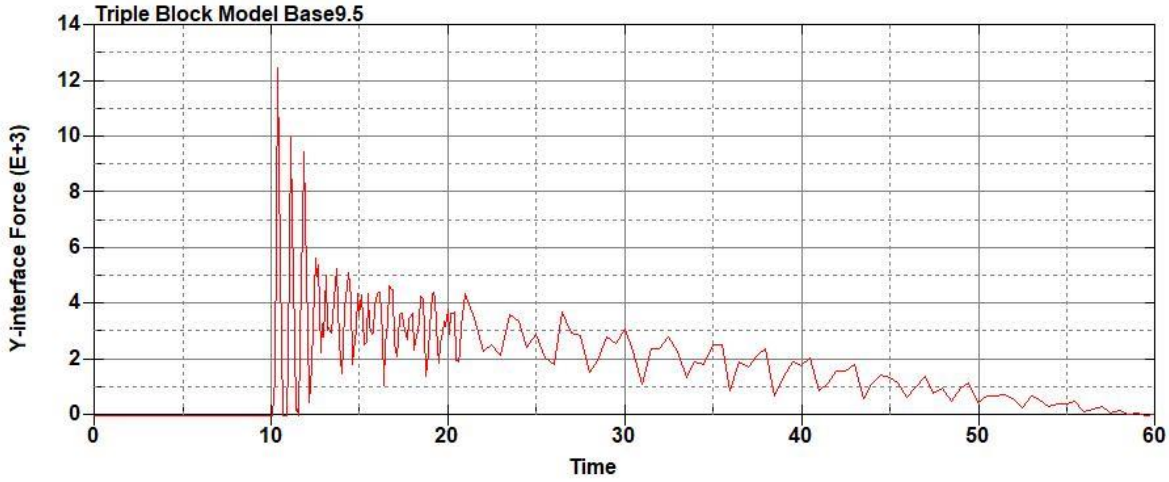


**Figure B-554: Base Run 9.5 Left Support Y-Interface Force (lbs) versus Time (ms) – 250 psi**

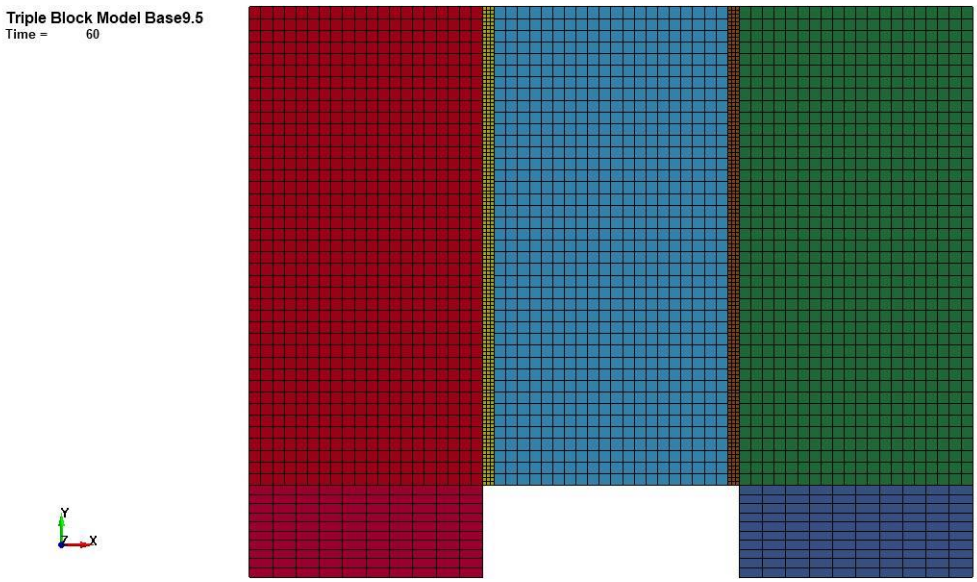


**Figure B-555: Last State at 60 Milliseconds for Base Run 9.5 – 250 psi**

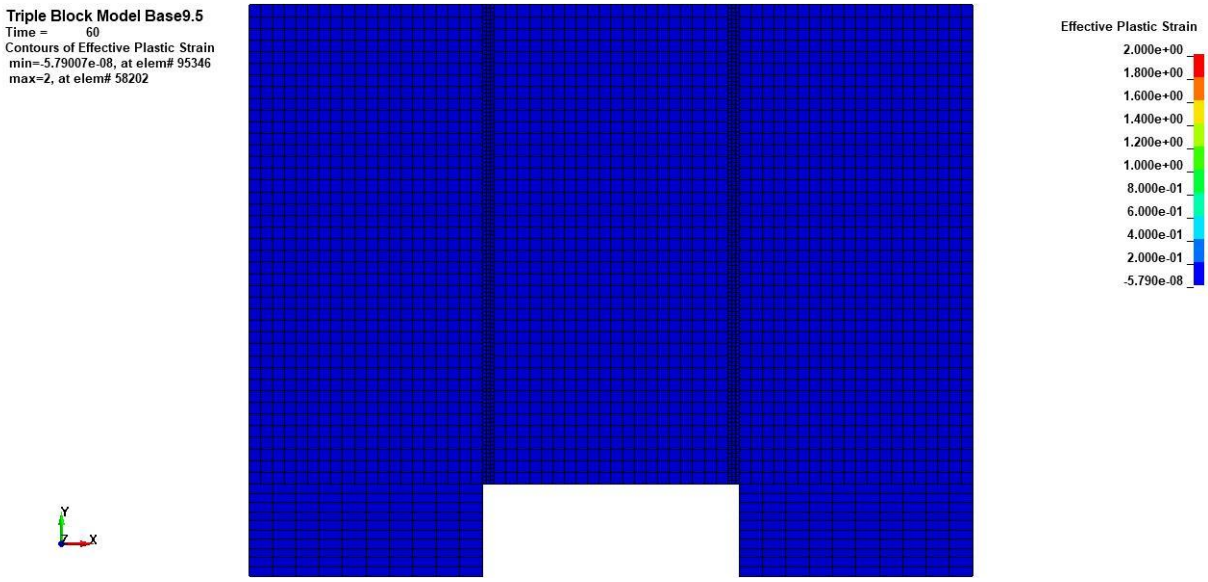


**Figure B-556: Effective Plastic Strain Fringe Plot for Last State at 60 Milliseconds for Base Run 9.5 – 250 psi**

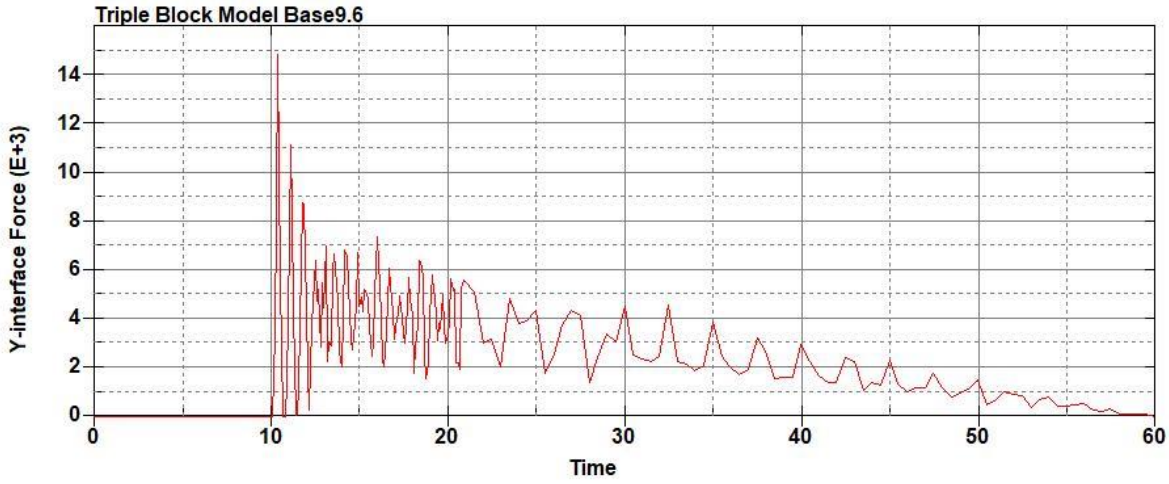


**Figure B-557: Base Run 9.6 Right Support Y-Interface Force (lbs) versus Time (ms) – 300 psi**

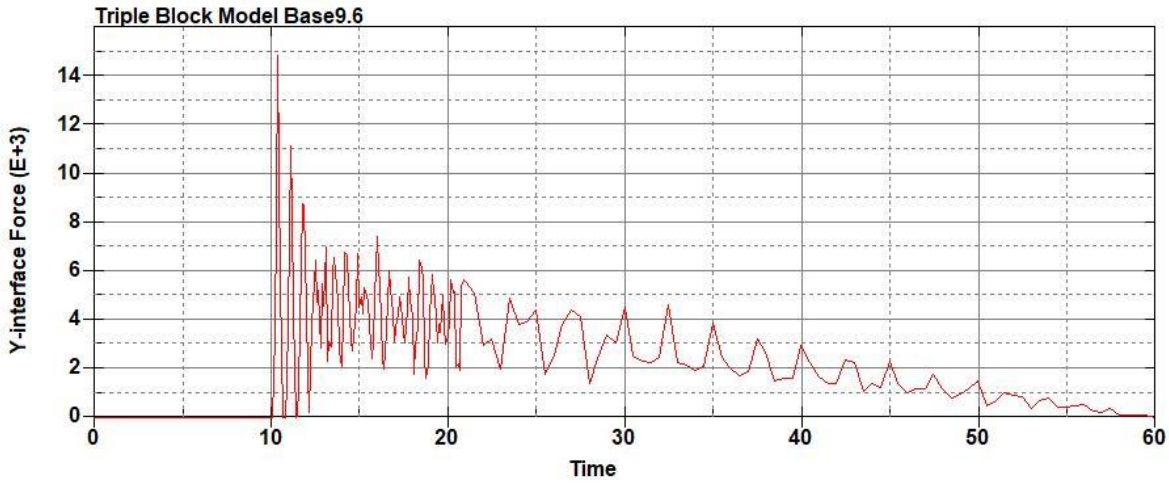


**Figure B-558: Base Run 9.6 Left Support Y-Interface Force (lbs) versus Time (ms) – 300 psi**

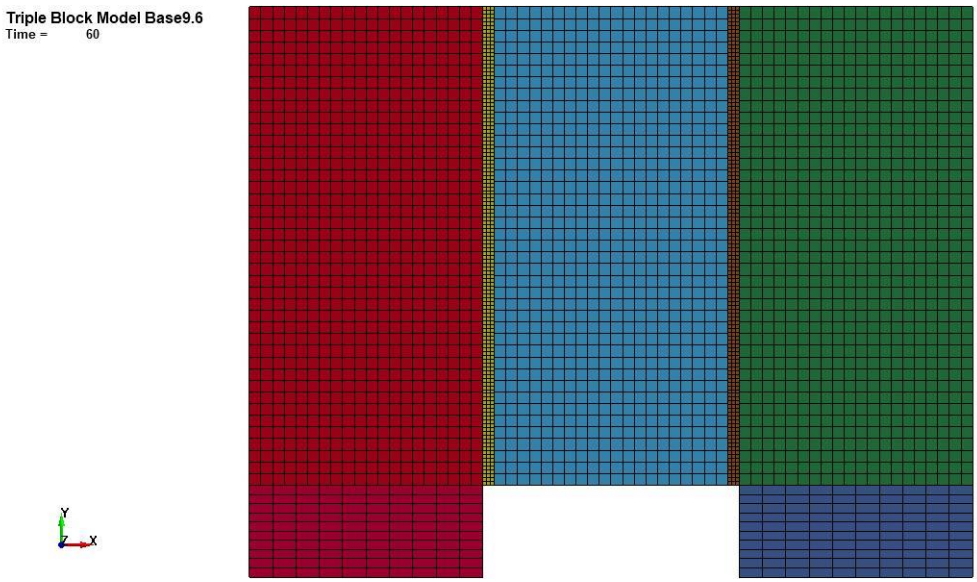


**Figure B-559: Last State at 60 Milliseconds for Base Run 9.6 – 300 psi**

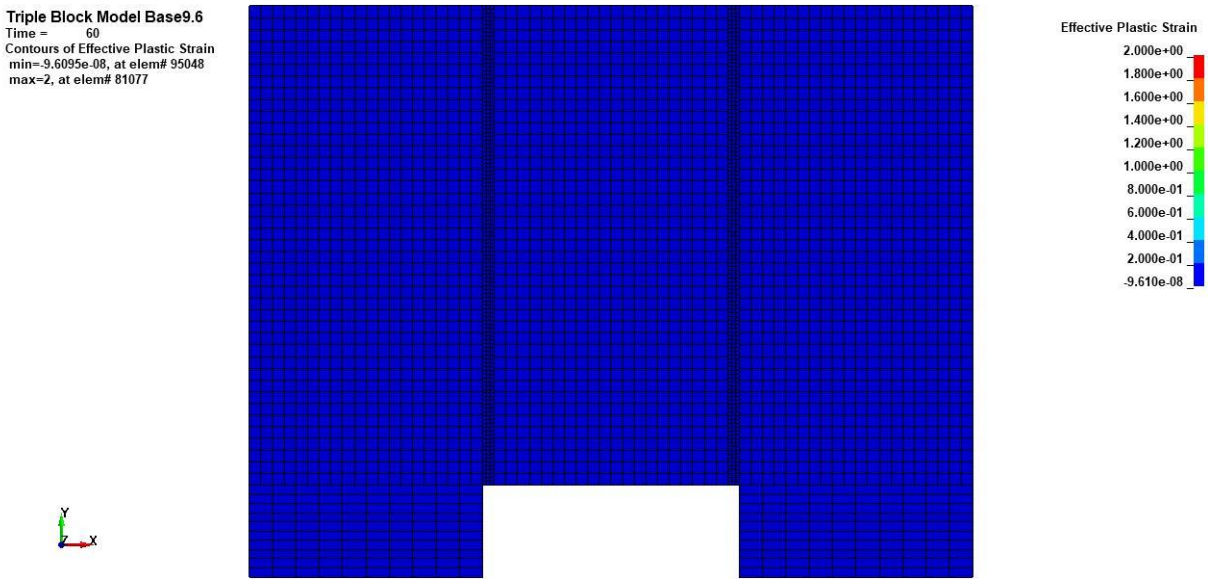


**Figure B-560: Effective Plastic Strain Fringe Plot for Last State at 60 Milliseconds for Base Run 9.6 – 300 psi**

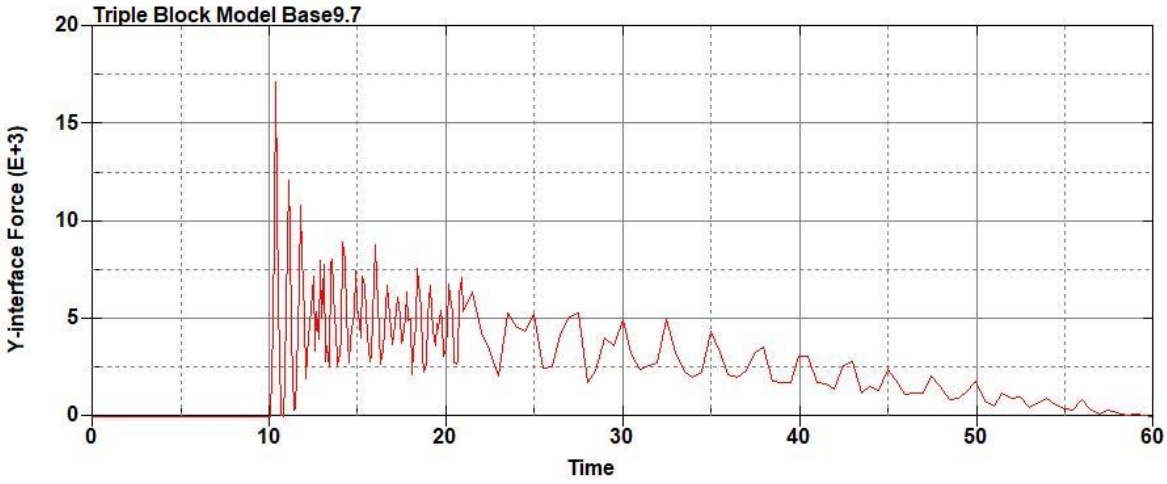


**Figure B-561: Base Run 9.7 Right Support Y-Interface Force (lbs) versus Time (ms) – 350 psi**

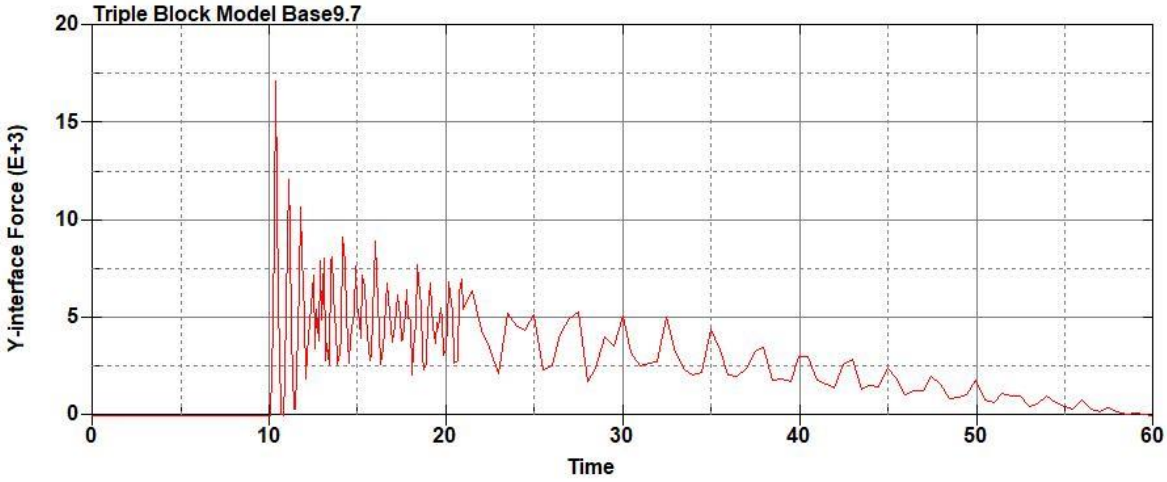


**Figure B-562: Base Run 9.7 Left Support Y-Interface Force (lbs) versus Time (ms) – 350 psi**

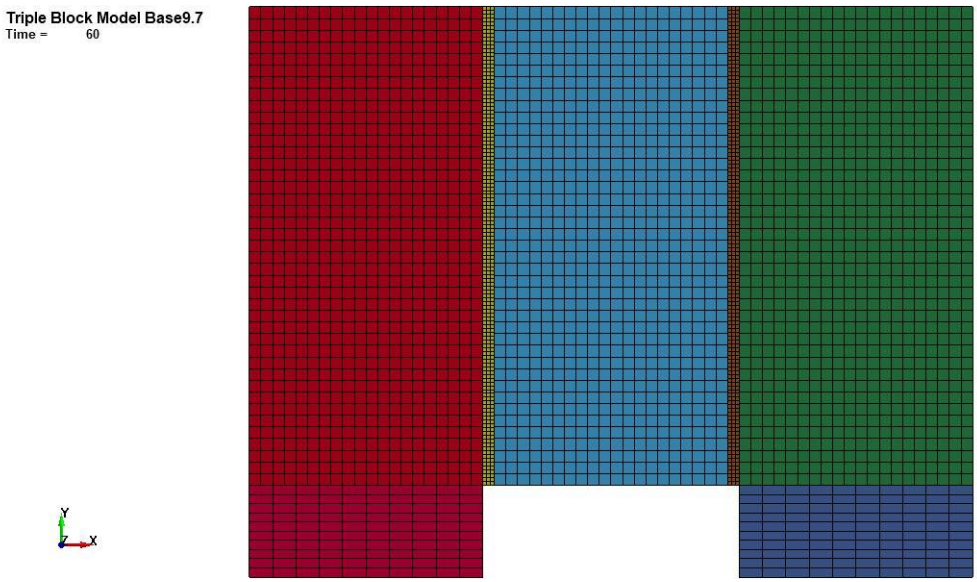


**Figure B-563: Last State at 60 Milliseconds for Base Run 9.7 – 350 psi**

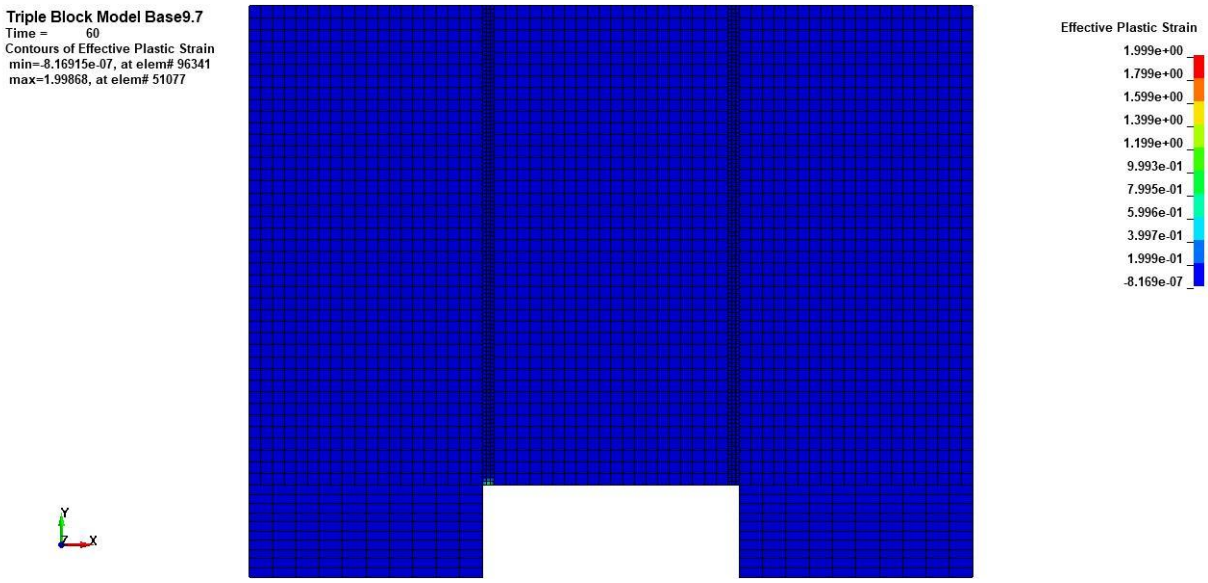


**Figure B-564: Effective Plastic Strain Fringe Plot for Last State at 60 Milliseconds for Base Run 9.7 – 350 psi**

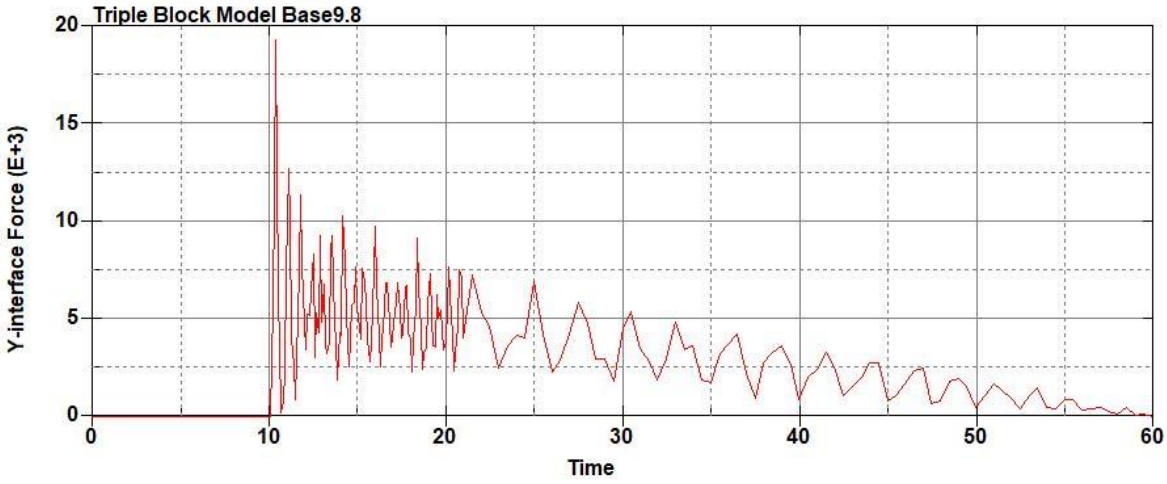


**Figure B-565: Base Run 9.8 Right Support Y-Interface Force (lbs) versus Time (ms) – 400 psi**

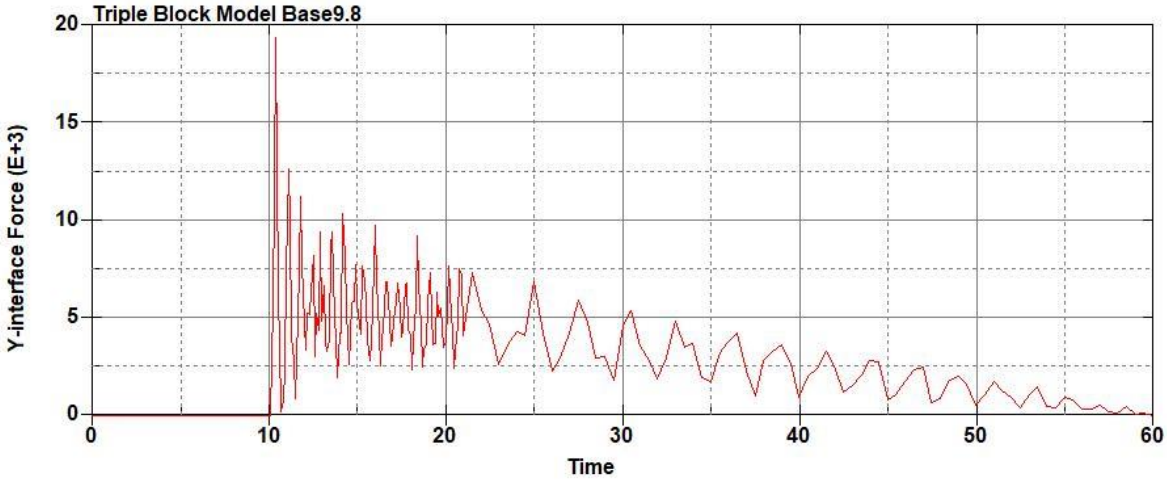


**Figure B-566: Base Run 9.8 Left Support Y-Interface Force (lbs) versus Time (ms) – 400 psi**

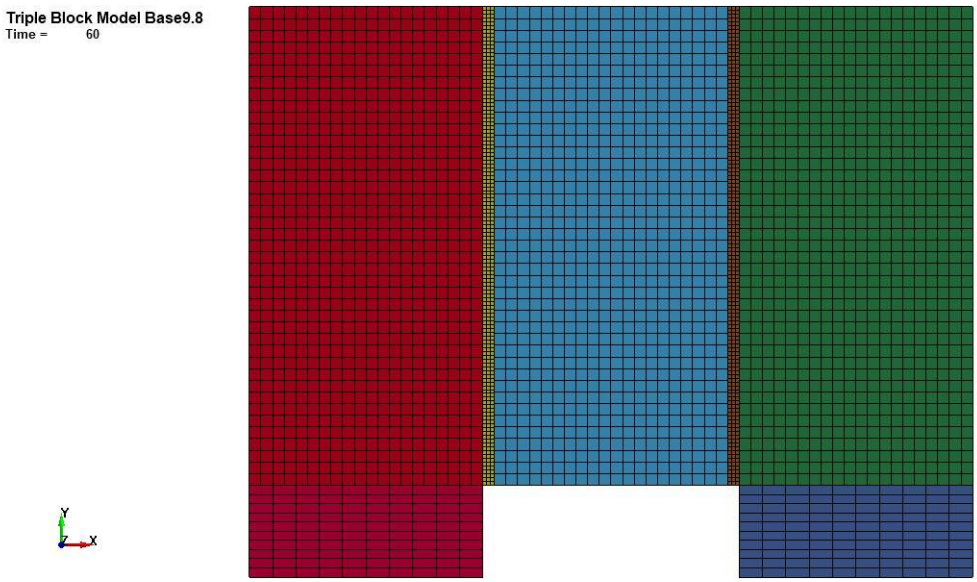


**Figure B-567: Last State at 60 Milliseconds for Base Run 9.8 – 400 psi**

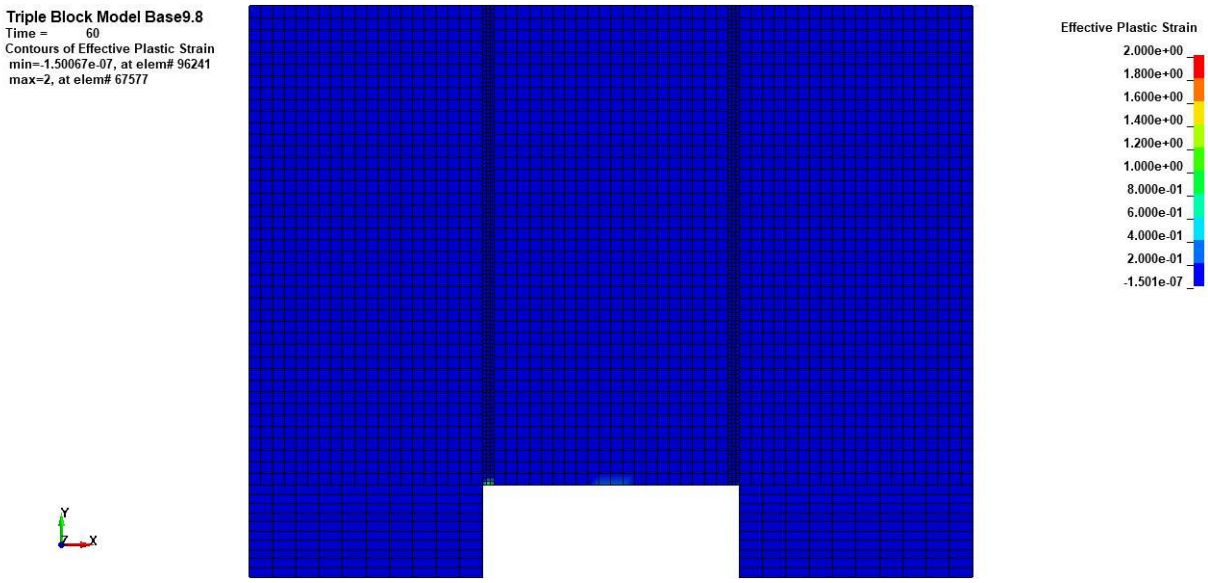


**Figure B-568: Effective Plastic Strain Fringe Plot for Last State at 60 Milliseconds for Base Run 9.8 – 400 psi**

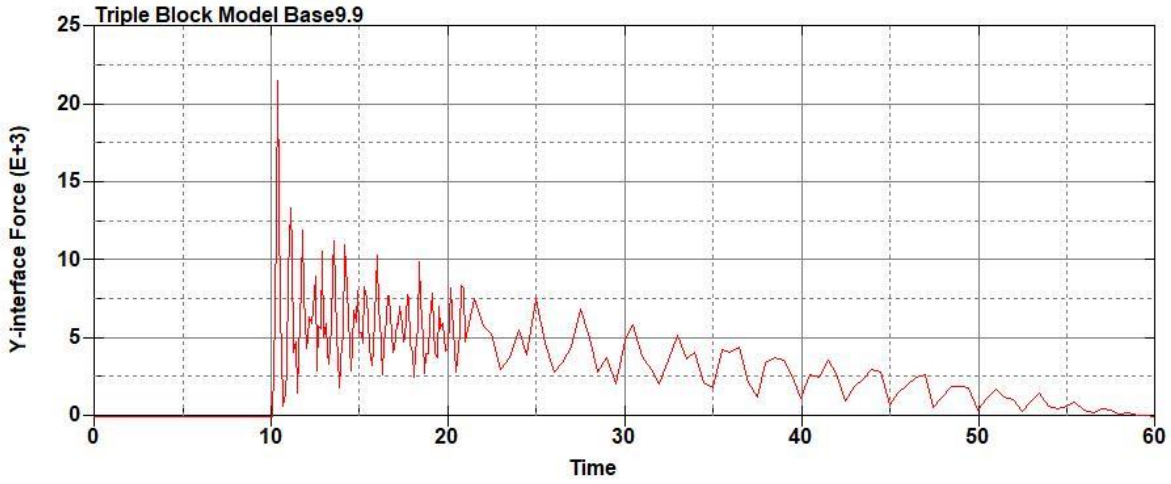


**Figure B-569: Base Run 9.9 Right Support Y-Interface Force (lbs) versus Time (ms) – 450 psi**

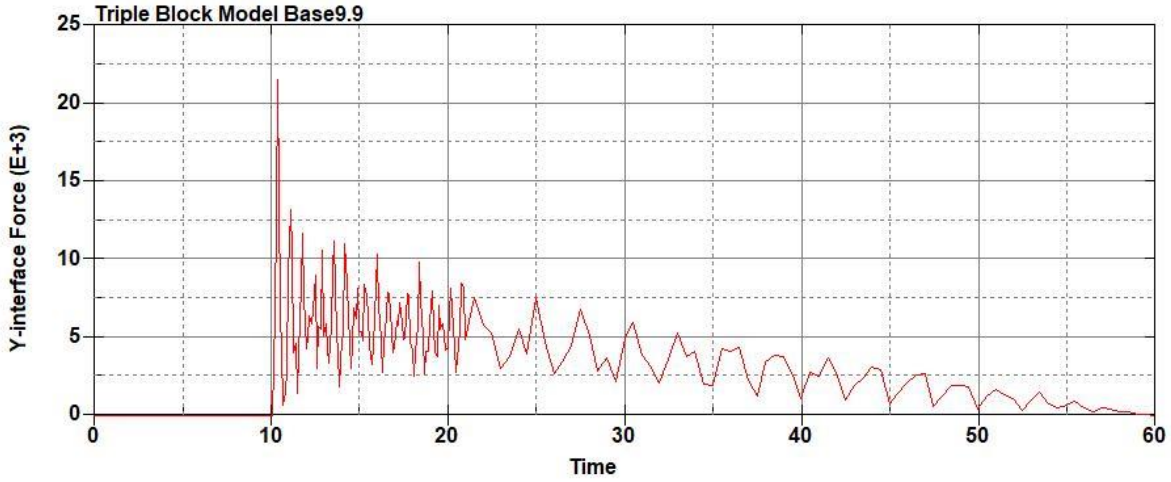


**Figure B-570: Base Run 9.9 Left Support Y-Interface Force (lbs) versus Time (ms) – 450 psi**

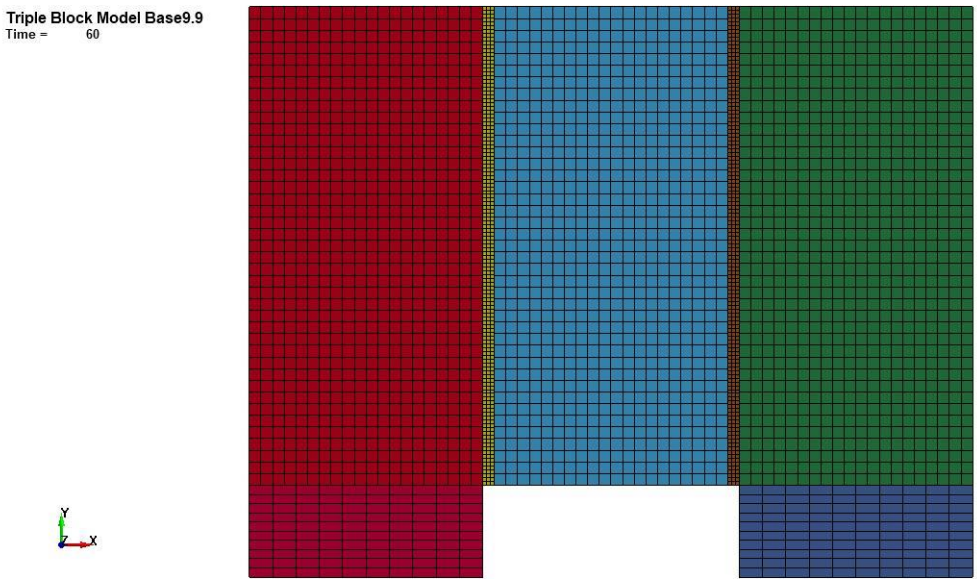


**Figure B-571: Last State at 60 Milliseconds for Base Run 9.9 – 450 psi**

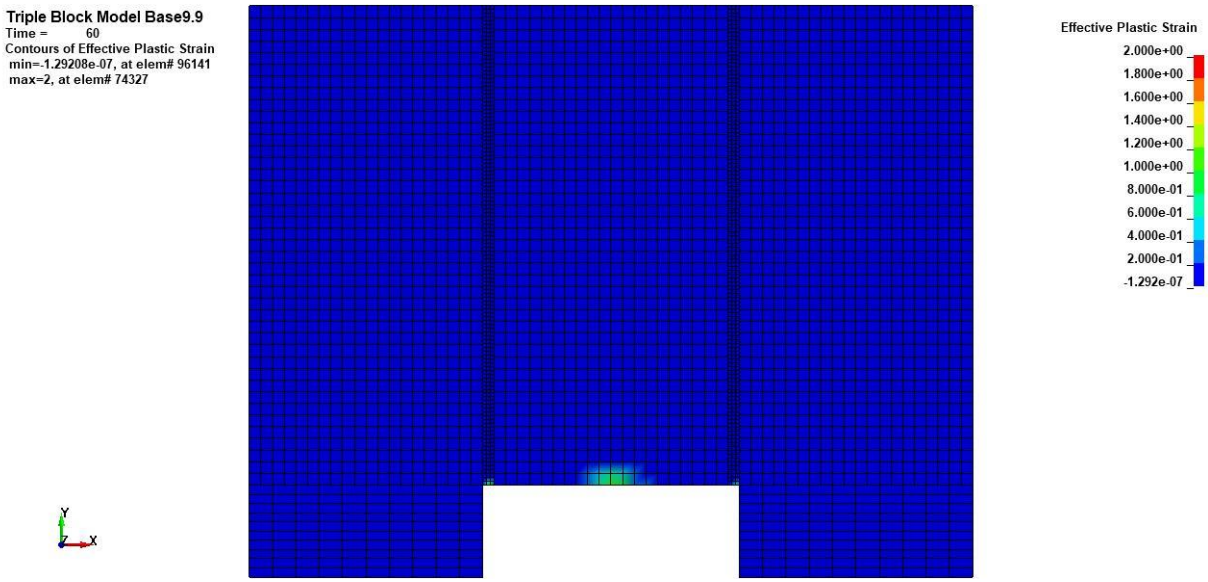


**Figure B-572: Effective Plastic Strain Fringe Plot for Last State at 60 Milliseconds for Base Run 9.9 – 450 psi**

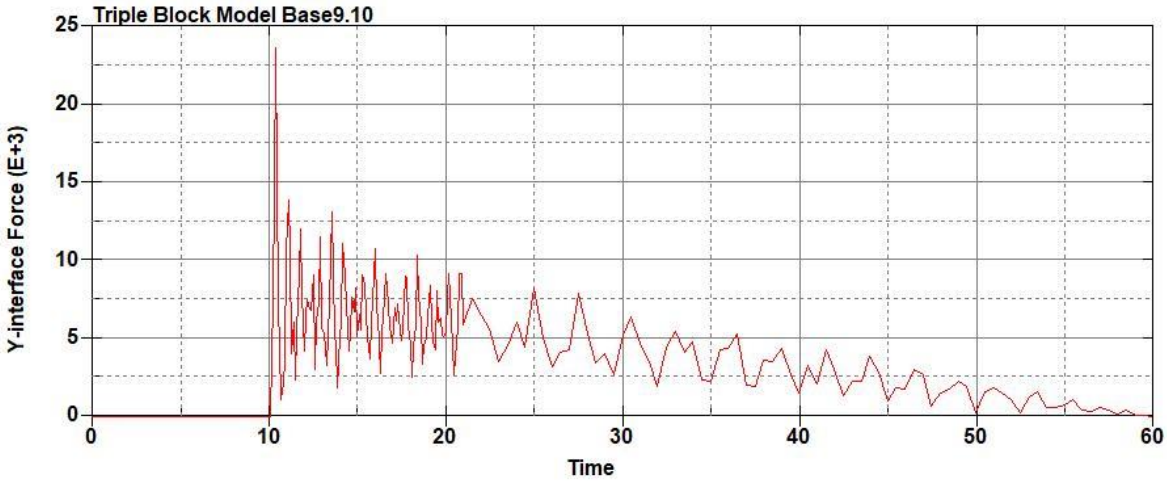


**Figure B-573: Base Run 9.10 Right Support Y-Interface Force (lbs) versus Time (ms) – 500 psi**

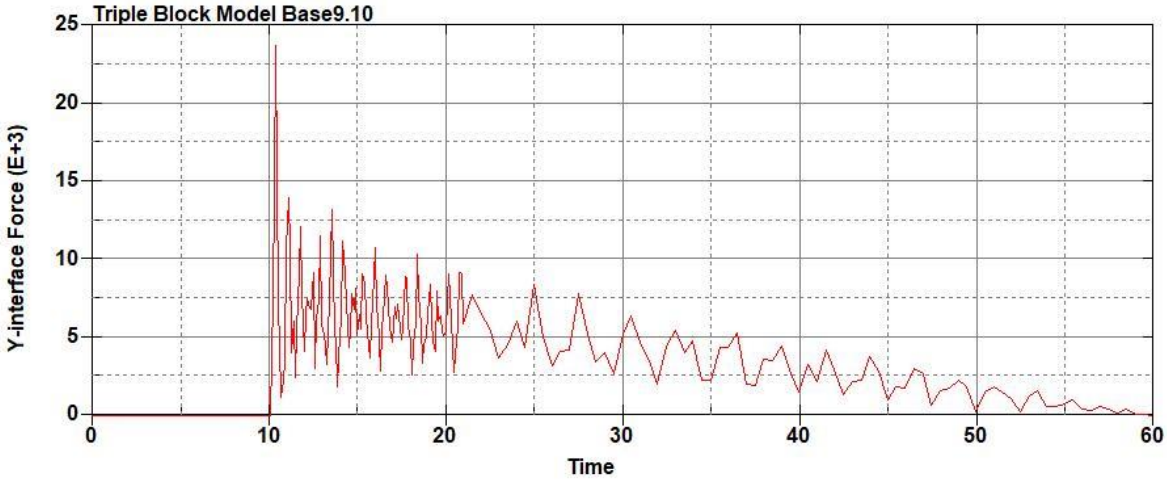


**Figure B-574: Base Run 9.10 Left Support Y-Interface Force (lbs) versus Time (ms) – 500 psi**

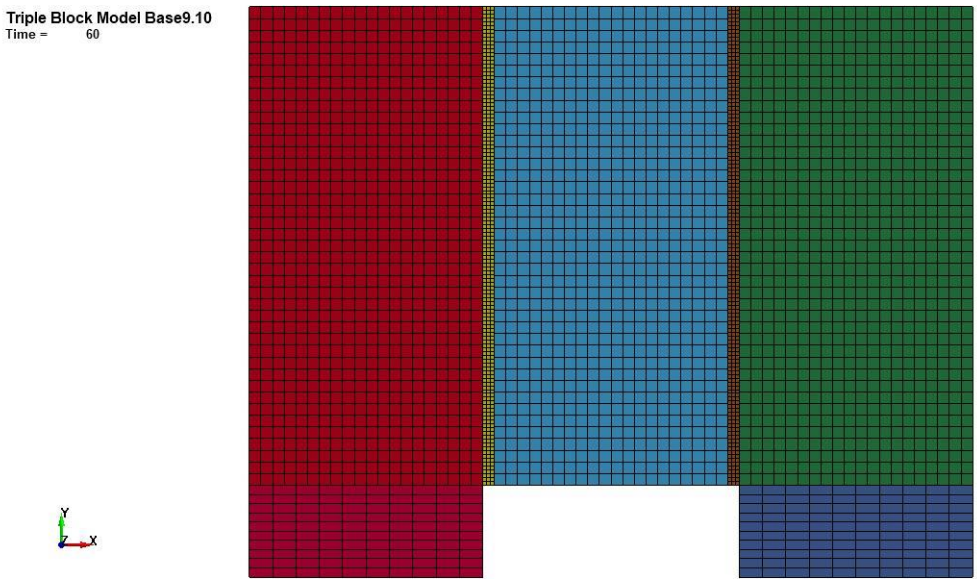


**Figure B-575: Last State at 60 Milliseconds for Base Run 9.10 – 500 psi**

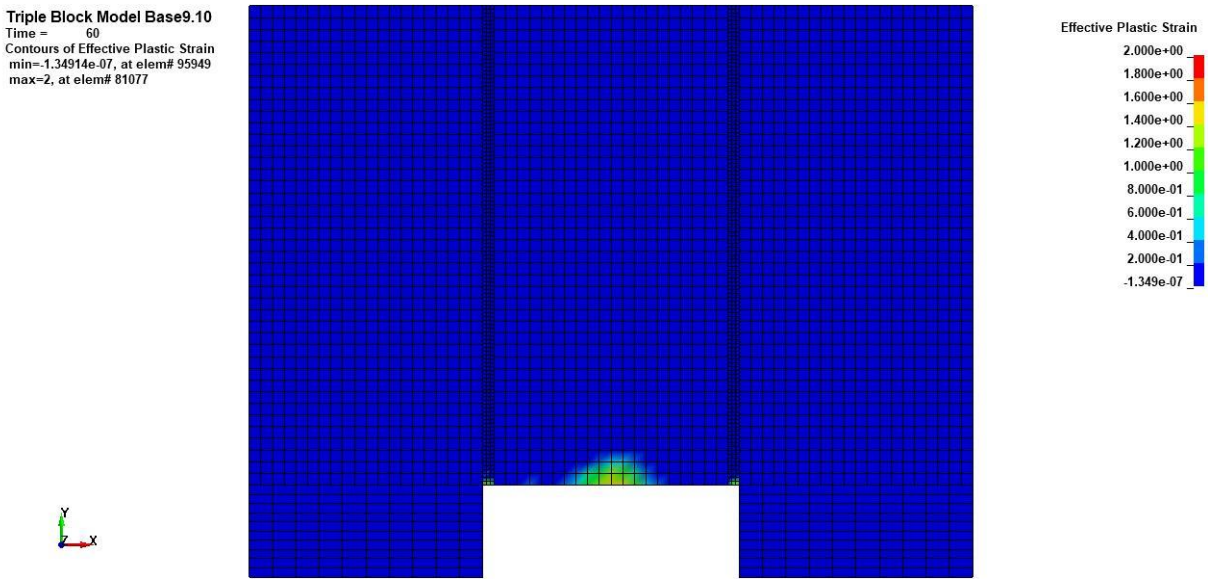


**Figure B-576: Effective Plastic Strain Fringe Plot for Last State at 60 Milliseconds for Base Run 9.10 – 500 psi**

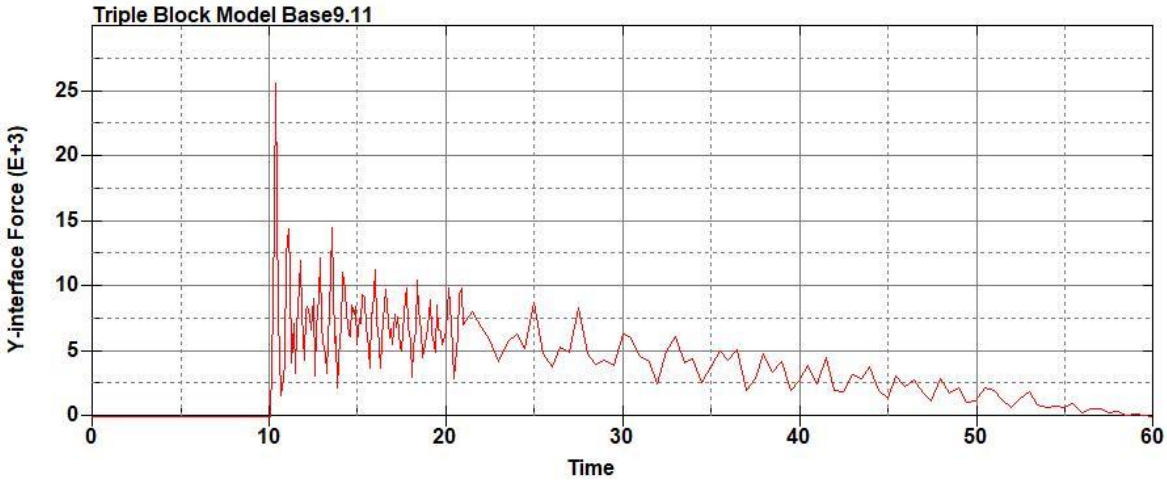


**Figure B-577: Base Run 9.11 Right Support Y-Interface Force (lbs) versus Time (ms) – 550 psi**

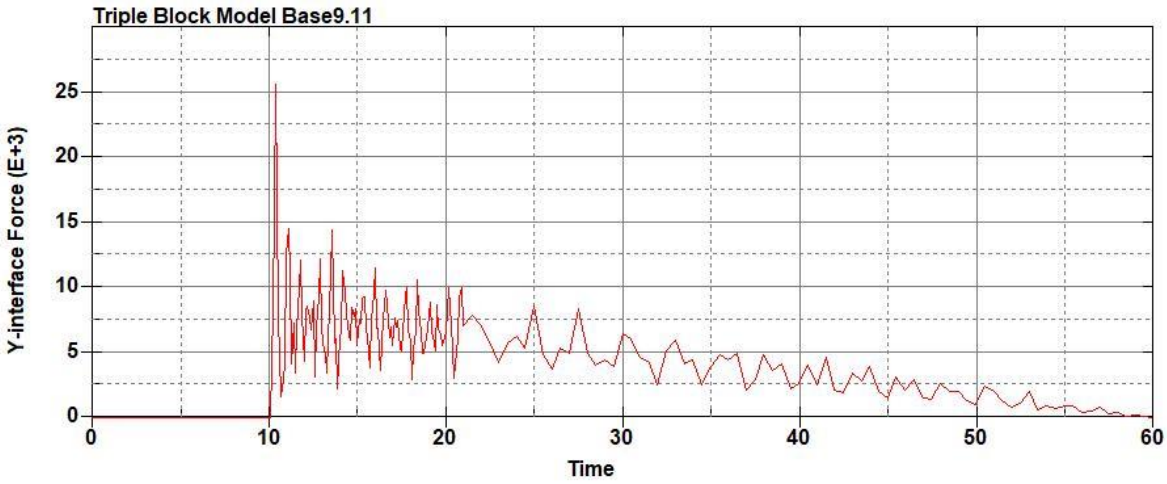


**Figure B-578: Base Run 9.11 Left Support Y-Interface Force (lbs) versus Time (ms) – 550 psi**

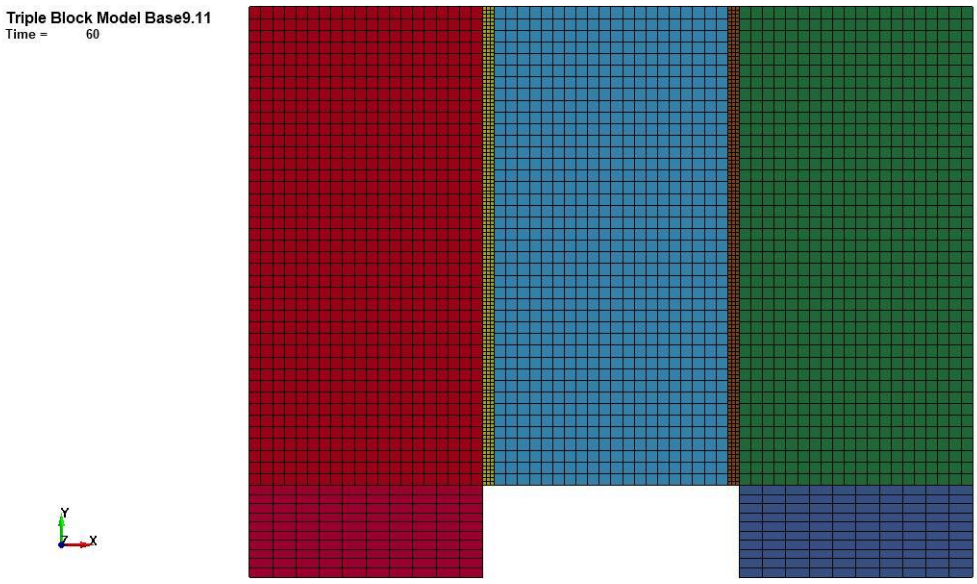


**Figure B-579: Last State at 60 Milliseconds for Base Run 9.11 – 550 psi**

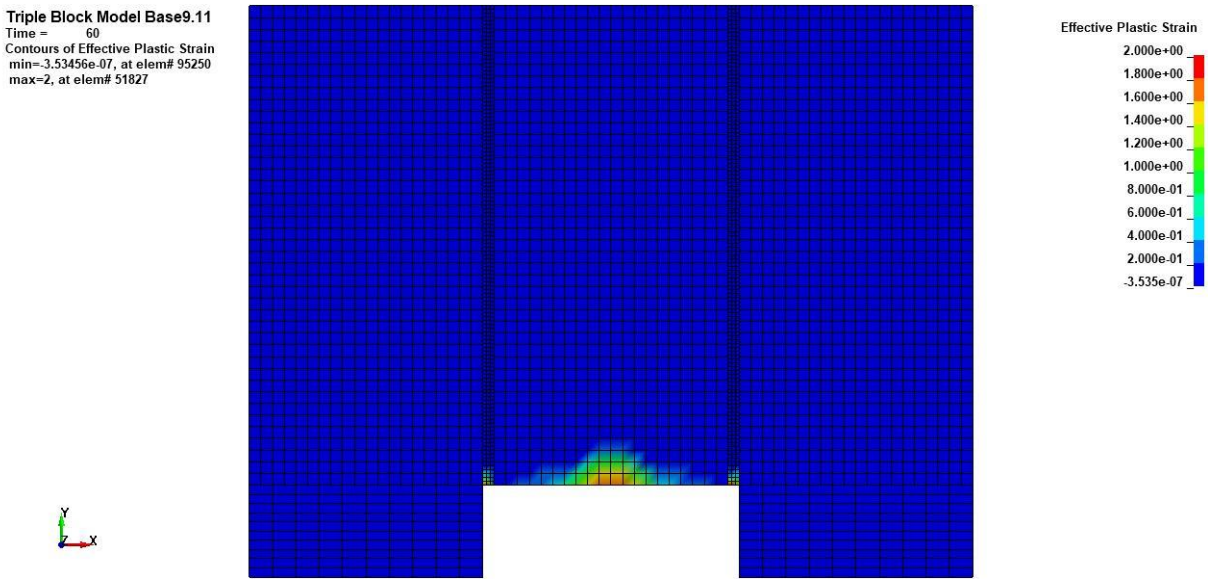


**Figure B-580: Effective Plastic Strain Fringe Plot for Last State at 60 Milliseconds for Base Run 9.11 – 550 psi**

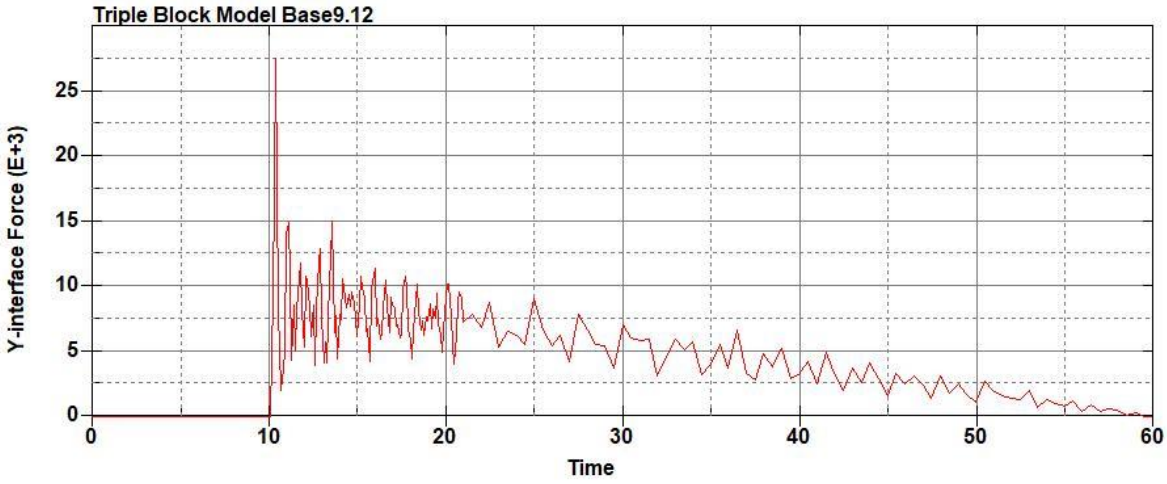


**Figure B-581: Base Run 9.12 Right Support Y-Interface Force (lbs) versus Time (ms) – 600 psi**

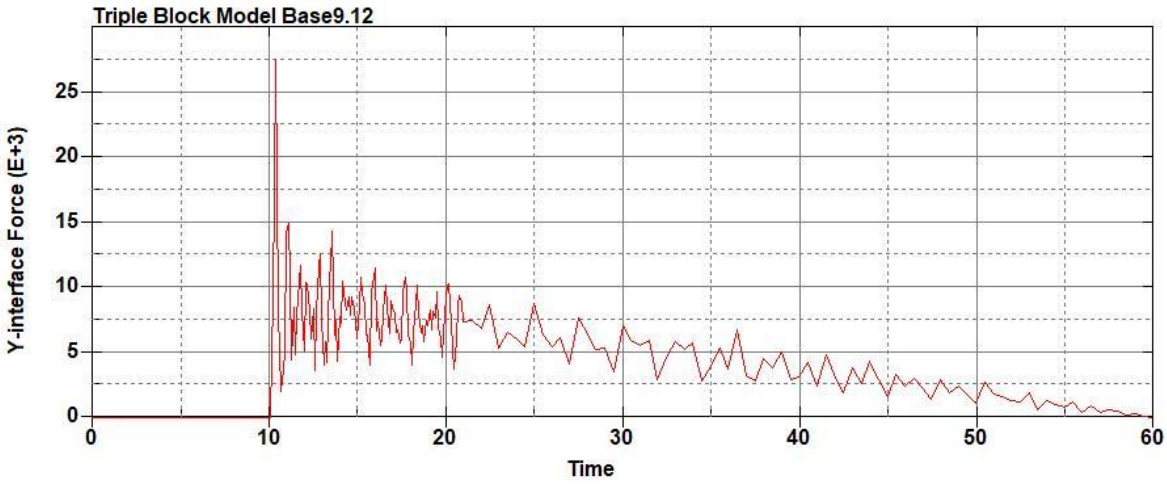


**Figure B-582: Base Run 9.12 Left Support Y-Interface Force (lbs) versus Time (ms) – 600 psi**

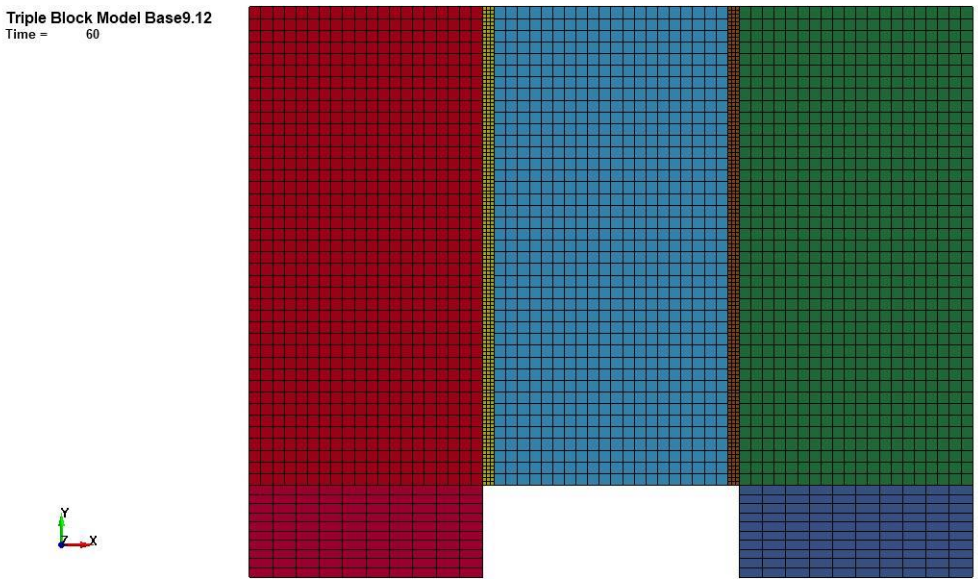


**Figure B-583: Last State at 60 Milliseconds for Base Run 9.12 – 600 psi**

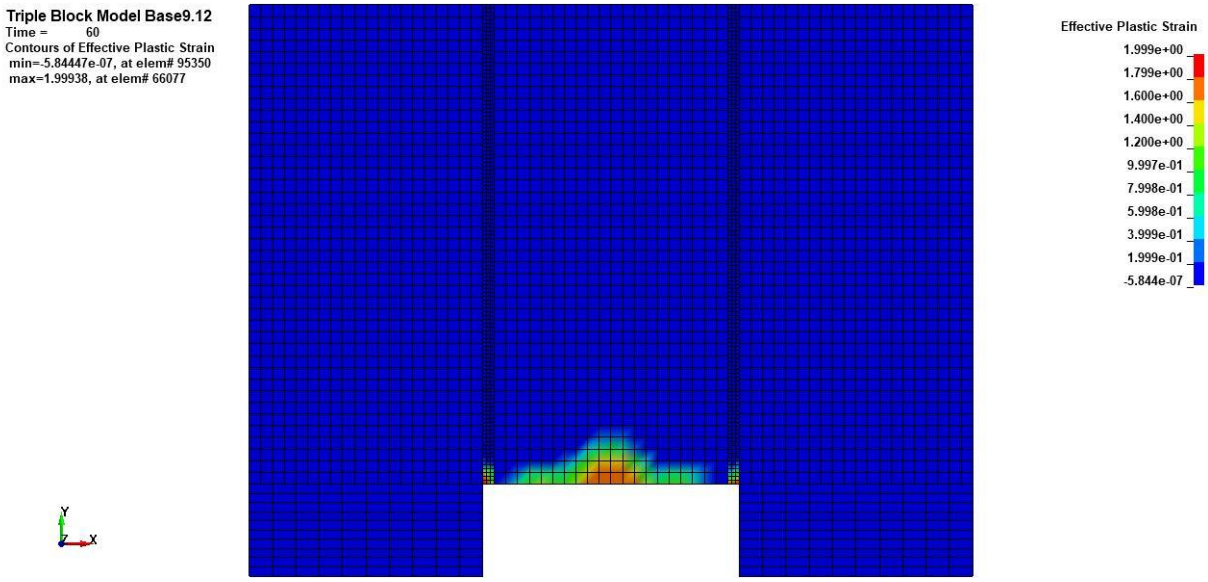


**Figure B-584: Effective Plastic Strain Fringe Plot for Last State at 60 Milliseconds for Base Run 9.12 – 600 psi**

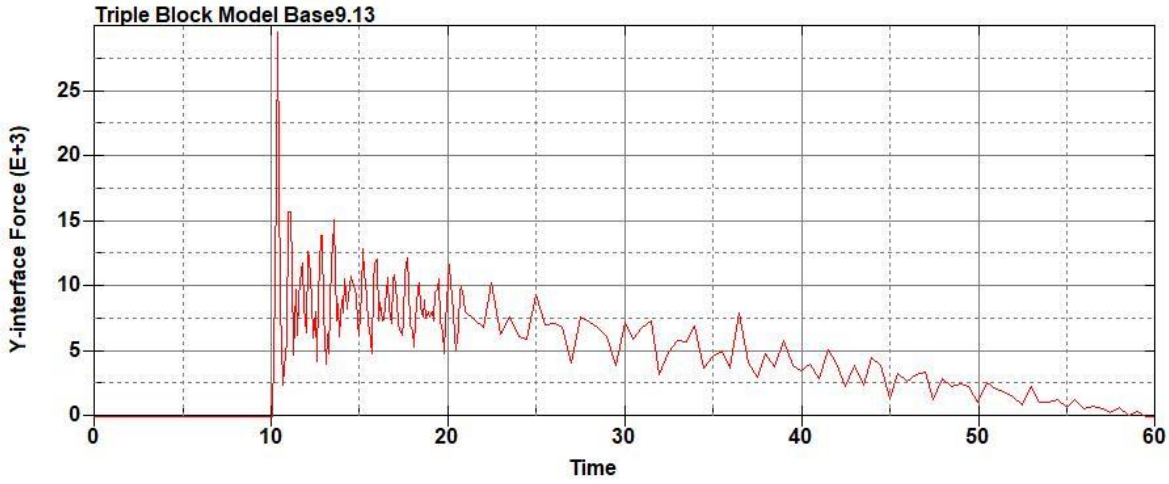


**Figure B-585: Base Run 9.13 Right Support Y-Interface Force (lbs) versus Time (ms) – 650 psi**

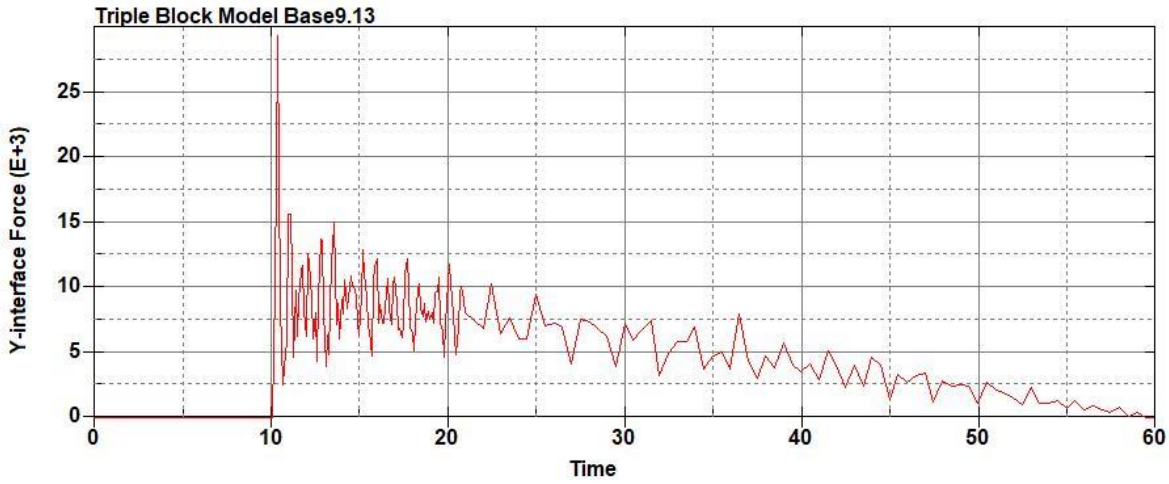


**Figure B-586: Base Run 9.13 Left Support Y-Interface Force (lbs) versus Time (ms) – 650 psi**

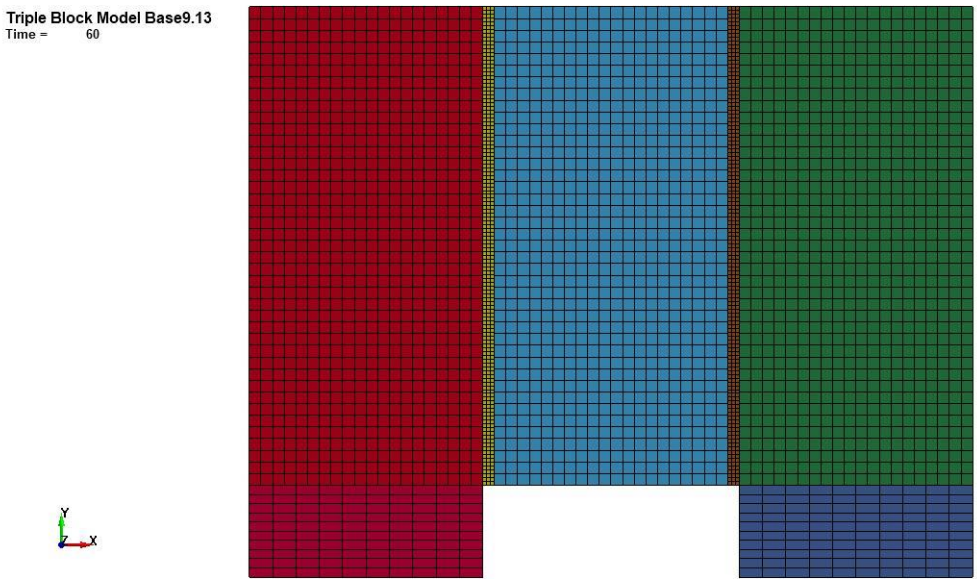


**Figure B-587: Last State at 60 Milliseconds for Base Run 9.13 – 650 psi**

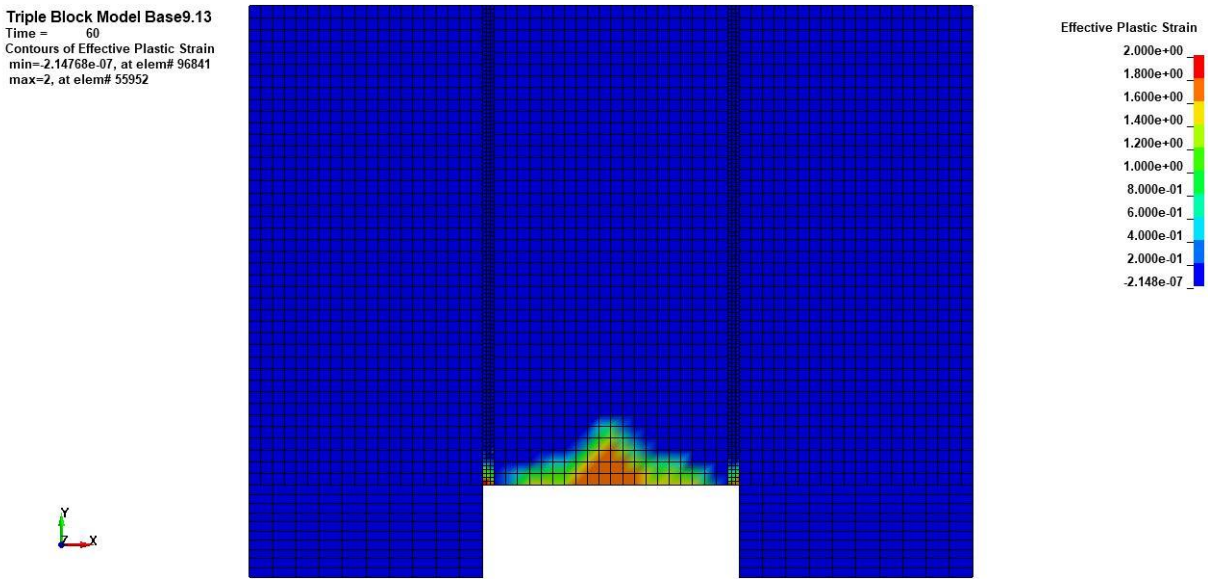


**Figure B-588: Effective Plastic Strain Fringe Plot for Last State at 60 Milliseconds for Base Run 9.13 – 650 psi**

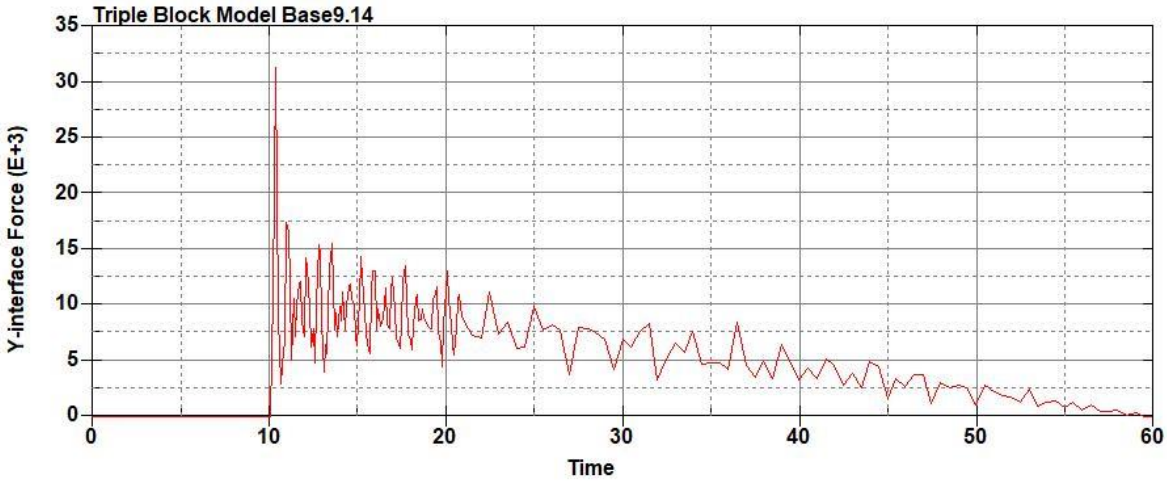


**Figure B-589: Base Run 9.14 Right Support Y-Interface Force (lbs) versus Time (ms) – 700 psi**

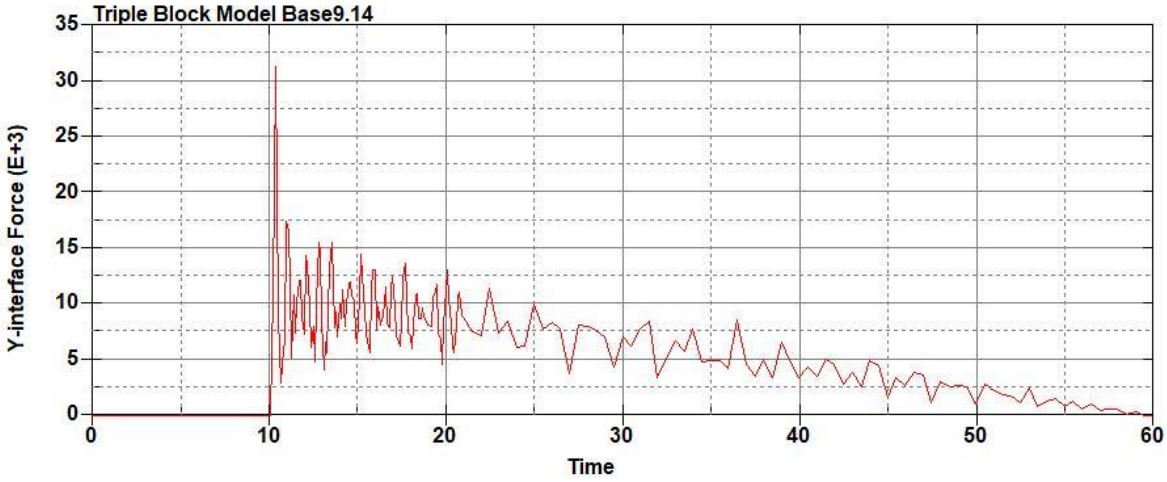


**Figure B-590: Base Run 9.14 Left Support Y-Interface Force (lbs) versus Time (ms) – 700 psi**

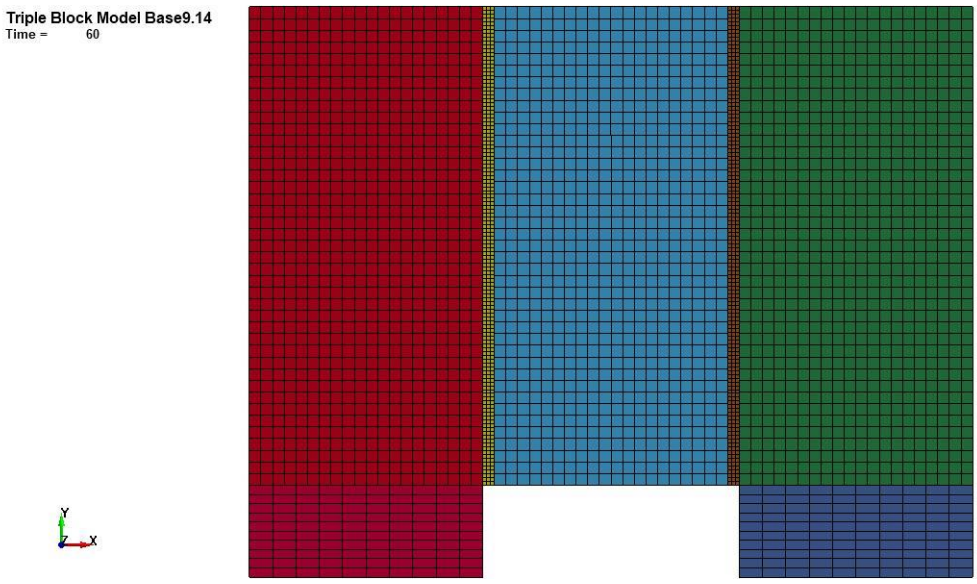


**Figure B-591: Last State at 60 Milliseconds for Base Run 9.14 – 700 psi**

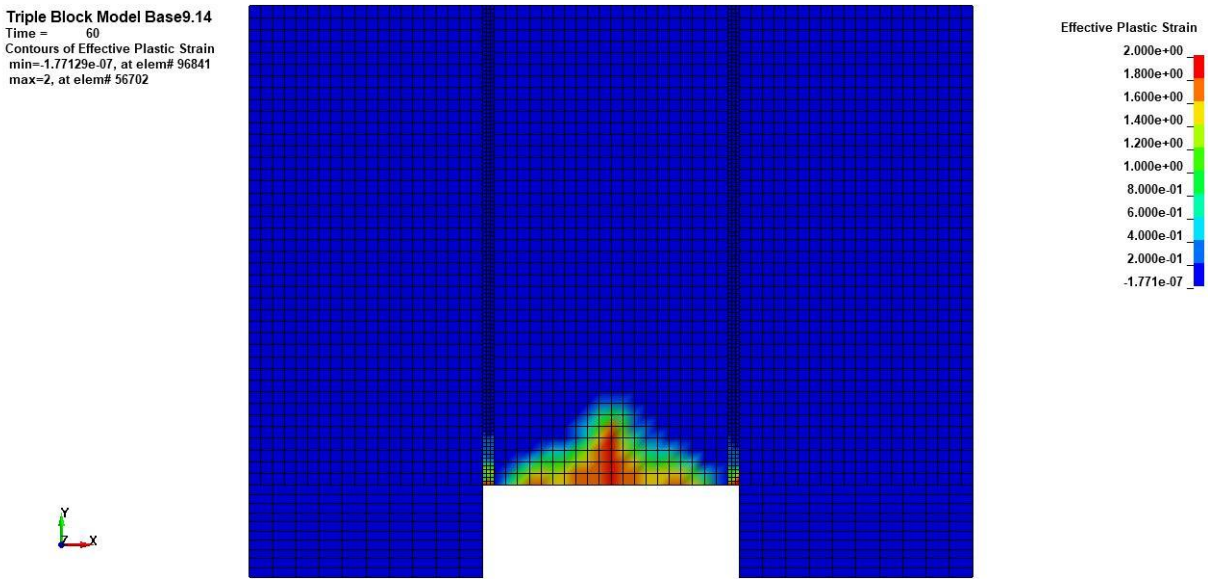


**Figure B-592: Effective Plastic Strain Fringe Plot for Last State at 60 Milliseconds for Base Run 9.14 – 700 psi**

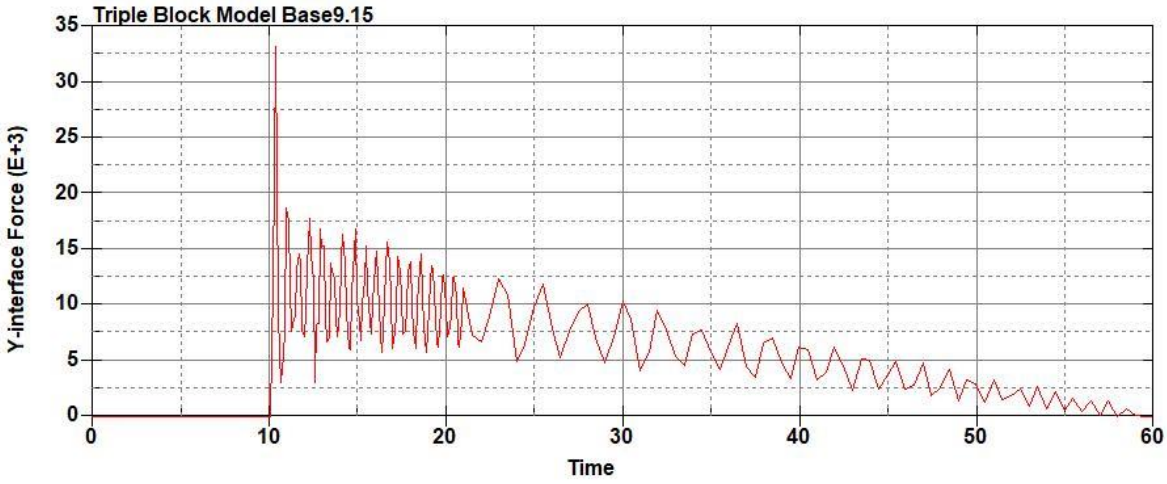


**Figure B-593: Base Run 9.15 Right Support Y-Interface Force (lbs) versus Time (ms) – 750 psi**

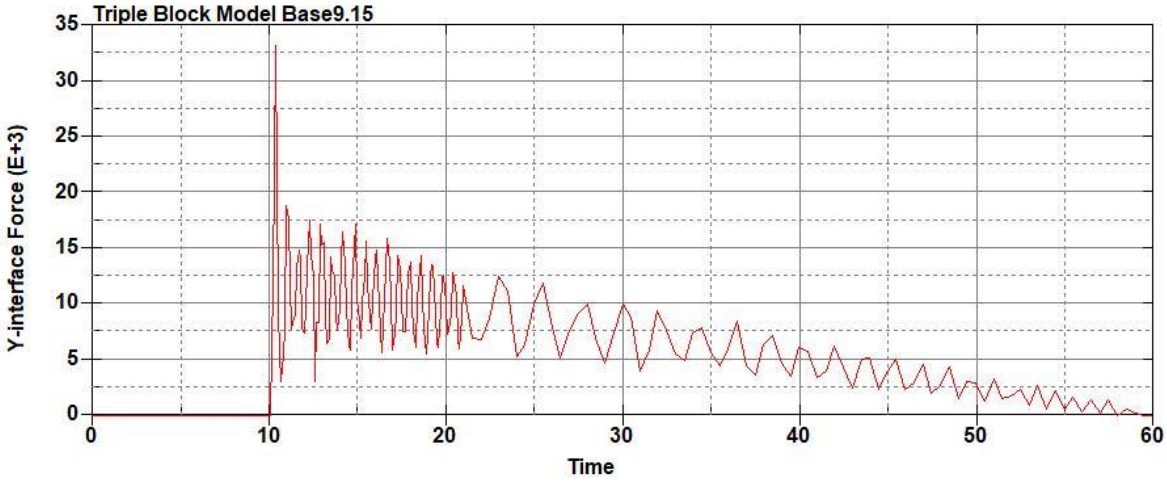


**Figure B-594: Base Run 9.15 Left Support Y-Interface Force (lbs) versus Time (ms) – 750 psi**

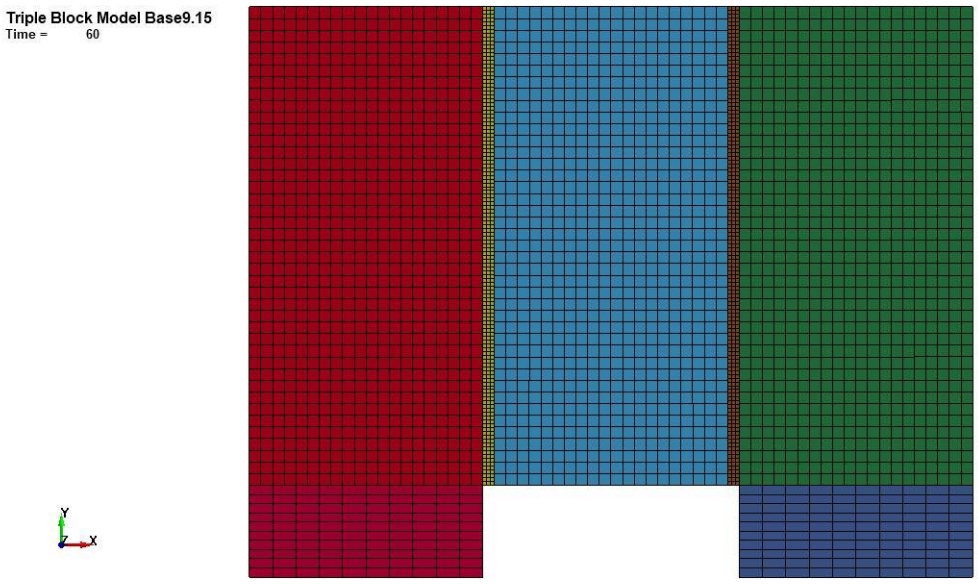


**Figure B-595: Last State at 60 Milliseconds for Base Run 9.15 – 750 psi**

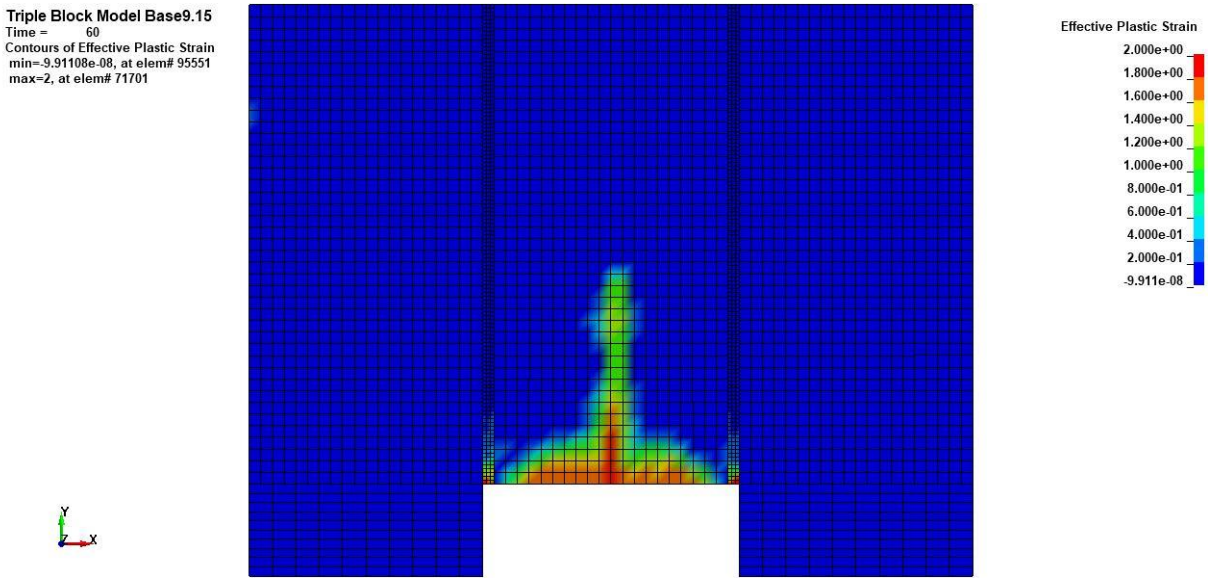


**Figure B-596: Effective Plastic Strain Fringe Plot for Last State at 60 Milliseconds for Base Run 9.15 – 750 psi**

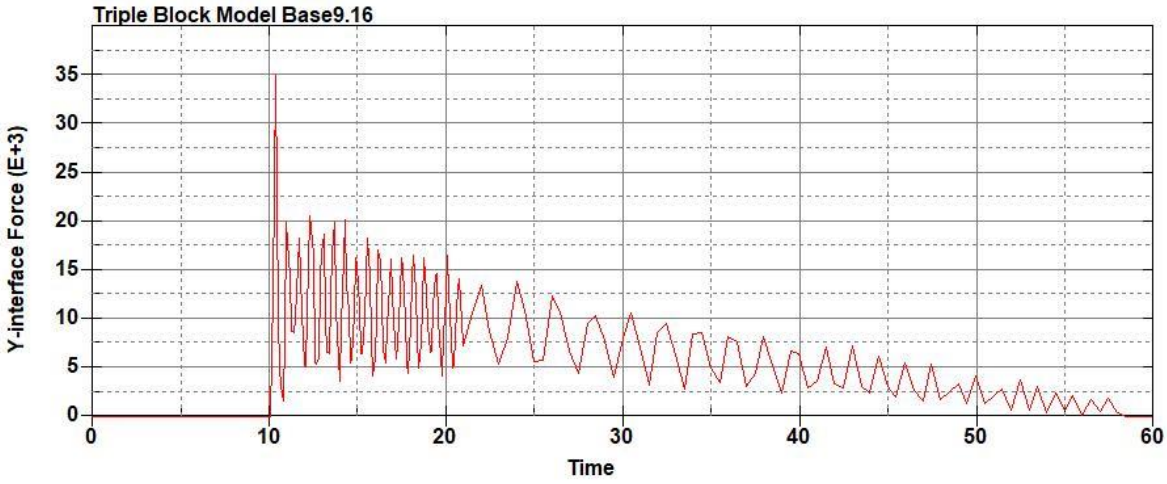


**Figure B-597: Base Run 9.16 Right Support Y-Interface Force (lbs) versus Time (ms) – 800 psi**

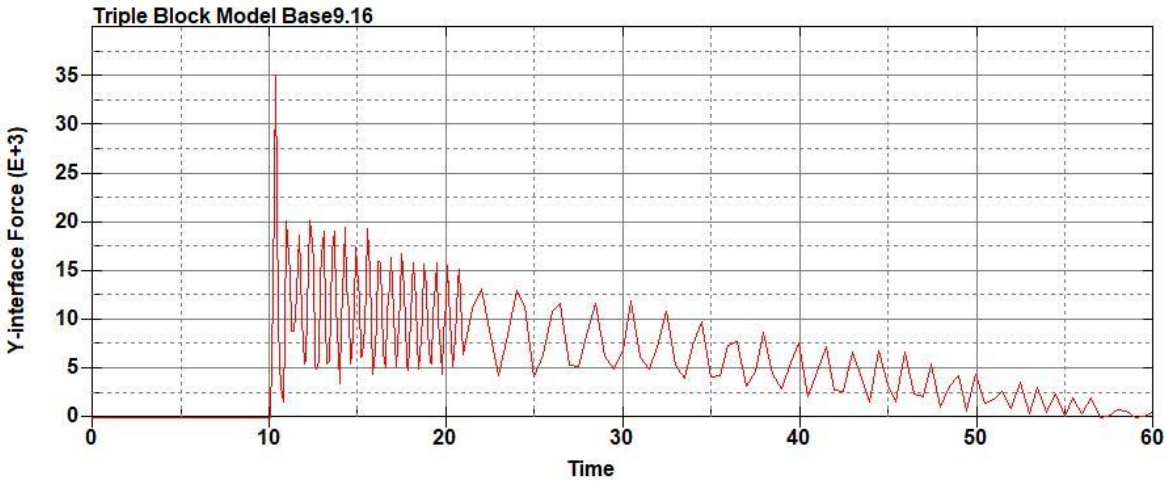


**Figure B-598: Base Run 9.16 Left Support Y-Interface Force (lbs) versus Time (ms) – 800 psi**

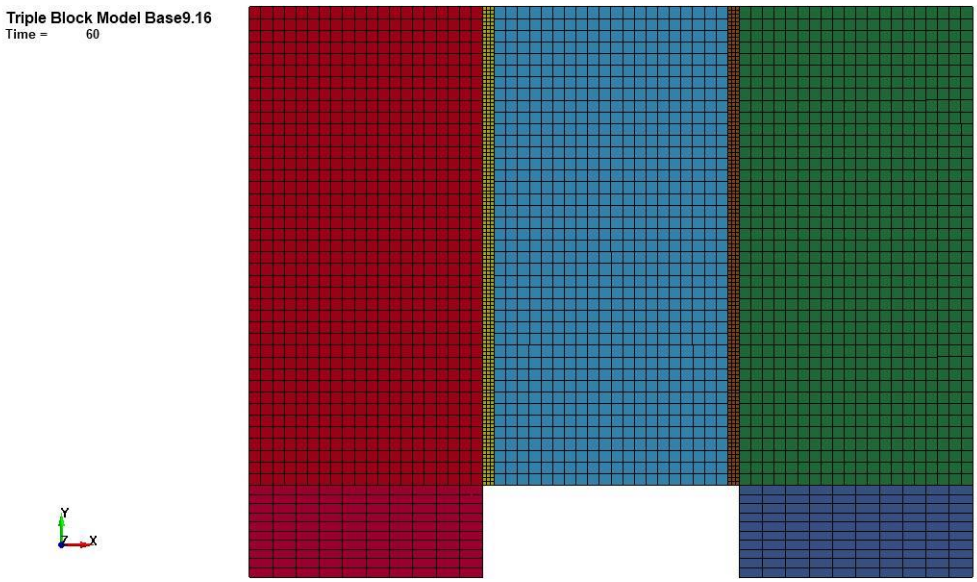


**Figure B-599: Last State at 60 Milliseconds for Base Run 9.16 – 800 psi**

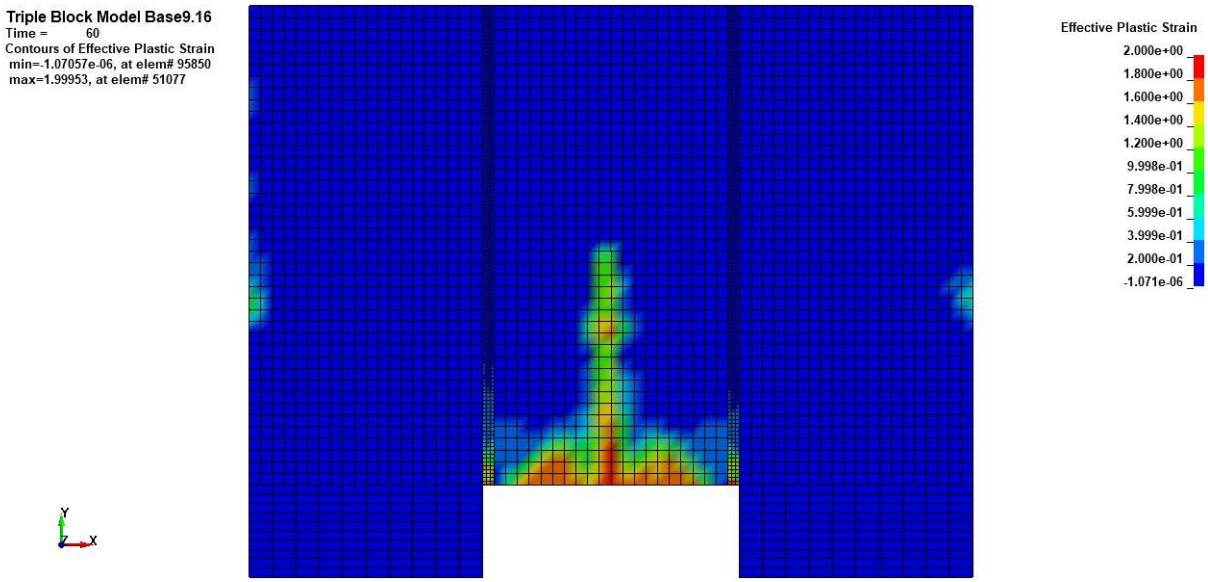


**Figure B-600: Effective Plastic Strain Fringe Plot for Last State at 60 Milliseconds for Base Run 9.16 – 800 psi**

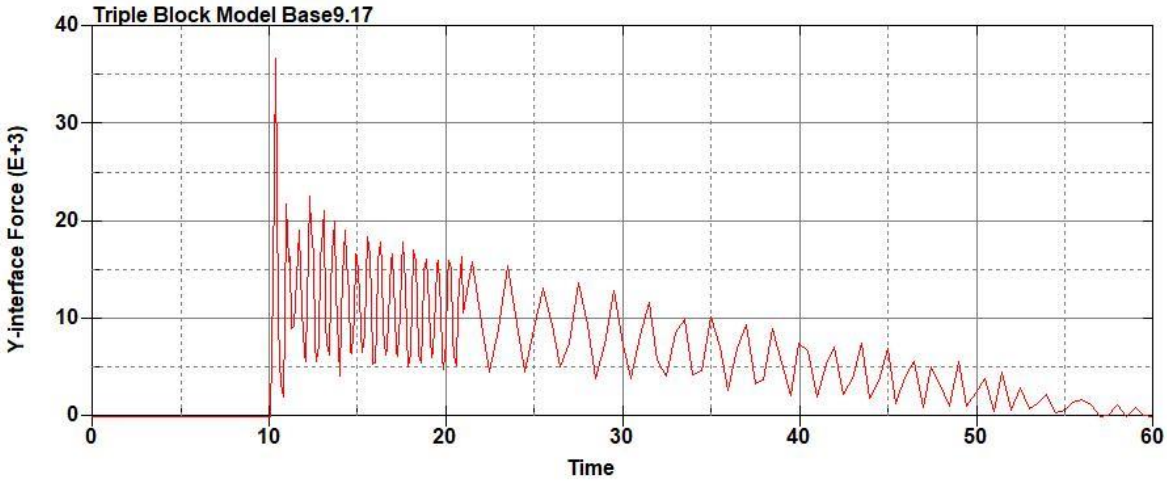


**Figure B-601: Base Run 9.17 Right Support Y-Interface Force (lbs) versus Time (ms) – 850 psi**

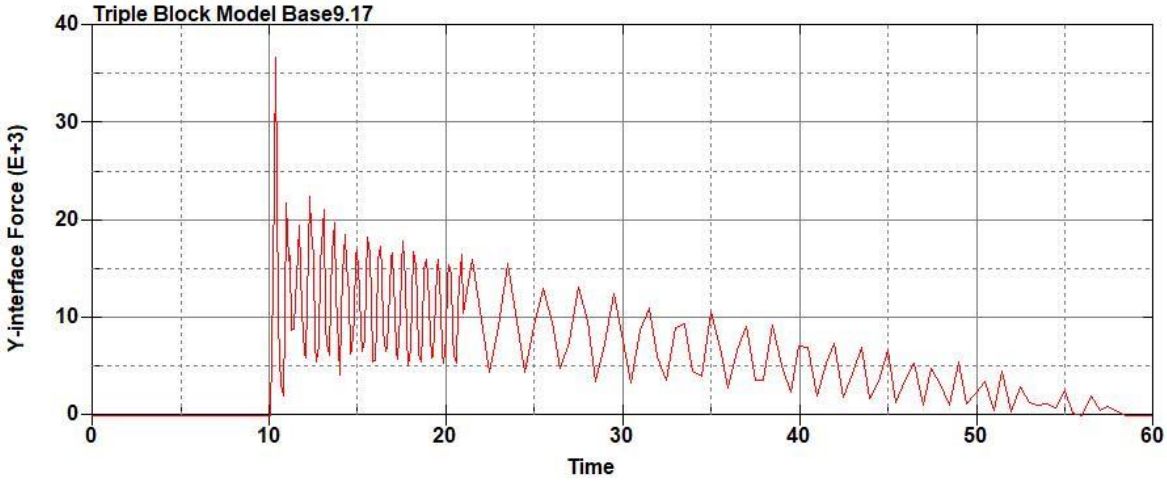


**Figure B-602: Base Run 9.17 Left Support Y-Interface Force (lbs) versus Time (ms) – 850 psi**

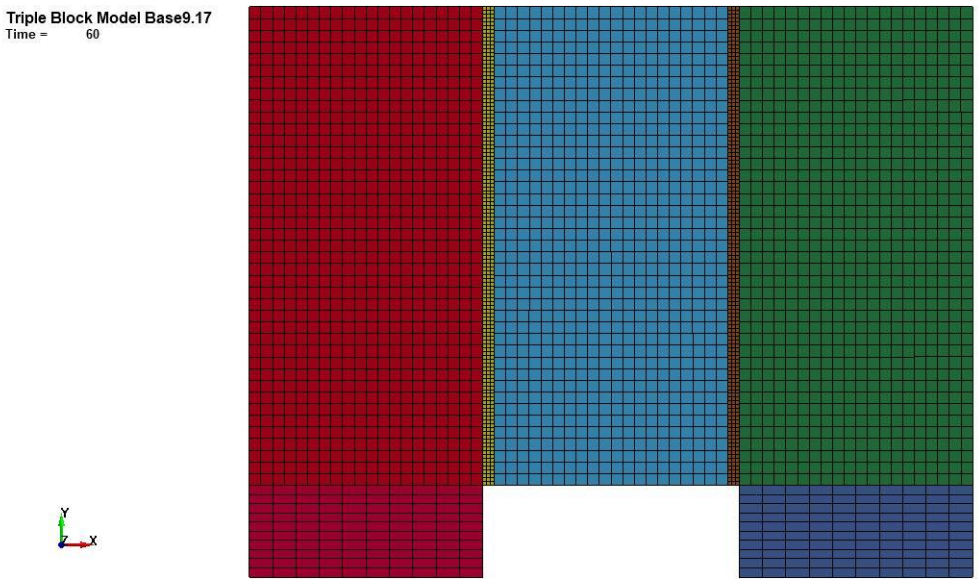


**Figure B-603: Last State at 60 Milliseconds for Base Run 9.17 – 850 psi**

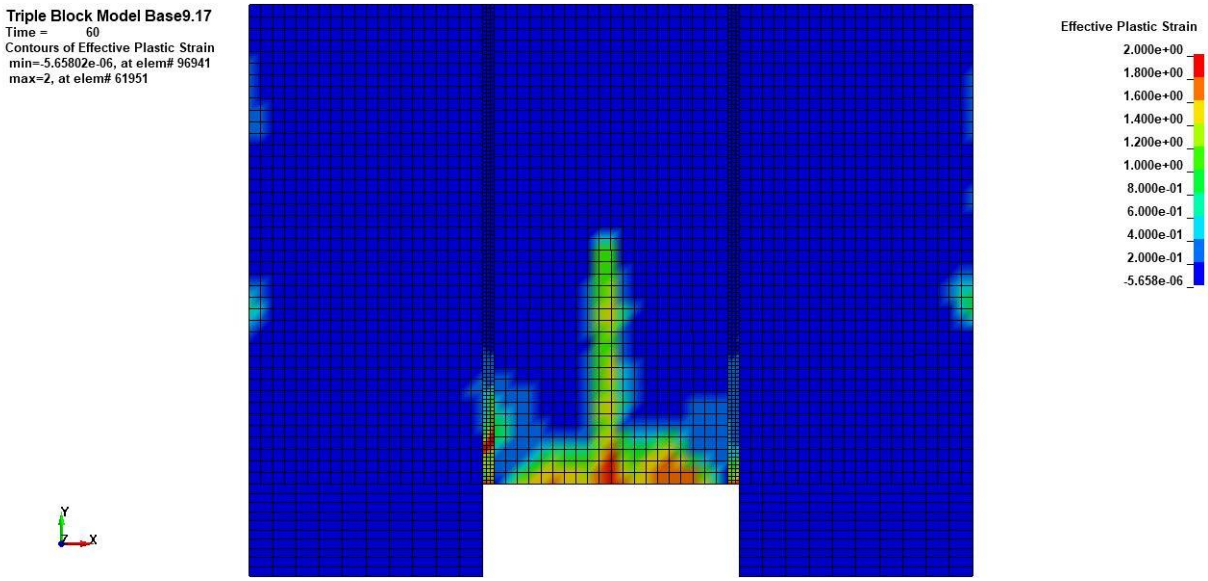


**Figure B-604: Effective Plastic Strain Fringe Plot for Last State at 60 Milliseconds for Base Run 9.17 – 850 psi**

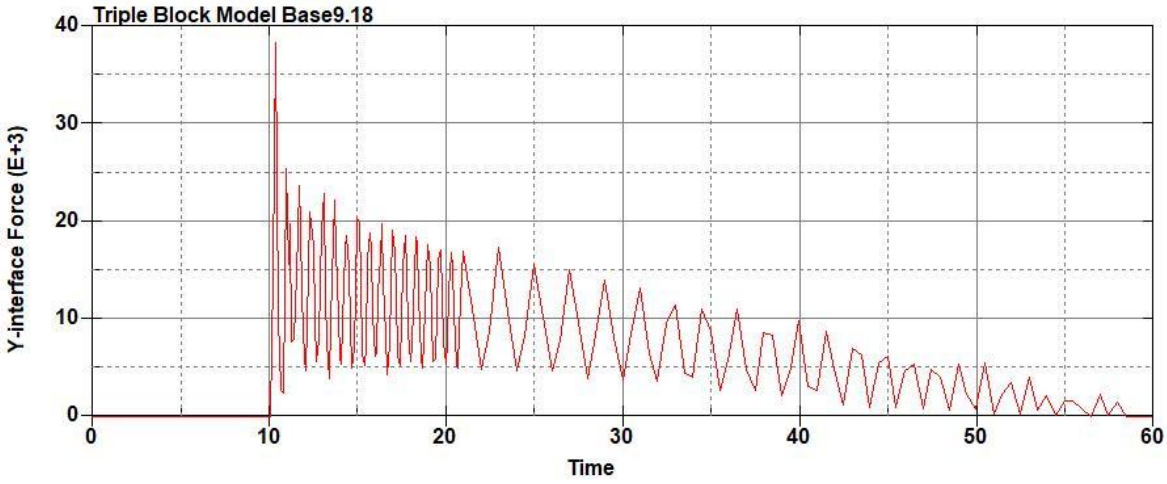


**Figure B-605: Base Run 9.18 Right Support Y-Interface Force (lbs) versus Time (ms) – 900 psi**

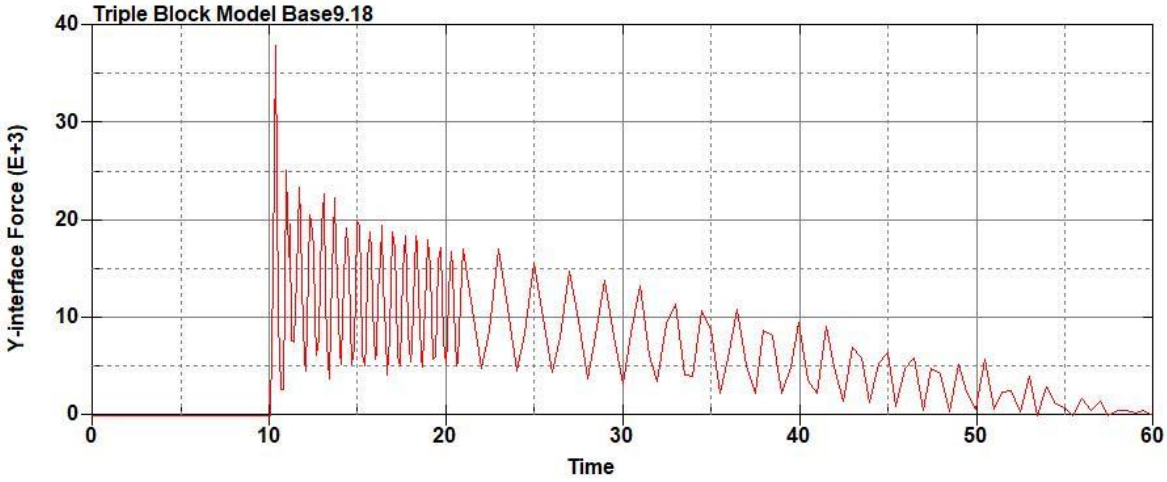


**Figure B-606: Base Run 9.18 Left Support Y-Interface Force (lbs) versus Time (ms) – 900 psi**

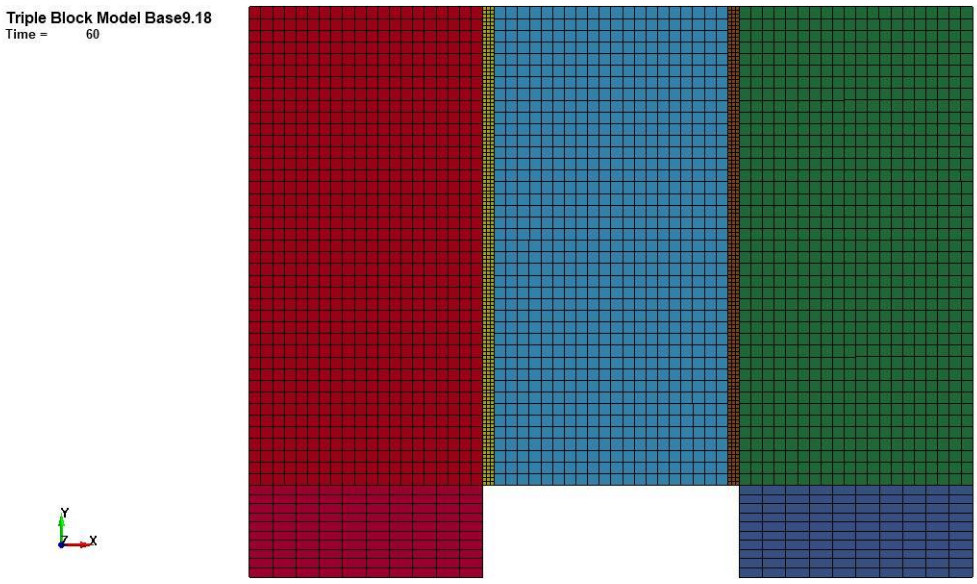


**Figure B-607: Last State at 60 Milliseconds for Base Run 9.18 – 900 psi**

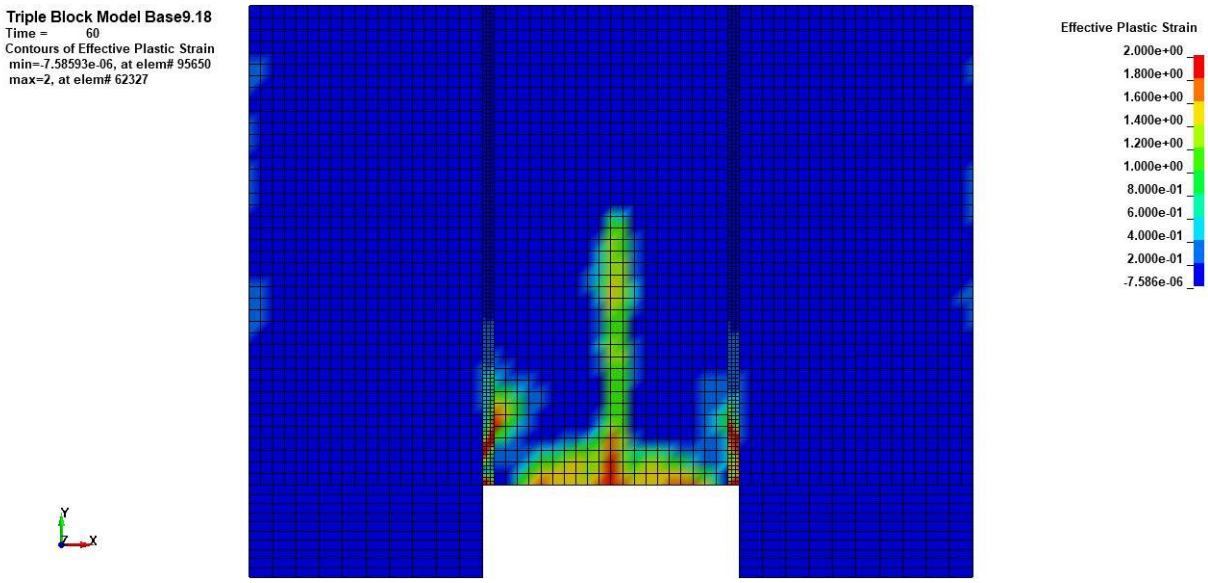


**Figure B-608: Effective Plastic Strain Fringe Plot for Last State at 60 Milliseconds for Base Run 9.18 – 900 psi**

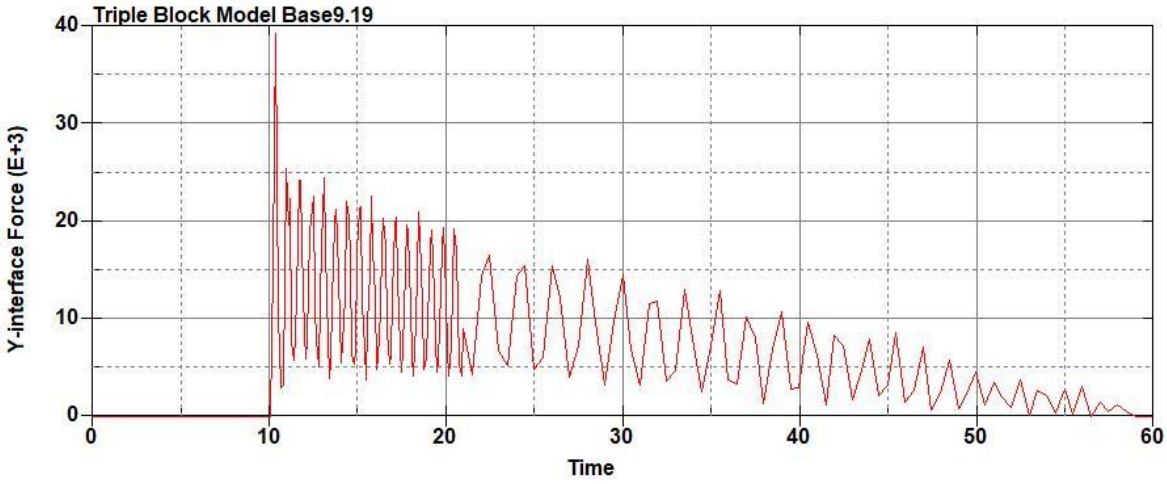


**Figure B-609: Base Run 9.19 Right Support Y-Interface Force (lbs) versus Time (ms) – 950 psi**

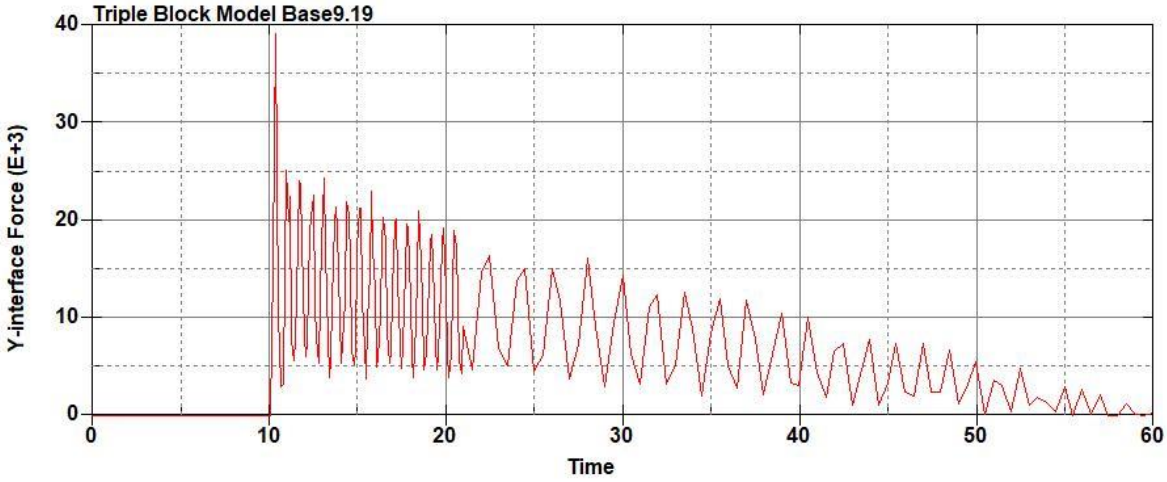


**Figure B-610: Base Run 9.19 Left Support Y-Interface Force (lbs) versus Time (ms) – 950 psi**

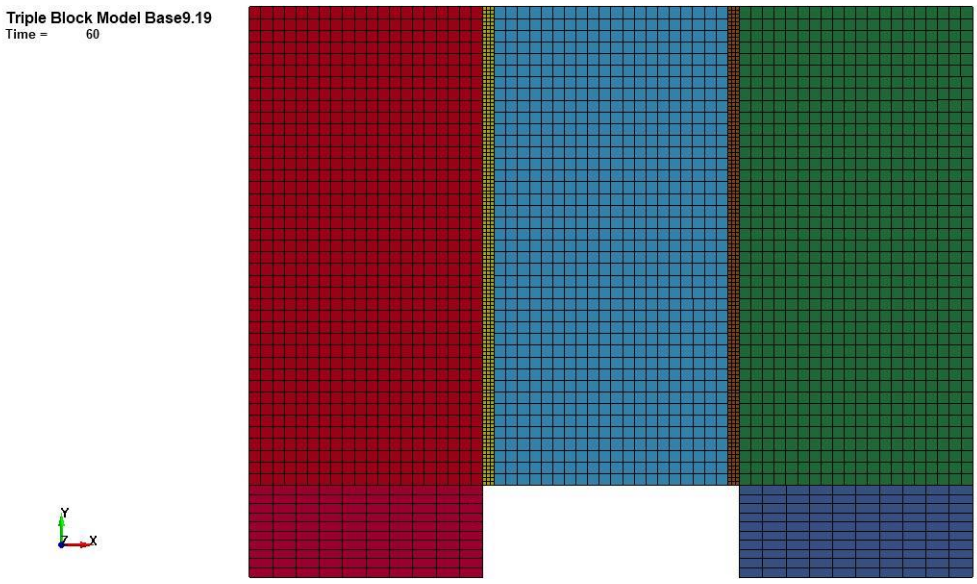


**Figure B-611: Last State at 60 Milliseconds for Base Run 9.19 – 950 psi**

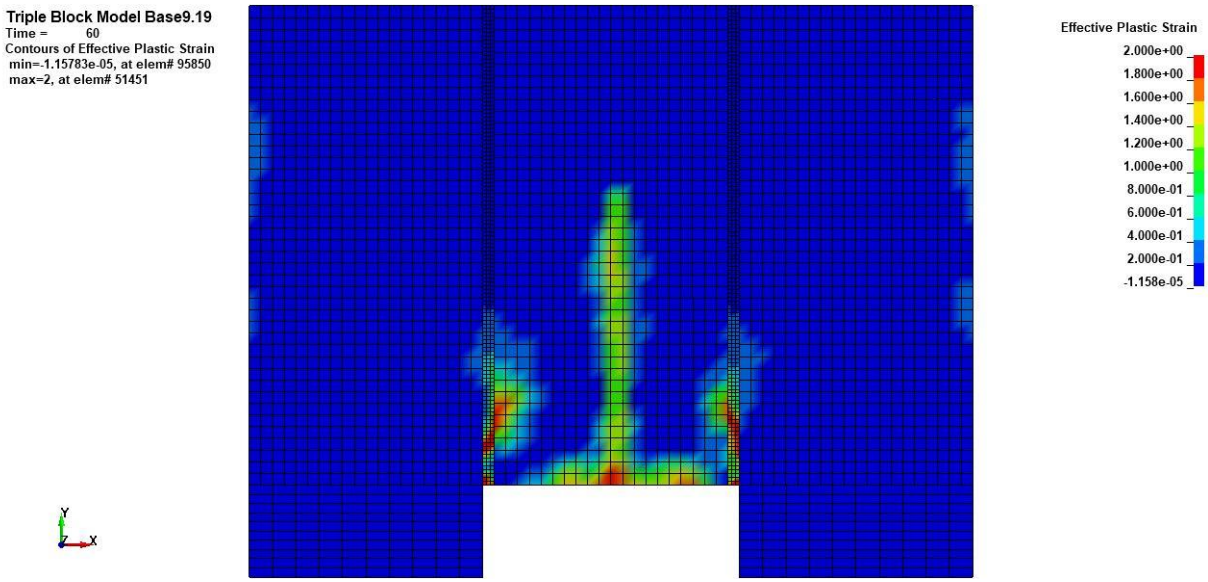


**Figure B-612: Effective Plastic Strain Fringe Plot for Last State at 60 Milliseconds for Base Run 9.19 – 950 psi**

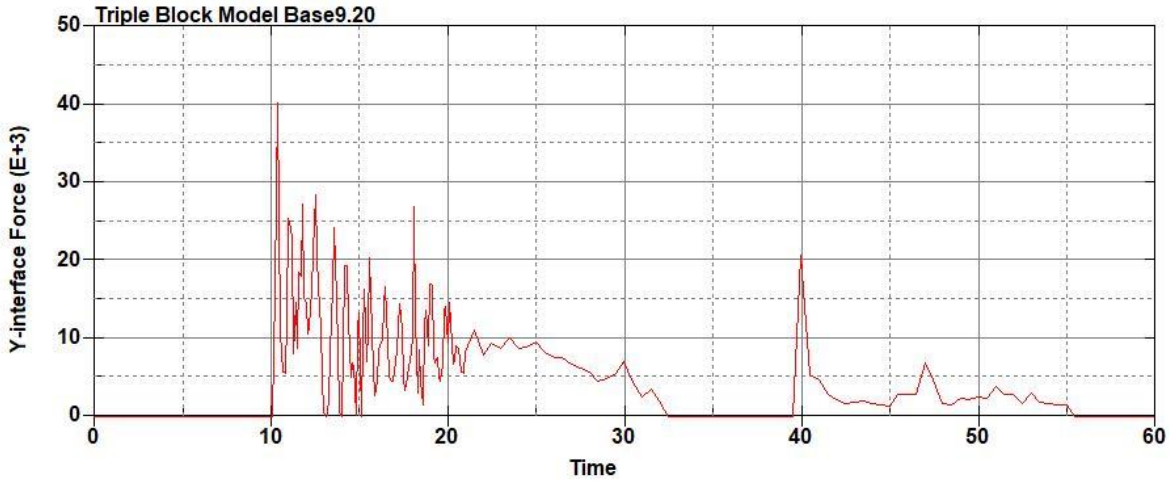


**Figure B-613: Base Run 9.20 Right Support Y-Interface Force (lbs) versus Time (ms) – 1000 psi**

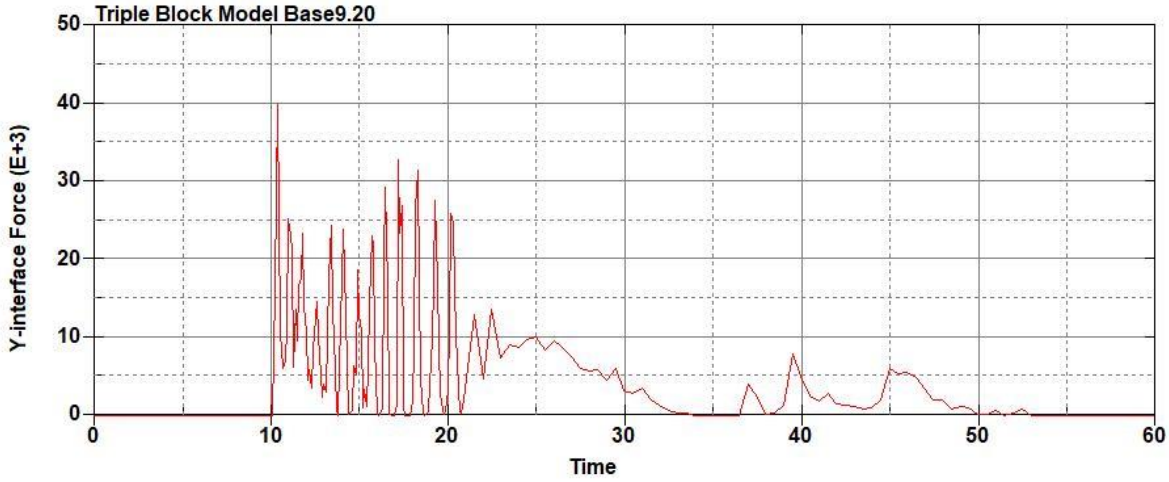


**Figure B-614: Base Run 9.20 Left Support Y-Interface Force (lbs) versus Time (ms) – 1000 psi**

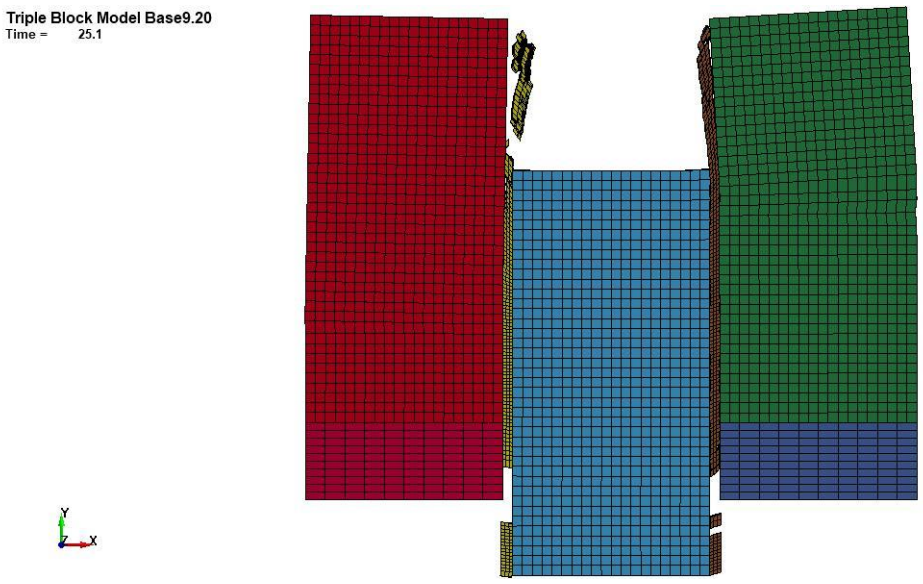


**Figure B-615: Last State at 25.1 Milliseconds for Base Run 9.20 – 1000 psi**

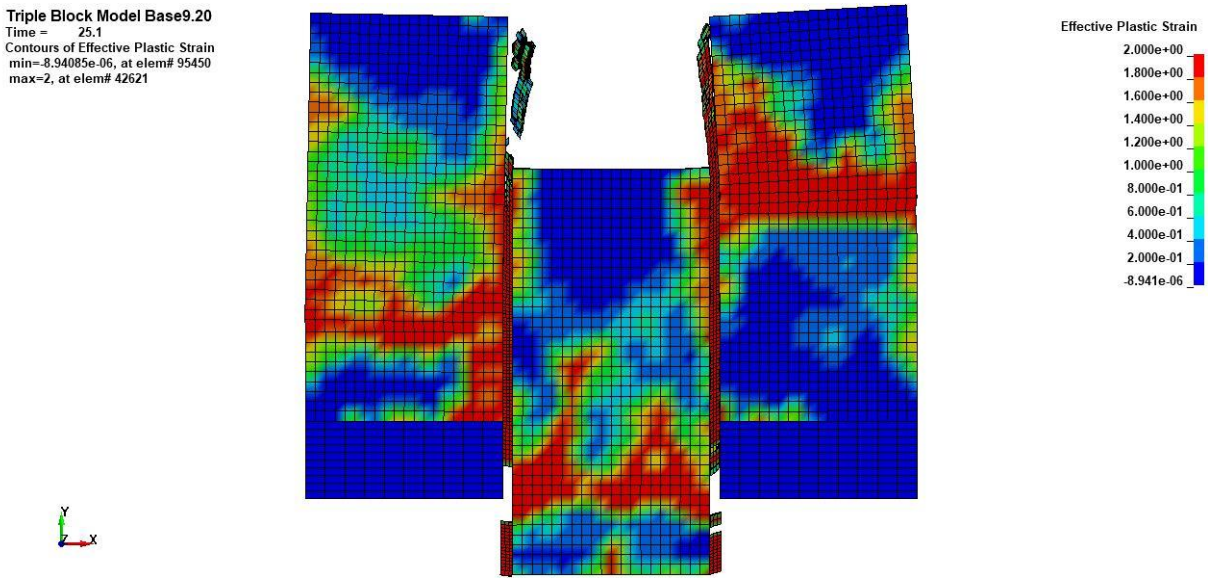


**Figure B-616: Effective Plastic Strain Fringe Plot for Last State at 25.1 Milliseconds for Base Run 9.20 – 1000 psi**

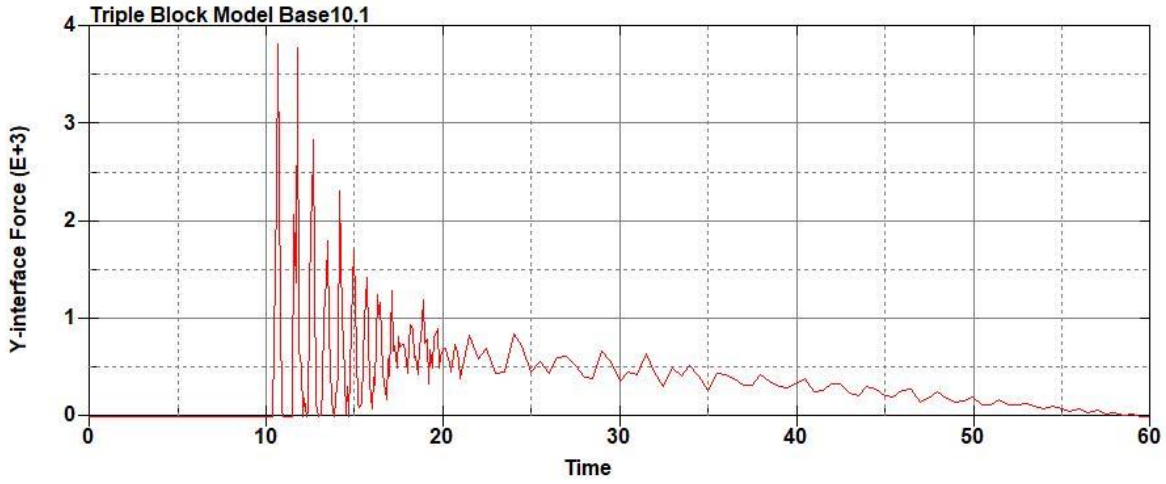


**Figure B-617: Base Run 10.1 Right Support Y-Interface Force (lbs) versus Time (ms) – 50 psi**

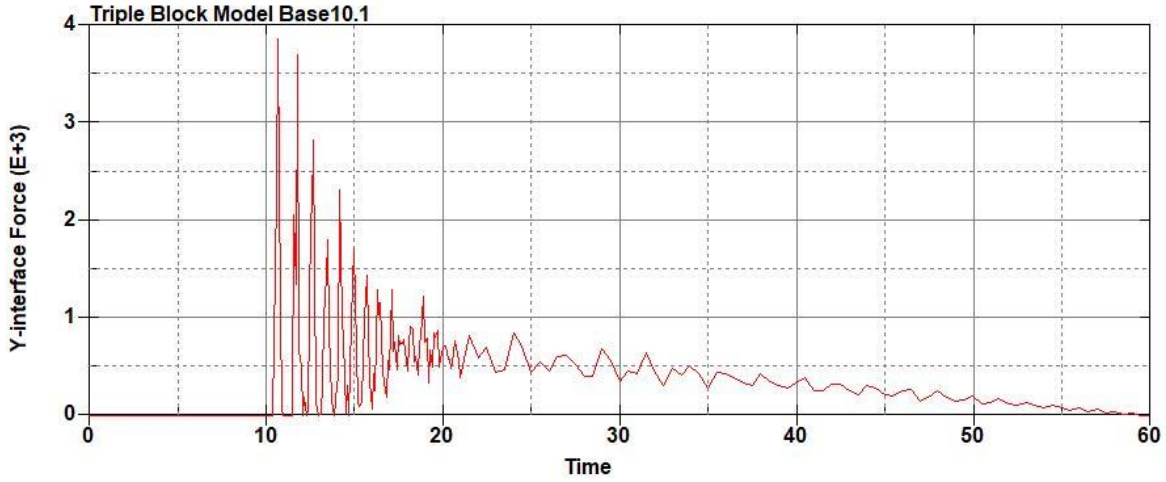


**Figure B-618: Base Run 10.1 Left Support Y-Interface Force (lbs) versus Time (ms) – 50 psi**

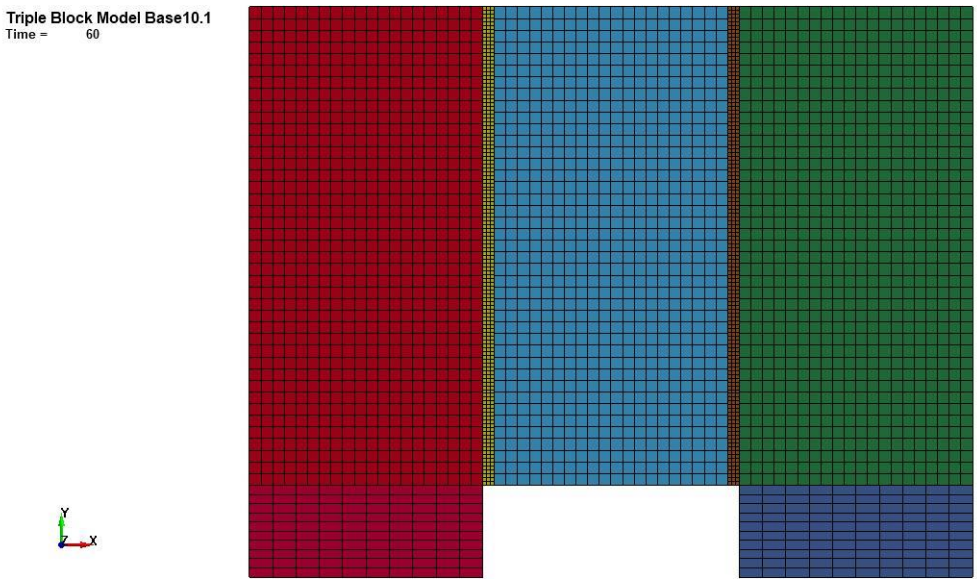


**Figure B-619: Last State at 60 Milliseconds for Base Run 10.1 – 50 psi**

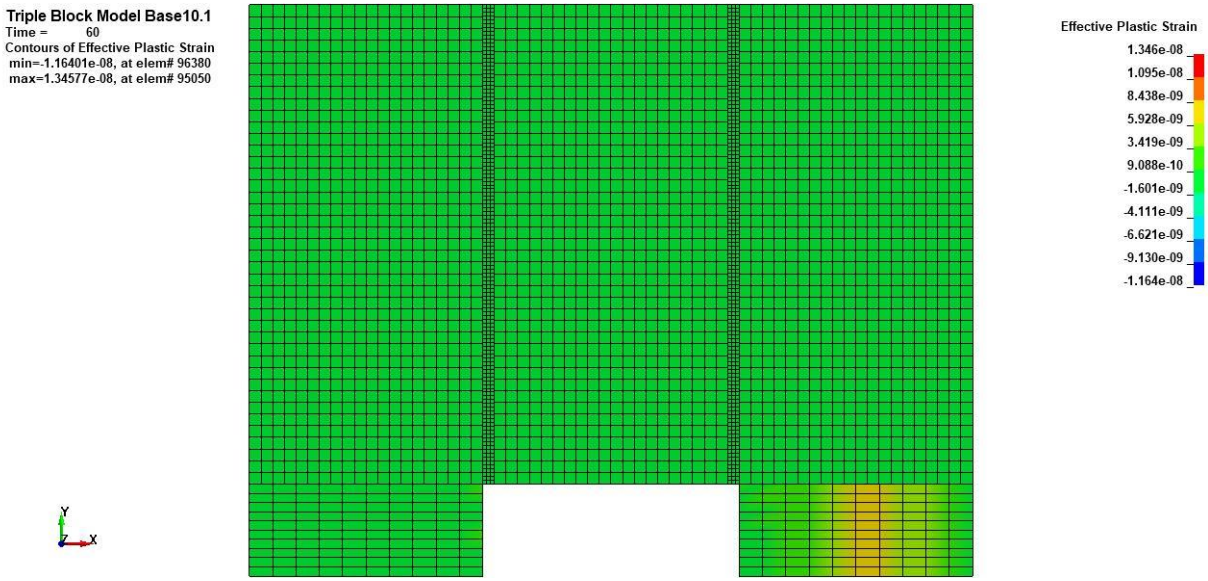


**Figure B-620: Effective Plastic Strain Fringe Plot for Last State at 60 Milliseconds for Base Run 10.1 – 50 psi**

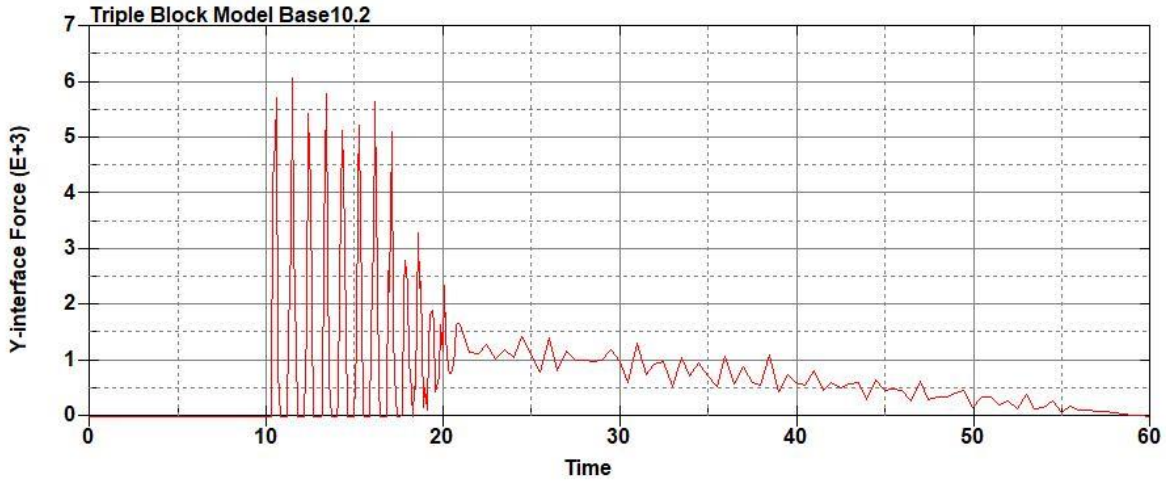


**Figure B-621: Base Run 10.2 Right Support Y-Interface Force (lbs) versus Time (ms) – 100 psi**

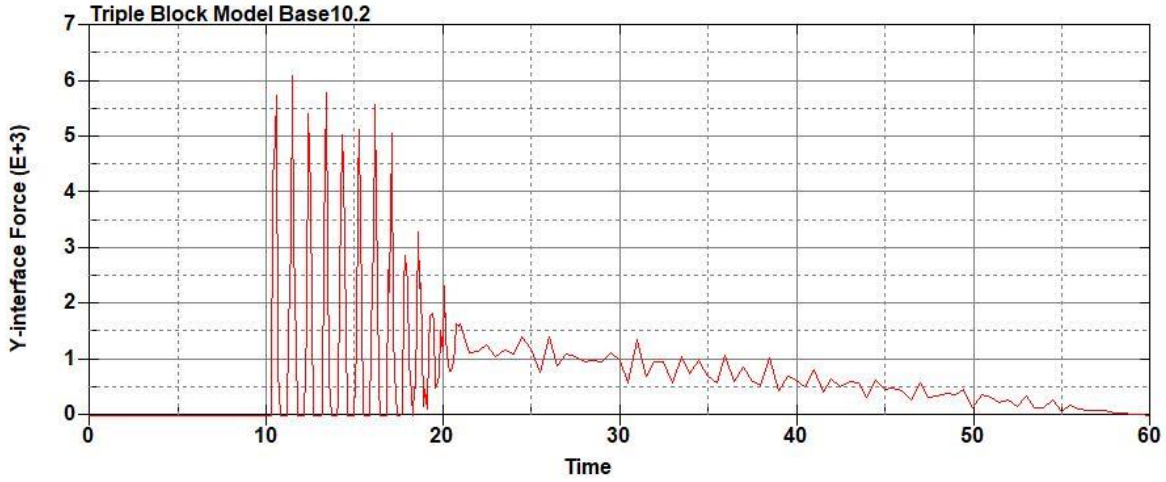


**Figure B-622: Base Run 10.2 Left Support Y-Interface Force (lbs) versus Time (ms) – 100 psi**

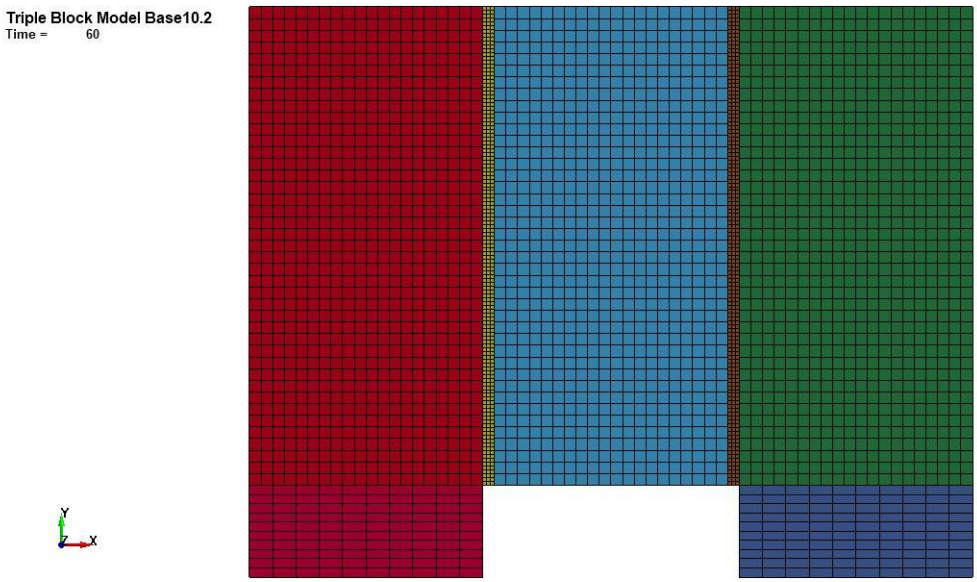


**Figure B-623: Last State at 60 Milliseconds for Base Run 10.2 – 100 psi**

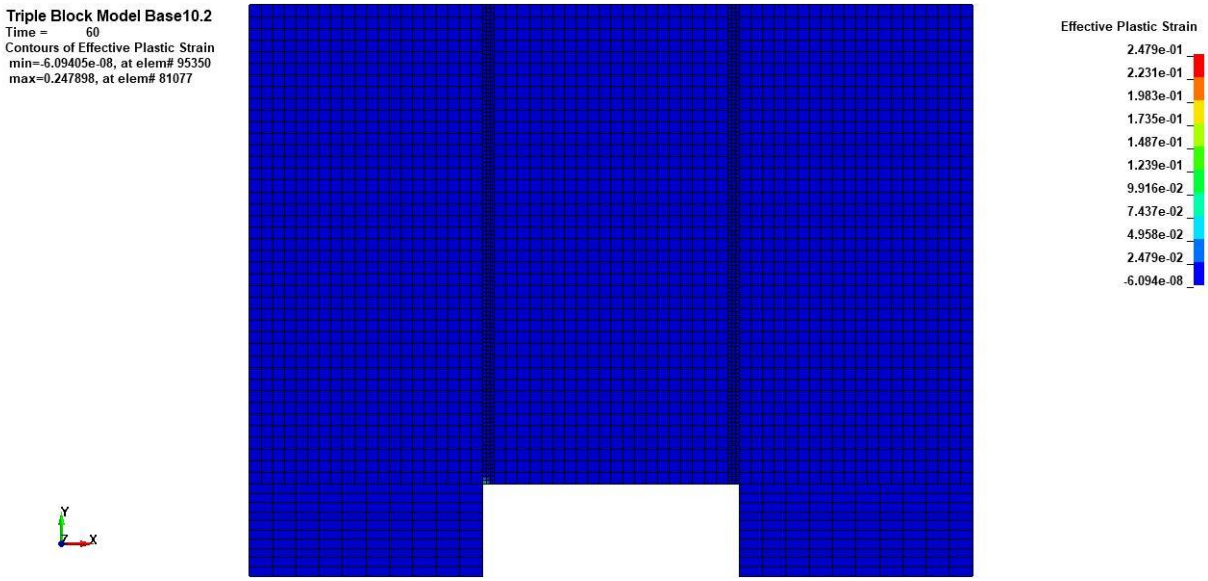


**Figure B-624: Base Run 10.2 Left Support Y-Interface Force (lbs) versus Time (ms) – 100 psi**

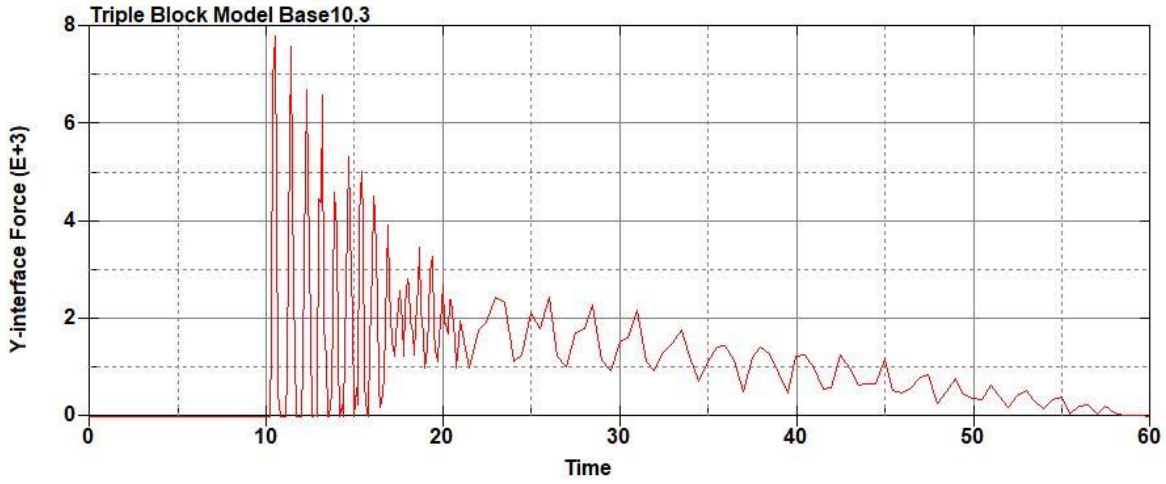


**Figure B-625: Base Run 10.3 Right Support Y-Interface Force (lbs) versus Time (ms) – 150 psi**

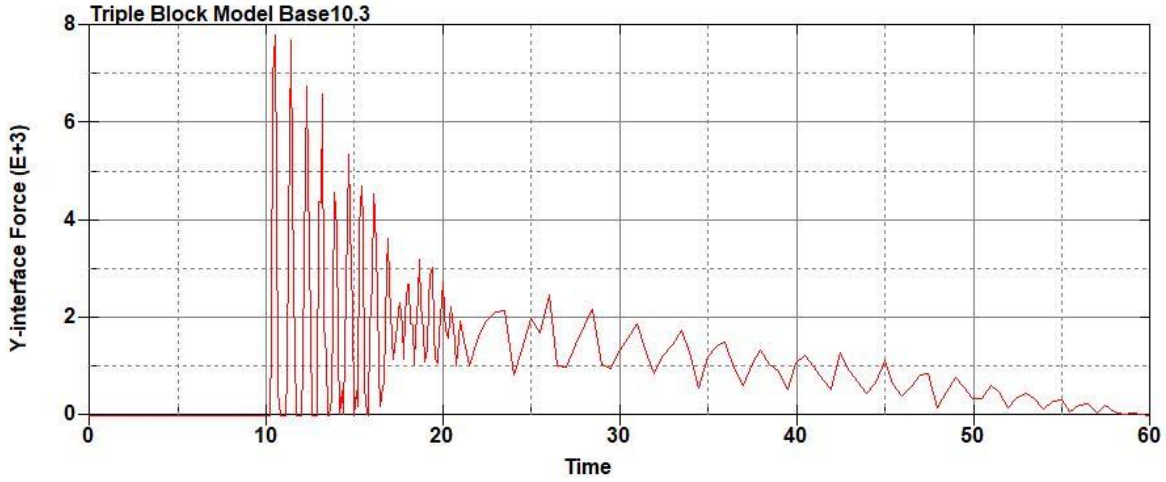


**Figure B-626: Base Run 10.3 Left Support Y-Interface Force (lbs) versus Time (ms) – 150 psi**

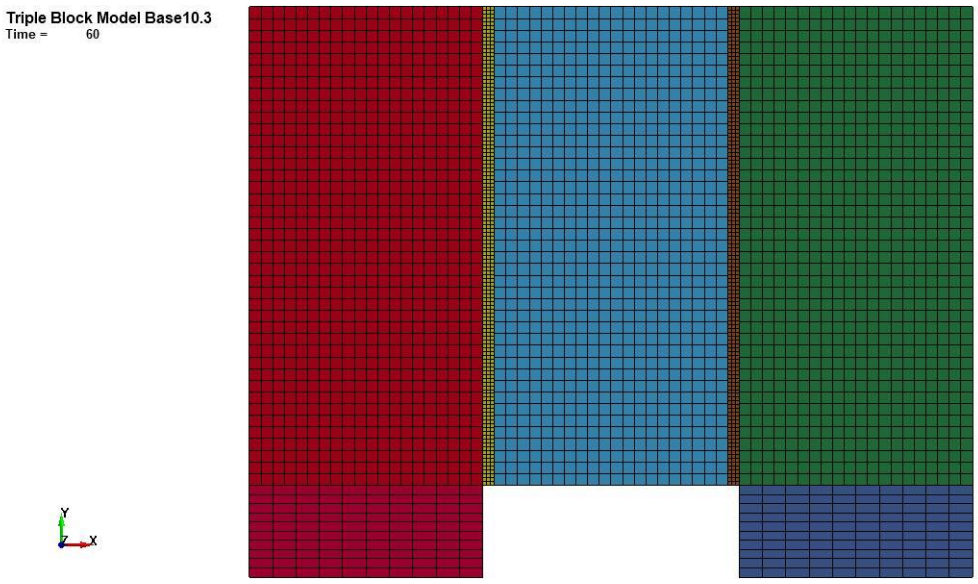


**Figure B-627: Last State at 60 Milliseconds for Base Run 10.3 – 150 psi**

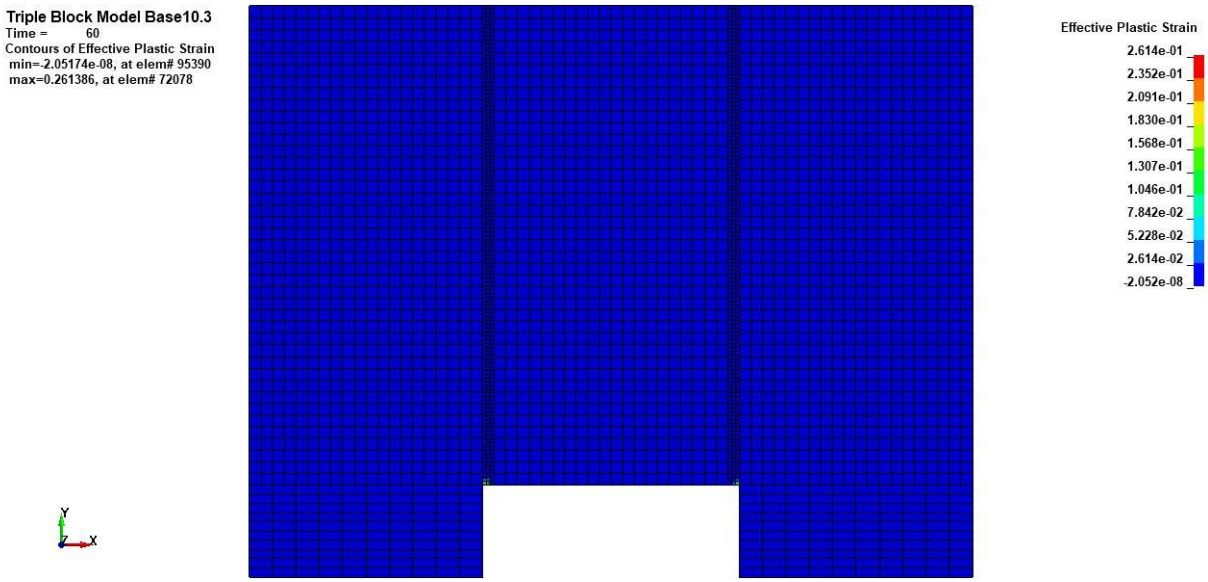


**Figure B-628: Effective Plastic Strain Fringe Plot for Last State at 60 Milliseconds for Base Run 10.3 – 150 psi**

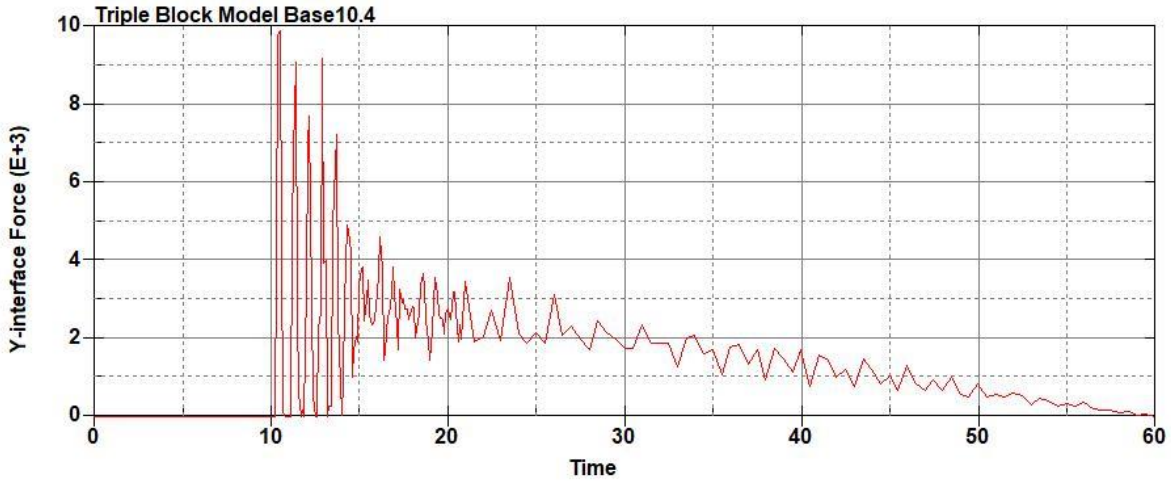


**Figure B-629: Base Run 10.4 Right Support Y-Interface Force (lbs) versus Time (ms) – 200 psi**

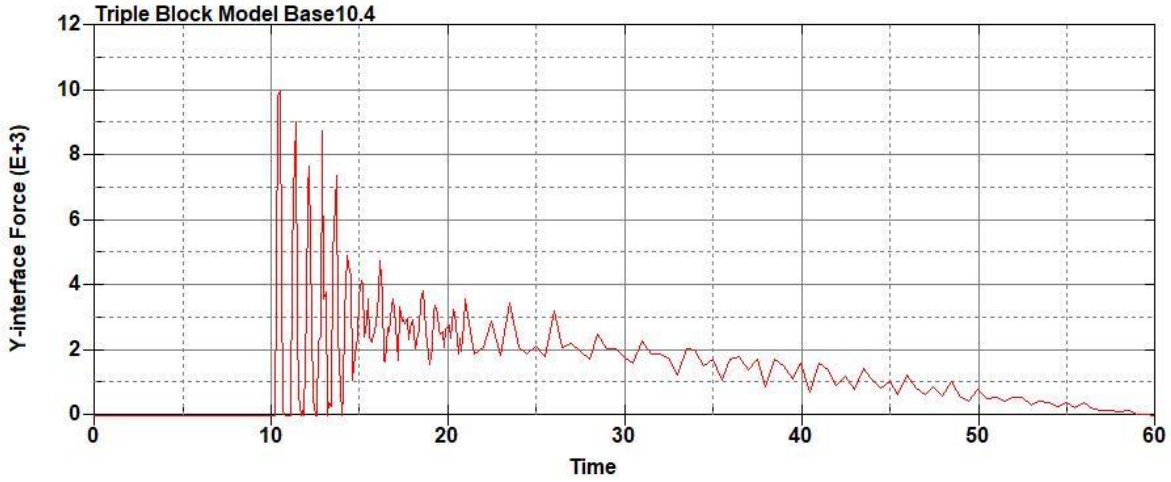


**Figure B-630: Base Run 10.4 Left Support Y-Interface Force (lbs) versus Time (ms) – 200 psi**

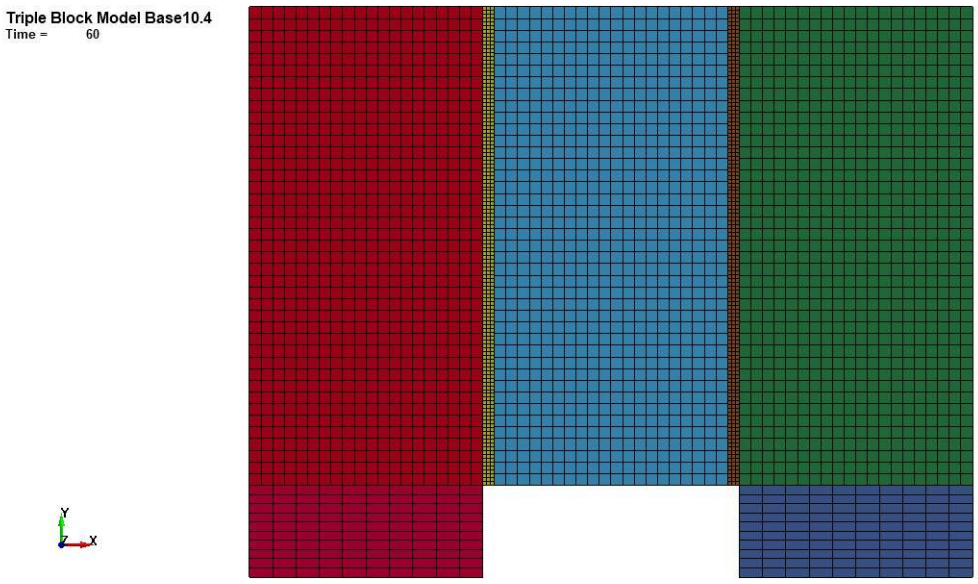


**Figure B-631: Last State at 60 Milliseconds for Base Run 10.4 – 200 psi**

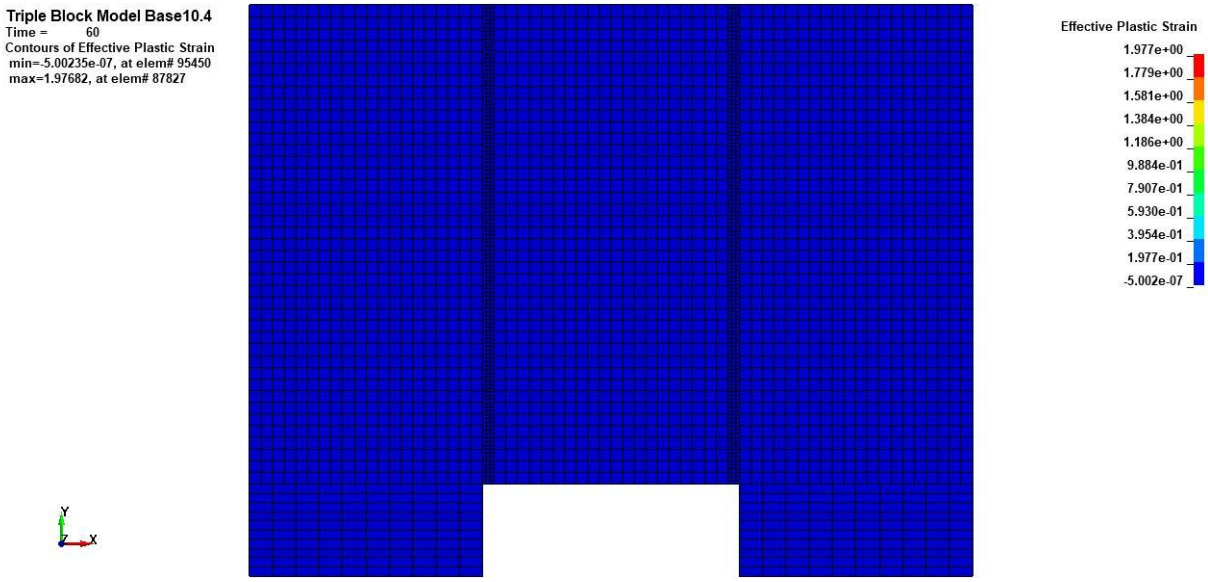


**Figure B-632: Effective Plastic Strain Fringe Plot for Last State at 60 Milliseconds for Base Run 10.4 – 200 psi**

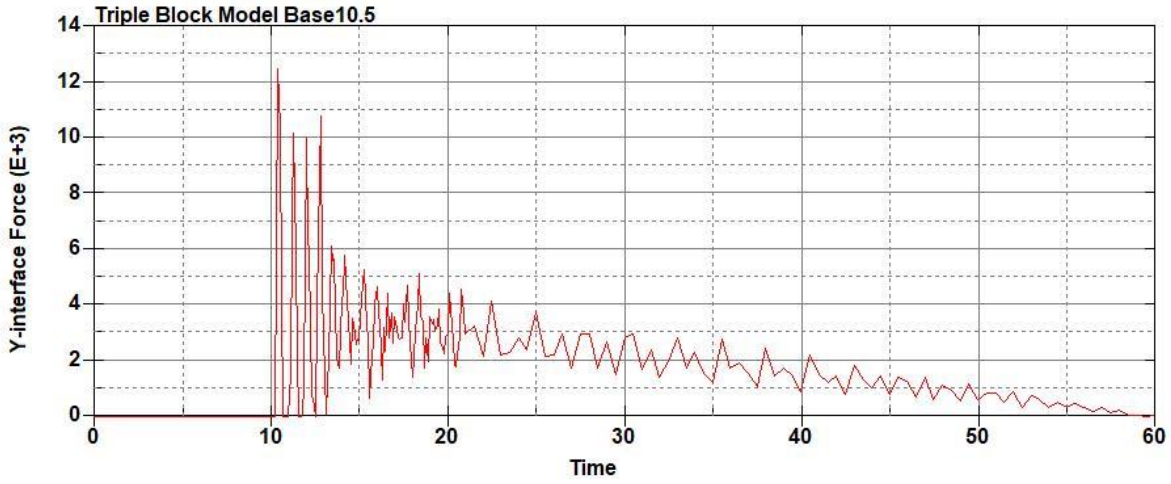


**Figure B-633: Base Run 10.5 Right Support Y-Interface Force (lbs) versus Time (ms) – 250 psi**

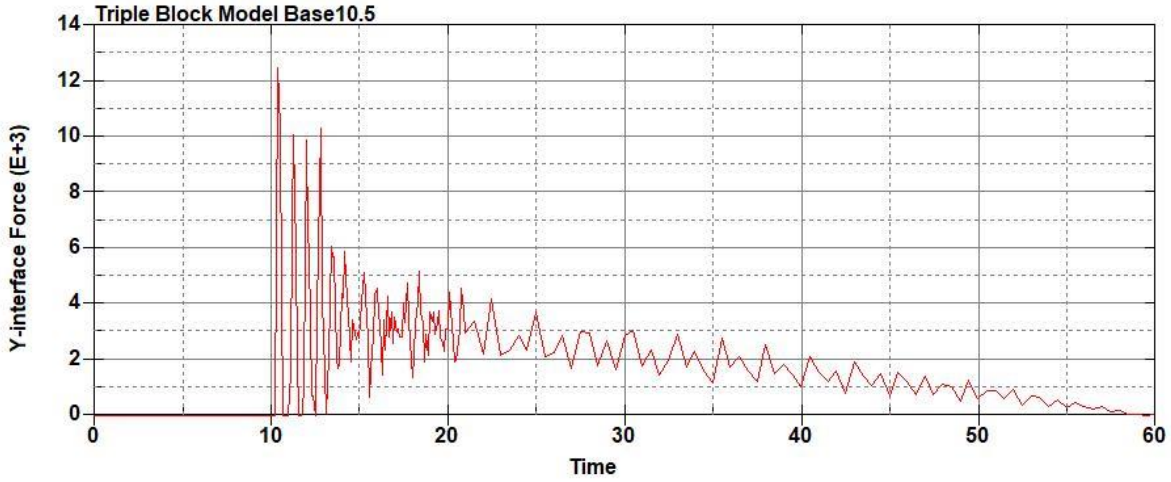


**Figure B-634: Base Run 10.5 Left Support Y-Interface Force (lbs) versus Time (ms) – 250 psi**

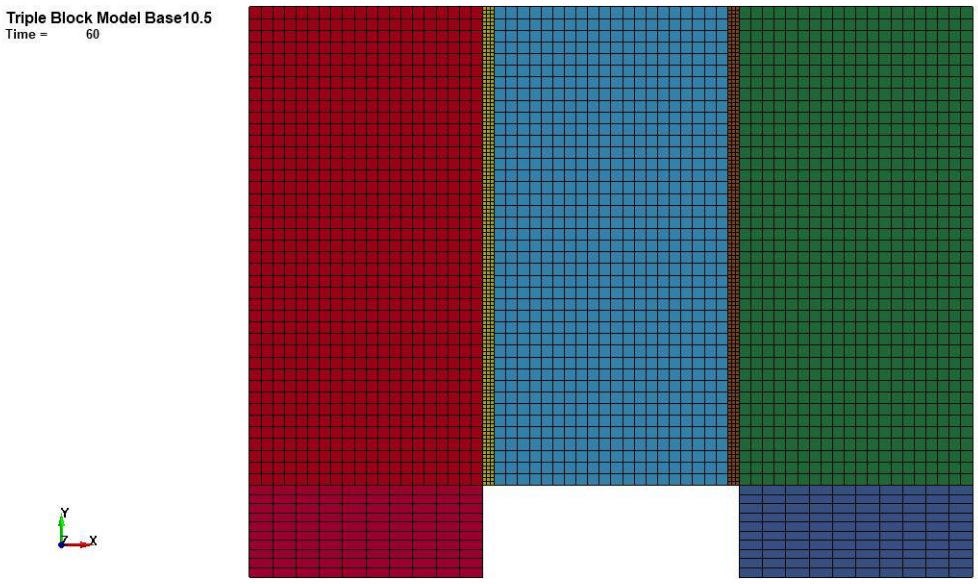


**Figure B-635: Last State at 60 Milliseconds for Base Run 10.5 – 250 psi**

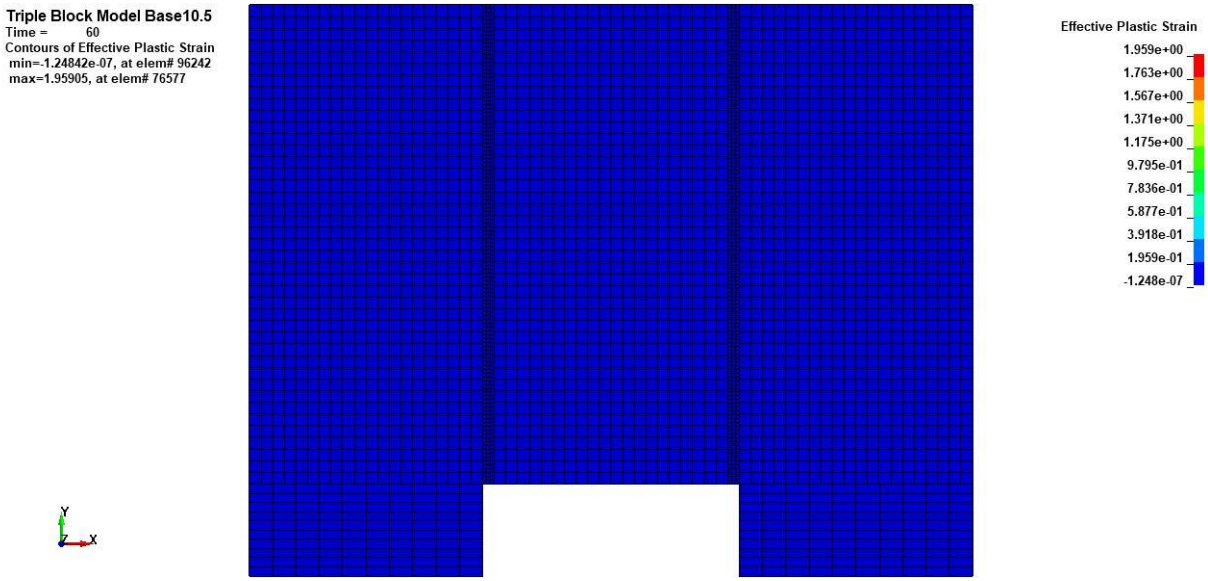


**Figure B-636: Effective Plastic Strain Fringe Plot for Last State at 60 Milliseconds for Base Run 10.5 – 250 psi**

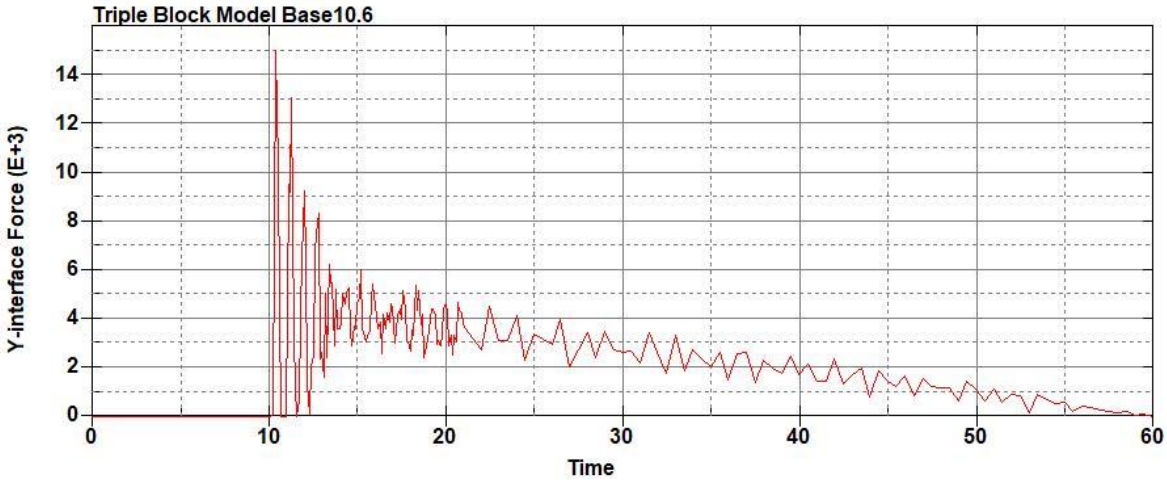


**Figure B-637: Base Run 10.6 Right Support Y-Interface Force (lbs) versus Time (ms) – 300 psi**

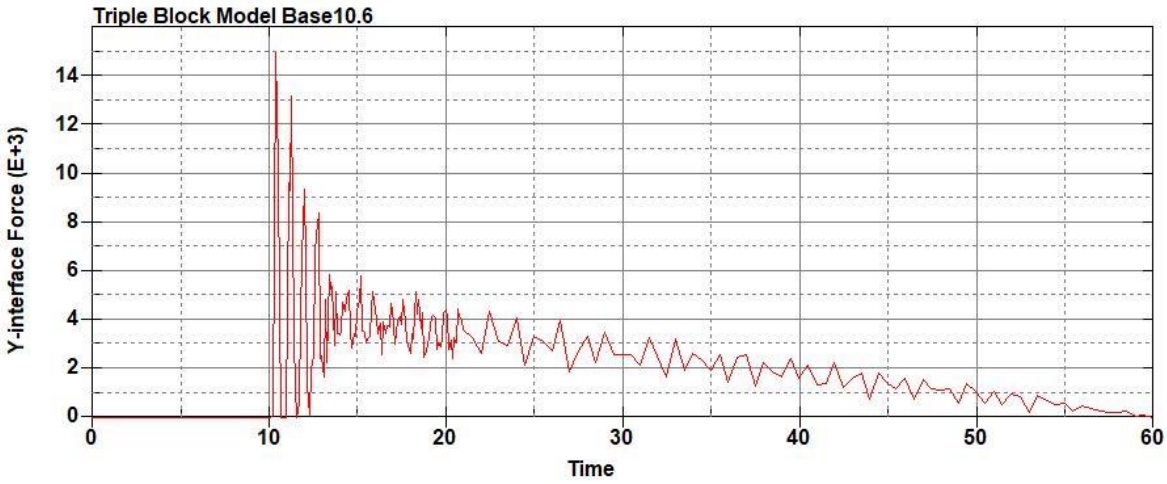


**Figure B-638: Base Run 10.6 Left Support Y-Interface Force (lbs) versus Time (ms) – 300 psi**

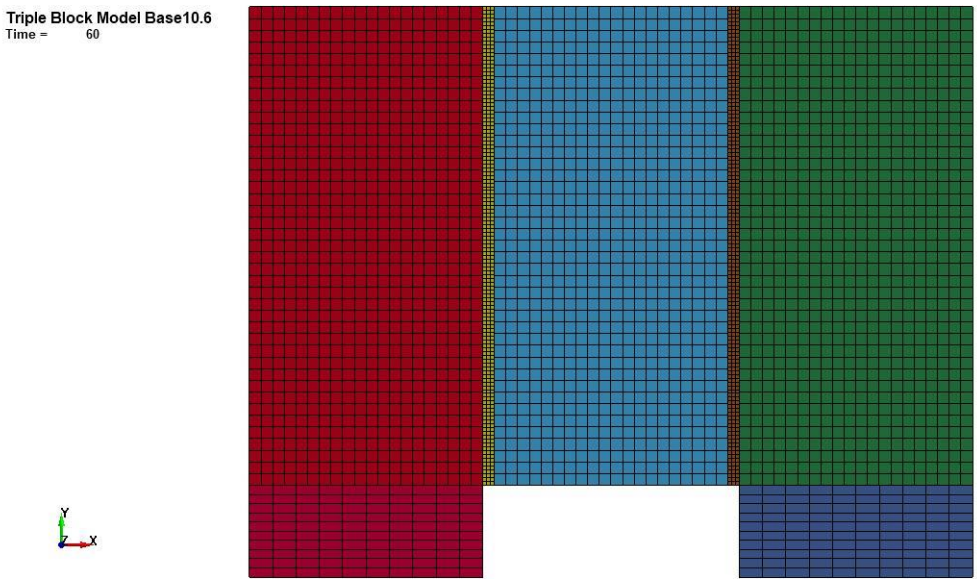


**Figure B-639: Last State at 60 Milliseconds for Base Run 10.6 – 300 psi**

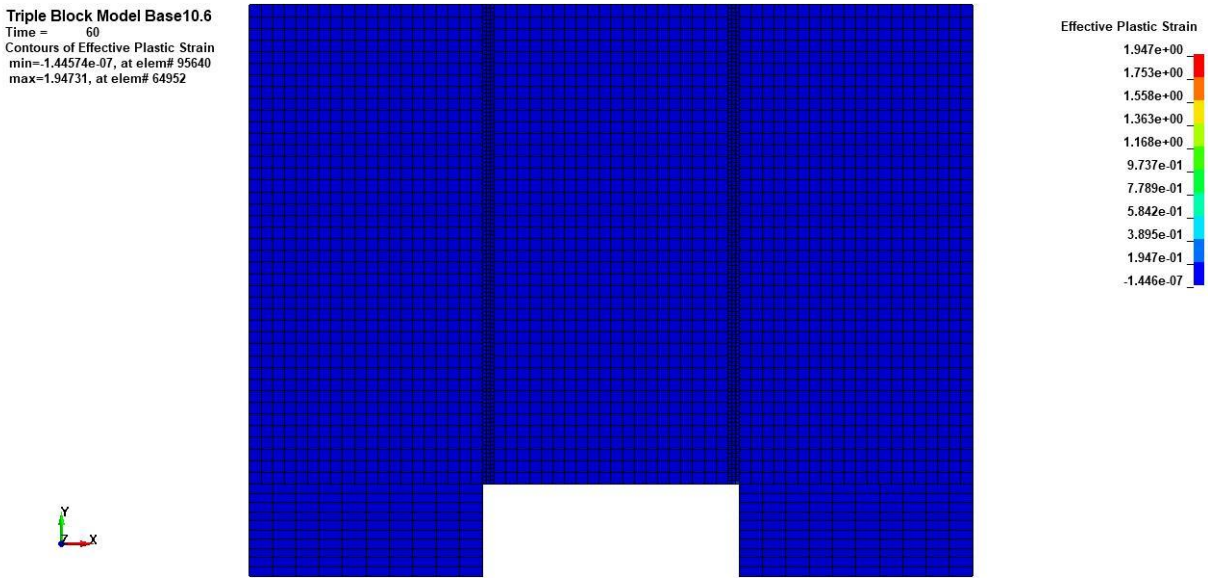


**Figure B-640: Effective Plastic Strain Fringe Plot for Last State at 60 Milliseconds for Base Run 10.6 – 300 psi**

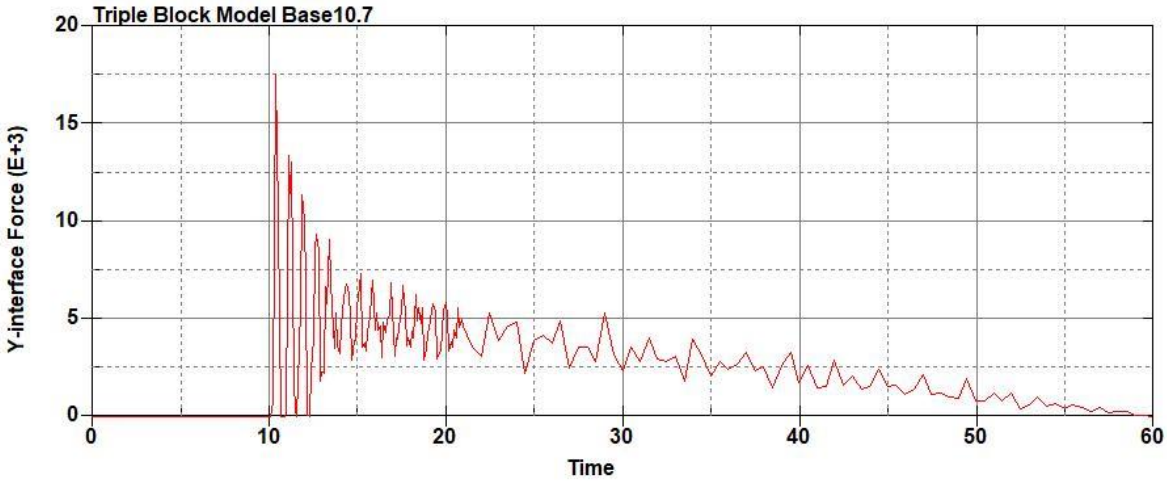


**Figure B-641: Base Run 10.7 Right Support Y-Interface Force (lbs) versus Time (ms) – 350 psi**

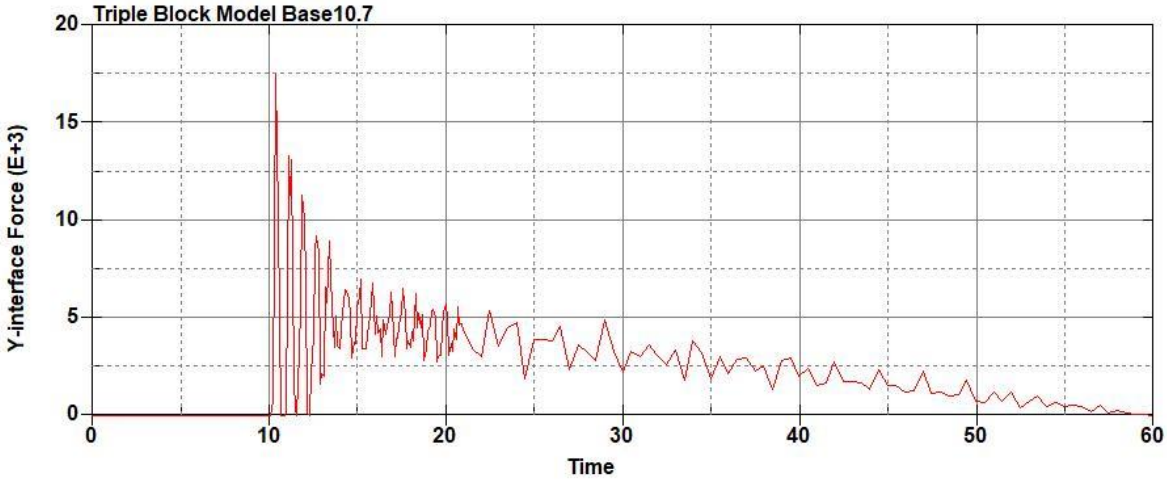


**Figure B-642: Base Run 10.7 Left Support Y-Interface Force (lbs) versus Time (ms) – 350 psi**

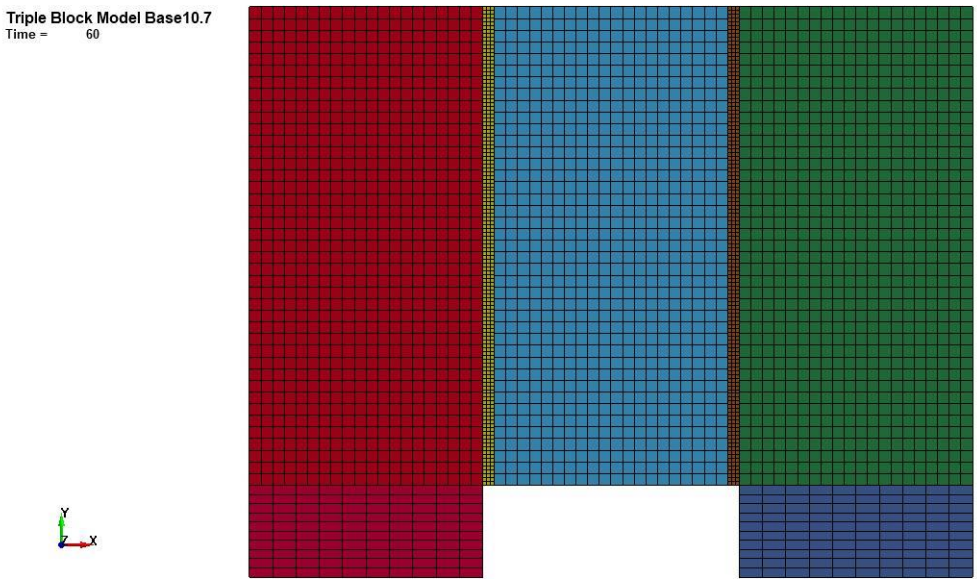


**Figure B-643: Last State at 60 Milliseconds for Base Run 10.7 – 350 psi**

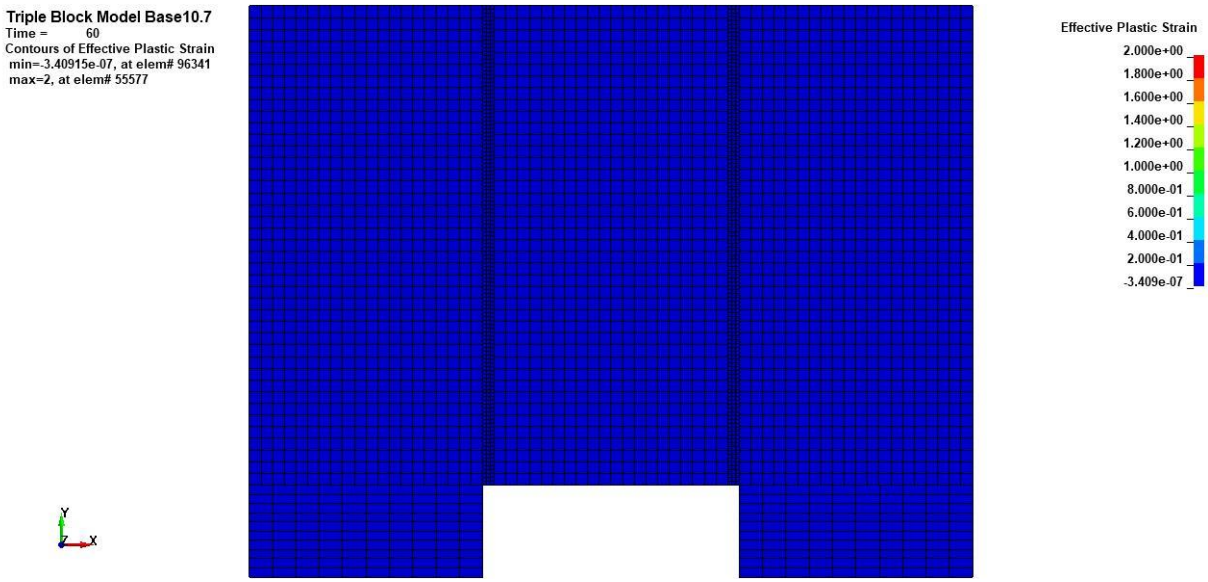


**Figure B-644: Effective Plastic Strain Fringe Plot for Last State at 60 Milliseconds for Base Run 10.7 – 350 psi**

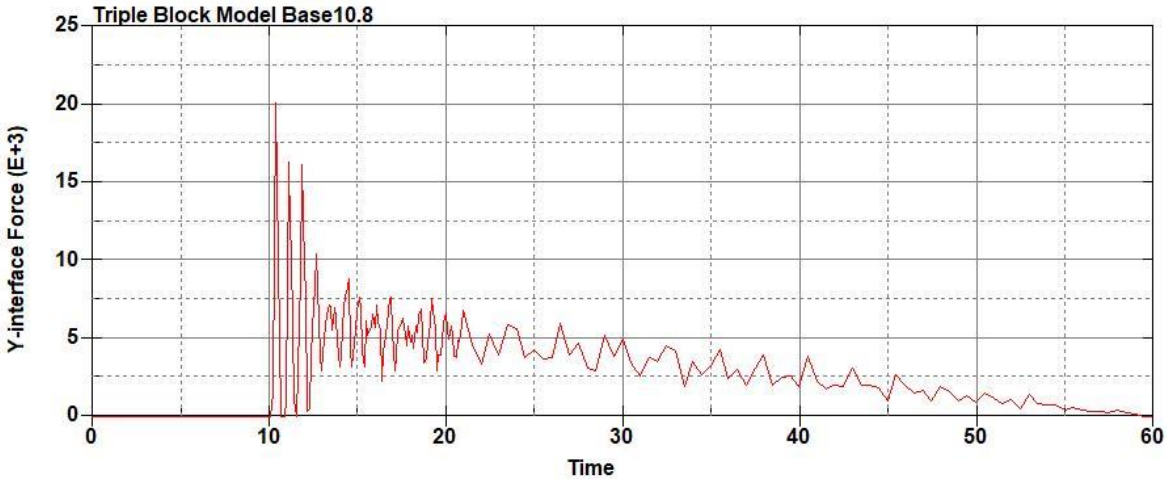


**Figure B-645: Base Run 10.8 Right Support Y-Interface Force (lbs) versus Time (ms) – 400 psi**

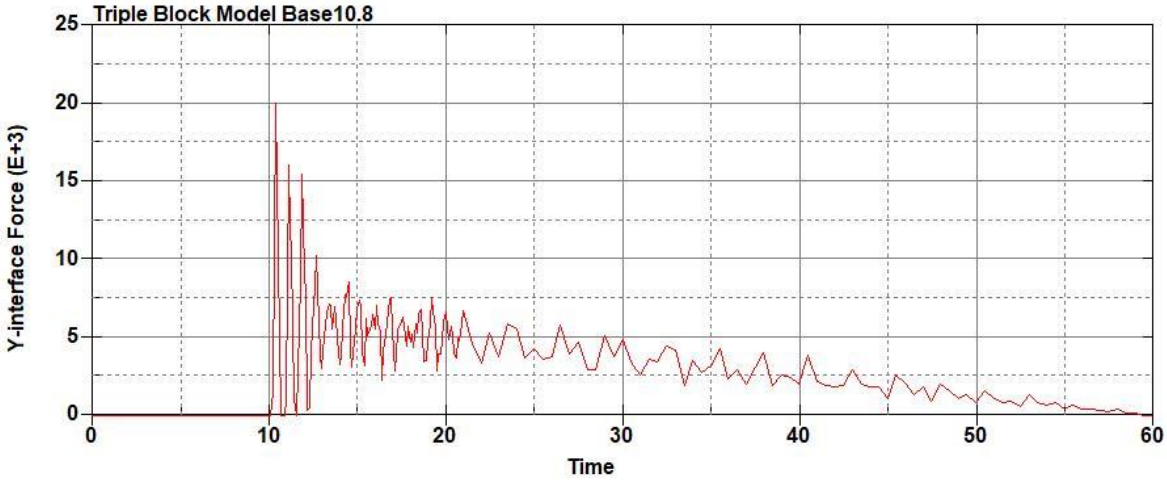


**Figure B-646: Base Run 10.8 Left Support Y-Interface Force (lbs) versus Time (ms) – 400 psi**

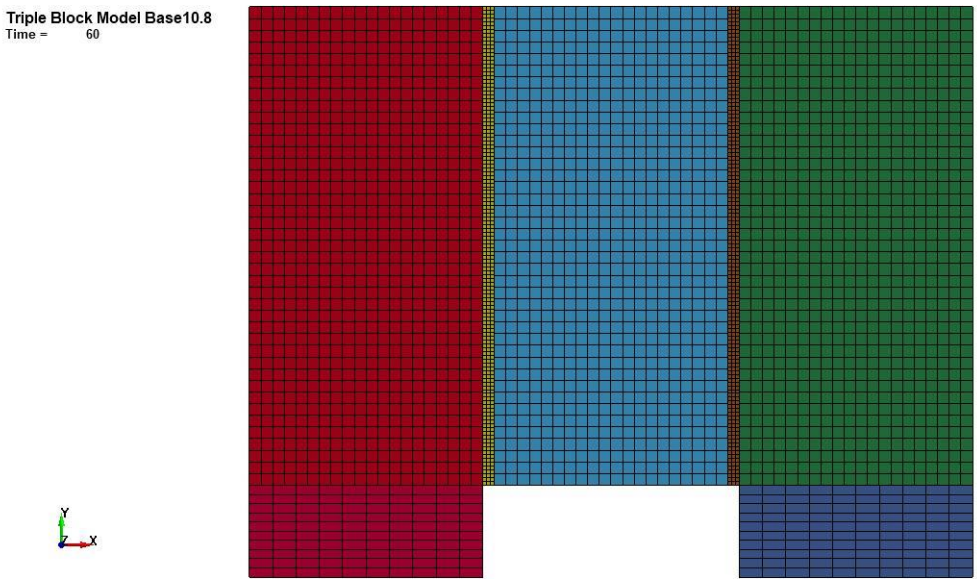


**Figure B-647: Last State at 60 Milliseconds for Base Run 10.8 – 400 psi**

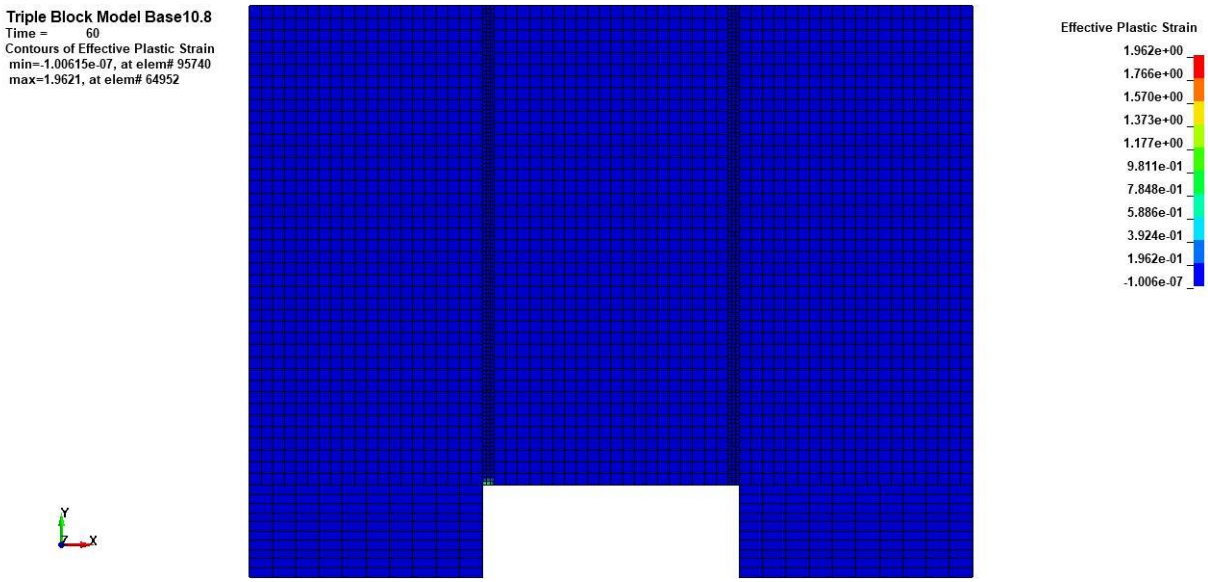


**Figure B-648: Effective Plastic Strain Fringe Plot for Last State at 60 Milliseconds for Base Run 10.8 – 400 psi**

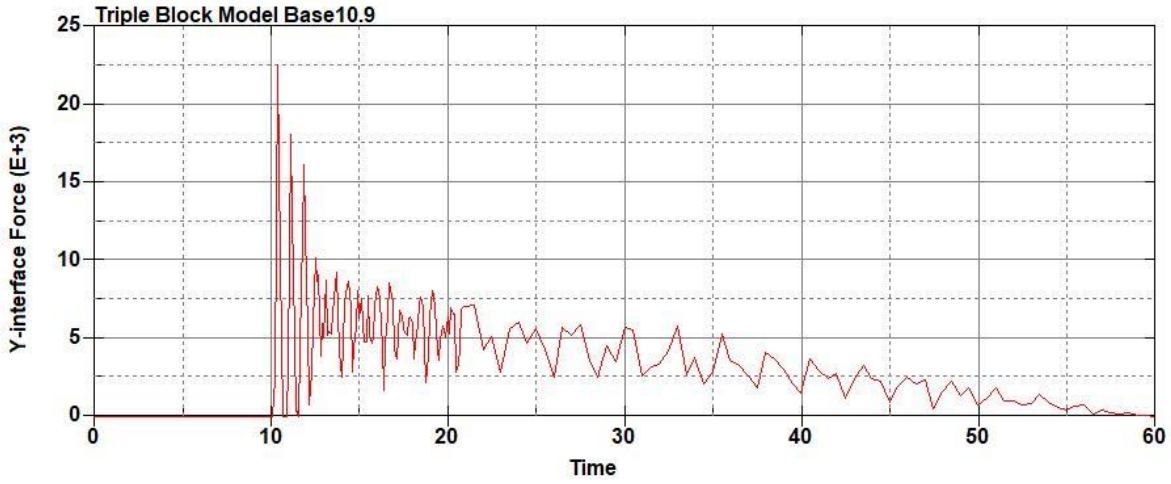


**Figure B-649: Base Run 10.9 Right Support Y-Interface Force (lbs) versus Time (ms) – 450 psi**

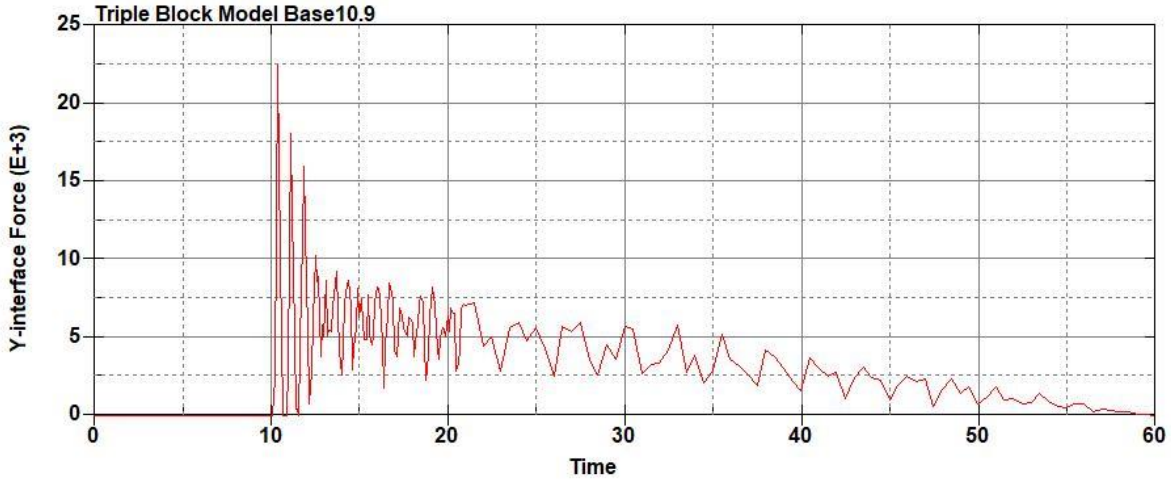


**Figure B-650: Base Run 10.9 Left Support Y-Interface Force (lbs) versus Time (ms) – 450 psi**

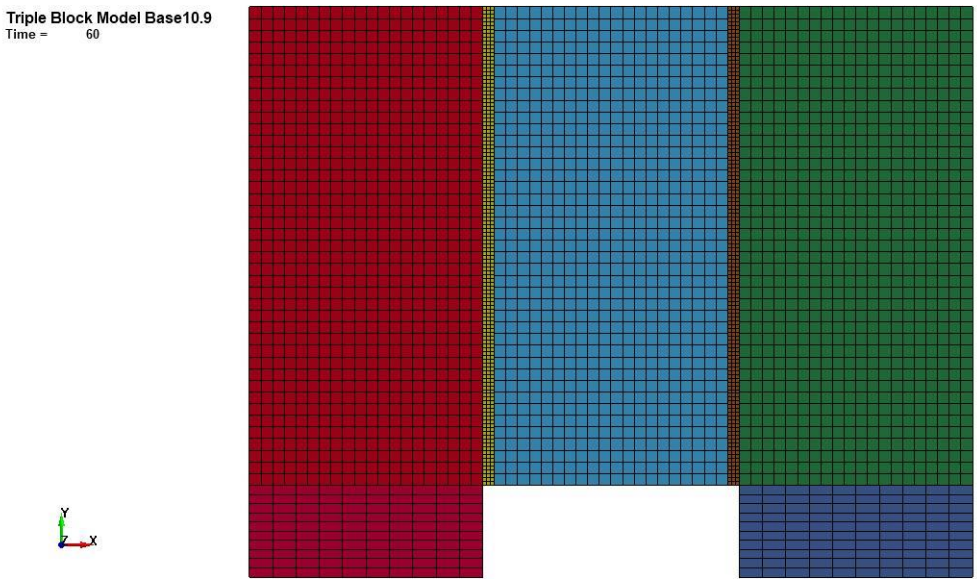


**Figure B-651: Last State at 60 Milliseconds for Base Run 10.9 – 450 psi**

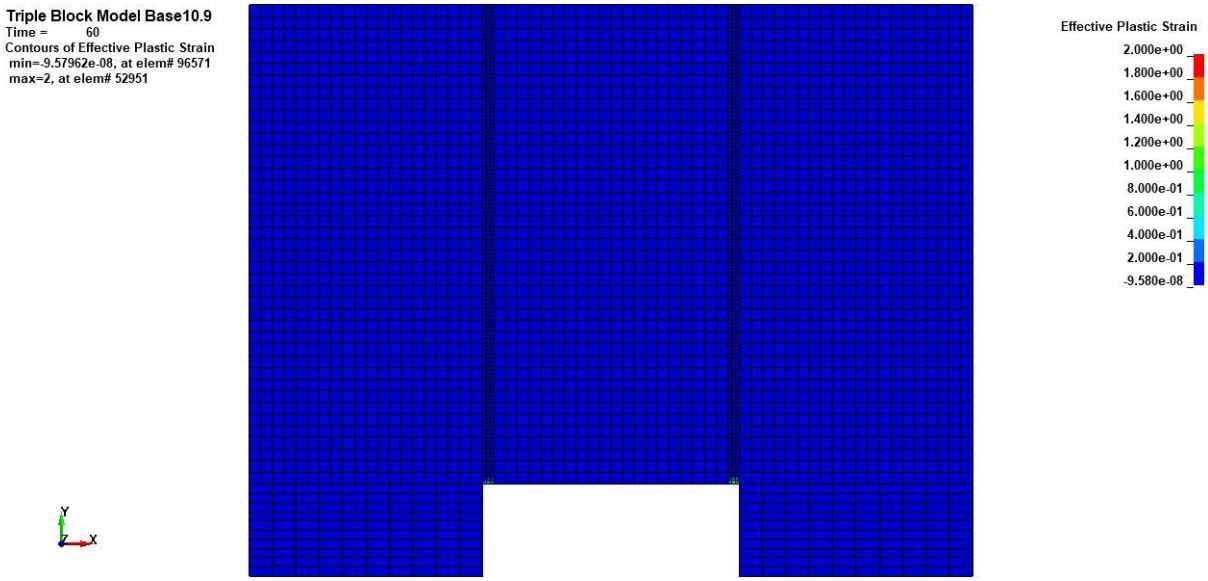


**Figure B-652: Effective Plastic Strain Fringe Plot for Last State at 60 Milliseconds for Base Run 10.9 – 450 psi**

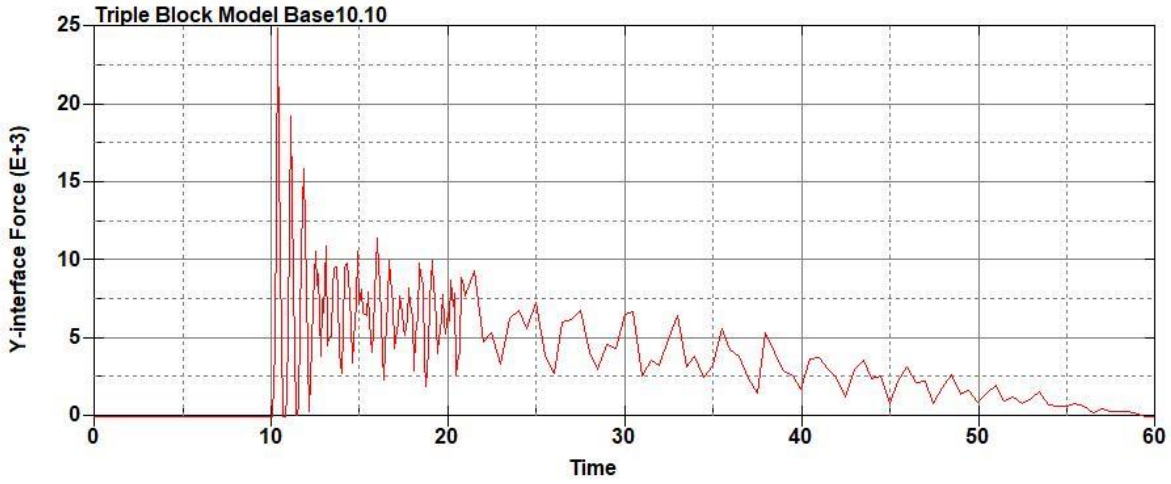


**Figure B-653: Base Run 10.10 Right Support Y-Interface Force (lbs) versus Time (ms) – 500 psi**

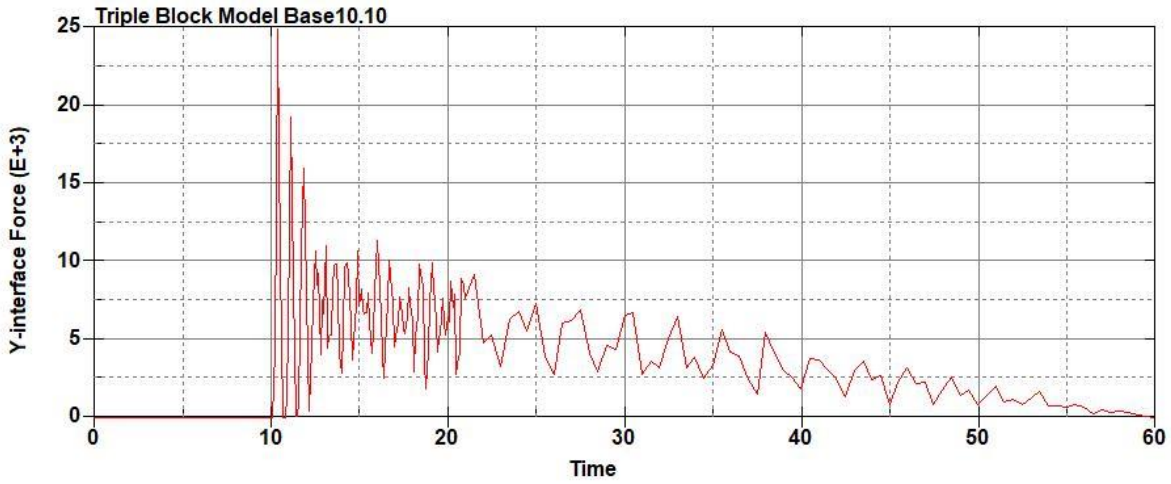


**Figure B-654: Base Run 10.10 Left Support Y-Interface Force (lbs) versus Time (ms) – 500 psi**

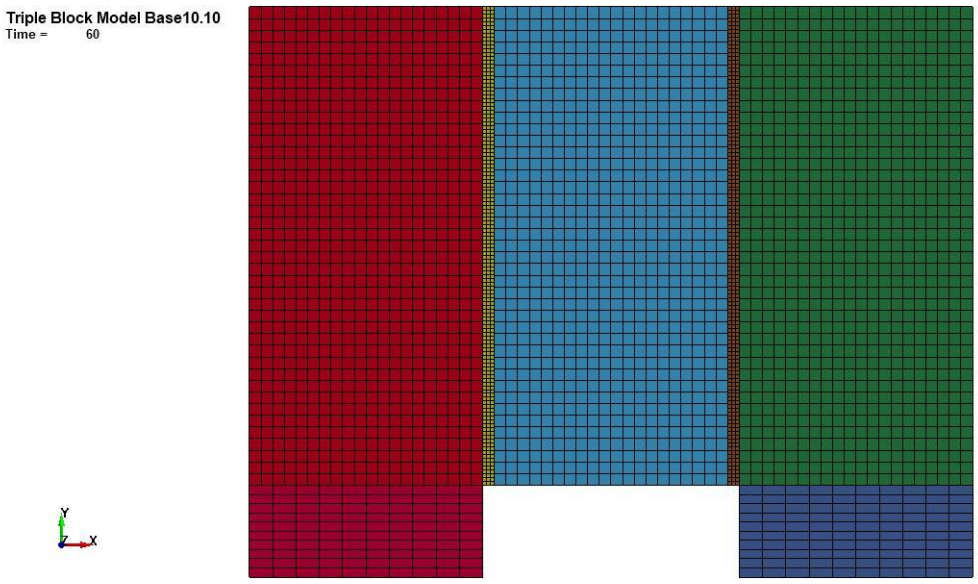


**Figure B-655: Last State at 60 Milliseconds for Base Run 10.10 – 500 psi**

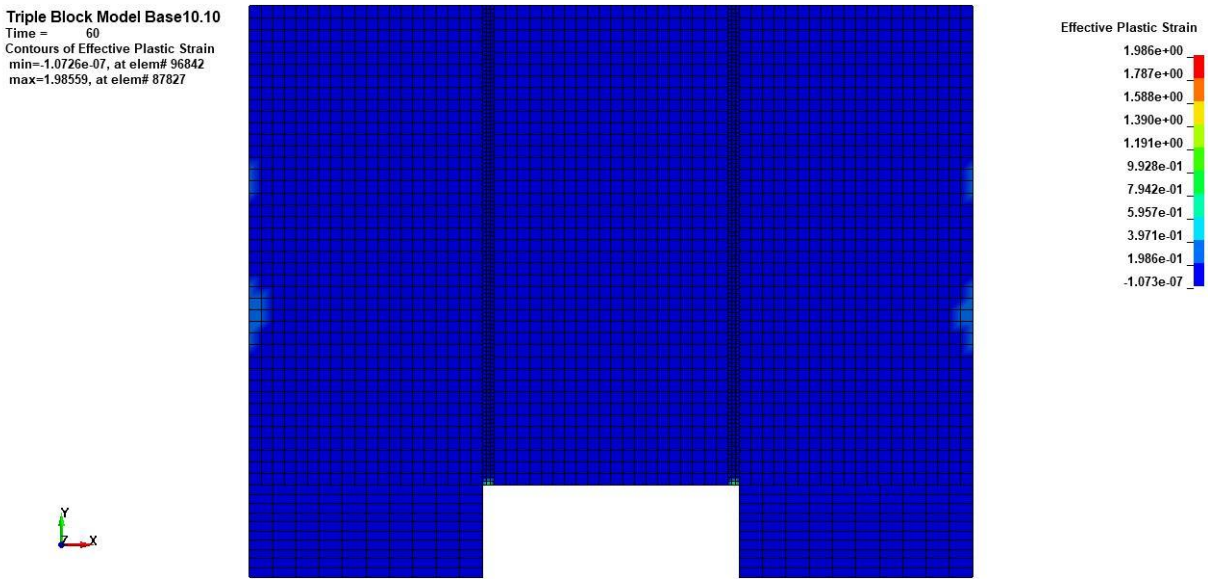


**Figure B-656: Effective Plastic Strain Fringe Plot for Last State at 60 Milliseconds for Base Run 10.10 – 500 psi**

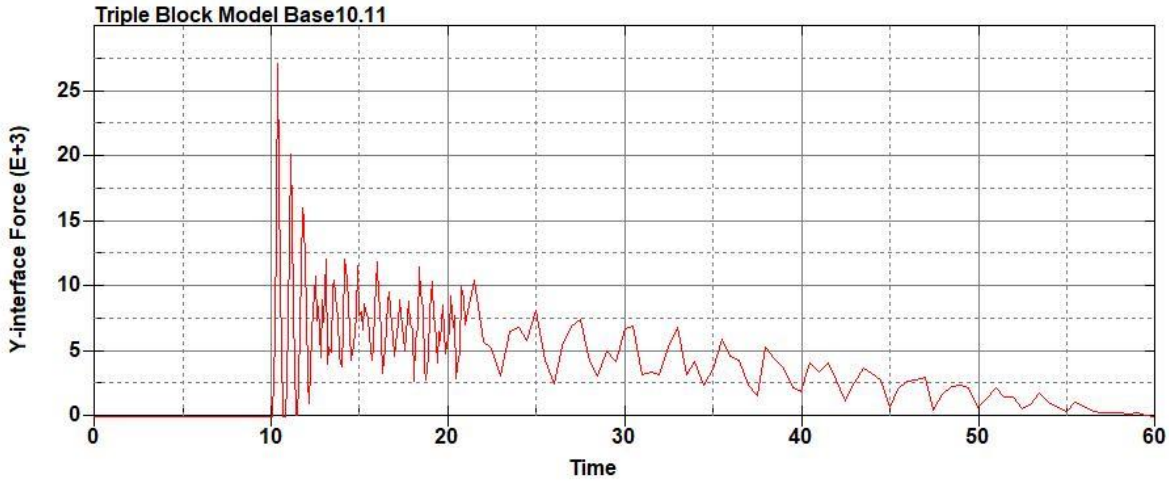


**Figure B-657: Base Run 10.11 Right Support Y-Interface Force (lbs) versus Time (ms) – 550 psi**

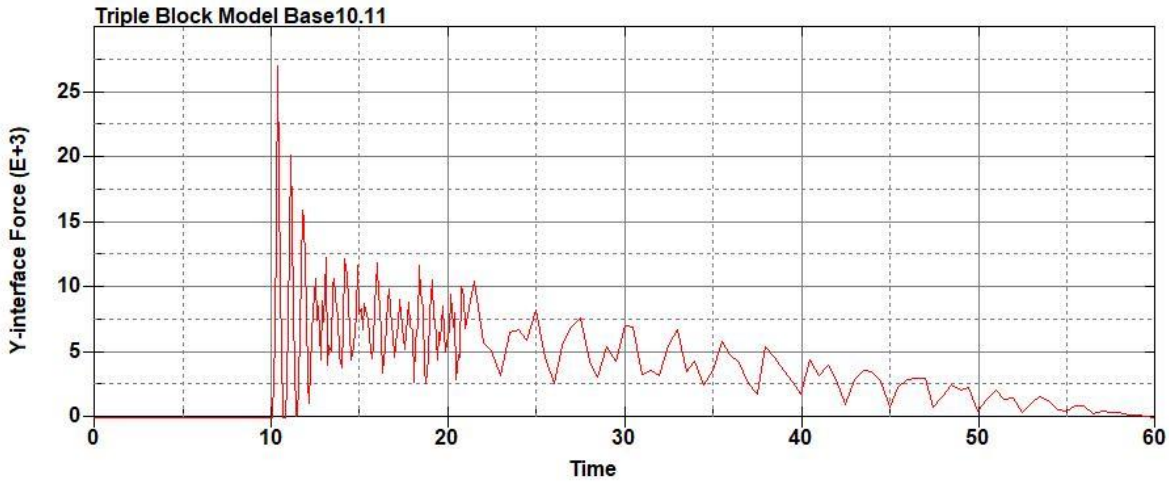


**Figure B-658: Base Run 10.11 Left Support Y-Interface Force (lbs) versus Time (ms) – 550 psi**

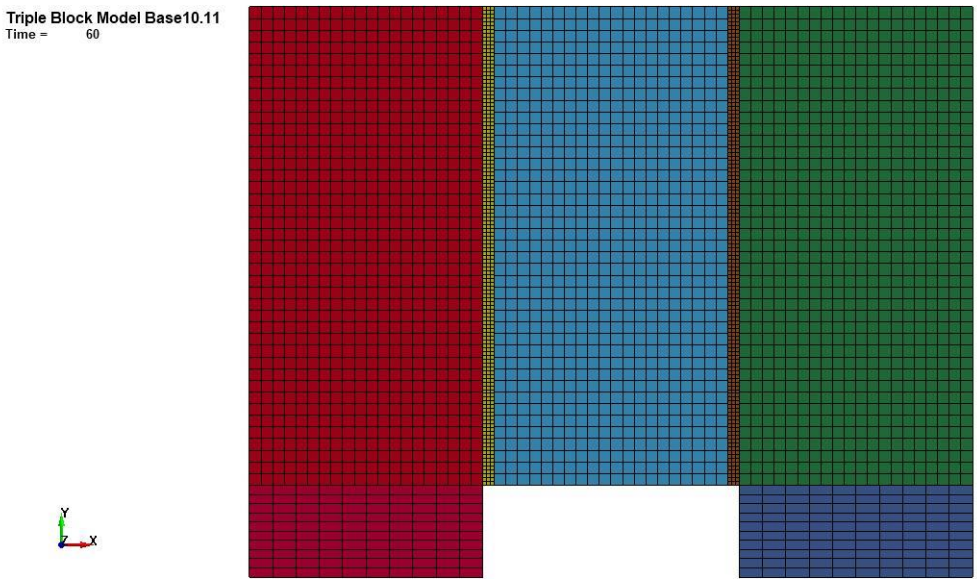


**Figure B-659: Last State at 60 Milliseconds for Base Run 10.11 – 550 psi**

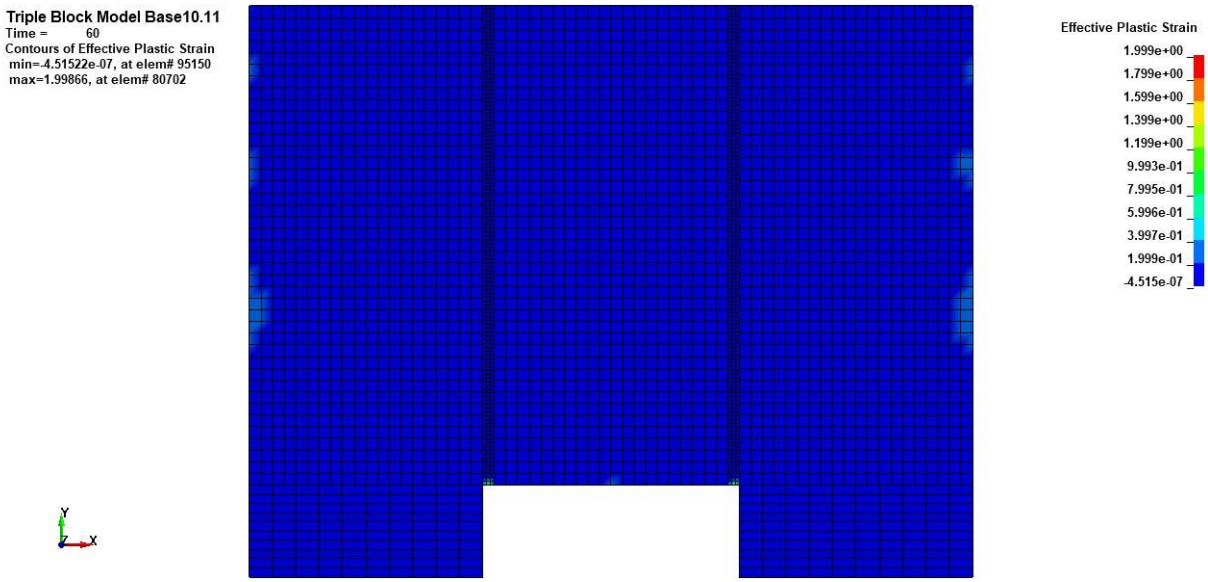


**Figure B-660: Effective Plastic Strain Fringe Plot for Last State at 60 Milliseconds for Base Run 10.11 – 550 psi**

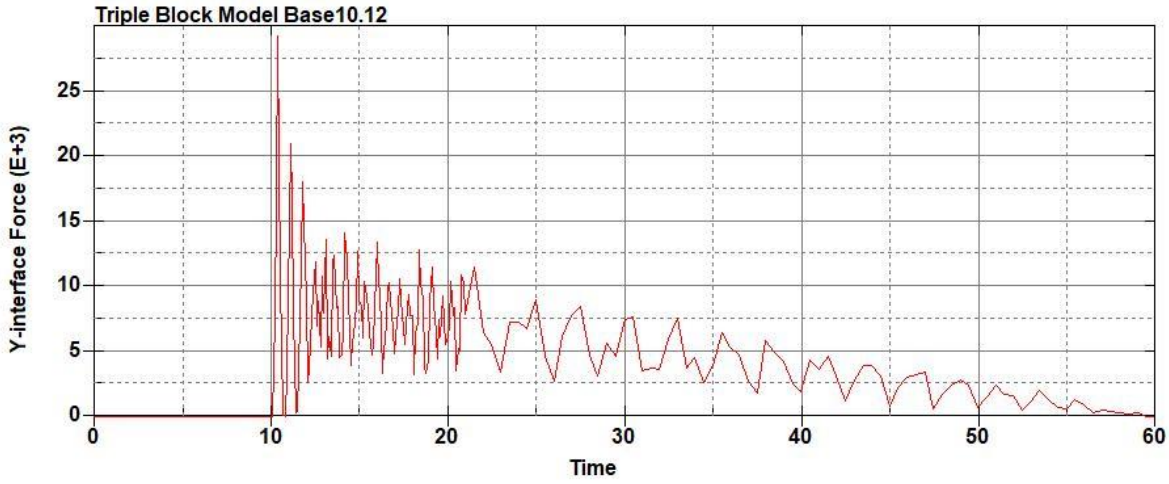


**Figure B-661: Base Run 10.12 Right Support Y-Interface Force (lbs) versus Time (ms) – 600 psi**

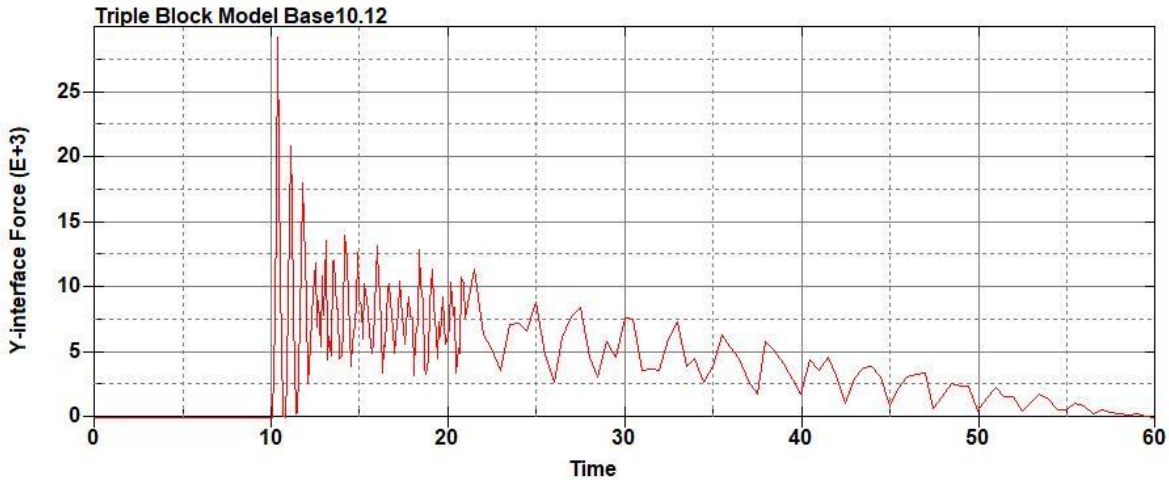


**Figure B-662: Base Run 10.12 Left Support Y-Interface Force (lbs) versus Time (ms) – 600 psi**

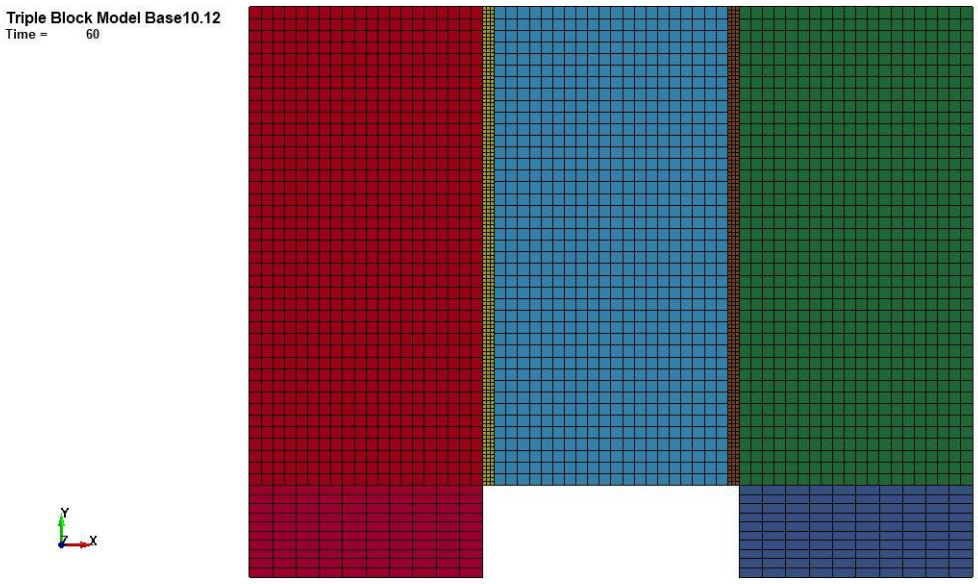


**Figure B-663: Last State at 60 Milliseconds for Base Run 10.12 – 600 psi**

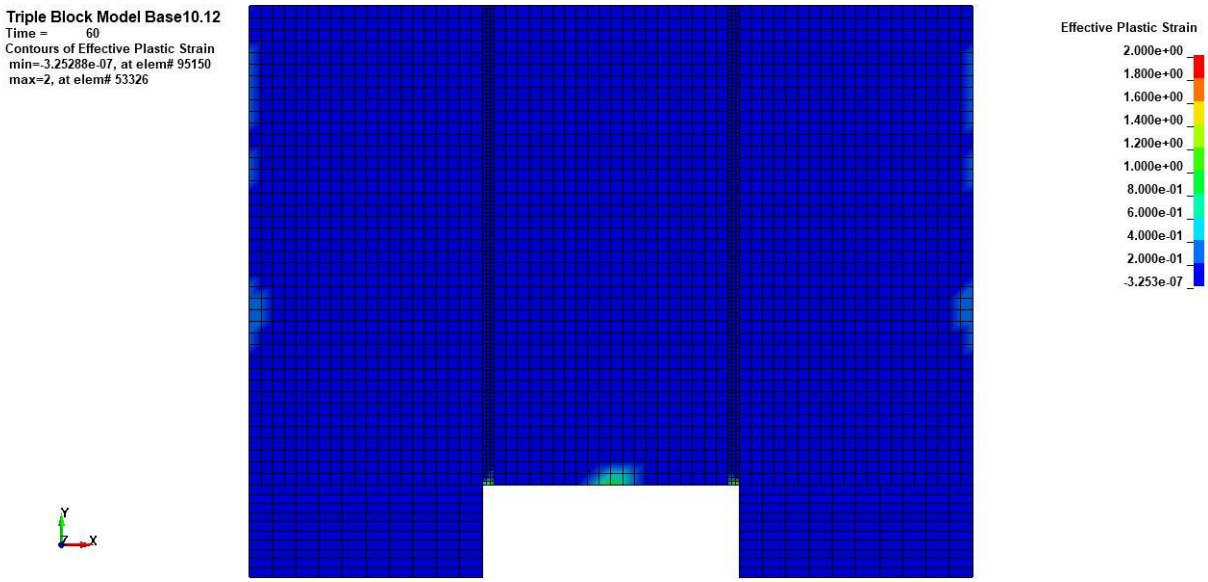


**Figure B-664: Effective Plastic Strain Fringe Plot for Last State at 60 Milliseconds for Base Run 10.12 – 600 psi**

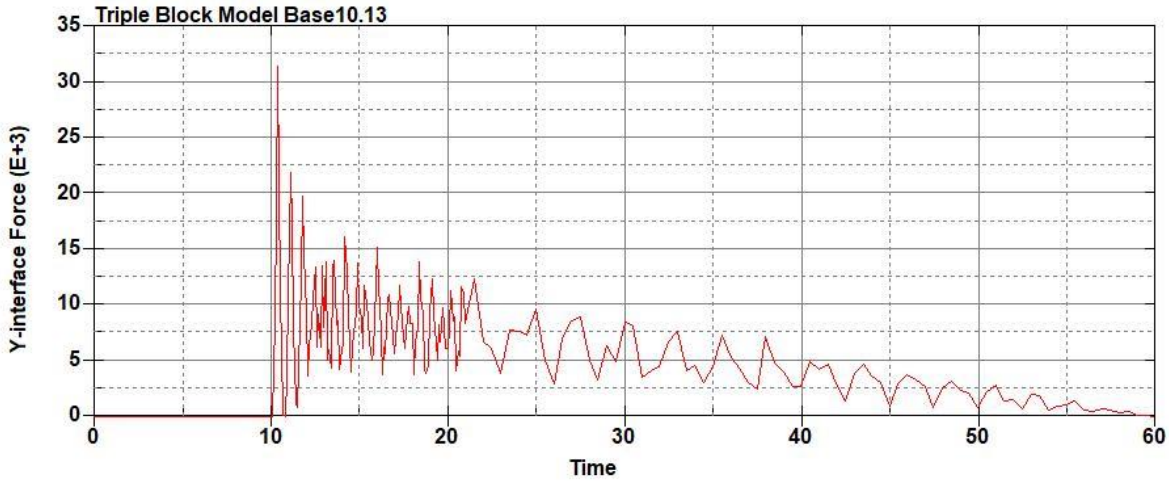


**Figure B-665: Base Run 10.13 Right Support Y-Interface Force (lbs) versus Time (ms) – 650 psi**

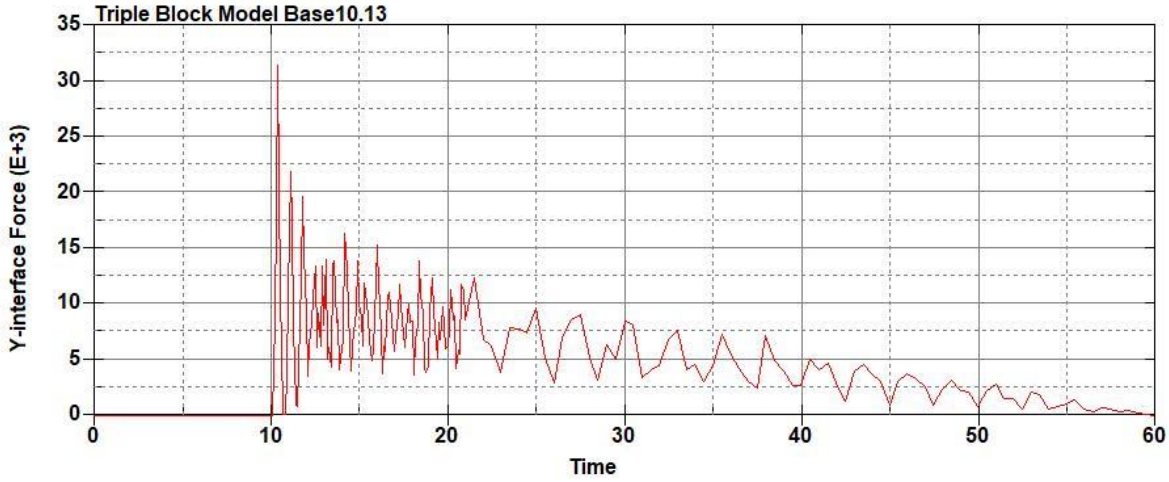


**Figure B-666: Base Run 10.13 Left Support Y-Interface Force (lbs) versus Time (ms) – 650 psi**

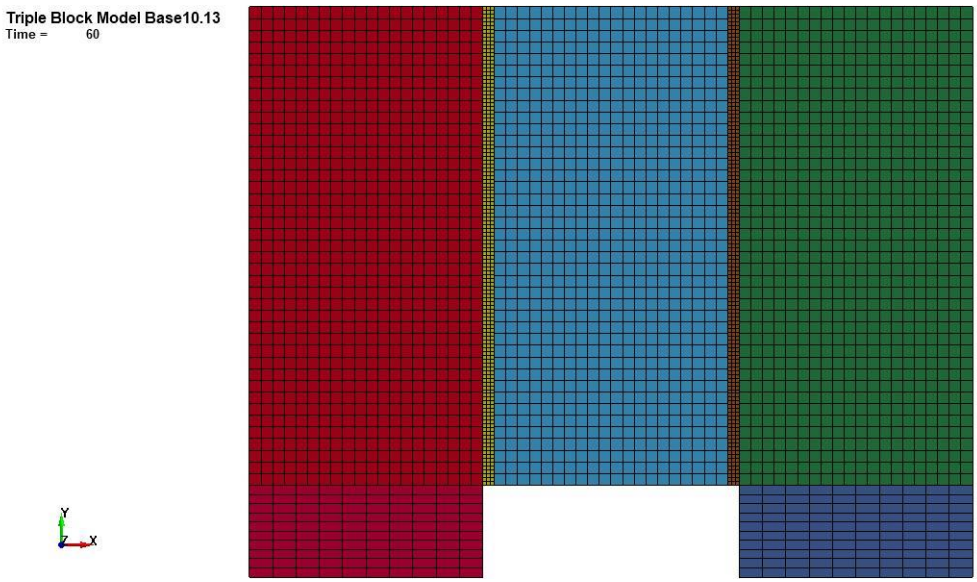


**Figure B-667: Last State at 60 Milliseconds for Base Run 10.13 – 650 psi**

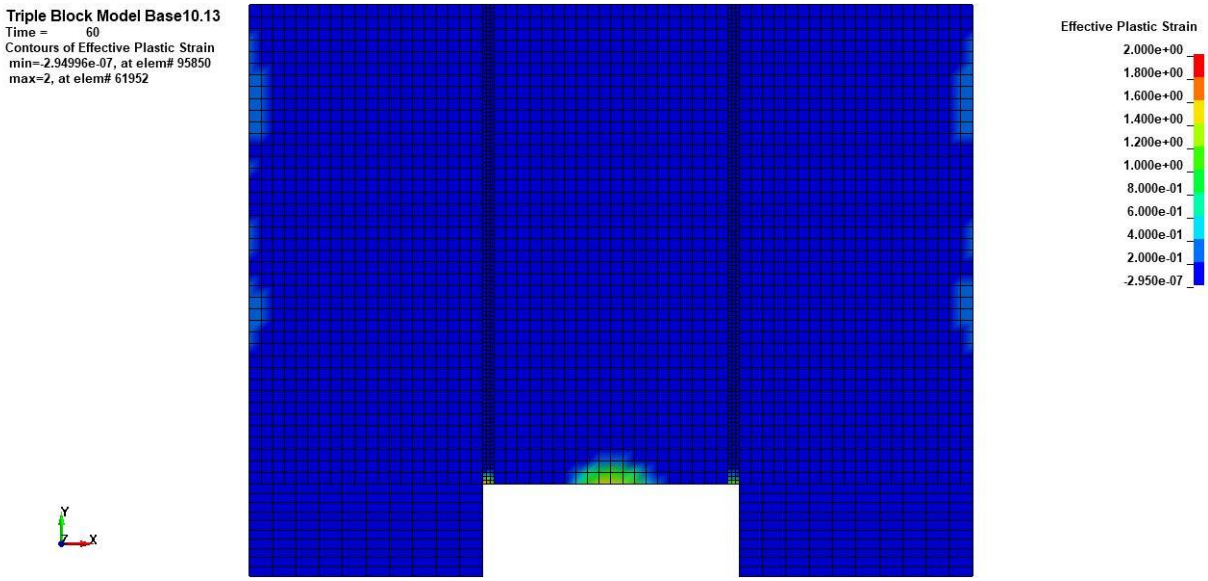


**Figure B-668: Effective Plastic Strain Fringe Plot for Last State at 60 Milliseconds for Base Run 10.13 – 650 psi**

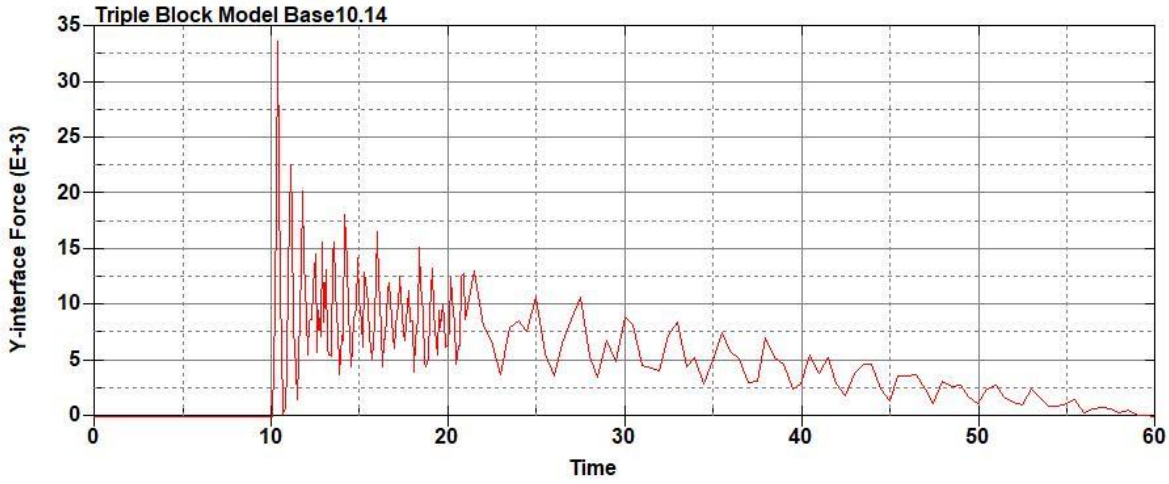


**Figure B-669: Base Run 10.14 Right Support Y-Interface Force (lbs) versus Time (ms) – 700 psi**

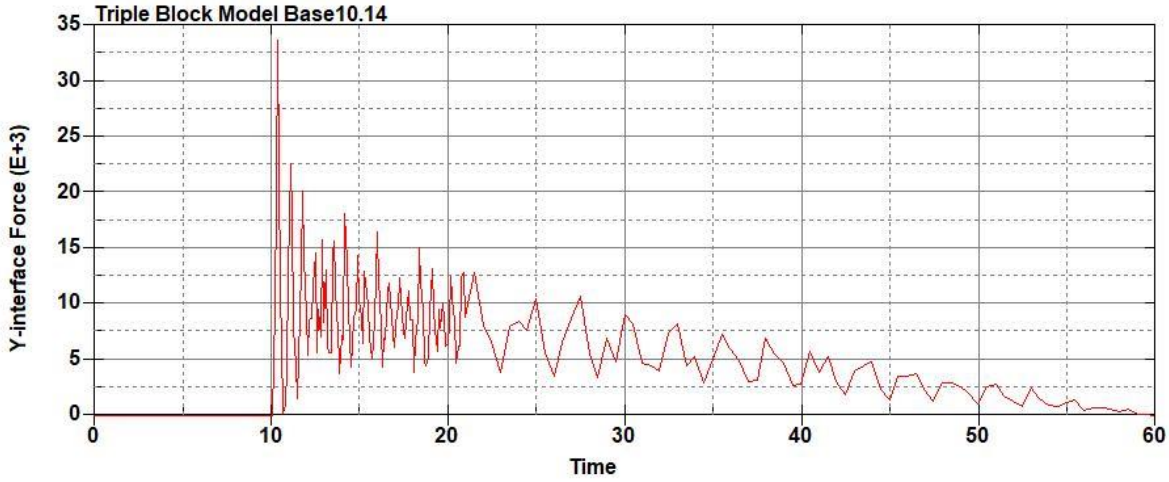


**Figure B-670: Base Run 10.14 Left Support Y-Interface Force (lbs) versus Time (ms) – 700 psi**

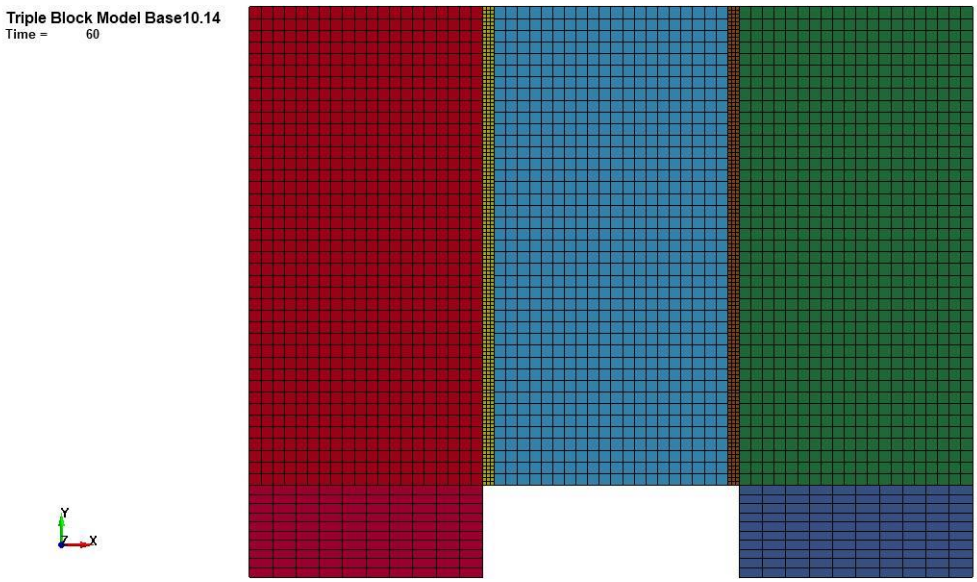


**Figure B-671: Last State at 60 Milliseconds for Base Run 10.14 – 700 psi**

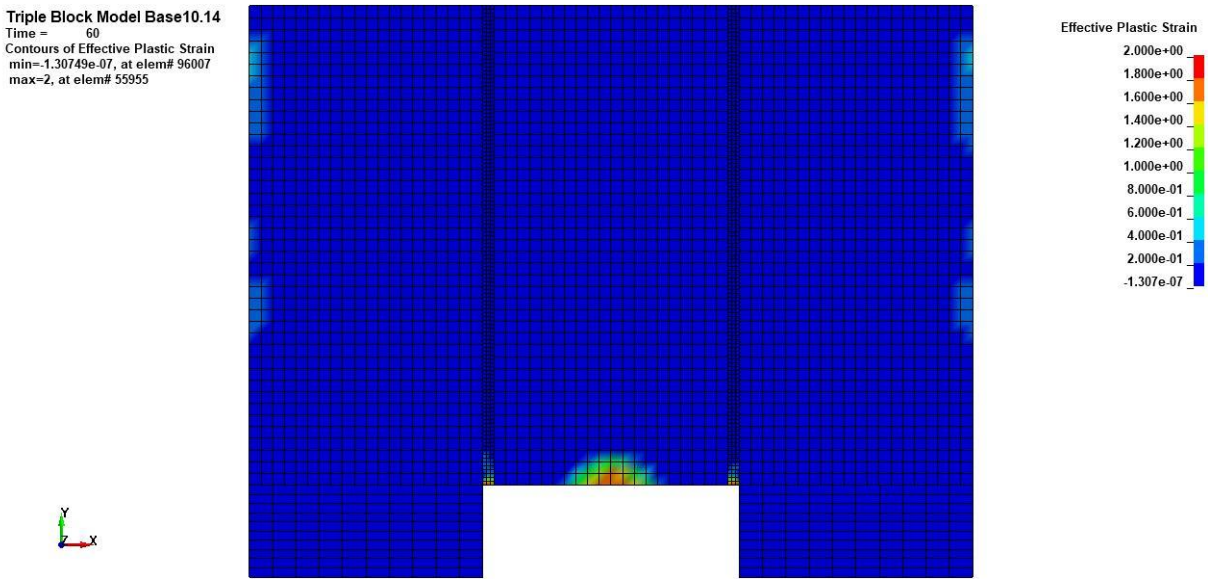


**Figure B-672: Effective Plastic Strain Fringe Plot for Last State at 60 Milliseconds for Base Run 10.14 – 700 psi**

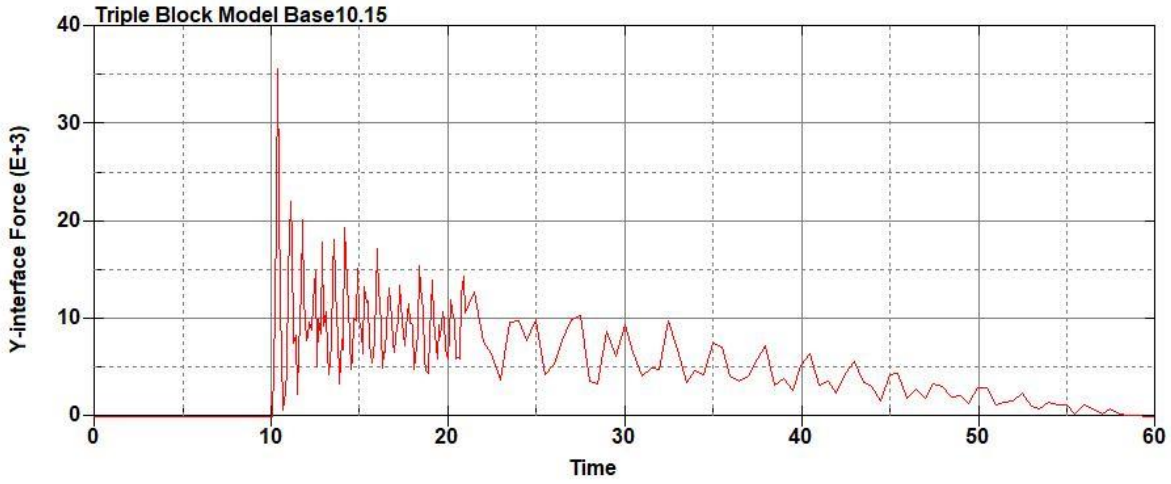


**Figure B-673: Base Run 10.15 Right Support Y-Interface Force (lbs) versus Time (ms) – 750 psi**

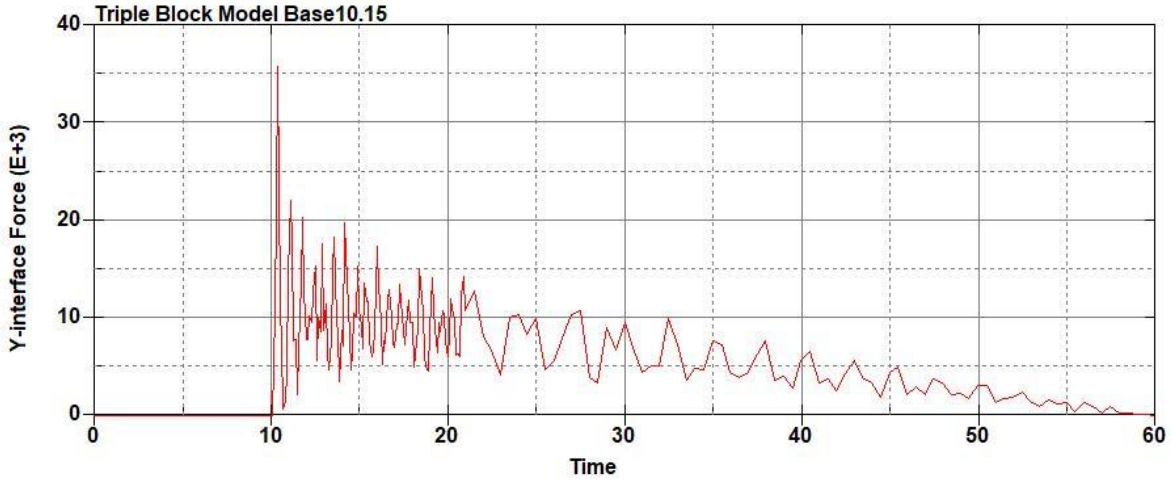


**Figure B-674: Base Run 10.15 Left Support Y-Interface Force (lbs) versus Time (ms) – 750 psi**

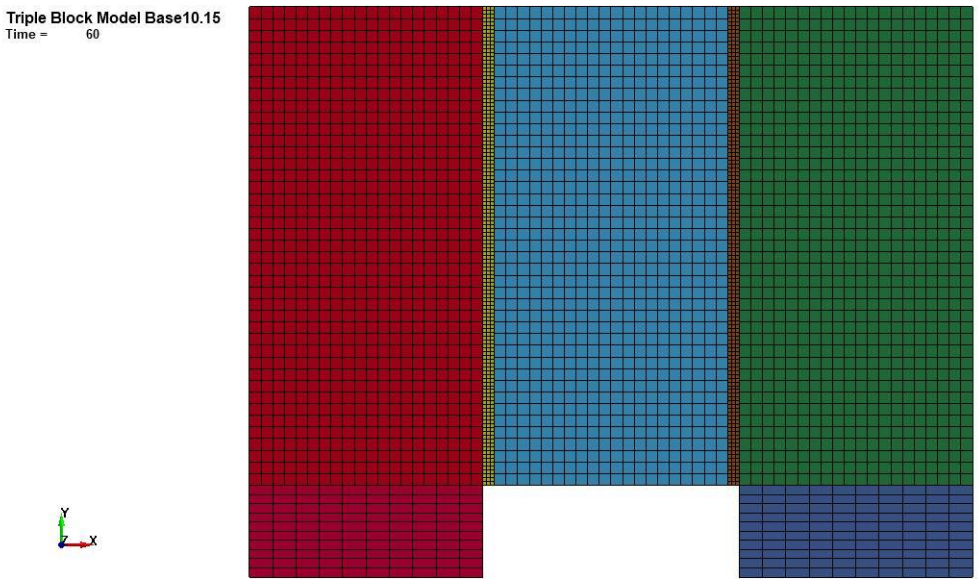


**Figure B-675: Last State at 60 Milliseconds for Base Run 10.15 – 750 psi**

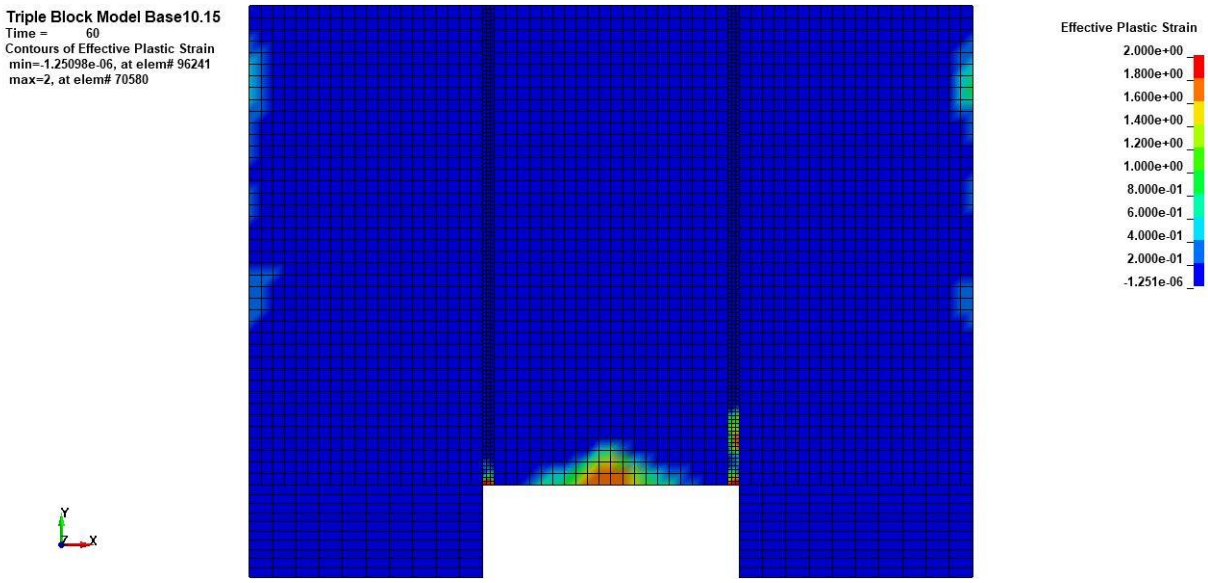


**Figure B-676: Effective Plastic Strain Fringe Plot for Last State at 60 Milliseconds for Base Run 10.15 – 750 psi**

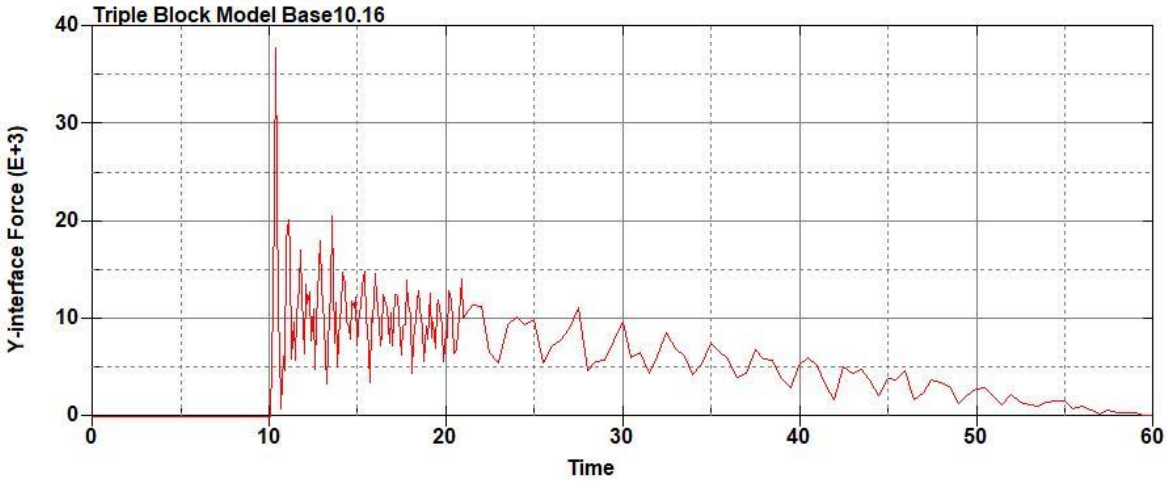


**Figure B-677: Base Run 10.16 Right Support Y-Interface Force (lbs) versus Time (ms) – 800 psi**

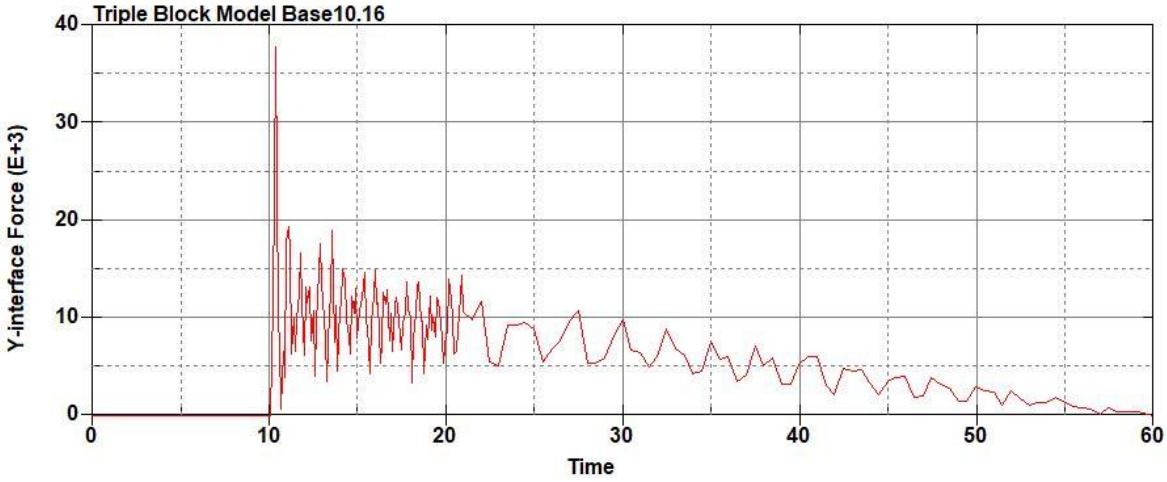


**Figure B-678: Base Run 10.16 Left Support Y-Interface Force (lbs) versus Time (ms) – 800 psi**

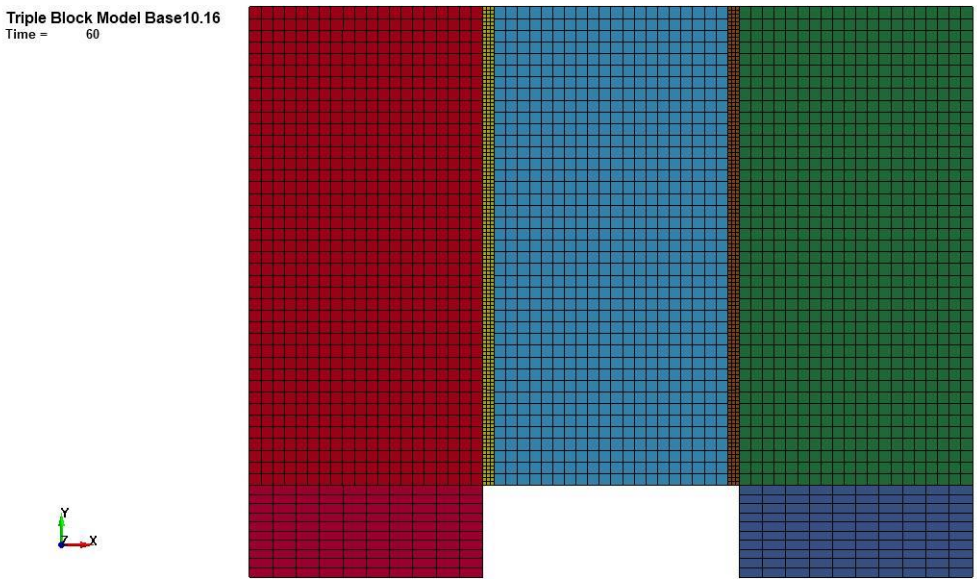


**Figure B-679: Last State at 60 Milliseconds for Base Run 10.16 – 800 psi**

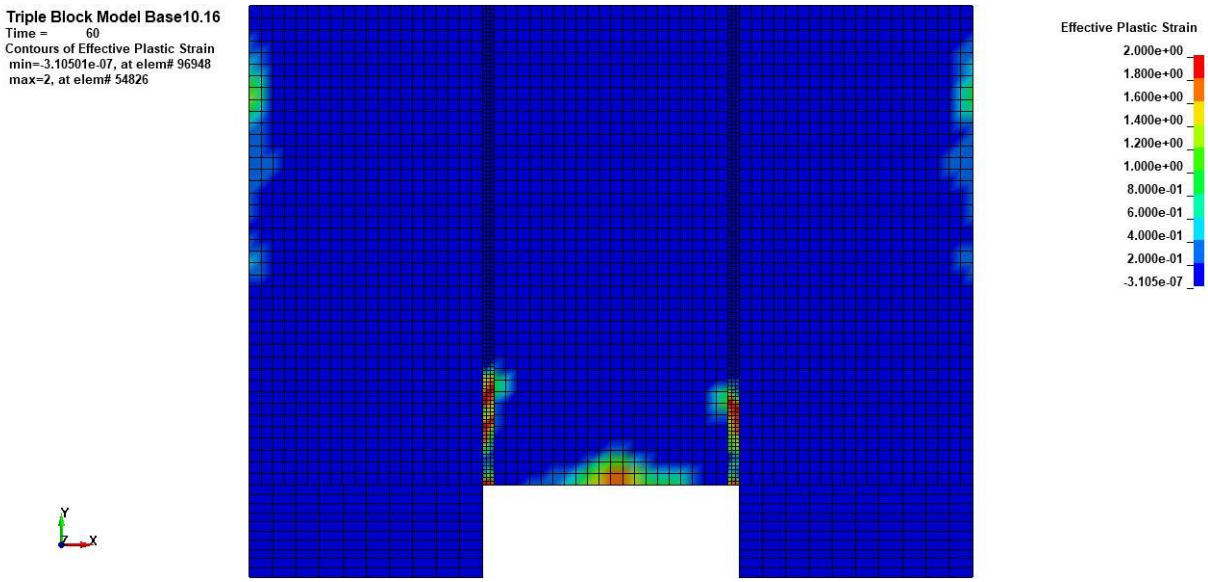


**Figure B-680: Effective Plastic Strain Fringe Plot for Last State at 60 Milliseconds for Base Run 10.16 – 800 psi**

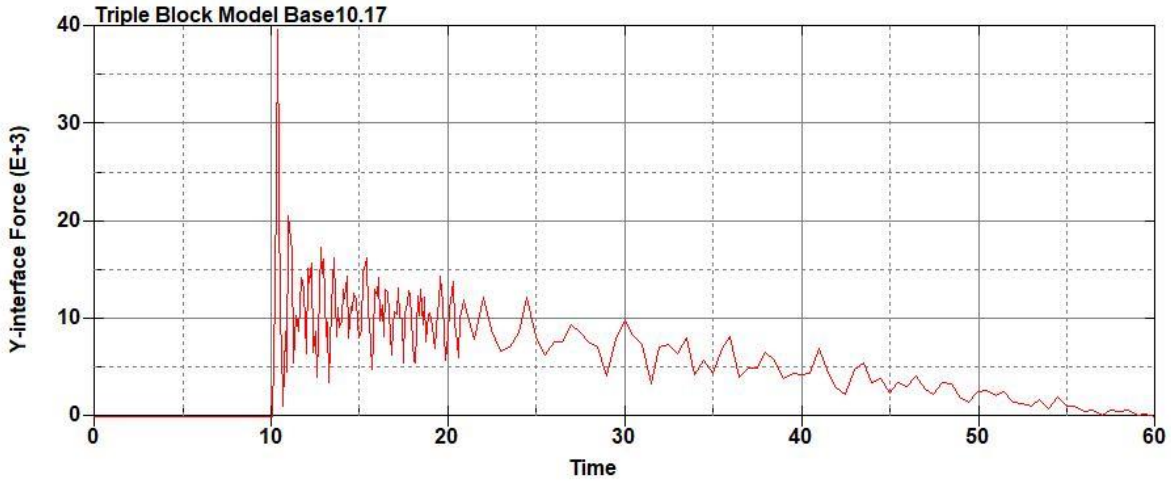


**Figure B-681: Base Run 10.17 Right Support Y-Interface Force (lbs) versus Time (ms) – 850 psi**

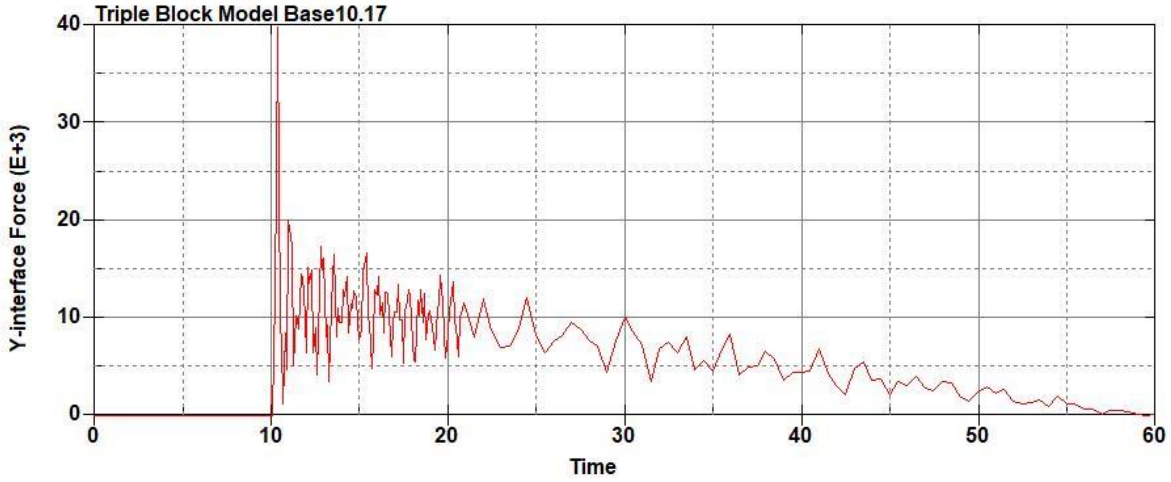


**Figure B-682: Base Run 10.17 Left Support Y-Interface Force (lbs) versus Time (ms) – 850 psi**

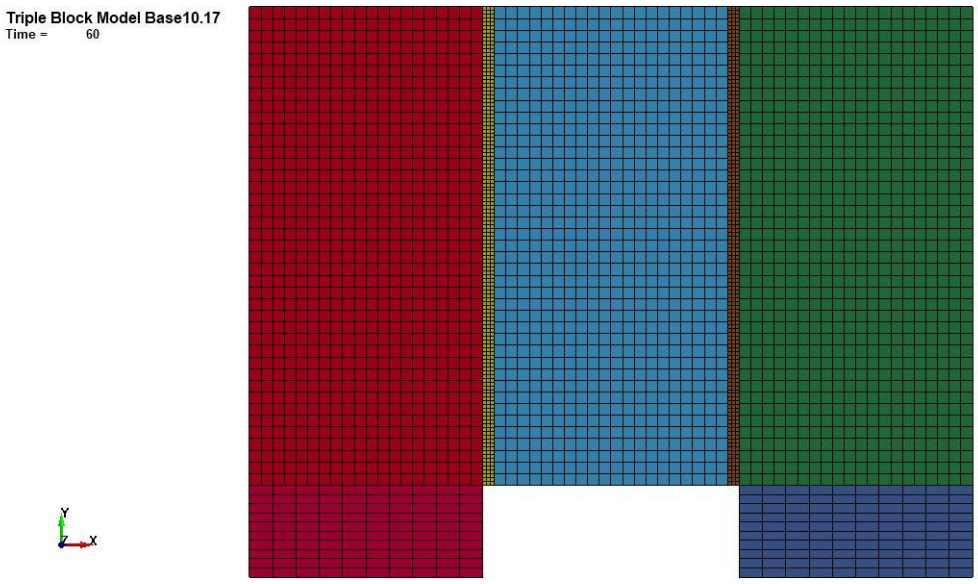


**Figure B-683: Last State at 60 Milliseconds for Base Run 10.17 – 850 psi**

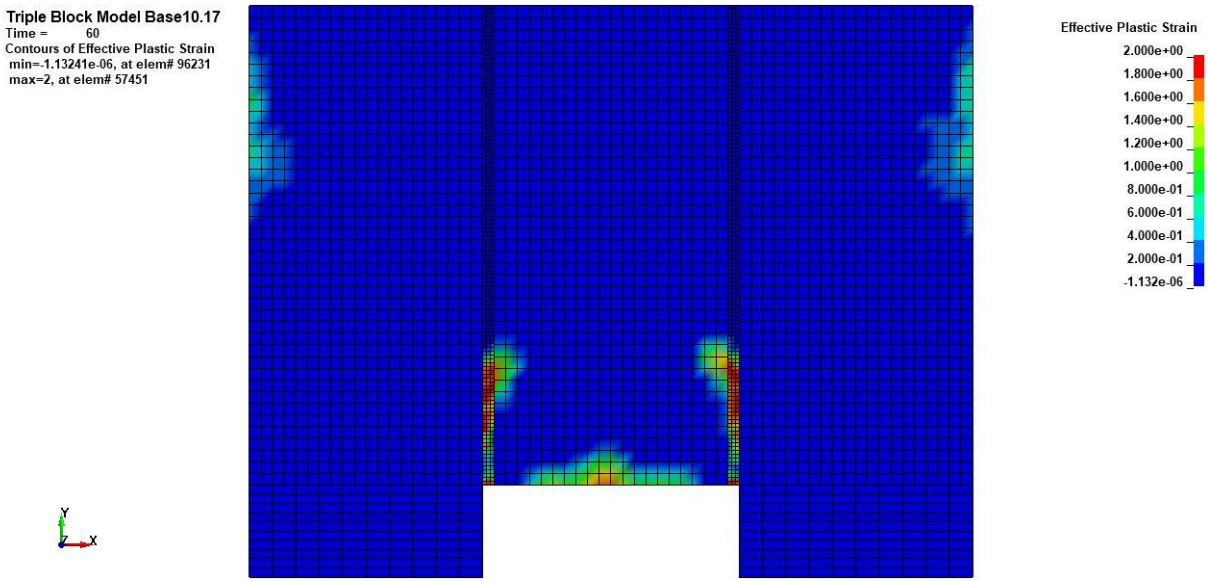


**Figure B-684: Effective Plastic Strain Fringe Plot for Last State at 60 Milliseconds for Base Run 10.17 – 850 psi**

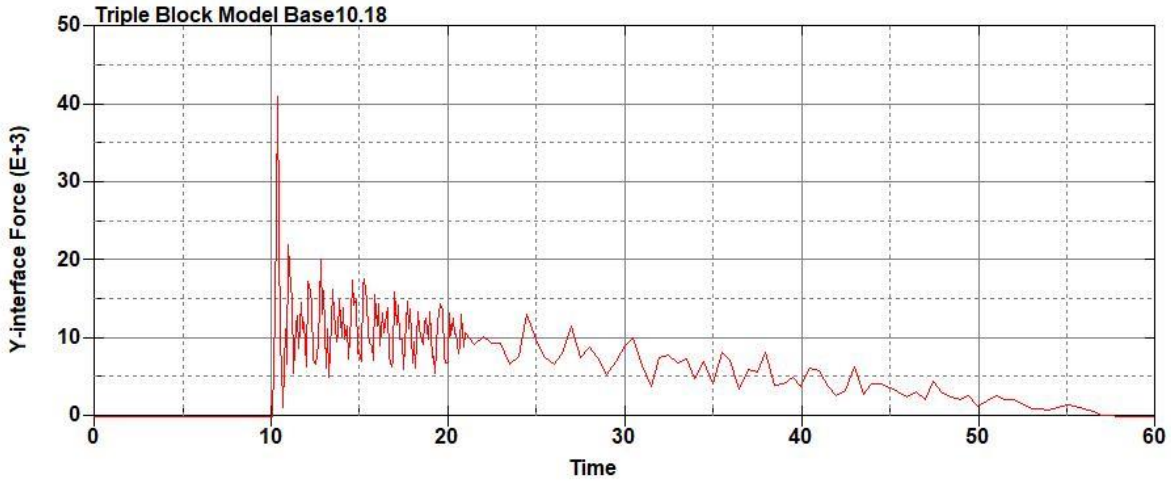


**Figure B-685: Base Run 10.18 Right Support Y-Interface Force (lbs) versus Time (ms) – 900 psi**

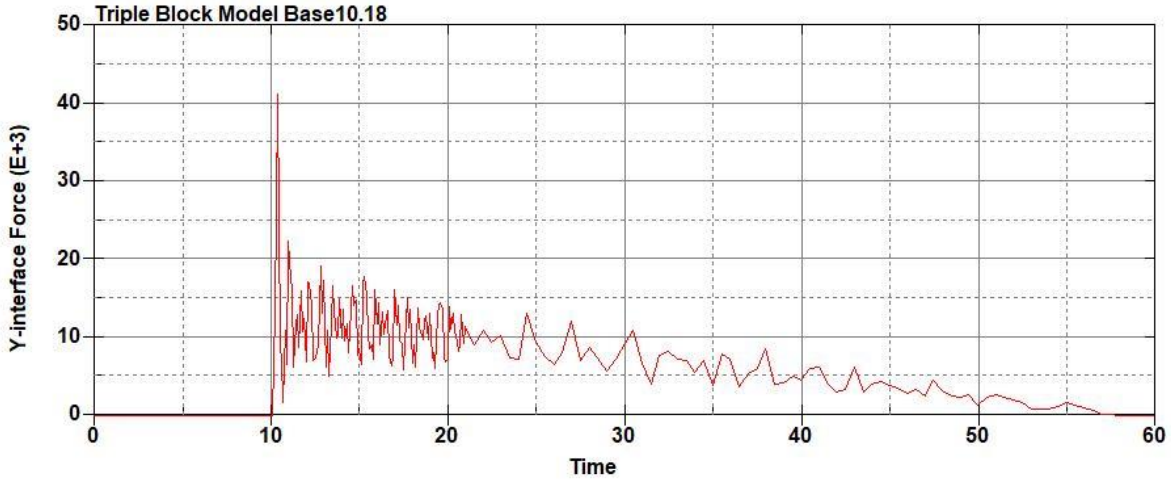


**Figure B-686: Base Run 10.18 Left Support Y-Interface Force (lbs) versus Time (ms) – 900 psi**

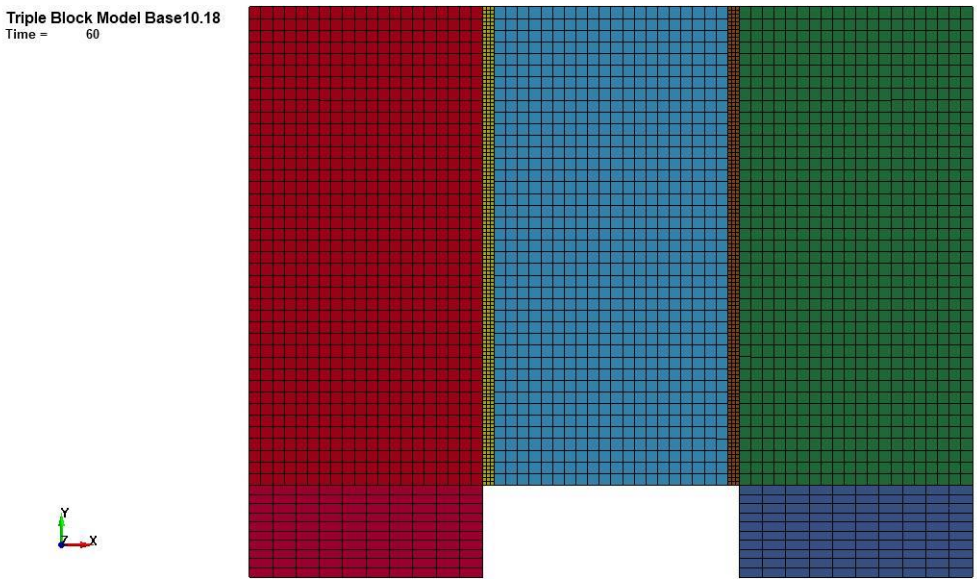


**Figure B-687: Last State at 60 Milliseconds for Base Run 10.18 – 900 psi**

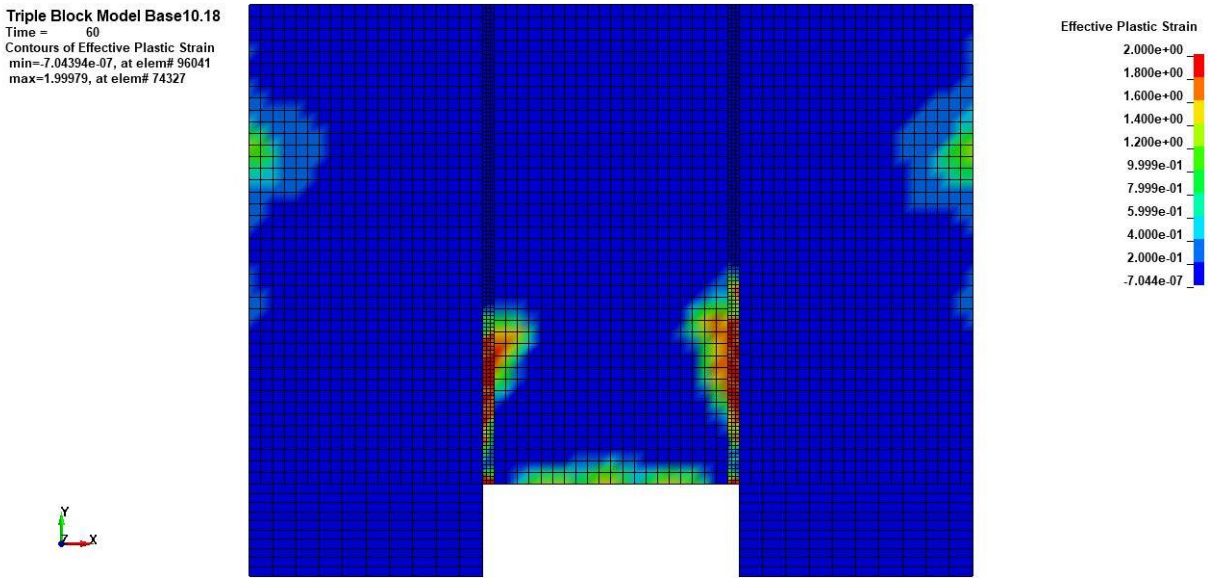


**Figure B-688: Effective Plastic Strain Fringe Plot for Last State at 60 Milliseconds for Base Run 10.18 – 900 psi**

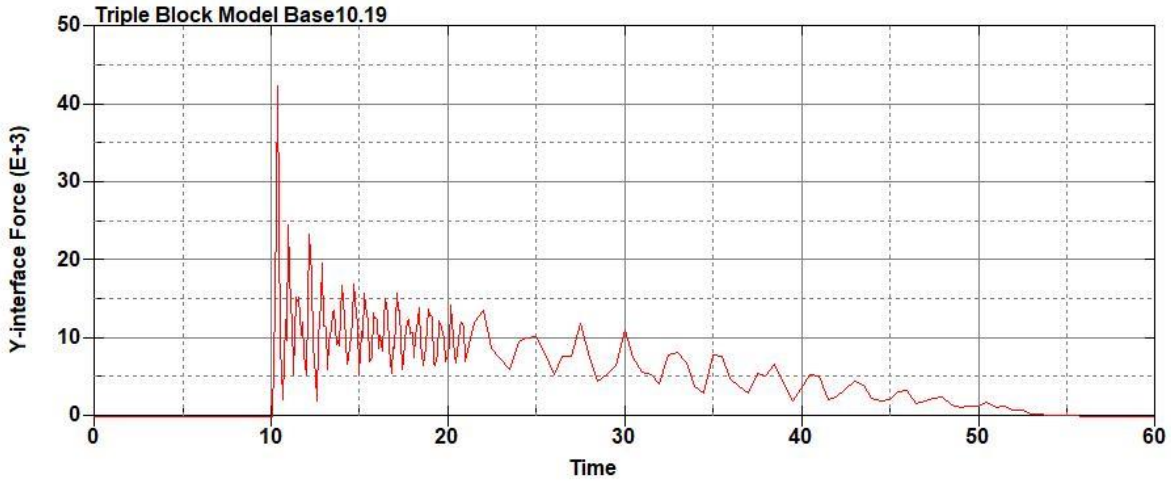


**Figure B-689: Base Run 10.19 Right Support Y-Interface Force (lbs) versus Time (ms) – 950 psi**

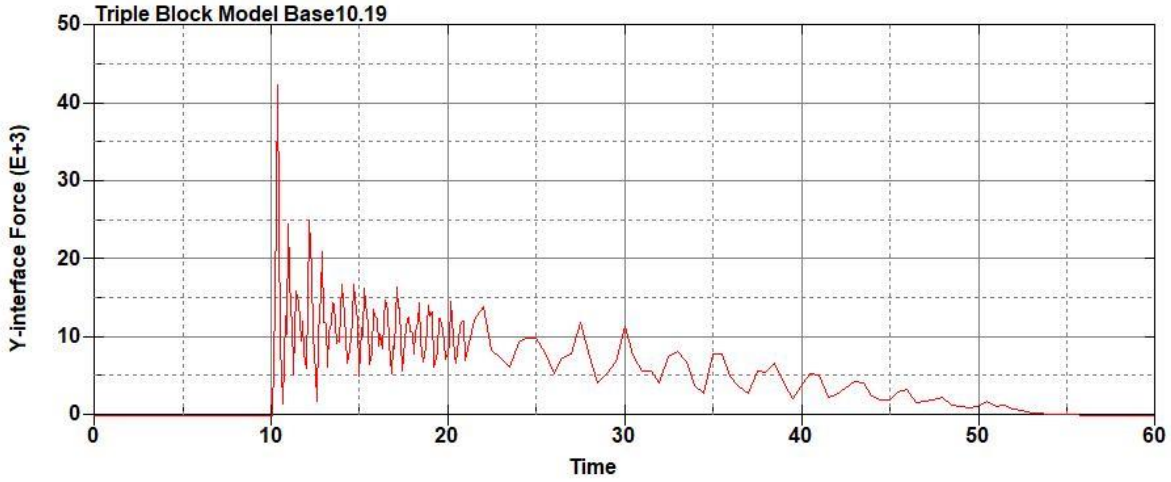


**Figure B-690: Base Run 10.19 Left Support Y-Interface Force (lbs) versus Time (ms) – 950 psi**

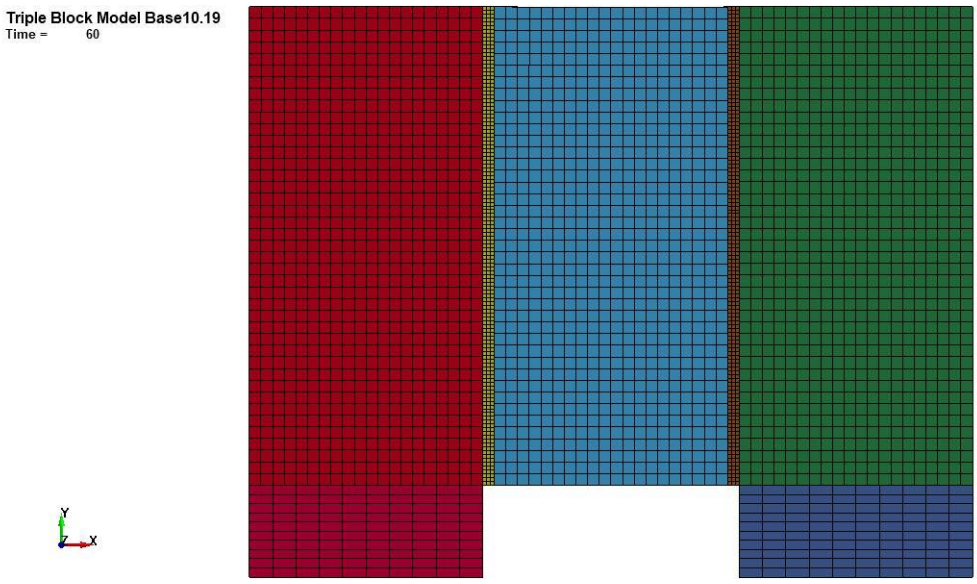


**Figure B-691: Last State at 60 Milliseconds for Base Run 10.19 – 950 psi**

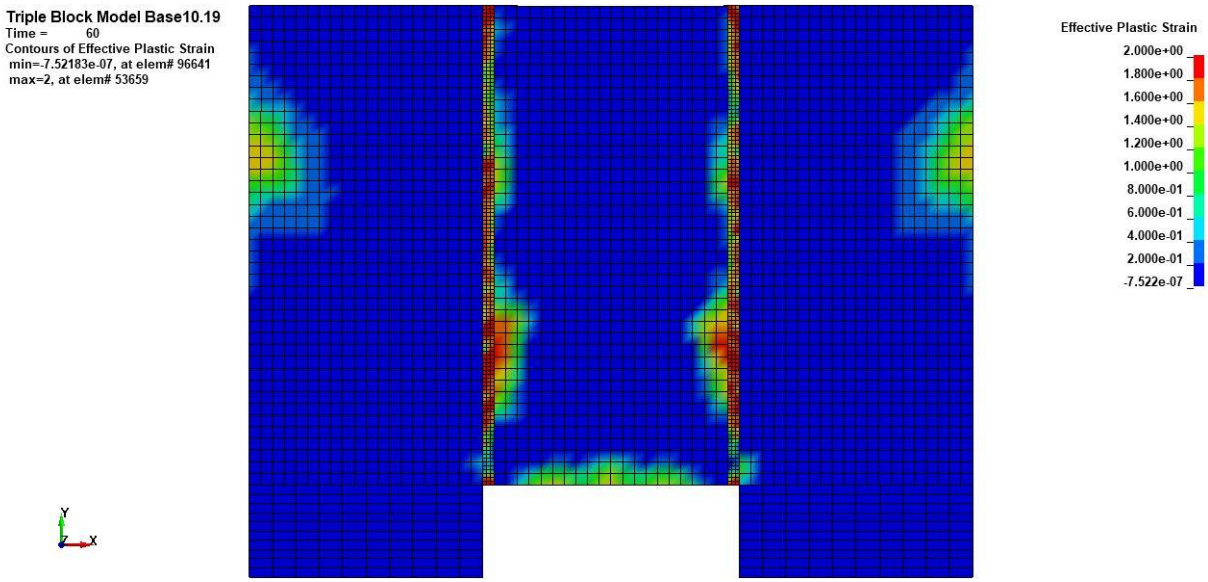


**Figure B-692: Effective Plastic Strain Fringe Plot for Last State at 60 Milliseconds for Base Run 10.19 – 950 psi**

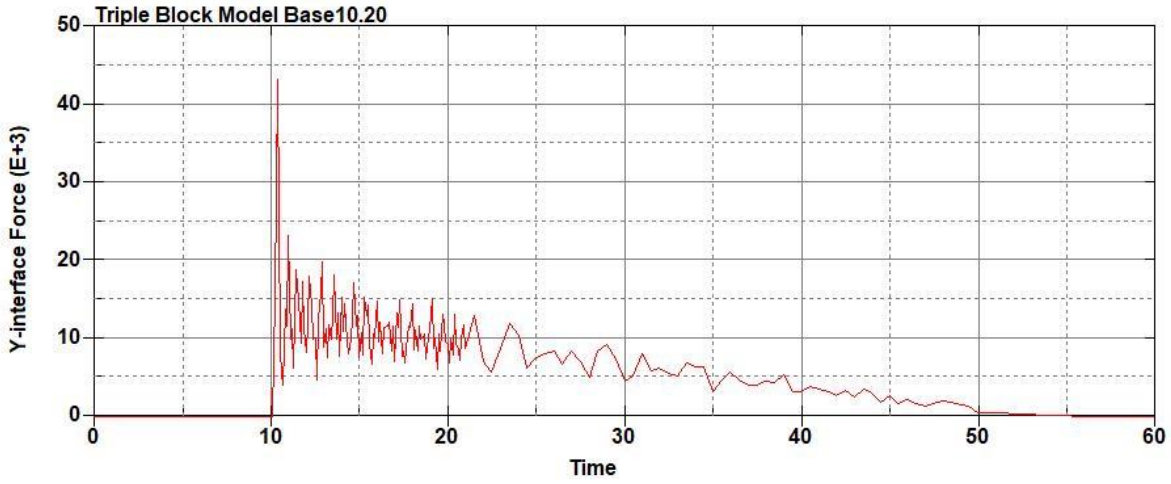


**Figure B-693: Base Run 10.20 Right Support Y-Interface Force (lbs) versus Time (ms) – 1000 psi**

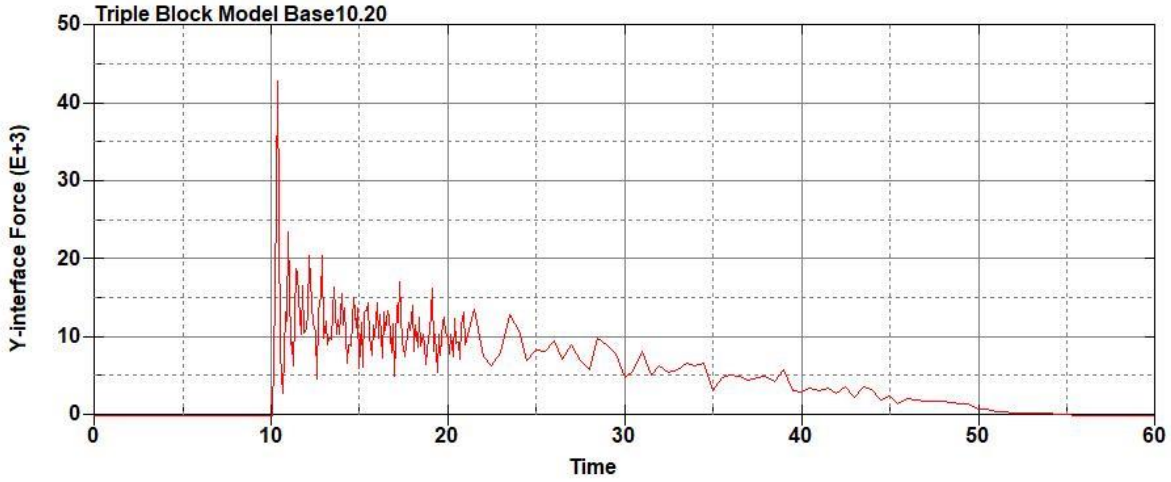


**Figure B-694: Base Run 10.20 Left Support Y-Interface Force (lbs) versus Time (ms) – 1000 psi**

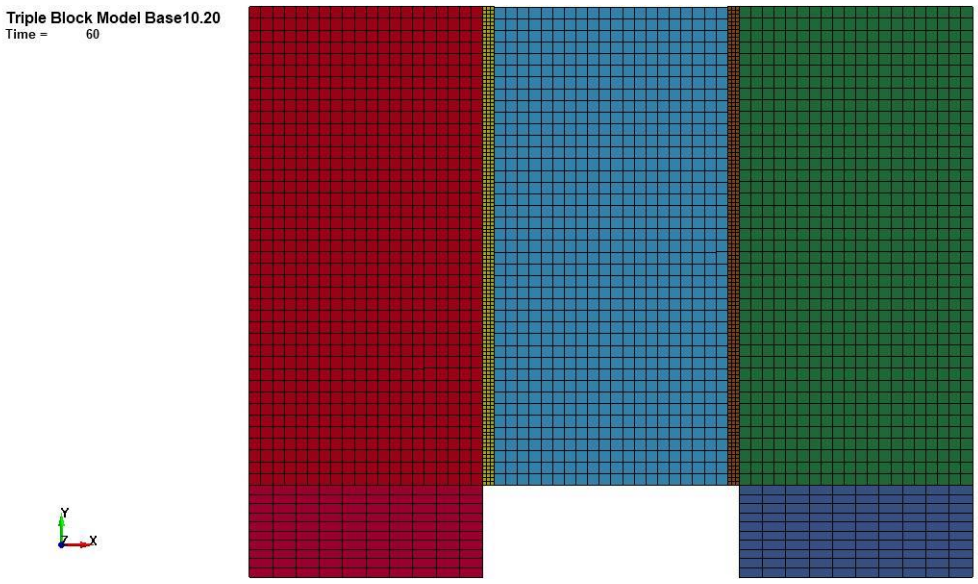


**Figure B-695: Last State at 60 Milliseconds for Base Run 10.20 – 1000 psi**

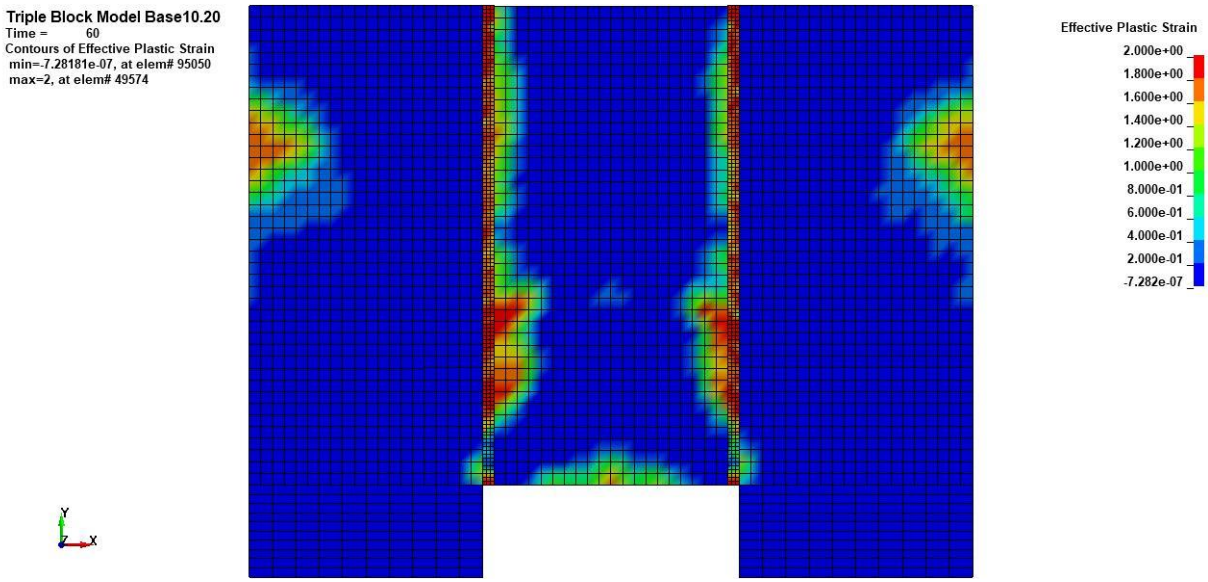


**Figure B-696: Effective Plastic Strain Fringe Plot for Last State at 60 Milliseconds for Base Run 10.20 – 1000 psi**

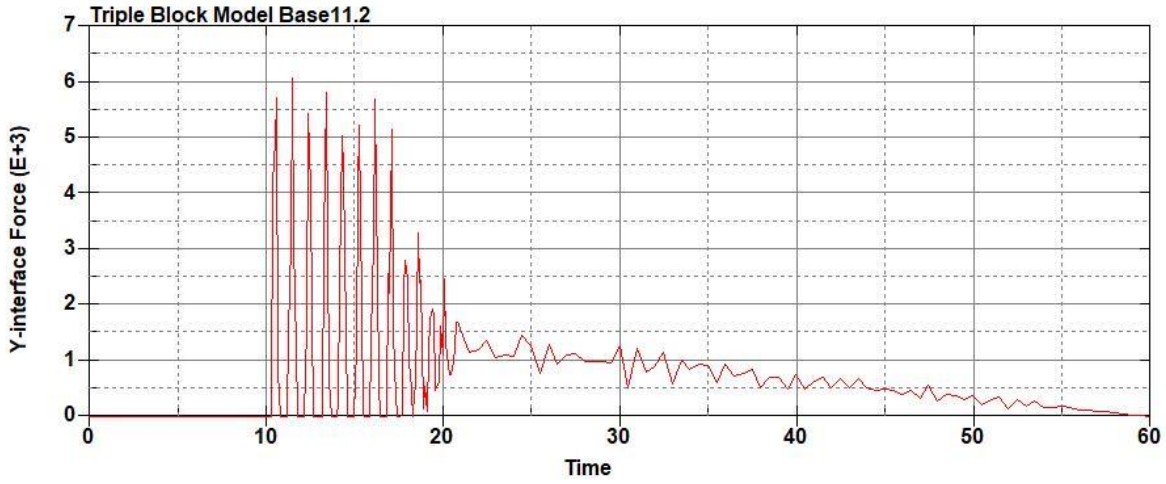


**Figure B-697: Base Run 11.2 Right Support Y-Interface Force (lbs) versus Time (ms) – 100 psi**

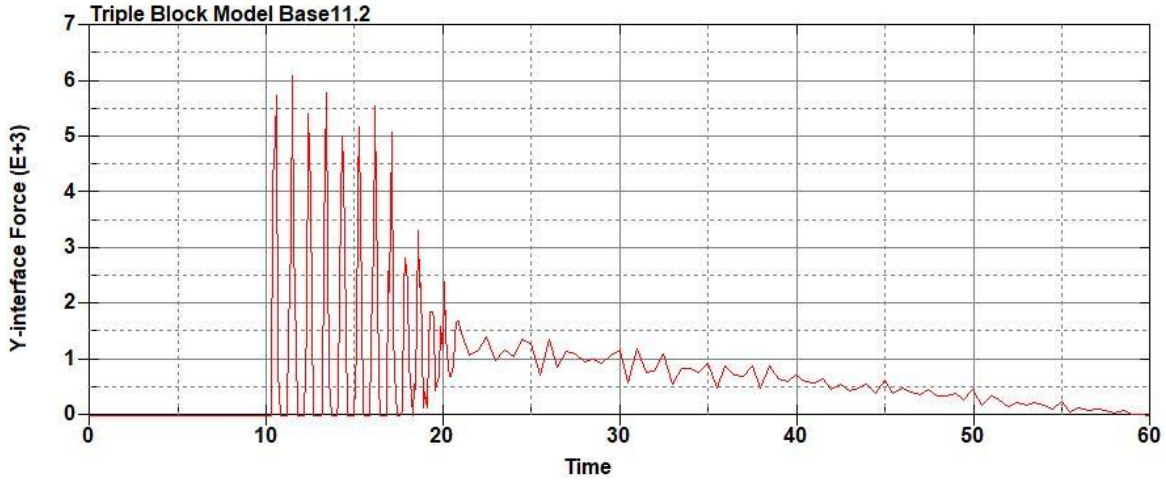


**Figure B-698: Base Run 11.2 Left Support Y-Interface Force (lbs) versus Time (ms) – 100 psi**

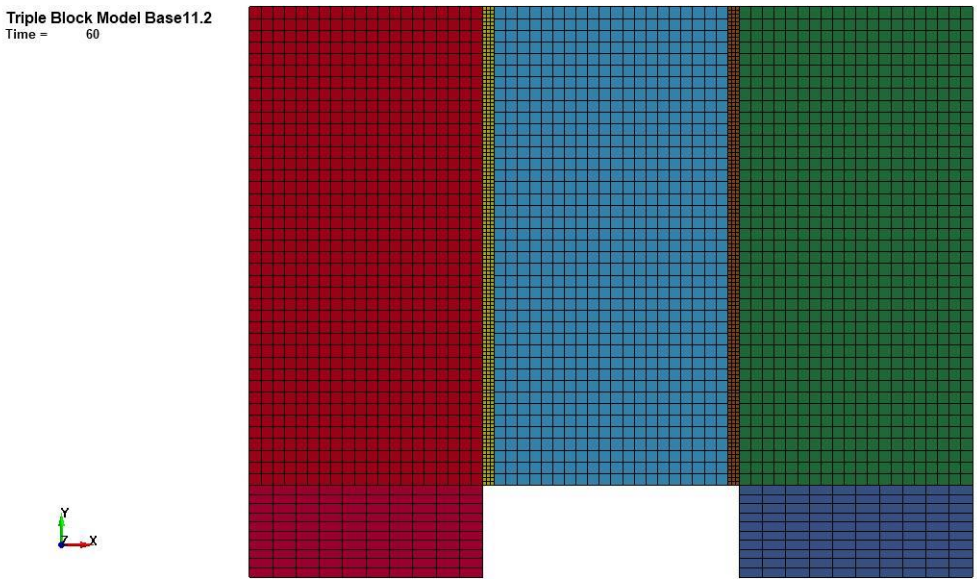


**Figure B-699: Last State at 60 Milliseconds for Base Run 11.2 – 100 psi**

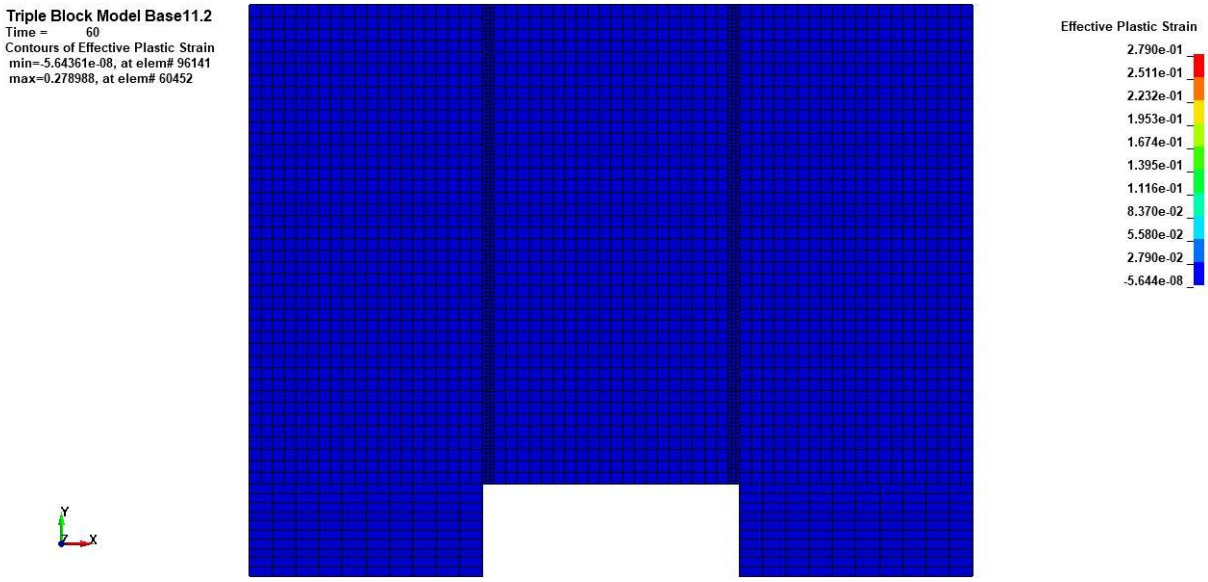


**Figure B-700: Effective Plastic Strain Fringe Plot for Last State at 60 Milliseconds for Base Run 11.2 – 100 psi**

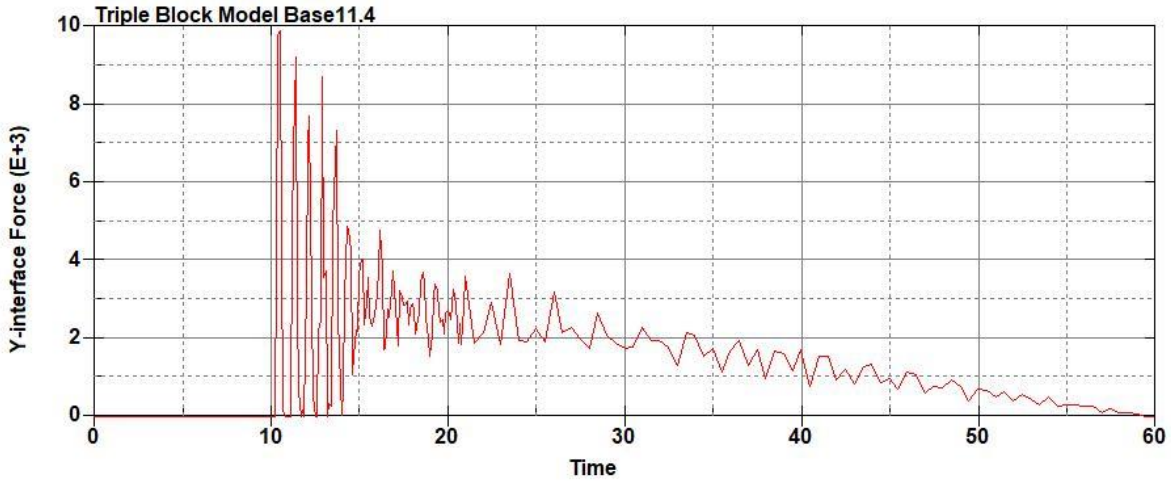


**Figure B-701: Base Run 11.4 Right Support Y-Interface Force (lbs) versus Time (ms) – 200 psi**

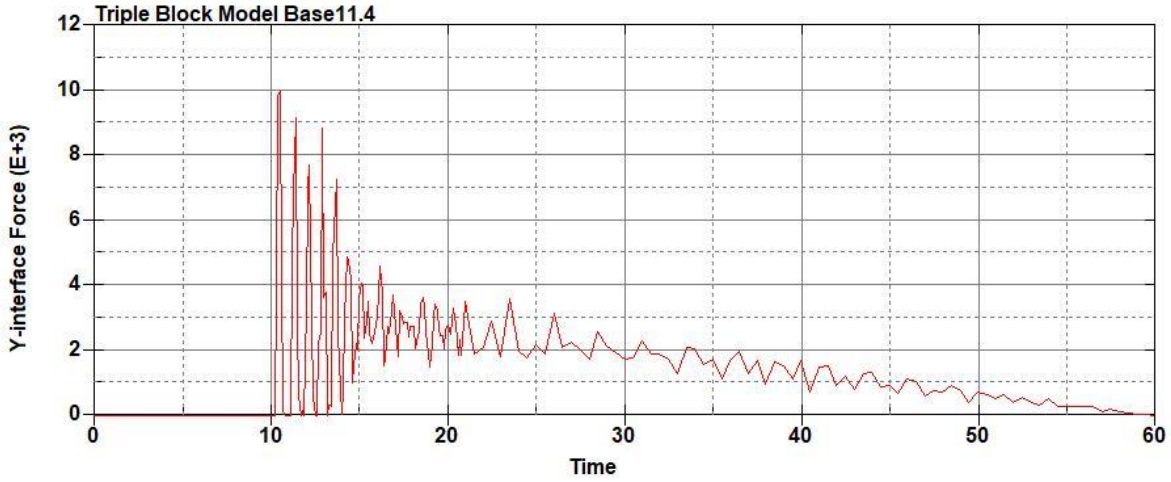


**Figure B-702: Base Run 11.4 Left Support Y-Interface Force (lbs) versus Time (ms) – 200 psi**

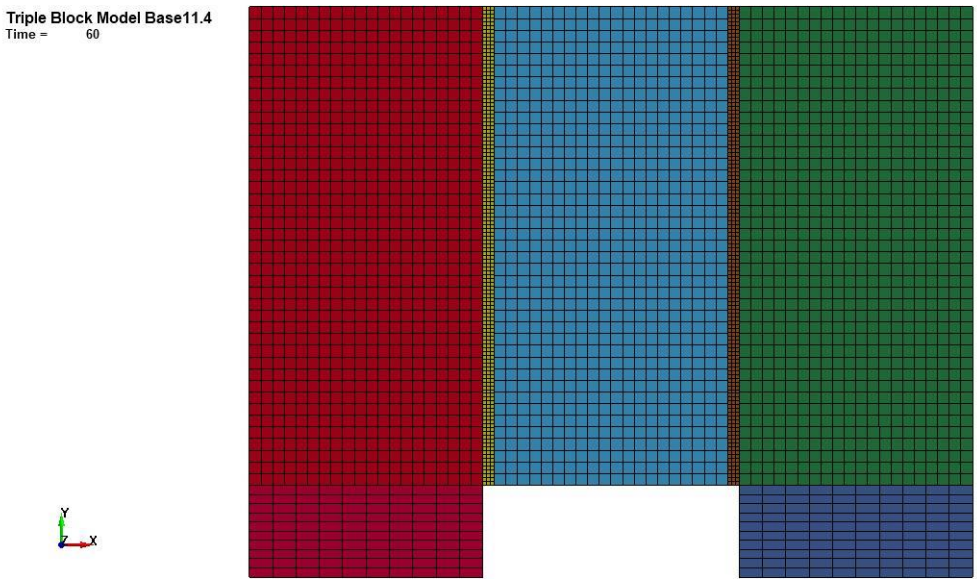


**Figure B-703: Last State at 60 Milliseconds for Base Run 11.4 – 200 psi**

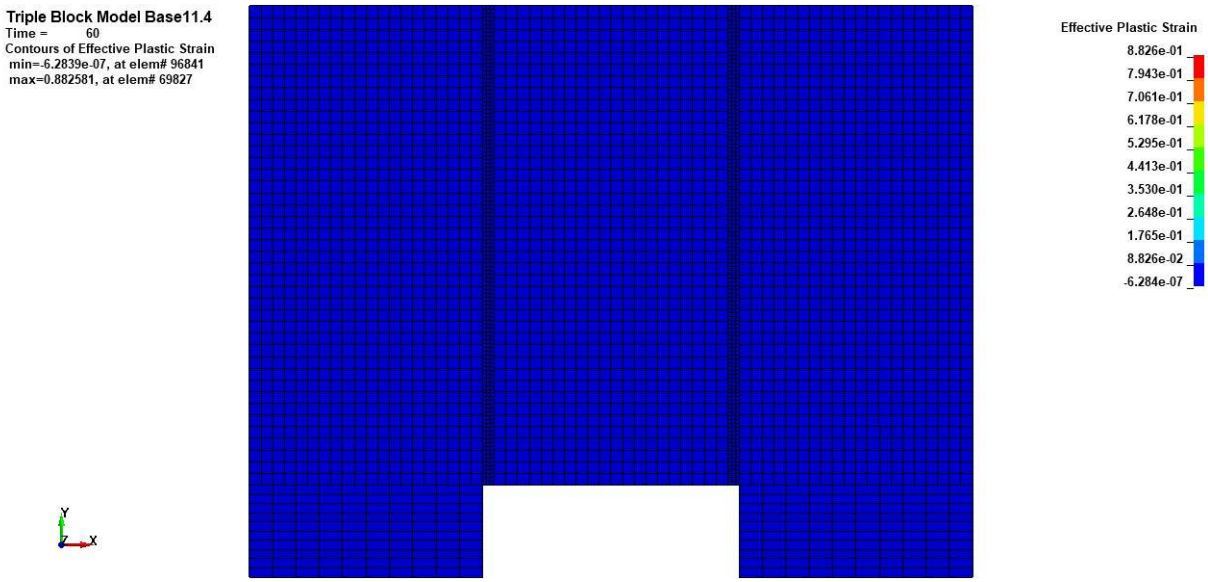


**Figure B-704: Effective Plastic Strain Fringe Plot for Last State at 60 Milliseconds for Base Run 11.4 – 200 psi**

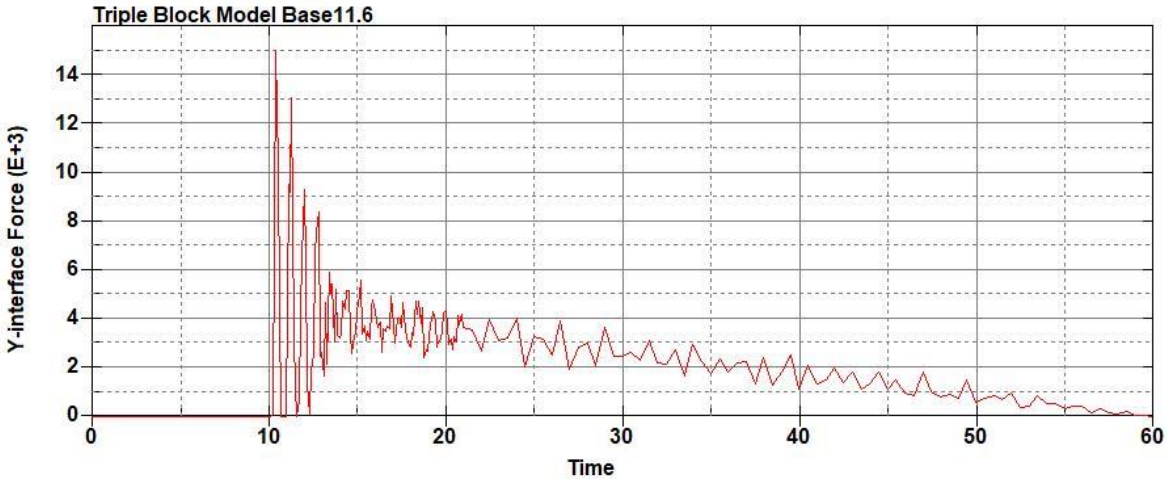


**Figure B-705: Base Run 11.6 Right Support Y-Interface Force (lbs) versus Time (ms) – 300 psi**

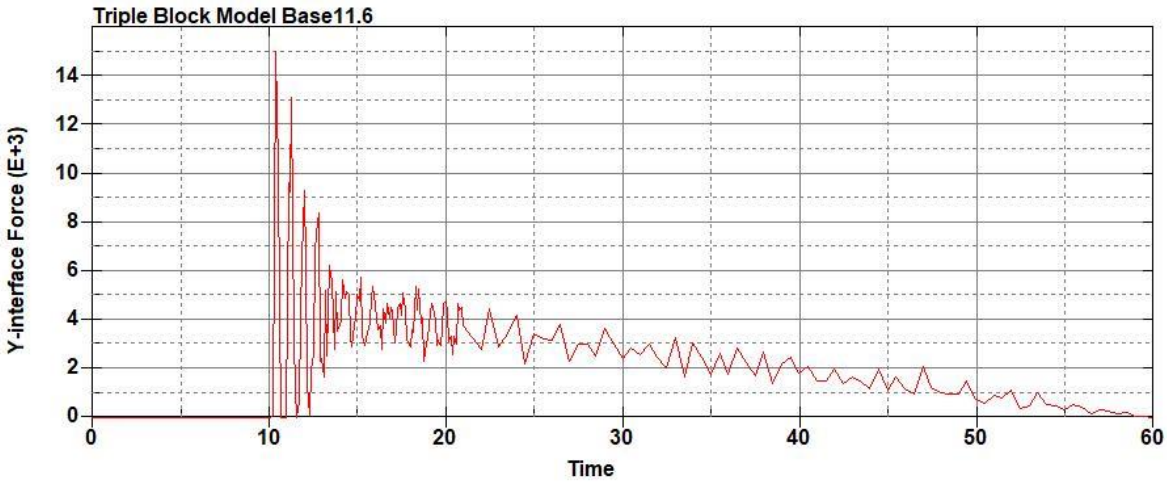


**Figure B-706: Base Run 11.6 Left Support Y-Interface Force (lbs) versus Time (ms) – 300 psi**

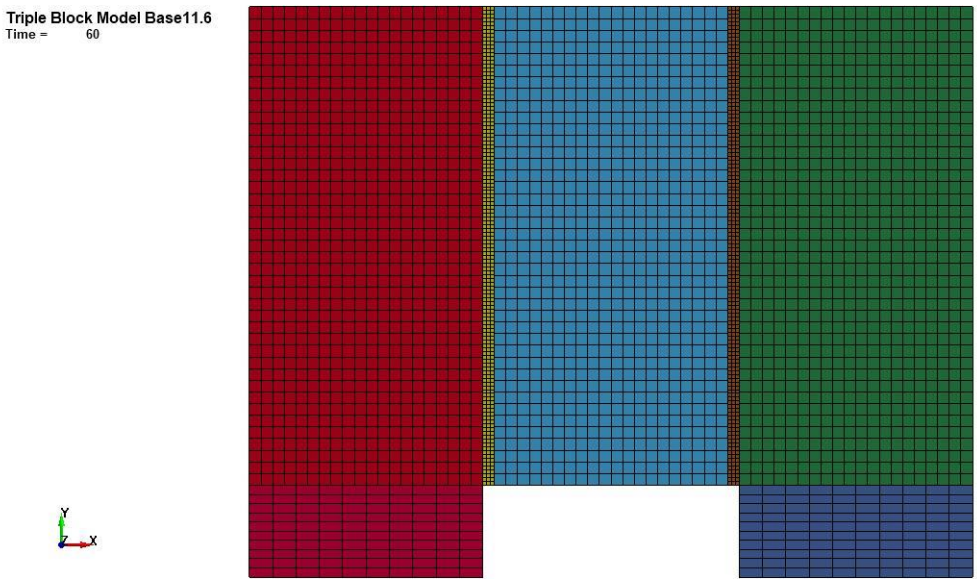


**Figure B-707: Last State at 60 Milliseconds for Base Run 11.6 – 300 psi**

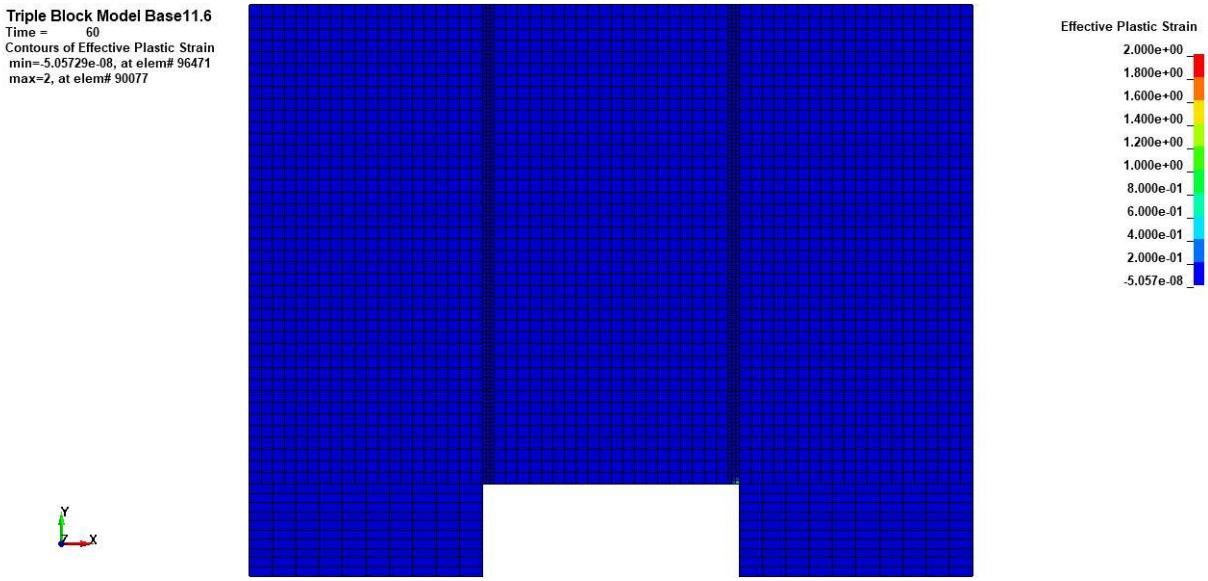


**Figure B-708: Effective Plastic Strain Fringe Plot for Last State at 60 Milliseconds for Base Run 11.6 – 300 psi**

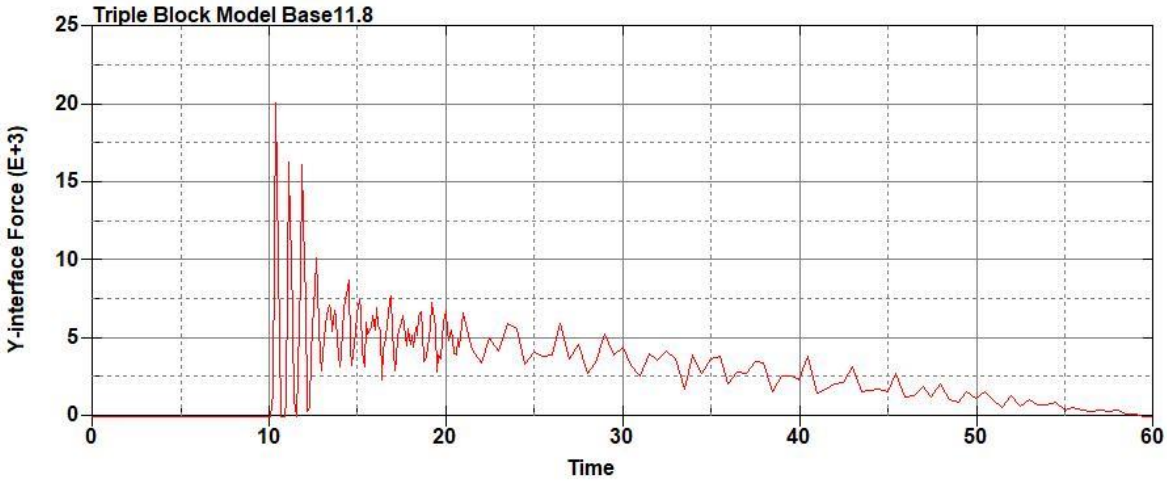


**Figure B-709: Base Run 11.8 Right Support Y-Interface Force (lbs) versus Time (ms) – 400 psi**

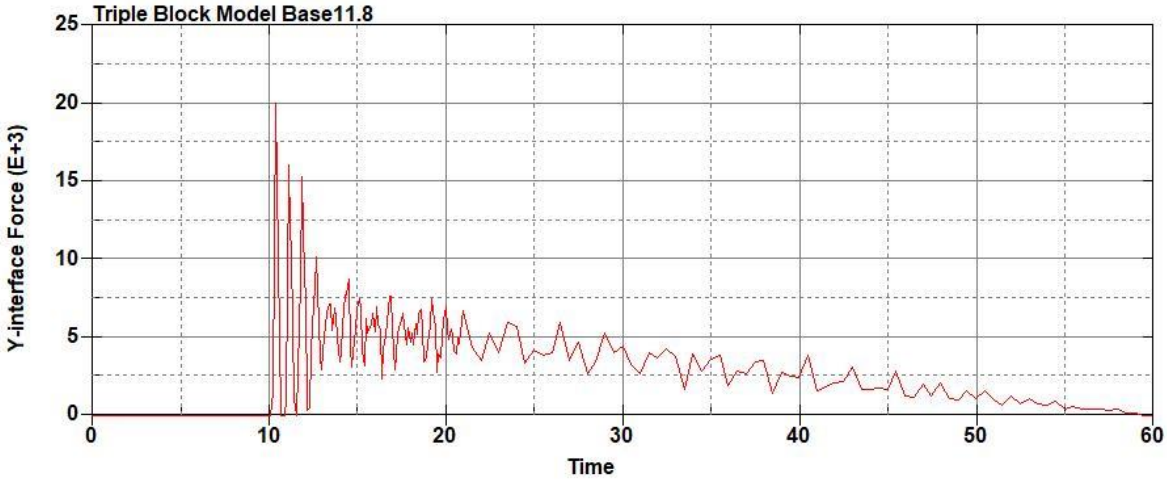


**Figure B-710: Base Run 11.8 Left Support Y-Interface Force (lbs) versus Time (ms) – 400 psi**

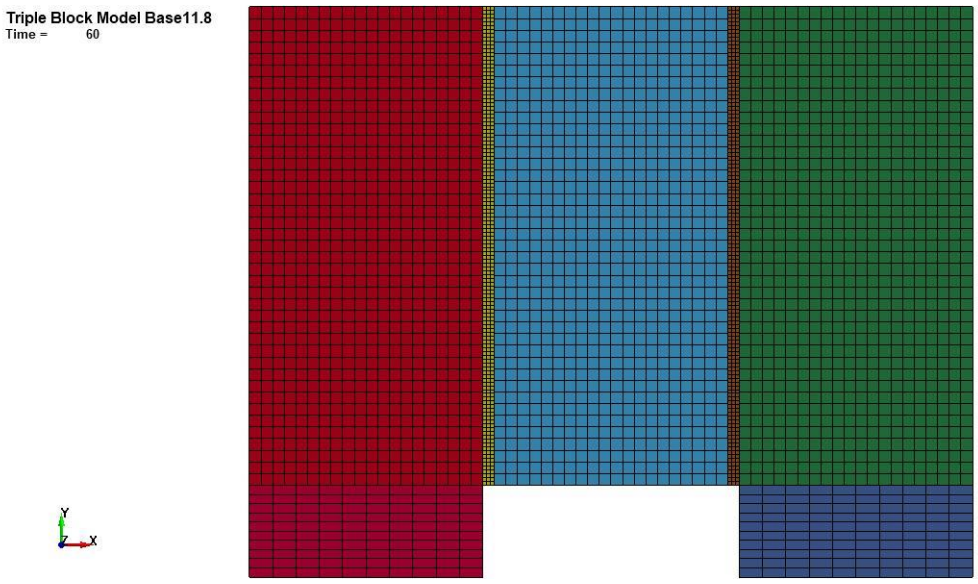


**Figure B-711: Last State at 60 Milliseconds for Base Run 11.8 – 400 psi**

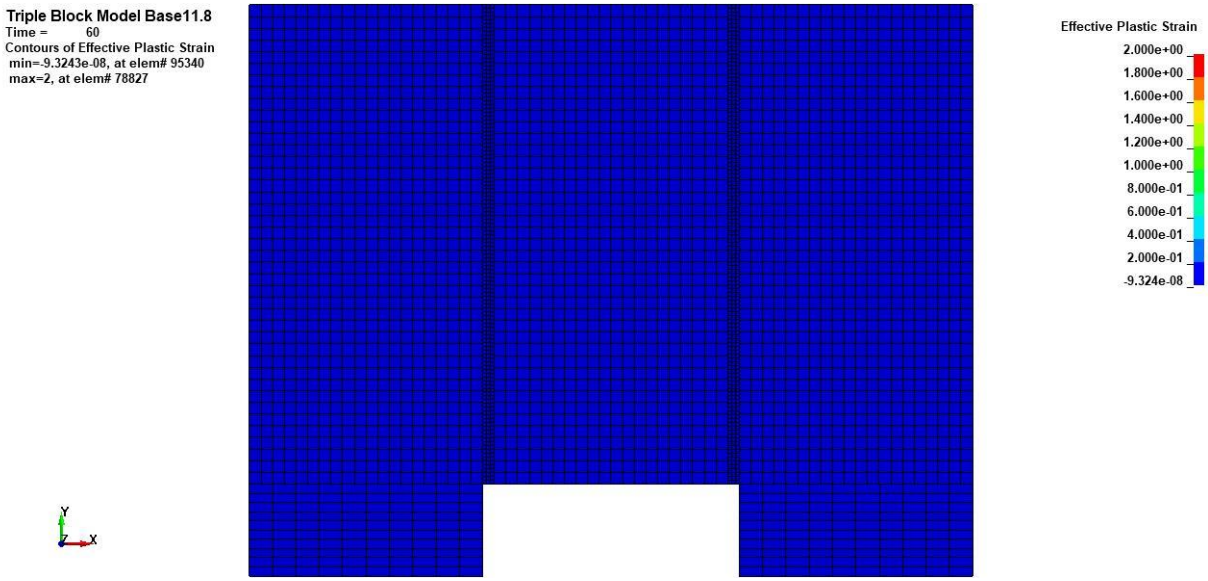


**Figure B-712: Effective Plastic Strain Fringe Plot for Last State at 60 Milliseconds for Base Run 11.8 – 400 psi**

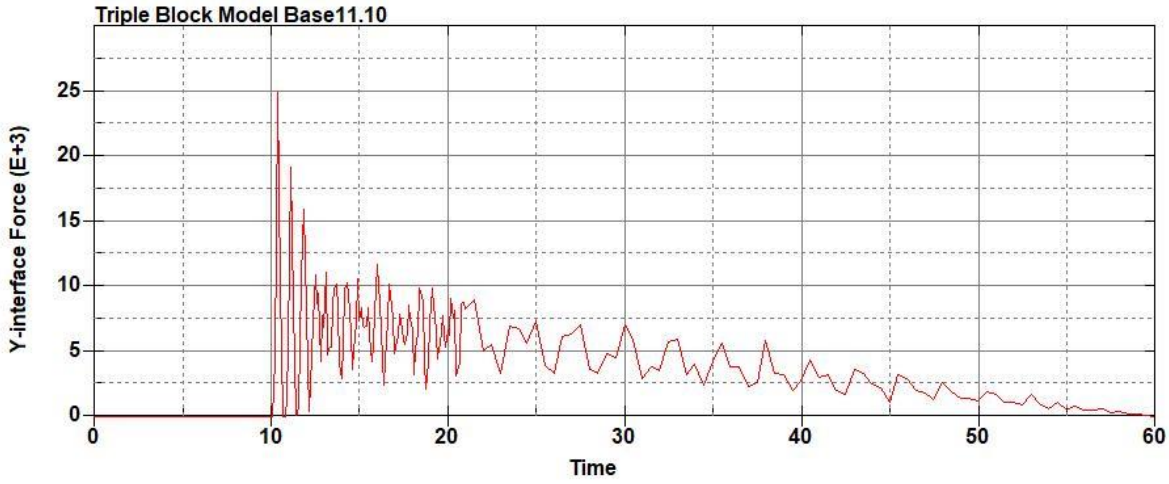


**Figure B-713: Base Run 11.10 Right Support Y-Interface Force (lbs) versus Time (ms) – 500 psi**

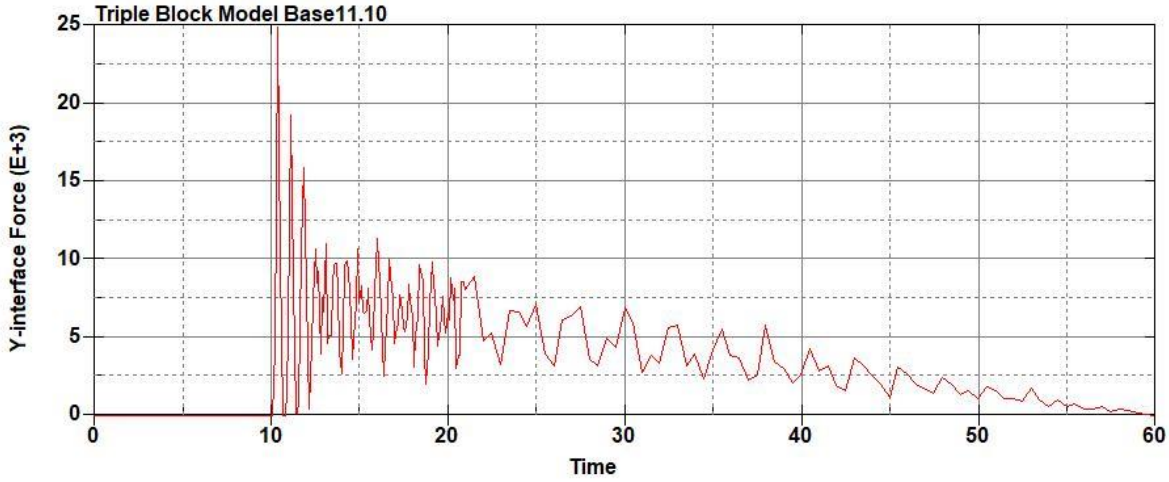


**Figure B-714: Base Run 11.10 Left Support Y-Interface Force (lbs) versus Time (ms) – 500 psi**

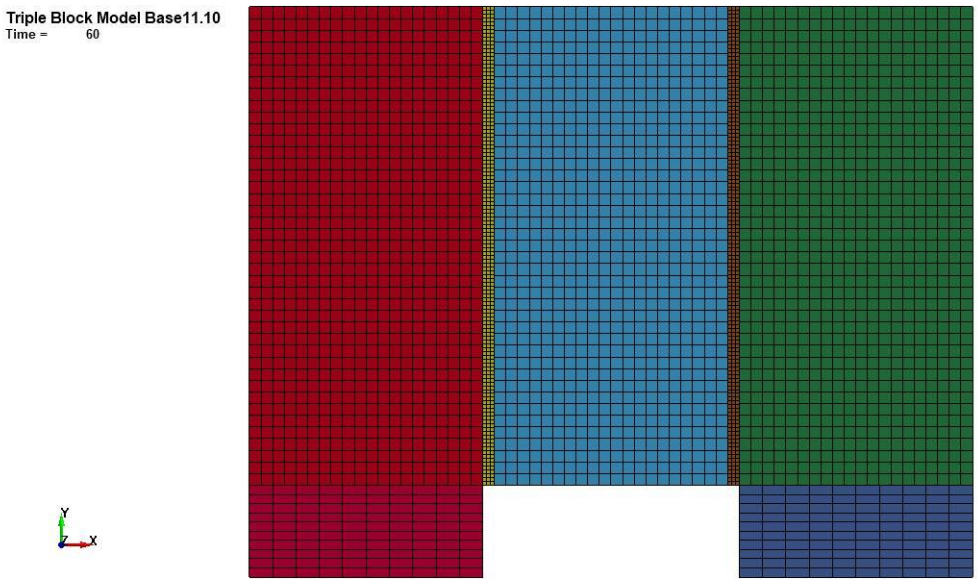


**Figure B-715: Last State at 60 Milliseconds for Base Run 11.10 – 500 psi**

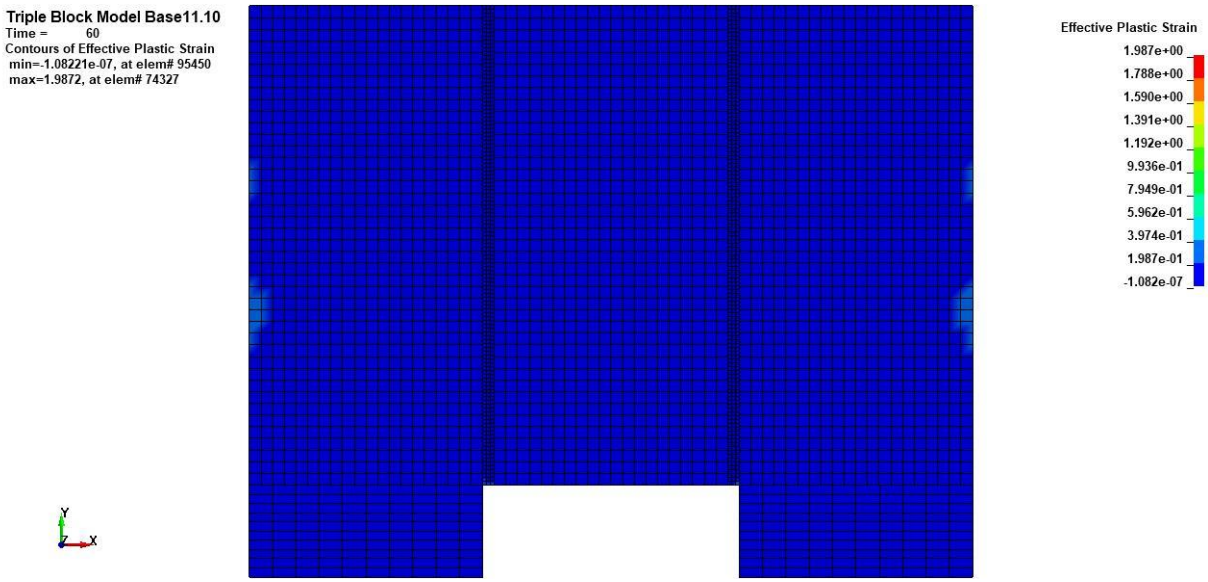


**Figure B-716: Effective Plastic Strain Fringe Plot for Last State at 60 Milliseconds for Base Run 11.10 – 500 psi**

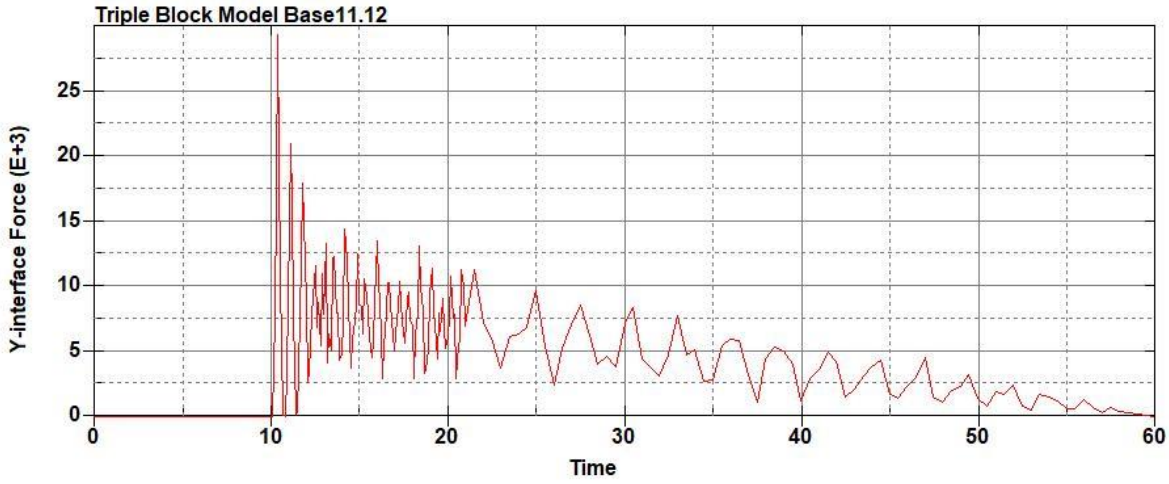


**Figure B-717: Base Run 11.12 Right Support Y-Interface Force (lbs) versus Time (ms) – 600 psi**

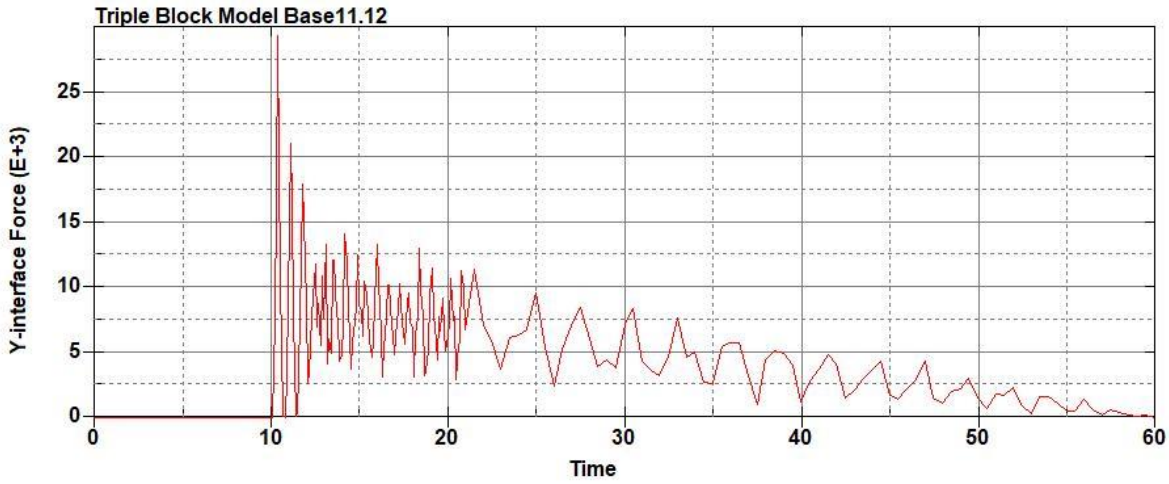


**Figure B-718: Base Run 11.12 Left Support Y-Interface Force (lbs) versus Time (ms) – 600 psi**

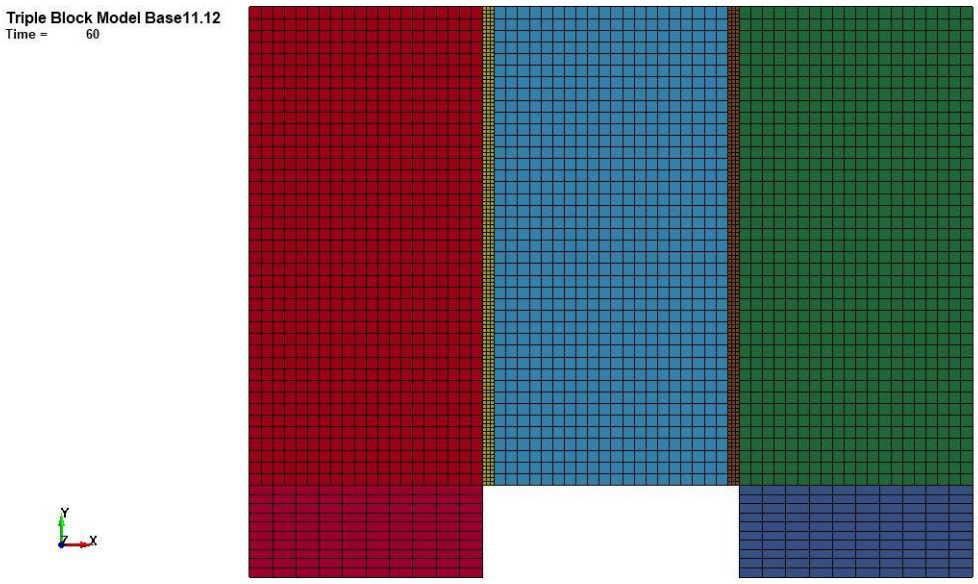


**Figure B-719: Last State at 60 Milliseconds for Base Run 11.12 – 600 psi**

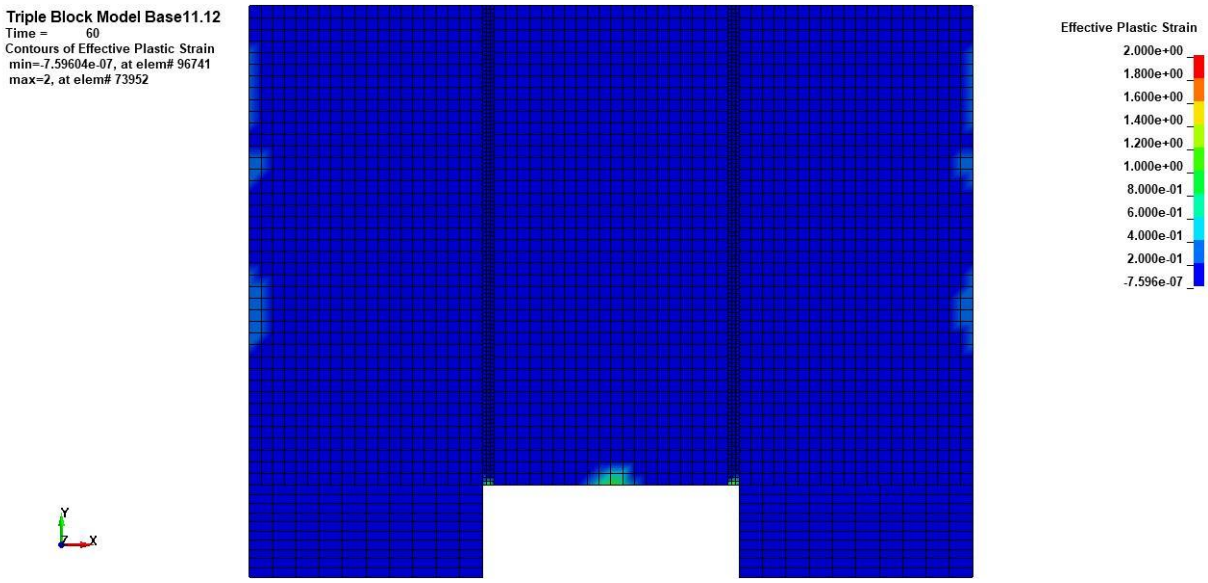


**Figure B-720: Effective Plastic Strain Fringe Plot for Last State at 60 Milliseconds for Base Run 11.12 – 600 psi**

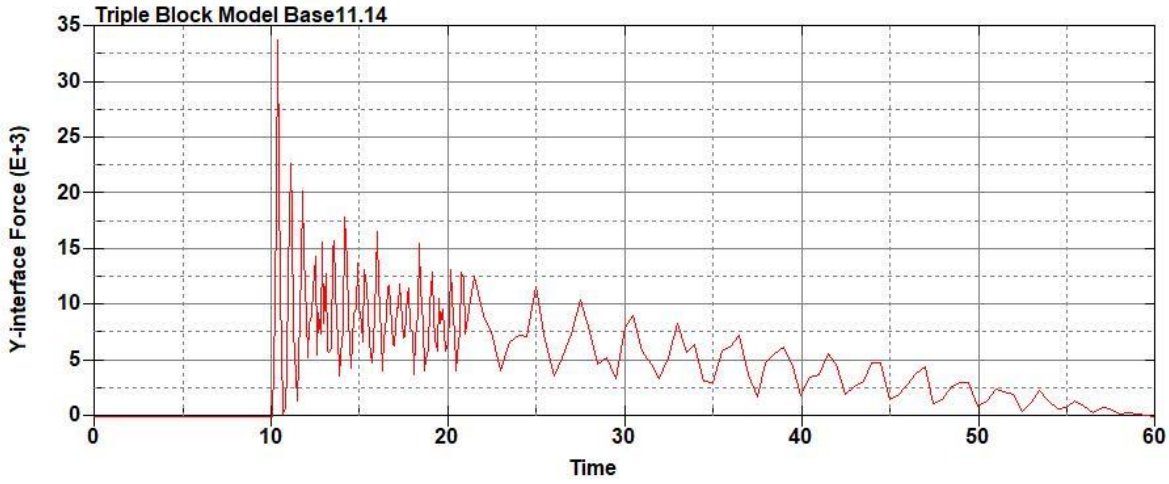


**Figure B-721: Base Run 11.14 Right Support Y-Interface Force (lbs) versus Time (ms) – 700 psi**

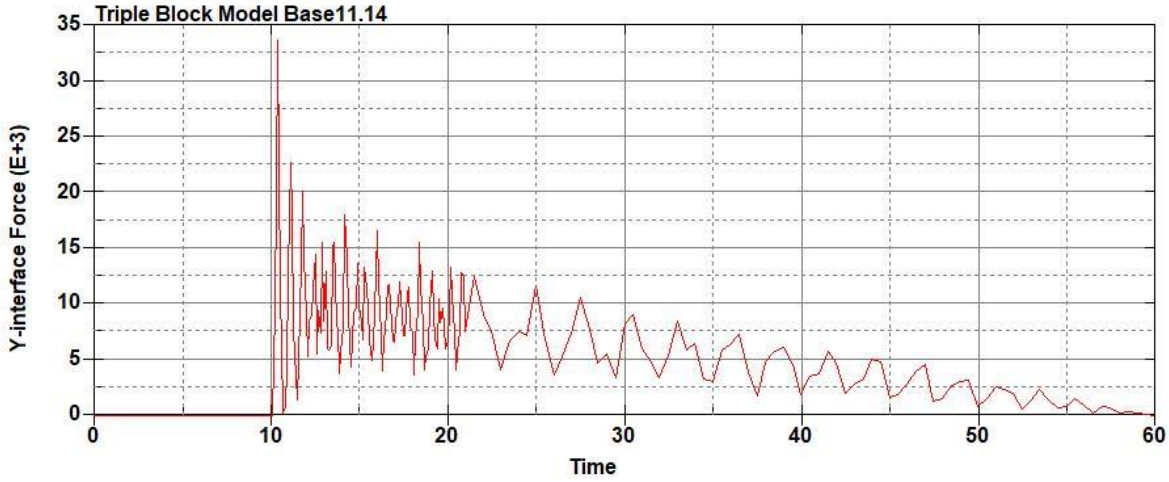


**Figure B-722: Base Run 11.14 Left Support Y-Interface Force (lbs) versus Time (ms) – 700 psi**

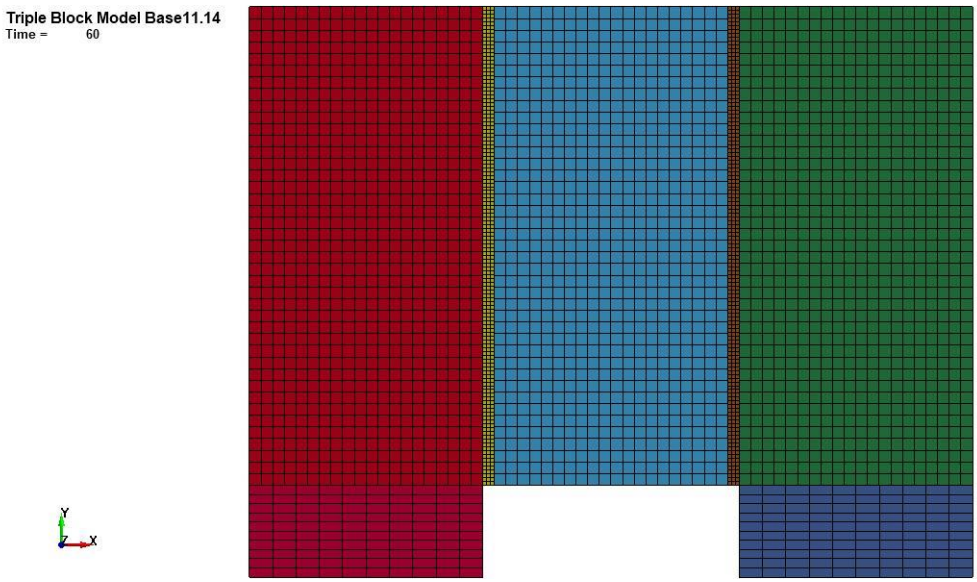


**Figure B-723: Last State at 60 Milliseconds for Base Run 11.14 – 700 psi**

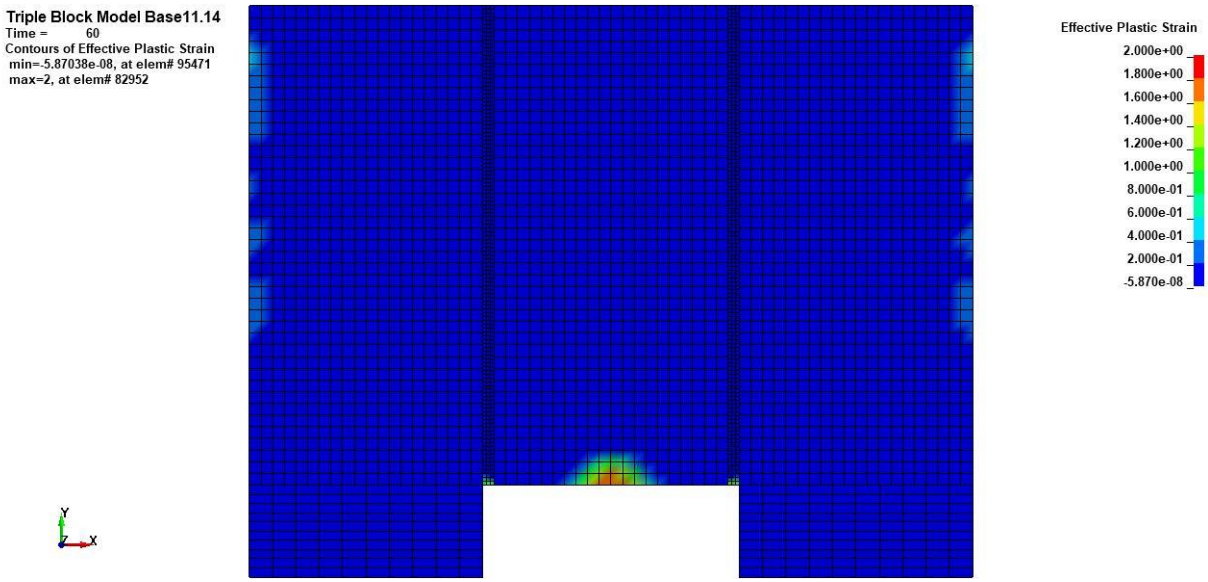


**Figure B-724: Effective Plastic Strain Fringe Plot for Last State at 60 Milliseconds for Base Run 11.14 – 700 psi**

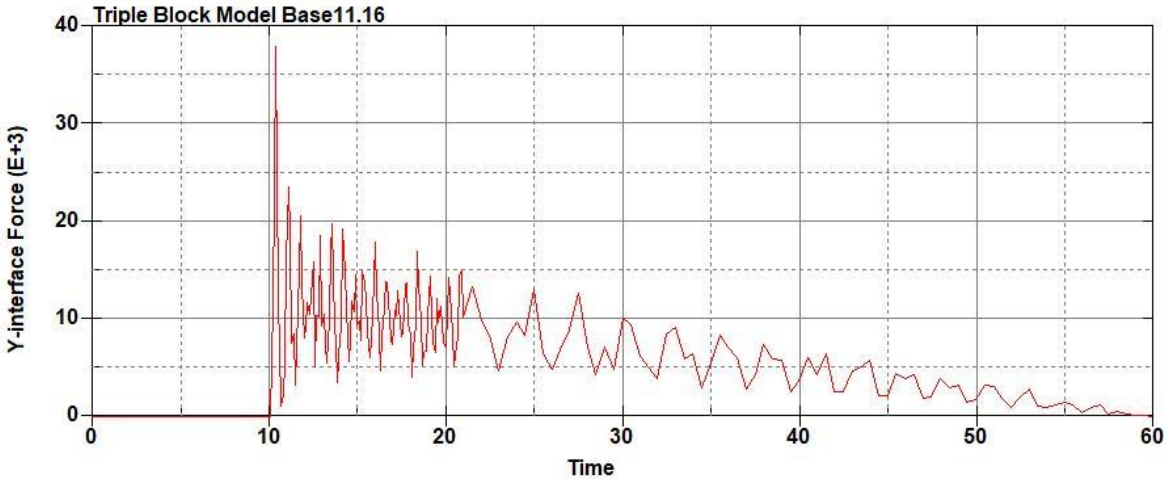


**Figure B-725: Base Run 11.16 Right Support Y-Interface Force (lbs) versus Time (ms) – 800 psi**

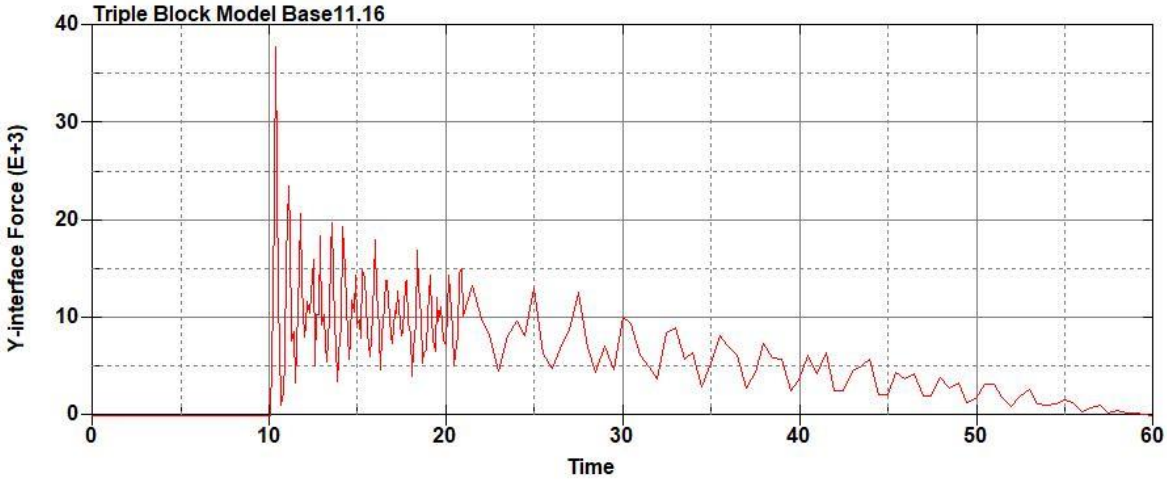


**Figure B-726: Base Run 11.16 Left Support Y-Interface Force (lbs) versus Time (ms) – 800 psi**

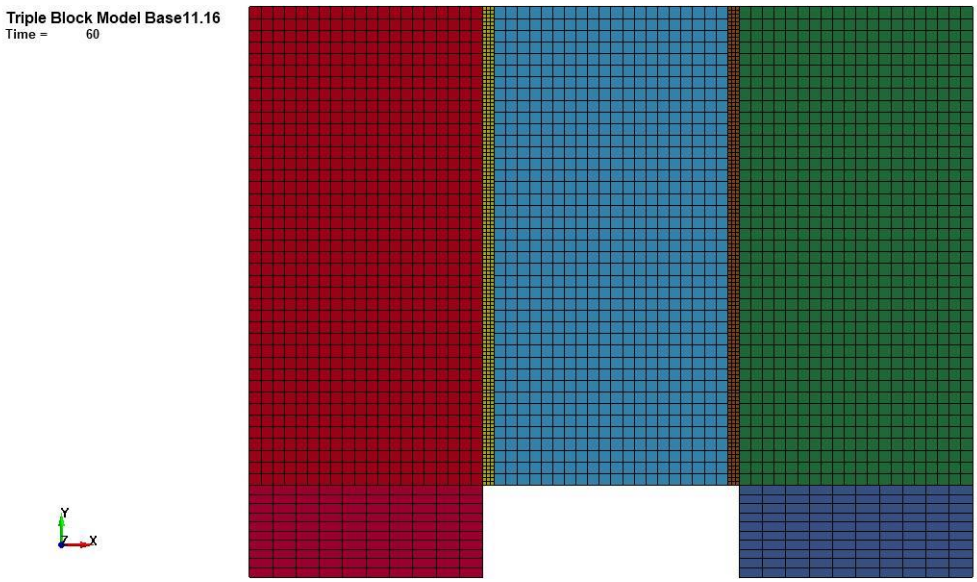


**Figure B-727: Last State at 60 Milliseconds for Base Run 11.16 – 800 psi**

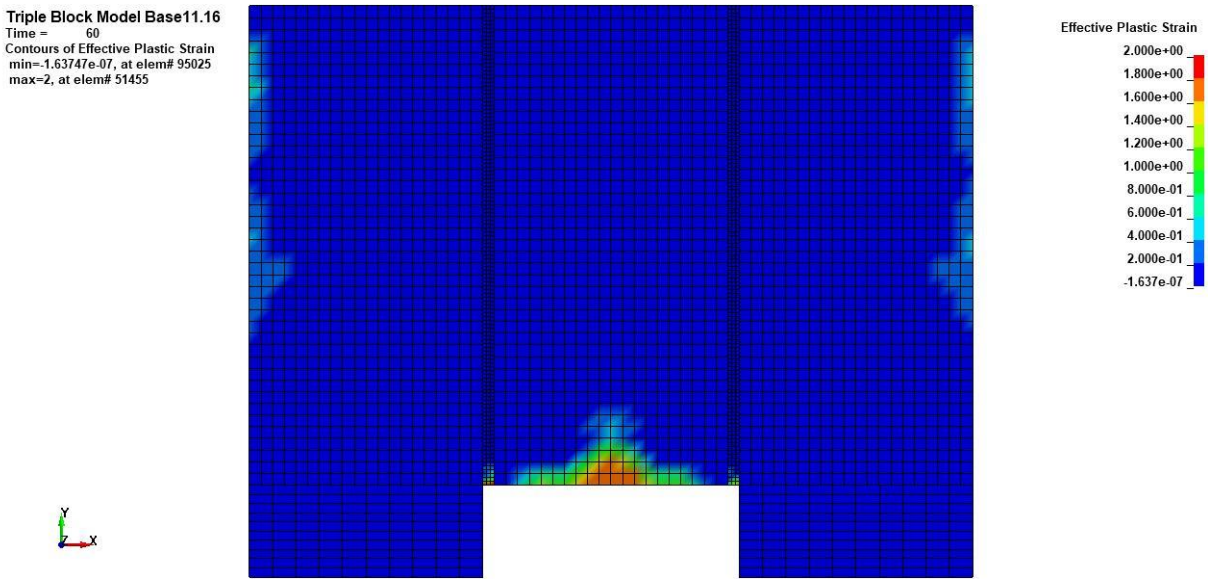


**Figure B-728: Effective Plastic Strain Fringe Plot for Last State at 60 Milliseconds for Base Run 11.16 – 800 psi**

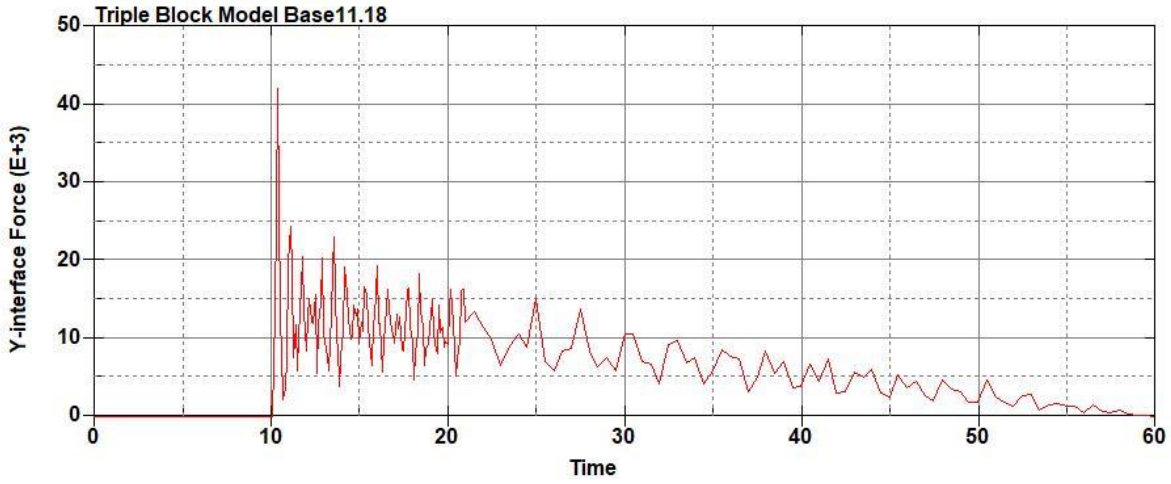


**Figure B-729: Base Run 11.18 Right Support Y-Interface Force (lbs) versus Time (ms) – 900 psi**

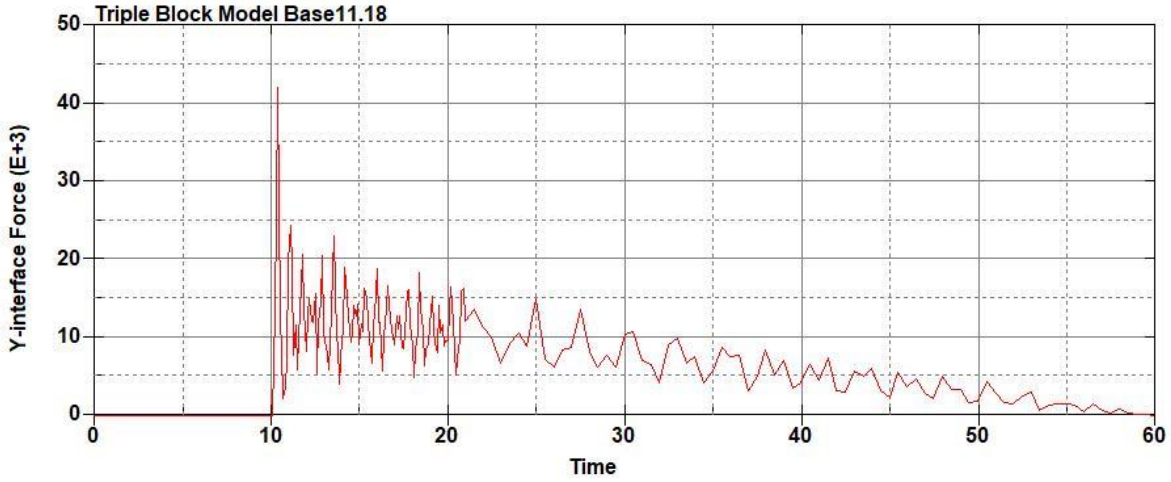


**Figure B-730: Base Run 11.18 Left Support Y-Interface Force (lbs) versus Time (ms) – 900 psi**

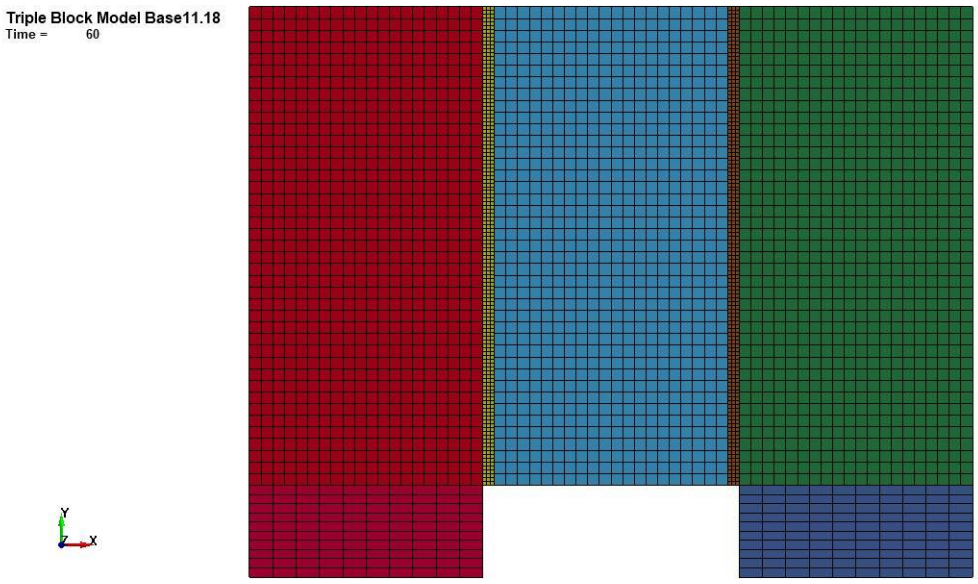


**Figure B-731: Last State at 60 Milliseconds for Base Run 11.18 – 900 psi**

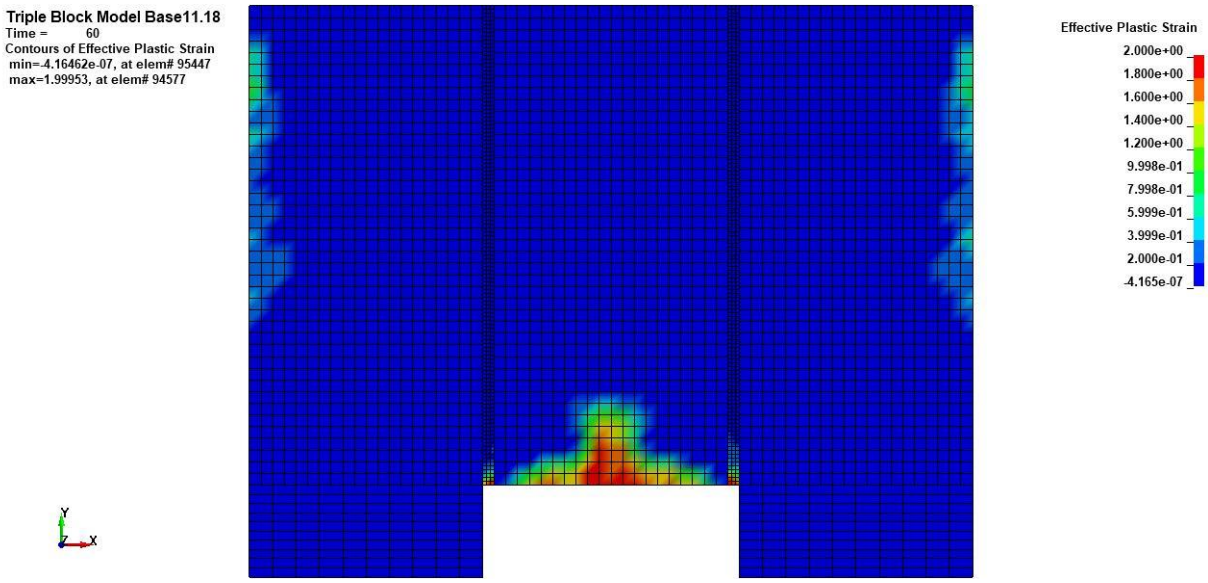


**Figure B-732: Effective Plastic Strain Fringe Plot for Last State at 60 Milliseconds for Base Run 11.18 – 900 psi**

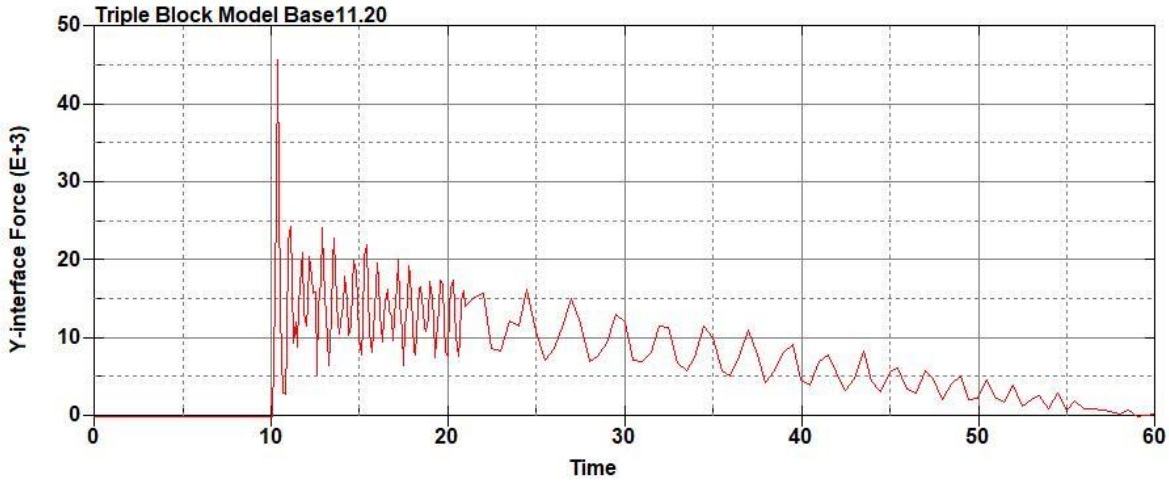


**Figure B-733: Base Run 11.20 Right Support Y-Interface Force (lbs) versus Time (ms) – 1000 psi**

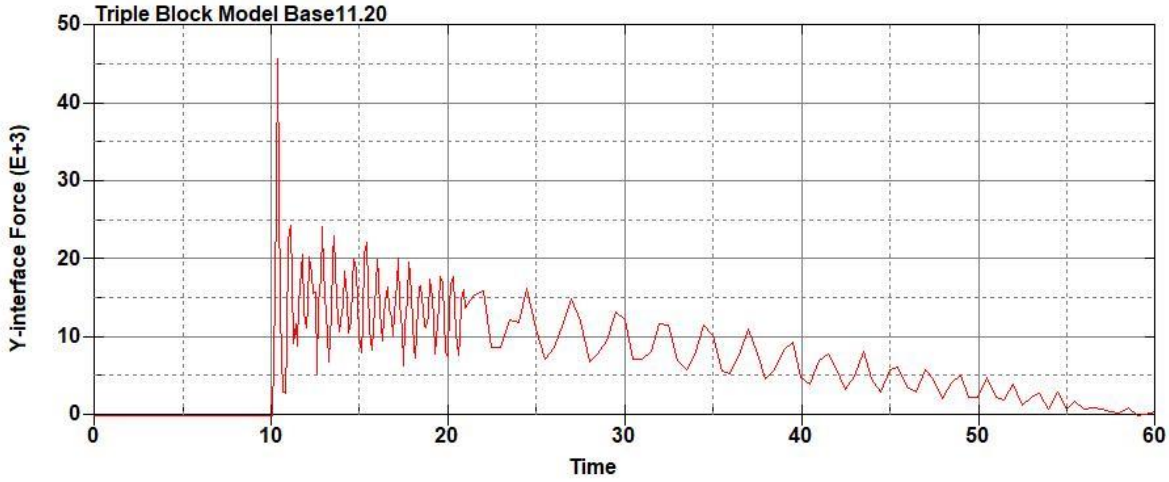


**Figure B-734: Base Run 11.20 Left Support Y-Interface Force (lbs) versus Time (ms) – 1000 psi**

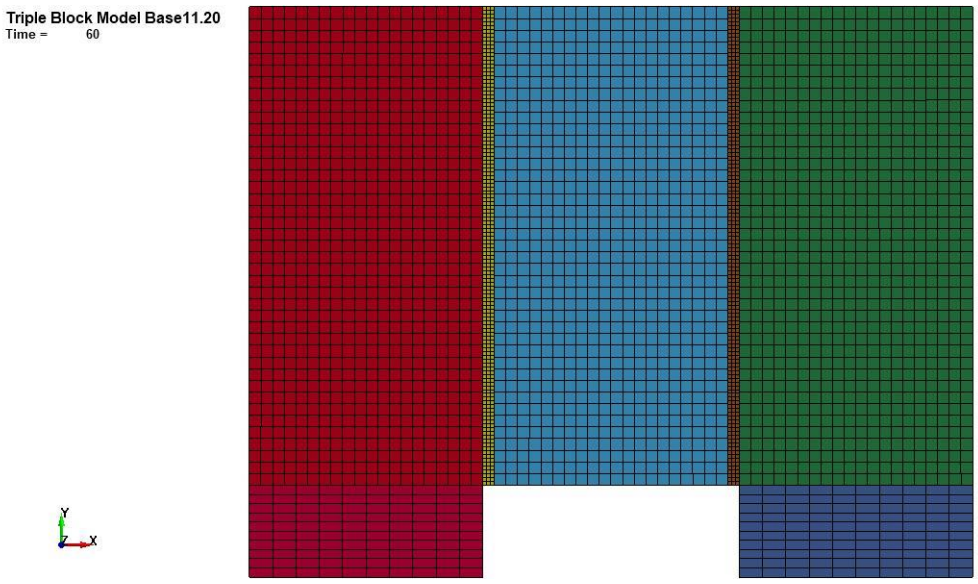


**Figure B-735: Last State at 60 Milliseconds for Base Run 11.20 – 1000 psi**

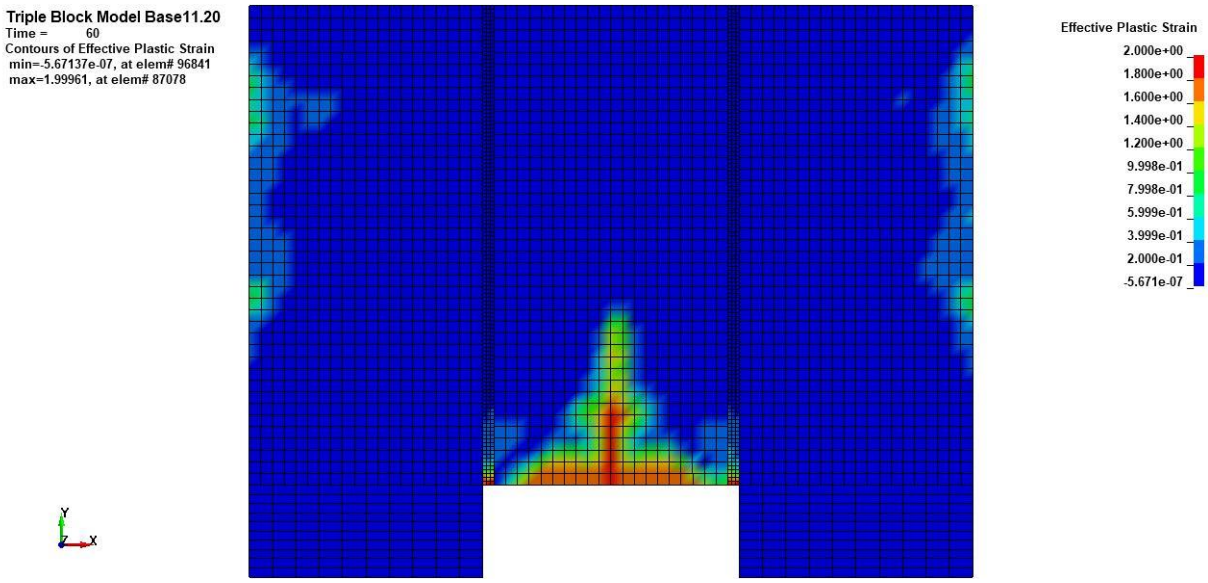


**Figure B-736: Effective Plastic Strain Fringe Plot for Last State at 60 Milliseconds for Base Run 11.20 – 1000 psi**

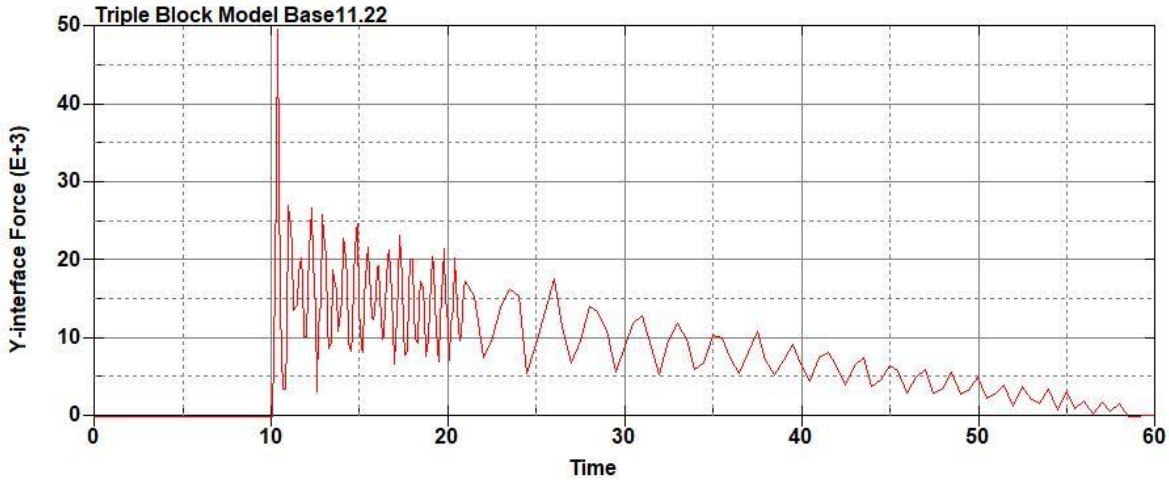


**Figure B-737: Base Run 11.22 Right Support Y-Interface Force (lbs) versus Time (ms) – 1100 psi**

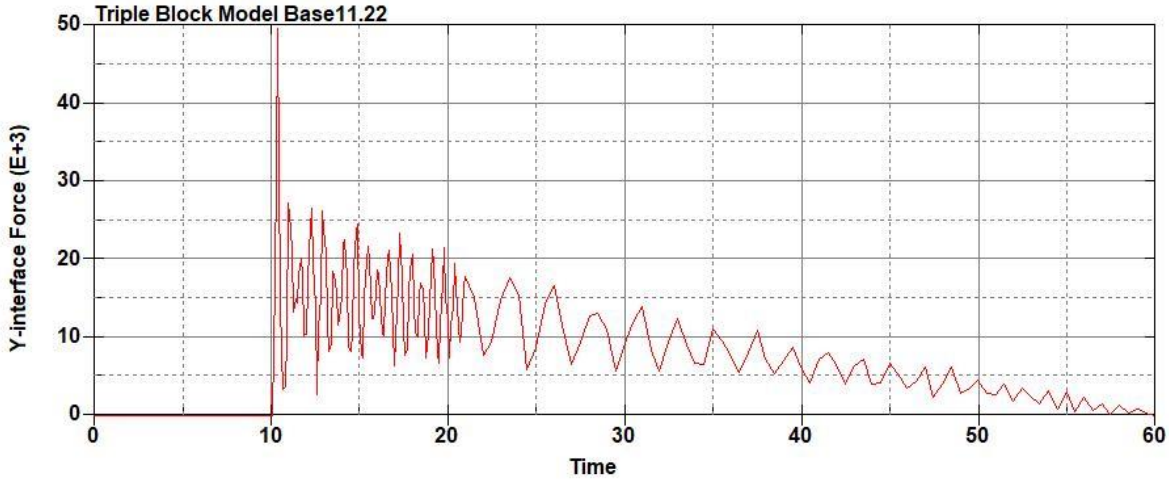


**Figure B-738: Base Run 11.22 Left Support Y-Interface Force (lbs) versus Time (ms) – 1100 psi**

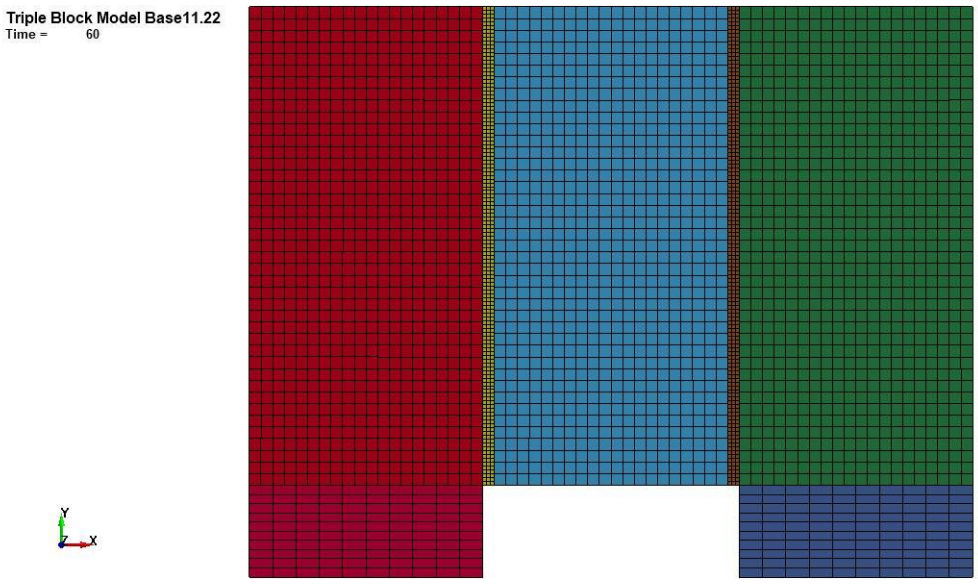


**Figure B-739: Last State at 60 Milliseconds for Base Run 11.22 – 1100 psi**

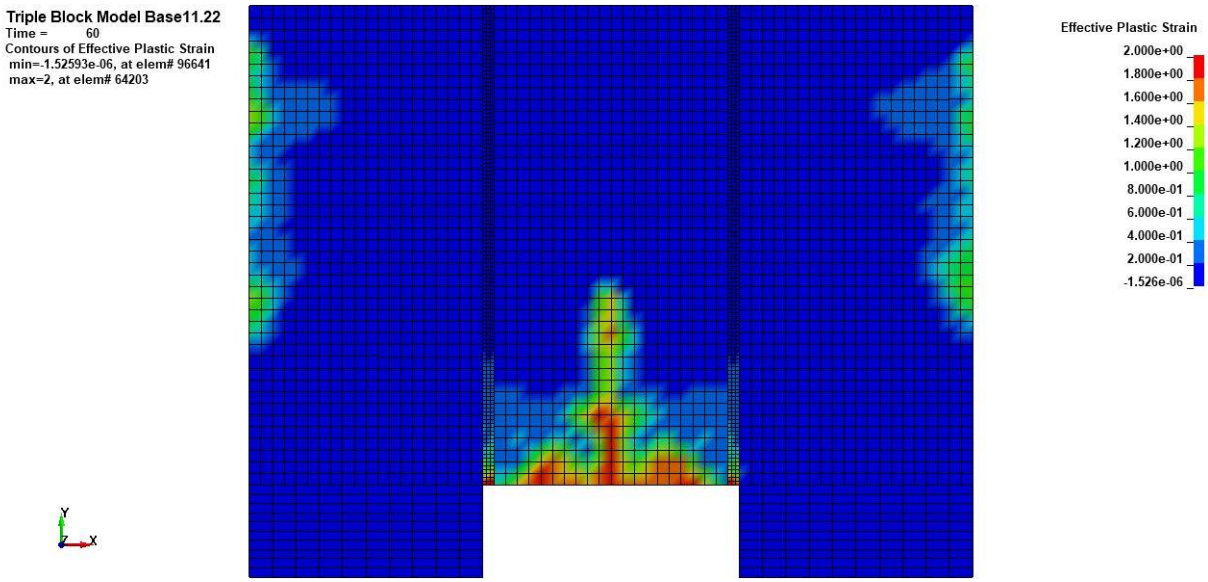


**Figure B-740: Effective Plastic Strain Fringe Plot for Last State at 60 Milliseconds for Base Run 11.22 – 1100 psi**

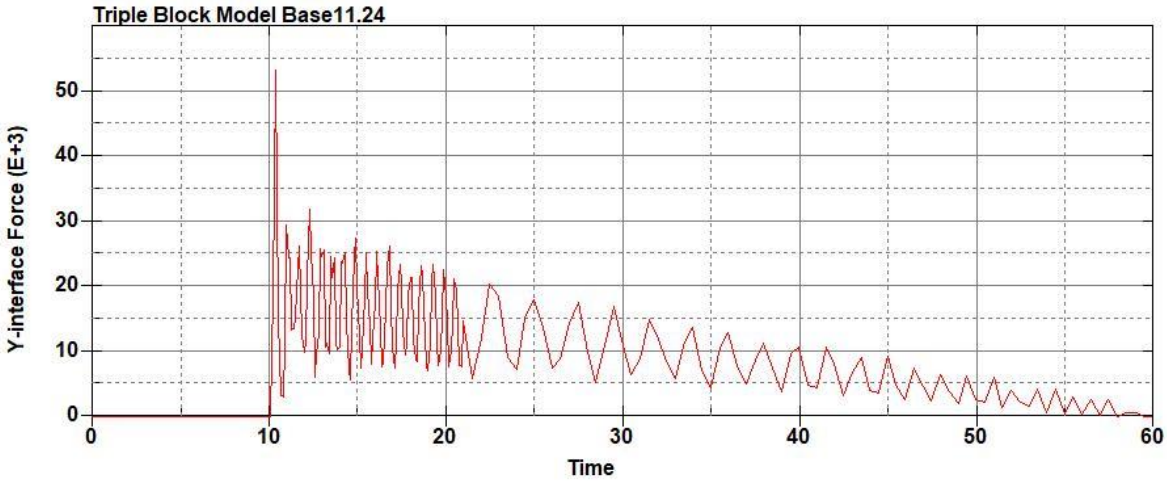


**Figure B-741: Base Run 11.24 Right Support Y-Interface Force (lbs) versus Time (ms) – 1200 psi**

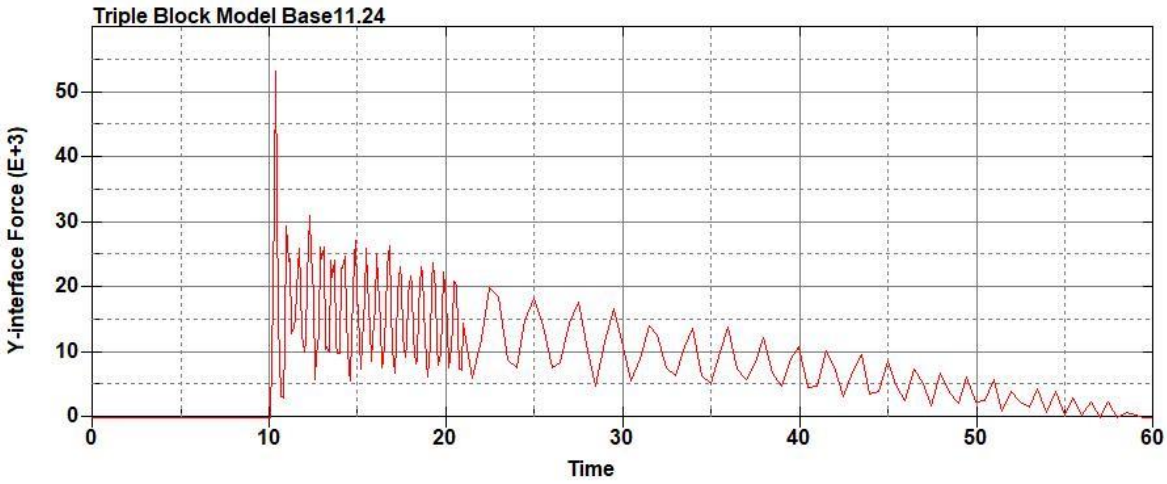


**Figure B-742: Base Run 11.24 Left Support Y-Interface Force (lbs) versus Time (ms) – 1200 psi**

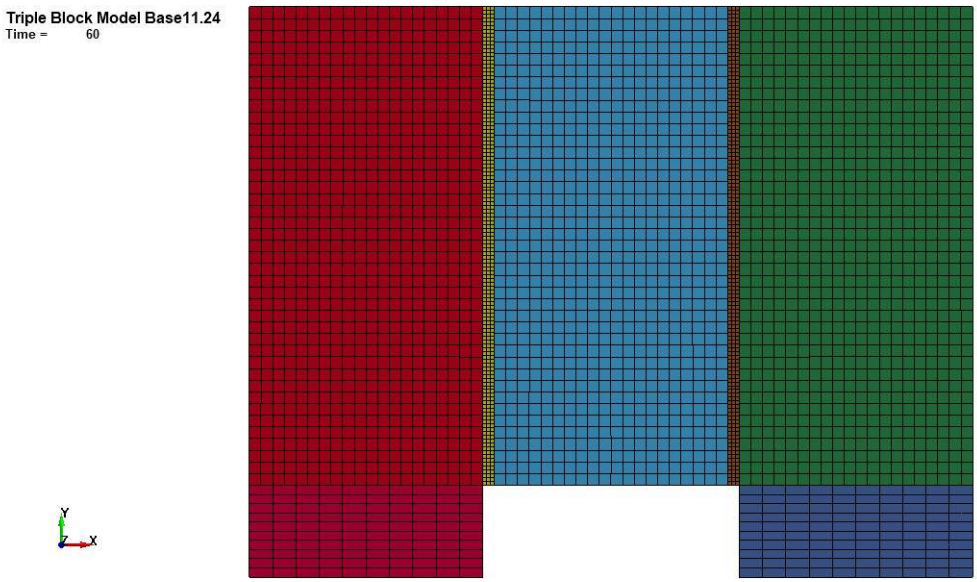


**Figure B-743: Last State at 60 Milliseconds for Base Run 11.24 – 1200 psi**

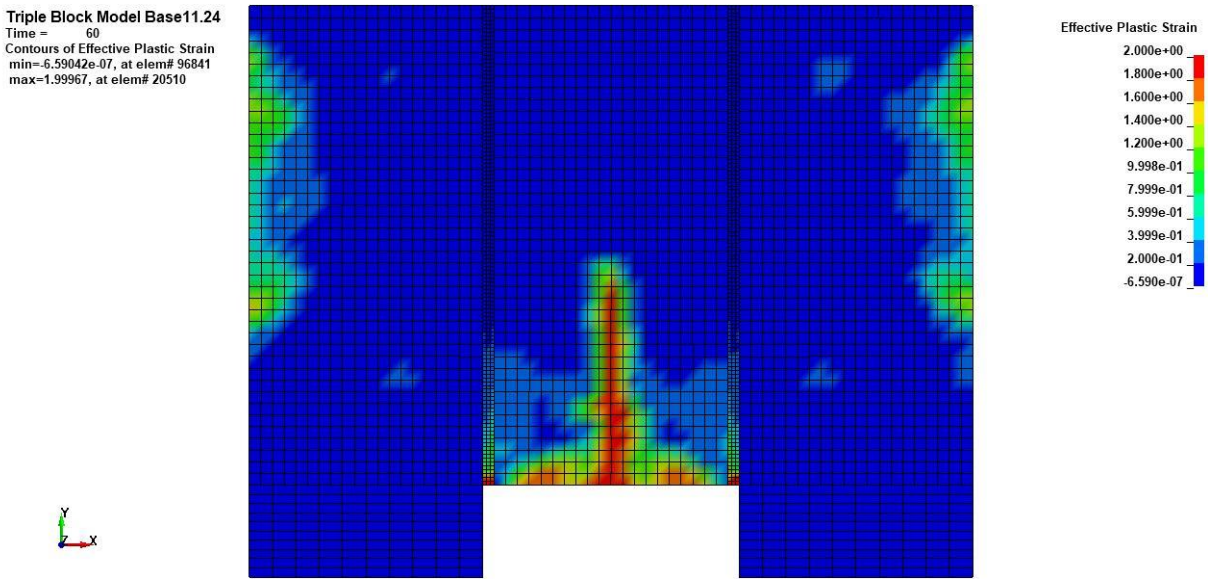


**Figure B-744: Effective Plastic Strain Fringe Plot for Last State at 60 Milliseconds for Base Run 11.24 – 1200 psi**

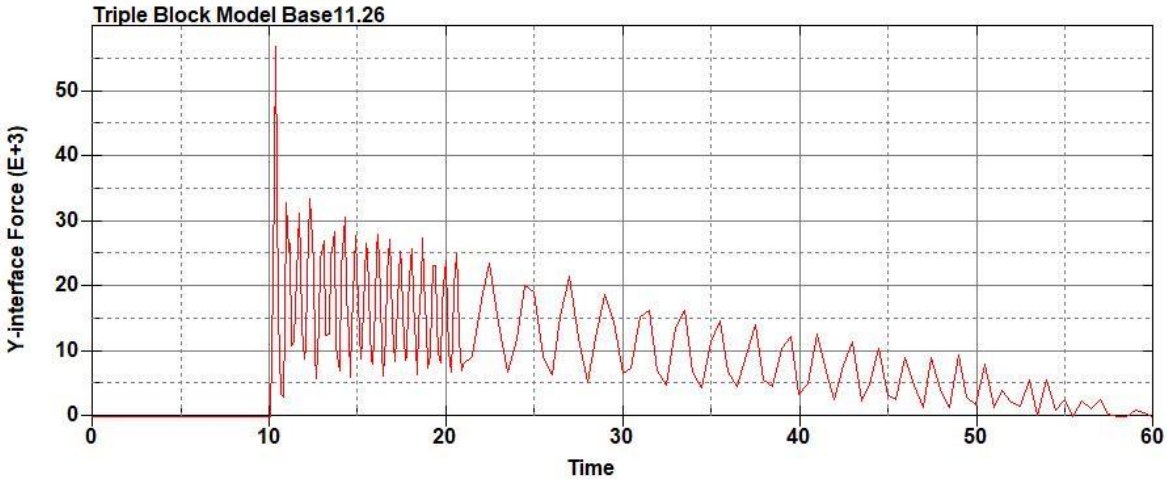


**Figure B-745: Base Run 11.26 Right Support Y-Interface Force (lbs) versus Time (ms) – 1300 psi**

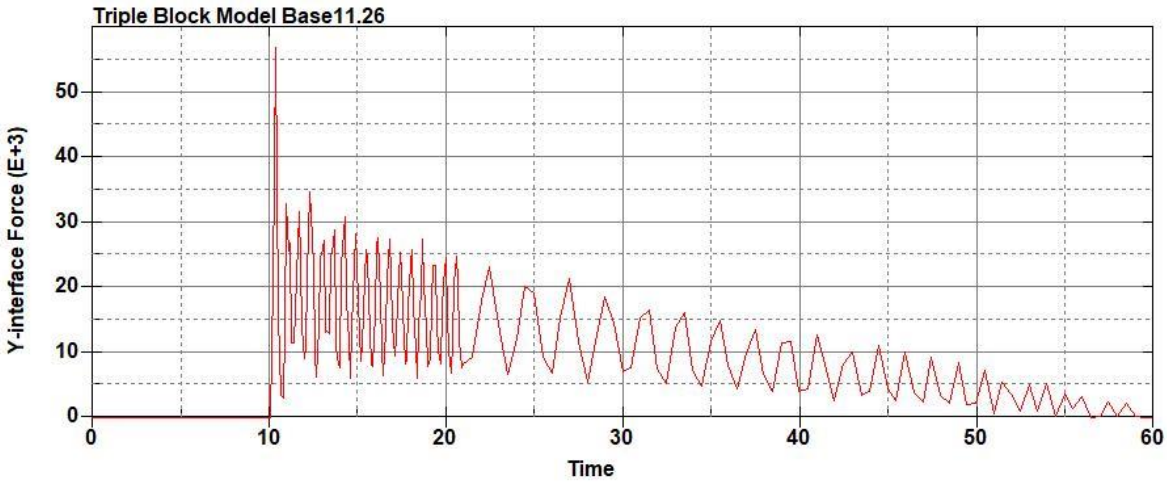


**Figure B-746: Base Run 11.26 Left Support Y-Interface Force (lbs) versus Time (ms) – 1300 psi**

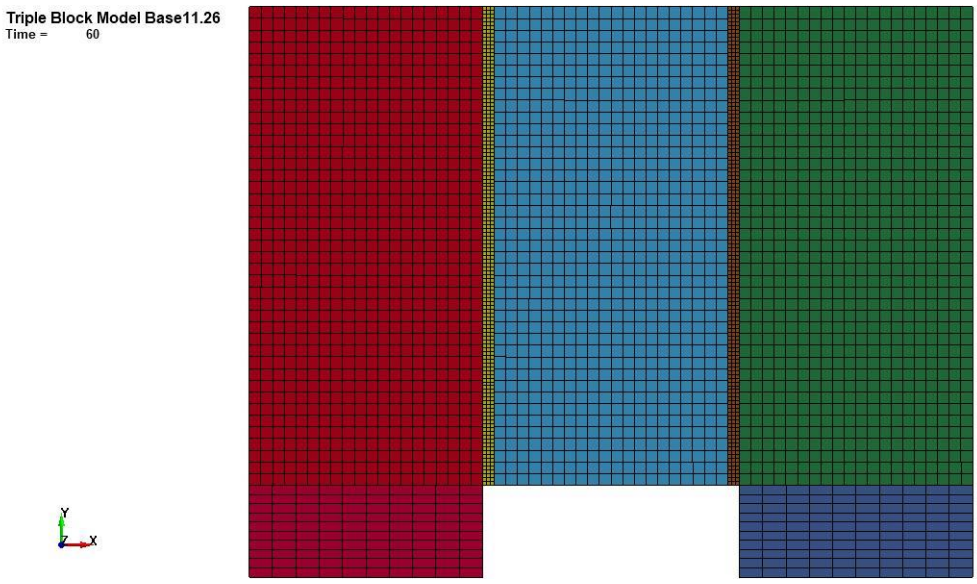


**Figure B-747: Last State at 60 Milliseconds for Base Run 11.26 – 1300 psi**

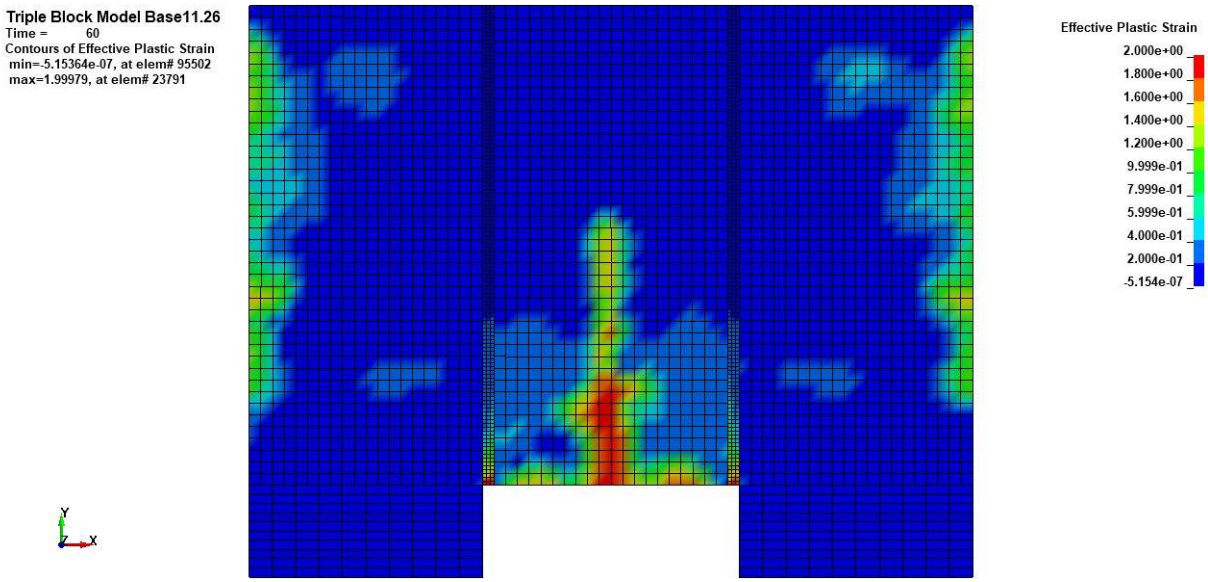


**Figure B-748: Effective Plastic Strain Fringe Plot for Last State at 60 Milliseconds for Base Run 11.26 – 1300 psi**

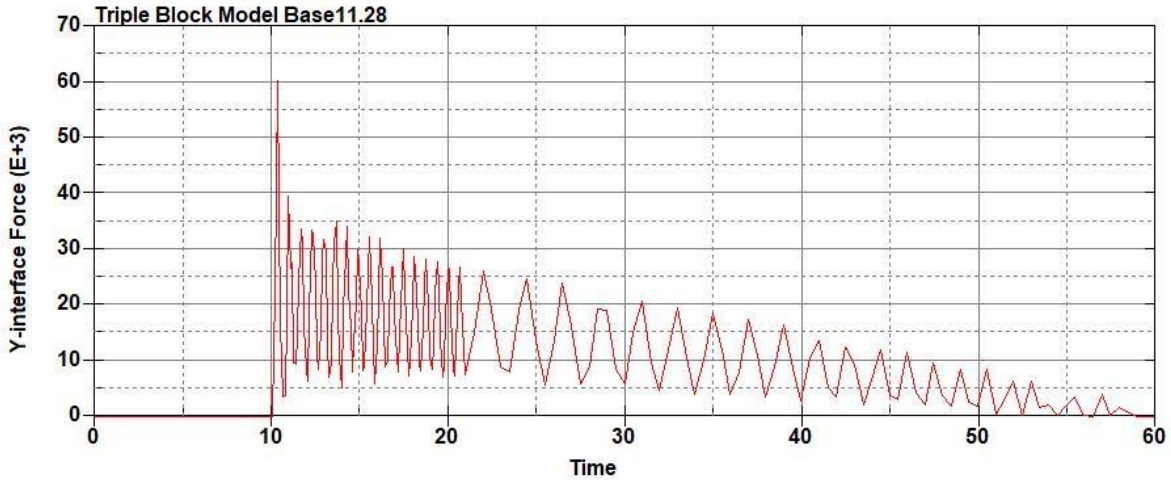


**Figure B-749: Base Run 11.28 Right Support Y-Interface Force (lbs) versus Time (ms) – 1400 psi**

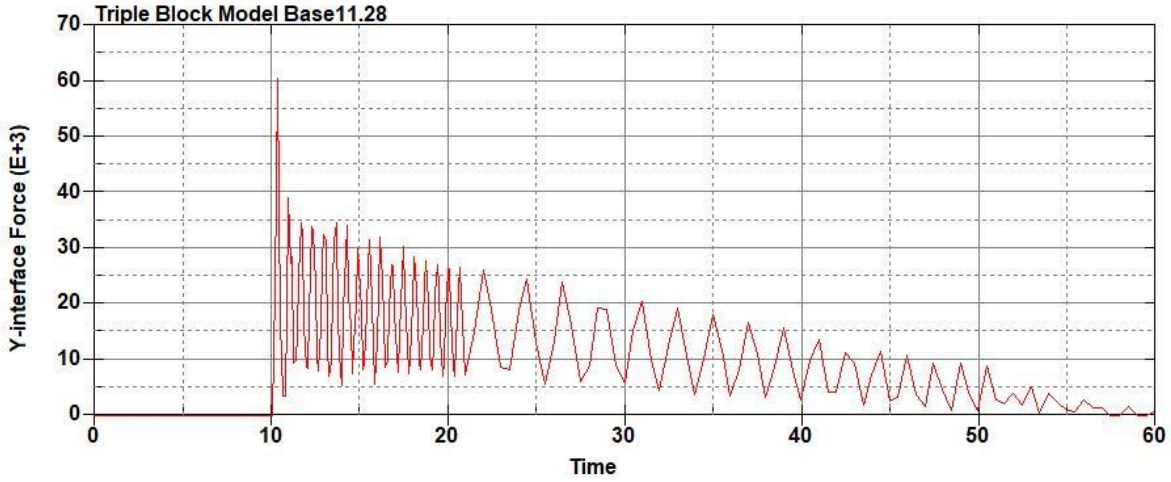


**Figure B-750: Base Run 11.28 Left Support Y-Interface Force (lbs) versus Time (ms) – 1400 psi**

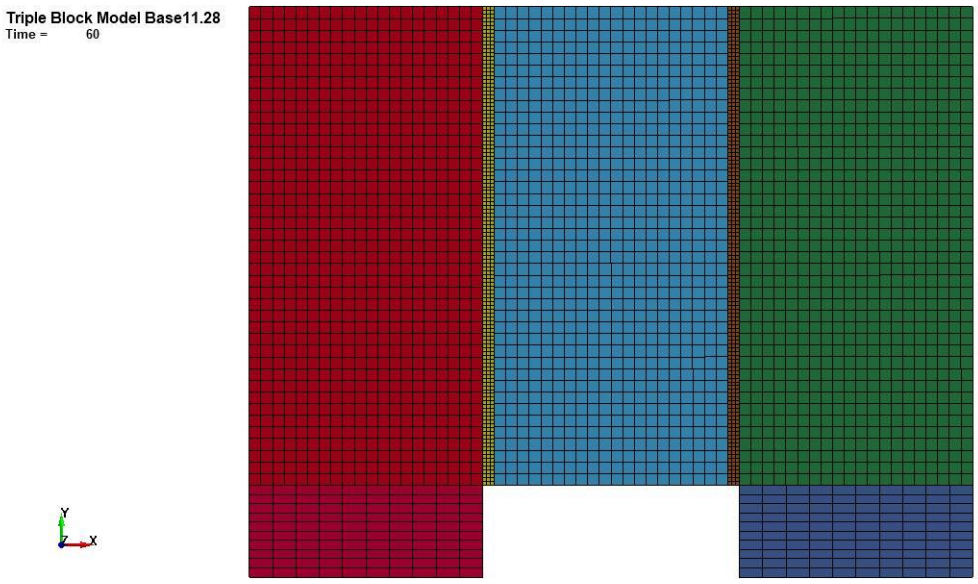


**Figure B-751: Last State at 60 Milliseconds for Base Run 11.28 – 1400 psi**

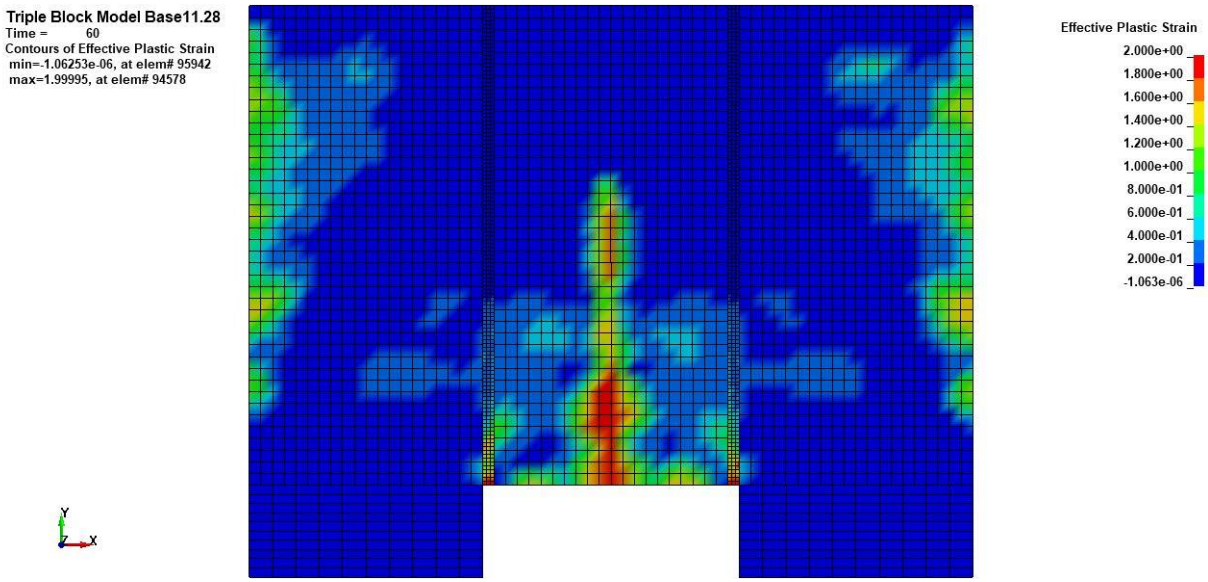


**Figure B-752: Effective Plastic Strain Fringe Plot for Last State at 60 Milliseconds for Base Run 11.28 – 1400 psi**

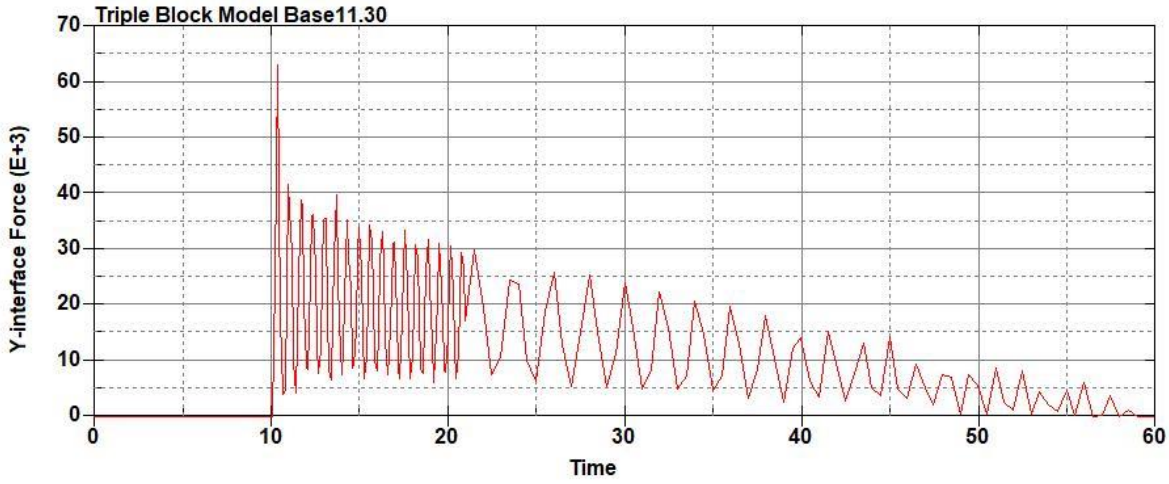


**Figure B-753: Base Run 11.30 Right Support Y-Interface Force (lbs) versus Time (ms) – 1500 psi**

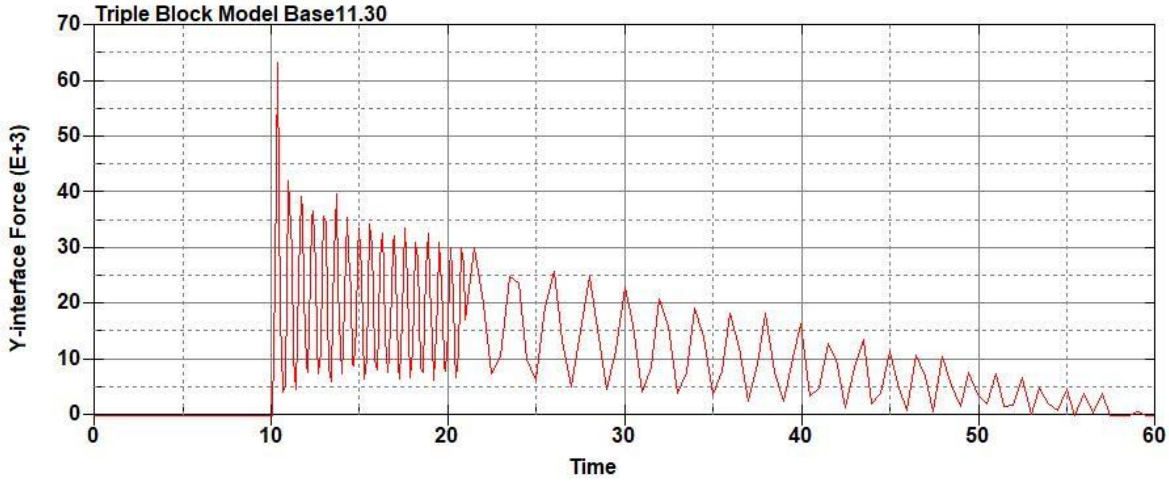


**Figure B-754: Base Run 11.30 Left Support Y-Interface Force (lbs) versus Time (ms) – 1500 psi**

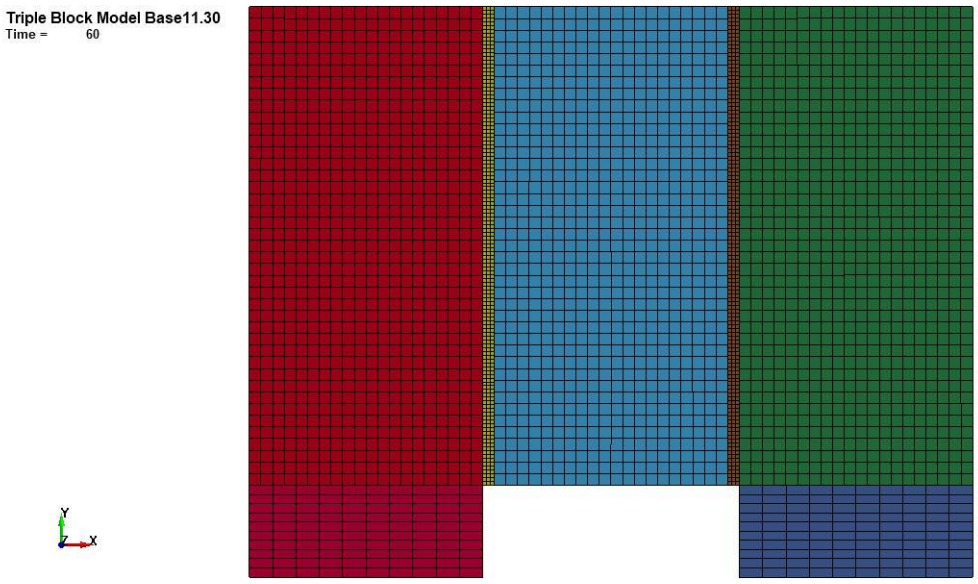


**Figure B-755: Last State at 60 Milliseconds for Base Run 11.30 – 1500 psi**

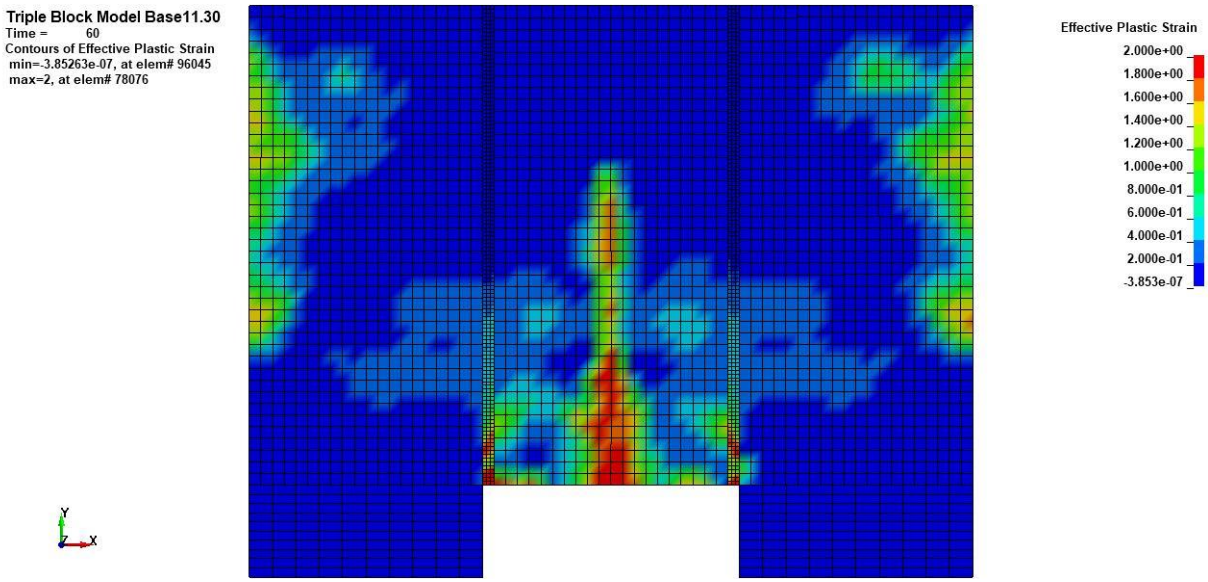


**Figure B-756: Effective Plastic Strain Fringe Plot for Last State at 60 Milliseconds for Base Run 11.30 – 1500 psi**

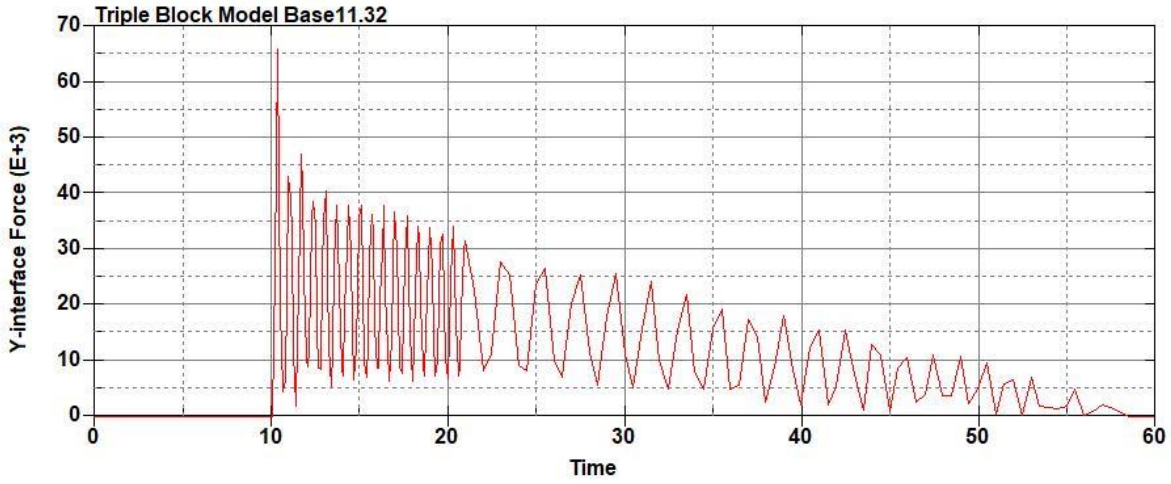


**Figure B-757: Base Run 11.32 Right Support Y-Interface Force (lbs) versus Time (ms) – 1600 psi**

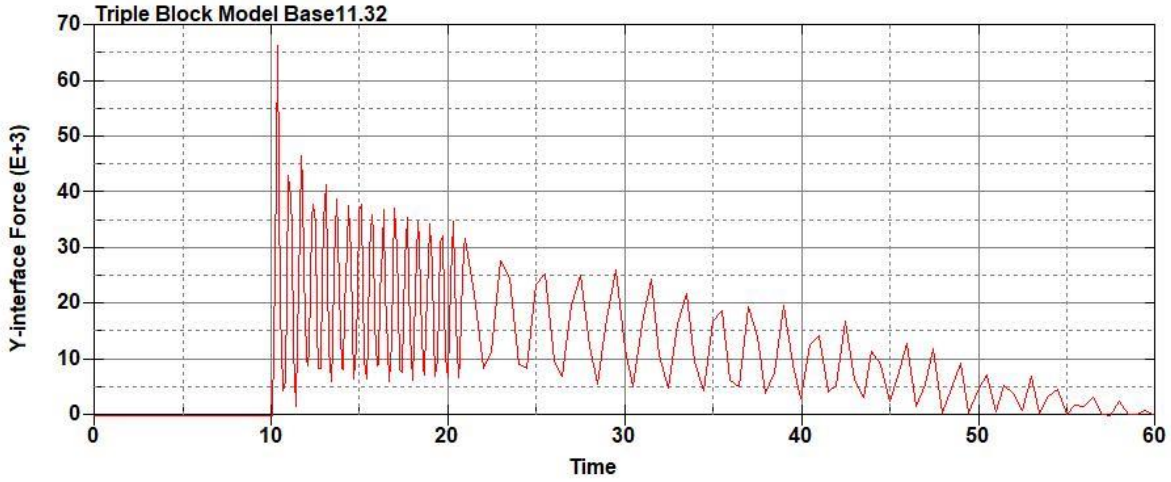


**Figure B-758: Base Run 11.32 Left Support Y-Interface Force (lbs) versus Time (ms) – 1600 psi**

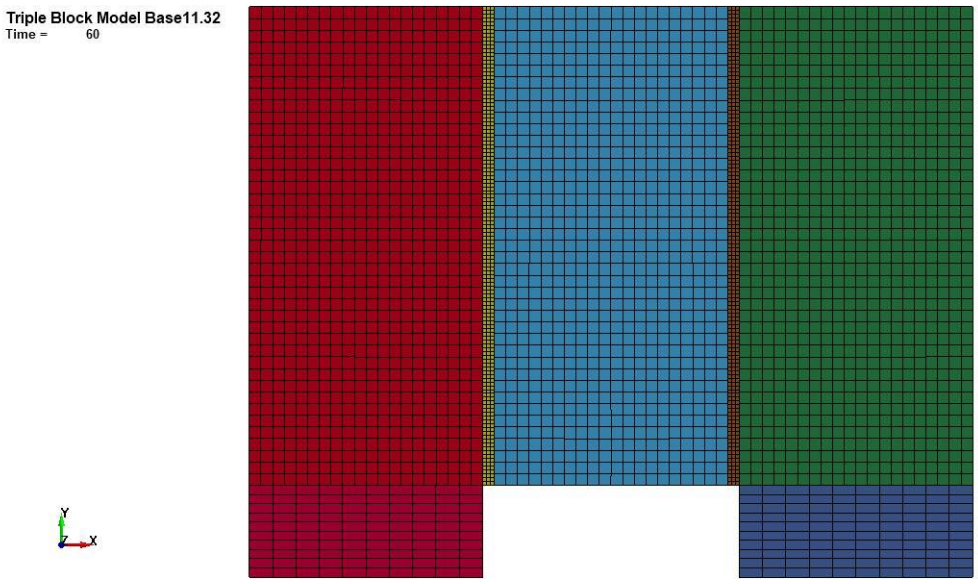


**Figure B-759: Last State at 60 Milliseconds for Base Run 11.32 – 1600 psi**

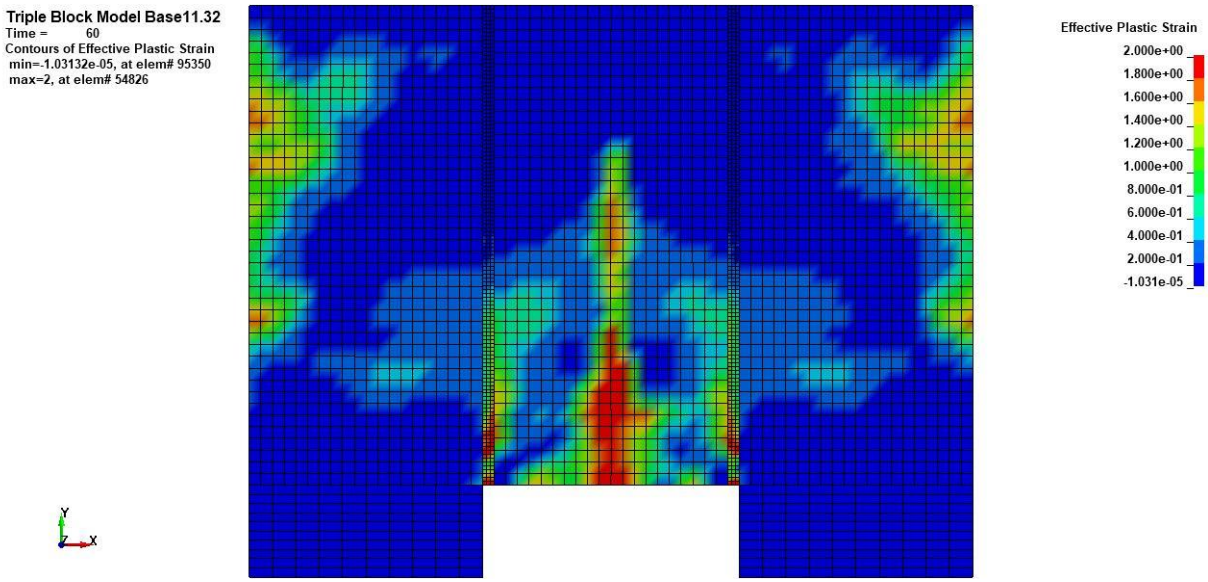


**Figure B-760: Effective Plastic Strain Fringe Plot for Last State at 60 Milliseconds for Base Run 11.32 – 1600 psi**

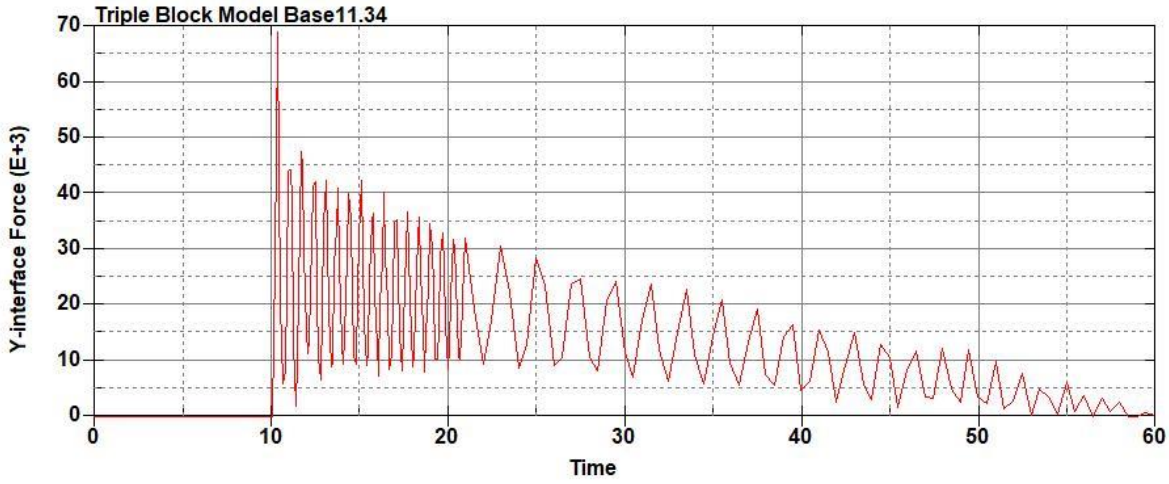


**Figure B-761: Base Run 11.34 Right Support Y-Interface Force (lbs) versus Time (ms) – 1700 psi**

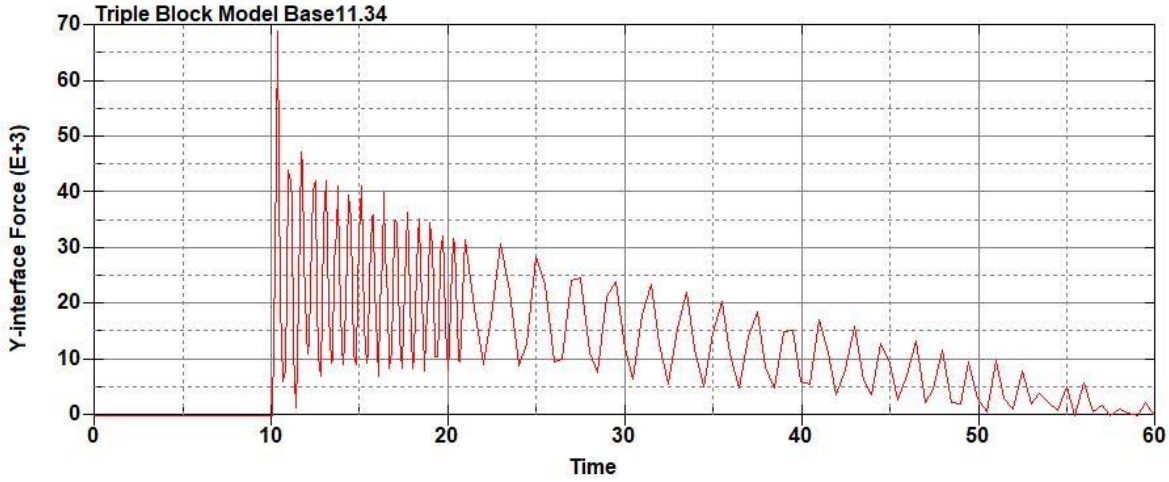


**Figure B-762: Base Run 11.34 Left Support Y-Interface Force (lbs) versus Time (ms) – 1700 psi**

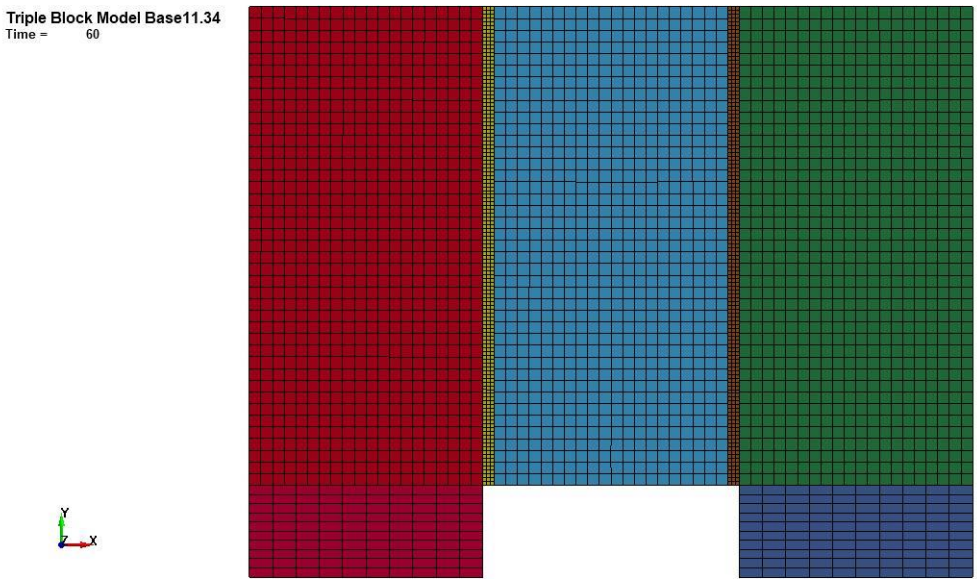


**Figure B-763: Last State at 60 Milliseconds for Base Run 11.34 – 1700 psi**

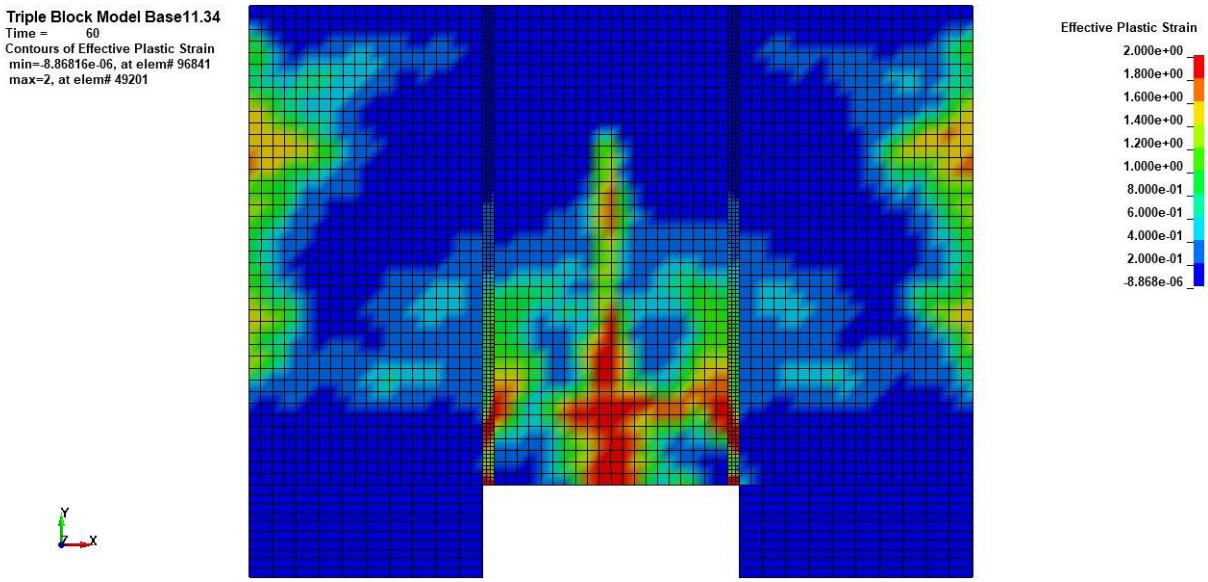


**Figure B-764: Effective Plastic Strain Fringe Plot for Last State at 60 Milliseconds for Base Run 11.34 – 1700 psi**

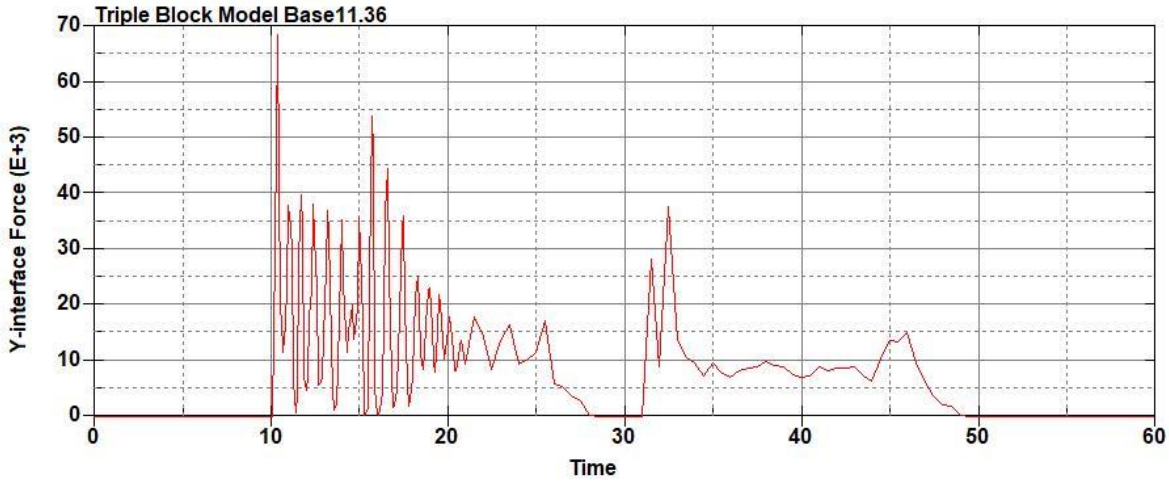


**Figure B-765: Base Run 11.36 Right Support Y-Interface Force (lbs) versus Time (ms) – 1800 psi**

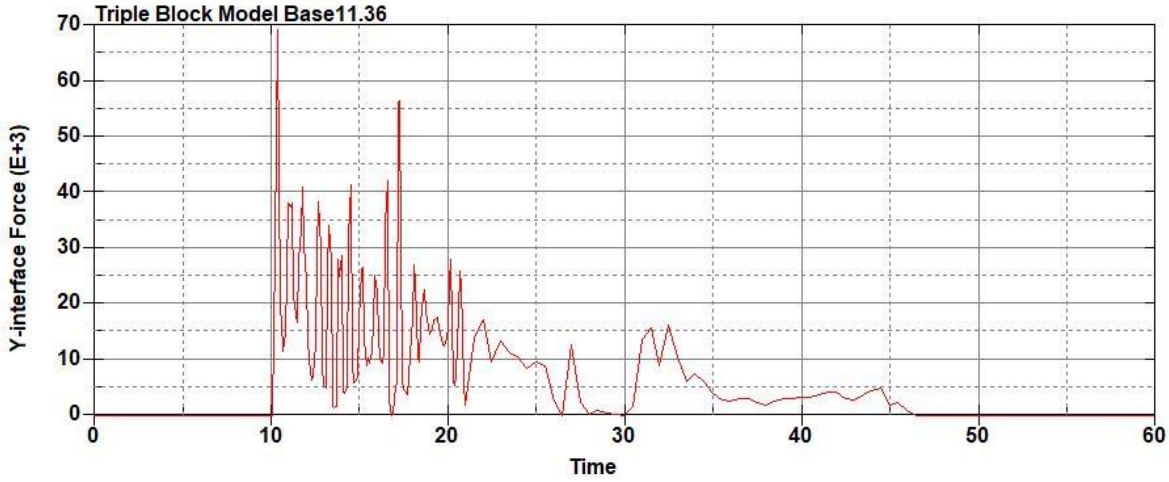


**Figure B-766: Base Run 11.36 Left Support Y-Interface Force (lbs) versus Time (ms) – 1800 psi**

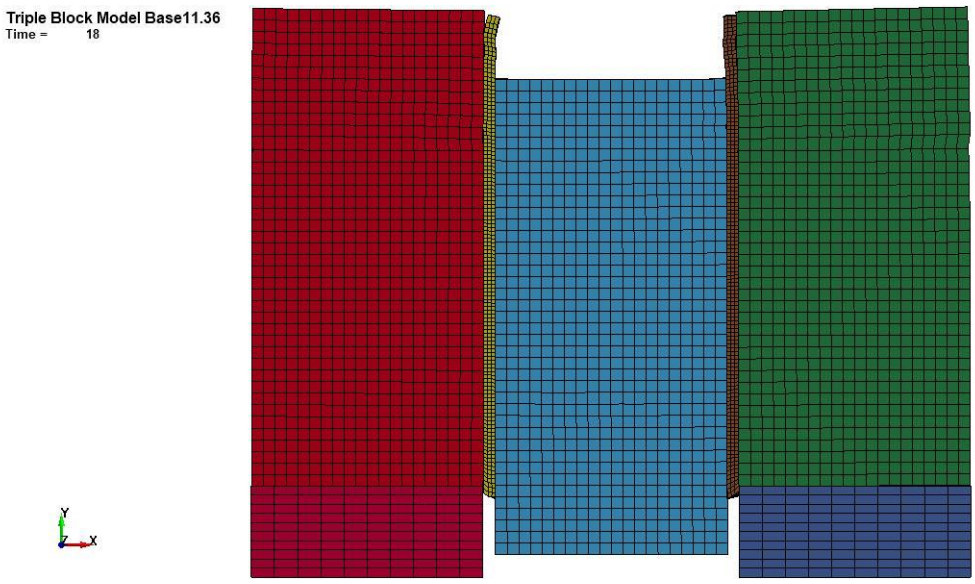


**Figure B-767: Last State at 18 Milliseconds for Base Run 11.36 – 1800 psi**

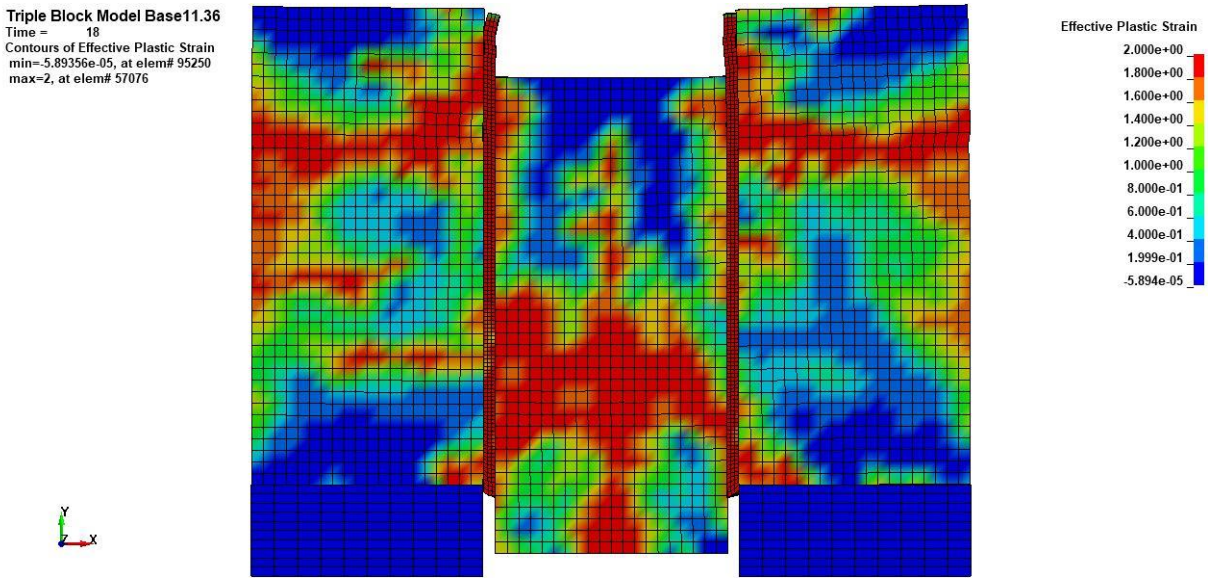


**Figure B-768: Effective Plastic Strain Fringe Plot for Last State at 18 Milliseconds for Base Run 11.36 – 1800 psi**

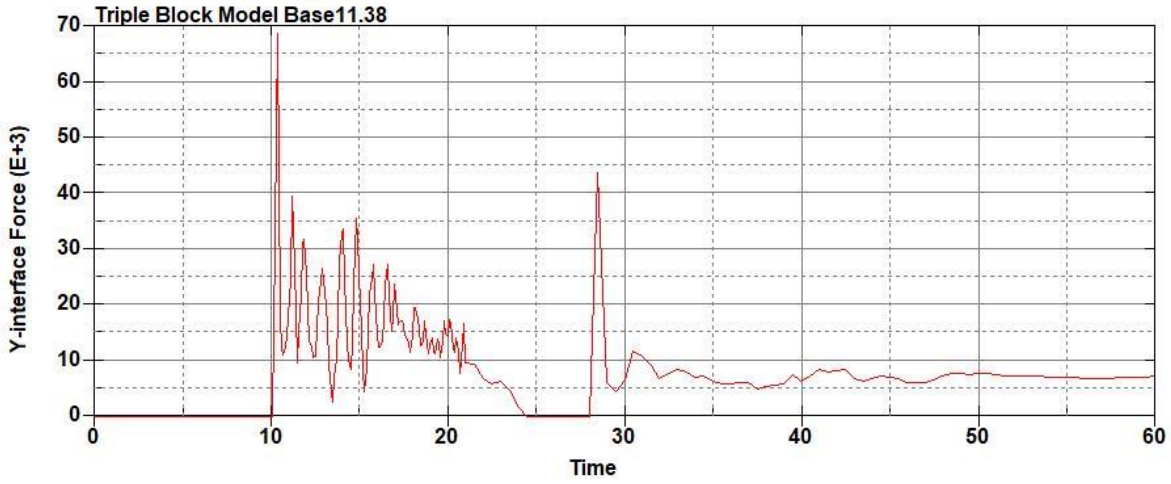


**Figure B-769: Base Run 11.38 Right Support Y-Interface Force (lbs) versus Time (ms) – 1900 psi**

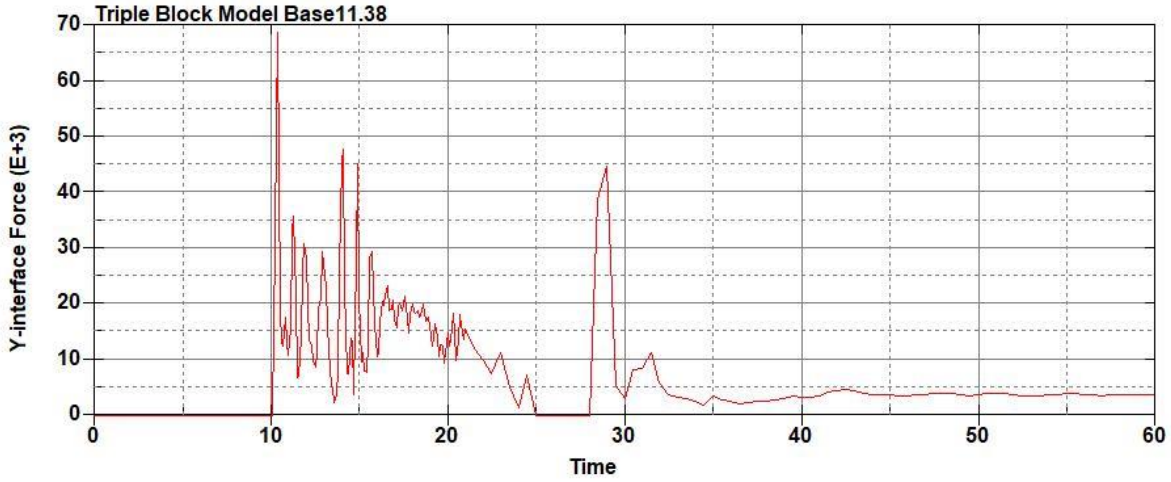


**Figure B-770: Base Run 11.38 Left Support Y-Interface Force (lbs) versus Time (ms) – 1900 psi**


**Figure B-771: Last State at 18 Milliseconds for Base Run 11.38 – 1900 psi**

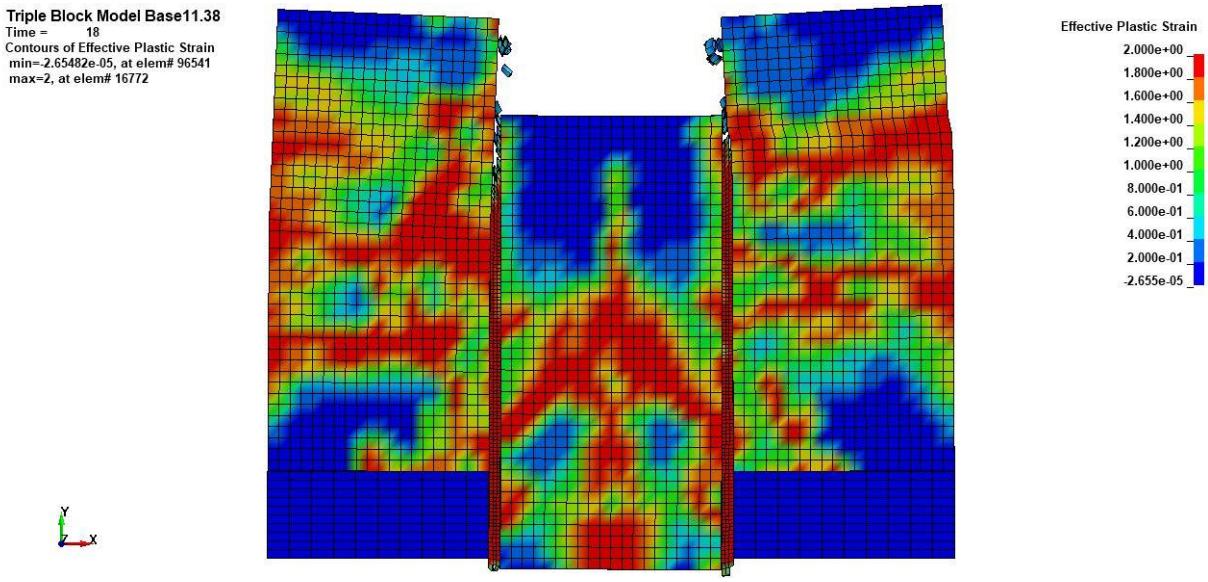


**Figure B-772: Effective Plastic Strain Fringe Plot for Last State at 18 Milliseconds for Base Run 11.38 – 1900 psi**

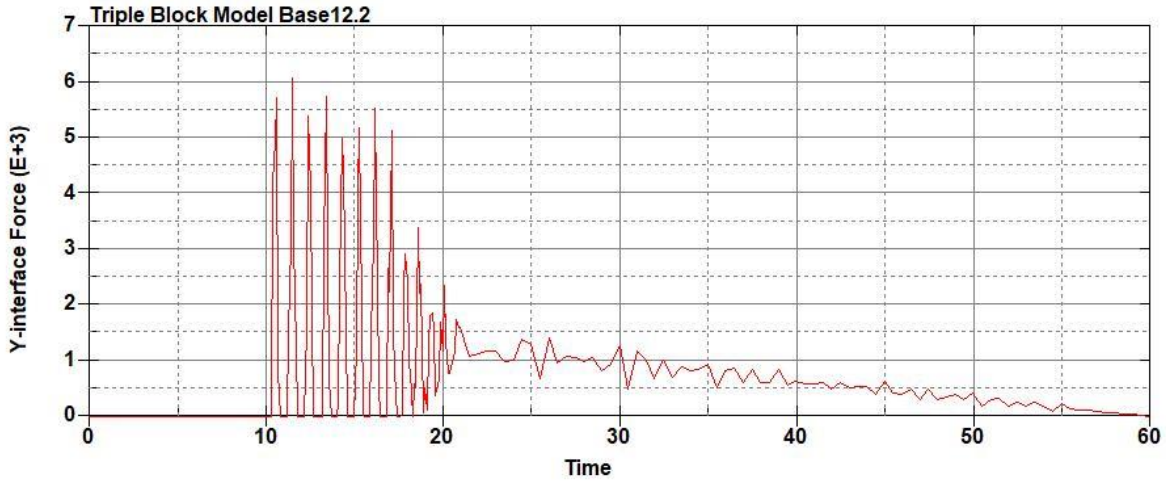


**Figure B-773: Base Run 12.2 Right Support Y-Interface Force (lbs) versus Time (ms) – 100 psi**

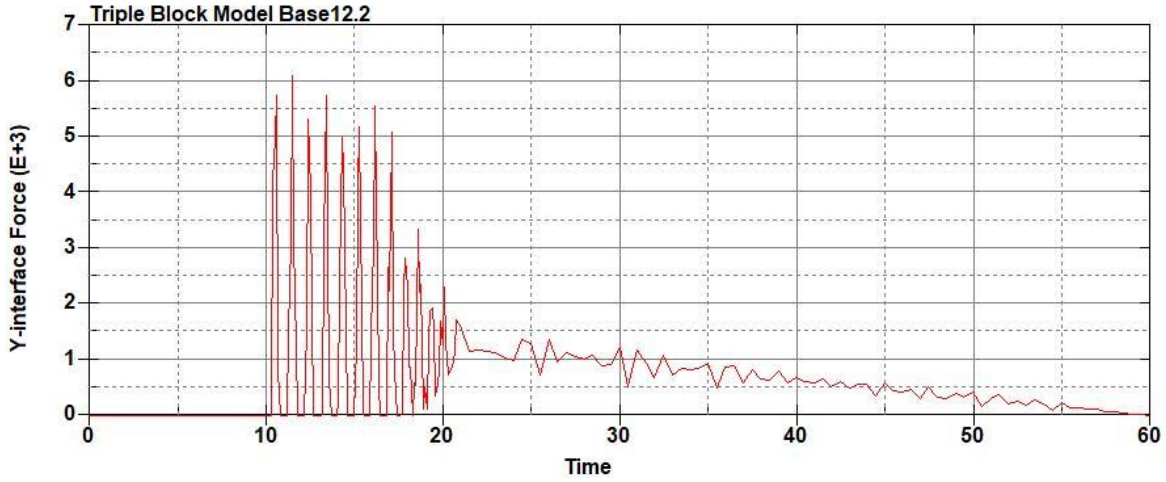


**Figure B-774: Base Run 12.2 Left Support Y-Interface Force (lbs) versus Time (ms) – 100 psi**

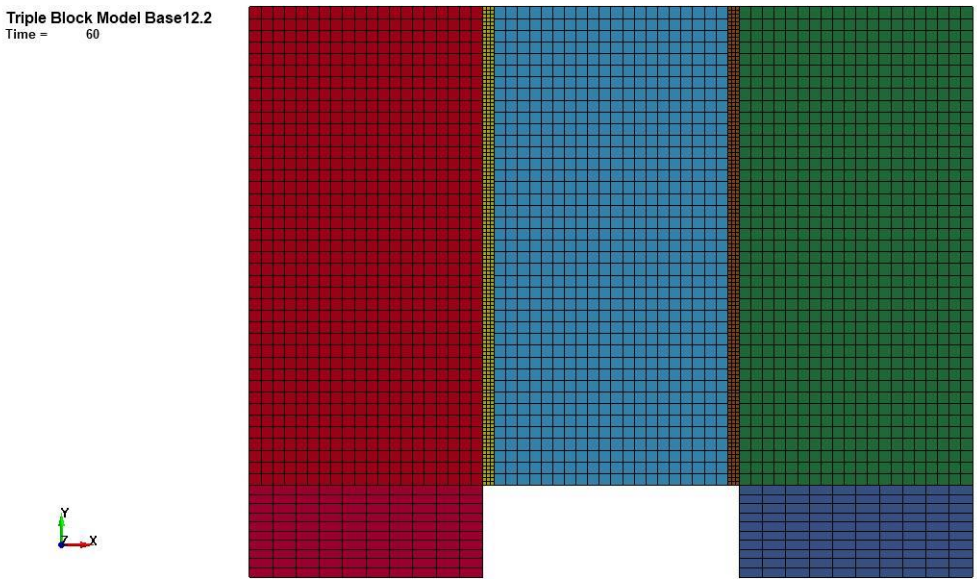


**Figure B-775: Last State at 60 Milliseconds for Base Run 12.2 – 100 psi**

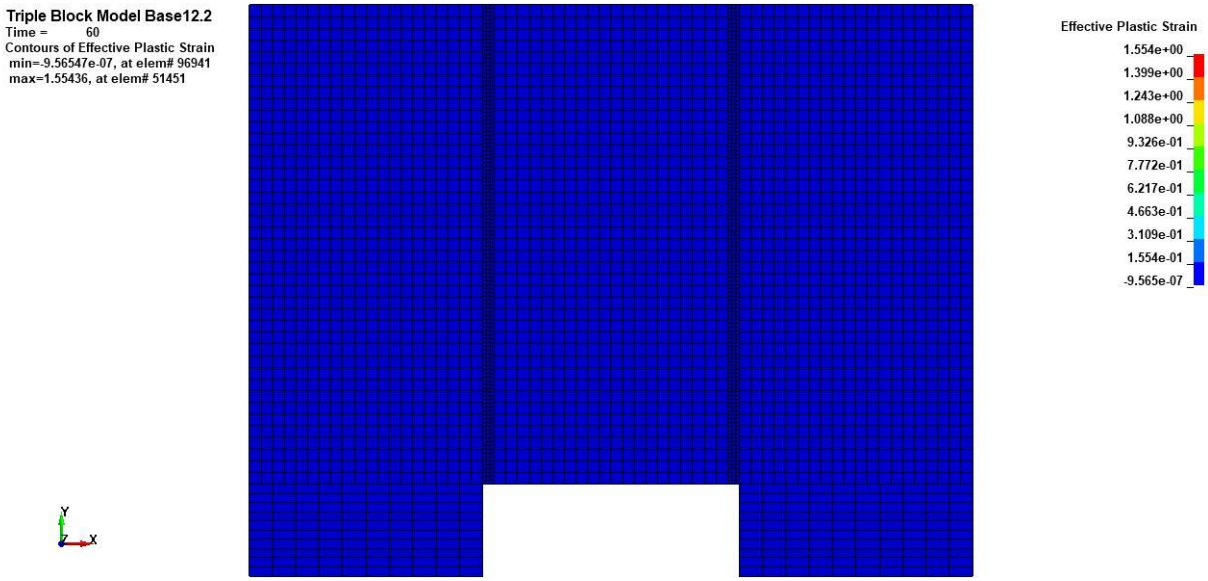


**Figure B-776: Effective Plastic Strain Fringe Plot for Last State at 60 Milliseconds for Base Run 12.2– 100 psi**

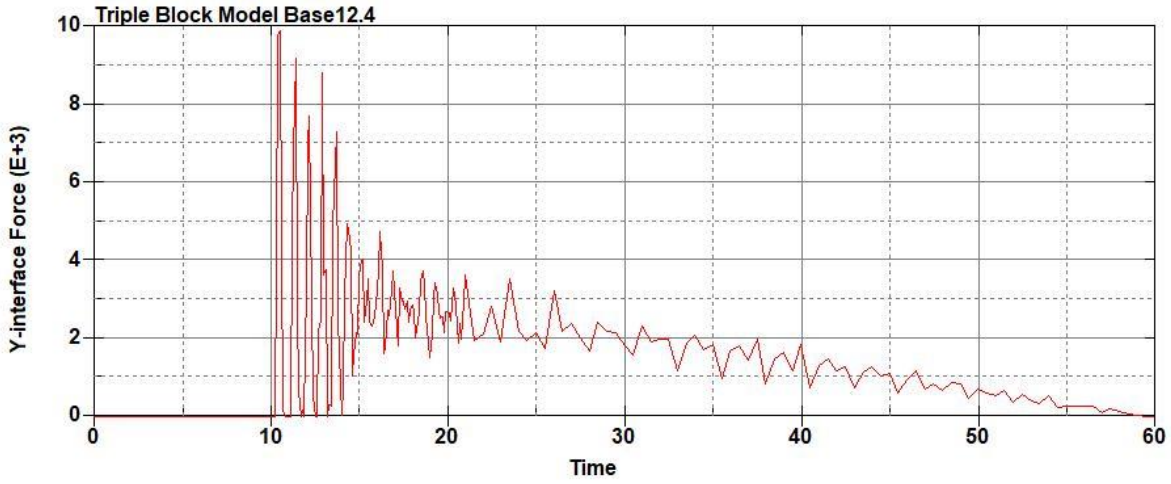


**Figure B-777: Base Run 12.4 Right Support Y-Interface Force (lbs) versus Time (ms) – 200 psi**

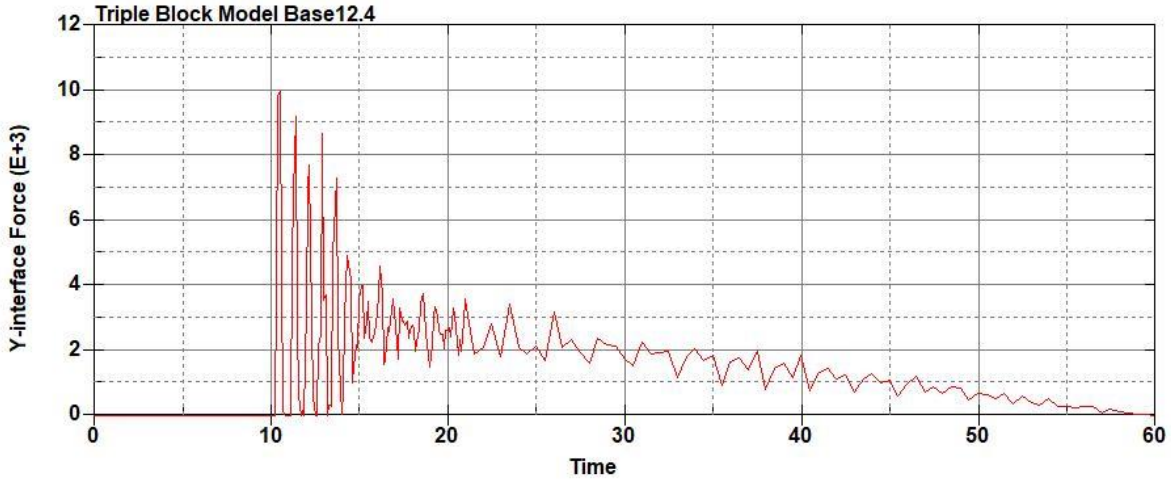


**Figure B-778: Base Run 12.4 Left Support Y-Interface Force (lbs) versus Time (ms) – 200 psi**

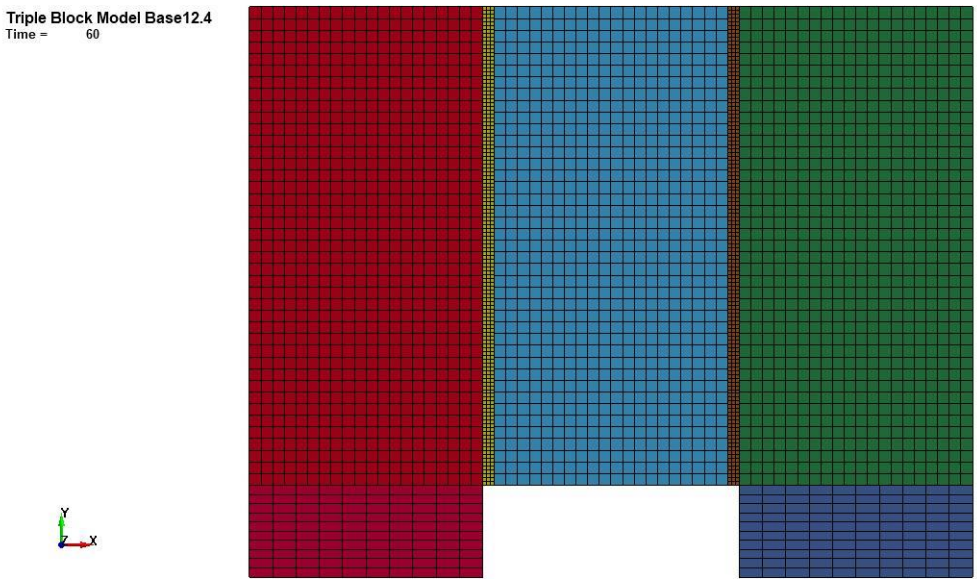


**Figure B-779: Last State at 60 Milliseconds for Base Run 12.4 – 200 psi**

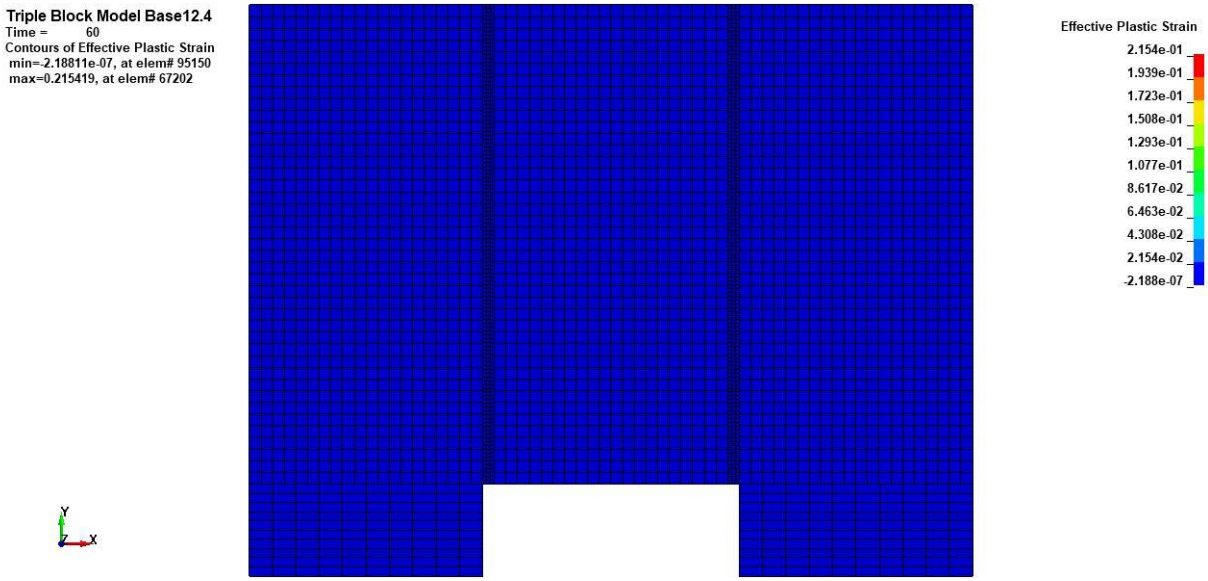


**Figure B-780: Effective Plastic Strain Fringe Plot for Last State at 60 Milliseconds for Base Run 12.4 – 200 psi**

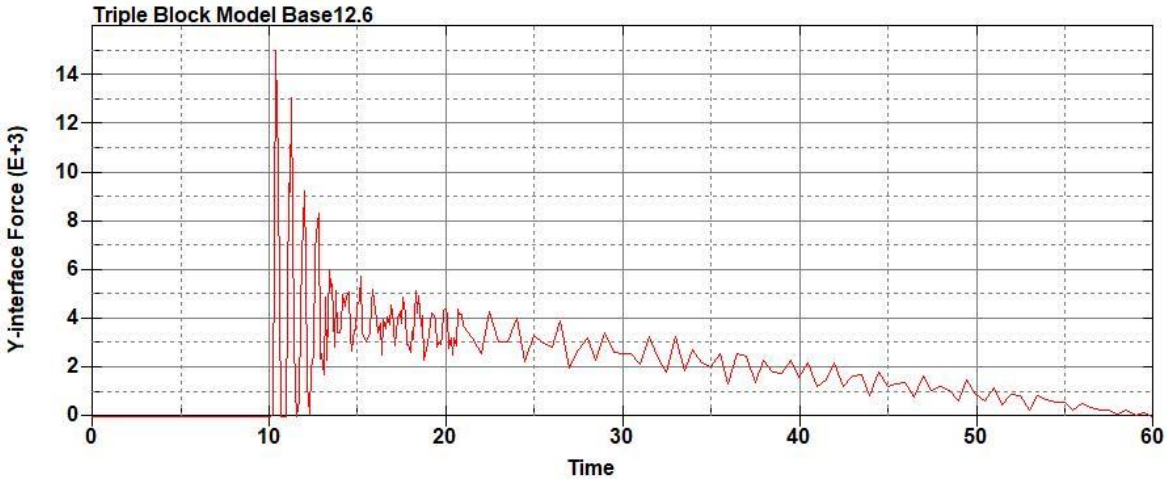


**Figure B-781: Base Run 12.6 Right Support Y-Interface Force (lbs) versus Time (ms) – 300 psi**

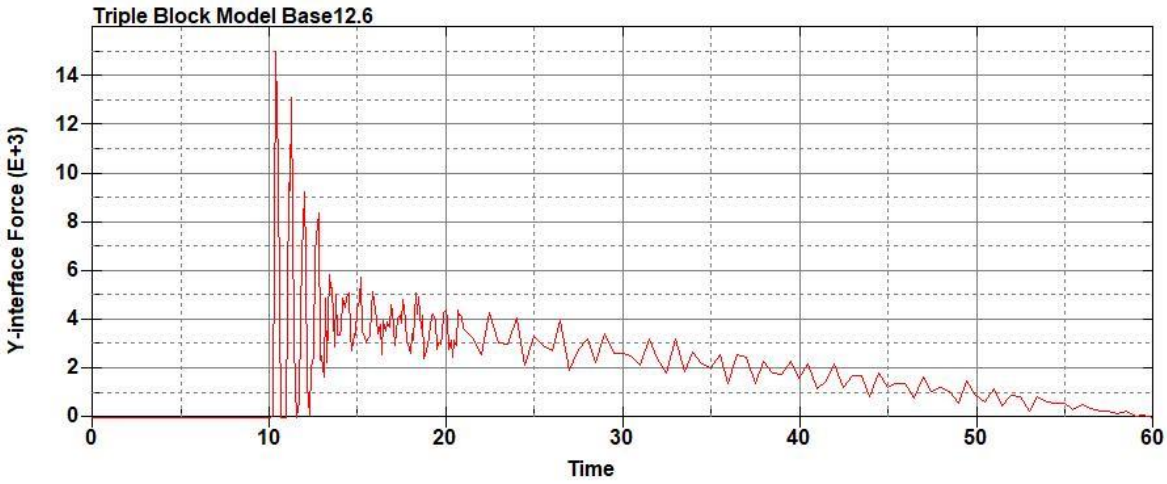


**Figure B-782: Base Run 12.6 Left Support Y-Interface Force (lbs) versus Time (ms) – 300 psi**

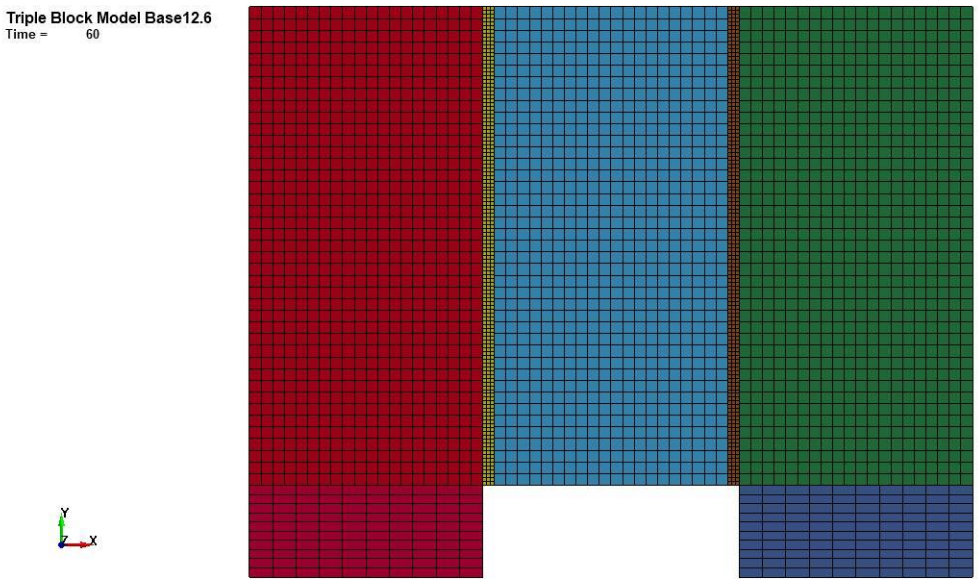


**Figure B-783: Last State at 60 Milliseconds for Base Run 12.6 – 300 psi**

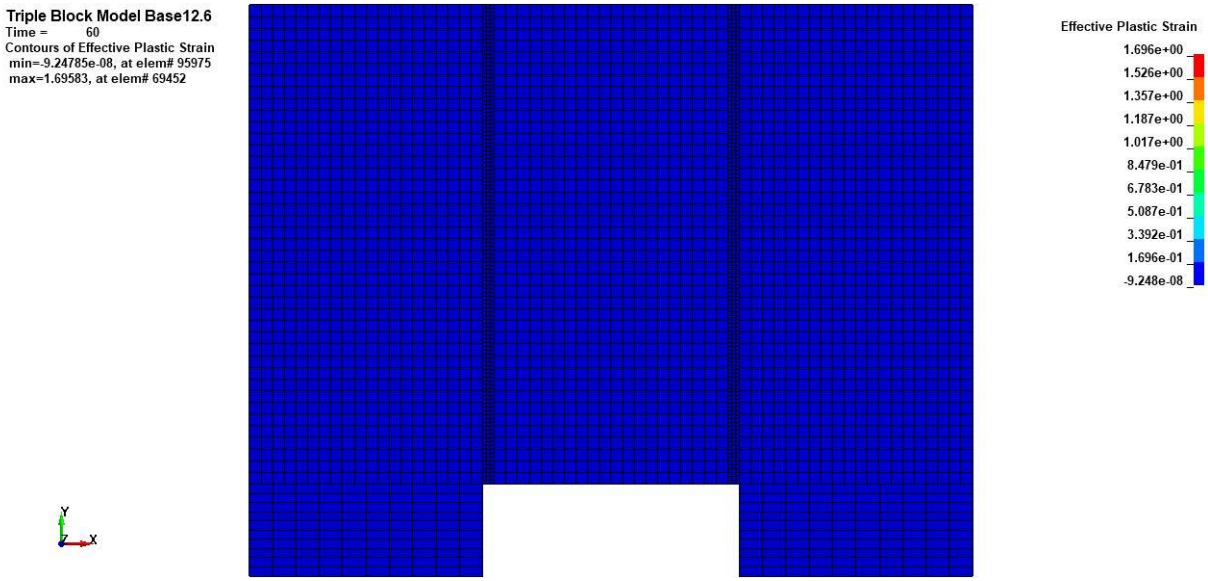


**Figure B-784: Effective Plastic Strain Fringe Plot for Last State at 60 Milliseconds for Base Run 12.6 – 300 psi**

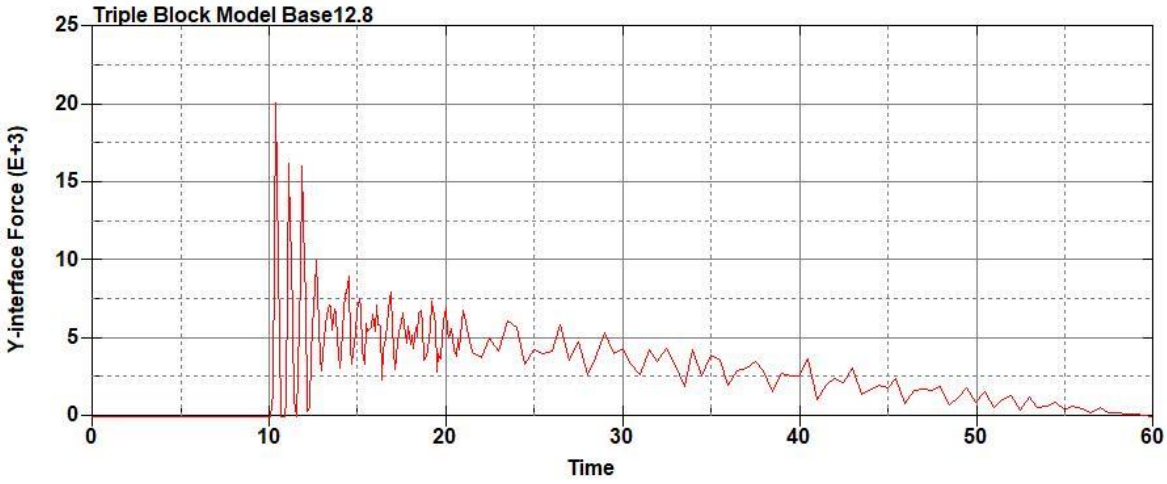


**Figure B-785: Base Run 12.8 Right Support Y-Interface Force (lbs) versus Time (ms) – 400 psi**

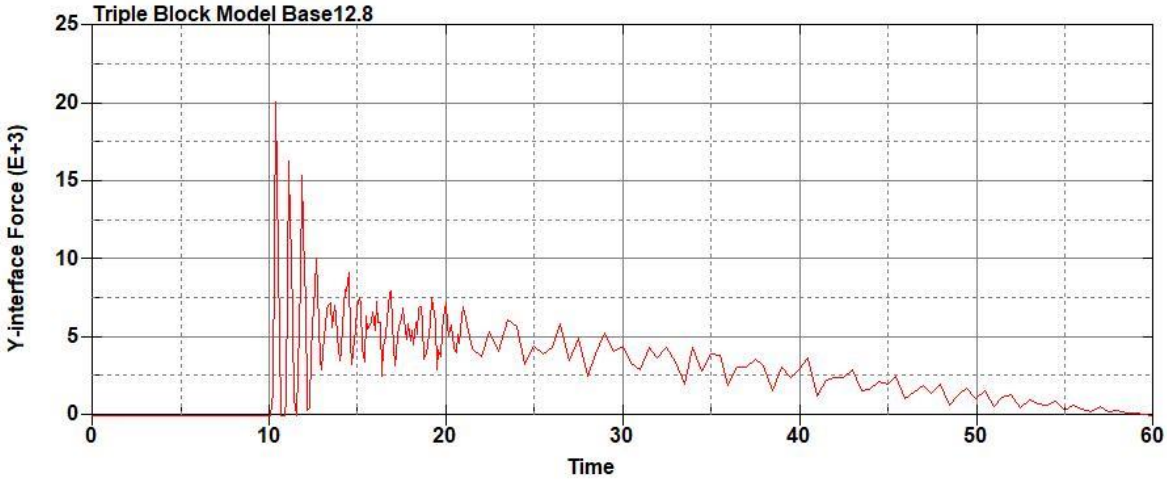


**Figure B-786: Base Run 12.8 Left Support Y-Interface Force (lbs) versus Time (ms) – 400 psi**

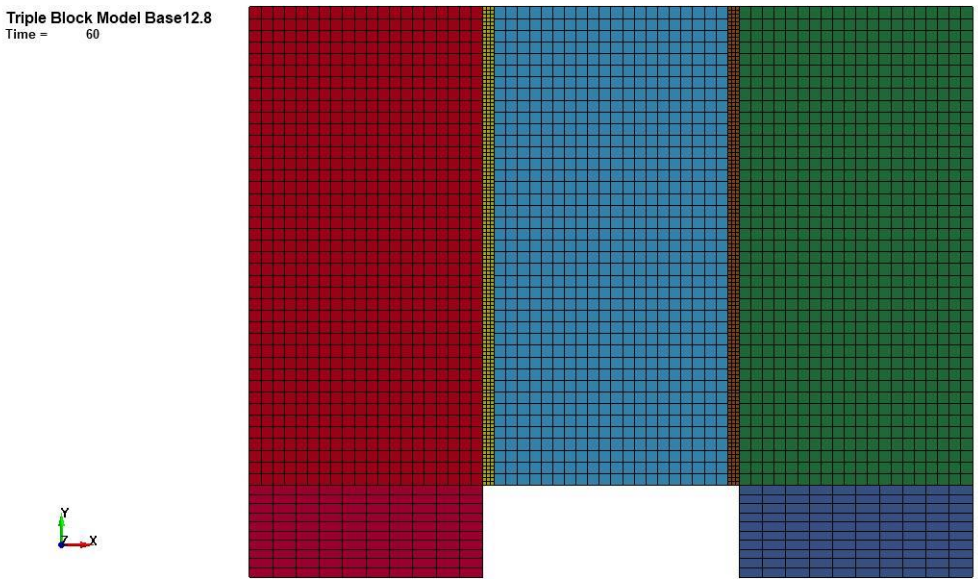


**Figure B-787: Last State at 60 Milliseconds for Base Run 12.8 – 400 psi**

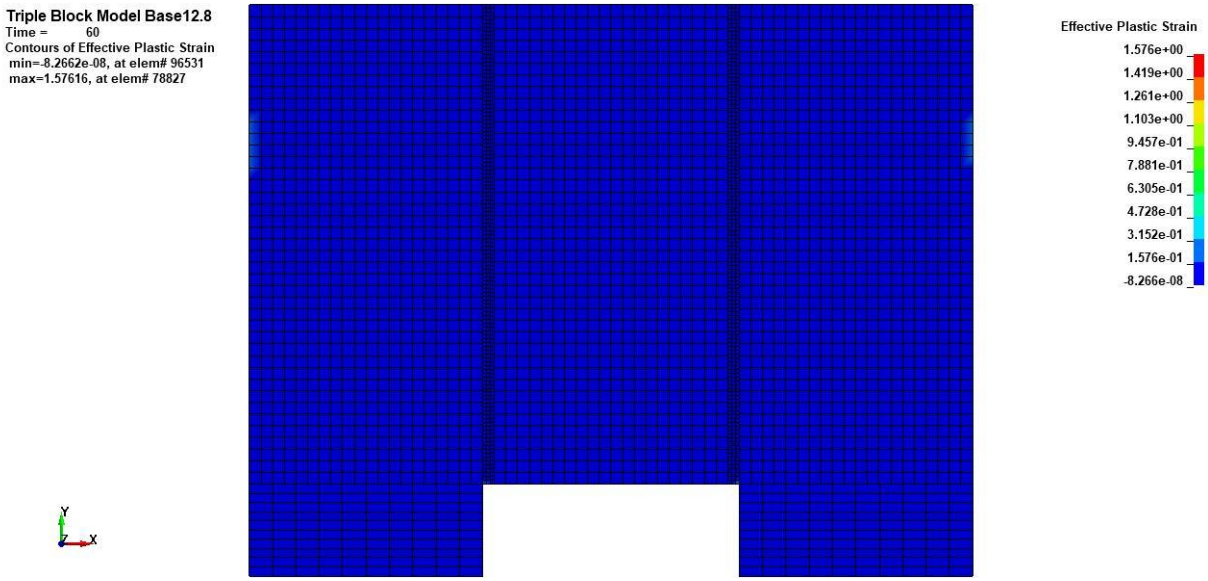


**Figure B-788: Effective Plastic Strain Fringe Plot for Last State at 60 Milliseconds for Base Run 12.8 – 400 psi**

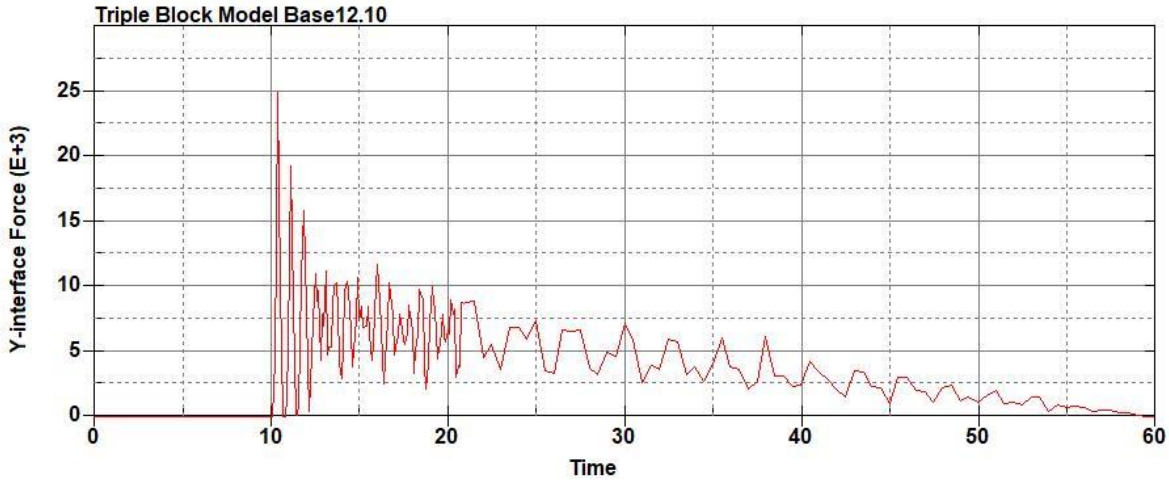


**Figure B-789: Base Run 12.10 Right Support Y-Interface Force (lbs) versus Time (ms) – 500 psi**

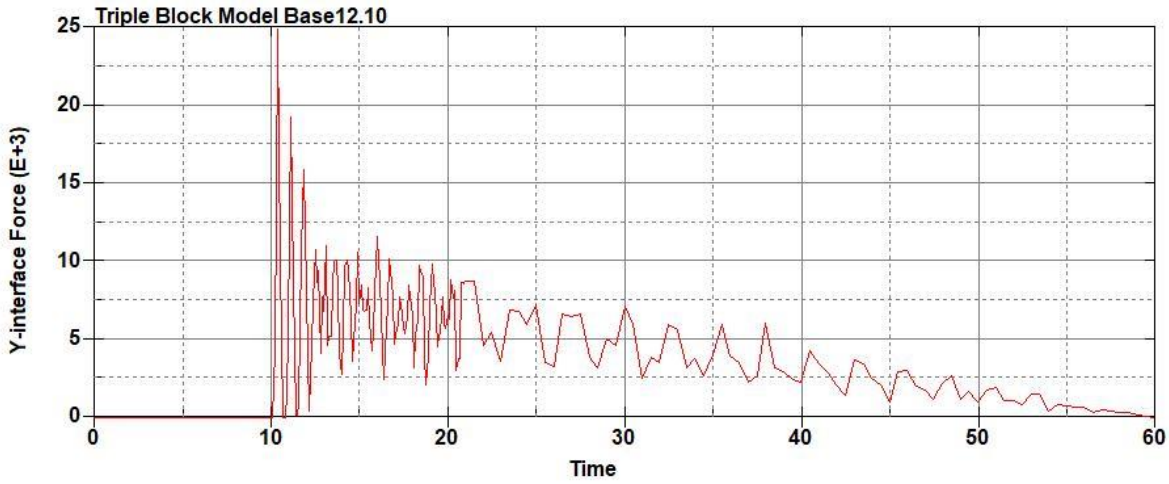


**Figure B-790: Base Run 12.10 Left Support Y-Interface Force (lbs) versus Time (ms) – 500 psi**

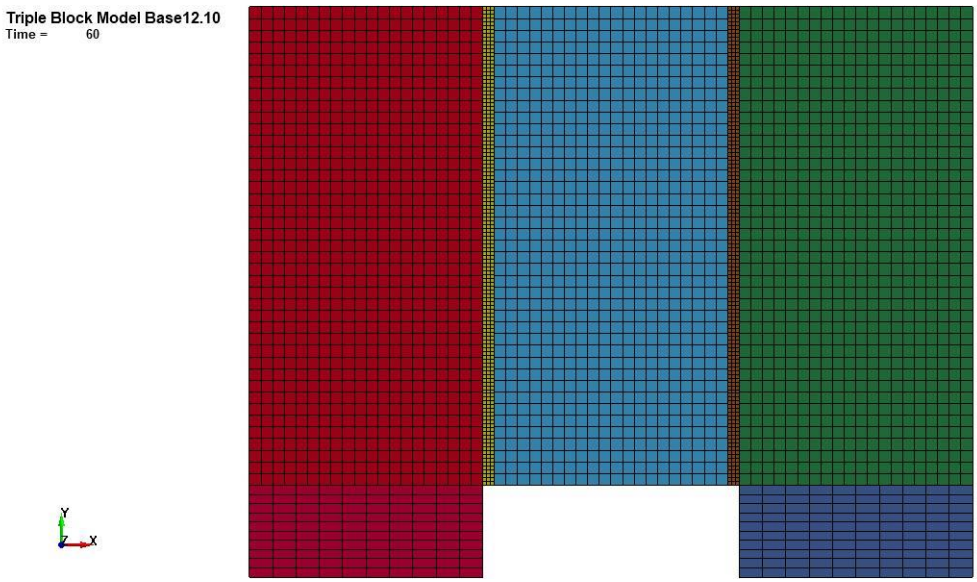


**Figure B-791: Last State at 60 Milliseconds for Base Run 12.10 – 500 psi**

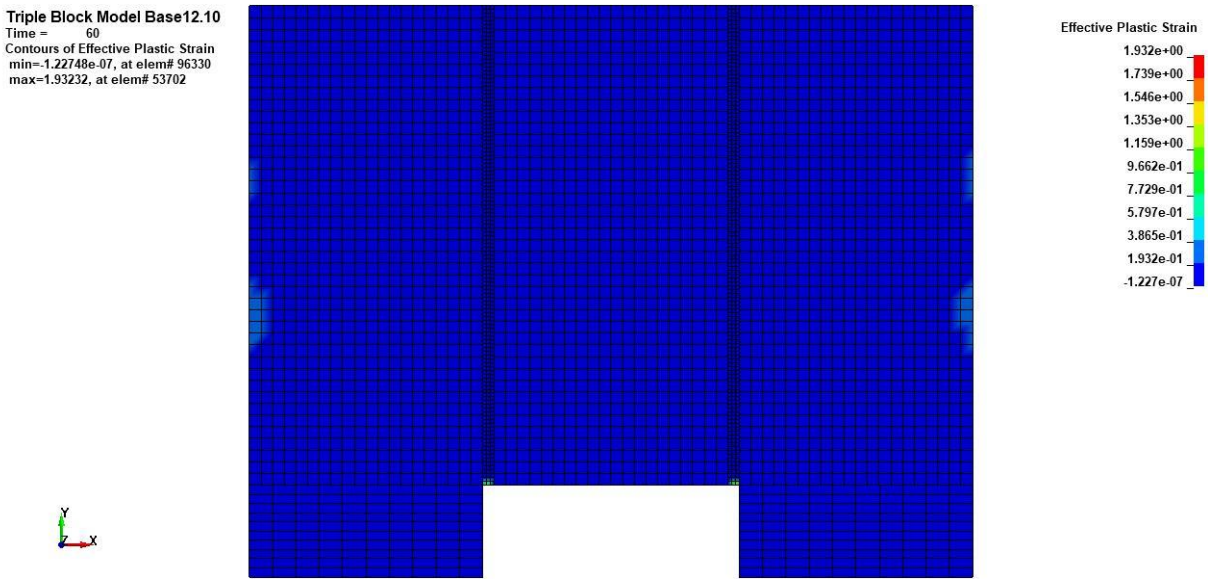


**Figure B-792: Effective Plastic Strain Fringe Plot for Last State at 60 Milliseconds for Base Run 12.10 – 500 psi**

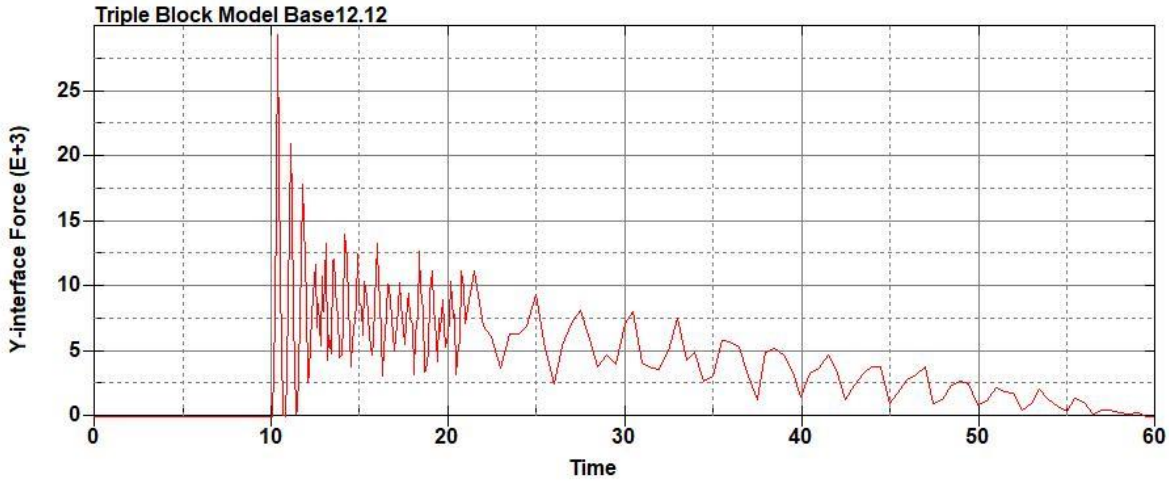


**Figure B-793: Base Run 12.12 Right Support Y-Interface Force (lbs) versus Time (ms) – 600 psi**

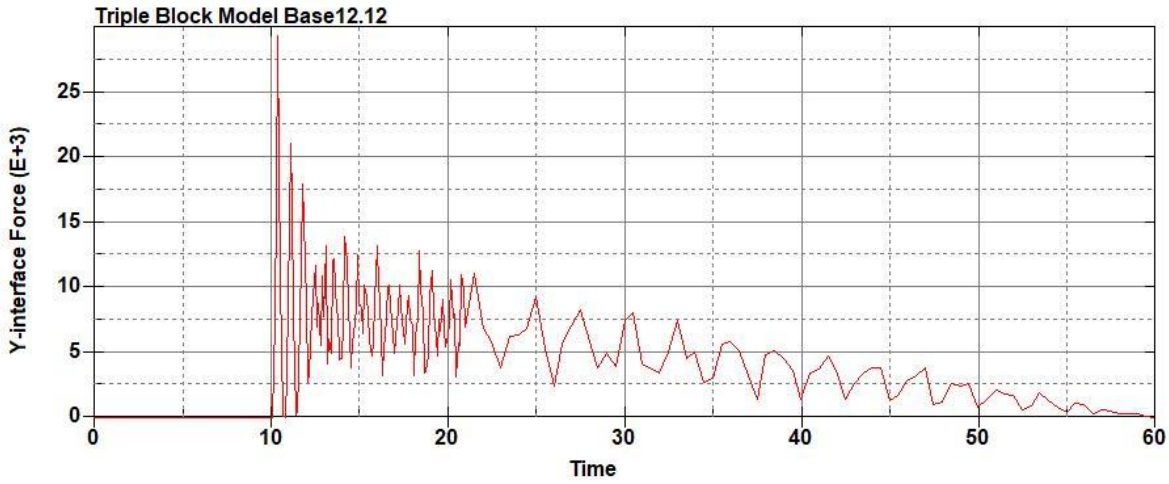


**Figure B-794: Base Run 12.12 Left Support Y-Interface Force (lbs) versus Time (ms) – 600 psi**

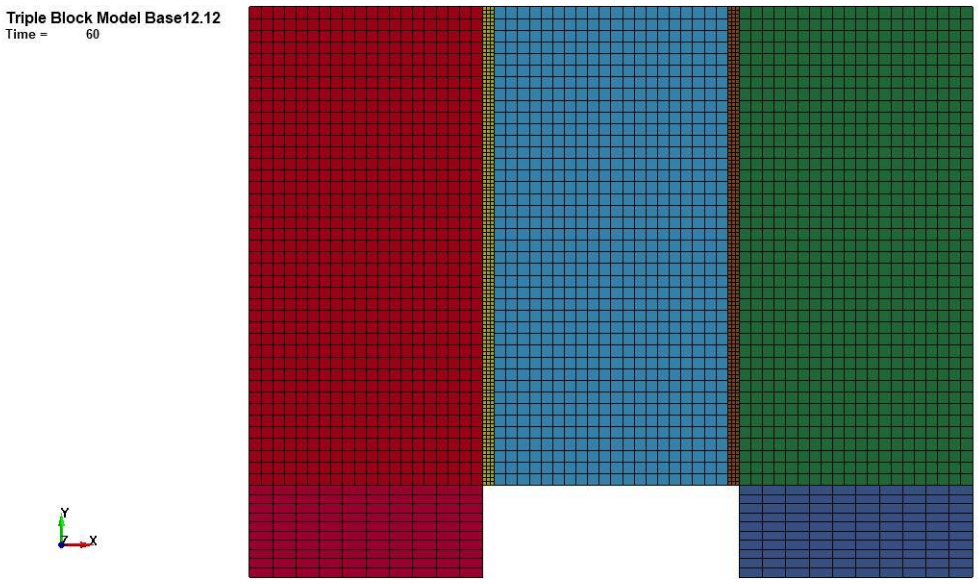


**Figure B-795: Last State at 60 Milliseconds for Base Run 12.12 – 600 psi**

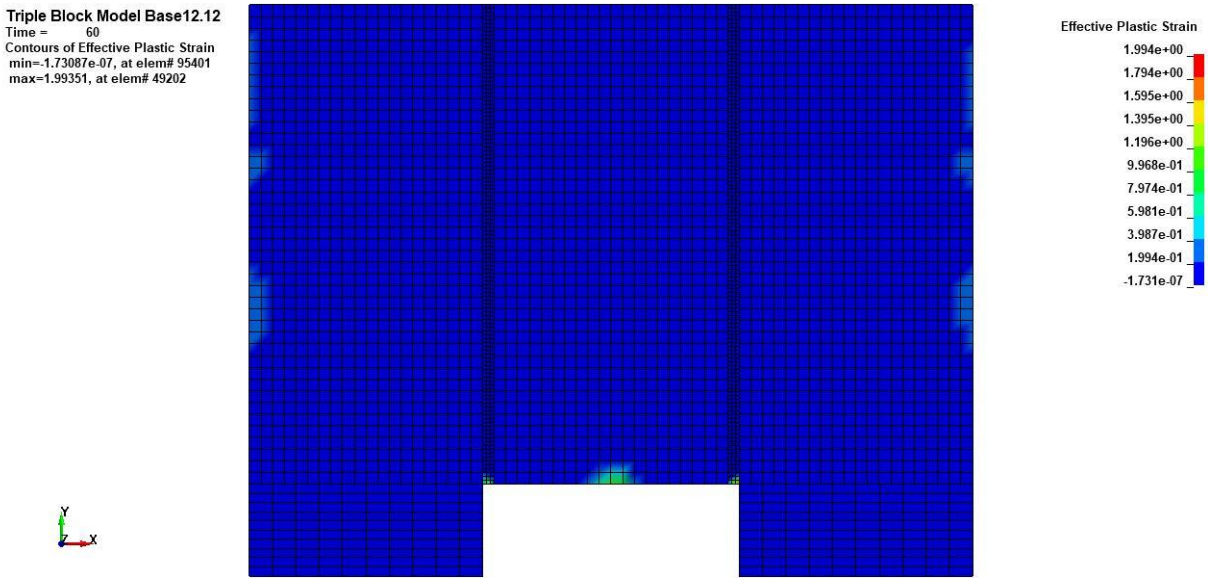


**Figure B-796: Effective Plastic Strain Fringe Plot for Last State at 60 Milliseconds for Base Run 12.12 – 600 psi**

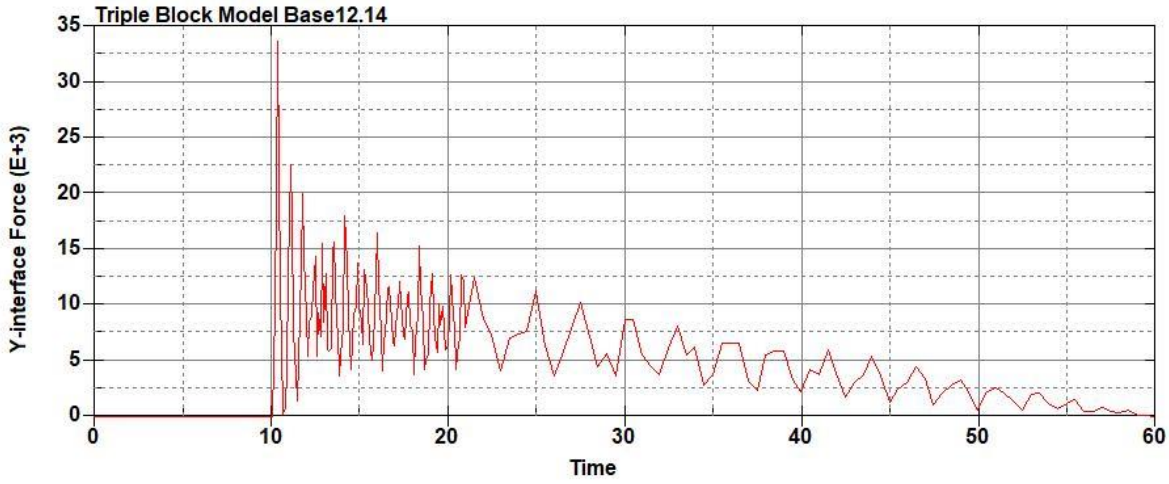


**Figure B-797: Base Run 12.14 Right Support Y-Interface Force (lbs) versus Time (ms) – 700 psi**

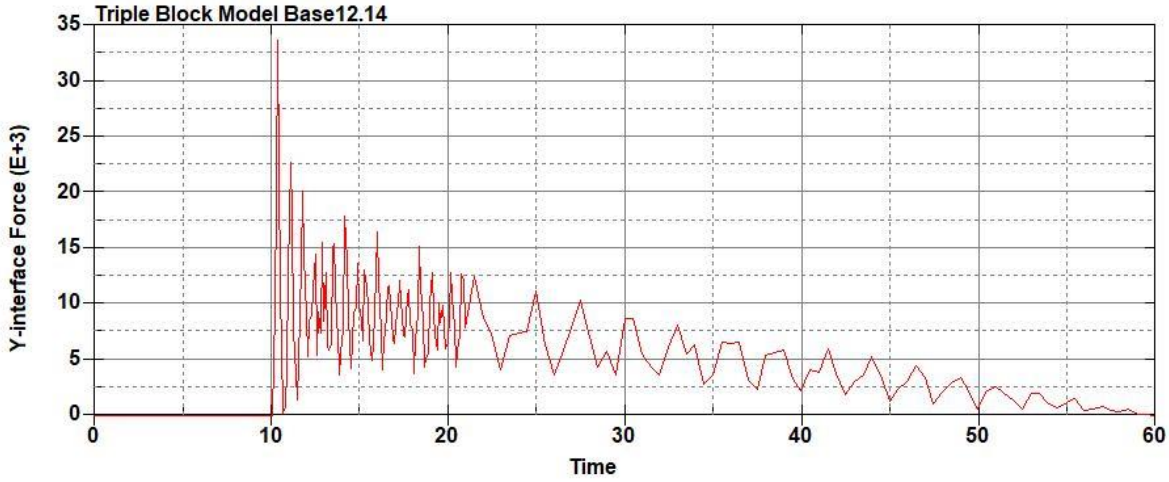


**Figure B-798: Base Run 12.14 Left Support Y-Interface Force (lbs) versus Time (ms) – 700 psi**

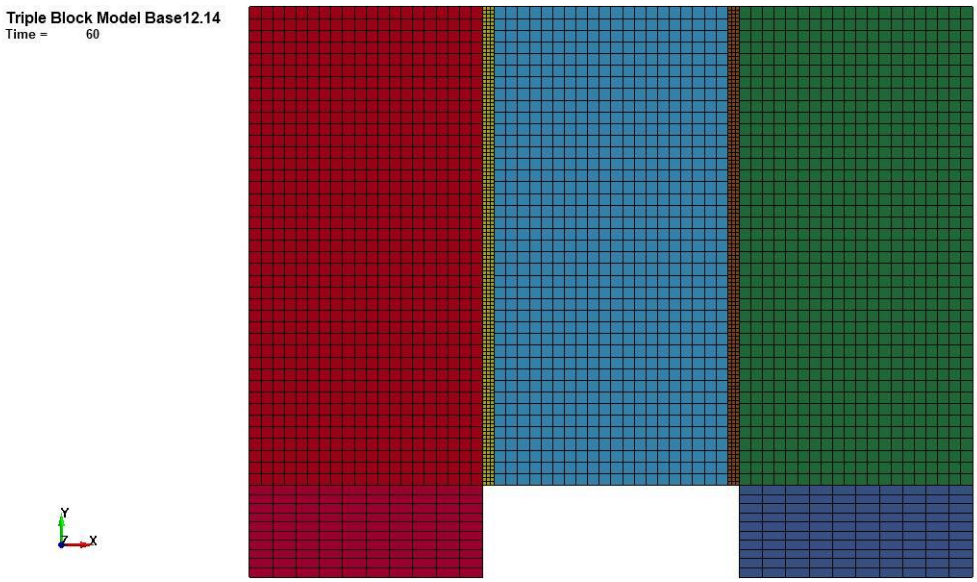


**Figure B-799: Last State at 60 Milliseconds for Base Run 12.14 – 700 psi**

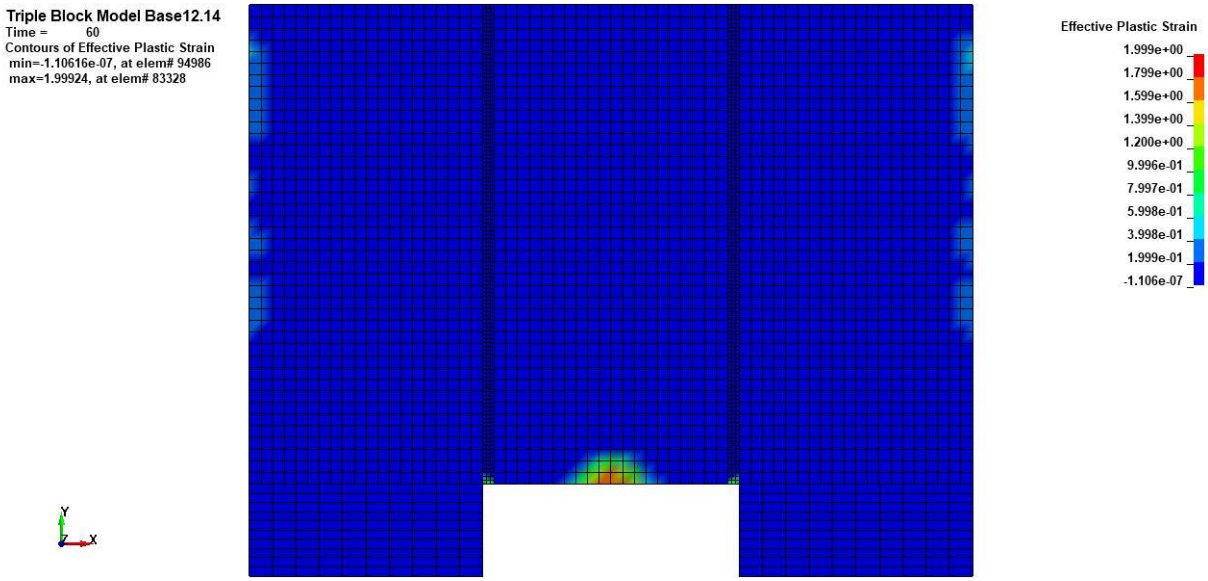


**Figure B-800: Effective Plastic Strain Fringe Plot for Last State at 60 Milliseconds for Base Run 12.14 – 700 psi**

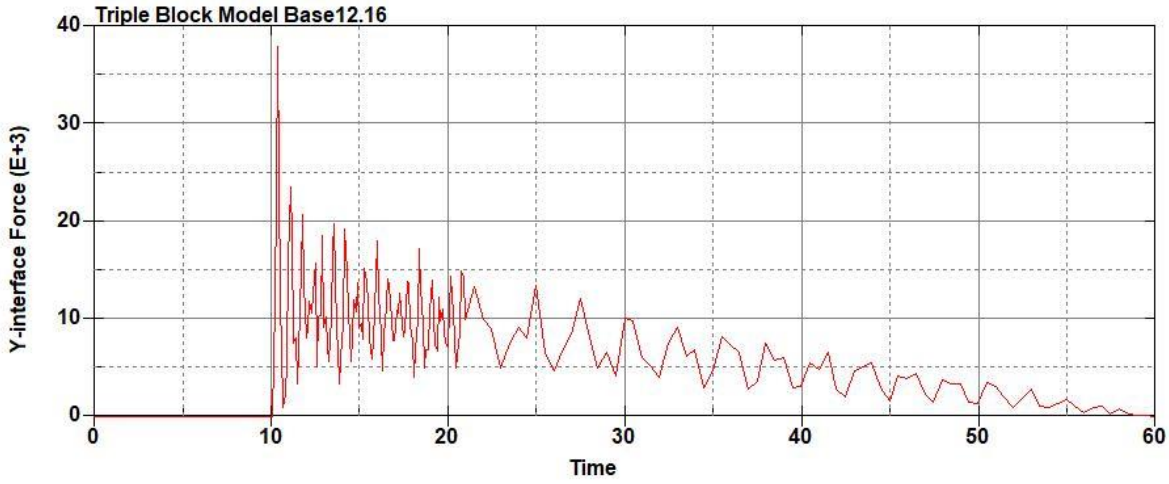


**Figure B-801: Base Run 12.16 Right Support Y-Interface Force (lbs) versus Time (ms) – 800 psi**

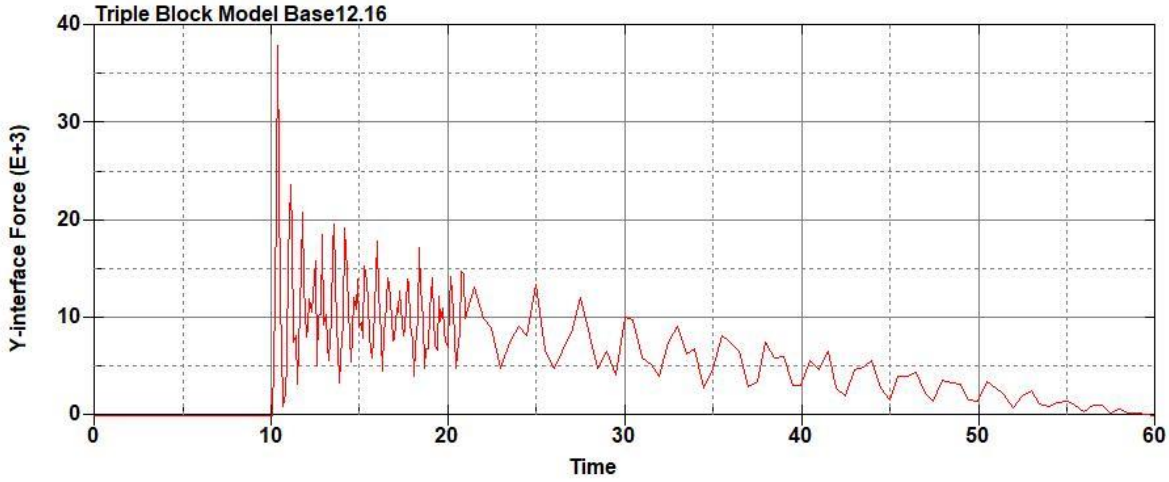


**Figure B-802: Base Run 12.16 Left Support Y-Interface Force (lbs) versus Time (ms) – 800 psi**

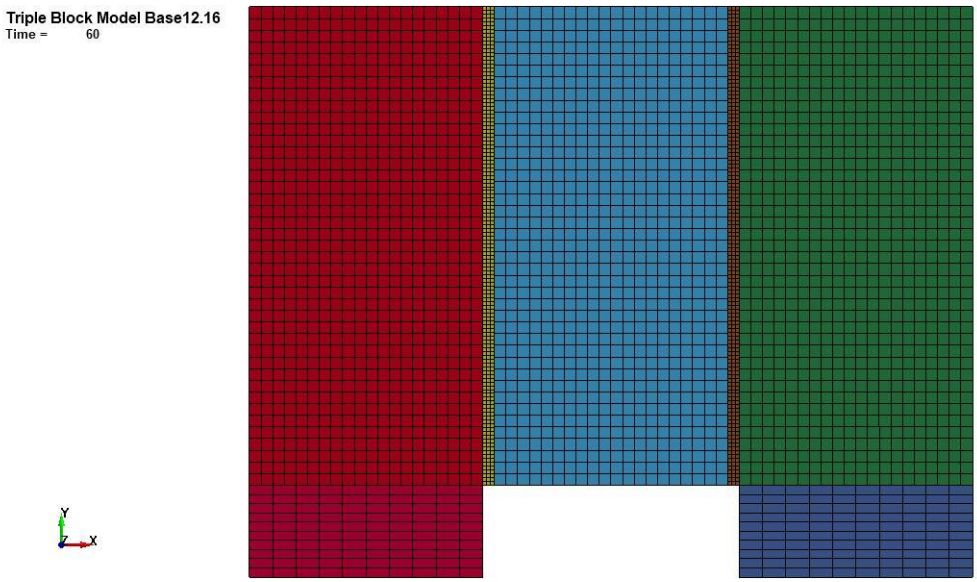


**Figure B-803: Last State at 60 Milliseconds for Base Run 12.16 – 800 psi**

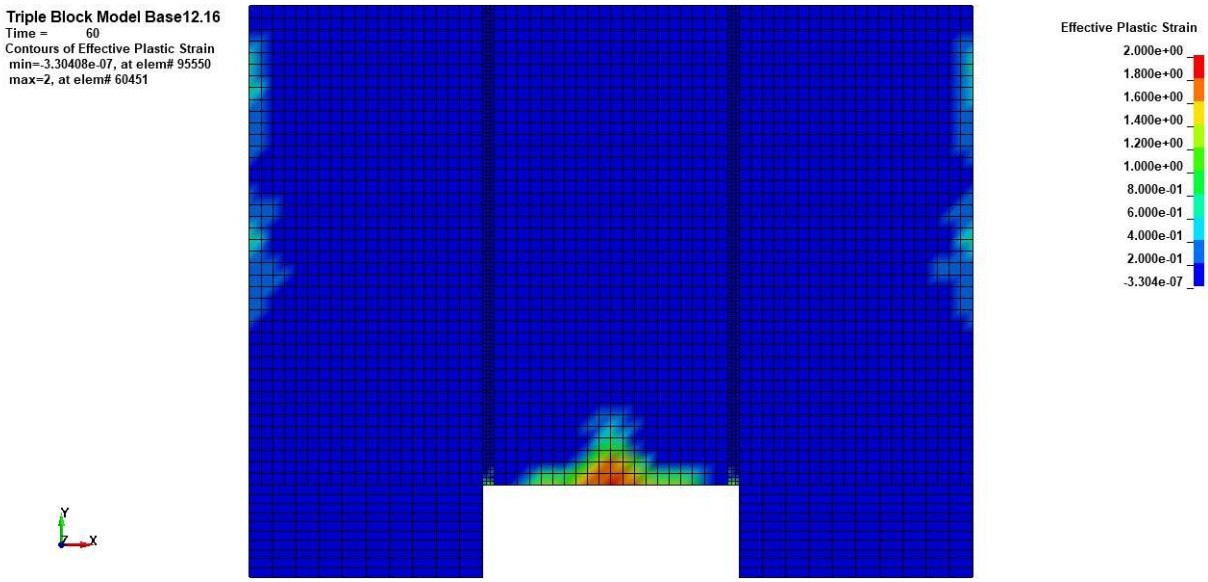


**Figure B-804: Effective Plastic Strain Fringe Plot for Last State at 60 Milliseconds for Base Run 12.16 – 800 psi**

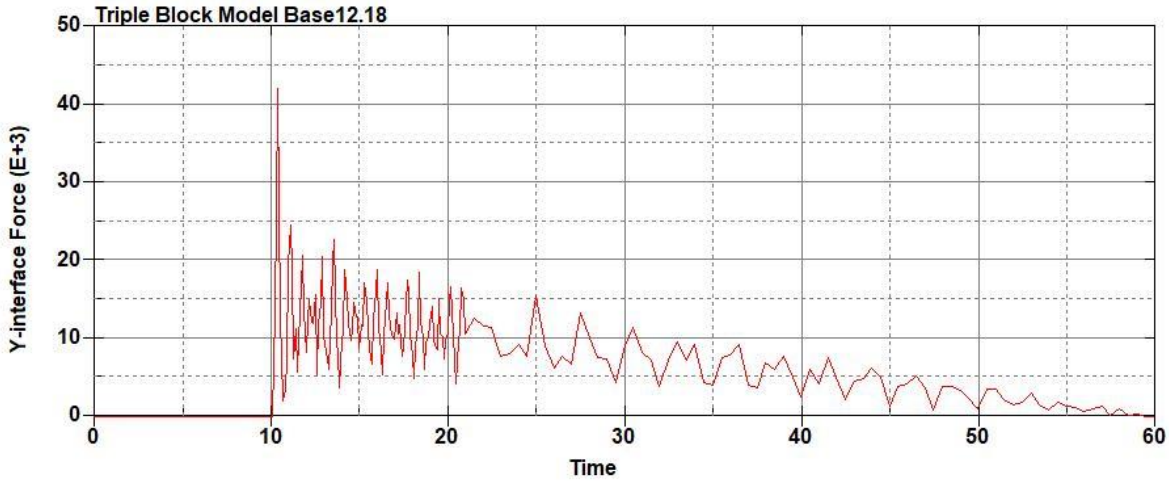


**Figure B-805: Base Run 12.18 Right Support Y-Interface Force (lbs) versus Time (ms) – 900 psi**

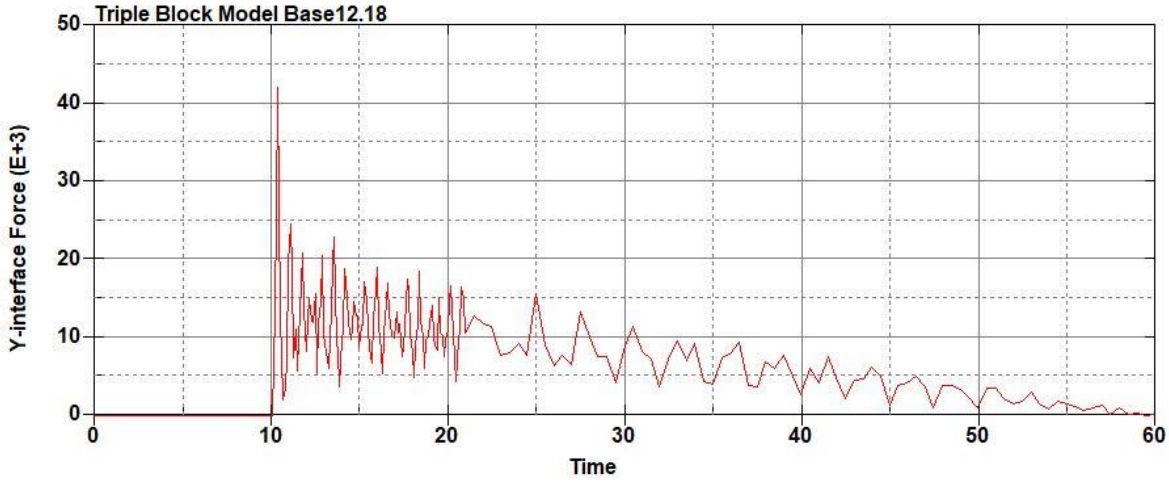


**Figure B-806: Base Run 12.18 Left Support Y-Interface Force (lbs) versus Time (ms) – 900 psi**

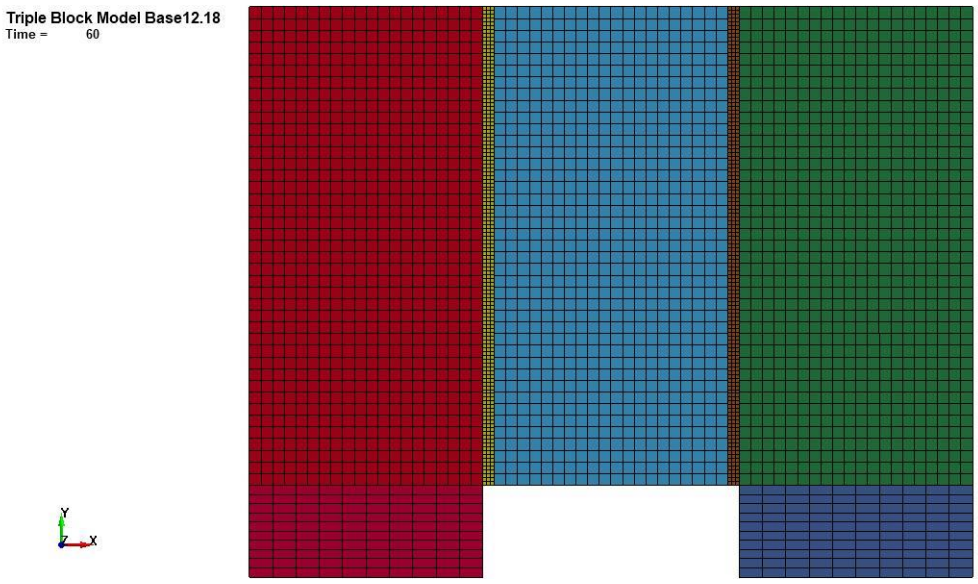


**Figure B-807: Last State at 60 Milliseconds for Base Run 12.18 – 900 psi**

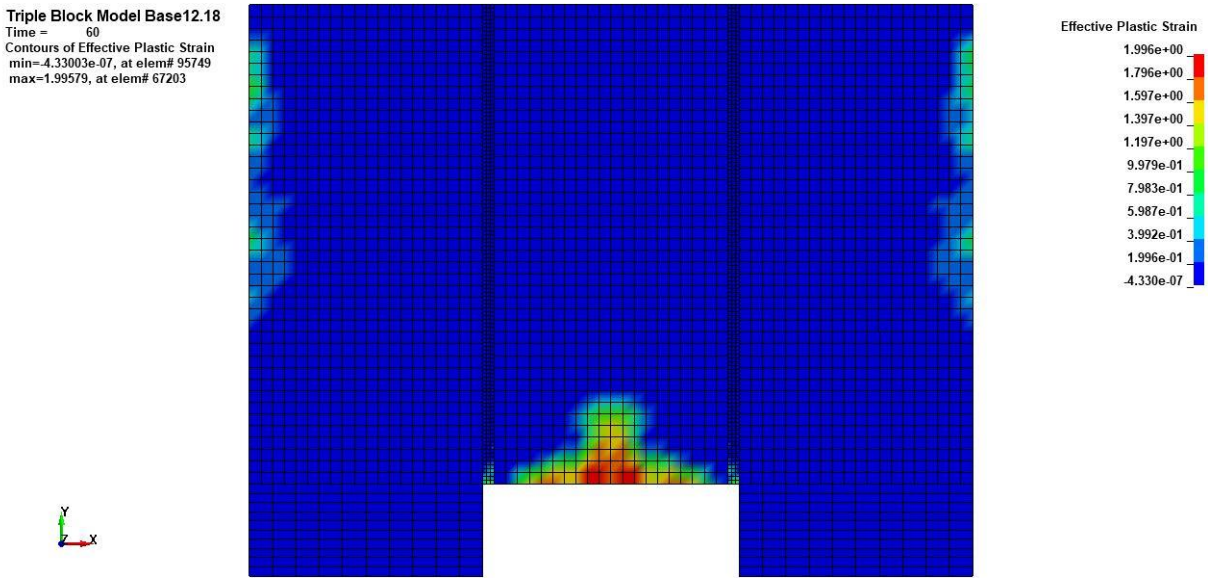


**Figure B-808: Effective Plastic Strain Fringe Plot for Last State at 60 Milliseconds for Base Run 12.18 – 900 psi**

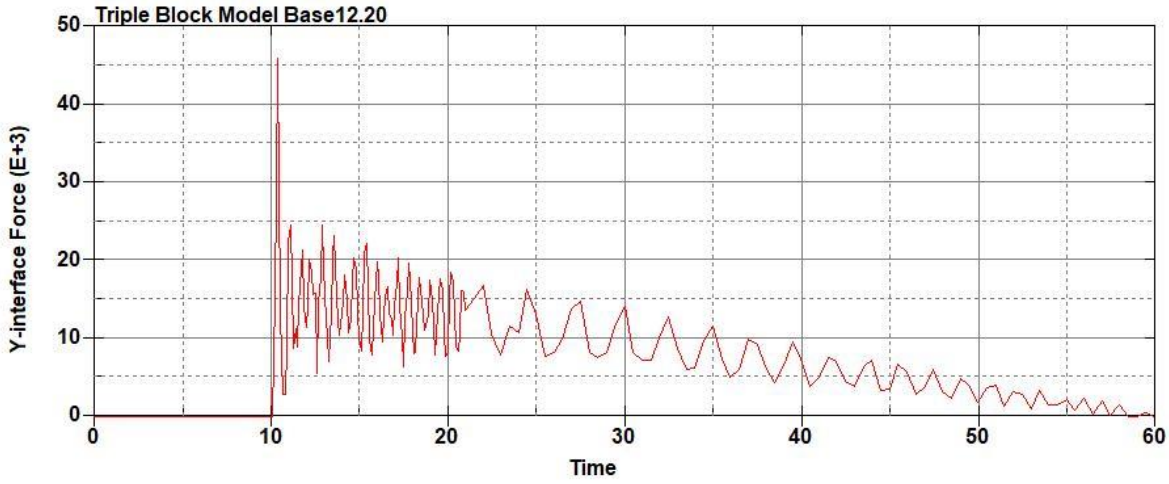


**Figure B-809: Base Run 12.20 Right Support Y-Interface Force (lbs) versus Time (ms) – 1000 psi**

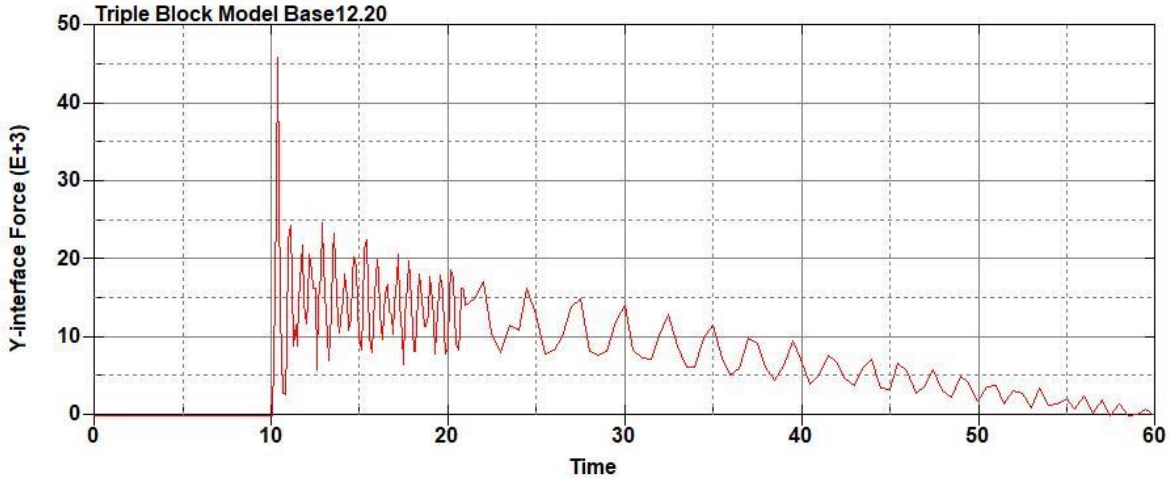


**Figure B-810: Base Run 12.20 Left Support Y-Interface Force (lbs) versus Time (ms) – 1000 psi**

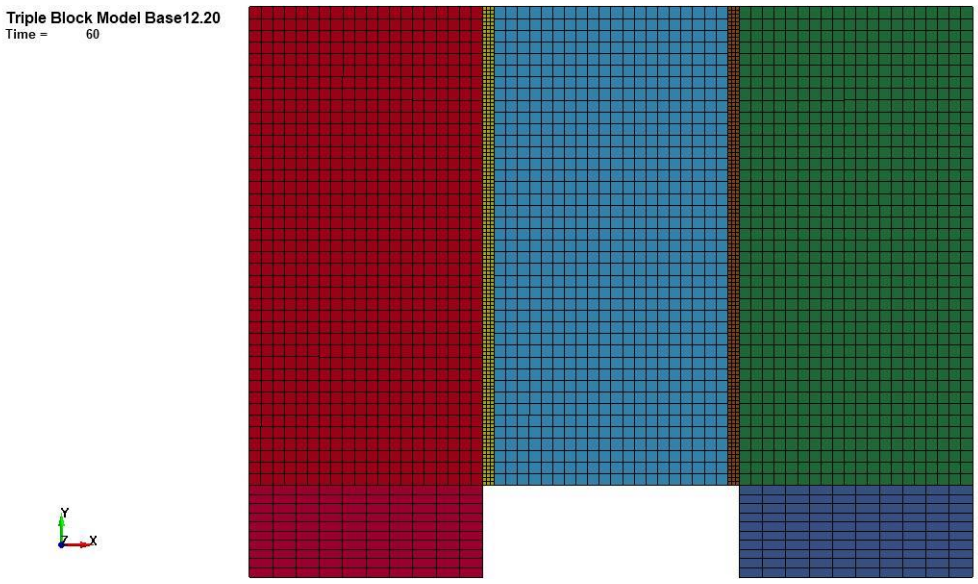


**Figure B-811: Last State at 60 Milliseconds for Base Run 12.20 – 1000 psi**

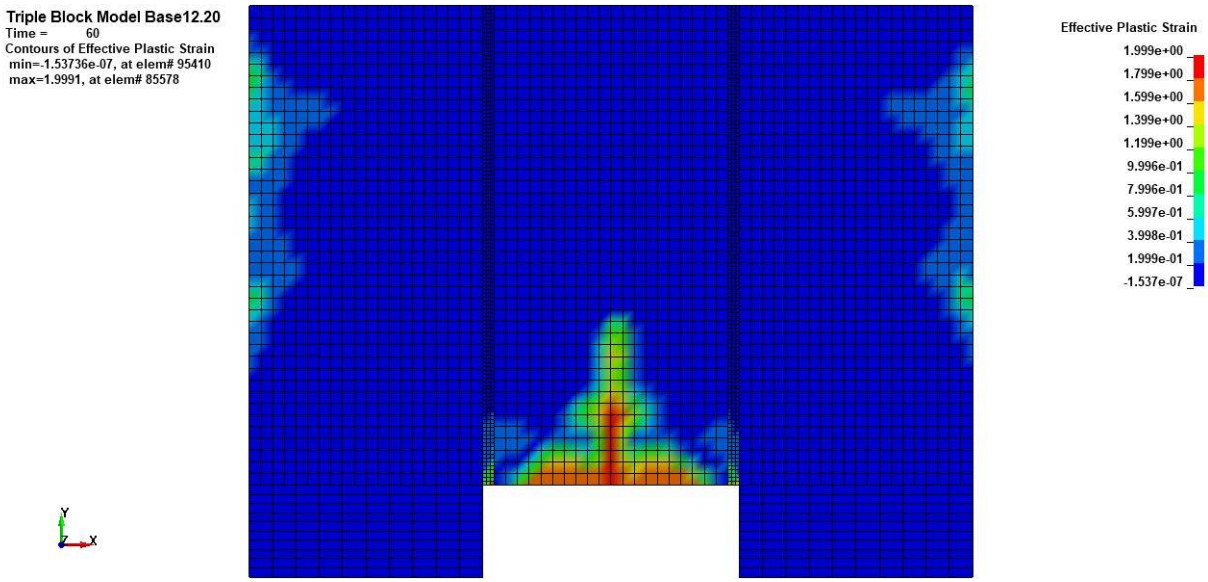


**Figure B-812: Effective Plastic Strain Fringe Plot for Last State at 60 Milliseconds for Base Run 12.20 – 1000 psi**

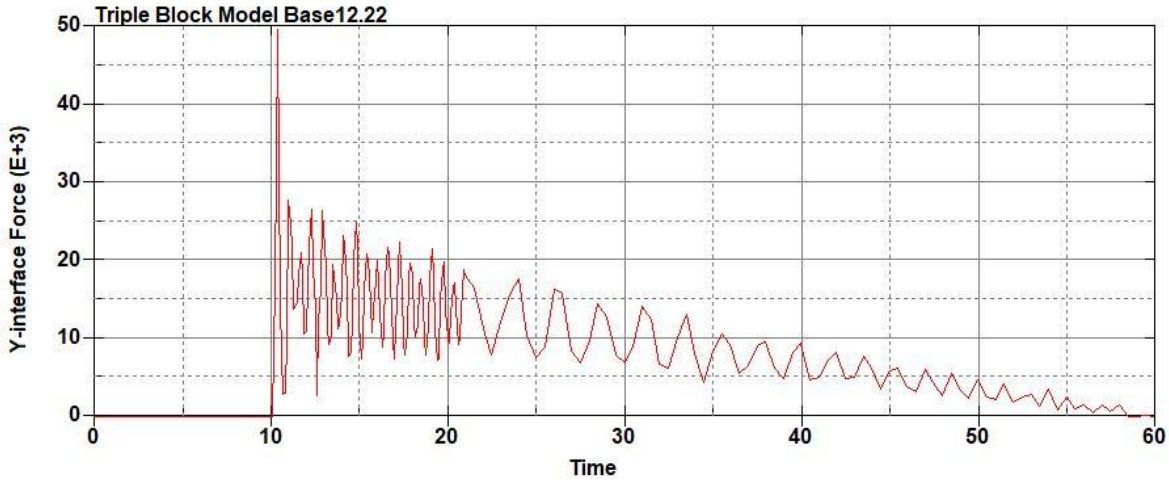


**Figure B-813: Base Run 12.22 Right Support Y-Interface Force (lbs) versus Time (ms) – 1100 psi**

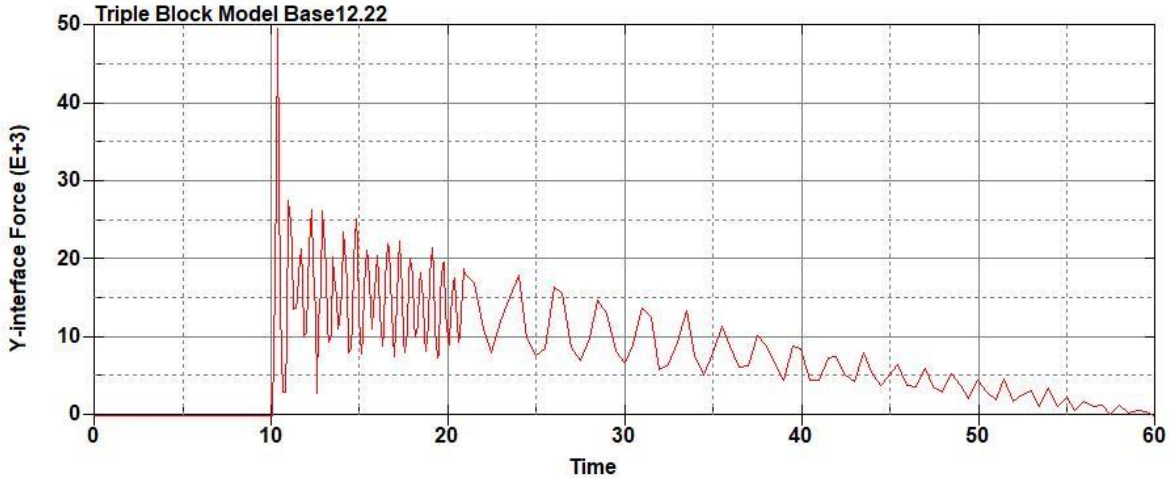


**Figure B-814: Base Run 12.22 Left Support Y-Interface Force (lbs) versus Time (ms) – 1100 psi**

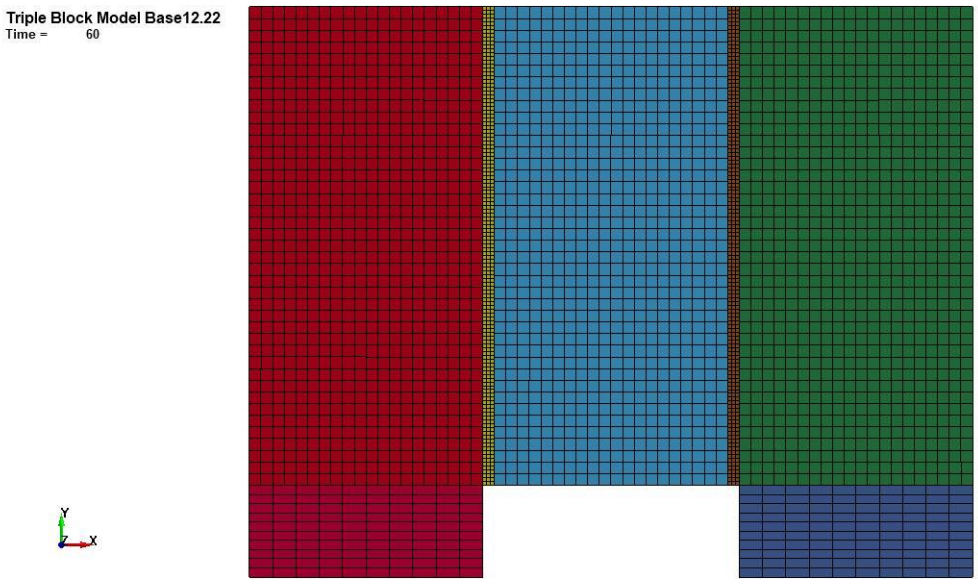


**Figure B-815: Last State at 60 Milliseconds for Base Run 12.22 – 1100 psi**

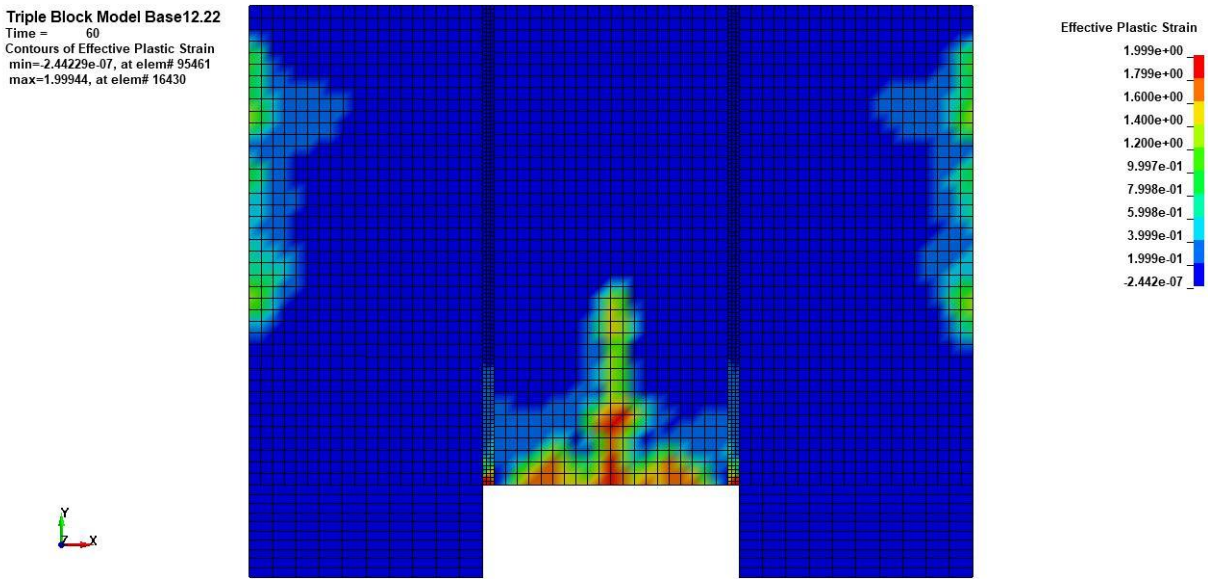


**Figure B-816: Effective Plastic Strain Fringe Plot for Last State at 60 Milliseconds for Base Run 12.22 – 1100 psi**

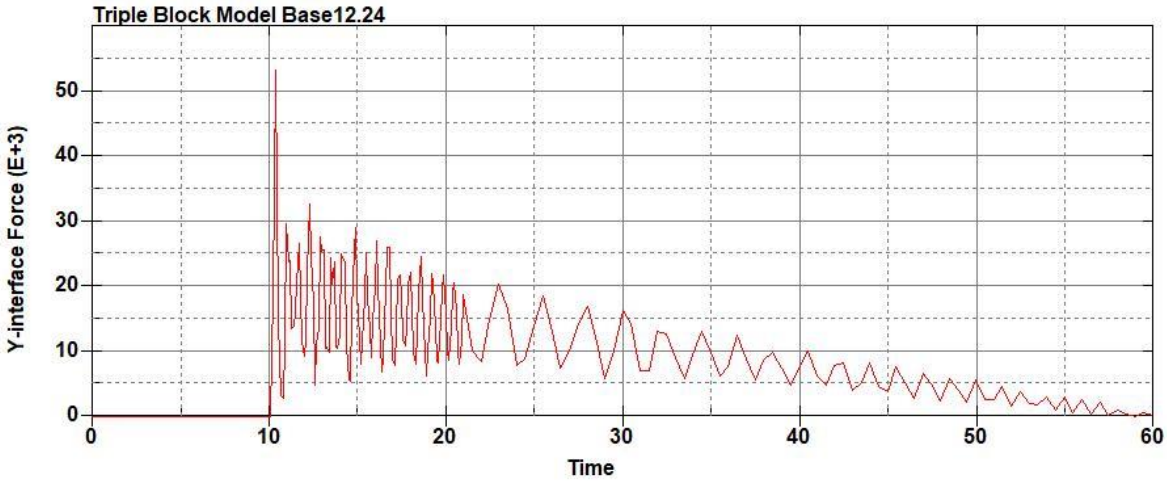


**Figure B-817: Base Run 12.24 Right Support Y-Interface Force (lbs) versus Time (ms) – 1200 psi**

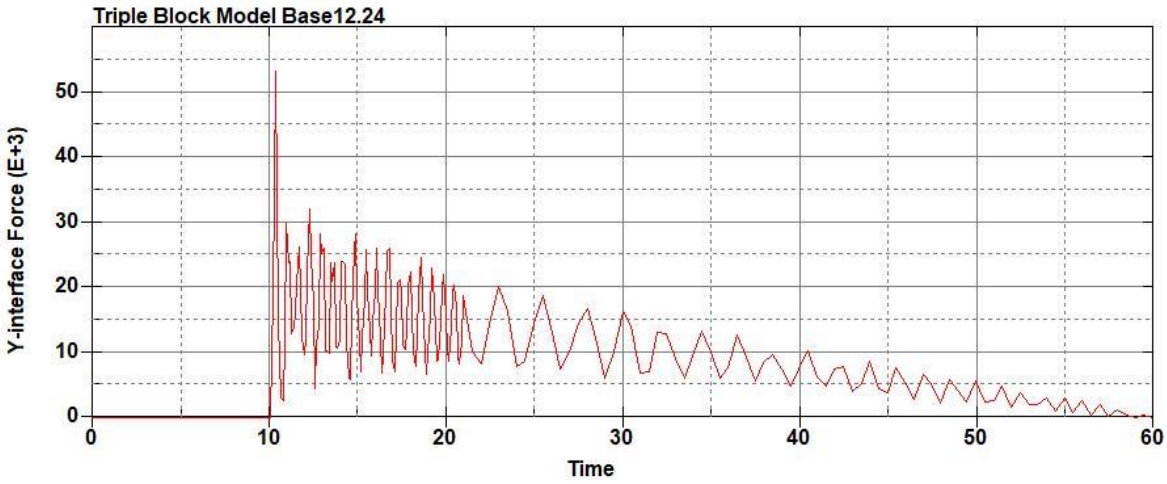


**Figure B-818: Base Run 12.24 Left Support Y-Interface Force (lbs) versus Time (ms) – 1200 psi**

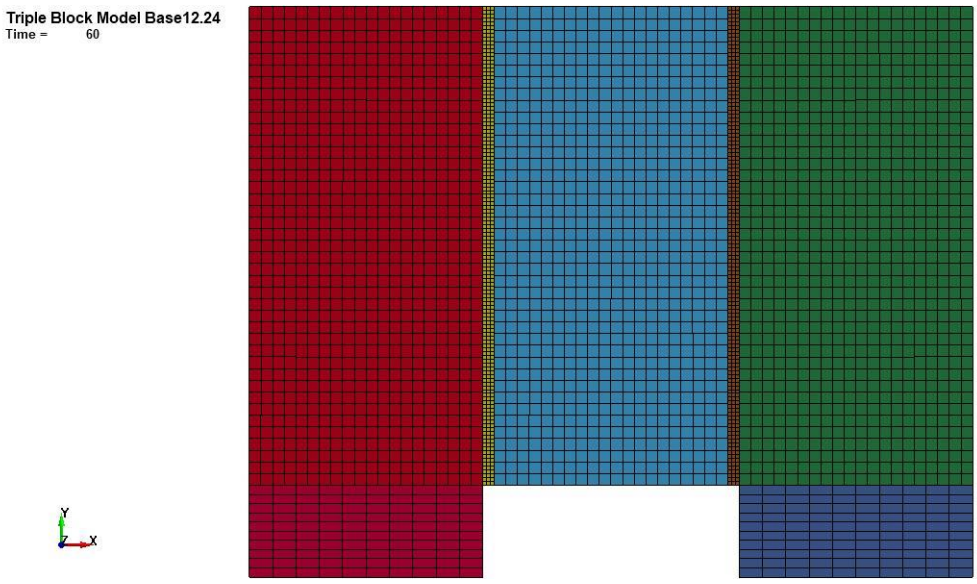


**Figure B-819: Last State at 60 Milliseconds for Base Run 12.24 – 1200 psi**

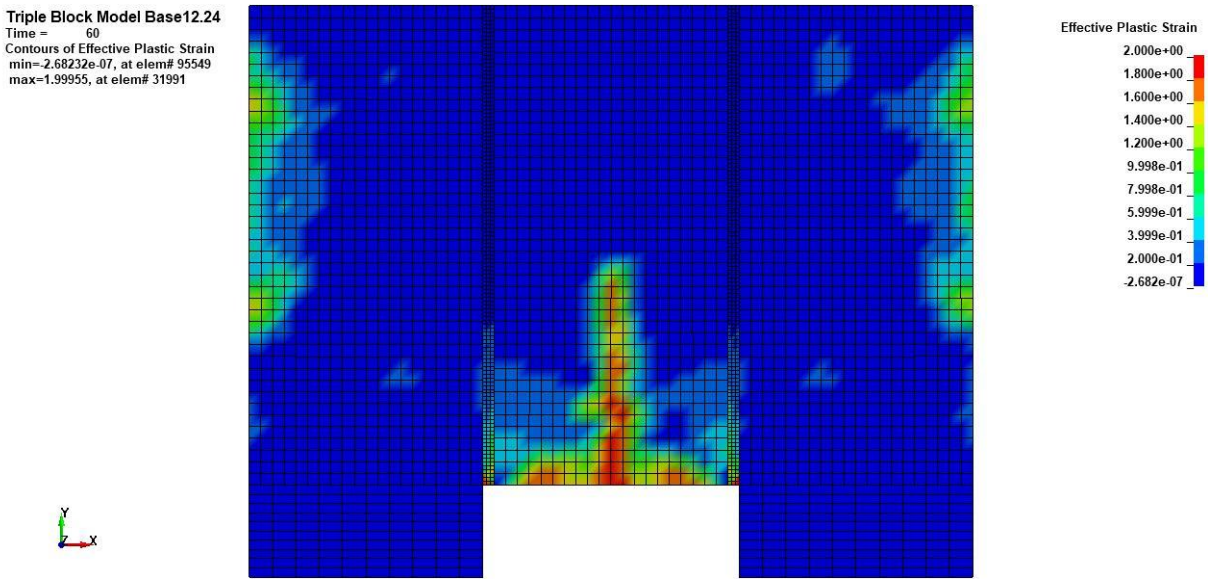


**Figure B-820: Effective Plastic Strain Fringe Plot for Last State at 60 Milliseconds for Base Run 12.24 – 1200 psi**

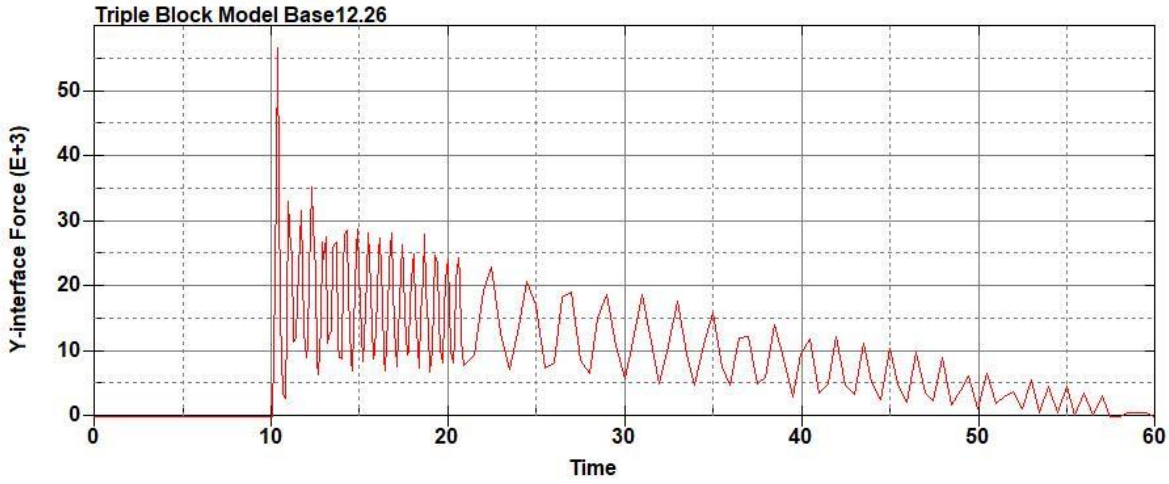


**Figure B-821: Base Run 12.26 Right Support Y-Interface Force (lbs) versus Time (ms) – 1300 psi**

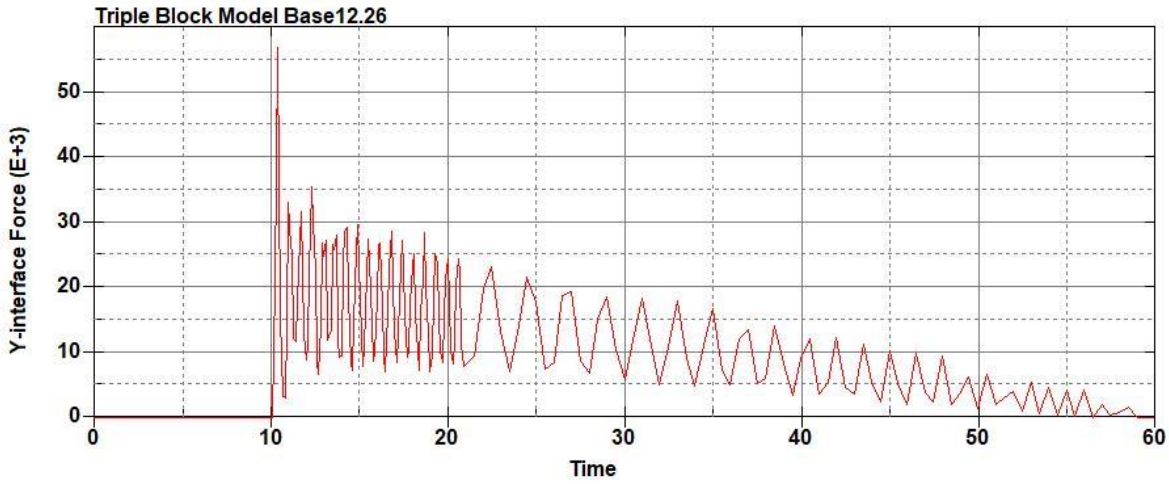


**Figure B-822: Base Run 12.26 Left Support Y-Interface Force (lbs) versus Time (ms) – 1300 psi**

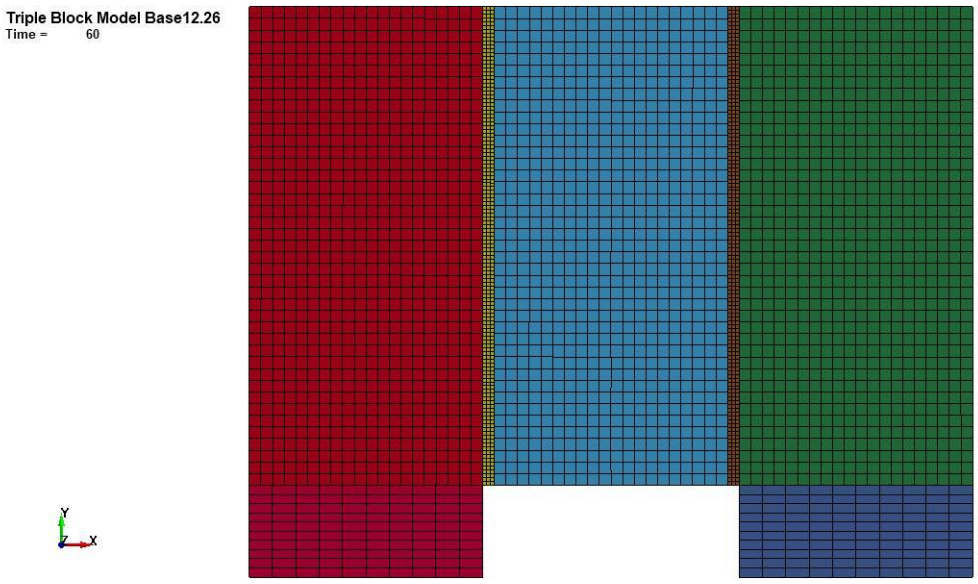


**Figure B-823: Last State at 60 Milliseconds for Base Run 12.26 – 1300 psi**

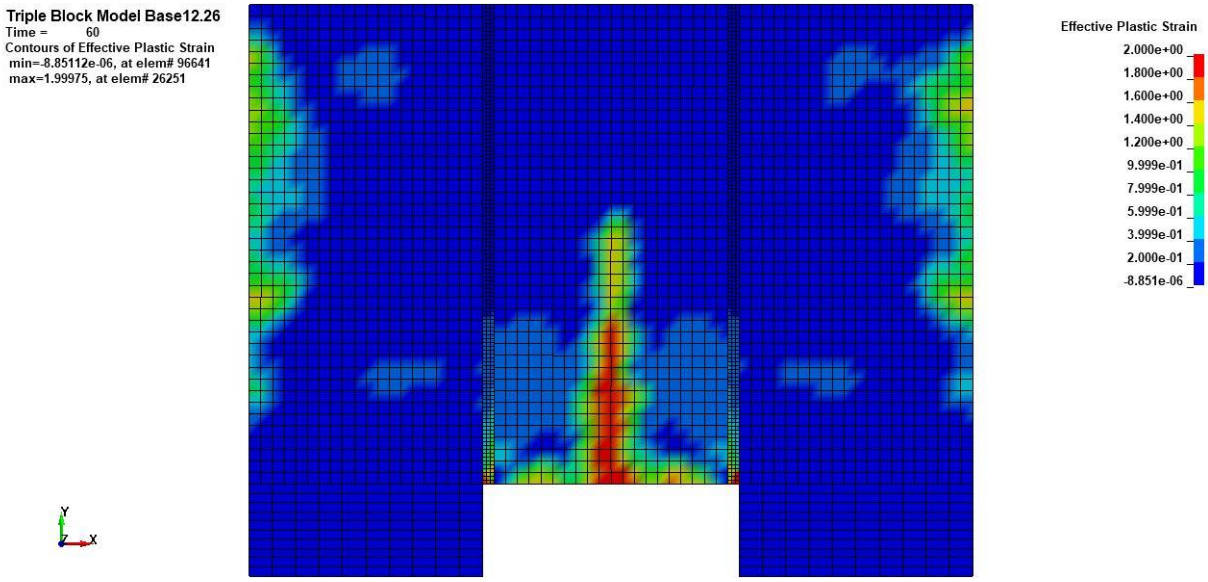


**Figure B-824: Effective Plastic Strain Fringe Plot for Last State at 60 Milliseconds for Base Run 12.26 – 1300 psi**

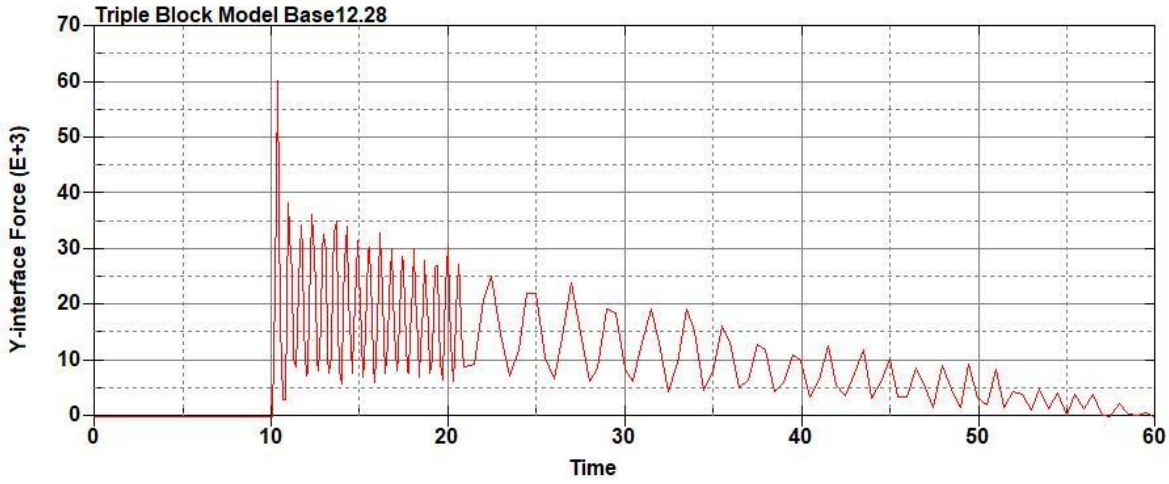


**Figure B-825: Base Run 12.28 Right Support Y-Interface Force (lbs) versus Time (ms) – 1400 psi**

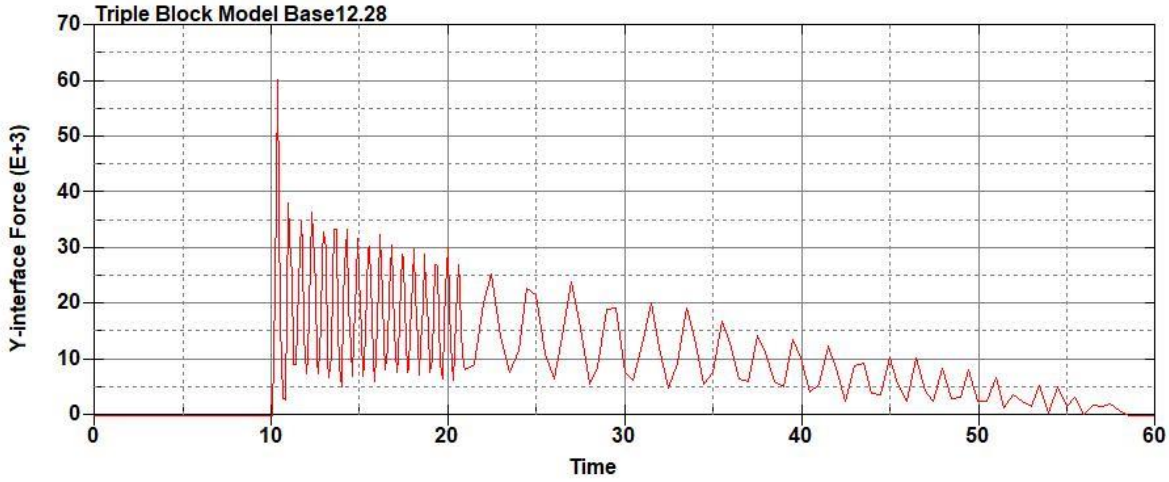


**Figure B-826: Base Run 12.28 Left Support Y-Interface Force (lbs) versus Time (ms) – 1400 psi**

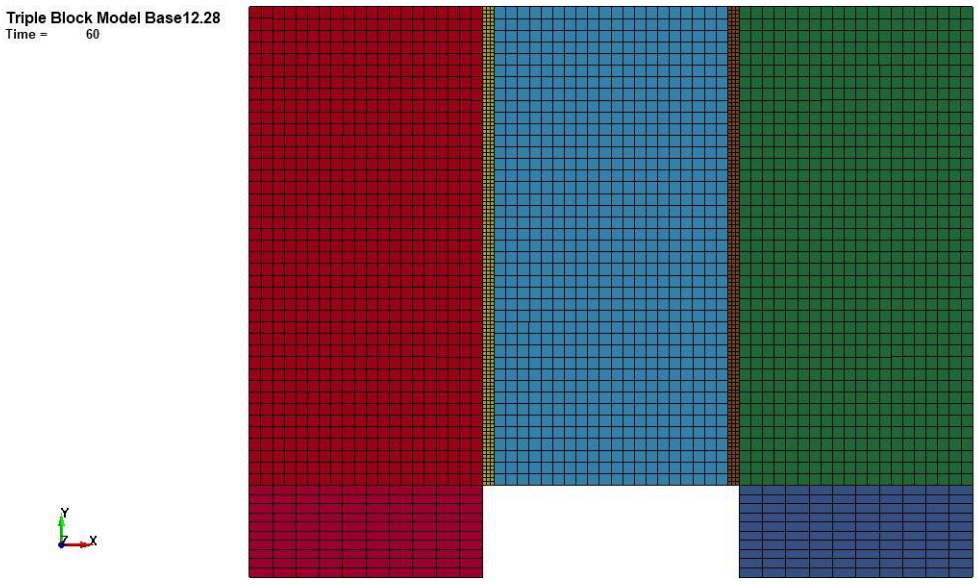


**Figure B-827: Last State at 60 Milliseconds for Base Run 12.28 – 1400 psi**

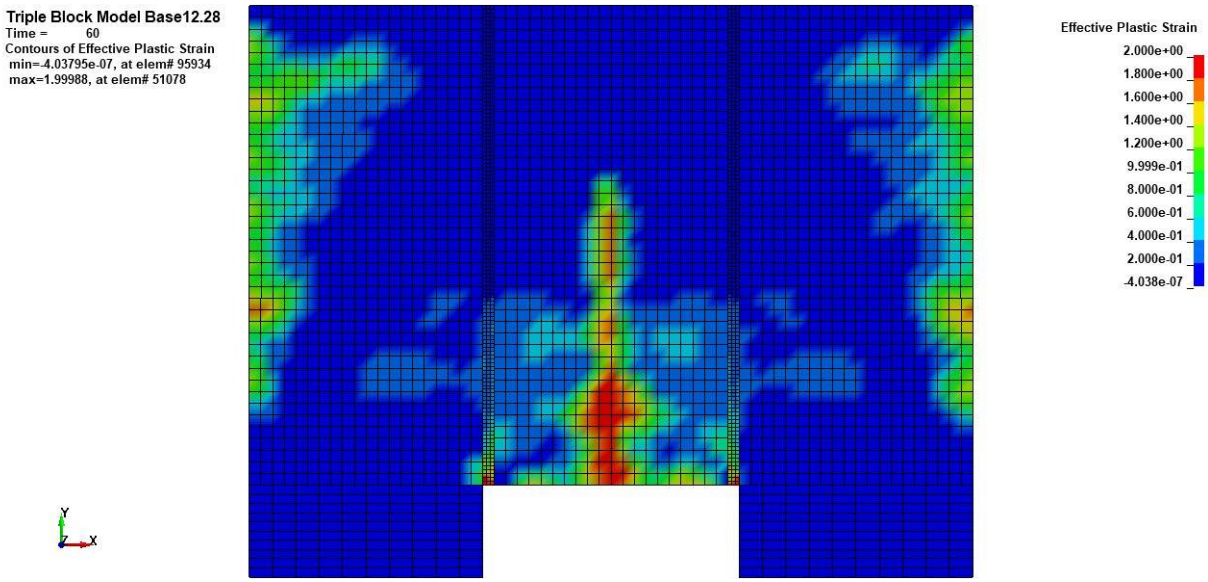


**Figure B-828: Effective Plastic Strain Fringe Plot for Last State at 60 Milliseconds for Base Run 12.28 – 1400 psi**

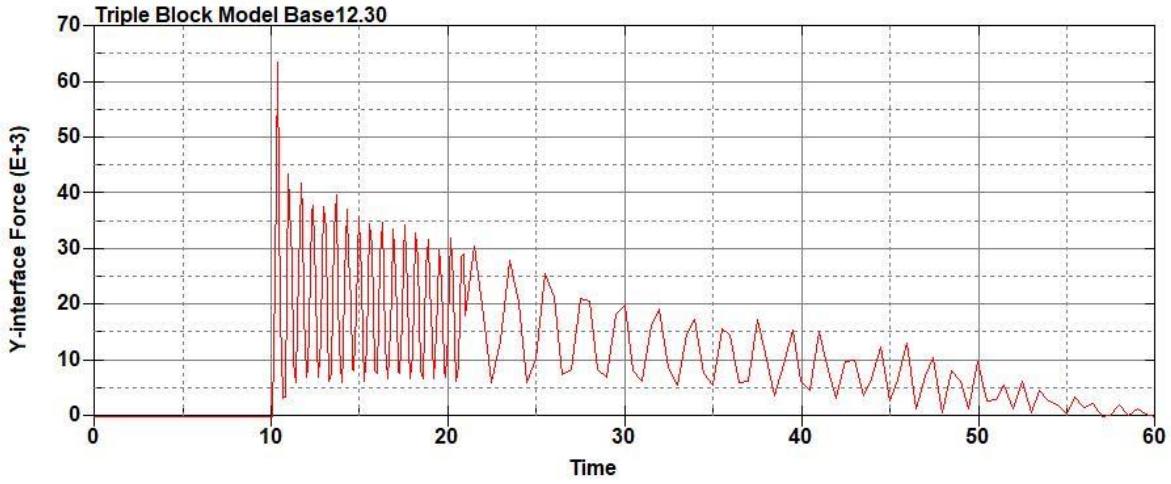


**Figure B-829: Base Run 12.30 Right Support Y-Interface Force (lbs) versus Time (ms) – 1500 psi**

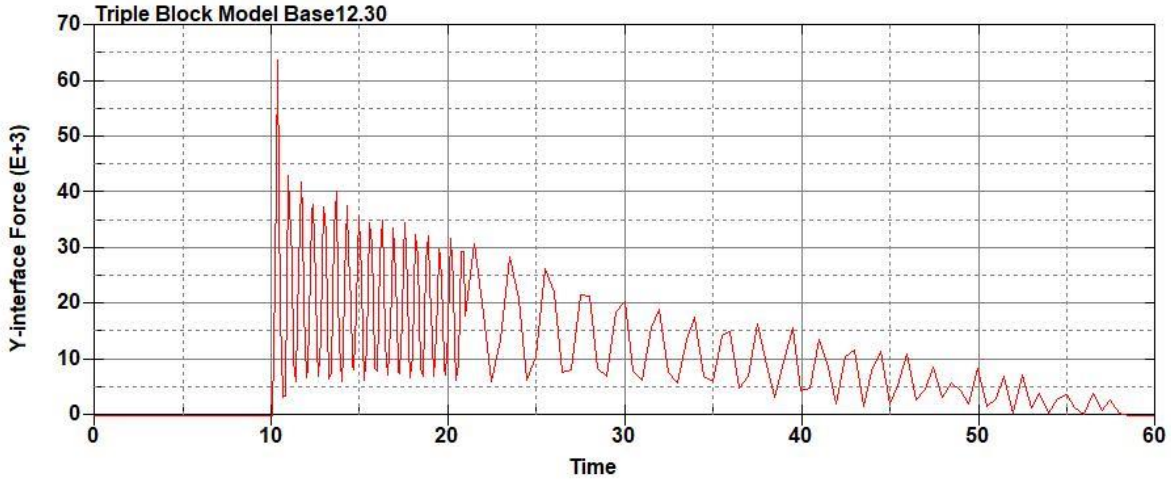


**Figure B-830: Base Run 12.30 Left Support Y-Interface Force (lbs) versus Time (ms) – 1500 psi**

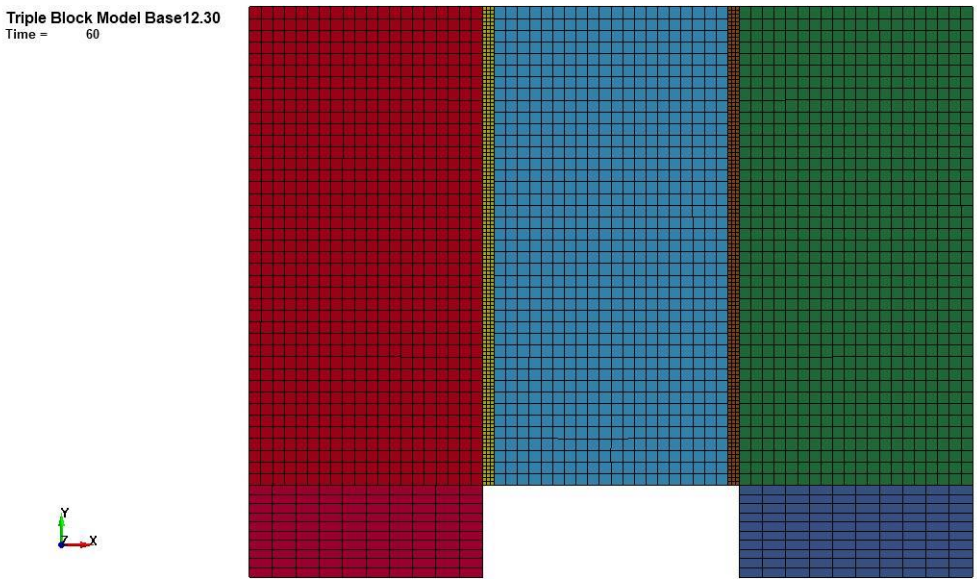


**Figure B-831: Last State at 60 Milliseconds for Base Run 12.30 – 1500 psi**

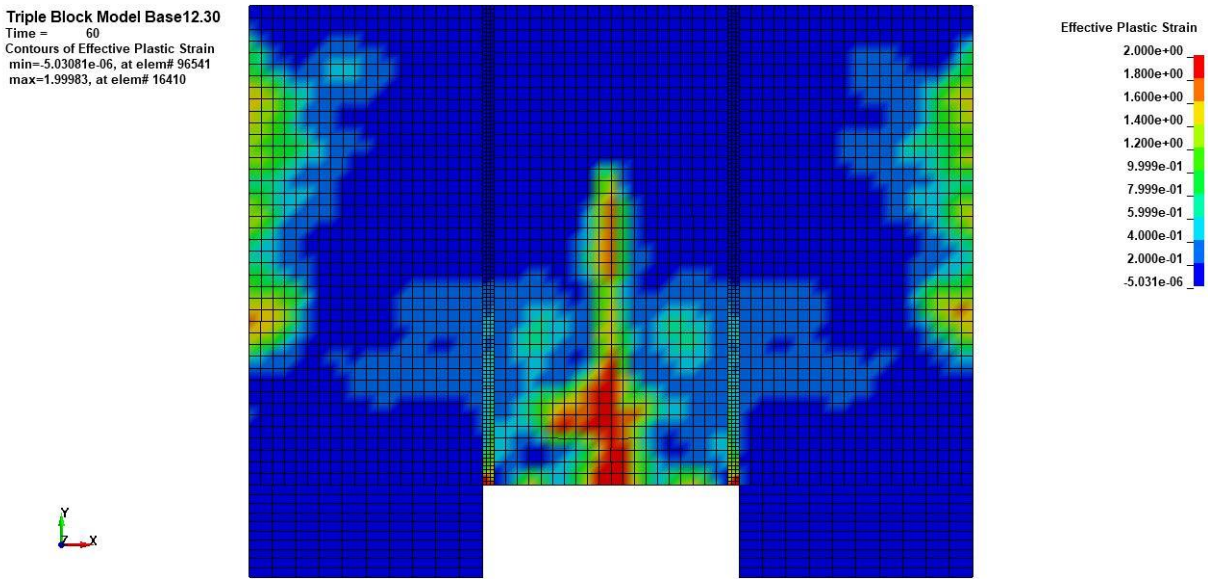


**Figure B-832: Effective Plastic Strain Fringe Plot for Last State at 60 Milliseconds for Base Run 12.30 – 1500 psi**

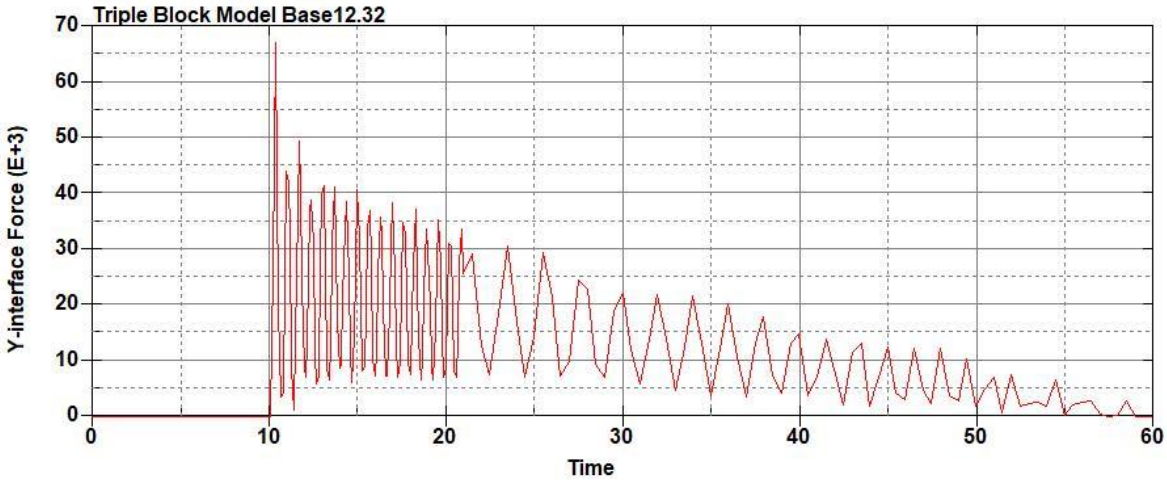


**Figure B-833: Base Run 12.32 Right Support Y-Interface Force (lbs) versus Time (ms) – 1600 psi**

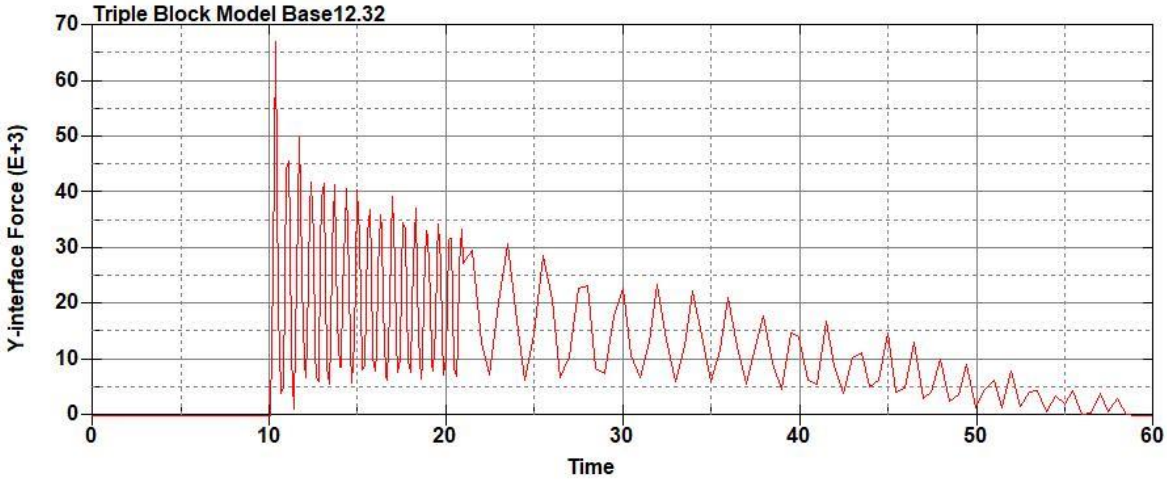


**Figure B-834: Base Run 12.32 Left Support Y-Interface Force (lbs) versus Time (ms) – 1600 psi**

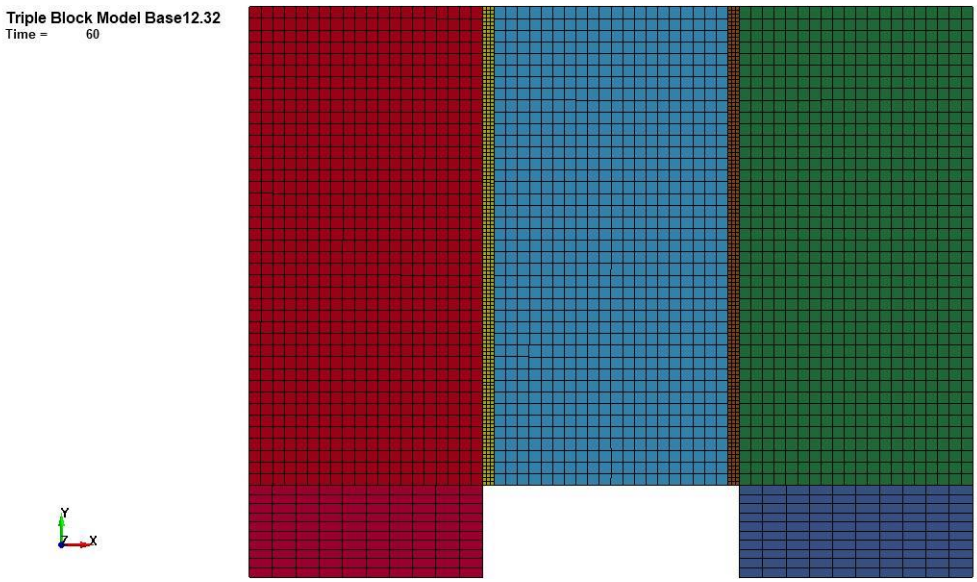


**Figure B-835: Last State at 60 Milliseconds for Base Run 12.32 – 1600 psi**

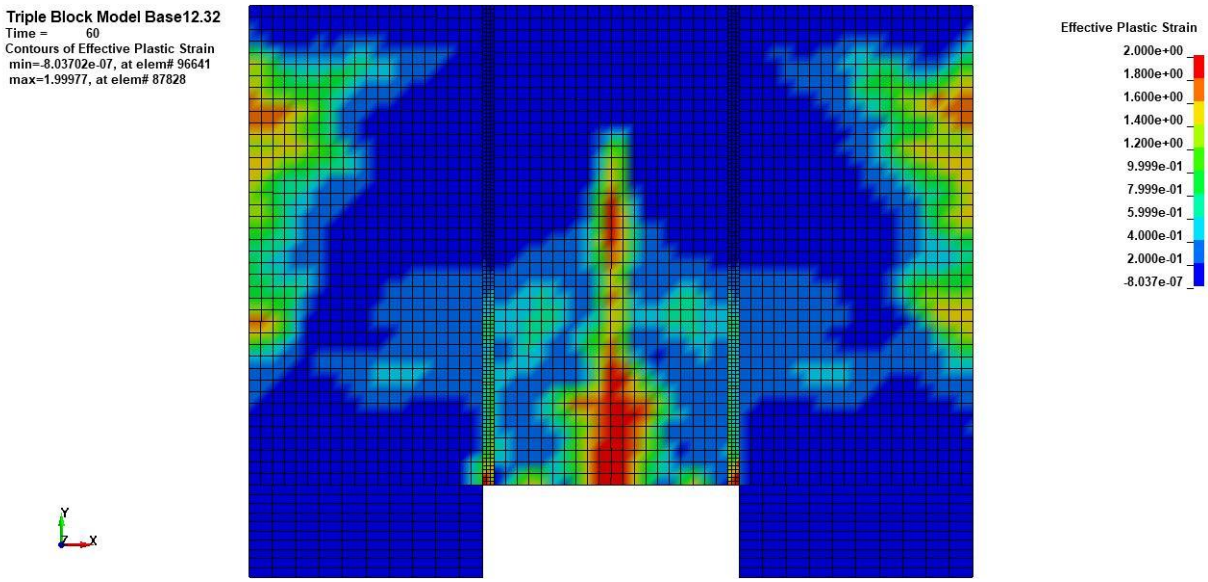


**Figure B-836: Effective Plastic Strain Fringe Plot for Last State at 60 Milliseconds for Base Run 12.32 – 1600 psi**

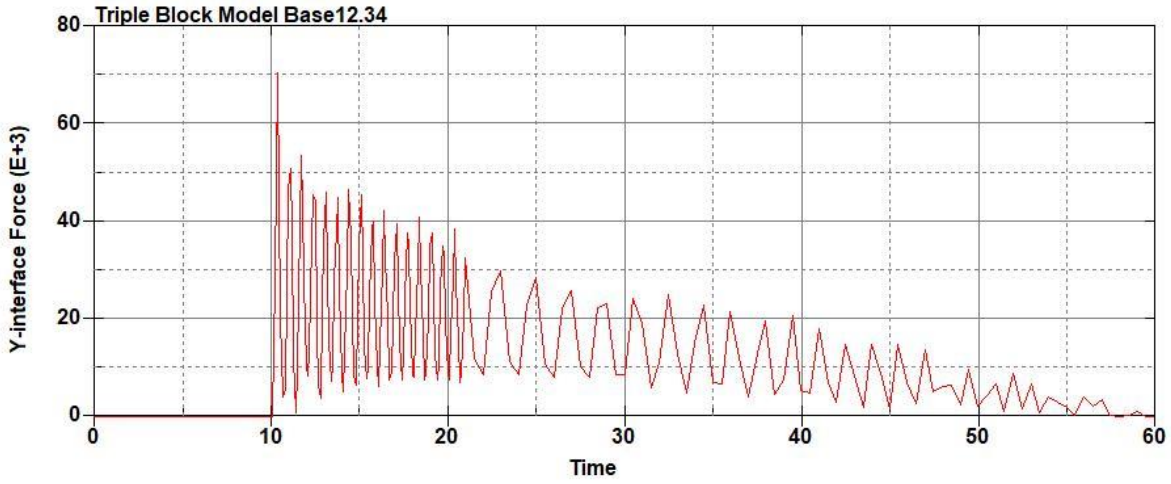


**Figure B-837: Base Run 12.34 Right Support Y-Interface Force (lbs) versus Time (ms) – 1700 psi**

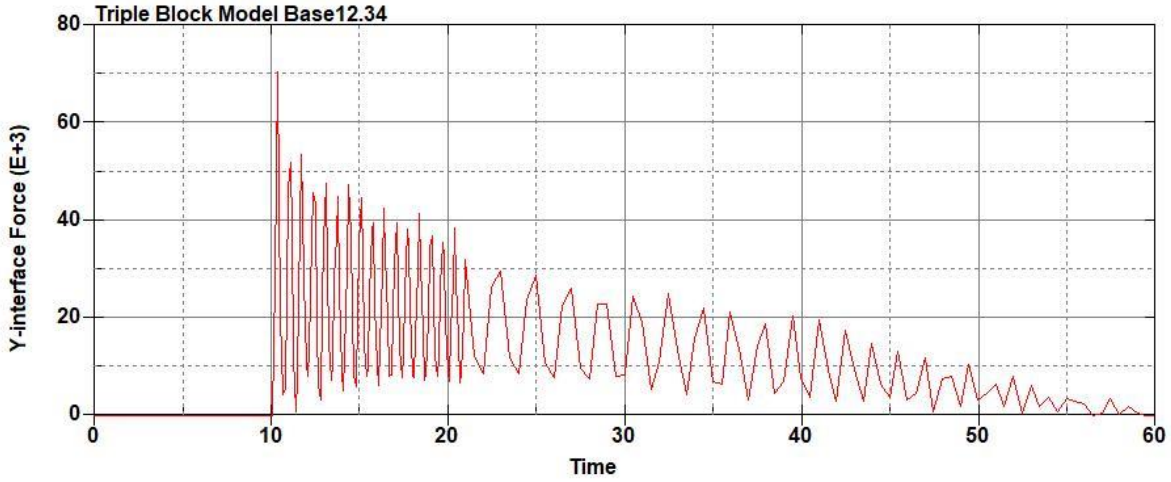


**Figure B-838: Base Run 12.34 Left Support Y-Interface Force (lbs) versus Time (ms) – 1700 psi**

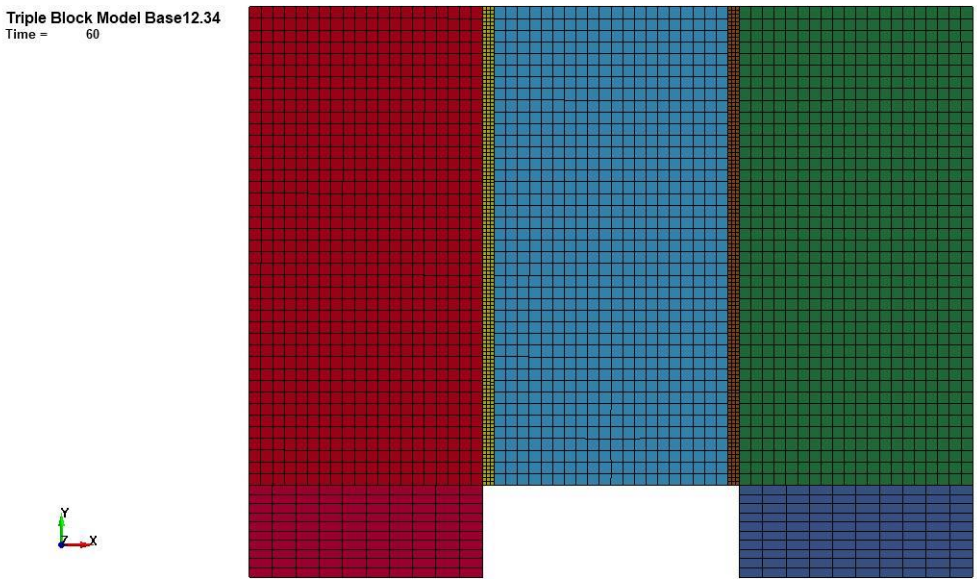


**Figure B-839: Last State at 60 Milliseconds for Base Run 12.34 – 1700 psi**

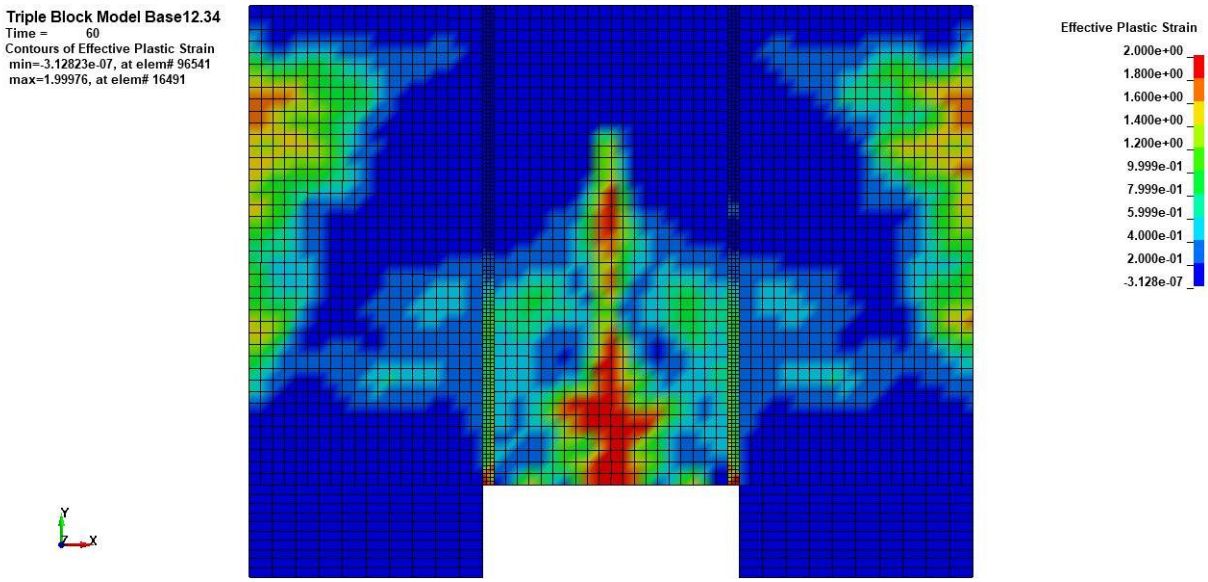


**Figure B-840: Effective Plastic Strain Fringe Plot for Last State at 60 Milliseconds for Base Run 12.34 – 1700 psi**

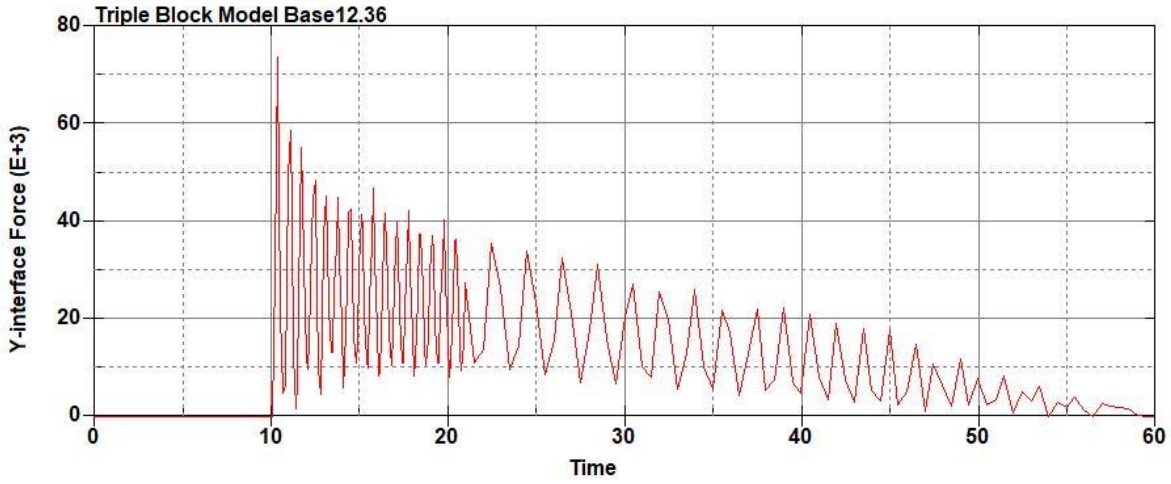


**Figure B-841: Base Run 12.36 Right Support Y-Interface Force (lbs) versus Time (ms) – 1800 psi**

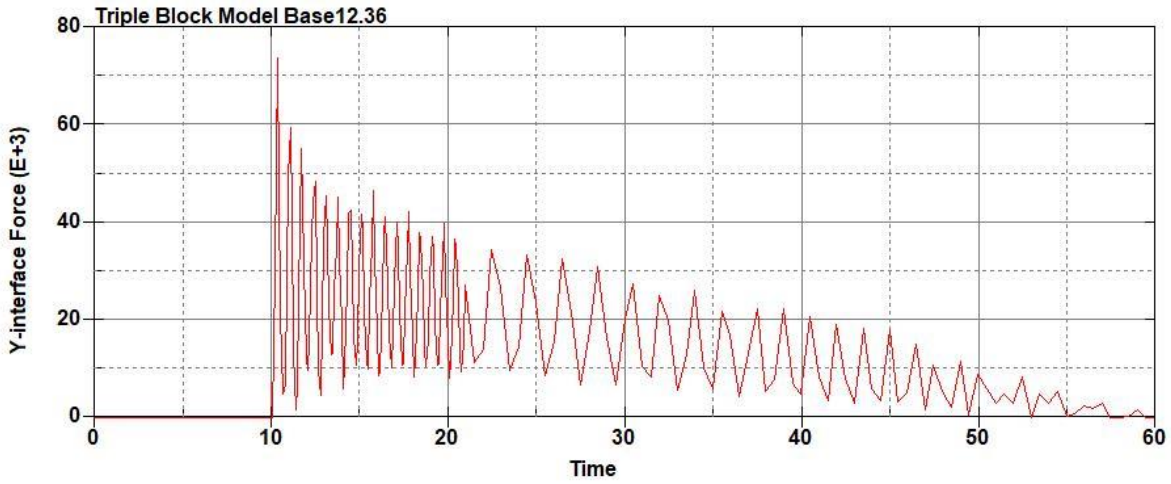


**Figure B-842: Base Run 12.36 Left Support Y-Interface Force (lbs) versus Time (ms) – 1800 psi**

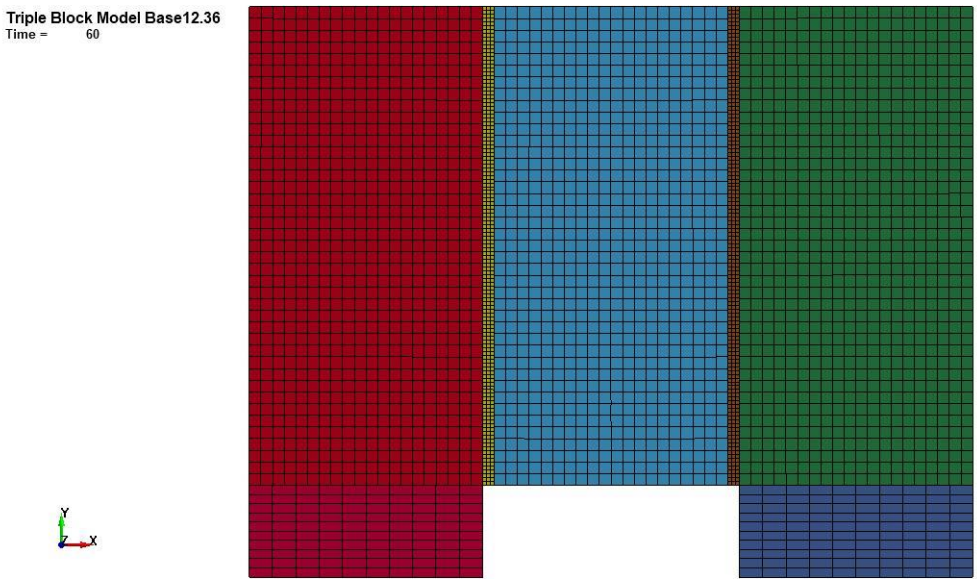


**Figure B-843: Last State at 60 Milliseconds for Base Run 12.36 – 1800 psi**

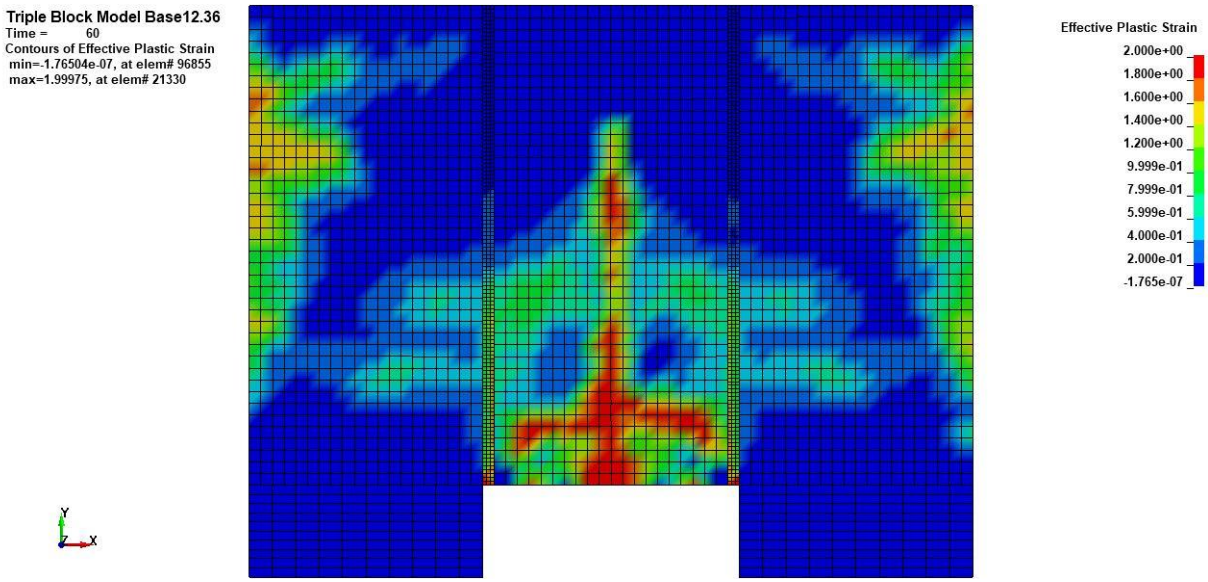


**Figure B-844: Effective Plastic Strain Fringe Plot for Last State at 60 Milliseconds for Base Run 12.36 – 1800 psi**

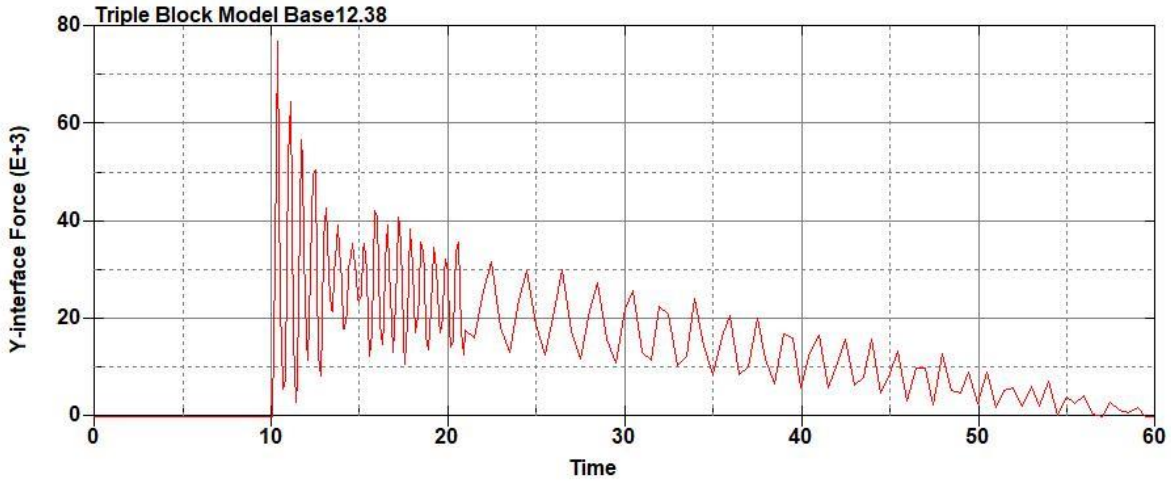


**Figure B-845: Base Run 12.38 Right Support Y-Interface Force (lbs) versus Time (ms) – 1900 psi**

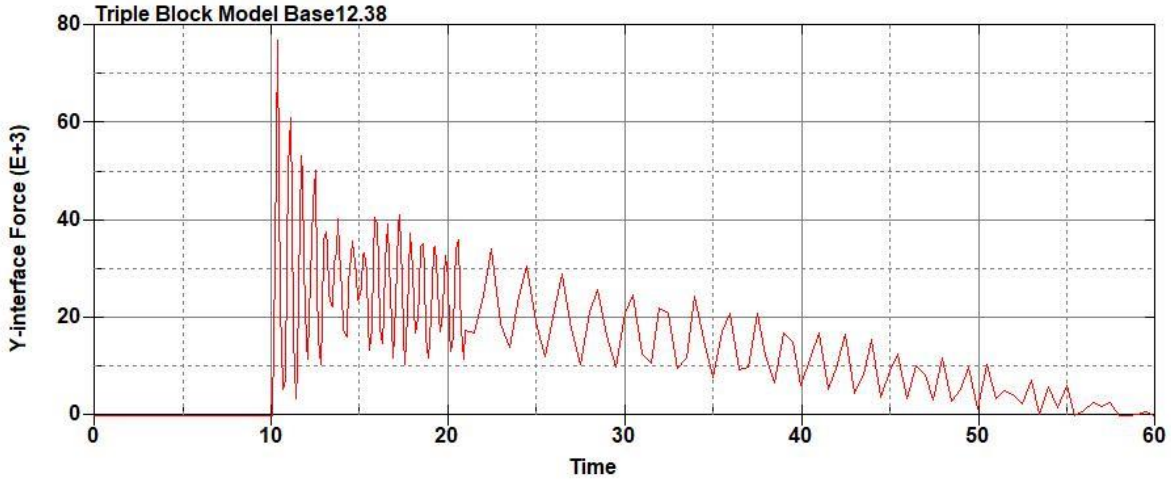


**Figure B-846: Base Run 12.38 Left Support Y-Interface Force (lbs) versus Time (ms) – 1900 psi**

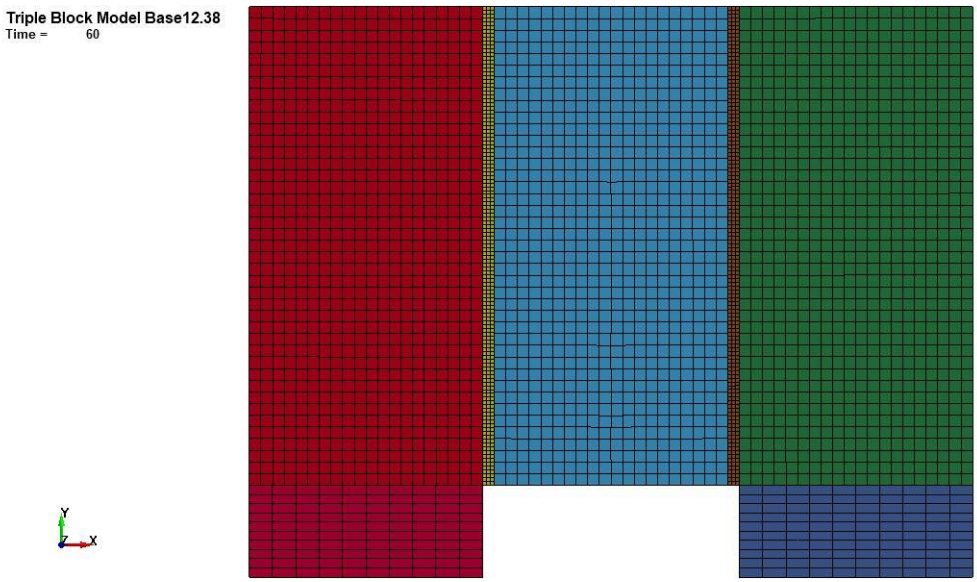


**Figure B-847: Last State at 60 Milliseconds for Base Run 12.38 – 1900 psi**

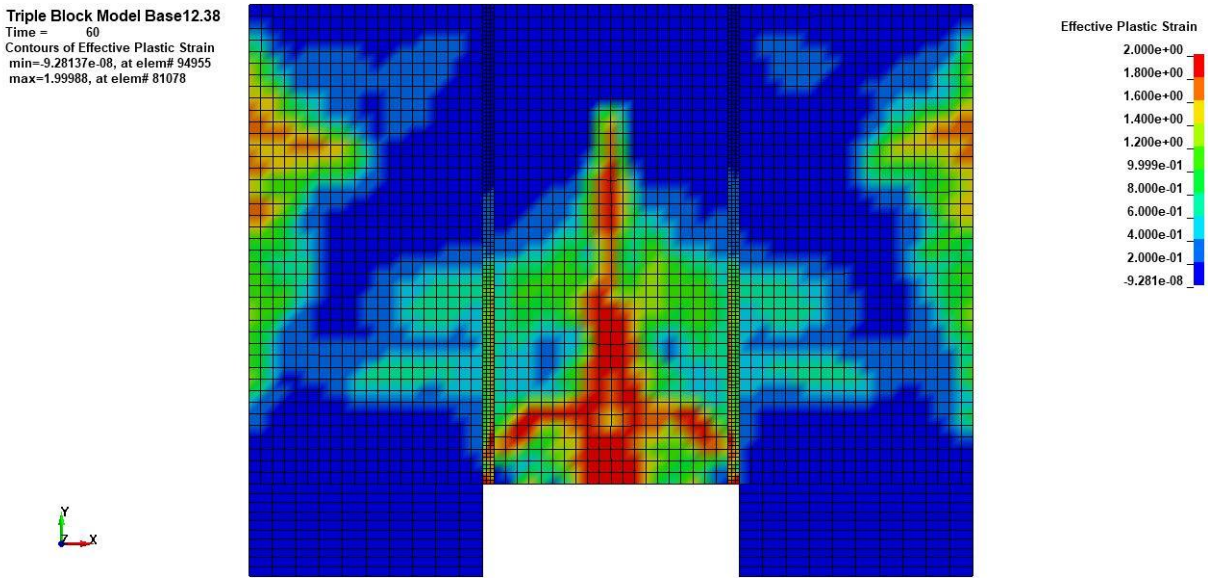


**Figure B-848: Effective Plastic Strain Fringe Plot for Last State at 60 Milliseconds for Base Run 12.38 – 1900 psi**

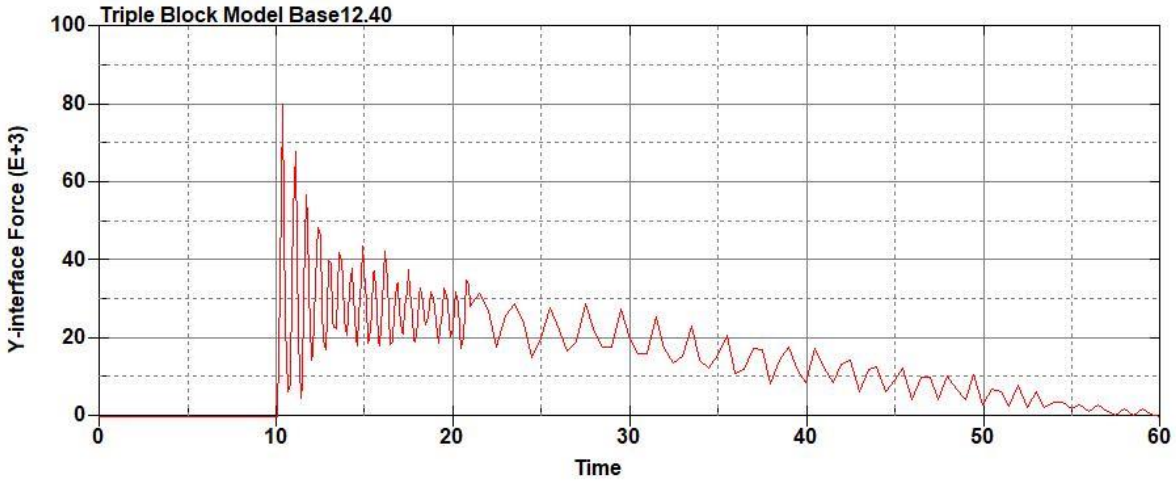


**Figure B-849: Base Run 12.40 Right Support Y-Interface Force (lbs) versus Time (ms) – 2000 psi**

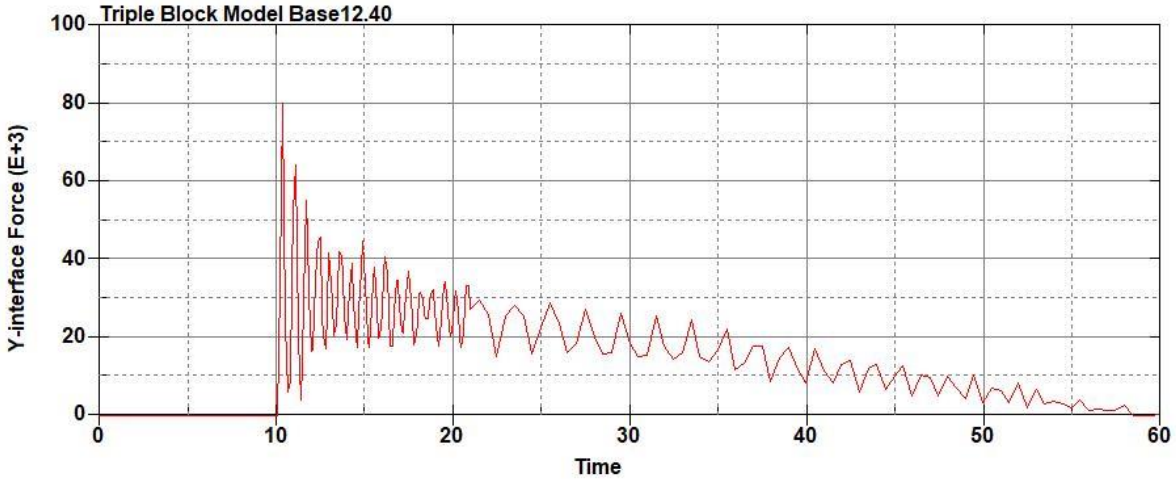


**Figure B-850: Base Run 12.40 Left Support Y-Interface Force (lbs) versus Time (ms) – 2000 psi**

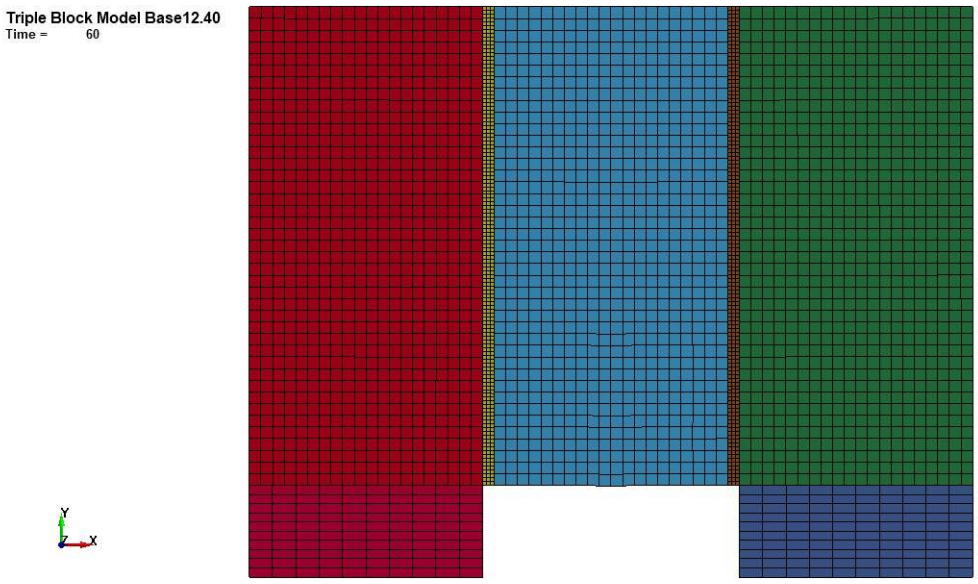


**Figure B-851: Last State at 60 Milliseconds for Base Run 12.40 – 2000 psi**

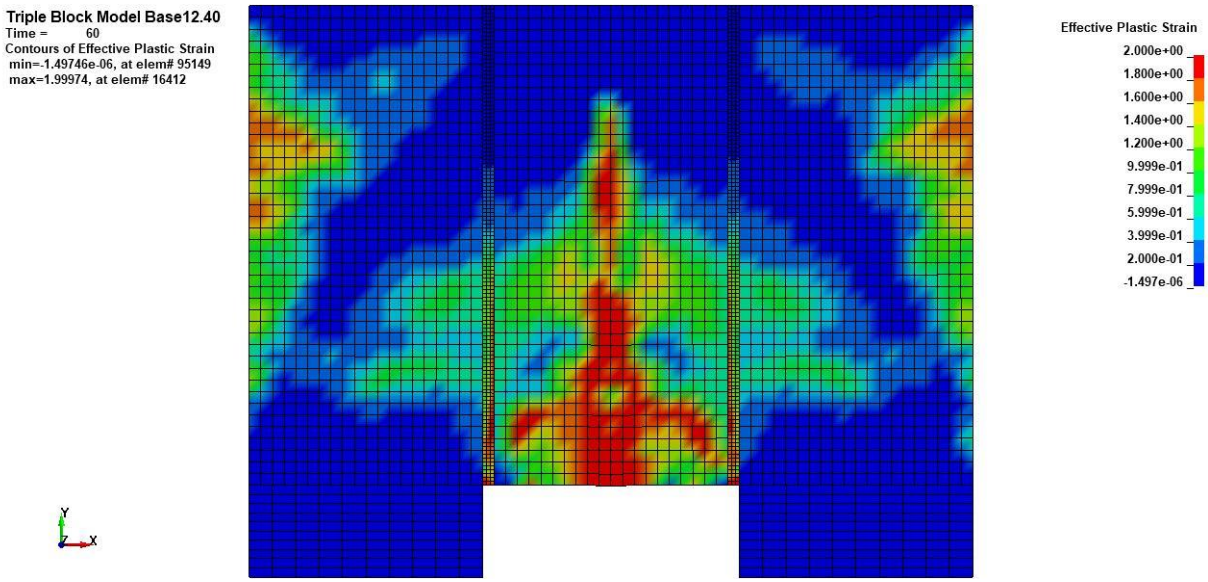


**Figure B-852: Effective Plastic Strain Fringe Plot for Last State at 60 Milliseconds for Base Run 12.40 – 2000 psi**

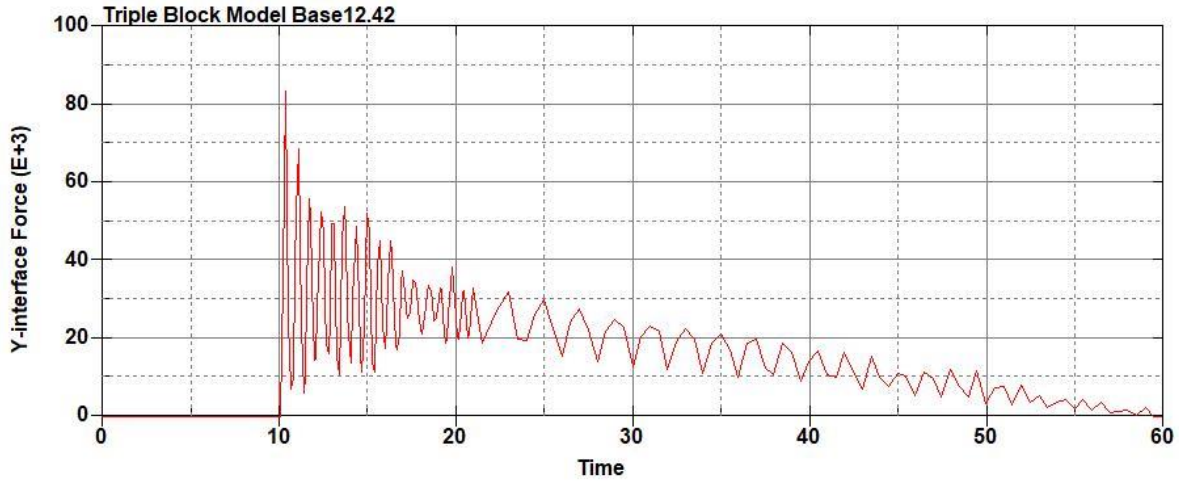


**Figure B-853: Base Run 12.42 Right Support Y-Interface Force (lbs) versus Time (ms) – 2100 psi**

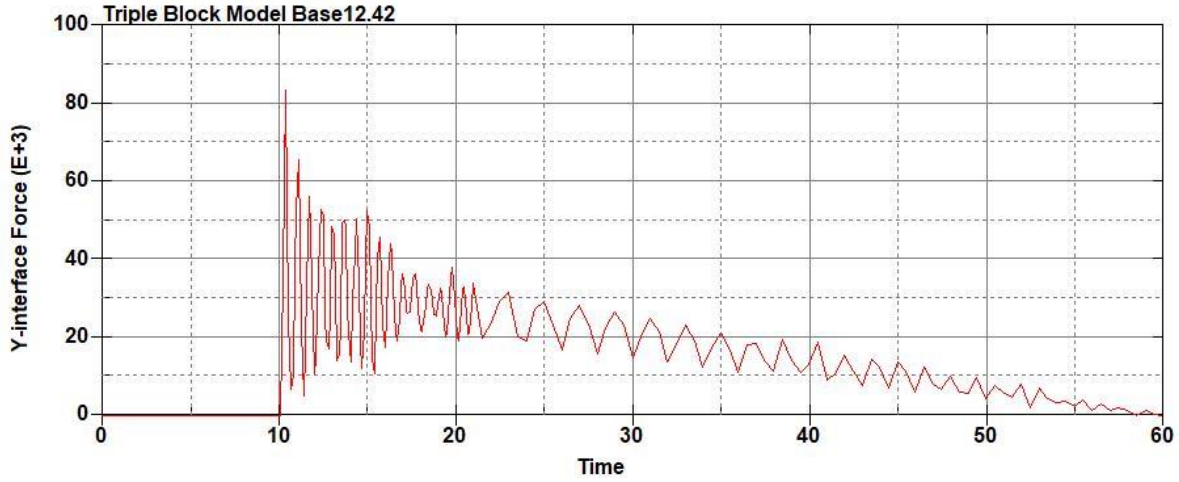


**Figure B-854: Base Run 12.42 Left Support Y-Interface Force (lbs) versus Time (ms) – 2100 psi**

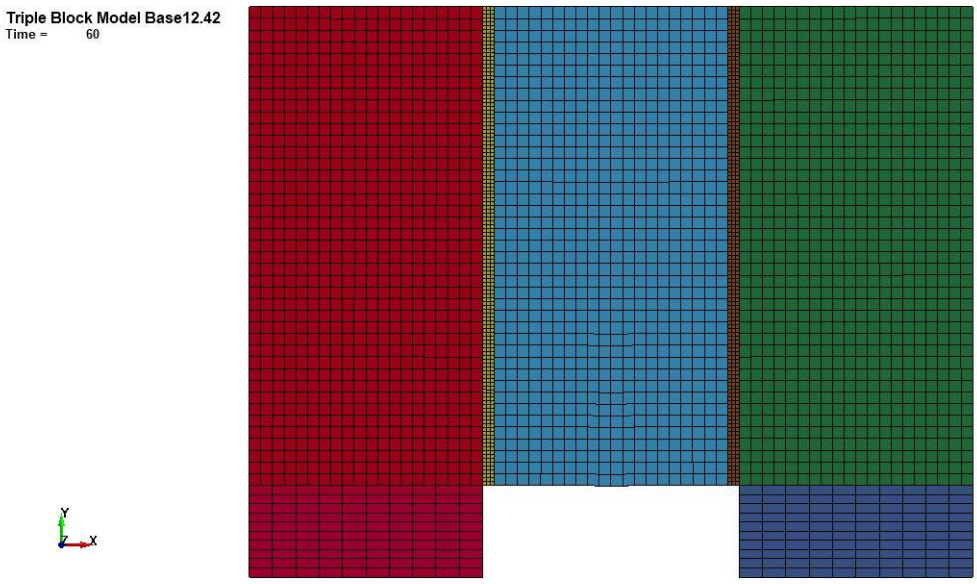


**Figure B-855: Last State at 60 Milliseconds for Base Run 12.42 – 2100 psi**

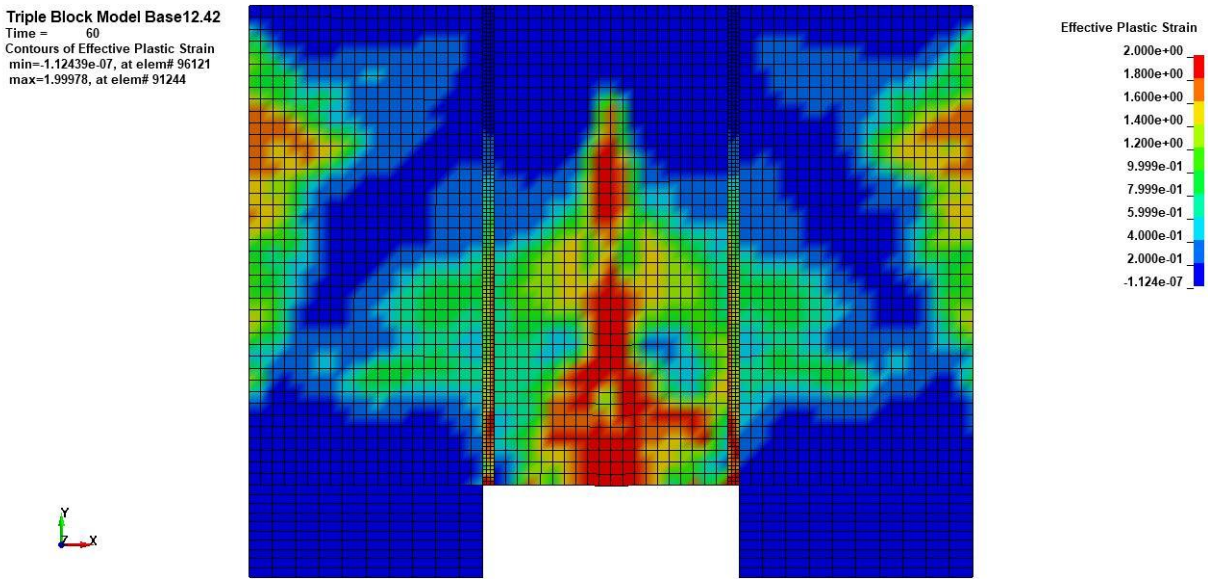


**Figure B-856: Effective Plastic Strain Fringe Plot for Last State at 60 Milliseconds for Base Run 12.42 – 2100 psi**

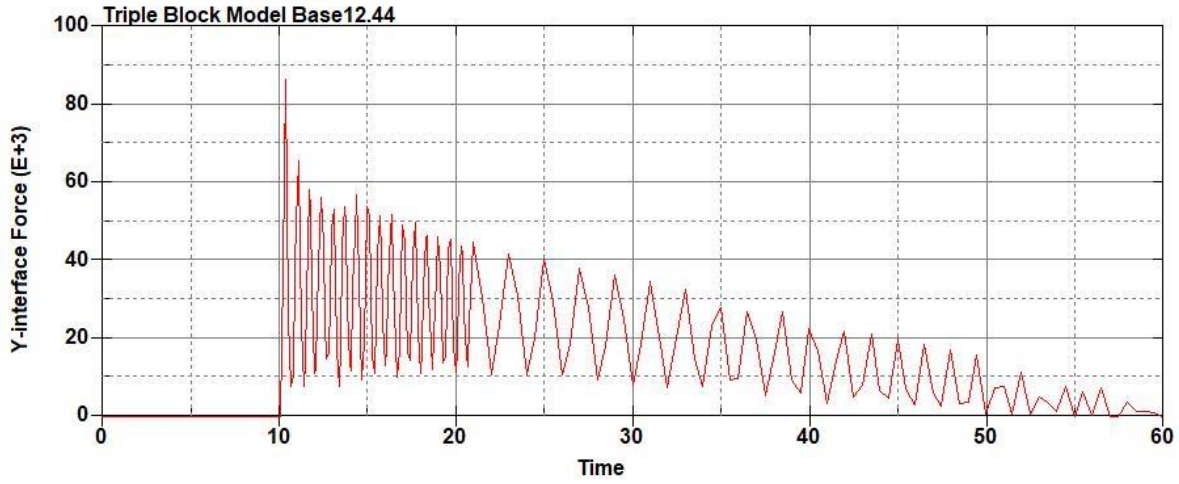


**Figure B-857: Base Run 12.44 Right Support Y-Interface Force (lbs) versus Time (ms) – 2200 psi**

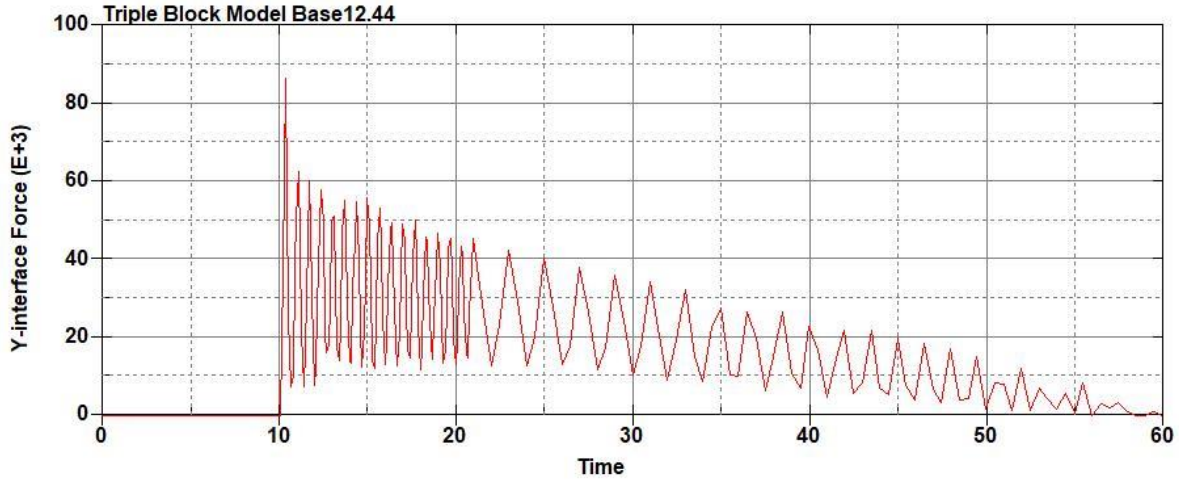


**Figure B-858: Base Run 12.44 Left Support Y-Interface Force (lbs) versus Time (ms) – 2200 psi**

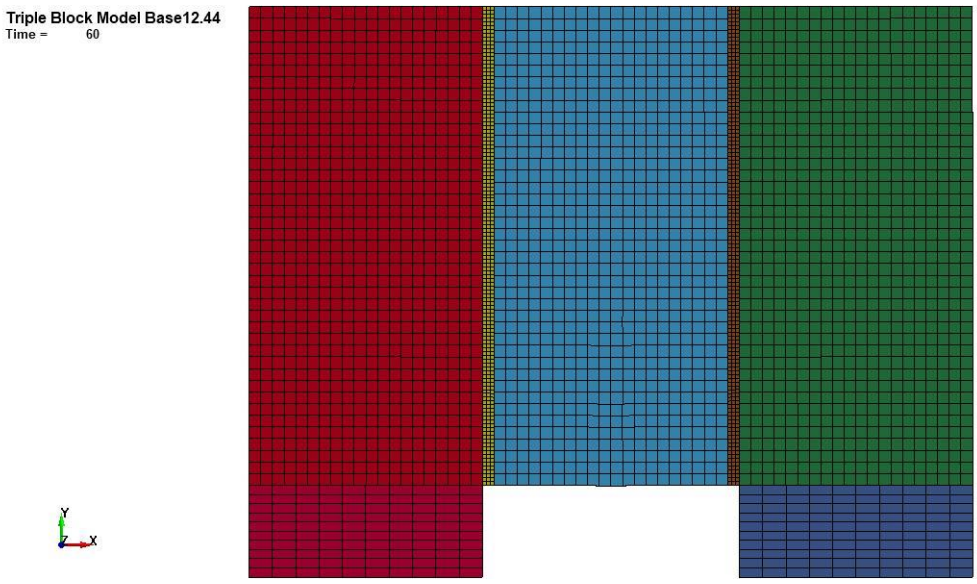


**Figure B-859: Last State at 60 Milliseconds for Base Run 12.44 – 2200 psi**

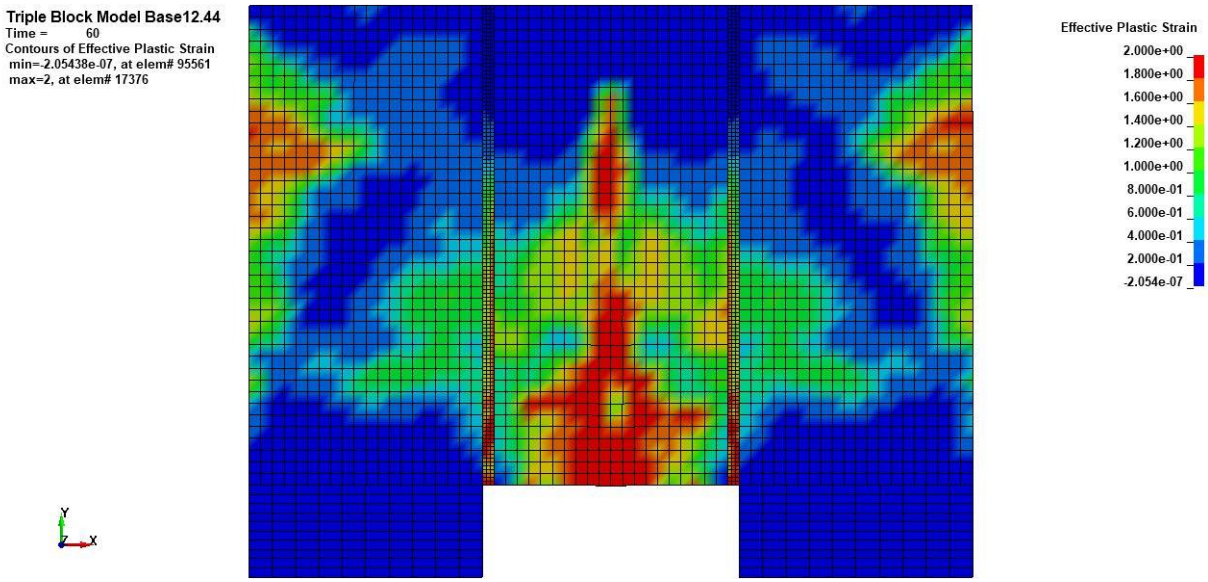


**Figure B-860: Effective Plastic Strain Fringe Plot for Last State at 60 Milliseconds for Base Run 12.44 – 2200 psi**

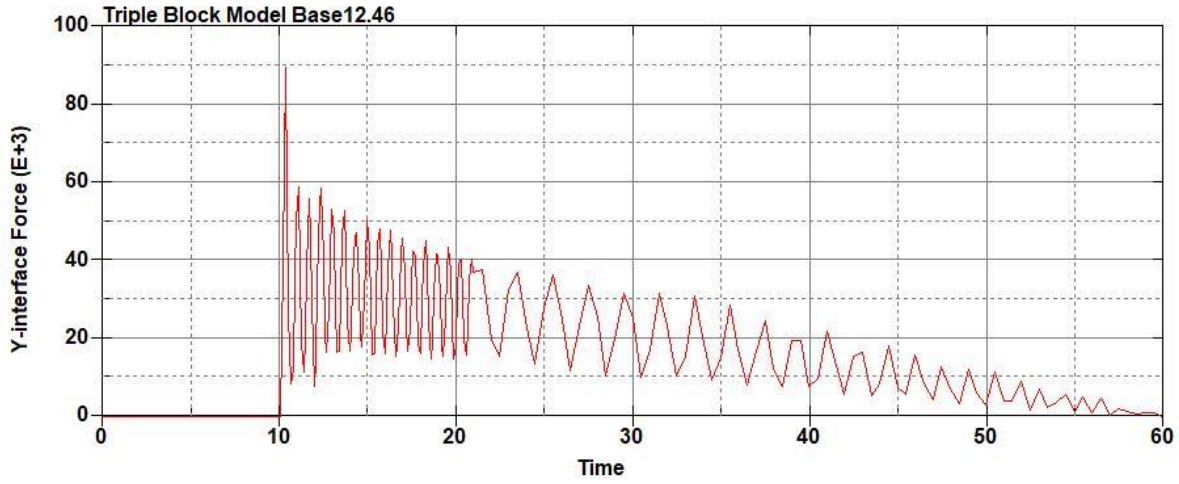


**Figure B-861: Base Run 12.46 Right Support Y-Interface Force (lbs) versus Time (ms) – 2300 psi**

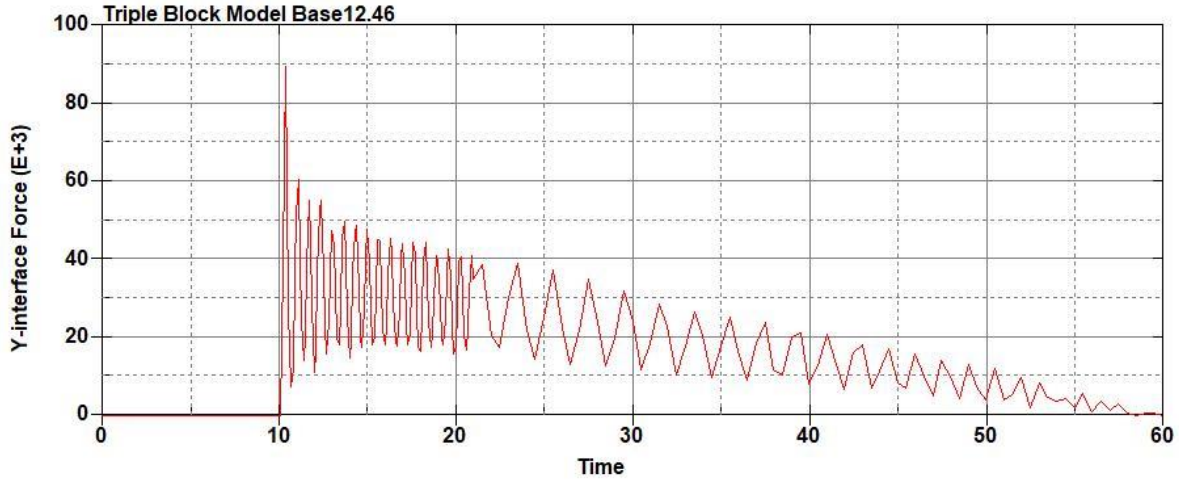


**Figure B-862: Base Run 12.46 Left Support Y-Interface Force (lbs) versus Time (ms) – 2300 psi**

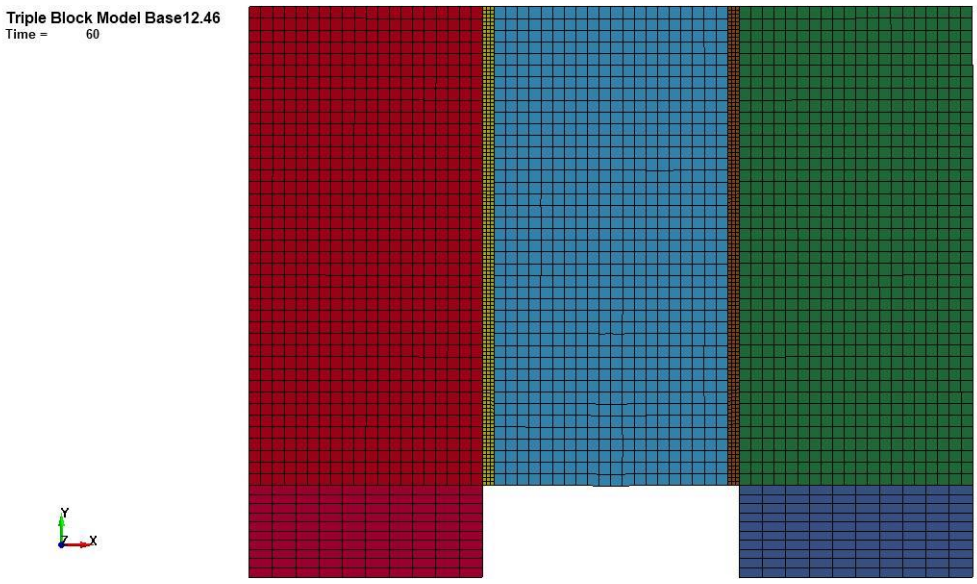


**Figure B-863: Last State at 60 Milliseconds for Base Run 12.46 – 2300 psi**

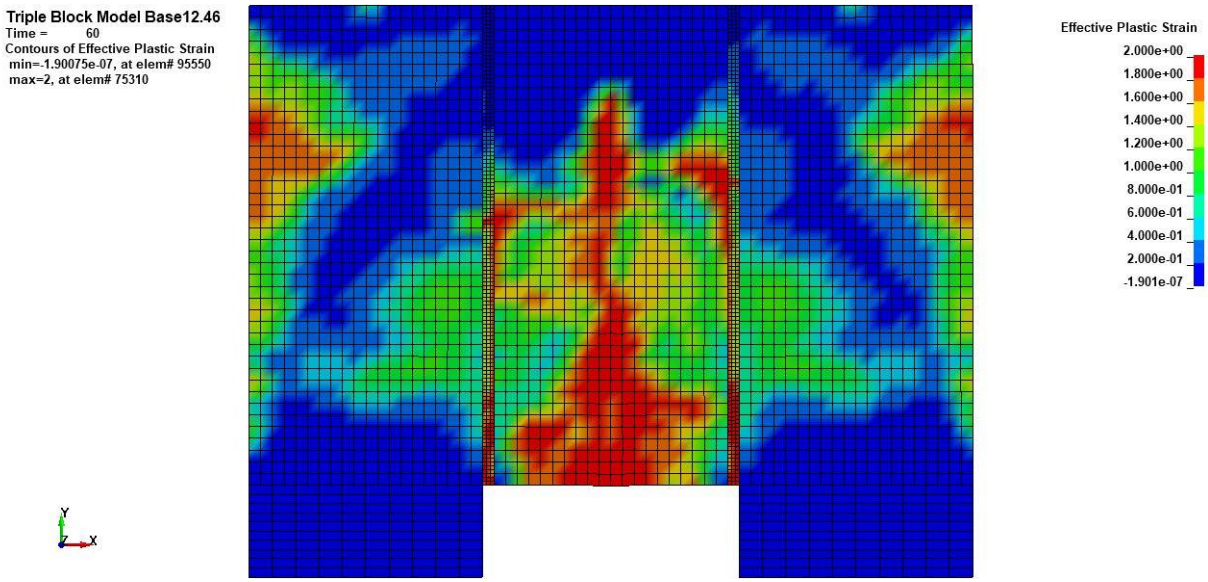


**Figure B-864: Effective Plastic Strain Fringe Plot for Last State at 60 Milliseconds for Base Run 12.46 – 2300 psi**

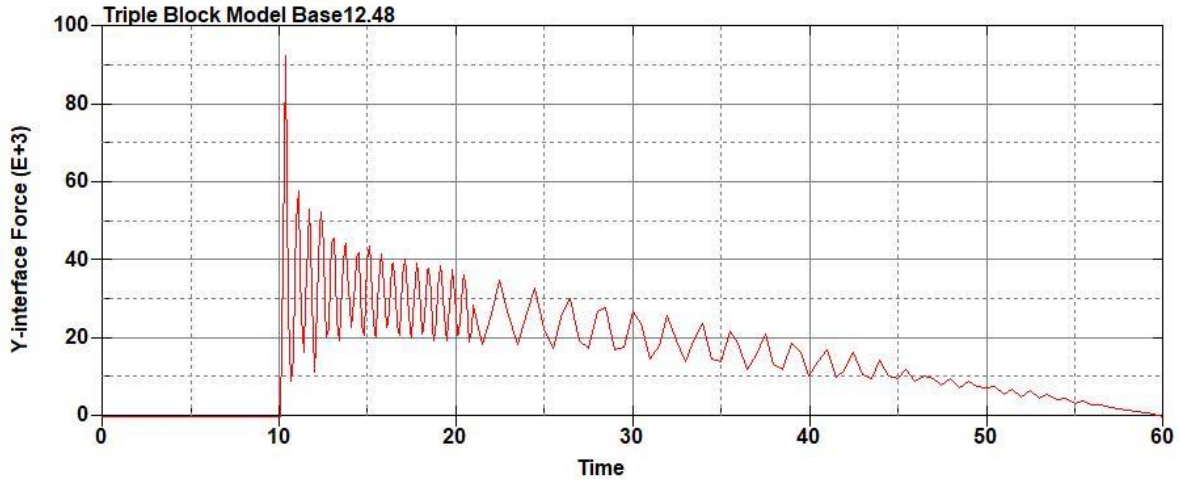


**Figure B-865: Base Run 12.48 Right Support Y-Interface Force (lbs) versus Time (ms) – 2400 psi**

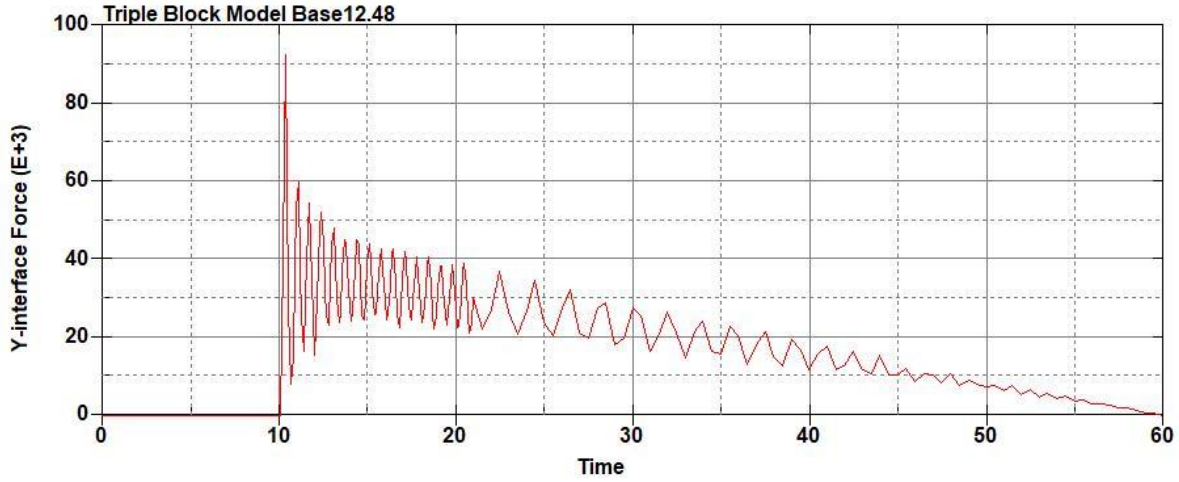


**Figure B-866: Base Run 12.48 Left Support Y-Interface Force (lbs) versus Time (ms) – 2400 psi**

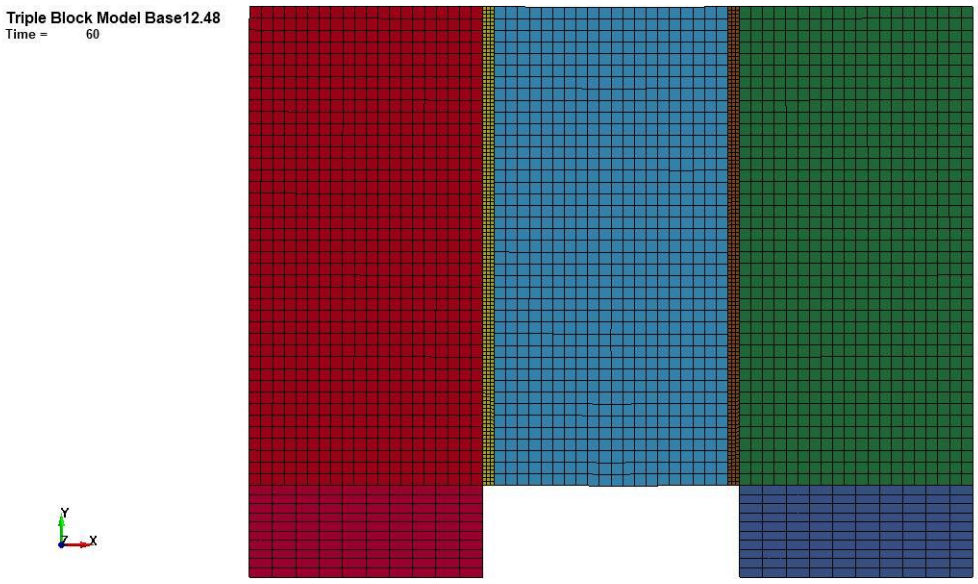


**Figure B-867: Last State at 60 Milliseconds for Base Run 12.48 – 2400 psi**

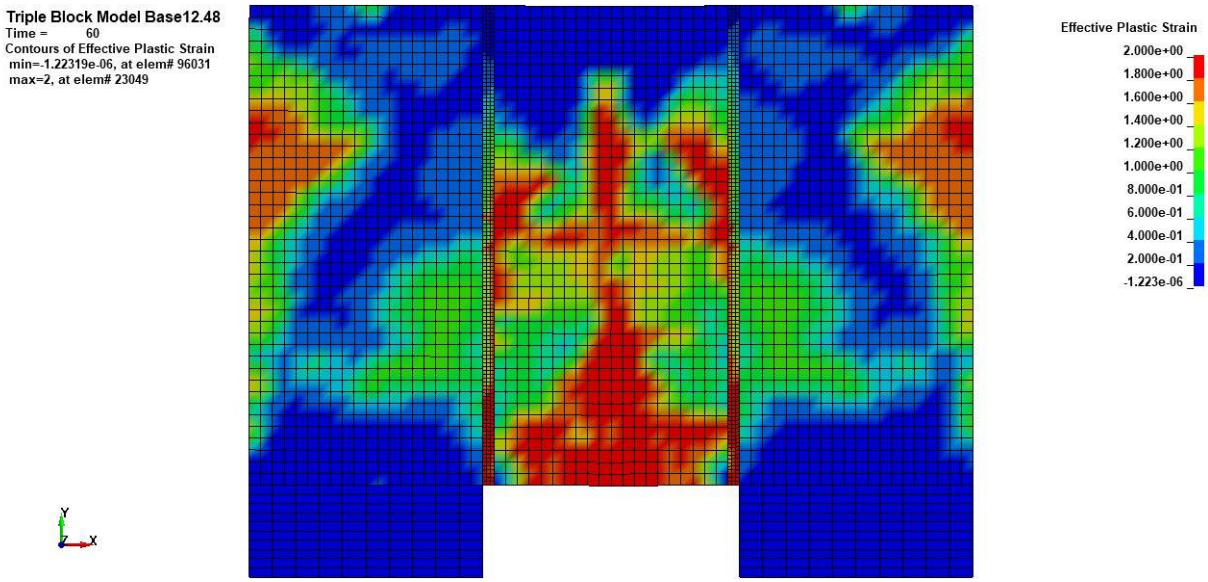


**Figure B-868: Effective Plastic Strain Fringe Plot for Last State at 60 Milliseconds for Base Run 12.48 – 2400 psi**

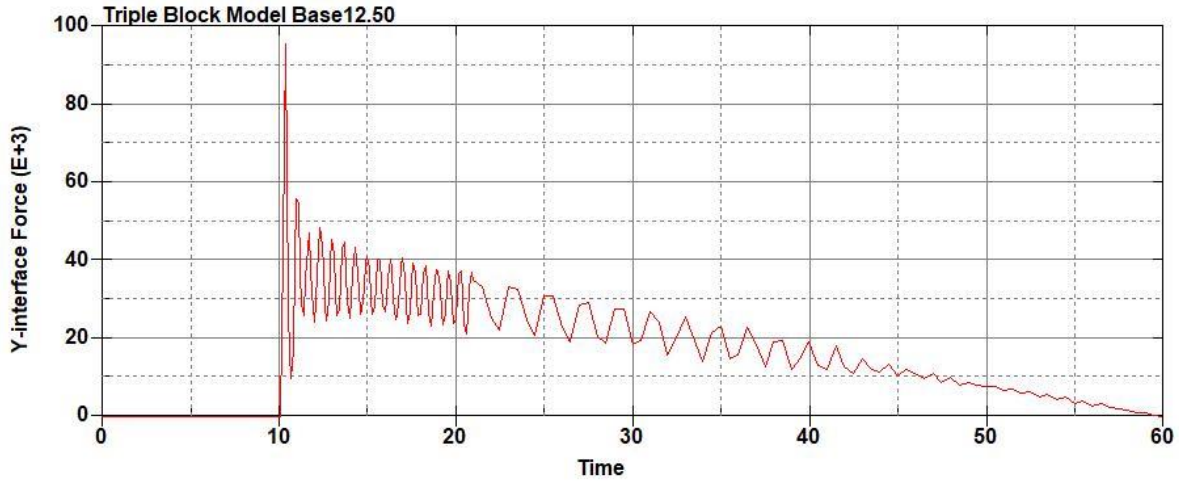


**Figure B-869: Base Run 12.50 Right Support Y-Interface Force (lbs) versus Time (ms) – 2500 psi**

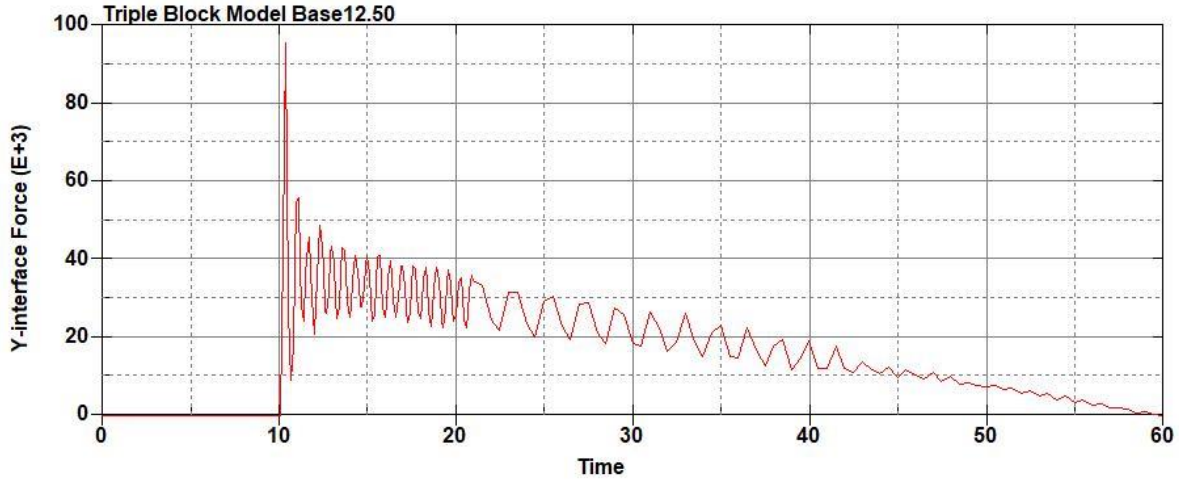


**Figure B-870: Base Run 12.50 Left Support Y-Interface Force (lbs) versus Time (ms) – 2500 psi**

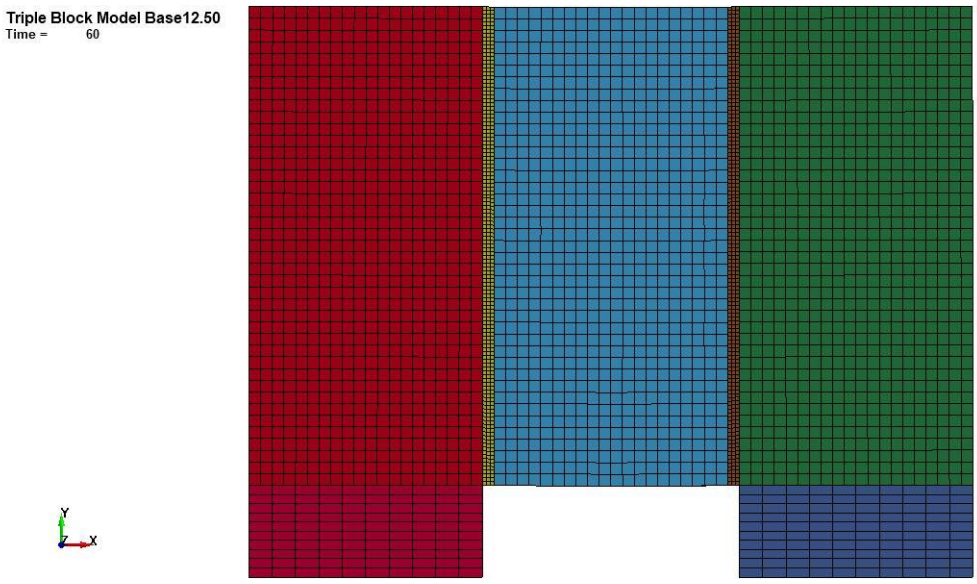


**Figure B-871: Last State at 60 Milliseconds for Base Run 12.50 – 2500 psi**

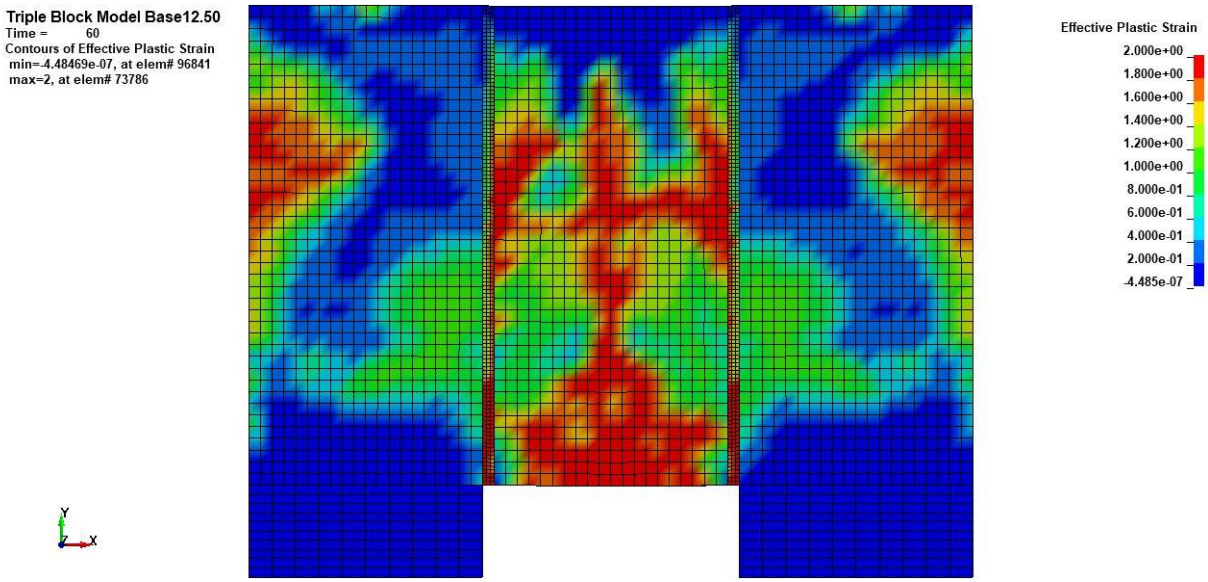


**Figure B-872: Effective Plastic Strain Fringe Plot for Last State at 60 Milliseconds for Base Run 12.50 – 2500 psi**

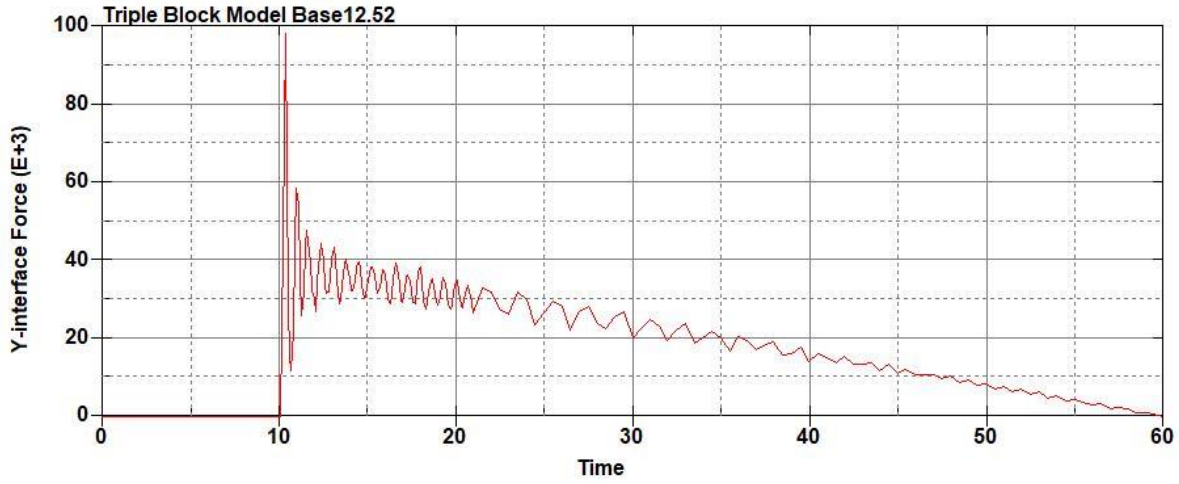


**Figure B-873: Base Run 12.52 Right Support Y-Interface Force (lbs) versus Time (ms) – 2600 psi**

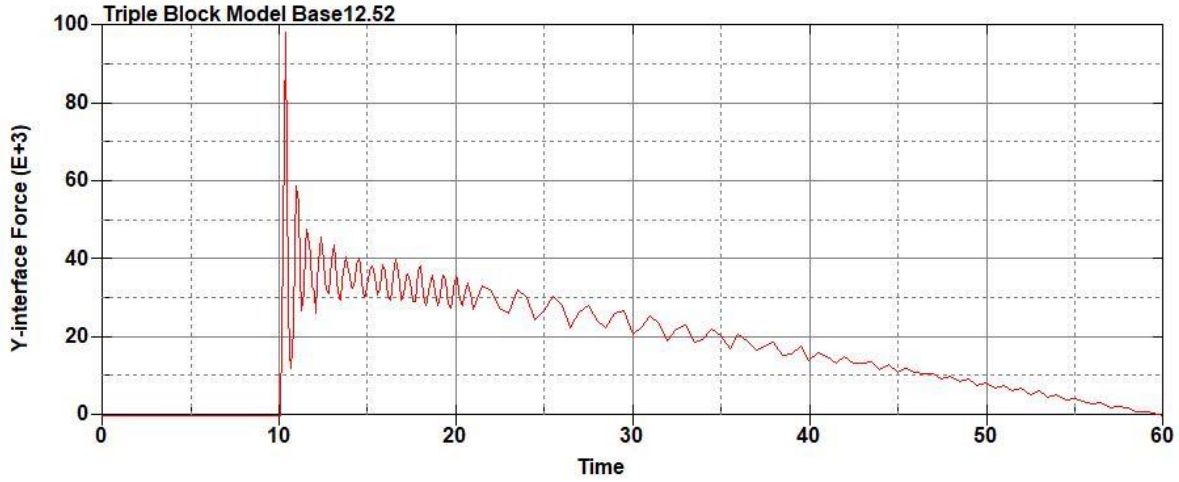


**Figure B-874: Base Run 12.52 Left Support Y-Interface Force (lbs) versus Time (ms) – 2600 psi**

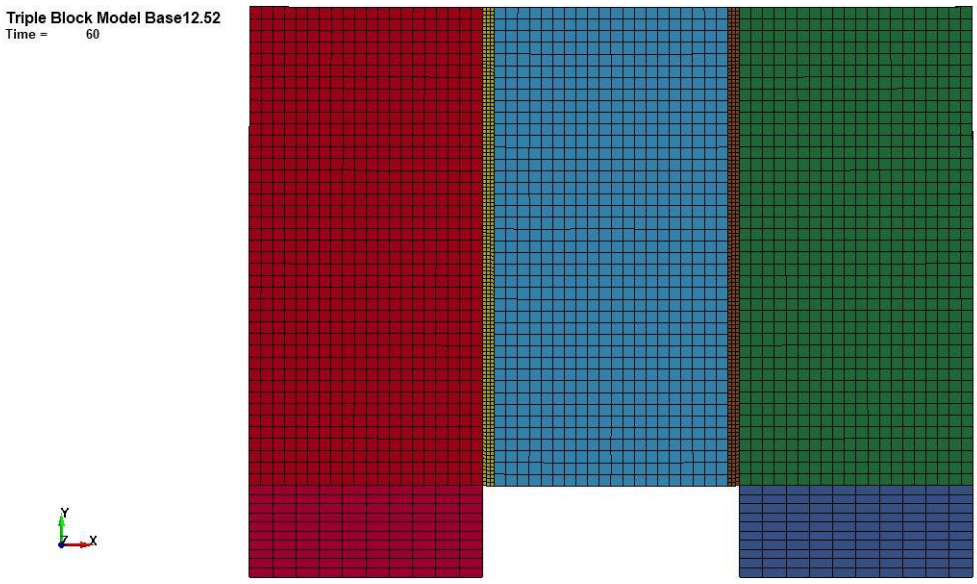


**Figure B-875: Last State at 60 Milliseconds for Base Run 12.52 – 2600 psi**

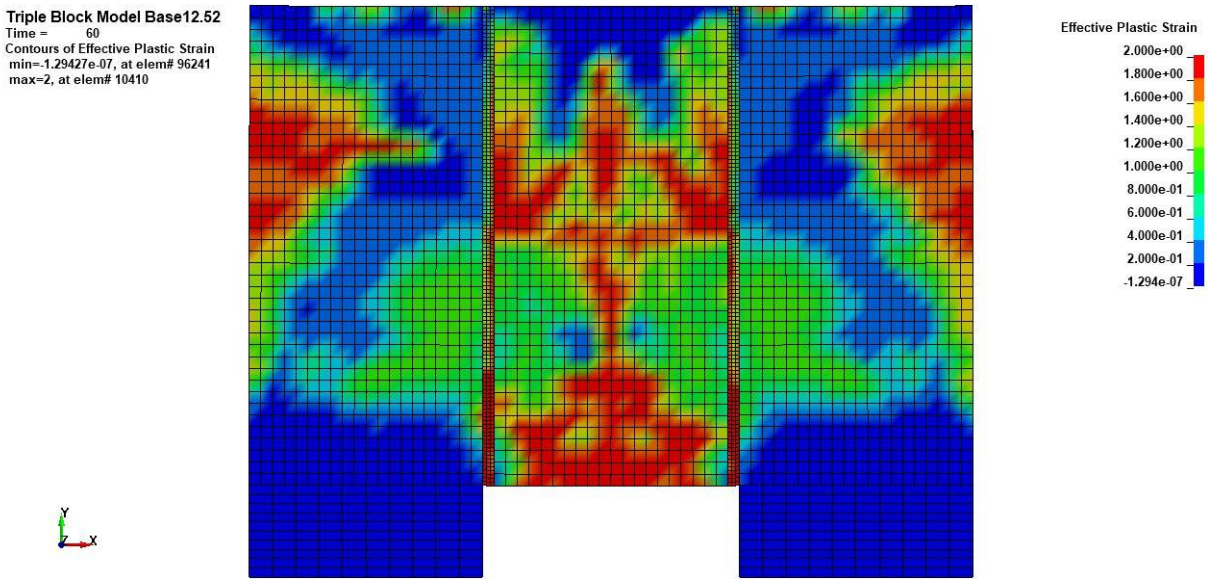


**Figure B-876: Effective Plastic Strain Fringe Plot for Last State at 60 Milliseconds for Base Run 12.52 – 2600 psi**

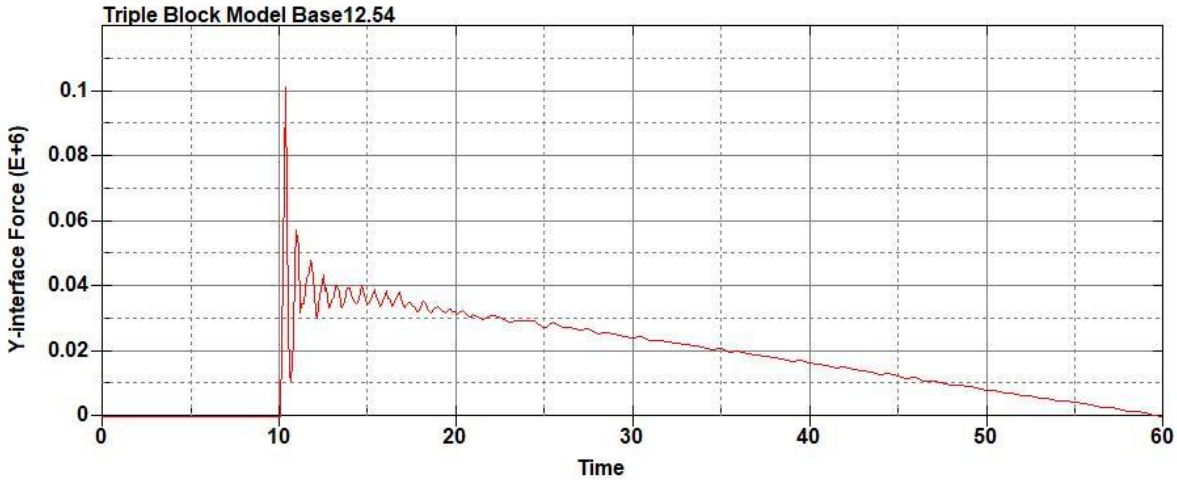


**Figure B-877: Base Run 12.54 Right Support Y-Interface Force (lbs) versus Time (ms) – 2700 psi**

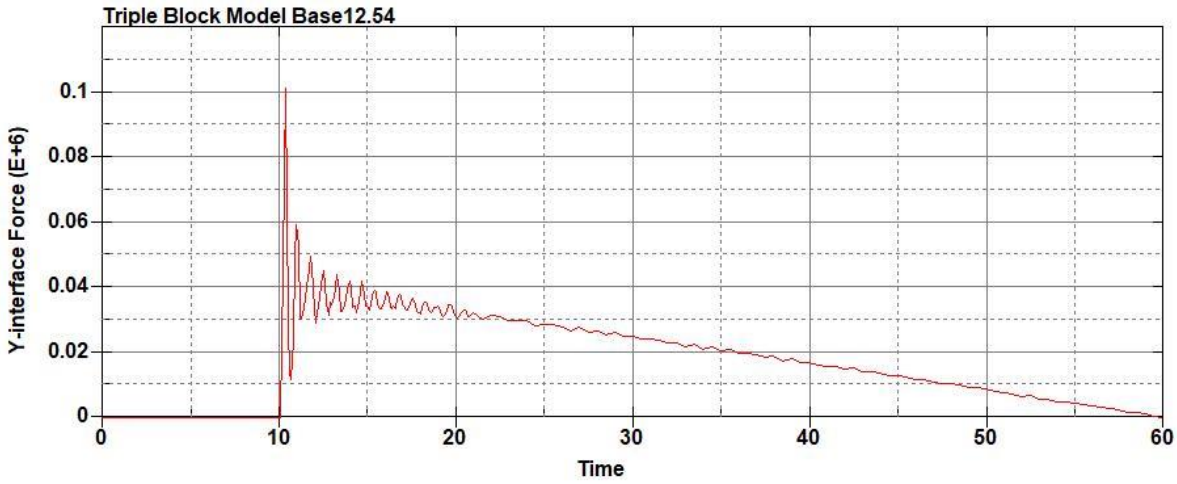


**Figure B-878: Base Run 12.54 Left Support Y-Interface Force (lbs) versus Time (ms) – 2700 psi**

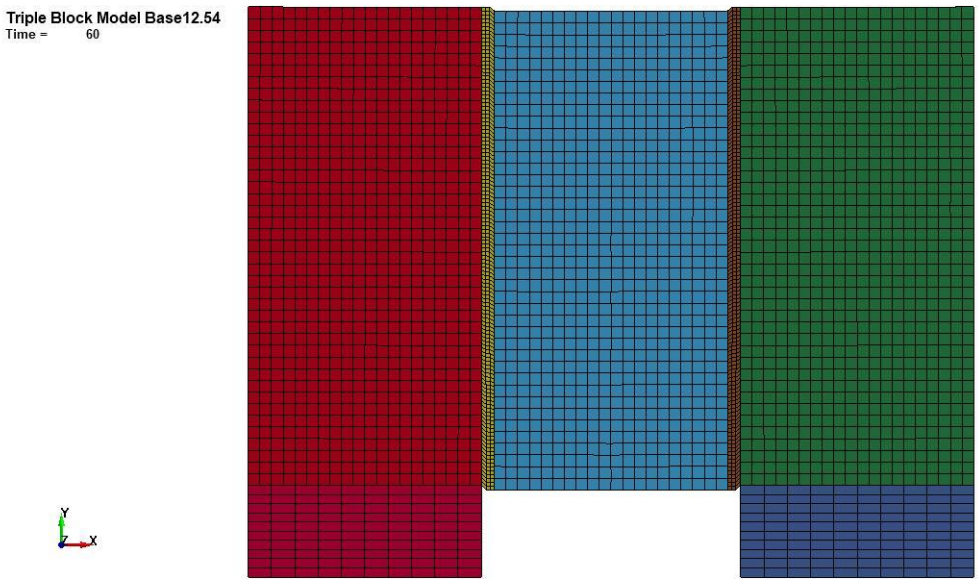


**Figure B-879: Last State at 60 Milliseconds for Base Run 12.54 – 2700 psi**

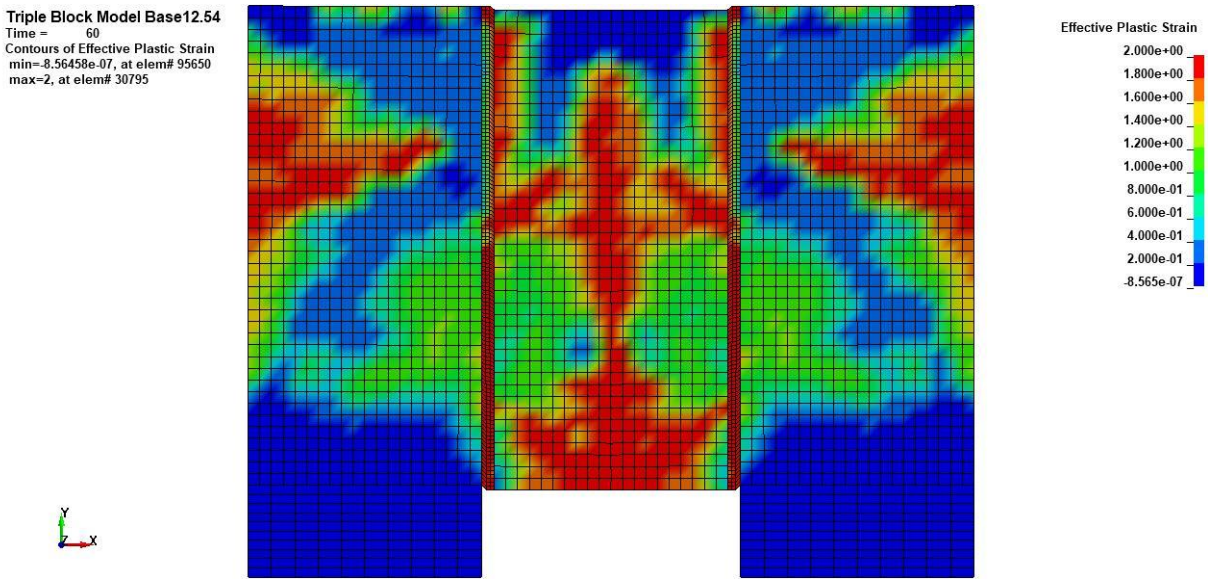


**Figure B-880: Effective Plastic Strain Fringe Plot for Last State at 60 Milliseconds for Base Run 12.54 – 2700 psi**

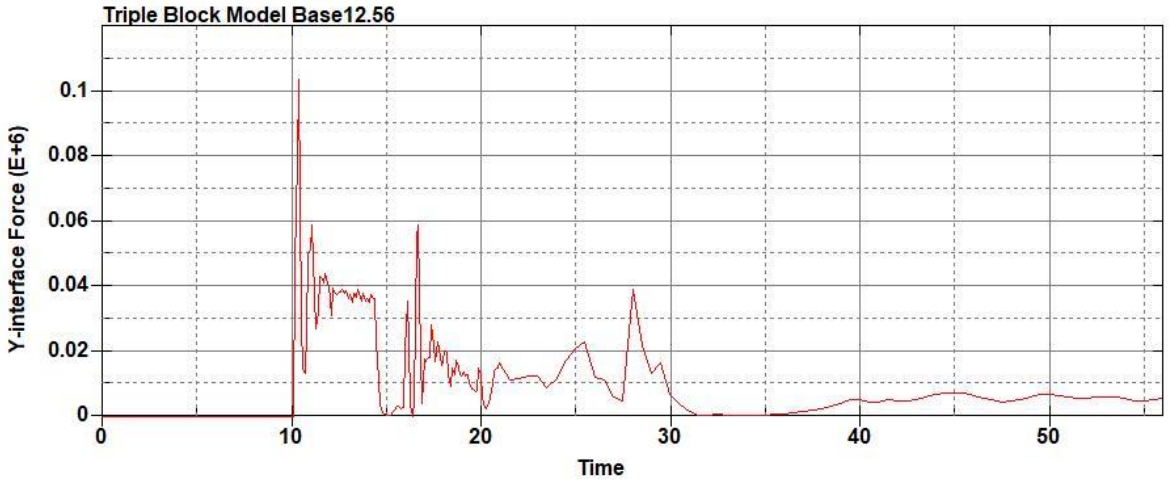


**Figure B-881: Base Run 12.56 Right Support Y-Interface Force (lbs) versus Time (ms) – 2800 psi**

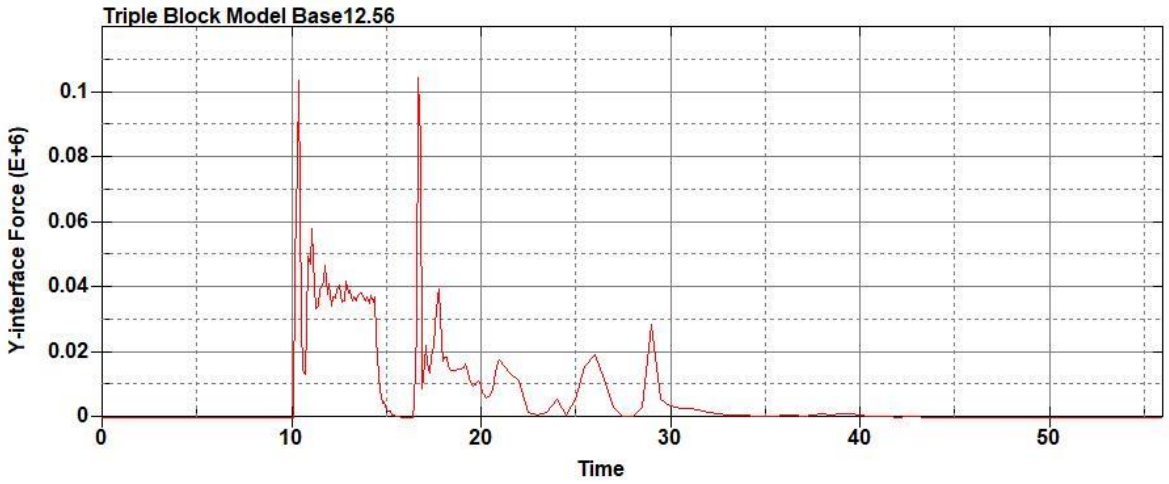


**Figure B-882: Base Run 12.56 Left Support Y-Interface Force (lbs) versus Time (ms) – 2800 psi**


**Figure B-883: Last State at 18 Milliseconds for Base Run 12.56 – 2800 psi**

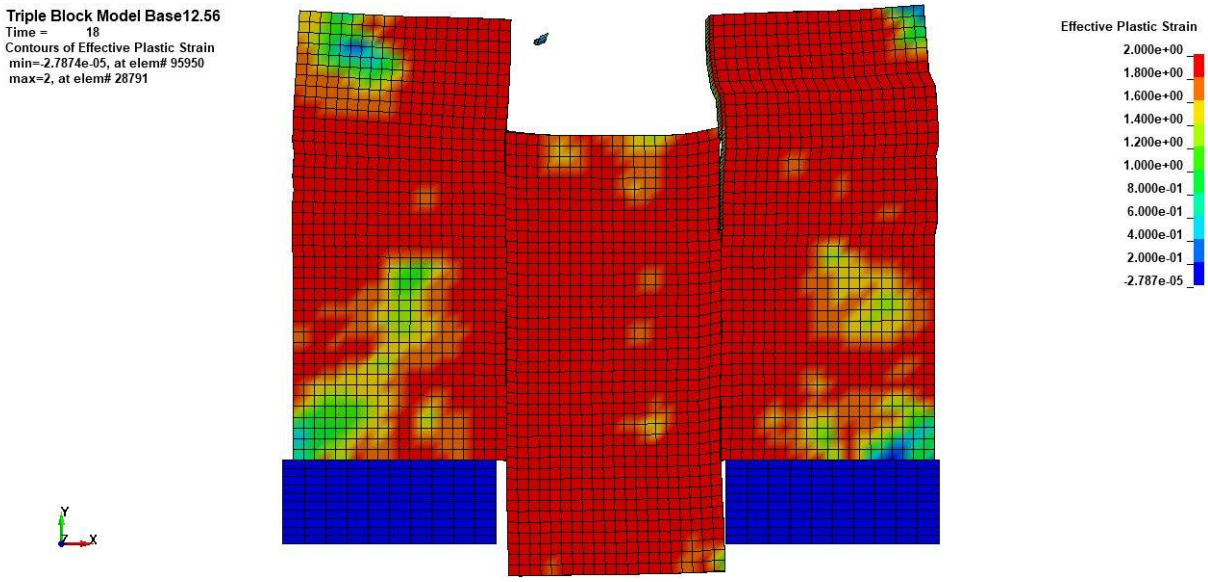


**Figure B-884: Effective Plastic Strain Fringe Plot for Last State at 18 Milliseconds for Base Run 12.56 – 2800 psi**

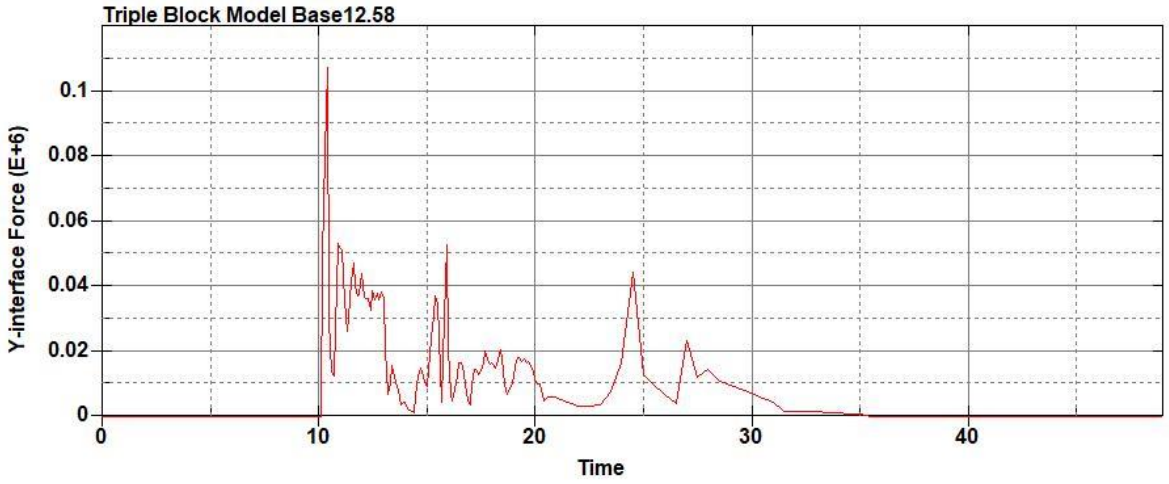


**Figure B-885: Base Run 12.58 Right Support Y-Interface Force (lbs) versus Time (ms) – 2900 psi**

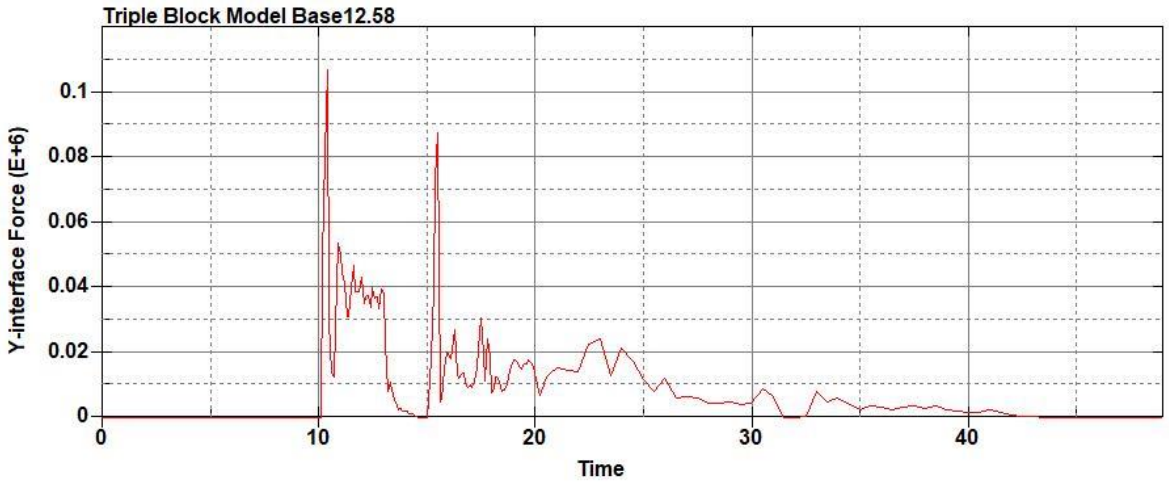


**Figure B-886: Base Run 12.58 Left Support Y-Interface Force (lbs) versus Time (ms) – 2900 psi**

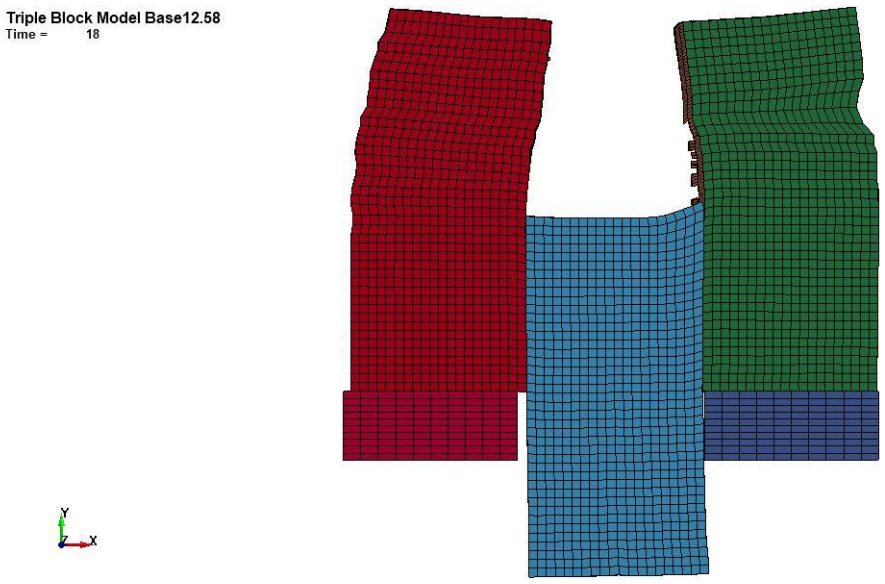


**Figure B-887: Last State at 18 Milliseconds for Base Run 12.58 – 2900 psi**

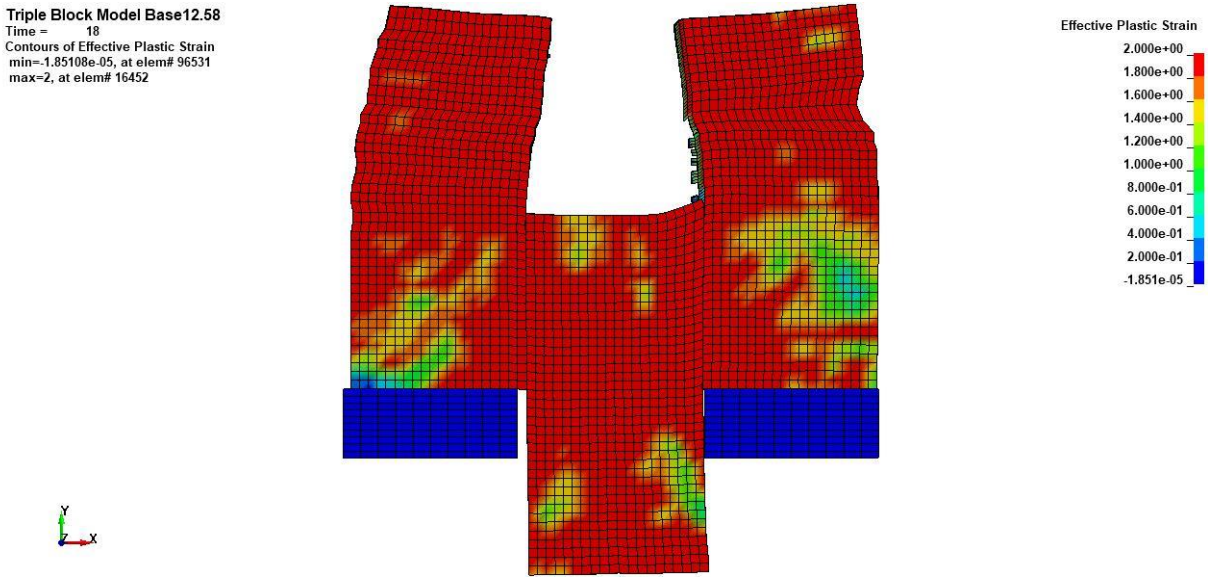


**Figure B-888: Effective Plastic Strain Fringe Plot for Last State at 18 Milliseconds for Base Run 12.58 – 2900 psi**

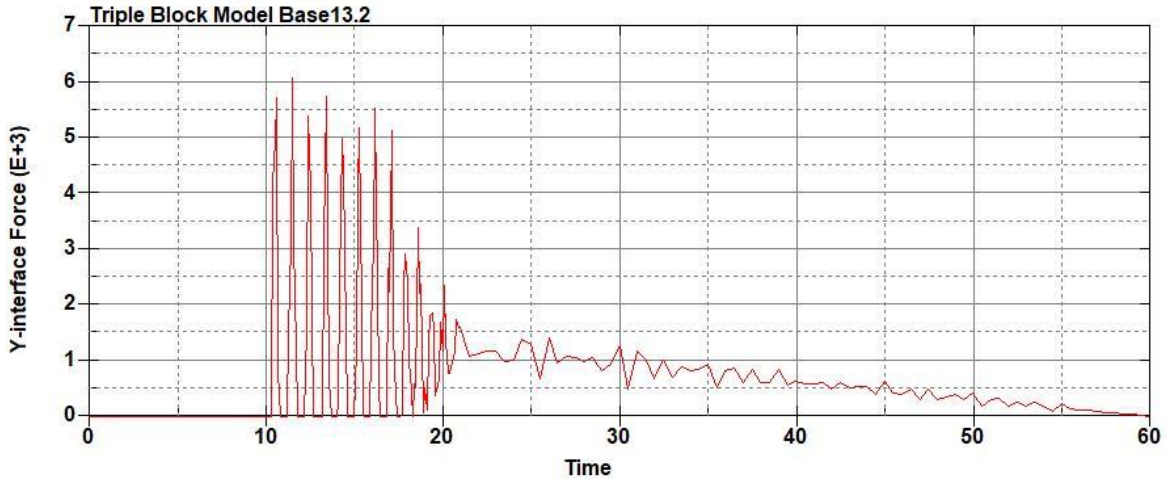


**Figure B-889: Base Run 13.2 Right Support Y-Interface Force (lbs) versus Time (ms) – 100 psi**

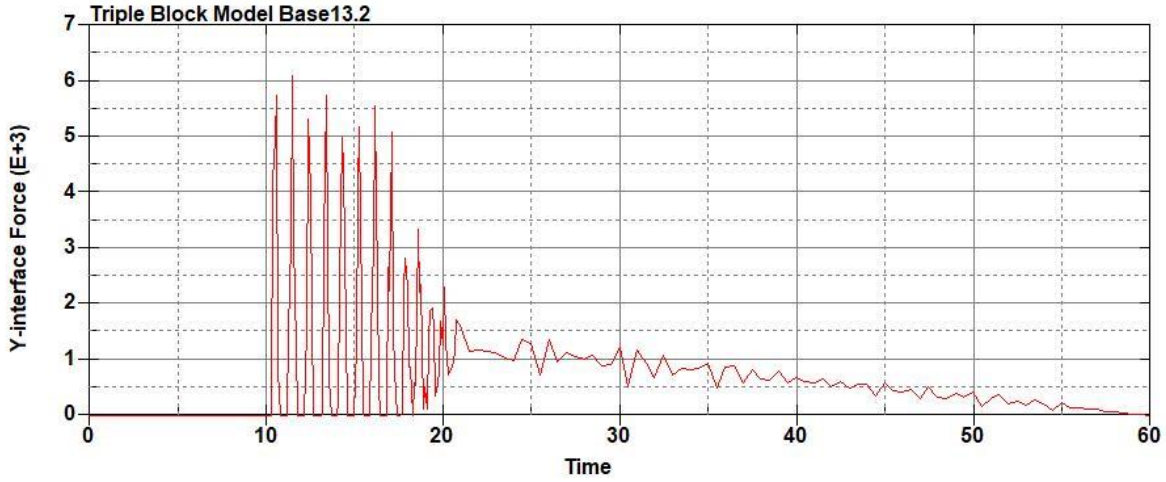


**Figure B-890: Base Run 13.2 Left Support Y-Interface Force (lbs) versus Time (ms) – 100 psi**

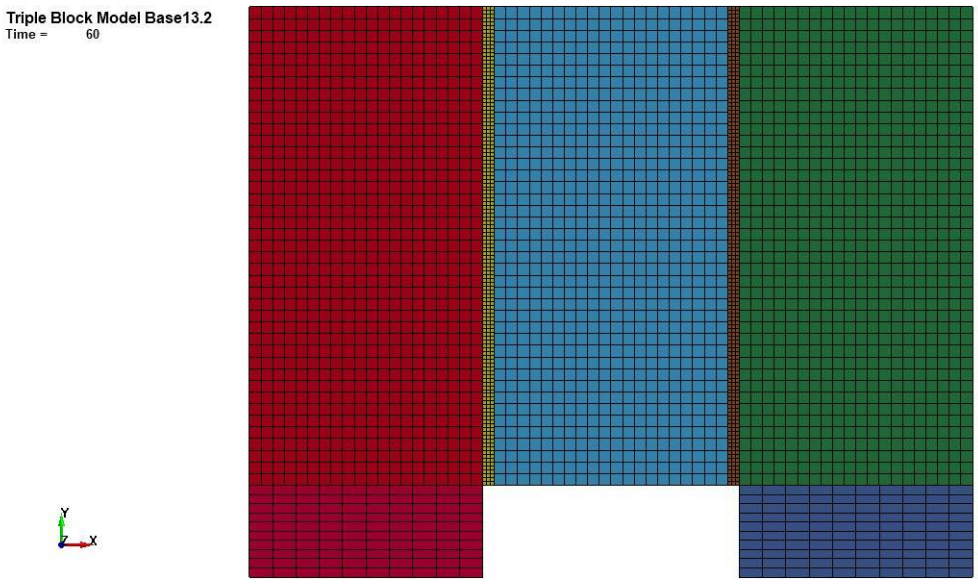


**Figure B-891: Last State at 60 Milliseconds for Base Run 13.2 – 100 psi**

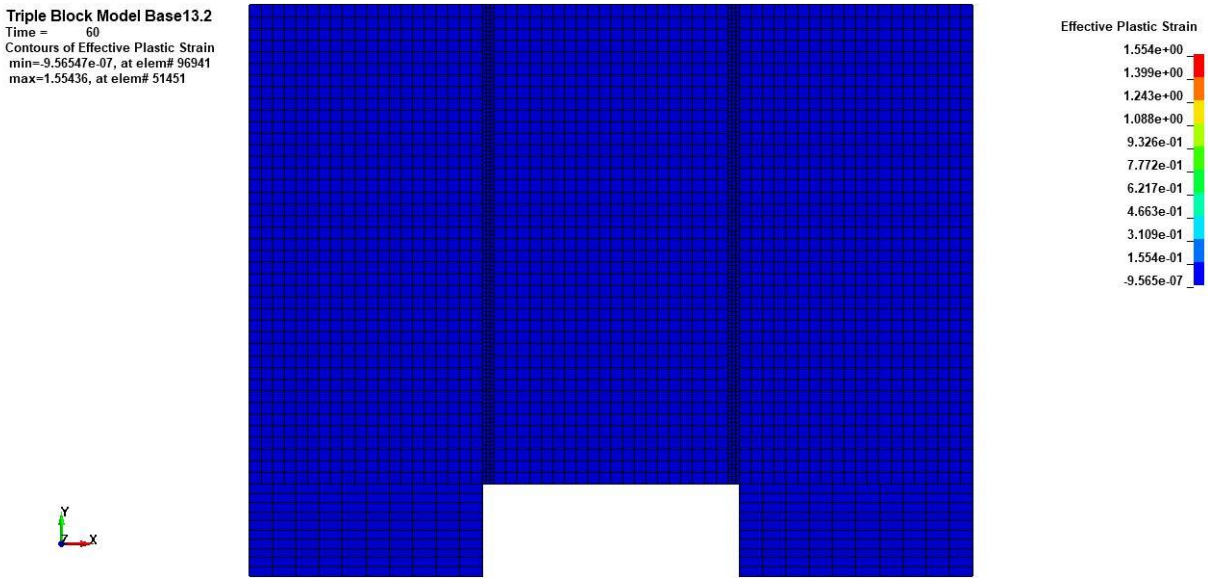


**Figure B-892: Effective Plastic Strain Fringe Plot for Last State at 60 Milliseconds for Base Run 13.2 – 100 psi**

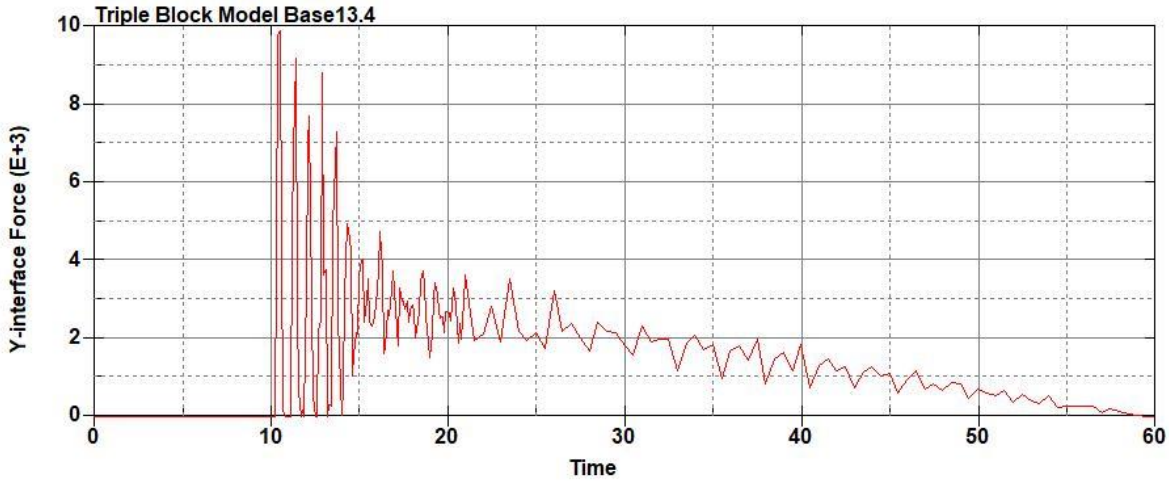


**Figure B-893: Base Run 13.4 Right Support Y-Interface Force (lbs) versus Time (ms) – 200 psi**

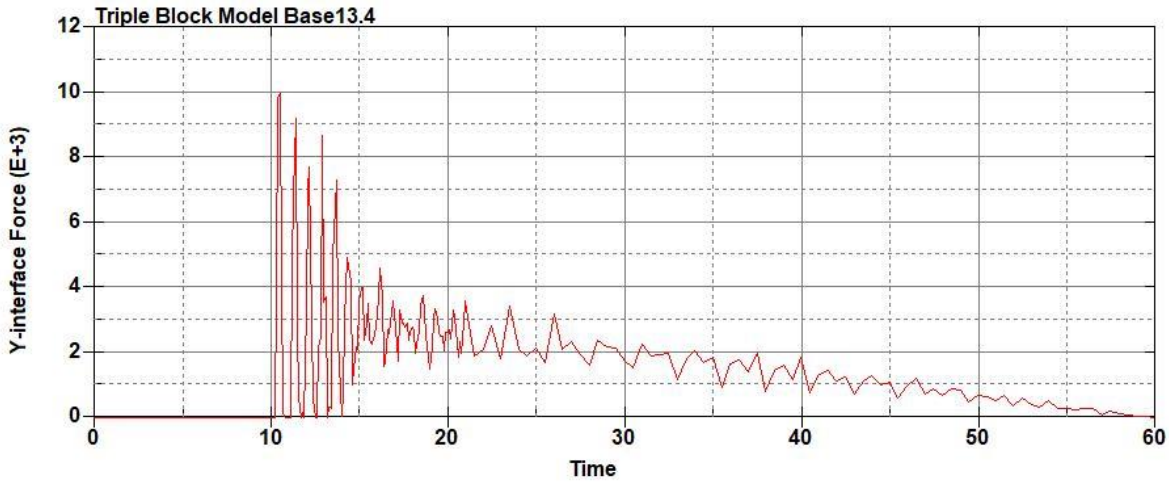


**Figure B-894: Base Run 13.4 Left Support Y-Interface Force (lbs) versus Time (ms) – 200 psi**

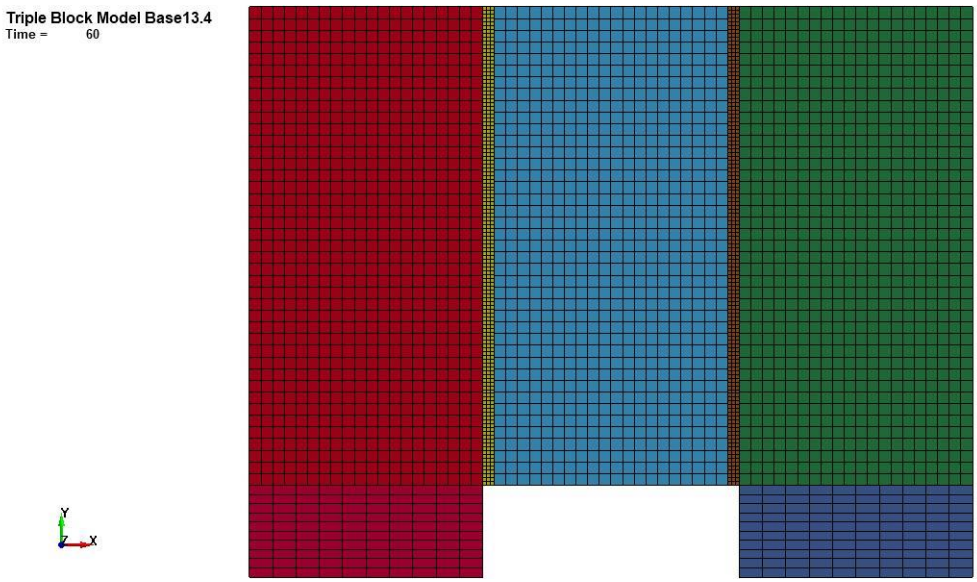


**Figure B-895: Last State at 60 Milliseconds for Base Run 13.4 – 200 psi**

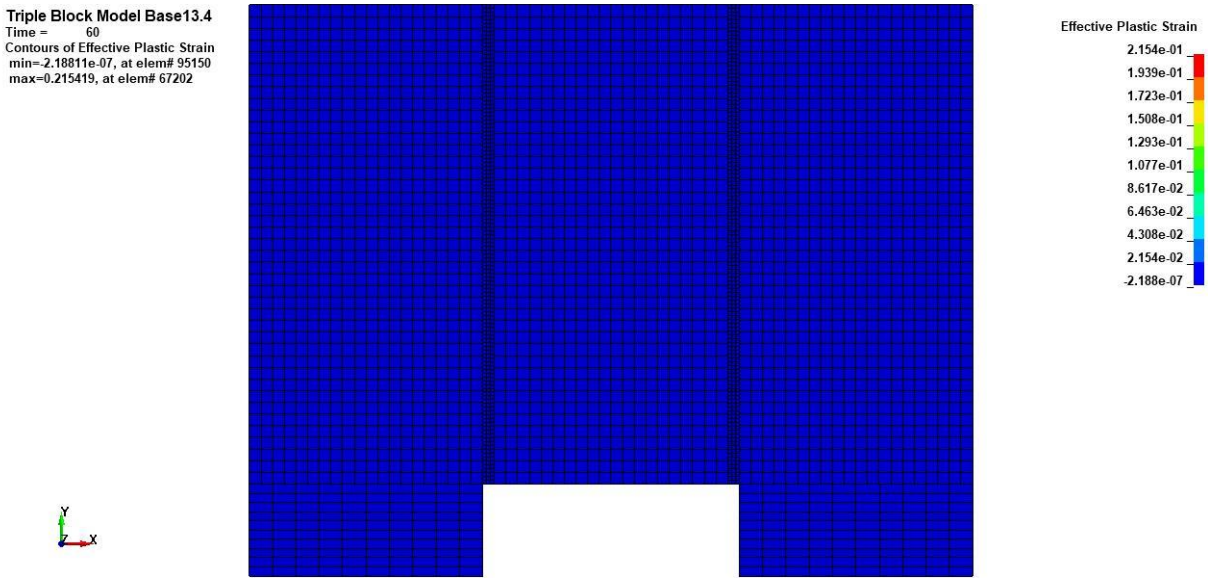


**Figure B-896: Effective Plastic Strain Fringe Plot for Last State at 60 Milliseconds for Base Run 13.4 – 200 psi**

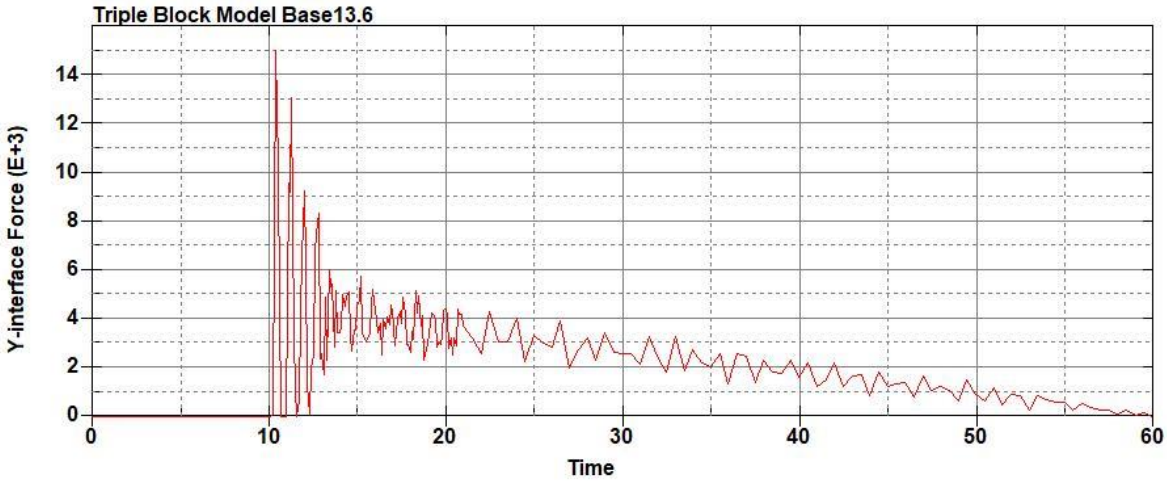


**Figure B-897: Base Run 13.6 Right Support Y-Interface Force (lbs) versus Time (ms) – 300 psi**

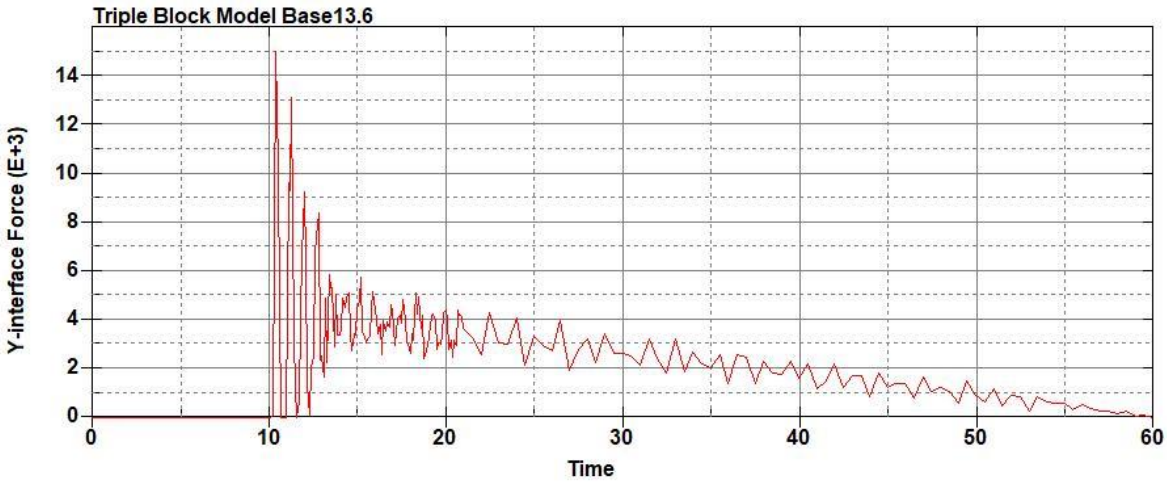


**Figure B-898: Base Run 13.6 Left Support Y-Interface Force (lbs) versus Time (ms) – 300 psi**

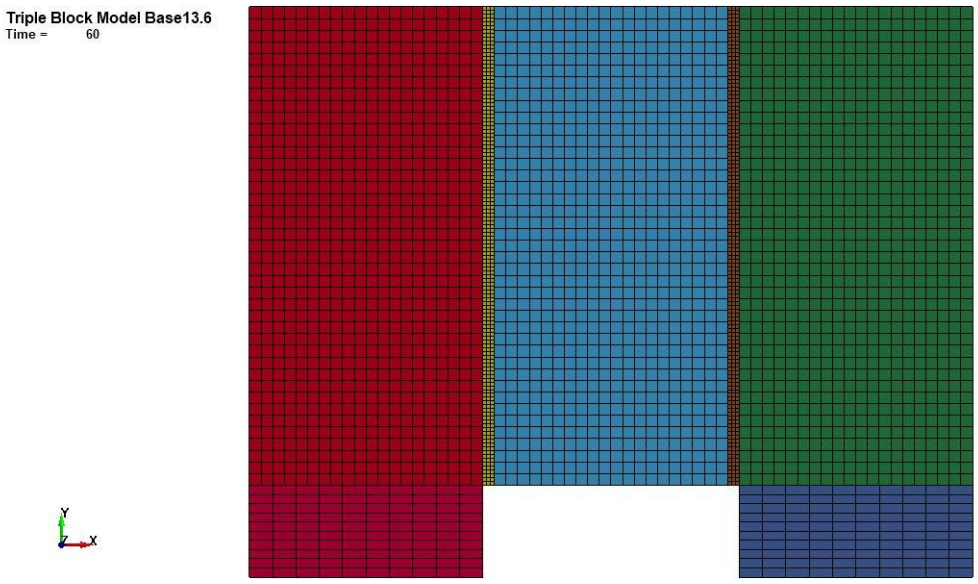


**Figure B-899: Last State at 60 Milliseconds for Base Run 13.6 – 300 psi**

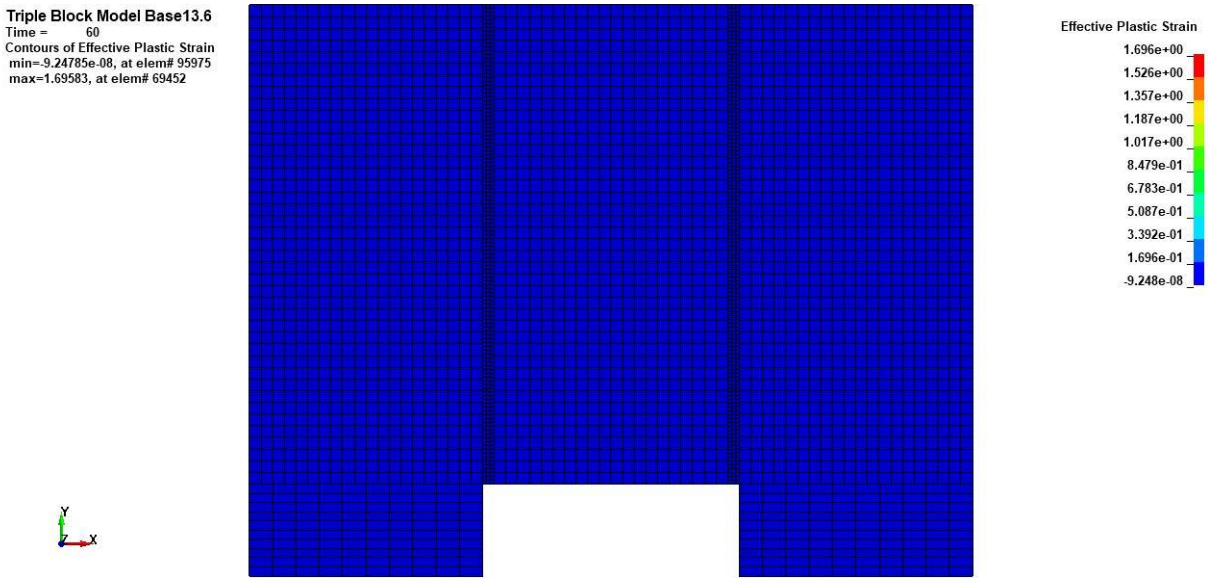


**Figure B-900: Effective Plastic Strain Fringe Plot for Last State at 60 Milliseconds for Base Run 13.6 – 300 psi**

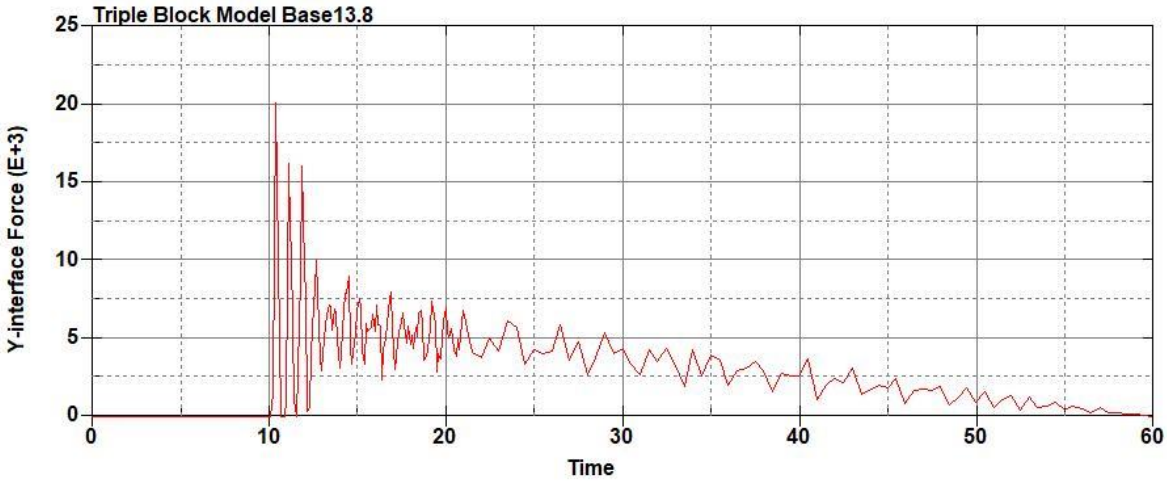


**Figure B-901: Base Run 13.8 Right Support Y-Interface Force (lbs) versus Time (ms) – 400 psi**

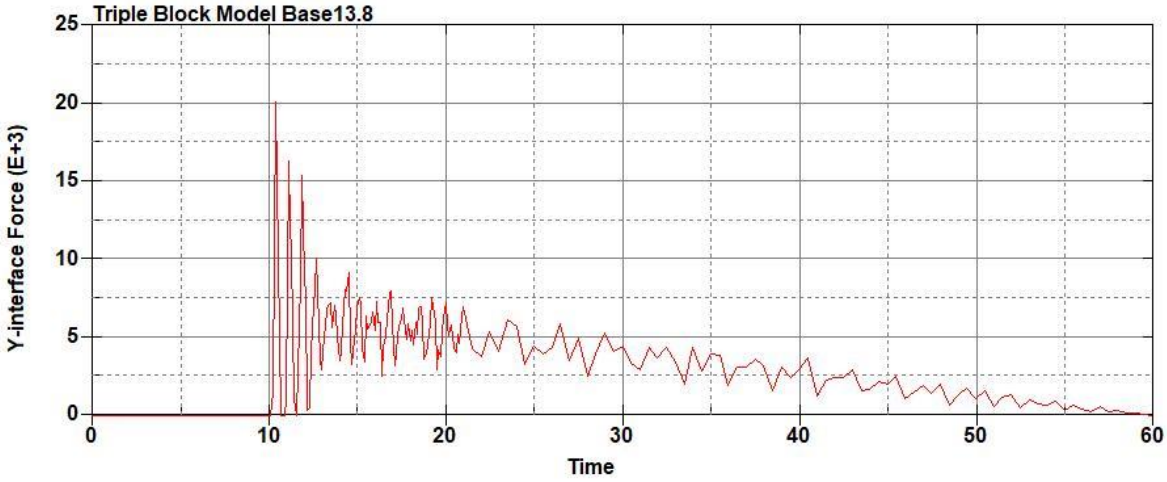


**Figure B-902: Base Run 13.8 Left Support Y-Interface Force (lbs) versus Time (ms) – 400 psi**

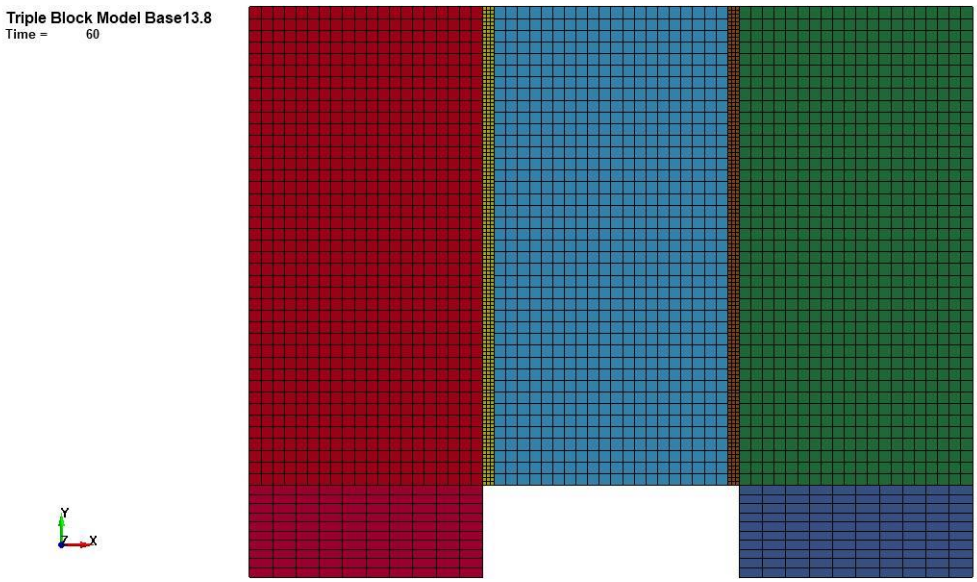


**Figure B-903: Last State at 60 Milliseconds for Base Run 13.8 – 400 psi**

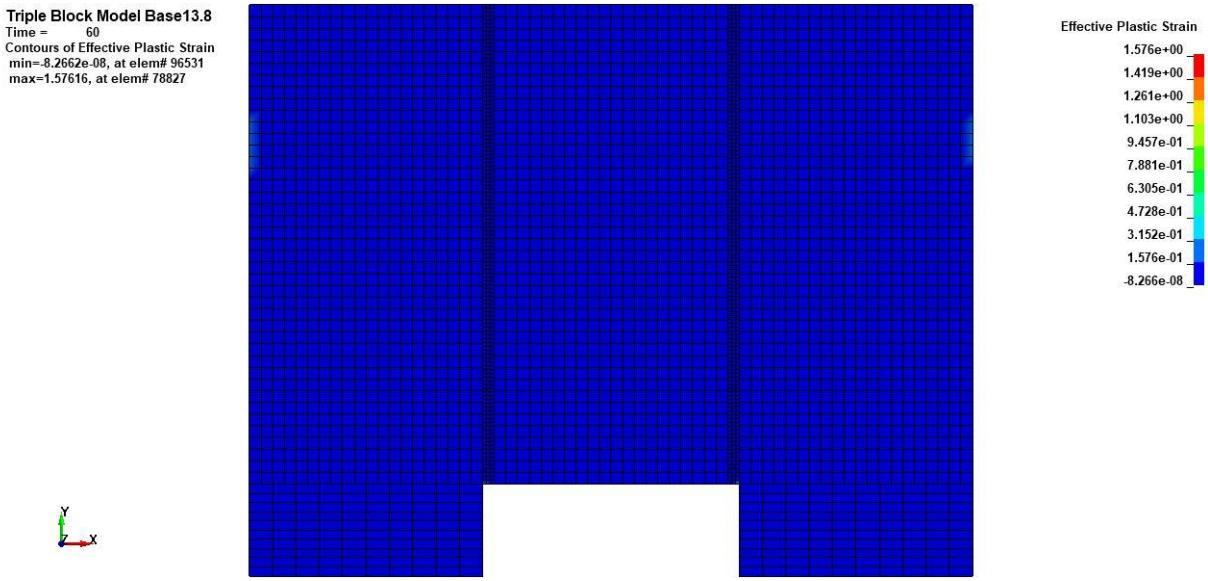


**Figure B-904: Effective Plastic Strain Fringe Plot for Last State at 60 Milliseconds for Base Run 13.8 – 400 psi**

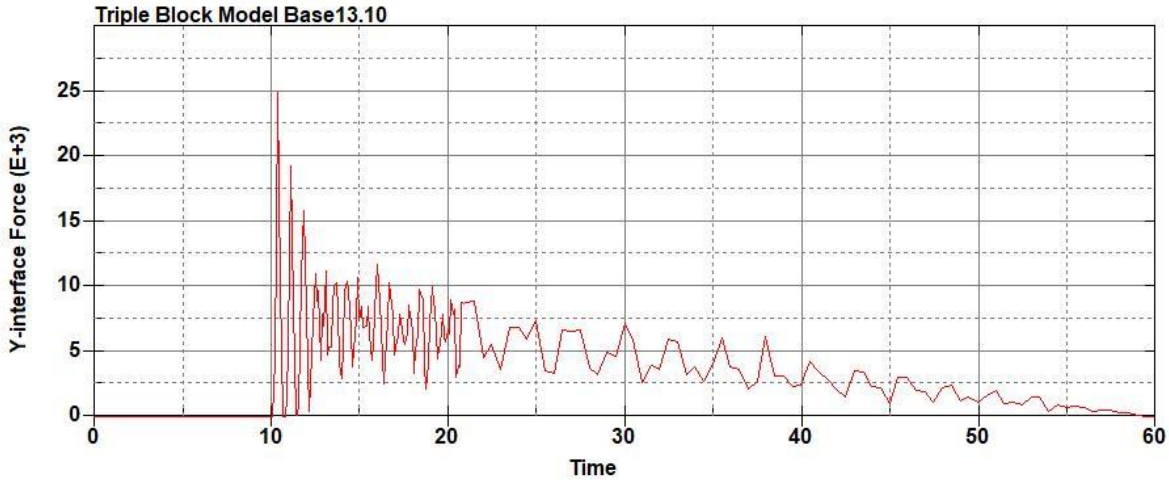


**Figure B-905: Base Run 13.10 Right Support Y-Interface Force (lbs) versus Time (ms) – 500 psi**

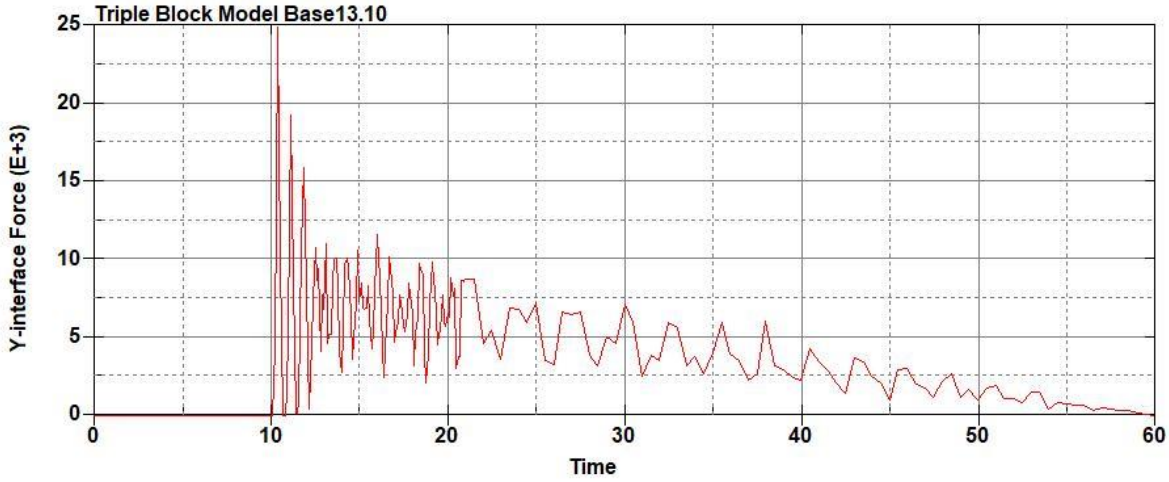


**Figure B-906: Base Run 13.10 Right Support Y-Interface Force (lbs) versus Time (ms) – 500 psi**

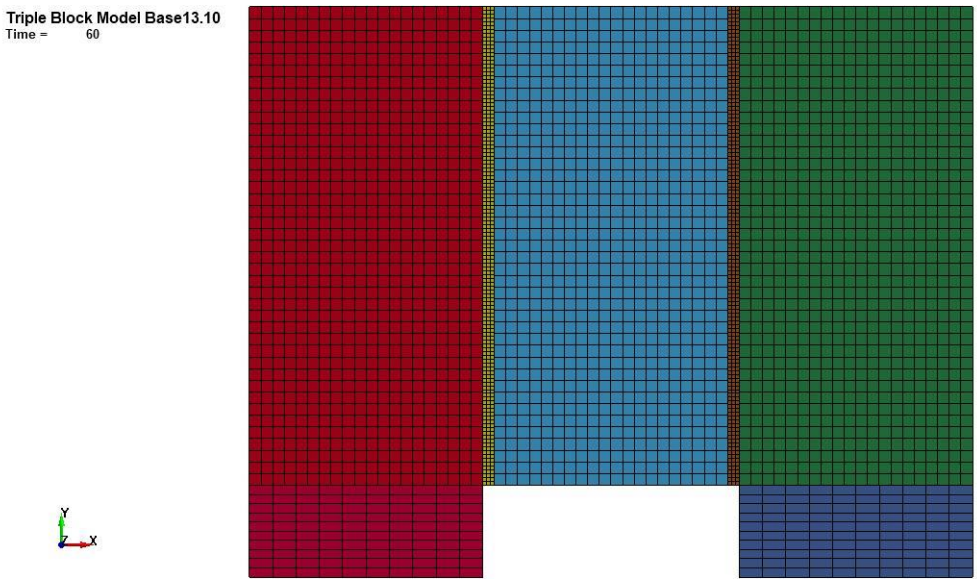


**Figure B-907: Last State at 60 Milliseconds for Base Run 13.10 – 500 psi**

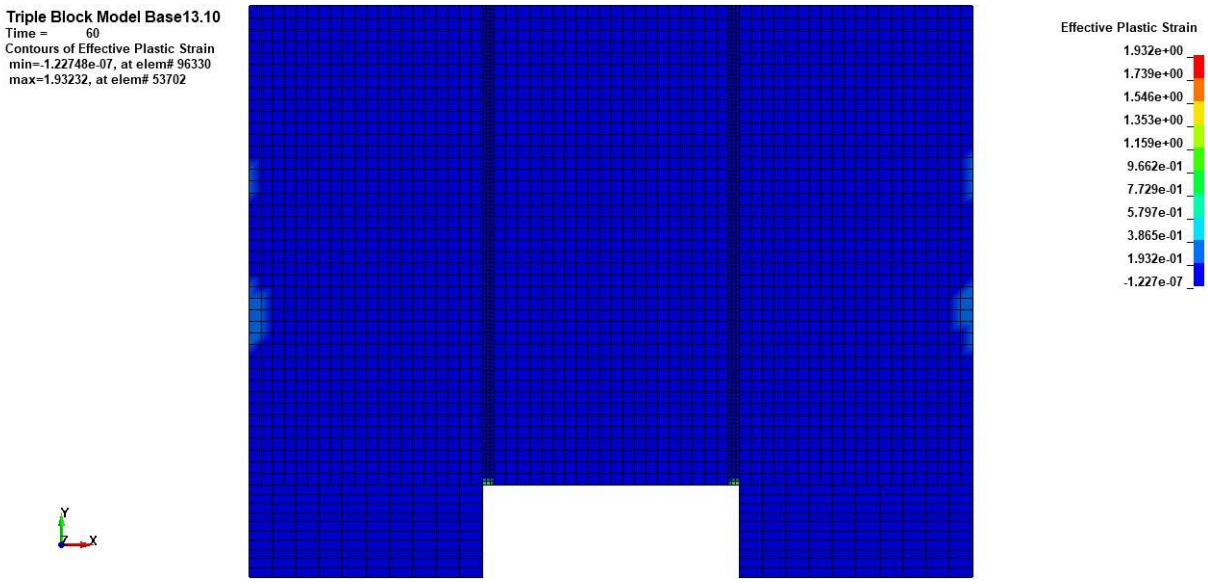


**Figure B-908: Effective Plastic Strain Fringe Plot for Last State at 60 Milliseconds for Base Run 13.10 – 500 psi**

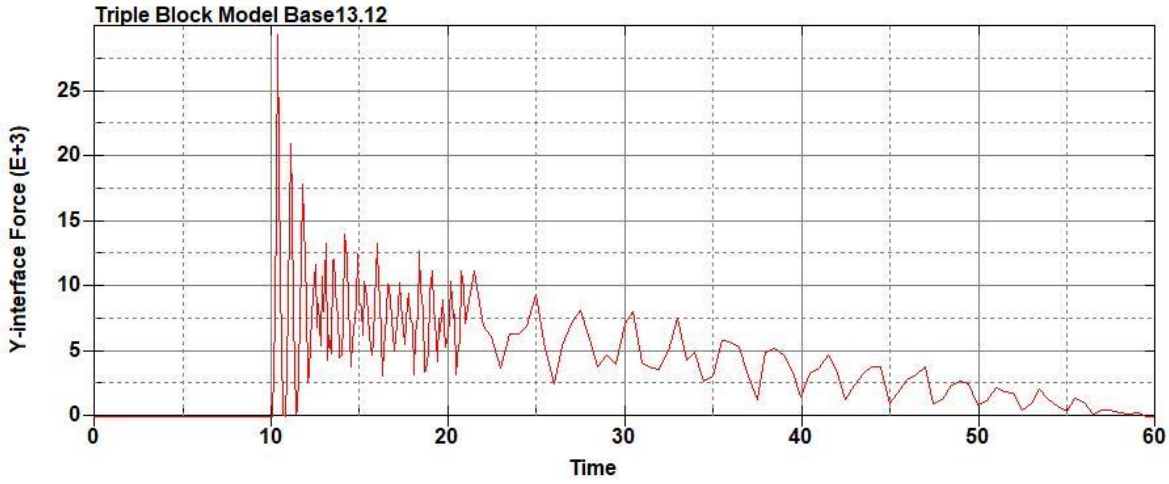


**Figure B-909: Base Run 13.12 Right Support Y-Interface Force (lbs) versus Time (ms) – 600 psi**

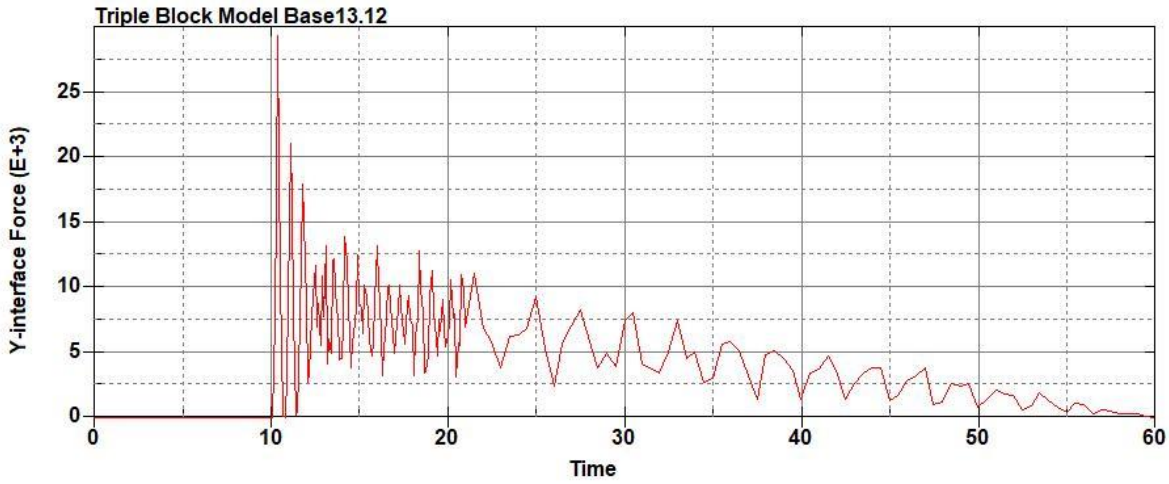


**Figure B-910: Base Run 13.12 Left Support Y-Interface Force (lbs) versus Time (ms) – 600 psi**

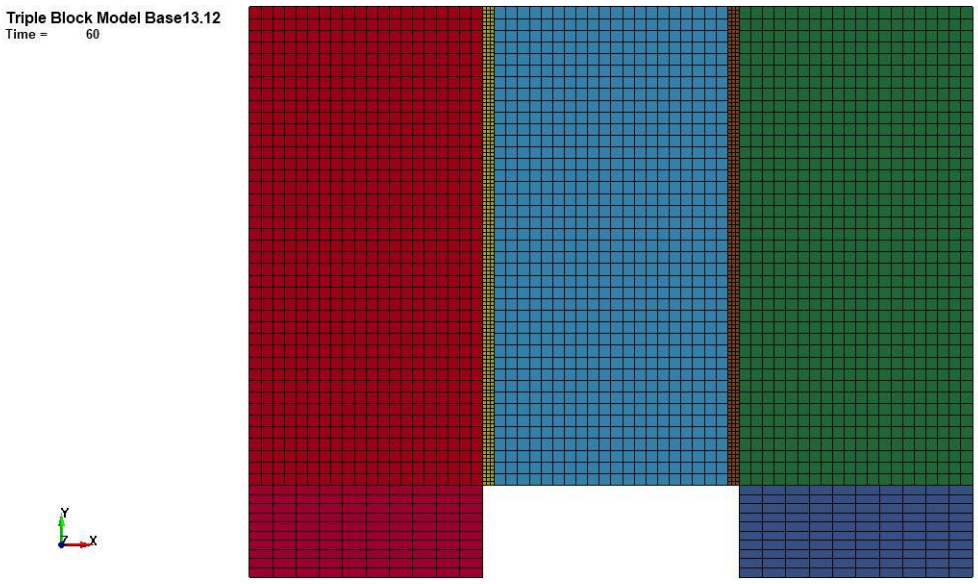


**Figure B-911: Last State at 60 Milliseconds for Base Run 13.12 – 600 psi**

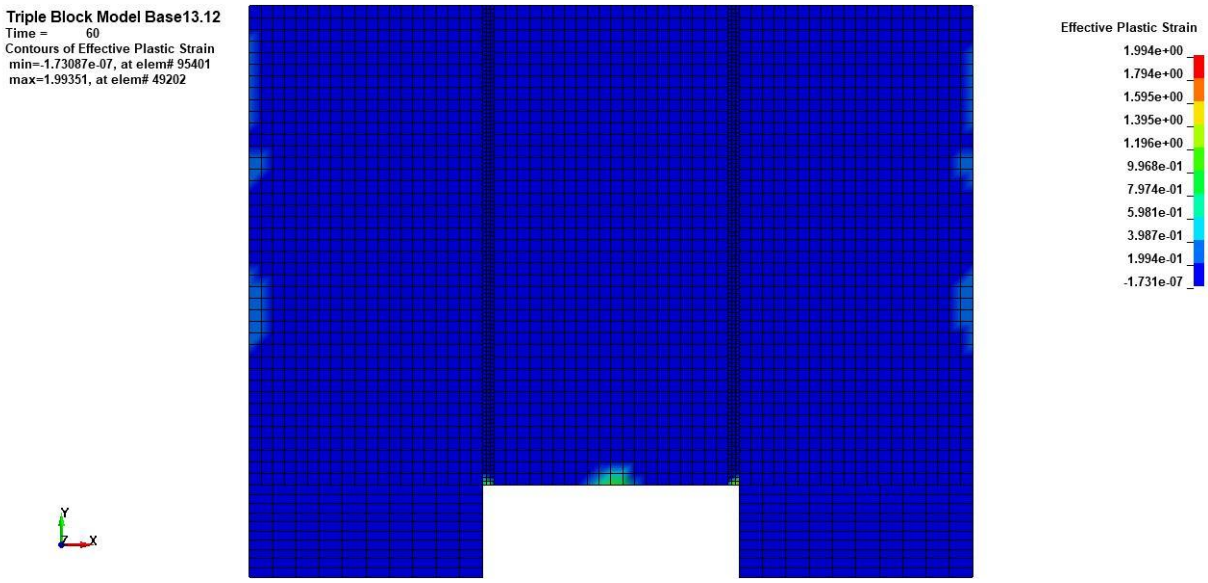


**Figure B-912: Effective Plastic Strain Fringe Plot for Last State at 60 Milliseconds for Base Run 13.12 – 600 psi**

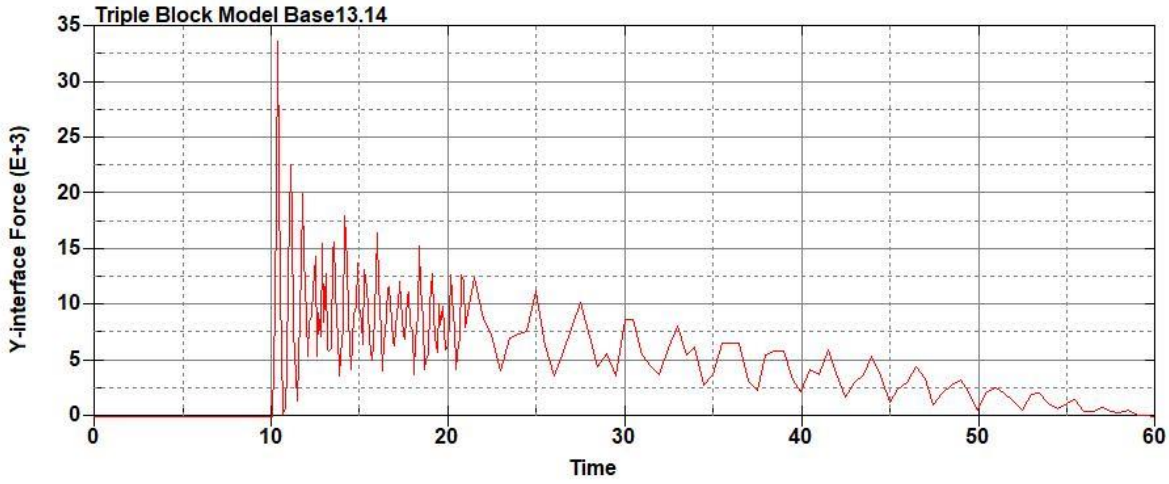


**Figure B-913: Base Run 13.14 Right Support Y-Interface Force (lbs) versus Time (ms) – 700 psi**

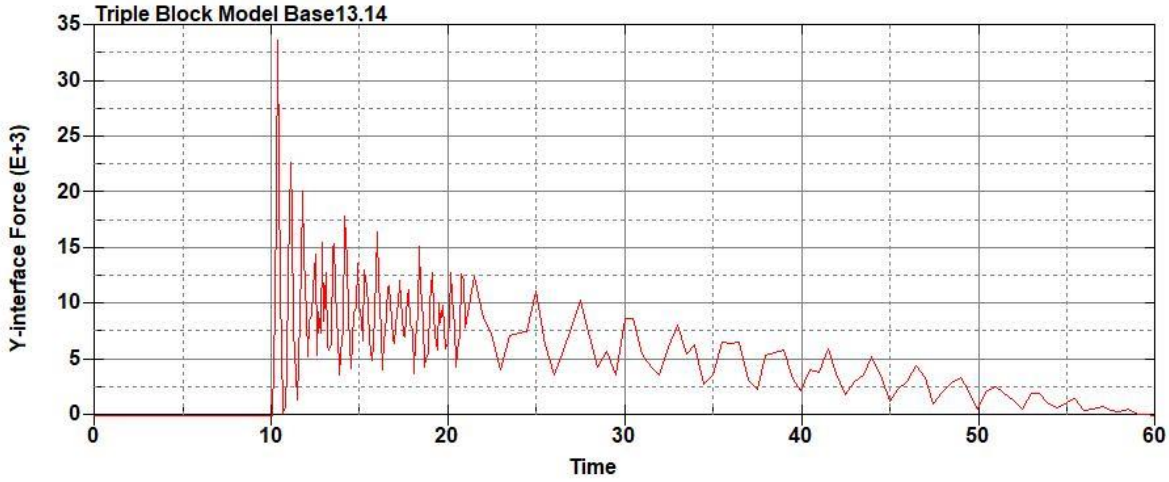


**Figure B-914: Base Run 13.14 Left Support Y-Interface Force (lbs) versus Time (ms) – 700 psi**

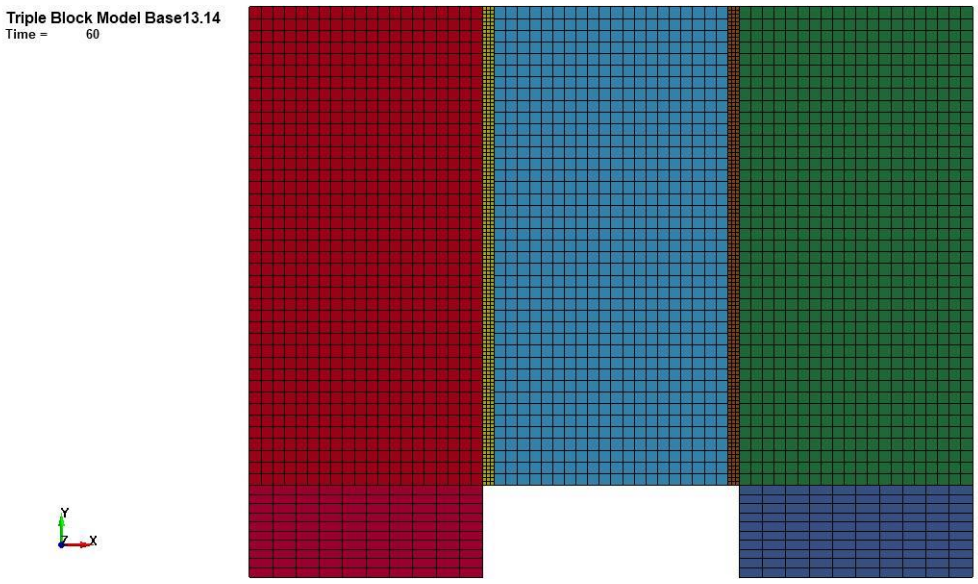


**Figure B-915: Last State at 60 Milliseconds for Base Run 13.14 – 700 psi**

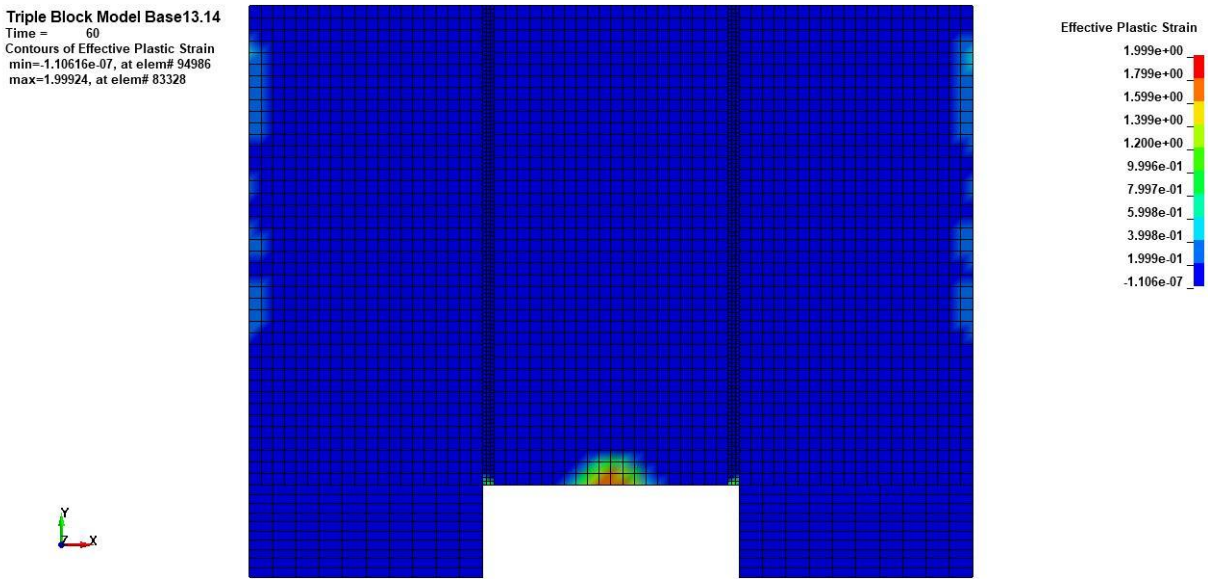


**Figure B-916: Effective Plastic Strain Fringe Plot for Last State at 60 Milliseconds for Base Run 13.14 – 700 psi**

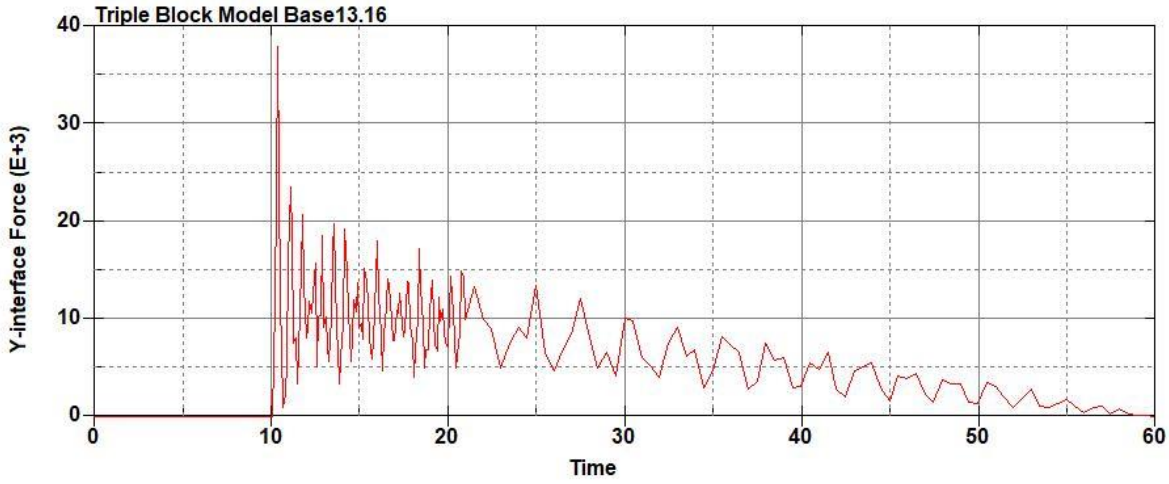


**Figure B-917: Base Run 13.16 Right Support Y-Interface Force (lbs) versus Time (ms) – 800 psi**

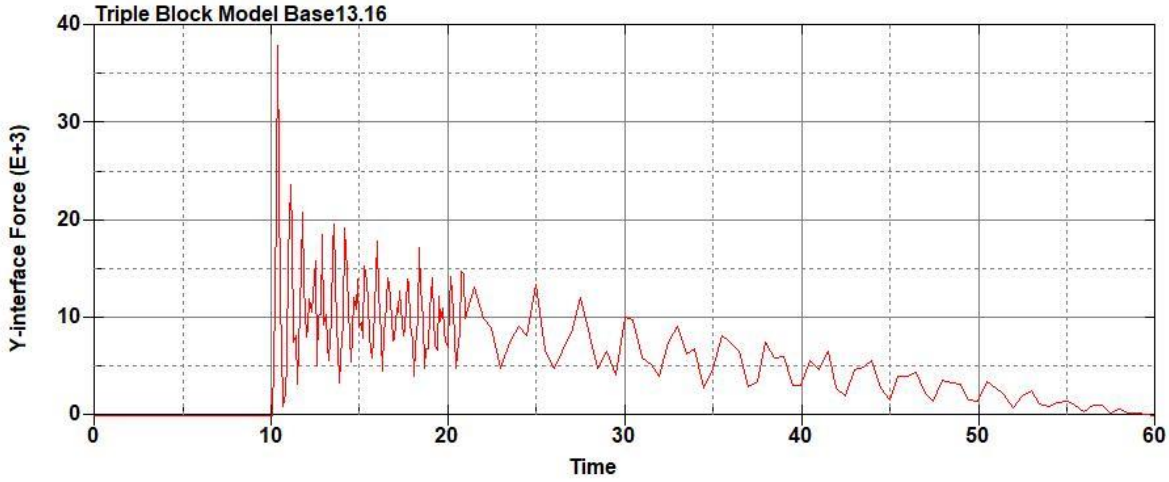


**Figure B-918: Base Run 13.16 Left Support Y-Interface Force (lbs) versus Time (ms) – 800 psi**

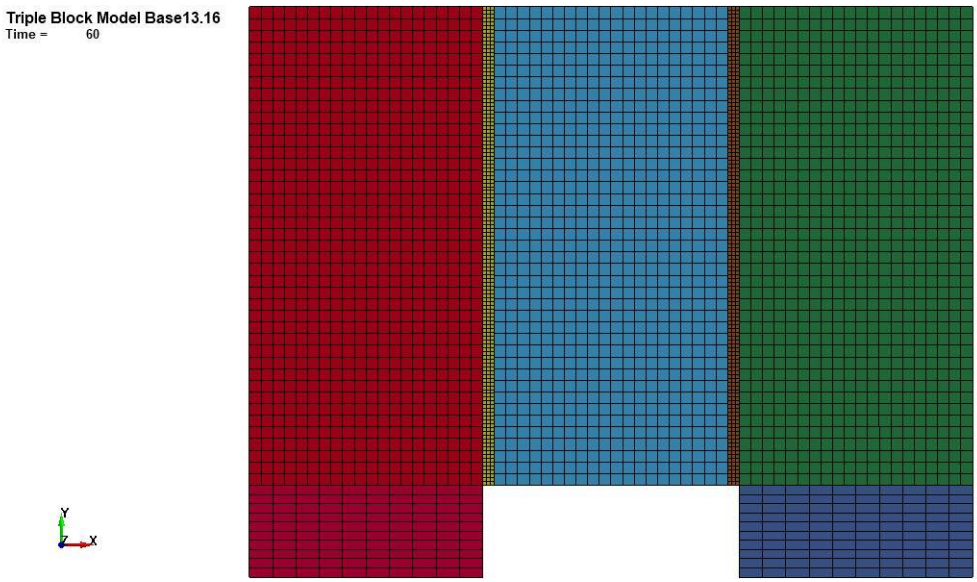


**Figure B-919: Last State at 60 Milliseconds for Base Run 13.16 – 800 psi**

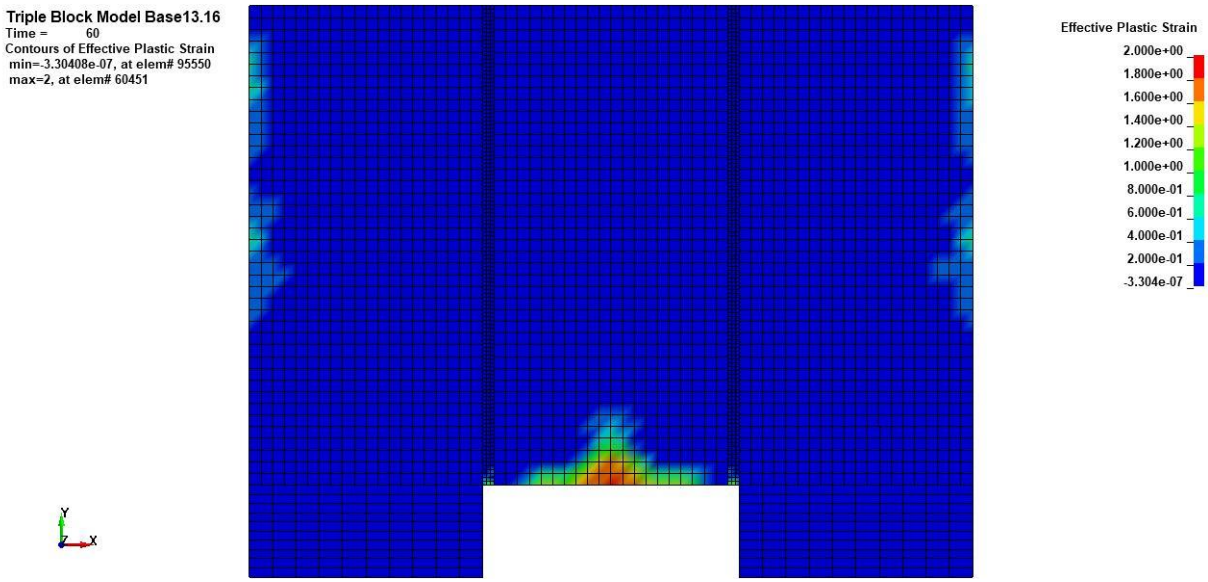


**Figure B-920: Effective Plastic Strain Fringe Plot for Last State at 60 Milliseconds for Base Run 13.16 – 800 psi**

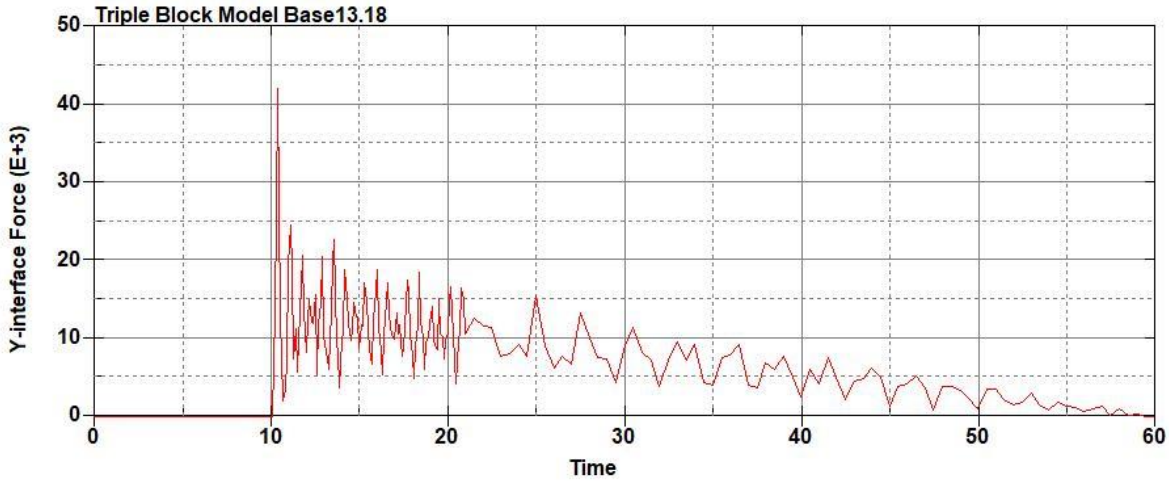


**Figure B-921: Base Run 13.18 Right Support Y-Interface Force (lbs) versus Time (ms) – 900 psi**

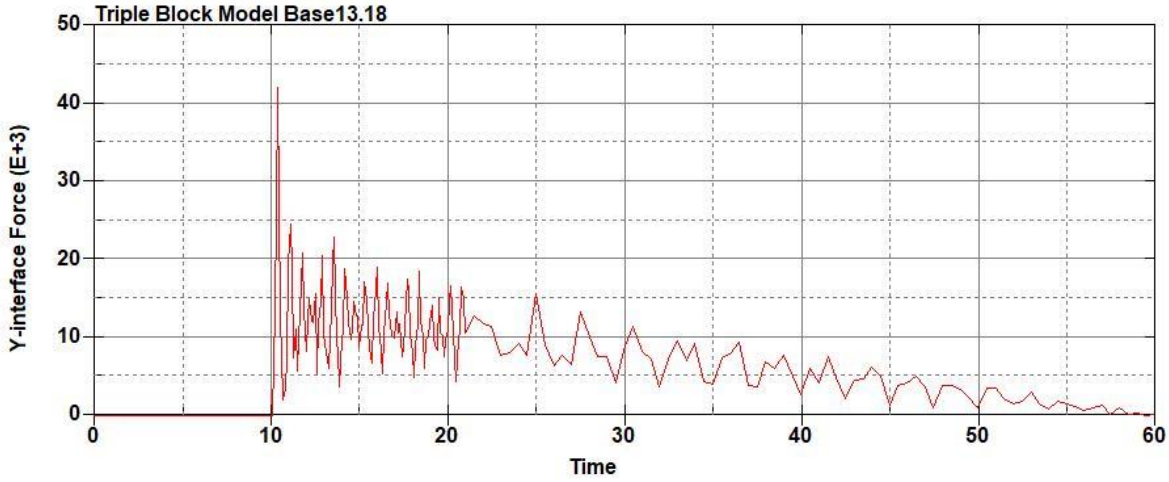


**Figure B-922: Base Run 13.18 Left Support Y-Interface Force (lbs) versus Time (ms) – 900 psi**

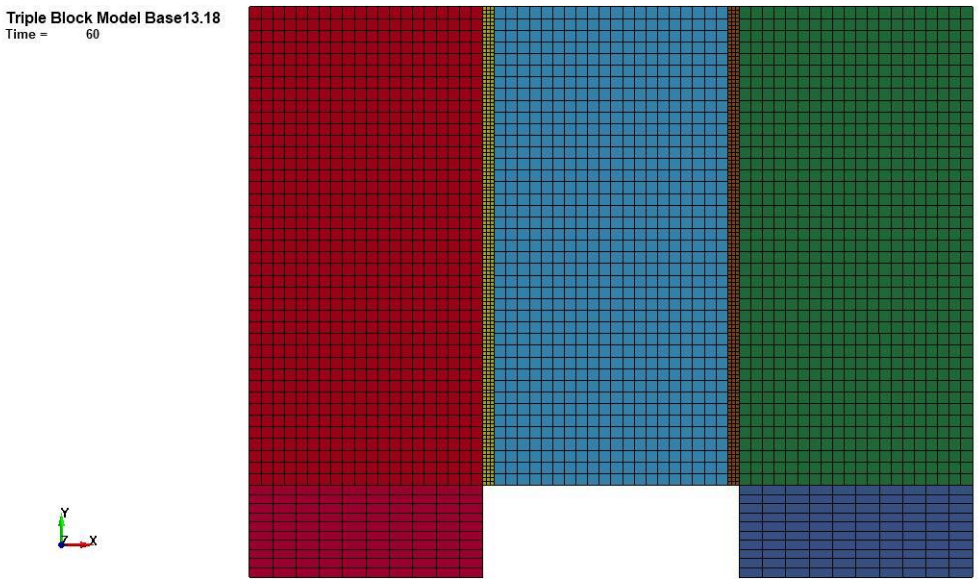


**Figure B-923: Last State at 60 Milliseconds for Base Run 13.18 – 900 psi**

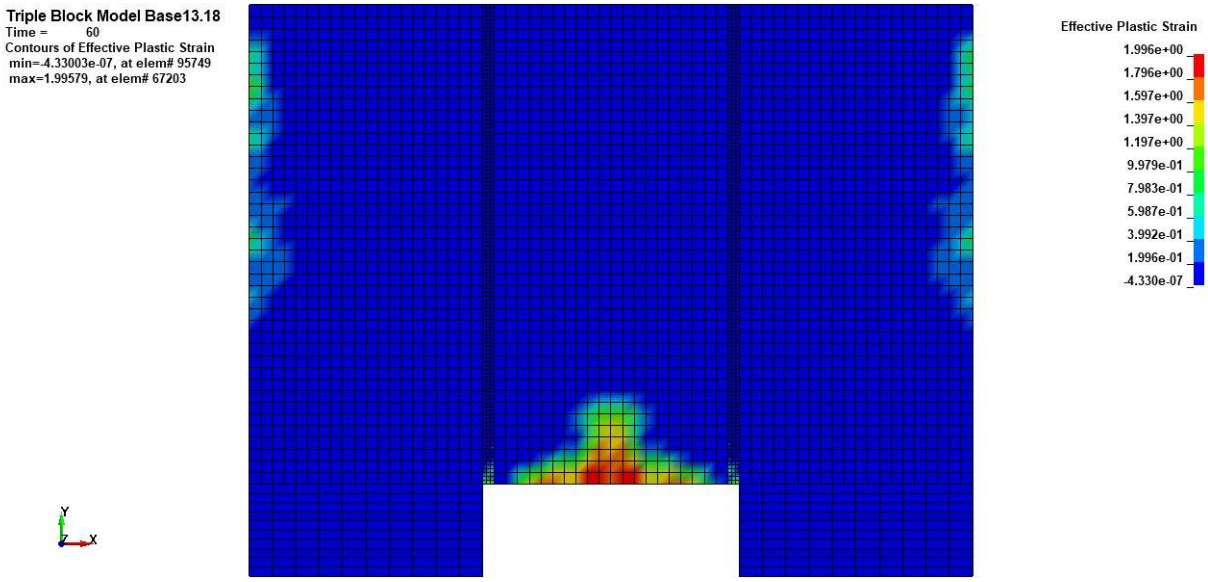


**Figure B-924: Effective Plastic Strain Fringe Plot for Last State at 60 Milliseconds for Base Run 13.18 – 900 psi**

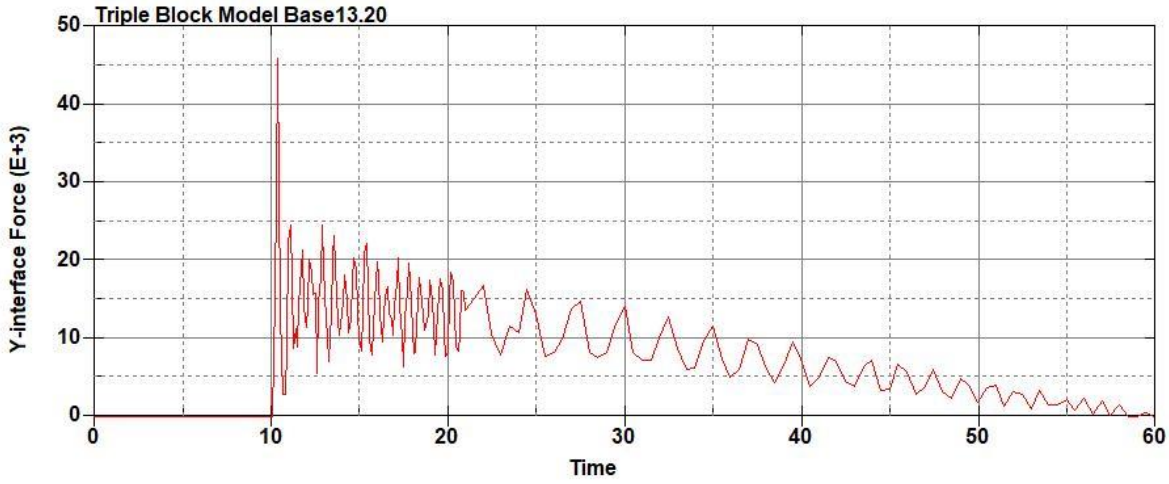


**Figure B-925: Base Run 13.20 Right Support Y-Interface Force (lbs) versus Time (ms) – 1000 psi**

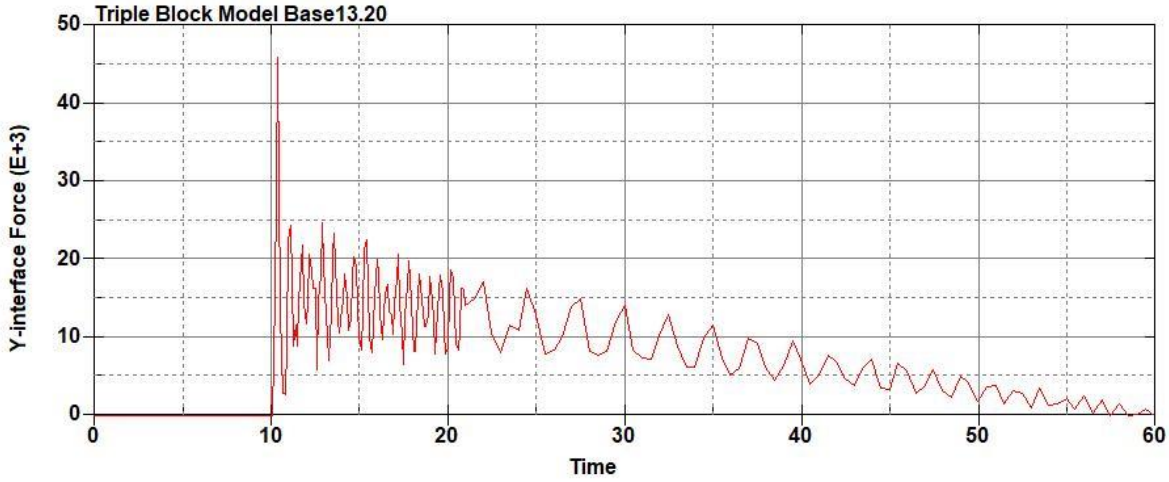


**Figure B-926: Base Run 13.20 Left Support Y-Interface Force (lbs) versus Time (ms) – 1000 psi**

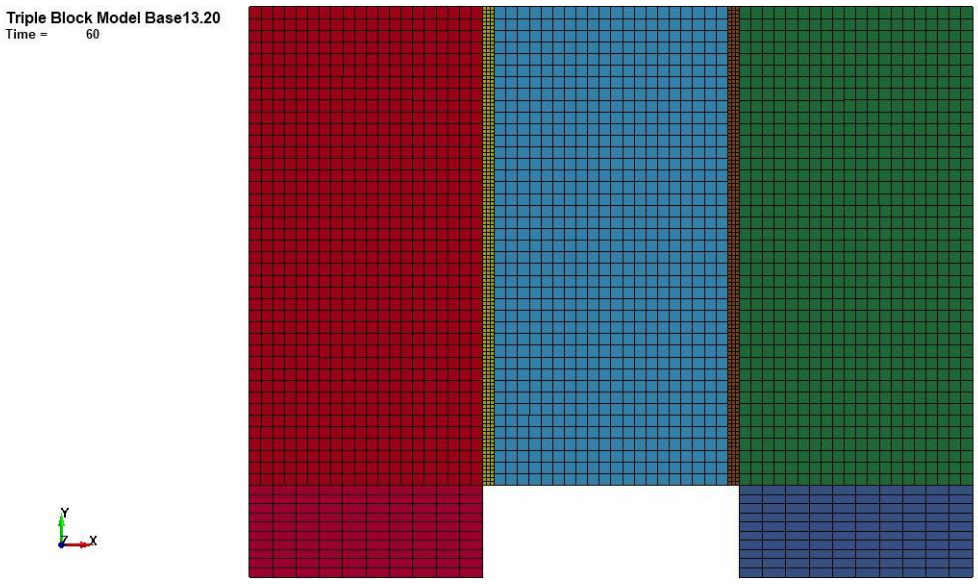


**Figure B-927: Last State at 60 Milliseconds for Base Run 13.20 – 1000 psi**

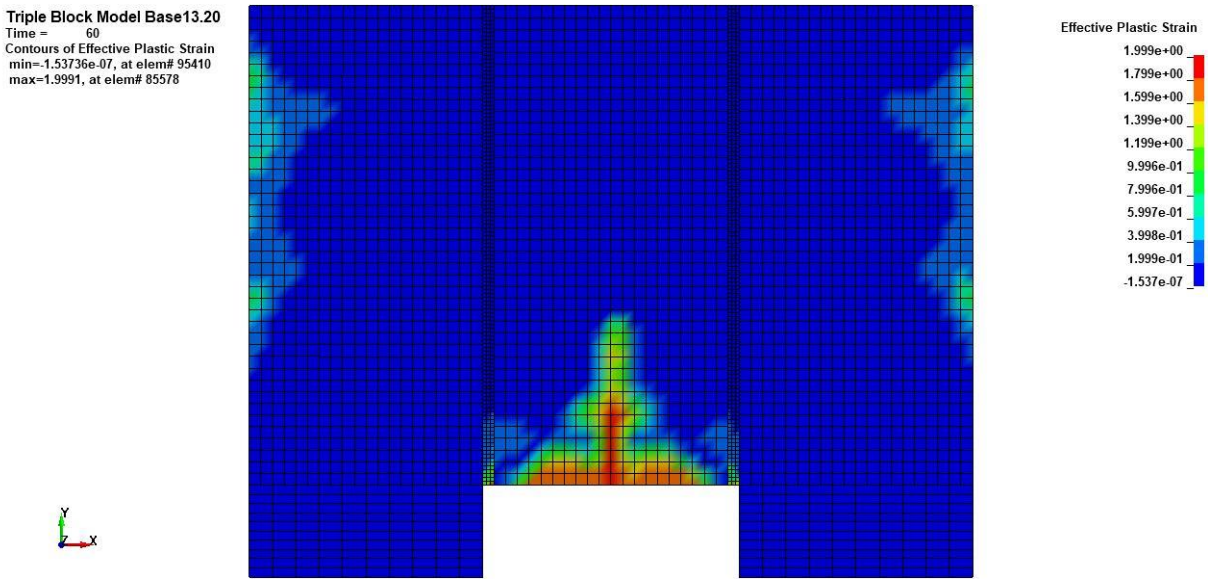


**Figure B-928: Effective Plastic Strain Fringe Plot for Last State at 60 Milliseconds for Base Run 13.20 – 1000 psi**

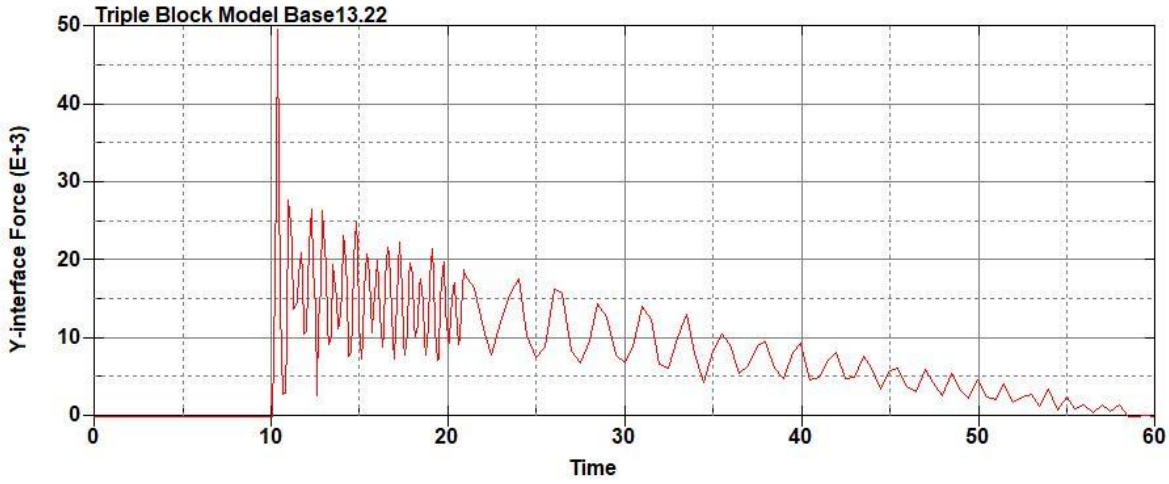


**Figure B-929: Base Run 13.22 Right Support Y-Interface Force (lbs) versus Time (ms) – 1100 psi**

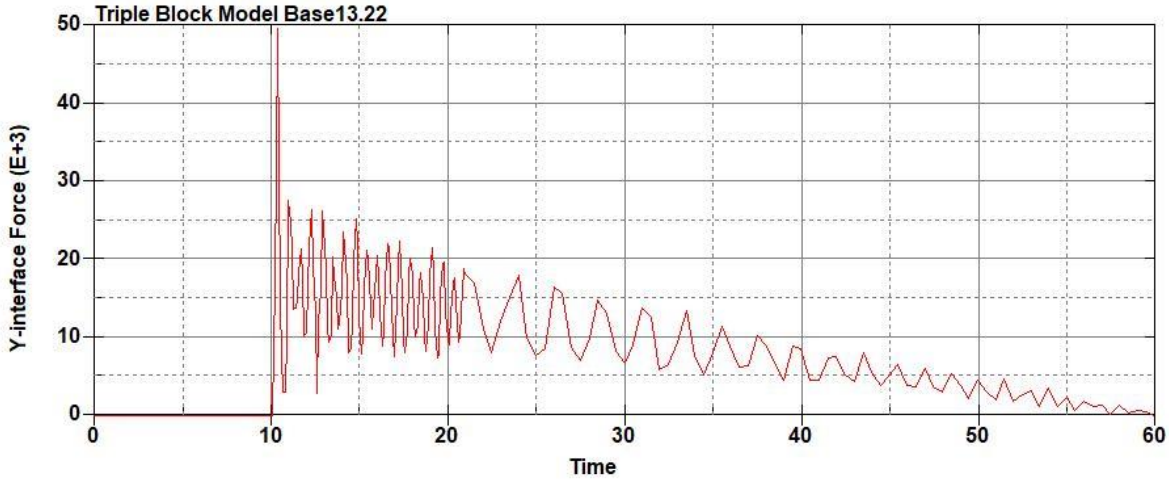


**Figure B-930: Base Run 13.22 Left Support Y-Interface Force (lbs) versus Time (ms) – 1100 psi**

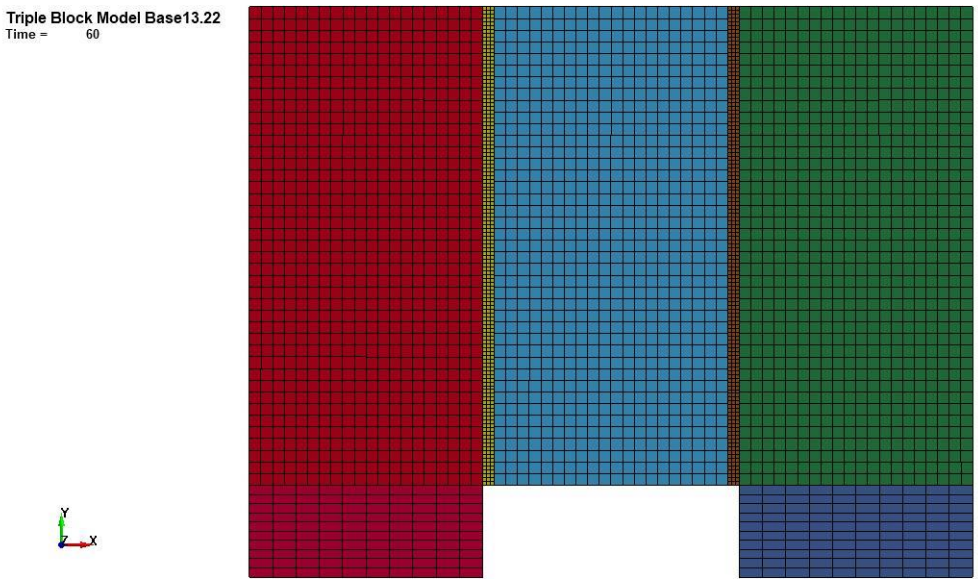


**Figure B-931: Last State at 60 Milliseconds for Base Run 13.22 – 1100 psi**

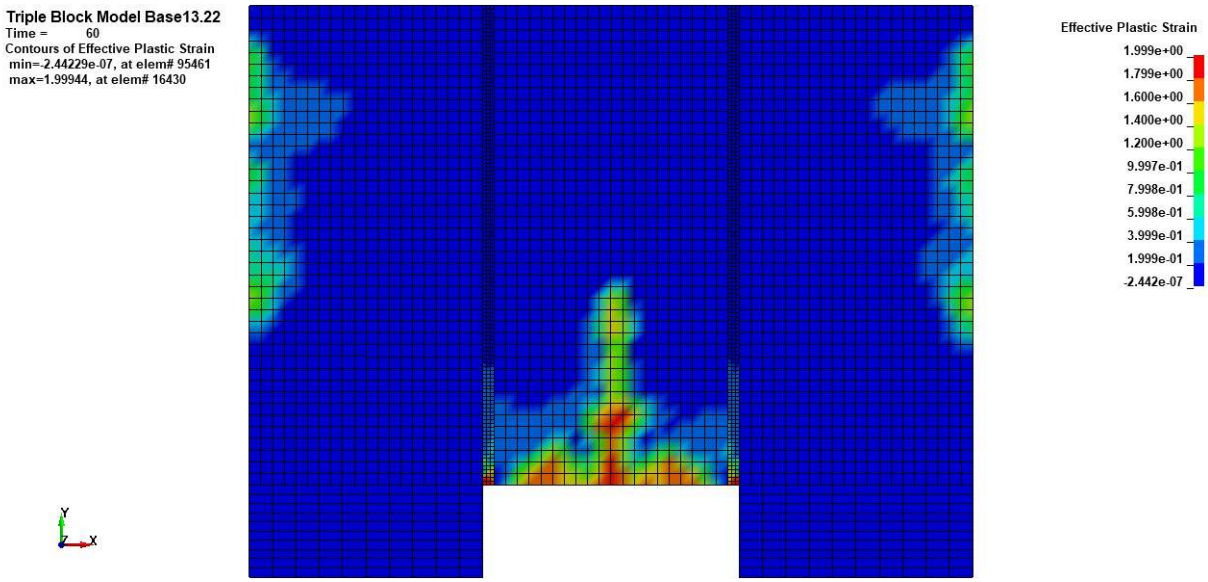


**Figure B-932: Effective Plastic Strain Fringe Plot for Last State at 60 Milliseconds for Base Run 13.22 – 1100 psi**

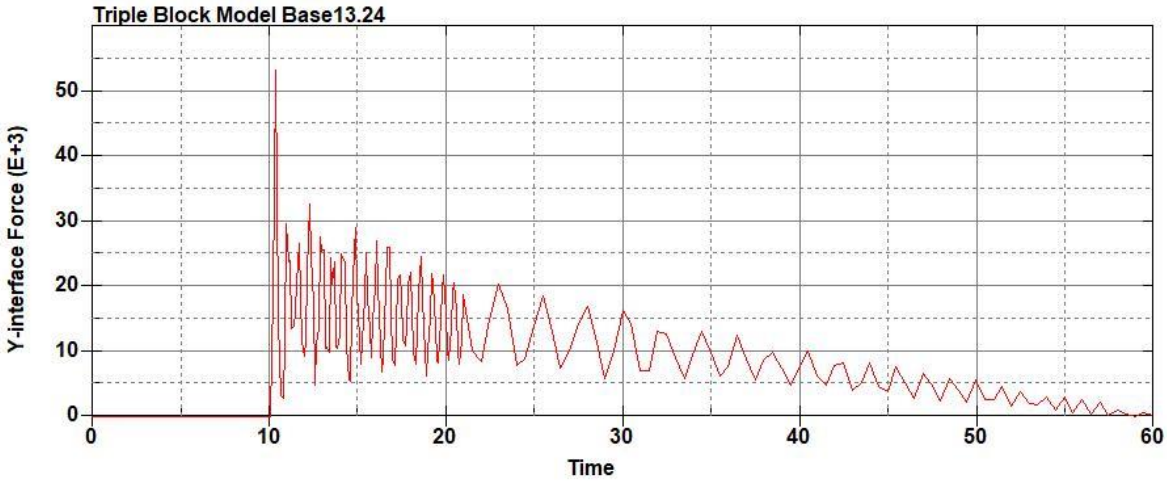


**Figure B-933: Base Run 13.24 Right Support Y-Interface Force (lbs) versus Time (ms) – 1200 psi**

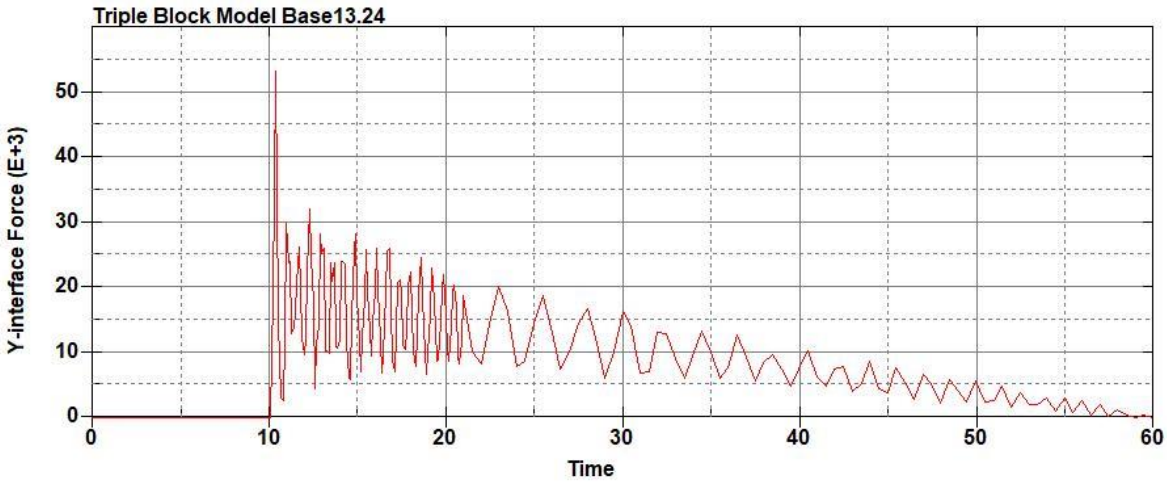


**Figure B-934: Base Run 13.24 Left Support Y-Interface Force (lbs) versus Time (ms) – 1200 psi**

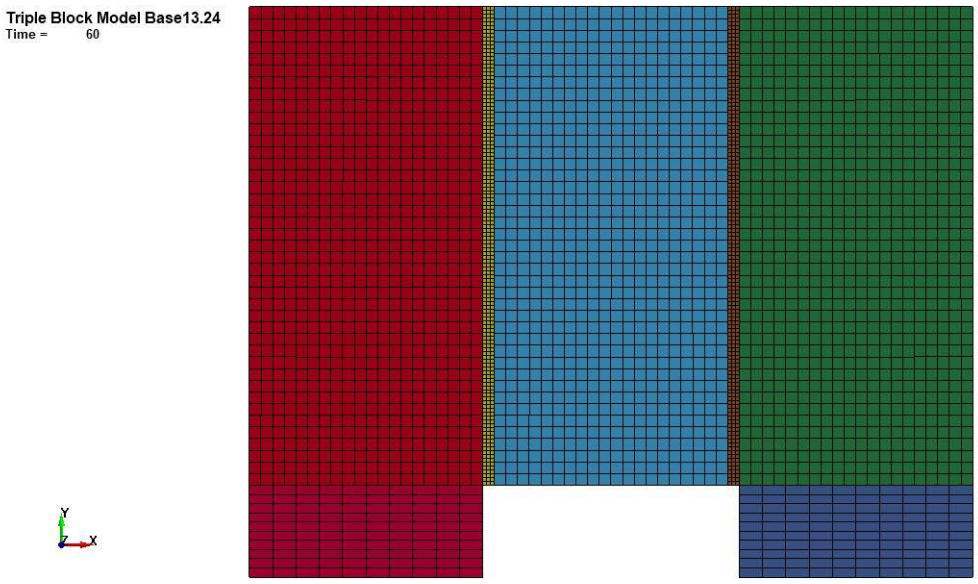


**Figure B-935: Last State at 60 Milliseconds for Base Run 13.24 – 1200 psi**

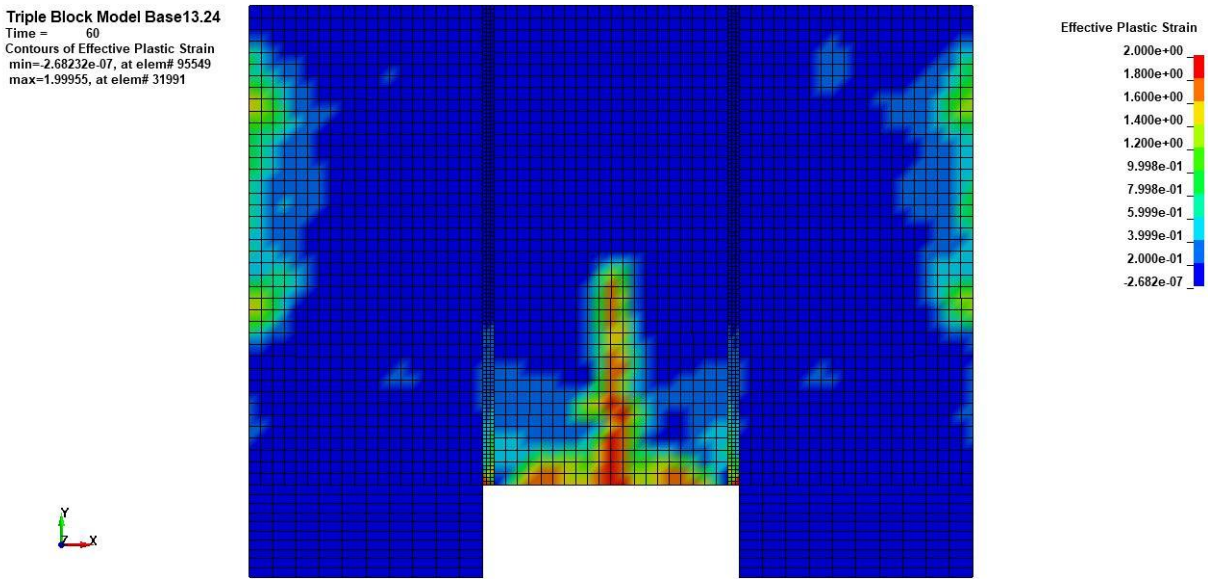


**Figure B-936: Effective Plastic Strain Fringe Plot for Last State at 60 Milliseconds for Base Run 13.24 – 1200 psi**

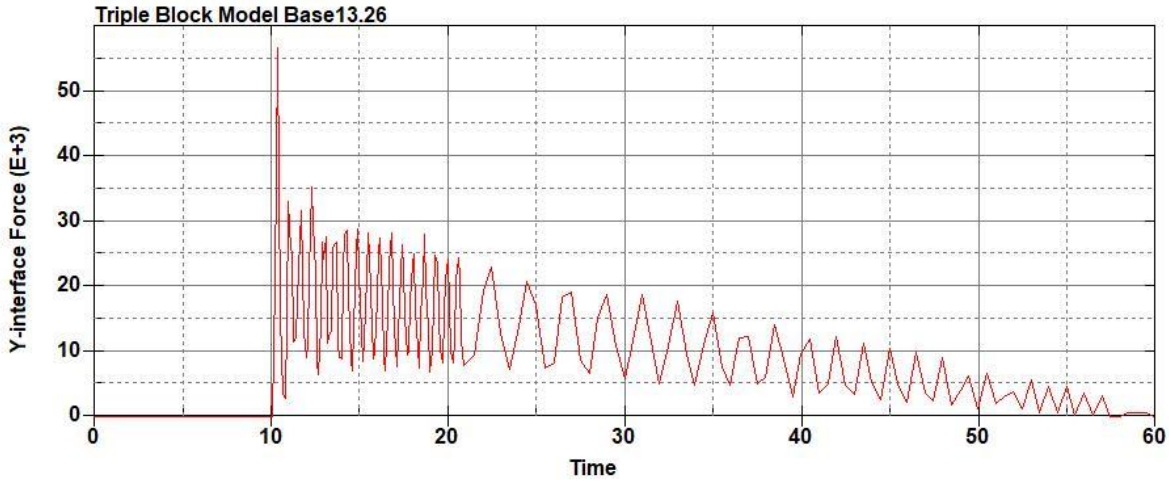


**Figure B-937: Base Run 13.26 Right Support Y-Interface Force (lbs) versus Time (ms) – 1300 psi**

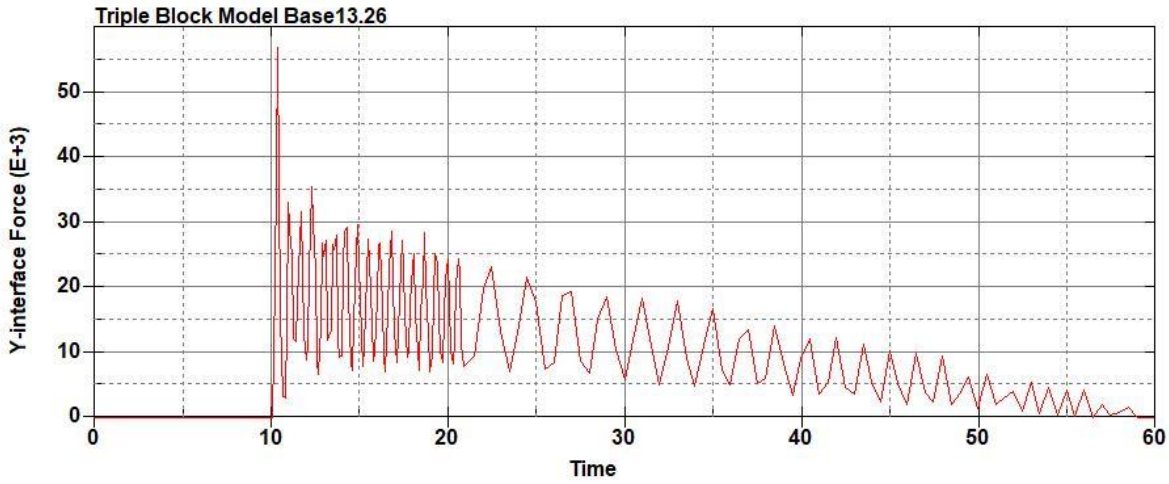


**Figure B-938: Base Run 13.26 Left Support Y-Interface Force (lbs) versus Time (ms) – 1300 psi**

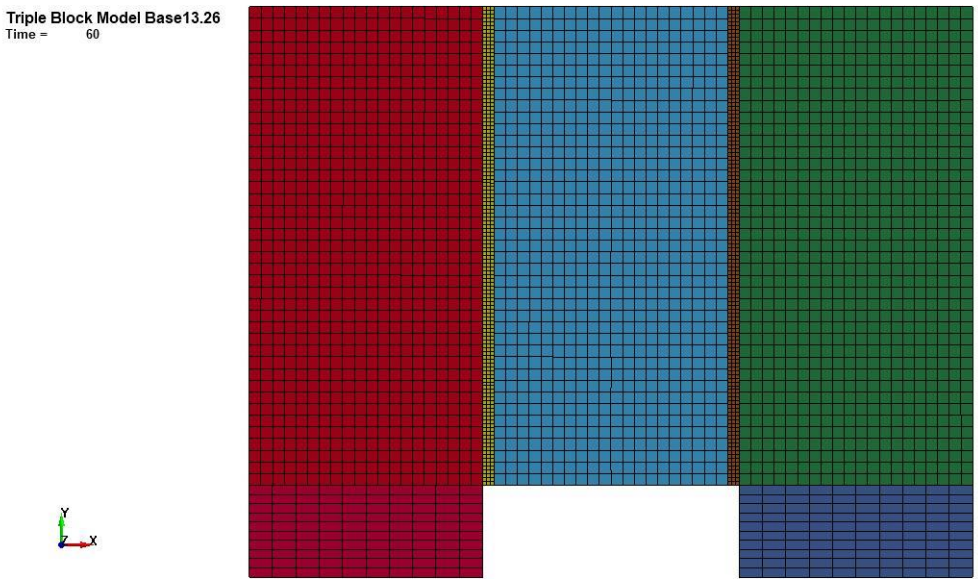


**Figure B-939: Last State at 60 Milliseconds for Base Run 13.26 – 1300 psi**

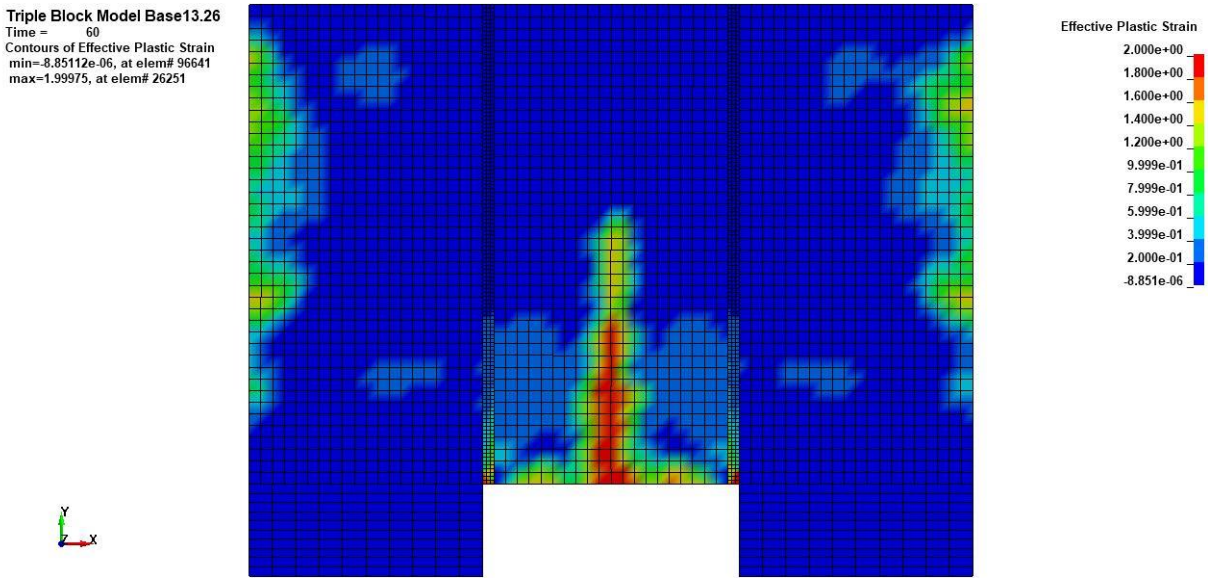


**Figure B-940: Effective Plastic Strain Fringe Plot for Last State at 60 Milliseconds for Base Run 13.26 – 1300 psi**

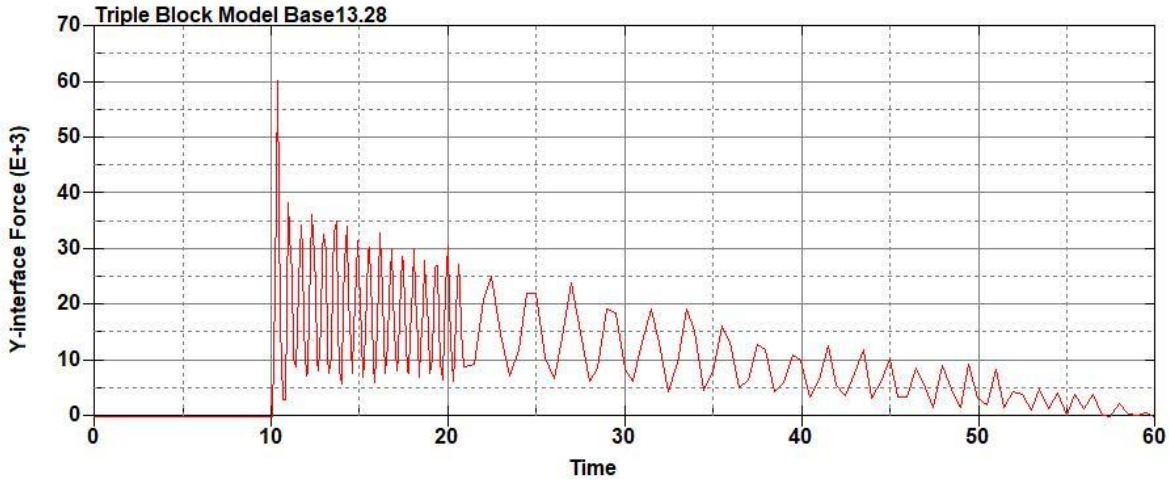


**Figure B-941: Base Run 13.28 Right Support Y-Interface Force (lbs) versus Time (ms) – 1400 psi**

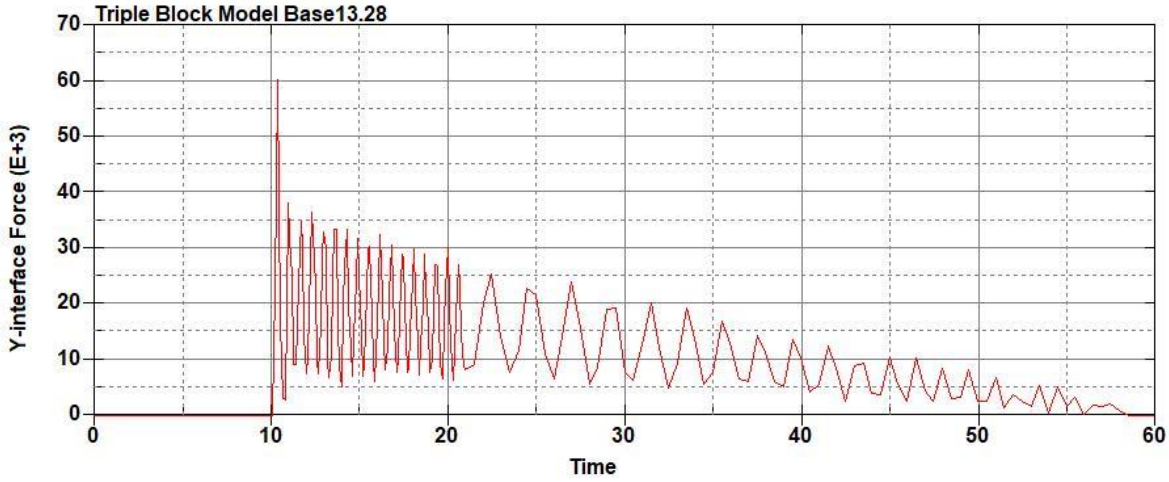


**Figure B-942: Base Run 13.28 Left Support Y-Interface Force (lbs) versus Time (ms) – 1400 psi**

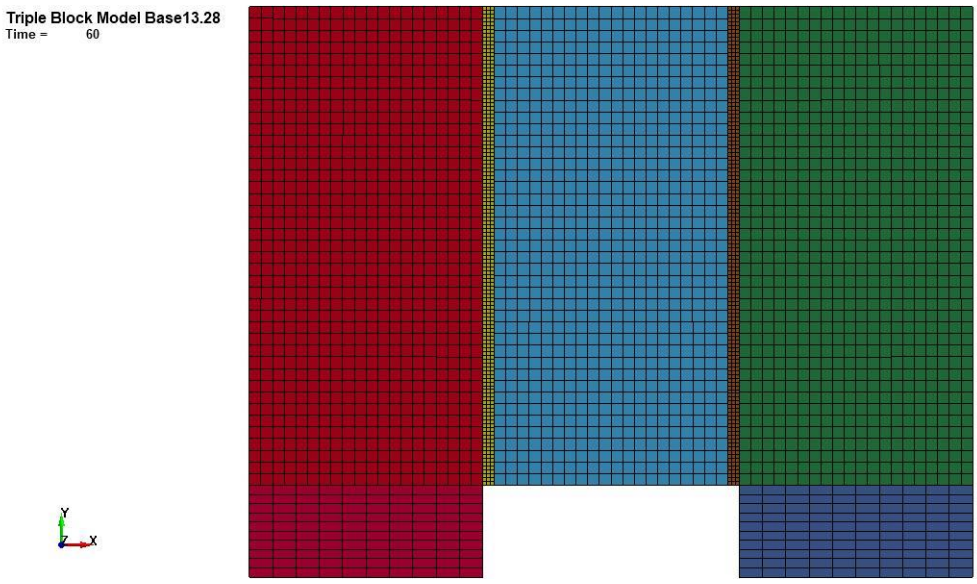


**Figure B-943: Last State at 60 Milliseconds for Base Run 13.28 – 1400 psi**

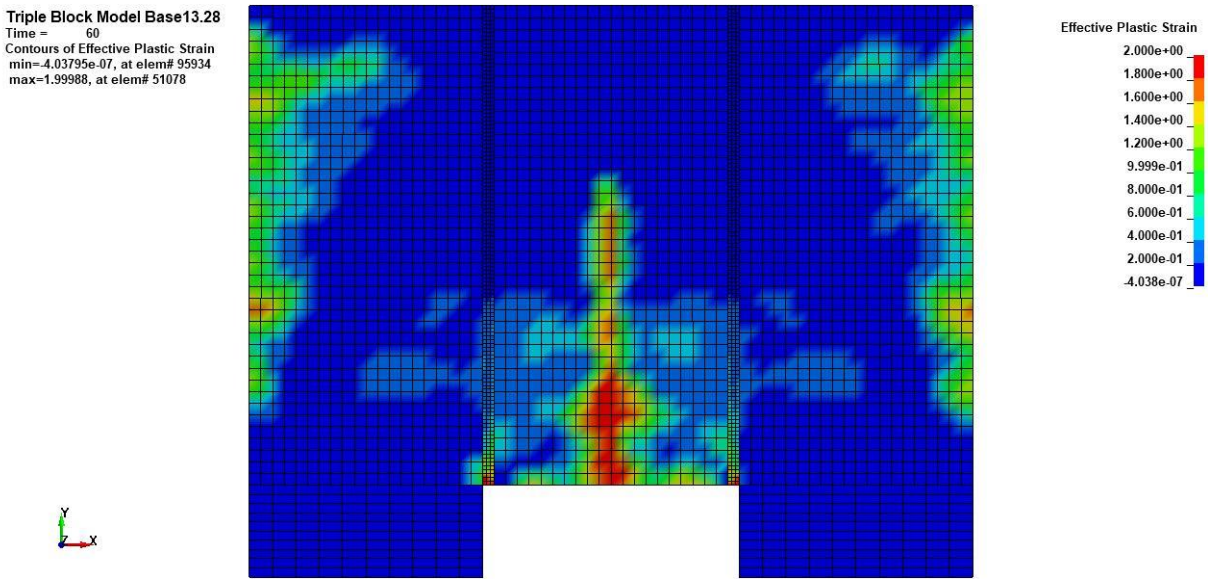


**Figure B-944: Effective Plastic Strain Fringe Plot for Last State at 60 Milliseconds for Base Run 13.28 – 1400 psi**

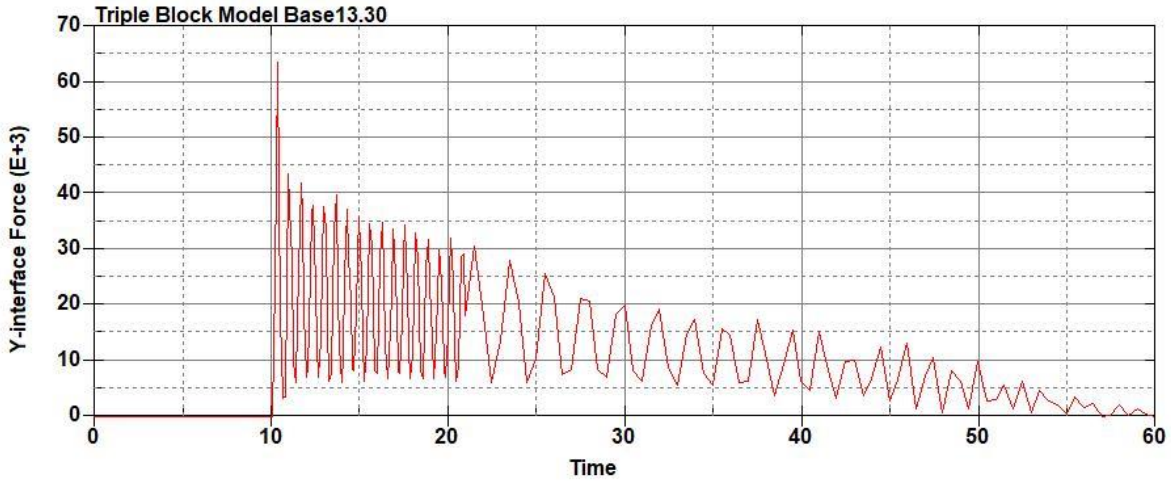


**Figure B-945: Base Run 13.30 Right Support Y-Interface Force (lbs) versus Time (ms) – 1500 psi**

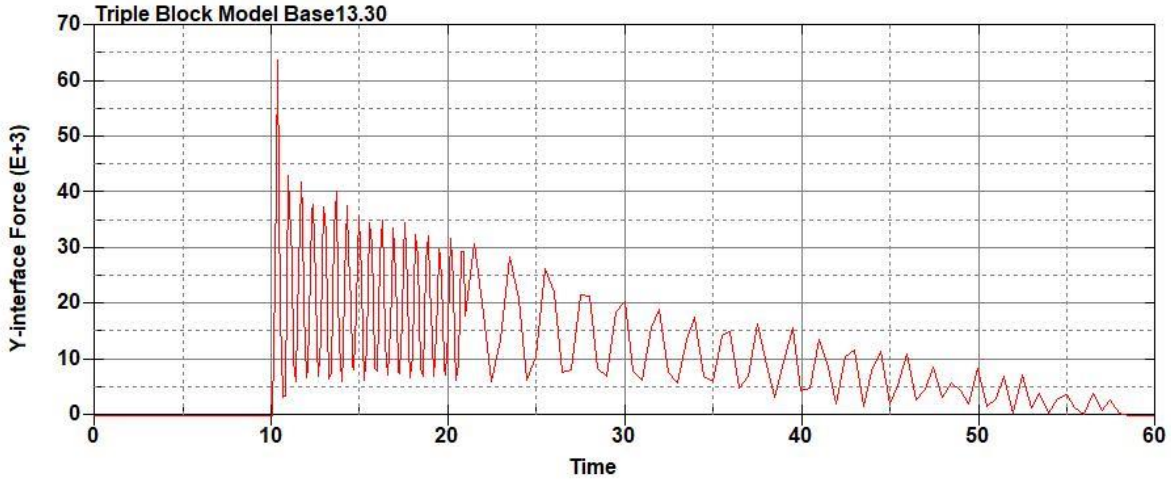


**Figure B-946: Base Run 13.30 Left Support Y-Interface Force (lbs) versus Time (ms) – 1500 psi**

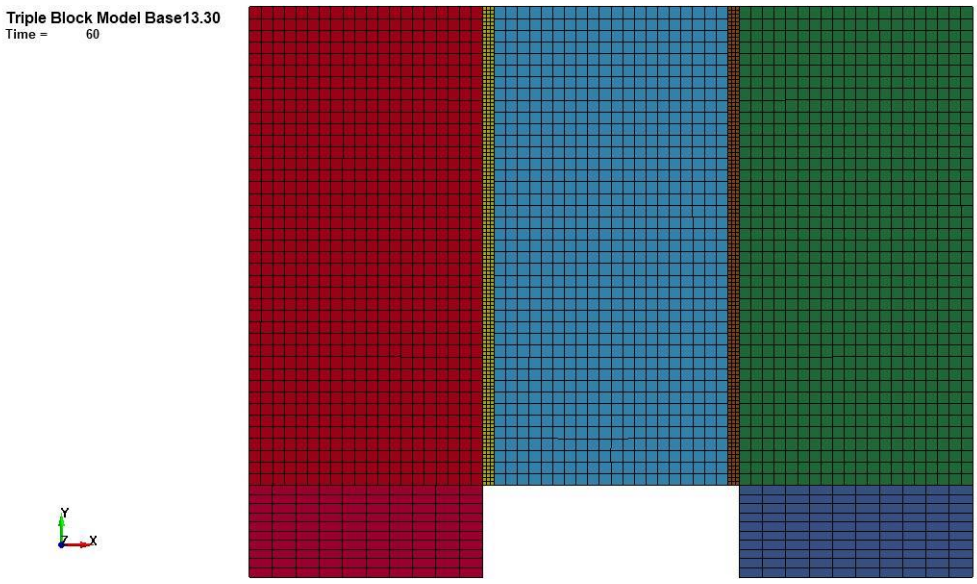


**Figure B-947: Last State at 60 Milliseconds for Base Run 13.30 – 1500 psi**

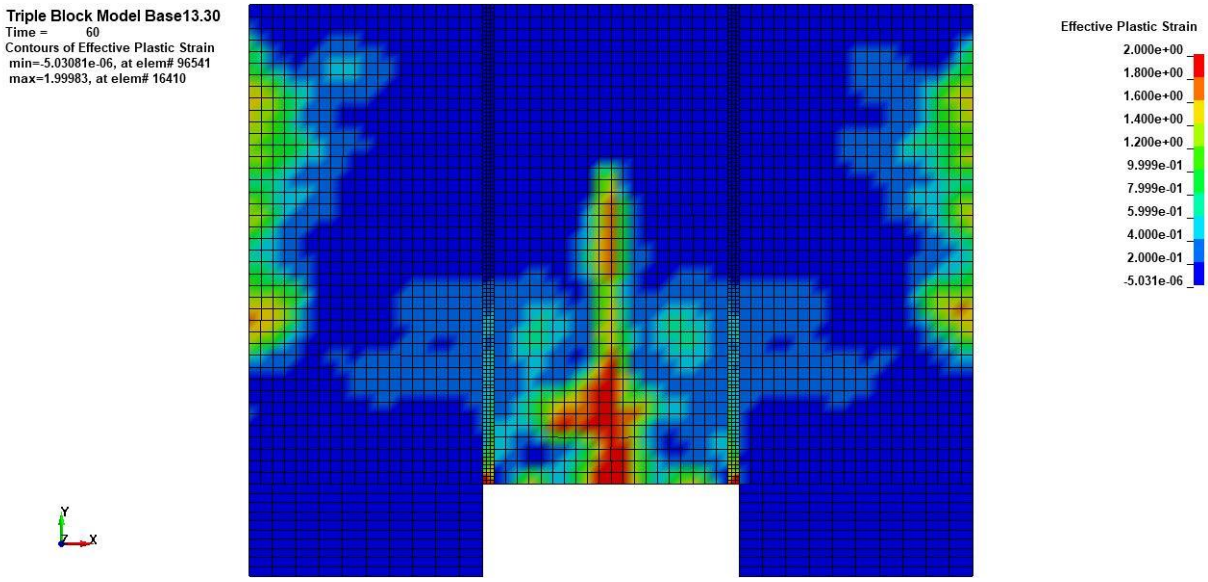


**Figure B-948: Effective Plastic Strain Fringe Plot for Last State at 60 Milliseconds for Base Run 13.30 – 1500 psi**

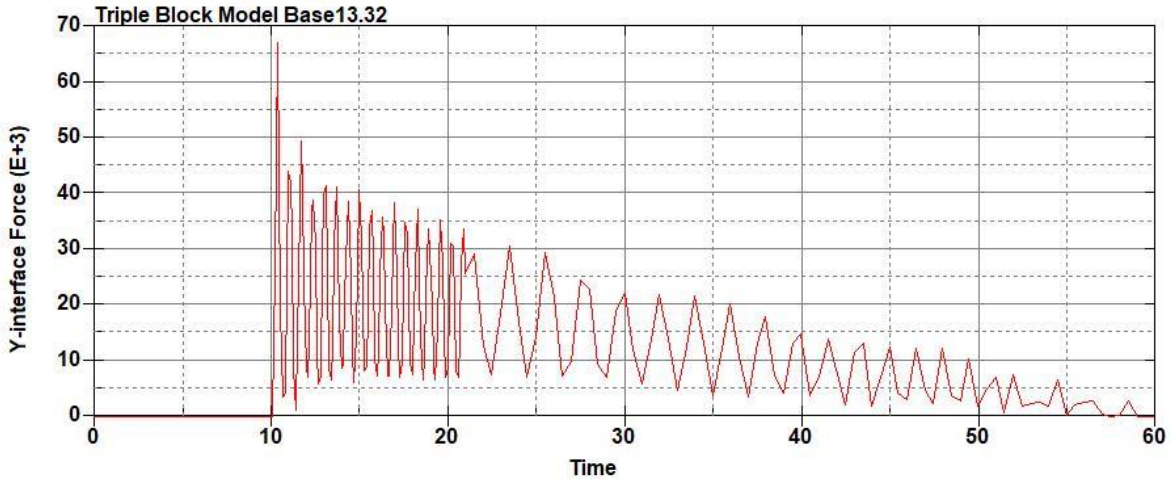


**Figure B-949: Base Run 13.32 Right Support Y-Interface Force (lbs) versus Time (ms) – 1600 psi**

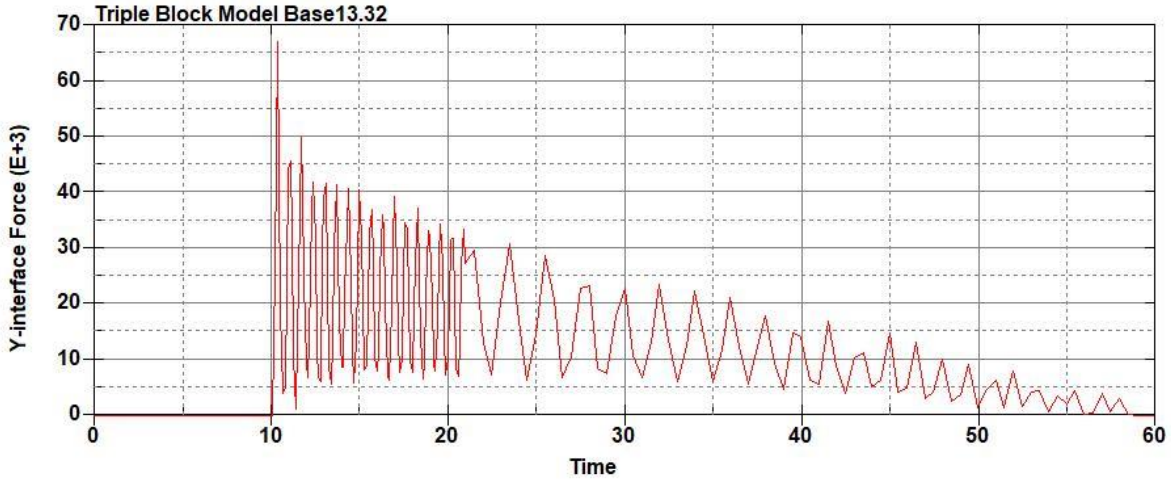


**Figure B-950: Base Run 13.32 Left Support Y-Interface Force (lbs) versus Time (ms) – 1600 psi**

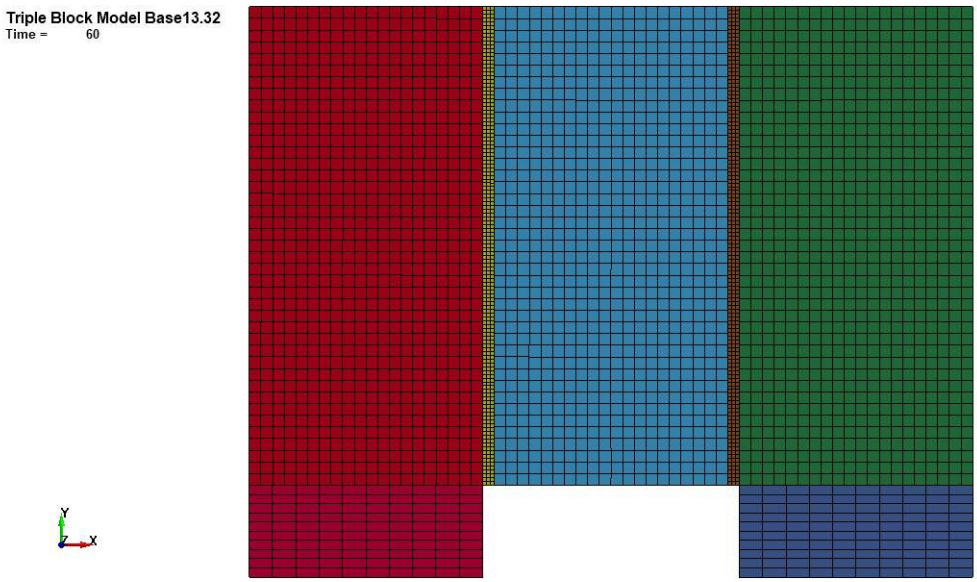


**Figure B-951: Last State at 60 Milliseconds for Base Run 13.32 – 1600 psi**

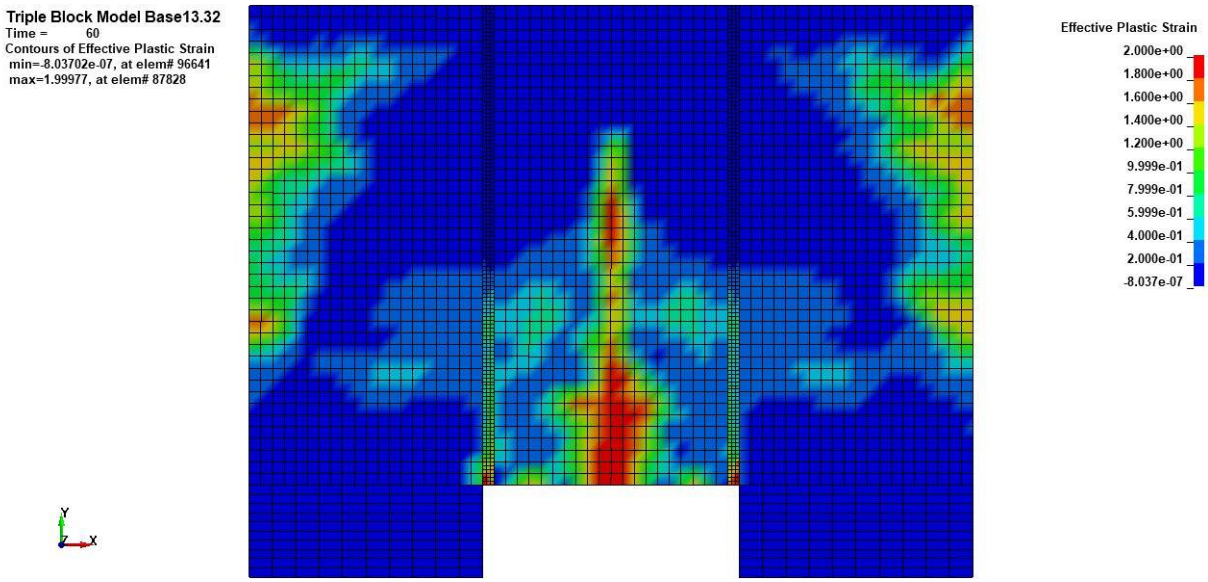


**Figure B-952: Effective Plastic Strain Fringe Plot for Last State at 60 Milliseconds for Base Run 13.32 – 1600 psi**

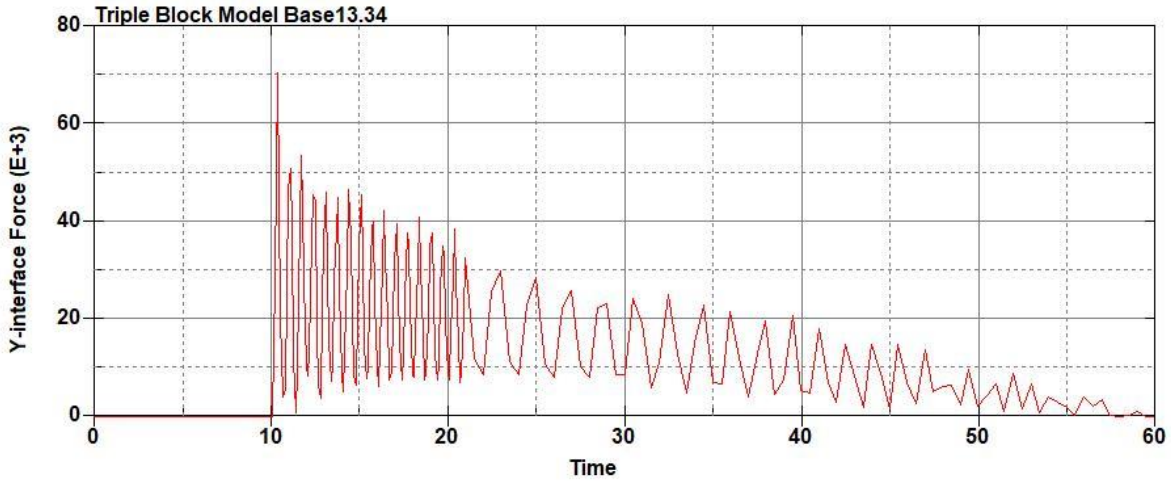


**Figure B-953: Base Run 13.34 Right Support Y-Interface Force (lbs) versus Time (ms) – 1700 psi**

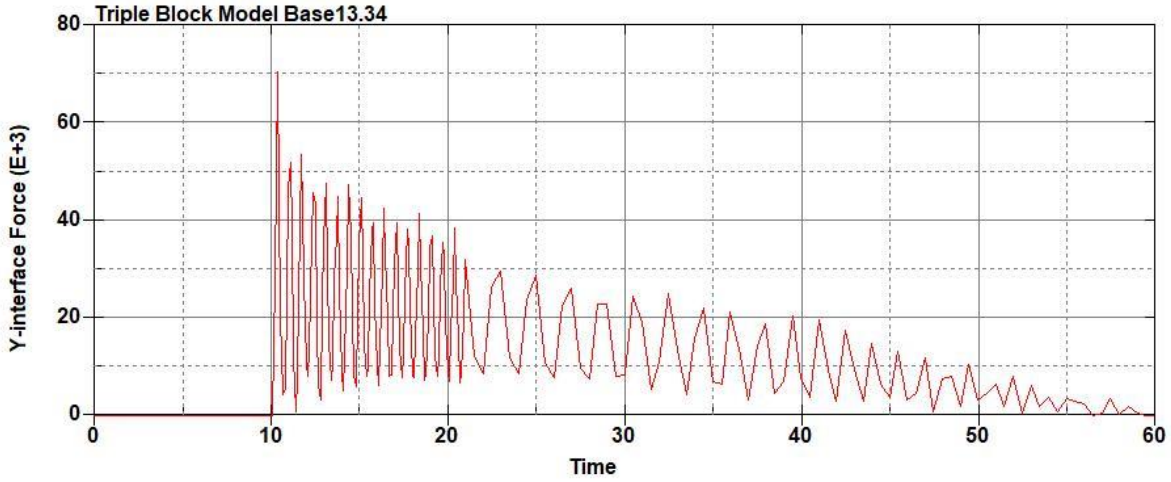


**Figure B-954: Base Run 13.34 Left Support Y-Interface Force (lbs) versus Time (ms) – 1700 psi**

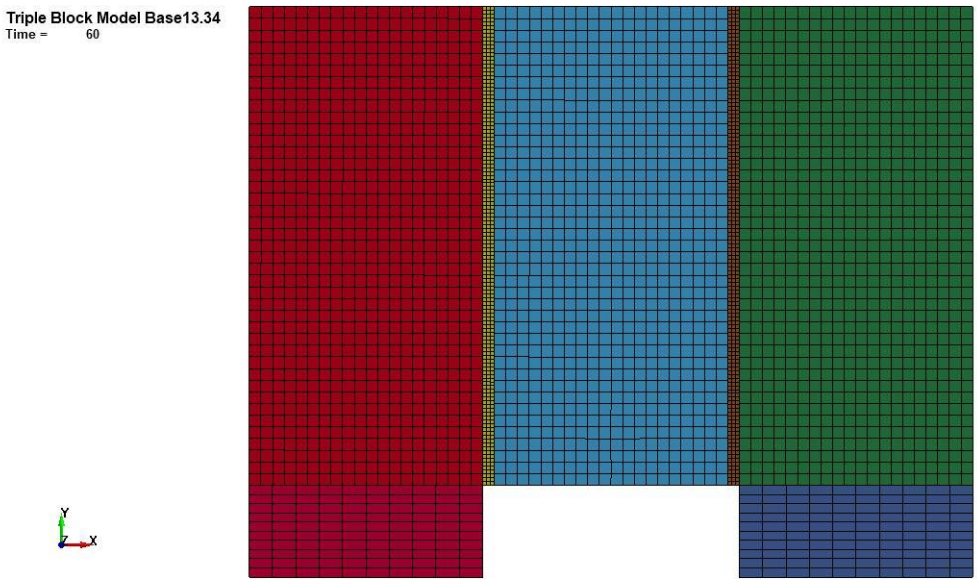


**Figure B-955: Last State at 60 Milliseconds for Base Run 13.34 – 1700 psi**

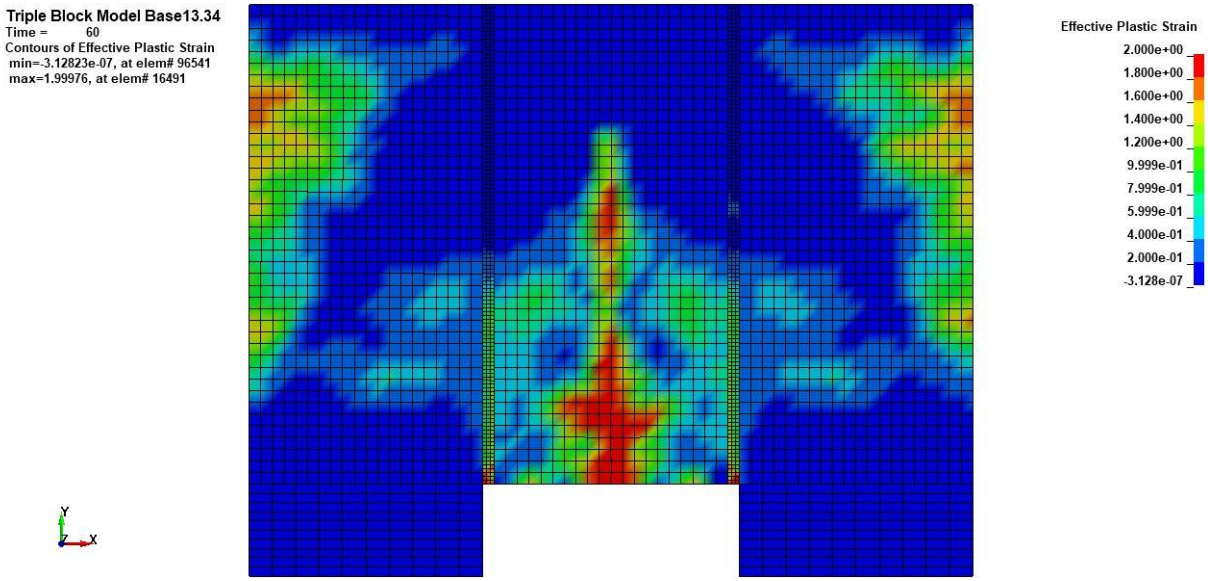


**Figure B-956: Effective Plastic Strain Fringe Plot for Last State at 60 Milliseconds for Base Run 13.34 – 1700 psi**

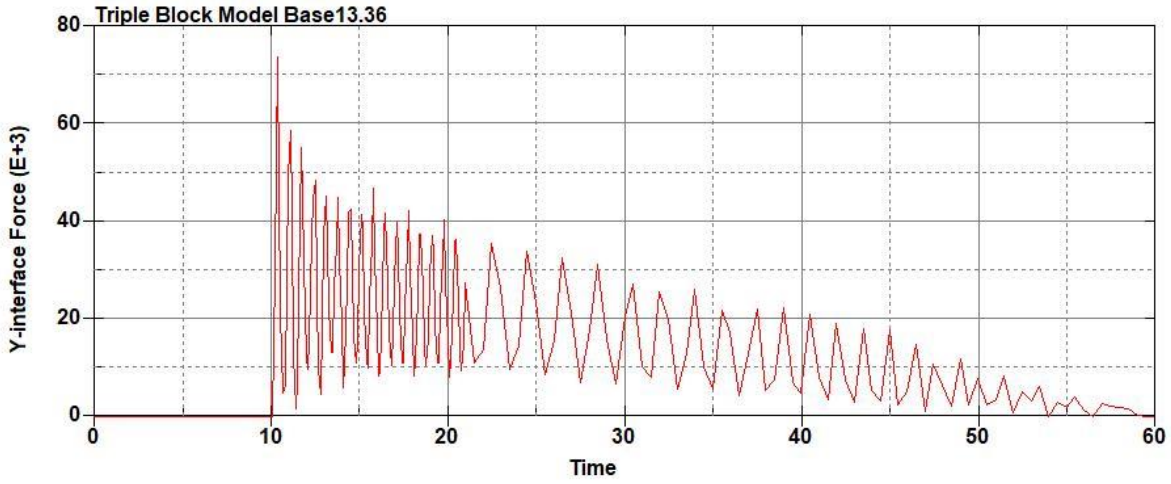


**Figure B-957: Base Run 13.36 Right Support Y-Interface Force (lbs) versus Time (ms) – 1800 psi**

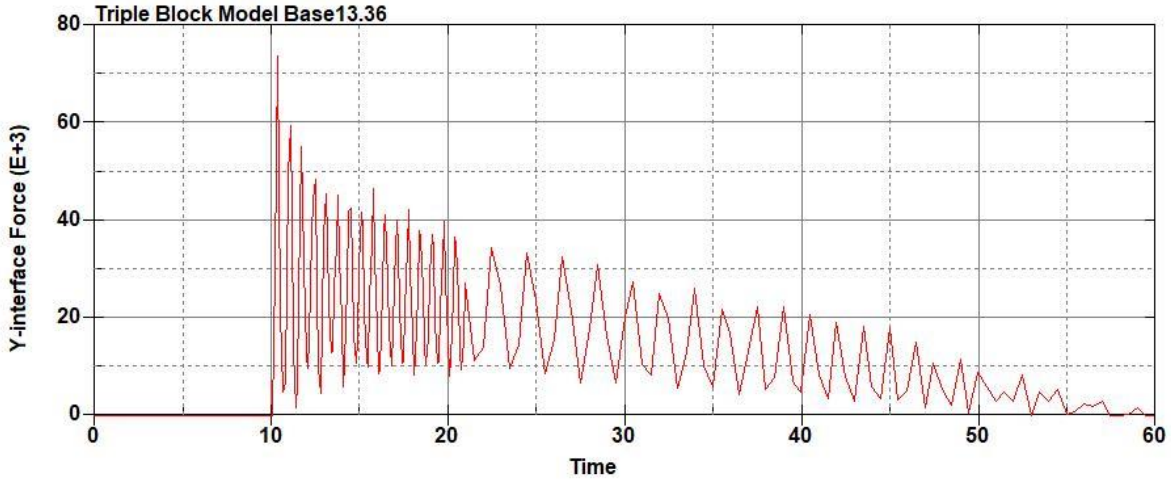


**Figure B-958: Base Run 13.36 Left Support Y-Interface Force (lbs) versus Time (ms) – 1800 psi**

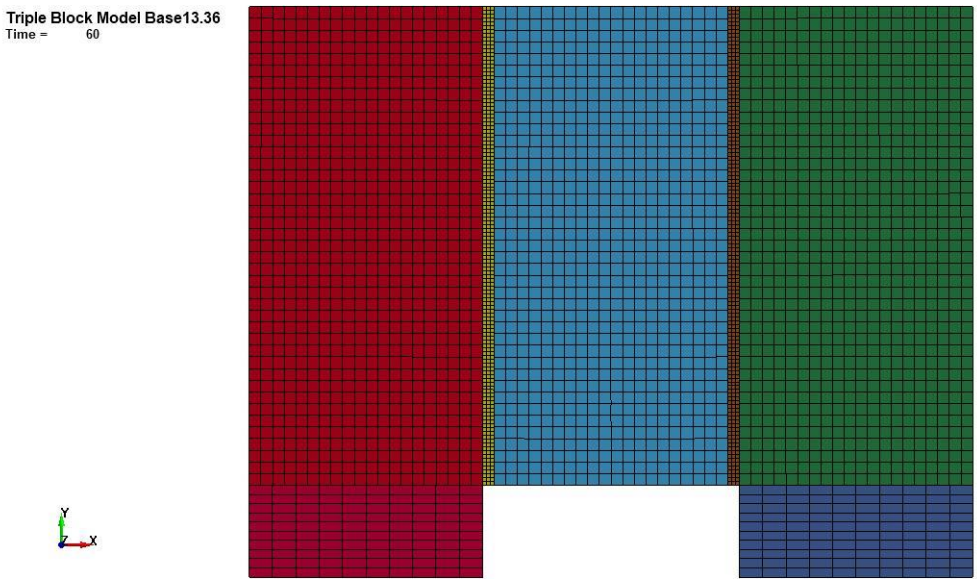


**Figure B-959: Last State at 60 Milliseconds for Base Run 13.36 – 1800 psi**

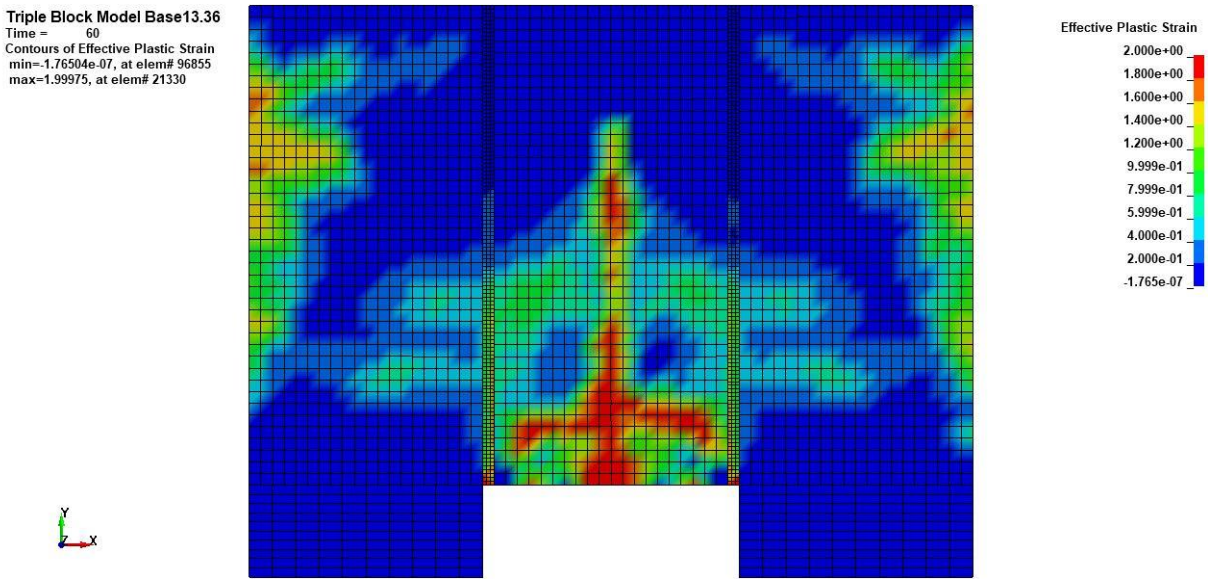


**Figure B-960: Effective Plastic Strain Fringe Plot for Last State at 60 Milliseconds for Base Run 13.36 – 1800 psi**

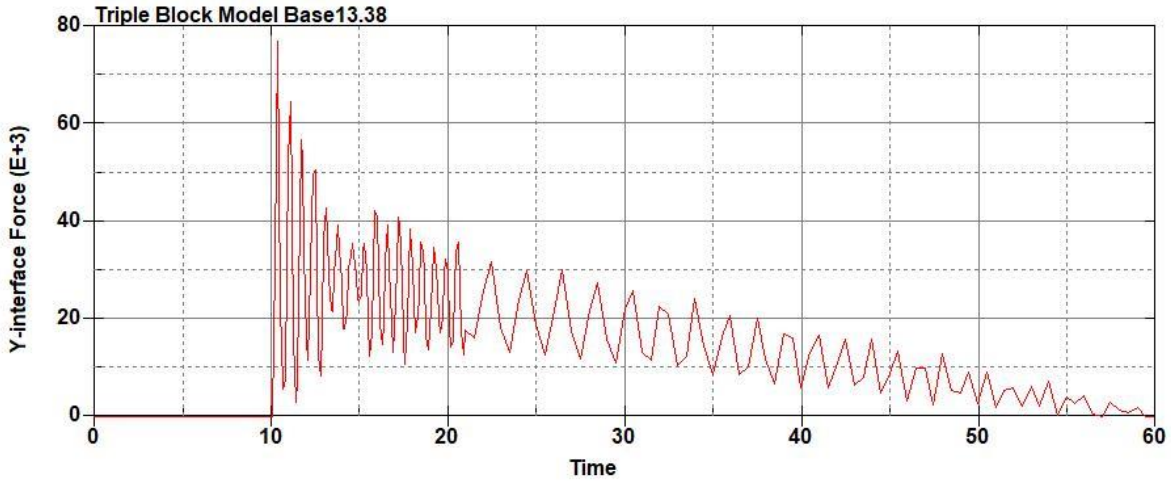


**Figure B-961: Base Run 13.38 Right Support Y-Interface Force (lbs) versus Time (ms) – 1900 psi**

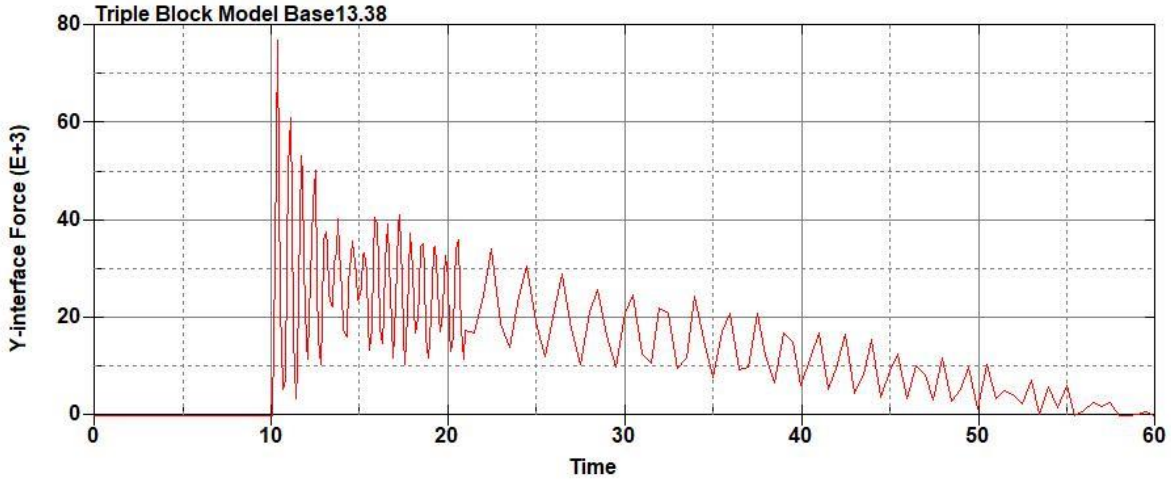


**Figure B-962: Base Run 13.38 Left Support Y-Interface Force (lbs) versus Time (ms) – 1900 psi**

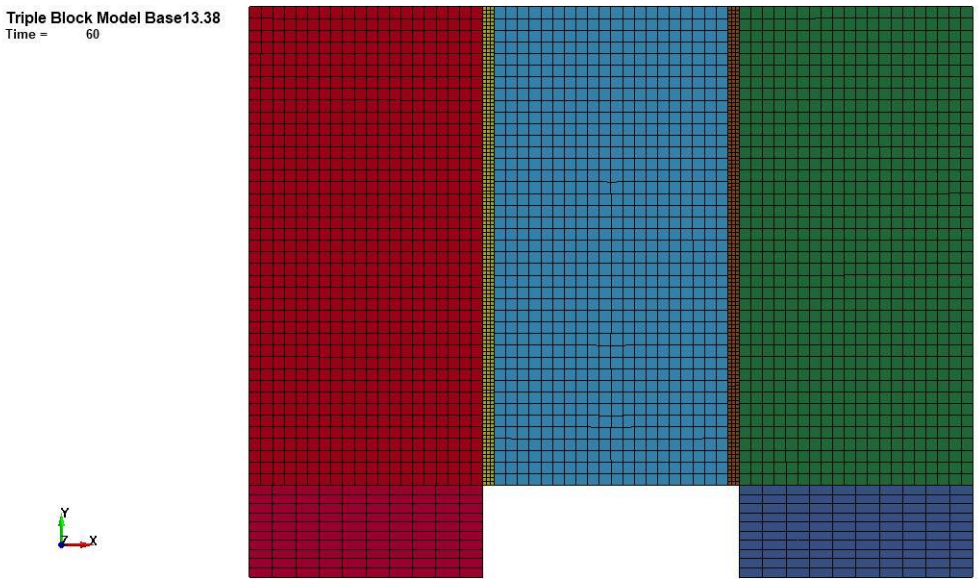


**Figure B-963: Last State at 60 Milliseconds for Base Run 13.38 – 1900 psi**

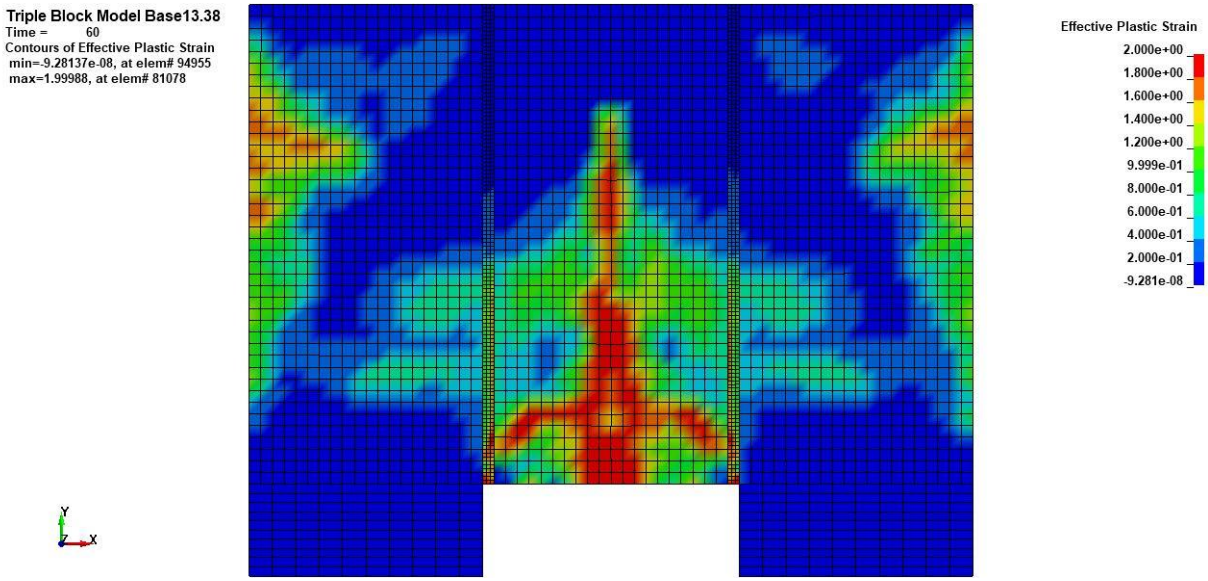


**Figure B-964: Effective Plastic Strain Fringe Plot for Last State at 60 Milliseconds for Base Run 13.38 – 1900 psi**

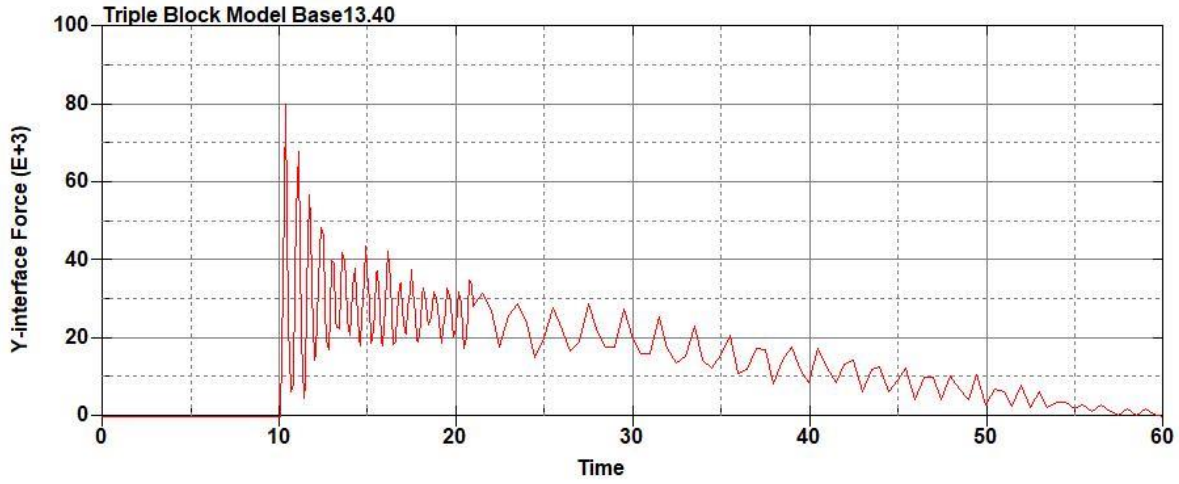


**Figure B-965: Base Run 13.40 Right Support Y-Interface Force (lbs) versus Time (ms) – 2000 psi**

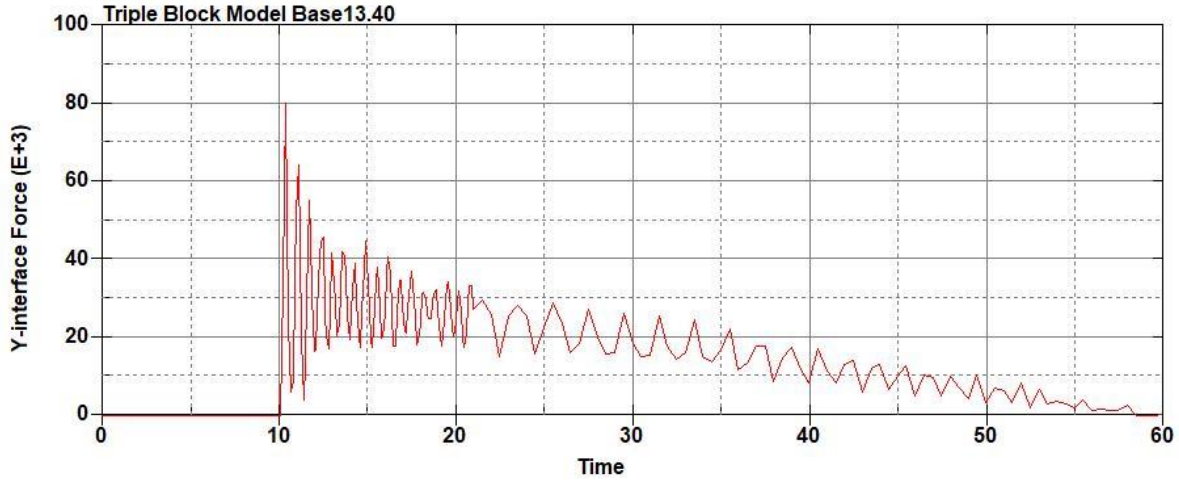


**Figure B-966: Base Run 13.40 Left Support Y-Interface Force (lbs) versus Time (ms) – 2000 psi**

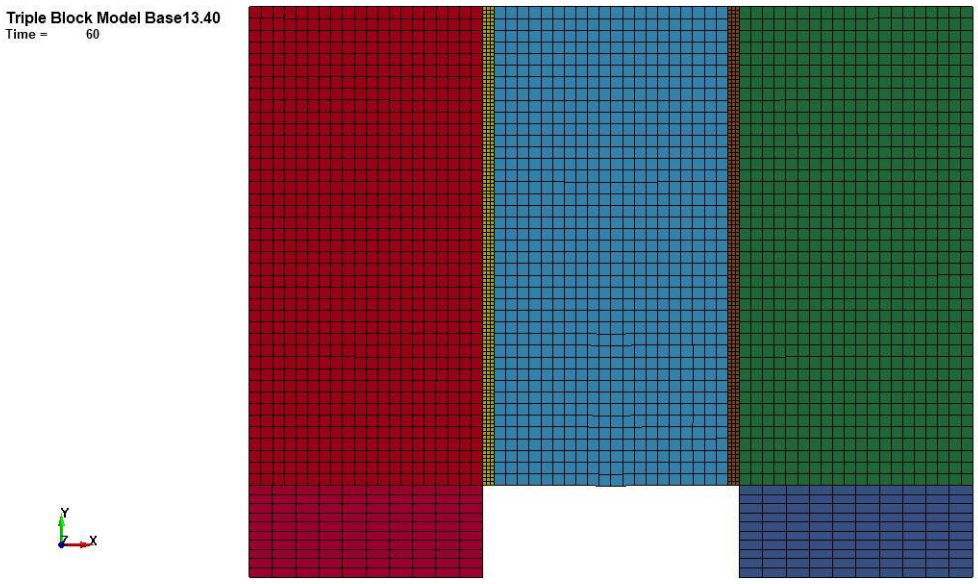


**Figure B-967: Last State at 60 Milliseconds for Base Run 13.40 – 2000 psi**

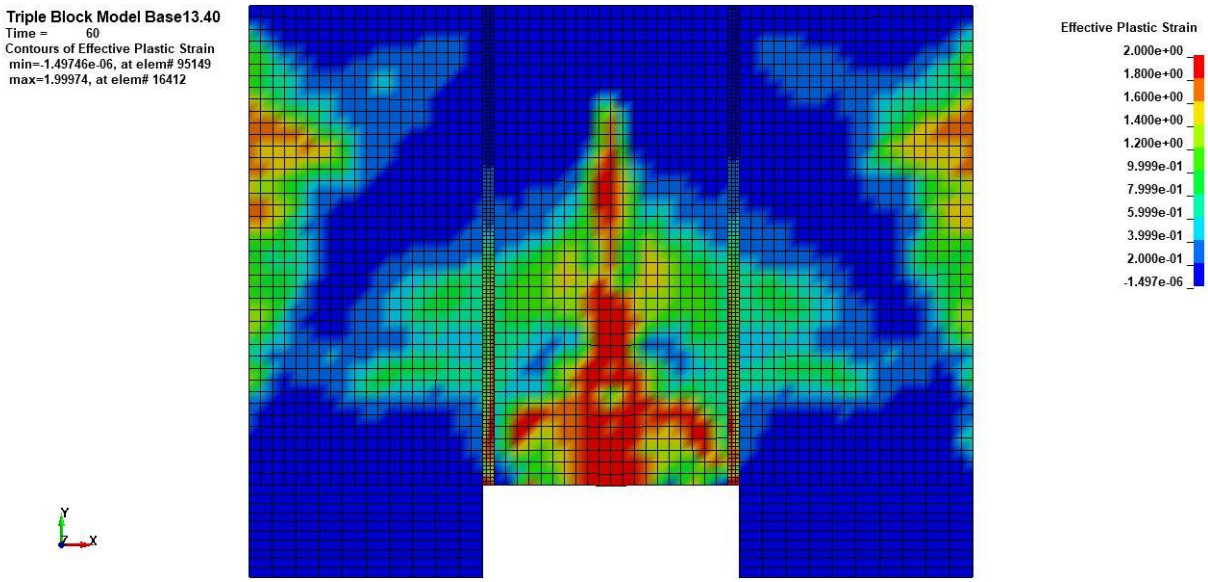


**Figure B-968: Effective Plastic Strain Fringe Plot for Last State at 60 Milliseconds for Base Run 13.40 – 2000 psi**

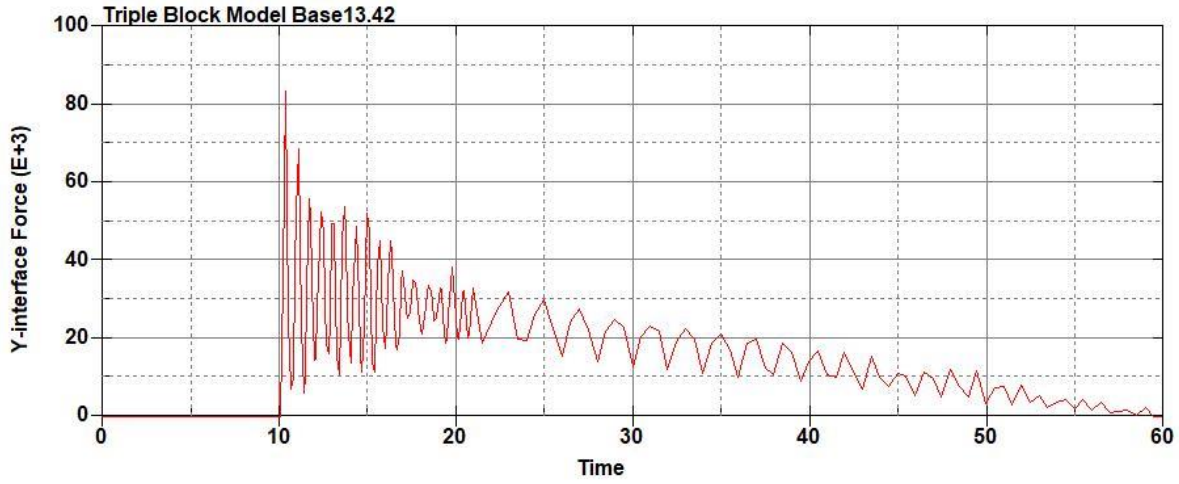


**Figure B-969: Base Run 13.42 Right Support Y-Interface Force (lbs) versus Time (ms) – 2100 psi**

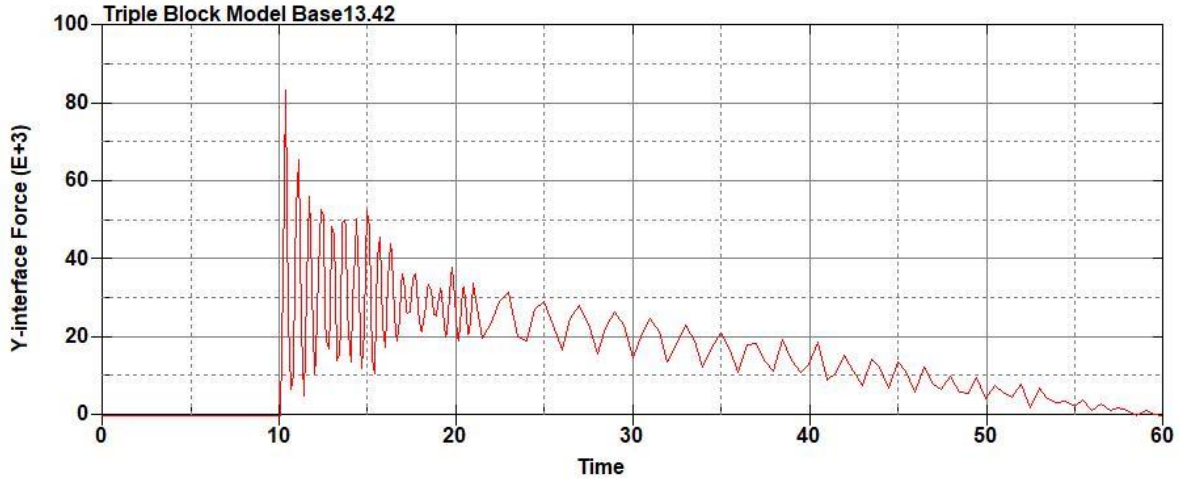


**Figure B-970: Base Run 13.42 Left Support Y-Interface Force (lbs) versus Time (ms) – 2100 psi**

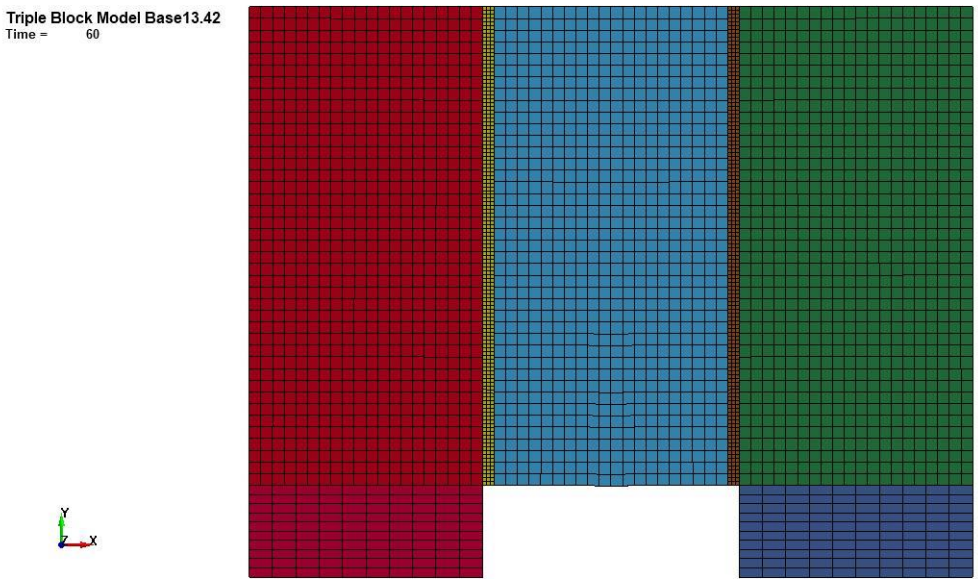


**Figure B-971: Last State at 60 Milliseconds for Base Run 13.42 – 2100 psi**

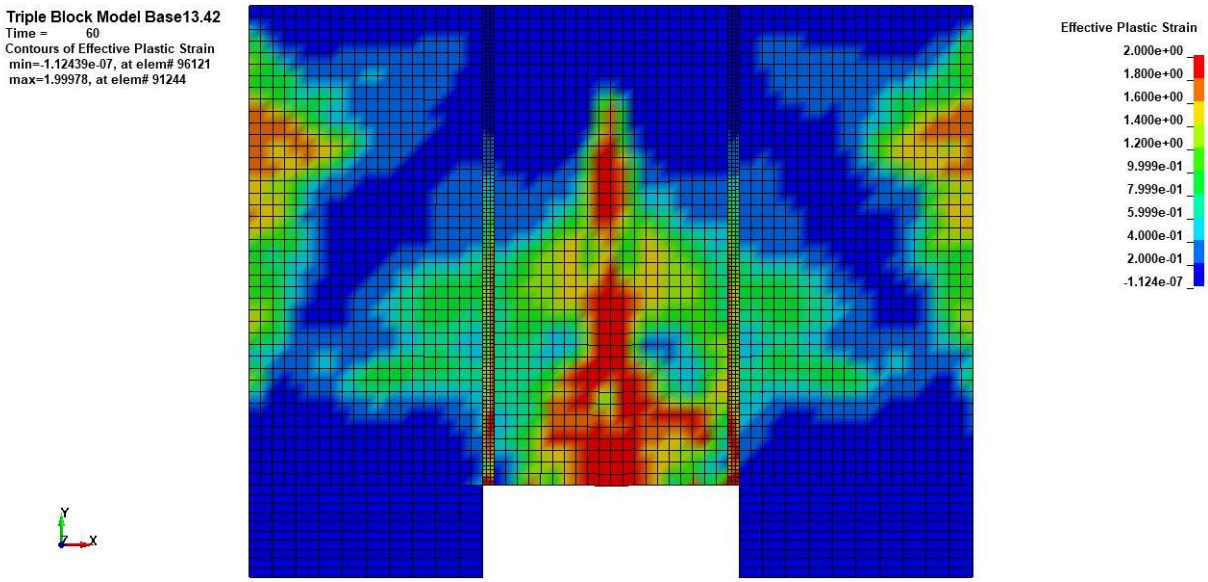


**Figure B-972: Effective Plastic Strain Fringe Plot for Last State at 60 Milliseconds for Base Run 13.42 – 2100 psi**

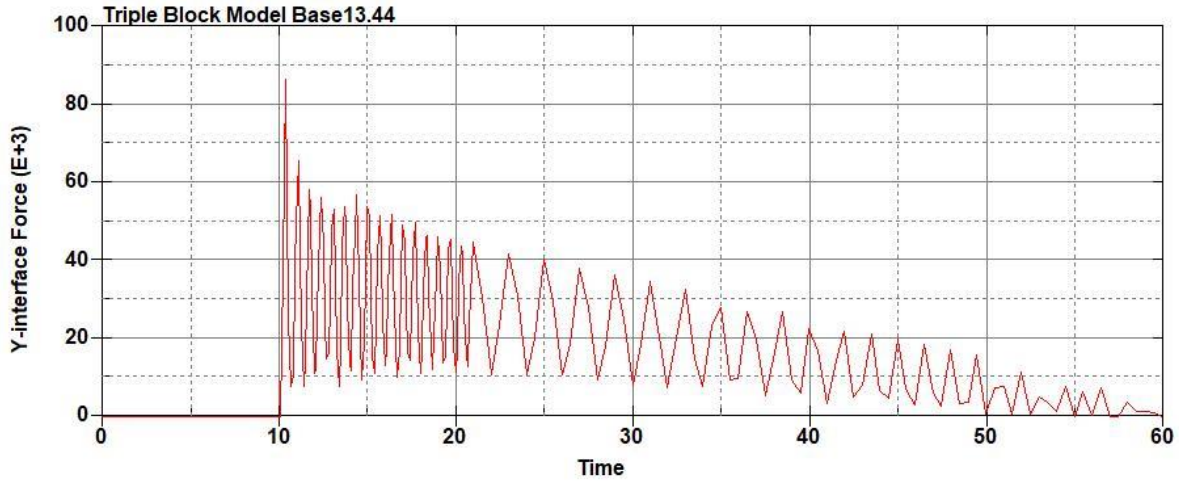


**Figure B-973: Base Run 13.44 Right Support Y-Interface Force (lbs) versus Time (ms) – 2200 psi**

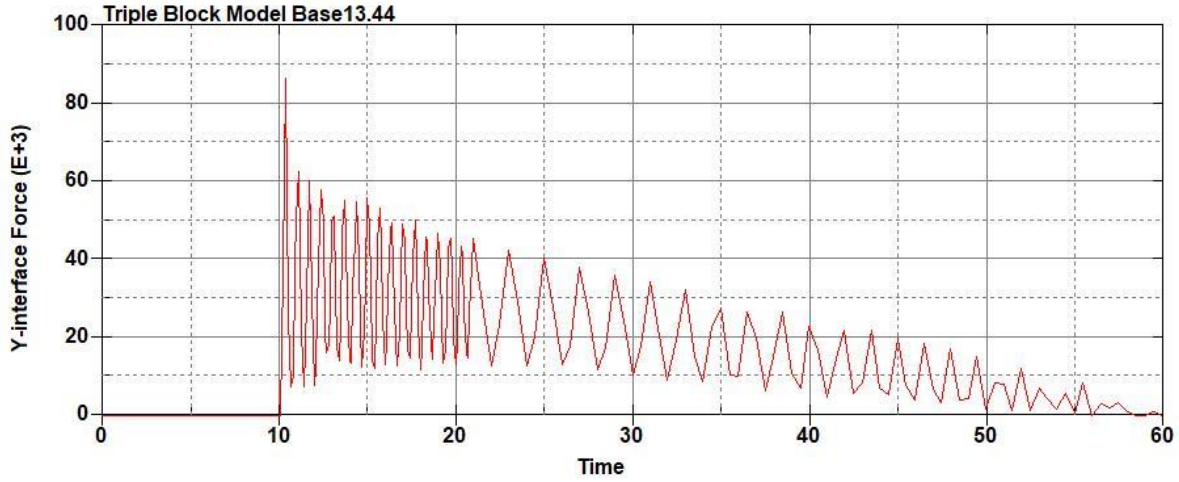


**Figure B-974: Base Run 13.44 Left Support Y-Interface Force (lbs) versus Time (ms) – 2200 psi**

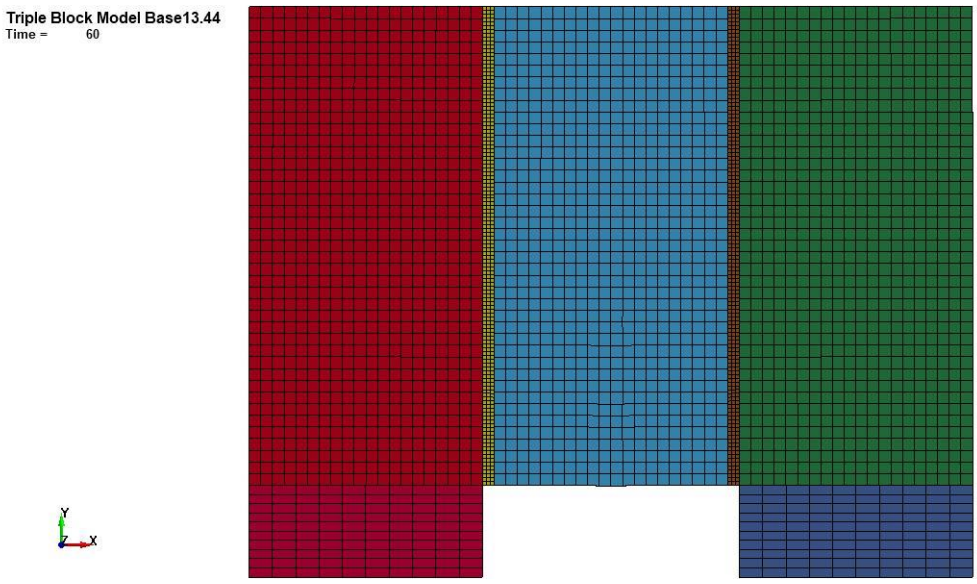


**Figure B-975: Last State at 60 Milliseconds for Base Run 13.44 – 2200 psi**

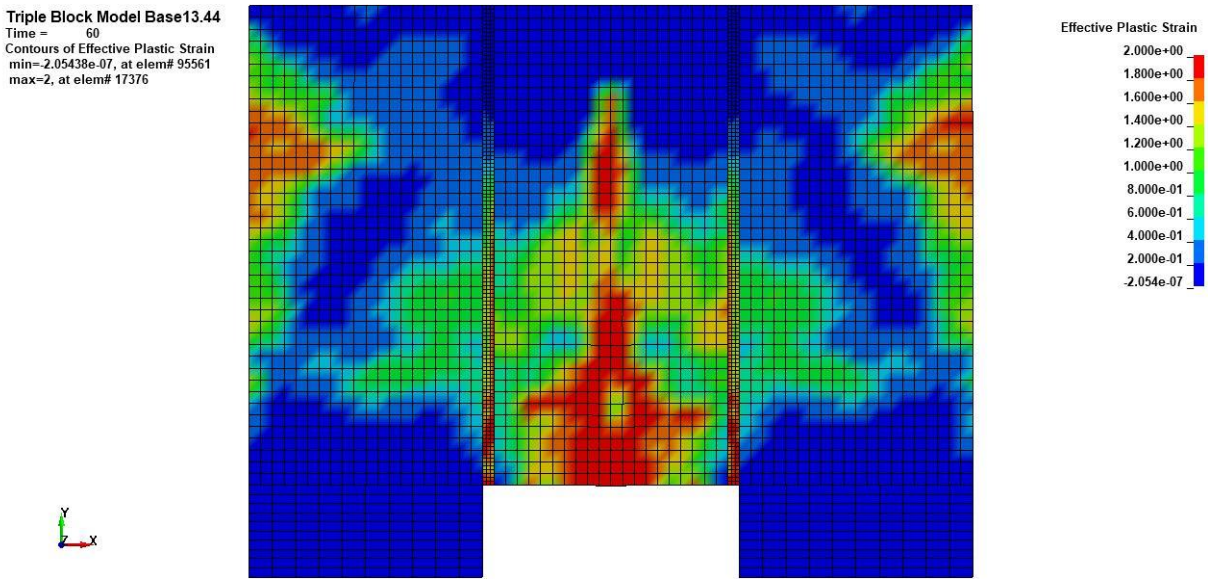


**Figure B-976: Effective Plastic Strain Fringe Plot for Last State at 60 Milliseconds for Base Run 13.44 – 2200 psi**

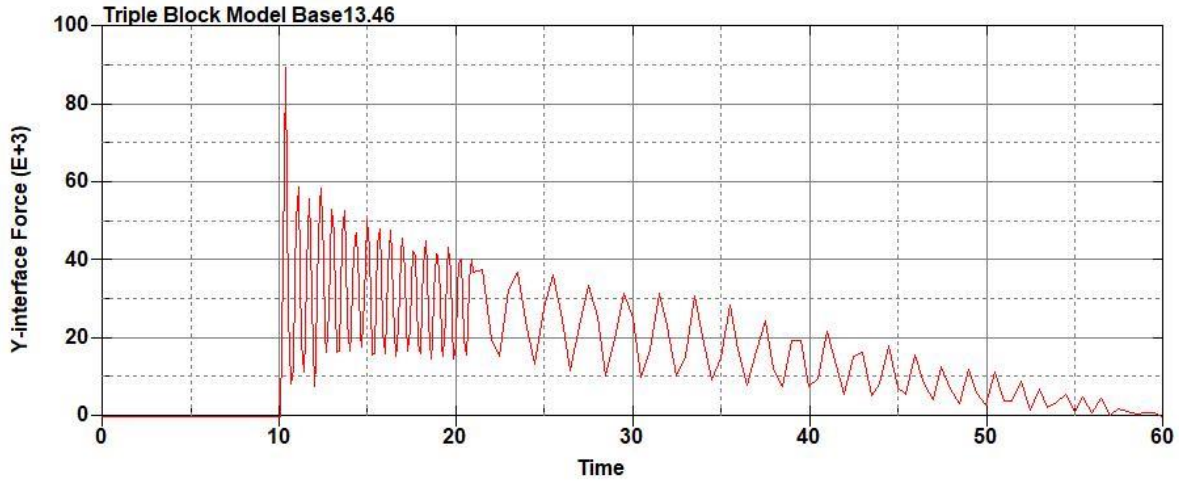


**Figure B-977: Base Run 13.46 Right Support Y-Interface Force (lbs) versus Time (ms) – 2300 psi**

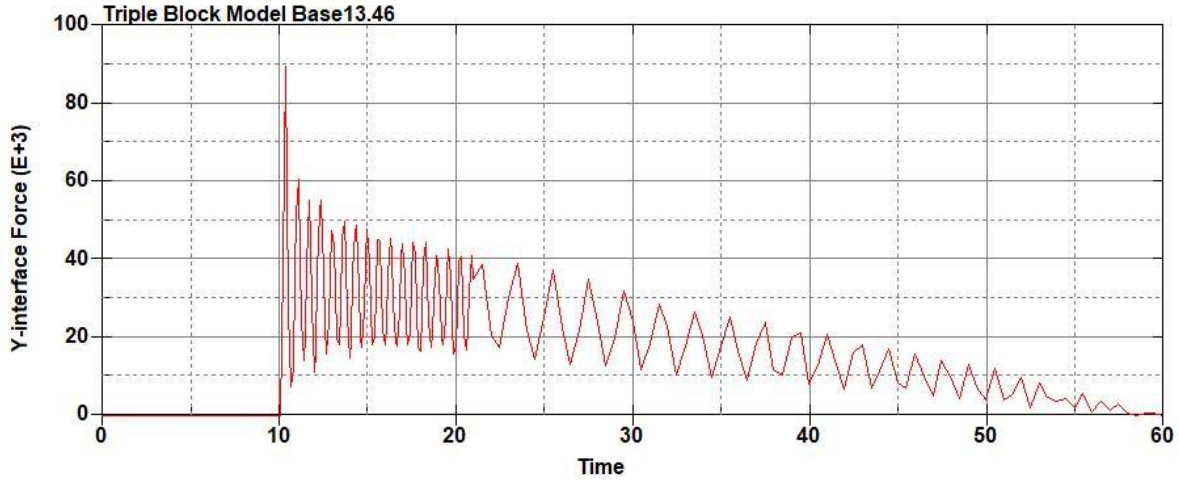


**Figure B-978: Base Run 13.46 Left Support Y-Interface Force (lbs) versus Time (ms) – 2300 psi**

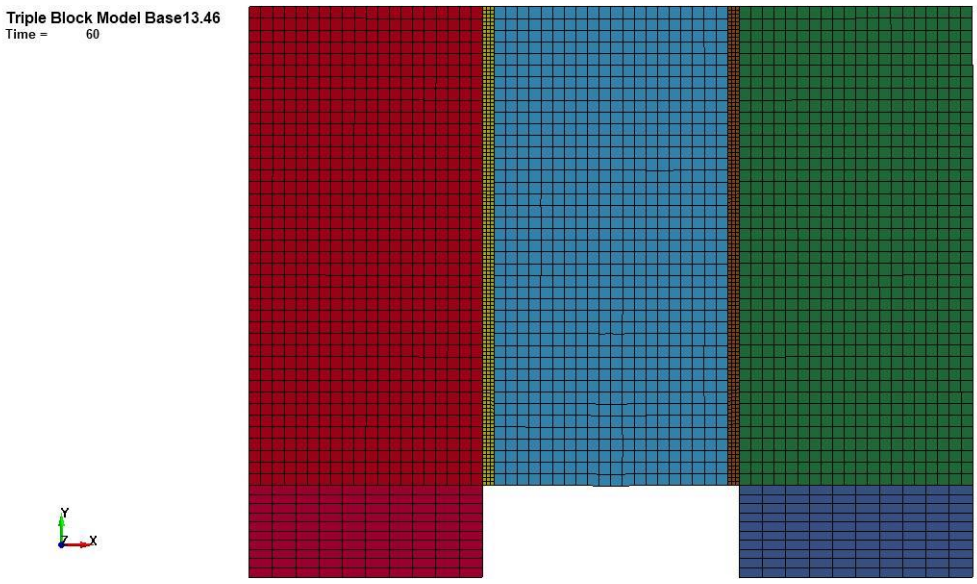


**Figure B-979: Last State at 60 Milliseconds for Base Run 13.46 – 2300 psi**

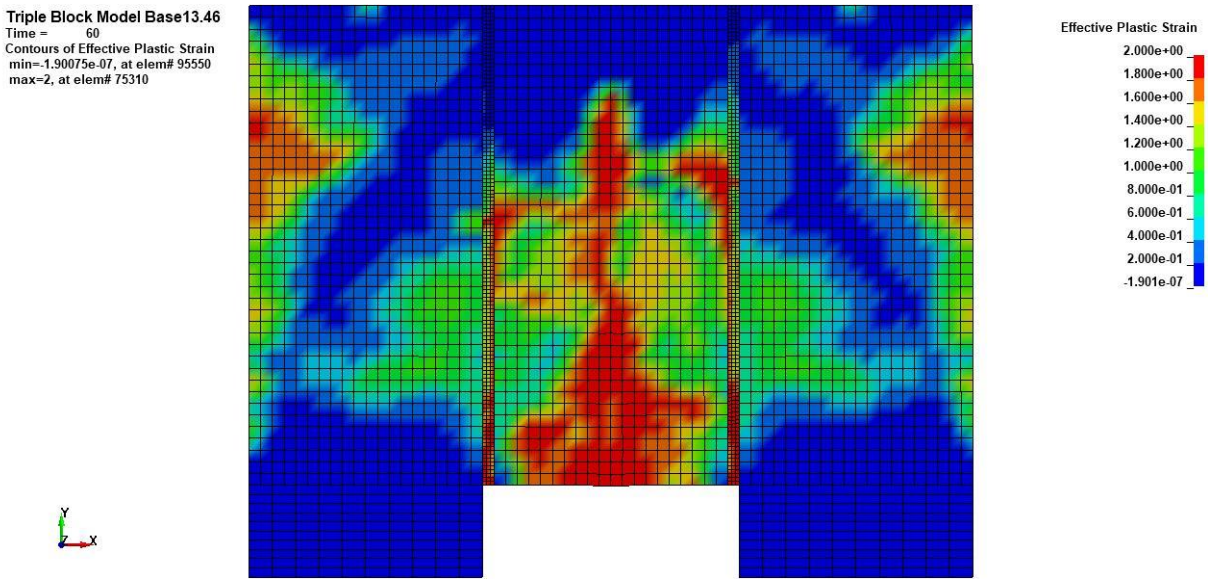


**Figure B-980: Effective Plastic Strain Fringe Plot for Last State at 60 Milliseconds for Base Run 13.46 – 2300 psi**

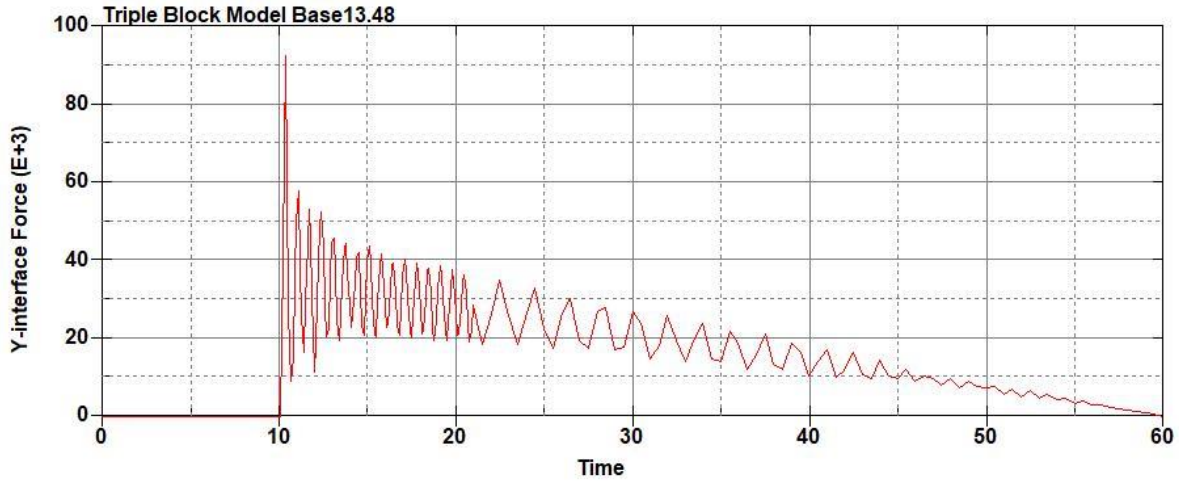


**Figure B-981: Base Run 13.48 Right Support Y-Interface Force (lbs) versus Time (ms) – 2400 psi**

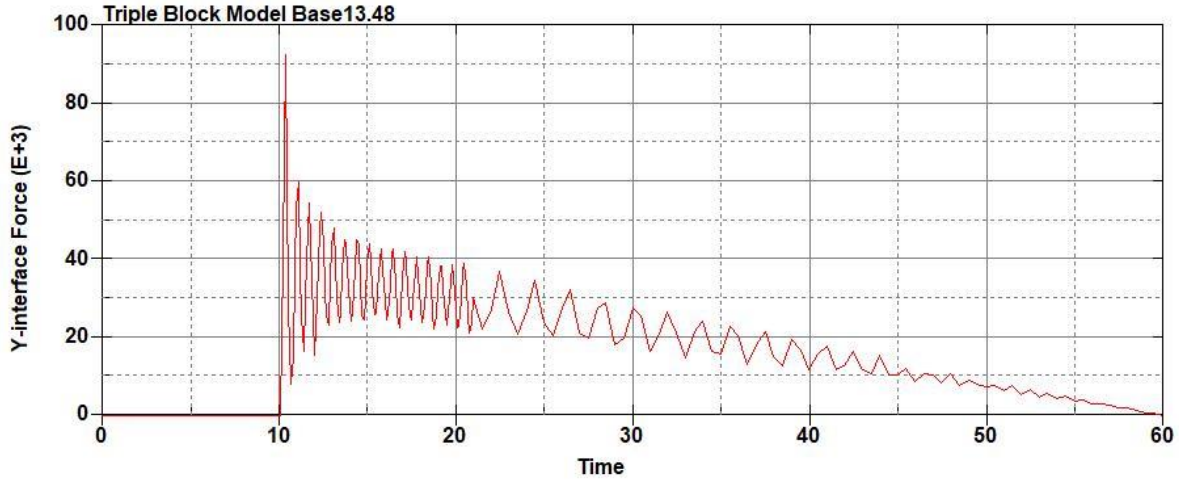


**Figure B-982: Base Run 13.48 Left Support Y-Interface Force (lbs) versus Time (ms) – 2400 psi**

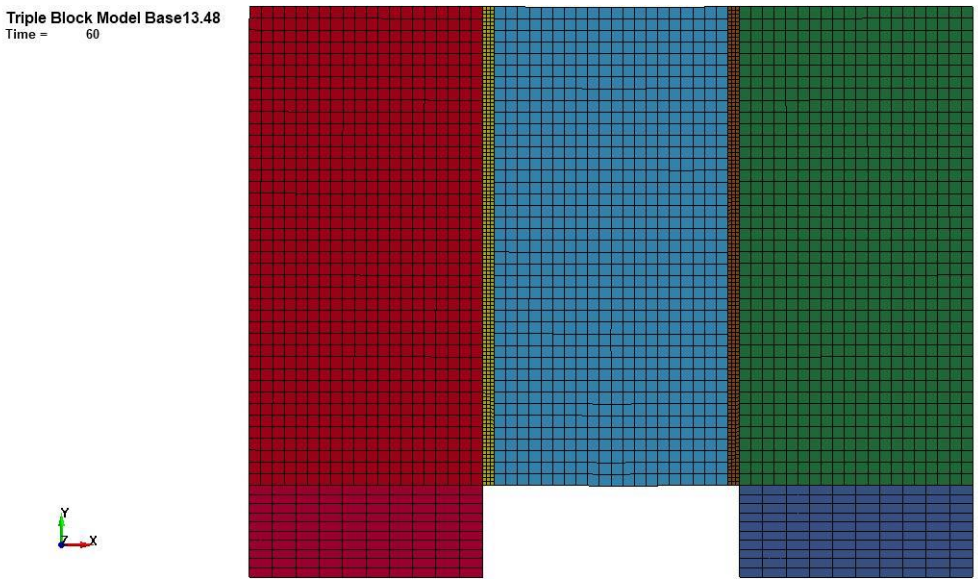


**Figure B-983: Last State at 60 Milliseconds for Base Run 13.48 – 2400 psi**

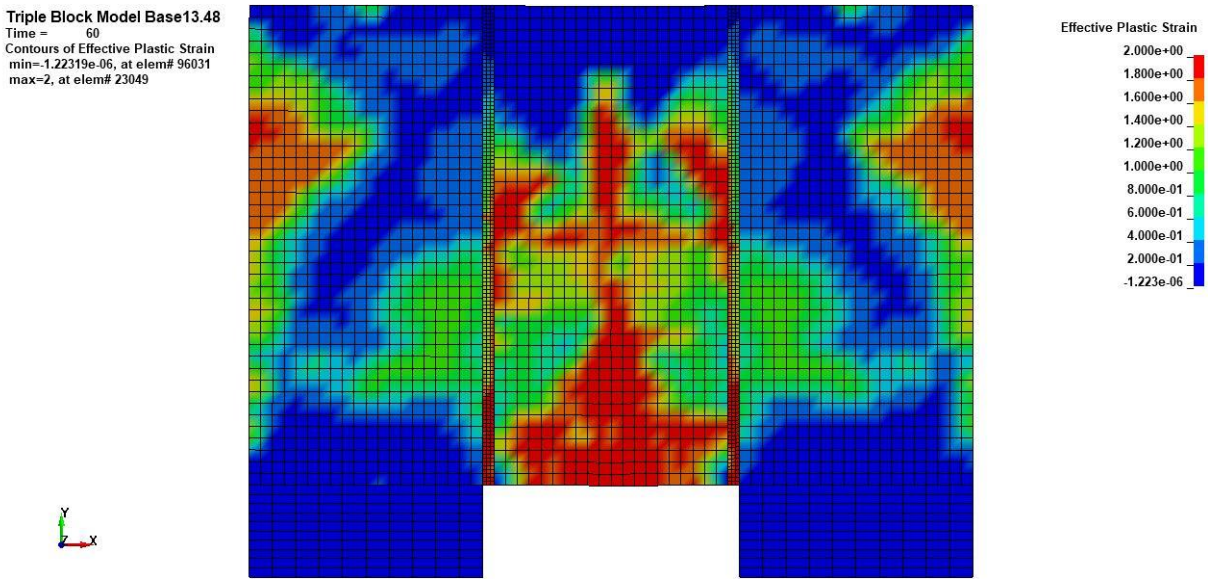


**Figure B-984: Effective Plastic Strain Fringe Plot for Last State at 60 Milliseconds for Base Run 13.48 – 2400 psi**

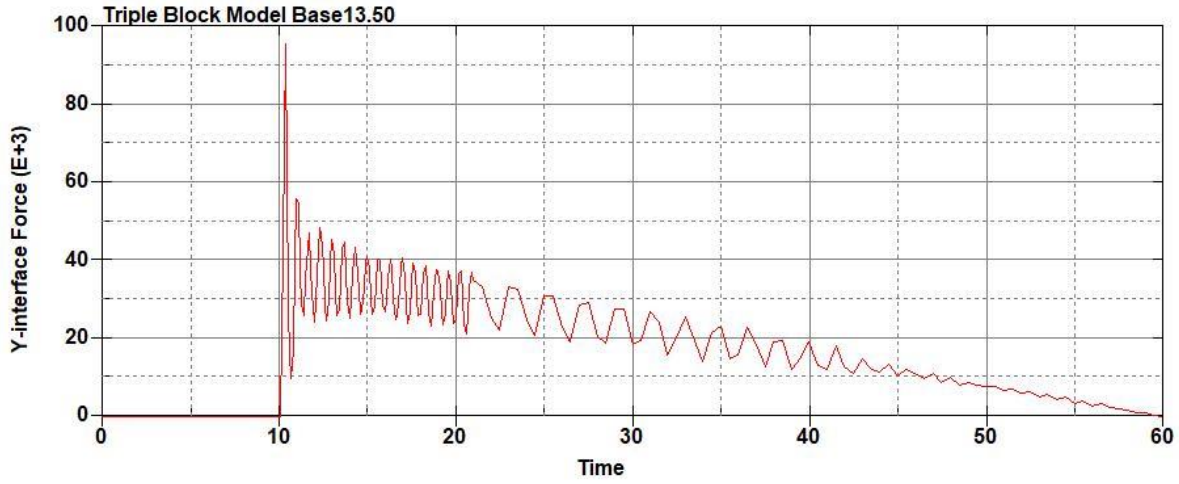


**Figure B-985: Base Run 13.50 Right Support Y-Interface Force (lbs) versus Time (ms) – 2500 psi**

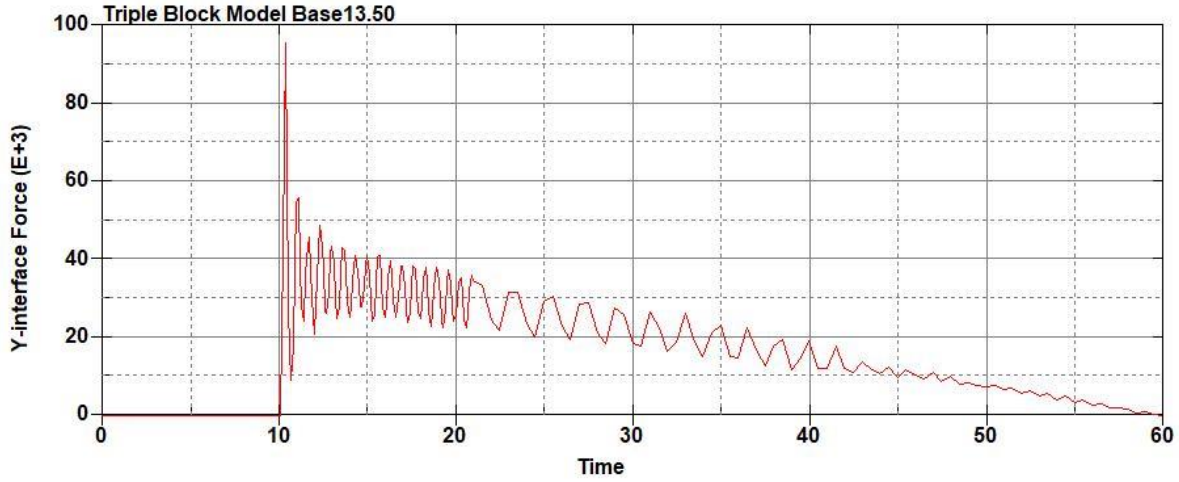


**Figure B-986: Base Run 13.50 Left Support Y-Interface Force (lbs) versus Time (ms) – 2500 psi**

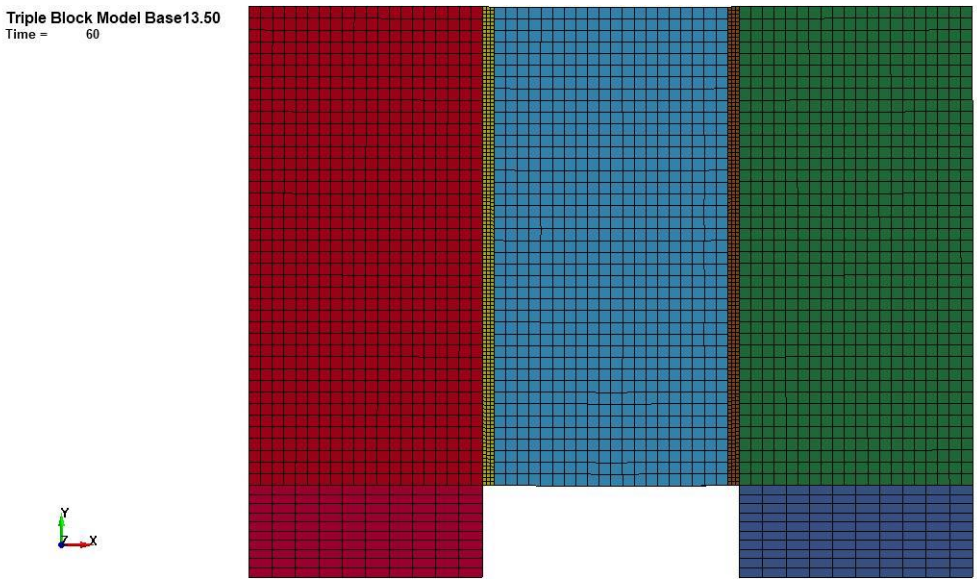


**Figure B-987: Last State at 60 Milliseconds for Base Run 13.50 – 2500 psi**

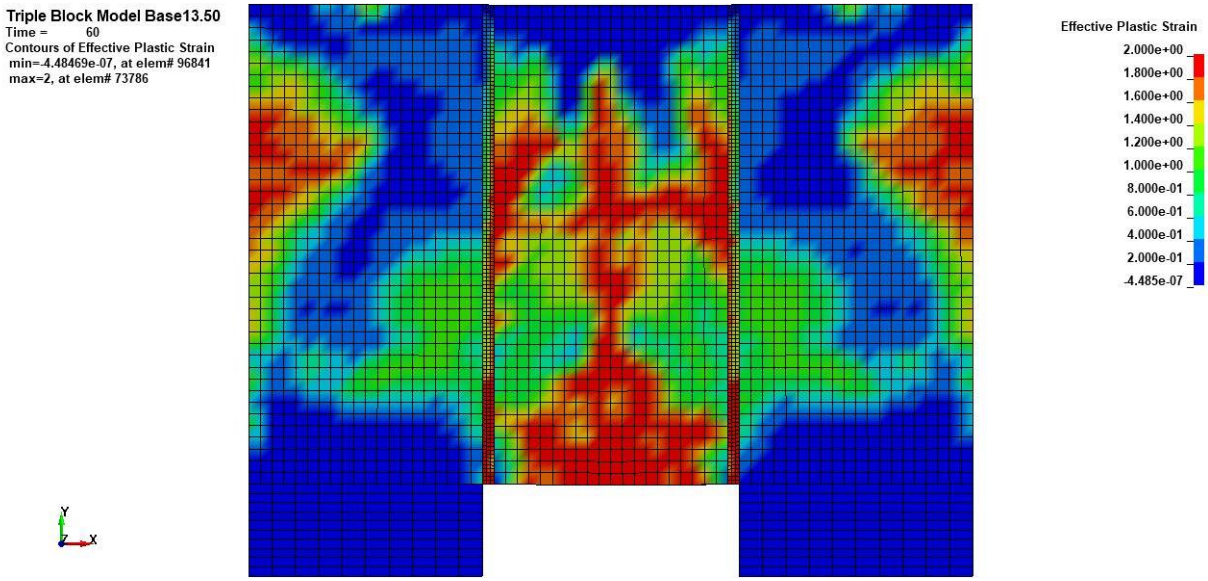


**Figure B-988: Effective Plastic Strain Fringe Plot for Last State at 60 Milliseconds for Base Run 13.50 – 2500 psi**

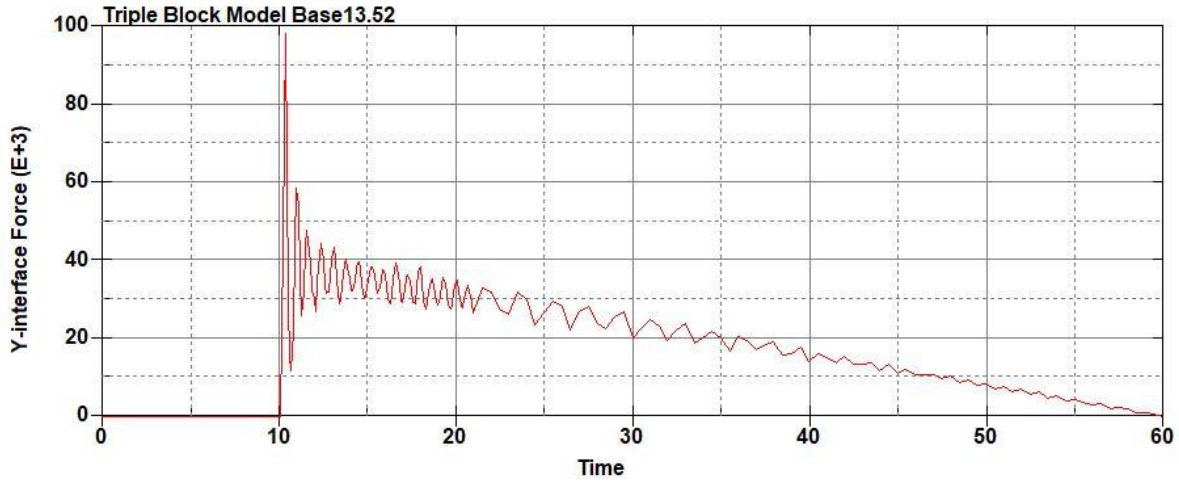


**Figure B-989: Base Run 13.52 Right Support Y-Interface Force (lbs) versus Time (ms) – 2600 psi**

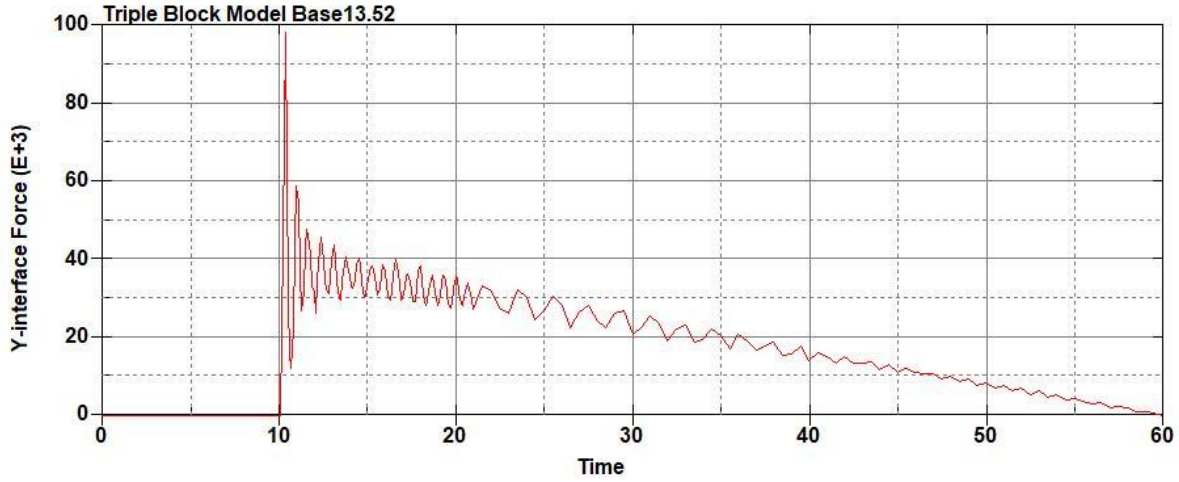


**Figure B-990: Base Run 13.52 Left Support Y-Interface Force (lbs) versus Time (ms) – 2600 psi**

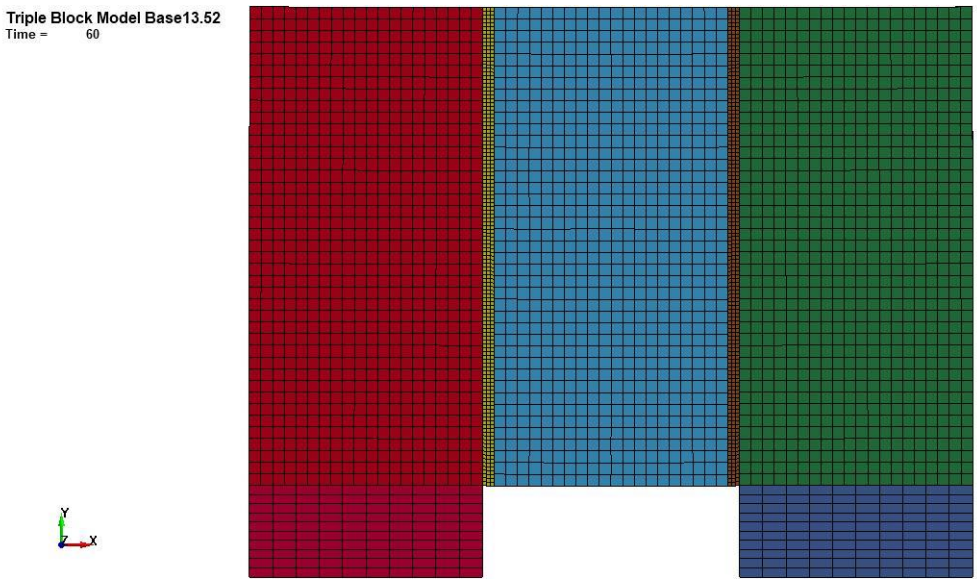


**Figure B-991: Last State at 60 Milliseconds for Base Run 13.52 – 2600 psi**

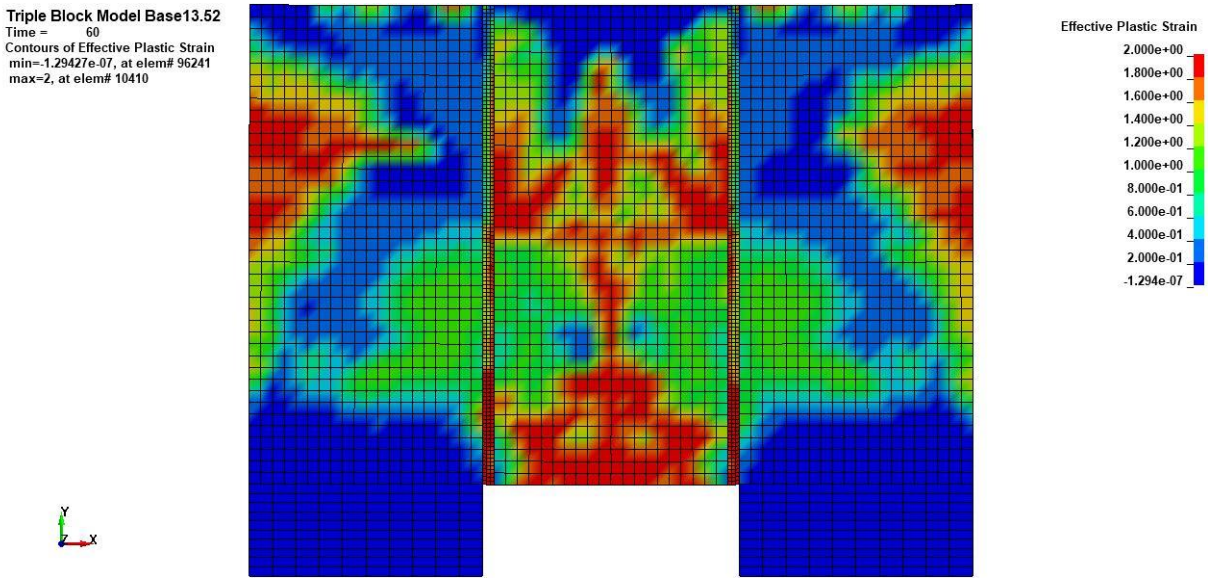


**Figure B-992: Effective Plastic Strain Fringe Plot for Last State at 60 Milliseconds for Base Run 13.52 – 2600 psi**

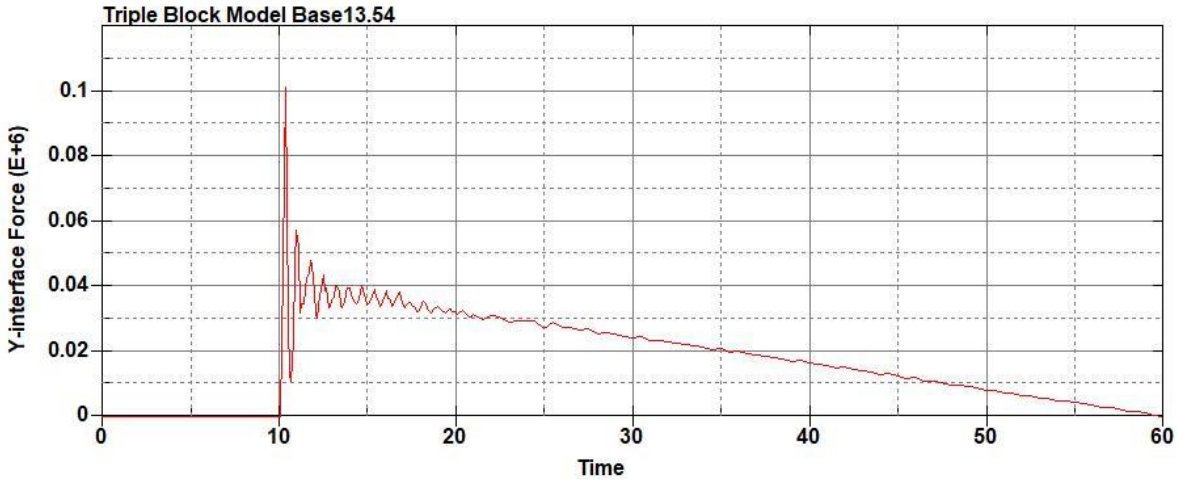


**Figure B-993: Base Run 13.54 Right Support Y-Interface Force (lbs) versus Time (ms) – 2700 psi**

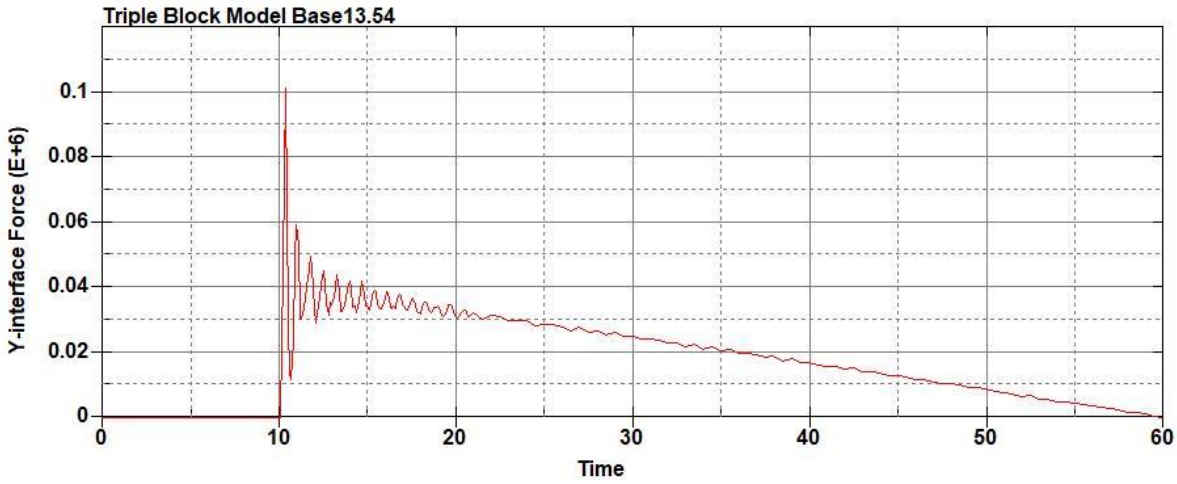


**Figure B-994: Base Run 13.54 Left Support Y-Interface Force (lbs) versus Time (ms) –2700 psi**

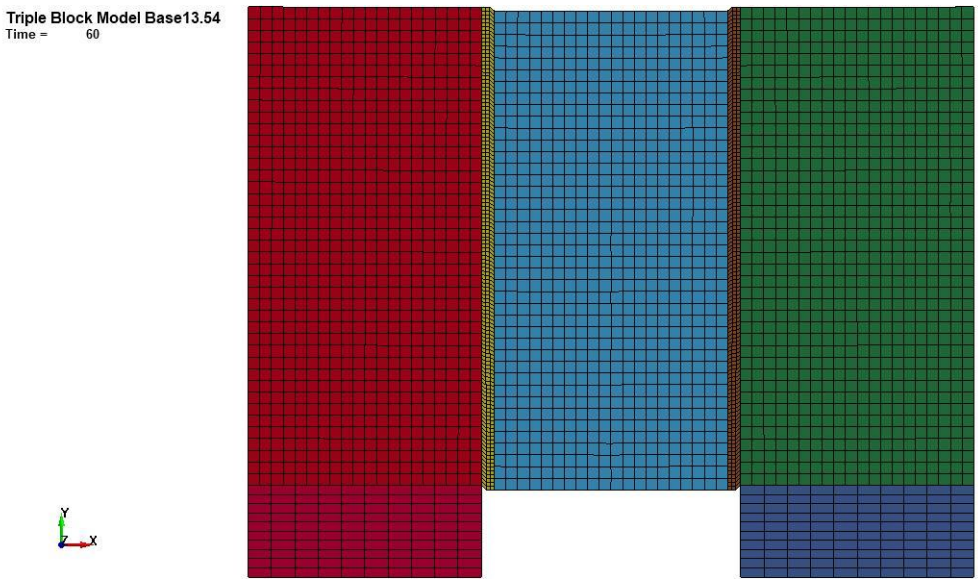


**Figure B-995: Last State at 60 Milliseconds for Base Run 13.54 – 2700 psi**

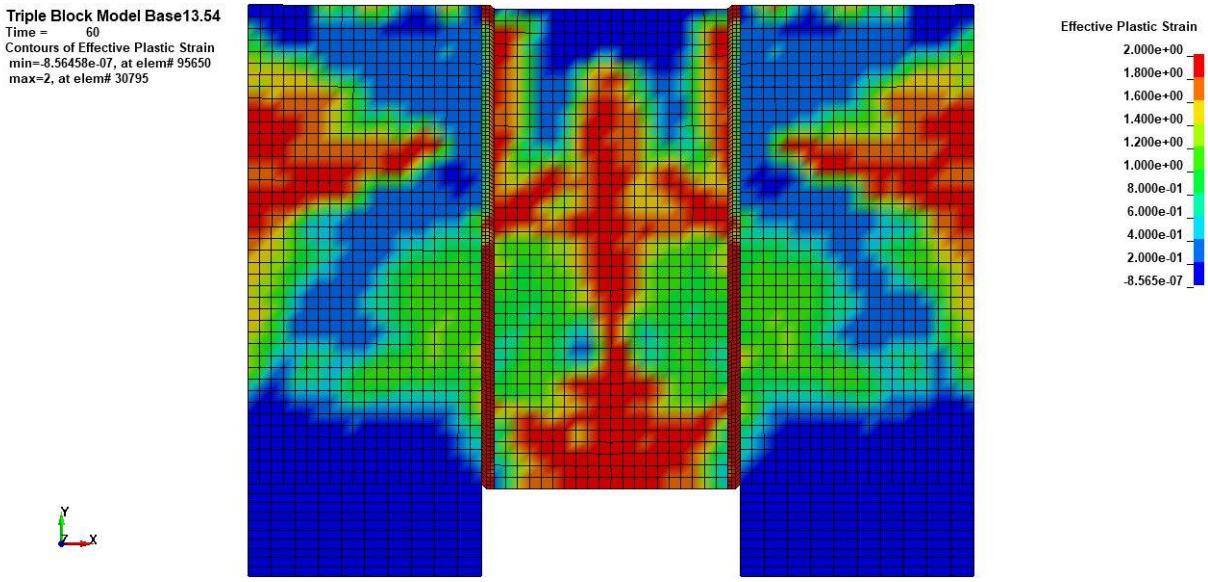


**Figure B-996: Effective Plastic Strain Fringe Plot for Last State at 60 Milliseconds for Base Run 13.54 – 2700 psi**

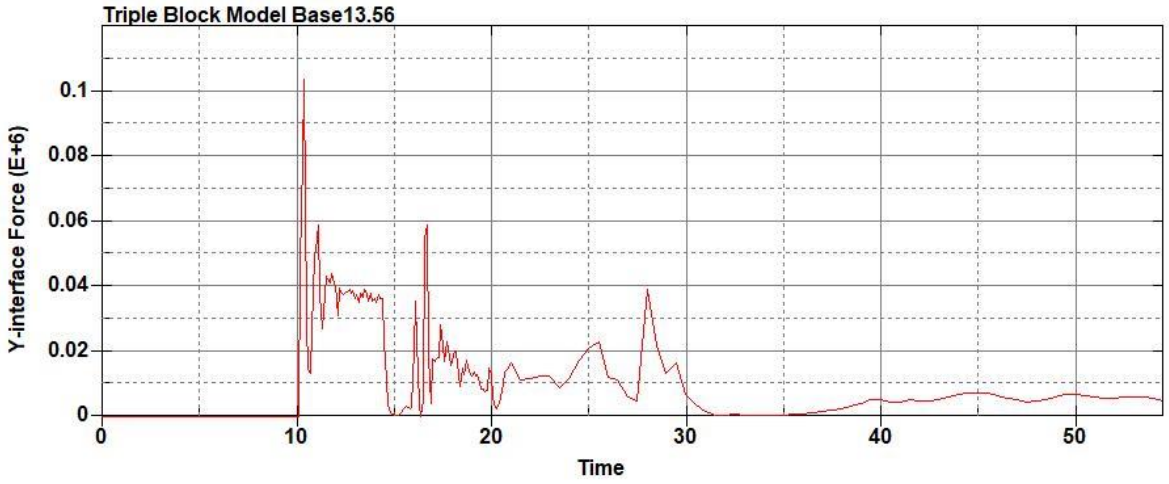


**Figure B-997: Base Run 13.56 Right Support Y-Interface Force (lbs) versus Time (ms) – 2800 psi**

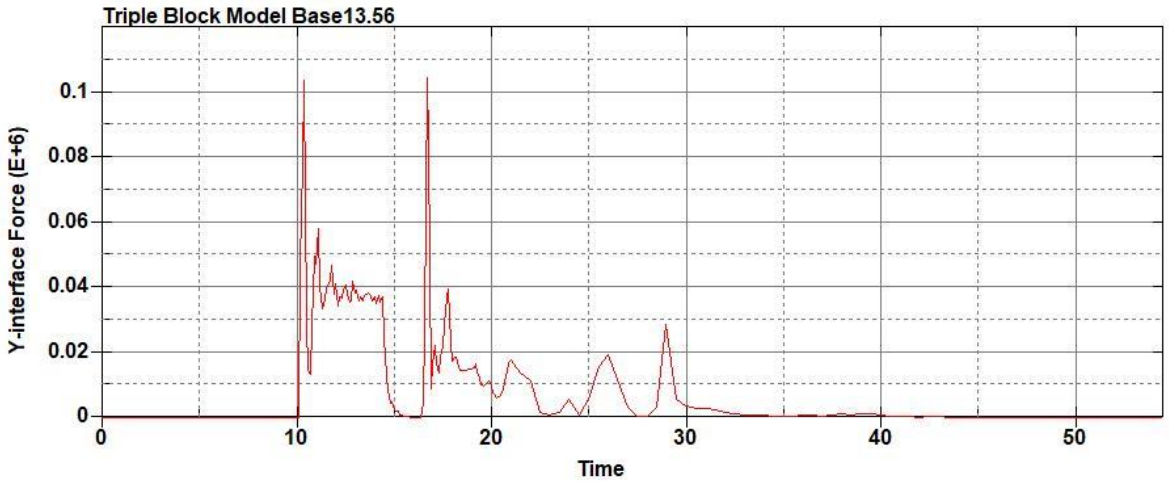


**Figure B-998: Base Run 13.56 Left Support Y-Interface Force (lbs) versus Time (ms) – 2800 psi**


**Figure B-999: Last State at 18 Milliseconds for Base Run 13.56 – 2800 psi**

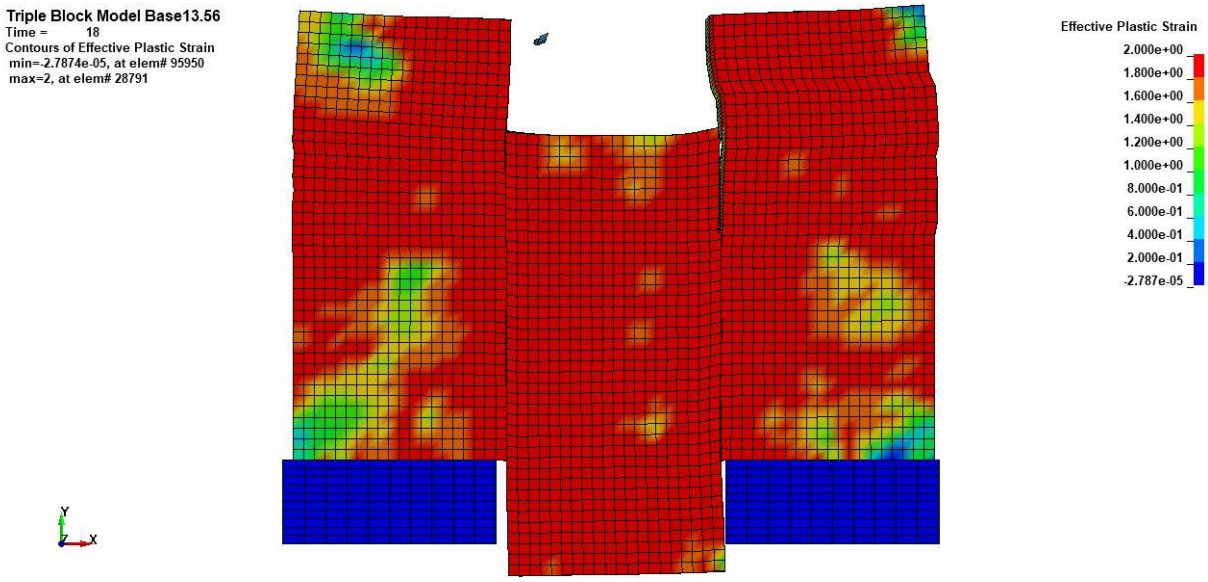


**Figure B-1000: Effective Plastic Strain Fringe Plot for Last State at 18 Milliseconds for Base Run 13.56 – 2800 psi**

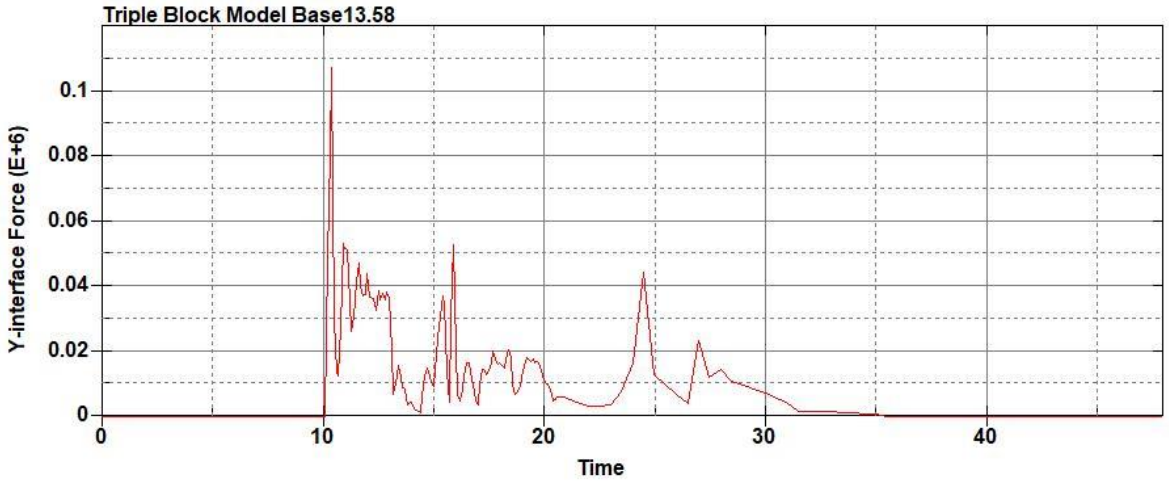


**Figure B-1001: Base Run 13.58 Right Support Y-Interface Force (lbs) versus Time (ms) – 2900 psi**

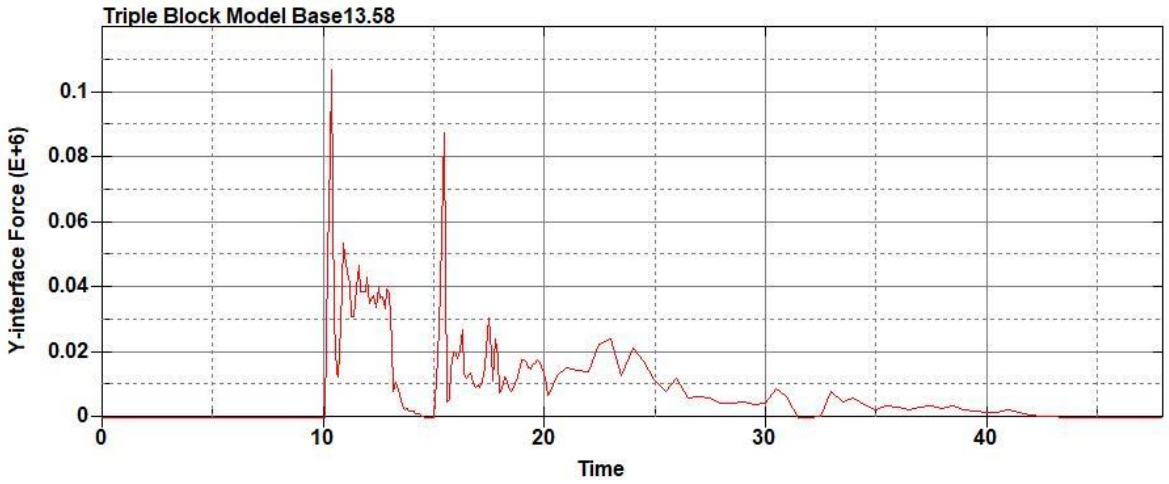


**Figure B-1002: Base Run 13.58 Left Support Y-Interface Force (lbs) versus Time (ms) – 2900 psi**

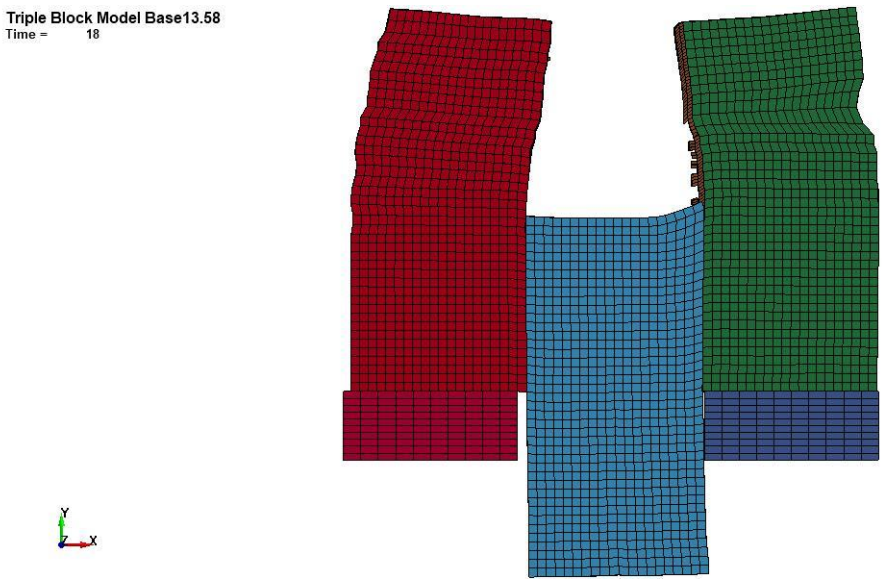


**Figure B-1003: Last State at 18 Milliseconds for Base Run 13.58 – 2900 psi**

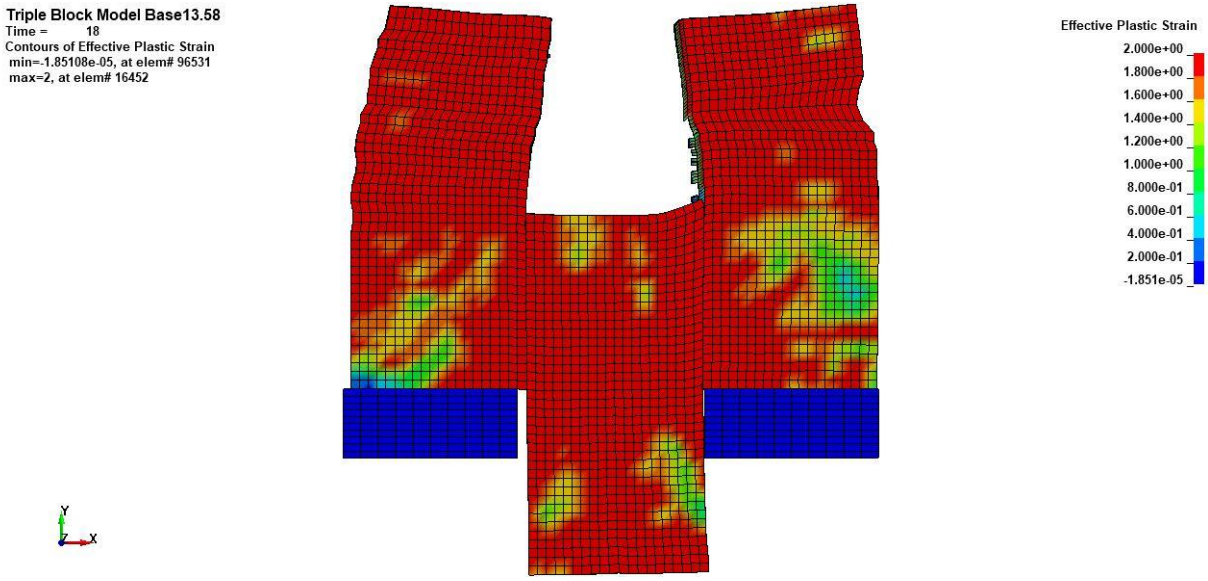


**Figure B-1004: Last State at 18 Milliseconds for Base Run 13.58 – 2900 psi**

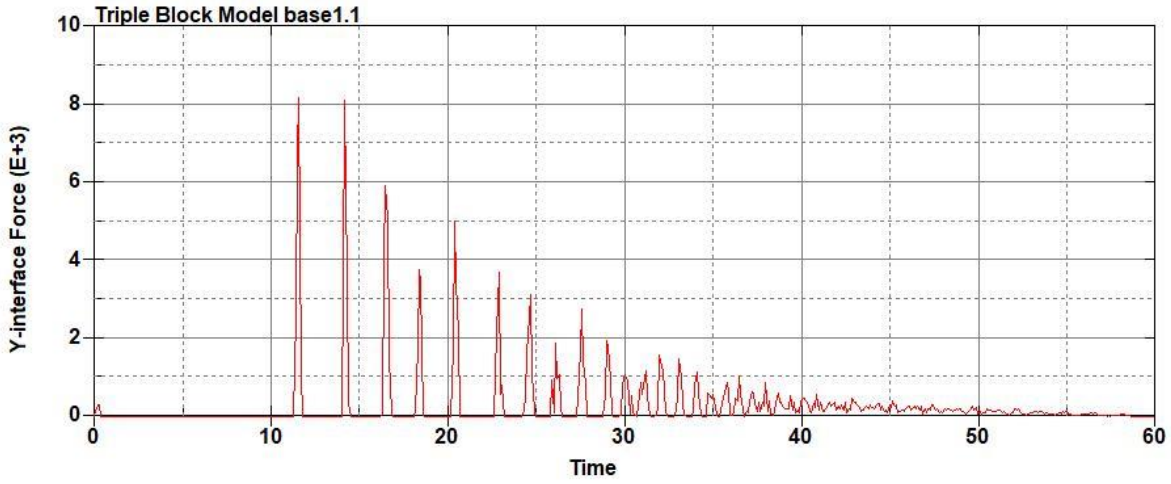


**Figure B-1005: Model Run 1.1 Right Support Y-Interface Force (lbs) versus Time (ms) – 50 psi**

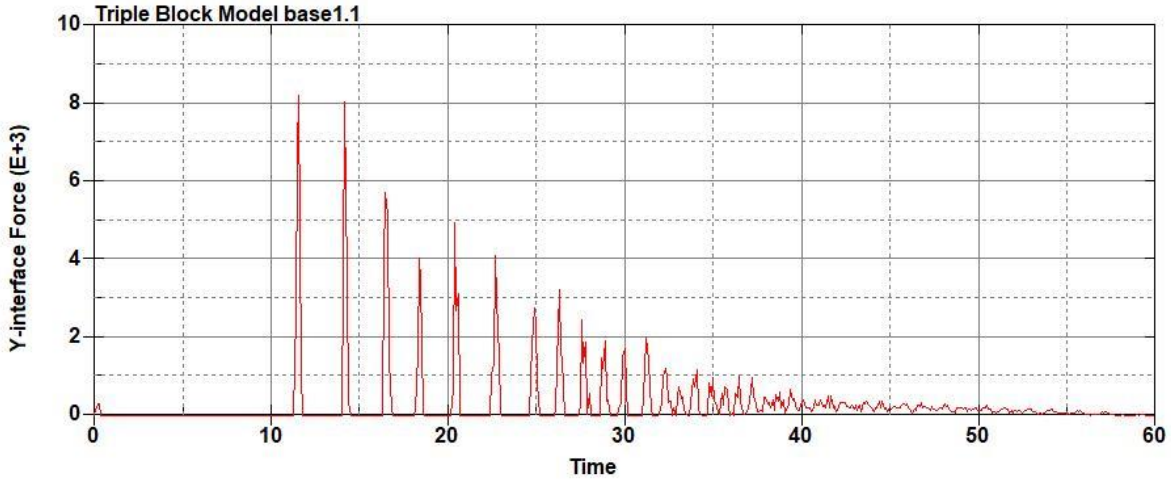


**Figure B-1006: Model Run 1.1 Left Support Y-Interface Force (lbs) versus Time (ms) – 50 psi**

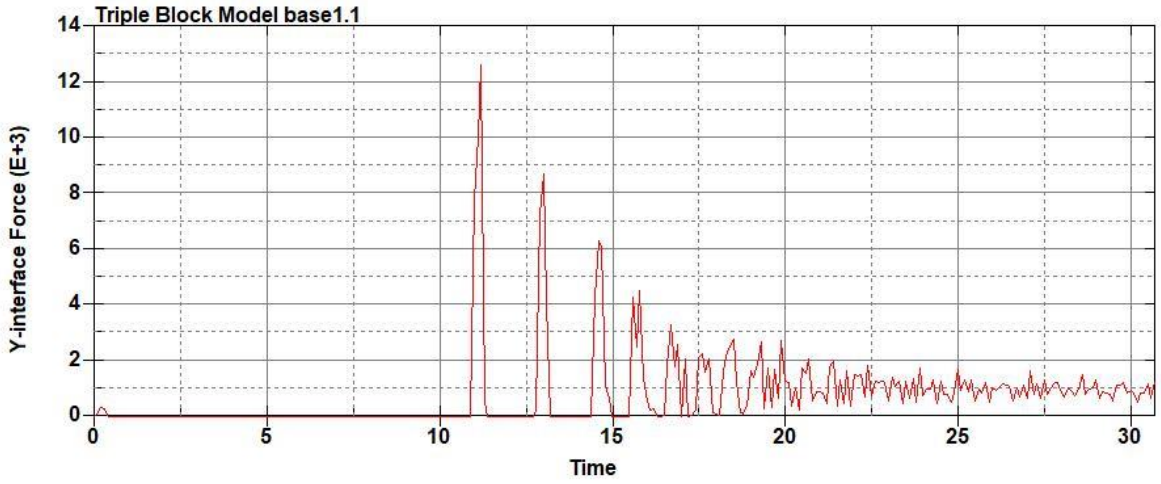


**Figure B-1007: Model Run 1.2 Right Support Y-Interface Force (lbs) versus Time (ms) – 100 psi**

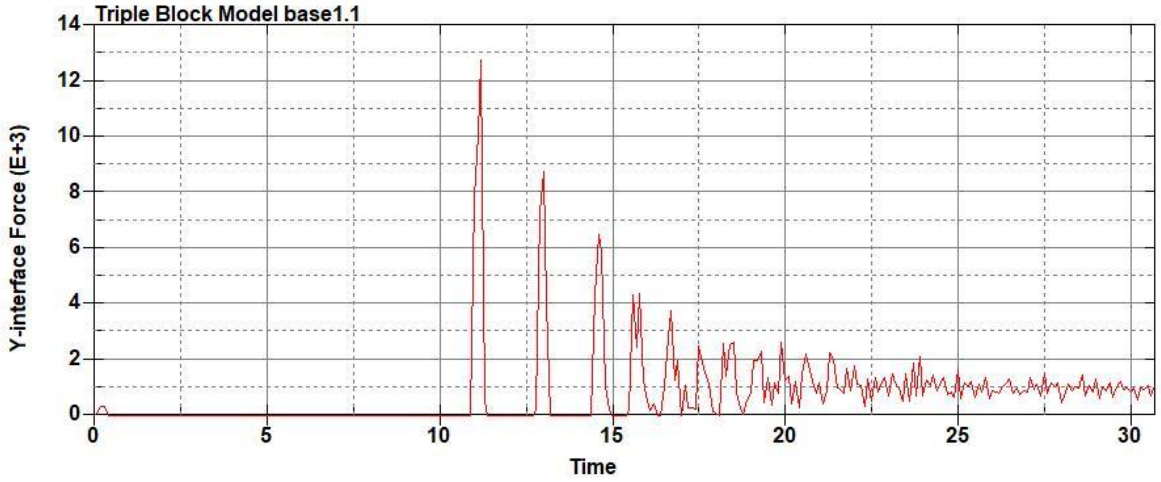


**Figure B-1008: Model Run 1.2 Left Support Y-Interface Force (lbs) versus Time (ms) – 100 psi**

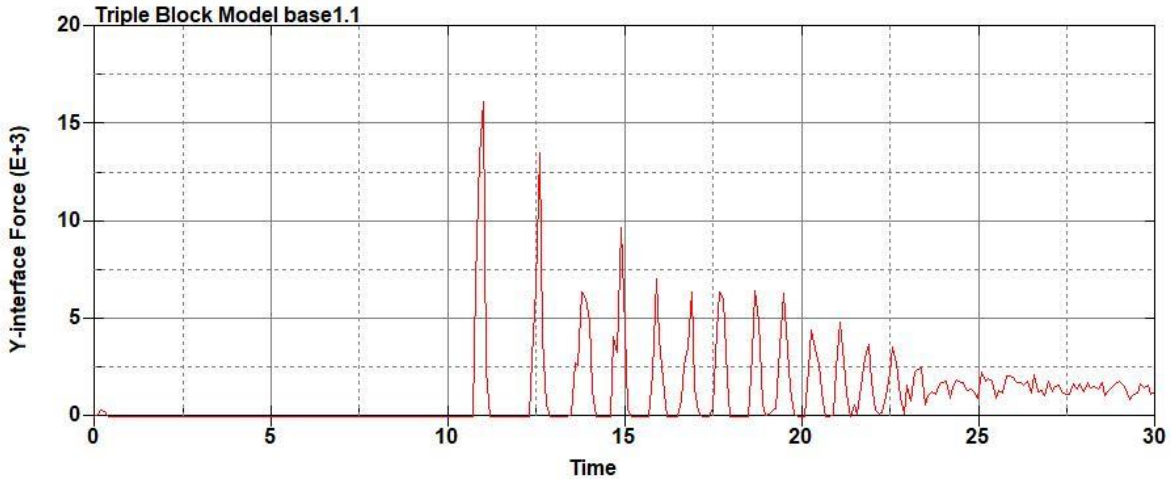


**Figure B-1009: Model Run 1.3 Right Support Y-Interface Force (lbs) versus Time (ms) – 150 psi**

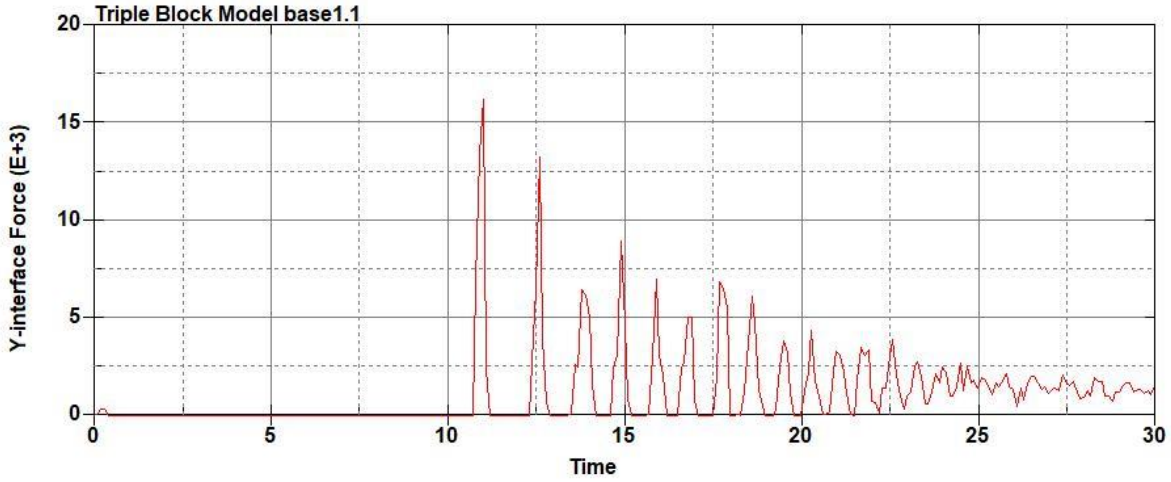


**Figure B-1010: Model Run 1.3 Left Support Y-Interface Force (lbs) versus Time (ms) – 150 psi**

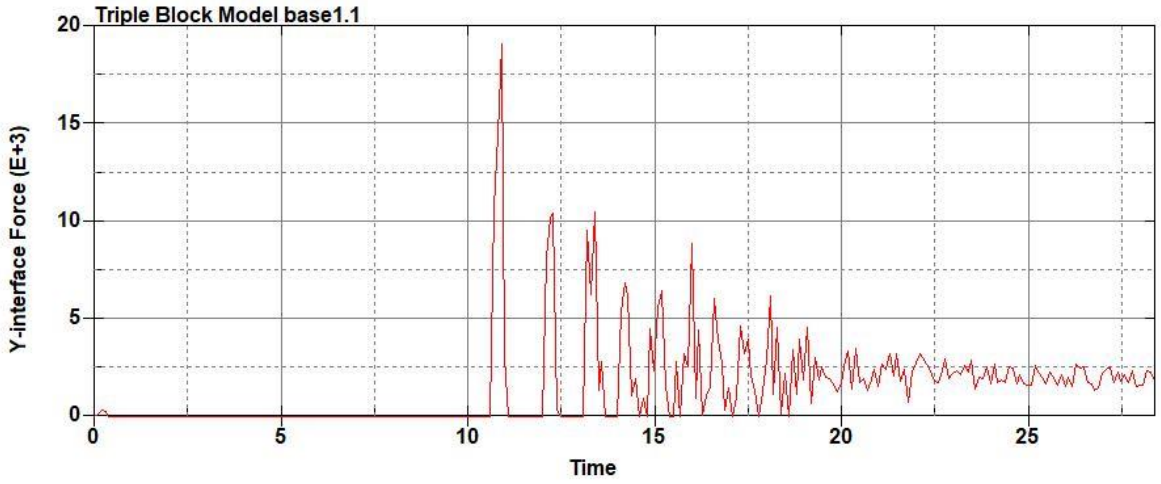


**Figure B-1011: Model Run 1.4 Right Support Y-Interface Force (lbs) versus Time (ms) – 200 psi**

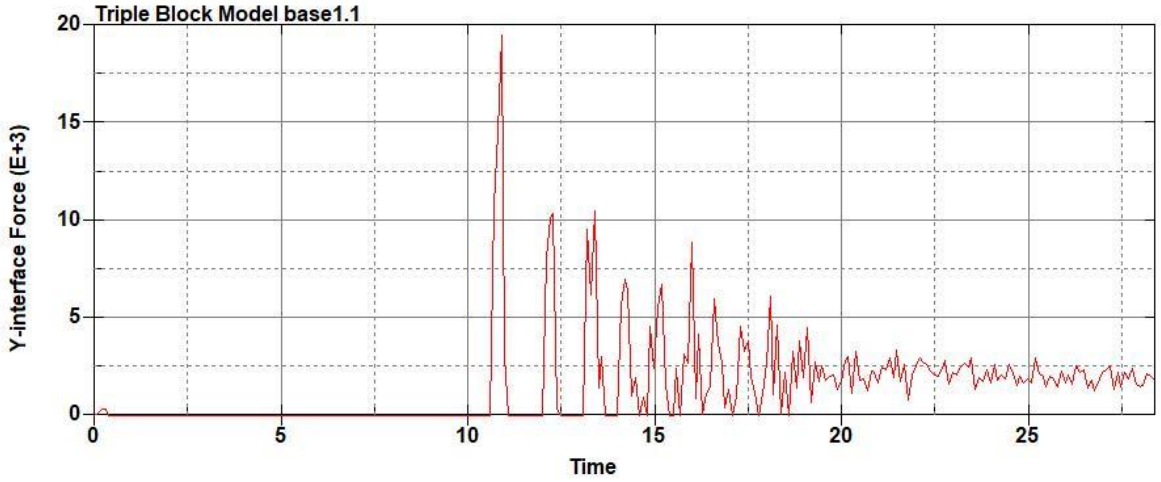


**Figure B-1012: Model Run 1.4 Left Support Y-Interface Force (lbs) versus Time (ms) – 200 psi**

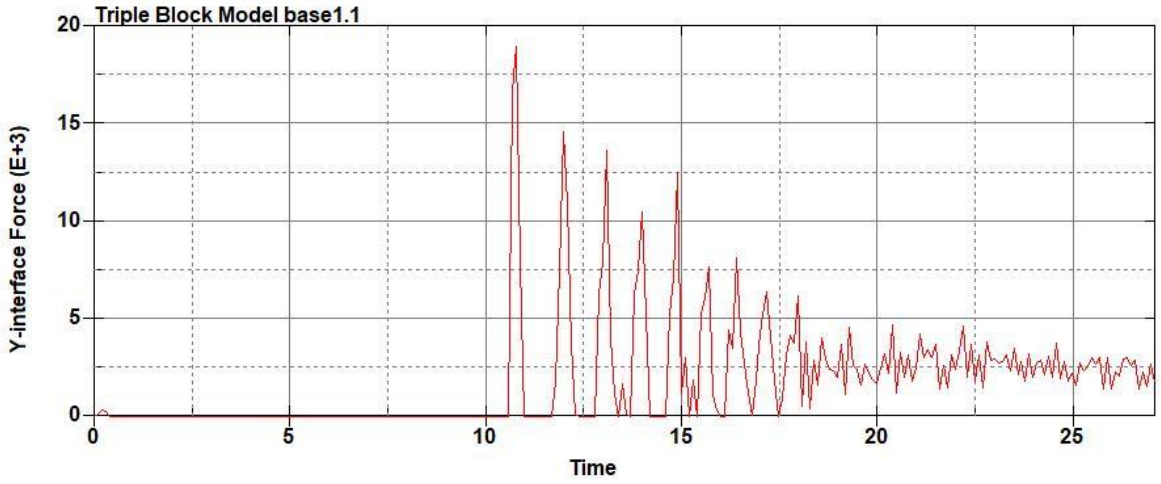


**Figure B-1013: Model Run 1.5 Right Support Y-Interface Force (lbs) versus Time (ms) – 250 psi**

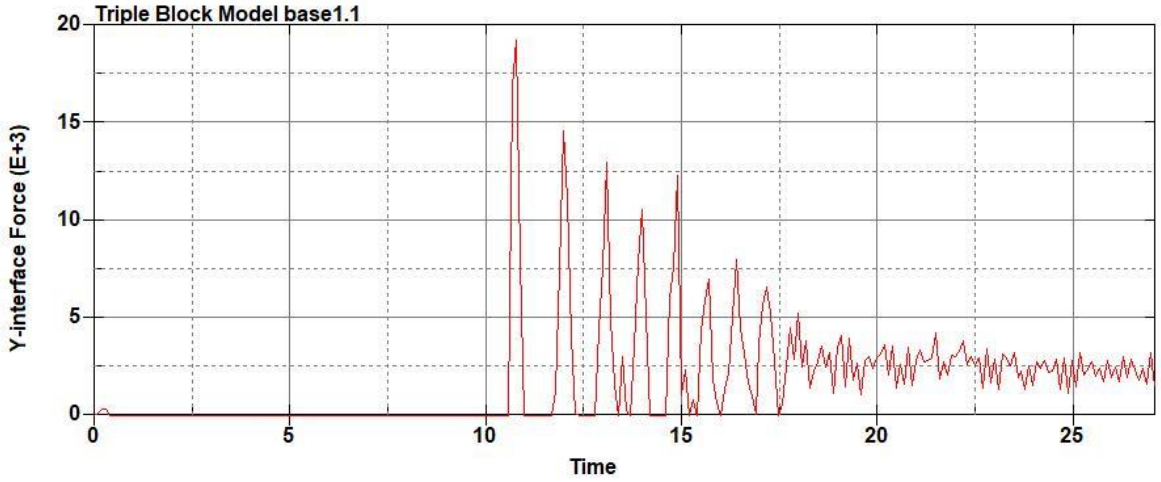


**Figure B-1014: Model Run 1.5 Left Support Y-Interface Force (lbs) versus Time (ms) – 250 psi**

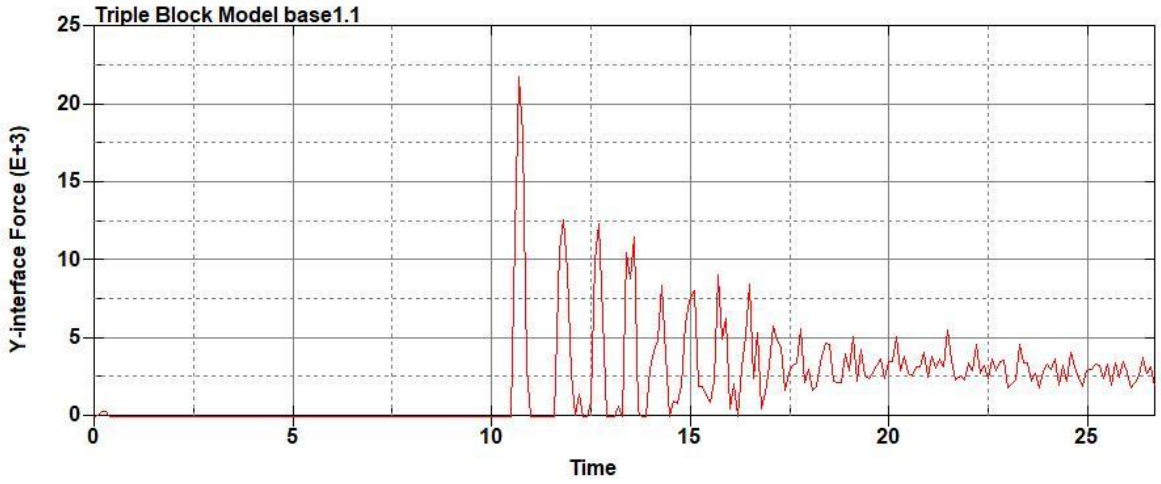


**Figure B-1015: Model Run 1.6 Right Support Y-Interface Force (lbs) versus Time (ms) – 300 psi**

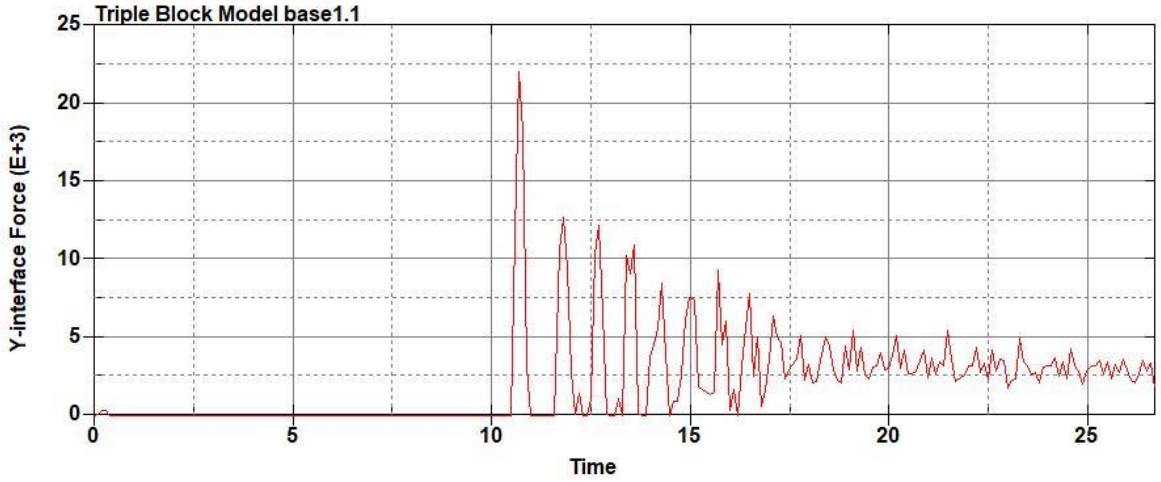


**Figure B-1016: Model Run 1.6 Left Support Y-Interface Force (lbs) versus Time (ms) – 300 psi**

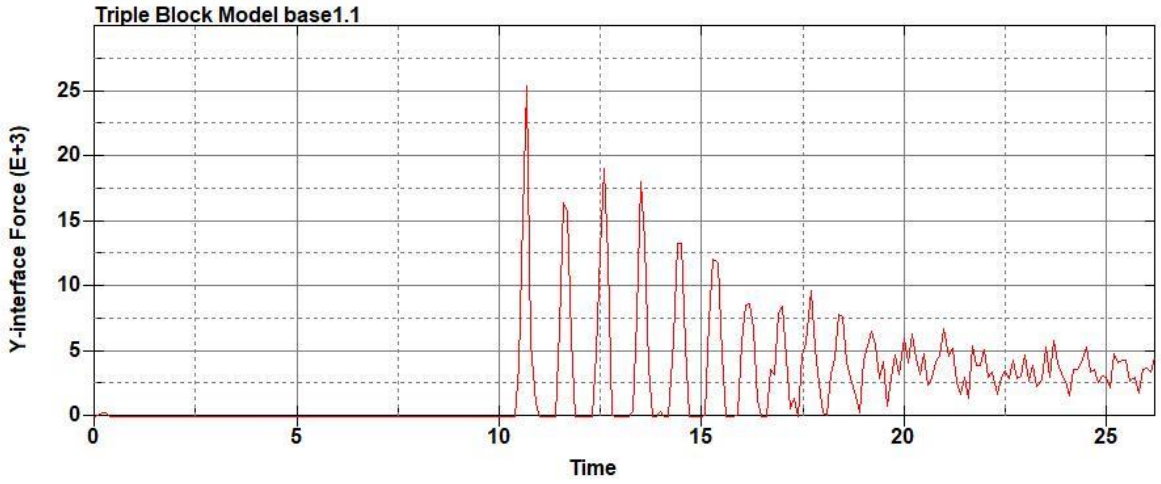


**Figure B-1017: Model Run 1.7 Right Support Y-Interface Force (lbs) versus Time (ms) – 350 psi**

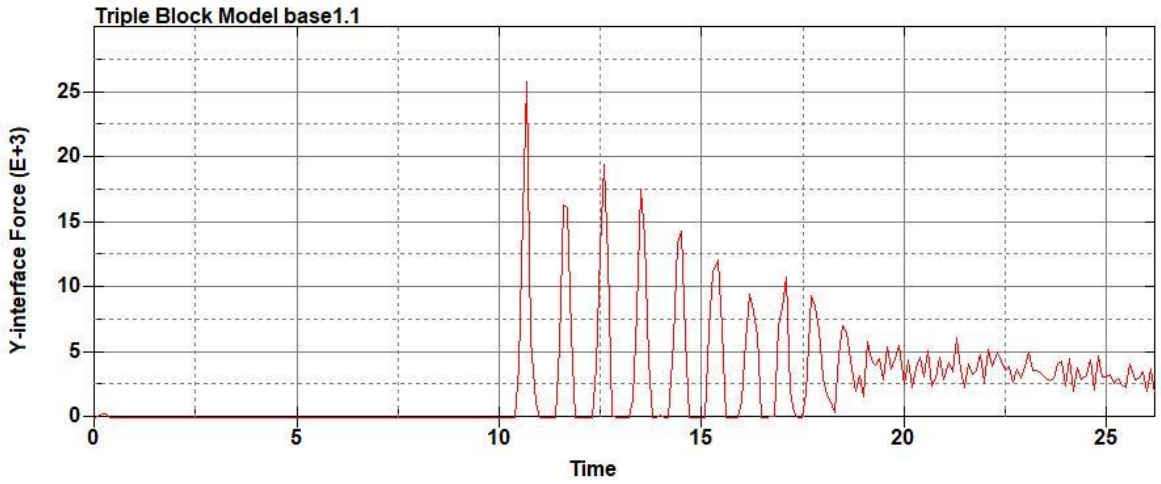


**Figure B-1018: Model Run 1.7 Left Support Y-Interface Force (lbs) versus Time (ms) – 350 psi**

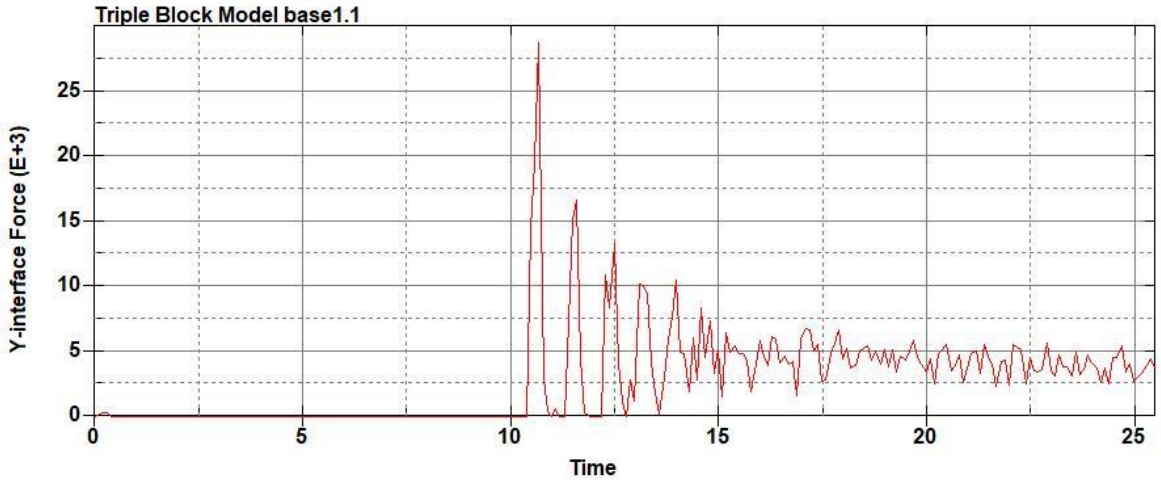


**Figure B-1019: Model Run 1.8 Right Support Y-Interface Force (lbs) versus Time (ms) – 400 psi**

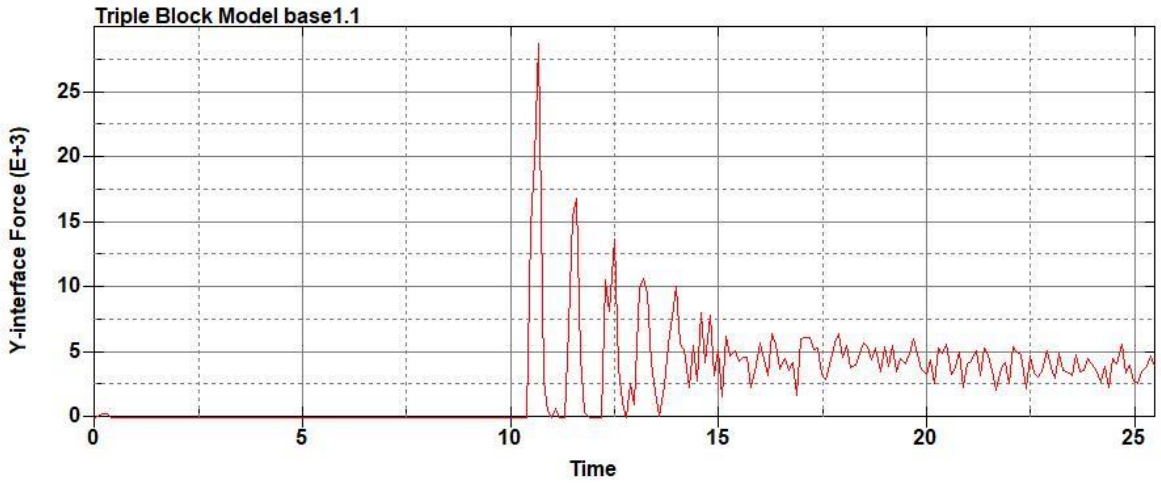


**Figure B-1020: Model Run 1.8 Left Support Y-Interface Force (lbs) versus Time (ms) – 400 psi**

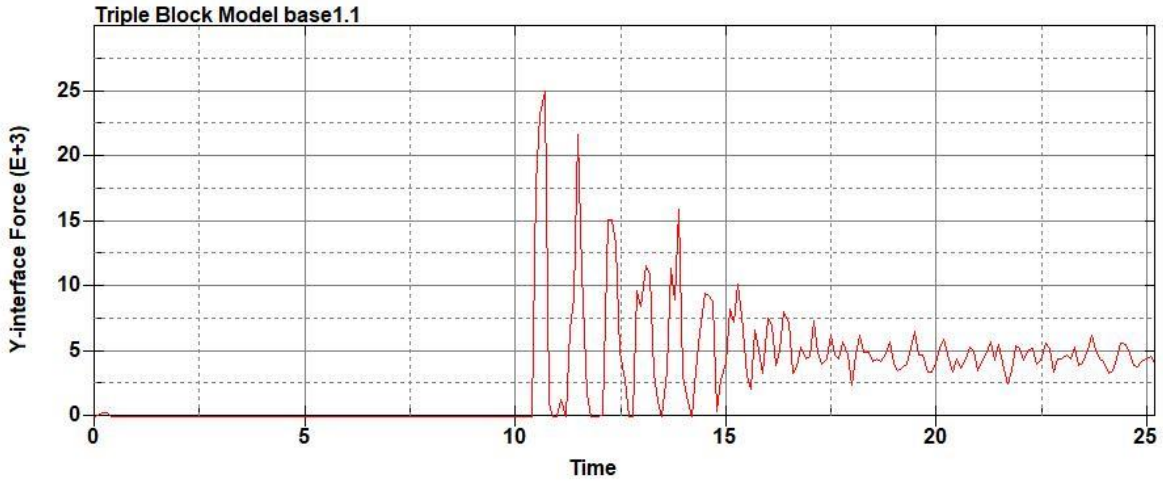


**Figure B-1021: Model Run 1.9 Right Support Y-Interface Force (lbs) versus Time (ms) – 450 psi**

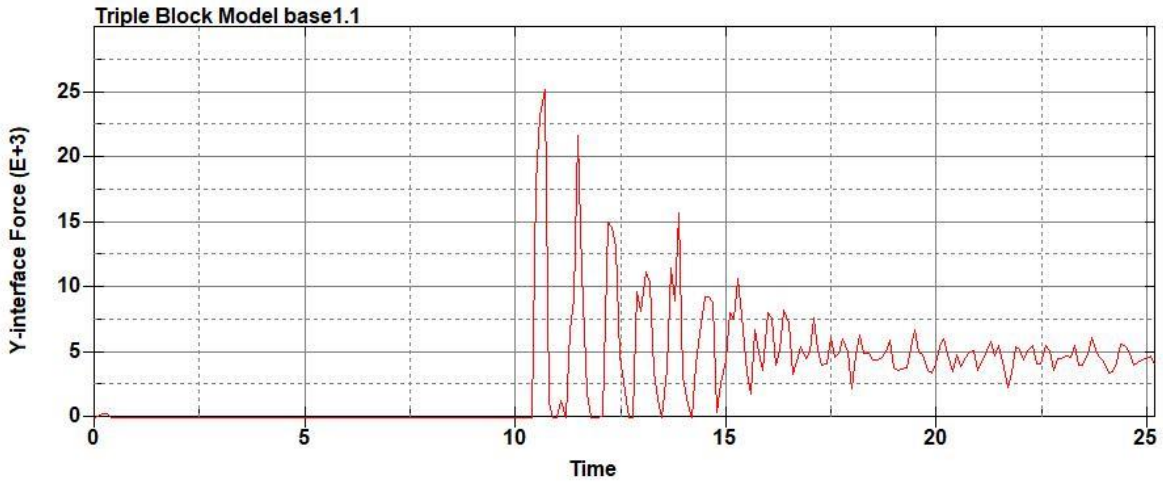


**Figure B-1022: Model Run 1.9 Left Support Y-Interface Force (lbs) versus Time (ms) – 450 psi**

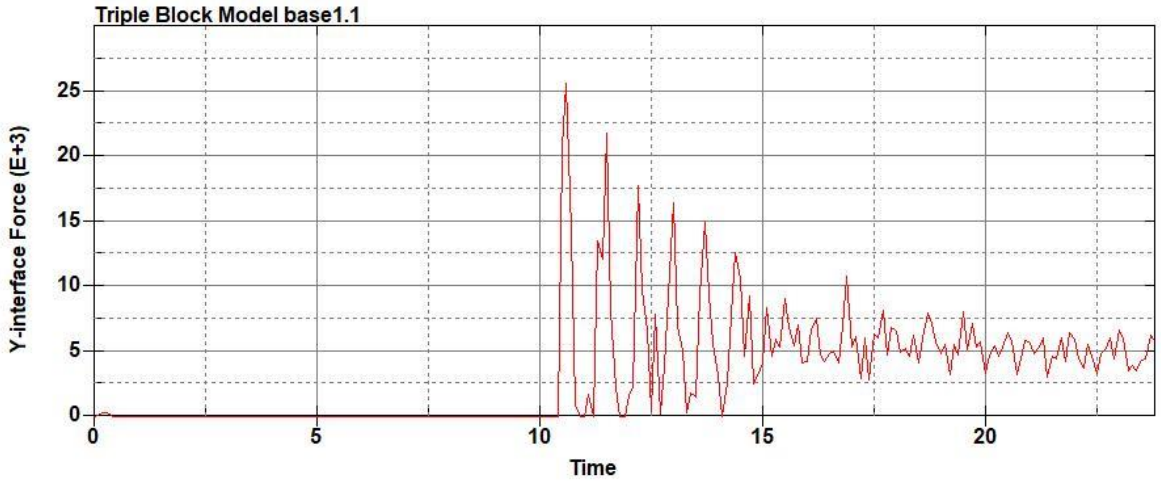


**Figure B-1023: Model Run 1.10 Right Support Y-Interface Force (lbs) versus Time (ms) – 500 psi**

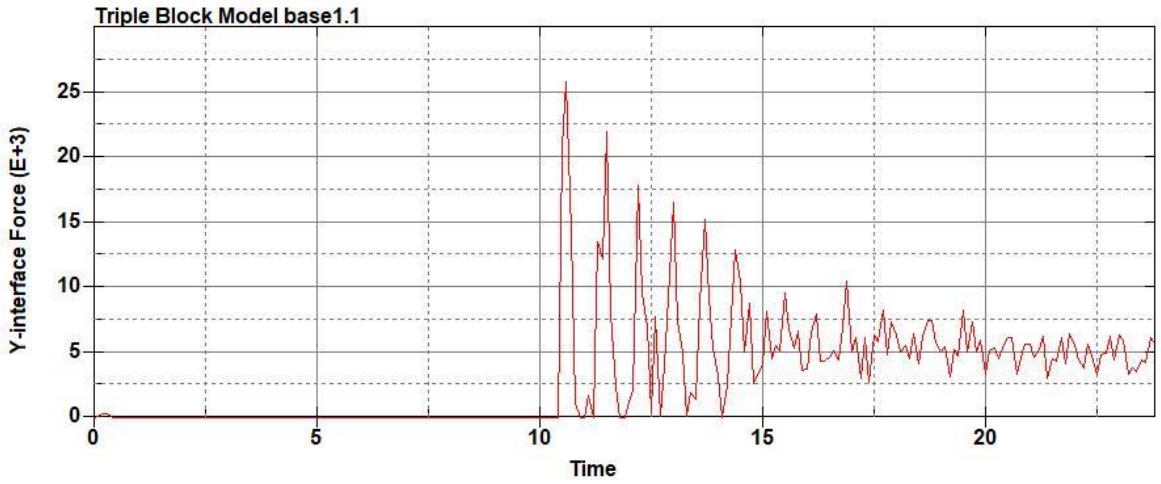


**Figure B-1024: Model Run 1.10 Left Support Y-Interface Force (lbs) versus Time (ms) – 500 psi**

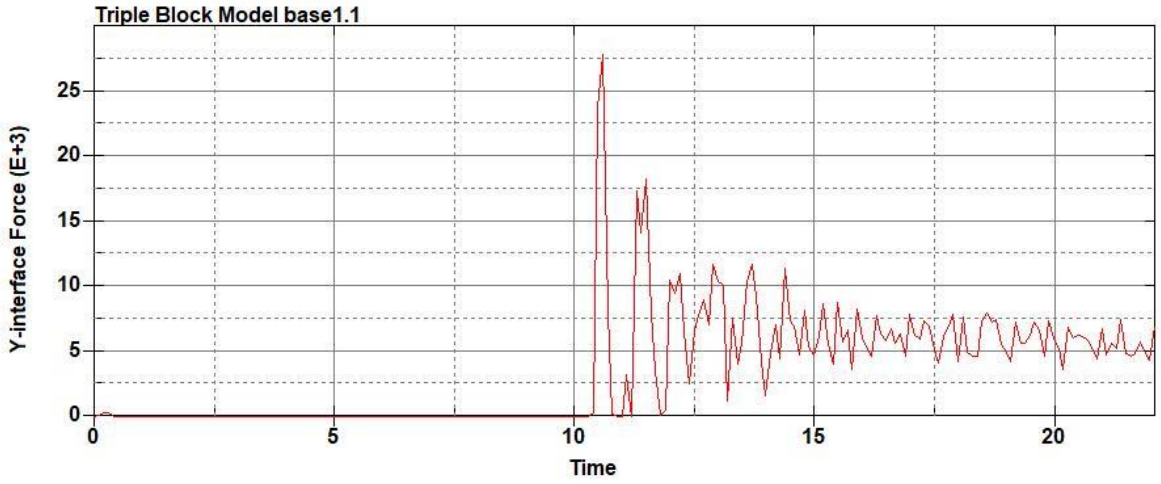


**Figure B-1025: Model Run 1.11 Right Support Y-Interface Force (lbs) versus Time (ms) – 550 psi**

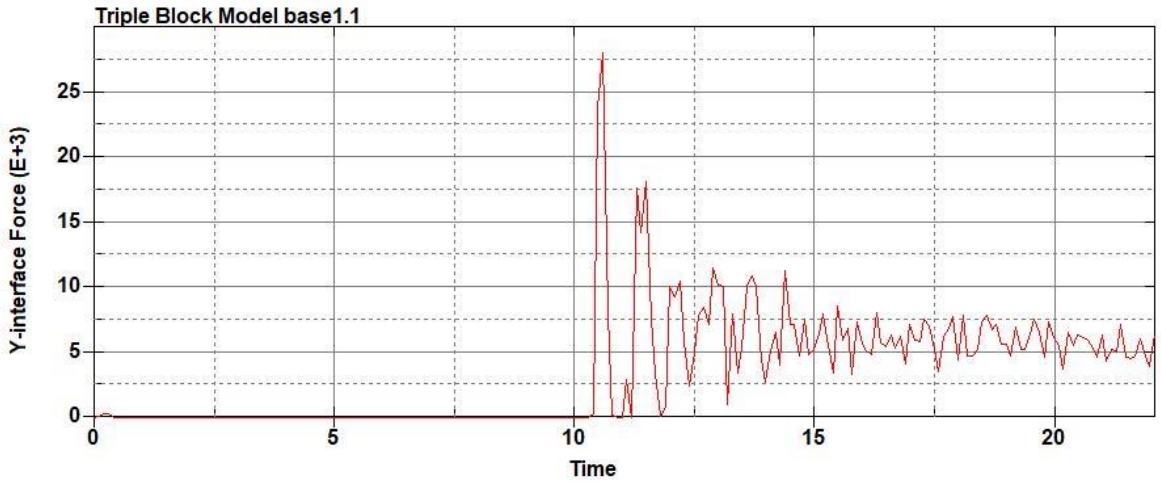


**Figure B-1026: Model Run 1.11 Left Support Y-Interface Force (lbs) versus Time (ms) – 550 psi**

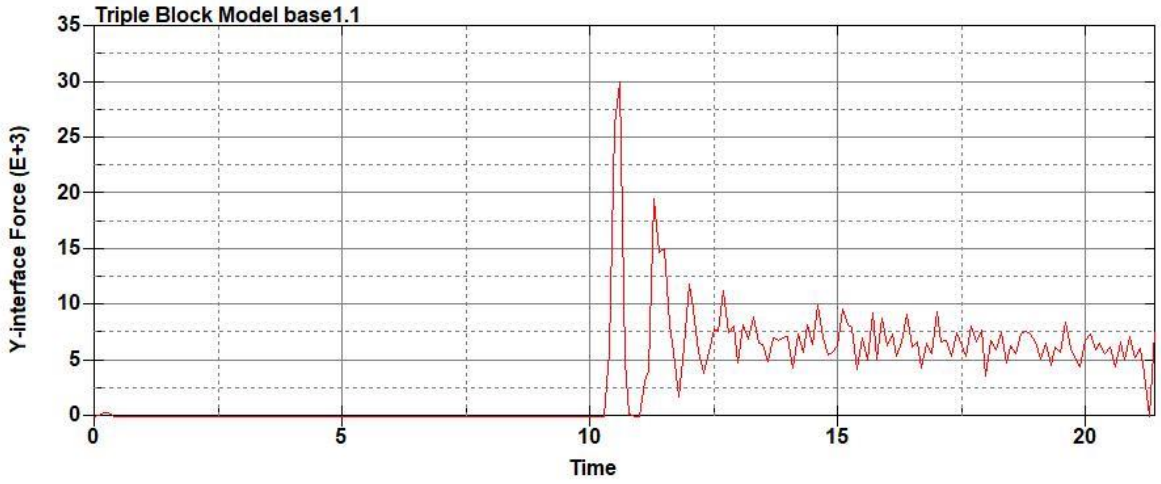


**Figure B-1027: Model Run 1.12 Right Support Y-Interface Force (lbs) versus Time (ms) – 600 psi**

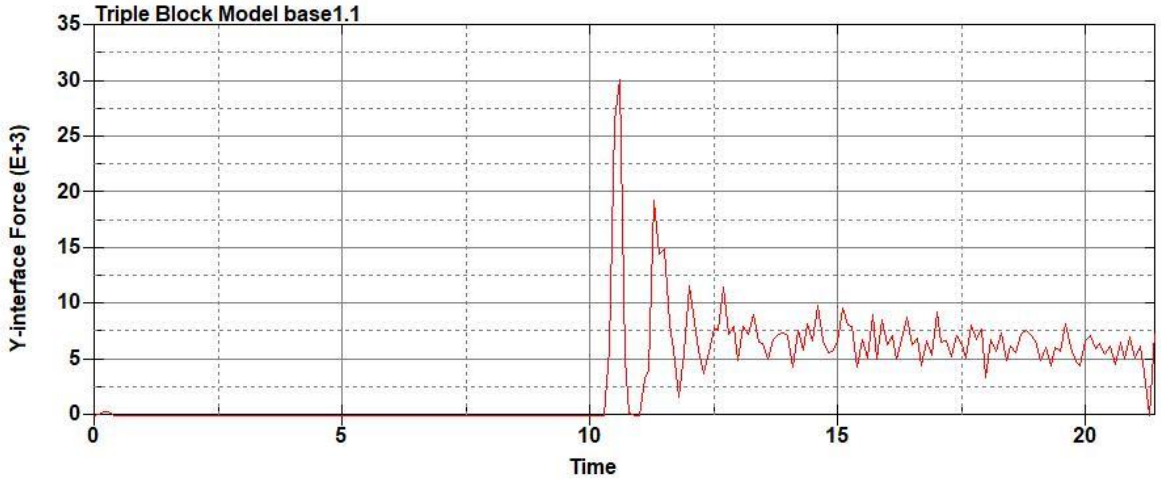


**Figure B-1028: Model Run 1.12 Left Support Y-Interface Force (lbs) versus Time (ms) – 600 psi**

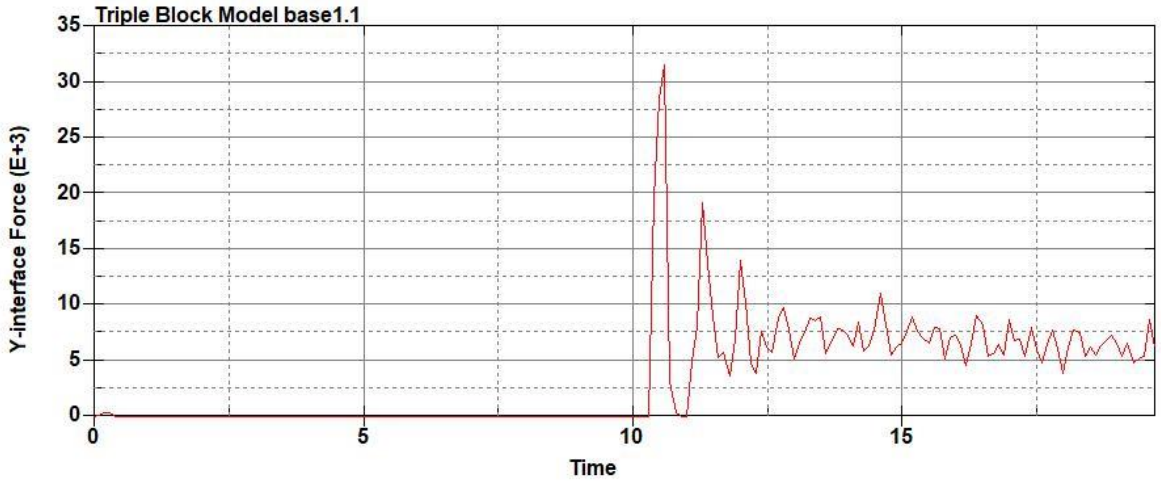


**Figure B-1029: Model Run 1.13 Right Support Y-Interface Force (lbs) versus Time (ms) – 650 psi**

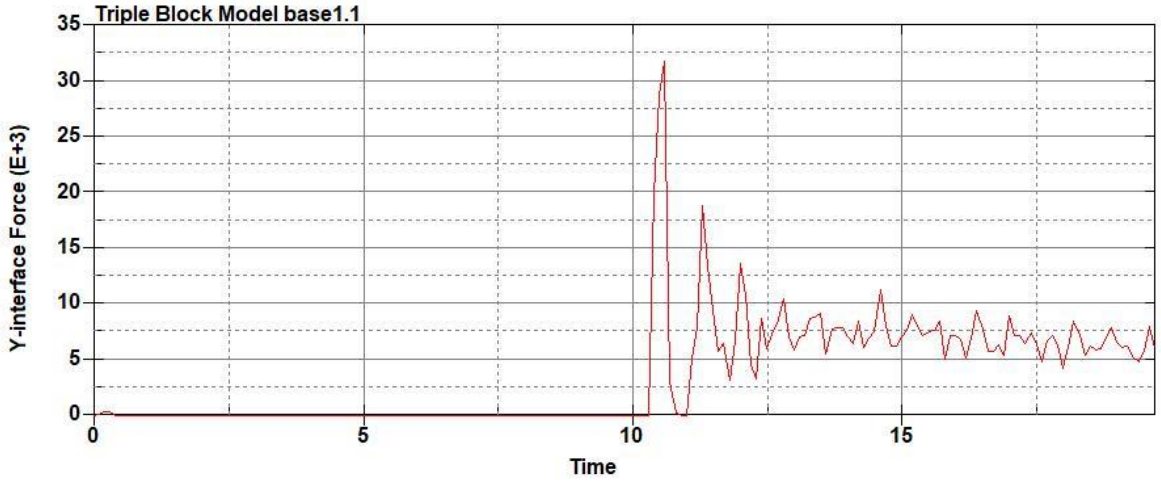


**Figure B-1030: Model Run 1.13 Left Support Y-Interface Force (lbs) versus Time (ms) – 650 psi**

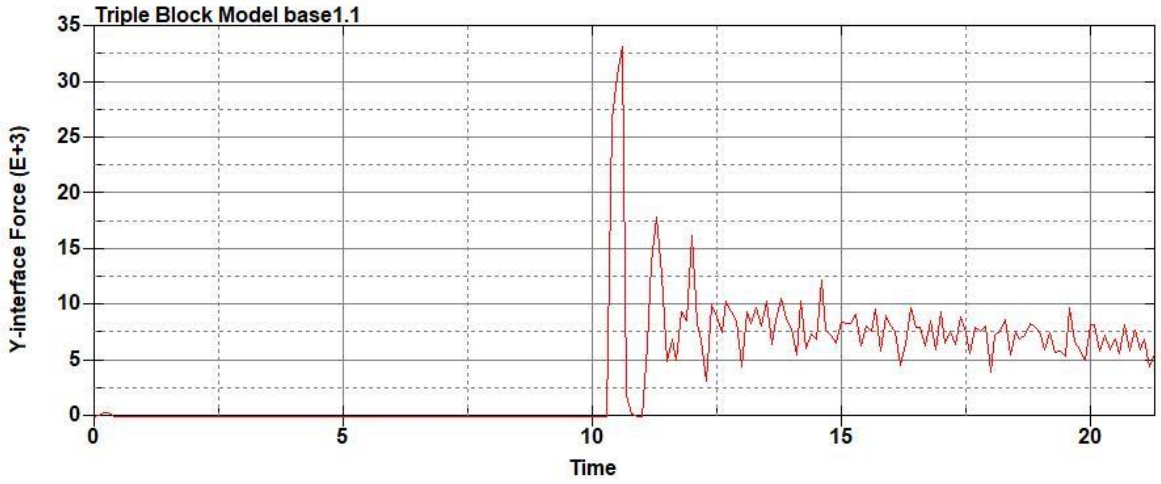


**Figure B-1031: Model Run 1.14 Right Support Y-Interface Force (lbs) versus Time (ms) – 700 psi**

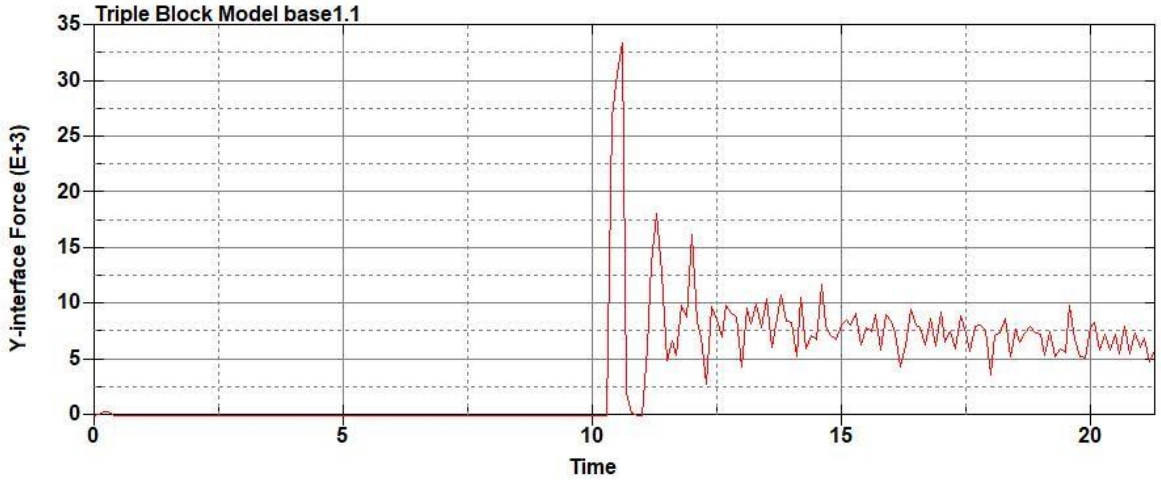


**Figure B-1032: Model Run 1.14 Left Support Y-Interface Force (lbs) versus Time (ms) – 700 psi**

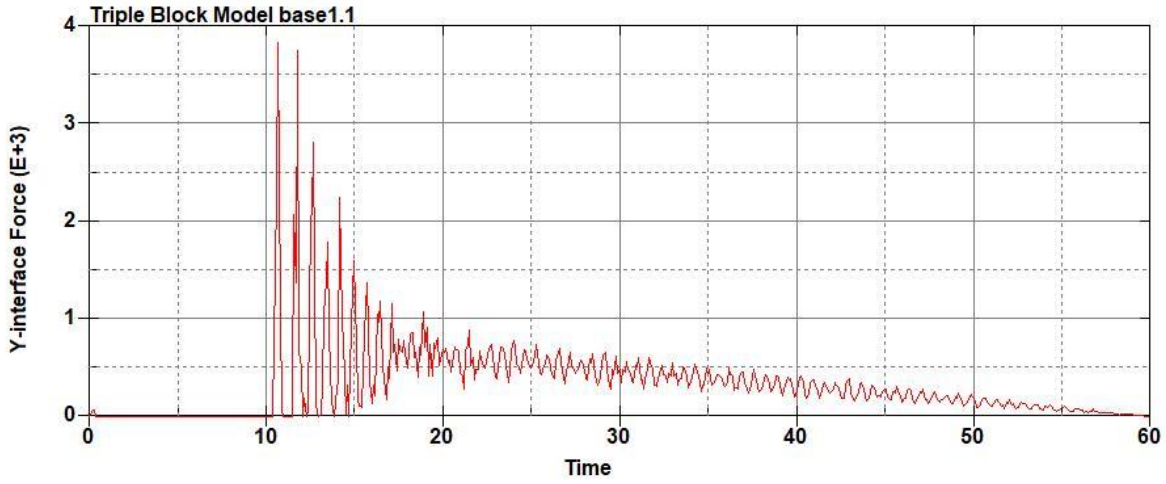


**Figure B-1033: Model Run 7.1 Right Support Y-Interface Force (lbs) versus Time (ms) – 50 psi**

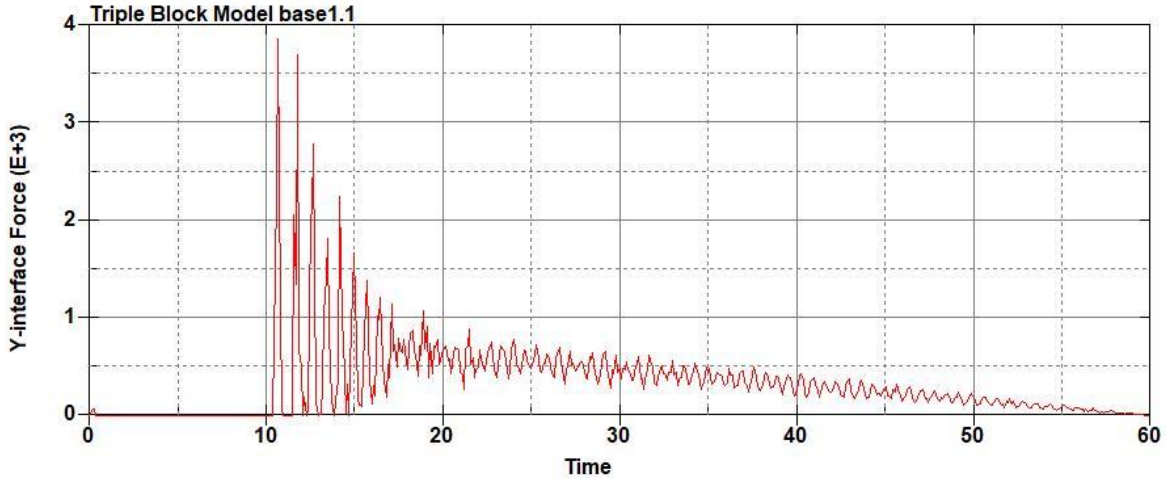


**Figure B-1034: Model Run 7.1 Left Support Y-Interface Force (lbs) versus Time (ms) – 50 psi**

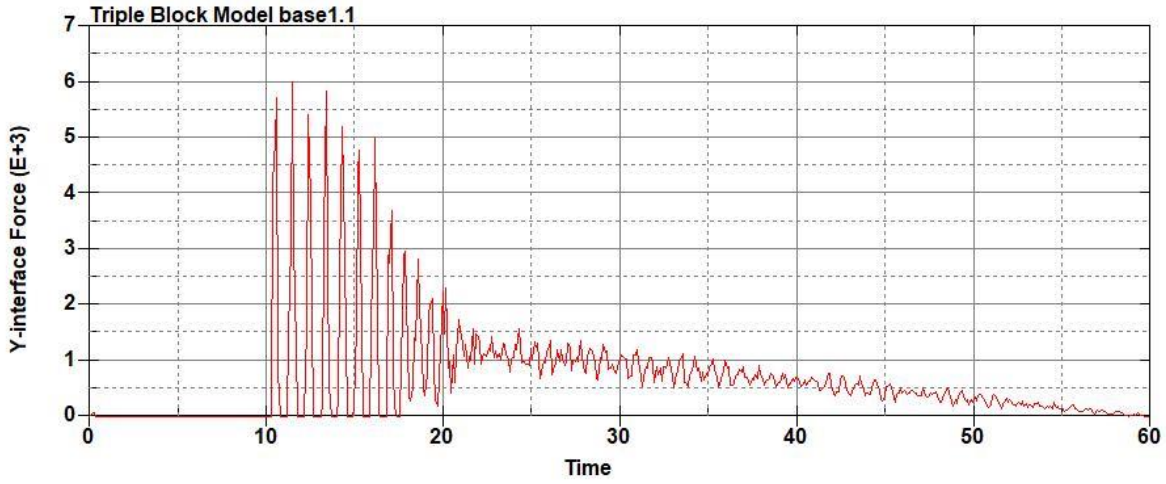


**Figure B-1035: Model Run 7.2 Right Support Y-Interface Force (lbs) versus Time (ms) – 100 psi**

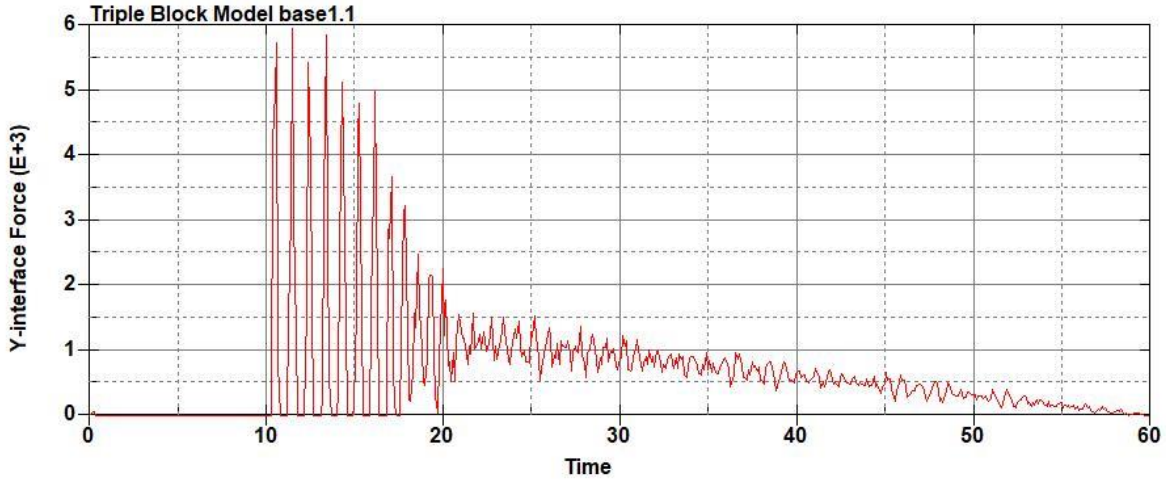


**Figure B-1036: Model Run 7.2 Left Support Y-Interface Force (lbs) versus Time (ms) – 100 psi**

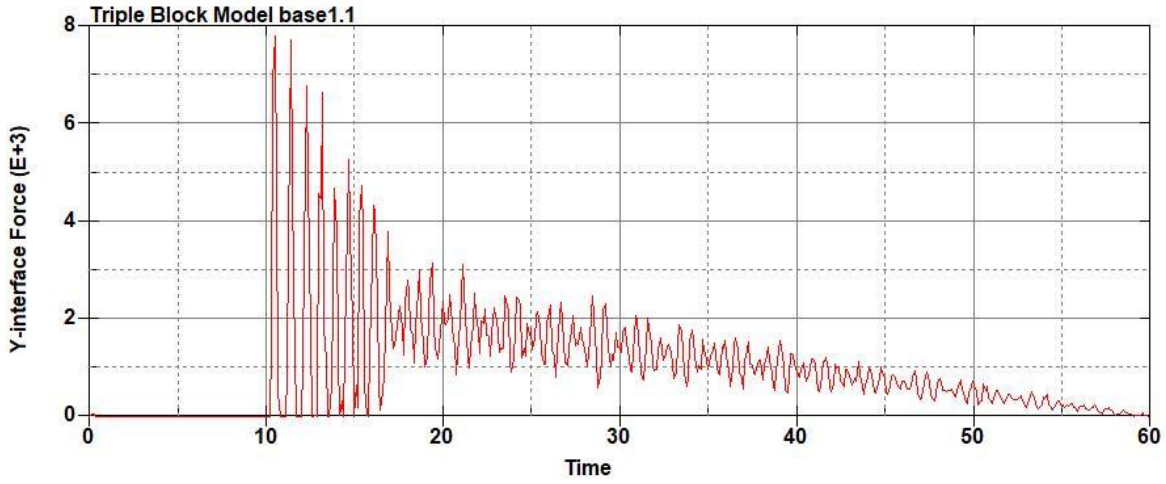


**Figure B-1037: Model Run 7.3 Right Support Y-Interface Force (lbs) versus Time (ms) – 150 psi**

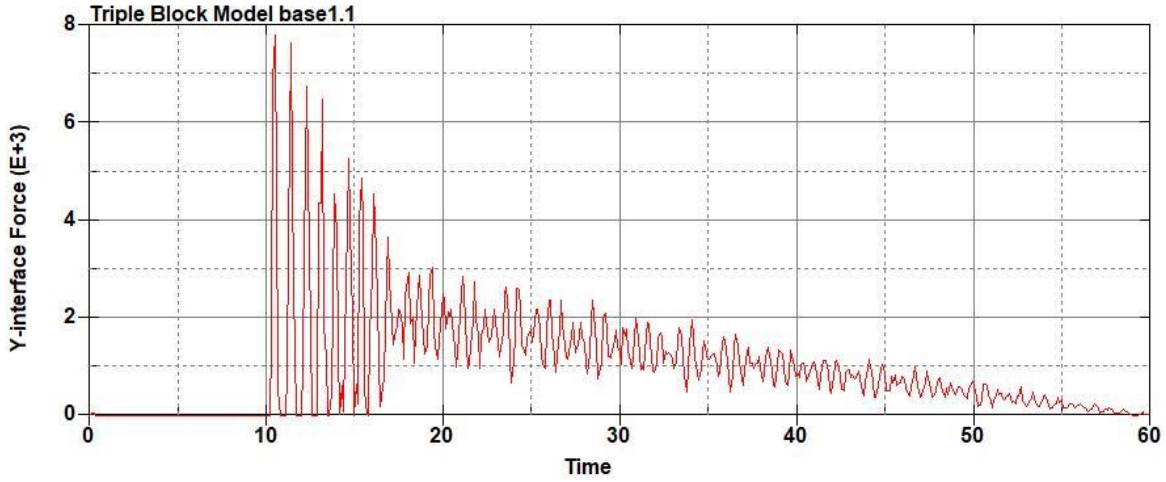


**Figure B-1038: Model Run 7.3 Left Support Y-Interface Force (lbs) versus Time (ms) – 150 psi**

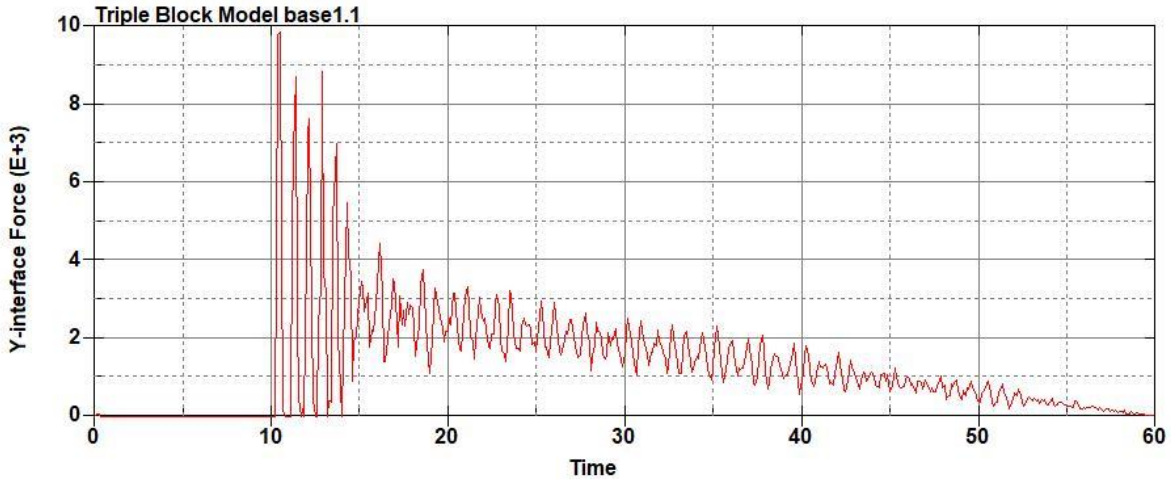


**Figure B-1039: Model Run 7.4 Right Support Y-Interface Force (lbs) versus Time (ms) – 200 psi**

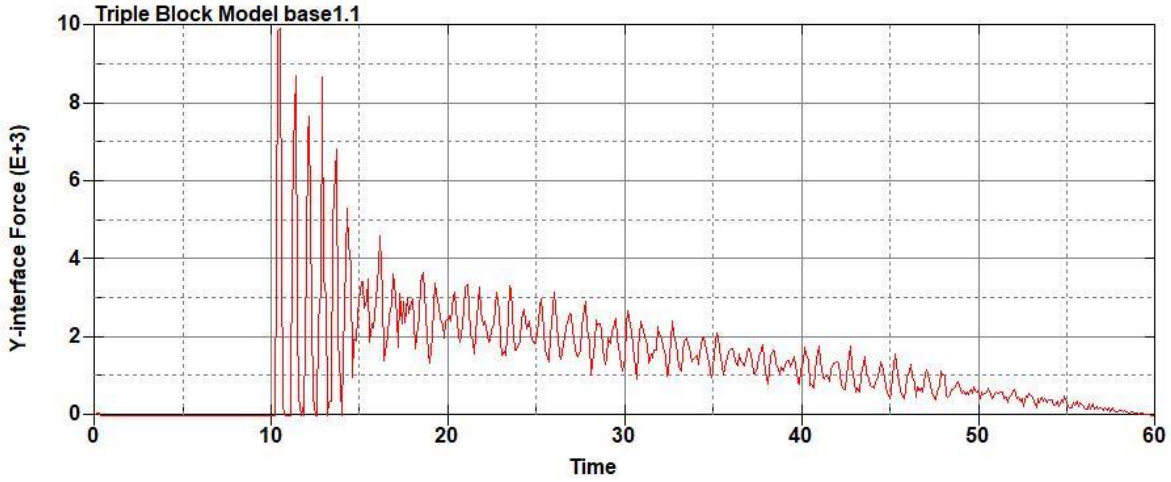


**Figure B-1040: Model Run 7.4 Left Support Y-Interface Force (lbs) versus Time (ms) – 200 psi**

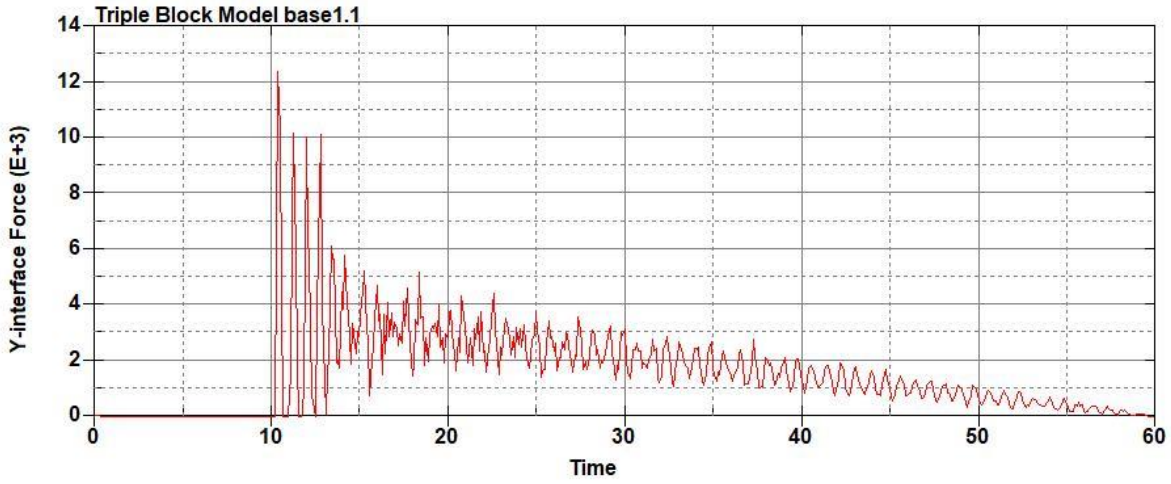


**Figure B-1041: Model Run 7.5 Right Support Y-Interface Force (lbs) versus Time (ms) – 250 psi**

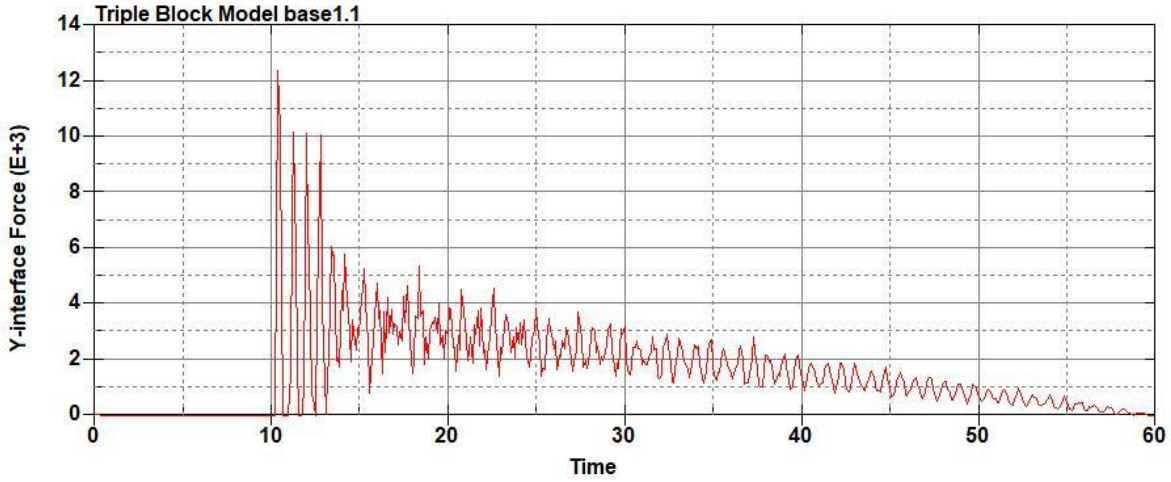


**Figure B-1042: Model Run 7.5 Left Support Y-Interface Force (lbs) versus Time (ms) – 250 psi**

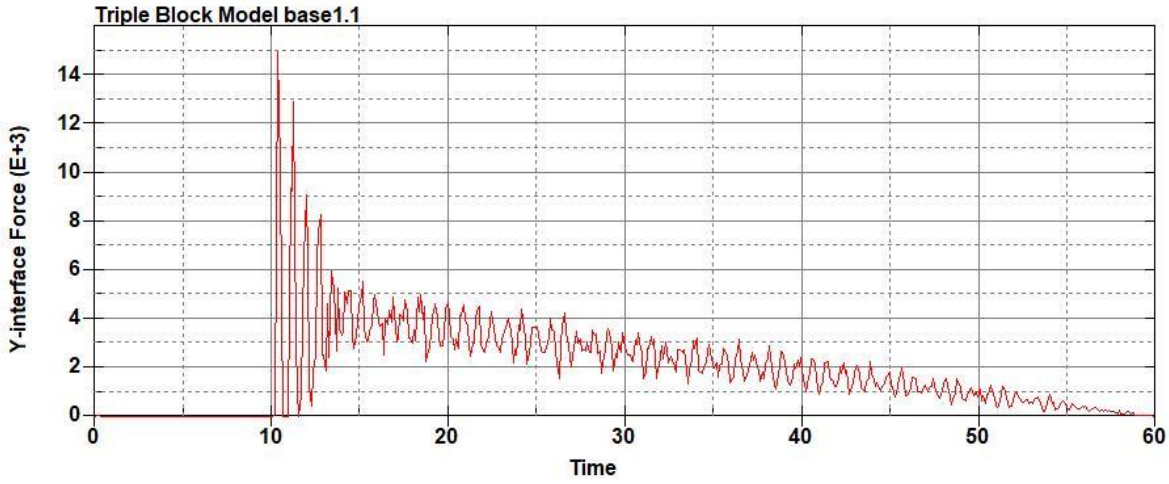


**Figure B-1043: Model Run 7.6 Right Support Y-Interface Force (lbs) versus Time (ms) – 300 psi**

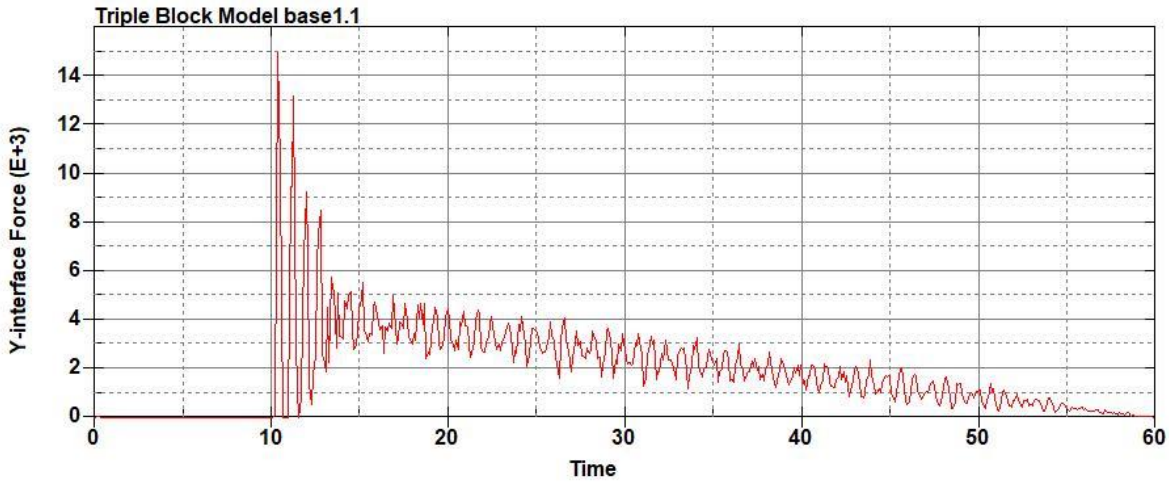


**Figure B-1044: Model Run 7.6 Left Support Y-Interface Force (lbs) versus Time (ms) – 300 psi**

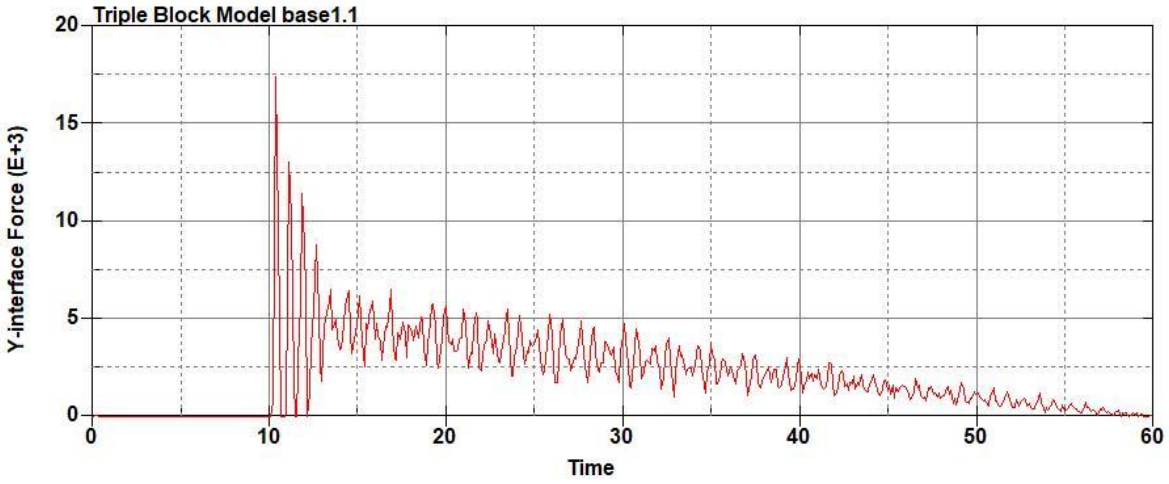


**Figure B-1045: Model Run 7.7 Right Support Y-Interface Force (lbs) versus Time (ms) – 350 psi**

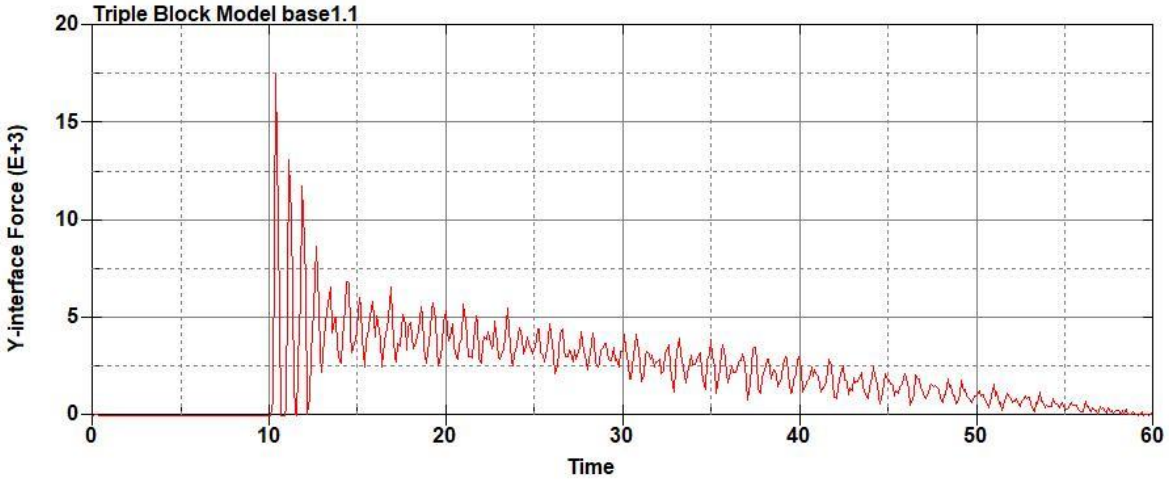


**Figure B-1046: Model Run 7.7 Left Support Y-Interface Force (lbs) versus Time (ms) – 350 psi**

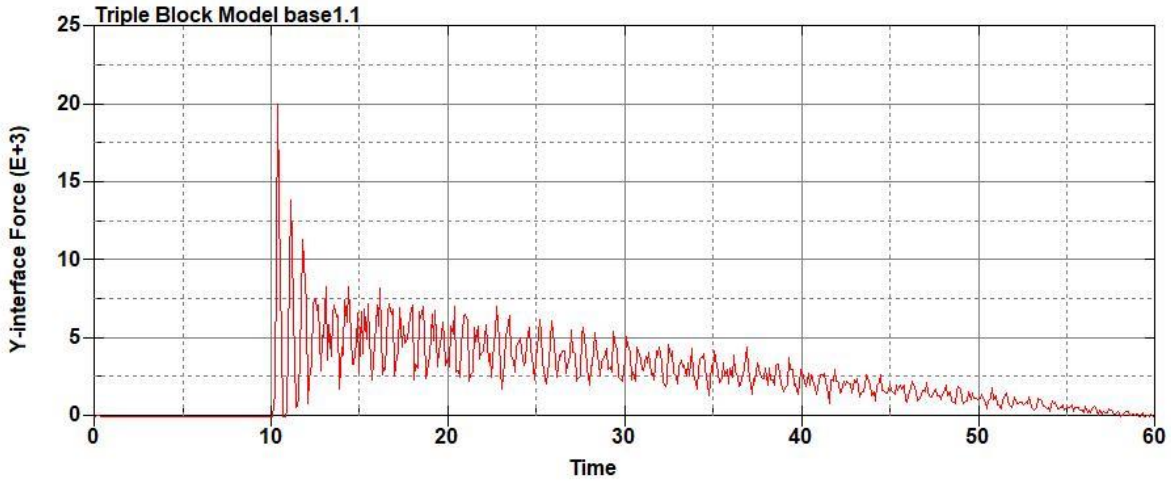


**Figure B-1047: Model Run 7.8 Right Support Y-Interface Force (lbs) versus Time (ms) – 400 psi**

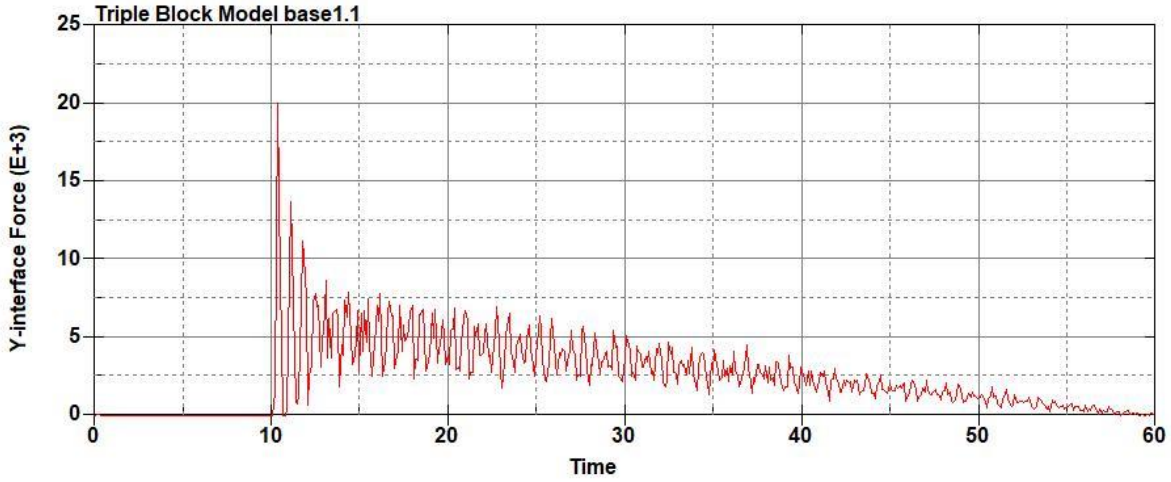


**Figure B-1048: Model Run 7.8 Left Support Y-Interface Force (lbs) versus Time (ms) – 400 psi**

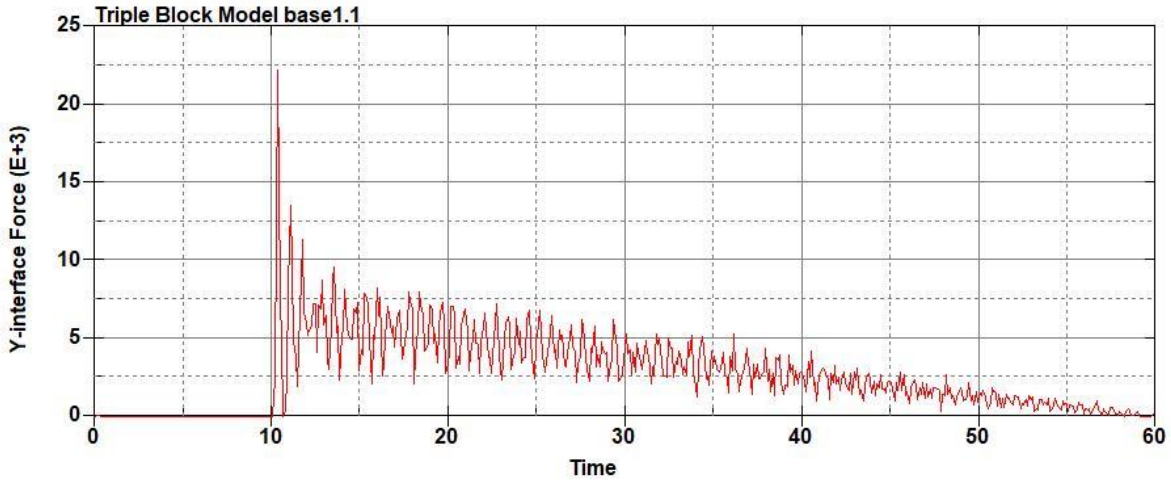


**Figure B-1049: Model Run 7.9 Right Support Y-Interface Force (lbs) versus Time (ms) – 450 psi**

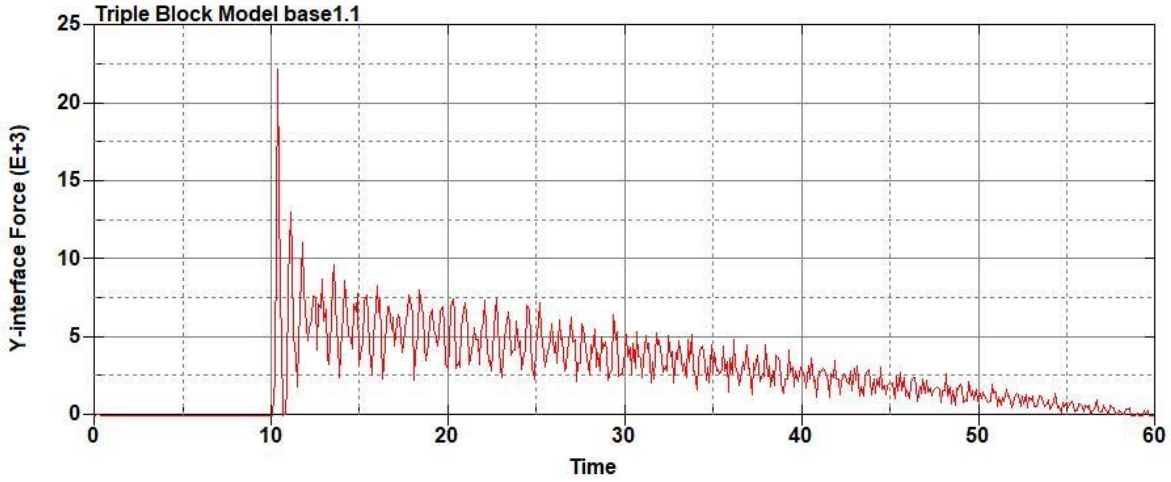


**Figure B-1050: Model Run 7.9 Left Support Y-Interface Force (lbs) versus Time (ms) – 450 psi**

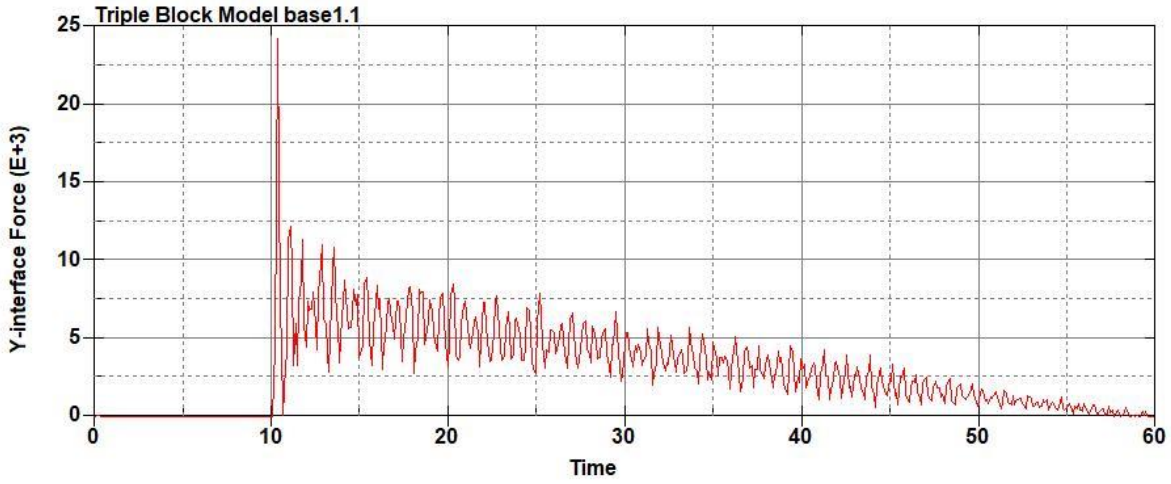


**Figure B-1051: Model Run 7.10 Right Support Y-Interface Force (lbs) versus Time (ms) – 500 psi**

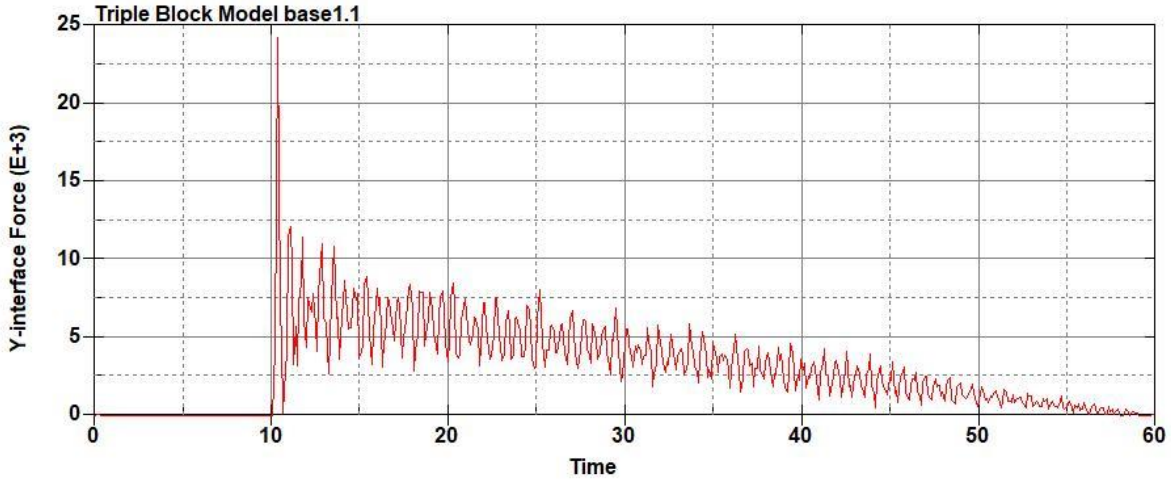


**Figure B-1052: Model Run 7.10 Left Support Y-Interface Force (lbs) versus Time (ms) – 500 psi**

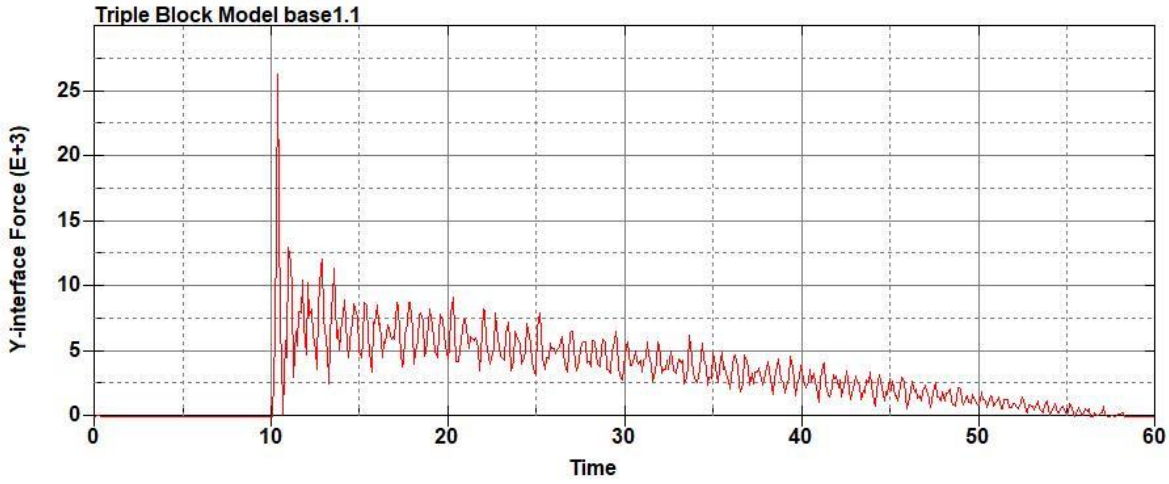


**Figure B-1053: Model Run 7.11 Right Support Y-Interface Force (lbs) versus Time (ms) – 550 psi**

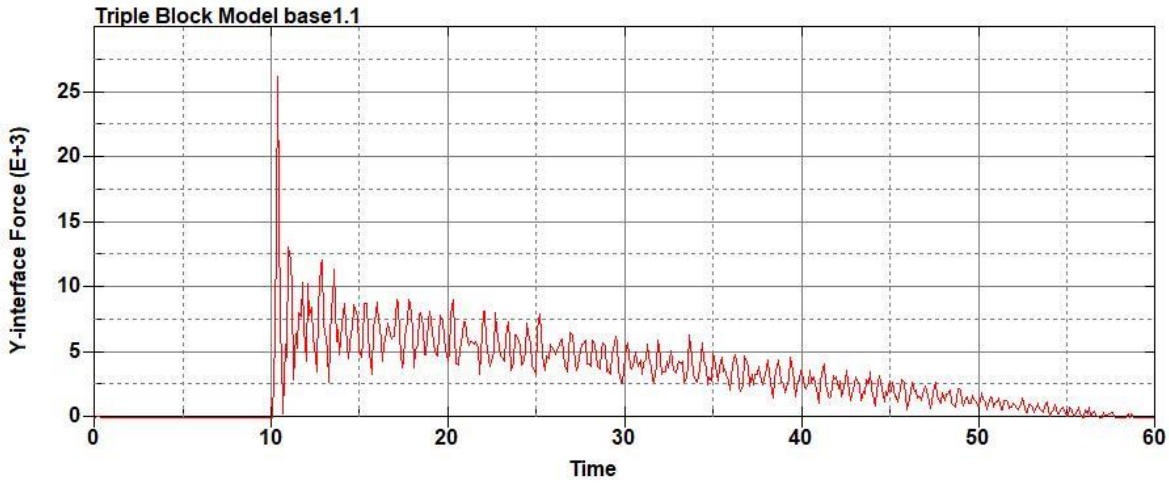


**Figure B-1054: Model Run 7.11 Left Support Y-Interface Force (lbs) versus Time (ms) – 550 psi**

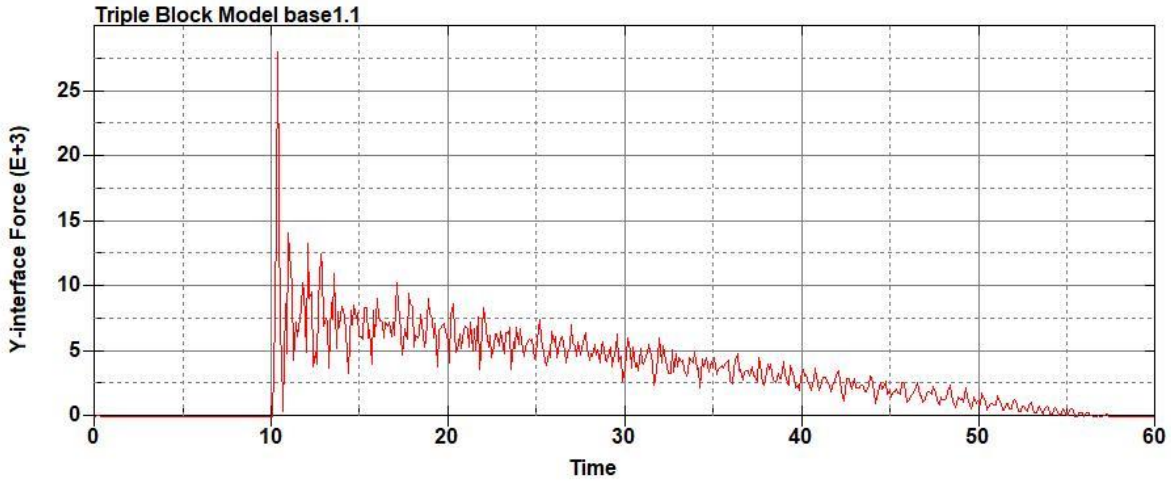


**Figure B-1055: Model Run 7.12 Right Support Y-Interface Force (lbs) versus Time (ms) – 600 psi**

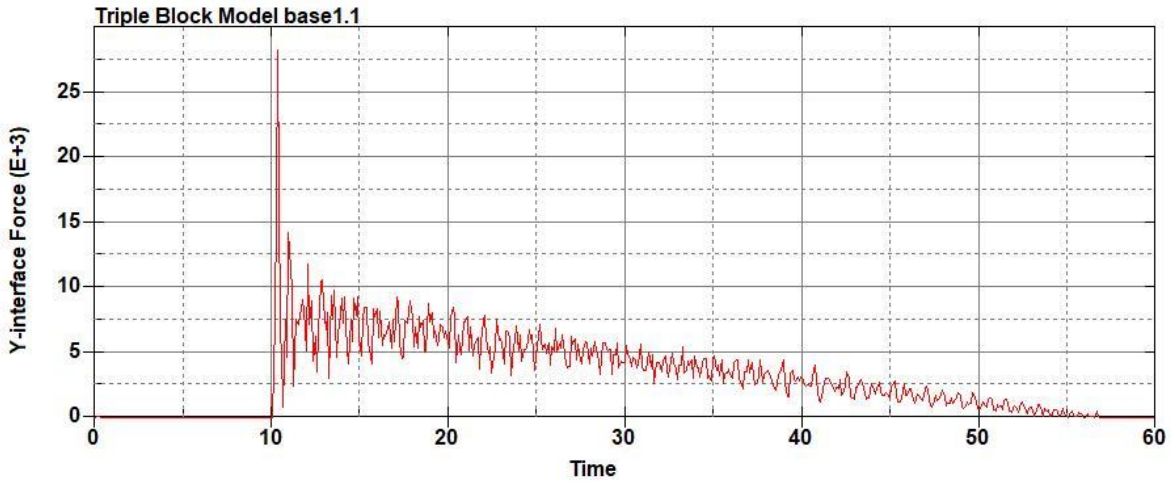


**Figure B-1056: Model Run 7.12 Left Support Y-Interface Force (lbs) versus Time (ms) – 600 psi**

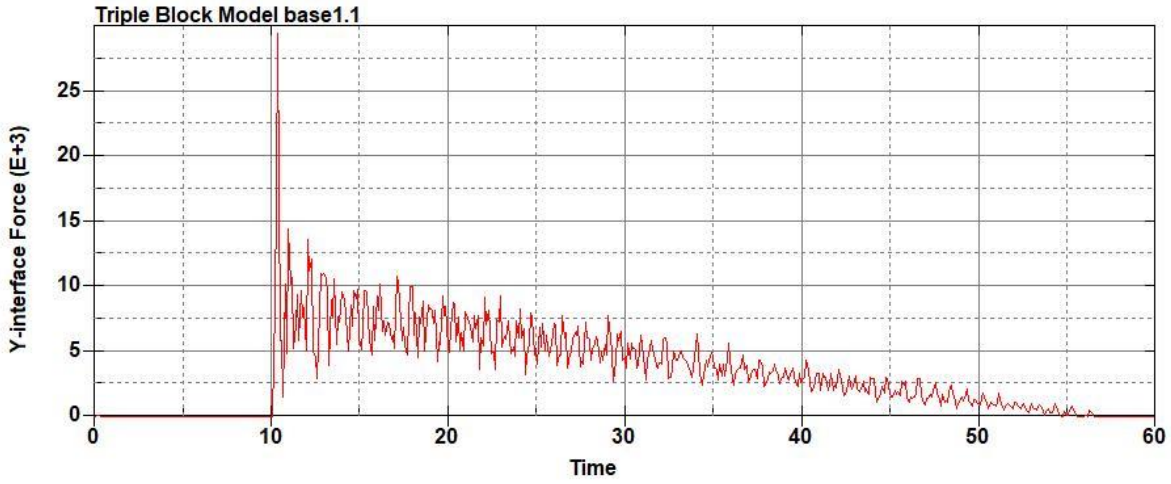


**Figure B-1057: Model Run 7.13 Right Support Y-Interface Force (lbs) versus Time (ms) – 650 psi**

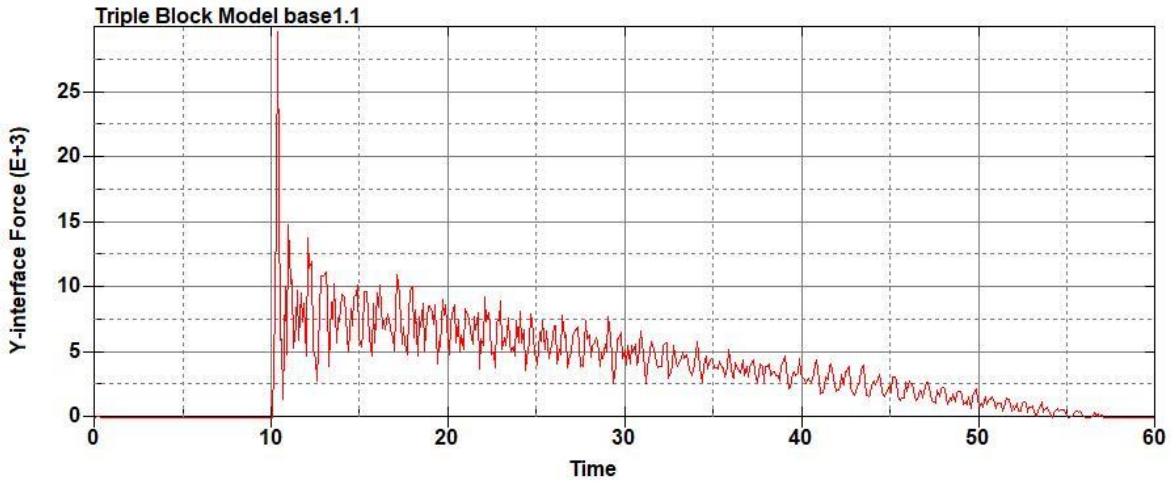


**Figure B-1058: Model Run 7.13 Left Support Y-Interface Force (lbs) versus Time (ms) – 650 psi**

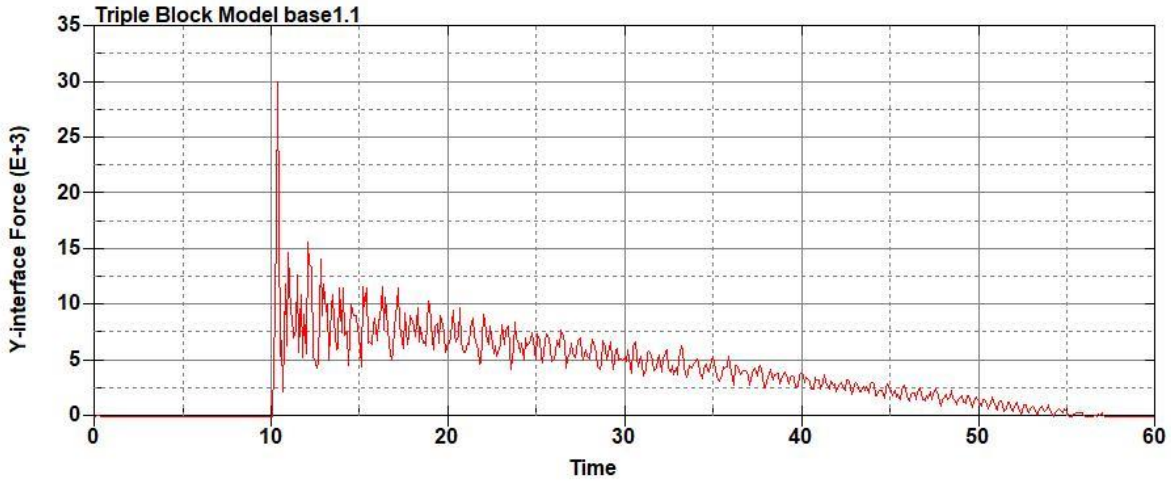


**Figure B-1059: Model Run 7.14 Right Support Y-Interface Force (lbs) versus Time (ms) – 700 psi**

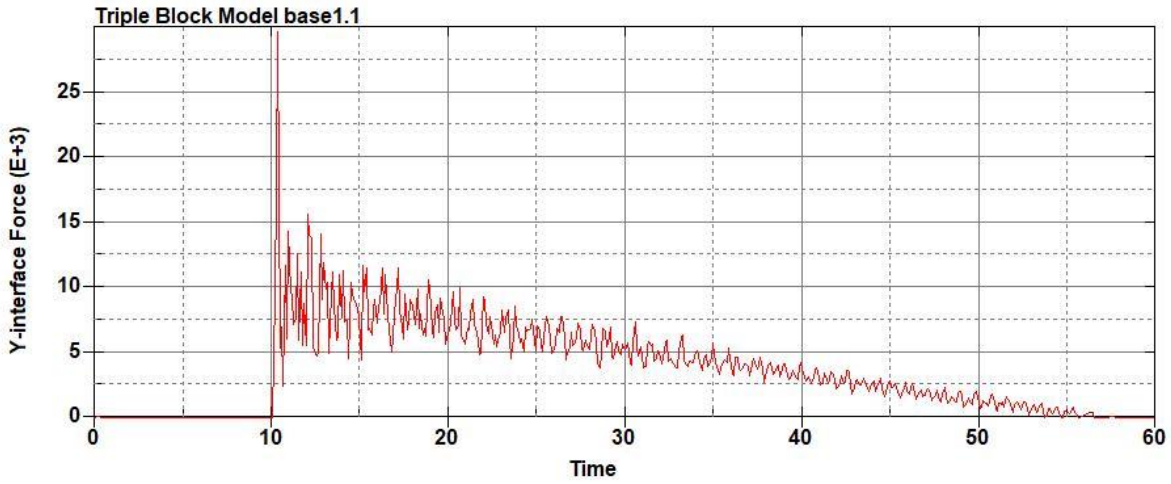


**Figure B-1060: Model Run 7.14 Left Support Y-Interface Force (lbs) versus Time (ms) – 700 psi**

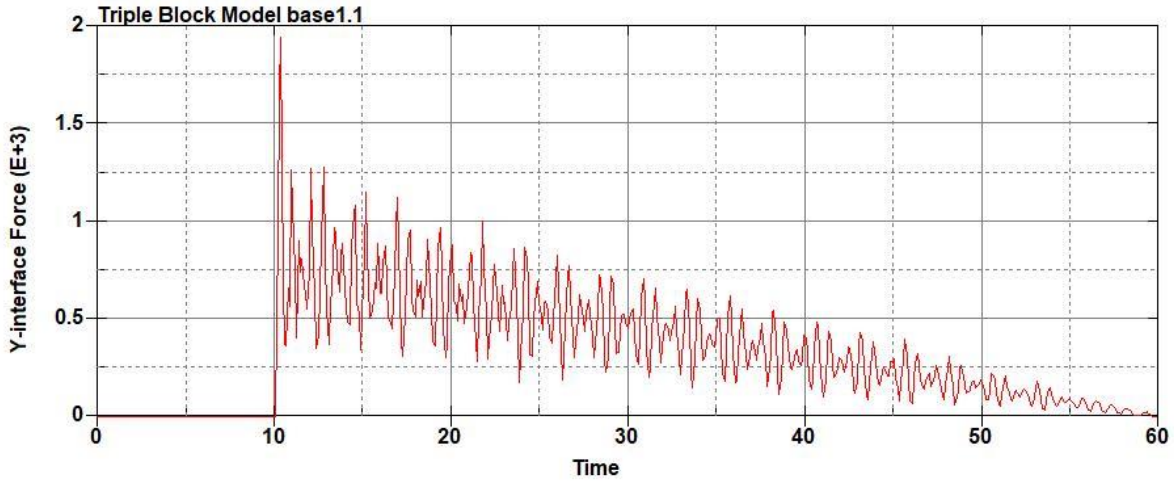


**Figure B-1061: Model Run 8.1 Right Support Y-Interface Force (lbs) versus Time (ms) – 50 psi**

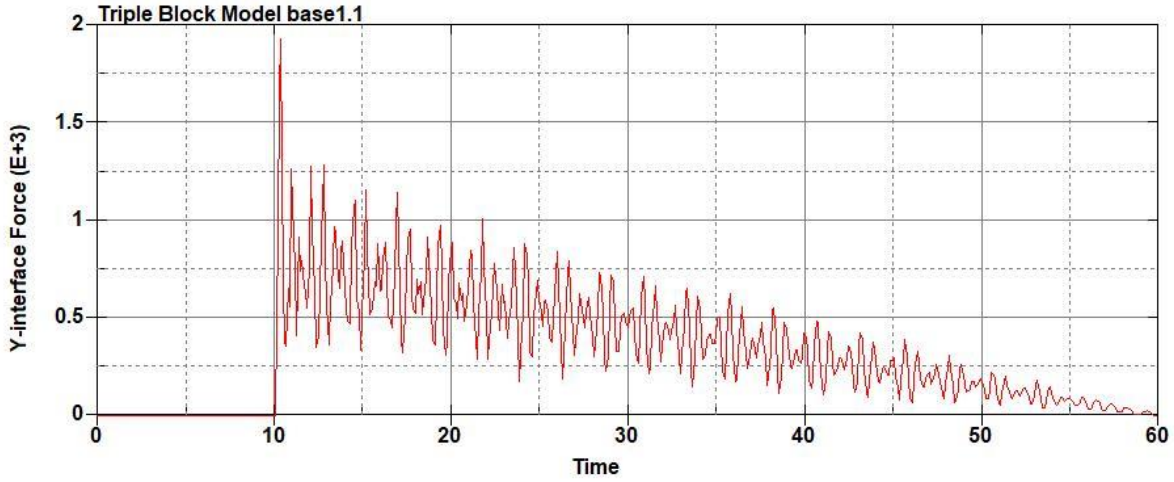


**Figure B-1062: Model Run 8.1 Left Support Y-Interface Force (lbs) versus Time (ms) – 50 psi**

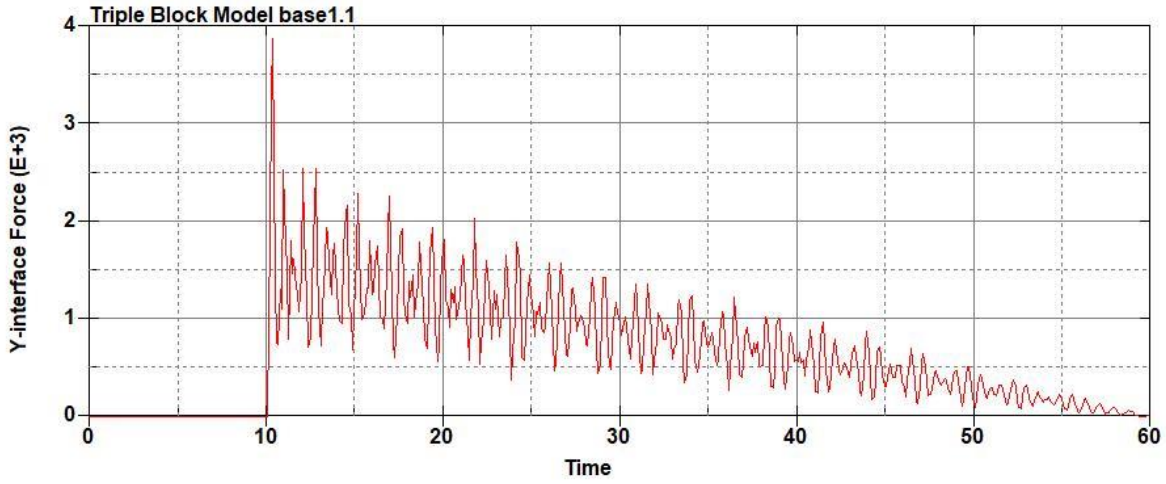


**Figure B-1063: Model Run 8.2 Right Support Y-Interface Force (lbs) versus Time (ms) – 100 psi**

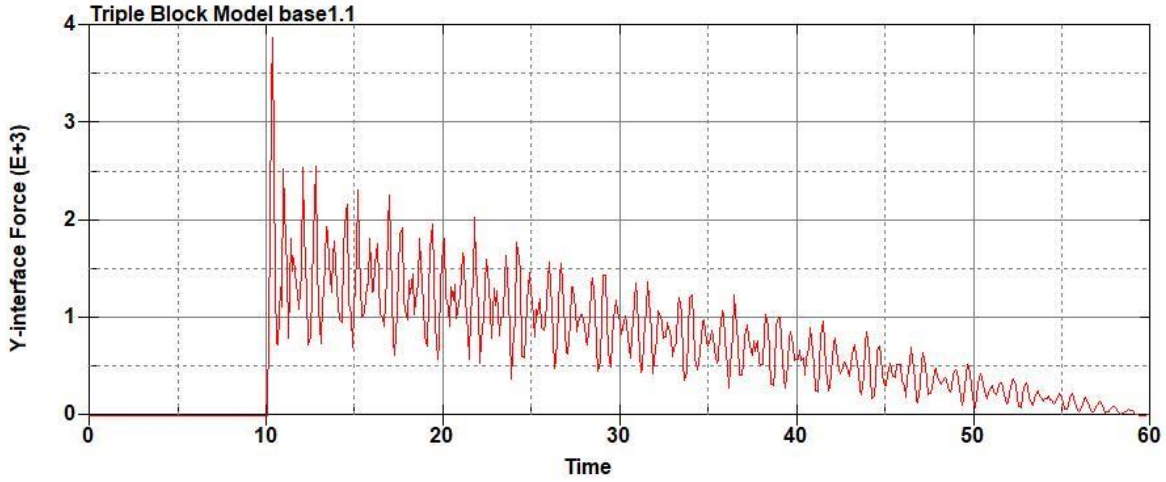


**Figure B-1064: Model Run 8.2 Left Support Y-Interface Force (lbs) versus Time (ms) – 100 psi**

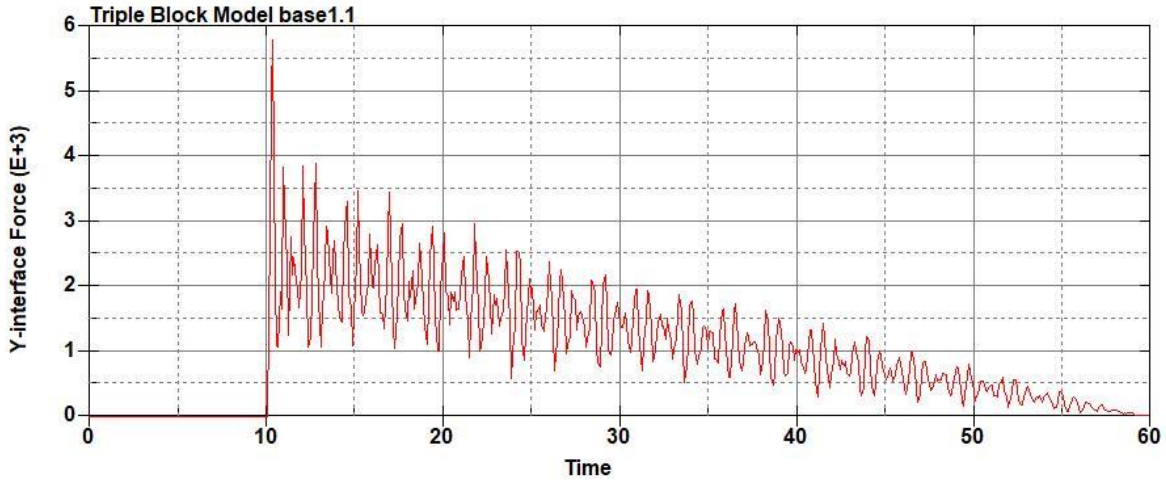


**Figure B-1065: Model Run 8.3 Right Support Y-Interface Force (lbs) versus Time (ms) – 150 psi**

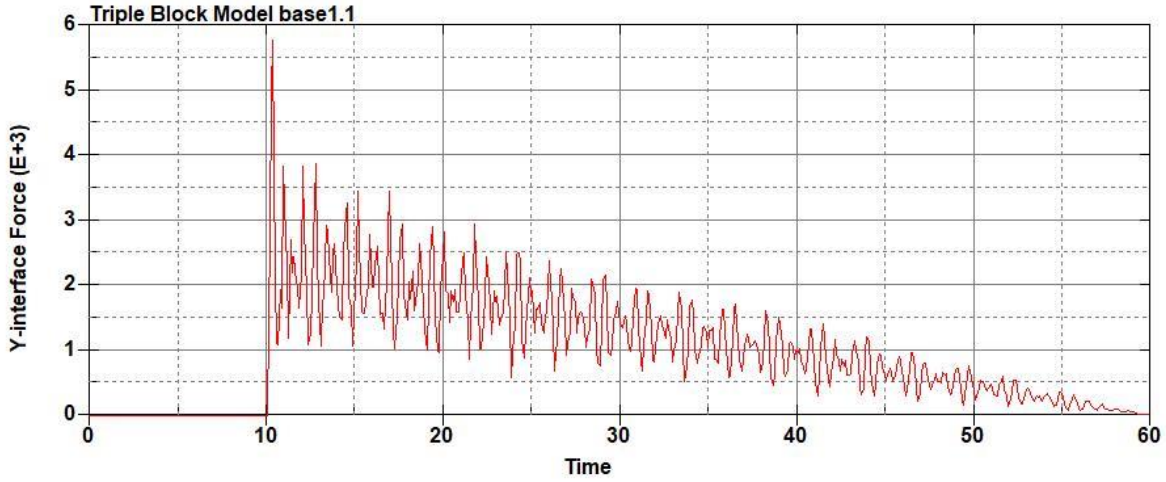


**Figure B-1066: Model Run 8.3 Right Support Y-Interface Force (lbs) versus Time (ms) – 150 psi**

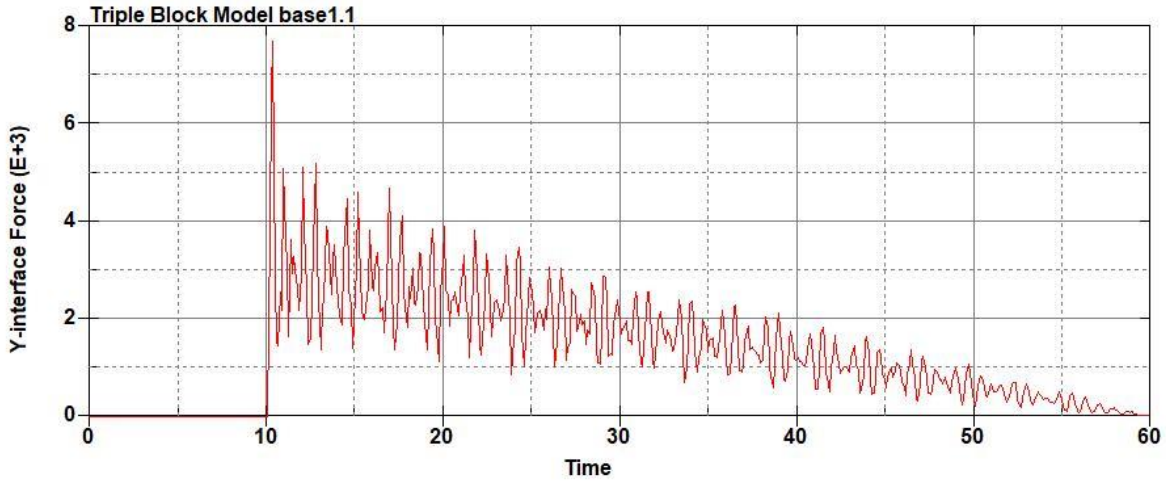


**Figure B-1067: Model Run 8.4 Right Support Y-Interface Force (lbs) versus Time (ms) – 200 psi**

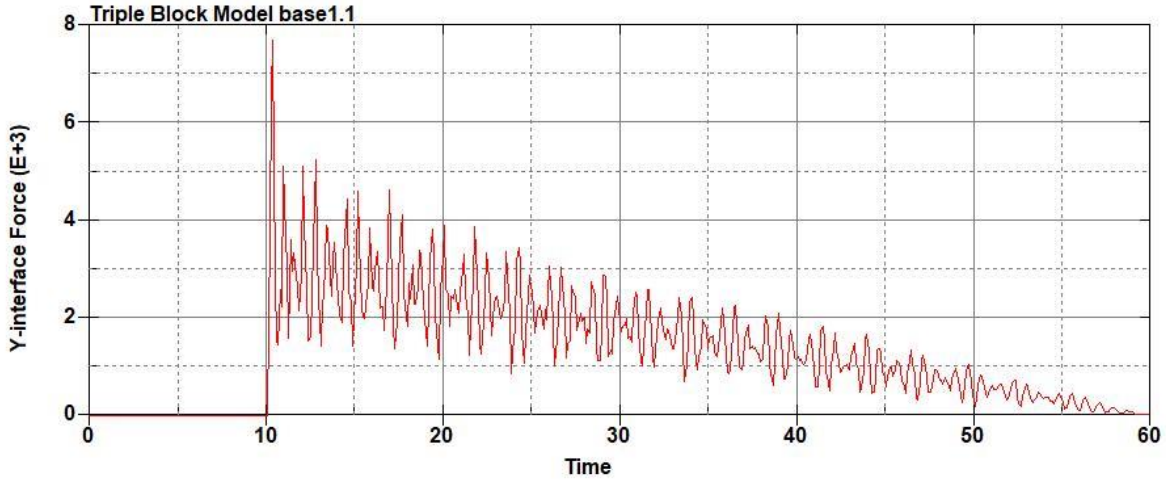


**Figure B-1068: Model Run 8.4 Left Support Y-Interface Force (lbs) versus Time (ms) – 200 psi**

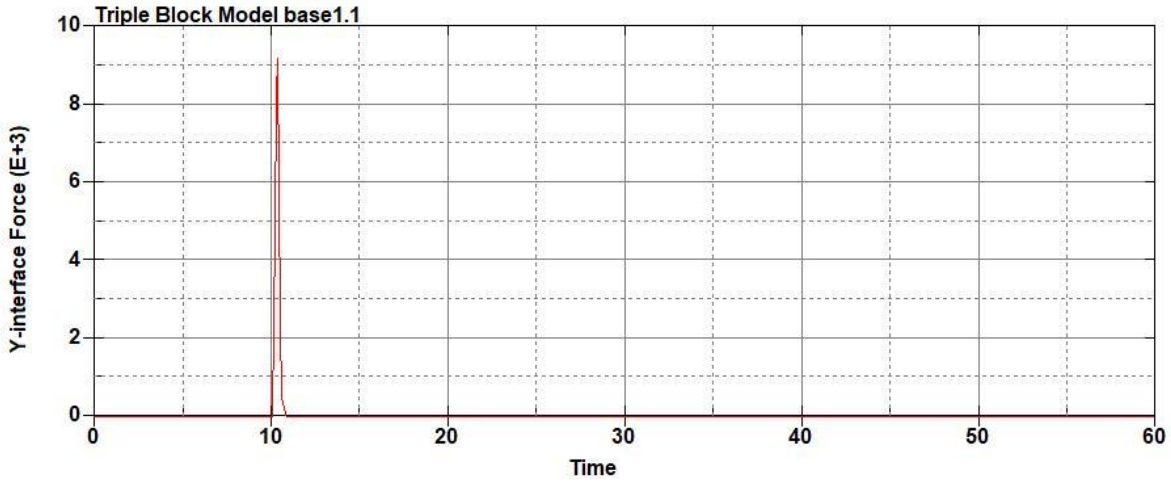


**Figure B-1069: Model Run 8.5 Right Support Y-Interface Force (lbs) versus Time (ms) – 250 psi**

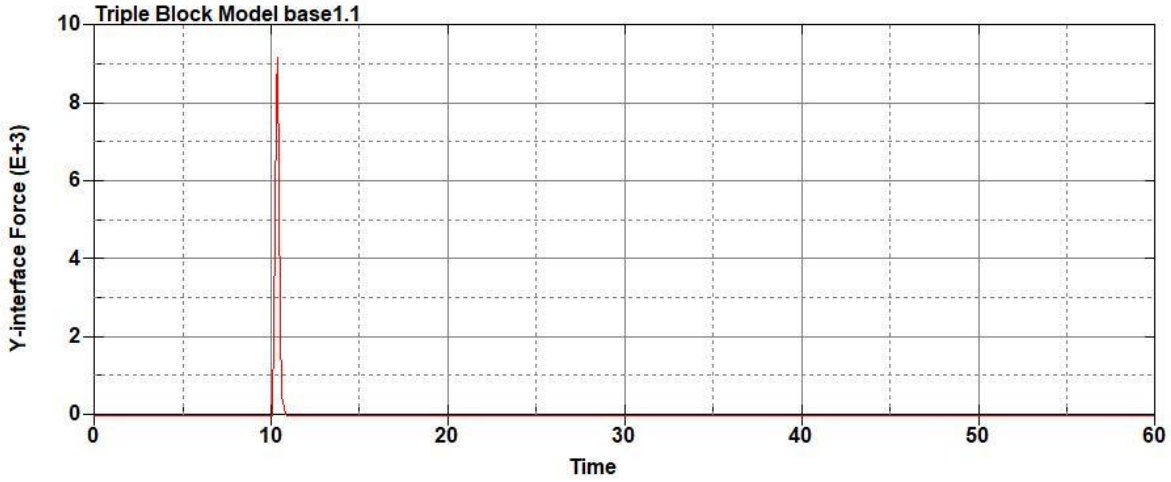


**Figure B-1070: Model Run 8.5 Left Support Y-Interface Force (lbs) versus Time (ms) – 250 psi**

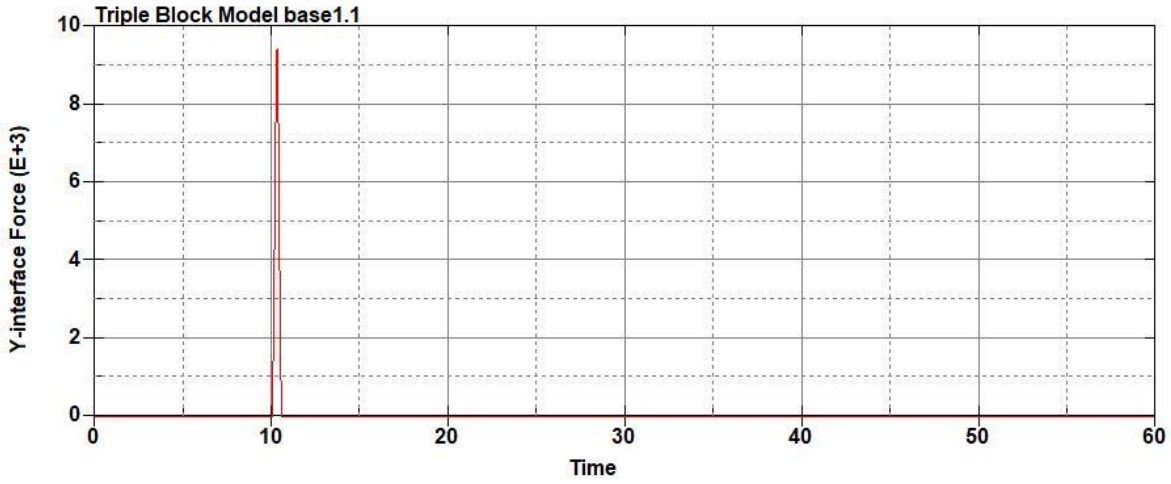


**Figure B-1071: Model Run 8.6 Right Support Y-Interface Force (lbs) versus Time (ms) – 300 psi**

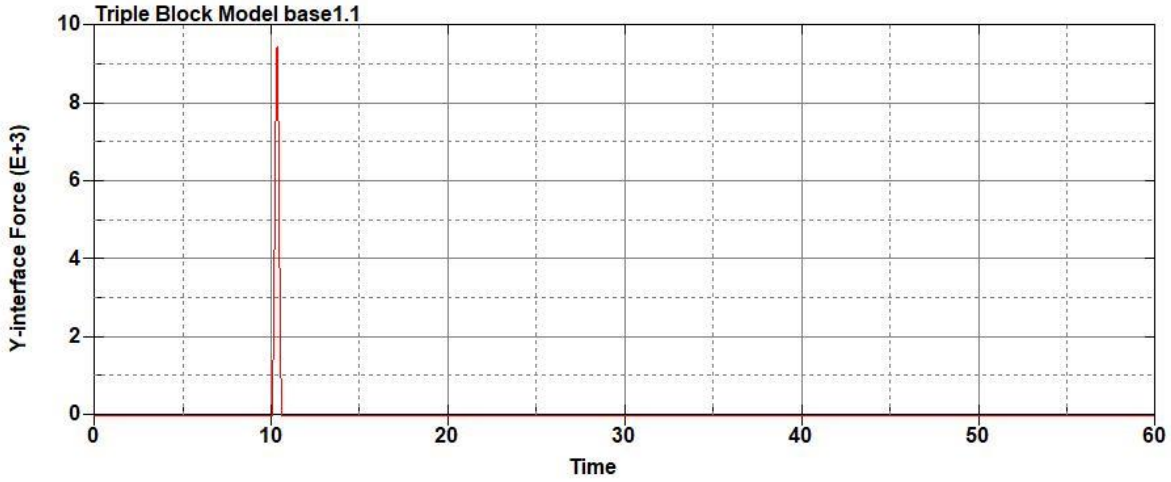


**Figure B-1072: Model Run 8.6 Left Support Y-Interface Force (lbs) versus Time (ms) – 300 psi**

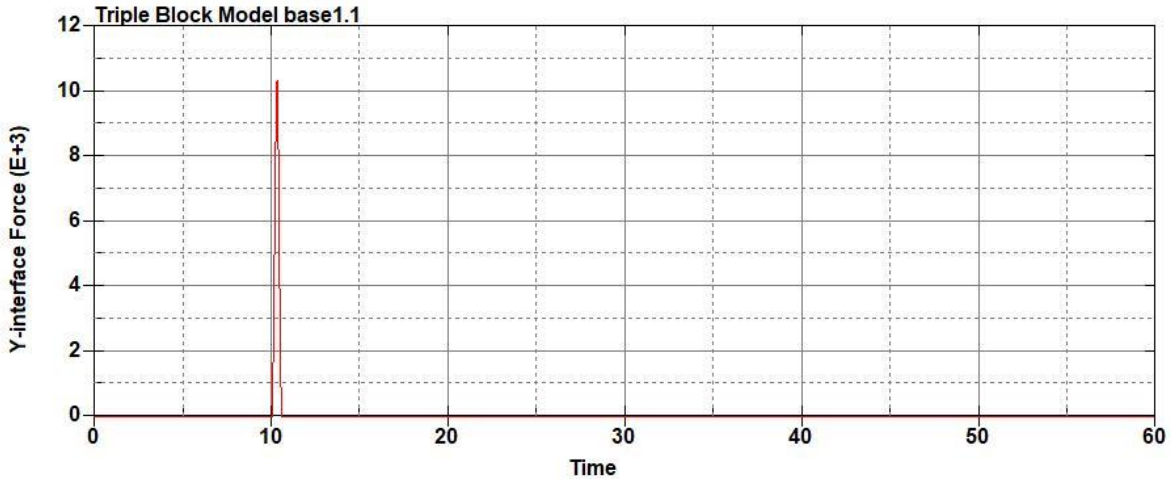


**Figure B-1073: Model Run 8.7 Right Support Y-Interface Force (lbs) versus Time (ms) – 350 psi**

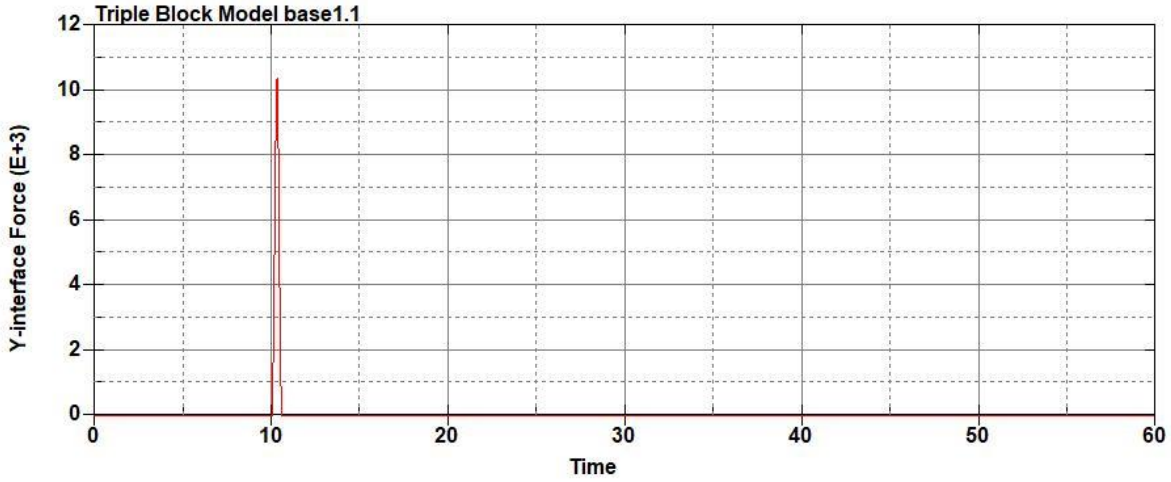


**Figure B-1074: Model Run 8.7 Left Support Y-Interface Force (lbs) versus Time (ms) – 350 psi**

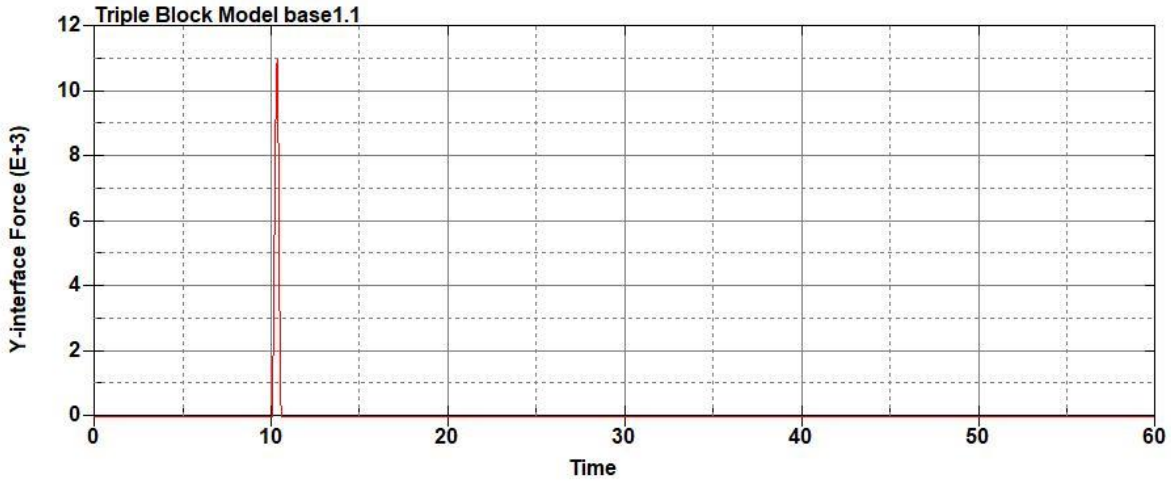


**Figure B-1075: Model Run 8.8 Right Support Y-Interface Force (lbs) versus Time (ms) – 400 psi**

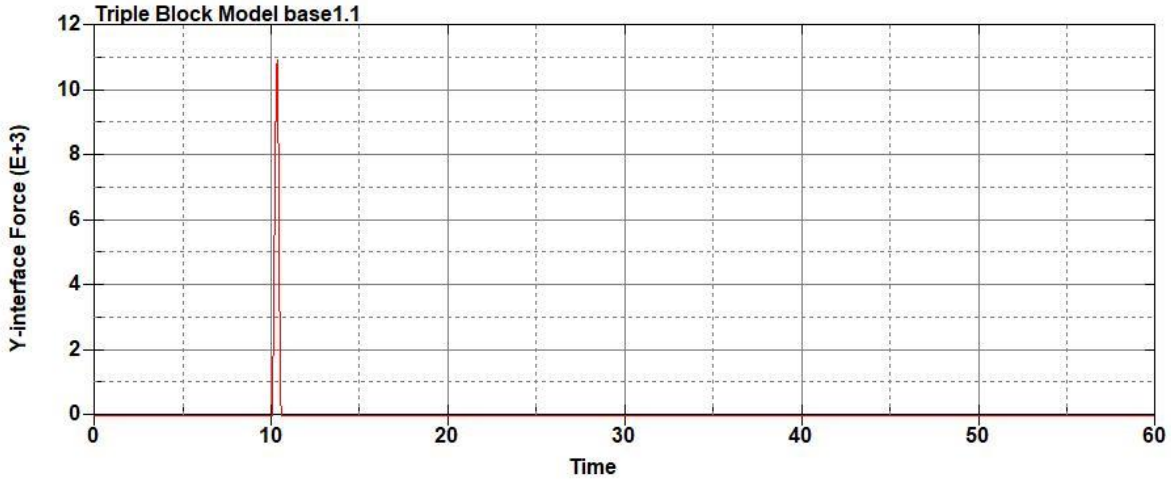


**Figure B-1076: Model Run 8.8 Left Support Y-Interface Force (lbs) versus Time (ms) – 400 psi**

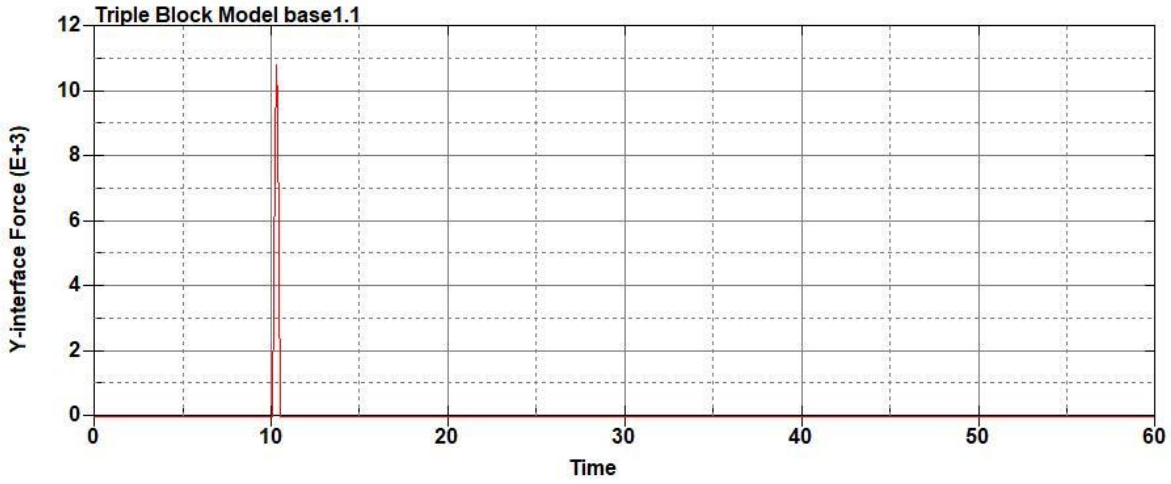


**Figure B-1077: Model Run 8.9 Right Support Y-Interface Force (lbs) versus Time (ms) – 450 psi**

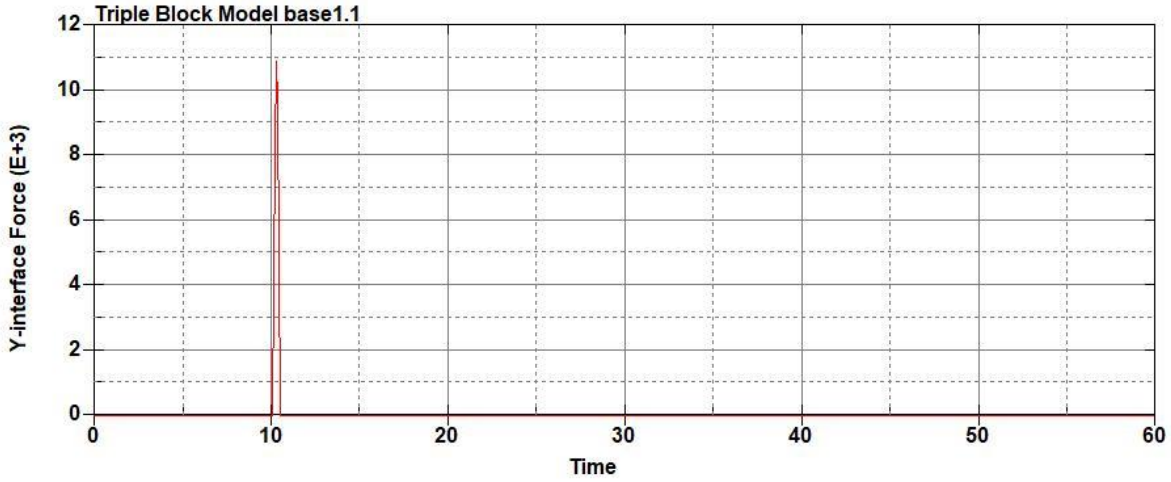


**Figure B-1078: Model Run 8.9 Left Support Y-Interface Force (lbs) versus Time (ms) – 450 psi**

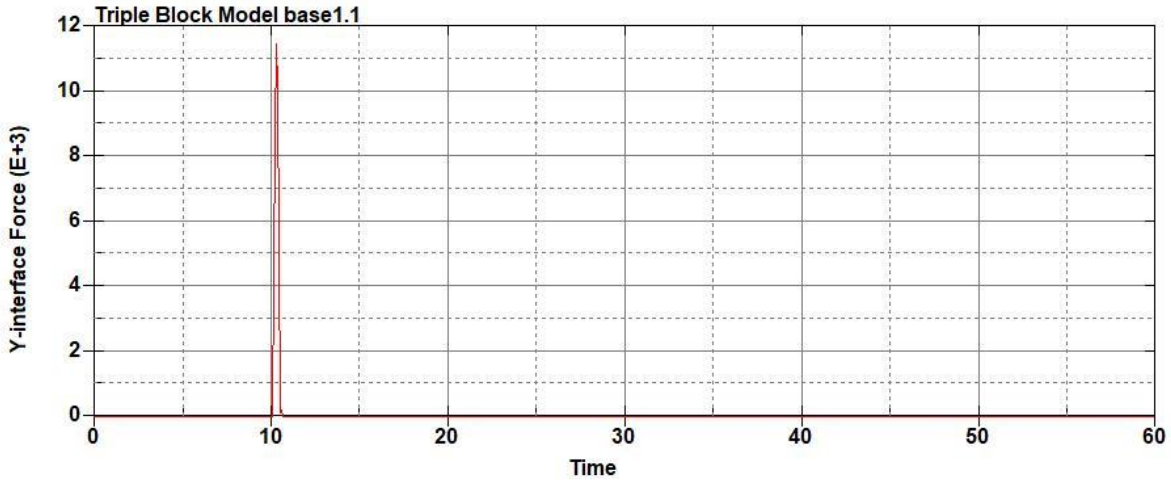


**Figure B-1079: Model Run 8.10 Right Support Y-Interface Force (lbs) versus Time (ms) – 500 psi**

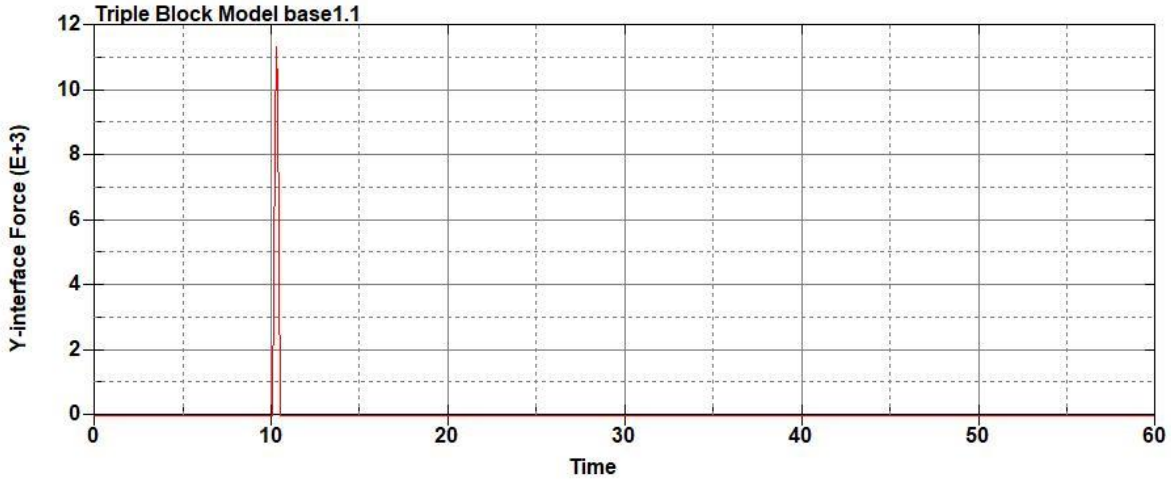


**Figure B-1080: Model Run 8.10 Left Support Y-Interface Force (lbs) versus Time (ms) – 500 psi**